British Columbia

Ministry of Energy and Mines
Energy and Minerals Division
Geological Survey Branch

Paper 2002-1

Geological Fieldwork 2001

A Summary of Field Activities and Current Research

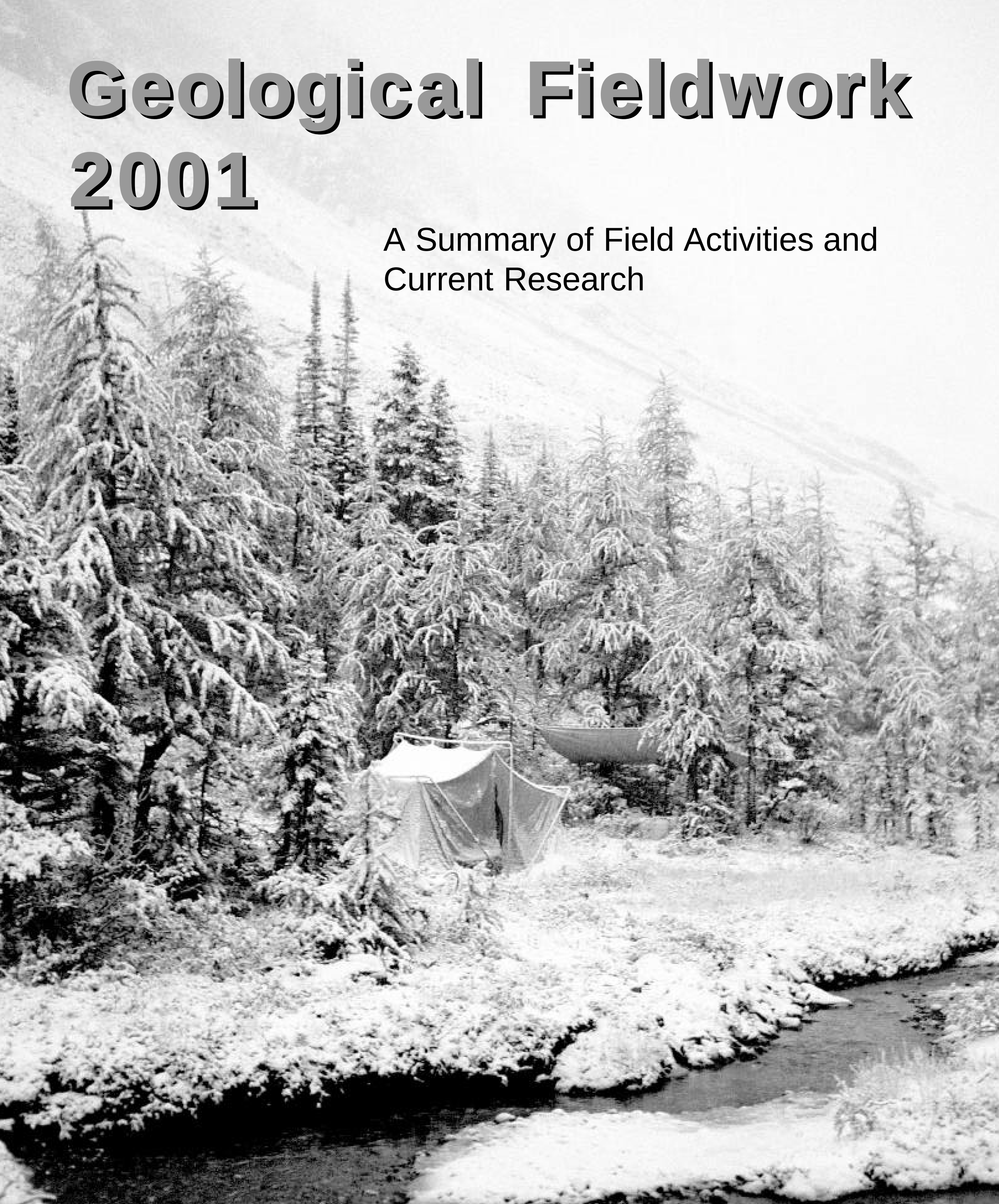

BRITISH COLUMBIA
Ministry of Energy and Mines
Energy and Minerals Division

GEOLOGICAL FIELDWORK 2001

A Summary of Field Activities and Research

PAPER 2002-1

Energy and Minerals Division
Geological Survey Branch

Parts of this publication may be quoted or reproduced if credit is given. The following is the recommended format for referencing individual works contained in this publication:

Mihalynuk, M.G. and Lowe, C. (2002): Atlin TGI, Part I: An introduction to the Atlin targeted geoscience initiative; *in* Geological Fieldwork 2001, *B.C. Ministry of Energy and Mines*, Paper 2002-1, p. 1-12.

British Columbia Cataloguing in Publication Data

Main entry under title:

Geological Fieldwork: - 1974 -

Annual.

Issuing body varies

Vols. For 1978-1996 issued in series: Paper / British Columbia. Ministry of Energy, Mines and Petroleum Resources; vols for 1997- 1998, Paper / British Columbia. Ministry of Employment and Investment; vols for 1999- , Paper / British Columbia Ministry of Energy and Mines.

Includes Bibliographical references.

ISSN 0381-243X=Geological Fieldwork

1. Geology - British Columbia - Periodicals. 2. Mines and mineral resources - British Columbia - Periodicals. 3. Geology - Fieldwork - Periodicals. 4. Geology, Economic - British Columbia - Periodicals. 5. British Columbia. Geological Survey Branch - Periodicals. I. British Columbia. Geological Division. II. British Columbia. Geological Survey Branch. III. British Columbia. Geological Survey Branch. IV. British Columbia. Dept. of Mines and Petroleum Resources. V. British Columbia. Ministry of Energy, Mines and Petroleum Resources. VI. British Columbia. Ministry of Employment and Investment. VII. British Columbia Ministry of Energy and Mines. VIII. Series: Paper (British Columbia. Ministry of Energy, Mines and Petroleum Resources). IX. Series: Paper (British Columbia. Ministry of Employment and Investment). X. Series: Paper (British Columbia Ministry of Energy and Mines).

QE187.46 622.1'09711 C76-083084-3 (Rev.)

Cover photo by Brian Grant - geological field camp in East Kootenays, British Columbia.

Ministry internet website address:
www.em.gov.bc.ca/geology

VICTORIA
BRITISH COLUMBIA
CANADA

JANUARY 2002

TABLE OF CONTENTS

MAPPING

M.G. Mihalynuk and C. Lowe: Atlin TGI, Part I: An Introduction to the Atlin Targeted Geoscience Initiative . . . 1

M.G. Mihalynuk, S.T. Johnston, C. Lowe, F. Cordey, J.M. English, F.A.M. Devine, K. Larson and Y. Merran: Atlin TGI Part II: Preliminary Results from the Atlin Targeted Geoscience Initiative, Nakina Area, Northwest British Columbia. 5

J.M. English, M.G. Mihalynuk, S.T. Johnston and F.A. Devine: Atlin TGI Part III: Geology and Petrochemistry of Mafic Rocks within the Northern Cache Creek Terrane and Tectonic Implications 19

K. Larson: Microstructural Analysis of the Teslin Fault, Northwestern British Columbia 31

M.G. Mihalynuk and L.M. Heaman: Age of Mineralized Porphyry at the Logtung deposit W-Mo-Bi-Be (Beryl, Aquamarine), Northwest BC 35

J. Nelson: Tracking Yukon-Tanana Terrane VMS Host Stratigraphy and Intrusion-Related Gold in the Southern Sylvester Allochthon. 41

F. Ferri and B.H. O'Brien: Preliminary Geology of the Cariboo Lake Area, Central British Columbia . . . 59

P. Schiarizza, S. Heffernan and J. Zuber: Geology of Quesnel and Slide Mountain Terranes West of Clearwater, South-Central BC 83

R. Friedman, G. Ray and I. Webster: U-Pb Zircon and Titanite Dating of Intrusive Rocks in the Heffley Lake Area, South-Central British Columbia 109

L.J. Diakow, J.B. Mahoney, T.G. Gleeson, M.G. Hrudey, L.C. Struik and A.D. Johnson: Middle Jurassic Stratigraphy Hosting Volcanogenic Massive Sulphide Mineralization in Eastern Bella Coola Map Area, Southwest British Columbia. 119

R.M. Friedman and J.K. Mortensen: U-Pb Zircon and Titanite Dating in Support of British Columbia Geological Survey Regional Mapping Studies. 135

ECONOMIC GEOLOGY

D. J. Alldrick and W. Jackaman: Metal Zoning in the Ecstall VMS Belt, Northwest British Columbia 151

G.T. Nixon and D.A. Archibald: Age of Platinum-Group-Element Mineralization in the Sappho Alkaline Complex, South-Central B.C. 171

K.P.E. Dunne and R. H. Pinsent: Depositional Setting of Silver-Rich Quartz-Sulphate-Carbonate Deposits of the Upper Kitsault River Area, Northwest BC 177

C. Ash: Geology of the East Harrison Lake Belt, SW BC. . 197

R.H. Pinsent: Ni-Cu-PGE Potential of the Giant Mascot and Cogburn Ultramafic-Mafic Bodies, Harrison-Hope Area, Southwestern British Columbia 211

J.M. Logan: Intrusion-Related Gold Mineral Occurrences of the Bayonne Magmatic Belt. 237

A.S. Legun: Overview of Coalbed Methane Geology in Northeast British Columbia 247

G. Ray, I. Webster, P. Megaw, J. McGlasson and K. Glover: The Lustdust Property in Central British Columbia: A Polymetallic Zoned Porphyry-Skarn-Manto-Vein System 257

K.P.E. Dunne and G. E. Ray: Constraints on Fluid Evolution at the Polymetallic Lustdust Porphyry-Skarn-Manto-Vein Prospect, North-Ccentral British Columbia 281

V.M. Levson, D.J. Mate and T. Ferbey: Platinum-Group-Element (PGE) Placer Deposits in British Columbia: Characterization and Implications for PGE Potential 303

INDUSTRIAL MINERALS

G.J. Simandl: Tantalum Market and Resources: An Overview 313

B. Ryan: Note on Desorption Results of Comox Formation Coals from the Courtenay Area, Vancouver Island, British Columbia 319

B. Ryan and B. Lane: Adsorption Characteristics of Coals with Special Reference to the Gething Formation, Northeast British Columbia 331

B. Ryan, M. Fournier and M. Dittrick: Selenium Concentrations in Mine Refuse and Mist Mountain Rocks; Evaluation of Variations Laterally and Over Time . . . 347

EXPL0RATION SERVICES

R. Lett and W. Jackaman: PGE Stream Sediment Geochemistry in British Columbia 365

W. Jackaman, R. Lett and P. Friske: National Geochemical Reconnaissance Surveys in the B.C. Cordillera to Target and Attract Mineral Exploration 377

D. Lefebure, W. Jackaman, M. Mihalynuk and J. Nelson: Anomalous RGS Survey Results West of Dease Lake - New Massive Sulphide Targets 383

R . Lett, V. Levson and C. Dunn: A Provisional Geochemical Exploration Model (GEM) for the Sappho Property, BC 389

P. Bobrowsky, M. Cathro and R. Paulen: Quaternary Geology Reconnaissance Studies 397

A.J. Bichler, E. D. Brooks and P.T. Bobrowsky: Sunshine Coast Aggregate Potential Mapping Project . . . 403

L. Jones, D. MacIntyre and P. Desjardins: The MapPlace - An Internet-based Mineral Exploration Tool. 409

Atlin TGI, Part I: An Introduction to the Atlin Targeted Geoscience Initiative

By Mitchell G. Mihalynuk[1] and Carmel Lowe[2]

KEYWORDS: *Geology, aeromagnetic, survey, mineral potential, resource, volcanogenic massive sulphide, pluton related gold, geochemistry, fossil, geochronology, Cache Creek Terrane, Atlin, Nakina.*

INTRODUCTION

Placer gold exploration and mining within the Atlin camp has been an economic driving force for the region during much of the last century. However, the area is well endowed with geological environments prospective for other types of mineral deposits. Unfortunately exploration for commodities other than gold has received relatively little attention, in part because the existing regional geological framework for the Atlin area (104N) stems from mapping in the early 1950's, predating the advent of plate tectonic theory (Aitken, 1959).

To help address the disparity between high mineral potential values and low mineral exploration expenditures, a proposal to study the Atlin area was chosen from numerous geoscience proposals from across Canada to receive funding under the Targeted Geoscience Initiative of the Geological Survey of Canada (GSC). The Atlin Targeted Geoscience Initiative is a three-year, multi-disciplinary project aimed at a fundamental revision of the geological and mineral resource knowledgebase for the Atlin area of north-western British Columbia. Principal project components are regional aeromagnetic and geological mapping surveys within the Atlin map area (NTS 104N; Figure 1). Collection of high-resolution aeromagnetic data over the entire project area was initiated in 2000. During 2001, matching funding by the British Columbia Geological Survey(BCGS) permitted systematic bedrock mapping at a 1:50 000 scale in the

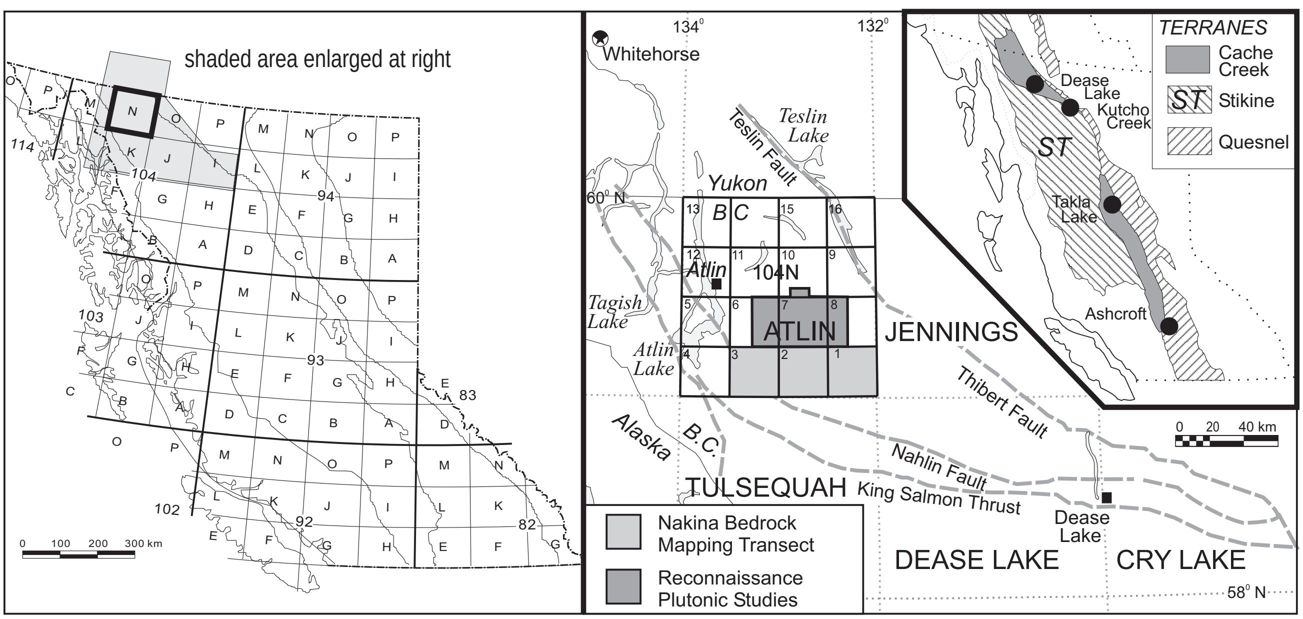

Figure 1. Location of the Atlin Integrated Geoscience Project in northwestern British Columbia. Bold outlined box (104N) shows extent of aeromagnetic survey. Regional geological mapping surveys were conducted over the eastern and central Nakina transect (104N/1 and 2). Reconnaissance plutonic studies covered parts of 104N/6, 7, 8 and 10.

[1] *British Columbia Ministry of Energy and Mines*
[2] *Geological Survey of Canada*

south-eastern project area (104N/1 and 2), as well as follow-up ground based magnetic and geologic surveys of post-accretionary plutonic bodies. Work conducted in 2001 involves researchers from the University of Victoria (UVic), The University of British Columbia (UBC) and Université Claude Bernard (UCB), Lyon, France. Geological map data collected in 2001 will be enhanced by geochemical, isotopic, and biogeochronological interpretations. Three university thesis studies initiated under the auspices of TGI will evaluate limestone sequence stratigraphy (Y. Merran, UCB), volcanic environments and petrogenesis (J. English, UVic) and tectonic evolution of serpentinite melange belts (F. Devine, UBC). A thesis study on the origin of ultramafites (G. Shellnut, UVic) received logistical support from the Atlin TGI, as did a CO_2 sequestration study (G. Dipple, UBC). *See* Table 1 for a detailed list of Atlin TGI participants and affiliated researchers.

PROJECT TIMELINE AND DELIVERABLES

Addressing Atlin TGI project objectives began early in 2000 with the production of shaded-relief digital elevation

TABLE 1
PRODUCTS PLANNED FOR THE ATLIN TGI

Topic	Person(s)	Affiliation	Product(s)	Status
Regional aeromagnetics	Dumont, R., Coyle, M. and Potvin, J.	GSC Ottawa	16 - 1:50 000 sheets	Complete
Aeromagnetic thematic studies	C. Lowe	GSC	Thematic maps and topical report(s)	Analysis underway
Regional mapping	M. Mihalynuk, S. Johnston, F. Cordey, F. Devine, J. English, Y. Merran, K. Larson	BCGS, UVic, UCB	1:50 000 sheets: 104N/1, 2 and 3	Compilation complete for 104N1&2
Magmatic rocks study	R. Anderson	GSC Vancouver	Input for magnetic modelling, topical report(s)	Samples in preparation
Radiolarian micropaleontology	F. Cordey	UCB	Fossil age database; approximately 80 age determinations	Results from first 24 samples in TGI Part II
Conodont micropaleontology	M. Orchard	GSC Vancouver	Fossil age database; approximately 25 samples in 2001	Sample preparation
Coral paleontology and paleobiogeography	W. Bamber	GSC Calgary	Fossil age database and paleobiogeographical interpretations	Preliminary identifications completed
Fusulinid paleontology and paleobiogeography	L. Rui	Paleontological contractor, Calgary	Fossil age database and paleobiogeographical interpretations	In preparation
Atlin geoscience lecture series	Johnston, S.T., Mihalynuk, M. Lowe, C. and Cordey, F.	UVic, BCGS, GSC, UCB	Four free public lectures in Atlin, summer 2001	Completed
Atlin Geoscape Poster	Anderson and others	GSC Vancouver	Public information in popular wall poster format	Mock-up complete
Petrogenesis of volcanic	J. English	UVic	M.Sc. thesis, presentations and papers	1st paper completed -see Atlin TGI Part III
Carbonate facies	Y. Merran	UCB	M.Sc. thesis, presentations and papers	Samples in preparation
Evolution of serpentinite mélange	F. Devine	UBC	B.Sc. thesis, presentations and paper	Geochronology samples in preparation
Ultramafites of the Cordillera	G. Shellnut	UVic	Ph.D. thesis, presentations and papers	1st paper in preparation for *Yukon Exploration and Geology*
Atlin area geochronology	M. Villeneuve	GSC Ottawa	Geochronological database and topical report(s)	Samples in preparation
CO_2 Sequestering potential of ultramafites	G. Dipple and students	UBC	Reconnaisance in 2001	Samples in preparation
Whitehorse Geoscience Forum presentation	C. Lowe and Mihalynuk, M.	GSC, BCGS	Oral presentations	Delivered
Cordilleran Roundup presentations	C. Lowe and others	GSC and others	Oral presentation (Lowe), 4 poster sessions	In preparation

models from Provincial 1:20 000 scale Terrain and Resource Information Management (TRIM) elevation data. This base was used to produce a colour-enhanced surficial geology map of the Atlin placer district. Existing geoscience information was compiled for the Atlin 1:250 000 sheet, based largely on an extensive compilation effort in the mid-nineties (Mihalynuk *et al*., 1996), but also using additional sources, such as unpublished 1:25 000 scale mapping by Jim Monger (GSC emeritus; cf. Monger, 1975). This new compilation map has been presented draped over the shaded relief elevation model. Also in 2000, a coincident release of reanalysed Regional Stream Sediment geochemical survey pulps by the BCGS (Jackaman *et al.*, 2000) aided in focusing the Atlin project in areas with stream sediment geochemical anomalies.

Approximately 32,000 line kilometres of aeromagnetic data was acquired over the entire project area in 2000 and early 2001. Flight lines were spaced 500 m apart and drape flown at a minimum terrain clearance of 200 m. To assist in interpretations of the airborne data, magnetic susceptibility measurements were made on archival hand samples, mainly from the BCGS rock stores. The aeromagnetic survey results have been published at 1:50 000 scale as a series of sixteen aeromagnetic anomaly maps (Dumont *et al*., 2001a, b, c and 13 others). Summer field programs in 2001 focused on geological mapping of NTS map sheets 104N/1 and 2 and ground investigations of selected magnetic anomalies. A preliminary report of the geological findings can be found in Atlin TGI Parts II and III (Mihalynuk *et al*., this volume; English *et al*., this volume).

Aeromagnetic data will be modeled and a geological map of 104N/1 will be produced for release in early 2002. In the summer of 2002, TGI project plans call for completion of mapping of 104N/2 and /3, and timely publication as Open File maps in early 2003.

AEROMAGNETIC SURVEY RESULTS SUMMARY

A summary of the Atlin aeromagnetic survey results is presented in Lowe and Anderson (2002). Highlights of the new aeromagnetic data set include:

1. Several, small (<5 km) sub-oval, positive and negative magnetic anomalies punctuate the subdued magnetic field that characterizes regions underlain by the Kedahda assemblage (dominated by cherts, argillites, siltstone and limestone) in the central part of the project area. At least two of these anomalies correlate with reported outcrops and subcrops of porphyry intrusions and with known copper mineralization.
2. Several E- to ENE-trending magnetic lineaments are imaged in the new data set. Two are more than 30 km long. They are not explained by known surface geology in the Atlin project area, although ENE-trending faults have been mapped in the Tagish map area farther to the west (Mihalynuk, 1999). These lineaments mark the southern boundary of some of the intrusive bodies and may be related to their emplacement or exhumation; as such they may represent important mineralizing conduits.
3. Crustal-scale faults such as the Nahlin, Llewellyn and Teslin correspond with strong northwest-trending magnetic lineaments. Magnetic lineaments with similar orientations transect the eastern portion of the Surprise Lake batholith and adjacent aureole where no faults have been mapped previously. Veins enriched with magnetite and base metals infill fractures at a number of localities along these lineaments.
4. Plutonic rocks show markedly different magnetic responses: the Fourth of July, Coconino, and Slaughter House intrusions correlate with strong, positive and relatively homogeneous magnetic anomalies; the Surprise Lake Suite of plutons are weakly magnetic; the magnetic fields observed over the Llangorse, Mount McMaster and Chichoida plutons are heterogeneous with distinct zones of positive and negative magnetic anomalies observed within each body.
5. Magnetic anomalies over exposures of the Nahlin ultramafite are the most intense within the map area. Data collected in the southern project area indicate that the body is a relatively shallowly north-dipping slab.

GEOLOGICAL SURVEY RESULTS SUMMARY

Preliminary results from mapping in the Nakina area are detailed in TGI Part II that follows this introduction (Mihalynuk *et al*., 2002). As part of the mapping program, extensive sample suites were collected for petrographic analysis, micro- and macro-paleontology, major and trace element lithogeochemistry, detailed stratigraphy, and isotope geochronology. At this stage, analysis of these samples is incomplete; results will be reported in succeeding papers.

Geological mapping conducted in other parts of the Atlin sheet focused on plutonic rocks with a six day reconnaissance mapping and sampling program over the McMaster and Llangorse plutons, their adjacent thermal aureoles and satellite stocks (cf. Lowe and Anderson, 2002), in part to explain aeromagnetic anomalies. Reconnaissance and detailed mapping of intrusions within the Atlin map area, including the Surprise Lake batholith, will resume during the 2002 field season. Questions addressed will concern the origin, timing and mode of emplacement of the intrusions and why anomalously high Regional Geochemical Survey stream sediment gold values are concentrated in streams draining the plutons and their aureoles.

CO_2 SEQUESTERING IN SERPENTINITE

Quartz-carbonate-mariposite altered serpentinites (listwanites) are widespread in the Atlin area where they have been the focus of lode gold exploration for most of the past century. They represent a geologic storehouse of carbon dioxide sequestered from mineralizing fluids during carbonation of magnesium silicate. They are also possible sinks for atmospheric CO_2, and are under investigation as part of an international effort to reduce greenhouse gases produced by combustion of fossil fuels. Greg Dipple (UBC) joined the Atlin TGI to initiate an NSERC funded study of

CO_2 sequestration in geologic systems. Media under investigation for industrial scale injection of CO_2 are asbestos waste rock piles and *in situ* serpentinite bodies. Critical for the efficacy of *in situ* sequestration are the initial and evolving state of serpentinite reservoir permeability and reaction kinetics as carbonation reactions proceed. Analysis of large-scale fossil CO_2 sequestering systems (listwanites) preserved in the Atlin area should provide insight into these questions. Dipple plans to have two thesis-based projects in place for the 2002 field season.

PUBLIC OUTREACH

Delivery and dissemination of geoscience information to a broad audience is a key objective of the Atlin TGI. To this end a series four free public geoscience lectures were delivered during the field season in Atlin. Continued delivery of project results will be by a combination of public lectures, posters sessions and conventional maps and reports (*see* Table 1). ***Atlin Geoscape***, a wall poster product aimed directly at public education is currently in production (Anderson). A project web site (http://www.pgc.nrcan.gc.ca/atlintgi) presents a project overview, current activities and project news.

REFERENCES CITED

Aitken, J.D. (1959): Atlin map-area, British Columbia, *Geological Survey of Canada*, Memoir 307, 89 pages.

Dumont, R., Coyle, M. and Potvin, J. (2001a): Aeromagnetic total field map British Columbia: Nakina Lake, NTS 104N/1; *Geological Survey of Canada*, Open File 4091.

Dumont, R., Coyle, M. and Potvin, J. (2001b): Aeromagnetic total field map British Columbia: Nakina, NTS 104N/2; *Geological Survey of Canada*, Open File 4092.

Dumont, R., Coyle, M. and Potvin, J. (2001c): Aeromagnetic total field map British Columbia: Sloko River, NTS 104N/3; *Geological Survey of Canada*, Open File 4093.

English, J.M., Mihalynuk, M.G., Johnston, S.T. and Devine, F.A.M. (2002): Atlin TGI Part III: Geology and Petrochemistry of mafic rocks within the northern Cache Creek terrane and tectonic implications; *in* Geological Fieldwork 2001, *BC Ministry of Energy and Mines*, Paper 2002-1, this volume.

Jackaman, W. (2000): British Columbia Regional Geochemical Survey, NTS 104N - Atlin; *BC Ministry of Energy and Mines*, BC RGS 51.

Lowe, C. and Anderson, R.G. (2002): Preliminary interpretations of new aeromagnetic data for the Atlin Map area, British Columbia - preliminary interpretations; *in* Current Research, Part A, *Geological Survey of Canada*, Paper 2002-A/7, 10 pages.

Lowe, C. and Mihalynuk, M.G. (2002): Overview of the Atlin Integrated Geoscience Project, northwestern British Columbia - *in* Current Research, Part A, *Geological Survey of Canada*, Paper 2002-A6, 7 pages.

Mihalynuk, M.G. (1999): Geology and Mineral Resources of the Tagish Lake Area; *BC Ministry of Energy and Mines,* Bulletin 105, 117 pages.

Mihalynuk, M.G., Bellefontaine, K.A., Brown, D.A., Logan, J.M., Nelson, J.L., Legun, A.S. and Diakow, L.J. (1996): Geological compilation, northwest British Columbia (NTS 94E, L, M; 104F, G, H, I, J, K, L, M, N, O, P; 114J, O, P); *B.C. Ministry of Energy, Mines and Petroleum Resources*, Open File 1996-11.

Mihalynuk, M.G., Johnston, S.T., Lowe, C., Cordey, F., Devine, F.A.M., English, J.M., Merran, Y. and Larson, K. (2002): Atlin TGI Part II: Preliminary results from the Nakina area, northwestern British Columbia; *in* Geological Fieldwork 2001; *BC Ministry of Energy and Mines*, Paper 2002-1, this volume.

Monger, J.W.H. (1975): Upper Paleozoic rocks of the Atlin Terrane, northwest British Columbia and south-central Yukon; *Geological Survey of Canada*, Paper 74-47, 63 pages.

Atlin TGI Part II: Preliminary Results from the Atlin Targeted Geoscience Initiative, Nakina Area, Northwest British Columbia

By Mitchell G. Mihalynuk[1], Stephen T. Johnston[2], Carmel Lowe[3], Fabrice Cordey[4], Joseph M. English[2], Fionnuala A.M. Devine[5], Kyle Larson[2] and Yann Merran[4]

KEYWORDS: *Regional geology, aeromagnetic, mineral potential, resource, volcanogenic massive sulphide, geochemistry, fossil, geochronology, Cache Creek Terrane, Atlin, Nakina, oceanic arc, seamount, mélange, accretionary complex.*

INTRODUCTION

In 1898, Fritz Miller and his partner Kenneth McLaren discovered rich placers near the town site of Atlin (Bilsland, 1952). Since that time, placer mining and vein lode exploration have been an important economic force in the region, and economic vitality has been largely determined by the price of gold. Economic diversification in the mining sector has not materialized, as exploration for commodities other than gold has been comparatively minimal, despite prospective geological environments in the area.

In 1999, the Atlin area was selected, along with several others across Canada, under the federally funded Targeted Geoscience Initiative (TGI), as one of those most likely to benefit from a modernized geoscience database. The Atlin TGI was launched in 2000 with a regional aeromagnetic survey of the entire Atlin map sheet, about 14000 square kilometres (Dumont *et al.*, 2001a; b; c and 13 others). In 2001, a regional geological mapping program was launched under the TGI with joint federal, provincial, and university support. Scientists from the British Columbia Geological Survey Branch, Canadian and European universities, and the Geological Survey of Canada have contributed to this mapping effort. The first published results are presented here together with a synopsis of aeromagnetic survey results. These results show that the area harbours potential for mineralization other than placer gold. For example, new mapping has revealed an extensive magnetite exhalite, as well as submarine felsic volcanic rocks, both of which are known to occur in the neighbourhood of polymetallic massive sulphide accumulations.

[1] British Columbia Ministry of Energy and Mines
[2] University of Victoria
[3] Geological Survey of Canada
[4] Université Claude Bernard
[5] The University of British Columbia

LOCATION, ACCESS AND PHYSIOGRAPHY

Regional geologic mapping at 1:50 000 scale was conducted across the southeast corner of the Atlin mapsheet in the Nakina Lake - Nakina River area, NTS mapsheets 104N/1 and 2. NTS mapsheet 104N/3 is scheduled for mapping in 2002. These three mapsheets are herein referred to as the Nakina area. When mapping is completed it will encompass an area between 38 and 115 kilometres southeast of the town site of Atlin (Figure 1).

Access to the Nakina area is most effectively achieved by use of helicopter, available for charter in Atlin. Parts of the area can also be accessed from lakes that are large enough for floatplanes. There are no all-season roads within the area. One road extends to the northern limit of 104N/3, but it requires fording the O'Donnel River during low water and is suitable only for four wheel drive or all-terrain vehicles. The old Telegraph Trail was cut diagonally across the western two thirds of the study area (104N/2 and 3) between 1900 and 1902 (Bilsland, 1952), but it has long since fallen into disuse and is thoroughly overgrown in most places. Likewise, the Taku Trail that joined Atlin with tidewater on Taku Inlet and followed the Silver Salmon River in the Nakina area has overgrown with the ebb of traffic in the post gold rush era.

Once in the Nakina area, travel by foot is easy, particularly on dry south-facing slopes where fir, spruce, aspen and pine forest are open, or where recent forest fire scars have yet to be established with willow, alder and dwarf birch. North-facing or poorly drained slopes can be a challenge, particularly near tree line where they are a tangle of stunted spruce. Precipitous canyons and white water impede travel across the lower Nakina River, Horsefeed Creek and "Paint Creek" (Photo 1; Figure 2; note that informal place names are enclosed in quotes).

From east to west, the area spans parts of the low, swampy Kawdy Plateau and the elevated, deeply dissected Taku Plateau. Most of the area is below tree line, which is around 1400 metres elevation. Mountain peaks are mainly less than 1900 metres elevation, although Paradise peak, just outside the western boundary of the area, is over 2180 metres. Most mountain slopes are easily negotiated.

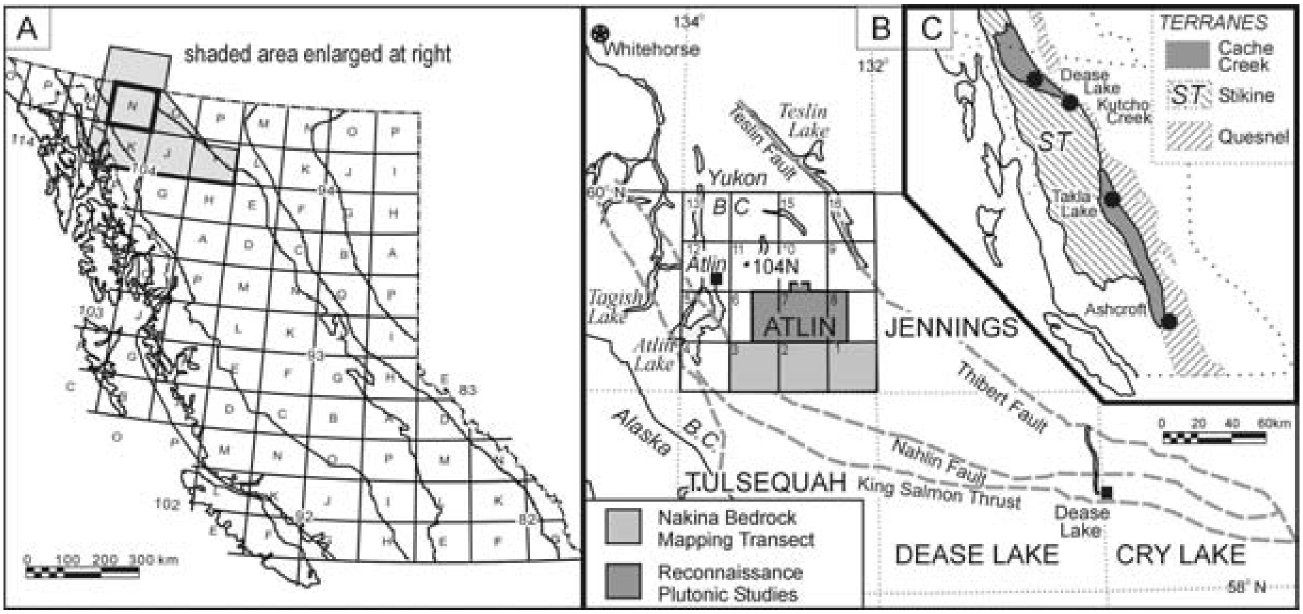

Figure 1. A. Location of the Atlin Integrated Geoscience Project in northwestern British Columbia. Bold outlined box (104N) shows extent of aeromagnetic survey. Regional geologic setting of the Atlin area. B. Regional geological mapping surveys were conducted over the eastern and central Nakina transect (104N/1 and 2). Reconnaissance plutonic studies covered parts of 104N6, 7, 8 and 10. C. Distribution of Cache Creek Terrane in BC and Yukon.

Photo 1. Deeply incised plateau underlain by carbonate of the Horsefeed Formation.

PREVIOUS WORK

Much of the Atlin area is underlain by oceanic crustal rocks of the Cache Creek Terrane (Coney *et al.*, 1980). Existing regional map coverage is of early to mid 1950’s vintage (Aitken, 1959), pre-dating the advent of plate tectonics. Thematic revision mapping in the mid to late 1960’s by Monger (1975) covered a significant portion of the central Nakina area. Monger (1975) focused on the Paleozoic stratigraphy, and suggested that the Nahlin mafic and ultramafic rocks may be obducted ocean basin crust.

Terry (1977) argued that the Nahlin body is part of a classical ophiolite, analogous to the Pindos ophiolites of Greece. Ash (1994) drew similar conclusions based on study of the ultramafic rocks near the town site of Atlin. The tectonic history of the Cache Creek Terrane within a Cordilleran context is presented in Mihalynuk *et al.* (1994).

A compilation of Atlin geology was completed as part of a provincial mineral potential evaluation (Mihalynuk *et al.*, 1996). Sources of information drawn upon for the compilation include mineral tenure assessment reports, 1:50 000 scale revision mapping (Lefebure and Gunning, 1988; Bloodgood and Bellefontaine, 1990; Mihalynuk and Smith, 1992) and regional stream sediment survey results. Results of reanalysis of archival Regional Geochemical Survey (RGS) stream sediment samples were recently released for the Atlin area (Jackaman, 2000). Unlike the old RGS data, these new data include a broad suite of elemental determinations including many rare earth elements and gold.

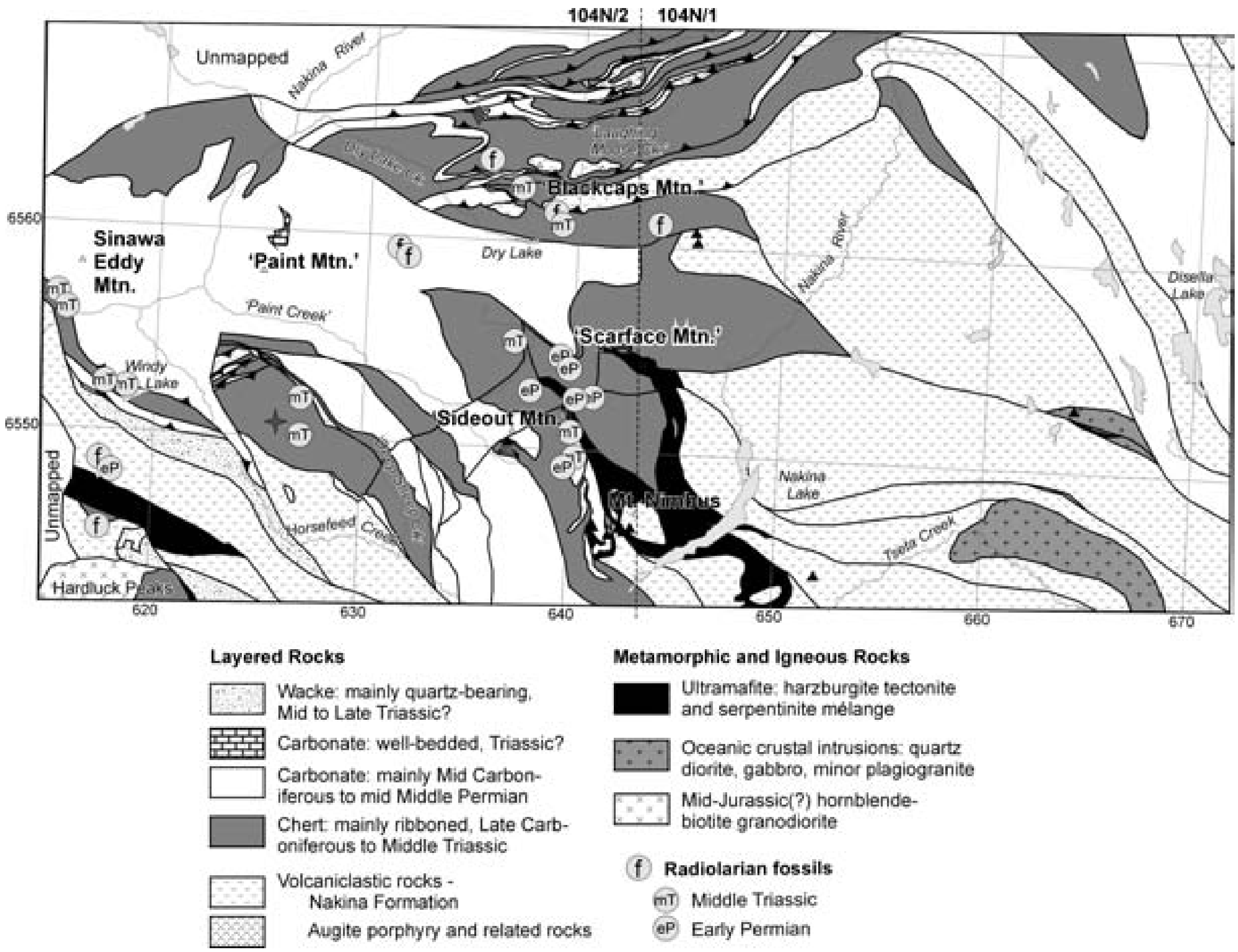

Figure 2. Generalized geology map of the Nakina map area based on fieldwork in 2001.

REGIONAL GEOLOGY RESULTS

At this reporting, 1:50 000 scale mapping is nearly complete for 104N/1 and about 70% complete for 104N/2. In general, the map area consists of an eastern mafic volcanic-dominated oceanic crustal domain and a western carbonate platform. Between these is a serpentinite mélange belt, and north of these is a heterolithic domain. Harzburgite of the Nahlin ultramafite crops out in south western-most corner of map sheet 104N/2 where it is structurally overlain by a basalt-diorite complex. This complex is separated from the carbonate platform by a beltof structurally intercalated volcaniclastic rocks, chert and wacke that are interpreted as part of an accretionary prism. Regional metamorphic grade is prehnite-pumpellyite facies. Biotite-actinolite grade rocks observed along the eastern margin of the map area may be attributed to contact metamorphism due to nearby intrusions. Thermal upgrading is also observed in the northern map area where it may be due to buried intrusions or an older regional (ocean floor) hydrothermal system.

NOMENCLATURE OF REGIONAL MAP UNITS

Almost all of the Nakina transect lies within the "southwestern facies belt" of the Cache Creek Terrane (Monger, 1975). Monger (1975) considered the this facies belt as consisting of three formations: thick lenses of Mississippian to Permian Horsefeed Formation carbonate; chert and pelite of the KedahdaFormation that host the carbonate lenses; and mafic volcanic rocks of the Nakina Formation that are intercalated with and underlie the Kedahda Formation. Much of the northern Cache Creek Terrane, especially along its margins, is highly disrupted and most units are bounded by faults. Various lithologies occur as structurally inter-leaved panels, as spectacular mélanges, and as polymictic breccias. Thus, difficulties arise in applying formal rock-stratigraphic nomenclature to the Cache Creek Terrane. Monger (1975, page 2) addressed these issues and elected to apply uniform nomenclature over the entire northern Cache Creek Terrane, conforming as much as possible to original usage (*e.g.* Watson and Mathews, 1944). We continue to use Monger's formation names within the bounds of their stated limitations, acknowledging that formation designations are locally inappropriate (Figure 2). In some areas, new age, geochemical and map data demand that we define separate units. As more such data becomes available, future workers will probably be forced into finer subdivisions, as is done for the accretionary belts of Japan (*e.g.* Isozaki *et al.*, 1990). Indeed, English *et al.* (2002, this volume) argue that volcanic rocks included in the Nakina Formation comprise assemblages that may have formed in disparate tectonic settings, and they have assigned local geographic names to distinct volcanic assemblages.

OCEANIC CRUST: INCLUDING NAKINA FORMATION

Rocks included in the oceanic crustal domain include primitive basalt and ultramafic rocks typical of oceanic crust. However, they lack pillowed flows and sheeted dikes of a classical ophiolite succession (although knockers comprised of dikes within dikes are found in the serpentinite mélange belt). The dominant unit of the oceanic crustal domain is Nakina Formation basaltic volcaniclastic rocks. These rocks are the focus of a paper by J. English *et al.* in this volume, and are dealt with here in only a cursory fashion. Basaltic rocks are interleaved with less abundant diorite, gabbro and rare plagiogranite. Basalt is comprised mainly of lapilli and ash-sized fragments which have been altered, commonly to prehnite, pumpellyite and chlorite. Less common are authigenic carbonate, and in the eastern portions, actinolite. Strongly weathered outcrops are orange, dark brown or olive green. Fresh surfaces are a distinctive mint green colour with grey and pink filaments (fine shear bands with clay and iron oxides). Homogeneous regions of volcanic rock locally form entire mountainsides. Locally this unit contains exotic clasts of diorite, chert, and rare carbonate.

Gabbro and diorite occur as isolated intrusions. Only rarely are tabular intrusive bodies seen cutting the volcaniclastic rocks. Gabbro and diorite are most abundant in the southeast and southwest corners of the map area where they are discontinuously exposed over areas of up to 40 km^2. They also occur as knockers in the serpentinite mélange where they range from a metre to hundreds of metres in long dimension. In the poorly exposed eastern map area, the covered spaces between outcrops could be underlain by less resistant units, such as ribbon chert or serpentinite. However, juxtaposition of such contrasting magnetic lithologies should disrupt the magnetic field. As no such disruption is observed (see Aeromagnetic Survey Results below), large bodies are shown on Figure 2.

Gabbro and diorite are medium-grained plagioclase and pyroxene or amphibole-phyric rocks; pyroxene is porphyritic in some samples. Ophitic and diabasic textures are common. Pyroxenes show exsolution lamellae and are probably calcic augite. Plagioclase is variably altered, from fresh to totally turbid; authigenic minerals include white mica, prehnite, quartz and carbonate. Mesoscopic and microscopic strain zones with semi-ductile to brittle deformation are common.

Plagiogranite occurs as a plexus of thin, irregular pegmatitic dikes cutting dioritic rocks in southern 104N/1, and as medium-grained knockers within the serpentinite mélange. Petrographic analysis of the pegmatitic plagiogranite shows that it is composed of fresh plagioclase and hornblende with 10% interstitial quartz and accessory titanite. Weak chlorite alteration affects the edges of some of the hornblende crystals. U-Pb and $^{40}Ar/^{39}Ar$ isotopic age dates are pending.

Tectonized harzburgite forms a 1.5 km thick tabular body with an exposed length of 10 kilometres in southwest 104N/2. Considered part of the Nahlin ultramafite (Terry, 1977), it is a resistant, poorly vegetated, dun-weathering body with strongly foliated zones. Lineated bastite (serpentinized enstatite orthopyroxene) are up to 2cm in long dimension, in a matrix of serpentinized olivine (Photo 2). Subidiomorphic chromite grains occur in streaky clusters several millimetres across. Magnetite is not common. Harzburgite also occurs as knockers, generally less than 2 m in diameter, within the serpentinite mélange belt. A 30 cm thick dunite dike intrudes one knocker, composed primarily of chilled diabase dikes.

KEDAHDA FORMATION CHERT SUCCESSIONS

Chert occurs throughout the map area. It is typically ribboned, black, grey, green or tan - weathering, with similarly coloured fresh surfaces. Outcrops are commonly rusty and rubbly, forming tenuous spires on steep slopes. Locally the chert is massive and blocky-weathering. Massive chert is normally black in colour.

Ribbon chert occurs as irregular 1-15 cm thick chert layers alternating with 0.2 - 2 cm argillaceous layers (Photo 3). Exceptions are common as chert beds can reach a metre or more in thickness; rarely chert beds are continuous and

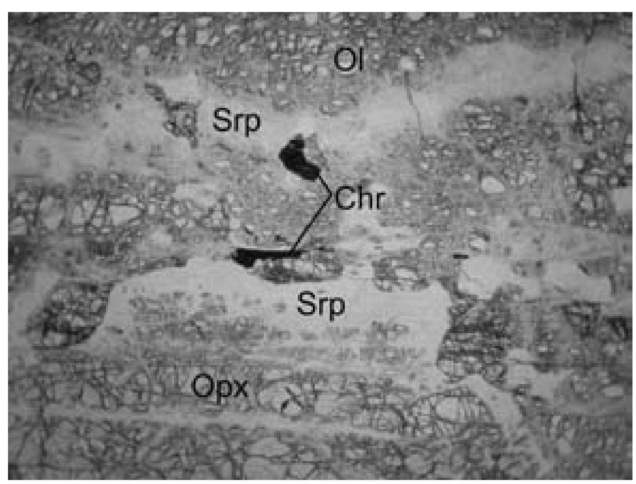

Photo 2. Photomicrograph of serpentinized harzburgite showing orthopyroxene (Opx) and olivine (Ol) now altered to serpentine (Srp). Chromite (Chr) is a common accessory. Long dimension of the photo represents 4 mm.

Photo 3. A representative view of well bedded ribbon chert. Note tight fold hinge (under hammer) plunging towards photographer.

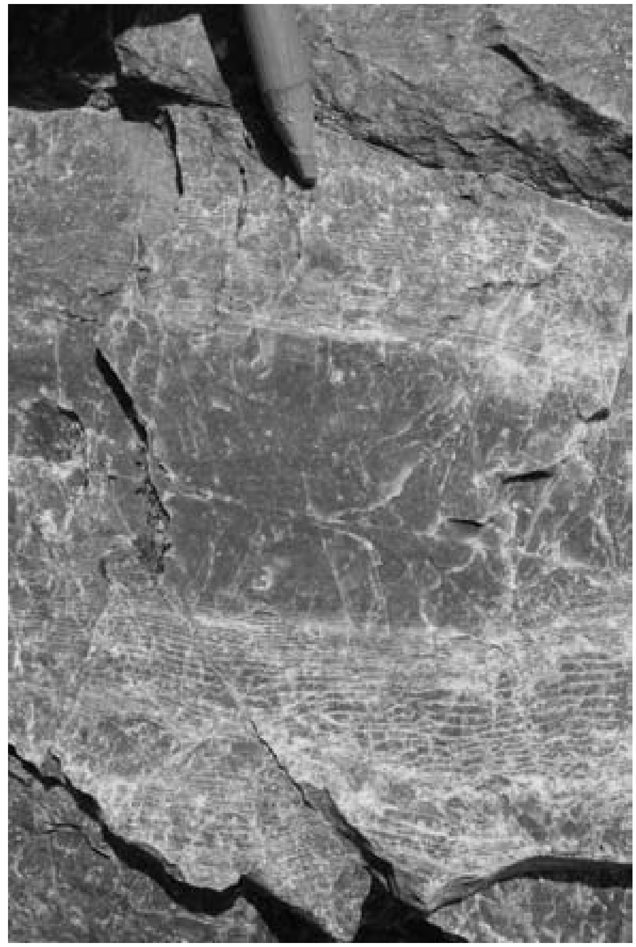

Photo 4. Well laminated chert probably originated as argillite, now silicified.

ruler straight. Massive chert may display fine, millimetre-thick laminae (Photo 4), possibly indicating an argillite progenitor that was subsequently silicified.

Ribbon chert is the dominant lithology in some highly disrupted zones where it is admixed with other lithologies, particularly volcaniclastics. Some of these disrupted zones may be "broken formation", a lithology typical within accretionary prisms.

Radiolaria are common in most ribbon chert, less common in massive chert and uncommon in laminated chert. Preliminary radiolarian identifications indicate ages of Early Permian to Mid Triassic; although ages of Late Carboniferous and Upper Triassic are possible (Table 1). Most radiolaria are of Middle Triassic age and Early Permian chert is also common. Late Permian and Early Triassic forms have not been conclusively identified. Age determinations are based upon field identifications and will be refined further (by F.C. at UCB, Lyon, France).

HORSEFEED FORMATION - CLASTIC CARBONATE

Horsefeed Formation carbonate rocks are located in the eastern, western and northern parts of the map area. In the east (104N/1E), extensively recrystallized carbonate occurs in three poorly exposed, north-northwest-trending belts of carbonate outcrops. In the west (south and central 104N/2), massive to thick-bedded and locally well-bedded and fossiliferous carbonate successions are dissected by the Nakina River and Horsefeed and "Paint" creeks, providing the most complete sections of the Horsefeed Formation. In the north (northwest 104N/1 and northeast 104N/2), fault-bounded panels carry sparsely fossiliferous limestone that is intercalated with volcanic rocks and chert.

Carbonate of the western map area is dominated by massive calcarenite, shallow water fusulinid packstone, turbiditic calcareous sandstone, conglomerate and micrite. One apparently homoclinal, sparsely fossiliferous carbonate section north of upper Horsefeed Creek exceeds 2800m in thickness. However, thrust repetitions that are common elsewhere in the carbonate package may thicken this sec-

TABLE 1
PRELIMINARY RADIOLARIAN IDENTIFICATIONS AND AGE DETERMINATIONS PERFORMEDIN THE FIELD

Sample Number	UTM east	UTM north	±	Lithology	Preser-vation	Radiolarian taxa	Age
FCO01-17-11	627845	6550565		ribbon chert	poor	*Triassocampe* sp.	Middle or Late Triassic
FCO01-17-5	627465	6552526	7	ribbon chert	moderate	*Triassocampe* sp. *Yeharaia* sp.	Middle Triassic
FCO01-18-1	637094	6555462	7	grey ribbon chert	good	*Plafkerium* sp. *Praesarla* sp. *Yeharaia* sp.	Middle Triassic
FCO01-23-1a	631228	6560060	8	ribbon chert contact w. breccia	poor	unidentified spumellarians	Phanerozoic
FCO01-23-1b	631228	6560060	8	ribbon chert contact w. breccia	poor	*Entactinia* sp. ?*Scharfenbergia* sp.	possibly Late Paleozoic
FCO01-27-4	617145	6552880		black ribbon chert	moderate	?*Pseudostylosphaera* sp. *Triassocampe* sp.	Middle or Late Triassic
FCO01-27-5	619073	6551883		black ribbon chert	moderate	*Sarla* sp. *Triassocampe* sp. *Yeharaia* sp.	Middle Triassic
MMI01-10-2	639744	6547919	6	ribbon chert	good	*Latentibifistula* sp. *Pseudoalbaillella scalprata*	Early Permian
MMI01-10-4	640237	6548581	4	ribbon chert	fair	?*Plafkerium* sp. *Pseudostylophaera compacta* *Triassocampe* sp.	Middle Triassic
MMI01-10-7	640470	6548881	5	small clast of red chert	poor	unidentified spumellarians	non diagnostic
MMI01-18-3a	614817	6556399	8	ribbon chert	moderate	*Plafkerium* sp. *Praesarla* sp. *Triassocampe* sp. *Yeharaia* sp.	Middle Triassic
MMI01-18-3b	614817	6556399	8	ribbon chert	good	*Plafkerium* sp. *Praesarla* sp. *Pseudostylosphaera* sp. *Yeharaia* sp.	Middle Triassic
MMI01-18-4b	614906	6556456	7	ribbon chert	moderate	*Yeharaia* sp. *Praesarla* sp.	Middle Triassic
MMI01-23-19d	643810	6561084		ribbon chert	poor	unidentified spumellarians	non diagnostic
MMI01-3-10	639743	6554556	4	ribbon chert	moderate	*Latentibifistula* sp. *Pseudoalbaillella scalprata* *Pseudoalbaillella* sp. cf. lomentaria	Early Permian
MMI01-3-7	639819	6554835	8	ribbon chert	good	*Pseudoalbaillella scalprata* *Polyfistula* sp. *Quadriremis* sp.	Early Permian
MMI01-4-18	639980	6553130		ribbon chert	moderate	*Pseudoalbaillella* sp. cf. *scalprata* *Quadriremis* sp.	Early Permian
MMI01-4-4	640188	6551702	7	ribbon chert	good	*Pseudostylosphaera* sp. *Triassocampe* sp.	Middle Triassic
MMI01-5-1	641050	6553290	18	ribbon chert	moderate	*Albaillella* sp. cf. *sinuata* *Haploaxon* sp. *Latentibifistula kamigoriensis* *Quinqueremis* sp.	Early-Middle Permian
MMI01-6-11	638253	6562083	7	ribbon chert	poor	unidentified spumellarians	non diagnostic
MMI01-6-7	638650	6561050	5	ribbon chert	moderate	*Pseudostylosphaera* sp. *Yeharaia* sp.	Middle Triassic
MMI01-6-8	638584	6561508	8	ribbon chert	poor	*Triactofenestrella* sp. large *Latentifistulidae* spumellarians	Late Paleozoic; Carboniferous or Permian
MMI01-7-19	635165	6563535	5	ribbon chert	poor	arms *Latentifistulidae* (large morphotypes)	Late Paleozoic; Carboniferous or Permian
MMI01-7-6a	636692	6562413	5	ribbon chert	moderate	*Triassocampe* sp. *Yeharaia* sp.	Middle Triassic
YME01-2-1a	617234	6548431		ribbon chert	poor	*Latentifistulidae*	Late Paleozoic; Carboniferous or Permian
YME01-2-1b	617234	6548431		ribbon chert	moderate	*Latentibifistula kamigoriensis* *Pseudoalbaillella* sp. cf. *lomentaria*	Early Permian
YME01-2-9	617628	6545501		ribbon chert	poor	large *Latentifistulidae* *Scharfenbergia* sp.	Late Paleozoic; Carboniferous or Permian
YME01-5-27	638662	6553152	8	ribbon chert	moderate	*Latentibifistula kamigoriensis* *Pseudoalbaillella* sp. cf. *scalprata*	Permian, probably Early
YME01-7-6	637681	6566429	6	ribbon chert	poor	recrystallized spumellarians	non diagnostic

tion. Without fossil age control, assessment of true stratigraphic thickness will be difficult.

Massive calcarenitic limestone is the most conspicuous unit in 104N/2. It is white to grey with hues of yellow. Outcrops vary from dense, smooth whalebacks to fractured rubbly slopes. A sense of layering can commonly be seen from a distance, although the source of the layering is not always clear. Locally layering can be attributed to bedding, while less commonly it results from jointing. In detail, calcareous grains are comprised of foraminifera, oolites, pelloids, fragments of echinoids, fenestrate bryozoa and algae, fusulinids, and invariably, crinoid ossicles. Rare bryozoan build-ups occur within the massive carbonate. Minor accumulations of alkaline volcanic tuff and flow units within the massive carbonate occur north of Horsefeed Creek headwaters and at “Sideout Mtn.” At these localities the volcanics form a substrate on which coralline reefs nucleated. At “Sideout Mtn.”, a debris-rich back reef and a shelly/algal lagoonal facies are developed. Intense dolomitization has been observed in one locality, north of “Deep Sheep Creek”. The massive unit may have been deposited as shallow water shoals.

Thick-bedded fusulinid packstone is the characteristic unit of the western carbonate. Beds range from decimetres to several metres thick; they generally lack internal structure and rarely have distinct tops and bottoms. Nevertheless, individual beds can be traced for hundreds of metres, recognized by abundant fusulinids commonly comprising more than 80% of the rock. Fusulinids are typically 0.5 to 1 cm in diameter and are commonly best displayed at the soil line or beneath moss, probably due to etching by humic acid. Fusulinid packstone is light grey to cream coloured and is more resistant than other carbonate lithologies. One resistant set of packstone beds, 20-50 m thick, can be traced along the westernmost fault-bounded edge of the main carbonate body in western 104N/2 (Figure 2, Photo 5).

Well-bedded sections within the massive western carbonate are best displayed in the Nakina River canyon, on the flanks of Mt. Sinawa Eddy, east of “Deep Sheep Creek” and south of lower Dry Lake Creek. Of these, the most continuous exposures are on the south and west flanks of Mt. Sinawa Eddy (Photo 6).

Photo 5. A view to the north of resistant fusulinid packstone beds of Permian age in fault contact with Middle Triassic ribbon chert. Photo 6 is a view of southwestern Sinawa Eddy Mountain, taken from the location denoted by the star.

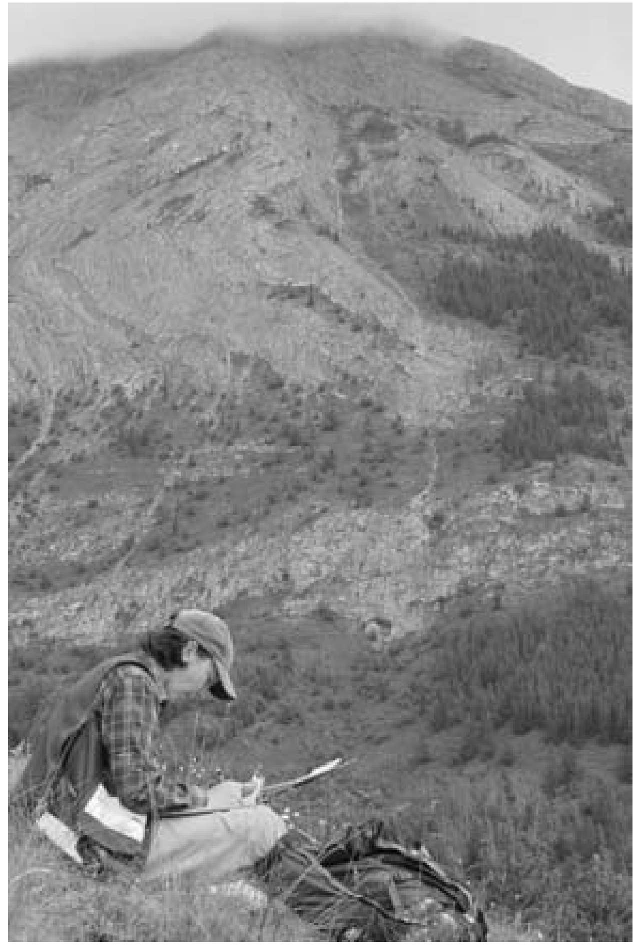

Photo 6. Well-bedded carbonates on Sinawa Eddy Mountain. View is to the northeast.

AUGITE PORPHYRY UNIT

A prominent unit of coarse augite porphyry breccia and ash tuff is repeated by folding and faulting in the “Laughing Moose Creek” area, where it is a key marker unit used to define the fold and thrust belt developed in that area. It forms dark green, locally orange weathering, highly compact, blocky outcrops with joint spacing in excess of 2m. Euhedral augite is conspicuous and crowded in some fragments. A compaction fabric and subparallel tuffaceous layering are common and may reflect rapid deposition and cooling during compaction.

Map patterns indicate thicknesses in excess of 250 m; however, folding probably thickens the unit in these areas. Where both the upper and lower contacts are exposed, the true stratigraphic thickness is between 15 and 80 metres. Basal contacts are with chert. Topographic irregularities and the local development of chert cobble conglomerate at lower contact point to an erosional unconformity. Near its southernmost occurrence, a 3 to >5 m thick lahar sits on the chert (the contact is not well exposed). Farther to the north, along a creek west of “Laughing Moose Creek”, the contact chert unit rests on rhythmically interbedded, turbiditic limestone granule conglomerate and argillaceous chert that is several tens of metres thick. A paleochannel within the rhythmically bedded section is 30 m across, more than 5 m deep, and is filled with coarse debris. Underlying the turbidites is an equal thickness of 5-40 cm thick beds of white chert and tan limestone. Farther west, along the same contact, decimetre-sized blocks of bivalve-bearing limestone occur near the base of the augite porphyry unit. Upper contacts are gradational with overlying tuffaceous carbonate. Local development of red, cross-stratified tuffaceous and calcarenitic sands indicate a subaerial environment. English *et al.* (this volume) show that the unit is subalkaline, and most like mafic volcanics erupted in an ocean island/plateau environment. The persistence of calcareous turbidite units interbedded with chert beneath the augite porphyry unit suggests that an elevated area with carbonate production, perhaps an ocean island, existed nearby prior to eruption of the augite porphyry unit.

FELSIC VOLCANIC AND INTERCALATED UNITS

Alpine ridges between the lower stretches of Horsefeed and “Paint” creeks are underlain primarily by bedded chert of Middle Triassic age (Table 1). Intercalated

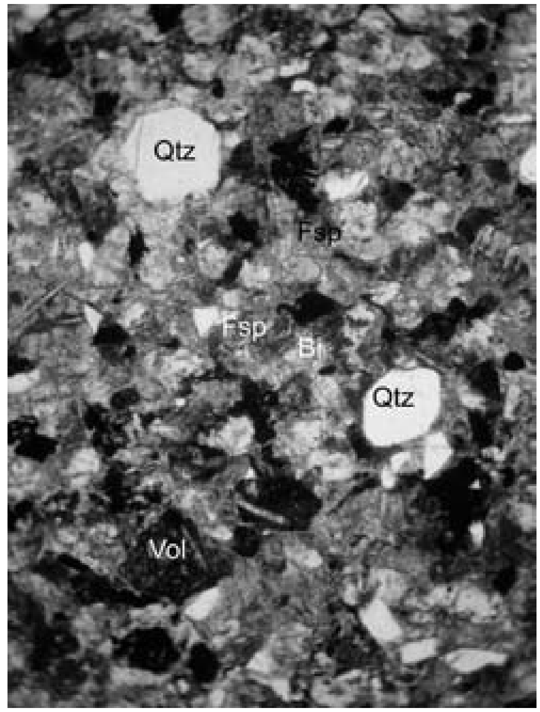

Photo 8. Photomicrograph of volcaniclastic rock within chert succession under plane polarized light. Note subidiomorphic quartz grains (Qtz) admixed with turbid feldspar (Fsp), mafic volcanic grains (Vol) and calcareous bioclasts (Bi). Width of photo represents 1.5 mm.

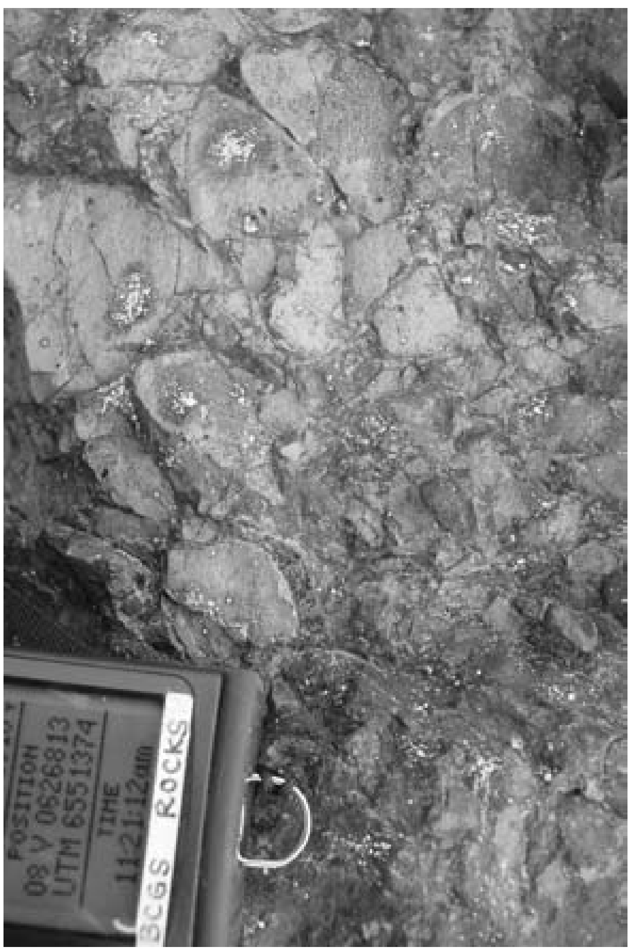

Photo 7. Basaltic pillow breccia within ribbon chert unit.

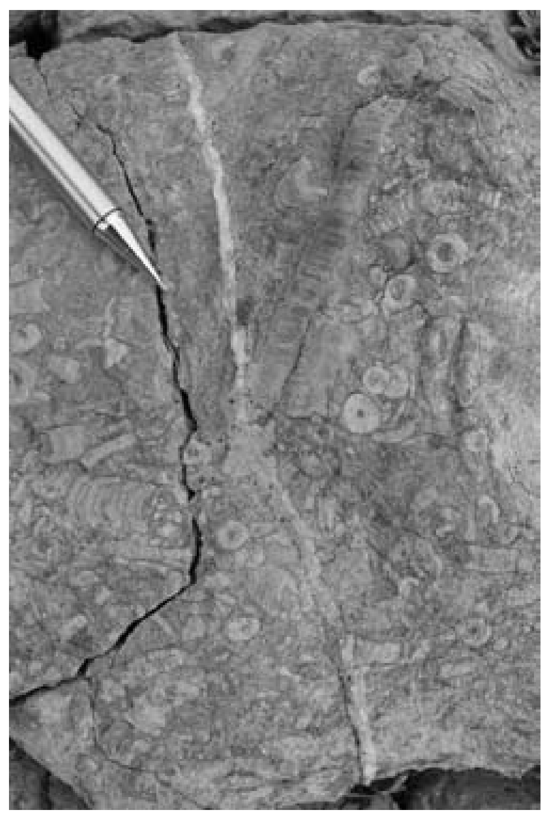

Photo 9. Crinoid and bivalve packstone with quartz-rich tuffaceous interlayers.

with the chert are bimodal volcanics: mafic pillow breccia (Photo 7) and quartz-rich tuff. In both cases the contacts with the chert appear to be primarily depositional. However, the quartz-rich tuffaceous layers grade laterally into shallow-water carbonates in which coarse quartz grains derived from the volcanics are admixed with calcareous fossil debris (Photo 8). The carbonate layer is at most 20 m thick. It is dark grey weathering, fetid and very fossiliferous, containing thick crinoid stems (up to 1.5 cm diameter, Photo 9) and bivalves.

Felsic volcanic rocks are dominantly coarse epiclastics, but breccia-sized trachyte clasts and a possible rhyolite flow were found within the same stratigraphic interval. Due to their economic potential, these felsic volcanics warrant further work to define their thickness and extent (see *Mineral Potential* below).

WACKE

Two types of wacke are common within the map area: those that are mainly siliceous mud matrix, and those that are mainly silt and sand-sized grains. Siliceous mud-rich wacke is brown and less commonly dark grey, black or blue-grey. Locally it grades into chert or volcaniclastics, and commonly contains chert grains and cobbles, volcanic grains and clasts up to lapilli size. Quartz is not common, but does occur in rare clasts of foliated quartz diorite. Because the unit tends to be siliceous and "grades" into chert, the field term "proto-chert" was used to describe all variants.

Wacke that is mainly sand or silt-sized grains is common, but only locally are quartz grains abundant. Clear contact relationships with adjacent strata are only known from the north flank of "Scarface Mountain", on the western ridge of Mount Nimbus, between lower Horsefeed and "Paint" creeks, and on the ridge north of Hardluck Peak. Samples from these localities contain as much as 20% monocrystalline quartz; in rare instances quartz grains comprise more than 30% of the rock. Near "Scarface Mountain" a chert-dominated fault panel contains between 1 and 3 metres of well-bedded, coarse, olive coloured, quartz-rich volcanic sandstone (Photo 10) that caps a section of volcanic flows and reefal carbonate 18m thick. The wacke has been collected for detrital zircon age determination.

West of Mount Nimbus a fault-bounded lens of wacke 5 to more than 20 m thick is sandwiched between fault-bounded panels of mafic volcanic and pure carbonate; each more than 1 km thick. Grains within the wacke are mainly silt-sized (coarser in Photo 11). Thin beds and lamellae have been strongly disrupted by synsedimentary microfaults. Fault planes are outlined by paper-thin carbonate veinlets. Detrital zircons have been extracted from this unit and are to be dated (F.D. at UBC).

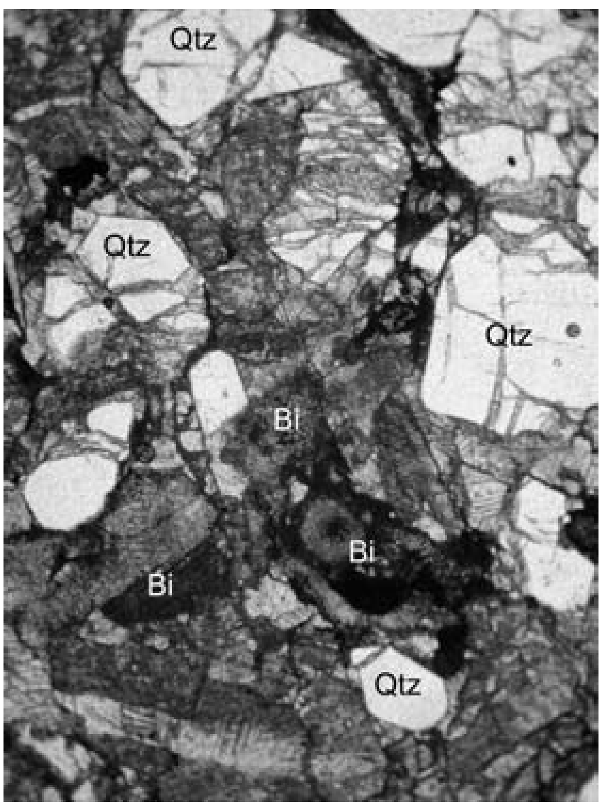

Photo 10. Photomicrograph of quartz-rich volcanic and calcareous bioclast-rich sandstone (sample MMI01-27-7). Note that coarse idiomorphic quartz (Qtz) has not been significantly abraided. Height of photo represents approximately 4mm, Bi = bioclast.

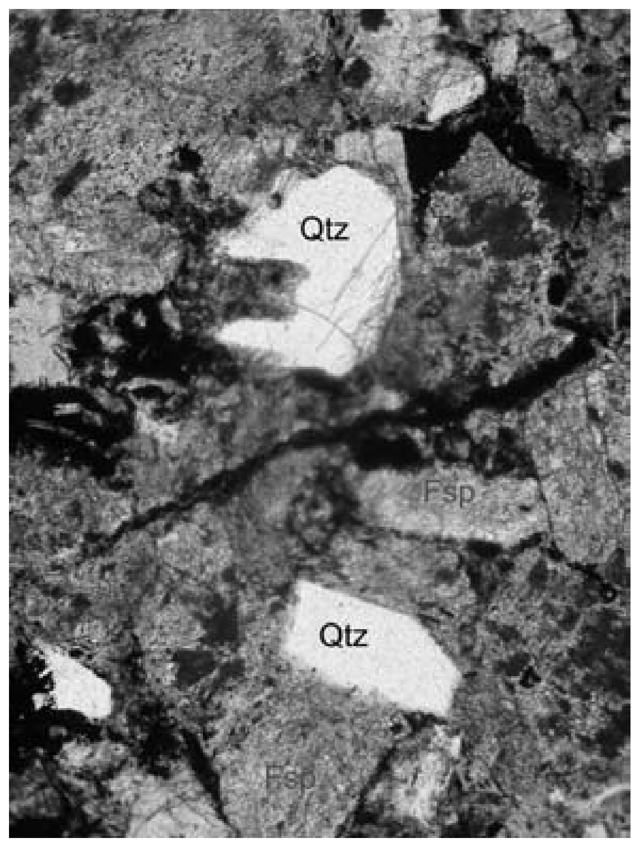

Photo 11. Photomicrograph of quartz-bearing (Qtz) arkose from near Mount Nimbus (sample MMI01-33-1). Height of photo represents approximately 1 mm.

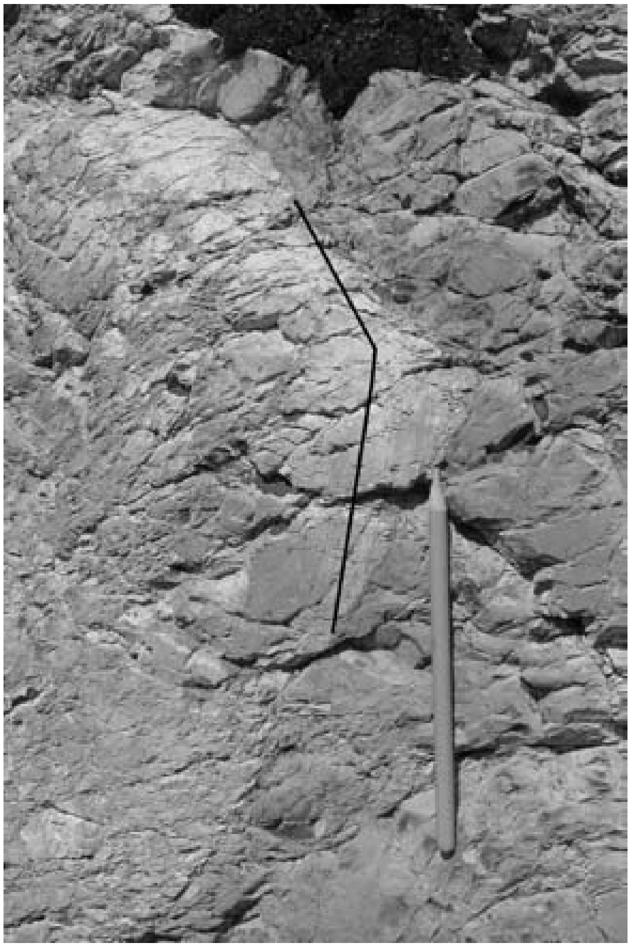

Photo 12. A westerly view of a small-scale reverse fault in quartz-bearing wacke between Horsefeed and “Paint” creeks. A black line approximates the outcrop surface^bedding plane intersection. The pencil crayon points to the clay-lined fault surface. The light-coloured wacke is interpreted to have been thrust in a northerly direction over hemipelagite.

Between lower Horsefeed and “Paint” creeks, well-exposed fault-bounded panels of orange-weathering, olive brown to green, quartz-rich wacke are tectonically interleaved with “proto-chert”, ribbon chert and lesser carbonate. Individual panels may range from a few metres to a few hundred metres in thickness. In detail, the panels display abundant evidence for soft-sediment deformation and small-scale reverse faults (Photo 12).

Coarse quartz wacke unconformably overlies mafic volcanic rocks in a well-exposed section on the ridge north of Hardluck Peaks. A red-weathering basal conglomerate containing oxidized cobbles of volcanic rocks grades rapidly upwards into quartz-rich silt, coarse sandstone, and boulder conglomerate containing abundant exotic intrusive clasts up to 1 m diameter, as well as intraclasts up to several metres long. Fusulinid limestone, chert and sparse serpentinite clasts are interpreted to have been derived from the surrounding Cache Creek Terrane lithologies however, no nearby source is apparent for porphyritic and coarse-grained granitic boulders (Photo 13). Carbonate layers up to 5 m thick occur near the middle of the exposed unit. Sam-

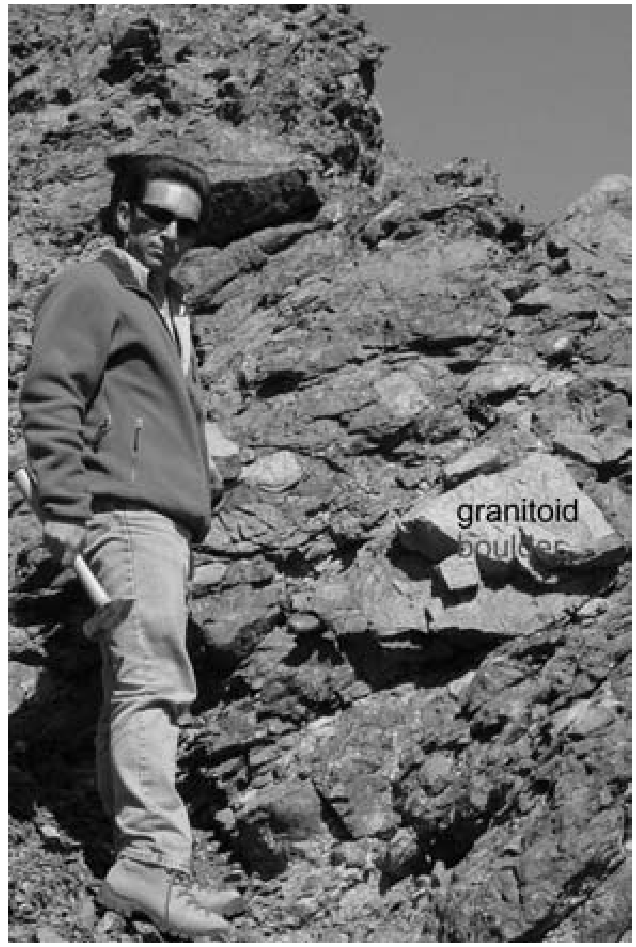

Photo 13. Conglomerate on the ridges north of Hardluck Peaks contains exotic granitic boulders up to 1 m diameter.

ples were collected for conodont extraction; however, contamination from older sources is expected. The unit is younger than the Cache Creek lithologies that it contains as clasts, and is older than an unfoliated granodiorite pluton that thermally metamorphoses the unit. Aitken (1959) mapped this unit as wacke of possible Triassic age. Six samples were collected for detrital zircon age determinations in order to better constrain the age of the unit.

LATE SYN- TO POST-ACCRETIONARY INTRUSIVE ROCKS

Intrusive bodies that cut structural fabrics within the Nakina area are known from two localities: on the north flanks of Hardluck Peaks in southwestern-most 104N/2, and on northern Sinawa Eddy Mountain. The body near Hardluck Peaks is herein called the “Hardluck pluton”. It is a blocky, grey-weathering, medium to coarse-grained hornblende biotite granodiorite. Hornblende clots and xenoliths are common. The pluton has steep contacts and a thermal metamorphic halo >100 m thick in which phyllite is locally developed. Within a few metres of the contact, ribbon chert has a sucrosic texture due to recrystallization of quartz. Within 50 cm of the contact the pluton is chilled.

A sample was collected for $^{40}Ar/^{39}Ar$ age determination. Based on comparison with similar dated plutons elsewhere in the Atlin area (Mihalynuk *et al.*, 1992), the pluton is thought to be Middle Jurassic to Eocene age.

On the north flank of Sinawa Eddy Mountain, 3 km north of the peak, a quartz porphyritic rhyolite stock 100 m in diameter is poorly exposed. The rhyolite is flaggy weathering, dusty tan to pale mauve and contains about 10% medium-grained quartz phenocrysts. A similar body has been mapped 1 km to the ENE, based upon the presence of similarly weathering felsenmeer.

STRUCTURAL STYLES

The degree of structural disruption and complexity of structural relationships within the Nakina area is difficult to convey on a map of 1:50 000 or smaller scale. For this reason, previous maps (*i.e.* Aitken, 1959; Monger, 1975), as well as that shown in Figure 2, under-represent structural complexity. Although a general northwest-striking structural fabric parallels the Nahlin body, there is significant discordance at the mountainside or more detailed scale. Our mapping at 1:20 000 scale, compiled at 1:50 000, and further simplified on Figure 2 (about 1:200 000 if entire page. As is, ~1:335 000) is of sufficient detail to resolve four structural elements not previously shown on maps; (1) a fold and thrust belt, (2) a serpentinite mélange belt, (3) parts of an accretionary prism, and (4) flow around resistant buttresses.

A fold and thrust belt is best defined in the north-central map area near "Laughing Moose Creek" and "Blackcap Mountain". Shallow to moderately north-dipping shear zones and truncation of hangingwall units are consistent with south verging thrust faults. Radiolarian fossil ages from chert in adjacent structural panels show that older strata are thrust over younger strata (Carboniferous and Permian over Middle Triassic). The fold and thrust belt has not been traced through massive carbonates at Sinawa Eddy Mountain, although at least two thrust faults placing limestone on limestone are recognized there. This together with the abrupt termination of turbidite beds and argillaceous bands strongly suggests a continuation of the belt. A resistant band of Permian fusulinids packstone that marks the western limit of the massive carbonate at Sinawa Eddy Mountain, structurally overlies Middle Triassic chert for 12 km along strike, and appears to extend a further 13 km to the northwest. Steep northeast dips on the fault contact suggest a southwest-verging thrust.

A serpentinite mélange belt extends north from Nakina Lake bifurcates and appears to pinch out south of Dry Lake valley (Figure 2). The belt is up to 4 km thick and contains knockers up to 2.5 km across. Knockers of almost all Cache Creek Terrane lithologies were recognized, but the most abundant are those composed of mafic volcanic rocks and of diorite. Knockers composed of chert and mafic intrusive rocks are of lesser and approximately equal abundance; other knocker types are rare. Where knockers are best exposed, they appear to be subvertical cigar-shaped bodies (Photo 14).

Many of the fault-bounded units in the Nakina area MAY have been first assembled in an accretionary prism. The best evidence of structural panels of sediments that appear to have been interleaved within an accretionary prism comes from between Horsefeed and "Paint" creeks. Here quartz-rich wacke of possible inner trench slope derivation are interleaved with pelagic sediments. Thrust faults apparently verge north-northwest, based upon small-scale low angle fault cut-offs (Photo 12).

Deformation that post-dates original assembly of the lithologic elements recognized in the Nakina area has modified most contacts, tightened folds, and resulted in flow of incompetent lithologies around more resistant buttress-forming lithologies. An example of flow around a buttress was observed 5 km south of Dry Lake where a resistant buttress of carbonate is wrapped by panels of chert admixed with minor amounts of other rock types including mafic volcanics and ultramafite.

Wacke and conglomerate north of Hardluck Peaks forms a 7 km by 1.7 km west-northwest-trending belt that is cut and offset in an apparent dextral sense by a northwest-trending fault. Serpentinite occurs along the fault on the

Photo 14. Resistant knockers in serpentinite mélange are here mainly composed of mafic volcaniclastic and intrusive lithologies. Dashed lines are parallel with long axes of knockers.

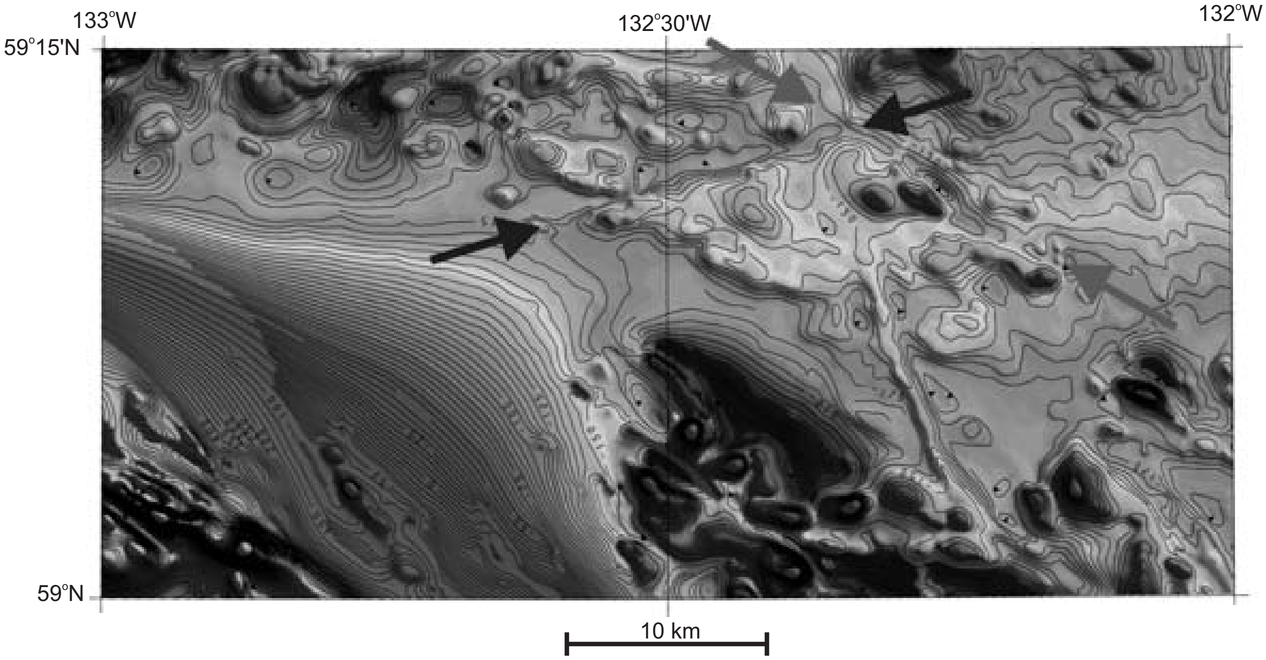

Figure 3. Aeromagnetic results for the Nakina map area, NTS 104N/1 and 2. Arrows show the location of linear negative anomalies as discussed in text. (*See* web page for colour version).

southern margin of the map. The fault appears to terminate in serpentinized harzburgite south of "Windy Lake".

AEROMAGNETIC SURVEY RESULTS

Magnetic anomaly data covering the 104N/1 and 2 map areas are shown in Figure 3. These data were acquired as part of the high-resolution aeromagnetic survey conducted over the 1:250 000 Atlin map area during the first phase of the Atlin Targeted Geoscience Initiative (Dumont *et al.*, 2001a, b). For a synopsis of the aeromagnetic data that is more thorough than that presented here, please see Lowe and Anderson (2002).

The magnetic field is dominated by a positive (up to 2100 nT) anomaly that extends over the southern two thirds of 104N/2 and continues some 30 km farther to the northwest. The source of the anomaly is interpreted to be serpentinized harzburgite in the northwest-trending Nahlin ultramafic body, because magnetic intensities are largest where these rocks are exposed at surface. In addition, magnetic susceptibility data (Lowe and Anderson, 2002) indicate that serpentinite has significantly higher values than any other Cache Creek Terrane lithology in the area. The spatial extent of the magnetic anomaly suggests that much of the map area to the south of Mt. Sinawa Eddy and "Paint Mtn." is likely underlain, at relatively shallow depths, by serpentinized ultramafic rocks. Such an interpretation requires that the Nahlin ultramafic body dips shallowly to the northeast, although previous workers have interpreted the northeast boundary of the body to be a near-vertical fault (Souther, 1971; Monger, 1975).

Numerous small, sub-oval to elliptical, positive magnetic anomalies punctuate the otherwise low amplitude magnetic field observed in the southern part of 104N/1 (Figure 3). Some of the anomalies correlate with discrete exposures of ultramafic rocks previously mapped in this area (Aitken, 1959; Monger, 1975) and ground investigation of others has led to the discovery of serpentinite mélange in areas previously thought to be underlain by mafic volcanic and associated rocks in the Nakina Formation (*e.g.* serpentinite mélange on Figure 2). The peak amplitudes (typically < 400 nT) and small aerial extent of most of these anomalies indicate that the source bodies unlikely persist to significant depths.

A prominent NNW-trending lineament, characterized by a narrow (<1 km) zone of moderately elevated (35 nT) magnetic anomaly values extends for more than 20 km through the central part of 104N/1. This lineament marks the eastern extent of the chert succession that underlies "Scarface Mtn." (compare Figures 2 and 3). Bedrock exposures in the vicinity of the lineament are not known and ground investigations failed to identify the magnetic source. Possible explanations include a mafic intrusion or secondary magnetization around an unmapped fault zone.

Two other notable lineaments, each approximately 17 km long, are imaged in the northern part of 104N/1. The lineaments are magnetic troughs, one northeast-trending and the other northwest-trending (shown by arrows on Figure 3), that intersect in the Nakina River valley approximately 16 km northeast of Dry Lake (Figure 2). The southern margins of both lineaments correspond to higher magnetic anomaly values where volcaniclastic rocks are exposed in the “Blackcaps Mtn.” area. The northeast-trending lineament parallels the boundary between these volcaniclastic rocks and the weakly magnetic chert succession that underlies much of the area between “Blackcaps Mtn.” and “Laughing Moose Creek”. The northwest-trending lineament parallels the boundary between the volcaniclastic rocks and weakly magnetic carbonate and chert units that underlie much of the northeastern part of the 104N/1 map area.

MINERAL POTENTIAL

Despite prospective geology, no metallic mineral occurrences area known from within the area mapped. Thus, a principal objective of the Nakina transect mapping was to evaluate the mineral potential of the area, especially for volcanogenic massive sulphide mineralization. Our discovery of a magnetite exhalite unit as well as submarine felsic volcanic rocks underlying parts of drainages with elevated RGS metal values, points to vigorous hydrothermal systems in a setting prospective for a Cyprus-style mineralization, and the right composition of submarine volcanic rocks for Kuroko-style mineralization.

MAGNETITE EXHALITE UNIT

A substantial thickness of magnetite exhalite is located 3.5 km northwest of “Blackcaps Mtn.” in dark green aquagene ash and dust tuff (diamond on Figure 2). Fine-grained magnetite comprises up to 50% of the rock across true thicknesses of at least 5 metres. Geochemical analysis of this unit has returned values of 16% Fe and 900-1200 ppm Ba over 5.3 metres, but background values for base and precious metals. The magnetite layers occur intermittently across a width of 25 m and can be traced for more than 700 metres along strike. Sparse quartz microlites seen in thin section may have been sourced in distal felsic eruptions that were coeval with the more abundant mafic tuff of the exhalite host unit.

RGS results are unavailable for the drainage basin directly underlying the exhalite, but values from the creeks draining areas underlain in part by correlative tuffite are elevated (with respect to the remainder of the Atlin sheet) in Au (41 ppb), As (31 ppm), Cu (64 ppm) and Zn (118 ppm; samples 9215, 9224 in Jackaman, 2000).

FELSIC VOLCANICS AND RGS DATA

Submarine quartz-phyric felsic volcanic rocks with volcanogenic massive sulphide potential were discovered in central 104N/2 (filled square on Figure 2). They appear intercalated with chert that has yielded Middle Triassic radiolaria along strike to the east. RGS data from creeks that drain the area are elevated (with respect to the remainder of the Atlin sheet) in copper (80 ppm), lead (6ppm), molybdenum (6 ppm), zinc (122 ppm), mercury (230 ppm) and gold (10 ppb; samples 9695, 9700, 9895 in Jackaman, 2000).

SUMMARY AND FUTURE WORK

Regional geological mapping in the Nakina Lake and River sheets (104N/1, 2) reveals a complexity not evident on previously published maps. Recognition of a fold and thrust belt, a serpentinite mélange belt, parts of an accretionary prism and widespread indications of felsic volcanism are among the most significant regional mapping contributions arising from this study. Production of 1:50 000 scale maps will be aided by 80 new radiolarian collections, 50 new collections of Carboniferous to Permian fusulinids and numerous macrofossil collections including Permian ammonoids and corals. Surprisingly, much of the hemipelagic stratigraphy is of Middle Triassic age, younger than expected on the basis of previous fossil age determinations. Oceanic crustal rocks are presumably the basement on which all strata were deposited and should yield some of the oldest ages in the Cache Creek Terrane. They will be dated using a combination of U/Pb and $^{40}Ar/^{39}Ar$ techniques.

Of key importance has been the discovery of submarine felsic volcanic rocks in an area underlain by drainage basins showing anomalous base metal RGS values. Abundant volcanic quartz in detrital sediments from a variety of places across the map area points to widespread felsic volcanism within or on the margins of the ancient Cache Creek ocean basin. The possibility that Cache Creek Terrane felsic or mafic volcanic successions might be associated with exhalites is demonstrated by our discovery of evidence for a vigorous fossil hydrothermal system. This large magnetite exhalite unit, exposed over 25m x 700 m, points to the viability of the Cache Creek Terrane as a host for volcanogenic mineral deposits.

ACKNOWLEDGEMENTS

We would not have been able to cover the ground without the dollar-stretching, aerial choreography of Norm Graham of Discovery Helicopters in Atlin. Thanks also to the people of Atlin for their generous support of our field program and enthusiastic attendance of our summer geo-lecture series. Jackie Williams and Alice Carlick kindly provided us with historically correct geographic place names for the Nakina Lake and River map areas. At the time of writing, pending cuts to government funding are anticipated to impact on delivery of some products planned under the Atlin Targeted Geoscience Initiative.

REFERENCES CITED

Aitken, J.D. (1959): Atlin map-area, British Columbia; *Geological Survey of Canada*, Memoir 307, 89 pages.

Ash, C.H. (1994): Origin and tectonic setting of ophiolitic ultramafic and related rocks in the Atlin area, British Columbia (NTS 104N); *B.C. Ministry of Energy, Mines and Petroleum Resources*, Bulletin 94, 48 pages.

Bilsland, W.W. (1952): Atlin, 1898-1910: The story of a gold boom; *British Columbia Historical Quarterly*, Volume 16, Numbers 3 and 4 (Reprinted in 1971 by the Atlin Centennial Committee, 63 pages with pictorial supplement).

Coney, P.J., Jones, D.L. and Monger, J.W.H. (1980): Cordilleran suspect terranes; *Nature (London)*, Volume 288, pages 329-333.

Dumont, R., Coyle, M. and Potvin, J. (2001a): Aeromagnetic total field map British Columbia: Nakina Lake, NTS 104N/1; *Geological Survey of Canada*, Open File 4091.

Dumont, R., Coyle, M. and Potvin, J. (2001b): Aeromagnetic total field map British Columbia: Nakina, NTS 104N/2; *Geological Survey of Canada*, Open File 4092.

Dumont, R., Coyle, M. and Potvin, J. (2001c): Aeromagnetic total field map British Columbia: Sloko River, NTS 104N/3; *Geological Survey of Canada*, Open File 4093.

English, J.M., Mihalynuk, M.G., Johnston, S.T. and Devine, F.A. (2002): Atlin TGI Part III: Geology and Petrochemistry of mafic rocks within the northern Cache Creek terrane and tectonic implications; *in* Geological Fieldwork 2001, *B.C. Ministry of Energy and Mines*, Paper 2002-1.

Isozaki, Y., Maruyama, S. and Furuoka, F. (1990): Accreted oceanic materials in Japan; *Tectonophysics*, Volume 181, pages 179-205.

Jackaman, W. (2000): British Columbia Regional Geochemical Survey, NTS 104N/1 - Atlin; *BC Ministry of Energy and Mines*, BC RGS 51.

Lefebure, D.V. and Gunning, M.H. (1988): Atlin; *in* Exploration in British Columbia; 1987, *British Columbia Ministry of Mines and Petroleum Resources*, 1987, pages B87-B95.

Lowe, C. and Anderson, R.G. (2002): Preliminary interpretation of new aeromagnetic data for the Atlin Map area, British Columbia; *in* Current Research, Part A, *Geological Survey of Canada*, Paper 2002-A17, page 10.

Mihalynuk, M.G., Smith, M.T., Gabites, J.E., Runkle, D. and Lefebure, D. (1992): Age of emplacement and basement character of the Cache Creek Terrane as constrained by new isotopic and geochemical data; *Canadian Journal of Earth Sciences*, Volume 29, pages 2463-2477.

Mihalynuk, M.G., Nelson, J. and Diakow, L.J. (1994): Cache Creek Terrane entrapment; oroclinal paradox within the Canadian Cordillera; *Tectonics*, Volume 13, pages 575-595.

Mihalynuk, M.G., Bellefontaine, K.A., Brown, D.A., Logan, J.M., Nelson, J.L., Legun, A.S. and Diakow, L.J. (1996): Geological compilation, northwest British Columbia (NTS 94E, L, M; 104F, G, H, I, J, K, L, M, N, O, P; 114J, O, P); *B.C. Ministry of Energy and Mines*, Open File 1996-11.

Monger, J. (1975): Upper Paleozoic rocks of the Atlin Terrane, northwestern British Columbia and south-central Yukon; *Geological Survey of Canada*, 63 pages.

Souther, J.G. (1971): Geology and mineral deposits of Tulsequah map-area, British Columbia; *Geological Survey of Canada*, Memoir 362, 84 pages.

Terry, J. (1977): Geology of the Nahlin ultramafic body, Atlin and Tulsequah map-areas, northwestern British Columbia; *in* Current Research, Part A, *Geological Survey of Canada*, pages 263-266.

Watson, K.D. and Mathews, W.H. (1944): The Tuya-Teslin area, northern British Columbia; *British Columbia Department of Mines*, Bulletin 19, 52 pages.

Atlin TGI Part III: Geology and Petrochemistry of Mafic Rocks Within the Northern Cache Creek Terrane and Tectonic Implications

By Joseph M. English[1], Mitchell G. Mihalynuk[2], Stephen T. Johnston[1] and Fionnuala A. Devine[3]

KEYWORDS: *Cache Creek terrane, Nakina, regional geology, volcaniclastic, basalt, geochemistry, oceanic arc, seamount, accretionary complex.*

INTRODUCTION

The Cache Creek terrane is a belt of oceanic rocks that extend the length of the Cordillera in British Columbia, where they occupy a central position within the accreted terranes (Coney *et al*., 1980; Figure 1). Fossil fauna in this belt are uniquely exotic with respect to the remainder of the Canadian Cordillera as they are typical of the equatorial Tethyan realm, contrasting with coeval faunas in adjacent terranes that show closer linkages with ancestral North America (Monger and Ross, 1971; Orchard *et al*., 2001). Fossil data in the Atlin area suggest an age range from Mississippian through to Lower Jurassic for these rocks (Monger, 1975; Cordey *et al*., 1991; Orchard, 1991). The bounding island arc terranes of Stikinia and Quesnellia, to the west and east respectively, may have developed in response to Palaeozoic through Mesozoic destruction of the Cache Creek ocean basin (Cordey *et al.*, 1987; Mihalynuk, 1999). Petrochemical analysis of the volcanic rocks of Cache Creek provides an opportunity to constrain the tectonic setting of the Cache Creek terrane throughout much of its early history. This terrane has played a pivotal role in the evolution of the Canadian Cordillera and improvements in understanding the Cache Creek terrane bear on the Cordillera as a whole.

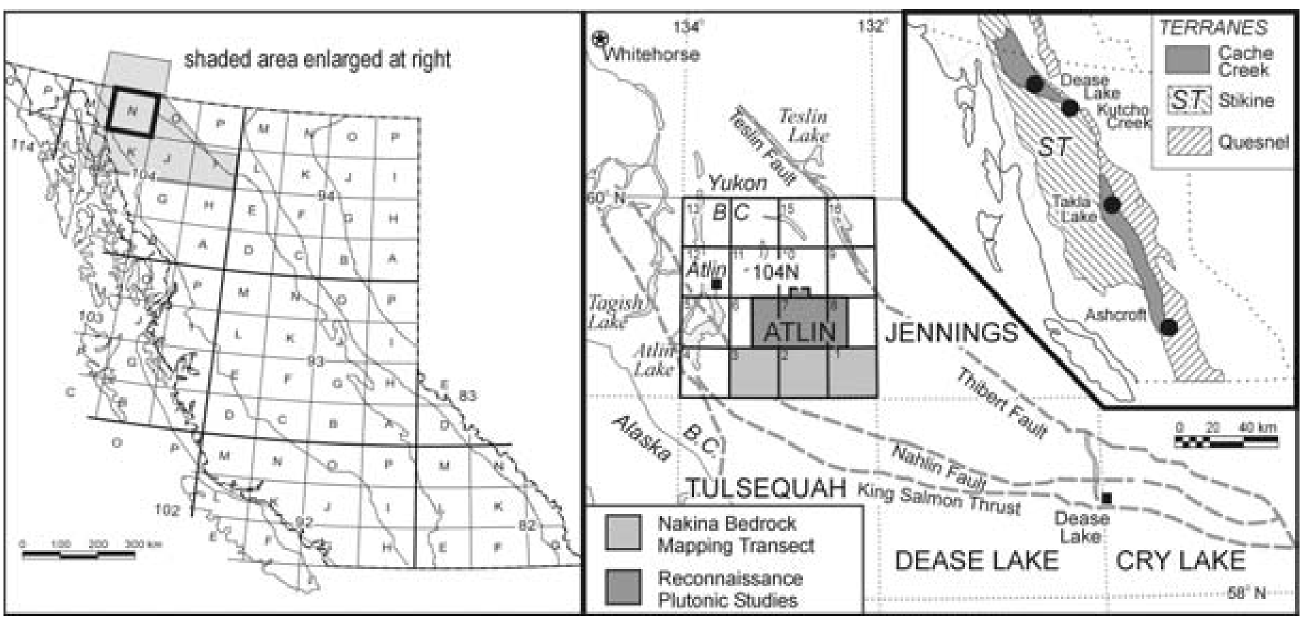

Figure 1. General location map of north-western British Columbia showing the Atlin Targeted Geoscience Initiative study area (1:250 000 sheet 104N), and the Nakina regional mapping project area (1:50 000 sheets 104N/1, 2, 3).

[1] *University of Victoria*
[2] *British Columbia Ministry of Energy and Mines*
[3] *The University of British Columbia*

PREVIOUS WORK

The existing regional geological context of the Nakina area of the Cache Creek terrane is based upon mapping conducted in the early to mid 1950s by Aitken (1959), prior to the origin of plate tectonic theory. Parts of the area were mapped by Monger (1975), who was the first to interpret the terrane as a dismembered ophiolite. Terry (1977) argued that the Nahlin Ultramafic body, the largest in the Canadian Cordillera, is part of a classical ophiolite. However, caution should be exercised in applying the term 'ophiolite' *sensu stricto*, as widespread exposures of pillow basalts and sheeted dykes of a pristine ophiolitic section are not known. In a more recent study, Ash (1994) drew similar conclusions from ultramafic rocks near Atlin and also demonstrated a MORB-chemistry for associated basalts.

Monger (1977) suggested that long-lived (Upper Mississippian–Upper Permian) carbonate-dominated successions in the Nakina region (the Horsefeed Formation) were founded on volcanic pediments and interpreted these as ancient seamounts or an oceanic plateau within the Cache Creek ocean basin. This concept is supported by geochemical analysis of Cache Creek rocks in central British Columbia, where Permian limestones are associated with basaltic rocks of ocean-island affinity (Ash and McDonald, 1993; Tardy *et al*., 2001). However, this hypothesis remains untested within the Nakina area, where the age, petrogenesis and geologic setting of volcanic strata remain incompletely understood.

GEOLOGY OF NAKINA AREA

The Cache Creek Terrane is characterised by tectonically imbricated slices of chert, argillite, volcaniclastics, limestone and wacke, as well as ultramafics, gabbro and basalt. These lithologies represent two distinctive lithotectonic elements: Upper Triassic to early Jurassic, subduction-related accretionary complexes, and dismembered basement assemblages (Monger *et al.*, 1982; Gabrielse and Yorath, 1989; Coney, 1989; Ash, 1994) emplaced during the closure of the Cache Creek ocean basin in the Middle Jurassic (Thorstad and Gabrielse, 1986; Mihalynuk *et al.*, 1999). Mapping undertaken in the Nakina region (Figure 2) during the 2001 field season appears to support this concept (*see* Mihalynuk *et al.*, this issue).

The structural complexity of this region precludes substantial stratigraphic preservation. However, a number of distinct mafic igneous assemblages have been recognised. These include the magmatic "knockers" of the Nimbus ser-

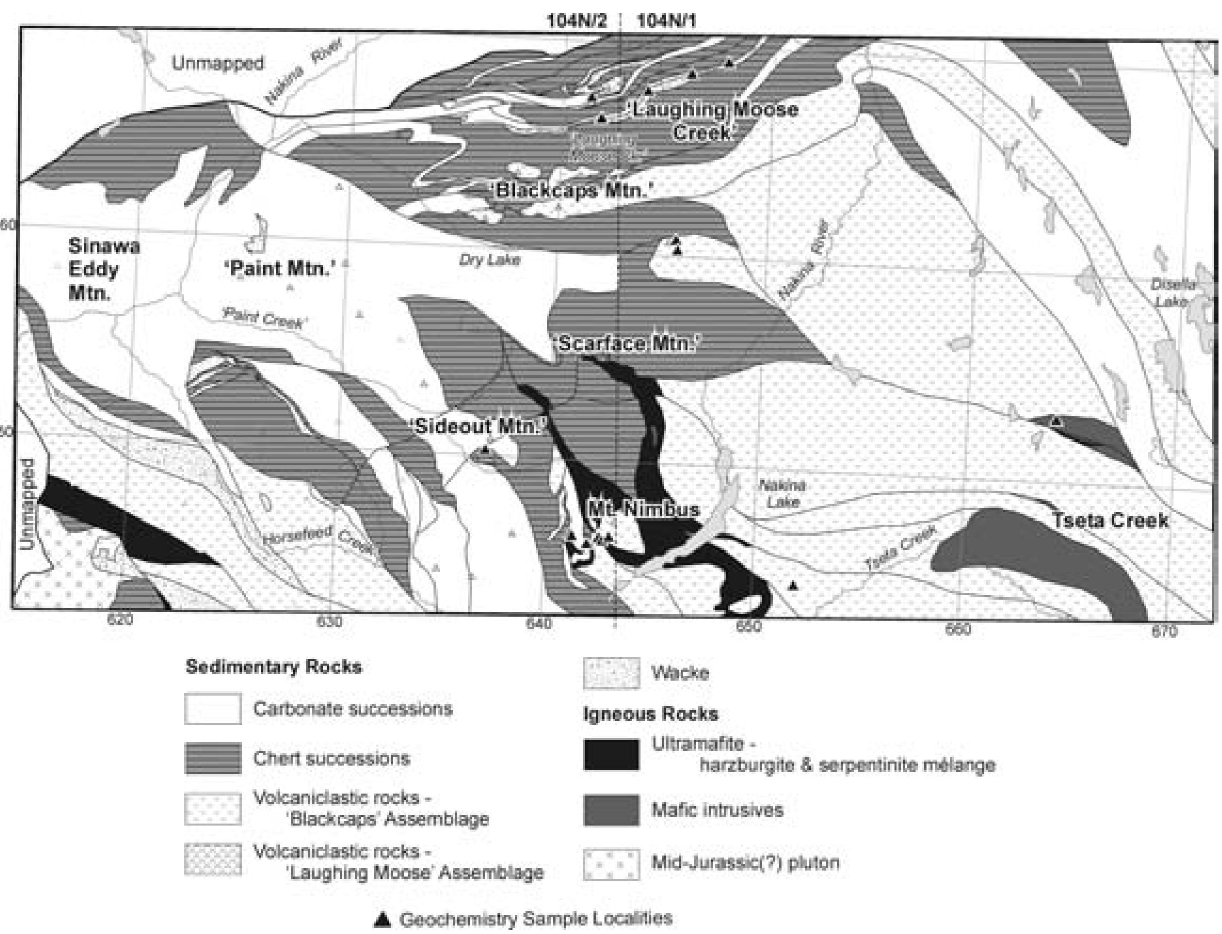

Figure 2. Generalized geologic map of the Nakina study area, NTS 104N/1 and 2 with a 10km UTM grid superimposed.

pentinite mélange; the mint-green tuffs of 'Blackcaps' Mountain; the coarse, augite-phyric breccia of 'Laughing Moose' Creek; as well as volcanic pediments to reef-forming carbonates. Mapping also revealed quartz-phyric felsic volcanic rocks (Mihalynuk *et al.*, this issue); their extent and nature is poorly defined and is not discussed further here.

NIMBUS MÉLANGE AND OTHER BASEMENT ROCKS

The Nimbus serpentinite mélange is exposed most extensively in the Mt. Nimbus region and extends eastward across Nakina Lake and north to the hills across 'Paint' Creek. The mélange belt has mafic volcanic rocks at its eastern margin, and to the west: chert, limestone and clastic sedimentary units. All bounding units display a layering that trends obliquely into the fault-bounded mélange belt. Blocks of mafic volcanics, up to 2 kilometres across, are surrounded by serpentinite within the mélange belt. Smaller, more lithologically varied blocks also occur within the mélange, enveloped in a scaly serpentinite matrix. These "knockers" are typically 1 to 50 metres across and include mafic volcanics, chert, harzburgite, limestone (rare), and plutonic rocks of gabbroic to granitic composition. The intrusive rocks are thought to be derived from the Cache Creek ocean basement or perhaps parts of a dismembered arc complex that was built atop such basement.

Southeast of Nakina Lake, the Nimbus mélange belt turns south and mafic volcanic rocks border it to the east and west. Farther east, in the Tseta Creek area, a transition to dominantly gabbroic rocks has been recognised. These gabbros display a broad range of grain size and degree of deformation. Some are intensely sheared while others are relatively undeformed. Similar textural variability is displayed by knockers within the Nimbus mélange.

\`BLACKCAPS' TUFF

The 'Blackcaps' Tuff occurs within a series of thrust sheets with associated chert and limestone breccias. This unit is comprised mainly of mint-green, monomictic lapilli and ash tuff. Coarse lapilli tuff and tuff breccia is relatively uncommon, displaying a fragmental texture on weathered surfaces, with angular clasts up to 10 cm in size. These clasts are typically basaltic andesite with relict plagioclase and pyroxene phenocrysts. Locally the fine tuff is also pyroxene-phyric. Pyroxene crystals are generally fresh and euhedral, without obviously abraded surfaces. Disseminated pyrite, pyrhhotite and minor chalcopyrite, less than 1-2%, are common. The fine-grained matrix and plagioclase crystals have been subjected to alteration, principally the formation of prehnite, pumpellyite, white mica, clay minerals and calcite. However, protolith textures are everywhere apparent. Shear fabrics can be ubiquitous over entire mountainsides. As such, they are interpreted as produced during deposition/resedimentation; although, tectonic fabrics that are superimposed on the earlier depositional fabrics are common locally.

The base of the succession at 'Blackcaps' consists of chert. Radiolarian identification reveals an age of Carboniferous or Permian based upon the presence of the relatively poorly preserved fusulinid ***Latentifistulidae*** extracted from well-bedded grey chert along strike to the west (identified by F. Cordey, *see* Mihalynuk *et al*. this volume). The chert unit grades progressively upwards, through a transitional argillaceous chert unit, and into the 'Blackcaps' Tuff. The transitional unit is siliceous containing fine volcanic ash and occasional crystals that mark the onset of volcaniclastic deposition.

The 'Blackcaps' Tuff may attain a thickness of 500m, although a paucity of bedding and marker horizons makes it difficult to rule out structural repetition. Some chert bands, up to several metres thick, are useful local markers, but the dominance of the tuff appears to represent deposition rates that greatly exceed those of biogenic chert accumulation. High in the succession, a planar-bedded calcarenitic unit can be traced for several hundred metres and is interpreted as turbiditic in origin. Both the calcareous and chert units probably reflect periods of relative quiescence in volcanic activity. Upper contacts of the 'Blackcaps' Tuff are marked by a limestone breccia. As of yet, no fossil ages have been extracted from this unit.

'LAUGHING MOOSE' AUGITE PORPHYRY BRECCIA

Basaltic breccia with coarse augite phenocrysts comprises a distinctive unit within the 'Laughing Moose' area, which lies just north of the 'Blackcaps' area. The Laughing Moose augite porphyry is a laterally extensive, monomictic matrix-supported breccia reaching up to 250m in thickness. The blocks are up to 1m across. It displays some variability, both flow-banding, presumably of pyroclastic origin, and coarse epiclastic sandstones containing well rounded clasts and crystals. Tuffs contain as much as 30% strikingly zoned euhedral augite crystals that are up to 1cm in diameter, and less abundant plagioclase phenocrysts. The groundmass is dominated by plagioclase and Fe-oxides. Some exposures illustrate syn-sedimentary deformation with microfaults offsetting graded beds. One isolated exposure of diorite is potentially co-magmatic, but contains a different phenocryst assemblage, predominantly hornblende and plagioclase.

The augite porphyry succession rests with angular unconformity on folded chert. Where observed, the base of the augite porphyry unit contains cm to dm-sized chert clasts.

In the upper part of this succession, the volcaniclastic sequence becomes more calcareous and eventually grades into limestones. No micro- or macrofossil data have yet been obtained from this limestone. The sequence is capped by carbonate granule conglomerates, tentatively interpreted as debris-flows.

TABLE 1
WHOLE ROCK MAJOR ELEMENTAL ABUNDANCES FOR MAFIC ROCKS IN THE NAKINA AREA

Sample	Assemblage	Easting	Northing	SiO2	TiO2	Al2O3	Fe2O3	FeO	MnO	MgO	CaO	Na2O	K2O	P2O5	Cr2O3	LOI	C	S	SUM
FDE01-14-12	'Laughing Moose' basalt	640750	6567060	44.64	2.97	11.06	11.44	-	0.13	10.3	11.07	2.33	0.98	0.47	0.074	4.4	0.64	<.01	99.96
FDE01-23-6	'Blackcaps' basalt	651840	6544708	53.61	0.65	13.66	8.63	-	0.14	6.96	9.37	3.54	0.12	0.06	0.04	3.2	0.11	0.02	99.99
FDE01-31-1A	Mt. Nimbus basanite	641345	6546812	39.21	4.54	13.33	12.22	-	0.17	6.93	9.55	1.87	1.88	2.07	0.011	7.6	0.71	<.01	99.52
FDE01-31-1B	Mt. Nimbus basanite	641345	6546812	38.51	4.96	14.25	12.91	-	0.16	7.27	8.17	1.29	2.34	2.49	0.017	6.8	0.28	0.01	99.31
FDE01-31-3	Mt. Nimbus basanite	641300	6546796	40.47	4.43	12.84	11.64	-	0.13	7.06	9	2.6	1.6	1.94	0.012	7.2	0.76	0.04	99.1
FDE01-31-4	Nimbus mélange basalt	641880	6546544	48.88	1.83	13.34	10.84	-	0.17	6.66	10.11	3.71	0.08	0.24	0.012	4	0.25	0.16	99.89
FDE01-31-6	Nimbus mélange gabbro	642538	6546533	46.58	0.21	19.48	5.42	-	0.1	7.45	13.2	2.25	0.52	<.01	0.017	4.8	<.01	<.01	100.1
FDE01-31-7	Nimbus mélange gabbro	642538	6546483	50.17	0.82	15.73	9.07	-	0.13	7.09	10.15	3.51	0.02	0.06	0.005	3.1	0.03	0.01	99.87
FDE01-31-10	Nimbus mélange basalt	642711	6546740	47.25	1.42	14.93	11.17	-	0.17	6.45	11.31	2.42	0.26	0.09	0.016	4.6	0.05	0.18	100.1
FDE01-31-12	Nimbus mélange tonalite	642536	6546483	77.23	0.12	12.93	0.23	-	<.01	0.32	1.17	5.4	1.46	<.01	0.008	0.9	0.09	<.01	99.79
JEN01-23-8	'Blackcaps' basalt	645368	6560715	48.67	1.32	15.34	10.48	-	0.16	6.17	11.16	1.53	0.26	0.16	0.013	4.7	0.01	0.02	99.98
JEN01-23-12	'Blackcaps' basalt	645419	6560010	48.24	1.33	15.38	10.49	-	0.14	6.56	11.41	2.2	0.32	0.08	0.019	3.9	0.04	0.11	100.1
JEN01-26-5A	Tseta Creek gabbro	665924	6551936	48.48	0.87	15.71	9.46	-	0.14	7.97	10.09	3.23	0.09	0.05	0.029	3.8	0.08	<.01	99.94
JEN01-27-6	'Blackcaps' basalt	644156	6567988	53.28	1.09	14.79	9.94	-	0.14	6.56	7.2	4.46	0.49	0.12	0.008	1.8	0.03	0.03	99.98
JEN01-32-1B	'Laughing Moose' basalt	646677	6568948	38.86	2.59	9.46	9.83	-	0.17	7.46	16.48	1.7	2.15	0.38	0.052	10	2.48	<.01	99.47
JEN01-32-8	'Laughing Moose' diorite	645724	6568619	52.65	1.79	16.46	8.38	-	0.11	5.06	5.74	4.19	0.96	0.41	0.002	3.9	0.33	0.13	99.71
MMI01-15-4	'Laughing Moose' basalt	641793	6566487	45.4	3.12	11.42	12.02	-	0.14	9.6	11.38	2.4	1.11	0.49	0.055	2.5	0.05	0.01	99.69
YME01-31-7C	'Sideout Mt.' trachyte	637065	6550442	70.47	0.93	12.39	4.82	-	0.04	1.01	1	6.11	0.54	0.09	<.001	2.2	0.11	0.18	99.87
N-MORB	global average[1]	-	-	50.4	1.36	15.2	1.3	8.14	0.18	8.96	11.4	2.3	0.09	0.14	-	-	-	-	99.47
E-MORB	global average[1]	-	-	51.2	1.69	16	9.4	-	0.16	6.9	11.5	2.74	0.43	0.15	-	-	-	-	100.17
OIB	global average[1]	-	-	49.2	2.57	12.8	-	11.4	0.17	10	10.8	2.12	0.51	0.25	-	-	-	-	99.82
IAT	Lau Basin[2]	-	-	56.76	1.39	14.58	-	11.5	0.22	3.74	7.66	3.37	0.52	0.16	-	-	-	-	99.92
RE: FDE01-31-7	Nimbus mélange gabbro			50.46	0.81	15.85	9.02	-	0.13	7.1	10.14	3.56	0.06	0.06	0.005	2.7	0.02	<.01	99.9
RE: JEN01-23-12	'Blackcaps' basalt	645419	6560010	47.99	1.32	15.28	10.46	-	0.14	6.55	11.37	2.19	0.33	0.13	0.018	4.2	0.05	0.07	100
% Difference	-	-	-	0.55	1	0.75	0.45	-	-	0.15	0.25	0.95	150	31.3	2.8	11.3	37.5	18.2	0.05
Std. SY4	-	-	-	49.9	0.29	20.69	6.21	2.86	0.108	0.54	8.05	7.1	1.66	0.13	-	4.56	-	-	102.14
RE: Std. SY4	-	-	-	49.84	0.3	20.93	6.24	-	0.1	0.51	8.22	6.79	1.58	0.07	<.001	5	1.1	0.03	99.63
% Difference	-	-	-	0.1	4.5	1.2	0.5	-	8	5.9	2.1	4.6	5.1	87.1	-	9.2	-	-	0.03

[1] Sun and McDonough (1989)
[2] Jenner *et al*. (1987)

VOLCANIC UNITS WITHIN CARBONATE

Isolated volcanic accumulations occur within carbonate units. At three localities, the volcanic rocks form the substrate of carbonate reefs. At another locality, glassy pillow lava flows occur within bioclastic limestone adjacent to the Nimbus mélange on the southwest flank of Mt. Nimbus. Here the volcanic rocks are highly fractured, as is the entire carbonate unit. Flows are brown-weathering, and pinkish maroon fresh, with pillows containing zones of elongate, calcite-filled vesicles and separated by interpillow hyaloclastite. Rounded to angular carbonate blocks comprise irregular interlayers within the volcanics; they are interpreted to be of olistostromal origin.

The most extensive framework reef constructed on an isolated accumulation of volcanics occurs on the southwest flank of 'Sideout Mountain', north of 'Paint Creek' (Monger, 1977; see also Mihalynuk *et al*., this issue). Here, Upper Mississippian reef/lagoonal carbonates were deposited on volcanic breccias. The breccia clasts are plagioclase-phyric (60-70%) and display a trachytic texture.

GEOCHEMISTRY

A representative suite of 18 intrusive and extrusive rocks from the Nakina area was analysed for major and trace element abundance in order to establish their composition and petrogenetic affiliation. Major oxides were determined by $LiBO_2$ fusion and ICP analysis and minor and trace element geochemistry was determined using ICP MS analysis, both at ACME Analytical Laboratories, Vancouver. These results are listed in Table 1, along with published data from volcanic rocks formed in various tectonic set-

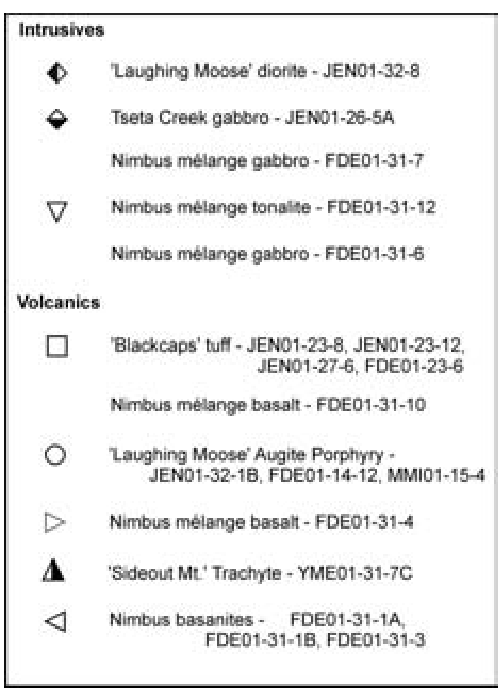

Figure 3. Key to the symbols used in geochemical diagrams.

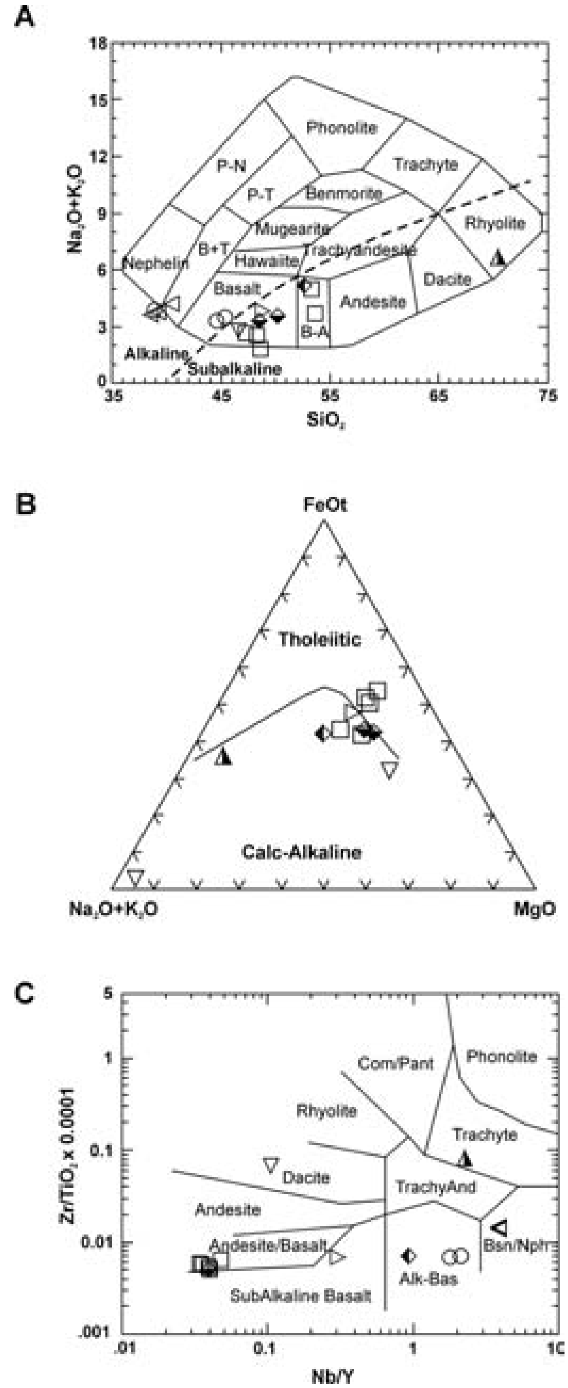

Figure 4. (a) Samples collected and analysed as part of this study are classified by using Na2O+K2O versus SiO2 (from Cox et al., 1979). This diagram also distinguishes between the fields for alkaline and subalkaline rocks (thick dashed line). Abbreviations: P-N – phonolite-nephelinite, P-T – phonolite-tephrite, B+T – basanite + tephrite, B-A – basaltic andesite. (b) The AFM (alkalis-FeOt-MgO) diagram of Irvine and Baragar (1971) can be used for subalkaline rocks to separate tholeiitic from calc-alkaline rocks. (c) Immobile trace element abundances are also used for classification (from Winchester and Floyd, 1977), particularly in altered volcanic rocks where elemental mobility is suspected. In this case little elemental mobility is shown - compare with (a). Abbreviations: Bsn/Nph – Basanite/Nephelinite; Com/Pant – Comendite/Pantellerite.

TABLE 2
WHOLE ROCK TRACE AND RARE EARTH ELEMENTAL ABUNDANCES FOR MAFIC ROCKS IN THE NAKINA AREA

Sample	Ba	Rb	Sr	Cs	Ga	Tl	Ta	Nb	Hf	Zr	Y	Th	U	Ni	Co	Sc	V	Cu	Pb	Zn	Bi
FDE01-14-12	341	31.5	165.1	1.1	18.4	0.1	2.8	50.5	5.3	207.5	23.5	4.7	0.9	105	47.7	35	234	84	<2	74	<.5
FDE01-23-6	11	1.1	66	<.1	13.3	0.1	<.1	0.8	1.2	42.6	16.8	0.1	0.1	36	34.3	35	205	66	<2	27	<.5
FDE01-31-1A	1113	52.7	985.6	31.7	24.6	0.2	9.2	162.1	14.5	659.1	41.8	16.4	3.1	81	41.5	20	215	24	7	138	<.5
FDE01-31-1B	1183	60	1082	29.8	23.3	0.2	9.7	172.7	15.9	687.9	44.7	15.9	2.6	86	43.7	21	224	27	6	177	<.5
FDE01-31-3	1464	38.3	1878	16.3	24.5	0.1	9.3	155.7	13.2	627.7	39.9	16.1	4.3	92	39	19	195	25	7	134	<.5
FDE01-31-4	69	1.5	152.9	0.5	17.9	0.1	0.2	9.2	2.8	127.3	30.2	0.6	0.4	32	39.2	43	264	77	<2	62	<.5
FDE01-31-6	20	5.7	173.5	0.7	14.3	0.2	<.1	<.5	<.5	6.5	6.6	<.1	<.1	85	28.2	28	97	30	<2	12	<.5
FDE01-31-7	12	<.5	146.2	<.1	13.9	0.1	<.1	0.7	1.1	41.3	18	<.1	<.1	29	37.4	38	225	5	<2	21	<.5
FDE01-31-10	23	2.4	105.5	<.1	18.3	0.2	<.1	1.2	2.4	80.3	33.8	0.1	<.1	48	44.5	38	304	81	<2	90	<.5
FDE01-31-12	94	17.9	150.8	0.2	8.7	0.2	<.1	2	3	82	19.1	1.9	0.5	11	0.5	3	<5	1	<2	1	<.5
JEN01-23-8	34	5.6	52.2	0.2	18.2	0.2	<.1	1.2	2	71.8	30.7	<.1	<.1	51	39.4	39	291	53	<2	68	<.5
JEN01-23-12	26	8.1	85.1	0.8	16.5	0.4	<.1	1.2	1.8	67.4	29.9	0.2	0.4	48	40.6	39	301	61	<2	67	<.5
JEN01-26-5A	24	1.1	101.3	<.1	14.5	0.3	<.1	<.5	1.3	37.2	20	0.2	<.1	60	41.6	41	259	70	<2	55	<.5
JEN01-27-6	735	7.1	145.8	0.1	14.4	1.1	<.1	0.9	1.7	63.5	26.1	0.2	<.1	23	33.6	37	293	14	<2	25	<.5
JEN01-32-1B	2792	52.6	445.2	3.4	14.5	0.6	2	38.5	4.4	176.5	21.5	3.5	0.6	121	39.1	33	264	94	<2	59	<.5
JEN01-32-8	473	17.1	611.2	1.4	21	0.9	0.6	17.8	3.1	125	19.1	2.4	1.2	49	27.1	14	136	22	2	89	<.5
MMI01-15-4	274	25.5	294.6	1.1	16.9	0.2	2.9	54.7	5	217.9	25.4	4.6	0.6	110	53.8	38	305	77	<2	71	<.5
YME01-31-7C	2401	14.8	516.2	0.5	25.6	0.2	9.5	182	16.5	756	80.9	12.5	2.6	5	12.7	6	26	5	4	38	<.5
N-MORB	6	0.6	90	0	-	-	-	2.3	2.1	74	28	0.12	0.05	177	50	40	262	-	-	-	-
E-MORB	57	5	155	0.1	-	-	-	8.3	2	73	22	0.6	0.18	-	-	-	-	-	1	-	-
OIB	350	31	660	0.4	-	-	-	48	7.8	280	29	4	1.02	-	-	-	-	-	3	-	-
IAT	102	8.2	169	0.2	-	-	0.1	1.1	2.3	79	34	0.41	0.18	25	-	32	350	-	-	114	-
RE: FDE01-31-7	12	<.5	153.4	<.1	16	0.2	<.1	0.6	1.5	41.9	18.4	0.2	<.1	60	36.4	38	238	5	<2	21	<.5
RE: JEN01-23-12	24	7.7	86	0.9	17.1	0.5	<.1	1.2	2	66.9	30.7	<.1	0.2	74	38.4	38	306	57	<2	62	<.5
% Difference	4.15	2.6	3	6.25	9.35	62.5	-	8.35	23.75	1.1	2.45	>100	25	13.23	4.2	1.3	3.75	3.5	-	4.05	-
Std. SY4	340	55	1191	1.5	35	-	0.9	13	10.6	517	119	1.4	0.8	9	2.8	1.1	8	7	10	93	-
RE: Std. SY4	335	56.6	1253	1.6	36.2	0.1	0.3	12.7	9.7	521.7	132.1	1.4	1	22	2.5	1	5	3	2	49	<.5
% Difference	1.5	2.9	5.2	6.7	3.4	-	200	2.4	9.3	0.9	11	-	25	144.4	12	10	60	133.3	400	89.8	-

tings. A key to the symbols used in the various plots is illustrated in Figure 3.

MAJOR AND TRACE ELEMENTS

Mafic rock samples from the Nakina area are both alkaline and subalkaline (Figure 4a). On the total alkalis versus silica (TAS) diagram of Cox *et al*. (1979), the 'Laughing Moose' augite porphyry breccia and carbonate-associated volcanics from Mt. Nimbus are classified as alkaline, whereas the rest of the samples are subalkaline. All of the samples reveal a basaltic to basaltic andesite composition, except for one sample representing an isolated volcanic accumulation in carbonate. Three of the representative intrusive rock samples were collected in the Mt. Nimbus area from blocks within the mélange. These include a medium grained, chloritised gabbro (FDE01-31-6); a green, vari-textured gabbro (FDE01-31-7), and a grey, recrystallised tonalite (FDE01-31-12). The other two intrusive samples are from the Tseta Creek gabbro (JEN0126-5A) and the 'Laughing Moose' diorite (JEN01-32-8). The 'Laughing Moose' diorite reveals a subalkaline chemistry and does not display any obvious similarities to its associated volcaniclastic rocks. The subalkaline rocks are plotted on an AFM diagram (Irvine and Baragar, 1971; Figure 4b). Most of these rocks appear to be calc-alkaline, although the 'Blackcaps' Tuff straddles the boundary.

Oxides in rocks, particularly alkalis, can move around during alteration and metamorphism (Smith and Smith, 1976). Petrographic analyses of samples considered in this study reveal varying degrees of alteration. The elevated LOI and C content of the Mt. Nimbus basanites is attributable to hydration of the glassy matrix and the presence of microscopic carbonate veinlets. High LOI content is also observed in one 'Laughing Moose' sample (JEN01-32-1B), and this is attributable to the presence of phyllosilicates and carbonate. However, compositional groupings based on major element profiles are consistent with those based on immobile trace element compositions, although classification may vary slightly. For example, rock classification based on the TAS diagram compares well with that based on the immobile element Zr/TiO_2 versus Nb/Y diagram (Figure 4c; Winchester and Floyd, 1977). The only major difference between these plots is that the porphyritic trachyte from 'Sideout Mountain' (YME01-31-7C) plots in the subalkaline field in major element classification of Figure 4a, but in the alkaline field in the trace element classification of Figure 4c. This sample is

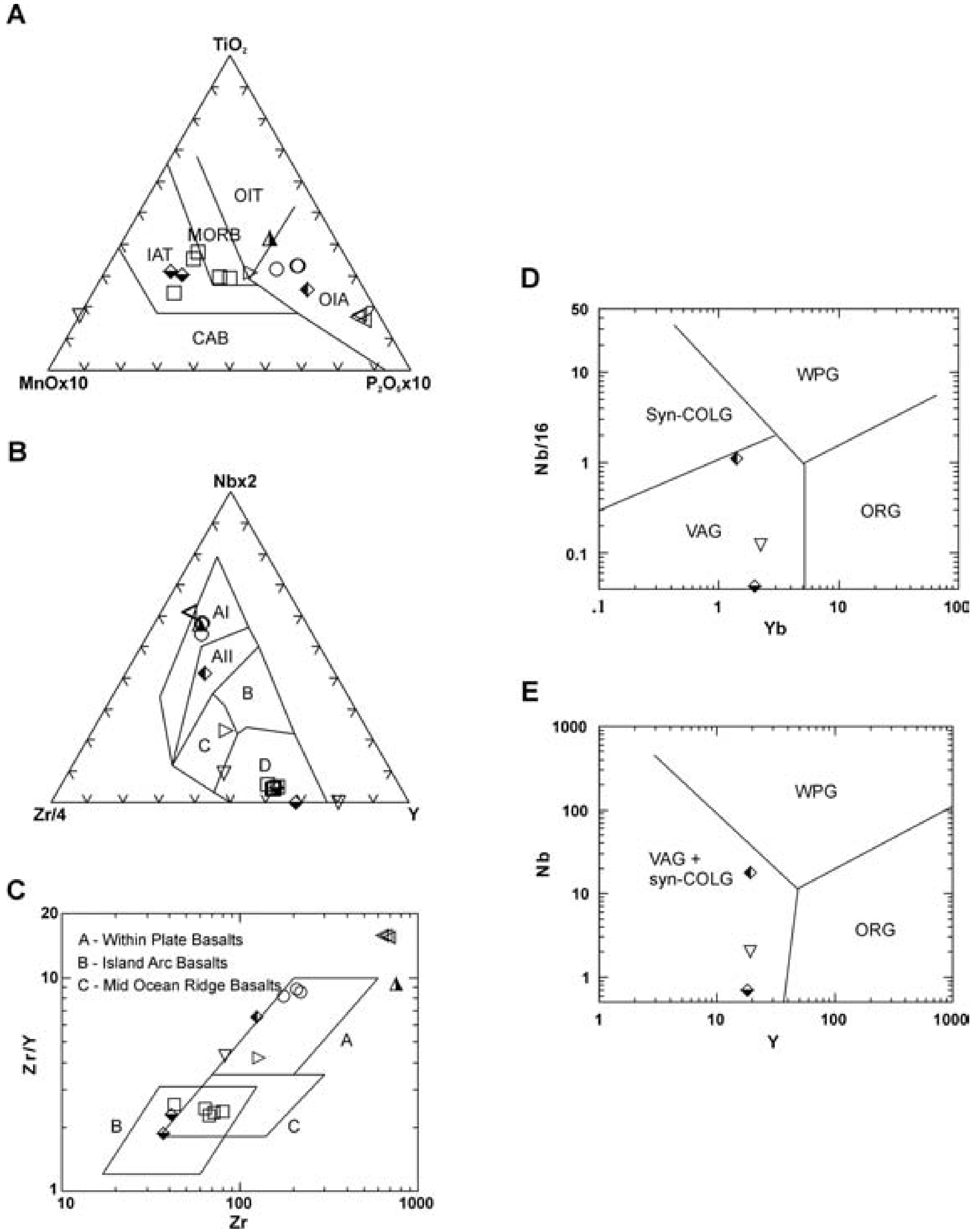

Figure 5. Trace element discriminant diagrams for rocks of basaltic composition following the methods of (a) Mullen (1983); (b) Meschede (1986) and Pearce and Norry (1979). Abbreviations when not given are: OIT – ocean island tholeiite; OIA – ocean island andesite; MORB – mid-ocean ridge basalt; IAT – island arc tholeiite; CAB – calc-alkaline basalt; AI – within-plate alkali basalts; AII – within-plate alkali basalts and within-plate tholeiites; B – E-type MORB; C – within-plate tholeiites and volcanic arc basalts; D – N-type MORB and volcanic arc basalts. Trace element discriminant diagrams for rocks of granitic composition are used in (d) and (e) (after method of Pearce *et al.*, 1984). Figure (d) is modified from the original, with Nb/16 used as a proxy for Ta. Abbreviations: syn-COLG – syn-collisional granites; VAG – volcanic arc granites; WPG – within plate granite; ORG – ocean ridge granite.

plagioclase-rich, and contains centimetre-sized alkali feldspar phenocrysts, which may skew the analyses due to their high Si and Na content (~65%), and very low Mg, Fe and Ca concentrations.

Major oxide and trace element distributions can also be used as indicators of the tectonic environment in which the sample was formed. Figure 5a shows tectonic discriminations based upon the TiO_2-MnO*10-P_2O_5*10 ternary plot of Mullen (1983). This plot indicates that the alkaline rocks, including the intrusive from the 'Laughing Moose' area, are of within-plate affinity. However, the tectonic affinity of the 'Blackcaps' Tuff is not entirely conclusive as it appears to straddle the island arc tholeiite (IAT) and mid-ocean ridge (MORB) fields. Although gabbroic rocks are not ideal for tectonic discrimination purposes, it is noted that these samples plot in the IAT field. The Nb*2-Zr/4-Y plot of Meschede (1986) (Figure 5b) further supports these basic observations.

A clearer picture is presented by Figure 5c, a Zr/Y versus Zr logarithmic discrimination plot of Pearce and Norry (1979). Yet again, a highly enriched within-plate source is suggested for the carbonate-associated volcanics and a within-plate setting also for the 'Laughing Moose' volcaniclastics. Gabbroic rocks plot in the island arc field and the 'Blackcaps' Tuff plots in the overlap between MORB and arc.

Further indication of a volcanic arc origin for the majority of the intrusive samples, is provided by the trace element diagrams of Pearce *et al.* (1984). Though these graphs were originally intended to show variations in tectonic origin of granitic rocks based on trace element versus SiO_2 values, the trend of the field division lines are well constrained at the low SiO_2 values, and we have extrapolated into lower SiO_2 values. Figure 5(d, e) illustrates that all of three intrusive rock samples lie within the volcanic arc field. Multi-element plots will now be utilised to probe the origin of these intrusive and volcanic rocks.

RARE EARTH ELEMENT (REE) AND MULTI-ELEMENT PLOTS

Primitive mantle normalised multi-element plots are used here to investigate the geochemical signature of these samples. The primitive mantle normalising values are those of Sun and McDonough (1989) and the element order is adopted from Jenner (1996). The Low Field Strength Element (LFSE) thorium is the only element used here that is acknowledged as being mobile during alteration.

In Figure 6a, samples from the 'Blackcaps' Tuff, the gabbroic body near Tseta Creek and from the basalt and gabbro within the Nimbus serpentinite mélange are plotted together with normal mid-ocean ridge basalt (N-MORB) and island-arc tholeiite (IAT) values. There is a striking consistency between all of the seven samples analysed, although some are slightly more enriched relative to others. All are characterised by a negative Nb anomaly, a characteristic signature of arc volcanic rocks (Jenner, 1996). However, this simple pattern is distorted by significant variability in the Th values. Apart from the negative Nb

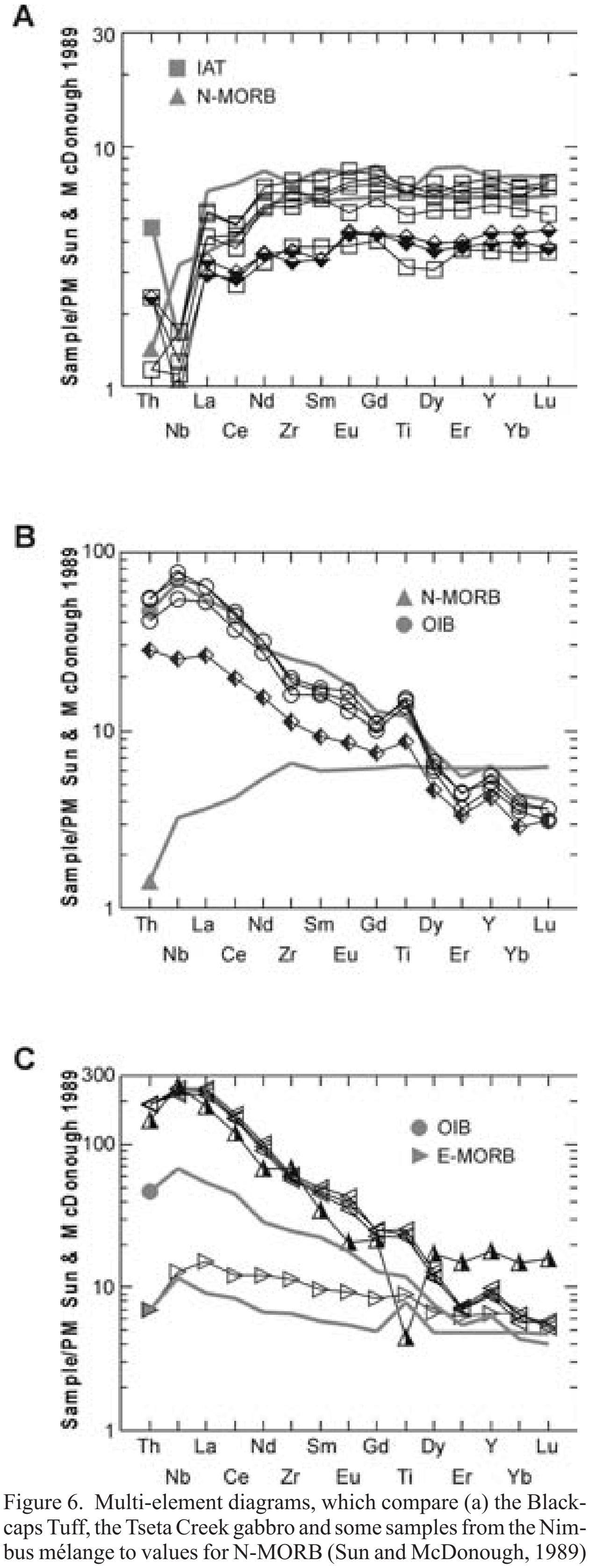

Figure 6. Multi-element diagrams, which compare (a) the Blackcaps Tuff, the Tseta Creek gabbro and some samples from the Nimbus mélange to values for N-MORB (Sun and McDonough, 1989) and IAT (Jenner *et al.,* 1987); (b) Laughing Moose rocks to values for N-MORB and OIB (Sun and McDonough, 1989), and (c) carbonate associated volcanics and one sample from Nimbus to values for OIB and E-MORB (Sun and McDonough, 1989).

anomaly, it is difficult to separate island-arc tholeiites from those volcanics of N-MORB affinity, as evidenced in the discrimination diagrams. However, the clastic nature of these volumetric deposits, and the presence of interbedded chert and bioclastic turbidites is consistent with an arc setting.

The 'Laughing Moose' augite porphyry displays enrichment in most of the incompatible elements relative to MORBs (Figure 6b). This humped pattern is characteristic of ocean-island basalts (OIB; Pearce, 1982, 1983), supporting interpretations drawn from discrimination diagrams. The intrusive rock sampled from this region (JEN01-32-8) appears to follow a similar trend, although it is relatively depleted in the light REEs, possibly reflecting its more evolved nature. This suggests that the diorite is comagmatic with the 'Laughing Moose' augite porphyry.

The final multi-element plot illustrated here (Figure 6c) displays the trends of the carbonate-associated basanite flows, as well as another sample from the Mt. Nimbus area (FDE01-31-4). The three samples of basanite are highly enriched in the incompatible elements, plotting at values three-times that of modern OIB. The solitary sample from 'Sideout Mountain' (YME01-31-7C) displays enrichment in both light and heavy REEs and a striking negative Ti anomaly. One possibility is that this enrichment in these samples may reflect a localised rifting event, tapping a very fertile mantle source. The final sample from Nimbus (FDE01-31-4) appears to reflect an enriched mid-ocean ridge (E-MORB) source, with a slight enrichment in LREE relative to N-MORB. This block, from near the margin of the mélange, had faint indications of calcite-filled vesicles and was thought to be a part of the pillowed basanite unit.

DISCUSSION

A rigorous evaluation of the Cache Creek terrane paleotectonic setting cannot be made based upon the limited data presented here. However, data obtained thus far from the Nakina region show it to be dominated by two different petrogenetic components; alkaline volcanic rocks of within-plate affinity, and primitive arc-related, subalkaline volcaniclastic rocks and intrusives.

First of all, there is a spatial association of alkali basalts of ocean-island affinity with the thick Horsefeed Formation platformal carbonate. Monger (1975) originally suggested that seamounts and/or oceanic plateaus in the Cache Creek ocean basin were the elevated oceanic basement on which the carbonate platforms were constructed, a contention supported by our data. Palaeontological and geochronological age-dating constrain the age of seamounts to older than the Permo-Carboniferous carbonate that caps them (Monger, 1975; see also Mihalynuk *et al*., this volume). Secondly, the mafic volcanic rocks in the 'Blackcaps' area are of oceanic arc affinity, and share this characteristic with some of the intrusive rocks that have been analysed. This may explain the paucity of sheeted dykes and pillow basalts in the Nakina region while thick sequences of volcaniclastics are preserved.

These observations pose an interesting question. Although arc volcanics have been documented within the Cache Creek terrane (*e.g.* the Kutcho Formation - Thorstad and Gabrielse, 1986; Sitlika Assemblage - Schiarizza and Payie, 1997; Hall Lake and French Range volcanics - Mihalynuk and Cordey, 1997; Ashcroft - Childe *et al.*, 1997), is their volumetric importance in the Nakina area greater than was previously appreciated? Accretionary complexes of deep ocean sediments are often associated with oceanic arcs, and the incorporation of carbonate platforms, volcanic seamounts and MORB-type pillow basalts from the subducting oceanic crust has been documented at modern island arcs (*e.g.* Taira *et al.*, 1989; Bloomer *et al.*, 1995; Johnson *et al.*, 1990; Johnson *et al.*, 1991). Therefore, an accretionary prism/oceanic arc origin may provide a mechanism to explain the lithological diversity within the Nakina area.

CONCLUSIONS

A number of distinct mafic igneous assemblages are recognised in the dominantly volcaniclastic rocks of the Nakina area. These include the magmatic "knockers" of the Nimbus serpentinite mélange; the mint-green tuffs of 'Blackcaps' Mountain; the coarse, augite-phyric breccia of 'Laughing Moose' Creek; as well as volcanic pediments to reef-forming carbonates.

No N-MORBs have been identified based upon preliminary geochemical investigation of the Nakina area basalts, despite having been documented elsewhere in the terrane (*e.g.* Ash and MacDonald, 1993; Ash, 1994; Mihalynuk, 1999). Alkaline volcanic rocks of 'Sideout Mountain', Mt. Nimbus and 'Laughing Moose Creek' were most likely sourced in an ocean island/plateau environment, consistent with the early suggestions of Monger (1977).

Other mafic rocks in the region have textural and geochemical characteristics consistent with formation in an oceanic arc environment. Juxtaposition of basaltic crustal fragments with disparate petrogenesis has been documented in accretionary prisms worldwide. An accretionary prism/oceanic arc origin for much of the volcanic rocks of the Nakina area is supported by the geochemistry and geology of the area.

ACKNOWLEDGEMENTS

Thanks to Fabrice Cordey, Yann Merran and Kyle Larson, who also participated in the fieldwork and lively discussions about the enigmatic Cache Creek terrane during the 2001 field season. Thanks also to Norm Graham of Discovery Helicopters in Atlin, who put us where we needed to go. Discussions with Kaesy Gladwin, Greg Shellnut and Sean Bailey were appreciated. Sample preparation occurred under the direction of Ray Lett. This study is being carried out as part of the Nakina Project, under the auspices of the Atlin Targeted Geoscience Initiative directed by Carmel Lowe of the Pacific Geoscience Centre.

REFERENCES CITED

Aitken, J.D., (1959): Atlin map-area, British Columbia; *Geological Survey of Canada,* Memoir 307, 89 pages.

Ash, C.H. (1994): Origin and tectonic setting of ophiolitic ultramafic and related rocks in the Atlin area, British Columbia (NTS 104N); *B.C. Ministry of Energy, Mines and Petroleum Resources,* Bulletin 94, 48 pages.

Ash, C.H. and Macdonald, R.W.J. (1993): Geology, mineralization and lithogeochemistry of the Stuart Lake area, central British Columbia (Parts of 93K/7, 8, 10 and 11); *in* Geological Fieldwork 1992, *B.C. Ministry of Energy, Mines and Petroleum Resources,* Paper 1993-1, pages 69-86.

Bloomer, S.H., Taylor, B., MacLeod, C.J., Stern, R.J., Fryer, P., Hawkins, J.W. and Johnson, L. (1995): Early arc volcanism and the ophiolite problem: A perspective from drilling in the western Pacific; *in* Active Margins and Marginal Basins of the Western Pacific, Taylor, B. and Natland, J. (Editors), *American Geophysical Union*, Geophysical Monograph 88, pages 1-30.

Childe, F., Friedman, R.M., Mortensen, J.K. and Thompson, F.H. (1997): Evidence for early Triassic felsic volcanism in the Ashcroft (92I) map area, British Columbia; *in* Geological Fieldwork 1996, *B.C. Ministry of Employment and Investment*, Paper 1997-1, pages 117-123.

Coney, P.J. (1989): Structural aspects of suspect terranes and accretionary tectonics in western North America; *Journal of Structural Geology*, Volume 11, No. 112, pages 107-125.

Coney, P.J., Jones, D.L. and Monger, J.W.H. (1980): Cordilleran suspect terranes; *Nature*, Volume 288, pages 329-333.

Cordey, F., Gordey, S.P and Orchard, M.J. (1991): New biostratigraphic data from the northern Cache Creek terrane, Teslin map area, southern Yukon; *in* Current Research, Part E; *Geological Survey of Canada*, Paper 91-1E, pages 67-76.

Cordey, F., Mortimer, N., DeWeever, P. and Monger, J.W.H. (1987): Significance of Jurassic radiolarians from the Cache Creek terrane, British Columbia; *Geology*, Volume 15, pages 1151-1154.

Cox, K.G., Bell, J.D. and Pankhurst, R.J. (1979): The interpretation of igneous rocks; *George Allen and Unwin*, London, pages 450.

Gabrielse, H. and Yorath, C.J. (1989): Decade of North American Geology #4, The Cordilleran Orogen in Canada; *Geoscience Canada*, Volume 16, Number 2, pages 67-83.

Irvine, T.N. and Baragar, W.R.A. (1971): A guide to the chemical classification of the common volcanic rocks; *Canadian Journal of Earth Sciences*, Volume 8, pages 523-548.

Johnson, L.E. and Fryer, P. (1990): The first evidence for MORB-like lavas from the outer Mariana forearc: geochemistry, petrography and tectonic implications; *Earth and Planetary Science Letters*, Volume 100, pages 304-316.

Johnson, L.E., Fryer, P., Taylor, B., Silk, M., Jones, D.L., Sliter, W.V., Itaya, T. and Ishii, T. (1991): New evidence for crustal accretion in the outer Mariana fore arc: Cretaceous radiolarian cherts and mid-ocean ridge basalt-like lavas; *Geology*, Volume 19, pages 811-814.

Jenner, G.A. (1996): Trace element geochemistry of igneous rocks: geochemical nomenclature and analytical geochemistry; *in* Trace element geochemistry of volcanic rocks: Applications for massive sulphide exploration, Wyman, D.A. (Editor), *Geological Association of Canada,* Short Course Notes, Volume 12, pages 51-77.

Jenner, G.A., Cawood, P.A., Rautenschlein-M and White, W.M. (1987): Composition of back-arc basin volcanics, Valu Fa Ridge, Lau Basin: evidence for a slab-derived component in their mantle source; *Journal of Volcanology and Geothermal Research,* Volume 32, pages 209-222.

Meschede, M. (1986): A method of discriminating between different types of mid-ocean ridge basalts and continental tholeiites with the Nb-Zr-Y diagram; *Chemical Geology*, Volume 56, pages 207-218.

Mihalynuk, M.G. (1999): Geology and mineral resources of the Tagish Lake area (NTS 104M/8, 9, 10E, 15 and 104N/12W) northwestern British Columbia; *B.C. Ministry of Energy, Mines and Petroleum Resources,* Bulletin 105, 217 pages.

Mihalynuk, M.G. and Cordey, F. (1997): Potential for Kutcho Creek volcanogenic massive sulphide mineralization in the northern Cache Creek terrane: A progress report; *in* Geological Fieldwork 1996, *B.C. Ministry of Employment and Investment*, Paper 1997-1, pages 157-170

Mihalynuk, M.G., Erdmer, P., Ghent, E.D., Archibald, D.A., Friedman, R.M., Cordey, F., Johannson, G.G. and Beanish, J. (1999): Age constraints for emplacement of the northern Cache Creek terrane and implications of blueshist metamorphism; in Geological Fieldwork 1998, *B.C. Ministry of Energy, Mines and Petroleum Resources,* Paper 1999-1, pages 127-141.

Monger, J.W.H. (1975): Upper Paleozoic rocks of the Atlin terrane; *Geological Survey of Canada,* Paper 74-47, 63 pages.

Monger, J.W.H. (1977): Upper Paleozoic rocks of the northwestern British Columbia; *Geological Survey of Canada*, Paper 77-1A, pages 255-262.

Monger, J.W.H. and Ross, C.A. (1971): Distribution of fusulinaceans in the western Canadian Cordillera; *Canadian Journal of Earth Sciences*, Volume 8, pages 259-278.

Monger, J.W.H., Price, R.A. and Tempelman-Kluit, D.J. (1982): Tectonic accretion and the origin of the two major metamorphic and plutonic welts in the Canadian Cordillera; *Geology*, Volume 10, pages 70-75.

Mullen, E.D. (1983): $MnO_2/TiO_2/P_2O_5$: a minor element discriminant for basaltic rocks of oceanic environments and its implications for petrogenesis; *Earth and Planetary Science Letters*, Volume 62, pages 53-62.

Orchard, M.J. (1991): Conodonts, time and terranes: An overview of the biostratigraphic record in the western Canadian Cordillera; *in* Ordovician to Triassic conodont palaeontology of the Canadian Cordillera; Orchard, M.J. and McCracken, A.D., Editors; *Geological Survey of Canada*, Bulletin 417, pages 1-25.

Orchard, M.J., Struik, L.C., Rui, L., Bamber, E.W., Mamet, B., Sano, H. and Taylor, H. (2001): Palaeontological and biogeographical constraints on the Carboniferous to Jurassic Cache Creek terrane in central British Columbia; *Canadian Journal of Earth Sciences*, Volume 38(4), pages 551-578.

Pearce, J.A. (1982): Trace element characteristics of lavas from destructive plate boundaries; *in* Andesites, Thorpe, R.S. Editor; *John Wiley and Sons Inc.*, New York, pages 525-548.

Pearce, J.A. (1983): Role of the sub-continental lithosphere in magma genesis at active plate margins; *in* Continental basalts and mantle xenoliths, Hawkesworth, C.J. and Norry, M.J. (Editors), *Shiva Publishing Limited*, pages 230-249.

Pearce, J.A. and Norry, M.J. (1979): Petrogenetic implications of Ti, Zr, Y and Nb variations in volcanic rocks; *Contributions to Mineralogy and Petrology*, Volume 69, pages 33-47.

Pearce, J.A., Harris, N.B.W. and Tindle, A.G. (1984): Trace element discrimination diagrams for the tectonic interpretation of granitic rocks; *Journal of Petrology*, Volume 25, pages 956-983.

Schiarizza, P. and Payie, G. (1997): Geology of the Sitlika Assemblage in the Kenny Creek - Mount Olson area (93N/12, 13), central British Columbia; *in* Geological Fieldwork 1996, *B.C. Ministry of Employment and Investment*, Paper 1997-1, pages 79-100.

Smith, R.E. and Smith, S.E. (1976): Comments on the use of Ti, Zr, Y, Sr, K, P and Nb in classification of basalt; *Earth and Planetary Science Letters*, Volume 32, pages 114-120.

Sun, S.S. and McDonough, W.F. (1989): Chemical and isotopic systematics of oceanic basalts: Implications for mantle composition and processes; *in* Magmatism in the ocean basins, *Geological Society of London*, Special Publication 42, pages 313-345.

Taira, A., Tokuyama, H. and Soh, W. (1989): Accretion tectonics and evolution of Japan; *in* The evolution of the Pacific Ocean Margins, Ben-Avraham, Z. (Editor), *Oxford University Press,* New York, pages 100-123.

Tardy, M., Lapierre, H., Struik, L.C., Bosch, D. and Brunet, P. (2001): The influence of mantle plume in the genesis of Cache Creek oceanic igneous rocks: implications for the geodynamic evolution of the inner accreted terranes of the Canadian Cordillera; *Canadian Journal of Earth Sciences*, Volume 38, pages 515-534.

Terry, J. (1977): Geology of the Nahlin ultramafic body, Atlin and Tulsequah map-areas, northwestern British Columbia; *in* Current Research, *Geological Survey of Canada*, Paper 77-1A, pages 263-266.

Thorstad, L.E., and Gabrielse, H. (1986): The Upper Triassic Kutcho Formation, Cassiar Mountains, north-central British Columbia; *Geological Survey of Canada*, Paper 86-16, 53 pages.

Winchester, J.A. and Floyd, P.A. (1977): Geochemical discrimination of different magma series and their differentiation products using immobile elements; *Chemical Geology*, Volume 20, pages 325-343.

Microstructural Analysis of the Teslin Fault, Northwestern British Columbia

By Kyle Larson[1]

KEYWORDS: *Teslin Fault, microstructure, shear indicators, Jennings River, Yukon-Tanana Terrane, Cache Creek Terrane.*

INTRODUCTION

The Canadian Cordillera is host to numerous crustal-scale shear zones, including the Tintina and Denali faults (Gabrielse, 1985). Study of these faults is necessary in order to determine motions of allochthonous terranes subsequent to their accretion onto the west margin of ancestral North American. Accurate knowledge of past motions on crustal scale faults is critical these paleogeographic reconstructions.

The Teslin Fault is a crustal-scale fault located approximately midway between the Denali and Tintina faults (Wheeler and McFeely, 1991). It separates the Cache Creek and Yukon-Tanana Terranes in the Jennings River area (Figure 1; Mihalynuk *et al*., 2001). Only a single exposure of the

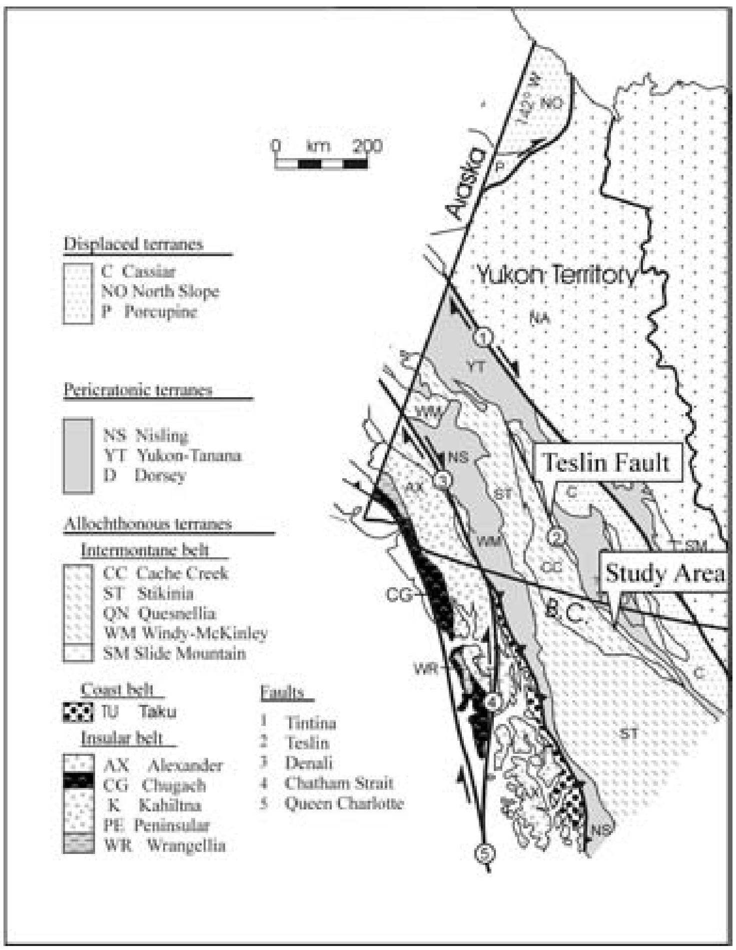

Figure 1. General overview of the Northern Cordillera depicting the relative position of the Teslin Fault, related terranes, and study area (modified from de Keijzer, 1995).

[1] *University of Victoria*

Teslin Fault is known. It is located below high water along the Jennings River. A preliminary study of the fault at this locality by de Keijzer *et al.* (2000) showed the dominant ductile deformation to be sinistral. This report augments that of de Keijzer *et al.* (2000) by focusing on micro-structural analysis of mylonites collected from the Jennings River location.

MINERALOGY AND STRUCTURAL FABRICS

A greenschist facies metamorphic mineral assemblage is exhibited by the Jennings River mylonites. It consists of partially recrystallized quartz, muscovite, and epidote, with lesser amounts of chlorite, actinolite, and biotite. Some of the epidote replaces plagioclase (Photo1). Euhedral pyrite cubes modified by cataclasis are locally common, but account for less than 1 % of the rock.

Jennings River mylonites display a well-developed steeply plunging lineation within a pervasive, steeply east-dipping foliation. The ductile fabric is well developed in the Yukon-Tanana Terrane greenstone but not in the rocks of the adjacent Cache Creek Terrane (de Keijzer *et al.,* 2000). A later brittle-ductile shear fabric overprints the ductile fabric in the greenstone providing evidence for two distinct episodes of deformation along the fault zone.

DUCTILE SINISTRAL MICRO-FABRICS

Micro-structural shear sense indicators characteristic of ductile fabrics in the Yukon-Tanana Terrane greenstone are of dominantly sinistral sense. The most common shear indicator consists of quartz and minor calcite fiber trails that nucleated on rotating pyrite porphyroblasts (Figure 2). Undulose fiber extinction suggests deformation coeval with fiber growth, while the fiber geometry shows face-controlled displacement. Fiber geometry indicates

Photo 1. Plagioclase grain with epidote replacement. Field of view (across) is 1.2 mm.

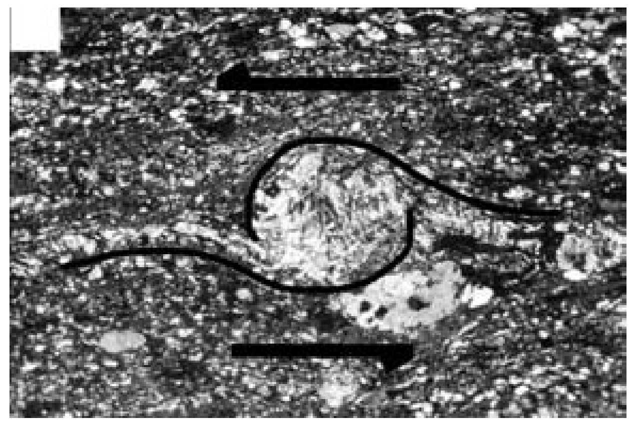

Photo 2. Delta-type porphyroclast showing sinistral shear. The porphyroclast and its tails are principally epidote. Field of view across is 1.6 mm.

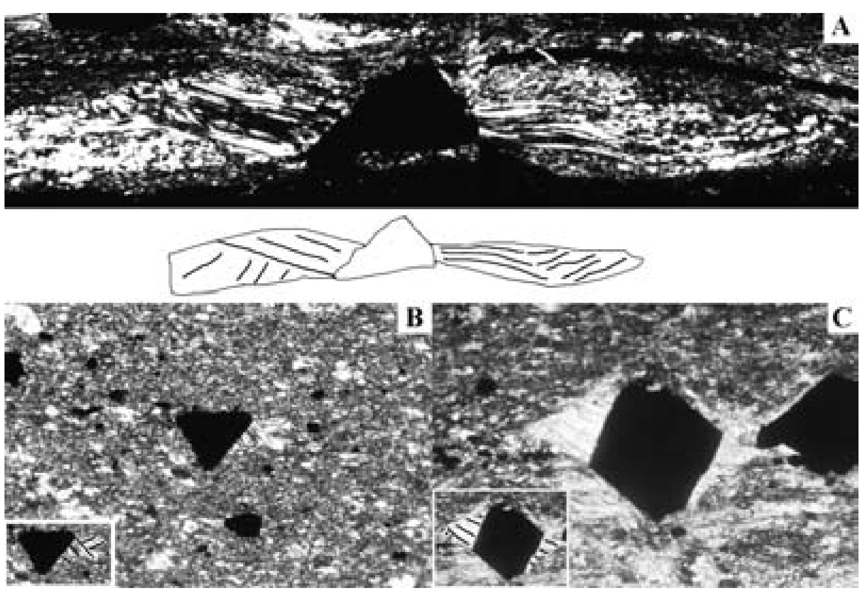

Figure 2. Quartz fibers on pyrite grains. Scale (a) 5 mm across (b) 1.2 mm across (c) across 0.6 mm.

counterclockwise vorticity and sinistral shearing during growth.

Sigma and delta-type porphyroclasts show a predominant sinistral shear sense, consistent with the mineral fibers. Tails emanating from delta porphyroclasts wrap down into the foliation plane indicating a counterclockwise rotation (Photo 2). The sigma-type porphyroclasts exhibit tangential tails that do not wrap down into a foliation plane, instead they originate directly from the edge of the porphyroblast with stair-step type geometry.

BRITTLE-DUCTILE DEXTRAL DEFORMATION

Evidence for dextral shearing is preserved in quasi-ductile micro-shears that cut across the earlier ductile fabrics (Photo 3). Little offset is apparent across these shears and most commonly, foliation planes bend into and out of the shear zone with minimal disturbance. This quasi-ductile shearing is not pervasive (with the exception of one sample within which the shearing is entirely penetrative), and probably represents much less displacement relative to the dominant sinistral fabric.

METAMORPHISM DURING DEFORMATION

The mylonitic greenschist mineral assemblage constrains the pressure and temperature range for these rocks to

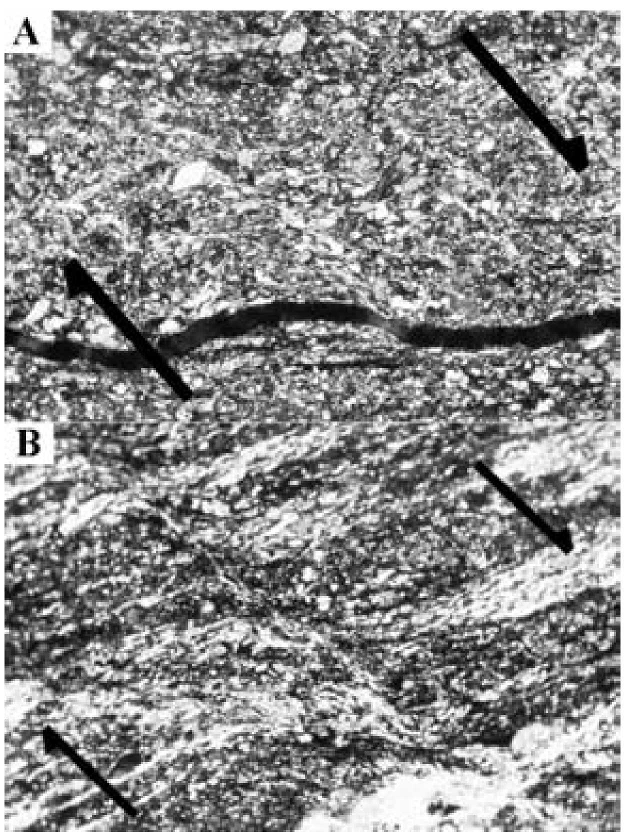

Photo 3. Dextral micro-faults clearly crosscutting ductile foliation planes. Field of view (a) across is 3 mm (b) across is 1.6 mm.

Photo 4. Type III calcite twins indicating a temperature of >200°C. Field of view across is 0.6 mm.

between 250-420 C° and 2 -10 kbars pressure (Klein and Hurlbut, 1999). Type III calcite twins in the greenstone rocks (Photo 4) require temperatures of >200 C° (Ferril, 1998; Passchier and Trouw, 1998) during shearing which is consistent with the greenschist metamorphism indicated by the authigenic mineral assemblage.

DISCUSSION

Timing of motion on the Teslin Fault is poorly constrained. Three plutons, the 57 Ma Charlie Cole stock, the 196 Ma Coconino tonalite and unnamed 184 Ma syenites all lie within 10 km of the projected fault trace. The Charlie Cole and Coconino intrusions are strongly foliated, while the 184 Ma syenites are largely undeformed. The differential deformation suggests that strain subsequent to the crystallization of the deformed 57 Ma Charlie Cole stock was partitioned such that the 184 Ma syenites escaped shearing or the syenites had cooled sufficiently to act as a rigid body.

General plate motion models (Engebrertson *et al.*, 1985) may help constrain the timing of translation on the Teslin Fault. Oblique sinistral convergence between the Pacific and North American plates took place between the Early Jurassic and mid-Cretaceous. Sinistral ductile shear along the Teslin Fault may have occurred during this interval. Brittle-ductile dextral shearing of the older ductile fabric may be attributable to oblique dextral convergence and coupling of plates in the late Cretaceous and Tertiary times.

Futher data suggests another dextral transpression event peaking between 174 Ma and 172 Ma (Mihalynuk et al., 1999). However, the 184 Ma syenites associated with the Teslin Fault are undeformed providing no direct evidence for Middle Jurassic deformation. More geochronologic control is required to test these speculations and constrain the motion history of the Teslin Fault.

CONCLUSIONS

An early ductile sinistral shearing event is preserved in the gross foliation of the rocks, fibrous crystal growth on pyrite crystals, and delta and sigma-type porphyroclasts. This ductile deformation is crosscut by later, more localized, dextral and quasi-ductile shear characterized by micro-faults offsetting foliation. This data is important to developing a motion history on the Teslin fault; however, more geochronologic data are needed to provide accurate fault motion and timing data.

ACKNOWLEDGEMENTS

Thanks are given to Mitch Mihalynuk and Stephen Johnston for the opportunity to work on this project as well as logistical support, expertise, and time taken out of their busy lives to markup drafts with red lines. Microscope work was preformed at the British Columbia Geological Survey Branch with most manuscript preparation undertaken at the University of Victoria in the Structure and Tectonics Group laboratory. This study is part of the Ancient Pacific Margin NATMAP project.

REFERENCES CITED

de Keijzer, M. (1995): Tectonic evolution of the Teslin Zone and the Western Cassiar Terrane, Northern Canadian Cordillera; unpublished Ph. D. thesis, *Univeristy of New Brunswick*, 391 pages.

de Keijzer, M., Mihalynuk, M.G. and Johnston, S.T. (2000): Structural Investigation of an Exposure of the Tintina Fault; *in* Current Research, *Geological Survey of Canada*, Paper 2000-A5, 10 pages.

Engebretson, D.C., Cox, A. and Gordon, R. G. (1985): Relative motions between oceanic and continental plates in the pacific basin; *Geological Society of America*, Special Paper, 206, 59 pages.

Ferril, D.A. (1998): Critical re-evaluation of differential stress estimates from calcite twins in coarse grained limestone; *Tectonophysics*, Volume 285, pages 77-86.

Gabrielse, H. (1985): Major dextral transcurrent displacements along the Northern Rocky Mountain Trench and related lineaments in north-central British Columbia; *Geological Society of America Bulletin*, Volume 96, pages 1-14.

Hurlbut, C. S. Jr. and Klein, C. (1977): *Manual of Mineralogy*, 19th edition, John Wiley and Sons, New York, 681 pages.

Mihalynuk, M.G., Nelson, J.L., de Keijzer, M., Friedman, R.M., Roots, C.F. and Gleeson, T.P. (2001): Geology of Goodwin Creek (104N/9E); *BC Ministry of Energy and Mines*, Open File 2001-5, 1:50 000 scale.

Mihalynuk, M.G., Erdmer, P., Ghent, E.D., Archibald, D.A., Friedman, R.M., Cordey, F., Johannson, G.G. and Beanish, J. (1999): Age constraints for emplacement of the Northern Cache Creek Terrane and implications of blueschist metamorphism; *in* Geological Fieldwork 1998, *BC Ministry of Energy and Mines*, Paper 1999-1, pages 127-141.

Passchier, C.W. and Trouw, R.A.J. (1998): *Microtectonics*; Springer – Verlag, Berlin, 281 pages.

Wheeler, J.O. and McFeely, P. (1991): Tectonic assemblage map of the Canadian Cordillera and adjacent portions of the United States of America, *Geological Survey of Canada,* Open File, 1712A, scale 1:2 000 000.

Age of Mineralized Porphyry at the Logtung deposit W-Mo-Bi-Be (Beryl, Aquamarine), Northwest BC

By Mitchell, G. Mihalynuk[1] and Larry M. Heaman[2]

KEYWORDS: *Logtung, tungsten, molybdenum, beryl, beryllium, aquamarine, bismuth, wolframite,*

INTRODUCTION

Logtung is a large tonnage, low-grade tungsten-molybdenum deposit that straddles the BC-Yukon border between Watson Lake and Whitehorse (Figure 1; MINFILE 104O016). Current unclassified resources are estimated at 162 million tonnes grading 0.052% MoS_2 and 0.13% WO_3 (Noble *et al.*, 1984). Bismuth and copper occur in lesser concentrations with traces of gold and tin. Gangue minerals include sky blue beryl. Small crystals of transparent blue beryl (var. aquamarine) less than 2mm in diameter are common, with some transparent crystals reaching more than 1 cm in diameter (P. Wojdak, personal communication, 2001), but gemstones cut from Logtung beryl have not been reported. Approximately 2 km south of the deposit, beryl is sufficiently abundant to be considered a source of beryllium, although the locality has yet to be drill tested (Wojdak, 1998). Both porphyritic and skarn mineralization are associated with monzonitic granite and a monzonite porphyry dike swarm (Noble *et al.*, 1984) that intrude calcareous, quartz-rich metasediments of Paleozoic to Triassic age (Mihalynuk *et al.*, 2000; Roots *et al.*, 2002). Objectives of this report are to briefly describe the petrography and U-Pb isotopic age data from the mineralized monzonite.

PREVIOUS WORK

Logtung was discovered in 1976 by Cordilleran Engineering Ltd. as a result of tracing tungsten stream sediment geochemical anomalies to their source in the Two Ladder Creek and Logjam Creek areas (Christopher, 1978). Canamax Resources (then Amax Potash Ltd.) optioned the property in 1977 and conducted an extensive property evaluation including the construction of a dirt road, and a 496 m decline for collection of a bulk sample. The dirt road provides access from the Alaska Highway at kilometre 1210.3 and winds north for about 15 km to the headwaters of south-flowing Logjam Creek. The last large program conducted on the British Columbia portion of the property was an electromagnetic survey in 1984 (Roth, 1984) for Canamax Resources Inc.

Early reconnaissance geological mapping north of the border was conducted by W.H. Poole who first mentioned

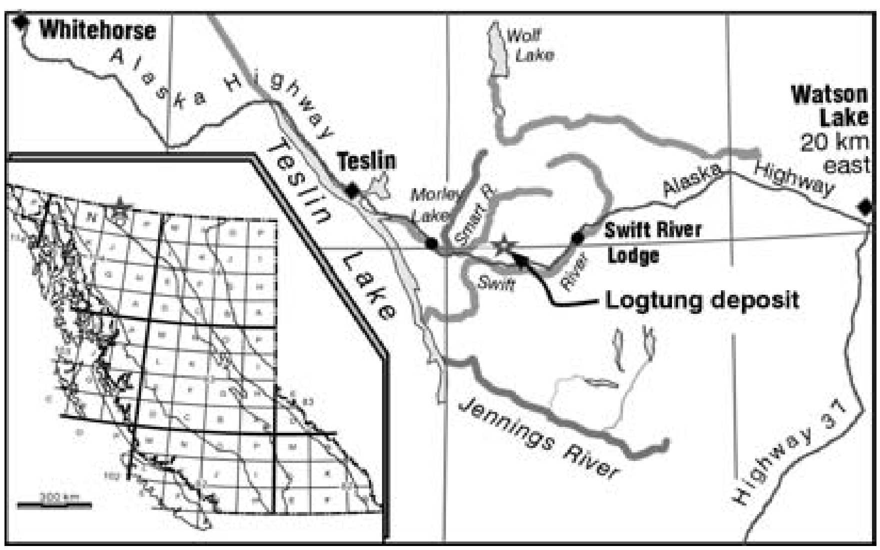

Figure 1. Location of the Logtung Porphyry near the BC - Yukon border.

[1] *British Columbia Ministry of Energy and Mines*
[2] *University of Alberta*

tungsten mineralization in the area (Poole, 1956; Poole *et al.*, 1960). Parts were remapped by Abbott (1981) during study of the Seagull tin district. Reconnaissance mapping of the adjacent area south of the border was conducted by H. Gabrielse (1969). Thesis studies by Noble (1982) and Stewart (1983) addressed the mineralization and related plutons at Logtung.

GEOLOGIC SETTING AND MINERALIZATION

Mineralization at Logtung is developed within monzonitic granite and crosscutting porphyritic felsic dikes and adjacent hornfelsed country rocks. Country rocks are Paleozoic to Triassic clastic strata that have been thermally metamorphosed by an en-echelon set of northwest-elongated Early Jurassic plutons (Mihalynuk *et al.*, 2000; Poole *et al.*, 1960; C.F. Roots, written communication, 2000, 2001). Jurassic bodies crop out within two kilometres, both southwest and northeast, of the Logtung deposit (Figure 2).

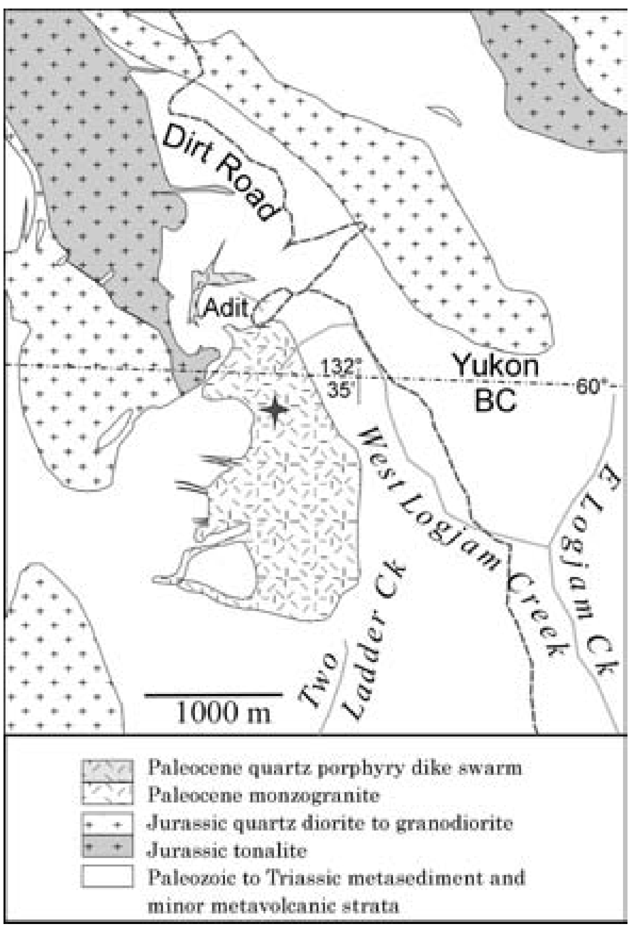

Figure 2. Generalized geological map of the Logtung area. Geology from Mihalynuk *et al*. (2000), Noble *et al.* (1984) and C.F. Roots (written communication, 2001). U-Pb age date sample locality is denoted by the star.

Logtung monzogranite is an orange-pink colour with phenocrysts of greasy grey quartz, white feldspar and black biotite (Figure 3a). Petrographic analysis shows that the monzogranite also contains fine-grained muscovite, sphene and intergranular fluorite (Figure 4a). Feldspar is dominated by perthite and normally zoned plagioclase (Figure 4b). Biotite contains abundant apatite and zircon inclusions. Fission of radioactive uranium and thorium within the zircon inclusions has caused extensive lattice damage in the biotite, resulting in broad halos (Figure 4a). Noble *et al.* (1984) also report primary scheelite, ilmenite, magnetite, pyrite and allanite.

Porphyritic felsic dikes such as that in Figure 3b are white and fine to medium-grained with subidiomorphic to idiomorphic quartz phenocrysts. Smokey quartz and interstitial fluorite are common, as in the monzogranite. Muscovite occurs as fine-grained glomerocrysts and as matrix alteration.

Molybdenum and tungsten are believed sourced from the monzonite and porphyritic dikes. Petrographic textures indicate that scheelite and fluorite are intergrown with quartz and feldspar, and geochemical analysis of unaltered samples reveal highly anomalous W and Mo values (Stewart, 1983). Paragenesis of the molybdenite and scheelite mineralization is related to four quartz vein systems according to (Noble *et al.*, 1984). Earliest quartz-molybdenite-scheelite veins (system I) formed in the thermo-metamorphic halo during late crystallization of the monzogranite stock. Quartz- molybdenite and quartz-scheelite veins (systems II and III) formed before and during felsic dike emplacement. Sheeted W-Mo veins (system IV) post-date most, but not all of the felsic dikes. Mineralization at Logtung has characteristics of both molybdenite skarn and tungsten porphyry (deposit models K07

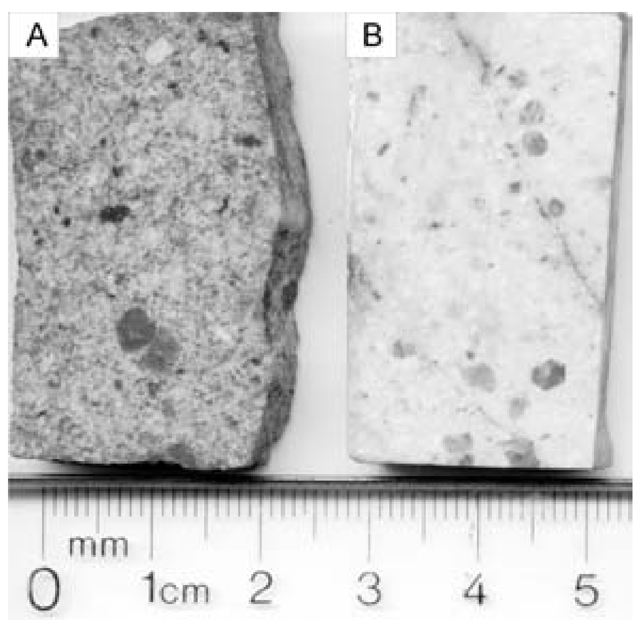

Figure 3. Rock slabs from the Logtung monzogranite (a) and felsic porphyry dikes (b). Dark crystals are smoky quartz phenocrysts.

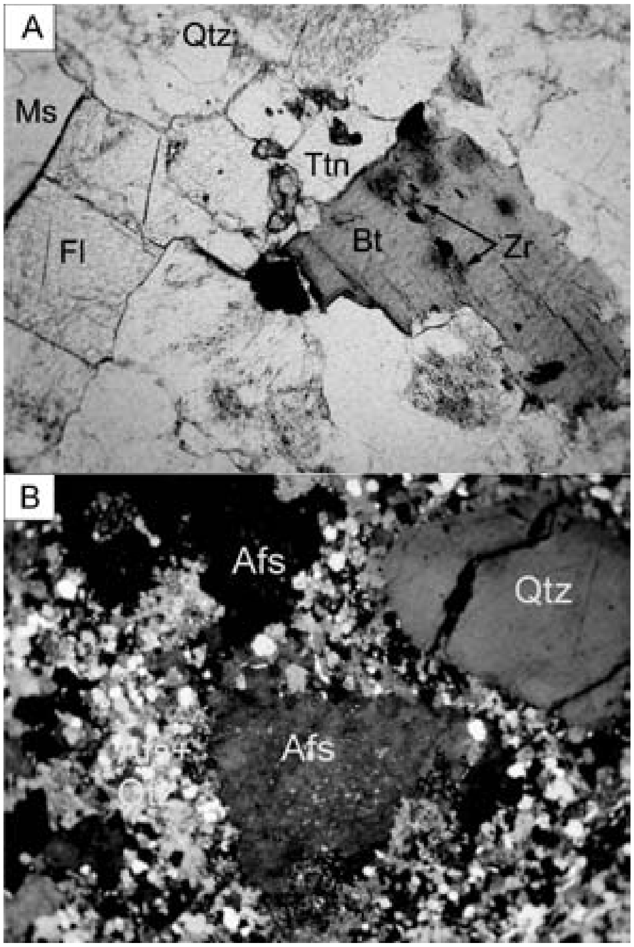

Figure 4. Representative thin section views of the Logtung monzogranite. Width of the photomicrographs represents approximately 2mm. Mineral abbreviations are: Afs = alkali feldspar; Bt = biotite; Fl = fluorite; Ms = muscovite; Qtz = quartz; Py = pyrite; Tnt = titanite; and Zr = zircon?

and L07 of Lefebure *et al.,* 1995), but it is generally acknowledged as a porphyry deposit (cf. Noble *et al.*, 1984).

Woodsworth *et al.* (1992) included the Logtung pluton with the Mid Cretaceous Cassiar suite, presumably based upon the preliminary 118±2 Ma Rb/Sr age determination on the monzogranite stock that is reported in Stewart (1983; published in Noble *et al.*, 1984); recalculated as 117.6 ±3.5 in Mortensen (1999). The age of the stock should place a maximum age on the mineralizing event because the monzogranite stock crystallization is synchronous with the oldest mineralization.

ISOTOPIC AGE DATING

A sample of monzogranite was collected from outcrops near the Yukon border and mineralized porphyry was collected from the test dumps near the Logtung exploration adit, on the Yukon side of the border. In order to best constrain the maximum age of mineralization, the monzogranite was crushed for U-Pb age determination (sample number 99-Th-03-02). Relatively abundant zircon was recovered using standard techniques (Heaman and Machado, 1992). Most of the zircon has an unusual morphology, occurring as irregular, faint tan grains with rare well-developed facets, often forming inclusions within fragments of quartz. These are characteristics observed in other examples of hydrothermal zircon. However, the Th/U ratios of 0.7 and 0.4 are within the typical range for igneous zircon crystallizing from felsic magmas, and such an origin cannot be ruled out. A few resorbed tips of zircons were also recovered, as was abundant molybdenite.

Two fractions of "hydrothermal" zircon were analyzed and the U-Pb results are presented in Table 1 and Figure 5. Uncertainties associated with these two analyses are large reflecting the low uranium content (17-23 ppm). The $^{206}Pb/^{238}U$ age of 58±6 Ma obtained for fraction #1 is interpreted as the best estimate for the time of hydrothermal zircon growth. Clearly additional zircon analyses are required to confirm this interpretation. Analysis of additional fractions is in progress and when completed the data will be available on-line, together with an updated age date. Persons interested in this data should refer to Geofile 2002-1 at http://www.em.gov.bc.ca/Mining/Geolsurv/Publications/catalog/cat_geof.htm.

DISCUSSION

Monzonitic porphyries of Late Cretaceous and Early Tertiary age that contain W-Mo, and more commonly Mo+/-W mineralization, are known in British Columbia and Yukon. However, most are dated by K-Ar techniques; we know of none other than Logtung that have been dated by the more robust U-Pb technique. One such deposit is Red Mountain, located nearly along strike approximately

TABLE 1
U-Pb RESULTS FOR THE ANCIENT CONTINENTAL MARGIN PROJECT

Description	Weight (ug)	Concentration (ppm) U	Pb	Th	Th/U	TCPb (pg)	$^{206}Pb/^{204}Pb$	Atomic Ratios ± 2σ error $^{206}Pb/^{238}U$	$^{207}Pb/^{235}U$	$^{207}Pb/^{206}Pb$	Apparent age ± 2σ error (Ma) $^{206}Pb/^{238}U$	$^{207}Pb/^{235}U$	$^{207}Pb/^{206}Pb$	% Dis.
99-TH-03-02														
8 irregular grains in qtz faint tan some eu faces M0	11.2	23	4	15	0.7	43	21	0.0090 ± 10	0.017 ± 68	0.0139 ± 545	58.0 ± 6.4	17.4 ± 67.2		
10 irregular grains faint tan M0	51.0	17	8	7	0.4	372	24	0.0468 ± 22	0.444 ± 147	0.0687 ± 230	295.1 ± 13.6	372.7 ± 102.4	888.9 ± 200	68.3

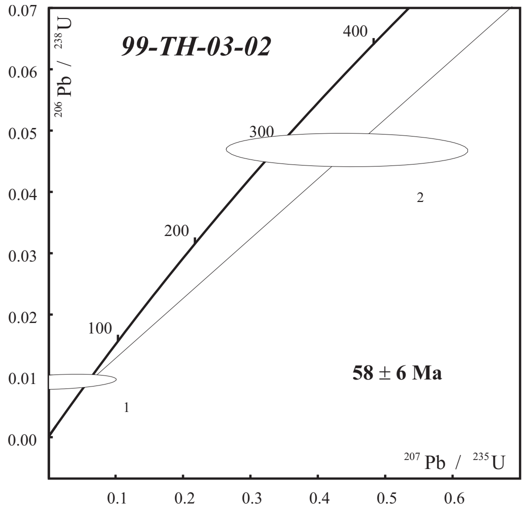

Figure 5. Concordia plot for geochronological data presented in Table 1. The best estimate for the age of the Logtung monzogranite stock is 58 +/- 6Ma.

150 km northwest of Logtung. It is a molybdenum deposit with calculated resources of 187 270 000 tonnes grading 0.167% MoS_2 (Brown and Kahlert, 1995), minor tungsten mineralization is associated with the latest mineralizing porphyries. Hydrothermal biotite that grew along with molybdenite is dated by the K-Ar technique as 87.3±2.0 Ma according to W.D. Sinclair (personal communication, 1985; *in* Brown and Kahlert, 1995); whereas the post-mineralization porphyry is 79.0±1.8 (*ibid.*).

About 100 km southwest of Logtung, a polyphase, dominantly porphyritic stock at the Adanac (Ruby Creek) deposit is mineralized with molybdenite as disseminations and in quartz veins that may also contain traces of scheelite +/-fluorite. Ages on four of the quartz monzonite phases range from 70.3±2.4 to 71.6±2.1Ma (Christopher and Pinsent, 1982).

Molybdenum-tungsten fracture and vein-dominated porphyry mineralization characterizes the Glacier Gulch deposit (Hudson Bay Mountain) near Smithers in northwest-central BC. Mineralization at Glacier Gulch is attributed to a quartz monzonite-granodiorite stock and comagmatic radial porphyry dike swarms. K-Ar age determinations on biotite from the stock have returned 67 ±5 (Kirkham, 1966) and 73.3 ±3.4Ma (Carter, 1974); 60 ±5 (Kirkham, 1966) on the porphyry dikes.

Molybdenite +/- tungsten mineralization at Trout Lake, southeastern BC, is hosted in Lower Paleozoic Lardeau Group. Pelitic quartzite, marble, calcareous phyllite and quartzite and metavolcanic rocks that host the mineralization are similar to lithologies hosting mineralization marginal to the Logtung monzogranite stock. Mineralization at Trout Lake is attributed to the nearby 76 Ma (Boyle and Leitch, 1983) granodiorite to tonalite intrusion. Tungsten production was recorded in 1942 (Stevenson, 1943). Resources are reported as 49 Mt grading 0.19% MoS_2 (Linnen *et al.*, 1995).

Molybdenum porphyry deposits with associated tungsten mineralization are scattered throughout BC and southern Yukon. Representatives of this type of deposits have an association with intrusions in the 60-87 Ma age range. Whether or not this mineralizing age is significant will be borne out as U-Pb age dating is completed.

Several intrusive bodies located in the same region as the Logtung deposit lack significant mineralization but are of Paleocene age, similar to the Logtung monzogranite. In areas to the west they are included in the ~53-59 Ma Sloko plutonic suite by Mihalynuk (1999). Woodsworth *et al*. (1992) included Early Tertiary intrusions of this region in the Bennett suite, but this name has been abandoned upon the recommendation of Hart (1995) principally because many of the included plutons in the Bennett Lake area are actually of Jurassic age. Bennett suite is restricted to plutons in the 175-178 Ma age range (*see* discussion in Mihalynuk, 1999). In areas to the immediate east, less than 10 km from Logtung, the Seagull batholith has yielded a K-Ar age of 60±6 Ma (Lowdon, 1960). Reanalysis of biotite from this sample returned an age of 101±5 (Wanless *et al*., 1972), consistent with a clustering of five other K-Ar ages from the batholith reported by Mortensen (1999), which range from 94±4 to 102.8±1.1Ma (average 99.6). The 60±6 Ma age appears to be erroneous (*see* Mortensen, 1999).

SUMMARY

A preliminary U-Pb age determination on zircon from the monzogranite stock at the Logtung deposit places a maximum age constraint on the oldest mineralized vein set. This new age of 58 Ma, if correct, is significantly younger than the ~118 Ma Rb-Sr age previously accepted for the Logtung monzogranite stock. Analyses are underway to further refine this U-Pb age. When the data are available they will be posted on-line as Geofile 2002-1 at http://www.em.gov.bc.ca/Mining/Geolsurv/Publications/ catalog/cat_geof.htm.

ACKNOWLEDGEMENTS

We thank Steve Gordey (Geological Survey of Canada, Vancouver) and Tekla Harms (Amherst College, Amherst, Massachusetts) who helped collect the sample dated here. George Simandl and Paul Wojdak (BC Ministry of Energy and Mines, Victoria and Smithers) contributed information on the occurrence of blue beryl (var. aquamarine). Thanks to Doug Eaton, for sharing his extensive knowledge of the Logtung deposit and providing access to an unpublished report. Doug's comments post-date submission of this article, but will hopefully be included in Geofile 2002-1. This work was made possible through the Ancient Pacific Margin NATMAP program, and the organizational vigilance of C.F. Roots.

REFERENCES CITED

Abbott, J. (1981): Geology of the Seagull tin district; in Yukon Geology and Exploration 1979-80, Department of Indian and Northern Affairs, pages 32-44.

Boyle, H.C. and Leitch, C.H.B. (1983): Geology of the Trout Lake molybdenum deposit, B.C.; Canadian Institute of Mining and Metallurgy Bulletin, Volume 76, pages 115-124.

Brown, P. and Kahlert, B. (1995): Geology and mineralization of the Red Mountain porphyry molybdenum deposit, south-central Yukon; in Porphyry deposits of the northwestern Cordillera of North America, Schroeter, T. G. (Editor), Canadian Institute of Mining, Metallurgy and Petroleum, Volume 46, pages 747-756.

Carter, N.C. (1974): Geology and geochronology of porphyry copper and molybdenum deposits in west-central British Columbia; The University of British Columbia, Vancouver, unpublished Ph.D. thesis, 236 pages.

Christopher, P.A. (1978): Logtung (104/13E, 105B/4E); in Geological Fieldwork 1977, BC Ministry of Energy and Mines, Paper 1978-1, pages 47-50.

Christopher, P.A. and Pinsent, R.H. (1982): Geology of the Ruby Creek and Boulder Creek area near Atlin (104N/ 11W); BC Ministry of Energy, Mines and Petroleum Resources, Preliminary Map 52, 10 pages.

Gabrielse, H. (1969): Geology of Jennings River map-area; Geological Survey of Canada, Paper 68-55, 37 pages.

Hart, C.J.R. (1995): Magmatic and tectonic evolution of the Intermontane Superterrane and Coast Plutonic Complex in Southern Yukon Territory; unpublished M.Sc. thesis, The University of British Columbia, 198 pages.

Heaman, L. and Machado, N. (1992): Timing and origin of midcontinent rift alkaline magmatism, North America: evidence from the Coldwell Complex; Contributions to Mineralogy and Petrology, Volume 110, pages 289-303.

Kirkham, R.V. (1966): Glacier Gulch molybdenum deposit; in Annual Report, BC Department of Mines, pages 86-91.

Lefebure, D.V. and Ray, G.E. (1995): British Columbia mineral deposit profiles, Volume 2 - metallics and coal; *BC Ministry of Energy and Mines*, Open File 1995-20, 135 pages.

Linnen, R., Williams-Jones, A., Leitch, C. and Macauley, T. (1995): Molybdenum mineralization in a fluorine-poor system: The Trout Lake stockwork deposit, southeastern British Columbia; *in* Porphyry deposits of the northwestern Cordillera of North America, Schroeter, T. G. (Editor), *Canadian Institute of Mining, Metallurgy and Petroleum, Volume 46, pages 771-780.*

Lowdon, J.A. (1960): Age determinations by the Geological Survey of Canada, Report 1; *Geological Survey of Canada,* Paper 60-17, 51 pages.

Mihalynuk, M.G. (1999): Geology and Mineral Resources of the Tagish Lake area (NTS 104M/8,9,10E, 15 and 104N/12W), Northwestern British Columbia; *BC Ministry of Energy and Mines*, Bulletin 105, 217 pages.

Mihalynuk, M.G., Nelson, J.L., Gleeson, T.P., Roots, C.F. and deKeijzer, M. (2000): Geology of Smart River area (NTS 104O/13); *BC Ministry of Energy and Mines*, Open File 2000-6.

Mortensen, J.K. (1999): YUKONAGE, An isotopic age database for the Yukon Territory; in Yukon Digital Geology, Gordey, S. P. and Makepeace, A. J. (Editors), *Geological Survey of Canada*, Open File D3826.

Noble, S.R. (1982): Petrology and fluid inclusion study of W-Mo mineralization at the Logtung deposit, south-central Yukon Territory; *University of Toronto*, Toronto, unpublished M.A.Sc. thesis, 286 pages.

Noble, S.R., Spooner, E.T.C. and Harris, F.R. (1984): The Logtung large tonnage, low-grade W (scheelite)-Mo porphyry deposit, south-central Yukon Territory; *Economic Geology*, Volume 79, pages 848-868.

Poole, W.H. (1956): Geology of the Cassiar Mountains in the vicinity of the Yukon-B.C. boundary; *Princeton University*, unpublished Ph.D. thesis

Poole, W.H., Roddick, J.A. and Green, A.H. (1960): Geology Wolf Lake map-area, Yukon Territory; *Geological Survey of Canada*, Map 10-1960.

Roots, C.F., Harms, T., Simard, R-L., Orchard, M. and Heaman, L. (2002): Constraints on the age of the Klinkit Succession east of Teslin Lake, northern BC (104O/11); *in* Current Research, Part A, *Geological Survey of Canada*, Paper 2002-A, in press.

Roth, J. (1984): Report on helicopter electromagnetic and magnetic surveys by Aerodat Ltd., Jam Claims, Logtung Project; *BC Ministry of Energy and Mines*, Assessment Report 12715, 28 pages.

Stevenson, J. (1943): Tungsten deposits of British Columbia; *BC Department of Mines and Petroleum Resources*, Bulletin 10, pages 130-133.

Stewart, J. (1983): Petrology and geochemistry of the intrusives spatially associated with the Logtung W-Mo Prospect, south-central Yukon Territory; *University of Toronto*, Toronto, unpublished M.Sc. thesis, 243 pages.

Wanless, R.K., Stevens, R.D., Lachance, G.R. and Delabio, R.N. (1972): Age determinations and geological studies, A-Ar isotopic ages, Report 10; *Geological Survey of Canada*, Paper 72-2.

Wojdak, P.J. (1998): Overview of Exploration Activity, Northwest Region; in Exploration and Mining in British Columbia, *BC Ministry of Energy and Mines*, pages 19-31.

Woodsworth, G.J., Anderson, R.G., Armstrong, R.L., Struik, L.C. and Van der Heyden, P. (1992): Plutonic regimes; *in* Geology of the Cordilleran Orogen in Canada, Gabrielse, H. and Yorath, C. J. (Editors), *Geological Survey of Canada*, pages 493-531.

Tracking Yukon-Tanana Terrane VMS Host Stratigraphy and Intrusion-Related Gold in the Southern Sylvester Allochthon (Beale Lake Map Area, 104I/14N)

By JoAnne Nelson

KEYWORDS: *Mississippian, Sylvester Allochthon, Dorsey assemblage, Yukon-Tanana Terrane, northern British Columbia, volcanogenic massive sulphides, gold veins.*

INTRODUCTION

This report describes a new mapping project in the Cassiar Mountains, located 70 kilometres northeast of Dease Lake in northern British Columbia. The area is attractive for two reasons. First, it contains rocks that are likely correlative with those of the Yukon-Tanana Terrane, a tract with known volcanogenic massive sulphide potential. Second, combined geological and regional geochemical data suggest possible intrusion-related gold mineralization within it.

The Beale Lake area, bordering the northeast side of the mid-Cretaceous Cassiar Batholith, is largely underlain by the Sylvester Allochthon, a stack of thrust sheets of oceanic to pericratonic arc affinity that overlies the para-autochthonous Cassiar Terrane (Figure 1).

The structurally highest sheet is a highly deformed pericratonic assemblage (Gabrielse, 1998). Like the Yukon-Tanana Terrane, it contains early Mississippian intrusions. The YTT in the Finlayson Lake belt in southern Yukon hosts several significant volcanogenic massive sulphide deposits associated with early Mississippian volcanic suites. Over the past 4 years, the Ancient Pacific Margin Natmap project has traced pericratonic Yukon-Tanana Terrane stratigraphy continuously southwards from the Finlayson belt into the Jennings River map area of northern B.C., where equivalent strata, including Mississippian felsic volcanic rocks and exhalative units, occur within the Big Salmon Complex and Dorsey assemblage (Mihalynuk *et al.* 1998, 2000, Nelson 1999, 2000). It has been suggested that the pericratonic assemblage in the Sylvester Allochthon is a direct southeastward extension of the Dorsey assemblage, interrupted by the Cassiar batholith (Harms, 2000; Nelson, 2001). The present project is in hot pursuit of these crucial early Mississippian volcanogenic hosts.

The second rationale for this study sprang from identification of strong gold and related anomalies (Bi, As, Hg) in the Cry Lake Regional Geochemical Survey (RGS) release (Jackaman, 1996), a suite of elements commonly associated with intrusion-related gold mineralization. Sets of gold-bearing veins are known in the area, notably the Nizi and Beale Lake properties; but RGS anomalies occur outside areas of documented mineralization as well. The Nizi veins in the northeastern corner of the Beale Lake map area have been interpreted as Eocene in age and epithermal in origin (Plint *et al.*, 1997), whereas the Beale Lake veins show at least in part a bismuth-tungsten association that may place them at a deeper level in a intrusion-related system (Durfeld and Fleming, 2001). The regionally extensive mid-Cretaceous Cassiar batholith underlies most of southern Beale Lake map area, and the Eocene Major Hart pluton is located 20 kilometres to the southeast (Figure 2).

Field mapping in 2001 completed the northern half of the Beale Lake map sheet, 104I/14. The adjacent map area, 104I/15, will be covered in future work. Results of exploration significance are: recognition of bipartite Dorsey assemblage in the uppermost, pericratonic unit of the Sylvester Allochthon, with felsic volcanic rocks in its upper part; and discovery of several new mineral showings, including veins that enlarge the potential area of interest for intrusion-related gold significantly beyond that previously reported.

REGIONAL GEOLOGY

The northern Cry Lake map area is partly underlain by the Sylvester Allochthon, which outcrops between the Cassiar Batholith to the southwest, and subadjacent Paleozoic continental shelf strata of the Cassiar Terrane to the northeast and south (Figure 2, from Gabrielse, 1998). Previous mapping in the McDame map area to the north showed that the allochthon comprises three distinctive, stacked tectonic elements (Nelson, 1993). Structurally lowest are late Paleozoic oceanic rocks of the Slide Mountain Terrane, overlain (depositionally?) by Middle to Late Triassic sedimentary strata. Above a thrust fault lie late Paleozoic island arc rocks assigned to the Harper Ranch subterrane of Quesnellia. Early Mississippian and older pericratonic and arc rocks occur at the structurally highest level. This pericratonic unit was first recognized by Gabrielse and Harms (1989). Harms (1990) and Harms *et al*. (1993) referred to it as the Rapid River tectonite. In northern Cry Lake area, Gabrielse (1998) distinguished the pericratonic unit, which he called the siliceous tectonite unit, from the rest of the allochthon. He also defined two large mid-Permian plutons. His work has provided an excellent framework for further subdivision.

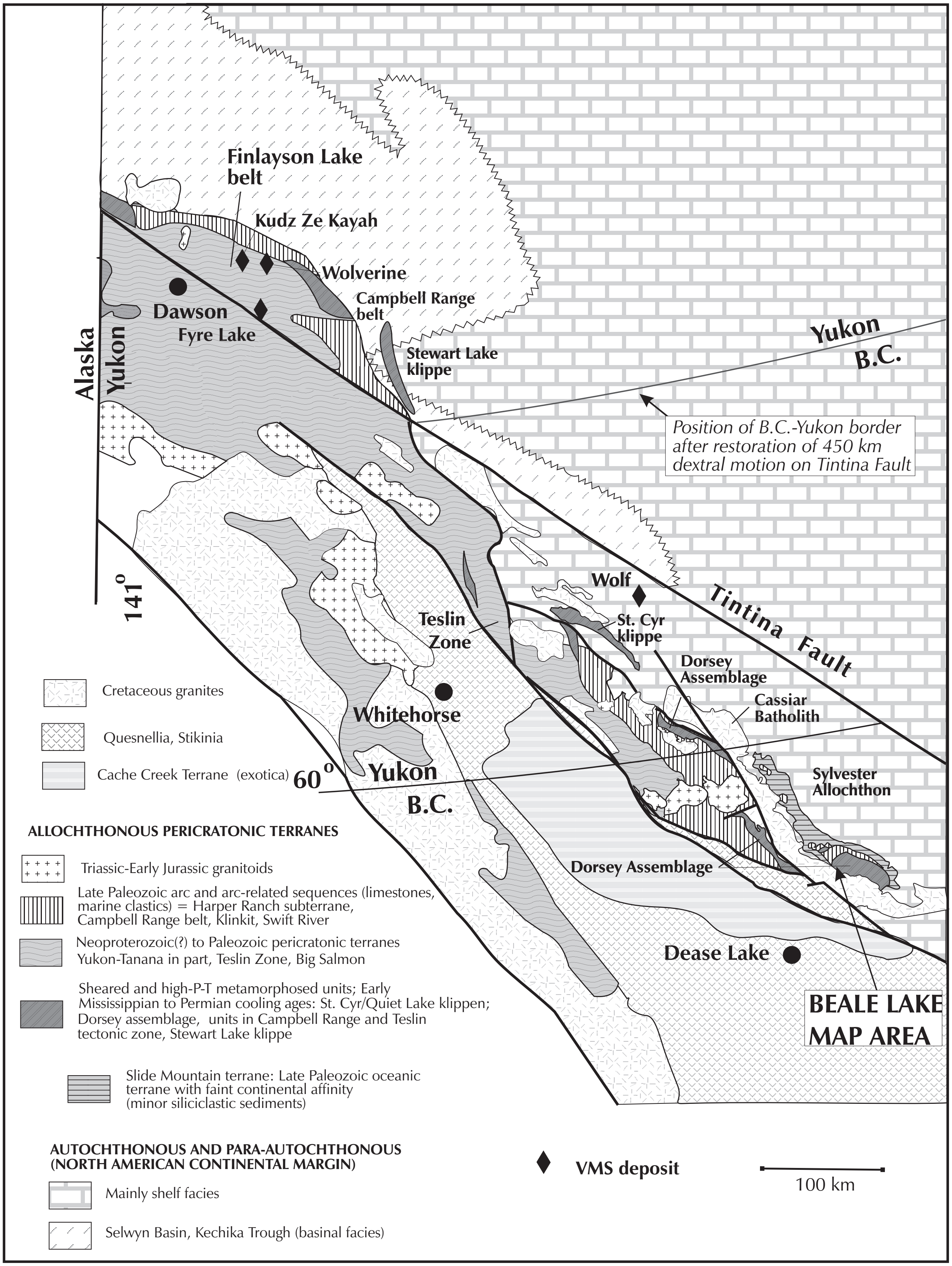

Figure 1. Regional geological setting of the Yukon-Tanana and surrounding terranes, Yukon and northern British Columbia.

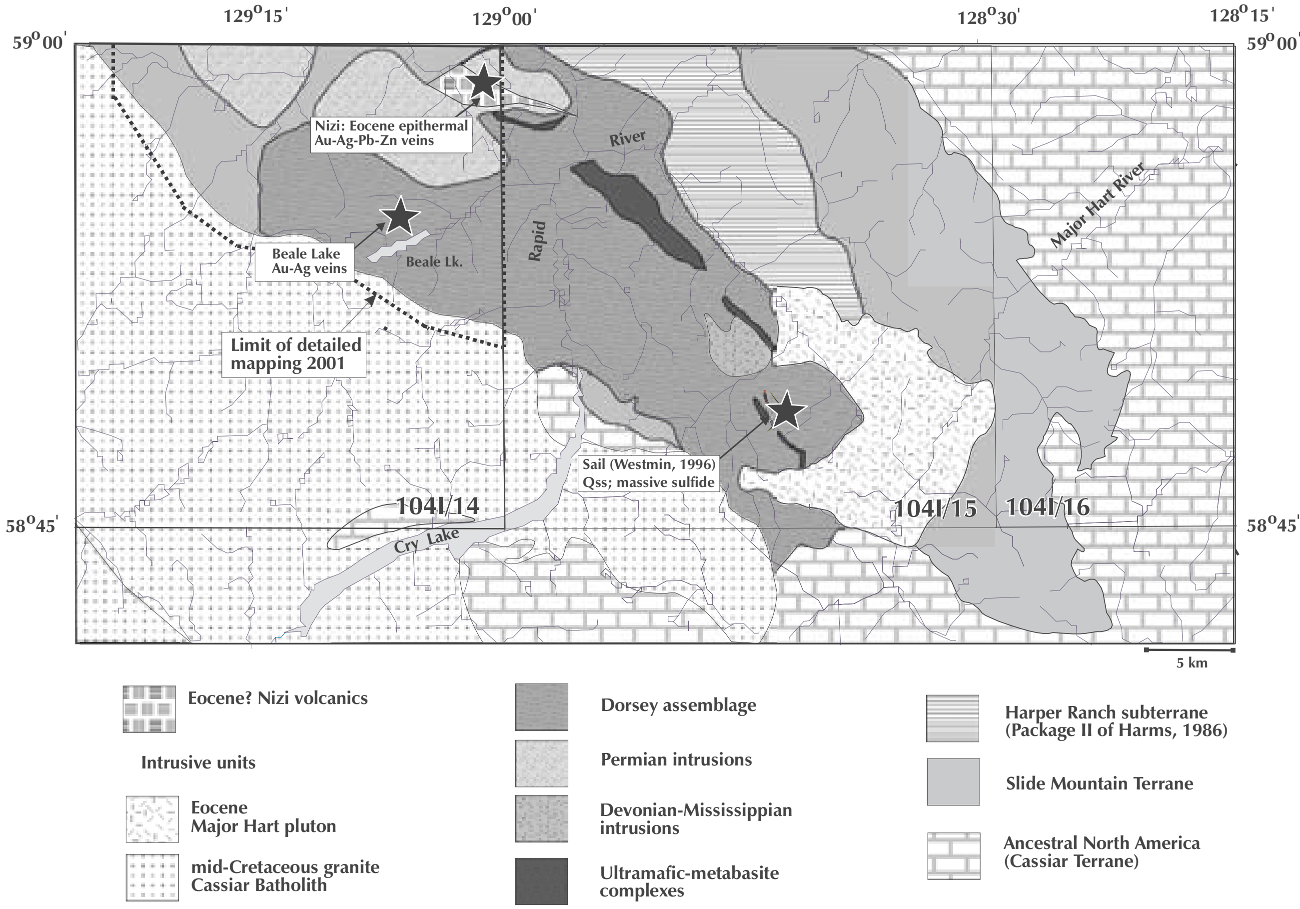

Figure 2. Geological setting of northern Cry Lake map area, prior to this project. Geology from Gabrielse (1998), Harms (1986), and Plint *et al.* (1997).

LOCAL GEOLOGY

The Sylvester Allochthon in northern Beale Lake map area comprises a set of stacked thrust slices folded into an upright syncline-anticline pair (Figure 3, 4).

Its general structure mirrors that seen farther north between the Dease River and the Yukon border. The structurally lowest slivers, truncated to the southwest by the Cassiar Batholith, are ultramafite, gabbro and basalt; they probably form a southern strike extension of Slide Mountain Terrane exposures along the Stewart-Cassiar Highway near Cassiar. They also correspond to Package I of Harms (1986). Above them, across a highly sheared contact, lies the Four Mile assemblage, a set of thrust slices of more diverse character, including widespread felsic to intermediate volcanic rocks of probable arc affinity. The volcanic rocks are intruded by the mid-Permian Meek and Nizi plutons. These rocks show a similar tectonic environment to Harper Ranch subterrane panels exposed farther north, for instance the Huntergroup volcanics and an unnamed Permian pluton in the headwaters of Big Creek near the Yukon border (Nelson and Bradford, 1993).

The Beale Mountain Thrust, exposed for many kilometres on the western face of Beale Mountain above the Four Mile River valley, spectacularly marks the base of the deformed and metamorphosed pericratonic allochthon (Figure 6a). It juxtaposes amphibolite and metasedimentary rocks, which were ductilely deformed in early Mississippian time, above a virtually undeformed Pennsylvanian-Permian volcanic/plutonic footwall. Above the thrust, the deformed rocks can be divided into two units, which correspond to the lower and upper Dorsey assemblage in the southern Yukon and northern British Columbia west of the Cassiar Batholith (Roots and Heaman, 2001; Nelson, 1999, 2000). The lower unit consists of strongly deformed, garnet grade basinal sedimentary rocks - metachert, meta-argillite, pelite and quartzite - with large lenses of amphibolite and metagabbro. The well-foliated but less tectonized upper unit contains phyllite, quartzite, metachert and most significantly, quartz-feldspar porphyry rhyolite and dacite flows and tuffs.

The youngest rocks in the area are the Zinc Lake volcanic/intrusive suite, which outcrops near the informally named Zinc Lake on the Nizi property in the northeastern corner of the map area. Fine grained, undeformed andesite,

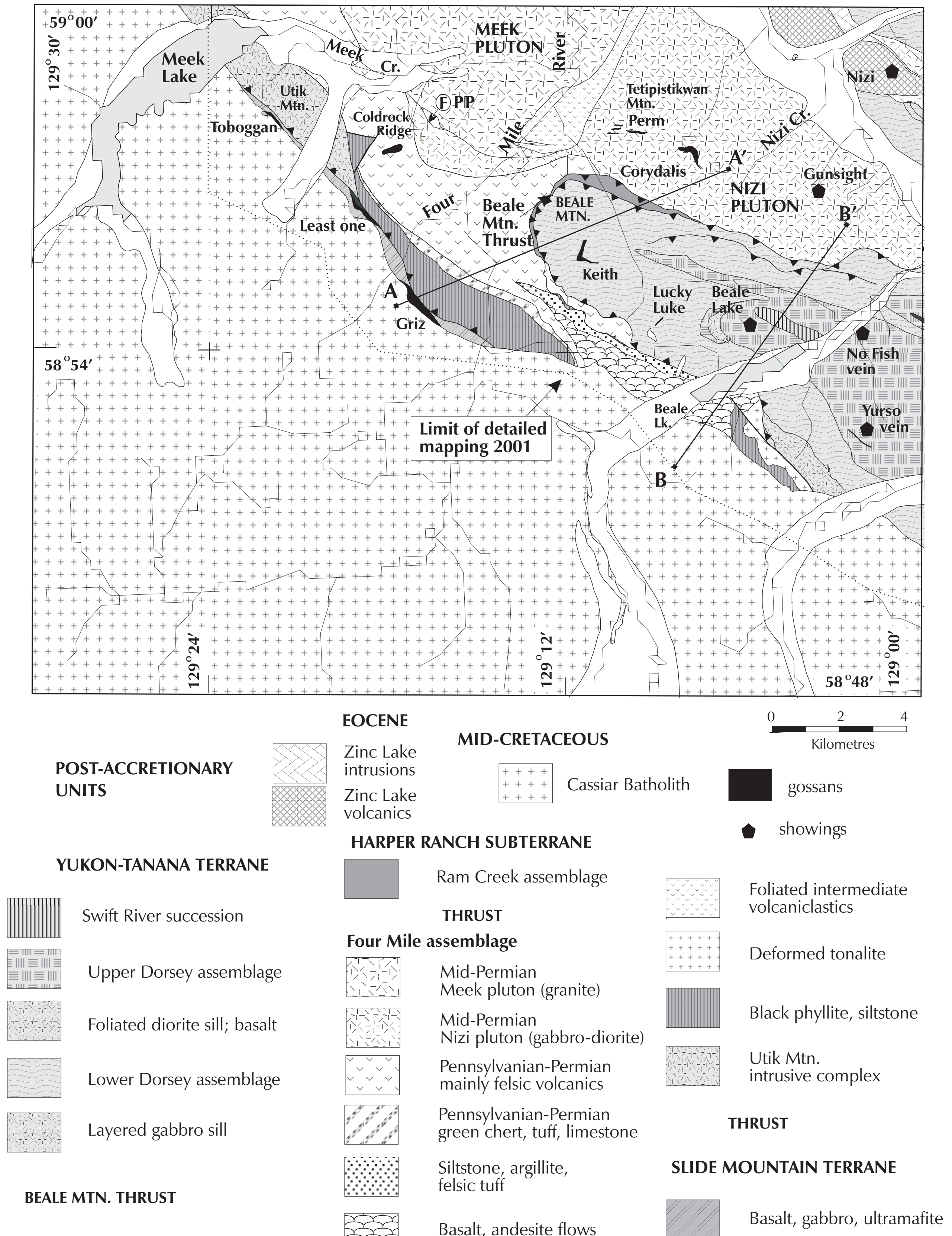

Figure 3. Geology of northern Beale Lake map area (104I/14), based on field mapping 2001. Some topographic names from Kaska elders of Dease River Band (personal communication, 2001).

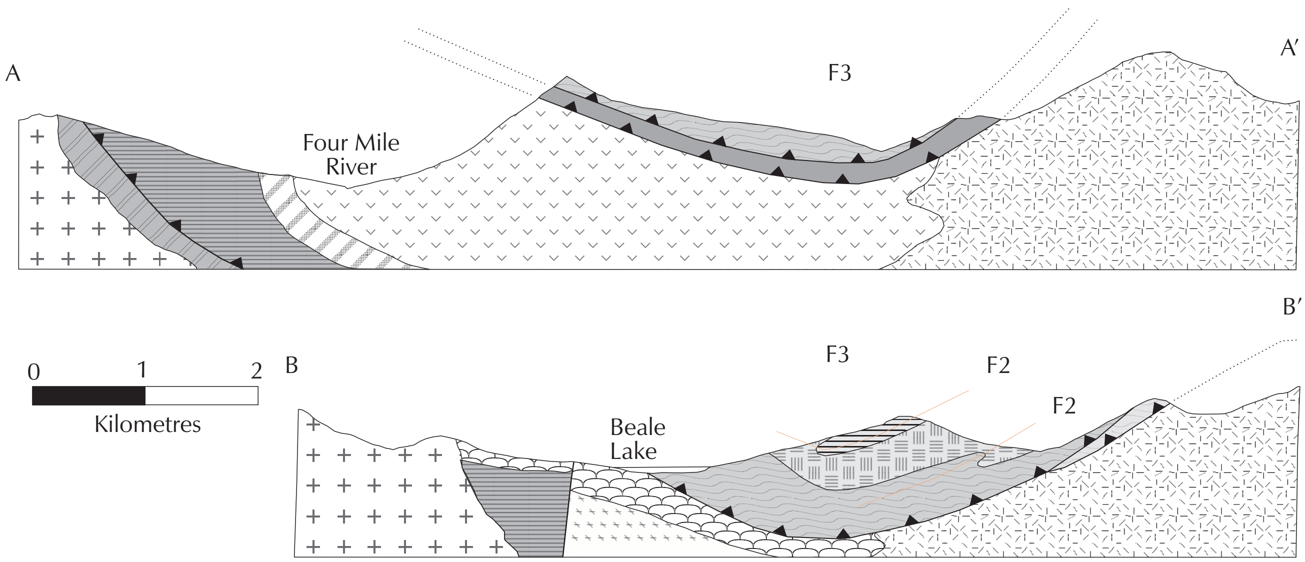

Figure 4. Cross sections of the Sylvester allochthon in the Beale Lake map area. *See* Figure 3 for geological legend and location of lines.

dacite and rhyolite flows and pyroclastic deposits are intruded by rhyolite and quartz-feldspar megacrystic dikes. This suite hosts the Nizi vein system. Galena lead signatures from the veins resemble other epigenetic, Cretaceous-Tertiary deposits of the Cassiar Terrane; the nearest correlative of the felsic intrusions is the Eocene Major Hart pluton. These observations led Plint *et al*. (1997) to assign an Eocene age to the suite. They termed it the Nizi volcanic sequence. The name Zinc Lake suite is proposed for the volcanic and associated intrusive rocks, to avoid confusion with the nearby Permian Nizi pluton.

SYLVESTER ALLOCHTHON

Rocks of the Sylvester allochthon are described in ascending structural order, *i.e.* Slide Mountain Terrane, Harper Ranch subterrane, and Yukon-Tanana Terrane (Dorsey assemblage). This order also corresponds to their pre-accretionary paleogeographic positions vis-à-vis North America, with a late Paleozoic Slide Mountain ocean the most inboard, a Yukon-Tanana pericratonic fragment most allochthonous, and a late Paleozoic Harper Ranch arc located between.

Slide Mountain Terrane

Ultramafic rocks, gabbro, basalt and minor argillite outcrop in a narrow northwesterly-trending strip located immediately northeast of the Cassiar Batholith. They lie structurally at the lowest exposed level in the Sylvester Allochthon in the Beale Lake map area (Figure 3). A few enclaves of texturally intact, serpentinized harzburgite tectonite hint at the ophiolitic affinity of this assemblage. Most rocks are highly sheared. The assemblage has been metamorphosed in greenschist facies with actinolite stable throughout. Most of the ultramafic bodies have been strongly altered to quartz-carbonate (-mariposite). No age control is available locally; however Slide Mountain basalt-sedimentary and ultramafite- gabbro panels near Cassiar have been dated as Mississippian through mid-Permian by conodonts and U-Pb methods (Nelson and Bradford, 1993).

Four Mile Assemblage (Harper Ranch Subterrane)

This group of thrust slices, informally termed the Four Mile assemblage, is bounded below by the Slide Mountain ultramafite/gabbro/basalt panel, and above by the Beale Mountain Thrust (Figure 3). The lowest slice, outcropping near Meek Lake in the northwestern part of the map area, consists of the Utik Mountain intrusive complex, a variable mafic complex with metasedimentary and metavolcanic screens. The main slice extends from south of Beale Lake, though the Meek Creek and Four Mile River drainages, into Nizi Creek to the northeast. It is structurally repeated on a secondary fault below the Beale Mountain Thrust on south Beale Mountain. Within these two repeated and related slices, undeformed volcanic rocks of varied compositions directly overlie a basement of polydeformed black phyllite, siltstone and argillite, which is cut by a tectonized tonalite/granodiorite pluton in exposures south of Beale Lake. The age of the undeformed volcanic rocks is constrained by a single Pennsylvanian-Permian conodont collection from a locality 6 kilometres east of Meek Lake (Gabrielse, 1998; *see* Figure 3). The mid-Permian Meek and Nizi plutons both show unequivocal intrusive contacts against volcanic country rocks in the main slice. The highest slice, directly below the Beale Mountain Thrust, consists of highly sheared, greenschist-grade metaplutonic and metavolcanic rocks that range from quartz-feldspar porphyries to gabbro. It is correlated with the Ram Creek assemblage, a strongly deformed, greenschist-grade assemblage with Mississippian plutonic and volcanic protoliths, which directly underlies the Dorsey assemblage west of the Cassiar batholith (Harms and Stevens, 1996; Nelson 2000).

The Utik Mountain intrusive complex is restricted to a single thrust slice, and does not resemble any other unit in the assemblage. Its component intrusions vary considerably in texture and composition, from clinopyroxene and hornblende gabbros cut by actinolite pegmatites, to fine grained hornblende-phyric basalt dikes with chilled margins. It contains rafts of chert and thin-bedded tuff and argillite, and at least one enclave of quartz-sericite schist, deformed and metamorphosed before intrusion. The variability of this complex, along with the prevalence of phenocrystic hornblende, suggests arc rather than oceanic affinity.

The black phyllite/siltstone/argillite unit forms the bases of both the main thrust sheet and of the structurally repeated sliver on south Beale Mountain. It is dominantly black and very fine grained. Laminated and cross-laminated siltstone beds are seen in places. This unit is characteristically foliated and crenulated, with several generations of folding evident. Post-kinematic andalusite, probably related to the Cassiar Batholith, is common in exposures north of Beale Lake. Diopside porphyroblasts occur in more calcareous lithologies south of Beale Lake. South of Beale Lake, this unit exhibits interfingering intrusive contacts with a coarse grained tonalite/granodiorite pluton. Textures in the pluton range from pristine, with only moderate replacement of original hornblende by biotite, to laminated mylonite unrecognizable as to protolith. This unit resembles polydeformed carbonaceous Devonian-Mississippian metasedimentary units, such as the autochthonous Earn Group and the Nasina Series of the Yukon-Tanana Terrane. It is overlain on abrupt, unsheared contacts in two well-exposed localities by undeformed volcanic and associated sedimentary strata.

The undeformed sequence is subdividable into several map units. The most widespread unit, which extends from south Beale Mountain to the northern border of the map area, is dominated by felsic, nearly aphanitic rhyolite and dacite flows and related pyroclastic deposits. The felsic unit reaches thicknesses of more than 2 kilometres. In outcrop the flow rocks are pale green, aphanitic, and commonly seamed with reticulating networks of fine chlorite veinlets. Lapilli tuffs, composed of matrix-supported angular felsic fragments, form pods and crude beds interspersed within the flows. Both Kspar-rich (rhyolitic) and Kspar-absent (dacitic) compositions have been confirmed by staining. In the northern part of the area, the felsic flow/tuff unit makes up most of the upper volcanic portion of the main thrust slice, above 100-300 metres of tuff, argillite and limestone. Excellent exposures of this steeply northeast-dipping sequence are seen on Coldrock Ridge between Meek Creek and the Fourmile River. Gabrielse (1998) reports recovery of Pennsylvanian-Permian conodonts from an outcrop that lies between the Meek pluton and a northwestern finger of the Nizi pluton (Figure 3). The locality is a breccia that contains limestone and felsic volcanic clasts in a pale green tuffaceous matrix (H. Gabrielse, pers. comm. 2001), underlain by sea-green, ribbon-bedded chert. Southward across the Four Mile River, the monotonous felsic unit interfingers with hornblende-plagioclase phyric andesites, well-bedded waterlain tuffs, and basalt, giving way along strike to other units. Farther to the southeast, two units predominate: a right side-up, northeast-facing volcanic-sedimentary unit, and an underlying basalt/basaltic andesite flow unit. The volcanic-sedimentary unit includes dark brown-grey argillite, siltstone, limestone, and tuff. The lapilli tuffs consist of white ash fragments in a brownish-grey, silt-mudstone matrix; they are in direct, depositional contact with dark green, nearly aphanitic basalt to andesite flows of the underlying unit. This relationship exhibits the compositional heterogeneity of the volcanic rocks in the Four Mile assemblage. They are thought to be of volcanic arc affinity, based on their basalt to rhyolite compositions, the predominance of felsic compositions, features like coarse lapilli tuffs and large phenocrysts, interfingering with clastic sediments, and their deformed metasedimentary basement.

The Meek and Nizi plutons are two compositionally distinct bodies arranged along regional trend in the northeastern part of the map area (Figure 3). They are mostly separated by a mildly foliated volcanic/volcaniclastic inlier, which consists of green porphyritic andesite to dacite flows and lapilli tuff. A finger of the Nizi pluton, extending along the western margin of the Meek pluton, is intruded by granitic and quartz-feldspar-phyric rhyolite dikes from it (Figure 5a).

Apophyses of both plutons intrude the felsic volcanic unit (Figure 5b). The southern boundary of the Nizi pluton below the deformed pericratonic rocks is not an intrusive contact, as reported in Gabrielse (1998), but a thrust fault with shear zones developed in both hanging and footwall (Figure 5c). Therefore the revised map interpretation is that both plutons lie in the footwall of the Beale Mountain Thrust, with the geologically younger Meek pluton intruding the Nizi pluton and both intruding rocks as young as Pennsylvanian-Permian.

The Nizi pluton is a very heterogeneous, multiphase body dominated by gabbro and diorite, with minor felsic tonalite and clinopyroxenite. Like compositions, textures in its component phases are strongly variable; hornblende in particular ranges from equant and poikilitic, replacing augite, to acicular. By contrast, the Meek pluton is a homogeneous granite. Typically coarse grained and equigranular, it consists of convex quartz intergrown with stubby plagioclase and orthoclase and lesser biotite. Neither pluton is strongly deformed, although zones of weak cataclasis affect them. Compositional layering and weak foliation are observed in the Nizi pluton, and its upper part adjacent to the Beale Mountain Thrust is highly sheared. The Meek pluton has been dated at 270±4 Ma by U-Pb methods on zircon, from a locality 1.5 kilometres west of the Four Mile River and .5 kilometres north of the Beale Lake map area. The same sample site yielded a 262±2 Ma U/Pb age on titanite, and a 266±4 Ma K/Ar age on biotite (Gabrielse *et al*., 1993). A K/Ar hornblende analysis from the Nizi pluton gave an

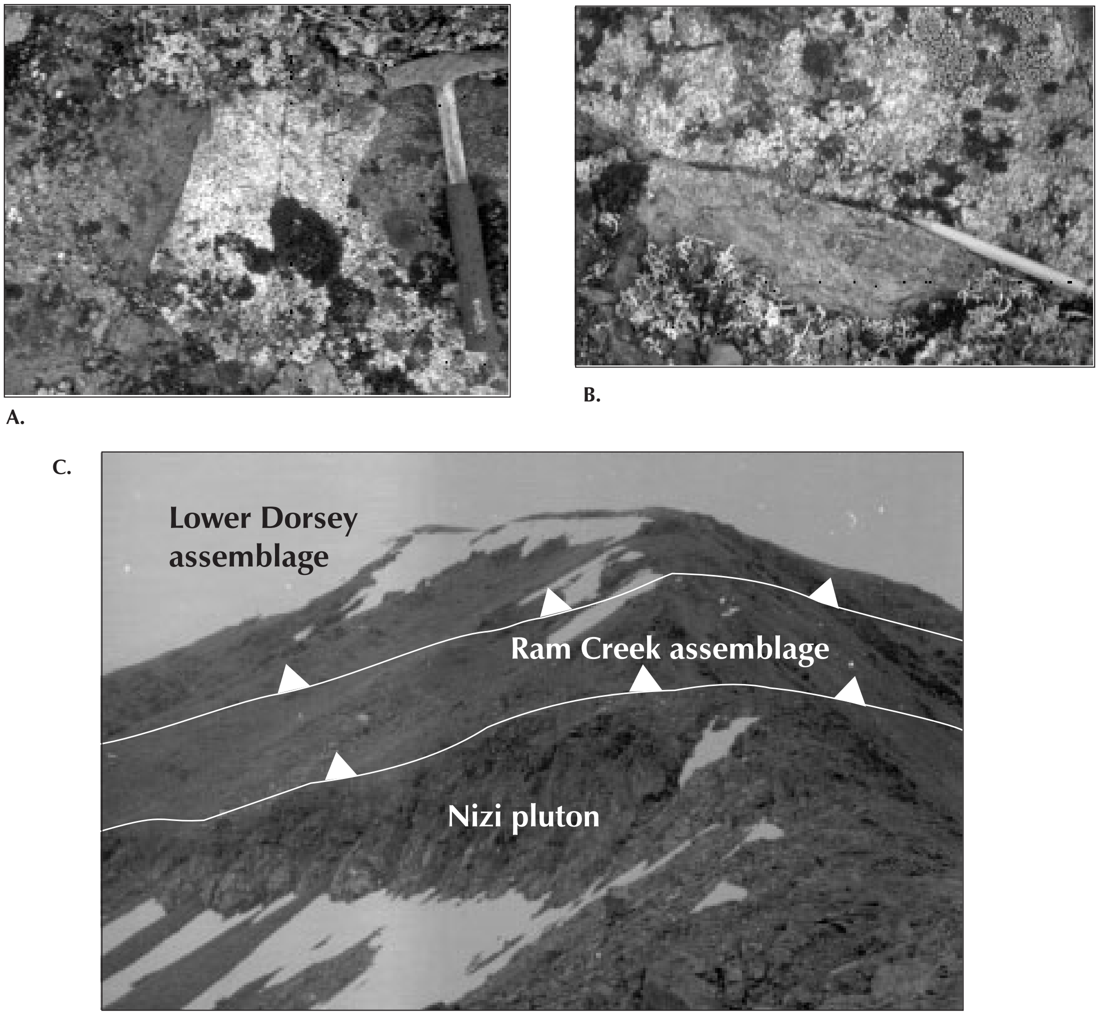

Figure 5. Key field relationships of the mid-Permian plutons. A) Dike of granite, texturally similar to, and probably an offshoot of Meek Pluton, cutting gabbro in an apophyse of the Nizi pluton. B) Nizi pluton diorite cutting undeformed felsic volcanic country rock of Four Mile assemblage. C) Upper thrust contact of the Nizi pluton below the Ram Creek and lower Dorsey assemblages.

age of 262±8 Ma (Hunt and Roddick, 1988). Therefore, although the Meek granite is geologically younger than the heterogeneous and more mafic Nizi pluton, in terms of available isotopic ages they are indistinguishable.

Dorsey Assemblage

The Dorsey assemblage is a layered sequence of metamorphic rocks intruded by deformed early Mississippian plutons, which lies structurally above the undeformed and weakly metamorphosed late Paleozoic rocks of the Four Mile assemblage. It occupies the core of a syncline that trends from Beale Mountain southeastwards across Beale Lake, and on the northeastern flank of the anticline that exposes the footwall Nizi pluton (Figure 3). It comprises two units, the upper and lower Dorsey assemblages, which are in contact across a layering-parallel, transitional zone. In spite of considerable penetrative deformation, and shearing particularly in the lower unit, these two units constitute an original and still readily interpretable stratigraphy. The term "tectonite" should be applied to these rocks with some caution, as they constitute neither broken formation nor tectonic melange.

Previous work suggested that the Permian Nizi pluton was emplaced into the metamorphic unit, constituting a common element with coeval plutons in the underlying panels (Gabrielse *et al.*, 1993). This study has documented a major fault, the Beale Mountain Thrust, between them. The existence of a Permian intrusive suite within the pericratonic assemblage, similar to the Ram Stock in the lower Dorsey Terrane near Swift River, Yukon (Stevens and Harms, 1995) and small pegmatites farther south in British Columbia (Nelson, 1999), has thus lost a major support. There is now only one known Permian intrusion within it, a small body between the Dease and Four Mile rivers in southern McDame map area (sample 89-SY-72A; Gabrielse *et al.*, 1993). However, a large, heterogeneous, unfoliated, diorite to tonalite body cuts the lower Dorsey assemblage northeast of Nizi Creek; part of it is exposed in the northeastern corner of Figure 3. In composition and texture it strongly resembles the nearby Nizi pluton, and could be its displaced roof. It has been sampled for U/Pb dating. In addition, sparse, greenish-black amphibolite rafts in the Nizi pluton indicate that it penetrated a basement not unlike the amphibolite-bearing lower Dorsey assemblage.

Lower Dorsey Assemblage

The lower Dorsey assemblage is an interlayered sequence of siliceous metasedimentary strata, amphibolite and metagabbro. The metasedimentary rocks, now fine grained quartzites, quartz-biotite-muscovite(-garnet-plagioclase) schists, marble and calc-silicates, probably had mostly chert, argillite and impure limestone protoliths. True pelites are rare; most micaceous rocks are dirty quartzites. Coarse-grained, pure, thickly layered orthoquartzites are also rare; the best example occurs near the exposed top of the unit on the west-facing spur north of Beale Lake. The interpreted metacherts form grey, ribbon-layered sequences. They tend to be highly pyritic. Some contain abundant garnets which may indicate manganese-rich compositions, and minor quartz-sericite schist suggests alteration.

Kyanite occurs in two samples from the lower Dorsey assemblage in the Sylvester Allochthon. In both cases it is relict, partly resorbed, and overgrown by muscovite. In one of these, from the west side of Beale Mountain, later fibrolitic sillimanite grows in the predominant fabric. This paragenetic sequence of kyanite to sillimanite mirrors aluminosilicate growth recorded in the lower Dorsey assemblage west of the Cassiar Batholith (Nelson, 2000). Harms *et al.* (1993) report amphibolite-grade assemblages of garnet-muscovite-zoisite and biotite-garnet-staurolite from pelites elsewhere in the deformed pericratonic assemblage.

Amphibolite occurs on all scales, from fine layers alternating with metachert and siliceous pelite to mountain-scale, lensoid bodies. Mineralogy varies from simple hornblende-plagioclase-quartz-titanite to garnet- and garnet-diopside-calcite-bearing varieties. The latter have a calcareous component in excess of that for normal basaltic rocks. It could be due to admixture with carbonate sediments, or seafloor alteration. In general these rocks show thoroughly metamorphic fabrics. Very fine, continuous titanite laminae could possibly reflect tuffaceous parentage. One example of plagioclase-quartz-garnet-filled amygdules(?) was noted.

Metamorphic fabrics in the amphibolites range from extremely foliated to nearly isotropic. The most foliated varieties consist of ribbons of very well aligned hornblende prisms, alternating with more felsic quartz-plagioclase-bearing laminae. Fine titanite trains parallel the layering. More equant and randomly oriented hornblende overgrows these textures, suggesting that peak metamorphism succeeded peak deformation. It is possible that the extremely foliated amphibolites inherited their fabrics from earlier phyllonites developed at lower metamorphic grade (J. Ryan pers. comm. 2001).

The metagabbros form a distinct, geologically younger suite than the amphibolites. Although foliated and sheared, they show clear relict plutonic textures, and never contain garnet. They may be cogenetic with a large layered gabbro body that intrudes the lower Dorsey assemblage south of Beale Lake. This body has strongly foliated and sheared margins. Apophyses of it show cross-cutting relationships with surrounding schists and amphibolites. Its unfoliated core is cumulate layered, involving sets of coarse and fine-grained gabbro, gabbro/leucogabbro, and gabbro/hornblendite rhythmites.

The lower Dorsey assemblage represents a pericratonic basin in which both intrusive and extrusive mafic material accumulated, possibly an intracontinental rift. Petrochemical analysis of amphibolites from west of the Cassiar Batholith shows a progression from N-MORB to E-MORB to within-plate compositions (Nelson, 2001). The metagabbros may belong to the syntectonic Mississippian intrusive suite identified by Gabrielse *et al.* (1998).

Upper Dorsey Assemblage

The upper unit of the Dorsey assemblage contrasts strongly with the lower unit. On both sides of Beale Lake, amphibolites abruptly disappear upsection, and well-foliated quartz-feldspar phyric metavolcanic rocks become important. They are accompanied by dark grey, grey, tan and green phyllite, quartzite with remnant quartz grains, and metachert. The identification of abundant felsic metavolcanic and epiclastic material in the upper part of the pericratonic unit is an important step in regional geological and metallogenetic correlations, since such rocks characterize both the metal-rich Finlayson Lake belt and, more locally, the upper Dorsey assemblage near Swift River (Roots and Heaman, 2001). U-Pb analyses are pending.

The felsic rocks include metamorphosed flows in which sparse quartz and feldspar porphyroclasts occur in finely (flow?-)laminated, dense, very fine grained quartz-plagioclase-Kspar matrix. Tuffaceous sequences show interbedding of phyllite, quartz- and feldspar-eye phyllite, and coarse volcaniclastics with abundant large quartz, plagioclase and Kspar augen in quartzo- feldspathic matrix. These are not mylonites; the textural variety is due to original interbedding of volcanic and clastic material, not to strain recrystallization. No papery, rusty quartz-sericite schists indicative of early hydrothermal alteration were seen in this area, although minor quartz-muscovite schists are present.

South of Beale Lake, large parts of the upper Dorsey assemblage are dominated by green and grey phyllite and quartzite. Sequences like this, which outcrop near Oblique Creek in southern Jennings River map area, were assigned to the Swift River succession (Nelson 1999). However, in the Beale Lake area the phyllite and quartzite clearly interfinger with quartz-feldspar phyric metatuffs. Perhaps the Oblique Creek metasedimentary sequences are a variant on the upper Dorsey assemblage, rather than the structurally overlying Swift River succession.

Mafic sills - well foliated metagabbros and in a few cases hornblendites - intrude the upper Dorsey assemblage. These bodies may belong to the same generation as the gabbros in the lower Dorsey assemblage.

Although well foliated, the upper Dorsey assemblage exhibits less obvious penetrative shearing than the lower Dorsey. Its metamorphic grade is apparently lower. Phyllites predominate over schists, original quartzite textures are preserved, and pale green, actinolitic hornblende is developed instead of deep green hornblende in the metagabbros. Mineralogically however, the metasedimentary rocks contain similar assemblages of muscovite, biotite and less common garnet.

Swift River Succession

A small area of dark-coloured chert, argillite, phyllite and white quartzite occurs in the synclinal core, structurally above the felsic metatuffs north of Beale Lake. These rocks are tentatively assigned to the Swift River succession, by analogy with sequences west of the Cassiar Batholith (Nelson, 1999, 2000).

POST-ACCRETIONARY UNITS

Cassiar Batholith

A portion of the regional, northwesterly-trending Cassiar Batholith (Figure 1) occupies the southern part of the map area. This body consists mainly of coarse grained granite and granodiorite, with pegmatitic and aplitic phases also present. One K/Ar biotite age of 107 Ma is available from this map area (GSC K/Ar 4063). This is typical of K/Ar ages for the batholith (Gabrielse, 1998, Table 8). Farther north, the eastern side of the batholith is cut by younger, Late Cretaceous stocks, which are asssociated with porphyry-skarn-manto mineralization (Panteleyev, 1980; Nelson and Bradford, 1993). In the Beale Lake area, distinct, cross-cutting bodies have not been identified, perhaps because the detailed mapping project terminated near the batholith margin. However, potentially younger, relatively fine-grained, quartz-feldspar megacrystic dikes lie along fractures in the country rocks east of the batholith; they may belong to the Late Cretaceous suite.

Zinc Lake Volcanics and Intrusions

Undeformed volcanic and volcaniclastic rocks and felsic intrusions outcrop in a northwesterly-striking belt in the northeastern corner of the map area, extending onto adjacent 104I/15 where Zinc Lake itself lies. These rocks were described in detail by Plint *et al.* (1997). Their contacts with the surrounding Dorsey assemblage and its intrusive bodies are unconformable or cross-cutting, and may in part be controlled by synvolcanic faults. Their overall outcrop pattern is that of a northwesterly-elongate graben. The felsic intrusions, which range from fine grained, glassy, flow-banded rhyolite to quartz-feldspar megacrystic granite, concentrate along the northeastern margin of the complex. Volcanic and volcaniclastic rocks range from andesites and andesite lapilli tuffs with tiny hornblende phenocrysts through dacites to flow-banded, aphanitic rhyolites. Two bulbous rhyolite bodies, possibly flow domes, were mapped on the ridge above Zinc Lake. The highest gold values on the property occur in this area (Plint *et al.*, 1997).

STRUCTURE

The Sylvester Allochthon is built of stacked, internally imbricated thrust packages, separated by major thrust faults, such as the Beale Mountain Thrust (Figure 6a).

Attitudes of these thrust faults, and of the units between them, have been affected by post-emplacement folding. Units and structures on the southwestern side of the allochthon, near the Cassiar Batholith, dip steeply northeast (Figure 4). This is a common feature along the length of the batholith, defining the western side of the “McDame synclinorium” of Gabrielse (1963). Forceful intrusion combined with crustal compression apparently caused the layered rocks to arch up over the eastern side of the batholith. Farther northeast, major contacts within the allochthon are warped into a series of upright, open, regional folds; for instance the syncline between Beale Mountain and Beale Lake, and the anticline that exposes the Nizi pluton (Figure 3). Prior to this (mid-Cretaceous?) folding event the allochthons probably lay above the Cassiar Terrane on nearly flat contacts.

Development of penetrative structures within the Four Mile assemblage was minimal, except for the black phyllite unit and Ram Creek assemblage. Strong shear fabrics are developed in the late Paleozoic volcanic rocks only within tens of metres of the Beale Mountain Thrust. By contrast, the Ram Creek assemblage is foliated, sheared, and mylonitized throughout. This is partly due to its position in the immediate footwall of the Beale Mountain Thrust; however, its degree of deformation vastly exceeds that developed in the Nizi pluton or the late Paleozoic volcanic rocks, even where they lie adjacent to the Beale Mountain Thrust. A twofold deformation history is suggested. A plagioclase porphyry dike, which cuts across structures in the Ram Creek assemblage but does not penetrate its external contacts, was collected for U/Pb dating.

The Dorsey assemblage is characterized by at least two episodes of penetrative deformation and shearing. One episode occurred in the early Mississippian, as shown by late synkinematic plutons of that age (Gabrielse *et al.*, 1993). A second, later shearing event accompanied its emplacement on top of the Four Mile assemblage as the hanging wall of the Beale Mountain Thrust (Figure 6a). This event must have postdated the youngest footwall rocks, the mid-Permian Meek and Nizi plutons. Distinct sets of fabrics and strain gradients can be related to these two events.

Ductile strain diminishes gradually upwards within the entire tectonite. The lower Dorsey assemblage contains sheath folds and very strong quartz stretching (E1) and mineral streaking (M1) lineations, associated with shear bands and c-s fabrics in appropriate lithologies. These features decrease to uncommon occurrence in the upper Dorsey assemblage. Rootlessly folded small leucosomes, a common feature of lower Dorsey amphibolites, do not appear in the upper Dorsey assemblage.

The E1 stretching and M1 streaking lineations show a pronounced northeasterly maximum at 58/18, and a lesser southwesterly one (Figure 6c). These represent measurements on the two limbs of the upright, F3

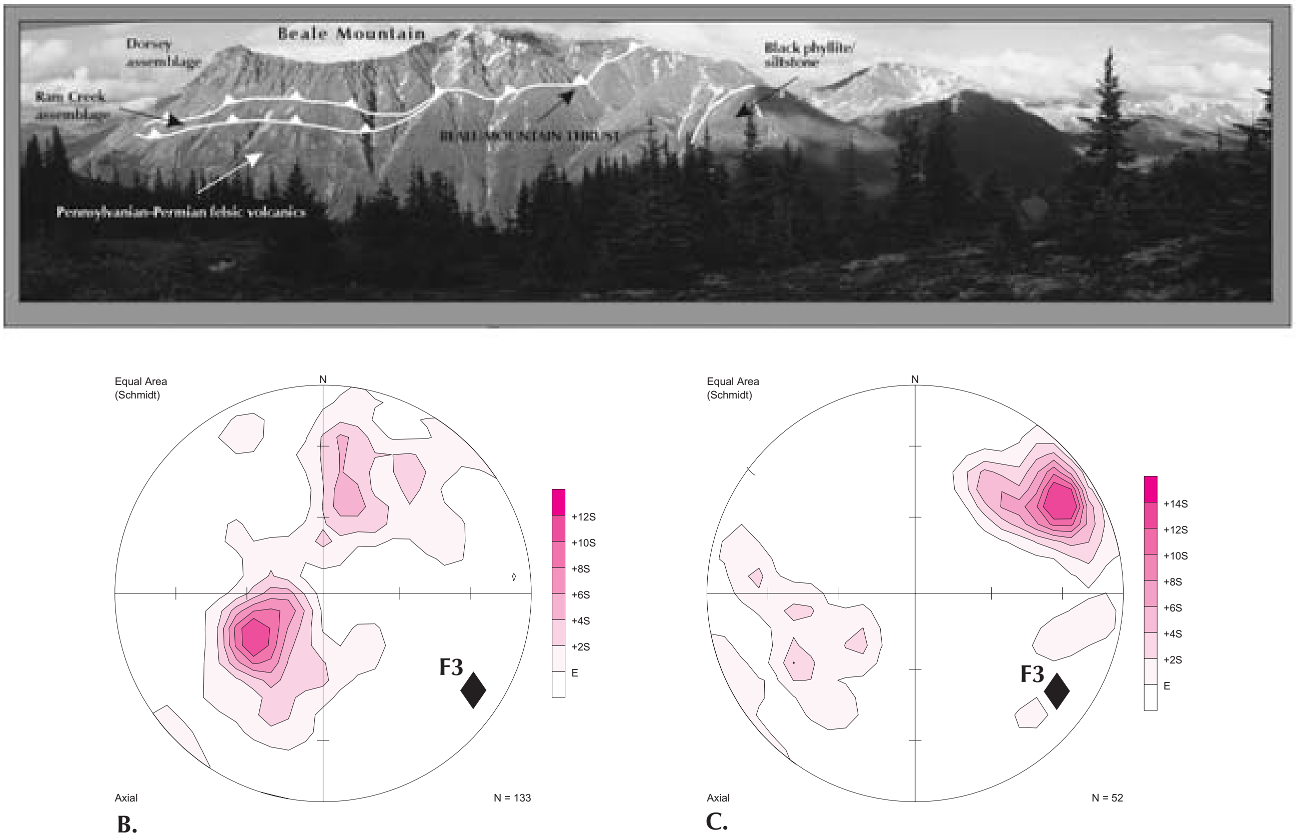

Figure 6. Structures in and around the Dorsey assemblage. A) The Beale Mtn. Thrust on Beale Mountain,. Note the gently dipping base of the upper pericratonic allochthon above rocks of the Harper Ranch subterrane. B) Attitudes of S1 foliation and transposed layering in the Dorsey assemblage. C) Early quartz stretching (E1) and mineral alignment (M1) in the Dorsey assemblage.

syncline, which also folded transposed layering and schistosity (S1) in the Dorsey assemblage (Figure 6b). Shear bands and asymmetric porphyryoclasts both in outcrop and thin section indicate tops to the northeast. Tentatively, this early tectonic event is assigned to the early Mississippian, probably immediately after deposition of the upper Dorsey assemblage. A pegmatite has been collected for U/Pb dating. Although it is cut by prominent mylonite zones, it locally crosscuts foliation in the amphibolite, and does not exhibit the stretching lineation that is so well-developed in its country rocks. These features fix its emplacement as late in the ductile shearing event.

Close-spaced shear zones are developed in rocks tens of metres from the Beale Mountain Thrust, including the lower Dorsey assemblage, the Ram Creek assemblage and the otherwise undeformed Four Mile assemblage. Shear bands indicate top-to-the-northeast motion on these subsidiary shears, and thus by implication on the main thrust fault. Interestingly, the post mid-Permian emplacement of the Dorsey assemblage on top of the subadjacent late Paleozoic arc assemblage followed the same sense as its much earlier internal deformation. Either the same large-scale crustal architecture controlled both, or crustal geometries shaped during the early Mississippian event influenced later accretion.

MINERAL OCCURRENCES AND MINERAL POTENTIAL

The Beale Lake map area is host to a diverse set of mineral occurrences and exploration possibilities, many of them documented here for the first time. Types of deposits represented include the following (Table 1):

1. Intrusion-related gold-silver-polymetallic veins.
2. Epithermal gold-silver-polymetallic veins.
3. Porphyry-style copper mineralization associated with zones of intrusive breccias and silicification in the Nizi pluton.

In addition, geological evidence supports the possible occurrence of the following deposit types in the area:

1. Syngenetic massive sulphide occurrences associated with pyrite-garnet-bearing (exhalative?) metachert in lower Dorsey assemblage.
2. Syngenetic massive sulphide occurrences associated with felsic volcanics and pyrite-garnet-bearing (exhalative?) metachert in upper Dorsey assemblage.
4. Mesothermal gold-quartz veins associated with quartz-carbonate-mariposite alteration in Slide Mountain ultramafic rocks.

Exhalites in Lower Dorsey Assemblage

Very rusty, pyritic metachert layers occur at two localities roughly at the same structural (and thus stratigraphic?) level in the lower Dorsey assemblage (Figure 3, Table 1). The layers are continuous over hundreds of metres to a kilometre of strike length, and are overall 5-10 metres thick. They contain two compositional varieties: dark grey, pyrite-rich chert with trace to abundant garnet, and white pyritic chert with minor, discontinuous quartz-sericite schist. Their mineralogy is consistent with that described from coticules, or metamorphosed Fe-Mn-silica exhalites. Geochemically, they are characteristically anomalous in manganese and barium (Table 2).

A sample from one very small occurrence, 01JN16-3, from near the top of the lower Dorsey assemblage 4 kilometres north of Beale Lake, contains over 17,000 ppm barium.

Potential for Syngenetic Sulphide Occurrences in Upper Dorsey Assemblage

The upper Dorsey assemblage near Beale Lake contains significant accumulations of felsic volcanic and volcaniclastic products. Exposures of blue-grey, yellow-stained phyllite similar to the "gunsteel" slates of the autochthonous Earn Group are associated with the felsic rocks. This suite is a probable equivalent of the early Mississippian upper Dorsey assemblage in the Swift River area, which in turn has been correlated with the felsic volcanic hosts of syngenetic massive sulfide deposits in the Finlayson Lake belt (Roots and Heaman, 2001). Thus, a geologically favorable environment for such deposits also exists within the upper Dorsey assemblage in the Sylvester Allochthon.

A 10 metre-thick section of rusty, pyritic chert, overlain by garnetiferous quartz-muscovite schist with unusually abundant tourmaline and apatite, is exposed on the west-facing spur north of Beale Lake. It is probably of sili-

TABLE 1
MINERAL OCCURRENCES, SHOWINGS AND ALTERATION ZONES, BEALE LAKE MAP AREA

	UTM east	UTM north	MINFILE number	Deposit type	Capsule description
Nizi A, B Zone	498637	6538060	104I032	Polymetallic veins Ag-Pb-Zn±Au.	samples assayed up to 12.0 g/tonne gold and up to 3428 g/tonne silver. These base metal zones are generally <20 centimetres wide and traceable for tens of metres.
Nizi H Zone	499240	6537900	104I032	Polymetallic veins Ag-Pb-Zn±Au.	Vein samples assayed up to 2.33 g/tonne gold and 627.43 g/tonne silver, 18.3% zinc and 7.% lead.
Nizi Surprise vein	499380	6537663	104I032	Polymetallic veins Ag-Pb-Zn±Au.	Chip/channel samples assayed up to 27.09 g/tonne gold and 1220.58 g/tonne silver over 2 metres.
Gunsight	496483	6534714	104I041	Polymetallic veins Ag-Pb-Zn±Au.	quartz vein with argentiferous galena, pyrite and sphalerite. One 20-centimetre sample contained .09 g/tonne Au, 110 g/tonne Ag, 8.36% Pb and 3.09% Zn.
Beale upper vein	494235	6529734	104I098	Polymetallic veins Ag-Pb-Zn±Au.	quartz vein + Au, Ag
Beale lower vein	494146	6530533	104I098	Polymetallic veins Ag-Pb-Zn±Au.	quartz-arsemopyrite-galena vein+Au, Ag
Yurso vein	498116	6525956		Polymetallic veins Ag-Pb-Zn±Au.	grab sample: Au (to 1250 ppb), Ag (greater than measurable using ICPMS technique), Bi (to 413 ppm), Pb (to 23,000 ppm), Sb (to 8000 ppm), anomalous Se, Te, Cu and Zn.
No Fish vein	497824	6529441		Polymetallic veins Ag-Pb-Zn±Au.	pyritiferous quartz vein with anomalous values of Cu, Te, Se, Ag, Mn
Perm	490989	6536006		Porphyry Cu	silicified intrusion breccia with disseminated pyrite, trace chalcopyrite
Corydalis	492624	6535272		Porphyry Cu	silicified intrusion breccia with disseminated pyrite, trace chalcopyrite
Keith	489414	6531816		Siliceous exhalite	chert + pyrite, garnet
Lucky Luke	491403	6529879		Siliceous exhalite	chert + pyrite, garnet
Toboggan	479062	6536436.6		Listwanite alteration	Fe-Mg carbonate-altered ultramafite, anomalous As, Sb, Mn
Least one	482128	6533259		Listwanite alteration	Fe-Mg carbonate-altered ultramafite, anomalous As, Sb, Mn
Griz	483689	6530499		Listwanite alteration	Fe-Mg carbonate-altered ultramafite, anomalous As, Sb, Mn

TABLE 2
LITHOGEOCHEMICAL DATA, 2001 SAMPLES, BEALE LAKE MAP AREA
(104I/14N)

				Element	Au	Au	Ag	Ag	As	W	Bi	Sb	Hg	Se	Te	Cd	Cu	Pb	Zn	Mn	Ba	Ni	Co	Cr
				Units	ppb	ppb	ppb	g/tonne	ppm	ppm	ppm	ppm	ppb	ppm	ppm	ppm	ppm	ppm	ppm	ppm	ppm	ppm	ppm	ppm
				Dect'n Limit	0.1		2		0.1	0.2	0.02	0.02	5	0.1	0.02	0.01	0.01	0.01	0.1	1	0.5	0.1	0.1	0.5
Field Number	Showing	Description	UTM east	UTM north		Fire assay		ICES																
					Polymetallic veins																			
01JN14-10	Beale upper vein	quartz vein in trench	494216	6529765	2964.4	2716.2	29299	31.9	954.6	2.9	17.23	18.15	676	5	0.24	1.34	101.8	4707.86	155.9	70	17.2	9.3	0.8	123.4
01LL10-4	Beale lower vein	quartz vein + aspy	493526	6529703	816.6		556		2954.7	228.3	100.62	1.46	< 5	0.8	0.58	0.18	167.18	18.71	20.2	124	11.9	13.5	9.1	151.2
01LL10-1b	Beale Lake	quartz vein + gn, sp, py	494113	6530374	548.6		20871	23.4	95513.7	4.4	40.57	194.71	386	15.4	0.63	65.97	222.15	1776.76	5176.2	< 1	35.1	11.7	9.5	77.8
01JN24-5	Yurso vein	quartz vein + tetrahedrite	498167	6525917	1135.4	1142.1	99999	1824.5	99999	0.5	413.24	8159.74	527	10.4	0.38	174.56	916.03	22378.92	395	< 1	59.7	9	0.7	67.8
01JN24-5B	Yurso vein	weathered vein	498167	6525917	1254.8	1119.9	99999	797.2	99999	0.3	401.28	864.47	1112	9.9	0.19	149.21	289.02	23557.87	557.7	< 1	35.5	3.5	< 1	21
01JN25-4	Yurso vein	rusty brecciated qz vein	497570	6526455	161.7		10408	10.9	2004.6	1.2	3.05	46.12	36	0.2	0.03	1.27	21.87	548.41	13	196	49.9	6.4	2.9	103.7
01JN25-4B	Yurso vein	quartz vein + tetrahedrite	497612	6526413	394.1		99999	1040.7	4056.1	1.1	6.7	1051.97	1294	129.7	1.64	77.18	606.28	24188.76	2037.9	32	64.3	11.8	0.3	113.3
01JN25-5	Yurso vein	quartz vein + tet, aspy, sb	498046	6526102	523.7		99999	140.9	24687.9	< 2	0.45	7573.33	1746	1.1	0.03	777.3	124.89	10013.88	10382.2	180	59.5	10.5	5.3	131.2
01JN26-9	Nizi	quartz vein NW of main showings	497270	6540126	4.7		1665		687.8	1.5	0.31	17.75	359	0.3	0.04	20.01	14.94	343.19	587.4	1350	66.8	687.8	39.9	450.2
01LL20-5	No Fish vein	quartz vein + py, grey sulphide	497870	6529465	3.5		1253		15.1	4	0.66	5.56	7	13.1	0.24	0.05	136.95	8.67	18.2	217	64.2	25.9	85.7	135.7
01LL20-5rep	No Fish vein	quartz vein + py, grey sulphide	497870	6529465	3.1		1323		13	1.1	0.66	6.09	10	14.3	0.25	0.04	130.39	7.61	19.1	204	43.3	21	84.6	72.6
					Veins associated with listwanite-altered ultramafites																			
01JN1-6	Least one	listwanite-altered ultramafite	481660	6533747	21.6		137		21.7	1.4	0.83	48.48	35	0.2	0.04	0.05	9.96	0.71	25	551	54.8	822.7	52.5	458.9
01JN6-5A	Least one	quartz vein in carbonate-altered ultramafite	482361	6533140	1.9		1088		179.2	0.7	0.15	49.29	8	0.6	0.04	< .01	12.19	0.8	9.6	756	31.1	815	47.3	390.7
01JN6-5B	Least one	quartz vein in carbonate-altered ultramafite	482361	6533140	0.3		437		99.4	0.5	0.54	9.07	40	0.5	0.09	0.02	19.56	0.47	8.9	686	34.4	1513.5	79.6	319.2
01JN7-6	Griz	quartz vein in carbonate-altered ultramafite	483924	6530173	0.6		138		142.3	0.6	1.27	2.97	7	2.1	0.06	0.04	5.88	0.4	11.9	684	25.8	1404.9	81.2	218
01JN8-1	Griz	quartz vein in carbonate-altered ultramafite	483688	6530463	0.5		263		62.5	0.5	0.5	6.2	113	1.1	0.04	0.09	6.11	1.17	12.4	431	41.4	517.6	36.1	230.8
01JN8-2	Griz	quartz vein in carbonate-altered ultramafite	483484	6530644	3.3		1179		229.8	3.4	0.24	56.25	50	1.7	0.1	0.01	8.87	1.6	5.7	459	80	592	44.9	278.4
01JN9-6B	Toboggan	silicified zone in fault	478807	6536738	8		524		50.1	1.1	0.28	5.5	13	5.1	0.06	< .01	10.23	9.29	11.5	42	111.7	10.7	2.7	83.6
					Pyrite-garnet cherts (coticules)																			
01JN13-2	Keith	pyritic chert/coticule	489071	6532542	0.9		260		1	1.2	0.37	0.11	17	3.5	0.41	0.1	110.92	8	33.7	1006	41.7	20.6	12.1	97.2
01LL8-3	Keith	rusty chert + scorodite	489553	6531843	0.5		291		26.3	1.8	0.2	0.45	10	0.4	0.18	0.19	44.95	26.2	53.6	658	112.3	22	9.6	99.3
01LL8-3B	Keith	rusty chert boulder	489553	6531843	0.2		338		17.5	2.5	0.19	3.31	9	2	0.11	0.65	104.81	20.17	37	143	28.1	32.5	9.7	140.5
01JN18-3		pyrite-graphite chert (coticule)	492061	6532135	2.8		158		3.9	1.5	0.12	0.22	55	2.8	0.04	1.67	78.81	5.93	90.1	103	17411.5	53.3	10.1	118.2
01JN20-7		blonde chert, top of black phyllite unit	487568	6529831	2.2		90		3.9	0.9	0.14	1.16	12	0.3	0.04	0.45	62.63	11.26	27.7	112	223.1	6.6	2.1	54.4
01JN23-6		pyritic chert	499851	6529299	1.4		467		9.1	4.8	0.12	1.51	60	2.6	0.11	1.41	45.78	10.58	53.2	63	14.6	23.4	9.7	156.2
01LL7-7A		pyritic chert (coticule)	493008	6529711	1.6		1161		73.4	2.5	0.3	1.87	17	1.4	0.09	0.62	59.15	45.74	35.7	268	2024	24.9	3	148.1
01LL11-2		dissem. pyrite	491600	6529971	6.8		244		50.1	7.5	0.43	0.22	< 5	0.7	0.08	0.1	103.72	9.44	76.3	658	364.2	65.2	28	121.1
01LL11-4B	Lucky Luke	pyritic chert	491482	6529821	1.4		184		138	1.1	0.36	0.89	6	1.6	< .02	0.33	60.47	12.38	42.9	359	99.7	10.1	3.9	60.1
01LL11-4C	Lucky Luke	pyritic chert	491482	6529821	1.5		303		7	1.5	0.76	0.12	< 5	0.5	0.03	0.23	75.38	9.1	80.7	756	199	61.5	34	99.5
01LL11-5A	Lucky Luke	quartz vein + minor pyrite	491423	6529780	0.7		91		35.8	1.9	0.06	1.06	< 5	0.1	< .02	0.23	19.95	6.18	17.5	587	8.3	21.2	8.4	139.5
01LL11-5B	Lucky Luke	black chert, dissem. pyrite	491423	6529780	2.7		182		5.6	0.4	0.07	0.32	6	1	0.04	0.37	62.94	4.19	75.5	603	86.3	86.1	42.5	76.9
01LL11-5C	Lucky Luke	rusty dike	491423	6529780	1.1		282		6	0.4	0.09	0.28	5	2.1	< .02	0.38	85.61	5.77	80.6	460	53.7	43.8	5.6	133.9
01LL12-7B		pyritic chert	494387	6532219	2.3		121		8.9	1.1	0.05	0.32	6	0.8	0.05	0.18	58.69	4.01	47.3	67	13.7	11.5	13.7	83.9
01LL13-4		chert + pyrite, graphite	492549	6532954	< 2		218		9.7	1.4	0.18	0.53	13	1.5	0.13	0.32	62.81	15.3	38.9	186	19.3	24.7	15.5	129.6

TABLE 2
LITHOGEOCHEMICAL DATA, 2001 SAMPLES, BEALE LAKE MAP AREA (104I/14N)

					Disseminated sulfides with intrusive breccias in Permian intrusions																			
01JN17-3		silicified intrusive breccia + sulfides	490164	6535444	2		62		4.4	0.9	0.06	0.27	34	1.6	< .02	< .01	27.37	5.65	4.3	44	34.1	4.6	3.8	48.5
01JN17-5	Perm	silicified intrusive breccia + sulfides	491017	6535998	1.3		211		1	0.6	0.58	0.07	17	3	0.06	0.01	82.96	14.58	8.8	242	35.7	15.1	59.7	65
01JN18-4	Corydalis	silicified intrusive breccia + sulfides (py, po, cpy)	492691	6535145	1.3		1226		17.5	1	0.18	0.72	222	1.1	< .02	1.3	1139.98	2.91	490.9	183	20.6	18	16.9	99.6
01JN18-4rep	Corydalis	silicified intrusive breccia + sulfides (py, po, cpy)	492691	6535145	0.9		1824		42.7	0.5	0.28	5.84	253	1.6	0.02	1.72	1405.63	18.31	476.7	192	22.6	15.3	18.7	97
					Gossans in felsic volcanics of Four Mile package																			
01JN3-11		pyrrhotite-pyrite gossan in Penn-Perm felsic volx	482961	6535472	1.6		99		11.9	0.6	0.13	1.17	29	< .1	0.02	0.09	21.35	14.86	50.8	435	730	4.8	5.5	31.4
01JN15-4		silicified felsic flow with dissem., veinlet pyrite	490114	6530011	3.3		38		2.3	0.4	0.09	0.31	< 5	0.2	0.04	0.04	63.97	10.25	64.2	868	406.7	8.3	11	51.6
01JN15-5		silicified felsic flow with dissem., veinlet pyrite	489983	6529464	4.3		355		108	0.9	0.25	1.04	11	1.2	0.06	0.24	83.8	16.68	73.6	770	107.2	11.5	13.8	52.7
01JN10-2		rusty dacite	480926	6540001	14.9		190		62.9	1.4	1.42	4.3	51	0.1	0.03	0.04	14.38	15.45	12.4	57	253.2	7.3	1.9	60.5
					Other gossans																			
01LL1-3		gossan in mafic intrusive complex	479544	6537016	2		640		59.1	0.6	0.14	19	9	2.1	< .02	1.2	75.41	49.01	38.8	375	50.4	4.2	11.8	53.8
01LL17-5		gossan in basalt, abundant pyrite	493156	6526692	53.9		434		8.1	0.3	0.55	0.64	12	6.2	1.25	0.1	229.79	5.96	16.5	96	35.8	65.9	139.2	64.1
01LL17-1		pyritic black argillite	494666	6525387	< .2		1976		4	1.9	0.23	0.23	< 5	20.7	0.06	1.65	76.23	7.43	260.1	237	219.2	88.3	8.2	219.9
01LL12-5		amphibolite + dissem. pyrite	494071	6532127	92.9		63		14.7	0.8	0.14	0.32	< 5	0.4	< .02	0.04	70.97	2.31	34.8	443	9.4	14.5	14.4	32.7
01LL12-8		sheared garnet amphib. + pyrite	494182	6532628	3.2		150		3	0.4	0.2	0.3	15	0.6	0.08	0.09	109.86	14.98	131.4	923	106.3	28	38.3	25.2
NOTES																								
Analysis of steel milled crushed rock prepared by ACME Analytical																								
ARMS = Aqua regia digestion - ICPMS																								
ACM = ACME Analytical, Vancouver																								
99999 = recommended re-assay																								

ceous exhalative origin. Like the pyritic-garnetiferous cherts of the lower Dorsey assemblage, it contains anomalous manganese and barium (sample 01LL7-7a, Table 2).

Porphyry-Style Mineralization in the Nizi Pluton

Prominent gossans, including the Perm and Corydalis showings, occur within the Nizi pluton. They are cross-cutting, linear, probably fracture-controlled zones, with west-northwesterly trends. The Perm is a prominent gossan on the bare west face of Tetipistikwan Mountain above the Four Mile River, roughly 50 metres across and 600 metres in strike length. The Corydalis gossan crosses a spur ridge of the mountain in the headwaters of Nizi Creek. Somewhat less intense than the Perm, it is 200 metres across and 600 metres in strike length. Within the gossans, plagioclase-porphyry dikes and zones of finely comminuted intrusive breccia cut the main-phase tonalites, diorites and gabbros of the pluton. The intrusive breccias incorporate angular clasts of their country rocks. They characteristically contain rounded, milled single-crystal plagioclase and hornblende fragments in a matrix of dust-sized rock debris cemented by secondary silica. Many are laced with fine quartz veinlets. Disseminated pyrite and lesser chalcopyrite occur throughout the matrix, as well as in fractures in the surrounding country rock. Samples from these gossans contain 1100-1400 ppm Cu, with anomalous Ag, Zn and Hg (Table 2).

These gossans are not described in assessment reports, although very old claim posts lie on them. The posts may date from early exploration of the Kirk or Four Mile property (MINFILE 104P 027; Gabrielse, 1963, p. 113). The Four Mile property, a shear-hosted copper-silver prospect, is located in McDame map area 10 kilometres to the north in the Four Mile River valley. It was staked for the first time by Beale Carlick, the Kaska trapper and prospector after whom Beale Lake and Beale Mountain were named.

Quartz-Carbonate-Mariposite Alteration Zones and Mesothermal Gold Vein Potential

Ultramafic bodies in the belt of Slide Mountain rocks along the eastern margin of the Cassiar Batholith are extensively altered to orange-weathering iron-magnesium carbonate, veined with quartz and carrying significant mariposite in some areas. This type of alteration is associated with the gold-quartz veins of the Cassiar camp (Pantaleyev and Diakow, 1982, Nelson and Bradford, 1993). Three alteration zones are exposed on ridges, separated by overburden-covered valleys. Overall the system extends over 8 kilometres along strike. Our samples were mildly anomalous in As, Sb, and Mn, as well as the ultramafite-related suite Ni-Co-Cr.

Polymetallic Veins

Polymetallic veins are the best-known deposit type in the Beale Lake map area. The Nizi property has been the target of several advanced exploration programs, including drilling. The current Beale Lake claims (previously held as the Keel and the Flag claims) and the RN claims have been systematically prospected and geochemically sampled. This report and the companion geological map (Nelson and Lepage, 2002) document and precisely locate the known showings, as well as previously unreported veins discovered in the course of field work this year.

Nizi Epithermal Vein System (MINFILE 104I-032)

Mineralization on the Nizi property is a vein-stockwork system with associated hydrothermal brecciation, cospatial and probably cogenetic with the relatively young Zinc Lake volcanic/intrusive suite ("Nizi volcanics" of Plint *et al.,* 1997). Known veins occur over a northwesterly-elongate area 2 kilometres long by 1 kilometre wide.Two distinct mineralization styles are present: sulphide-poor, gold-silver-quartz veins and stockworks associated with pervasive silicification, and sulphide-rich iron carbonate-sphalerite-galena veins associated with pervasive carbonate alteration. Six main mineralized areas have been outlined, the Zinc Lake Zone, Discovery Vein/Surprise Vein, Grizzly Ridge Vein, H Zone, Gully A Zone and B Zone, mainly through the exploration and drilling programs of Gold Giant Minerals Incorporated in 1987-1992 (Cavey and Chapman, 1992; McIntosh and Scott, 1991). In 1996, Madrona Mining drilled six holes, five in the Discovery/Surprise vein area, and one to test the southeastern extension of the Zinc Lake Zone (Plint *et al*., 1997). The core from this project is stored at the east end of Beale Lake.

The Discovery/Surprise Vein area represents the best exploration target identified to date on the Nizi Property. It is characterized by multistage, microcrystalline quartz-carbon-sulphide-barite stockworks with very fine-grained pyrite, galena, sphalerite, chalcopyrite, tetrahedrite and acanthite. Assay values up to 41.0 g/t Au were obtained from these veins, with typical channel samples returning 1.5 to 30 g/tonne Au and 190 to 1200 g/tonne Ag over 1-2 metres (Bond, 1993).

The Gully A and B zones are iron carbonate-microcrystalline quartz-rhodochrosite-sphalerite-galena-pyrite veins; the H Zone, banded carbonate-quartz-sphalerite-galena-pyrite veins. Both are controlled by north-striking subvertical fractures and/or shears. A 1.8 metre chip sample of H Zone sphalerite-galena- pyrite-carbonate-rhyolite breccia returned values of 2.26 g/t Au, 278.1 g/t Ag; best grab sample assays from the Gully Zone are 11.38 g/t Au and 22.4 g/t Ag (Bond 1993).

Plint *et al*. (1997) show that the galena lead isotopic signature of the Nizi plots above, and near the very young end of the shale curve defined by Godwin and Sinclair (1982). It is similar to lead from veins and skarns near the Seagull Batholith, the Cassiar gold-quartz veins, Midway, Butler Mountain and other Cretaceous-Early Tertiary epigenetic deposits in the Cassiar area (Bradford, 1988). The coincident centering of the alteration halo and the gold-quartz veins around the rhyolites near Zinc Lake strongly favors cogenesis between Nizi volcanic activity and the epithermal event. Gabrielse (1994) assigned the kaolinized quartz-orthoclase porphyry rhyolite on the Nizi property to the Eocene suite, by correlation with the Major Hart pluton

(Figure 2). The entire Zinc Lake volcanic/intrusive sequence is tentatively assigned to the Eocene. It is thus possible that igneous/hydrothermal systems ranging from intrusion-related to epithermal may extend from the Major Hart pluton as far north as the Four Mile River.

Beale Lake Intrusion-Related Vein System (MINFILE 104I-098)

Gold and silver-bearing quartz-sulphide veins were first discovered on the ridge north of Beale Lake in 1982-3 by the Cassiar Joint Venture, who conducted grid soil sampling and prospecting (Fleming, 1983). In 1996, following the Cry Lake regional geochemical data release (Jackaman, 1996), the ground was restaked in 1996 by Westmin Resources Ltd., and contour soil sampling and limited prospecting carried out (Jones, 1997), mainly aimed at volcanogenic massive sulphide-style targets. The current property owners have collected new, and reinterpreted existing, soil geochemical data; and conducted further prospecting (Durfeld and Fleming, 2001). Their work identifies a set of veins with overall dimensions of 1 by 2 kilometres, which comprises two compositionally and spatially distinct styles of gold mineralization. To the west, quartz-arsenopyrite- pyrite-scheelite veins are associated with Au-As-W-Bi anomalies. To the east, quartz-base metal sulphide veins are associated with anomalous values of Au, As, Pb, and local Ag, Zn, Sb, Cu and Bi. They suggest a zoned, intrusion-related gold system.

The Beale Lake veins are hosted by metamorphosed sedimentary and volcaniclastic rocks of the upper Dorsey assemblage. Our traverses in 2001 relocated some of the sampled veins, including a prominent trench in silicified vein breccia from which Durfeld and Fleming (2001) report 27 and 41 g/tonne Au in grab samples, and a quartz-arsenopyrite-galena vein from which they report 2.5 g/tonne Au, 5.5 g/tonne Ag. Repeat grab samples from these veins returned geochemically highly anomalous Au and Ag (Au to 2716 ppb by fire assay) (Table 2). Although in the alpine, much of the property is covered by overburden. Mineralized quartz vein float throughout the area hints at additional, unexposed veins.

Gunsight (MINFILE 104I-041)

The Gunsight showing was discovered during preliminary exploration in 1992, on claims adjoining the Nizi property to the south (RN Group; Termuende, 1993). It is a west-northwesterly-striking quartz vein with argentiferous galena, pyrite and sphalerite. One 20-centimetre sample contained .09 g/tonne Au, 110 g/tonne Ag, 8.36% Pb and 3.09% Zn. The vein is associated with brecciated hornblende granodiorite of the Permian Nizi pluton. This vein may relate to the Nizi system, to the Beale Lake veins, or to the porphyry-style occurrences near the headwaters of Nizi Creek. It was not visited this season.

New Discoveries

Two polymetallic veins were encountered during 2001 traverses southeast of Beale Lake, on ground not covered by assessment reports. One, the No Fish vein, outcrops in a waterfall in a north-draining creek. It is 2-8 centimetres wide and strikes west-northwest. The other, the Yurso vein, outcrops in the pass at the head of the creek, where it has been traced as subcrop over 1000 metres along a northwesterly strike (Nelson and Lepage, 2002). The No Fish vein contains pyrite, and a grey metallic mineral. It is anomalous in Cu, Se, Te, Ag, Mn and Co (Table 2). The Yurso vein contains arsenopyrite, pyrite, stibnite and tetrahedrite. Analyses show it to be highly anomalous in a broad suite of metals, including gold (to 1250 ppb), silver (to 1824 g/t), bismuth (to 413 ppm), lead (to 23,000 ppm), antimony (to 8000 ppm), as well as Se, Te, Cu and Zn. Heavily oxidized vein fragments of secondary base metal sulphates and carbonates, such as anglesite and smithsonite, are abundant in float downslope from the projected vein trace. The largest pieces of vein material are 20-30 centimetres in their shortest dimension (Figure 7).

The fracture that hosts the Yurso vein is also occupied by granite porphyry dikes that contain round quartz and orthoclase megacrysts. They may be offshoots from the nearby Cassiar Batholith, or younger, Late Cretaceous-Eocene intrusions. Some show strong argillic alteration, which also affects rocks of the upper Dorsey assemblage around the vein.

These vein occurrences are on strike with, and 2 to 5 kilometres southeast of the Beale Lake vein set. They suggest that it may extend through the low-lying country around Beale Lake and, potentially, onto 104I/15. The granite porphyry dikes that accompany them lend strength to the inferred connection between late plutonic activity and gold mineralization.

CONCLUSIONS

This investigation of the Beale Lake map area has produced some significant changes to our understanding of the southern Sylvester Allochthon. Most important, it has firmly established and made specific the correlation of the uppermost, deformed pericratonic allochthon with the Dorsey assemblage west of the Cassiar Batholith. This relationship was previously published only in abstracts, as a suggestion based on perceived general similarities. It is now clear that the same two twofold unit subdivision can be

Figure 7. Typical chunk of the Yurso vein, rusty-stained quartz with pyrite, arsenopyrite, tetrahedrite and stibnite.

equally applied to the Dorsey assemblage in its type area, and to the pericratonic assemblage in the Sylvester Allochthon. The lower unit, with its extensive cliff-forming amphibolites, is recognizable in localities from the Swift River valley in southern Yukon (Stevens and Harms, 1985) to the west face of Beale Mountain. The upper unit, with its felsic volcanic component, is probably equivalent to Mississippian felsic units in the Yukon-Tanana Terrane, including those known to host volcanogenic massive sulphide deposits.

Structurally below the Dorsey assemblage, the Sylvester Allochthon can be divided into two distinct assemblages, a lower one of oceanic and a middle one of island arc affinity. This accords with the gross structure of the allochthon between the Dease River and the Yukon border. The mid-Permian Meek and Nizi plutons form parts of a single complex that intrudes the middle, arc-related, assemblage. Referred to here as the Four Mile assemblage, it shares a broad age and affinity with Division III, the middle unit of the allochthon farther north. However, in detail these two units differ significantly enough to warrant separate unit names. As exposed in the Huntergroup Range and on Juniper Mountain near Cassiar, Division III is dominated by Pennsylvanian-Permian augite-phyric basaltic andesites and limestone-limestone breccia-chert sequences (Nelson and Bradford, 1993). In contrast, the most extensive unit in the Four Mile assemblage is a complex of nearly aphanitic dacite to rhyolite flows. The deformed phyllite is also unique to this area. This diversity is typical of island arc sequences, which can comprise a wide variety of volcanic sources and evanescent sedimentary environments.

Polymetallic, precious metal-bearing veins are widespread in the eastern part of the map area, including the epithermal Nizi vein system associated with young volcanic rocks in the north, and the deeper, intrusion-related Beale Lake system. The latter is now shown by new discoveries this summer to extend at least 5 kilometres south of Beale Lake. These results, combined with the pattern of Au and Ag and As, Sb, Bi and Hg in stream sediments that extends from Beale Lake area to the eastern border of Cry Lake map area (Jackaman 1996), suggests that the potential for further intrusion-related gold discoveries is alive and well in the Cassiars.

ACKNOWLEDGEMENTS

The study area lies within the traditional territory of the Kaska Dene. We acknowledge the warm welcome of the Dease River Band, in particular Mr. Frank Dennis, Band Chief, and Mr. Walter Carlick, Band Manager. Two members of the band, Damian Leonard and Christian Carlick, participated in the field work. Their enthusiasm and interest in mineral exploration in the Beale Lake area were much appreciated.

This project would never have happened without the astute observations of Hu Gabrielse and Tekla Harms. Luc Lepage helped make the map happen, from negotiating hairy gullies, to discovering new showings and geological gems, to alligator wrestling with printer drivers in the dreaded Blanshard Bayou. Thanks to Dave Lefebure for a good job of textual tuning. Aesthetics by Janet Holland.

REFERENCES

Bond, W.D. (1993): Geological, geochemical and diamond drill report on the Nizi mineral claims, Gold Fields Canadian Mining Ltd. *British Columbia Ministry of Energy, Mines and Petroleum Resources*, Assessment Report 22840.

Bradford, J.A. (1988): Geology and genesis of the Midway silver-lead-zinc deposit, north-central British Columbia, unpublished M.Sc. thesis, *The University of British Columbia*, 280 pages.

Cavey, G. and Chapman, J. (1992): Report on the Nizi Project for Gold Giant Minerals Inc., Liard Mining Division, British Columbia, NTS 104I/14,15 and 104P2,3. Private Report.

Durfeld, R.M. and Fleming, D.B. (2001): Summary report on the Beale Lake gold property; Private Report.

Fleming, D.B. (1983): Beale Lake property, 1983 geochemical assessment report, *British Columbia Ministry of Energy, Mines and Petroleum Resources,* Assessment Report 12181.

Gabrielse, H. (1963): McDame Map Area, Cassiar District, British Columbia, *Geological Survey of Canada*, Memoir 319, 138 pages.

Gabrielse, H. (1994): Geology of Cry Lake (104I) and Dease Lake (104J/E) Map Areas, North Central British Columbia; *Geological Survey of Canada*, Open File Map 2779.

Gabrielse, H. (1998): Geology of Cry Lake and Dease Lake map areas, north-central British Columbia, *Geological Survey of Canada*, Bulletin 504, 147 pages.

Gabrielse, H., and Harms, T.A., (1989). Permian and Devonian plutonic rocks in the Sylvester allochthon, Cry Lake and McDame map areas, northern British Columbia; *in* Current Research Part E, *Geological Survey of Canada,* Paper 89-1E, pages 1-4.

Gabrielse, H., Mortensen, J.K., Parrish, R.R., Harms, T.A., Nelson, J.L., and van der Heyden, P. (1993): Late Paleozoic Plutons in the Sylvester Allochthon, Northern British Columbia; *in* Radiogenic Age and Isotopic Studies, Report 7, *Geological Survey of Canada*, Paper 93-1, pages 107-118.

Godwin, C.J. and Sinclair, A.J. (1982): Average lead isotope growth curves for shale-hosted zinc-lead deposits, Canadian Cordillera: *Economic Geology*, Volume 7, pages 675-690.

Harms, T.A. (1986): Structural and tectonic analysis of the Sylvester Allochthon, SW McDame map area, northern British Columbia: Implications for paleogeography and accretion. Unpublished Ph. D. thesis, University of Arizona, 80 pages.

Harms, T.A. (2000): Proposed terrane affinities of pericratonic assemblages in northern British Columbia and southern Yukon, Canada; *Geological Society of America,* Abstracts with Programs, Volume 32, page A-17.

Harms, T.A. and Stevens, R.A. (1996): Assemblage analysis of the Dorsey Terrane; Slave-Northern Cordillera Lithospheric Evolution (SNORCLE) and Cordilleran Tectonics Workshop, Report of the 1996, Combined Meeting; pages 199-201.

Hunt, P.A. and Roddick, J.C. (1988): A compilation of K-Ar ages, Report 18, *in* Radiogenic Age and Isotopic Studies: Report 2, *Geological Survey of Canada*, Paper 88-2, pages 127-153.

Jackaman, W. (1996): British Columbia Regional Geochemical Survey: NTS 104/I - Cry Lake; Stream Sediment and Water Geochemical Data; B.C. RGS 44; *British Columbia Ministry of Employment and Investment* Open File; B.C. RGS 44, 52 pages.

Jones, M.I. (1997): Flag property, 1996 assessment report, Flag 1 to 4 claims; Geological mapping and soil sampling surveys, Liard Mining Division, NTS map area 104I/14, Latitude 58°54'00"N, Longitude 129°09'00"W, British Columbia Ministry of Energy and Mines Assessment Report 25044.

McIntosh, R. and Scott, G. (1991): Report on the Cry Lake Project for Omega Gold Corporation, Liard Mining Division, British Columbia, NTS 104I; Internal Company Report.

Mihalynuk, M. Nelson, J.L. and Friedman, R.M. (1998): Regional geology and mineralization of the Big Salmon Complex (104N NE and 104O NW), *in* Geological Fieldwork 1997, British Columbia Ministry of Employment and Investment, *Geological Survey Branch*, Paper 1998-1, pages 6-1 to 6-20.

Mihalynuk, M.G., Nelson, J., Roots, C.F. and Friedman, R.M. (2000): Ancient Pacific Margin part III: Regional geology and mineralization of the Big Salmon Complex (104N/9,10 & 104O/12,13,14W); *in* Geological Fieldwork 1999, *British Columbia Ministry of Energy and Mines*, Geological Survey Branch, Paper 2000-1, pages 27-46.

Nelson, J.L. (1993): The Sylvester Allochthon: Upper Paleozoic marginal basin and island-arc terranes in northern British Columbia; *Canadian Journal of Earth Sciences*, Volume 30, pages 631-643.

Nelson, J. (2001): Cross sections of the allochthonous units west of the Cassiar Batholith and the Sylvester Allochthon: Pancake tectonic stratigraphy above the Cassiar Platform; *in* Slave-Northern Cordillera Lithospheric Evolution (SNORCLE) and Cordilleran Tectonics Workshop, Report of the 2001 Combined Meeting; pages 76-77.

Nelson, J. (1999): Devono-Mississippian VMS Project: Continuing studies in the Dorsey Terrane, northern British Columbia; *in* Geological Fieldwork 1998, *British Columbia Ministry of Energy and Mines,* Geological Survey Branch, Paper 1999-1, pages 143-155.

Nelson, J.L. (2000): Ancient Pacific Margins Part VI: Still heading south: Potential VMS hosts in the eastern Dorsey Terrane, Jennings River(104O/1; 7,8,9,10); *in* Geological Fieldwork, 1999, *British Columbia Ministry of Employment and Investment,* Geological Survey Branch, Paper 2000-1, pages 107-126.

Nelson, J. and Bradford, J.A. (1993): Geology of the Midway-Cassiar area, northern British Columbia; *British Columiba Ministry of Energy, Mines and Petroleum Resources,* Bulletin 83, 94 pages.

Nelson, J., and Lepage, L.D. (2002): Geology and mineral occurrences, Beale Lake map area (NTS 104I/14N) . *British Columbia Ministry of Energy and Mines,*Open File Map 2002-6, 1:50,000 scale.

Pantaleyev, A. (1980): Cassiar Map-Area. *British Columbia Ministry of Energy, Mines and Petroleum Resources*, Geological Fieldwork 1979, Paper 1980-1, pages 51-60.

Pantaleyev, A., and Diakow, L.J. (1982): Cassiar Gold Deposits, McDame Map Area (104P/4,5), *British Columbia Ministry of Energy, Mines and Petroleum Resources,* Geological Fieldwork 1981, Paper 1982-1 pages 156-161.

Plint, H., McMillan, W.J. , Nelson, J. and Pantaleyev, A. (1997): The Nizi property: a classic (Eocene?) epithermal gold system in far northern British Columbia;) *in* Geological Fieldwork, 1997, *British Columbia Ministry of Employment and Investment,* Geological Survey Branch, Paper 1998-17, pages 17-1 to 17-13.

Roots, C.F. and Heaman, L.M. (2001): Mississippian U-Pb dates from Dorsey terrane assemblages in the upper Swift River area, southern Yukon; *in* Current Research, *Geological Survey of Canada,* Paper 2001-A1, 9 pages.

Stevens, R.A. and Harms, T.A. (1995): Investigations in the Dorsey Terrane, Part I: Stratigraphy, structure and metamorphism in the Dorsey Range, southern Yukon Territory and northern British Columbia; *in* Current Research, *Geological Survey of Canada,* Paper 1995A, pages 117-127.

Termuende, T. (1993): Assessment Report for the RN claim group, Liard Mining Division, NTS 104I/14E, 104I/15W, Latitude 59°00'N, Longitude 129°15'W, *British Columbia Ministry of Energy and Mines,* Assessment Report 22946.

Preliminary Geology of the Cariboo Lake Area, Central British Columbia (093A/11, 12, 13 AND 14)

By Filippo Ferri[1] and Brian H. O'Brien[2]

KEYWORDS: *Barkerville Terrane, Cariboo Terrane, Kootenay Terrane, Snowshoe Group, Keithley, Harveys Ridge, Agnes conglomerate, Goose Peak quartzite, Downey, Ramos, Frank Creek volcanics, Mount Barker volcanics, geochemistry, Unlikely, Frank Creek, Ace, volcanogenic massive sulphide, VMS, besshi, sedimentary exhalative, SEDEX.*

INTRODUCTION

This paper summarizes work in the second year of the Barkerville Mapping Project, a multi-year program examining the stratigraphic and structural setting of massive sulphide mineralization hosted by Snowshoe Group stratigraphy in the Cariboo Lake area. These relatively new sulphide occurrences are of volcanogenic or sedimentary exhalative origin and are best represented by the Ace Cu-Pb-Zn-Au-Ag (MINFILE 093A 142) and Frank Creek Cu-Pb-Zn-Au-Ag (MINFILE 093A 152) showings (Figure 1).

The main aims of this project are: 1) a better understanding of the geological setting of the Frank Creek and Ace mineral occurrences; 2) define the regional extent, nature and significance of metavolcanic rocks associated with the Frank Creek showing; 3) evaluate the nature and significance of metavolcanic rocks within the Downey succession, and, 4) test a model suggesting the inversion of Snowshoe stratigraphy (Höy and Ferri, 1998a). The objectives of the 2001 field program were to extend mapping northeastward toward Little River, northwestward across Cariboo Lake and onto the Snowshoe Plateau (Figure 2). This latter area is dominated by sub-amphibolite grade sections of Snowshoe stratigraphy and it was anticipated that it would provide an opportunity to recognize stratigraphic units delineated during the 2000 season.

Approximately 60 days were spent in the field from the beginning of June to the third week of August. A base was set up in Likely, which is the nearest source of supplies for the Cariboo Lake area. This small centre is reached by paved road from a turn-off some 20 kilometres south of Williams Lake on Highway 97 (Figure 2). Logging roads extend westward from Likely and cover a large portion of the sub-alpine regions of the map area. A very rough, 4-wheel drive quad road traverses the Snowshoe Plateau and connects the Keithley and Cunningham creek valleys.

[1] *British Columbia Ministry of Energy and Mines*
[2] *Geological Survey of Newfoundland and Labrador*

Two principal areas were mapped: 1) An area within the Goose Range which is bounded by Little River to the north, Ishkloo Creek to the west, Barkers Creek to the east and the headwaters of Grain Creek to the southwest; 2) a region that occupies the northwest side of Cariboo Lake and is bounded by Kangaroo and Spinks creeks to the southwest and Sixbee Creek to the northeast. The northwest boundary is within the Snowshoe Plateau, and roughly corresponds to a line between Roundtop Mountain, Yanks Peak and Coyote Hill (Figure 3a).

The Snowshoe Plateau and Goose Range represent the first large area of elevated terrain as one leaves the interior plateau and before entering the rugged Cariboo Mountains to the east. Relief is moderate with peaks reaching 2100 metres and alpine occurring at approximately 1700 metres. Many of the ridges within the Snowshoe Plateau occur just above timberline and allow easy travel.

This work builds on mapping south of Cariboo Lake by Ferri (2001a, b). A detailed account of previous work within the Barkerville - Wells area is given by Struik (1988). The present map area was covered at a regional scale by Campbell (1978) and at a more detailed level by Struik (1983a, b; 1988). Lang (1938, 1939) first mapped the area around Keithley Creek and the region between Yanks Peak and Roundtop Mountain. Holland (1954) re-examined this latter area in hopes of shedding new light on this economically important region. Panteleyev *et al*. (1996) mapped Quesnel Terrane rocks to the west and also gave a good account of regional geology. Rees (1987), as part of a Ph.D. dissertation, examined in considerable detail the boundary between the Quesnel and Barkerville terranes between Cariboo Lake and Mount Brew. Höy and Ferri (1998a, b) described Pb-Zn deposits of the Cariboo and Barkerville terranes, and Ferri *et al.* (1999) detailed the age, composition and tectonic significance of the western Quesnel Lake Gneiss.

REGIONAL SETTING

The Late Proterozoic to Paleozoic Snowshoe Group is a dominantly siliciclastic package of continental derivation that most likely represents the distal western edge of Ancestral North America. This fault-bounded sequence is stratigraphically distinct from other packages around it and as such has been called the Barkerville Subterrane, a subset of the Kootenay Terrane, with which it shares many similarities (Struik, 1986, 1988). East of the Snowshoe Group, across the westerly-verging Pleasant Valley thrust, are rocks

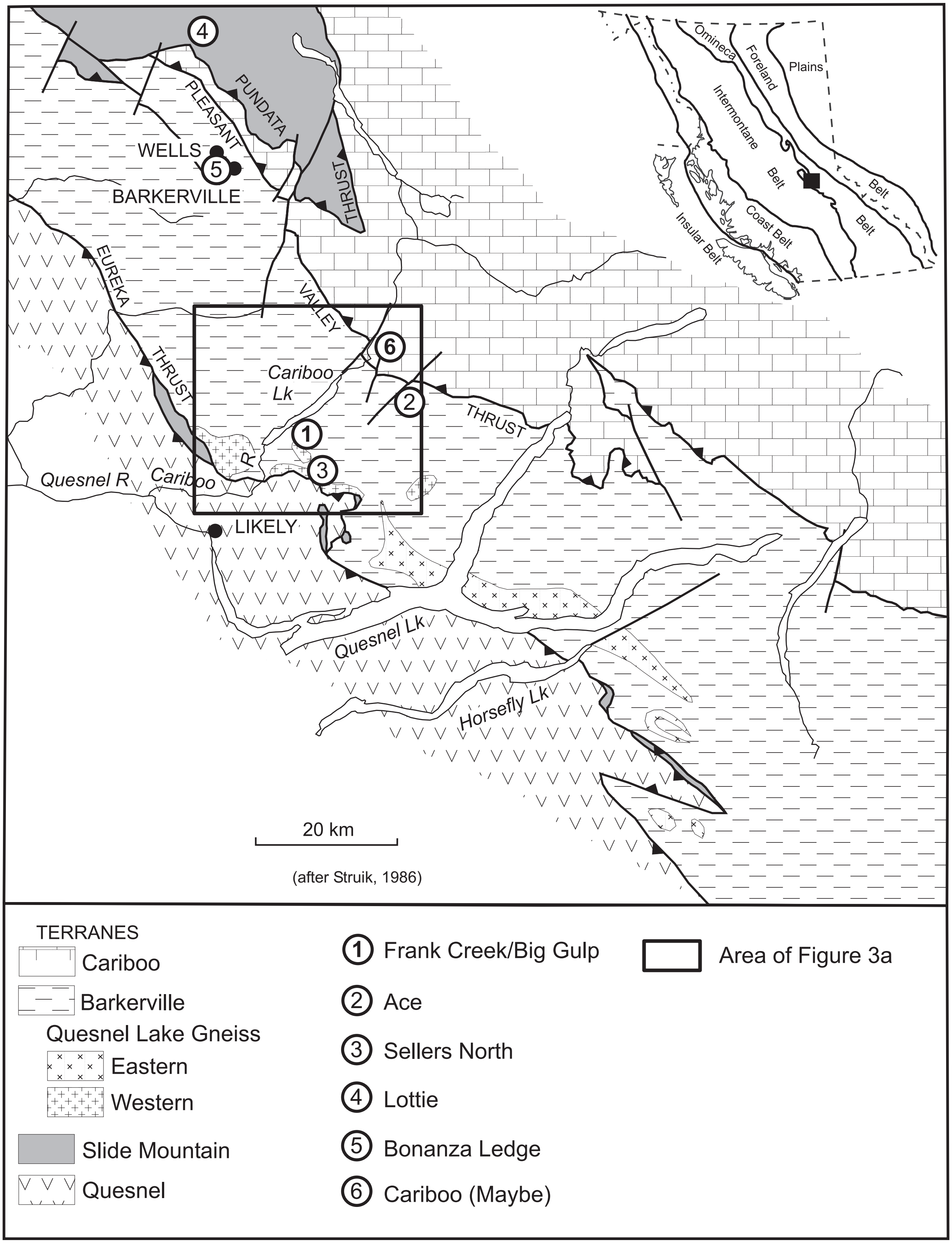

Figure 1. Generalized geological setting of the study area, together with some of the more significant mineral showings in the Barkerville and Cariboo terranes.

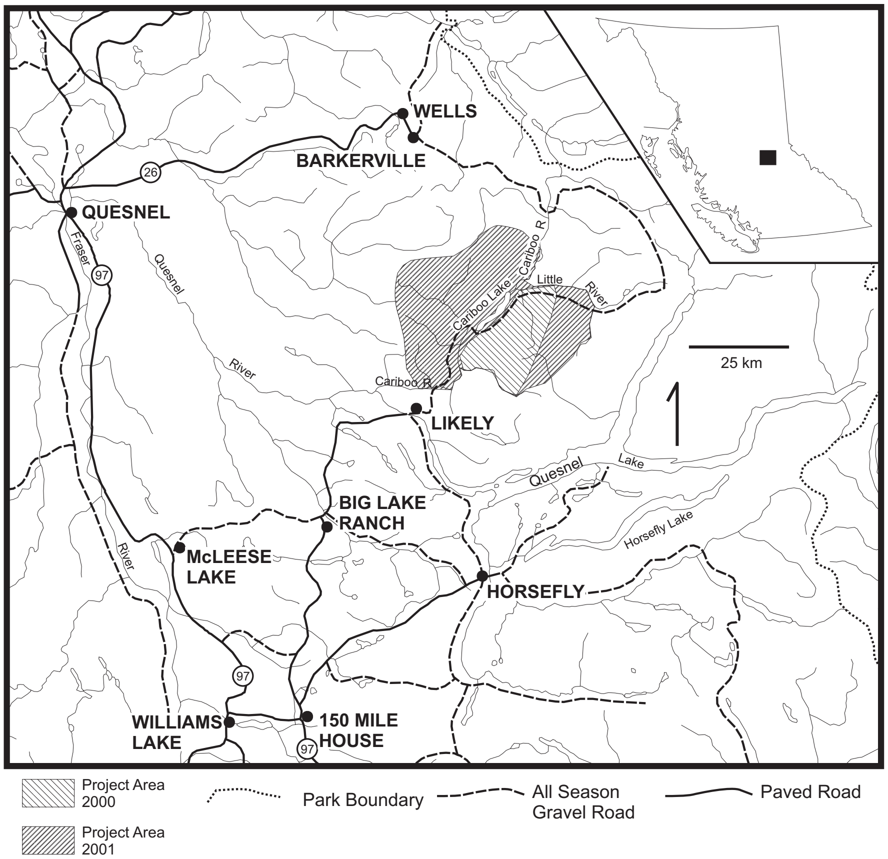

Figure 2. Location of the Cariboo Lake study area.

of the Kaza, Cariboo and Black Stuart groups, which also contain an abundance of siliciclastics, but with facies which suggest a more proximal continental shelf setting. Many of these units can be correlated with similar stratigraphy within Ancestral North American rocks. These rocks are placed within the Cariboo Subterrane, representing, like the Cassiar Terrane to which it belongs, a displaced piece of Ancestral North America (Struik, 1986, 1988). The west flank of the Snowshoe Group is occupied by the Quesnel Terrane, a composite volcanic-arc sequence dominated by Mesozoic mafic to intermediate volcanic rocks. It is separated from the Snowshoe Group by the easterly-directed Eureka thrust fault along which are slivers of mafic and ultramafic rocks assigned to the Crooked Amphibolite. This latter package has been correlated with rocks of the Slide Mountain Terrane, an assemblage of ocean floor volcanic and sedimentary rocks which structurally straddle the Barkerville and Cariboo terrane lithologies along the Pundata Thrust north of Wells (Figure 1).

Although the Snowshoe Group has an overall stratigraphic sequence distinct from that of the Cariboo Subterrane, there are similarities between the two, particularly with rocks of the Cariboo Group (Figure 4). This resulted in early workers taking stratigraphic terminology developed within the Snowshoe Plateau and extending it eastward into rocks of Cariboo Mountains (*see* Struik, 1988). This led to stratigraphic problems until Campbell *et al*. (1973) realized that the two sequences were quite distinct and required redefinition and new type sections. As a result, Struik (1988) formally reassigned rocks within the Snowshoe Plateau to the Snowshoe Group.

The present structural interleaving of the various terranes and dominant structural fabrics resulted from deformation which began in early Middle Jurassic time, although there may be earlier events of Permo-Triassic or Devono-Mississippian age. The latter is supported by the presence of the Early Mississippian Quesnel Lake Gneiss, possibly related to arc volcanism (Ferri *et al.*, 1999). Jurassic deformation resulted from the easterly thrusting of the Quesnel and Slide Mountain terranes on to the Snowshoe Group along Eureka and Pundata thrusts. There are three sets of penetrative cross-cutting structural features within the map area with metamorphism reaching amphibolite grade during the second period of deformation.

The Snowshoe Group has been subdivided into several informal units or successions by Struik (1988; Figure 4). It is dominated by siliciclastic rocks with lesser carbonate and volcanic sequences. Due to the penetrative fabric and lack of suitable lithologies for geochronology and preservation of fossils, there are few age constraints for this package. Regional correlations and scant fossil remains indicate a Late Proterozoic to Late Paleozoic age (Figure 4). The lower to middle Snowshoe Group is broadly correlative with the Kaza and lower to middle Cariboo Group (Figure 4, Struik,

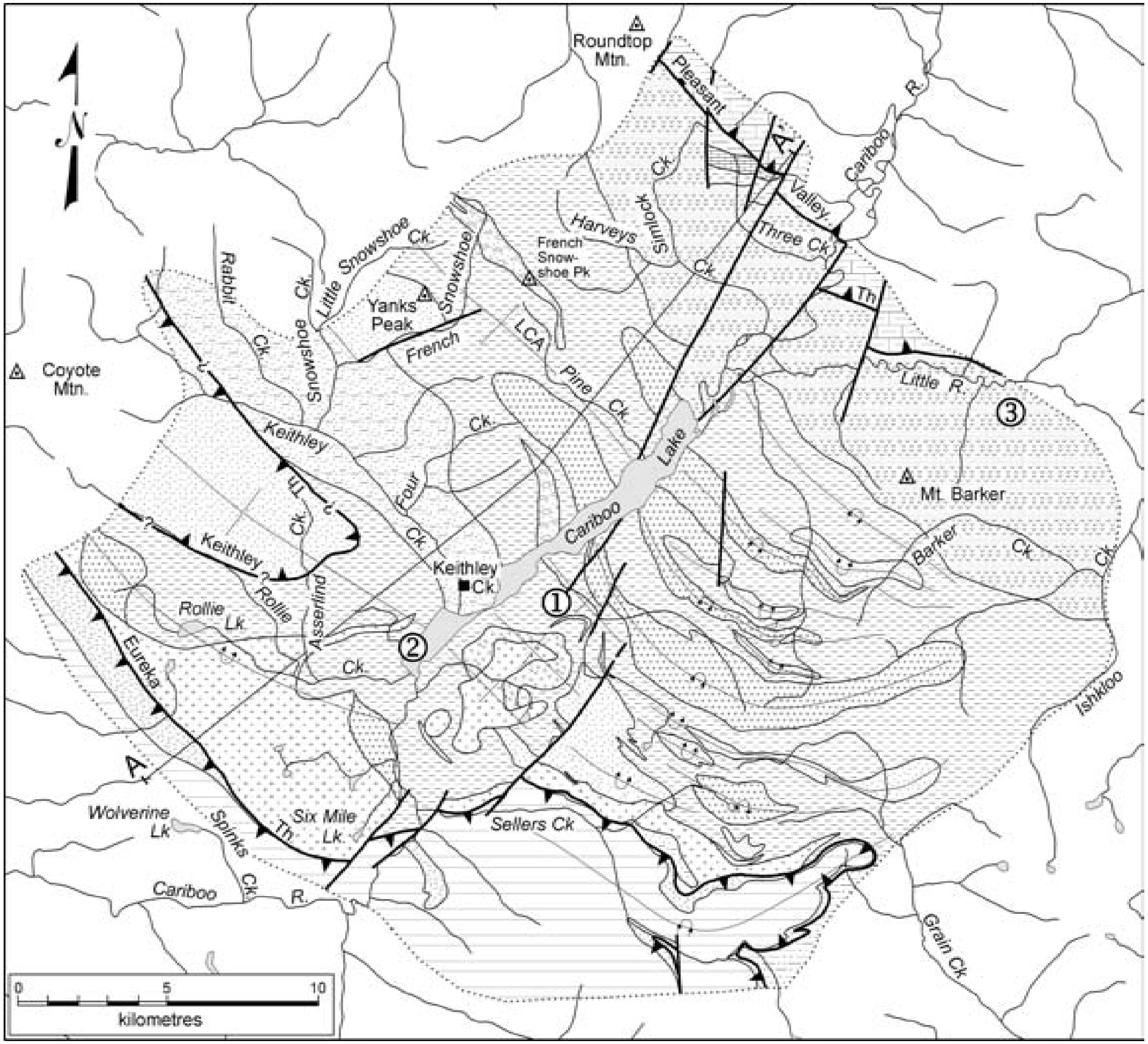
N
Roundtop Mtn.
Pleasant
Valley
Three Ck
Cariboo R.
A'
Simlock Ck.
Harveys
French Snow-shoe Pk
Th
Little R.
③
Mt. Barker
Barker Ck.
Ck.
Ishkloo
Little Snowshoe Ck.
Snowshoe
Snowshoe Ck.
Rabbit Ck.
Yanks Peak
French
LCA
Pine Ck.
Coyote Mtn.
Keithley
Th
Ck.
Keithley
Four Ck.
Cariboo Lake
Keithley Ck.
①
②
Rollie
Rollie Lk.
Asserlind
Ck.
Eureka
A
Wolverine Lk
Spinks Ck.
Th
Six Mile Lk.
Sellers Ck
Cariboo R.
Grain Ck
0
5
10
kilometres

Figure 3a.

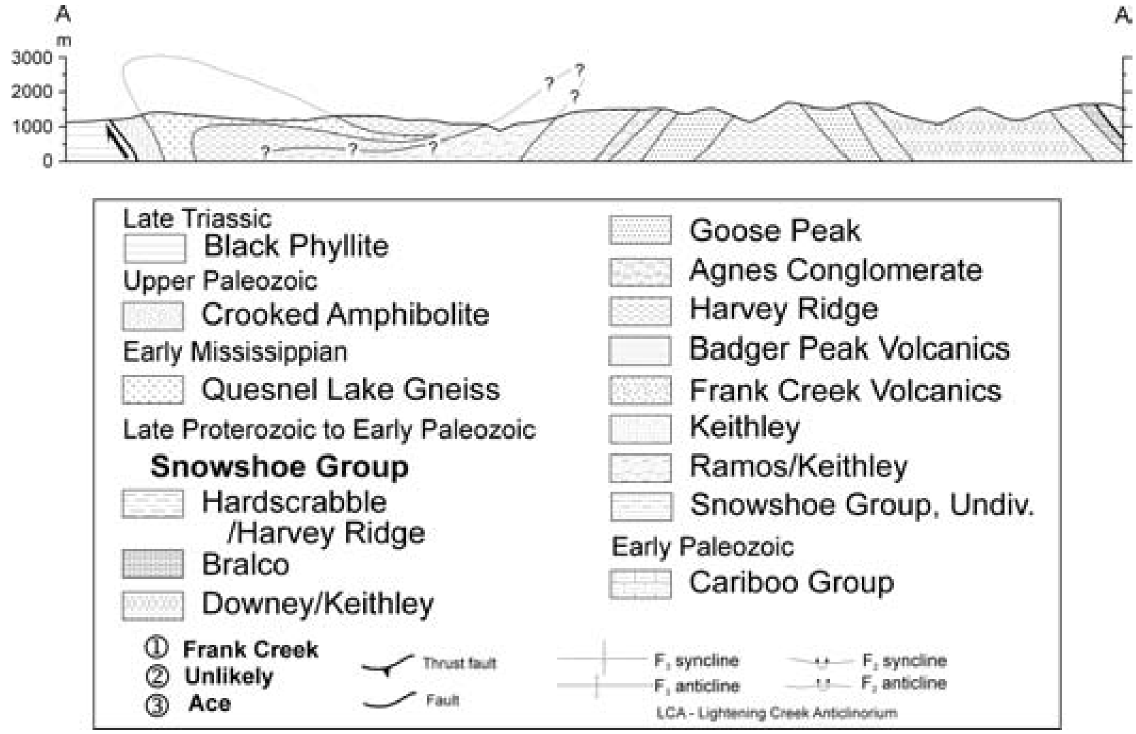

Figure 3. (a) Simplified preliminary geologic map of the Cariboo Lake area. (b) Simplified structural cross-sesction.

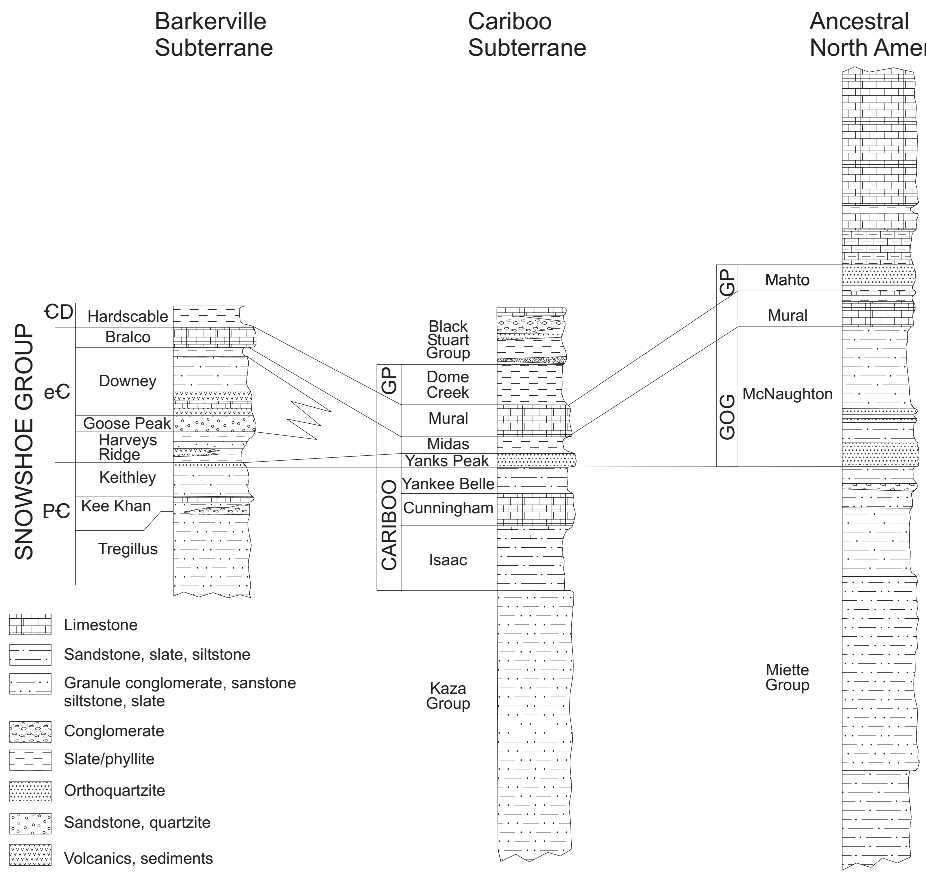

Figure 4. Generalized stratigraphic columns of the Barkerville and Cariboo subterranes and Ancestral North American rocks showing possible correlations of Snowshoe Group stratigraphy (modified from Struik, 1986).

1986). The coarse clastics of the Goose Peak quartzite, in conjunction with the volcanics of the Downey and inferred post-Early Cambrian age for the Bralco Limestone, have no direct correlatives within rocks of the Cariboo Subterrane. This would be resolved, in part, if the Bralco limestone (of the Snowshoe Group) correlates with the Mural Formation, a suggestion indirectly inferred by Struik (1988) who correlates the Bralco with the Archaeocyathid-bearing Tshinakin limestone of the Eagle Bay Formation (Schiarizza and Preto, 1987) implying it is age-equivalent to the Mural Formation.

LITHOLOGIC UNITS

Mapping this past summer encountered all units delineated during the 2000 field season (Ferri, 2001a, b). These include rocks of the Keithley, Harveys Ridge, and possibly Downey successions together with the Goose Peak quartzite and Agnes conglomerate. In addition, clastics, marble and minor igneous rocks along Keithley Creek that are assigned to the Ramos succession by Struik (1988, 1983a), may be all, or in part, equivalent to the Keithley succession. Early Mississippian foliated granite of the Quesnel Lake Gneiss intrudes Snowshoe rocks along the southwestern margin of the map area. Geologically, the southern part of the map area is structurally bounded by mafic to ultramafic rocks of the Crooked Amphibolite and dark grey phyllites and siltstones of Late Triassic age which belong to the basal Nicola Group (as per Panteleyev *et al*., 1996) and have been informally termed the "Black Phyllite" (Rees, 1987).

The light coloured, relatively thin and intermittent, orthoquartzite at the top of the Keithley succession was used as an excellent marker during the 2000 field season. Although sporadic and poorly exposed in sub-alpine areas, this unit can be used in conjunction with the contrasting lithologies of the Keithley schists and sandstones, and dark phyllites and sandstones of the Harveys Ridge, to establish overall map patterns. This was also the case during the 2001 field season, although the Keithley quartzite was only encountered in several areas, either due to limited outcrop or non-deposition.

BLACK PHYLLITE

The Black phyllite was only seen in sporadic outcrops in the Spinks Creek area and along the main logging road on the west side of the Quesnel River, south of Cariboo Lake. These rocks consist primarily of grey to rusty-weathering dark grey to blue grey or silvery phyllite. Thin horizons or bands of siltstone, with or without argillaceous partings, may be present. Some of the siltstone beds are up to 5 centimetres thick and locally grade into very fine-grained sandstone. A section of grey to dark grey quartz-feldspar-bearing schist to phyllite was encountered within an area assigned to this unit. It is an unusual lithology for this unit, but quartzose rocks are described from the base of the Black Phyllite south of the map area (Bloodgood, 1990). Phyllite and siltstone of this unit is usually quite friable in comparison to similar, denser and more indurated Harveys Ridge lithologies.

Black Phyllite rocks are believed to be Late Triassic in age (*see* Panteleyev *et al*., 1996) and form basement to the Nicola arc to the west. Western exposures of the Black phyllite contain sections of mafic tuffaceous sediments which interfinger with volcanic rocks typical of the Nicola Group (Panteleyev *et al., ibid.*)

CROOKED AMPHIBOLITE

Mafic and ultramafic rocks of the Crooked Amphibolite crop out immediately east of Wolverine Lake and extend, intermittently, northwestward onto the high ridge west of Rollie Lake. Mapping this past summer, in conjunction with work by Struik (1983a) and Rees (1987), suggests that the unit is approximately 1 kilometre thick in the north and thins southeastward and disappears in the vicinity of Six Mile Lake. The unit re-appears across the Cariboo River valley and shows the same thickness variations.

Much of the exposure west of Rollie Lake consists of grey to brown weathering, massive to strongly foliated and variably serpentinized ultramafite. Relict light brown weathering, dark green pyroxene crystals, up to 2 centimetres in size, are visible locally. These comprise up to 80 % of exposures in areas and may form a crude layering. Asbestos veining is present locally.

Southeast of this ridge, the Crooked Amphibolite consists of chlorite schist together with talc and iron carbonate altered gabbro and pyroxenite. Relict breccia textures (intrusive?) within gabbro can be observed locally. The Crooked Amphibolite displays a strong fabric (mylonitic) at its contact with the Quesnel Lake Gneiss. This is particularly well developed in exposures immediately north of Wolverine Lake. In this area, the western-most part of the Quesnel Lake Gneiss contains fine to medium-grained, chlorite-hornblende?-plagioclase gneiss in sections up to tens of metres thick. These are roughly on strike with Crooked Amphibolite lithologies and may be part of this unit. Similar mafic gneiss lithologies occur within the main part of the Quesnel Lake Gneiss and can be traced into less deformed sections and appear to have originally been gabbroic dikes. However, on the west side of the Quesnel Lake Gneiss, mafic gneiss of possible Crooked Amphibolite affinities appear to be intruded by the former unit casting doubt on the correlation of all mafic gneisses with the Crooked Amphibolite.

QUESNEL LAKE GNEISS

The large body of Quesnel Lake Gneiss, north of the Cariboo River, is a northern continuation of two similar units to the southwest. This felsic intrusion is actually a folded sill to transgressive sill-like body (Figure 3a, b). In the southwest, the unit is only preserved on the limbs of a large F_2 fold. This structure plunges northwest and is well outlined by the trace of the Quesnel Lake Gneiss (Figure 3a).

This unit is fairly uniform in composition consisting of a coarsely crystalline foliated potassium feldspar megacrystic granite to granodiorite. It is locally highly deformed, commonly at its contact with the Crooked Amphibolite, and appears gneissic in composition, displaying layers or lenses of quartz, feldspar and possibly mica. Potassium feldspar megacrysts are up to 8 centimetres in length and can comprise up to 30 % of the unit. These are invariably aligned, resulting in a well defined mineral lineation. Quartz may be flattened to form ribbons up to several centimetres in length. Biotite and muscovite are accessory minerals, with the former commonly altered to chlorite. At the western margin of this body, a mica poor, felsic-looking, finer grained variety of foliated granite intrudes typical lithologies of the Quesnel Lake Gneiss.

This body of foliated granite is the northern terminus of a series of Early Mississippian intrusions, collectively termed the Quesnel Lake Gneiss. These are subdivided into two informal suites based on composition and rough geographic position: the peraluminous Western Quesnel Lake Gneiss and the meta-aluminous Eastern Quesnel Lake Gneiss (Ferri *et al.*, 1999). The significance of the Quesnel Lake Gneiss has been the subject of much debate and Ferri *et al.*, (1999) suggested that these bodies are related to Late Devonian to Early Mississippian arc volcanism, whereas others (Montgomery and Ross, 1989) proposed that the alkaline geochemistry found within parts of the Eastern Quesnel Lake Gneiss may imply intrusion in an extensional regime.

SNOWSHOE GROUP

One of the aims of the 2000 field season was to test a model, first put forth by Höy and Ferri (1998a), that suggested much of the Snowshoe stratigraphy is inverted. Although mapping could not demonstrate this, it indicated that parts of the stratigraphic succession are overturned. Examination of Snowshoe stratigraphy during the 2000 field season indicated that rocks presently assigned to the Downey succession may be equivalent to the Keithley succession (Ferri, 2001a, b). Evidence gathered during the 2001 field season is consistent with this hypothesis. South of Harveys Creek, facing directions, together with the presence of a Keithley-like quartzite at the contact between the Harveys Ridge succession and lithologies currently assigned to the Downey succession, re-enforce this assumption. This would then imply that the dark siliciclastic rocks of the Hardscrabble Mountain succession, which are now interpreted to sit stratigraphically above the Downey succession, are in fact equivalent to Harveys Ridge rocks. This is confirmed at the outcrop scale as lithologies of Harveys Ridge and Hardscrabble Mountain successions are indistinguishable, an observation also noted by Struik (1988). Struik (*ibid*.) suggested that to make the two units equivalent would require large southwest verging fold structures, the presence of which have been demonstrated within the map area (Ferri, 2001a, b; Rees, 1987).

Furthermore, rocks presently included within the Ramos Creek succession along the Keithley Creek valley may be part of the Keithley succession. This is based on tracing Keithley rocks southeastward from Yanks Peak, in conjunction with the facing direction of lithologies on either side of Keithley Creek. This also suggests that carbonate, siliciclastics and deformed mafic igneous rocks west of Yanks Peak are also part of the Keithley succession. Struik (1988) noted that parts of the Ramos may be equivalent to sections of the Keithley succession.

North of Sellers Creek, limestone and stratigraphically underlying clastics at the base of the Keithley succession have recently been tentatively assigned to the Kee Khan marble and Tregillus sediments by Ferri (2001b). Limestone at Sellers Creek is associated with overlying chloritic-rich, Cu-bearing sediments of possible volcanic origin. These rocks are very similar to Cu-bearing meta-volcanic-limestone associations along Harveys Creek (presently assigned to the Downly succession), suggesting they are equivalent. If the limestone and underlying clastics are part of the Keithley succession, the overall sequence would have similarities to Downey rocks to the north, suggesting the two packages are equivalent.

This re-interpretation of Snowshoe stratigraphy suggests that, within the map area, the number of stratigraphic units making up the Snowshoe Group can be reduced by 50 %. A similar condensation of Snowshoe stratigraphy can be achieved in the Wells-Barkerville area, although there are more units defined in this region (Tom, Tregillus, Eaglesnest, Island Mountain) that are not encountered in the Cariboo Lake area. This re-definition of Snowshoe stratigraphy suggests the presence of large southwesterly directed fold structures between the study area and the Wells-Barkerville region, an inference compatible with the structural style present within the map area.

It is interesting to note that Holland (1954) first subdivided present day Snowshoe rocks in the Yanks Peak area and used the terms Yankee Belle, Yanks Peak and Midas to describe key sections. Yankee Belle and Midas were derived from mineral claims in the Yanks Peak vicinity which were primarily underlain by the respective rock types (Holland, *ibid.*). Holland's Yankee Belle Formation and Yanks Peak quartzite correspond to the present Keithley succession and Keithley quartzite respectively, and the Midas formation represented the Harveys Ridge succession. The higher Harveys Ridge coarse clastics and Agnes conglomerate were part of his Snowshoe Formation.

Holland (1954) traced these units eastward to the Cariboo Mountains and later workers (Sutherland Brown, 1957, 1963; Campbell *et al*., 1973) applied this terminology to lithologies typical of these rocks west of the Pleasant Valley Thrust (*see* Struik, 1988). Campbell *et al*. (1973) first suggested that Yankee Belle, Yanks Peak and Midas rocks in the informal type area may have very little in common with similarly named stratigraphy throughout the bulk of the Cariboo Mountains. This, together with the plethora of formation terminology in the Wells-Barkerville area led to the re-definition of Snowshoe rocks by Struik (1988). As a result of this long history of formation definition, the original type areas for the Yankee Belle, Yanks Peak and Midas formations are now part of the Snowshoe Group and may or may not correlate with the with definitions of these units.

Keithley Succession

Keithley rocks are located on the west flank of Yanks Peak and east of Grain Creek. Upper greenschist to lower amphibolite schist along the ridge west of Keithley Creek are also tentatively grouped with this unit. Rocks presently assigned to the Ramos and Downey successions in the map area by Struik (1988, 1983a) may be part of the Keithley succession and will be described in later sections.

In the Yanks Peak area the Keithley succession is characterized by thinly interlayered rusty brown to grey weathering, grey to grey green or green shale, siltstone to very fine sandstone. Locally, sandstone layers approach a metre in thickness and occur as a coarse, granule conglomerate. This sandstone is feldspathic and contains blue-grey to dark grey vitreous quartz grains. These horizons are commonly graded and may be interbedded with quartzo-feldspathic wackes.

On the ridge west of Keithley Creek are poorly exposed sections of thinly interlayered rusty brown weathering, grey garnet?-biotite-muscovite schist and quartz schist. These can be traced to the southern end of this ridge where they contain large porphyroblasts of andalusite? and appear to sit structurally above Harveys Ridge and Goose Peak lithologies. Several hundred metres of garnet-bearing chlorite-actinolite schist and gneiss occur on the east flank of this ridge and occupy an area between these Keithley schists and underlying Harveys Ridge or Ramos lithologies. These mafic schists locally contain felsdspar segregations and can be traced into lithologies which suggest they may be, in part, metagabbro or metadiorite. The gneissocity is highly contorted and the intense fabric indicates the rocks are highly strained. One outcrop of rusty brown weathering, dark green magnetic, pyroxene phyric schist is located at the north end of this belt.

Southeast of Grain Creek the Keithley succession is characterized by 5 to 100-centimetre-thick beds of grey to beige, impure quartzite to micaceous quartzite separated by 0.1 to 10 centimetre sections of garnet-biotite-muscovite quartz schist. These latter beds contain between 10 and 70 % mica. The Keithley is considerably more quartzose in the Grain Creek area than in the region around Yanks Peak.

Up to 100 metres of Keithley quartzite outcrops along the top of Yanks Peak where it is repeated by folding or thrusting. This quartzite can be traced to the southwest where it is inferred to be cut by a late normal fault along the French Snowshoe Creek valley. The quartzite was not encountered southeastward along strike within the Keithley Creek valley and disappears before the Little Snowshoe Creek valley (Struik, 1988; 1983a). Southeast of Grain Creek it is only 5 metres thick.

Keithley quartzite is light grey, white to beige and commonly has a purplish colour. It is relatively pure and commonly approaches an orthoquartzite in composition. Bedding is thick or massive and occasionally there are thin to film-like phyllitic partings. On Yanks Peak, thin grey phyllite, siltstone to fine sandstone is interbedded with the quartzite. These sections locally show grading and cross-stratification. Where present, and in conjunction with the overlying Harveys Ridge black clastics, this unit forms an excellent marker.

The thickness of the Keithley succession is dependent on the interpretation of its basal sequence. If carbonate and clastics in the Sellers Creek area are part of the Kee Khan marble and Tregillus clastics, respectively, this unit is probably over 500 metres in thickness. If these units are part of the Keithley, then it is in excess of 1000 metres. Struik (1988) suggested it is no more than 300 metres, although current work indicates this is probably a minimum.

Harveys Ridge Succession

The Harveys Ridge succession is characterized by black clastics and minor dark grey carbonate and metavolcanics. The most common lithology is a dark grey to black carbonaceous phyllite to siltstone, the latter commonly characterized by very thin, discontinuous laminae of white quartz (Photo 1). This lithology is well exposed east of Yanks Peak and along ridges within the Snowshoe Plateau. These rocks are metamorphosed to amphibolite grade in the Grain Creek area where they contain porphyroblasts of garnet and biotite, although the bulk of the rock barely attains a schistose texture, possibly due to the carbonaceous content. The unit is also characterized by dark grey to black quartzite or quartz sandstone containing black vitreous quartz grains.

Along the Snowshoe Plateau, the unit commonly contains thin to thick horizons of quartz-feldspar wackes and quartz grains are commonly blue-grey to dark grey or black. Towards the east, sections of grey to beige fine to coarse quartz sandstone are found interbedded with these wackes. These are sometimes feldspathic and the entire sequence appears very similar to the transitional section of the Harveys Ridge, immediately below the coarse sandstones of the Goose Peak quartzite (Ferri, 2001). This influx of coarser clastics in the upper part of the Harveys Ridge sequence can be seen northeast of Keithley Creek, on the north side of Cariboo Lake.

The thickness of this unit is quite variable. Carbonaceous phyllite to siltstone varies from 50 to several hundred

Photo 1. Typical dark grey to black, carbonaceous siltstones and phyllites of the Harveys Ridge succession.

metres, whereas the coarser wacke and quartzite are probably in excess of 300 metres. The transitional section of Harveys Ridge clastics varies between 100 and greater than 500 metres and probably occupies a large portion of the Snowshoe Plateau. In some areas, no mappable section of carbonaceous phyllite was encountered and only lithologies of the transitional sequence were observed.

Several sections of mafic volcanics were seen within the Harveys Ridge section and may be equivalent to similar volcanics observed in the Frank Creek area. These occur along the ridge immediately north of the community of Keithley Creek and along road side exposures on the southwest side of Cariboo Lake. Volcanics north of Keithley Creek are only a few metres thick and consist of dark green carbonate altered chlorite schist, which locally is less deformed and includes relict feldspar and pyroxene crystals. On the north shore of Cariboo Lake 1 to 5-metre sections of brown weathering, iron-carbonate altered metavolcanics are interbedded with typical Harveys Ridge lithologies. These sections have smears or porphyroblasts of green mica suggesting a volcanic origin prior to alteration. Initial trace element chemical analysis of these two groups of volcanics indicate a mafic alkaline chemistry compatible with the mafic Frank Creek volcanics to the southwest (*see* below, Ferri, 2001a).

Outcrops of highly deformed greenish grey, actinolite-chlorite schist or phyllite similar in appearance to the intermediate Frank Creek metavolcanics occur in the vicinity of the Peacock showing (Minfile 093A 133) northwest of southern Cariboo Lake. These are associated with Goose Peak and possibly transitional Harveys Ridge lithologies and appear to contain relict volcanic clasts.

Several outcrops of grey to light grey weathering, light to dark grey finely laminated limestone with thin dark grey phyllitic partings occur south of Four Creek. Limestone is typically finely recrystallized, although locally it is a coarse marble.

Agnes Conglomerate

The Agnes conglomerate is a distinctive quartzite cobble conglomerate within the upper part of the Harveys Ridge succession, either stratigraphically near the beginning of the transitional part of the Harveys Ridge or just below the Goose Peak quartzite. It crops out in two main linear belts within the map area, occurring on either side of the Lightning Creek Anticlinorium (Figure 3a). It extends from the Cariboo Lake area, northwestward and thins out south of the headwaters of Four Creek reappearing along strike in the Yanks Peak region. The second area of good exposure is along the Snowshoe Plateau where it outcrops along the top of French Snowshoe Peak and can be traced north and south for approximately 10 kilometres. On the southwest side of French Snowshoe Creek, quartzite originally placed within the Keithley succession contains quartzite cobbles and is tentatively assigned to the Agnes conglomerate.

The most distinctive lithology of this unit is a grey to beige matrix to clast-supported granule to boulder quartzite conglomerate (Photo 2). Orange-weathering, grey carbonate clasts are present locally. The matrix to this conglomerate is a quartz sandstone to quartzite similar in composition to the clasts. Locally, conglomerate consists of light grey siltstone clasts floating in a dark grey phyllitic matrix. Conglomerate is commonly associated with beige to light brown, fine to coarse grained, thick to massively bedded quartz sandstone, and light greenish grey phyllite to siltstone. These light coloured sandstones and phyllites can be the most common lithology within the Agnes conglomerate sequence and sit immediately above black carbonaceous phyllite and siltstone of the Harveys Ridge succession along the Snowshoe Plateau. Quartz wackes and sandstones more akin to the transitional Harveys Ridge succession occur stratigraphically above the Agnes conglomerate.

On the north side of Pine Creek, dark grey to cream orthoquartzite horizons, up to 3 metres thick, occur within the Agnes conglomerate section. The light coloured quartzite appears very similar to Keithley quartzite whereas the dark grey variety is characterized by black vitreous quartz grains as per quartzites in the Harveys Ridge succession.

Goose Peak Quartzite

The extent of coarse feldspathic quartzite assigned to the Goose Peak is fairly limited within the present study area in comparison to the area south of Cariboo Lake. Two belts of exposure were seen on either side of Pine Creek and scattered outcrops of this unit were observed in the poorly exposed region around the large body of Quesnel Lake Gneiss.

The Goose Peak is characterized by thick to massive bedded, grey, poorly sorted coarse grained feldspathic impure quartzite to granule conglomerate. The micaceous and feldspar content of these rocks is usually less than 10 %, combined. Thin to moderately bedded dark grey to grey phyllite to siltstone partings are subordinate, although they increase in abundance towards the base of the unit. Relatively pure, well sorted grey to beige quartzite to micaceous quartzite is also present within sections assigned to this unit and bear a strong similarity with Keithley sandstones.

Photo 2. Stretched quartzite cobble to boulder conglomerate of the Agnes conglomerate.

Downey or Keithley Succession

It is suggested that rocks presently assigned to the Downey succession in the Harveys Creek area may be part of the Keithley succession (*see* also Ferri; 2001a, b) This is based on several lines of evidence. First, facing and structural evidence suggest that the eastern edge of Harveys Ridge rocks, south of Harveys Creek, occur on the southwesterly overturned limb of an F_2 anticlinal fold. Second, the contact between Harveys Ridge rocks and the presently named Downey sequence is marked by a grey to beige, impure to relatively pure quartzite similar to that at the upper contact of the Keithley succession.

The most common lithology consists of grey-green to green phyllite to siltstone, containing thin interbeds of grey to green sandstone to impure quartzite. Less common is grey to brown weathering, mottled to lustrous grey to dark grey phyllite, siltstone and wacke. These rocks are more highly metamorphosed southeast of Mount Barker and consist of grey to light grey garnet-biotite schist and quartz schist.

This succession also contains sections of chlorite schist of metavolcanic origin (alkaline composition; *see* section below). There are no relict tuffaceous textures within sections of mafic schist in the present study area, except for 0.5 to 1 centimetre ovoid smears of dark green chlorite observed within chlorite schist between Simlock and Harveys Creek. Chlorite schist is 100 to 200 metres thick in the Cariboo River area and thins northwestward. This mafic schist is commonly associated with sections of thinly interlayered, grey to dark grey limestone and phyllite up to several hundred metres thick. The limestone is commonly bleached to a white marble and may be orange to brown weathering. At the headwaters of Simlock Creek, and near the Cariboo Hudson Mine, these limestone horizons contain sections of limestone clast conglomerate (with a calcarenite matrix) or clastic carbonate (calcarenite) up to 15 metres thick. These carbonate horizons, especially the orange to brown weathering variety, are quite distinct from Bralco limestone.

South of Cariboo River the Downey/Keithley succession is locally coarser grained and contains sections of coarse feldspathic sandstone to granule conglomerate, which superficially resemble lithologies within the Goose Peak quartzite. North of Ishkloo Creek, dark grey to black garnet and biotite bearing phyllite to schist of the Harveys Ridge succession sit on dark green-grey garnet-biotite schist which contain sections of chlorite schist. There is no orthoquartzite present at the contact, but subangular beige orthoquartzite boulders up to 1 metre thick occur at this contact.

Parts of this sequence contain sills of metadiorite up to several hundred metres thick. These are abundant along the ridge including Mount Barker, where they form several mappable bodies, and they also occur north of the Cariboo River. The spatial association of these metadioritic bodies and metavolcanics suggests they are co-magmatic[3], although the volcanics are alkaline in composition whereas the meta-diorite display calc-alkaline signatures.

One of the few fossil localities within the Snowshoe Group occurs within rocks tentatively assigned to the Downey succession (Struik, 1988). Ostracod and bryozoa fragments were recovered from rocks very near the Pleasant Valley thrust fault north of Wells. There is some uncertainty as to the assignment of these rocks to the Downey succession (Struik, 1988).

Ramos or Keithley Succession

Exposures of brown weathering, grey to dark grey or green-grey phyllite with thin to thick beds of grey to greenish grey siltstone to fine sandstone occur along the lower Keithley Creek valley. Interbedded with these lithologies is moderately to thickly bedded grey feldspathic sandstone to wacke. These lithologies can be traced northward, beyond the mouth of Little Snowshoe Creek, where they are subordinate to greenish chloritic phyllite and schist. West of Rabbit Creek, a section of thinly interbedded dark grey weathering grey limestone and grey schist occurs with these schists and sandstone. This limestone sequence locally sits structurally above mafic volcanics and diorite.

Southwest of Keithley Creek, limestone is structurally succeeded by sheared mafic schist and banded gneiss. A thin band of dark grey to black phyllite and siltstone, similar to that within the Harveys Ridge succession, occurs between the two.

Struik (1988) placed these rocks within the Ramos succession and interpreted them as one of the oldest sequences within the Snowshoe Group, sitting below the Kee Khan marble and Keithley succession. Based on facing directions, structural attitudes and stratigraphic makeup, these may alternately be part of the Keithley succession. Keithley rocks from the top and west flank of Yanks Peak can be traced southward to French Snowshoe Creek and appear offset by a late, northeast trending normal fault. Quartzite on the south side of the creek was originally mapped as the upper part of the Keithley succession by Holland (1954) and Struik (1988). However, examination of this identified quartzite conglomerate horizons suggesting it is part of the Agnes conglomerate. Furthermore, this quartzite and conglomerate traces southeastward into Harveys Ridge lithologies and is on strike with Agnes conglomerate south of Four Creek.

Keithley quartzite is not encountered south of French Snowshoe Creek. The present interpretation of the southward extension of Keithley lithologies places them along the ridge tops northeast of Keithley Creek (Struik, 1988). The structural attitude of bedding and foliation in the Keithley Creek area together with tops being consistently overturned to the northeast, as seen on Yanks Peak, suggest these rocks sit stratigraphically below the Harveys Ridge succession. It is suggested here that the rocks along the Keithley Creek valley may be part of the Keithley succession. The presence of limestone and mafic metavolcanics along the northward extension of these rocks is similar to the sequence of limestone and chloritic schist north of Sellers Creek and to rocks along Harveys Creek, both of which are thought to be part of the Keithley succession.

If the above correlations are correct, this would require facies changes within the Keithley succession to account for the different lithologies. The rapid disappearance of the thick Keithley quartzite north of Yanks Peak is consistent with this.

Bralco Limestone

Several hundred metres of thin to thickly or massively bedded, grey weathering, grey to dark grey finely recrystallized limestone are found at the headwaters of Three Creek. Locally it is slightly dolomitized and beige weathering and may be coarsely recrystallized to a white marble. Bedding can be well developed and the unit breaks into thin sheets or has platy to flaggy partings. Limestone is locally argillaceous and thin grey phyllitic partings are sometimes present. A primary limestone breccia may be associated with these argillaceous regions. Locally ovoid or circular features up to 5 millimetres in diametre are found in 1 to 3 centimetre thick horizons and may be oolitic or pisolitic in origin. These appear silicified and have calcite cores. Discontinuous layers, up to 1 metre thick, of white to beige quartzite or recrystallized chert occur in two localities. This limestone can be traced to the southwest where it thins and occurs in the footwall of the Pleasant Valley Thrust, and consists of dark grey, platy argillaceous limestone to recrystallized limestone. The unit does not appear to extend north of Simlock Creek and could be cut by a late northeast-trending normal fault.

Dark grey to black phyllites and siltstones of the Hardscrabble/Harveys Ridge lie above the limestone. Although no exposure was identified structurally below the limestone, scattered rubble of dark grey to black siltstone and phyllite, not unlike that of the Harveys Ridge, extends over an area of 500 metres.

Struik (1988), from trace fossil information, indicated that the Bralco limestone may be younger than Cambrian, possibly Siluro-Devonian. This age or stratigraphic position would create some problems with the argument posed in this report equating Downey with Keithley stratigraphy. Alternatively, the dark grey to black fine siliciclastics on either side of the limestone may be part of the Harveys Ridge succession suggesting the Bralco Limestone overlies this unit and is found in the core of an F_2 synclinal fold. The assignment of Downey rocks to the Keithley requires the presence of Harveys Ridge lithologies above the Keithley succession. Furthermore, no Bralco limestone exists in the upper part of the Harveys Ridge succession west of Three Creek. There are only scattered occurrences of grey to dark grey limestone to the west of here suggesting that, if this stratigraphic re-interpretation is correct, the limestone has either not been deposited or has been removed and replaced by coarse clastics of the transitional Harveys Ridge or Goose Peak.

Another possibility is that the Bralco limestone is actually in the hanging wall of the Pleasant Valley Thrust and may be equivalent to the Mural limestone. Initially, Struik (1981, 1982) equated this carbonate with either the Cunningham or Mural formations. The associated lithologies and lack of a thick interbedded shale-limestone sequence, typical for the base of the Cunningham limestone, suggest it could be equated with the Mural Formation.

Hardscrabble Mountain/Harveys Ridge Successions

Dark grey to black phyllite and siltstone overlie the Bralco limestone along the ridge northwest of Three Creek. Siltstone contains thin, discontinuous layers of light grey to white quartz 0.5 to 2 centimetres apart. Minor lithologies include thin beds of black sandstone and altered mafic metavolcanic rocks. Rubble of the same material outcrops below the limestone over a length of about 500 metres.

These rocks have been assigned to the Hardscrabble Mountain succession by Struik (1988). Superficially these rocks are identical to basal Harveys Ridge lithologies and it is suggested here that these be placed with the Harveys Ridge succession. The repetition of these rocks around the Bralco limestone is explained by the presence of an F_2 fold. This is supported by the presence of green-grey to grey siltstones and phyllites further up the ridge which are identical to lithologies to the west within rocks presently assigned to the Downey succession.

To the northwest, near Hardscrabble Mountain, the Early Permian Sugar limestone sits stratigraphically above clastics of the Hardscabble Mountain succession (Struik, 1988). Struik (*ibid.*) suggests that the Sugar limestone sits uncomfortably above the Hardscrabble, with the latter being possibly Devono-Mississippian in age and equivalent to the Black Stuart Group of the Cariboo Terrane. The correlations suggested in this paper would indicate that the unconformity at the base of the Sugar limestone would be quite profound, placing Permian upon Cambrian lithologies.

MAFIC SILLS AND DIKES

Several parts of the map area contain abundant alkaline to subalkaline mafic intrusions. There are two areas where these are concentrated: in the region between Keithley and Rollie creeks and along the ridge containing Mount Barker and extending northwestward into the vicinity of Simlock Creek. Many of these are sills or dikes are up to 5 metres in thickness, although in the Mount Barker area they form large, mappable bodies several hundred metres in thickness. These are fine to coarse-grained diorite with between 40 and 60 % pyroxene and/or hornblende with the remaining being composed of plagioclase feldspar. The larger sill-like bodies north of Mount Barker may contain up to 5 % biotite and traces of quartz.

Most of the diorite bodies contain a foliation of varying intensity, which is parallel to the main foliation within surrounding meta-sediments. Some have an intense, to almost mylonitic, fabric, whereas others are essentially undeformed. Diorite between Keithley and Rollie creeks has similar geochemical characteristics as the Frank Creek or Mount Badger volcanics[4]. *See* section on Geochemistry below.

CARIBOO GROUP

Rocks belonging to the Cariboo Group were examined in a cursory manor along the northeastern edge of the map area. Lithologies belonging to the Yankee Belle, Yanks Peak, Midas and Mural formations occur between the confluence of Little and Cariboo rivers and Roundtop Mountain. Yankee Belle rocks consist of interlayered light grey to greenish grey siltstone and thin interbeds of fine-grained grey sandstone. Yanks Peak Formation is dominated by beige to white or light grey, thick to massively bedded, fine to coarse grained orthoquartzite to impure quartzite. Orthoquartzite forms sections up to 50 metres thick producing resistive exposures and forming an excellent marker horizon. Immediately above the orthoquartzite are several massive, metres-thick sections of black to dark grey quartzite containing fine to coarse grains of black vitreous quartz, presumably belonging to the Midas Formation. Stratigraphically above this are sections of grey to greenish grey siltstone with horizons of purplish grey sandstone (up to 1 metre thick) or dark grey sandstone and grey slate. Limestone of the Mural Formation was only seen in one locality and consists of massive looking, light grey to white (mottled) finely recrystallized limestone. Very few bedding surfaces were discerned and these were questionable. Locally, parts of the limestone are orange weathering and slightly dolomitic.

It is generally very difficult, at the outcrop level, to distinguish Yankee Belle from Midas rocks (this study and Struik, 1988). Generally, the Midas Formation forms a fining upwards sequence whereas the Yankee Belle is a coarsening upwards succession and contains limestone in its lower part. Lacking any fossils, it is also very easy to confuse Cunningham and Mural limestones in outcrop. The base of the Cunningham consists of a 100 metre thick section of interlayered limestone and calcareous phyllite or slate like that of the underlying Isaac Formation. The transition from Mural to Midas formations is relatively sharp and occurs over a few metres (Struik, 1988).

REGIONAL CORRELATIONS

Struik (1986, 1988) correlated parts of the Snowshoe stratigraphy with sections of the Eagle Bay Assemblage (Figure 5). Höy and Ferri (1998a) and Ferri (2001a) suggested that the Bralco limestone is equivalent to the Early Cambrian Tshinakin and equivalent limestones (Badshot, Mural). Höy and Ferri (1998a) also indicated that the sequence may be inverted and that the Downey sits above the Bralco limestone.

Work this past summer suggests that the Downey is stratigraphically below the Bralco limestone and may in fact lie underneath the Harveys Ridge succession. The stratigraphic sequence proposed for the map area, based on the revised structural interpretation, is shown in Figure 6. Rocks of the Downey would be equivalent to the Keithley succession and rocks of the Hardscrabble Mountain succession would simply be a repetition of Harveys Ridge rocks.

Parts of this new stratigraphic sequence correlate well with massive sulphide-bearing Eagle Bay Assemblage rocks in the Adams Plateau region. The similarity in lithologies, their relative sequence and similar style of mineralized occurrences lends further strength to the newly proposed stratigraphic column for the Cariboo Lake area.

Höy (1999) recently described several Pb-Zn-Cu volcanogenic massive sulphide occurrences in unit EBG of the Eagle Bay Assemblage in the Adams Plateau area (Figure 7). The Mosquito King, Spar, Lucky Coon, Elsie and King Tut occurrences and their relative position within the stratigraphic sequence, is shown in Figure 7. If one assumes Mount Barker volcanics sit below the Keithley quartzite, the

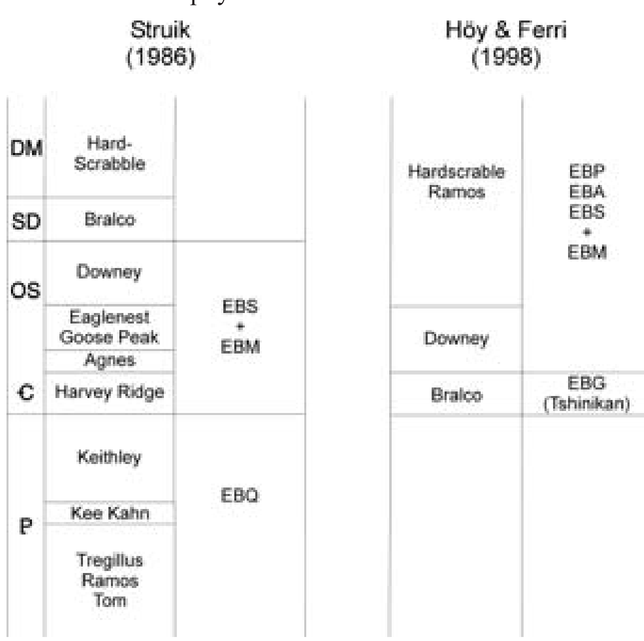

Figure 5. Generalized stratigraphic correlations of parts of the Snowshoe Group and Eagle Bay Assemblage, from Struik (1986) and Höy and Ferri (1998).

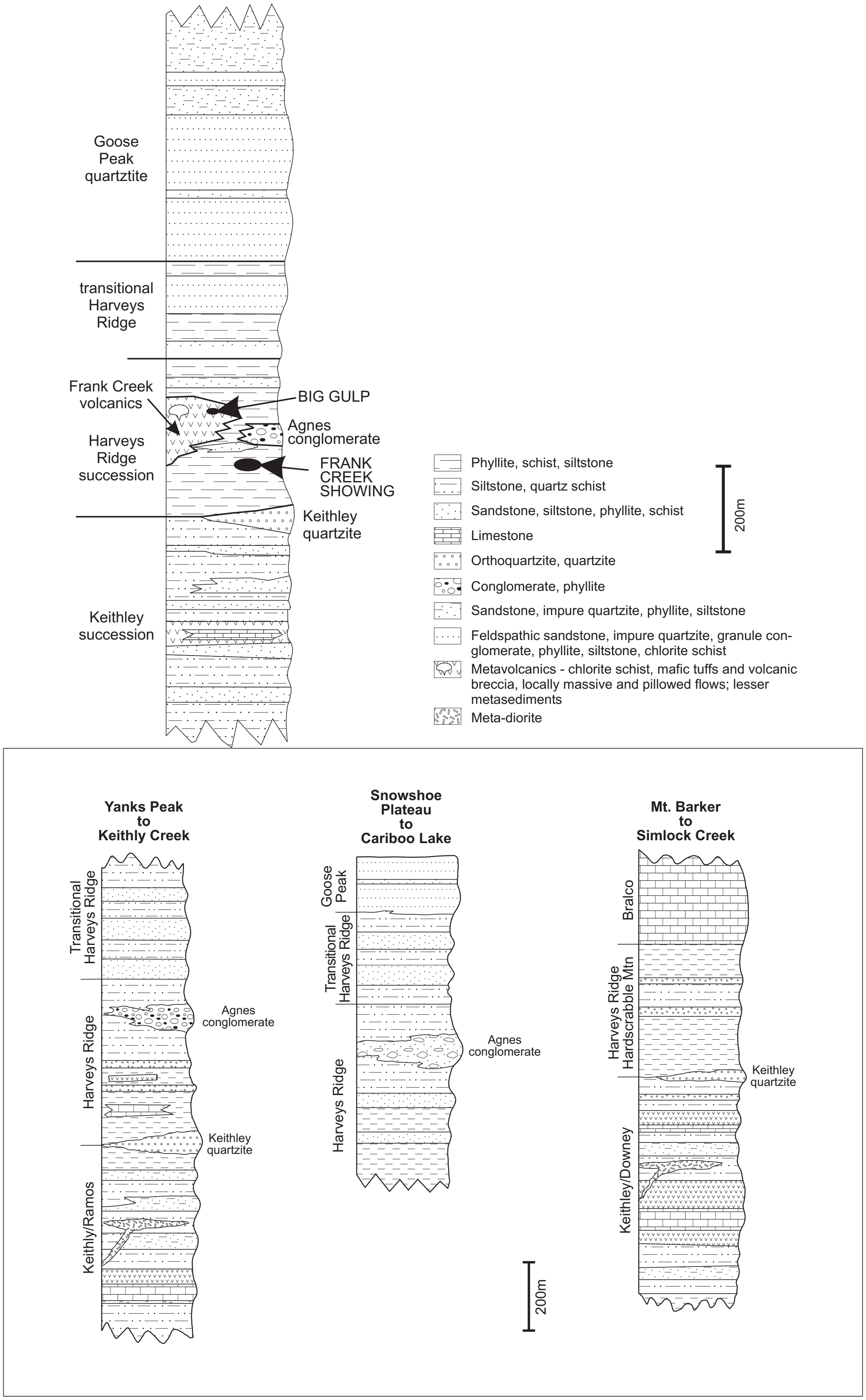

Figure 6. (a) Simplified stratigraphic column for sub-Downey/Keithley stratigraphy southeast of Cariboo Lake (from Ferri, 2001). (b) Generalized and composite stratigraphic columns from three different parts of the Snowshoe Group showing proposed stratigraphic order.

general stratigraphic sequence within each area are approximately correlative. Unit EBG_1 would equate with the Mount Barker volcanics, unit EBG_2 with the Keithley quartzite and the carbonaceous sediments and volcanics of units EBG_3 to EBG_6 being equivalent to the Harveys Ridge succession (including the Frank Creek volcanics). Chemically, the volcanics of unit EBG_1 display the same signature as those of the Mount Barker area. The quartzite of unit EBG_2 is relatively pure and displays the same thickness variations as the Keithley quartzite.

In general, the carbonaceous character of units EBG_3, EBG_5 and EBG_6, together with the volcanic sequence of unit EBG_4, has an overall similarity to that of the Harveys Ridge succession. Sporadic limestone occurrences are found in the Harveys Ridge succession, particularly north of Keithley Creek. Metavolcanics of unit EBG_4 are correlated with the Frank Creek or Badger Peak volcanics, although they sit below Lucky Coon mineralization. The EBG_3 to EBG_6 section is much more calcareous than the sequence in the Cariboo Lake area and may reflect lateral facies variations.

One of the other similarities between the two sections is the relative position of massive sulphide mineralization (Figure 7). Copper-rich occurrences within unit EBG_1 are similar to Ace and sporadic Cu mineralization within the Mount Barker volcanics. The mineralogy of Lucky Coon and related occurrences, as well as the host sequence of black carbonaceous sediments above a relatively pure quartzite horizon (EBG_2), are analogous to the Frank Creek and Unlikely showings.

PRELIMINARY GEOCHEMISTRY OF MAFIC IGNEOUS ROCKS

Although small mafic, post-tectonic plugs and dikes are found cross-cutting the Snowshoe Group, the bulk of mafic rocks are pre-tectonic and metavolcanic rocks are found intercalated within these sediments. Mafic metavolcanics and intrusive rocks are found within the Harveys Ridge, Ramos/Keithley and Downey/Keithley successions. They have been subdivided into the following groups: Mount Barker volcanics, Mount Barker metadiorite, Harveys Ridge volcanics, metadiorite between Keithley and Rollie creeks and sheared metavolcanics? and metadiorite southwest of Keithley Creek (Figure 8). Select samples of these rocks were analyzed to better understand their composition and tectonic setting (Table 1).

Many of the mafic igneous rocks within the map area have undergone upper greenschist to lower amphibolite grade metamorphism and have been multiply deformed. As a consequence, the analyses of these rocks using major oxides is suspect considering the mobility of these elements at these conditions. Since trace elements are less mobile during regional metamorphism, all the diagrams presented in the next section make use of these chemical components.

Utilizing the Zr/TiO_2 versus Nb/Y trace element rock classification diagram derived by Winchester and Floyd (1977), all of the mafic volcanic rocks range from alkaline to subalkaline basalts, although SiO_2 values range as high as basaltic andesites or andesites (Table 1, Figure 8). Dioritic bodies intruding Snowshoe rocks between Keithley and Rollie creeks form two clusters with one group having alka-

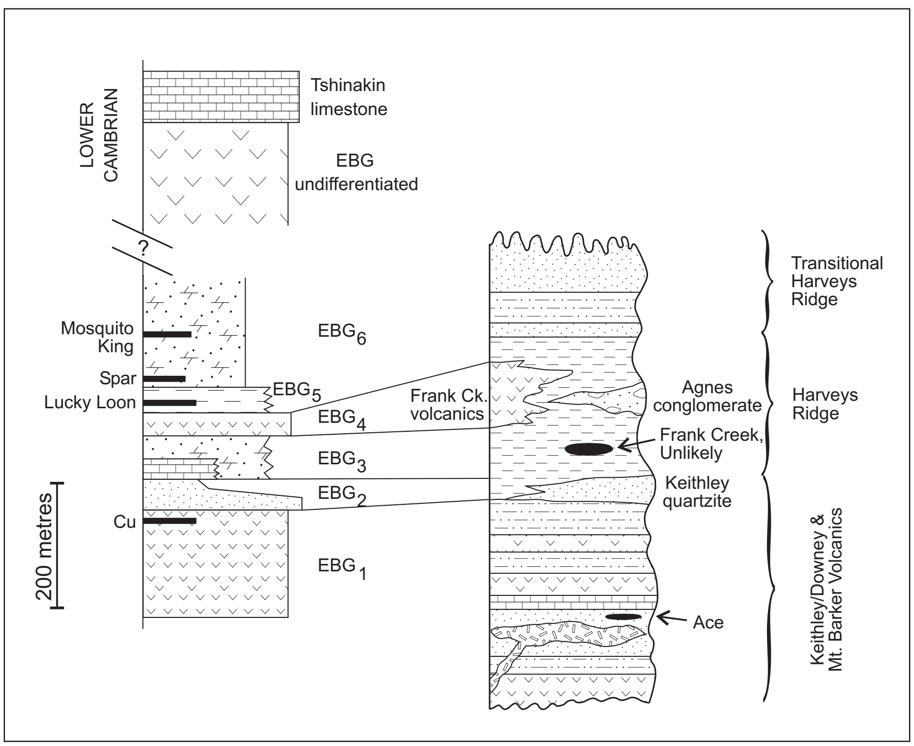

Figure 7. Correlation of EBG stratigraphy associated with Lucky Coon and Mosquito King mineralization on the Adams Plateau (Höy, 1999) and proposed stratigraphy and associated mineralization within the Cariboo Lake map area.

TABLE 1
WHOLE ROCK AND TRACE ELEMENT GEOCHEMISTRY OF SELECT IGNEOUS ROCKS WITHIN THE SNOWSHOE GROUP.

	01BO-06-03a	01BO-06-03b	01BO-06-06	01BO-11-01	01BO-15-07a	01BO-18-01	01BO-18-03a	01BO-18-05	01BO-21-06	01BO-21-07	01BO-29-05	01BO-31-05	01BO-33-03a	01BO-04-06	01FFE-03-01	01FFE-03-01A	01FFE-03-07	01FFE-06-09	01FFE-07-02	01FFE-07-05	01FFE-07-15	01FFE-08-07	01FFE-08-08
Unit	KR-D	KR-D	KR-D	KR-D	MB-V	MB-D	MB-D	MB-V	MB-V	MB-V	MB-V	MB-V	MB-V	KR-D	KR-D	KR-D	KR-D	KR-D	KR-D	KR-D	KR-D	HR-V	HR-V
Easting	602007	602007	603109	603382	613981	624228	624336	625052	623878	623987	614366	614857	626161	601826	597750	597750	59744	602549	602901	602729	603506	608792	608950
Northing	5844432	5844432	5845654	5848436	5857068	5850777	5849846	5850070	5846831	5846861	5863133	5862407	5849138	5848997	5845225	5845225	5846775	5845117	5846038	5846792	5847252	5849779	5849809
SiO2	52.4	53.47	43.38	50.54	45.04	50.29	48.5	47.18	62.2	57.9	41.33	49.75	48.61	50.9	50.56	47.24	46.18	44.13	54.02	44.83	49.27	47.54	44.29
TiO2	0.93	1.13	1.87	0.87	2.44	1.04	1.1	1.35	0.99	0.99	0.76	1.07	1	1.25	1.17	2.57	1.75	1.73	0.68	3.79	1.4	2.51	1.75
Al2O3	15.6	14.97	13.35	16.45	14.15	14.56	16.9	17.85	19.03	19.1	9.69	12.65	17.27	15.77	15.55	15.09	18.15	12.43	14.59	13.19	15.27	15.21	14.22
Fe2O3	10.14	10.35	13.65	8.26	12.4	14.22	11.1	11.18	7.44	10.65	10.09	11.52	13.89	9.65	10.65	14.06	10.8	12.9	9.25	13.73	11.15	12.56	11.43
MnO	0.15	0.15	0.2	0.15	0.09	0.23	0.2	0.17	0.07	0.1	0.1	0.11	0.18	0.14	0.17	0.21	0.12	0.18	0.15	0.18	0.17	0.14	0.14
MgO	6.01	5.42	7.76	5.65	8.18	3.49	3.3	2.06	1.61	2.34	9.27	10.78	4.36	6.71	6.26	6.34	6	13.1	7.44	8.47	6.55	5.76	7.46
CaO	8.8	8.44	12.43	14.07	6.11	6.21	5.9	5.26	0.34	0.43	5.32	5.42	7.07	9.09	10.36	9.1	9.43	9.93	9.36	9.44	11.06	7.3	5.84
Na2O	3.54	2.73	1.87	0.85	2.94	2.74	5.1	6.32	0.83	0.79	2.44	3.91	3.1	3.42	2.44	3.06	3.09	0.37	2.23	1.95	2.23	3.96	4.32
K2O	0.4	0.73	0.69	0.15	0.01	0.56	0.5	0.82	3.2	3.71	0.87	0.1	0.69	0.31	0.18	0.56	1.41	0.5	0.25	0.82	0.25	0.07	0.01
P2O5	0.07	0.1	0.46	0.07	0.27	0.3	0.4	0.55	0.12	0.1	0.07	0.11	0.25	0.09	0.07	0.33	0.18	0.4	0.03	0.66	0.1	0.25	0.27
LOI	1.27	1.75	3.83	2.14	8.06	6	6.57	6.75	3.6	3.52	19.34	3.97	2.92	2.24	2.21	0.95	2.36	3.61	1.4	2.54	2.07	4.32	9.97
SUM	99.32	99.29	99.56	99.21	99.7	99.66	99.54	99.53	99.5	99.7	99.32	99.4	99.35	99.58	99.63	99.54	99.67	99.35	99.42	99.69	99.54	99.63	99.71
Zr	66	77	139	66	154	106	122	123	155	144	60	73	87	73	73	166	126	142	58	305	77	158	120
Y	22	27	18	17	22	25	27	25	20	24	7	10	20	22	26	27	19	19	18	24	26	23	19
Sr	213	218	242	281	223	625	577	481	261	111	255	112	816	154	130	450	550	122	98	386	166	246	335
Nb	9	12	22	11	20	12	11	14	27	17	14	15	13	12	12	24	21	26	12	24	12	22	20
V	274	279	233	210	319	347	277	166	129	139	166	213	283	273	277	299	203	223	247	226	294	289	224
La	5	<5	13	<5	<5	26	24	33	34	42	16	19	24	5	9	18	14	16	12	5	10	<5	8
Ce	8	21	56	35	52	81	64	109	110	93	30	41	56	14	25	89	<5	40	20	55	12	56	59
Ba	63	487	706	50	70	156	89	444	748	715	398	94	137	98	128	285	1982	722	185	915	161	110	107
Rb	23	32	21	14	11	41	30	25	111	133	24	<3	34	18	11	12	35	22	17	37	14	8	8

	01FFE-09-02a	01FFE-09-04a	01FFE-09-04b	01FFE-11-04	01FFE-11-08	01FFE-11-09	01FFE-11-07a	01FFE-11-07b	01FFE-13-04	01FFE-17-01	01FFE-17-02	01FFe-24-07	01FFe-28-06	01FFe-35-02	01FFe-38-05	01FFe-39-01	01FFe-39-02	01FFe-40-07a	01FFe-40-07b	01FFe-41-01a	01FFe-41-01b
Unit	HR-V	HR-V	HR-V	KR-D	KC	KC	KC	KC	KR-D	MB-V	MB-V	MB-V	MB-V	HR-V	MB-D	MB-D	MB-D	KR-D	KR-D	KC	KC
Easting	605096	605812	605812	603458	601192	600110	601064	601064	602071	613099	613025	619060	627324	615548	627262	625052	624956	602880	602880	596524	596524
Northing	5844003	5845055	5845055	5849443	5849676	5849997	5850147	5850147	5852299	5858123	5858272	5852850	5845314	5860691	5848373	5850254	5850418	5846012	5846012	5856980	5856980
SiO2	35.33	43.65	31.15	53.7	42.38	36.63	43.52	45.13	51.38	50.56	44.38	50.58	56.81	34.15	47.08	47.45	46.52	55.13	54.18	47.86	44.72
TiO2	0.87	2.25	1.59	1.44	2.54	0.58	2.02	2.74	0.92	2.86	2.67	1.15	1.39	0.67	0.56	0.55	1.04	0.76	0.68	1.58	1.19
Al2O3	9.76	14.42	14.09	14.96	14.71	5.94	13.57	14.94	14.21	16.86	14.82	16.05	19.13	10.13	14.97	15.02	15.06	14.57	14.52	14.52	16.39
Fe2O3	9.38	12.5	17.15	11.31	13.15	17.59	12.73	12.39	9.89	15.13	12.47	11.1	11.47	11.78	9.39	9.48	10.43	9.61	9.48	11.17	11.03
MnO	0.14	0.14	0.18	0.17	0.15	0.2	0.18	0.15	0.17	0.07	0.12	0.2	0.05	0.14	0.15	0.17	0.17	0.15	0.15	0.15	0.15
MgO	12.39	9.81	23.84	4.51	8.64	28.19	13.11	9.09	7.71	3.64	5.59	4.61	1.66	14.48	7.78	8.6	3.42	6.28	7.21	8.31	9.13
CaO	5.69	9.22	1.94	7.78	12.02	2.52	9.4	9.73	11.18	1.38	6.92	4.61	0.5	9.1	11.06	9.13	8.31	9.36	9.28	8.55	8.81
Na2O	0.05	0.95	0.01	3.31	1.82	0.02	1	2.75	1.48	0.86	3.94	4.51	1.61	0.01	2.85	3.11	3.38	2.25	2.08	3.02	2.24
K2O	2.47	2.16	0.01	0.46	0.75	0.01	0.83	0.47	0.23	3.64	0.15	0.18	3.85	0.01	0.4	0.56	1.14	0.15	0.28	0.81	1.21
P2O5	0.11	0.31	0.23	0.15	0.4	0.05	0.2	0.5	0.07	0.43	0.34	0.27	0.15	0.05	0.11	0.1	0.28	0.05	0.05	0.2	0.23
LOI	22.87	3.83	9.68	1.73	2.93	7.23	2.85	1.65	2.34	4.21	8.28	6.57	3.04	18.79	4.55	5.15	9.56	1	1.48	3.07	3.2
SUM	99.13	99.56	99.88	99.53	99.53	98.97	99.51	99.57	99.59	99.77	99.69	99.84	99.74	99.32	98.92	99.35	99.34	99.32	99.41	99.62	99.12
Zr	77	158	85	115	177	37	114	158	67	193	183	118	258	48	60	52	90	56	53	113	98
Y	15	17	11	34	17	6	13	21	23	18	25	26	41	11	11	16	23	24	22	29	19
Sr	149	338	13	226	512	53	117	451	230	74	313	234	113	242	924	717	653	111	103	322	323
Nb	19	28	19	12	30	10	23	27	12	26	23	15	28	10	11	9	12	11	10	14	15
V	140	294	186	280	204	92	227	263	252	237	270	293	211	140	216	224	277	292	263	297	223
La	7	17	21	<5	12	10	19	16	9	12	16	27	42	18	16	26	18	13	9	<5	13
Ce	44	<5	47	19	58	20	40	83	31	43	98	82	97	33	42	22	53	23	9	<5	<5
Ba	667	3232	33	137	381	56	1015	286	83	1251	121	107	829	16	244	296	270	111	163	3763	8246
Rb	93	57	8	28	23	5	19	17	23	83	11	11	135	5	16	26	48	10	13	18	31

KR-D: Diorite between Keithley and Rollie creeks; HR-V: Harveys Ridge volcanics; KC: sheared metavolcanics and diorite southwest of Keithley Creek;
MB-V: Mount Barker volcanics; MB-G: Mount Barker diorite.
Major oxides in per cent; trace elements in ppm; Steel mill grinding at GSB; major oxides by Fused Disc - X-ray fluorescence; trace elements pressed pellet - X-ray fluorescence
Analysis performed at Cominco Research Laboratory, Vancouver, B.C. SUM = Sum of oxides

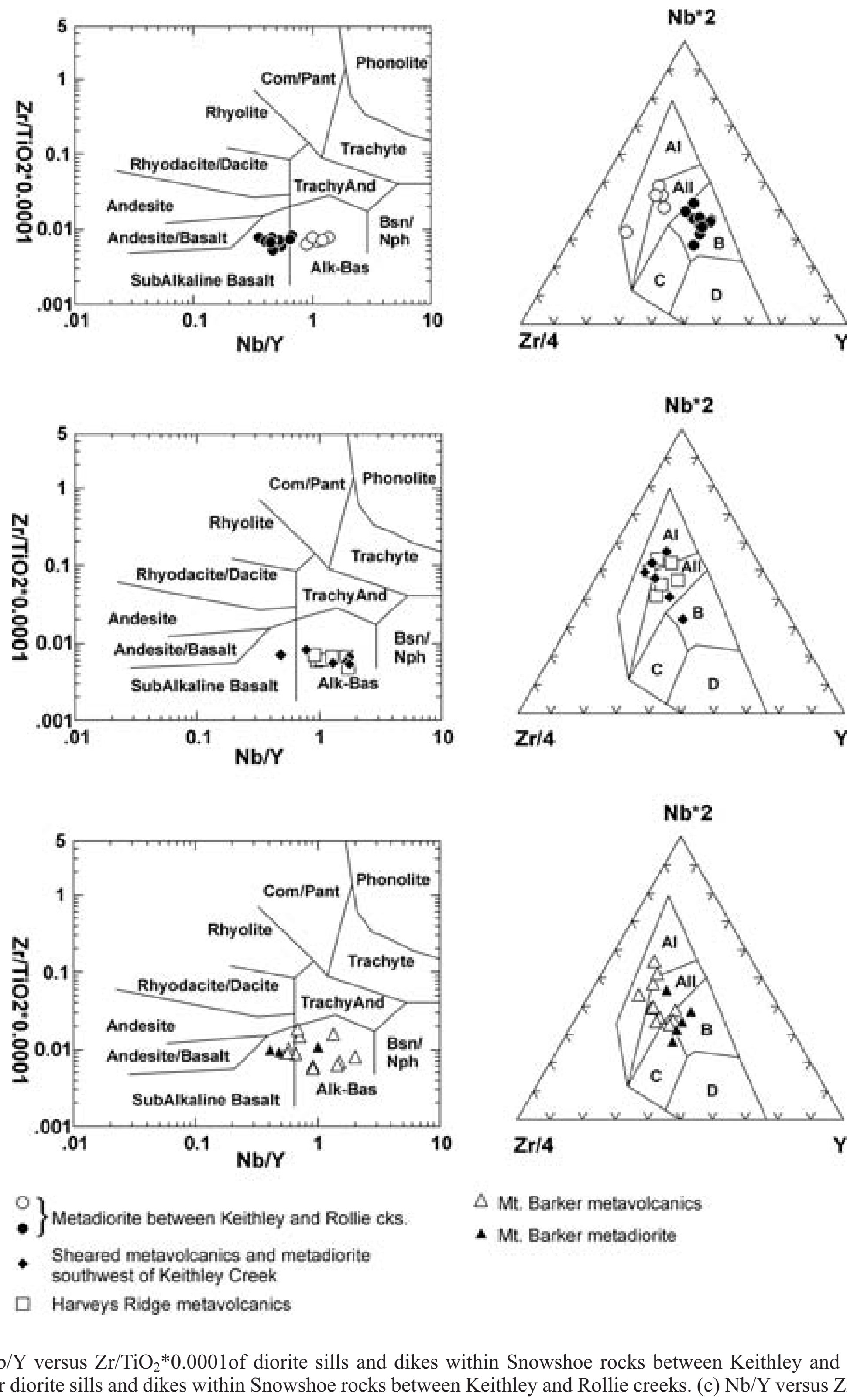

Figure 8. (a) Nb/Y versus Zr/TiO_2*0.0001of diorite sills and dikes within Snowshoe rocks between Keithley and Rollie creeks. (b) Nb*2-Zr/4-Y for diorite sills and dikes within Snowshoe rocks between Keithley and Rollie creeks. (c) Nb/Y versus Zr/TiO_2*0.0001 for sheared metavolcanics and diorite southwest of Keithley Creek and Harveys Ridge volcanics. (d) Nb*2-Zr/4-Y for sheared metavolcanics and diorite southwest of Keithley Creek and Harveys Ridge volcanics. (e) Nb/Y versus Zr/TiO_2*0.0001 for diorite and metavolcanics within the Mount Barker volcanics. (f) Nb*2-Zr/4-Y for diorite and metavolcanics within the Mount Barker volcanics. AI - within-plate alkali basalts; AII - within-plate alkali basalts and within-plate tholeiites; B - E-type MORB (mid-ocean ridge basalt); C - within-plate tholeiites and volcanic-arc basalts; D - N-type MORB and volcanic-arc basalts. Alk-bas - alkali-basalt; bsn - basinite; com - comendite; nph - nephelinite; pant - pantellerite; trachyand - trachyandesite.

line, within-plate signatures and the other having subalkaline compositions and suggesting a MORB setting (Figure 8). A very similar trend is exhibited for samples taken from the body of sheared mafic metavolcanic and dioritic rocks southwest of Keithley Creek (Figure 8). Harveys Ridge metavolcanics are entirely of alkaline composition and have a within-plate signature.

Mount Barker volcanics and metadiorite are part of the Downey/Keithley succession and plot within the alkaline and subalkaline fields, respectively (Figure 8). Furthermore, the values of Nb-Y and Zr also show within-plate and MORB tectonic signatures on the discrimination diagram proposed by Meschede (1986). It is interesting to note that several of the metadiorite sample points fall within the volcanic arc basalt field (C).

In summary, preliminary geochemistry of mafic igneous rocks within the Snowshoe Group indicate alkaline to subalkaline compositions and generally suggest an extensional tectonic setting.

STRUCTURE AND METAMORPHISM

Sedimentary and igneous rocks record at least three phases of penetrative deformation at the outcrop scale (Figure 9). The first consists of a layer-parallel fabric defined by the alignment of phyllosilicates and, in higher strain areas, the flattening of silicate minerals. The second phase of deformation was quite ductile and of such intensity that first phase foliation and bedding are approximately parallel to sub-parallel to second phase foliations along second phase fold limbs. It is only in the core of second phase fold structures that one can observe the layer parallel first phase foliation being crenulated. The last phase of ductile deformation is seen as a sub-vertical crenulation cleavage axial planar to open folds. These crenulations are not ubiquitous throughout the map area, being more evident in the upper greenschist to amphibolite grade regions. Locally, especially near northeast trending fault structures, northeast trending crenulations are developed across second phase foliations. The relationship of these to third phase crenulations is unclear.

No first phase folds or other large-scale structures were observed outside of the large shear zone at the contact between the Crooked Amphibolite and Quesnel Lake Gneiss. This shear zone is believed to be a first phase structure and resulted from the emplacement of Slide Mountain and Quesnel rocks overtop of the Snowshoe Group (Rees, 1987; Struik, 1988). Surprisingly, no large scale folds or faults have been recognized within Snowshoe stratigraphy that are unequivocally related to this convergence.

The geological pattern southeast of Cariboo Lake and in the region between Barker and Ishkloo creeks is dominated by second and third phase fold structures. The area between Barker and Ishkloo creeks, as with the area mapped during the 2000 field season, contains southeast to northwest trending second phase foliations which dip shallowly or moderately to the north and outline large-scale southwesterly verging fold structures (Ferri, 2001a, b). These general attitudes have been modified north of Cariboo Lake by upright third phase folding producing the large Lightening Creek Anticlinorium and related structures to the southwest. Large third phase folds similar to these were delineated in the region between Frank and Sellers creeks (Ferri, 2001a, b). There is a profound change in structural style north and south of Cariboo Lake. To the north of the lake, third phase structures, like the Lightening Creek Anticlinorium, are the dominant structures and control the map pattern. Second phase structures may be present here, but may have been refolded by these third phase structures.

Near Grain Creek, the Keithley quartzite outcrops on a ridge in the very southeastern part of the map area. Its disappearance to the south is interpreted to result from a second phase fold closure. To the northeast, poor exposure and the lack of a suitable marker within the large expanse of rocks tentatively assigned to the upper transitional Harveys Ridge made delineation of structures tentative, at best.

North of Cariboo Lake, the northeast trending axis of the Lightening Creek Anticlinorium can be traced from the eastern side of Yanks Peak down to Cariboo Lake. Second and first phase foliations are also broadly warped to the west of this structure (Figure 3a) suggesting the presence of similar structures. One of these is well outlined by the long, northeastward tongue of Quesnel Lake Gneiss which extends almost to the mouth of Keithley Creek (Figure 3a, b). The core of the Lightening Creek Anticlinorium occurs within the broad expanse of Harveys Ridge lithologies. The Agnes conglomerate is also repeated on either side of the axis. The steep dip of first and second foliations on either side of the axis, particularly to the northeast, further accentuates this large fold.

The stratigraphy on Yanks Peak poses some structural challenges. This overturned panel of Keithley stratigraphy, together with rocks tentatively assigned to the Keithley succession immediately to the southwest and Agnes and Harveys Ridge stratigraphy in the core of the Lightening Creek Anticlinorium, suggests the presence of a northeast verging fold or faulted fold structure which is tentatively shown in Figure 3b. The orientation of this fold is inconsistent with a third phase structure (*i*.e. parasitic fold to the Lightening Creek Anticlinorium) and, if correct, is most likely related to second phase deformation. Struik (1988) outlines similar structures in the Wells-Barkerville map sheet. If this interpretation is accurate, this second phase vergence reversal or confrontation zone would suggest the presence of box fold-like geometry similar to the west flank of the Porcupine Creek Anticlinorium (Likorish, 1993). Second phase fold structures and the relationship between second phase foliation and bedding between Yanks Peak and Keithley Creek, are consistent with a northeast-verging fold structure inferred in Figure 3b.

Highly deformed meta-volcanic and igneous rocks along the southwest side of Keithley Creek suggest the presence of a large ductile shear zone. No kinematic indicators could be discerned within these deformed rocks and the vergence of the fault zone is not known. This fault roughly coincides with the northeasterly directed Keithley Thrust first delineated by Struik (1983a; 1988). The southward extension of this fault is not known. It cannot be traced south-

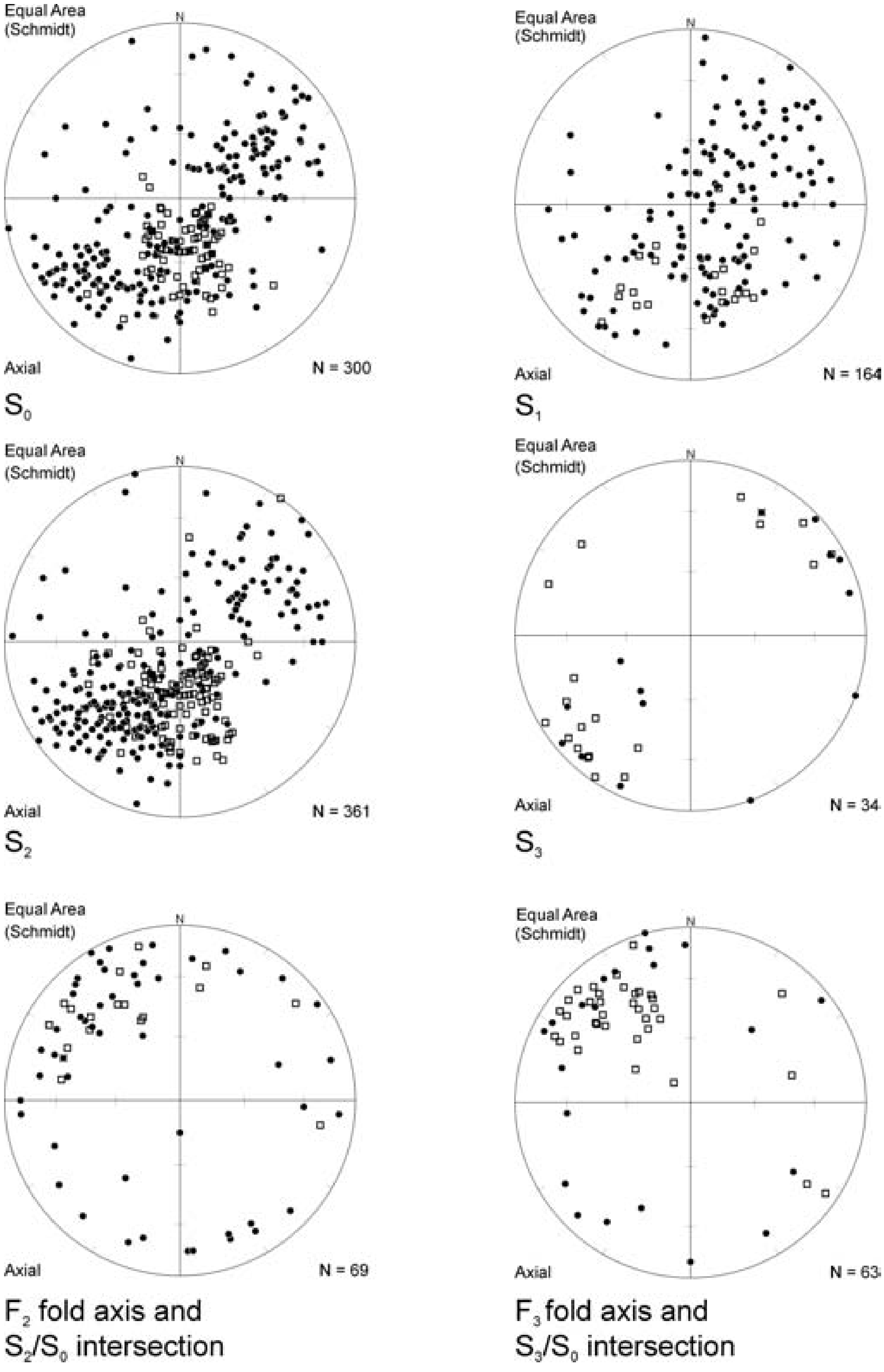

Figure 9. Equal area plots of structural data collected within the map area. Symbols refer to areas mapped during 2001 field season. These areas are shown in Figure 2.

eastward towards Cariboo Lake suggesting that it may trace an arcuate path along the headwaters of Asserlind Creek, following the general trend of foliation, and then swing around and up along Rollie Creek.

Higher grade metamorphic rocks were encountered in two areas: between Barker and Ishkloo creeks and in the area west of Keithley Creek. The area between Barker and Ishkloo creeks occurs within the garnet isograd and staurolite was observed locally. Metamorphic mineral assemblages suggest lower amphibolite conditions. Southwest of Keithley Creek garnet-biotite-muscovite schist and garnet-hornblende and actinolite bearing mafic metavolcanics occur, indicating upper greenschists to lower amphibolite environments. Outcrop is sporadic in this area and mapping of metamorphic isograds was not possible. Biotite-bearing schist can be traced up to the Crooked Amphibolite in the southwest, although the few outcrops of the Late Triassic Black phyllite seen further west are relatively unmetamorphosed.

Metamorphic rocks southwest of Keithley Creek are also characterized by the presence of large (up to 3 centimetres) idioblastic crystals of andalusite. The orientation of these crystals appears random or semi-random and this mineral suggests low pressure metamorphic conditions.

In general, peak metamorphic conditions, as shown by the growth of metamorphic index minerals, occurred during the latter parts of the second phase of deformation. The presence of muscovite and chlorite along third phase crenulations indicates that this period of deformation occurred during the waning stages of this metamorphic event. First phase deformation is believed to have begun in the late Early Jurassic (approximately 190 to 185 Ma; Rees, 1987). Metamorphic sphene in parts of the Quesnel Lake Gneiss suggest that second phase deformation occurred at approximately 175 Ma (Mortensen *et al*., 1987). Arguments put forth by Rees (1987) suggest that there was little or no break between second and third phase deformation, with the latter continuing to about 160 Ma. Thus the main ductile elements present within the map area occurred over a relatively short time period.

MINERAL OCCURRENCES

One of the main objectives of this mapping project was to examine the geologic setting of recently discovered massive sulphide mineralization in the Snowshoe Group. During the course of mapping, a new semi-massive sulphide occurrence was discovered within rocks of the Harveys Ridge succession and is here named the Unlikely showing. This, together with other indicators of mineralization within this unit and the more important Frank Creek occurrence, suggests this horizon has above average potential for hosting additional massive sulphide mineralization. It will also be argued later in this section that the revised stratigraphic sequence for the Snowshoe Group correlates well with Eagle Bay sections containing significant massive sulphide occurrences in the Adams Plateau region (Lucky Coon) and that this metallogenic horizon or time line extends northward into the Barkerville area.

In addition to massive sulphide mineralization, there are numerous other mineral occurrences within the map area. These include the abundant Ag-Au veins in the region around Yanks Peak (Holland, 1954), the Cariboo-Hudson gold mine and associated showings, numerous placer operations on Keithley, Pine and Harveys creeks and other minor vein occurrences. Mapping this summer also encountered several minor Cu-bearing veins and disseminations within volcanics of the Downey/Keithley succession. The following discussion focuses on the Ace and Frank Creek occurrences and the reader is directed towards the Minfile database for information on the other showings.

UNLIKELY

Mapping during the 2001 field season led to the discovery of the Unlikely Cu-bearing semi-massive sulphide occurrence (Photo 3). It is located along the main road on the north shore of Cariboo Lake, approximately 2.25 kilometres southwest of the small community of Keithley Creek. Mineralogy, overall characteristics and association with mafic metavolcanics suggest this may represent stratiform besshi-style sulphide mineralization similar to that at Frank Creek, immediately to the southeast.

Host rocks are grey to dark grey or black phyllites and siltstones of the Harveys Ridge succession. Locally, immediately adjacent to the sulphides, is a "stripped" sequence of alternating light grey to white and dark grey siltstone from 0.5 to 1 centimetre thick. Green-mica bearing, ankerite altered and silicified? horizons up to several metres thick occur structurally above the showing. Chemical analyses suggests these are highly altered mafic volcanic sequences originally of alkaline composition.

The showing is about 1.5 metres wide at its thickest point and gossanous sediments and sulphide can be traced for approximately 10 to 15 metres. The strike of the sulphide horizon is parallel to schistosity or cleavage presumably of second phase origin. Bedding is tightly folded locally, but is essentially parallel to the main schistosity. The mineralized zone is highly siliceous and appears to be silicified Harveys Ridge lithologies. The southwest part of the mineralized zone contains the highest concentrations of sulphides, with

Photo 3. The Unlikely mineral occurrence (outlined by the white line).

TABLE 2
GEOCHEMISTRY OF SEVERAL MINERALIZED HORIZONS AND OCCURRENCES WITHIN THE SNOWSHOE GROUP

	Easting	Northing	Mo 0.01	Cu 0.01	Pb 0.01	Zn 0.1	Ag 2	Ni 0.1	Co 0.1	Mn 1	Fe 0.01	As 0.1	U 0.1	Au 1	Th 0.1	Sr 0.5	Cd 0.01	Sb 0.02	Bi 0.02
01FFE-09-03	605535	5844523	4.27	2217.3	22.31	52.7	724	337.4	214.6	692	27.65	2875.4	1.1	12.4	0.6	12.6	0.06	1.71	33.36
01FFe-32-6	607045	5859165	18.14	114.86	16.58	513.6	295	62	6	364	10.88	67.2	3	1.2	1.4	11	0.63	8.52	0.17
01FFe-32-6a	607045	5859165	1.54	63.3	3.1	161.2	156	26.3	3.4	34	4.64	6.3	1.1	1.3	2	2.3	0.17	0.81	0.02
UNLIKELY 1	605535	5844523	4.84	1489.8	10.32	37.5	403	285.2	213.9	636	29.01	2901.2	1.4	8.1	0.7	7.6	0.11	1.94	16.13
UNLIKELY 2	605535	5844523	4.92	894.75	12.25	40.3	330	59.8	37.5	533	28.21	175.5	1.9	6	1	12.6	0.08	0.29	17.4
UNLIKELY 3	605535	5844523	3.49	3323.2	31.66	46	963	216.3	197.7	744	24.07	32.7	0.9	15.7	0.5	15	0.16	0.25	53.34
UNLIKELY 4	605535	5844523	2.58	518.58	13.95	162	146	64.6	72.7	1059	12.14	43.4	2.7	4.5	2.7	13	0.2	0.06	20.79
UNLIKELY 5	605535	5844523	2.08	1131.2	12.25	92.7	306	84.2	82.2	970	12.31	16.2	1.7	4.9	1.8	42.6	0.19	0.1	15.11
01FFE-9-2A	605096	5844003	0.84	172.84	4.38	61.4	119	257.4	56.4	964	6.9	187.5	0.3	1.9	1	123.7	0.18	0.32	2.57
01FFE-6-2	605096	5844003	2.83	46.36	1.08	28.2	31	6.2	14.1	571	4.11	0.1	0.4	1.3	3.2	69.2	0.01	0.07	0.28
01FFE-11-7	601064	5850147	1.42	37.9	0.74	51.5	11	3.7	11.6	354	3.45	0.3	0.7	0.5	3.8	34.4	0.06	0.02	< .02
01FFE-22-1	613924	5887034	0.09	15637	2.13	134.5	6211	23.8	50.3	1177	7.1	1.2	0.1	361.2	2.3	37.4	0.09	0.06	4.63
01FFE-22-2	613827	5858245	0.51	492.72	11.95	28.1	1277	104.1	49.2	3854	29.97	4.9	0.9	769.7	2.9	134.5	0.04	0.18	2.17

	V 2	Ca 0.01	P 0.001	La 0.5	Cr 0.5	Mg 0.01	Ba 0.5	Ti 0.001	B 1	Al 0.01	Na 0.001	K 0.01	W 0.2	Sc	Tl 0.02	S 0.02	Hg 5	Se 0.1	Te 0.02	Ga 0.02
01FFE-09-03	35	0.45	0.043	1.8	73.1	1.3	28.2	0.005	< 1	0.99	0.01	0.03	1.8	2.5	0.13	14.24	12	16.6	0.11	5.9
01FFe-32-6	53	0.01	0.077	3.2	100.3	0.03	124.5	0.001	4	0.57	0.003	0.14	0.5	1.6	0.05	0.12	24	6.8	0.14	1.9
01FFe-32-6a	22	0.01	0.046	9.3	68.1	0.01	132.4	0.003	1	0.48	0.021	0.09	< .2	1.7	0.04	0.07	6	1.6	0.05	0.9
UNLIKELY 1	3	0.26	0.01	1	43.6	0.36	19.4	0.003	< 1	0.13	0.013	0.03	1.7	0.6	0.2	16.07	20	16.5	0.15	0.8
UNLIKELY 2	13	0.17	0.023	1.5	40.3	0.16	59.9	0.01	< 1	0.29	0.017	0.04	1	1.1	0.03	2.34	5	6.7	0.05	1.9
UNLIKELY 3	6	0.72	0.006	0.8	51.1	0.27	19.9	0.002	< 1	0.18	0.016	0.02	2.1	0.9	0.02	15.93	< 5	25.3	0.1	1.6
UNLIKELY 4	44	0.31	0.08	1.8	84.3	1.26	53.7	0.004	1	0.99	0.044	0.04	0.4	2.9	0.02	2.86	< 5	6.2	0.03	5
UNLIKELY 5	21	1.73	0.037	1.3	67.4	1.04	64.6	< .001	< 1	0.55	0.022	0.06	0.4	1.6	0.03	5.41	< 5	9	0.05	2.5
01FFE-9-2A	14	3.72	0.067	3.3	63.3	5.25	84.6	0.012	< 1	0.42	0.012	0.17	< .2	6.6	0.07	1.22	< 5	1.7	0.02	1
01FFE-6-2	15	1.41	0.535	32.3	2.1	0.9	248.8	0.061	< 1	1.69	0.034	0.37	0.4	0.7	0.18	0.57	< 5	0.8	< .02	4.4
01FFE-11-7	16	1.42	0.454	21.6	1.4	0.68	81.6	0.069	1	1.55	0.045	0.12	< .2	0.8	0.02	0.15	< 5	0.2	< .02	4.1
01FFE-22-1	162	1.38	0.233	14	4.1	3.12	6.6	0.028	< 1	4.28	0.011	< .01	< .2	10	< .02	0.06	1159	3.5	0.05	19.1
01FFE-22-2	< 2	7.21	0.02	11.2	4.3	0.42	24.9	0.003	< 1	0.56	0.003	0.01	2.5	0.4	0.02	10.97	44	1.4	0.17	2.3

NOTES: Steel mill grinding at GSB; analysis by Aqua regia digestion (1 g sample)-mass spectroscopy at ACME Analytical Laboratory, Vancouver, B.C.; all results in ppm except Fe, Ca, P, Mg, Ti, Al, Na, K and S which are in per cent and Au in ppb

01FFe-09-03: grab sample of sulphides at the Unlikely showing (Harveys Ridge succession)

01FFe-32-6: grab sample of ferricrete on Harveys Ridge siltstone and phyllite

01FFe-32-6a: grab sample of pyritiferous Harveys Ridge siltstones and phyllites

UNLIKELY 1: grab sample of high grade zone (Harveys Ridge succession)

UNLIKELY 2: semi-continuous chip sample (1.5 metres) across the main mineralized zone. (Harveys Ridge succession)

UNLIKELY 3: grab sample from the middle of the main silicified zone. (Harveys Ridge succession)

UNLIKELY 4: grab sample of thinnly interlayered light and dark grey siltstone with minor sulphides. Approximately 5 m northeast of the main zone. (Harveys Ridge succession)

UNLIKELY 5: grab sample of spalled piece of siliceous Harveys Ridge with disseminated sulphides. (Harveys Ridge succession)

01FFe-9-2A: grab sample of altered volcanics within the Harveys Ridge succession.

01FFe-6-2: grab sample of 2 m wide gossanous siltstone and sandstone of Harveys Ridge succession. Up to 20 per cent pyrite.

01FFe-22-1: grab sample of chalcopyrite-bearing quartz-carbonate vein within Mount Barker volcanics.

01FFe-22-2: grab sample of pyrite-rich zone within limestone adjacent to Mount Barker volcanics (Downey/Keithley succession). Garnet? and diopside? Associated with this suggesting skarn-type mineralization one 1.5 by 3 metre area containing zones over 50 % sulphide, and averaging between 25 and 50 %. Sulphide content decreases to the northeast and disappears into the "stripped" Harveys Ridge lithology described above.

Sulphides consist of pyrite, pyrrhotite, arsenopyrite and chalcopyrite. Cu content varies from 0.05 to 0.3 % and some of the higher Cu values are associated with anomalous Au (Table 2). Sulphides commonly appear finely disseminated and have a dull lustre, although they are locally recrystallized into coarser masses. Sulphides also form more concentrated horizons or discontinuous lenses parallel to the main schistosity.

ACE

The Ace property is located south of the Little River, 35 kilometres northeast of Likely and is easily reached from the Wells-Barkerville road. A detailed description of the property history can be obtained from Höy and Ferri (1998a). The Little River valley, within which the Ace property occurs, contains extensive glacio-fluvial deposits and as such the only exposures are limited to the river valley, the ridge containing Mount Barker and some road cuts. Extensive trenching within the property was carried out in the mid-1990s but has either been subsequently back filled and/or slumped in or flooded. The lithologies exposed in the trenches were described in Höy and Ferri (1998a) and these rock types are entirely consistent with other sequences of the Downey/Keithley succession encountered northwest and southeast of the Ace property. Sulphide mineralization is semi-massive within quartzo-feldspathic schist and phyllite, and consists primarily of pyrite and pyrrhotite with lesser amounts of chalcopyrite, sphalerite and galena. As Höy and Ferri (1998a) point out, Cu/Pb and Zn/Pb ratios, together with the mixed mafic meta-volcanic and sedimentary sequence suggest a besshi-type setting for this occurrence.

Barker Minerals Ltd. drilled 7 holes on the property during the 1998 field season (Payne, 1999). The thickest, composite section of sulphide encountered was approximately 0.5 metres and was elevated in Au, Ag, Cu and Zn. Barker Minerals Ltd. suggest that sulphide mineralization sits above a felsic unit which is from 4 to 82 metres in thickness. This rock outcrops near the main road and Höy and Ferri (1998a) theorized that it may represent highly deformed intrusive rock. This unit was sampled during the 2000 field season for U-Pb geochronology. Recovered zircons had a morphology indicating they were detrital and subsequent analysis confirms this (Richard Freidman, Personal Communication, 2001). These results cast doubt on the felsic volcanic or intrusive origin of this unit.

Mafic volcanics and intrusive rocks associated with the meta-sedimentary sequence hosting the Ace property can be traced northwestward across the Cariboo River and to Harveys Creek. Bornite-bearing quartz veins were observed within metavolcanic rocks on the south side of Harveys Creek and are found in metamorphosed rocks in the Pennys Creek area northwest of the Cariboo-Hudson Mine. Malachite stained metadiorite or metavolcanics were also observed southwest and south of the Ace occurrence, within the Mount Barker volcanic sequence. Metavolcanic rocks disappear to the northwest and only a narrow section of chlorite schist is associated with limestone at Downey Pass, near Wells. These volcanics can be traced southeastward (Struik, 1983b) and it is argued that they form part of the stratigraphic sequence in the Adams Plateau area (Eagle Bay Assemblage).

MASSIVE SULPHIDE POTENTIAL IN THE HARVEYS RIDGE SUCCESSION

The presence of the Frank Creek and Unlikely besshi-style volcanogenic massive sulphide occurrences within the Harveys Ridge succession clearly shows that within Snowshoe stratigraphy, this unit has above average potential for hosting significant syngenetic mineralization. Mapping along the Snowshoe Plateau also encountered several sections of ferricrete incrusted sections of Harveys Ridge sediments. Sampling of one northeast of Yanks Peak returned elevated levels of Zn, although the levels of other elements are relatively low (Table 2). The presence of these ferricrete deposits indicates that the host rocks either have a high iron background level or contain zones of high iron concentration that are being leached by ground waters percolating along permeable layers, most likely a fault zone.

The Frank Creek showing is hosted by black to dark grey carbonaceous shales and siltstones which commonly lie immediately below the Agnes conglomerate. This is especially true on the Snowshoe Plateau where fine black clastics also contain ferricrete deposits. Conglomeratic rocks of the Agnes occur roughly at the same stratigraphic level as the Frank Creek volcanics (*see* Ferri, 2001b) and occur immediately above the Frank Creek occurrence. These two rock types suggest increased tectonic activity subsequent to the deposition of the fine black clastics. Furthermore, the deposition of alkalic volcanic rocks points to increased heat flow and extensional tectonics during this time. The presence of massive sulphide mineralization within the black clastics of the Harveys Ridge succession may also indicate that this horizon was experiencing precursor effects registered in immediately overlying lithologies. These fine, carbonaceous, black clastics indicate anoxic conditions which would have been an ideal environment for the deposition of sulphides from expelled metal-rich brines. Although this scenario is analogous to sedimentary exhalative-type massive sulphide mineralization (SEDEX) found elsewhere in the Cordillera (*i.e.* Kechika Trough) the elevated levels of Cu and pyrrhotite suggests higher temperatures and input from igneous sources, and is more akin to sediment-volcanic or besshi-type mineralization.

Correlation southward of the Harveys Ridge succession with massive sulphide-bearing stratigraphy of the Eagle Bay Assemblage in the Adams Plateau region suggests that this horizon represents a significant metallogenic period within the western part of the Kootenay Terrane. In the Adams Plateau area similar stratigraphy hosts several significant massive sulphide deposits (Lucky Coon, King Tut; Höy, 1999). These occurrences consist of Pb-Zn deposits with elevated levels of Cu and Au. Höy (1999) demonstrated that thickness and facies changes within local stratigraphy reflect the presence of growth faults which may have been channel ways for metalliferous brines that produced the deposits. There is not enough stratigraphic control in the present study area to suggest a similar scenario, although the nature of the deposits implies that some type of fault system may have been involved with their formation.

CONCLUSIONS

- A new Cu-rich massive sulphide showing named the Unlikely was discovered within rocks of the Harveys Ridge succession.
- The stratigraphic sequence hosting the Frank Creek and Unlikely occurrences is similar to Eagle Bay stratigraphy in the vicinity of the Lucky Coon and related showings within the Adams Plateau.
- Mapping suggests that rocks of the Downey and Ramos may be equivalent to the Keithley succession and that Hardscrabble Mountain and Harveys lithologies may also be time equivalent.

ACKNOWLEDGMENTS

The authors would like to thank Adrian Hickin and Jarrod Brown for competent and cheerful assistance this past summer. Their angling abilities kept us well fed during parts of the summer.

The senior author would also like to thank Bert Struik of the Geological Survey of Canada for providing him with his original field data for this area. This information was invaluable, especially in areas where we did not access due to time constraints.

The excellent hospitality of Donna and Allen Purdy of Neilsen's Lakeshore Cabins made our stay in Likely much more enjoyable. Flycamps were located and supported through the help of Tom Arduini of Arduini Helicopters.

We would like to thank Brian Grant and Trygve Höy for reading early versions of this manuscript and for providing useful and constructive criticism.

REFERENCES

Bloodgood, M. (1990): Geology of the Eureka Peak and Spanish Lake map areas, British Columbia; *B.C. Ministry of Energy, Mines and Petroleum Resources*, Paper 1990-3.

Campbell, R.B. (1978): Quesnel Lake, British Columbia; *Geological Survey of Canada,* Open File 574.

Campbell, R.B., Mountjoy, E.W., and Young, F.G. (1973): Geology of the McBride map area, British Columbia; *Geological Survey of Canada*, Paper 72-35.

Ferri, F. (2001a): Geological setting of the Frank Creek massive sulphide occurrence near Cariboo Lake, east-central B.C.; *in* Geological Fieldwork 2000, *B.C. Ministry of Energy and Mines*, Paper 2000-1, pages 31-49.

Ferri, F. (2001b): Geology of the Frank Creek - Cariboo Lake area, central British Columbia (NTS 93A/11,14); *B.C. Ministry of Energy and Mines* Open File 2001-11.

Ferri, F., Höy, T. and Friedman, R.M. (1999): Description, U-Pb age and tectonic setting of the Quesnel Lake Gneiss, east-central British Columbia; *in* Geological Fieldwork 1998, *B.C. Ministry of Energy and Mines*, Paper 1999-1, pages 69-80.

Holland, S.S. (1954): Geology of the Yanks Peak-Roundtop Mountain area, Cariboo District, British Columbia; *British Columbia Department of Mines and Petroleum Resources*, Bulletin 34.

Höy, T. (1999): Massive sulphide deposits of the Eagle Bay Assemblage, Adams Plateau, south central British Columbia (082M/3, 4); *in* Geological Fieldwork 1998, *B.C. Ministry of Energy and Mines*, Paper 1999-1, pages 223-245.

Höy, T. and Ferri, F. (1998a): Stratabound base metal deposits of the Barkerville Subterrane, central British Columbia (093A/NW); *in* Geological Fieldwork 1997, *B.C. Ministry of Employment and Investment*, Paper 1998-1, pages 13-1 - 13-12.

Höy, T. and Ferri, F. (1998b): Zn-Pb deposits in the Cariboo Subterrane, central British Columbia (093A/NW); *in* Geological Fieldwork 1997, *B.C. Ministry of Employment and Investment*, Paper 1998-1, pages 14-1 - 14-9.

Lang, A.H. (1938): Keithley Creek map area, Cariboo District, British Columbia; *Geological Survey of Canada*, Paper 38-16.

Lang, A.H. (1939): Keithley Creek map area; *Geological Survey of Canada*, Paper 38-16.

Likorish, W.H. (1993): Structural evolution of the Porcupine Creek anticlinorium, Western Main Ranges, Rocky Mountains, British Columbia; *Journal of Structural Geology*, Volume 15, Numbers 3-5, pages 477-489.

Meschede, M. (1986): A method of discriminating between different types of mid-ocean ridge basalts and continental tholeiites with the Nb-Zr-Y diagram; *Chemical Geology*, Volume 56, pages 207 - 218.

Montgomery, J.R., and Ross, J.V. (1989): A note on the Quesnel Lake Gneiss, Cariboo Mountains, British Columbia; *Canadian Journal of Earth Sciences*, Volume 26, pages 1503-1508.

Mortensen, J.K., Montgomery, J.M. and Fillipone, J. (1987): U-Pb zircon, monazite, and sphene ages for granitic orthogneiss of the Barkerville Terrane, east-central British Columbia; *Canadian Journal of Earth Sciences*, Volume 24, pages 1261-1266.

Panteleyev, A, Bailey, D.G., Bloodgood, M.A. and Hancock, K.D. (1996): Geology and mineral deposits of the Quesnel River-Horsefly map area, central Quesnel Trough, British Columbia; *Ministry of Employment and Investment*, Bulletin 97, 156 pages.

Payne, J. (1999): Geological, geochemical and geophysical report on the Ace property; *B.C. Ministry of Energy and Mines*, Assessment Report 25904.

Rees, C.J. (1987): The Intermontane - Omineca Belt boundary in the Quesnel Lake area, east-central British Columbia: Tectonic implications based on geology, structure and

[3] *The large body of meta-diorite northeast of Mount Barker has been dated by U-Pb geochronology and preliminary ages of 277.3 ± 4.8 Ma and 281.0 ± 5.2 Ma have been obtained (R. Friedman, Personal Communication, 2001) suggesting it is not co-magmatic with the meta-volcanics.*

[4] *A subalkaline sill southwest of Keithley Creek was samples and dated by U-Pb geochronology resulting in a preliminary age of 281 ± 12 Ma (R. Friedman, Personal Communication, 2001), very similar in age to meta-diorite along Mount Barker.*

paleomagnetism; Ph.D. Thesis; *Carleton University*, Ottawa, Ontario, 421 pages.

Schiarizza, P. and Preto, V.A. (1987): Geology of the Adams Plateau-Clearwater-Vavenby area; *B.C. Ministry of Energy, Mines and Petroleum Resources*, Paper 1987-2, 88 pages.

Struik, L.C. (1981): Snowshoe Formation, central British Columbia; *in* Current Research, Part A, *Geological Survey of Canada,* Paper 81-1A, pages 213-216.

Struik, L.C. (1982): Wells (93H/4), Spectacle Lakes (93H/3), Swift River (93A/13), and Cariboo Lake (93A/14) map areas; *Geological Survey of Canada*, Open File 858.

Struik, L.C. (1983a): Bedrock geology of Spanish Lake (93A/11) and parts of adjoining map areas, central British Columbia; *Geological Survey of Canada*, Open File 920.

Struik, L.C. (1983b): Bedrock geology of Quesnel Lake (93A/10) and part of Mitchell Lake (93A/15) map areas, central British Columbia; *Geological Survey of Canada*, Open File 962.

Struik, L.C. (1986): Imbricated terranes of the Cariboo Gold belt with correlations and implications for tectonics in southeastern British Columbia; *Canadian Journal of Earth Sciences*, Volume 23, pages 1047-1061.

Struik, L.C. (1988): Structural geology of the Cariboo Gold Mining District, east-central British Columbia; *Geological Survey of Canada*, Memoir 421, 100 pages.

Sutherland Brown, A. (1957): Geology of the Antler Creek area, Cariboo District, British Columbia; *British Columbia Department of Mines and Petroleum Resources*, Bulletin 38.

Sutherland Brown, A. (1963): Geology of the Cariboo River area, British Columbia; *British Columbia Department of Mines and Petroleum Resources*, Bulletin 47.

Winchester, J.A. and Floyd, P.A. (1977): Geological discrimination of different magma series and their differentiation products using immobile elements; *Chemical Geology*, Volume 20, pages 325-342.

Geology of Quesnel and Slide Mountain Terranes West of Clearwater, South-Central British Columbia (92P/9, 10, 15, 16)

By Paul Schiarizza[1], Scott Heffernan[2] and Joshua Zuber[3]

KEYWORDS: *Quesnel Terrane, Nicola Group, Harper Ranch Group, Triassic-Jurassic plutons, Thuya Batholith, Slide Mountain Terrane, Fennell Formation, Raft Batholith, copper, molybdenum, dextral strike-slip.*

INTRODUCTION

The Bonaparte project is a multi-year bedrock mapping program initiated by the British Columbia Geological Survey during the 2000 field season. The project is focused on Mesozoic arc volcanic and plutonic rocks of the Quesnel Terrane in the northeastern part of the Bonaparte Lake (92P) map sheet (Figure 1). This area encompasses a northwest-trending belt of high mineral potential that includes a number of interesting mineral occurrences, as well as numerous regional geochemical survey and till geochemical anomalies. The Bonaparte project will improve the quality and detail of bedrock maps for the area, which are based primarily on 1:250 000-scale mapping carried out by the Geological Survey of Canada in the 1960s. The new mapping will provide an improved geologic framework for interpreting the mineral occurrences and geochemical anomalies, and for predicting favourable settings for future discoveries.

The initial mapping for the Bonaparte Project covered about 700 square kilometres within and adjacent to the Nehalliston Plateau, and is summarized by Schiarizza and Israel (2001). Fieldwork in June through August, 2001, extended this mapping northward to the south margin of the Raft Batholith, covering an additional 900 square kilometres (Figure 1). Here, we present preliminary results from this second year of mapping, together with some revisions to the interpretations presented by Schiarizza and Israel (2001) based on new fossil data.

The area described in this report is bounded on the east by the North Thompson River, which is followed by Highway 5 and the main line of the Canadian National Railway. Highway 24 branches westward from Highway 5 at the town of Little Fort and cuts across the southern part of the area to eventually connect with Highway 97 south of 100 Mile House. An east-west transect across the northern part of the area is provided by the Camp 2 logging road between Clearwater and Canim Lake. An extensive network of secondary logging and Forest Service roads that branch from these major roads provides easy access to most parts of the map area.

The geological interpretations presented here build on the 1:250 000-scale mapping of Campbell and Tipper (1971), whose work incorporated earlier studies along the North Thompson River by Uglow (1922) and Walker (1931). Our work also incorporates the work of Preto (1970) who focused on mineral occurrences in the area north of Eakin Creek, and descriptions of geology and mineralization of a more local nature that are found in Assessment Reports and annual reports of the Ministry of Energy and Mines.

REGIONAL GEOLOGIC SETTING

The Bonaparte Project area is situated in the eastern Intermontane Belt, which is underlain mainly by Upper Paleozoic to Lower Mesozoic arc volcanic, plutonic and sedimentary rocks of the Quesnel Terrane. Farther west within the Intermontane Belt are coeval Paleozoic and Mesozoic rocks of the oceanic Cache Creek Terrane. At the latitude of the present study area, the boundary between the Cache Creek and Quesnel terranes is hidden beneath a broad area of Tertiary volcanic rocks and unconsolidated Quaternary sediments (Figure 1). Directly east of the Quesnel Terrane are rocks of the Omineca Belt, represented at this latitude by Upper Paleozoic basalt, chert, gabbro and associated rocks of the Slide Mountain Terrane, and Proterozoic and Paleozoic metasedimentary, metavolcanic and metaplutonic rocks of the pericratonic Kootenay Terrane. The latter succession is generally interpreted as an outboard facies of the North American miogeocline (*eg*. Colpron and Price, 1995), while the former may represent a marginal or back-arc basin that formed directly outboard of the continental margin in Late Paleozoic time (Klepacki and Wheeler, 1985; Schiarizza, 1989; Roback *et al*., 1994; Ferri, 1997). Jura-Cretaceous granitic rocks, including the Raft and Baldy batholiths, crosscut the boundaries between the Kootenay, Slide Mountain and Quesnel terranes. The youngest rocks in the region are valley-filling and plateau-capping flows of mainly Quaternary age that occur in the area of Clearwater and Wells Gray Park (Hickson and Souther, 1984).

The Quesnel Terrane is characterized by an Upper Triassic to Lower Jurassic magmatic arc complex that formed above an east-dipping subduction zone (Mortimer, 1987).

[1] *British Columbia Geological Survey*
[2] *The University of British Columbia*
[3] *University of Victoria*

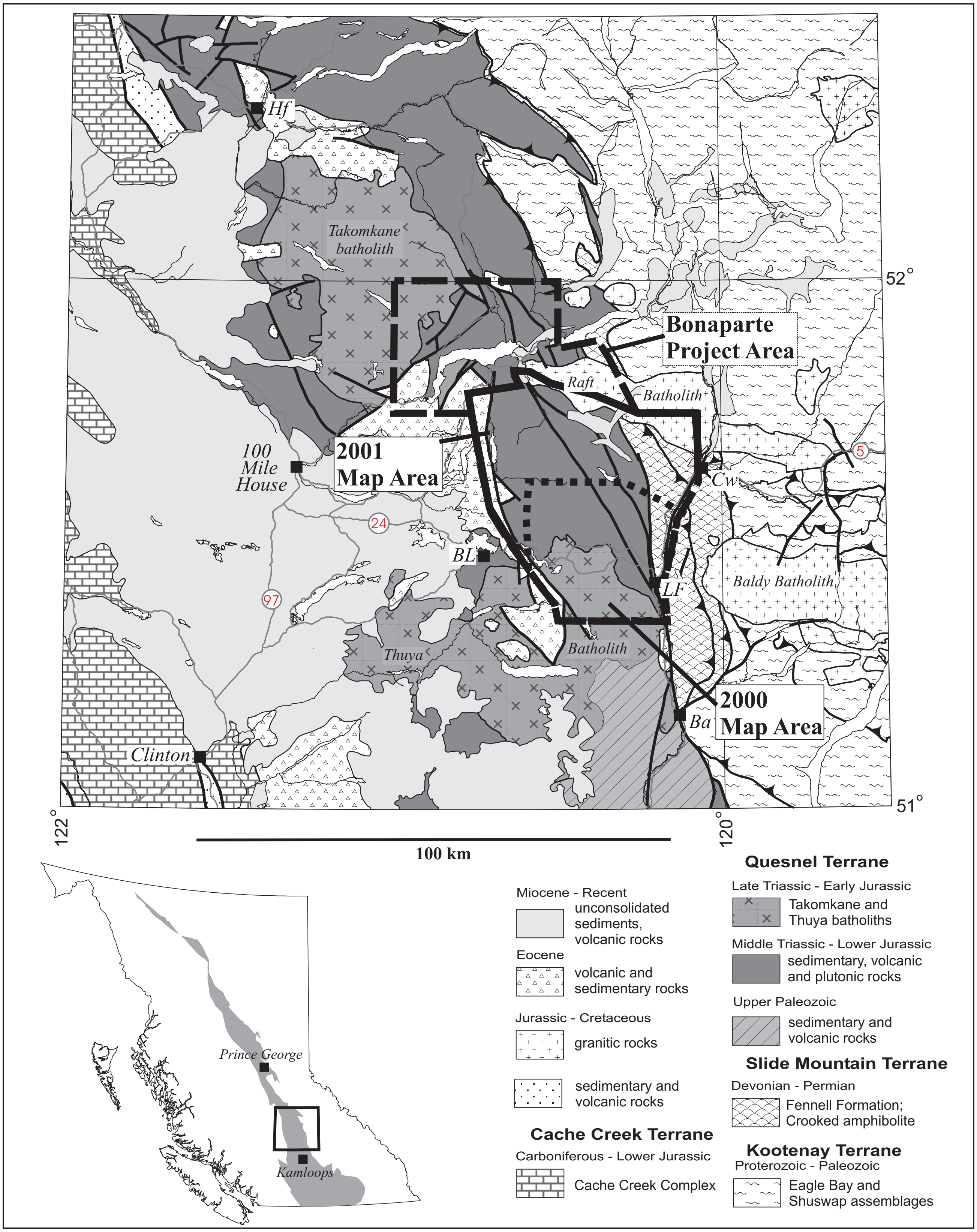

Figure 1. Regional geologic setting of the Bonaparte project area. Abbreviations: Ba, Barriere; BL, Bridge Lake; Cw, Clearwater; Hf, Horsefly; LF, Little Fort. Inset shows location of the map in south-central British Columbia, with distribution of the Quesnel Terrane shown in grey.

The Cache Creek Terrane to the west is inferred to include the remnants of the associated accretion-subduction complex (Travers, 1978). In southern and central British Columbia the early Mesozoic arc of the Quesnel Terrane is represented mainly by Upper Triassic volcanic and associated sedimentary rocks of the Nicola Group, together with abundant Late Triassic to Early Jurassic calc-alkaline to alkaline intrusions (Schau, 1970; Lefebure, 1976; Preto, 1977, 1979). Lower Jurassic volcanic rocks rest stratigraphically above Triassic arc volcanic rocks to the north of the Bonaparte project area, (Panteleyev *et al*., 1996; Nelson and Bellefontaine, 1996), but are apparently missing to the south, where this stratigraphic position is occupied by sedimentary rocks of the Lower to Middle Jurassic Ashcroft Formation (Travers, 1978; Monger and McMillan, 1989). However, Lower Jurassic arc volcanic rocks do occur in the easternmost part of the Quesnel Terrane in southern British Columbia, where they are represented by the Rossland Group (Höy and Dunne, 1997). In contrast to the Lower Jurassic volcanic rocks to the north of the Bonaparte area, these volcanic rocks rest above Triassic sedimentary rocks that were apparently deposited well east of the axis of Triassic arc magmatism.

In southern British Columbia, Mesozoic rocks of the Quesnel Terrane rest stratigraphically above a diverse assemblage of Paleozoic rocks, commonly across an angular unconformity (Read and Okulitch, 1977). Within and directly south of the Bonaparte project area, the Paleozoic part of the Quesnel Terrane comprises the Harper Ranch Group, which is interpreted as part of a late Paleozoic arc complex (Monger, 1977; Smith, 1979; Danner and Orchard, 2000). Elsewhere in southern British Columbia, Mesozoic rocks of the Quesnel Terrane rest stratigraphically above Paleozoic rocks of more oceanic aspect. These include rocks assigned to the Okanagan subterrane by Monger *et al*. (1991), and, along the eastern edge of the Quesnel Terrane, rocks included in the Slide Mountain Terrane (Campbell, 1971; Klepacki and Wheeler, 1985; Rees, 1987). In both southern and central British Columbia there is indirect evidence suggesting that Late Paleozoic arc rocks correlated with the Harper Ranch Group may have formed above a basement with North American affinities (Roback and Walker, 1995; Ferri, 1997). Furthermore, recent mapping directly south of the Bonaparte Lake map sheet, in the Vernon and Ashcroft map areas, suggests that pericratonic rocks correlative with those in the Kootenay Terrane extend farther west than previously thought, and underlie Permian and Triassic rocks of the Quesnel Terrane across an unconformable stratigraphic contact (Erdmer *et al*., 1999).

Deformation in the region included several pulses of Late Paleozoic to mid-Mesozoic contraction, as well as an important episode of dextral strike-slip and block faulting during Eocene time. Studies to the north of the Bonaparte project area document east-directed thrusting of Quesnel and Slide Mountain terranes over the Kootenay Terrane in late Early Jurassic time, followed by west-vergent folding and thrust faulting in the Middle Jurassic (Brown *et al*., 1986; Rees, 1987). A similar scenario, involving post-early Late Permian imbrication and emplacement above the Kootenay Terrane, followed by west-directed folding and thrust faulting, is documented for the Slide Mountain Terrane directly east of the project area (Schiarizza, 1983). There, the structural imbrication and emplacement of the Slide Mountain Terrane is interpreted as a Permo-Triassic event correlated with the Sonoma orogeny (Schiarizza, 1989).

LITHOLOGIC UNITS

The distribution of the main lithologic units within the southern and central parts of the Bonaparte project area, mapped during the 2000 and 2001 field seasons, is shown on Figure 2. Figure 3 provides a more detailed view of part of this area, including two-fold subdivisions of both the Nicola volcanic unit and the overlying Jurassic rocks. The cross sections of Figure 4 include the detailed subdivisions of Figure 3, and the lines of section are shown on both maps (although only partially represented on Figure 3). Most of the map units shown on Figures 2 and 3 are discussed in the following sections. However, some minor units in the southern part of the area, such as the Tintlhohtan Lake stock, are not mentioned because there is no new information to add to the descriptions provided by Schiarizza and Israel (2001).

FENNELL FORMATION

The Fennell Formation was defined by Uglow (1922) to include greenstone, gabbro and chert that he mapped along the east side of the North Thompson River valley between the Barriere River and Joseph Creek. It was traced northward by Walker (1931), who considered it to be mainly an intrusive body (the Fennell batholith), and then by Campbell and Tipper (1971) who, like Uglow, recognized that it included submarine volcanic and sedimentary rocks and local gabbroic intrusions. Campbell and Tipper correlated it with the Antler Formation of the Slide Mountain Group, which crops out 150 kilometres to the north in the Cariboo River area. The Fennell and Antler formations, together with similar rocks to the north and south, were subsequently assigned to the Slide Mountain Terrane, the most inboard tract of oceanic rocks within the Canadian Cordillera (Monger *et al*., 1982).

Detailed mapping of the Fennell Formation between the Barriere River and Clearwater by Schiarizza (1983, 1989) established that the formation could be separated into two major divisions. The structurally lower division is a heterogeneous assemblage of bedded chert, gabbro, diabase and pillowed basalt, with lesser amounts of sandstone, quartz-feldspar-porphyry rhyolite and intraformational conglomerate. Conodonts extracted from bedded chert range from Early Mississippian to early Late Permian in age (M.J. Orchard *in* Schiarizza and Preto, 1987), and their distribution demonstrates that the lower division comprises several imbricate thrust slices. The upper division consists almost entirely of pillowed and massive basalt, together with minor amounts of bedded chert and gabbro. Conodonts from chert intercalated with basalt at two localities are Pennsylvanian and Permian, respectively, indicating that the upper division spans at least part of the same age range as the lower division. Schiarizza (1983, 1989) therefore in-

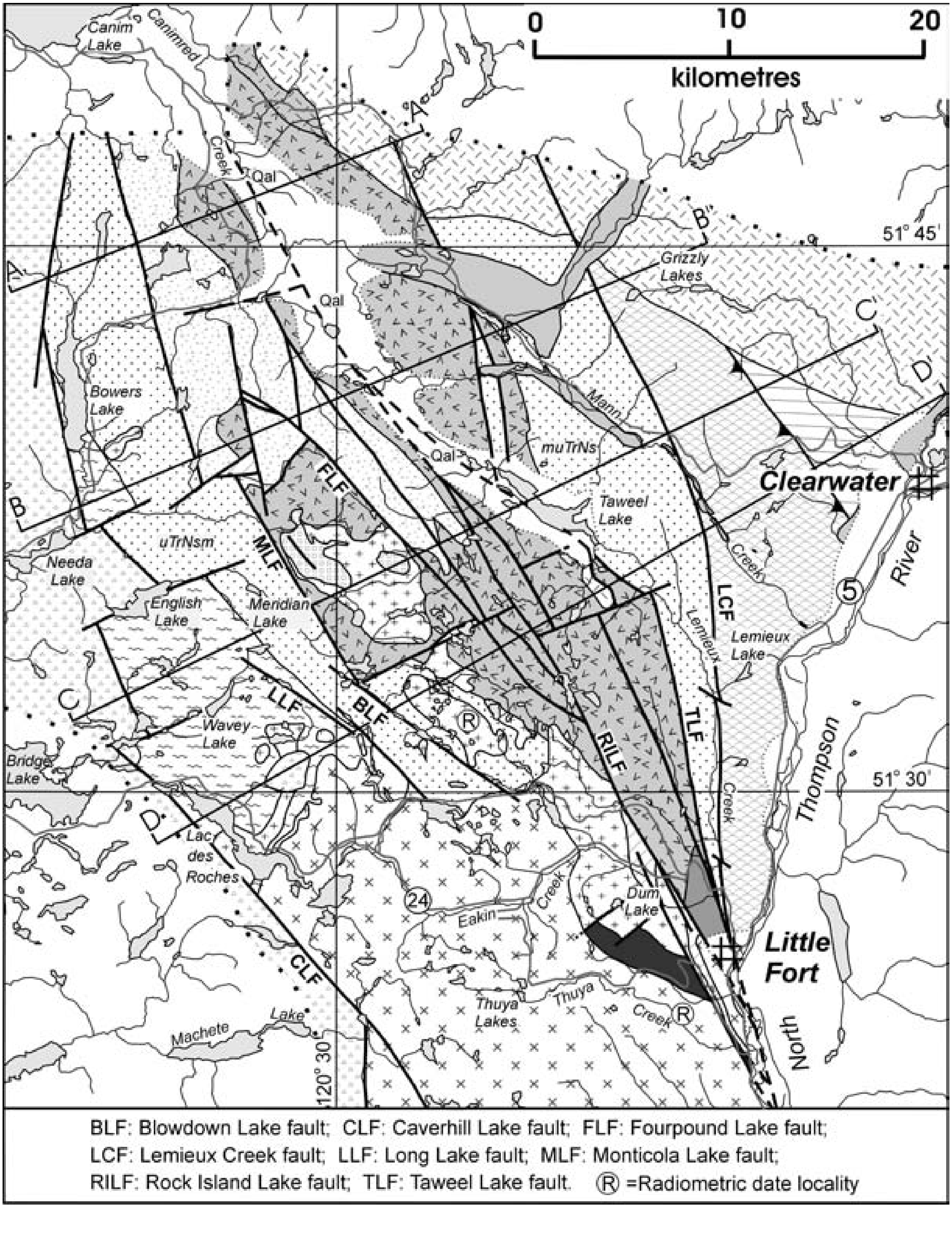

Figure 2a. Generalized geology of the southern and central parts of the Bonaparte project area.

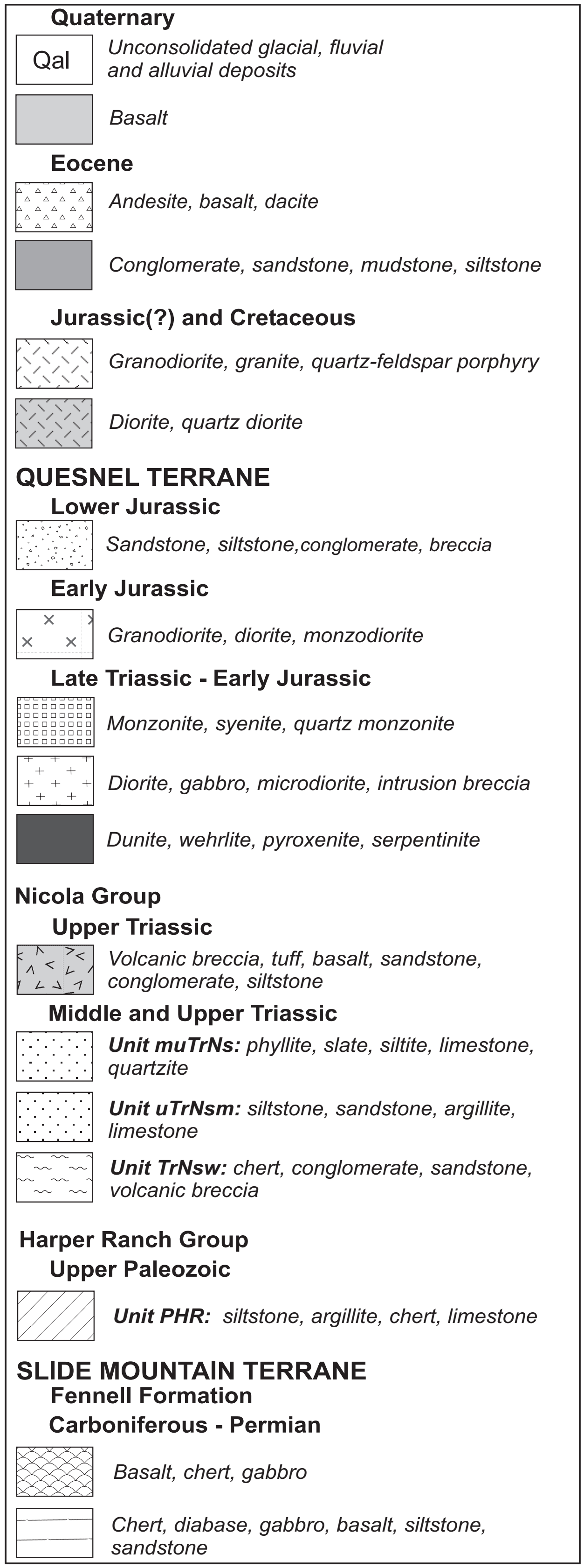

Figure 2b. Legend to accompany Figure 2a.

ferred that the two divisions are separated by a thrust fault similar to those that imbricate the lower division.

Within the present map area, the Fennell Formation forms a continuous belt that extends from Little Fort to the Raft Batholith. The western boundary of this belt is the Lemieux Creek fault, which separates the Fennell belt from Middle and Upper Triassic sedimentary rocks of the Lemieux Creek succession, the easternmost representative of Quesnel Terrane at this latitude. The Fennell belt is bounded by the North Thompson River valley to the east, which separates it from the more extensive exposures of the formation that were studied in detail by Schiarizza (1983, 1989).

Most of the Fennell Formation within the present map area comprises pillowed to massive basalt assigned to the upper division (Photo 1). The basalts form resistant brown-weathered exposures that form many of the more prominent mountains and ridges in the map area, including Mount Olie, Mount Loveway and Skwilatin Mountain in the south, and Clearwater, Grizzly and Grizzly Cub mountains in the north. The basalts include rare interbeds of bedded chert, and are locally intruded by dikes and sills of diabase and gabbro.

The lower structural division of the Fennell Formation crops out in a relatively small area west of Clearwater (Figure 2). It is not nearly as well exposed as the upper division, but is represented by scattered exposures of mainly chert, diabase, gabbro and basalt. The cherts occur in light to dark shades of grey to green, and commonly include interbeds of argillite, phyllite and siltstone. Bedding dips at moderate to steep angles to the southwest. The contact with structurally overlying basalts of the upper division is not well exposed, but is constrained to have a northwesterly strike. One isolated exposure along or near the contact, 3.5 kilometres northwest of the North Thompson River valley, shows basalt structurally above chert across a warped but mainly southwest-dipping fault contact. This observation is consistent with the interpretation that the two structural divisions are separated by a thrust fault.

HARPER RANCH GROUP

The Harper Ranch Group (Smith, 1979) consists of Upper Paleozoic sedimentary and volcanic rocks that rest stratigraphically beneath lower Mesozoic rocks of the Quesnel Terrane across an angular unconformity. The type area is on and near the Harper family ranch, located east of Kamloops on the north side of the South Thompson River, where the group comprises a Devonian to Upper Permian assemblage of carbonates, siltstones, mudstones, volcaniclastic sandstones and local andesitic volcanic rocks (Danner and Orchard, 2000). This belt of Paleozoic rocks extends northward to the south margin of the Thuya Batholith (Figure 1), and is also represented by several isolated fault and/or unconformity-bounded inliers farther north, within the Bonaparte Project area (Figures 2 and 3). These Paleozoic rocks were included in the Badger Creek Formation of Uglow (1922) and were assigned to the eastern Cache Creek Group by Campbell and Tipper (1971).

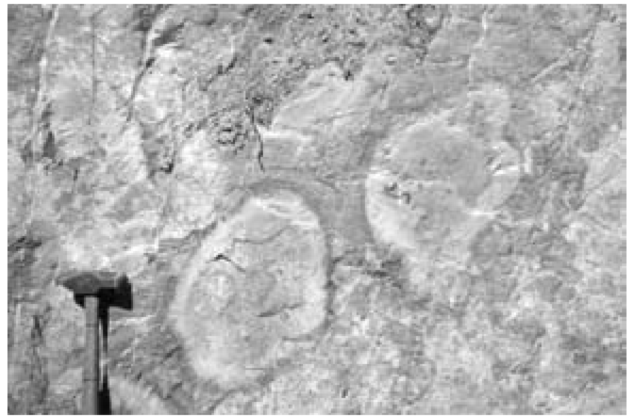

Photo 1. Pillowed basalt from the upper structural division of the Fennell Formation, 9 kilometres west of Clearwater.

Within the Bonaparte project area, the most extensive belt of rocks assigned to the Harper Ranch Group extends discontinuously from Highway 24 to Highway 5, along the west side of the Rock Island Lake fault (Figure 2). This assemblage, described by Schiarizza and Israel (2001), is dominated by siltstone and limestone, with local intercalations of chert and siliceous argillite. It is tentatively included in the Harper Ranch Group following Campbell and Tipper (1971), but is undated and may include Triassic rocks of Unit uTrNsm, which crop out along strike to the northwest (Figure 2).

Campbell and Tipper (1971) documented an occurrence of fossiliferous Permian limestone 3 kilometres northwest of Deer Lake. They did not map it as a separate unit, but included it in a belt of volcanic and sedimentary rocks assigned primarily to the Upper Triassic Nicola Group (their Unit 11). The fossiliferous limestone was located and resampled by Schiarizza and Israel (2001). They tentatively correlated it with more extensive, but undated exposures of limestone and mineralized skarn at Deer Lake, implying that the Harper Ranch Group underlies a large area north of the Thuya batholith. Subsequent fossil identifications (including Permian macrofossils by E.W. Bamber, Geological Survey of Canada, Calgary; and Permian and Triassic conodonts by M.J Orchard, Geological Survey of Canada, Vancouver) have confirmed the Permian age of the limestone 3 kilometres northwest of Deer Lake, but have shown that the limestone right at Deer Lake is Upper (to Middle?) Triassic. Therefore, most of the Deer Lake belt assigned to the Harper Ranch Group by Schiarizza and Israel is now included in Unit uTrNsm of the Nicola Group (described later in this report). The Permian rocks northwest of Deer Lake, comprising dark grey fossiliferous limestone with thin interbeds of dark grey argillite and chert, are apparently a small inlier of the underlying Harper Ranch Group. The Permian succession is only a few tens of metres thick and is truncated by a diorite pluton to the southwest. Its contact with sedimentary rocks of the Nicola Group to the northeast is not exposed, but is suspected to be an unconformity.

Permian rocks of the Harper Ranch Group also occur in a small, isolated fault block on the west slopes of Windy Mountain (Figure 3). The succession there is dominated by light to dark grey, locally green, laminated to massive chert and chert-rich sedimentary breccia. It also includes minor amounts of argillite and siltstone, as well as a lens of fossiliferous limestone. The limestone lens is up to 10 metres thick, at least 30 metres long, and is enclosed in a sedimentary breccia that contains millimetre to metre-scale clasts within a fine-grained clastic to cherty matrix. The clasts are dominated by chert and limestone, but also include aphyric and feldspar-phyric volcanic rocks, microdiorite, argillite and siltstone. A fossil collection from this limestone lens, which included brachiopods, corals and bryozoans, was assigned a Permian age by E.W. Bamber of the Geological Survey of Canada (Campbell and Tipper, 1971, page 22).

NICOLA GROUP

Campbell and Tipper (1971) assigned most Triassic volcanic and sedimentary rocks in the central and eastern Bonaparte Lake map sheet to the Nicola Group, but excluded the Triassic sedimentary succession along Lemieux Creek (their Unit 10; Lemieux Creek succession of this report). Schiarizza and Israel (2000) included the Lemieux Creek succession in the group, and also felt that substantial sections of rock mapped as Jurassic by Campbell and Tipper (their Unit 16, and parts of Unit 15) were more likely Triassic, so also included them in the Nicola Group. The reinterpretation of Campbell and Tipper's Unit 16 has been substantiated by a single microfossil call and continues to be applied here. Likewise, their Unit 15 continues to be regarded as partly Triassic (included in units uTrNsm and uTrNsv of this report) and partly Jurassic.

Schiarizza and Israel (2001) discussed the Nicola Group in terms of three fault-bounded belts of uncertain stratigraphic relationship. These included an eastern sedimentary belt, a central volcanic belt and a western belt of sedimentary rocks with local intercalations of volcanic rock. Our 2001 mapping program, together with some new microfossil dates, suggests that the eastern and western sedimentary belts are at least in part the same age, and that they both underlie the volcanic rocks of the central belt stratigraphically. This suggests that the pattern of volcanic versus sedimentary rocks may be primarily the result of preservation of the younger, volcanic part of the succession in the core of large synclinal structure. Local occurrences of volcanic breccia within the western sedimentary belt suggest, however, that there were also pulses of volcanism prior to deposition of the main volcanic units presently preserved in the core of the Nicola belt.

In the descriptions that follow, the Nicola Group is subdivided into 5 informal units. The Lemieux Creek succession comprises the easternmost element of the group and contains sedimentary rocks of Middle and Upper Triassic age. The Meridian Lake succession crops out on west side of the main belt of volcanic rocks within the group, but includes rocks that are lithologically similar and of the same age as the Lemieux Creek succession, so is thought to be largely its western equivalent. The Wavey Lake succession is an undated chert-rich unit that, at least in part, structurally underlies the Meridian Lake succession and forms the westernmost element of the Nicola Group in the map area. The main concentration of volcanic rocks form a belt that separates the Lemieux Creek and Meridian Lake successions. The rocks of this belt are undivided on Figure 2, but separated into a lower volcanic unit and an upper unit of mixed volcanic, volcaniclastic and sedimentary rocks on Figure 3. The upper mixed unit forms the top of the Nicola Group and is stratigraphically overlain by Jurassic rocks.

Lemieux Creek Succession (Unit muTrNs)

Triassic sedimentary rocks of the Lemieux Creek succession crop out within a single north-northwest-trending belt that extends from Little Fort to the Raft Batholith (Figure 2). This belt forms the easternmost element of the Quesnel Terrane and is juxtaposed with the Fennell Formation of the Slide Mountain Terrane across the Eocene(?) Lemieux Creek fault. The western contact of the Lemieux Creek succession is also marked by a young fault in the southern part of the belt, but north of Taweel Lake it is interpreted as a stratigraphic contact with overlying volcanic rocks of Unit uTrNv.

The Lemieux Creek succession consists mainly of medium to dark grey phyllites, slates and slaty siltstones that commonly contain thin beds and lenses of laminated siltstone or quartzose siltite. The succession also includes thin to thick beds of fine-grained quartzite and calcareous quartzite, and beds of medium to coarse-grained feldspathic to quartzose sandstone. Thin-section analysis of a sample of fine-grained quartzose sandstone collected a few kilometres southeast of Taweel Lake during the 2000 field season (Schiarizza and Israel, 2001) confirms that it contains a significant amount of detrital muscovite and biotite.

Limestone is common within eastern exposures of the Lemieux Creek succession between Highway 24 and Lemieux Lake. Much of it forms fractured and brecciated exposures within the Lemieux Creek fault zone, but it also occurs in well preserved intervals, up to 100 metres thick, comprising thin to thick limestone beds intercalated with siltstone and slate (Photo 2). Only a few scattered beds of limestone were noted in the northern part of the belt, although much of the siltstone, sandstone and quartzite is distinctly calcareous.

Campbell and Tipper (1971) report that collections of poorly preserved macrofossils from limestone exposures within Unit muTrNs north of Highway 24 suggest a Late Triassic age. Three samples collected from this same belt during the 2000 field season yielded conodonts of Early Carnian or Ladinian-Carnian age (northern two sample locations shown on Figure 3), whereas collections made from this belt by M.J. Orchard in 1985 yielded conodonts of Anisian, Ladinian and Early Carnian age (M.J. Orchard, written communication, May and June 2001). These fossil collections support correlation of the Lemieux Creek succession with lithologically similar Middle to Upper Triassic rocks that form the base of the Nicola Group in the Quesnel River - Horsefly map area (Unit 1 of Panteleyev *et al*., 1996).

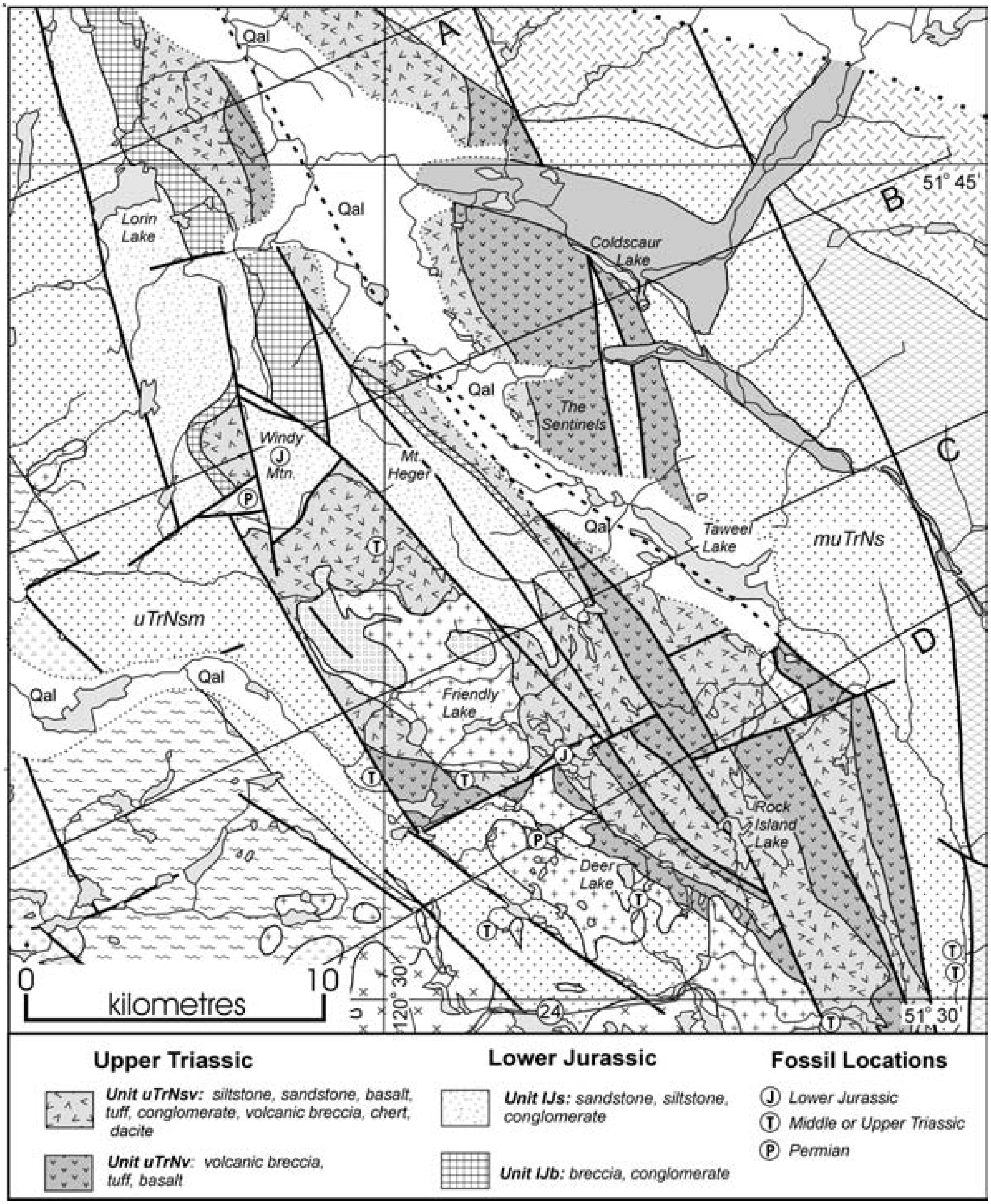

Figure 3. Generalized geology around the central part of the Nicola belt, showing subdivisions of the Nicola volcanic unit and overlying Lower Jurassic rocks. Other map units are shown with same patterns as Figure 2.

Photo 2. Well-bedded limestone from the Lemieux Creek succession, 1.5 kilometres southwest of Lemieux Lake.

Meridian Lake Succession (Unit uTrNsm)

Clastic sedimentary rocks and local limestone assigned to the Meridian Lake succession form a continuous belt that extends from the north margin of the Thuya Batholith to the northern limit of our mapping, just south of Canim Lake (Figure 2). The eastern contact is a fault along most of its length, but rocks included in the succession east of the Blowdown Lake fault may be in stratigraphic contact beneath volcanic rocks of Unit uTrNv. On its west side, the Meridian lake succession is in part underlain by the chert-rich Wavey lake succession, and in part faulted against Eocene volcanic rocks. The Meridian Lake succession includes rocks assigned to either the Nicola Group or an unnamed Lower Jurassic sedimentary unit (their Unit 15) by Campbell and Tipper (1971). It comprises the upper part of the Ripple Lake belt of Schiarizza and Israel (2001), but also includes rocks, east of the Blowdown Lake fault, that they tentatively assigned to the Paleozoic Harper Ranch Group. This assignment was based on the presence of Permian limestone at one locality, 3 kilometres northwest of Deer Lake. In the revised interpretation presented here, the Harper Ranch Group is thought to be restricted to a very small area that is either faulted against or stratigraphically beneath the Meridian Lake succession (Figure 3).

The Meridian Lake succession is dominated by thin-bedded intervals of laminated siltstone, dark grey argillite, weakly cleaved slate, and less common fine to medium-grained sandstone. Coarser-grained clastic rocks occur locally but are not common. These include layers and lenses of pebble conglomerate, up to several metres thick, that occur within a succession of mainly thin-bedded cherty argillites and siltstones east of the Blowdown Lake fault, 2.5 to 4 kilometres southeast of Monticola Lake. The conglomerate includes angular to subrounded pebbles of mainly argillite, chert and siltstone that are most commonly supported by a silty to siliceous argillite matrix. Clasts of feldspathic and pyroxene-feldspar-phyric volcanic rocks are also present, and rare limestone-matrix conglomerate units include limestone and sandstone clasts. Pebble to cobble conglomerate also occurs along the western margin of the Meridian Lake succession, southeast of Bowers Lake. There, however, it is dominated by clasts of pyroxene-phyric basalt, and is intercalated with volcanic sandstone containing mainly pyroxene and feldspar grains. Also present, to the east of Bowers Lake, are units of massive pyroxene porphyry interleaved with siltstone and argillite. It was not established, however, whether these are sills or flows.

Dark grey micritic limestone and limy argillite are fairly common in the southern part of the main Meridian Lake belt, as far north as the English Lake cross fault, and are also common in the belt east of the Blowdown Lake fault. The limestone occurs as thin to thick beds intercalated with siltstone, argillite and, locally, chert. Limestone samples collected from two separate exposures a short distance southeast of Deer Lake yielded conodonts that have been assigned Ladinian-Carnian and Early Carnian ages, respectively (M.J. Orchard, written communication, May 2001). Similar limestone on the west side of the Blowdown Lake fault, 5 kilometres west-southwest of Deer Lake, yielded conodonts that were assigned a Carnian age (Figure 3). Six kilometers northeast of this locality, just west of the Monticola Lake fault, is a fossil locality described by Campbell and Tipper (1971), comprising Halobiid fragments of probable Upper Triassic age.

The fossil dates described above indicate that the Meridian Lake succession is, at least in part, the same age as the Lemieux Creek succession. Correlation is supported by a strong lithologic similarity, although the Meridian lake succession does not apparently include the quartzites and quartzose sandstones that occur within the Lemieux Creek succession. The rocks of the Meridian Lake succession near Deer Lake are apparently in contact with rocks of the Nicola volcanic unit to the northeast, but this contact is not exposed. However, it is suspected to be a stratigraphic rather than a structural contact because diorite of probable earliest Jurassic age cuts across it, precluding a Jurassic or younger fault.

Wavey Lake Succession (Unit TrNsw)

The Wavey Lake succession is dominated by chert and volcaniclastic sandstone, but also includes substantial intervals of conglomerate and local occurrences of volcanic breccia. It forms a belt that is bounded by the Meridian Lake succession to the east, and is in fault contact with Eocene volcanic rocks to the west. This belt is close to 10 kilometres wide and extends from the northwest margin of the Thuya batholith to English Lake, where it is apparently truncated by a northeast-striking fault. The Wavey Lake succession was not recognized directly north of this fault, where the Meridian Lake succession extends westward to the Eocene volcanic rocks. It does occur locally farther north, however, where it is represented by a few exposures of chert and slate south-southeast of Bowers Lake. The rocks assigned to the Wavey Lake succession in this report were included in the Nicola Group by Campbell and Tipper (1971), and comprise the western, structurally lower part of the Ripple Lake belt described by Schiarizza and Israel (2001).

The most characteristic lithology within the Wavey lake succession is light to dark grey, locally green, chert that occurs as millimetre to centimetre-scale lenses and laminae interbedded with slate, argillite and siltstone. The chert intervals are interbedded with fine to medium-grained volcaniclastic sandstone that occurs as thin to medium beds, and locally forms channels that cut into the chert. Also common are thick lenses of poorly sorted and poorly stratified pebble to cobble conglomerate. The subangular to rounded clasts are dominated by laminated siltstone, cherty argillite and argillite, but also include chert, limestone, pyroxene and/or feldspar-phyric volcanic rocks and microdiorite. The conglomerates vary from clast to matrix-supported; the matrix commonly ranges from a siltstone to a gritty sandstone, and in places is distinctly calcareous.

A lens of coarse volcaniclastic rocks more than 200 metres thick was traced for about 4 kilometres within the eastern part of the Wavey Lake succession by Schiarizza and Israel (2001). It comprises pyroxene porphyry breccias and pyroxene-feldspar-crystal-lithic tuffs that are very similar to rocks found in units uTrNv and uTrNsv to the east. The base of the lens is defined by the (minor) Long Lake fault, but the top is a steeply-dipping northeast-facing stratigraphic contact across which the coarse volcaniclastic rocks are overlain by chert and fine to medium-grained volcaniclastic sandstone typical of the Wavey Lake succession. Isolated exposures of coarse volcaniclastic rock were noted at a few localities elsewhere in the succession, but do not constitute mappable bodies.

No macrofossils are known from the Wavey Lake succession, and chert samples processed after the 2000 field season did not yield conodonts or radiolaria. It is clearly intruded by the Early Jurassic Thuya batholith, as well as by small stocks of diorite that are suspected to be slightly older. Along its eastern margin the Wavey Lake succession rests structurally beneath the Upper Triassic Meridian Lake succession. This contact is not exposed, but is locally tightly constrained and there is no evidence of a fault or structural discordance across it. These relationships suggest that the Wavey lake succession constitutes a relatively low stratigraphic element within the Nicola Group, and that the coarse volcaniclastic lens northeast of the Long Lake fault reflects an earlier pulse of volcanism than that recorded by the main concentration of volcanic rocks that overlies the Meridian Lake succession to the east. Alternatively, the Wavey Lake succession might be a western, deeper water facies that includes stratigraphic equivalents of both the Meridian Lake succession and the overlying volcanic rocks.

Volcanic Unit (uTrNv)

Unit uTrNv comprises a thick succession of mafic volcanic rocks that overlie sedimentary rocks of the Lemieux Creek and Meridian Lake successions. It is dominated by mafic volcanic breccias containing clasts of pyroxene-phyric basalt (Photo 3), but also includes massive to pillowed pyroxene-phyric basaltic flows (Photo 4), well-bedded mafic tuffs and pyroxene-rich volcanic sandstones. This unit is represented by good exposures in several partially fault-bounded belts in the southern part of the project area, which are described by Schiarizza and Israel (2001). In the 2001 map area it is represented mainly by a

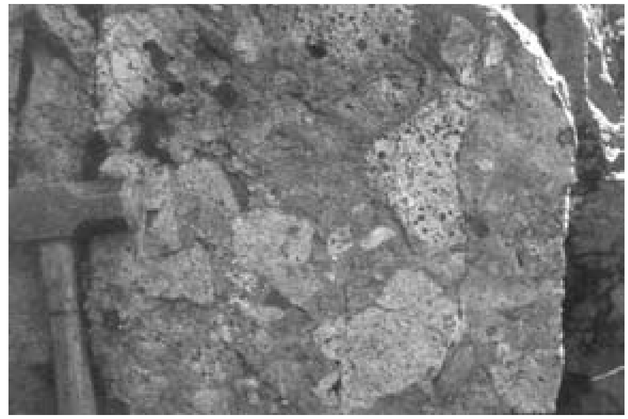

Photo 3. Volcanic breccia of Unit uTrNv, 2.5 kilometres east of Rock Island Lake.

Photo 4. Pillowed pyroxene-phyric basalt of Unit uTrNv, 3.5 kilometres east of Rock Island Lake.

wide belt of exposures that, in part, make up the Sentinels and the prominent ridges west of Coldscaur Lake (Figure 3). This belt is bounded by the Taweel Lake fault in the south, and extends northward to the Raft Batholith. It consists mainly of pyroxene porphyry breccias, but also includes massive pyroxene-phyric flows (or sills), and includes interbeds of pyroxene-rich sandstone near its basal contact with the Lemieux Creek succession. Unit uTrNv is also mapped in the northwestern part of the map area, where it is represented by sparse exposures of pillowed pyroxene-phyric basalt a short distance southwest of Canimred Creek (Figure 3).

The contact between Unit uTrNv and the Lemieux Creek succession is nowhere well exposed, but is inferred to be stratigraphic in the area east of the Sentinels, based on concordant bedding orientations and west-facing stratigraphic tops indicators in adjacent exposures of the respective units. The basal part of Unit uTrNv in this area comprises thin to thick beds of pyroxene-rich sandstone containing thin siltstone interbeds, interspersed with massive units of pyroxene porphyry breccia. In the Deer Lake area, on the opposite side of the volcanic belt, Unit uTrNv is inferred to overlie sedimentary rocks of the Meridian Lake succession, but the contact there is projected through a drift-covered area up to several hundred metres wide. However, as discussed previously, the contact is crosscut by a diorite stock of probable earliest Jurassic age, suggesting that it is more likely to be a stratigraphic contact than a fault.

Unit uTrNv is not dated directly. It is assigned an Upper Triassic age on the basis of its stratigraphic position above Middle and Upper Triassic sedimentary rocks of the Lemieux Creek and Meridian Lake successions, and below Upper Triassic rocks of Unit uTrNsv.

Mixed Volcanic-Sedimentary Unit (uTrNsv)

Unit uTrNsv comprises a succession of sedimentary, volcaniclastic and local volcanic rocks that overlies and interfingers with Unit uTrNv, and forms the uppermost unit within the Nicola Group. It includes pyroxene porphyry breccias and local flows identical to those found within Unit uTrNv, but these are intercalated with, and volumetrically subordinate to, sedimentary rocks that include siltstone, slate, pyroxene-rich sandstone and conglomerate, as well as minor amounts of chert and limestone (*see* detailed descriptions by Schiarizza and Israel, 2001). Unit uTrNsv is best represented by exposures in several fault panels on either side of the Rock Island Lake fault, between Highway 24 and Taweel Lake (Figure 3). It continues northward from there, along both sides of the Rock Island Lake - Taweel Lake fault system, to the northern limit of our 2001 mapping, but exposure is poor in this part of the area. Unit uTrNsv is also represented by fairly extensive exposures within the fault block that extends from Friendly Lake to Windy Mountain, where it is intruded by diorites and syenites of the Friendly Lake complex.

Several of the fault panels in the southern part of the map area contain the transition from Unit uTrNsv into stratigraphically lower volcanic rocks of Unit uTrNv (Schiarizza and Israel, 2001). This same stratigraphic relationship is inferred in the northern part of the map area, in separate panels on either side of the Rock Island Lake - Taweel Lake fault system (Figure 3), but is not well exposed. The stratigraphic top of Unit uTrNsv is defined by Lower Jurassic rocks of units lJb and lJs. This transition is mapped east and southeast of Mount Heger, west of Windy Mountain, and east of Lorin Lake, but is not well exposed in any of these areas (Figure 3).

A thin limestone bed intercalated with clastic and volcaniclastic rocks of Unit uTrNsv along Highway 24, 6 kilometres south-southeast of Rock Island Lake, was sampled during the 2000 field season and yielded Triassic conodonts (M.J. Orchard, written communication, May 2001). This sample comes from the west side of a west-facing fault panel that, 1.5 kilometres to the east, includes the transition into underlying volcanic rocks of Unit uTrNv (Figure 3). Campbell and Tipper (1971) report Triassic macrofossils from two separate localities within the Friendly Lake fault block, one from 1.5 kilometres south of the west end of Friendly Lake, and the other from 4.5 kilometres southeast of Windy Mountain (Figure 3). The locality south of Friendly Lake was sampled for microfossils during the 2000 field season and yielded conodonts of Early Carnian age (M.J. Orchard, written communication, May 2001). The fossils come from dark grey limestone that is intercalated with feldspathic sandstone and small-pebble conglomerate. Although these rocks are provisionally included in Unit uTrNsv, the conodont age and lithologic association suggest that they may comprise a small fault panel derived from the Meridian Lake succession. The other fossil locality within the Friendly Lake block, 4.5 kilometres southeast of Windy Mountain, was not located during our 2001 mapping program. A traverse through this area encountered well-bedded volcaniclastic sandstones and siltstones that are readily included in Unit uTrNsv.

TRIASSIC-JURASSIC PLUTONIC ROCKS

Calc-alkaline and alkaline plutons of Late Triassic to Early Jurassic age are a prominent feature of the Quesnel Terrane and are related to important porphyry Cu (±Au) and skarn deposits. Plutonic rocks are well represented in the southern part of the Bonaparte project area, which includes the northeastern part of the calc-alkaline Thuya batholith as well as numerous smaller, predominantly dioritic stocks and plugs that appear to have more alkaline affinities (Schiarizza and Israel, 2001). The latter are most prominent as a northwest-trending belt that includes, from southeast to northwest, the Dum Lake ultramafic-mafic intrusive complex, several diorite stocks near Deer Lake, and the Friendly Lake diorite-syenite intrusive complex (Figure 2). These rocks intrude the volcanic unit of the Nicola Group as well as underlying sedimentary rocks of the Meridian Lake succession and Harper Ranch Group. Small dioritic stocks are also common within more western exposures of the Meridian Lake succession and the adjacent Wavey Lake succession, particularly along the margins of the Thuya batholith (Figure 2).

Plutonic rocks are not a prominent component of the Quesnel Terrane in the central part of the Bonaparte project area, perhaps in part because a general northwest structural plunge has resulted in exposure of mainly Lower Jurassic sedimentary rocks, which may postdate much of the plutonism, along strike from the Dum Lake - Friendly Lake belt. However, a small body of diorite and syenite was mapped within Unit uTrNsv along Windy Creek, 2.5 kilometers northwest of the Friendly Lake complex, and an elongate body of microdiorite and microgabbro occurs 3 kilometres farther to the north, apparently as a fault-bounded lens along the Fourpound Lake fault (Figure 3). These intrusive units are apparently the northernmost exposed expressions of the plutonism associated with the Friendly Lake complex. The only other mappable intrusive body suspected to be this age in the 2001 map area comprises a plug of quartz-carbonate-altered microdiorite and hornblende-feldspar porphyry that intrudes sedimentary rocks of the Meridian Lake succession 7 kilometres west of Windy Mountain (Figure 3).

Age of the Deer Lake Diorite Stocks

During the 2001 field season a sample of leucocratic diorite/gabbro was collected from the largest of the Deer Lake diorite stocks, 1.3 kilometres west of the south end of Deer Lake (Figure 2). This sample yielded a U-Pb date of 197.8 ±1.4 Ma based on the overlap of 5 zircon fractions on concordia (R. Friedman, University of British Columbia, written communication, November 2001). This very Early Jurassic age is about 5 million years older than a U-Pb zircon date obtained from the Thuya Batholith (discussed below), consistent with the interpretation of Schiarizza and Israel (2001) that the Dum Lake - Deer Lake - Friendly Lake belt of intrusions predates emplacement of the batholith.

None of the other dioritic to syenitic intrusive units within the Nicola belt are dated at this time, but U-Pb work is in progress on samples collected from the Dum Lake and Friendly Lake complexes during the 2001 field season. An earlier attempt to date the largest monzonite/syenite unit within the Friendly Lake complex after the 2000 field season was unsuccessful because, due to a wide age range for inherited components and probable Pb loss in the modest amount of zircon recovered, the data could not be confidently regressed to yield a lower intercept age (R. Friedman, University of British Columbia, written communication, April 2001).

Age of the Thuya Batholith

Prior to the present study, the only U-Pb zircon date available for the Thuya batholith was an age of 205 ±9.3 Ma reported by Calderwood *et al*. (1990) for a sample of hornblende-biotite monzodiorite collected near Highway 24 a short distance east of Lac des Roches. Jung (1986) reports K-Ar dates of 186 ±6 Ma and 191 ±7 Ma on, respectively, hornblende and biotite separates from the same sample, as well as a Rb-Sr whole rock - mineral isochron date of 183.6 ±4.4 Ma, with an initial $^{87}Sr/^{86}Sr$ ratio of 0.7042. Other K-Ar dates on unaltered samples to the south and west of the Lac des Roches sample site, summarized by Jung (1986), range from 181 ±7 Ma to 203 ±6 Ma.

Following the 2000 field season, a sample of relatively unaltered hornblende-biotite granodiorite collected near Thuya Creek (Figure 2) was submitted to the Geochronology Laboratory at the University of British Columbia for U-Pb dating. This sample has an interpreted age of 192.7 ±0.9 Ma, based mainly on 2 overlapping concordant zircon fractions (R. Friedman, written communication, August 2001). This Early Jurassic crystallization age is, within error, identical to a tightly constrained U-Pb zircon date of 193 ±0.6 Ma reported by Whiteaker (1996) for the Takomkane Batholith. Similar U-Pb zircon dates of 196 ±1, 194 ±1 and 193 ±1 Ma are reported by Parrish and Monger (1992) for, respectively, the Wild Horse, Pennask and Bromley batholiths to the south. These 5 large batholiths define a linear north-northwest trending belt of Early Jurassic magmatism that extends for 300 kilometres within the central to eastern part of the Quesnel Terrane.

LOWER JURASSIC ROCKS

Lower Jurassic rocks crop out in a northwest-trending belt that has been traced for close to 30 kilometres in the northern part of the map area (Figure 2). The most distinctive lithology within this belt is conglomerate containing granitoid clasts. These conglomerates are interbedded with, and overlain by, a succession of finer-grained sedimentary rocks that contain Early Jurassic fossils at Windy Mountain (Campbell and Tipper, 1971). Breccia and conglomerate containing mainly pyroxene porphyry clasts forms a unit that underlies the Jurassic sedimentary rocks throughout most of the belt. This unit is tentatively included in the Jurassic succession because contacts with overlying granitoid-bearing conglomerates appear to be gradational. Sedimentary and volcanic rocks of Unit uTrNsv underlie the breccia unit, but this contact is not well exposed.

Lower Jurassic Breccia (Unit lJb)

The Lower Jurassic breccia unit is best exposed in a belt, up to 1.5 kilometres wide, that has been traced from the Fourpound Lake fault, just north of Windy Mountain, for more than 15 kilometres to the northern limit of our mapping (Figure 3). Its western boundary is a stratigraphic contact with overlying Lower Jurassic sedimentary rocks along the full length of this belt. Its eastern contact is a system of faults in the south, but may be a stratigraphic contact with Unit uTrNsv in the north. The unit is also represented by narrower belts of similar breccia that occur between Lower Jurassic sedimentary rocks and underlying volcaniclastic rocks of Unit uTrNsv in two separate fault-bounded domains, west and east of Windy Mountain respectively (Figure 3).

Unit lJb consists mainly of green, brown-weathering breccia dominated by angular to sub-rounded fragments of pyroxene porphyry that commonly range up to several tens of centimeters in size (Photo 5). The breccia is most commonly, but not exclusively, matrix-supported, and is typically massive, but locally displays crude stratification. Subordinate clast types include hornblende-feldspar porphyry, microdiorite, aphyric mafic volcanic rock, laminated

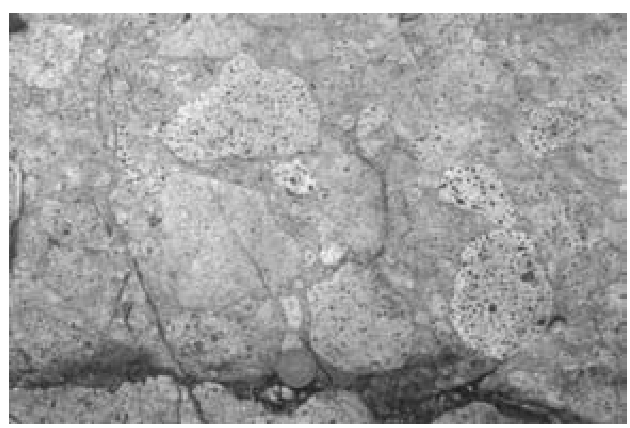

Photo 5. Matrix-supported breccia/conglomerate of Unit lJb, 5 kilometres north of Windy Mountain. Canadian one dollar coin for scale near bottom-centre of photo.

siltstone and argillite. These subsidiary clast types are most common in rare exposures of pebble to cobble conglomerate that contain a substantial proportion of sub-rounded to rounded clasts, but otherwise are similar to the more typical breccias. The unit also includes intercalations of pyroxene-rich sandstone and thin-bedded argillite/siltstone sequences that form intervals up to several metres thick. Locally, laminated siltstone/argillite sequences occur as isolated intraclasts, up to 2 metres in length, within the breccia. The unit also includes pyroxene-porphyry basalt with apparent pillow forms that was observed in a single exposure northeast of Lorin Lake (Figure 3).

Unit lJb is lithologically very similar to the Triassic breccias of Unit uTrNv, but is assigned to a separate unit on the basis of its stratigraphic position. With the exception of the pillows near Lorin Lake, most of the unit shows no evidence of primary volcanism, suggesting the possibility that much of it may have been derived from erosion of the Triassic volcanic rocks.

Lower Jurassic Sedimentary Rocks (Unit lJs)

Sedimentary rocks assigned to Unit lJs are well exposed in a fault-bounded block encompassing Windy Mountain (Figure 3). The section there includes a lower polymictic conglomerate unit containing clasts of granitic rock, which grades upwards into a succession dominated by thin-bedded sandstones and siltstones that locally contain Lower Jurassic fossils. Correlative rocks, including a basal section of granitoid-bearing conglomerates several hundred metres thick, crop out in a belt that extends north-northwestward from Windy Mountain to the limit of our mapping. This predominantly west-facing belt is stratigraphically underlain by pyroxene porphyry-dominated breccias of Unit lJb, and is inferred to be faulted against Triassic sedimentary rocks of the Meridian Lake succession to the west. Unit lJs is also represented by a northwest-trending belt of mainly sandstones and siltstones that crop out east and southeast of Windy Mountain, on the northeast side of the Fourpound Lake fault. Granitoid-bearing conglomerates, exposed locally east and southeast of Mount Heger, also occur at the base of the succession in this area, but form thin and discontinuous units. Underlying breccias of Unit lJb are likewise relatively thin and apparently discontinuous in this area.

The conglomerates at the base of Unit lJs commonly form resistant, brown-weathering exposures, as exemplified by those forming the prominent ridges south and southeast of Windy Mountain. They typically include poorly sorted pebbles, cobbles and boulders of a variety of rock types, supported by a sandy feldspathic matrix that also includes mafic mineral grains (largely hornblende), small lithic grains and quartz. The clasts range from angular to rounded, and commonly include granodiorite, tonalite, diorite, pyroxene±feldspar-phyric basalt, aphyric volcanic rocks and siltstone (Photo 6). Pebbles of limestone and chert are present in many exposures but form only a small percentage of the clast population. The conglomerates are typically unstratified, but locally exhibit very crude stratification and interbedded lenses of medium to coarse-grained arkosic sandstone.

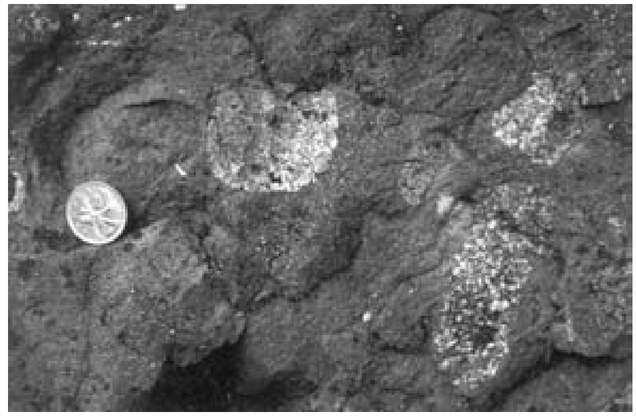

Photo 6. Matrix-supported conglomerate containing granodiorite and diorite clasts; Unit lJs south of Windy Mountain.

Photo 7. Thin bedded sandstone and siltstone of Unit lJs, Windy Mountain.

The conglomerate interval at the base of Unit lJs passes up-section into finer-grained clastic rocks across a zone of mixed-gradation that is fairly well exposed on the slopes southeast of Windy Mountain. Most of the unit above this contact zone consists of thin-bedded, fine to coarse-grained sandstones, laminated siltstones and silty argillites, with local thick beds of coarse sandstone and granule to small-pebble conglomerate (Photo 7). The sandstones are typically wackes that are rich in feldspar, mafic mineral grains and small lithic fragments.

There are no volcanic rocks within Unit lJs, but the sedimentary rocks within the unit are commonly cut by dikes of dark green pyroxene-phyric basalt that are very similar to, but clearly younger than, the pyroxene-rich basalts that characterize the volcanic rocks within the underlying Nicola Group.

Unit lJs is dated at Windy Mountain, where Campbell and Tipper (1971) made two fossil collections, which were assigned “possible Lower Jurassic” and “Sinemurian?” ages, respectively, by H. Frebold of the Geological Survey of Canada. Additional ammonite collections were made during our 2001 fieldwork, but had not yet been identified when this report was written. Nevertheless, their lithology and provisional Lower Jurassic age suggest that these rocks correlate with the Lower to Middle Jurassic Ashcroft Formation, which overlies the Nicola Group 100 kilometres southeast of the project area, and likewise contains a basal conglomerate unit that contains granitoid clasts (Travers, 1978; Monger and McMillan, 1989).

Jurassic sedimentary rocks are known from one other location within the project area, comprising a Lower Jurassic argillite-siltstone package of very limited extent that was identified by Preto (1970) just west of Lost Horse Lake. These rocks, which yielded poorly preserved ammonites of probable Late Sinemurian or Early Pliensbachian age, are mapped as a narrow fault-bounded sliver along the northeast-striking fault south of Friendly Lake (Figure 3). They are suspected to correlate with siltstones and argillites that are common in the upper parts of Unit lJs around Windy Mountain.

RAFT BATHOLITH

The Raft batholith is an elongate granitic pluton of Jurassic or Cretaceous age that extends for about 70 kilometres in a west-northwest direction, and cuts across the boundaries between Kootenay, Slide Mountain and Quesnel terranes (Figure 1). During the 2001 field season a substantial portion of the southern margin of the batholith was mapped, extending from Clearwater for about 40 kilometres westward to the west end of the pluton (Figure 2). The batholith clearly intrudes the Fennell Formation, the Lemieux Creek succession and the Nicola volcanic unit from east to west across this transect, although the contacts between these pre-batholith units are interpreted as steep faults that extend into that batholith and cause minor offsets and reorientations of its southern contact.

Most portions of the Raft Batholith covered during our 2001 mapping program consist of light grey, medium to coarse-grained hornblende-biotite granodiorite to monzogranite of rather uniform composition and appearance. Pinkish potassium feldspar crystals tend to be slightly larger than the plagioclase and quartz, and locally form phenocrysts more than 1 centimetre in size. Mafic minerals typically make up 10 to 20 percent of the rock, with biotite predominating over hornblende. The granodiorite is commonly intruded by dikes of pegmatite, aplite and quartz-feldspar porphyry, but these younger phases typically amount to only 1 or 2 percent of the rock exposed at any given outcrop.

A distinctly different phase, comprising medium-grained hornblende-biotite diorite, locally grading to quartz diorite, underlies a relatively small area along the southwest margin of the batholith (Figure 2). Unequivocal crosscutting relationships between these more mafic rocks and the granodiorite to the northeast were not observed. Campbell and Tipper (1971) note that narrow zones of hornblende diorite also occur near the north contact of the batholith just west of the Clearwater River.

Wanless *et al*. (1967) report K-Ar biotite dates of 140 ±9 Ma and 105 ±9 Ma on two separate samples from the Raft Batholith. The older date came from a sample collected on the west bank of the Clearwater River near the northern margin of the batholith, and the younger one came from a sample collected near the south margin of the batholith, about 8 kilometres northwest of Clearwater. Jung (1986) reports biotite K-Ar and Rb-Sr whole rock-mineral separates isochron dates from a granodiorite sample collected from the west side of the Clearwater River, about 8 kilometres north of Clearwater. He provisionally accepted the 104.3 ±3.3 Ma Rb-Sr date as the magmatic age, and suggested that the older K-Ar date of 138 ±6 Ma reflected excess radiogenic Ar in the biotite. Subsequent U-Pb dating of zircons from the same sample, however, yielded an upper intercept age of 168 +14/-12 Ma (Calderwood *et al*., 1990). Regional relationships suggest that ages near the lower or upper limits of these published dates might be permissible for the Raft batholith, as plutons of both late Middle Jurassic and mid-Cretaceous age are common within a belt that overlaps the Omineca and Intermontane belts from the present study area southward to the international boundary (Logan, 2002). A sample of granodiorite collected during the 2001 field season has been submitted for U-Pb isotopic dating in an attempt to clarify the crystallization age of the main phase of the batholith.

EOCENE(?) SEDIMENTARY ROCKS WEST OF CANIMRED CREEK

Thin-bedded sedimentary rocks that were observed in only two outcrops about 4 kilometres apart are interpreted as part of a succession that overlies volcanic and volcaniclastic rocks of the Nicola Group on the west side of Canimred Creek, near the northern limit of our mapping (Figure 2). Where observed, this succession consists mainly of friable, laminated to thin-bedded mudstones and siltstones in pale shades of purple, grey and green. Bedding dips at moderate angles to the east and is apparently discordant to that in the poorly exposed Nicola rocks to the west. Relationships to the east are masked by a wide belt of unconsolidated Quaternary sediments, but it is suspected that the thin-bedded sedimentary rocks dip into, and are bounded by, the northern extension of the Rock Island Lake fault system, which is inferred to follow the valley of Canimred Creek (Figure 4, section A). The sedimentary succession may correlate with an assemblage of thin-bedded lacustrine sedimentary rocks of Eocene age that crop out in the valley of the Horsefly River, about 60 kilometres to the north-northwest (Wilson, 1977; Unit 10 of Panteleyev *et al*., 1996). They are, therefore, provisionally assigned an Eocene age.

EOCENE VOLCANIC ROCKS (SKULL HILL FORMATION)

Campbell and Tipper (1971) assigned Eocene volcanic rocks in the Bonaparte Lake map sheet to the Skull Hill Formation of the Kamloops Group. The most extensive exposures of the formation within the sheet define a north-northwest trending belt that extends for almost 70 kilometres between Bonaparte and Canim lakes (Figure 1). The eastern side of this belt is in contact with Mesozoic rocks that are the focus of the Bonaparte mapping project,

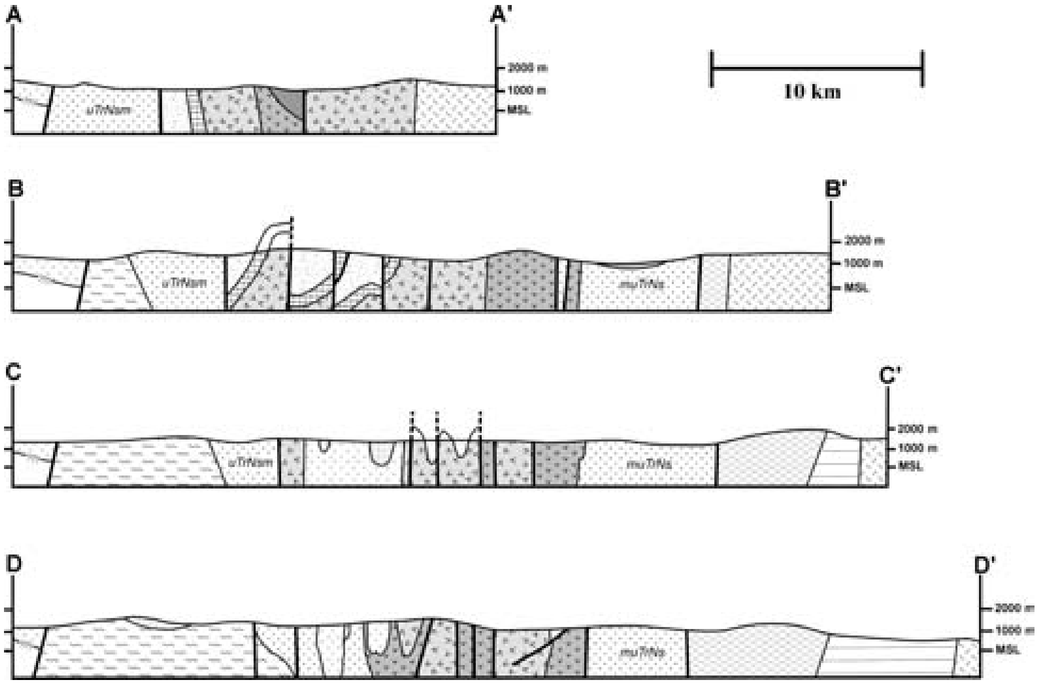

Figure 4. Schematic cross sections along lines shown on figures 2a and 3. *See* figures 2b and 3 for legend.

and was used as the western boundary of our mapping (Figure 2). The Skull Hill Formation is also represented by a small outlier of olivine-pyroxene-phyric basalt that overlies the Wavey Lake succession of the Nicola Group 3 kilometres north of Lac des Roches.

Most exposures of the Skull Hill Formation observed during the present study consist of dark grey to brown-weathered, pyroxene-phyric basalt flows. Also present are hornblende-phyric andesite flows, monolithic andesite and basalt breccias and dacite containing hornblende, biotite and feldspar phenocrysts. Minor amounts of sedimentary rock, including arkosic sandstone, granule to pebble conglomerate, and plant-rich shale, are intercalated with andesite and basalt southeast of Lac des Roches, but were not observed elsewhere. The Skull Hill Formation is suspected to be juxtaposed against the Mesozoic rocks to the east by a system of west-side-down normal faults, but evidence for such structures was observed only southeast of Lac des Roches, as described by Schiarizza and Israel (2001).

QUATERNARY VOLCANIC ROCKS

Flat-lying alkali olivine basalt flows within the Mann Creek and Clearwater River valleys comprise the south end of a volcanic field that extends 70 kilometres northward to form a prominent feature of Wells Gray Park (Figure 1). Campbell and Tipper (1971) recognized that some volcanic units in the northern part of the field were Pleistocene and younger, but correlated most of the volcanic rocks with the Miocene-Pliocene Chilcotin basalts, which cover much of the Interior Plateau to the west. More detailed study by Hickson and Souther (1984) and Hickson (1986) has shown that the Wells Gray - Clearwater volcanics are almost entirely Pleistocene and Holocene in age, and therefore are both spatially and temporally distinct from the compositionally similar Chilcotin Group.

The largest area inferred to be underlain by Pleistocene volcanic rocks within the present map area follows Mann Creek southwestward from the north boundary of the area, and then extends westward to cover a broad plateau north and northwest of Coldscaur Lake (Figures 2 and 3). Good exposures, however, are limited to the southeast corner of this lava field, along low scarps bounding Mann Creek southeast of Coldscaur Lake; the distribution elsewhere is inferred from the plateau-like topography and a positive anomaly on regional aeromagnetic maps. The volcanic rocks exposed southeast of Coldscaur Lake consist of several, thin, columnar-jointed subaerial flows with a total thickness of about 20 metres. The flows comprise dark grey to purplish-grey vesicular basalt that commonly contains small olivine phenocrysts. Similar flat-lying basalt flows are common as erosional remnants along the walls of Mann Creek for an additional 15 kilometres to the southeast (Figure 3), and a small remnant apparently occurs 5 to 6 kilometres beyond these, where Mann Creek enters the North Thompson River valley (Uglow, 1922). Hickson (1986) reports K-Ar whole rock isotopic dates from two separate sample localities along Mann Creek, southeast of Coldscaur Lake. One gave an age of 0.18 ±0.11 Ma and the other gave an age of 0.02 ±0.02 Ma.

Pleistocene volcanic rocks are also exposed along the east side of the Clearwater River at Clearwater, and in the west wall of the North Thompson River valley 3 kilometres to the south-southwest (Figure 2). These are remnants of volcanic units that become much more extensive within and adjacent to the Clearwater River valley farther north. The exposures near Clearwater are largely of subaerial flows similar to those along Mann Creek, but the base of the volcanic section 3 kilometres south-southwest of Clearwater comprises pillowed lava and pillow breccia (Walker, 1931; Hickson and Souther, 1984). Hickson and Souther report K-Ar whole rock dates of 0.35 ±0.09 Ma from the glassy rim of a quenched pillow at this locality, and 0.50 ±0.05 Ma from a subaerial flow directly overlying the pillowed deposit.

STRUCTURE

MESOSCOPIC STRUCTURES

Mesoscopic structures observed in the map area include a slaty to phyllitic cleavage that is axial planar to northwest to southeast-plunging mesoscopic folds, and a younger set of folds, with a locally developed crenulation cleavage, that deform the slaty cleavage. These structures are best developed in the Lemieux Creek succession, but comparable structures occur locally in fine-grained sedimentary intervals within all other Paleozoic and Mesozoic stratified rock units. Associated volcanic and coarse-grained clastic rocks are not generally foliated, except in local zones of high strain within fault zones or along the margins of some plutons (Schiarizza and Israel, 2001).

Within the Lemieux Creek succession the phase 1 slaty cleavage is highly variable in orientation, although steep west to southwest dips associated with east to northeast vergent folds are most common. The younger crenulation cleavage, which is best developed in exposures east of Taweel Lake, generally dips at moderate angles to the north-northeast. This pattern may relate to regional contractional deformation that is well documented along the Quesnel/Slide Mountain/Kootenay terrane boundaries to the north, where late Early Jurassic east-vergent thrust faults and associated folds are overprinted by early Middle Jurassic west-vergent backfolds (Brown *et al*., 1986; Rees, 1987).

MAP-SCALE STRUCTURES

The macroscopic structure of the study area is dominated by systems of northwest to north-striking faults, and less common northeast-striking cross faults (Figure 2). This intricate network of faults was recognized by Campbell and Tipper (1971) who noted that many of the faults cut Eocene rocks, but predate the Miocene. Schiarizza and Israel (2001) mapped the structures in the southern part of the Bonaparte project area in more detail, and confirmed that many of the faults were Eocene in age. However, like Campbell and Tipper, they suspected that some of the structures were older, but of uncertain age or sense of displacement. Schiarizza and Israel noted that Eocene faults in the western part of the area showed mainly west-side-down normal displacement, but that the structure in the east was dominated by a prominent system of dextral strike-slip faults, which they referred to as the Rock Island Lake fault system.

Schiarizza and Israel (2001) suggested that the structure of the south-central Bonaparte project area includes a northwest-trending syncline, which they called the Nehalliston syncline. The map pattern and stratigraphic relationships established during the 2001 field season confirm that the Nicola belt is generally synclinal in nature, comprising a core of Lower Jurassic rocks underlain by Nicola volcanic and volcaniclastic rocks, which in turn are flanked by underlying sedimentary rocks of units muTrNs and uTrNsm to the east and west, respectively. However, this synclinal structure has been fragmented by faults, mainly of Eocene age, to such an extent that no simple axial trace can be drawn to represent it. It is suspected that this synclinal structure developed as a Mesozoic compressional fold that was subsequently dissected and modified by younger faults. An alternative interpretation is that it reflects mainly a graben-like pattern of faulting during the Eocene.

Lemieux Creek Fault

The Lemieux Creek fault separates the Fennell Formation of the Slide Mountain Terrane from the Lemieux Creek succession of the Quesnel Terrane from the town of Little Fort to the south margin of the Raft Batholith (Figure 2). Parts of the fault zone are exposed locally over a distance of about 15 kilometres northward from where it crosses Highway 24. In this area the northerly-trending fault zone, in places more than 100 metres wide, is marked by brecciated and carbonate-altered rocks cut by anastomosing networks of steeply-dipping brittle faults with north-northeast to northwest strikes (Schiarizza and Israel, 2001). The fault's position is well constrained, but not exposed, northward from there, where it gradually changes to a north-northwesterly strike. It coincides with a prominent topographic lineament and a change in orientation of the southern contact of Raft Batholith, so is inferred to extend into, and cause minor offset of, these Jura-Cretaceous granitic rocks.

The relationships described above suggest that the latest movement on the Lemieux Creek fault postdates the Raft batholith, but that the post-batholith displacement is only minor. Nevertheless, this relatively young faulting, which is suspected to be Eocene in age, masks the pre-Tertiary configuration of the Fennell/Nicola contact in this area. Campbell and Tipper (1971) map this contact as a northeast-dipping thrust fault directly north of the Raft Batholith, while farther to the north the contacts between Quesnel, Slide Mountain and Kootenay terranes are mapped as a system of east-directed thrust faults that are overprinted by southwest-vergent folds (Brown *et al*., 1986; Rees, 1987). Campbell (1971) and Rees (1987) suggest that these Early to Middle Jurassic deformations may have overprinted an original stratigraphic relationship and that Middle to Upper Triassic rocks equivalent to the Lemieux Creek succession were deposited above Paleozoic rocks of the Slide Mountain Terrane, represented in that area by the Crooked Amphibolite.

Rock Island Lake Fault System

The system of steep faults that extends northwestward from Little Fort, through the eastern part of the Nicola belt, is referred to as the Rock Island Lake fault system by Schiarizza and Israel (2001). Brittle faults within the system cut rocks as young as the Eocene Chu Chua Formation, and kinematic indicators suggest mainly dextral strike-slip movement. The two main strands of this system, the Rock Island Lake fault and the Taweel Lake fault, are inferred to merge northwest of Taweel Lake and continue to the northern limit of our mapping (Figure 2). Their trajectories are not well constrained over most of this distance, however, as they are projected through a broad drift-covered area that extends from Taweel Lake to Canimred Creek. Evidence for a fault within the valley of Taweel Lake is provided by the apparent truncation of structures and a stratigraphic contact between units muTrNs and uTrNv that are mapped north of the lake (Figure 3). The faults' projected trace along Canimred Creek, at the northern limit of our mapping, is supported by the presence of east-dipping Eocene(?) sedimentary rocks west of the creek that may be bounded by the fault (Figure 4, section A).

Caverhill Lake Fault System

The Caverhill Lake fault is a southwest-side-down normal fault that separates Eocene volcanic rocks from Mesozoic rocks in the southwestern corner of the map area (Figure 2; Schiarizza and Israel, 2001). A related system of northwest to northerly-striking faults, locally offset by northeast-striking structures, is inferred to mark the eastern limit of the Eocene volcanic rocks along the full length of the map area (Figure 2). None of these faults was observed, however, and their presence is inferred mainly from the linear nature of the Eocene contact. Outliers of Eocene volcanic rocks are preserved east of the fault system, southeast and southwest of Wavey Lake (Figure 2), whereas inliers of Mesozoic rocks are exposed beneath the Eocene at Bridge Lake (Campbell and Tipper, 1971). These relationships suggest that west-side-down movement along the Caverhill Lake system amounts to only a few hundred metres of vertical offset.

Other Faults

The central part of the map area is transected by numerous northwesterly trending faults of unknown age, although it is suspected that most of these faults, like the adjacent Rock Island Lake and Caverhill Lake systems, formed in the Eocene. Several of the more prominent faults, such as those forming the eastern boundary of the Meridian Lake succession, the fault west of Windy Mountain and the Fourpound Lake fault, juxtapose older rocks on their west side against younger rocks to the east. These might be east-side-down conjugates to the Caverhill Lake fault system, but the fault dips and movement vectors along them are unconstrained. Some short fault segments are clearly truncated by other faults and cause duplications of local portions of the stratigraphy. These might be relicts of Mesozoic contractional structures. One of these faults duplicates the Jurassic stratigraphy northeast of Windy Mountain, and another duplicates Triassic stratigraphy between Deer Lake and the Rock Island Lake fault. Both are displayed as east-dipping faults, implying reverse movement, on Figure 4 (sections B and D), but their actual dip directions are unconstrained so other interpretations are equally viable.

MINERAL OCCURRENCES

Mineral occurrences within the southern and central parts of the Bonaparte project area are shown on Figure 5. These were extracted mainly from the B.C. Geological Survey Branch's MINFILE database, which was updated for the western part of the Bonaparte Lake (92P) map sheet in the late winter and spring of 2001. Most occurrences are within the southern part of the area, and were described by Schiarizza and Israel (2001). Here, we describe the MINFILE occurrences in the 2001 map area, as well as mineralization and alteration encountered during our mapping (Table 1 and Figure 5). We also provide updates on occurrences in the south that have been active subsequent to the report of Schiarizza and Israel.

RECENTLY ACTIVE PROSPECTS

Golden Loon Platinum (MINFILE 92P 043)

Cusac Gold Mines Limited optioned the Golden Loon claim group and initiated an exploration program for platinum group elements within ultramafic rocks of the Dum Lake igneous complex in the summer of 2000 (Clearwater Platinum project of Schiarizza and Israel, 2001). This program culminated in a drilling program during the spring of 2001. However, the option was subsequently dropped and there was little or no exploration work on the claim group during the following summer.

Worldstock (MINFILE 92P 145)

The Worldstock showing, comprising an isolated outcrop of carbonate-chlorite-pyrite-silica-altered rock with traces of chalcopyrite, was discovered in 1997 and returned 0.78 % copper over a 4 metre by 3 metre panel sample (Wells, 2000). Subsequent exploration by Christopher James Gold Corporation included soil geochemical, induced polarization and magnetic surveys. These programs generated a north-trending zone, more than 1200 metres long and 300 to 400 metres wide, with coincident copper-in-soils and IP chargeability anomalies. The more interesting targets were tested with a trenching and diamond drilling program during late spring 2001. Results of the diamond drilling had not been released when this report was written, but several trenches examined in June showed extensive areas of pyrite-sericite-silica-carbonate-altered rock cut by quartz and quartz-carbonate stockwork veins containing pyrite and chalcopyrite. The extent and nature of the alteration/mineralization are consistent with a porphyry-style environment. Host rocks appear to be mainly pyroxene porphyry breccias typical of Unit uTrNv. Outcrops of massive hornblende-pyroxene porphyry and

TABLE 1
GEOCHEMICAL DATA FOR SELECTED ROCK SAMPLES COLLECTED DURING THE 2001 FIELD SEASON

Element	Mo	Cu	Pb	Zn	Ni	Co	As	Cd	Sb	Bi	Cr	Ba	W	Hg	Ag	Au	Pt	Pd
Units	ppm	ppm	ppm	ppm	ppm	ppm	ppm	ppm	ppm	ppm	ppm	ppm	ppm	ppb	ppb	ppb	ppb	ppb
Method	ARMS	ARMS	ARMS	ARMS	ARMS	ARMS	ARMS	ARMS	ARMS	ARMS	ARMS	ARMS	ARMS	ARMS	ARMS	FA	FA	FA
Lab	ACM	ACM	ACM	ACM	ACM	ACM	ACM	ACM	ACM	ACM	ACM	ACM	ACM	ACM	ACM	ACM	ACM	ACM
Detection	0.01	0.01	0.01	0.1	0.1	0.1	0.1	0.01	0.02	0.02	0.5	0.5	0.2	5	2	2	2	2
Field #																		
O1PSC-122	107.51	114.7	163.36	35.7	12.9	6.5	2.9	0.48	0.28	232.09	118.6	70	86.6	< 5	42030	45	3	< 2
O1PSC-177	0.1	170.92	2.82	37.1	37.5	26.2	60.2	0.08	0.39	1	65.8	222	< .2	8	174	3	< 2	< 2
O1PSC-178	0.34	113.57	1.28	80.5	68.2	50.9	13.7	0.08	1.69	0.08	134.6	153	< .2	6	23	4	4	2
O1PSC-319	0.21	98.44	2.68	43.5	7.6	16.2	0.9	0.09	0.07	0.06	12.1	263.6	0.5	5	144	24	4	6
O1PSC-326	15.3	116.43	2.86	84	8.9	18.3	3.3	0.18	0.25	0.05	16	41.5	< .2	35	54	2	7	3
01SHE-36	2.27	6.19	8.07	3.5	4	1.2	2.5	0.1	0.09	0.14	133.4	13.9	< .2	7	183	77	4	< 2
01SHE-128-1	1.92	156.86	6.97	75.9	34.1	33.1	5.5	0.11	8.4	0.03	52.9	11.1	0.7	82	96	14	< 2	12
01SHE-128-2	1.37	53.55	4.5	13.8	25	21.2	122.1	0.18	6.53	0.02	18.1	32.5	< .2	33	70	14	7	5
01SHE-128-3	0.94	30.82	2.19	21.1	4.4	7.8	40.4	0.09	5.47	< .02	27.8	23.8	< .2	34	27	18	2	2
01SHE-172	0.75	322.95	40.33	257	178.5	47.8	69.5	8.31	7.14	1.25	237.9	114.7	10.3	6	2166	8	14	14
01SHE-174	7.6	2954.9	9199.2	15949	13.6	12.2	8.1	317.77	1.8	71.88	49.8	3.9	2.2	379	62027	3	3	2
01SHE-302	4.23	701.67	971.88	15988	89.5	35	99999	449.04	108.09	259.29	17.8	13.8	2.6	126	59273	810	2	2
01SHE-306	53.59	82.75	16.53	59	10.4	14.2	185.8	0.52	0.95	0.26	28	66.6	0.4	62	234	20	7	3
01SHE-378	7.03	41.38	69.37	188.4	20.9	6.3	7	4.16	0.54	1.66	61.2	62	1.2	7	886	4	3	2
01SHE-379	13.27	110.5	6.49	311.3	59.9	11	8.1	10.58	0.95	0.56	86.3	83	0.7	8	541	5	< 2	5
01SHE-397	0.56	565.32	6.66	35.7	5.7	8.4	9.1	0.31	0.32	0.25	39.3	72	< .2	< 5	235	8	3	9
01SHE-404	4.88	208.53	9.78	152.8	49.2	22.1	8.3	1.61	2	0.18	46.1	70.5	0.3	97	379	5	6	5
01SHE-405	14.78	122.12	18.87	126.7	18.5	6.5	87.9	2.01	4.47	0.4	32.6	121.6	< .2	184	592	6	5	3

Analysis of steel milled sample prepared by GSB.
ARMS = Aqua regia digestion - ICPMS
FA = Lead fire assay-ICP finish
ACM = ACME Analytical, Vancouver

fine-grained hornblende-pyroxene-feldspar microdiorite are located about 200 metres northeast of the mineralized rock, and may represent a small Late Triassic - Early Jurassic intrusive body.

Silver Lake - New Discovery

The Silver Lake property of Christopher James Gold Corporation includes the Worldstock showing and several precious metal vein systems on the PGR claims to the northwest (Schiarizza and Israel, 2001). In 2000, chalcopyrite-rich pebbles were discovered in glacial drift at two separate localities, 4.7 and 5.7 kilometres west-northwest, respectively, of the Worldstock showing, prompting an exploration program over this part of the property during the 2001 field season. The property was visited in early August, shortly after a trench had been excavated on a strong geophysical anomaly about 50 metres north-northeast of the southeastern float occurrence (referred to as New Discovery A). The trench exposed an impressive zone of copper mineralization, averaging about 1 metre wide, over a northwest strike-length of 25 metres. The mineralization comprises patches of massive chalcopyrite-pyrite and quartz within multiply-sheared, pyrite-magnetite-chlorite-altered pyroxene porphyry basalt. Systematic chip-panel sampling across the zone returned copper values in the 2 to 15 percent range with 34 to 177 grams per tonne silver and up to 0.33 gram per tonne gold over 0.6 to 1.5 metre sample widths (Christopher James Gold Corporation, News Release, July 30 2001). A diamond drilling program to test the geometry of this zone over an 85 metre strike-length returned encouraging copper and silver values in 3 of 6 holes. A phase two drilling program encountered copper values over a 700 metre strike-length along a strong northwest-trending geophysical and copper-in-soils anomaly between the original two float discoveries (Christopher James Gold Corporation, News Release, November 20 2001).

Crazy Fox Property (MINFILE 92P 185)

The Crazy Fox property, centred about 4 kilometres east of Rock Island Lake, was initially staked in the spring of 1998 to cover a multi-element anomaly detected by a BCGS till geochemical survey (Bobrowsky *et al*., 1998; Paulen *et al*., 2000). Subsequent work in 1998 and 1999 by Bourdon and Addie (2000a, 2000b) outlined a north-northwest trending belt, up to 500 metres wide and 10 kilometres long, containing highly anomalous values for Ag, As, Ba, Cd, Co, Cu, Se, Sb and Zn in till and soil samples. Coincident with this geochemical anomaly is a strong magnetic anomaly evident on the regional aeromagnetic map, and confirmed by a ground magnetic survey carried out by Inmet Mining Corporation in 2000 (Burge, 2001). The property is currently optioned by Cassidy Gold Corporation, who drilled one hole in August 2001. In an October news release, Cassidy management stated that more detailed geological mapping, slated for the spring of 2002, would be undertaken prior to any further drilling.

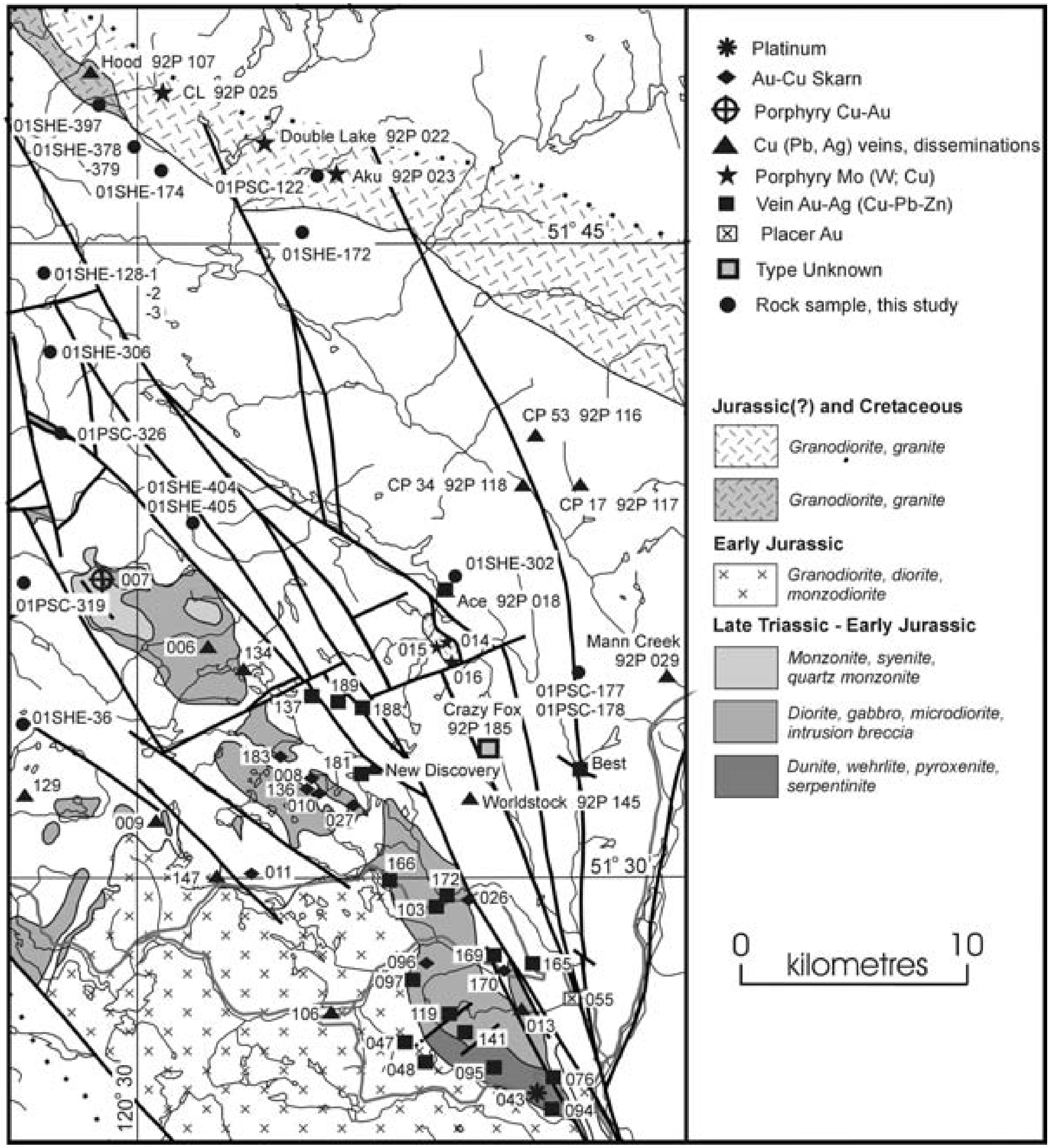

Figure 5. Locations of MINFILE occurrences in the southern and central parts of the Bonaparte project area, and selected rock samples collected during the 2001 field season. Base map is derived from Figure 2, with only plutonic rocks and faults shown. Occurrences discussed in text are shown with name and full MINFILE number. Other occurrences, discussed by Schiarizza and Israel (2001), are designated with only the last 3 digits of their 92P MINFILE number. *See* figures 2a and 3 for Place Names mentioned in text.

The Crazy Fox property straddles the contact between units uTrNv and uTrNsv of this report, and is underlain by a moderately to steeply west-dipping succession of volcanic breccias, pillowed flows and thick sedimentary intervals dominated by siltstone, argillite and volcanic sandstone. Flow-banded rhyolite to dacite occurs locally and is either part of the volcanic stratigraphy or a series of younger (Eocene?) sills. No mineralization is exposed on the property, but the current exploration program is targeting a potential volcanic-hosted massive sulphide occurrence.

VEIN OCCURRENCES IN THE LEMIEUX CREEK AND FENNELL BELTS

Ace (MINFILE 92P 018)

The Ace occurrence is hosted by metasedimentary rocks of Unit muTrNs along upper Lemieux Creek, a little more than 100 m downstream from the outlet of Taweel Lake (Davis, 1925, p. B152; Schiarizza and Israel, 2001). Mineralization at an old shaft on the southwest bank of the creek comprises lenses of massive pyrrhotite-pyrite-arsenopyrite with minor chalcopyrite. Individual sulphide lenses are up to several tens of centimetres wide, and are enclosed in dark grey phyllite containing contorted layers and fragments of lighter grey siltite and fine-grained quartzose metasandstone. Mineralization also occurs in trenches located about 700 metres northeast of the Lemieux Creek shaft, where massive sulphide lenses, including arsenopyrite, sphalerite, galena, chalcopyrite and pyrite, are hosted by similar brecciated and quartz-carbonate-pyrite-altered metasedimentary rocks (Jenks, 1999). A sample collected from one of these sulphide lenses during the 2001 field season returned 15 988 ppm Zn, 972 ppm Pb, 702 ppm Cu, 259 ppm Bi, 59273 ppb Ag and 810 ppb Au (Sample 01SHE-302 on Figure 5 and Table 1).

Alteration and Mineralization along the Lemieux Creek Fault

Brecciated, altered and locally mineralized rocks occur along the Lemieux Creek fault for a distance of at least 6 kilometres west of Lemieux Lake and Skwilatin Mountain. The southern part of this zone was covered by the Best claims and explored for epithermal gold mineralization from 1984 to 1989. There, brecciated and carbonate±quartz±pyrite-altered rocks of the Fennell Formation and Lemieux Creek succession, together with similarly altered feldspar porphyry dikes, are interleaved within a complex system of north to northwest-striking faults. Gilmour (1985) reports that an 18-metre chip sample that crossed the Nicola/Fennell contact, defined in that area by an altered feldspar porphyry dike, returned .007 oz/ton Au (located as "Best" on Figure 5).

About 5 kilometres north of the sampled area described above, a recently-constructed logging road exposes altered and mineralized rocks of the Fennell Formation that are within, or just east of, the projected trace of the Lemieux Creek fault. The rocks closest to the fault are breccias, comprising angular greenstone fragments within a matrix of carbonate with disseminated to semi-massive pyrite. Cutting the breccia are veins and stringers of white to pinkish calcite containing pyrrhotite and local traces of chalcopyrite, as well as rusty, vuggy quartz and quartz-calcite veins containing limonite-altered sulphides that may include pyrite, arsenopyrite, sphalerite, chalcopyrite and galena. The veins commonly strike northwest and dip steeply. Two samples were collected during our mapping, one from a pyrite-calcite-cemented breccia (01PSC-178), and one from a calcite vein containing pyrrhotite and traces of chalcopyrite (01PSC-177). Both samples contain anomalous arsenic and copper values, but are not enriched in other base or precious metals. A sample from one of the vuggy quartz-calcite-sulphide veins collected by prospector Paul Watt, who recently staked the Silver Pipe claims over this ground, returned 6.09% Zn, 0.15%Cd, 1666 ppm Cu, 128 ppm Pb, 55.8 ppm Ag and 20 ppb Au. In addition, a sample of semi-massive sulphides from the matrix of a calcite-pyrite-cemented breccia returned 330 ppb Au and 20.3 g/t Ag.

Mann Creek (MINFILE 92P 029)

The Mann Creek occurrence comprises several small showings containing either chalcopyrite or galena along the lower reaches of Mann Creek (Figure 5). This area was mentioned briefly by Uglow (1922), who reported that a modest exploration program was being directed at malachite and azurite-stained rocks on the south bank of the creek. More recent exploration included a program of geological mapping and soil and rock geochemistry in 1973 (McLeod, 1973), and prospecting in 1980 (Mirko, 1980). The mineralization is hosted in metabasalts of the Fennell Formation. It includes three separate occurrences of pyrite and minor chalcopyrite in calcite-epidote veins, and a single occurrence of galena in a quartz-carbonate stringer (McLeod, 1973). All four showings are contained within an area of about 0.15 square kilometre.

CP Occurrences (MINFILE 92P 116, 117, 118)

The CP showings comprise three separate occurrences of chalcopyrite within quartz veins between Clearwater Peak and Mann Creek (Figure 5). The mineralization was discovered in 1972 during an exploration program that was initiated after reconnaissance geochemical prospecting in the area revealed slightly anomalous values in copper, zinc and molybdenum (Dawson, 1972). Two of the occurrences are within metabasalts of the upper Fennell Formation, while the other, on the southwest bank of Mann Creek, is within slate of Unit muTrNs on the opposite side of the Lemieux Creek fault. Each occurrence comprises minor amounts of chalcopyrite within a single, narrow quartz vein. The only other mineralization discovered during the 1972 exploration program was a trace of galena in a quartz-carbonate vein cutting Unit muTrNs, 1300 metres northwest of the CP 34 showing (Dawson, 1972). There has been no exploration work recorded on any of the occurrences since their initial discovery.

OCCURRENCES ASSOCIATED WITH THE RAFT BATHOLITH

Aku (MINFILE 92P 023)

The Aku showings are located within the Raft Batholith, about 1.5 kilometres north of its south contact, 2 kilometres east of Patricia Lake (Figure 5). The area was first staked in 1966 after anomalous molybdenum values were encountered in stream silt samples. The mineralization was discovered during an exploration program carried out over the following two years, which included geological, geochemical and geophysical surveys, together with limited trenching and diamond drilling. Additional geochemical and geophysical surveys were carried out in 1974 and 1976, and again in 1980 after the showings were restaked as the D.D. claim group.

The area of the Aku showings is underlain by medium to coarse-grained monzogranite, cut by veins and patches of quartz-orthoclase pegmatite, and northwest-striking dikes of aplite and quartz-feldspar porphyry. Mineralization comprises molybdenite and pyrite, locally with traces of chalcopyrite, disseminated along hairline fractures and within narrow quartz veinlets. The mineralized veinlets typically dip steeply to the north-northeast, and are sporadically developed within a northwest-trending zone about 1 kilometre long and up to 400 metres wide (Gareau, 1981). However, narrow zones of sheeted quartz veinlets, dipping steeply to the north-northeast and containing pyrite, specularite and molybdenite, were also encountered more than 1 kilometre west of this main zone of mineralization. A sample of this western mineralized material contains 107.5 ppm Mo, 42030 ppb Ag and 45 ppb Au, and is highly anomalous in bismuth and tungsten (Figure 5 and Table 1, Sample 01PSC-122).

Double Lake (MINFILE 92P 022)

The Double Lake showing, located within the Raft Batholith about 1 kilometre south of Sicily Lake, was originally staked at the same time as the Aku showings, which are about 3 kilometres to the east-southeast. The most recent work recorded over the showing was in 1979, when it was covered by the Moly claims. This work included geological and soil geochemical surveys as well as a trenching and percussion drilling program (DeLeen, 1980). Mineralization consists of molybdenite, pyrite and chalcopyrite along fracture planes and as disseminations within coarse-grained monzogranite, and occurs discontinuously over a distance of at least 800 metres along a northeast-trending system of trenches (DeLeen, 1980).

CL (MINFILE 92P 025)

The CL molybdenum showing is located in the southwestern part of the Raft Batholith, about 4 kilometres west-southwest of Corsica Lake. The area was explored by soil sampling, geophysical surveys and 3 shallow diamond drill holes during the period 1966 through 1969. It was restaked as part of the DL claim block, which also included the Hood occurrence to the west, and explored with additional soil and geophysical surveys in 1980. The mineralization was not located during the present study but is reported to consist of molybdenite in quartz veins and on fracture surfaces (Dawson, 1981). The predominant host rock is granite to granodiorite of the main phase of the Raft Batholith.

Hood (MINFILE 92P 107)

The Hood showing is located near the southwest margin of the Raft Batholith, about 4.5 kilometres east of Canimred Creek. It comprises disseminated sulphides, including pyrrhotite, pyrite, chalcopyrite and traces of molybdenite, scattered over an area of about 500 metres by 200 metres within diorite that forms the western border phase of the batholith (Ney, 1972). The Hood claims were staked in 1971 after mineralized float was discovered along logging roads. The *in situ* mineralization was located during an exploration program that same year that included geological mapping, soil and rock geochemical sampling and an induced polarization survey (Ney, 1972). The showing was subsequently restaked as part of the DL claim block, and investigated with soil and geophysical surveys in 1980 (Dawson, 1981).

The Hood showing occurs along the northeast margin of the diorite border phase of the Raft Batholith, near its contact with granite that is typical of most of the batholith. During our 2001 mapping program additional mineralization was encountered along the south margin of the diorite unit, about 1.5 kilometres south of the Hood occurrence. The diorite there is rich in magnetite and biotite, contains disseminated pyrite, and locally hosts narrow, sheeted chlorite-sulphide veinlets that contain pyrite and traces of chalcopyrite. A sample that included this sheeted vein material returned 565 ppm Cu and 235 ppb Ag (Table 1 and Figure 5, Sample 01SHE-397).

Mineralization in Country Rocks on the Southwest Side of the Batholith

During the 2001 field season, mineralization was located at three separate localities, over a distance of 8.5 kilometres, within hornfelsed country rock near the southwest margin of the Raft Batholith. One occurrence, 3.5 kilometres southeast of the Hood showing, consists of pyrite and minor galena within quartz-epidote veinlets that cut fine-grained silicified metasedimentary rocks. Two separate samples of this material contained anomalous base metal and silver concentrations (Table 1 and Figure 5, Samples 01SHE-378 and 01SHE-379). The second locality, 1.5 kilometres to the south-southwest, comprises chalcopyrite, galena and sphalerite within a steeply-dipping, west-northwest striking brecciated fault zone that is up to 20 centimetres wide and cuts fine-grained silica-pyrite-pyrrhotite-altered metasedimentary rocks. A sample of this material contains 2955 ppm Cu, 9199 ppm Pb, 15949 ppm Zn and 62027 ppb Ag, and also yielded high values of bismuth and mercury (Sample 01SHE- 174). The third locality is 7 kilometres east-southeast of the second, and about 3.5 kilometres southwest of the Aku prospect. There, pyrite, pyrrhotite and traces of chalcopyrite occur in fractures and quartz-epidote veins within a west-northwest

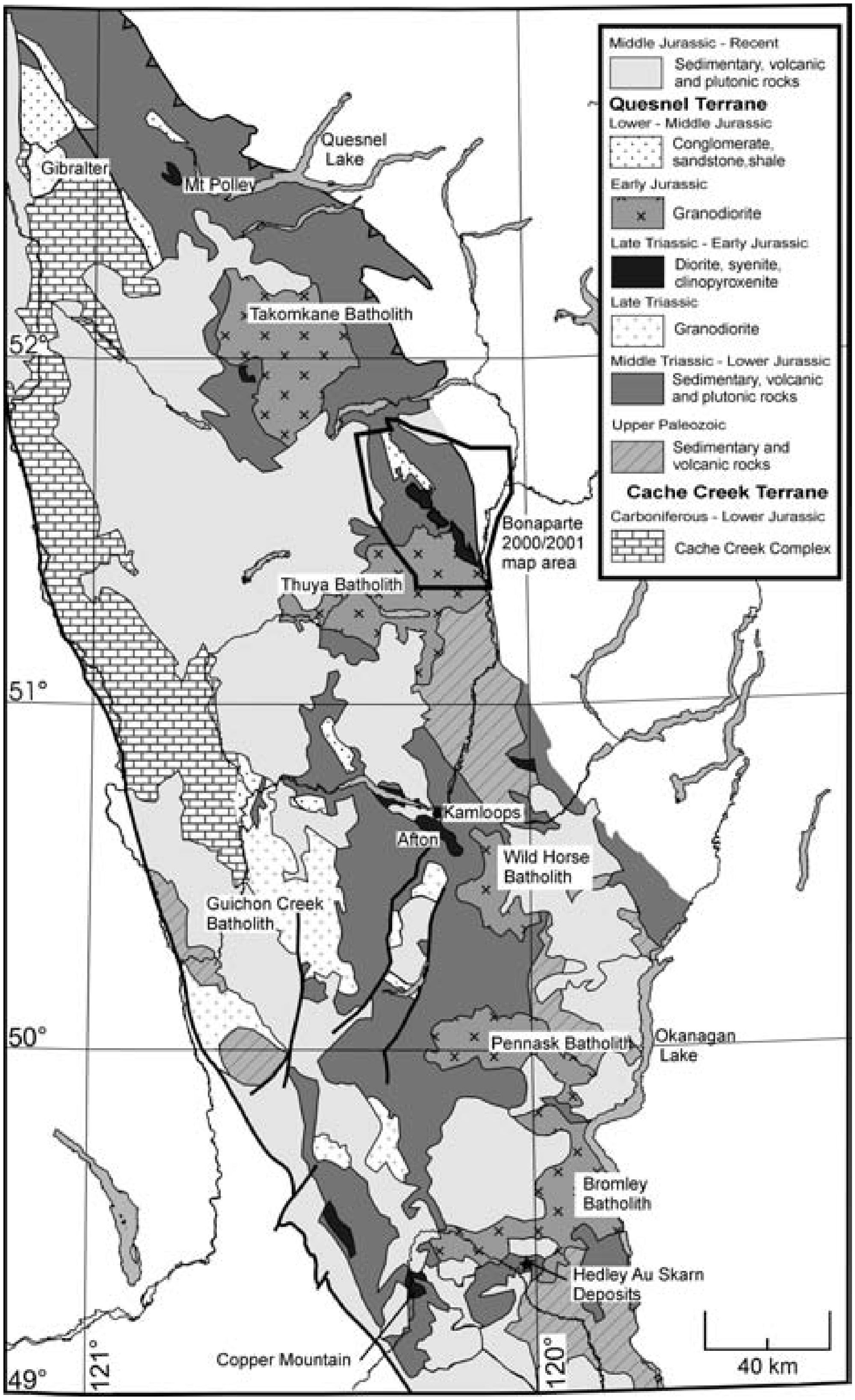

Figure 6. Simplified geologic map of south-central British Columbia highlighting the major belts of Late Triassic - Early Jurassic plutons of the Quesnel Terrane. Geology after Wheeler and McFeely (1991), modified with data from Parrish and Monger (1992), Ray and Dawson (1994), Mortensen *et al*. (1995), Whiteaker (1996), Ray and Webster (2000) and Ash and Riveros (2001).

striking, steeply north-dipping fault zone that cuts metasedimentary rocks of Unit muTrNs. A sample of this material returned 323 ppm Cu, 2166 ppb Ag, 8 ppb Au, 14 ppb Pt and 14 ppb Pd (Sample 01SHE-172).

INDICATIONS OF MINERALIZATION IN THE WEST-CENTRAL PART OF THE STUDY AREA

Southwest of Canimred Creek

The sparse bedrock exposures of Unit uTrNv and overlying Eocene(?) sedimentary rocks directly west of the broad area of drift covering the valley of Canimred Creek are commonly altered with disseminated pyrite and cut by quartz-carbonate veins containing variable amounts of pyrite and/or pyrrhotite. Samples 01SHE-128-1, 128-2 and 128-3 (Table 1 and Figure 5) were collected from, respectively, a brittle fault zone, a quartz-carbonate vein and pyritic volcanic host rocks of Unit uTrNv. All three samples returned weakly anomalous gold values of 14 to 18 ppb, as well as elevated concentrations of mercury, antimony and arsenic. A sample of carbonate-altered conglomerate from Unit lJs, 3.5 kilometres to the south, returned 53.59 ppm Mo and 20 ppb Au, and was also anomalous in mercury and arsenic (Sample 01SHE-306). These indications of epithermal-style alteration may be related to the systems of northwest and east-northeast trending Eocene(?) faults that transect this area.

Near the Fourpound Lake Fault

An exposure of microdiorite 1 kilometre north of Windy Mountain, apparently part of a lens of intrusive rocks enclosed by strands of the Fourpound Lake fault, is in large part altered to a rusty gossanous rock containing pyrite, pyrrhotite and relict feldspar grains. Sample 01PSC-326 from this rusty material returned 15.3 ppm Mo and 116.43 ppm Cu (Figure 5 and Table 1).

Eight kilometers to the southeast of the sample described above, and about 1 kilometre northeast of the trace of the Fourpound Lake fault, two adjacent outcrops of sedimentary rock within Unit lJs include areas of pyrrhotite-bearing gossan. Samples collected from these outcrops (01SHE- 404 and 01SHE-405) returned slightly elevated base metal and mercury values, and 379 and 592 ppb Ag, respectively.

West of the Monticola Lake Fault

An exposure about 1.4 kilometres north of the north end of Wavey Lake includes a complex mixture of microdiorite, diorite and granodiorite cutting chert and associated sedimentary rocks of the Wavey Lake succession. Pyrrhotite occurs as disseminations and stringers within the intrusive rocks and the adjacent country rock. A sample of altered country rock returned 77 ppb Au (Figure 5 and Table 1, Sample 01SHE-36). Similar dioritic intrusions are common within the Wavey Lake succession to the southeast, and host sparse chalcopyrite and molybdenite mineralization at the Ellen occurrence (MINFILE 92P 129; Wares and MacDonald, 1972).

A traverse through the eastern part of the Meridian Lake belt, west of the Friendly Lake intrusive complex, encountered several exposures of rusty silicified rock with variable amounts of disseminated pyrite, at least in part derived from sedimentary rocks of the Meridian Lake succession. Sample 01PSC-319 (Figure 5 and Table 1) from an exposure of this silicified rock returned 24 ppb Au. These exposures are just east of the recently-staked Need claims, which cover several zones of highly anomalous gold in soil and rock grab samples (Cassidy Gold Corporation, News Release, October 22 2001).

SUMMARY OF MAIN CONCLUSIONS

The Nicola Group is represented in the southern and central parts of the Bonaparte project area by Upper Triassic volcanic and volcaniclastic rocks together with underlying Middle to Upper Triassic sedimentary rocks represented by the Lemieux Creek succession in the east and the Meridian Lake succession to the west. The Wavey Lake succession is an undated assemblage of mainly cherts and volcaniclastic sandstones that occurs west of and structurally beneath the Meridian Lake succession. It is interpreted as a western facies of the Nicola Group.

The Meridian Lake succession is underlain by Upper Paleozoic carbonate, chert and siltstone of the Harper Ranch Group. The Lemieux Creek succession is faulted against the Upper Paleozoic Fennell Formation of the Slide Mountain Terrane, and north of the study area is inferred to have been deposited above the Crooked Amphibolite, an oceanic assemblage also included in the Slide Mountain Terrane. The Meridian Lake and Lemieux Creek successions contain similar assemblages of siltstone, slate and limestone, but the Lemieux Creek succession also includes quartzites and quartzose metasandstones, perhaps reflecting a depositional setting more proximal to Proterozoic and Paleozoic quartzose metasedimentary rocks of the pericratonic Kootenay Terrane.

The Thuya batholith, part of which intrudes the Nicola Group in the southwestern part of the Bonaparte project area, has yielded an Early Jurassic U-Pb crystallization age of 192.7 ±0.9 Ma. It is one of five large calc-alkaline batholiths, also including the Takomkane Batholith to the north, and the Wild Horse, Pennask and Bromley batholiths to the south, that define a linear north-northwest trending belt of Early Jurassic magmatism that extends for 300 kilometres within the central to eastern part of the Quesnel Terrane (Figure 6).

A prominent belt of ultramafic - mafic - syenitic plutonic rocks, only partially shown on previous maps, extends northwestward from the northeast margin of the Thuya batholith. One of these stocks, a diorite unit near Deer Lake, has yielded a U-Pb crystallization age of 197.8 ±1.4 Ma. These pre-Thuya intrusive rocks are correlated with a suite of small alkaline plutons of latest Triassic to earliest Jurassic age that are scattered along and just west of the magmatic axis defined by the large Early Jurassic calc-alkaline plutons described above (Figure 6). Within the project area, base and precious metal mineral occurrences are concentrated within and adjacent to this belt of Late Triassic(?) - Early Jurassic plutons. These include copper-gold skarns associated with the Deer Lake diorite stocks, and porphyry-style copper mineralization within the Friendly Lake diorite-syenite complex. Correlative rocks elsewhere along this magmatic belt host economic copper-gold porphyry deposits at Mount Polley, Afton and Copper Mountain, and potentially correlative dioritic rocks are associated with the gold skarns at Hedley (Figure 6).

The Nicola Group is stratigraphically overlain by a succession of Lower Jurassic sedimentary rocks that includes distinctive granitoid-bearing conglomerates in its lower part. These sedimentary rocks are correlated with the Lower to Middle Jurassic Ashcroft Formation, which overlies the Nicola Group in the western part of the Quesnel Terrane to the south. The granitic clasts in Lower Jurassic conglomerate must be older than the Thuya batholith. They are most prominent in western exposures, and may have been derived from a source now buried beneath Tertiary and Quaternary deposits to the west of the map area. A buried pre-Jurassic granitic pluton in this area might have economic potential, as the western part of Quesnel Terrane includes a belt of Late Triassic calc-alkaline plutons that host the important copper porphyry deposits of the Highland Valley (Guichon Creek Batholith) and(?) Gibralter (Figure 6).

The Middle Jurassic or younger Raft Batholith, and the mid-Cretaceous Tintlhohtan Lake stock represent younger magmatism in the project area. These belong to suites of plutons that extend across the boundaries between Kootenay, Slide Mountain and Quesnel terranes. Within the Bonaparte project area, both the Raft Batholith and the Tintlhohtan Lake stock host porphyry molybdenum mineralization.

The structure of the Bonaparte project area is characterized by panels of steeply-dipping strata bounded by systems of mainly northwest-striking Eocene faults. Epithermal-style alteration and mineralization occurs along or adjacent to some of these faults. The Eocene structures include a network of dextral strike-slip faults referred to as the Rock Island Lake fault system. The main strands of this system, the Rock Island Lake and Taweel Lake faults, have been traced from Little Fort to Canimred Creek, a distance of more than 50 kilometres, and may be part of a significant dextral strike-slip system that has not been well documented in this part of the cordillera.

ACKNOWLEDGMENTS

We thank Shawn Ling of Peaceful Cove Resort, and Jim and Bella Jackson of Birch Island for their hospitality during our fieldwork. Discussions in the field with Mike Cathro, Dave Lefebure, Ron Wells, Paul Watt, Vic Preto, Terry Poulton, Richard Friedman and Lori Kennedy were helpful and are gratefully acknowledged. We also thank Mike Orchard, Terry Poulton and Wayne Bamber for their fossil identifications, and Richard Friedman for his radiometric dating. Dave Lefebure and Brian Grant reviewed earlier versions of the manuscript and suggested improvements. We thank Janet Holland for formatting the final version of the paper.

REFERENCES

Ash, C.H. and Riveros, C.P. (2001): Geology of the Gibralter copper-molybdenite deposit, east-central British Columbia (93B/9); *in* Geological Fieldwork 2000, *British Columbia Ministry of Energy and Mines*, Paper 2001-1, pages 119-133.

Bobrowsky, P.T., Paulen, R., Little, E., Prebble, A., Ledwon, A. and Lett, R. (1998): Till geochemistry of the Louis Creek - Chu Chua Creek area (NTS 92P/1E and 92P/8E); *British Columbia Ministry of Energy and Mines*, Open File 1998-6.

Bourdon, B. and Addie, L. (2000a): Report on till, soil, rock and silt geochemistry, Crazy Fox property, Crazy Fox group; *British Columbia Ministry of Energy and Mines*, Assessment Report 26 290, 9 pages.

Bourdon, B. and Addie, L. (2000b): Report on till, soil, rock and silt geochemistry, Crazy Fox property, Fox group; *British Columbia Ministry of Energy and Mines*, Assessment Report 26 291, 9 pages.

Brown, R.L., Journeay, J.M., Lane, L.S., Murphy, D.C. and Rees, C.J. (1986): Obduction, backfolding and piggyback thrusting in the metamorphic hinterland of the southeastern Canadian Cordillera; *Journal of Structural Geology*, Volume 8, pages 255-268.

Burge, C. (2001): Geophysical assessment report, Demers property, Kamloops Mining Division; *British Columbia Ministry of Energy and Mines*, Assessment Report 26 521, 9 pages.

Calderwood, A.R., van der Heyden, P. and Armstrong, R.L. (1990): Geochronometry of the Thuya, Takomkane, Raft and Baldy batholiths, south-central British Columbia; *Geological Association of Canada - Mineralogical Association of Canada*, Annual Meeting, Vancouver. B.C., Program with Abstracts, Volume 15, page A19.

Campbell, K.V. (1971): Metamorphic petrology and structural geology of the Crooked Lake area, Cariboo Mountains, British Columbia; unpublished Ph.D. thesis, *The University of Washington*, 192 pages.

Campbell, R.B. and Tipper, H.W. (1971): Bonaparte Lake map area, British Columbia; *Geological Survey of Canada*, Memoir 363, 100 pages.

Colpron, M. and Price, R.A. (1995): Tectonic significance of the Kootenay terrane, southeastern Canadian Cordillera: An alternative model; *Geology*, Volume 23, pages 25-28.

Danner, W.R. and Orchard, M.J. (2000): Paleontology of the Cache Creek and Quesnellia terranes, southwestern British Columbia; *in* Guidebook for geological field trips in southwestern British Columbia and northern Washington, edited by G.J. Woodsworth, L.E. Jackson, Jr., J.L. Nelson and B.C. Ward, published by the Cordilleran Section, *Geological Association of Canada*, for the Geological Society of America, Cordilleran Section 2000 Annual Meeting, Vancouver, B.C., pages 117-173.

Davis, A.W. (1925): Central Mineral Survey District (No. 3); *in* Annual Report of the Minister of Mines for 1924, *British Columbia Bureau of Mines*, pages B134-B158.

Dawson, J.M. (1972): Geological and geochemical report on the CP group of claims, Kamloops Mining Division, British Columbia; *British Columbia Ministry of Mines and Petroleum Resources*, Assessment Report 3885, 17 pages.

Dawson, J.M. (1981): Geochemical and geophysical report on the DL claims, Kamloops Mining Division, British Columbia; *British Columbia Ministry of Energy, Mines and Petroleum Resources*, Assessment Report 9019, 13 pages.

DeLeen, J. (1980): Report on the Moly claims of Norsemont Mining Corporation; *British Columbia Ministry of Energy, Mines and Petroleum Resources*, Assessment Report 7920, 10 pages.

Erdmer, P., Thompson, R.I. and Daughtry, K.L. (1999): Pericratonic Paleozoic succession in Vernon and Ashcroft map areas, British Columbia; *in* Current Research 1999-A, *Geological Survey of Canada*, pages 205-213.

Ferri, F. (1997): Nina Creek Group and Lay Range Assemblage, north-central British Columbia: remnants of late Paleozoic oceanic and arc terranes; *Canadian Journal of Earth Sciences*, Volume 34, pages 854-874.

Gareau, M.B. (1981): Geological, geochemical and geophysical assessment report, D.D. claim group, Kamloops Mining District; *British Columbia Ministry of Energy, Mines and Petroleum Resources*, Assessment Report 8852, 17 pages.

Gilmour, W.R. (1985): Geochemical and geological assessment report on the Best property (Best 1-4 claims), Lemieux Creek area, Kamloops Mining Division, B.C.; *British Columbia Ministry of Energy, Mines and Petroleum Resources*, Assessment Report 13 312, 12 pages.

Hickson, C.J. (1986): Quaternary volcanism in the Wells Gray - Clearwater area, east-central British Columiba; unpublished Ph.D. thesis, *The University of British Columbia*, 357 pages.

Hickson, C.J. and Souther, J.G. (1984): Late Cenozoic volcanic rocks of the Clearwater - Wells Gray area, British Columbia; *Canadian Journal of Earth Sciences*, Volume 21, pages 267-277.

Höy, T. and Dunne, K.P.E. (1997): Early Jurassic Rossland Group, southern British Columbia: Part I - stratigraphy and tectonics, *British Columbia Ministry of Employment and Investment*, Bulletin 102, 123 pages.

Jenks, J. (1999): Assessment Report, Geological Mapping and Prospecting, Lem 1-3 Mineral Claims; *B.C. Ministry of Energy and Mines*, Assessment Report 25939, 16 pages.

Jung, A. (1986): Geochronometry and geochemistry of the Thuya, Takomkane, Raft and Baldy batholiths, west of the Shuswap metamorphic complex, south-central British Columbia; unpublished B.Sc. thesis, *The University of British Columbia*, 140 pages.

Klepacki, D.W. and Wheeler, J.O. (1985): Stratigraphic and structural relations of the Milford, Kaslo and Slocan groups, Goat Range, Lardeau and Nelson map areas, British Columbia; *in* Report of Activities, Part A, *Geological Survey of Canada*, Paper 85-1A, pages 277-286.

Lefebure, D.V. (1976): Geology of the Nicola Group in the Fairweather Hills, British Columbia; unpublished M.Sc. thesis, *Queens's University*, 179 pages.

Logan, J.M. (2002): Intrusion-related mineral occurrences of the Cretaceous Bayonne Magmatic Belt, southeast British Columbia; *British Columbia Ministry of Energy and Mines*, Geoscience Map 2002-1.

McLeod, J.W. (1973): Geological and geochemical report on the X claim group at Blackpool, B.C. in the Kamloops Mining District; *British Columbia Ministry of Mines and Petroleum Resources*, Assessment Report 4777, 12 pages.

Mirko, J.M. (1980): Prospecting report on the Billy mineral claim, Kamloops Mining Division, B.C.; *British Columbia Ministry of Energy, Mines and Petroleum Resources*, Assessment Report 8266, 4 pages.

Monger, J.W.H. (1977): Upper Paleozoic rocks of the Canadian Cordillera and their bearing on cordilleran evolution; *Canadian Journal of Earth Sciences*, Volume 14, pages 1832-1859.

Monger, J.W.H., Price, R.A., and Tempelman-Kluit, D.J. (1982): Tectonic accretion and the origin of the two major metamorphic and plutonic welts in the Canadian Cordillera; *Geology*, Volume 10, pages 70-75.

Monger, J.W.H. and McMillan, W.J. (1989): Geology, Ashcroft, British Columbia (92I); *Geological Survey of Canada*, Map 42-1989, sheet 1, scale 1:250 000.

Monger, J.W.H., Wheeler, J.O., Tipper, H.W., Gabrielse, H., Harms, T., Struik, L.C., Campbell, R.B., Dodds, C.J., Gehrels, G.E. and O'Brien, J. (1991): Part B. Cordilleran Terranes, *in* Upper Devonian to Middle Jurassic assemblages, Chapter 8 of Geology of the Cordilleran Orogen in Canada, edited by H. Gabrielse and C.J. Yorath, *Geological Survey of Canada*, Geology of Canada, Number 4, pages 281-327.

Mortensen, J.K., Ghosh, D.K. and Ferri, F. (1995): U-Pb geochronology of intrusive rocks associated with copper-gold porphyry deposits in the Canadian Cordillera; *in* Porphyry Deposits of the Northwestern Cordillera of North America, Schroeter, T.G., Editor, *Canadian Institute of Mining, Metallurgy and Petroleum*, Special Volume 46, pages 142-158.

Mortimer, N. (1987): The Nicola Group: Late Triassic and Early Jurassic subduction-related volcanism in British Columbia; *Canadian Journal of Earth Sciences*, Volume 24, pages 2521-2536.

Nelson, J.L. and Bellefontaine, K.A. (1996): The geology and mineral deposits of north-central Quesnellia; Tezzeron Lake to Discovery Creek, central British Columbia; *British Columbia Ministry of Employment and Investment*, Bulletin 99, 112 pages.

Ney, C.S. (1972): Kennco Explorations, (Western) Limited report on geochemical, geological and geophysical surveys, Orange Group and Red Group; *British Columbia Ministry of Mines and Petroleum Resources*, Assessment Report 3765, 8 pages.

Panteleyev, A., Bailey, D.G., Bloodgood, M.A. and Hancock, K.D. (1996): Geology and mineral deposits of the Quesnel River - Horsefly map area, central Quesnel Trough, British Columbia; *British Columbia Ministry of Employment and Investment*, Bulletin 97, 155 pages.

Parrish, R.R. and Monger, J.W.H. (1992): New U-Pb dates from southwestern British Columbia; *in* Radiogenic Age and Isotopic Studies: Report 5; *Geological Survey of Canada*, Paper 91-2, pages 87-108.

Paulen, R.C., Bobrowsky, P.T., Lett, R.E., Jackaman, W., Bichler, A.J. and Wingerter, C. (2000): Till geochemistry of the Chu Chua - Clearwater area, B.C. (parts of NTS 92P/8 and 92P/9); *British Columbia Ministry of Energy and Mines*, Open File 2000-17, 233 pages.

Preto, V.A.G. (1970): Geology of the area between Eakin Creek and Windy Mountain; *in* Geology, Exploration and Mining in British Columbia, *British Columbia Department of Mines and Petroleum Resources*, pages 307-312.

Preto, V.A. (1977); The Nicola Group: Mesozoic volcanism related to rifting in southern British Columbia; *in* Volcanic regimes in Canada, edited by W.R.A. Baragar, L.C. Coleman and J.M. Hall, *The Geological Association of Canada*, Special Paper 16, pages 39-57.

Preto, V.A. (1979): Geology of the Nicola Group between Merritt and Princeton; *British Columbia Ministry of Energy, Mines and Petroleum Resources*, Bulletin 69, 90 pages.

Ray, G.E. and Dawson, G.L. (1994): The geology and mineral deposits of the Hedley gold skarn district, southern British Columbia; *British Columbia Ministry of Energy, Mines and Petroleum Resources*, Bulletin 87, 156 pages.

Ray, G.E. and Webster, I.C.L. (2000): The Heff prospect at Heffley Lake, south-central B.C. (092INE 096): An unusual example of a mafic-ultramafic-related Cu-Au-REE-bearing magnetite skarn; *in* Geological Fieldwork 1999, *British Columbia Ministry of Energy and Mines*, Paper 2000-1, pages 273-286.

Read, P.B. and Okulitch, A.V. (1977): The Triassic unconformity of south-central British Columbia; *Canadian Journal of Earth Sciences*, Volume 14, pages 606-638.

Rees, C.J. (1987): The Intermontane-Omineca belt boundary in the Quesnel Lake area, east-central British Columbia: tectonic implications based on geology, structure and paleomagnetism; unpublished Ph.D. thesis, *Carleton University*, 421 pages.

Roback, R.C., Sevigny, J.H. and Walker, N.W. (1994): Tectonic setting of the Slide Mountain terrane, southern British Columbia; *Tectonics*, Volume 13, pages 1242-1258.

Roback, R.C. and Walker, N.W. (1995): Provenance, detrital zircon U-Pb geochronometry, and tectonic significance of Permian to Lower Triassic sandstone in southeastern Quenellia, British Columbia and Washington; *Geological Society of America*, Bulletin, Volume 107, pages 665-675.

Schau, M.P. (1970): Stratigraphy and structure of the type area of the Upper Triassic Nicola Group in south-central British Columbia; *in* Structure of the southern Canadian Cordillera, edited by J.O. Wheeler, The Geological Association of Canada, Special Paper 6, pages 123-135.

Schiarizza, P. (1983): Geology of the Barriere River-Clearwater area; *British Columbia Ministry of Energy, Mines and Petroleum Resources*, Preliminary Map 53.

Schiarizza, P. (1989): Structural and stratigraphic relationships between the Fennell Formation and Eagle Bay Assemblage, western Omineca Belt, south-central British Columbia: Implications for Paleozoic tectonics along the paleocontinental margin of western North America; unpublished M.Sc. thesis, *University of Calgary*, 343 pages.

Schiarizza, P. and Preto, V.A. (1987): Geology of the Adams Plateau-Clearwater-Vavenby area; *British Columbia Ministry of Energy, Mines and Petroleum Resources*, Paper 1987-2, 88 pages.

Schiarizza, P. and Israel, S. (2001): Geology and mineral occurrences of the Nehalliston Plateau, south-central British Columbia (92P/7, 8, 9, 10); *in* Geological Fieldwork 2000, *British Columbia Ministry of Energy and Mines*, Paper 2001-1, pages 1-30.

Smith, R.B. (1979): Geology of the Harper Ranch Group (Carboniferous-Permian) and Nicola Group (Upper Triassic) northeast of Kamloops, British Columbia; unpublished M.Sc. thesis, *The University of British Columbia*, 211 pages.

Travers, W.B. (1978): Overturned Nicola and Ashcroft strata and their relations to the Cache Creek Group, southwestern Intermontane Belt, British Columbia; *Canadian Journal of Earth Sciences*, Volume 15, pages 99-116.

Uglow, W.L. (1922): Geology of the North Thompson Valley map area, British Columbia; *in* Summary Report, 1921, Part A, *Geological Survey of Canada*, pages 72A-106A.

Walker, J.F. (1931): Clearwater River and Foghorn Creek map-area, Kamloops District, British Columbia; *in* Summary Report, 1930, Part A, *Geological Survey of Canada*, pages 125A-153A.

Wanless, R.K., Stevens, R.D., Lachance, G.R. and Edmonds, C.M. (1967): Age determinations and geological studies: K-Ar isotopic ages, Report 7; *Geological Survey of Canada*, Paper 66-17.

Wares, R. and MacDonald, A.L.J. (1972): Geological, geochemical and geophysical report on the Ellen-Gizelle claims, 92P/10E; *British Columbia Department of Mines and Petroleum Resources*, Assessment Report 4365, 21 pages.

Wells, R.C. (2000): Soil geochemical and prospecting report for the Worldstock copper-gold target; *British Columbia Ministry of Energy and Mines*, Assessment Report 26 180.

Wheeler, J.O. and McFeely, P. (1991): Tectonic Assemblage map of the Canadian Cordillera and adjacent parts of the United States of America; *Geological Survey of Canada*, Map 1712A, 1:2 000 000-scale.

Whiteaker, R.J. (1996): The geology, geochronology and mineralization of the Ann property: An Early Jurassic alkalic porphyry system near Lac La Hache, B.C.; unpublished B.Sc. thesis, *The University of British Columbia*, 65 pages.

Wilson, M.V.H. (1977): Paleoecology of Eocene lacustrine varves at Horsefly, British Columbia; *Canadian Journal of Earth Sciences*, Volume 14, pages 953-962.

U-Pb Zircon and Titanite Dating of Intrusive Rocks in the Heffley Lake Area, South-Central British Columbia

By Richard Friedman[1], Gerry Ray[2] and Ian Webster[2]

KEYWORDS: *U-Pb geochronology, radiometric ages, zircons, titanite, Heffley Creek Pluton, megacrystic syenite, Heff prospect, Fe oxide, Cu-Au, skarn, Nicola Group, Harper Ranch Group.*

INTRODUCTION

This paper presents new U-Pb data and interpreted magmatic ages for two intrusions in the Heffley Lake area. The oldest of these, the mafic-ultramafic Heffley Creek Pluton (Ray and Webster, 2000a and b) is a pre or syntectonic intrusion related to a swarm of altered dikes and the Fe oxide-Cu-Au Heff skarn (BC MINFILE 092INE096). The other intrusion is part of a younger suite of feldspar megacrystic alkalic intrusions of syenitic to quartz monzodiorite composition that post-date the main tectonic event. These new radiometric ages are significant in dating the structural, plutonic and mineralizing history of the Heffley Lake area.

LOCATION AND GENERAL GEOLOGY

INTRODUCTION

The Heffley Lake area lies within the Intermontane Belt approximately 26 km northeast of Kamloops. Metasedimentary rocks of the Quesnel Terrane and younger intrusive rocks dominate the area (Figure 1). The area includes the west-northwest trending contact between Late Triassic Nicola Group calcareous sediments and tuffs to the north, and Paleozoic sediments and volcaniclastics of the Harper Ranch Group to the south (Figures 1 and 2). The contact between these two groups has been intruded by the Heffley Creek Pluton (Figures 1 and 2; Ray and Webster, 2000a and b), an elongate, large (> 13 km^2) body which includes magnetite-rich ultramafic pyroxenites, mafic gabbros and diorites, and more felsic marginal phases. The Nicola Group limestones adjacent to the northern margin of the pluton contain some magnetite-Cu-Au-bearing skarns that make up the Heff prospect (also known as the Iron Range, Hal or Mesabi claims). These skarns are spatially associated with a swarm of deformed, highly altered dioritic dikes and sills related to the nearby Heffley Creek Pluton (Figure 3; Ray and Webster, 2000a).

Small bodies of feldspar megacrystic syenitic rocks intrude the Harper Ranch Group, south of Heffley Lake, and are probably part of the Mount Fleet Complex farther south (Figure 1; Kwak, 1964; Webster and Ray, 2001).

STRATIFIED ROCKS

The stratified rocks in this area were originally mapped as Cache Creek Group (Cockfield, 1944, 1947), but subsequently Monger and McMillan (1989) included them in the Quesnel Terrane. Recent mapping (Ray and Webster, 2000a and b) and microfossil identification (M.J. Orchard, personal communication, 2000) suggest they can be separated into northern and southern packages that belong to the Nicola and Harper Ranch groups, respectively (Figure 2). The rocks in both groups comprise mainly steeply dipping, northwest-striking argillites and calcareous siltstones with lesser andesitic ash and lapilli tuff and some limestone. These were intruded by the Heffley Creek Pluton, probably during a period of folding and lower to sub-greenschist facies metamorphism that produced slatey and phyllitic fabrics. Immediately northeast of the pluton, the Late Triassic Nicola Group limestones and a swarm of altered dioritic dikes host the Heff magnetite-bearing garnet-pyroxene Cu-Au skarns (Figure 2 and 3).

The Harper Ranch rocks south of the Heffley Creek Pluton include units of crinoidal limestones containing Carboniferous-Permian age microfossils (Figure 2; M.J. Orchard, personal communication, 2000). Adjacent to the pluton these carbonates are bleached and recrystallized to marble but, unlike the Nicola Group limestones farther north, skarns are not present. The Heffley lakes obscure the northwest-trending contact between the Nicola and Harper Ranch groups but the contact continues southeastwards along Armour Creek (Figure 2). This stratigraphic contact was intruded by the Heffley Creek Pluton and has subsequently been the locus of brittle movement along the Armour Creek Fault (Figure 2).

[1]*The University of British Columbia*
[2]*British Columbia Ministry of Energy and Mines*

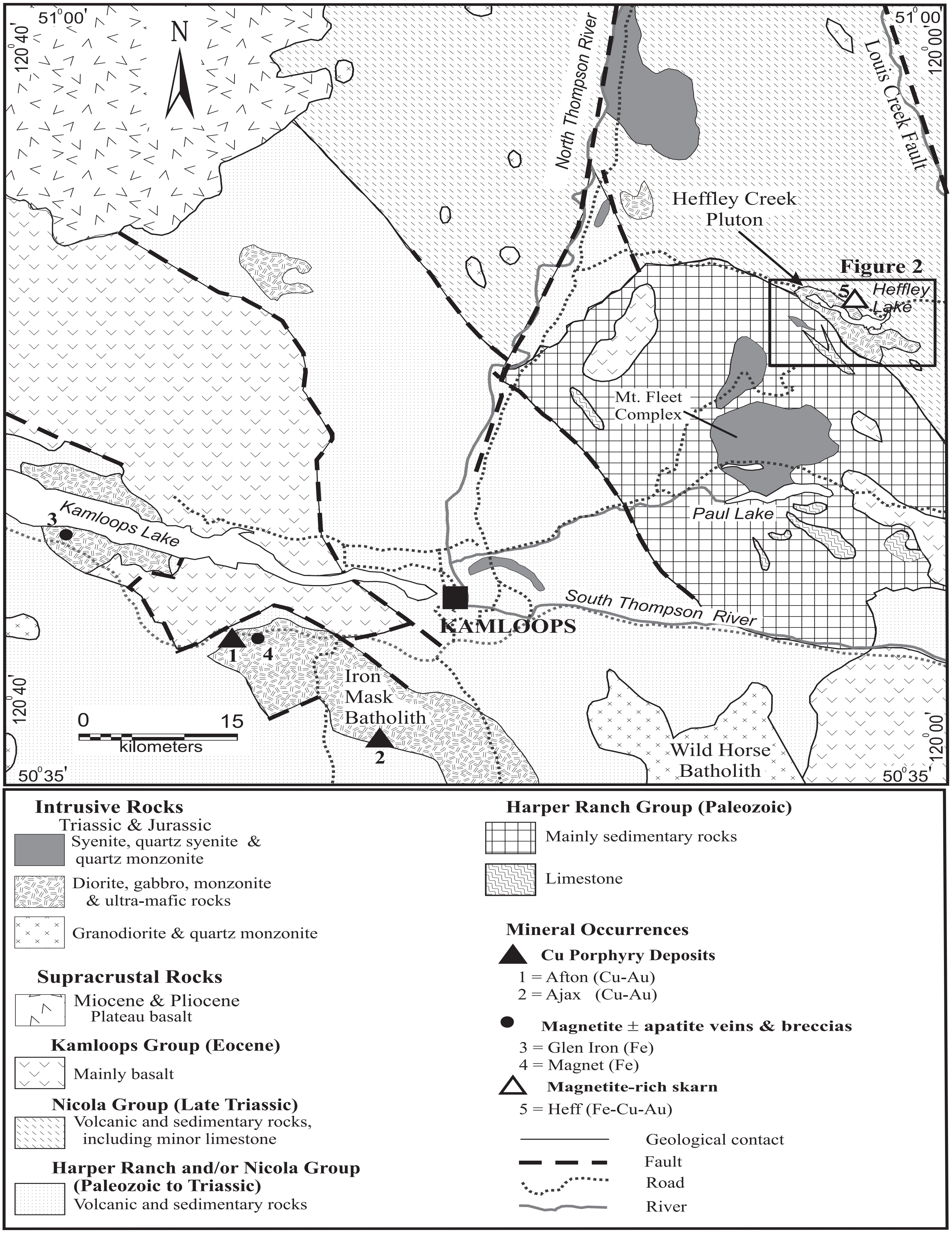

Figure 1. Regional geology and mineral occurrences in the Kamloops-Heffley Lake dis

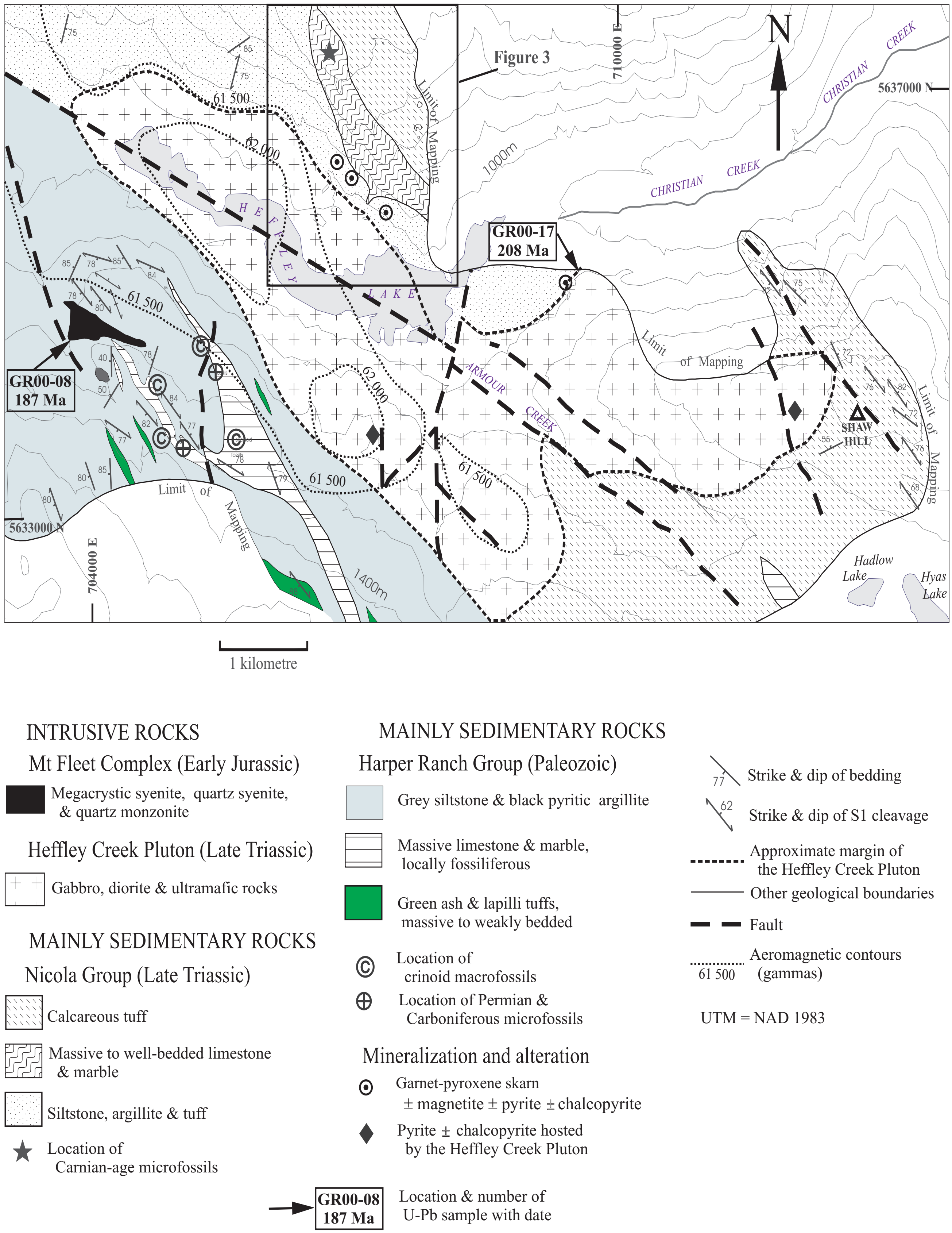

Figure 2. Geology of the Heffley Lake area showing location of the microfossil and U-Pb zircon samples. Geology after Ray and Webster (2000a and b).

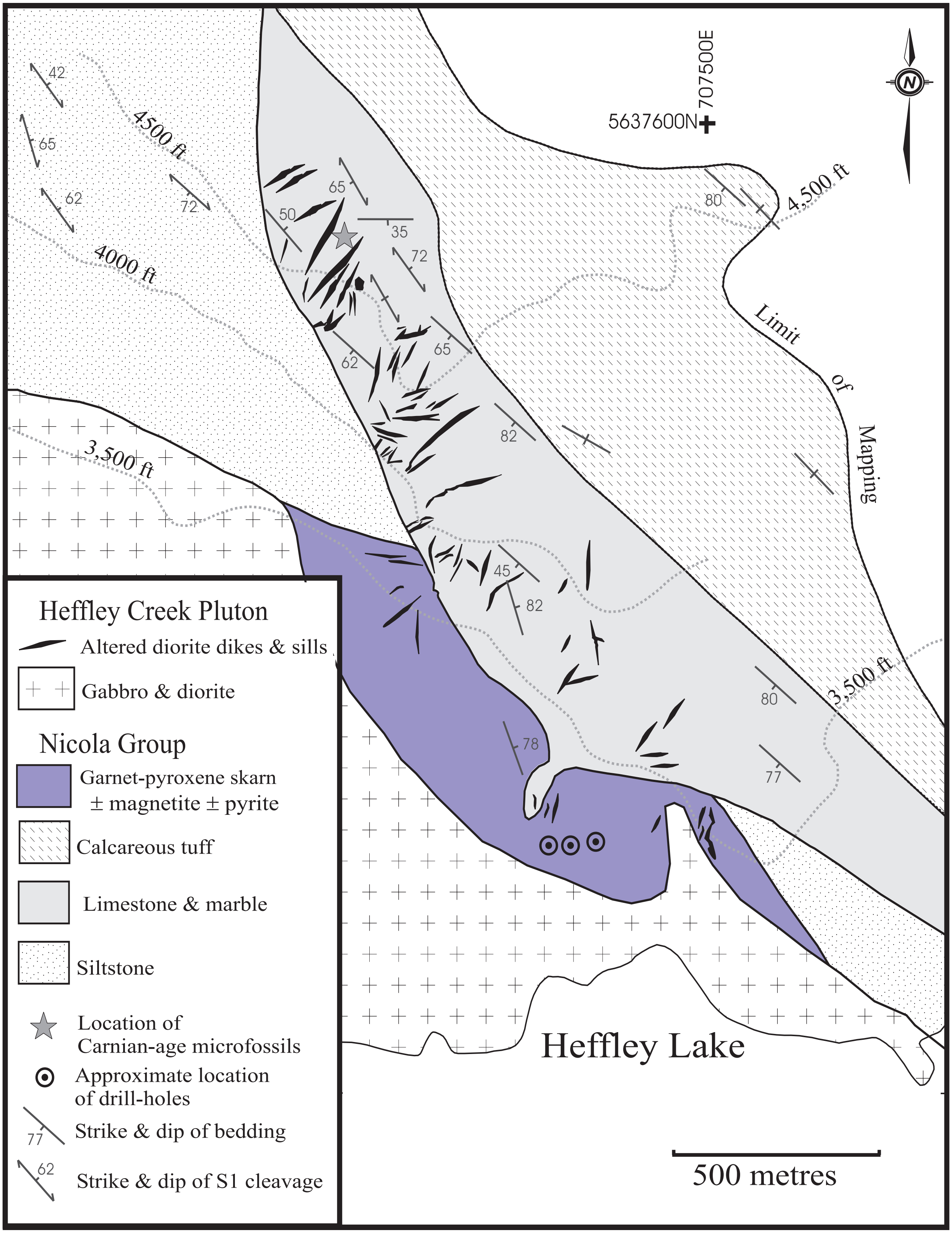

Figure 3. Geology of the Heff Fe-Cu-Au skarn, south-central British Columbia. After Casselman (1980), Arseneau (1997) and Ray and Webster (2000a and b).

INTRUSIVE ROCKS

Introduction

Two intrusive phases are recognized. The oldest and largest of these is the Heffley Creek Pluton and its marginal dike-sill swarm (Figure 2 and 3). This phase either predates or was coeval with the district-wide folding, and was affected subsequently by younger brittle movement along the Armour Creek Fault (Figure 2).

A younger generation of intrusions post-dates the folding but have undergone late brittle faulting. This phase resulted in several minor bodies of distinctive feldspar megacrystic syenitic intrusions, the largest of which outcrops 2 km southwest of Heffley Lake (Figure 2).

Heffley Creek Pluton and its Related Dike-Sill Swarm

The elongate Heffley Creek Pluton is traceable over a 13 km^2 area from Heffley Lake eastwards to Shaw Hill (Figure 2). The pluton, which intrudes the Nicola and Harper Ranch groups, includes early ultramafic rocks and younger gabbros and diorites. In addition, the swarm of sills and dikes on the Heff skarn property, north of Heffley Lake, is probably related to the pluton.

The ultramafic rocks, including pyroxenites and hornblendites, occupy the central parts of the pluton. They are dark, coarse grained (up to 0.5 cm) massive rocks that commonly contain up to 2 % disseminated pyrite and up to 10 % disseminated magnetite. The latter mineral gives rise to a 6 km-long magnetic anomaly as outlined by a government aeromagnetic survey (Map 4411G) (Figure 2).

Feldspar Megacrystic Syenitic Intrusions

These minor, <3 metre-thick dikes and sills are widely scattered throughout the area and they intrude both the Nicola and Harper Ranch groups. Southwest of Heffley Lake, however, larger bodies up to 300 m wide and 1 km in strike length occur (Figure 2). These syenitic rocks are believed to be a northern extension of the Mount Fleet Alkaline Complex, which intrudes Harper Ranch Group rocks farther south (Figure 1). The complex includes large subcircular bodies of quartz monzonite and megacrystic syenite as well as smaller bodies of garnetiferous and mafic shonkonite (Kwak, 1964). The Mount Fleet Complex has been identified as a potential host for platinum-group-element (PGE) mineralization (Webster and Ray, 2001).

The syenites in the Heffley Lake area form leucocratic, buff coloured rocks that contain up to 7 % remnant mafic amphibole and biotite, both of which are extensively chloritized, as well as trace to minor amounts of glassy quartz. The syenites are characterized by abundant (up to 30 %), elongate, euhedral to subhedral megacrystic feldspar laths which are generally between 2 and 4 cm long, although locally crystals exceed 15 cm. Some of these pale brown phenocrysts have thin, light coloured margins and are partially resorbed. Many crystals show a pronounced parallel orientation due to igneous flow. Where intrusive-country-rock contacts are exposed, no chilled margins are detectable, although thin (<0.5 m wide) zones of silicification and hornfels occur adjacent to some dikes. In areas of faulting, many syenitic outcrops are cut by sets of parallel, tension-filled white quartz veins up to 1 cm thick.

STRUCTURE

One episode of major folding is recognized (F1), which overprints both the Nicola and Harper Ranch rocks. This resulted in the moderately to steeply dipping beds and a southeast-trending axial planar slatey cleavage (S1). Very few minor F1 folds have been identified, but bedding-cleavage intersections in the Nicola Group limestones north of Heffley Lake reveal the presence of several tight synforms and antiforms.

During the F1 episode, limestones throughout the area underwent ductile deformation. The Heffley Creek Pluton generally lacks any S1 tectonic cleavage, although it occurs locally along the pluton margins. Many dikes on the Heff property were disrupted by boudinage and brittle extension, and some are folded and cut by the S1 slatey cleavage. Stereo plots of bedding and S1 cleavage measurements indicate that the tight F1 folds have subhorizontal to gently south-easterly plunging axes and their axial planes are southeast-striking and steeply northeast-dipping (Ray and Webster, 2000b). Most of the altered sills and dikes on the Heff property strike northeasterly (Figure 3) and are structurally controlled by a-c fractures developed during the F1 folding. The folding of some sills and dikes together with their a-c joint control is strong supportive evidence that both the intrusions and the skarns were coeval with the F1 deformation.

CHEMISTRY OF THE INTRUSIVE ROCKS

Figure 4 includes chemical plots of analytical data (Ray and Webster, 2000a and b) for the main body of the Heffley Creek Pluton, its related dike swarm, and the younger megacrystic syenites. All are metaluminous and representative of volcanic-arc granitoids, as defined by Pearce *et al*., 1984 (Figures 4F and G). The syenitic suite is alkalic (Figures 4A, D and E) and ranges in composition from syenite to quartz-monzodiorite. The gabbroic and dioritic samples from the main part of the Heffley Creek Pluton range from felsic quartz diorite to mafic gabbro-diorite, and their total alkali-silica content indicates a weak alkalic affinity (Figures 4A, D and E).

MINERALIZATION

The following two types of mineralization are identified in the Heffley Lake area, both of which are associated with the Heffley Creek Pluton (Ray and Webster, 2000a and b; Webster and Ray, 2001):

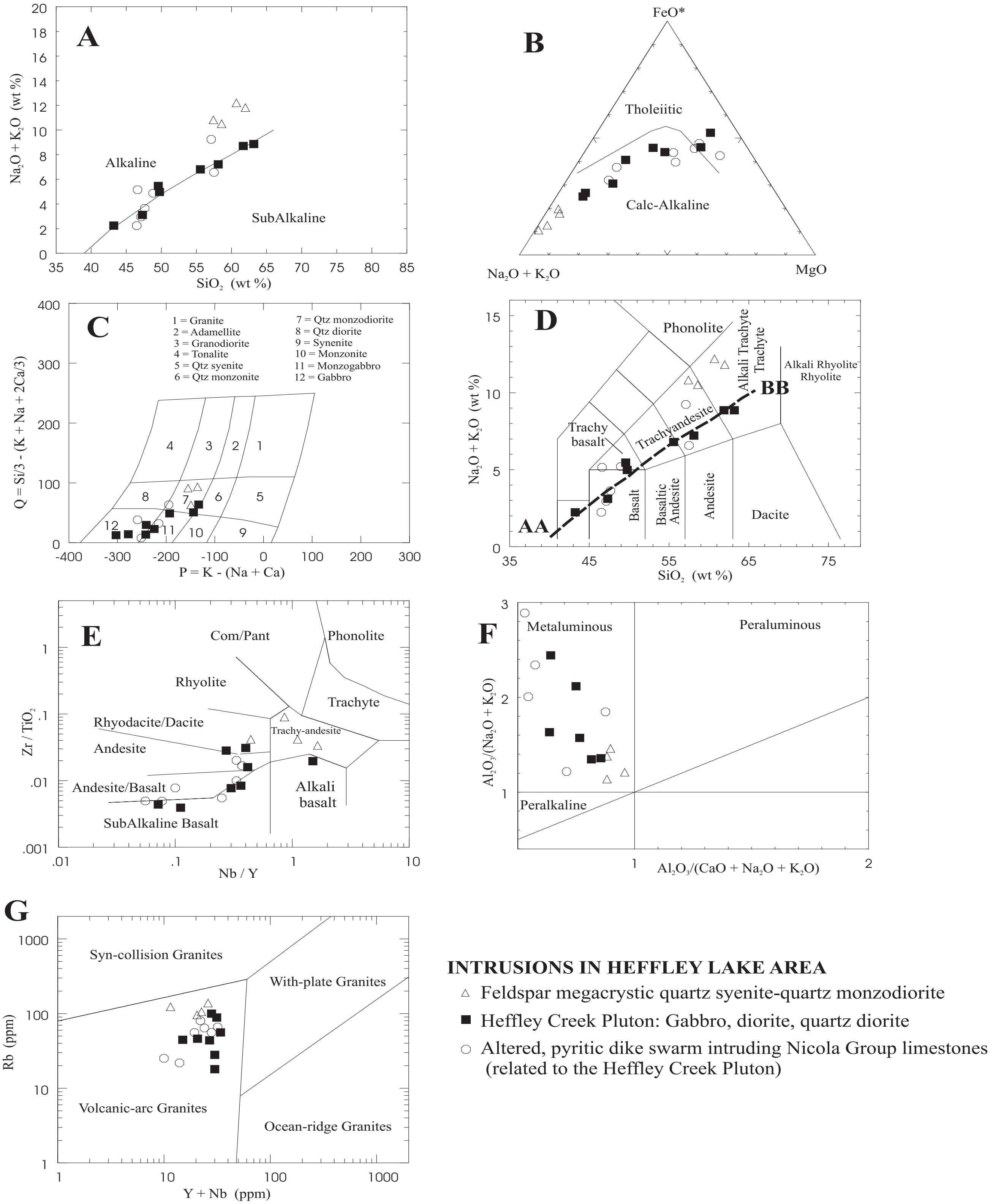

Figure 4. Major and trace element plots of the intrusive rocks, Heffley Lake area (data from Ray and Webster, 2000a and b).
A&B: Alkali-silica and AFM plot (after Irvine and Baragar 1971).
C: Q - P plot (after Debon and Le Fort, 1983).
D: Alkali versus silica plot (after Le Maitre *et al*., 1989). Line AA-BB represent alkaline-subalkaline line in Figure 4A.
E: Zr/TiO2 versus Nb/Y discrimination plot (after Winchester & Floyd, 1977).
F: Aluminum saturation plot (after Maniar and Piccolli, 1989).
G: Log Rb versus Log Y+Nb tectonic discrimination plot (after Pearce *et al*., 1984).

1. Magnetite-rich chalcopyrite ± Au ± REE garnet-pyroxene skarns as seen at the Heff prospect, and
2. Disseminations and veins of chalcopyrite ± magnetite-pyrite mineralization, possibly representing porphyry Cu-style mineralization as hosted by the Heffley Creek Pluton (Figure 2).

In addition, both the Heffley Creek Pluton and the younger megacrystic syenitic have a potential for hosting sulphide-rich PGE mineralization, similar to that identified in other alkalic complexes (Nixon *et al*., 2001).

U-Pb GEOCHRONOLOGY

Zircons for U-Pb dating were extracted from two samples collected from the Heffley Creek Pluton and a smaller syenitic body in the Heffley Lake area. Sample locations are shown in Figure 2 and listed in Table 1. The Heffley Creek Pluton material (GR00-17) is a leucocratic quartz diorite taken from the margin of the intrusion, while the other (sample GR00-08) is a megacrystic quartz-bearing syenite. The U-Pb data are presented in Table 1 and plotted at the 2 sigma level of uncertainty on standard concordia diagrams (Figure 5A, 5B). U-Pb analytical techniques at The University of British Columbia, Geochronology Laboratory, where all work was carried out, are given in Friedman *et al*. (2001).

The Heffley Creek Pluton sample (GR00-17) yielded good quality, clear, euhedral prismatic zircons and clear, pale yellow euhedral titanites. U-Pb results for four multi-grain zircon fractions and three multigrain titanite fractions are plotted on Figure 5A. Zircon and titanite data define a linear array interpreted as a Pb-loss chord; there is no indication of inherited components in any of the analyses. An interpreted age of 208.1 ± 6.1 Ma is based on the weighted mean of $^{207}Pb/^{206}Pb$ dates for all of the analyses, but is strongly controlled by relatively precise zircon data.

The syenite sample (GR00-08) yielded abundant clear, pale to vivid pink, euhedral, equant zircons. Many grains were broken or had a high density of cracks. Faint igneous zoning was observed in some grains but no cores were seen. The coarsest (>149 micrometres), unbroken, crack-free grains with the palest colour and highest clarity were selected for analysis. These were then strongly air abraded so that an estimated 15-25 volume percent of the outer portions of grains were removed. The abraded grains were divided into five multigrain fractions, consisting of five to eleven grains or pieces of grains in each (Table 1).

All analysed fractions give discordant results with $^{207}Pb/^{206}Pb$ dates of ~184-189 Ma (Table 1; Fig. 5B). Discordance is attributed to Pb loss in these very high uranium-bearing zircons (~1500-2000 ppm). An age estimate of 186.9 ± 1.7 Ma for the crystallization of this syenite is based on the weighted mean of $^{207}Pb/^{206}Pb$ dates for the five analysed fractions.

SUMMARY AND CONCLUSIONS

These new U-Pb zircon dates are important because they reveal the timing of the deformation, plutonism and skarn mineralization in the Heffley Lake area. They are interpreted as follows:

1. The 208 Ma (Late Triassic) age for the Heffley Creek Pluton (sample GR00-17) is believed to date both the emplacement of the pluton and the subsequent development of the Heff Fe-Cu-Au skarn mineralization.
2. The intrusion of the megacrystic syenite took place circa 187 Ma during the Early Jurassic. This probably also dates the emplacement of the Mount Fleet Alkalic Complex farther south (Figure 1).
3. Field evidence indicates that the Heffley Creek Pluton is likely a syntectonic intrusion while the younger syenites are post-tectonic. This suggests that the deformation in this district took place circa 208 Ma and was terminated by 187 Ma. The deformation that affected the Heffley Creek Pluton and its country rocks is probably related to the docking of Quesnellia with Ancestral North America.
4. The Heffley Creek Pluton and the megacrystic syenites are separated by a 20 million year time interval which strongly suggests the two suites are unrelated.
5. Chemical analyses provide evidence that the Heffley Creek Pluton has alkalic affinities. This and its Late Triassic age closely resemble the Iron Mask Batholith (Preto *et al*., 1979; Kwong, 1987) southwest of Kamloops (Figure 1). The batholith hosts the Afton and Ajax porphyry copper deposits (Carr and Reed, 1976; Ross *et al*., 1995) and, like the Heffley Creek Pluton, is associated with magnetite-apatite-bearing mineralization at the Glen Iron and Magnet occurrences (Figure 1; Cann and Godwin, 1983; Hancock, 1988). This implies that the Heffley Creek Pluton and any satellite bodies warrant prospecting as a porphyry copper target.

ACKNOWLEDGMENTS

The ideas and scientific opinions of the following persons were helpful to this program: D.A. Brown, M.S. Cathro, D.V. Lefebure, R.H. McMillan, G.T. Nixon, and V.A.G. Preto.

REFERENCES

Arseneau, G.J. (1997): Geological, geochemical and geophysical report on the 1997 field work, Mesabi property; submitted by Echo Bay Mines, October 1997, *B.C. Ministry of Energy, Mines and Petroleum Resources*, Assessment Report 25203, 79 pages.

Cann, R.M., and Godwin, C.I. (1983): Genesis of magmatic magnetite-apatite lodes, Iron Mask Batholith, south central British Columbia (92I); Geological Fieldwork 1982, *B.C. Ministry of Energy, Mines and Petroleum Resources*, Paper 1983-1, pages 267-284.

TABLE1

U-Pb ANALYTICAL DATA FOR INTRUSIVE ROCKS FROM THE HEFFLEY LAKE AREA

Fraction[1]	Wt (µg)	U^2 (ppm)	Pb^{*3} (ppm)	$^{206}Pb^4/^{204}Pb$	Pb^5 (pg)	$^{208}Pb^3$ (%)	Isotopic ratios (1 sigma, %)[6] $^{206}Pb/^{238}U$	$^{207}Pb/^{235}U$	$^{207}Pb/^{206}Pb$	Apparent ages (2 sigma, Ma)[6] $^{206}Pb/^{238}U$	$^{207}Pb/^{235}U$	$^{207}Pb/^{206}Pb$
GR00-17 hornblende quartz diorite, Heffley Creek Pluton; UTM: zone 10, E 709570, N 5635364, NAD83; interpreted age: 208.1 ± 6.1 Ma												
A c,cl,pp,b,2	17	1198	42	3843	10	25	0.02909 (0.12)	0.2016 (0.24)	0.05028 (0.18)	184.8 (0.6)	186.5 (0.8)	207.9 (8.4)
B c,cl,pp,p,b,6	21	930	31	3795	9	21	0.02899 (0.12)	0.2009 (0.30)	0.05026 (0.24)	184.2 (0.4)	185.9 (1.0)	207 (11)
D f,cl,vp,p,b,14	14	721	24	1579	12	21	0.02922 (0.12)	0.2029 (0.59)	0.05035 (0.55)	185.7 (0.4)	187.5 (2.0)	211 (25/26)
F ff,cl,pp,b,50	13	739	24	1617	10	22	0.02760 (0.16)	0.1916 (0.67)	0.05035 (0.63)	175.5 (0.6)	178.0 (2.2)	211 (29/30)
T1 cc,y,py,cl	527	61	3.1	139	472	48	0.02880 (0.45)	0.1988 (1.5)	0.05005 (1.3)	183.0 (1.6)	184.1 (5.2)	197 (58/60)
T2 cc,y,py,cl	479	130	3.8	114	1190	7.3	0.02995 (0.57)	0.2091 (1.9)	0.05064 (1.5)	190.3 (2.1)	192.8 (6.6)	224 (70/73)
T3 cc,y,py,cl	409	273	7.9	100	2550	4.7	0.03057 (0.68)	0.2131 (2.2)	0.05057 (1.8)	194.1 (2.6)	196.2 (7.9)	221 (82/86)
GR00-08 megacrystic syenitic body; UTM: zone 10, E 703982, N 5634867, NAD83; interpreted age: 186.9 ± 1.7 Ma												
A cc,cl,pp,b,5	40	1494	46	20598	5	19	0.02748 (0.09)	0.1888 (0.16)	0.04984 (0.08)	174.8 (0.3)	175.6 (0.5)	187.7 (3.9)
B cc,cl,pp,b,11	40	1679	54	24058	4	23	0.02733 (0.09)	0.1877 (0.16)	0.04981 (0.08)	173.8 (0.3)	174.7 (0.5)	186.3 (3.8)
C cc,cl,pp,b,5	40	2059	68	28543	7	27	0.02665 (0.12)	0.1830 (0.18)	0.04982 (0.08)	169.5 (0.4)	170.7 (0.6)	186.4 (3.7)
D cc,cl,pp,b,6	74	1676	53	21798	10	23	0.02727 (0.11)	0.1871 (0.17)	0.04975 (0.08)	173.4 (0.4)	174.1 (0.5)	183.5 (3.8)
E cc,cl,pp,b,5	44	1986	64	15270	10	24	0.02739 (0.11)	0.1883 (0.17)	0.04987 (0.09)	174.2 (0.4)	175.2 (0.6)	188.8 (4.0)

[1] Upper case letter = zircon fraction identifier; T1, T2, etc, for titanites. All zircon fractions air abraded. All titanites unabraded; Grain size, intermediate dimension: cc=>149µm, c=<149µm and >134µm, m=<134µm and >104µm, f=<104µm and >74µm, ff <74µm; Grain character codes: b= broken, cl=clear; eq=equant; p=prismatic; pp=pale pink; py=flattened pyramid; vp=vivid pink; y=pale yellow. Zircons nonmagnetic on Franz magnetic separator at field strength of 1.8A and sideslopes of 1°-2°. Titanites nonmagnetic at 0.6A and 20° sideslope, and magnatic at 1.8A and 5° sideslope. Front slope of 20° for all.

[2] U blank correction of 1pg ± 20%; U fractionation corrections were measured for each run with a double ^{233}U-^{235}U spike (about 0.004/amu).

[3] Radiogenic Pb

[4] Measured ratio corrected for spike and Pb fractionation of 0.0037/amu ± 20% (Daly collector), which was determined by repeated analysis of NBS Pb 981 standard throughout the course of this study.

[5] Total common Pb in analysis based on blank isotopic composition.

[6] Corrected for blank Pb (2-10 pg, zircon; 20 pg, titanite), U (1 pg, all) and common Pb concentrations based on Stacey and Kramers (1975) model Pb at the age or the $^{207}Pb/^{206}Pb$ age of the rock.

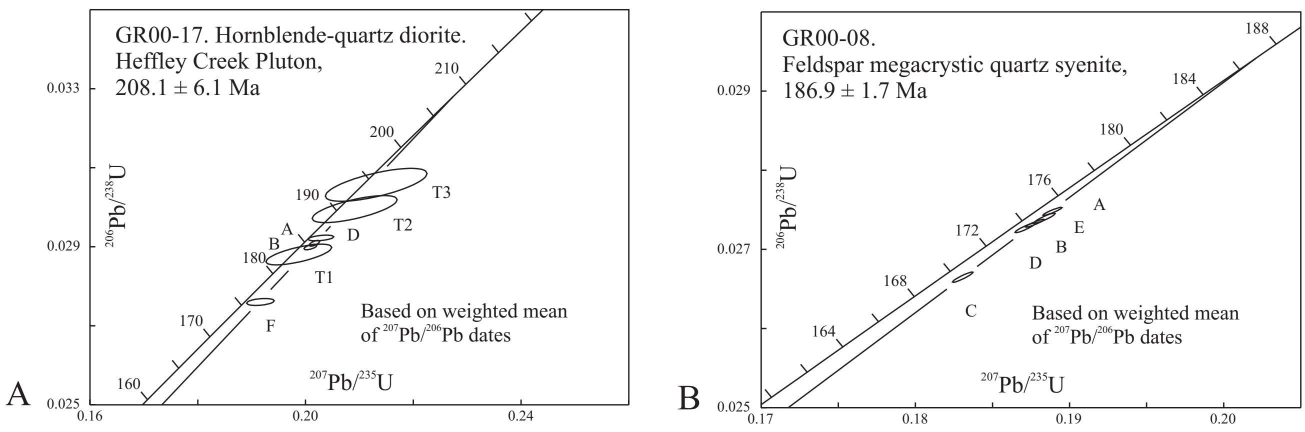

Figure 5. Concordia plots. A. Plot showing 2 sigma error ellipses for zircon fractions A, B, D and F and titanite fractions T1-T3, from quartz diorite of the Heffley Creek Pluton (sample GR00-17). B. Plot showing 2 sigma error ellipses for zircon fractions A-E from a sample of megacrystic syenite (sample GR00-08). *See* text for a discussion of these data.

Carr, J.M., and Reed, A.J. (1976): Afton; *In* Porphyry deposits of the Canadian Cordillera. (A. Sutherland Brown, ed.). *Canadian Institute of Mining and Metallurgy;* Special Volume 15, pages 376-387.

Casselman, M.J. (1980): Assessment report of line-cutting and geological, soil geochemical and magnetometer surveys on the Heff Lake Property; Unpublished report for *Cominco Limited*.

Cockfield, W.E. (1944): Nicola map area, British Columbia, *Geological Survey of Canada*, Paper 44-20. Map with descriptive notes, , Ottawa, 1944.

Cockfield, W.E. (1947): Nicola, Kamloops and Yale districts, British Columbia, *Geological Survey of Canada*, Map 886A, scale 1:253 440.

Debon, F., and Le Fort, P., 1983, A chemical-mineralogical classification of common plutonic rocks and associations: *Royal Society of Edinburgh*, Transactions, Earth Sciences 73 (for 1982), pages 135-149.

Friedman, R.M., Diakow, L.J., Lane R.A. and Mortensen, J.K. (2001): New U-Pb age constraints on latest Cretaceous magmatism and associated mineralization in the Fawnie Range, Nechako Plateau, central British Columbia: Canadian Journal of Earth Sciences, Volume 38, pages 619-637.

Hancock, K.D. (1988): Magnetite occurrences in British Columbia; *B.C. Ministry of Energy, Mines and Petroleum Resources*, Open File 1988-28, 153 pages.

Irvine, T.N., and Baragar, W.R.A. (1971): A guide to the chemical classification of the common volcanic rocks; *Canadian Journal of Earth Sciences*, Volume 8, pages 523-547.

Kwak, T.A.P. (1964): A garnet-bearing syenite near Kamloops, B.C.; unpublished M. Sc. thesis, *University of British Columbia*, 53 pages.

Kwong, Y.T.J. (1987): Evolution of the Iron Mask Batholith and its associated copper mineralization; *B.C. Ministry of Energy, Mines and Petroleum Resources*, Bulletin 77, 55 pages.

Le Maitre, R.W., Bateman, P., Dudek, A., Keller, J., Lameyre, J., Lebas, M.J., Sabine, P.A., Schmid, R., Sorensen, H., Streckeisen, A., Woolley, A.R., and Zanettin, B., Eds., (1989): A classification of igneous rocks and glossary of terms: recommendations of the International Union of Geological Sciences Subcommission on the systematics of igneous rocks, *Oxford Blackwell Scientific Publications*, 193 pages.

Maniar, P.D., and Piccoli, P.M. (989): Tectonic discrimination of granitoids: *Geological Society of America,* Bulletin, Volume 101, pages 635-643.

Monger, J.W.H. and McMillan, W.J. (1989): Geology, Ashcroft, British Columbia*; Geological Survey of Canada,* Map 42-1989, sheet 1, scale 1:250 000.

Nixon, G.T. and Carbno, B. (2001): Whiterocks Mountain Alkaline Complex, south-central British Columbia: geology and platinum-group-element mineralization; *in* Geological Fieldwork 2000, *British Columbia Ministry of Energy and Mine*s, Paper 2001-1, pages 191- 222.

Pearce, J.A., Harris, N.B.W., and Tindle, A.G., 1984, Trace element discrimination diagrams for the tectonic interpretation of granitic rocks: *Journal of Petrology*, Volume 25, pages 956-983.

Preto, V.A., Osatenko, M.J., McMillan, W.J., and Armstrong, R.L. (1979): Isotopic dates and strontium isotopic ratios for plutonic and volcanic rocks in the Quesnel Trough and Nicola Belt, south-central B.C., *Canadian Journal of Earth Science*, Volume 16, pages 1658-1672.

Ray, G.E. and Webster, I.C.L. (2000a): The Heff Prospect at Heffley Lake, South-Central B.C. (091INE096): An Unusual Example of a Mafic-ultramafic-related Cu-Au-REE-Bearing Magnetite Skarn; *in* Geological Fieldwork 1999, *British Columbia Ministry of Energy and Mines,* Paper 2000-1, pages 273-286.

Ray, G.E. and Webster, I.C.L. (2000b): Geology and mineral occurrences in the Heffley Lake Area, south-central B.C.; *B.C. Ministry of Energy and, Mines,* Open File Map 2000-10.

Ross, K.V., Godwin, C.I., Bond, L., and Dawson, K.M. (1995): Geology, alteration and mineralization of the Ajax East and Ajax West copper-gold alkalic porphyry deposits, southern Iron Mask batholith, Kamloops, British Columbia; *In* Porphyry Deposits of the Northwest Cordillera of North America. (T.G. Schroeter, ed.). *Canadian Institute of Mining, Metallurgy and Petroleum.* Special volume 46, pages 565-608.

Sangster, D.F. (1969): The contact metasomatic magnetite deposits of British Columbia; *Geological Survey of Canada,* Bulletin 172, 85 pages.

Stacey, J.S. and Kamers, J.D. (1975): Approximation of terrestrial lead isotopic evolution by a two-stage model; *Earth and Plantetary Science Letters*, Volume 26, page 207-221.

Webster, I.C.L., and Ray, G.E. (2001): The Mount Fleet Alkaline Complex (92I/16): A potential PGE target. *In Exploration and Mining in British Columbia - 2000, B.C. Ministry of Energy and Mines*, pages 71-76.

Winchester, J.A., and Floyd, P.A. (1977): Geological discrimination of different magma series and their differentiation products using immobile elements. *Chemical Geology*, Volume 20, pages 325-343.

Middle Jurassic Stratigraphy Hosting Volcanogenic Massive Sulphide Mineralization in Eastern Bella Coola Map Area (NTS 093/D), Southwest British Columbia

By L.J. Diakow[1], J.B. Mahoney[2], T.G. Gleeson[3], M.G. Hrudey[4], L.C. Struik[5] and A.D. Johnson[2]

KEYWORDS: *Regional Mapping, Bella Coola, Middle Jurassic, Hazelton Group, Volcanogenic Massive Sulphide, Nifty.*

INTRODUCTION

Eastern Bella Coola map area (NTS 93D) is considered highly prospective for metallic minerals because arc volcanic-sedimentary assemblages of both Middle Jurassic and Early Cretaceous age occur in the area. These rocks are potentially correlative with coeval strata known elsewhere to host important volcanogenic massive sulphide deposits, including the Jurassic Eskay Creek deposit to the north and the Early Cretaceous Britannia deposit to the south.

This work is a part of the Bella Coola Targeted Geoscience Initiative (TGI) whose primary objective is to improve understanding of the geology underlying the eastern half of the Bella Coola map area in order to evaluate the potential of arc-related volcano-sedimentary rocks for volcanogenic massive sulphide deposits. An additional goal is to place the geology of the eastern Bella Coola region into a regional context; for example, to evaluate potential linkages between this area and Late Cretaceous and Eocene porphyry belts found in the Whitesail Lake map area (NTS 93E) to the north.

This paper emphasizes results of the Bella Coola TGI related to Middle Jurassic volcano-sedimentary stratigraphy of the Hazelton Group. Regionally, the Middle Jurassic Hazelton Group in Stikinia locally hosts stratabound and stratiform massive sulphides deposited synchronously with submarine silica-bimodal volcanic rocks and sedimentary rocks. Our aim is to examine the internal character of volcanic sequences and contained mineral deposits to improve our understanding of the metallogenesis and history of Mesozoic arc generated magmatism along the western margin of the Stikine terrane in southwest and central British Columbia.

[1] *British Columbia Ministry of Energy and Mines*
[2] *University of Wisconsin*
[3] *Simon Fraser University*
[4] *University of Calgary*
[5] *Geological Survey of Canada*

ACCESS AND PHYSIOGRAPHY

The study area straddles a physiographic transition from mountainous terrain of the Kitimat Ranges in the west, sculpted by numerous active alpine glaciers, eastward to comparatively subdued forested topography of the Chilcotin Plateau. The majority of the Bella Coola area is rugged with steep-sided mountains covered at lower elevation by thick, nearly impenetrable coastal vegetation. Helicopter assistance is essential to gathering geological information efficiently during a relatively narrow window of suitable weather lasting from July into early September.

Highway 22 traverses the study area and provides an all-weather surface to Williams Lake, about 430 kilometres east. Relatively few logging roads extend from the highway up some of the major river valleys. Ground access to the historically most active exploration play in the area, the Nifty property, and a number of other nearby prospects is a challenging endeavor. The first part is via a good logging road that extends northward from the highway up Noosegulch River valley. The road ends at a bridge washout and beyond this point it is an arduous hike across steep talus slopes and through difficult bush to the Nifty property.

PREVIOUS AND PRESENT WORK

Systematic mapping of the Bella Coola map sheet by the Geological Survey of Canada was conducted between 1962 and 1965 as part of the Coast Mountain Project, an umbrella program involving several simultaneous mapping studies that collectively established the geological framework of remote mountainous coastal terrain stretching nearly 700 kilometres from Vancouver to Prince Rupert. This program, completed in the mid-1970s, generated a number of 1:250 000-scale geological maps and accompanying reports, including one for the Bella Coola map area (Baer, 1973). Since completion of the Coast Mountain Project, selected areas between Bella Coola and Prince Rupert have been the subject of more detailed geologic and tectonic analyses (*e.g.* Stowell and McClelland, 2000 and references therein).

The impetus for new bedrock mapping aimed at producing a modern geological map and mineral potential reassessment of the eastern half of Bella Coola map area stems from a number of factors. These include:

1) Existence of tracts of high mineral potential geology identified by reinterpretation of the geology and mineral potential of the Bella Coola area, as part of the British Columbia Mineral Potential Initiative-Mid-Coast Project (Bellefontaine and Alldrick, 1994, 1995);

2) Recognition of the importance and regional potential of Jurassic arc-volcanic rocks as host for significant volcanogenic massive sulphides of the Eskay Creek type (Massey *et al.,* 1999);

3) Recent work focused on the mineral occurrences in the eastern Bella Coola area. (Ray *et al*., 1998) characterized physical and chemical features of the Nifty occurrence, the principal stratiform sulphide occurrence in the region. This work yielded fundamental information useful for comparison to other potential exploration targets.

The Bella Coola Targeted Geoscience Initiative (TGI) is a new, two-year bedrock mapping program. Coordinated by the Geological Survey of Canada, it is implemented by scientists from both the federal and provincial geological surveys and the universities of British Columbia, and Wisconsin - Eau Claire. This program will examine a large region of volcanic strata underlying the eastern Bella Coola map area viewed as the most prospective for volcanic-hosted massive sulphide mineralization. In addition, the probability of southward extensions of Late Cretaceous or Eocene arc-magmatic suites associated with copper-molybdenum porphyry style deposits in the Whitesail Lake and Smithers map areas (Carter, 1981) will be examined. A regional stream sediment survey to quantify metal contents in watersheds of Bella Coola (NTS 93D) and adjoining parts of Laredo Sound (NTS 103A) map sheet is the focus of a joint Canada-Provincial geochemical survey that was conducted simultaneously with the bedrock programs in 2001 (Jackaman *et al.*, 2002; this volume).

In 2001, the Bella Coola TGI involved 1:50 000-scale bedrock mapping, encompassing roughly 2000 square kilometres situated between the Dean to Bella Coola rivers, and between Dean Channel and the boundary of Tweedsmuir Provincial Park. This region was arbitrarily subdivided into contiguous eastern and western study areas (Figure 1). Mapping data was digitally captured during more than 160 traverses in these areas. Geological results from the western study area are presented in a series of thematic geological reports that address Early Cretaceous stratigraphy (Struik *et al*., 2002), plutonic rock suites (Hrudey *et al*., 2002) and structural geology (Mahoney *et al*., 2002). This report focuses on the eastern study area, underlain mainly by Jurassic volcanic and sedimentary rocks that crop out to the east of the broad, deformed belt of Early Cretaceous rocks. We present a preliminary account of the lithological character,

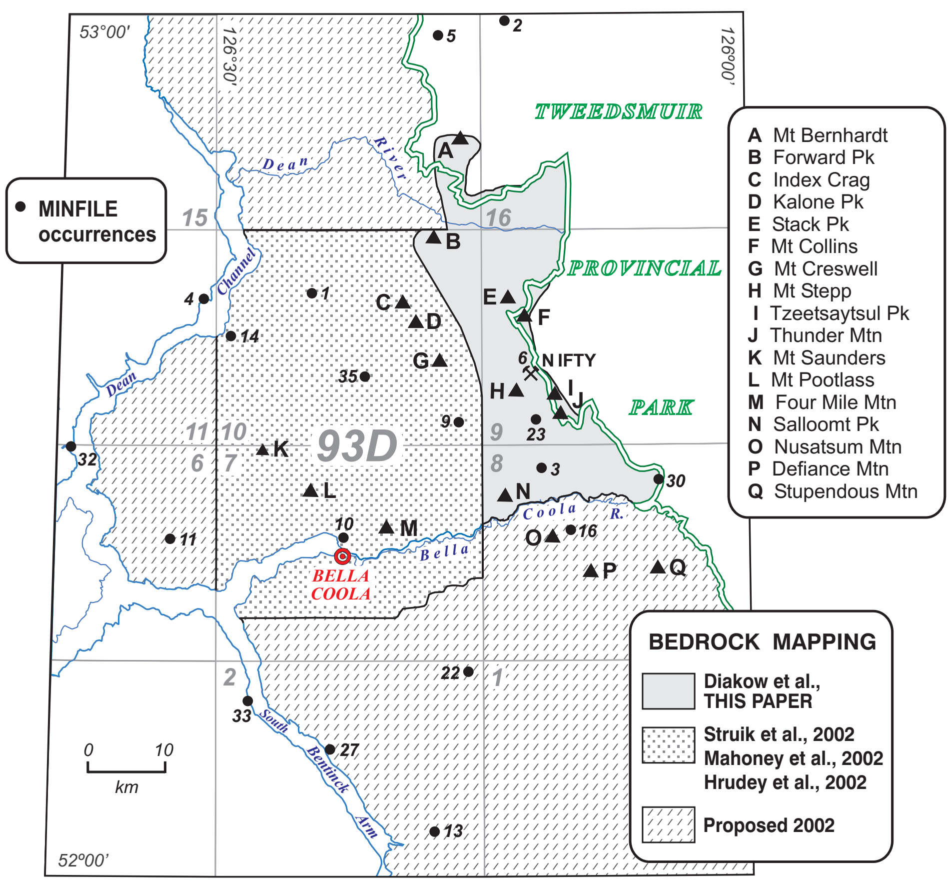

Figure 1. Geographic location map of eastern Bella Coola map area (93D), showing prominent peaks and major drainages. Field mapping during the 2001 field season was concentrated between the Bella Coola and Dean Rivers, in the area east of Dean Channel and west of Tweedsmuir Park. Letters refer to prominent peaks in the area, and dots correspond to MINFILE occurrences. Note location of Nifty prospect.

internal stratigraphic arrangement of various lithofacies and the relative position and setting of known mineral occurrences within this stratigraphy. A supplementary mapping project conducted in southern Tweedsmuir Provincial Park focused on structural and stratigraphic aspects of the Atnarko Complex (Isreal and Kennedy, 2002).

REGIONAL SETTING

The Bella Coola map area (93D) straddles the boundary between the Intermontane and Insular superterranes in west-central British Columbia. Intrusive and metamorphic rocks of the Coast Plutonic Complex dominate the western portion of the region, and separate rocks of Stikinia (Intermontane superterrane) from those of Wrangellia and possibly Alexander Terrane (Insular superterrane; Figure 2 inset). Metamorphic pendants of the Burke Channel Assemblage, a belt of supracrustal rocks exposed along the western margin of Stikinia, are exposed within the Coast Plutonic Complex east of the Coast Shear Zone (Figure 2; Boghossian and Gehrels, 2000). These rocks include quartzite, marble, biotite schist (metapelite) and lesser amphibolite (mafic volcanic rocks) and quartzite-cobble conglomerate. These rocks are lithologically and isotopically similar to continental margin assemblages to the north within the Coast Plutonic Complex (Boghossian and Gehrels, 2000).

At the latitude of Bella Coola, rocks of the Insular superterrane are restricted to the western side of the Coast Mountain Shear Zone (Figure 2). This structure is a 1200-kilometre long, northeast-side-up shear zone active mainly between approximately 65 and 55 Ma (Rusmore *et al*., 2000, and references therein). Andronicos *et al*. (1999) suggest this shear zone is a potentially major translational structure that may have accommodated 1000s of kilometres of displacement.

East of the Coast Mountain Shear Zone, granitic and metamorphic rocks of the Coast Plutonic Complex comprise the western boundary of Jurassic and Cretaceous arc-related volcano-sedimentary sequences spatially associated with a diverse suite(s) of syn- and post volcanic plutons. These two contrasting lithostratigraphic groups are exposed in parallel northwest-trending belts that include from east to west, 1) bimodal volcanic strata and related volcanogenic sedimentary rocks of the Hazelton Group (Baer, 1973); and 2) the informally named Monarch volcanics (van der Heyden, 1990, 1991; Rusmore *et al.*, 2000), a thick succession of Early Cretaceous volcanic and sedimentary rocks. Plutons of probable Jurassic to Tertiary age intrude both belts, but are volumetrically more abundant in the western belt (Baer, 1973).

Although this report focuses on the stratigraphy of the Hazelton Group, a summary of the Monarch volcanics, plutonic assemblages and the structural setting of the adjoining western belt, described in detail in companion papers (Struik *et al*., 2002; Hrudey *et al.*, 2002; Mahoney *et al*., 2002), is presented below.

The informally named Monarch sequence forms a thick succession of andesitic flows, fragmental rocks, volcaniclastic sandstone, tuffs and slates underlying a broad region west of Noosgulch River and Kalone Creek (Struik *et al*., 2002). Olive green dacite to andesite flows and associated tuff breccias dominate the succession, although intercalated sediments form continuous stratigraphic sections up to several hundred metres in thickness. Stratigraphy within this sequence is complicated by abrupt lateral facies changes and structural deformation. The base of the section is exposed in one locality north of Salloomt Peak, where polymictic conglomerate with plutonic and volcanic clasts gradationally overlie a quartz diorite pluton which yields a 134 ± 0.3 Ma U-Pb zircon age (van der Heyden, 1991). The contact between the Monarch volcanics and the Hazelton Group has not been found in the map area.

Probable Jurassic to Tertiary, on average intermediate composition, intrusive rocks form volumetrically significant plutons cutting both the Monarch sequence and the Hazelton Group to the east (Hrudey *et al*., 2002). These plutons range from very fine to medium-grained diorite and microdiorite associated with the Hazelton Group to fine to coarse-grained hornblende and pyroxene-bearing quartz diorite, diorite, granodiorite and gabbro, hornblende and biotite-bearing granodiorite and tonalite, and hornblende-biotite granite. These plutons are generally massive, and magmatic and structural foliations are evident locally. The oldest known intrusive rocks, inferred to be subvolcanic plutons associated with the Middle Jurassic Hazelton Group, consist of diorite and microdiorite that appears to have been intruded prior to deposition of the Early Cretaceous Monarch sequence

Rocks in the eastern Bella Coola map area have been affected by several distinct deformational events recording episodic extensional, contractional, and transpressional tectonism in the region (Mahoney *et al*., 2002; Isreal and Kennedy, 2002). The timing is equivocal; the contractional and transpressional events are relatively well constrained by crosscutting relations, whereas the timing of the extensional events is less clear. The widespread occurrence of north-trending basalt to andesite dikes and dike swarms spatially associated with both the Hazelton Group and the Monarch sequence suggests that east-west extensional events may have been an important factor in arc development during both Middle Jurassic and Early Cretaceous time.

A well developed system of northwest-trending, northeast-vergent folds and subordinate thrust faults is associated with the Monarch sequence in the central portion of the map area. Structures vary from outcrop-scale, close to tight, locally isoclinal, asymmetric to map-scale recumbent shallowly to steeply plunging folds. The northeast-vergent fold system is inferred to be Late Cretaceous based on the age of folded strata and regional correlation with the eastern Waddington thrust belt (Rusmore and Woodsworth, 1994). Although rocks of the Hazelton Group in the eastern Bella Coola map area are tilted and locally openly folded, it is unclear if these structures are the same age as the Cretaceous (?) folds to the west. Hazelton Group may underlie a sub-Lower Cretaceous rock decollement surface, like some of the sub-Monarch volcanic plutonic suites to the west.

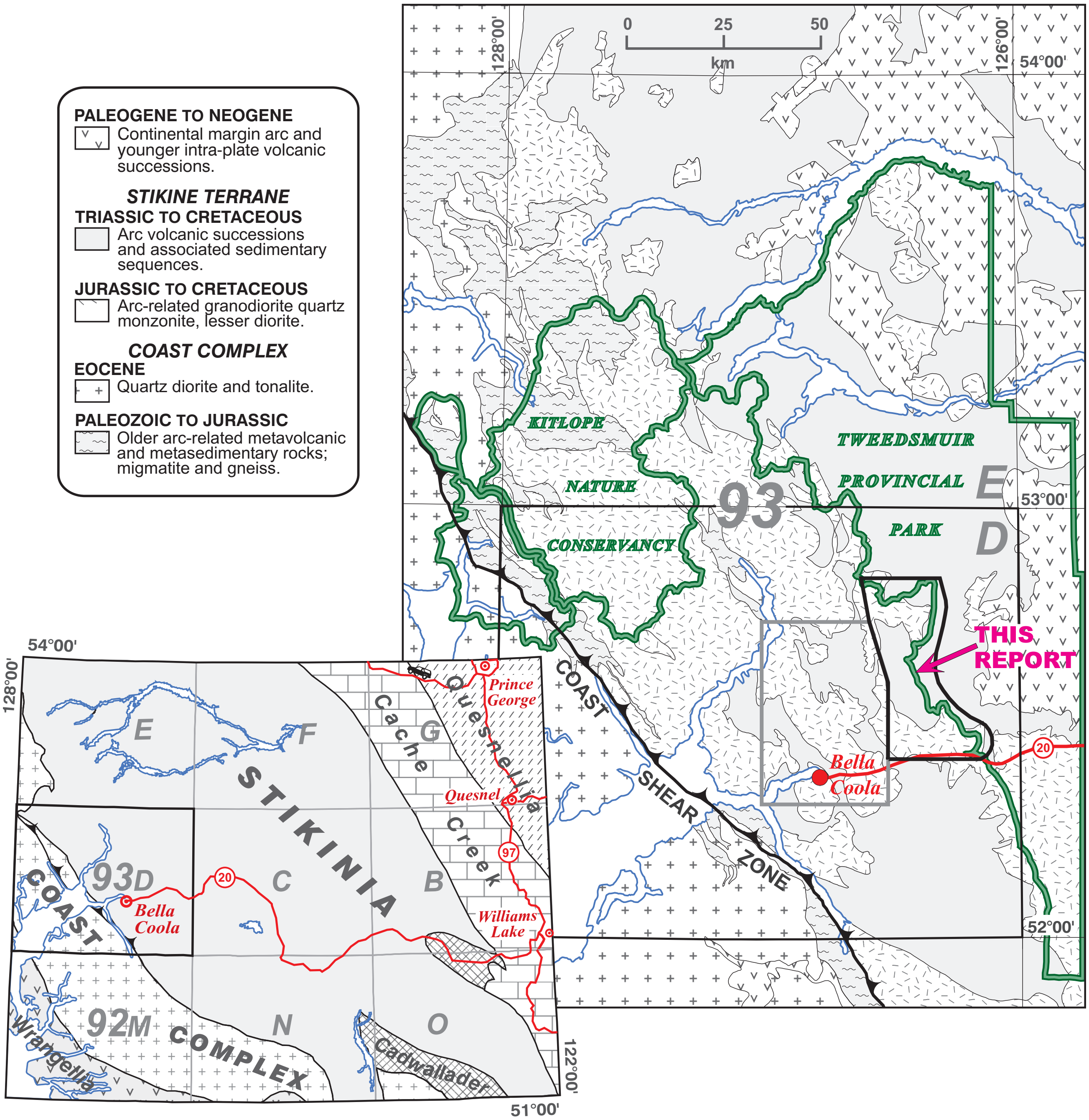

Figure 2. Schematic regional geologic map of Bella Coola (93D) and Whitesail Lake (93E) map areas and adjoining areas. Boxed areas indicate contiguous areas mapped during the 2001 field season. Inset map shows morphogeologic belts and terranes of the west-central Canadian Cordillera.

The contractional event is superceded by the development of a series of northwest-trending, steeply dipping ductile protomylonitic to mylonitic transpressional shear zones (10-1300 m wide), which affect most rocks in the western portion of the mapped area. These shear zones increase in concentration from east to west, although a similar deformational style is concentrated in the Atnarko Complex to the southeast (Israel and Kennedy, 2002). The shear system involves several different phases of Jurassic (?) to Cretaceous plutonic rocks and the Early Cretaceous Monarch sequence, and is itself cut by various probable Tertiary plutons. Shear sense indicators are equivocal; the shear zone apparently records extensive transpressional multi-directional flow. The high-angle shear zones are restricted to the western map area, and do not involve rocks of the Hazelton Group.

LITHOSTRATIGRAPHY

EARLY AND MIDDLE JURASSIC HAZELTON GROUP

The Hazelton Group is one of the most widely distributed Mesozoic arc-magmatic successions in the Canadian Cordillera, strung out along the entire length and breadth of the Stikine terrane. It is associated with significant mineral deposits, including Eskay Creek type volcanic-hosted massive sulphides (Roth *et al.*, 1999), epithermal gold, and associated copper-gold porphyry deposits in subvolcanic granitoids (Diakow *et al*., 1991; MacDonald *et al*., 1996). Over the past three decades, the Hazelton Group has attracted the attention of both the explorationist and geological surveys which resulted in considerable new and revised stratigraphic nomenclature that builds upon a Jurassic stratigraphic foundation established by Tipper and Richards (1976) in central British Columbia.

Rocks of the Hazelton Group consist of an island-arc volcano-sedimentary assemblage that broadly ranges in age from Early to Middle Jurassic (Hettangian to Bajocian). In general terms, the earliest record of arc constructional events in west-central Stikinia were subaerial and by Middle Jurassic time volcanism had waned. However, it still provided significant episodic input into a broad, shallow marine back-arc (?) or intra-arc (?) trough established to the east-southeast of the older, eroded subaerial centres.

Baer's (1973) work, coupled with fossil collections from pioneering reconnaissance exploration in central British Columbia (G.M. Dawson, 1878), show that Jurassic strata extend to the eastern boundary of the Bella Coola map sheet, well within Tweedsmuir Park. In that location, they are unconformably overlain by remnants of a moderately dissected peralkaline shield volcano forming the Rainbow Range (Bevier, 1981). The Rainbow Range is one of a number of Neogene volcanic centers and related alkaline plutons comprising the Anahim Volcanic Belt (Souther, 1977, 1986). Volcanic loci in this belt are scattered along a linear east-west tract at about 52° latitude, extending for 300 kilometres from the coast into the Chilcotin Plateau to the east (Souther and Yorath, 1992).

Jurassic rocks documented in the Bella Coola area by Baer (1973) were presumed to overlie an even more widely distributed greenstone assemblage of possible Triassic age. Recent findings of the Bella Coola TGI program reveal that the oldest Mesozoic rocks in the area include the Jurassic Hazelton Group, found mainly to the east (this report). These rocks pass farther west into a younger, Early Cretaceous volcano-sedimentary succession (Struik *et al.*, 2002). No Triassic or older strata have been found in the study area. An unconformable contact between Jurassic and Cretaceous sequences is suspected but has not yet been mapped. The Talcheazoone fault, inferred as steeply dipping, projects north northwesterly from east of Sallompt Peak and along much of its strike length separates folded and thrust faulted Cretaceous strata from tilted Hazelton Group strata. A belt dominated by dioritic intrusive complexes lies east of the Talcheazoone fault, although elements of these same intrusive complexes can be found in other parts of eastern Bella Coola map area (Figure 3; Hrudey *et al*., 2002).

Separation of Jurassic Hazelton Group from Early Cretaceous Monarch volcanics is sometimes equivocal in absence of interlayered fossil-bearing clastic rocks. However, in this study the differentiating field criteria included:

1) The Jurassic succession is dominated by crudely bedded, dark green, sometimes oxidized purplish flows of basalt to andesite composition containing plagioclase and augite phenocrysts. Rhyolitic pyroclastic rocks and less common aphanitic flows form areally restricted deposits bound by the more mafic rocks. These contrast with the Cretaceous volcanics in which fragmental rocks are generally more widespread than flows and have the bulk composition of andesite. These rocks are typically olive to light green-grey and exhibit aphanitic and plagiophryic textures, but also appear to contain notable hornblende phenocrysts.
2) Jurassic sedimentary rocks exhibit an intimate relationship with arc magmatism, manifest in volcanic interbeds and the high proportion of angular feldspar with or without quartz and volcanic lithic fragments in arkose, greywacke and volcanic lithic-bearing clastic rocks derived from nearby volcanic and/or plutonic sources. Tuffaceous argillite containing fossils are rare within the Jurassic succession. By contrast, Early Cretaceous strata include more prominent and regionally mapable black slate beds. These are interlayered with siltstone and sandstone that form discrete rusty weathered intervals 10s of metres thick within the volcanic rocks. Fossils including ammonites and other shelly fauna are abundant locally (Struik *et al.*, 2002).

In this study, the volcanic and sedimentary rocks comprising the Hazelton Group are subdivided into various lithofacies on the basis of continuity in overall lithologic characteristics and their original textures and structures. The distribution of these rocks is shown in figure 3. These lithofacies are described in order of decreasing relative prominence in which order of description makes no inference of superposition. Regionally, these rocks are in the sub-greenschist facies as the mafic rocks contain an assemblage of secondary chlorite, epidote and albite. The original

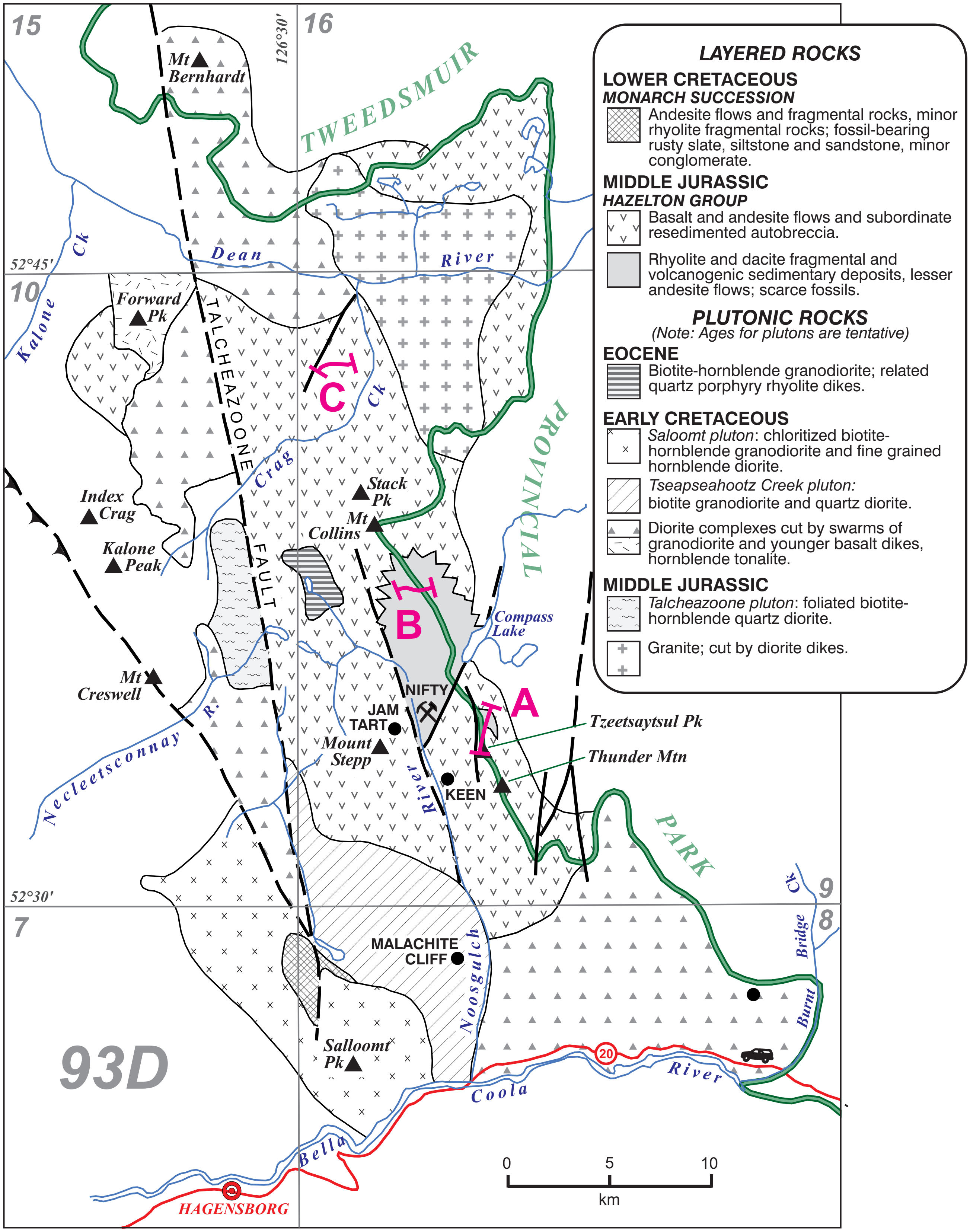

Figure 3. Schematic geology map of the eastern portion of the Bella Coola map sheet, bordering Tweedsmuir Provincial Park. Letters refer to stratigraphic columns (Figures 4,5 and 6) discussed in the text. Dots are MINFILE occurrences.

textures and fabrics within this mixed volcano-sedimentary succession are generally well preserved.

Bimodal Mafic-Intermediate and Lesser Rhyolitic Volcanic Rocks

Volumetrically, subaerial mafic to intermediate lava flows and associated breccias dominate probable Jurassic successions in the study area. Thick mafic volcanic sections are particularly well exposed at Tzeetsaytsul Peak and Thunder Mountain in the southeast. Thick accumulations of mafic to intermediate rocks crop out again farther northwest in the region between Mount Collins and Stack Peak, then across Crag Creek towards Forward Mountain. Locally these mafic volcanic rocks are interlayered with or faulted against felsic volcanic rocks. Representative stratigraphic sections described below are shown in figure 3 and detailed sections are presented in figures 4, 5 and 6. Composite diorite bodies cut by intermediate and mafic dike swarms, crop out immediately adjacent to the mafic volcanic unit in at least three areas leading us to speculate that they may be comagmatic. An alternate hypothesis is that such complexes may be Early Cretaceous (Hrudey *et al*., 2002) and related to extrusive rocks of the Monarch succession (Struik *et al.,* 2002); however, at this early stage of the program there is no compelling geochemical or geochronological data to verify either genetic association.

Tzeetsaytzul Peak and Thunder Mountain Area

At Thunder and Tzeetsaytzul mountains, more than 1100 metres of crudely layered volcanic strata dip between 25 and 40 degrees southwest toward the Noosgulch River valley. The volcanic rocks are dominated by basalt to andesite lava flows in excess of 750 metres thick, interlayered with related breccias. Dacite to rhyolite flows and tuffs have an aggregate thickness of about 250 metres. On the north side of Tzeetsaytzul Peak, these felsic rocks dominate the lower 200 metres of the section, and form a distinct interval within more mafic rocks approximately 120 metres down from the summit (Figure 4; Section A in Figure 3). A relatively short distance northwest of Tzeetsaytzul Peak, a high-angle fault trending northeast through Compass Lake truncates and juxtaposes the mafic succession against a dominantly felsic, shallow marine lithofacies.

The basalt and andesite flow and fragmental rocks have a massive character that at a distance, are discernable as a series of uniformly weathered, very thick planar beds. Oxidized reddish flow tops accompanied by autoclastic breccia have been observed only at one locality. The flows are typically dark grey-green to purplish green and exhibit amygdaloidal, porphyritic and aphanitic textures.

Amygdaloidal flow varieties are very common in the upper part of the section at Thunder and Tzeetsaytsul mountains. They contain rounded, irregular, and stretched amygdules ranging from several millimetres up to 30 millimetres in diameter, which are infilled with either quartz or chlorite or a combination of these minerals, with or without epidote. Quartz is generally clear and crystalline, growing inwards from an outer concentric shell composed of chlorite; however, in a few places it is a translucent variety of chalcedony. The porphyritic texture in the flows is imparted by randomly oriented blocky plagioclase phenocrysts 1-4 mm in amounts rarely more than 20 to 25%. Rare andesitic lavas may contain plagioclase laths between 6 and 13 millimetres. In addition to plagioclase, augite phenocrysts are ubiquitous, present as grains ranging from 1 to 3 millimetres in amounts commonly up to 7%. Rare hornblende phenocrysts accompany augite in some andesites. In thin section, the hornblende is corroded, surrounded typically by an opacite rim.

Autoclastic rocks forming irregular deposits between lava flows are relatively common in the vicinity of Tzeetsaytzul Peak. These deposits characteristically contain basaltic monomict porphyry fragments composed of fine-grained, crowded, plagioclase and lesser augite phenocrysts. They are poorly sorted and unstructured containing subangular to subrounded blocks that are fragment supported and matrix poor or in similar matrix composed of finer granulated fragments. Some of the fragments exceed one metre in diameter. These deposits may represent variably reworked and redeposited autobreccia, although, in general, the flow succession lacks in-situ fragmented and oxidized tops and bottoms common in subaerially erupted lavas.

Felsic rocks observed in two intervals on the north slope of Tzeetsaytzul Peak appear to be stratigraphically bound by mafic volcanic rocks. The lower section consists of as much as 200 metres of dacite to rhyolite lava flows having a somewhat bulbous cross section. Adjacent rocks are mafic breccias and the upper contact, which was not mapped, is assumed to be with massive mafic flows. Except for relict flow laminae and spherulitic texture, these flows are aphanitic and massive in appearance. Rare, volcanic breccia containing subangular blocks of laminated rhyolite is spatially associated with the more massive flows. The upper felsic interval, about 50 to 70 metres thick, is located near the top of Tzeetsaytsul Peak. It comprises mainly light green lapilli tuffs characterized by white weathering angular rhyolitic fragments. Welded texture is observed in several thin intervals within this otherwise massive nonwelded deposit.

Mount Collins to Forward Mountain Area

Mount Collins and connected ridges to the north and east are underlain by a large volume of mafic and intermediate flows lithologically similar to those at Thunder and Tzeetsaytsul mountains (Figure 3). East of Mount Collins coarse breccias identical to those described at Tzeetsaytsul Peak are prominent within the mafic sequence. Mainly porphyritic flows with plagioclase and lesser augite phenocrysts form the ridges across a drainage divide immediately west of Mount Collins. These flows are associated with volcanic breccia, finer bedded tuffs and thin lenticular interbeds of locally welded rhyolitic tuff.

The volcanic sequence west of Mount Collins area has a chlorite-rich aureole surrounding a biotite-hornblende granodiorite stock. Quartz-feldspar porphyry dikes ranging up to 20 metres wide appear to project outward from the stock cutting adjacent country rocks. Such felsic hypabyssal

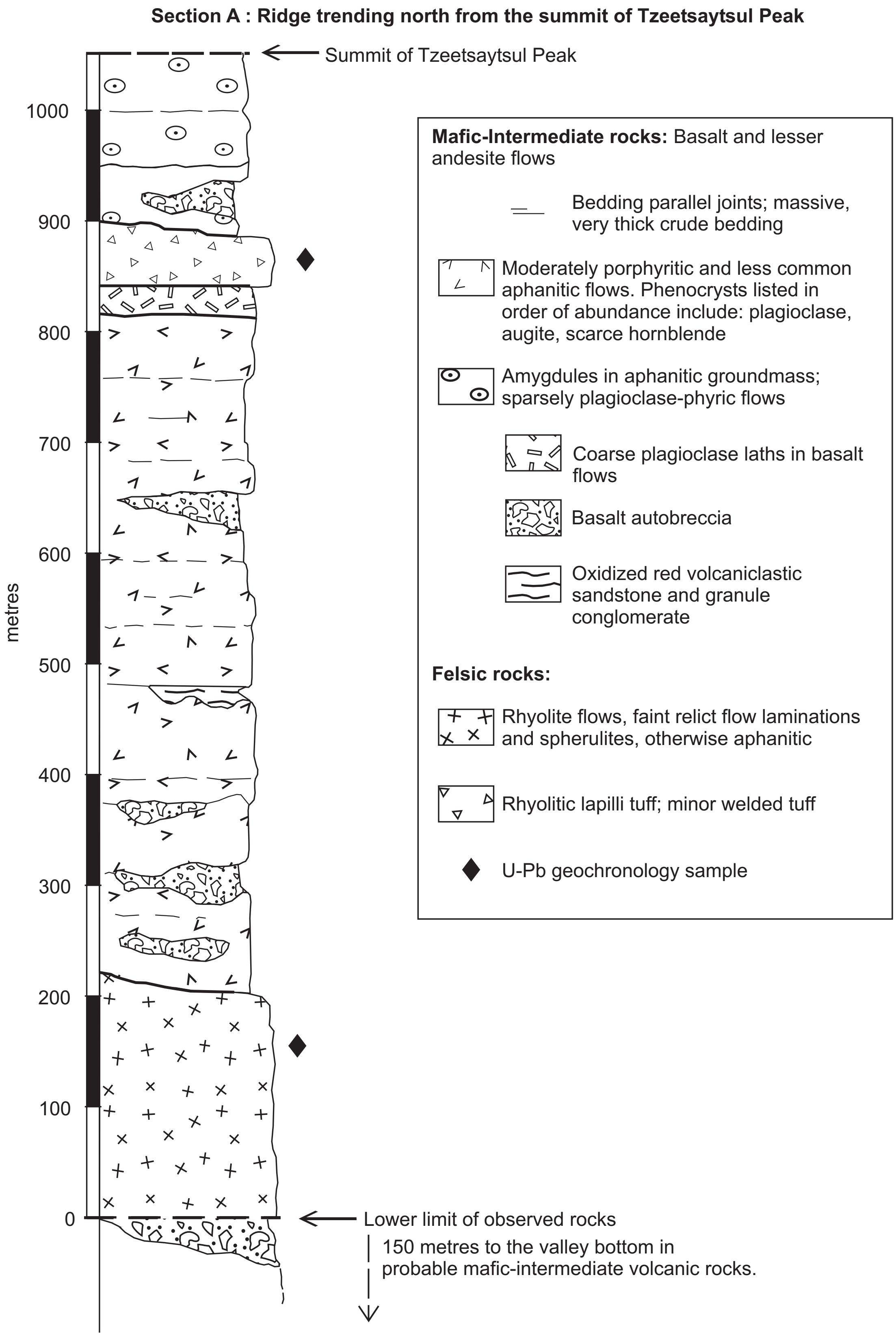

Figure 4. Stratigraphic section of the mafic volcanic facies exposed on the north flank of Tzeetsaytsul Peak. Base of section not exposed; upper limit is the modern erosion surface. Note the bimodal nature of the succession.

rocks are prominent mainly in the area between Stack Peak and Mount Collins where interestingly, they are also spatially associated with rhyolitic rocks that comprise a well-bedded subaqueous volcaniclastic succession.

Presently, the northern extent of the mafic volcanic sequence is in the vicinity of Forward Peak, occupying an area west of the inferred Talcheazoone fault. Aphanitic and lesser porphyritic basalts, similar to those found elsewhere, predominate. Additionally, there are significant lapilli tuffs, some with white felsic fragments, quartz-feldspar crystal tuffs and in a few places substantial rhyolite sills (?). A moderate foliation is developed in tuffs and is particularly noticeable in those containing stretched felsic fragments.

West of Crag Creek a sequence of mafic lavas having lithologic features similar to those near Mount Collins appear to unconformably overlie a distinctive sequence of sedimentary rocks (Figure 5; Section C in Figure 3). Because the lower contact of the sedimentary rocks was not observed, it is unclear whether these sediments are underlain by more mafic flows similar to those stratigraphically above, or are in fact an older unit. However, Baer (page 30, 1973) describes geology underlying a ridge south of the junction between Crag Creek and Dean River that is presumed to be an along strike extension immediately north of Section C. In this section a fossil-bearing thin carbonate unit, thought to be correlative with belemnite-bearing tuffaceous mudstones in Section C, appears to occupy a relatively thin interval in a mafic volcanic sequence.

In section C, the lower contact of the overlying mafic sequence is sharp, marked by a change in bedding that is inclined at a high angle relative to the underlying sedimentary rocks. In the west this sequence is truncated by a high angle fault that places it against quartz-bearing rhyolite lapilli tuffs. The lava flows are relatively thin and separated by clastic rocks derived from the flows. The clastic rocks consist of granule and pebble conglomerates and well-layered feldspar-rich sandstones. The clasts are composed of abundant angular pyroxene grains and, monomict basalt that are subrounded and tightly packed. The clasts commonly weather positively where the carbonate cement has been dissolved.

Fossil-bearing Sedimentary Rocks West of Crag Creek

Sedimentary rocks underlying mafic rocks in section C comprise about 75 metres of thinly bedded volcanogenic mudstone, siltstone and sandstone. Tuffaceous mudstone dominates the lower 25 metres of exposure. The sedimentary rocks exhibit distinctive parallel banding due to thinly bedded off-white ash tuff layers alternating with black mudstone. These are interbedded with feldspathic siltstone, sandstone, and minor granule conglomerate, which become more prevalent upsection. Welded tuff containing chloritic fiamme and an andesite flow or sill crop out in the middle of the section and attest to the volcanogenic origin of the interbedded sedimentary rocks. Fossils from wackes collected by Baer (1973) at this site were recently re-examined and reported to contain a diverse collection of bivalves and some belemnoids all of which are non diagnostic Jurassic forms (pers. comm. T.P. Poulton; Report No. J4-2001-TPP).

Rhyolitic Pyroclastic and Resedimented Pyroclastic Deposits

Mount Collins South to the Nifty Mineral Occurrence

Ridges south of Mount Collins are underlain by a thick succession of rhyolitic pyroclastic and resedimented pyroclastic strata that contrast markedly with the dominantly mafic character of the Hazelton Group to the north and south. This felsic succession seems to form an areally restricted lense enclosed by more mafic components of the Hazelton Group. Over 1000 metres of rhyolitic volcaniclastic rocks are well exposed in an east-dipping homocline south of Mount Collins (Figure 6; Section B in Figure 3). The base of the section is interpreted to gradationally overlie andesitic breccias and subordinate flows cut by hypabyssal sills and dikes. Near the top of the felsic succession interbeds of mafic volcaniclastic strata suggest a gradational or lateral interfingering relationship with mafic volcanogenic sedimentary rocks lying to the east and north.

The rhyolitic succession comprising section B (Figure 6) may be subdivided into two distinct lithofacies. These include a lower dominantly coarse tuff facies that passes gradationally upwards into thick planar bedded, volcanogenic sedimentary deposits.

Rhyolite Tuff Lithofacies

The lower ~420 metres of strata is characterized by diffusely bedded to massive rhyolitic lapilli tuff and tuff breccia, intercalated locally with resedimented pyroclastic debris. Individual beds are up to 5 metres thick, and are typically composed of poorly sorted, angular, pebble to cobble-sized clasts of aphanitic felsic volcanic rock floating in a coarse-grained volcaniclastic matrix. Rounded clasts and crude laminations are locally evident, suggesting reworking of volcaniclastic debris. Thick (>4 m) lenticular beds of clast-supported volcanic boulder conglomerate are locally evident. Quartz-phyric rhyolite dikes, sills and rare welded lapilli tuff occur sporadically throughout the sequence. Thin basaltic flows form a minor, yet genetically important, portion of the sequence. Units are distinctly lenticular, and the sequence is characterized by rapid lateral facies changes.

Resedimented Syn-eruptive Volcaniclastic Lithofacies

The rhyolite tuff lithofacies is sharply overlain by more than 600 metres of well-bedded volcaniclastic conglomerate, sandstone, siltstone and subordinate primary volcanic deposits comprised of welded and nonwelded lapilli tuff and rare accretionary lapilli tuff. The lowermost beds consist of a 20 to 30 metre section of tuffaceous black mudstone interbedded with dark gray, parallel and locally cross laminated, feldspathic sandstone and siltstone. White ash-tuff laminae in black mudstones mark the base, and closely resemble those found at the bottom of lithologically similar mudstones and feldspathic sandstone occupying the lower part of Section C, west of Crag Creek (*see* Figure 5 for details). This sequence is gradationally overlain by 100s of metres of thickly bedded to massive, coarse-grained feldspathic arenite and intercalated matrix-supported volca-

Section C : Ridge west of Crag Creek (starting point at treeline); 6.8 kilometres at 343° azimuth from the summit of Mount Collins (UTM 09 670287E, 5843542N)

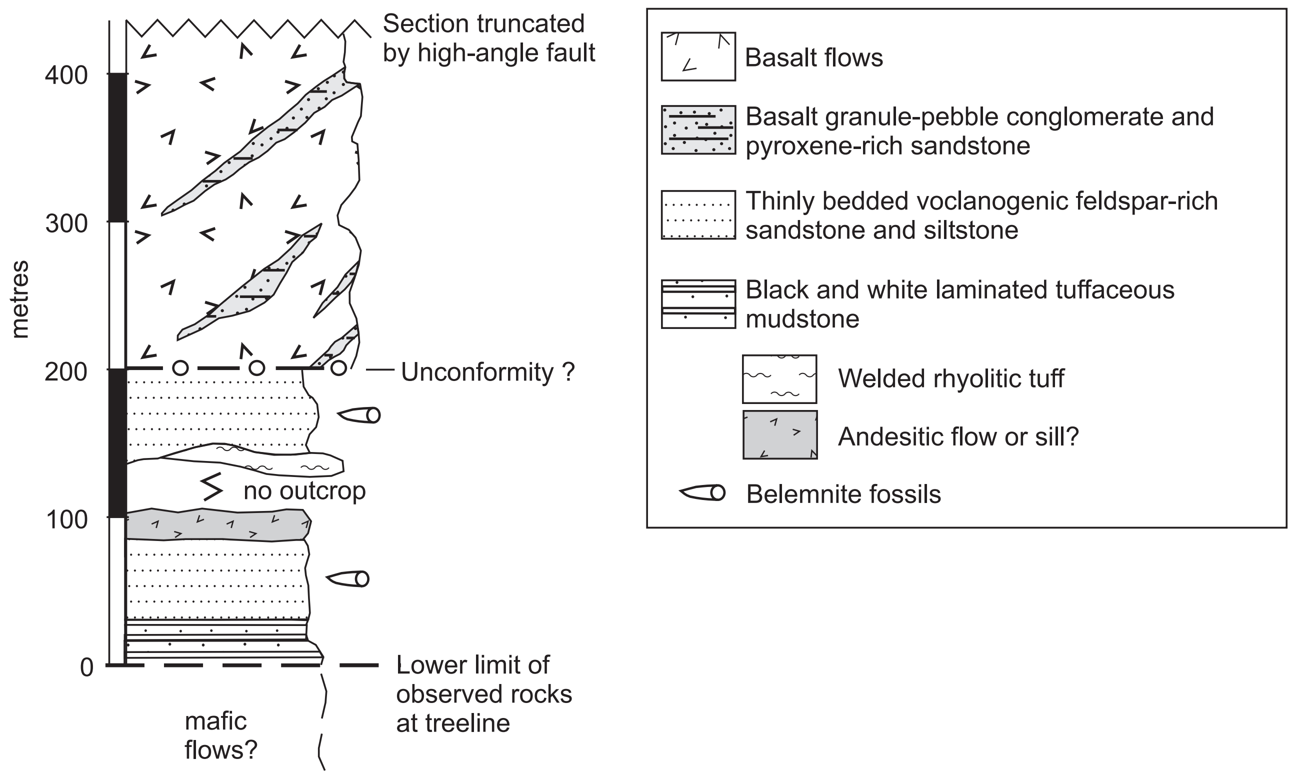

Figure 5. Stratigraphic section of the mafic volcanic facies and underlying volcanogenic sedimentary facies exposed on an east-facing slope west of Crag Creek. Base of the section is not exposed; upper limit is the modern erosion surface.

nic pebble conglomerate. Graded bedding and convolute laminations are common; most units appear tabular and laterally continuous. Rare welded quartz-bearing rhyolite ash-flow tuff occupies intervals up to 25 metres thick interbedded with quartz-rich sandstone and volcanic sharpstone conglomerate. Felsic fiamme define a pronounced eutaxitic texture in several intervals of the welded rhyolites. Quartz and feldspar arenite sandstones interlayered with lesser rhyolite granule and pebble conglomerates dominate massive beds in the upper portion of the section. Polycrystalline quartz, probably derived from a plutonic source, is found in some of these arenites. Laminated and massive ash tuffs up to 40 metres thick and a rare, accretionary lapilli tuff bed several metres thick are interlayered with these clastic rocks and attest to syn-sedimentary explosive volcanic eruptions.

Near the top of the exposed section light colored resedimented rhyolitic volcaniclastic rocks are gradationally overlain by 30 metres of dark green and purple basalt pebble conglomerate and coarse-grained sandstone. These conglomerates and sandstones are characterized by an abundance of coarse sand to granule-sized volcanic lithic clasts of finely amygdaloidal and vesicular basalt. A thin basaltic andesite sill or flow occurs within these mafic clastic rocks. These mafic conglomerates exhibit distinctive differential weathering in which tightly packed basalt clasts are separated by voids that evidently result from the dissolution of carbonate cement. A similar feature was also noted in nearly identical mafic conglomerates and sandstones found as lenticular beds within mafic flows directly overlying tuffaceous mudstone and feldspathic sandstone west of Crag Creek (*see* Figure 5 for details). In turn these mafic deposits are sharply overlain by reddish oxidized siltstone with oscillation ripples in the topmost bed of section B.

Felsic volcanogenic sedimentary rocks comprising most of section B dip moderately southeast, below topographically lower terrain west of Compass Lake. Felsic strata then continue to the southwest where they comprise part of the hangingwall succession for the stratiform mineralization at Nifty. Farther east-southeast of Nifty, the felsic volcanic succession is cut off by a northeast striking fault whose trace projects through Compass Lake. Across this structure the felsic sequence is juxtaposed against the mafic volcanic succession underlying Tzeetsaytsul and Thunder mountains.

On the north side of an east-west trending valley, occupied in part by Compass Lake, white weathered rhyolite forms a series of scattered low lying knolls. These rocks are aphanitic and locally display diffuse flow laminae. Although interpreted as lava flows, their uniform texture, ab-

Section B : Centred 3.1 kilometres at 149° azimuth from the summit of Mount Collins
(UTM 09 674000E, 5834370N)

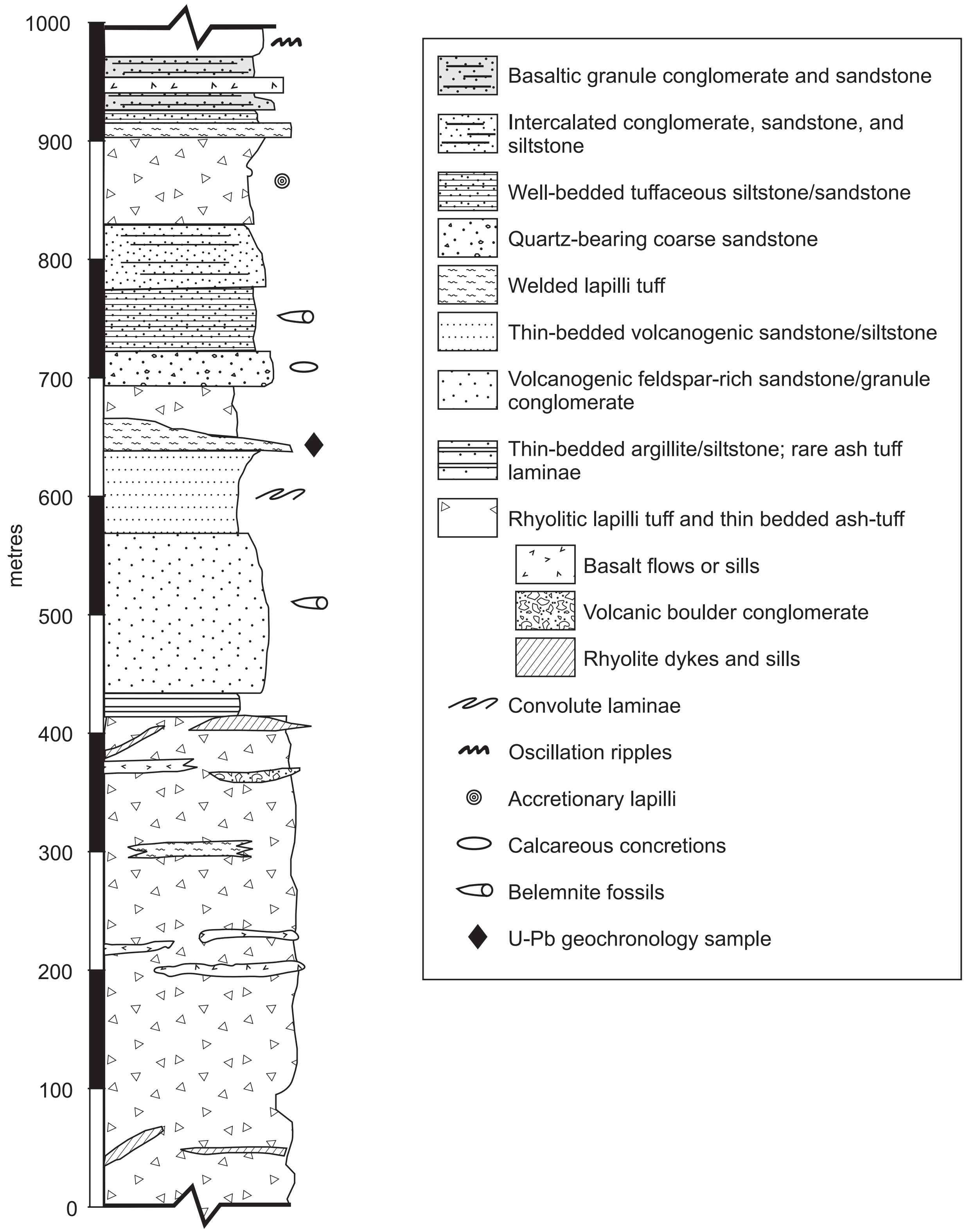

Figure 6. Stratigraphic section of the rhyolitic facies exposed on the west-facing slope of an unnamed mountain south of Mount Collins. Base of section is not exposed; upper limit is the modern erosion surface.

sence of related autoclastic rocks and common occurrence of finely disseminated pyrite suggests they might be part of a subvolcanic intrusive dome. South of the east-west trending valley, near the Nifty occurrence, aphanitic rhyolite is found, but accompanied by lesser lapilli tuffs. The fragments consist mainly of subangular aphanitic white rhyolite and fewer, fine-grained plagioclase porphyries. Quartz is often present in the matrix as grains several millimeters in diameter.

Volcanic strata hosting stratiform sulphides and barite at the Nifty occurrence were re-examined in some detail by Ray *et al.* (1998), who synthesized published geology and provided new information on the geochemistry of the host rocks and mineralization. Rocks immediately overlying the mineralized interval at Nifty have been disrupted by faults, which rotate the layered sequence from subvertical to gentler dips. In turn, strata have been cut by several generations of northeast to east trending steeply dipping post-mineralization dikes composed of andesite and quartz porphyry rhyolite.

Above the sulphide and capping barite mineralization near the adit, the stratigraphy consists of alternating orange and white weathering ash tuffs containing subordinate lapilli tuffs. Fragments invariably consist of aphanitic white rhyolite lapilli set in a finer aggregate of volcanic lithics, plagioclase and a few quartz crystals. These felsic tuffs are sharply overlain by a conformable sequence of dark green aphanitic rocks, which near the base comprise thin parallel-layered ash-tuff or volcanic siltstone and mudstone. In turn these rocks grade imperceptibly upwards into other dark green massive rocks with aphanitic texture, interpreted as lava flows.

Ray *et al.* (1998) shows that in the vicinity of Nifty the hangingwall stratigraphy is dominated by tholeiitic and calcalkaline basalt and andesite, interbedded with volumetrically lesser calcalkaline rhyodacite tuff and minor devitrified lava flows. Footwall strata were not examined during this study; however, Ray *et al*. (1998) documented pervasive bleaching accompanied by the addition of silica and pyrite to the tuffs and flows of probable dacite and andesite composition.

Mixed Mafic-felsic Clastic Lithofacies

Mafic clastic rocks near the top of section B are believed to grade upwards into a dominantly mafic volcanogenic sedimentary succession widely exposed at lower elevation immediately to the east and north of section B. Currently, little is known about these deposits other than that they consist of medium to thick bedded mafic volcaniclastic sandstone, siltstone and lesser conglomerate, estimated to be in the order of several hundred metres thick. These clastic rocks contain diagnostic quartz grains, angular black mudstone and basaltic debris, which suggests rapid dissection of a lithologically varied provenance region or mixing of detritus derived from both felsic and mafic sources. The exact nature of the transition with resedimented felsic volcaniclastic rocks dominant to the west in section B is unclear. The felsic and basaltic sedimentary successions may interfinger over a few 100 metres, or the contact may represent a buttress unconformity or fault.

DEPOSITIONAL ENVIRONMENT

Volcanic rocks in the study area are broadly divided into two compositional clans - a regionally prominent, mainly basalt flow sequence containing subordinate rhyolitic tuffs and scarce interflow sedimentary rocks, and an adjacent succession composed mainly of rhyolitic volcanogenic sedimentary rocks interspersed with rhyolitic pyroclastic deposits. These felsic pyroclastic rocks appear to change laterally into a more massive rhyolite flow-tuff facies that has a distinctly bimodal character and is associated with stratiform sulphide-barite mineralization and crosscutting felsic to intermediate dikes. The temporal relationship of these two contrasting packages is presently poorly constrained. They appear to interfinger laterally and are in part coeval volcanic sequences that evolved relatively close to one another. Although geochemical analysis for the volcanic rocks discussed are not yet available, geochemistry of country and hypabyssal rocks in the vicinity of Nifty suggest the rhyolites and basalts are volcanic arc related (Ray *et al*., 1998).

Tzeetsaytsul Peak-Thunder Mountain, Mount Collins and Stack Peak all composed of thick, crudely layered sequences of dark green and purplish basalt and lesser andesite flows. Individual flows, several 10s of metres thick, grade imperceptibly through combinations of aphanitic, plagiophyric and amygdaloidal textures. Very rarely is an actual flow contact observed, indicated by red oxidation accompanied by flow breccia. Interflow deposits of monomictic basalt breccia debris, that in places exhibit rounded clasts, are interpreted as redeposited autoclastic products derived possibly from flow breccias. Because the lava sequences are typically massive, uniformly layered and homogeneous, lacking pillows, hyaloclastites and well stratified waterlain tuffs; they probably reflect high volume and high effusion rate eruptions in a subaerial setting close to their source vent(s). Comparatively minor subaerial felsic flows and fragmental rocks evidently coalesce with the mafic rocks and indicate the bimodal nature of magmatism.

An abrupt change from mafic to felsic dominant successions corresponds with several steeply dipping faults which trend northwest, parallel to Noosgulch River, and an intersecting northeast fault passing through Compass Lake. These faults delimit rhyolitic rocks generally deposited in a shallow marine depocentre.

Topographically lowest and perhaps oldest rhyolitic rocks crop out south west of Compass Lake and consist of aphanitic rhyolites believed to be devitrified flows, and subordinate lapilli tuff and minor well-layered waterlain ash tuffs. To the north, the rhyolitic succession detailed at Section B, in the area south of Mount Collins, represents both subaerial and submarine deposition. The coarse pyroclastic lithofacies at the base of the section contains primary lapilli tuff, matrix-supported reworked pyroclastic debris, channelized clast-supported conglomerate, rare, thin, non-pillowed basalt flows and associated breccias and small rhyolitic flow domes. This assemblage suggests deposition on the relatively steep flanks of a rhyolitic eruptive centre adjacent to the distal reaches of a basaltic volcanic edifice. An abrupt change from underlying coarse pyroclastic lithofacies into overlying resedimented rhyolitic volcaniclastic lithofacies records a change towards sequential rhyolitic eruptive events punctuated by transport of large volumes of ash, crystals and lithic fragments in shallow water.

More than 600 metres of thick, uniformly bedded resedimented volcaniclastic rocks composed exclusively of rhyolitic fragments, crystals and ash, alternate with subordinate primary pyroclastic deposits in an overall shallowing upward sequence. The base of the sequence is composed of thin to medium-bedded, laterally continuous fine-grained rocks. These beds generally coarsen upward into thickly bedded coarse-grained sandstones with substantial pebble conglomerate. Sedimentary structures are abundant, and include graded bedding, parallel laminations, basal scour features, convolute laminations and matrix-supported pebble conglomerate. These features, together with distinctive thin to medium bedded couplets consisting of a basal structureless to parallel laminated sandstone overlain by a parallel to convolute laminated siltstone representing top-cut-out turbidite (AB) packets indicate submarine deposition by mass sediment gravity flow.

Submarine deposition is supported by the presence of belemnites and *Cruiziana* trace fossils. Water depth is equivocal, as these rocks could represent submarine fan deposition below normal wave base, or shallow marine deposition in a deltaic environment characterized by high sediment influx. Several measurements from convolute beds suggest sediment failure and transport on a northwest-southeast striking paleoslope that dipped west-southwest. The shallow water depositional setting is further supported by the presence of welded lapilli tuff and associated tuffaceous conglomerate and sandstone. An overall shallowing upward sequence is indicated by the increasing presence of primary volcanic rocks upsection including welded-tuff and lapilli tuff. Accretionary lapilli found immediately above a welded tuff record a brief interval of subaerial deposition and is followed by resumption in shallow water deposition marked by development of oscillatory wave ripples in siltstones occupying the upper portion of the lithofacies.

The rhyolitic succession interfingers with more mafic sediments in the upper 50 metres of the section. Oscillation ripples above and accretionary lapilli below these mafic strata indicate this interfingering occurred in a shallow marine depositional environment. Although the interfingering sediments appear compositionally distinct in outcrop, thin section petrography indicates sandstone beds are locally well mixed; containing a heterogeneous bimodal assemblage of basaltic tuff clasts intermixed with quartz and sanidine grains.

AGE OF VOLCANO-SEDIMENTARY ROCKS AND CORRELATION

The Middle Jurassic depositional ages for volcanic and sedimentary rocks of the Hazelton Group rocks of eastern Bella Coola map area are based on several isotopic dates from igneous rocks in the vicinity of the Nifty mineral prospect and inferred from ammonite fauna identified in sedimentary rocks lying outside the study area in the northeastern corner of the Bella Coola area.

Felsic volcaniclastic rocks exposed near Mount Collins are thought to be temporally equivalent to silica bimodal volcanic rocks that host the Nifty occurrence. In order to test this hypothesis, and to determine the timing of felsic volcanism locally associated with stratiform sulphide mineralization in the region, several samples have been collected for uranium-lead dating. A white weathered rhyolite north of Nifty (UTM Zone 09 675 208E, 5830012N) yields a range of provisional Middle Jurassic ages, and requires additional zircon fractions to obtain a more precise date (pers. comm., Mike Villeneuve, 2001). Ray *et al.* (1998) report a U-Pb date on zircon of 164.2+1.2/-0.9 Ma from a quartz rhyolite dike (UTM location: Zone 09 675150E, 5828850N). This dike is one in a swarm of northeast trending hypabyssal intrusives near the Nifty occurrence, where they cut volcanic strata hosting the sulphide-barite mineralization. This date, therefore, provides a minimum age for bimodal volcanism and syngenetic sulphide-barite mineralization in the Hazelton succession in the Bella Coola map area.

South of Mount Collins a welded ash-flow tuff about 25 metres thick, conformable with bounding subaqueous volcanogenic clastic rocks, is currently being processed for a U-Pb date (*see* Figure 6 for approximate position in section C; UTM location: Zone 09 673912E, 5834551N). The tuff contains fiamme up to 120 millimetres long in a white siliceous groundmass that contains sparse quartz phenocrysts and microscopic sanidine grains. This date will provide information on the contemporaneity of rhyolitic deposits near Mount Collins with those closer to Nifty.

Comparison of depositional ages for the felsic volcaniclastic facies and mafic flow facies will be achieved by dating two samples of felsic rocks occupying intervals within depositionally conformable mafic volcanic rocks at Tzeetsaytzul Peak. These age determinations will partly bracket the timing of mafic volcanism and provide a temporal relationship with bimodal volcanic rocks associated with massive sulphides at Nifty. The lower of the two sites is from the upper portion of approximately 250 metres of aphanitic rhyolite interpreted as a flow dome; and, the second sample is from a thin, welded zone in a rhyolite lapilli tuff succession near the top of Tzeetsaytzul Peak (*see* Figure 4 for approximate positions in section A; respective UTM locations Zone 09 677545E, 5828855N and 677417E, 5827245N).

Volcanic derived feldspar and quartz-bearing sedimentary rocks intercalated with primary volcanic rocks south of Mount Collins contain sparsely distributed, non-diagnostic belemnoids and *Cruiziana* trace fossils. However, at another locality close to Mount Collins a collection of bivalves have been previously identified by Dr. J.A. Jeletsky as Callovian to Early Oxfordian in age. At a new fossil locality, one and one half kilometres southeast of Mount Collins, ammonites occur within rare limey lenses in a twenty five metre thick interval of thinly bedded black siltstone and sandstone that occurs stratigraphically beneath coarse mafic sandstones that lay to the east and north of strata comprising Section B (GSC location C-306159; Zone 09 673800E, 583625N). Poor preservation of these ammonites prevents positive identification (pers. comm. J. Haggart; Report No. 2001-7), however, further examination of this locality is planned.

Recent re-examination of the Geological Survey of Canada's archived fossil collections from the Bella Coola area by Dr. T.P. Poulton include several collections made from a ridge south of the confluence of Crag Creek and Dean Rivers (GSC Locations 65045 and 65046). These collections, reported in Baer (1973, pages 32 and 33), are from a feldspathic wacke associated with limestone situated between massive basaltic lavas. Sedimentary strata in this section are believed to continue immediately south, correlating with a gently dipping sequence of volcanogenic sandstones and tuffaceous mudstones forming the lower part of Section C (Figure 5). Scarce belemnites were found in these shallow marine rocks in Section C and comparable strata to the north contain abundant shelly fauna, although non diagnostic, they are presumed to be of Jurassic age (pers. comm. T.P. Poulton, Report No. J4-2001-TPP). Argillites and greywackes believed to be correlative with volcanogenic sedimentary interbeds occur sporadically in widely separated areas near the eastern margin of the Bella Coola map area. Locally, they contain the Early Bajocian ammonite, *Stephanoceras*, associated with a variety of bivalves (Baer, 1973; pers. comm. T.P. Poulton, Report No. J4-2001-TPP).

Lithologically similar sedimentary rocks of Bajocian age, also containing *Stephanoceras* or other abundant shelly fauna, extend northward into Whitesail Lake map area (NTS 93E), thence eastward into the southern Nechako River map area (NTS 93F). A lithologic feature common in all areas is the presence of felsic volcanic interbeds manifest as ash tuff and coarser fragmental interbeds and, ubiquitous beds rich in angular feldspar grains and volcanic lithic clasts in wackes. These components indicate contemporaneous explosive felsic volcanic activity adjacent to or within a shallow marine depositional basin. If the rocks in the study area are proven to be Bajocian in age (Middle Jurassic) they are then most comparable to strata comprising the Naglico formation in the southern Nechako area (Diakow *et al.* 1997a) where time stratigraphic rocks are dominated by basalt and andesite flows containing local accumulations of fossil-bearing feldspathic and lithic arenites. However, the distinctive volcanogenic character of Bajocian strata is not unique to this specific time interval in the southern Nechako River and Whitesail Lake map areas. Fossil-bearing mudstones, feldspathic and lithic arenites containing significant components of felsic volcanic material have also been recognized in Middle Jurassic Aalenian, down into Early Jurassic Toarcian strata in these areas (Diakow and Levson, 1997b; Poulton and Tipper, 1991; Woodsworth, 1980). Therefore, the possibility exists that some of volcano-sedimentary sections exposed in the study area may well be older than fossiliferous Early Bajocian strata known in eastern Bella Coola map area.

MINERAL POTENTIAL OF JURASSIC VOLCANO-SEDIMENTARY ROCKS

The Jurassic Hazelton magmatic arc in Stikinia is an important metallotect for a variety of mineral deposits including copper-gold porphyries associated with subvolcanic plutons, epithermal gold-silver deposits in subaerial rocks and less common, but significant, stratiform massive sulphide in subaqueous volcano-sedimentary sequences. Evaluation of submarine volcanic-sedimentary sequences in British Columbia as potential hosts for massive sulphide accumulations reveals that remnants of the Hazelton arc are primary targets for exploration (Massey *et al.*, 1999).

The Eskay Creek deposit, in northwest British Columbia, is the premier example of massive sulphides hosted by strata of the Hazelton Group. The Eskay Creek mine, currently in its 6th year of operation, has reserves as of January 2001 of 705 200 tonnes of direct shipping ore containing 65.5 g/t gold and 3036 g/t silver and 761 800 tonnes of mill ore grading 25.8 g/t gold and 1092 g/t silver (Wojdak, 2001). At Eskay Creek, stratiform massive sulphide mineralization occurs in a carbonaceous mudstone interval deposited in a submarine environment during Aalenian to Bajocian (Middle Jurassic) time (Roth *et. al.*, 1999). Mineralized mudstone is depositionally bound by subaqueous bimodal tholeiitic volcanic rocks composed of rhyolite in the upper footwall unit and massive and pillowed basalts stratigraphically lower in the hangingwall unit where they may be locally interlayered with mudstone. Roth and coworkers (1999) envisage that the Eskay Creek deposit formed during waning Hazelton arc volcanism that coincided in space and time with extensional rift tectonism localizing basin development, which consequently focused volcanic and subvolcanic intrusive rocks and metalliferous hydrothermal fluids. The Eskay Creek deposit exhibits many characteristics typical of massive sulphide deposits. However, unusually elevated antimony, mercury and arsenic, accompanying extremely high gold and silver contents are mineralogic features more commonly associated with epithermal mineralization. Such precious metal enriched massive sulphide deposits have been termed Eskay Creek-type or subaqueous hot spring gold-silver in British Columbia (Alldrick, 1995).

In the Bella Coola area, investigation of the Nifty prospect, a significant volcanic- associated stratiform sulphide-barite prospect, indicates that it possesses features that suggest metal deposition may be related to relatively low temperature hydrothermal fluids vented in a shallow water environment (Ray *et al.* 1998). The Nifty mineralization is positioned beneath a hanging wall succession composed of waterlain felsic tuffs overlain by basaltic tuffs and probable flows. Overall this succession has transitional tholeiitic to calcalkaline chemistry. Stratiform barite forms a series of discontinuous stratabound lenticles above lenticular pods containing galena, sphalerite and pyrite. The mineralization is weakly enriched in Ag, As, Sb and Hg suggesting a lower temperature fluid that reflects a more epithermal character; however, gold values are negligible (Ray, *et al.*, 1998). Below the mineralized zone, primary intermediate volcanic rocks comprising the footwall are extensively bleached and enriched in potassium, sodium and magnesium, and associated with ubiquitous disseminated pyrite. Late post-mineral dikes, of both felsic and mafic compositions, and calcalkaline affinity cut the hangingwall-footwall successions along a preferred east-northeast trend.

Within the area mapped, a rhyolitic unit of probable Aalenian to Bajocian age is believed to be the most prospective host rocks for volcanic-related massive sulphide mineralization. This assemblage consists of more than 1000 metres of resedimented syn-erupted fragmental and subordinate primary volcanic rocks showing evidence of subaqueous and periodic subaerial deposition. The Nifty occurrence is situated adjacent to several intersecting high-angle faults that form the southern margin of a distinctive rhyolitic assemblage. These structures evidently post date deposition of the rhyolite unit; and, they may have caused an unknown portion of this rhyolitic facies to be uplifted and subsequently eroded. Unlike other parts of this rhyolitic unit, however, semi-concordant alteration and sulphide-barite mineralization are evident only in the vicinity of Nifty. Elsewhere, scant mineralization is limited to disseminated pyrite associated with massive aphanitic rhyolites interpreted either as flows or subvolcanic intrusives.

CONCLUSIONS

The Hazelton Group in the Bella Coola area is composed of bimodal volcano-sedimentary rocks that represent deposition in both submarine and subaerial environments. Subaqueous rhyolite volcanic facies host the Nifty prospect, a key stratiform sulphide-barite occurrence, and is presumed to be the most prospective unit in the study area. Regionally, the bimodal volcanic rocks and interbedded fossiliferous sediments are tentatively Bajocian in age, but possibly as old as Toarcian. We believe this volcano-sedimentary succession has good potential for the discovery of other VMS prospects in the region. Despite the difficulties associated with of exploring in steep forested coastal terrain as in the Bella Coola region, the new mapping supplemented by regional stream sediment geochemistry programs jointly conducted by the federal and provincial surveys will better focus prospecting and exploration in the area.

ACKNOWLEDGMENTS

Mapping contributions by Sarah Gordee, Heather Sparks, Sara White, Edna Kaiser and Lori Snyder are greatly appreciated. We thank Terry Poulton and Jim Haggart of the Geological Survey of Canada for identifying new fossil collections and re-examining archived collections from the Bella Coola area. Gerry Ray has been an advocate for further mapping in the Bella Coola area and is acknowledged for sharing his views on mineral occurrences in the study area. Richard Lapointe and Rob Skelley of West Coast Helicopters provided safe, reliable air support for the mapping program. Gaylene Binns and David Flegel of the B.C. Ministry of Forests, and Dawn and Kim Meiers helped out with operational logistics. Editorial comments by Brian Grant and figures prepared by Verna Vilkos and Alexandra Shaw improved the paper.

REFERENCES

Alldrick, D.J. (1995): Shallow Subaqueous Hot Spring Au-Ag; *in* Selected British Columbia Mineral Deposit Profiles, Volume 1, D.V. Lefebure and G.E. Ray, Editors, *British Columbia Ministry of Energy and Mines*, Open File 1995-20. pages 55-57.

Andronicos, C., Hollister, L.S., Davidson, C. and Chardon, D. (1999): Kinematics and Tectonic Significance of Transpressive Structures Within the Coast Plutonic Complex, British Columbia; *Journal of Structural Geology*, Volume 21, pages 229-243.

Baer, A.J. (1973): Bella Coola-Laredo Sound Map-Areas, British Columbia; *Geological Survey of Canada*, Memoir 372, 122 pages.

Bellefontaine, K.A. and Alldrick, D.J. (1994): Mineral Potential of the Mid-Coast Area; *B.C. Ministry of Energy and Mines*, Open File 1994-17, 1:250 000 scale.

Bellefontaine, K.A. and Alldrick, D.J. (1995): Highlights of the Mid-Coast Mineral Potential Project (92F,G,H,J,L,M,N,N, 93D, 102P, 103A); *in* Geological Fieldwork 1994, *B.C. Ministry of Energy and Mines*, Paper 1995-1, pages 449-458.

Bevier, M.L. (1981): The Rainbow Range, British Columbia: a Miocene Peralkaline Shield Volcano; *Journal of Volcanology and Geothermal Research*, Volume 11, pages 225-251.

Boghossian, N.D. and Gehrels, G.E. (2000): Nd Isotopic Signature of Metasedimentary Pendants in the Coast Mountains Between Prince Rupert and Bella Coola, British Columbia; *in* Tectonics of the Coast Mountains, southeastern Alaska and British Columbia; H.H. Stowell and W.C. McClelland, Editors, *Geological Society of America*, Special Paper 343, pages 77-88.

Carter, N.C. (1981): Porphyry Copper and Molybdenum Deposits of West-Central British Columbia; *B.C. Ministry of Energy, Mines and Petroleum Resources*, Bulletin 64, 150 pages.

Dawson, G.M. (1878): Explorations in British Columbia, Chiefly in the Basins of the Blackwater, Salmon, and Nechako Rivers, and on Francois Lake; *Geological Survey of Canada*, Report on Progress 1876-77, pages 17-94.

Diakow, L.J., Panteleyev, A. and Schroeter, T.G. (1991): Jurassic Epithermal Deposits in the Toodoggone River Area, Northern British Columbia: Examples of Well-Preserved, Volcanic-Hosted, Precious Metal Mineralization; *Economic Geology*, Volume 86, Number 3, pages 529-554.

Diakow, L.J., Webster, I.C.L, Richards, T.A. and Tipper, H.W. (1997a): Geology of the Fawnie and Nechako Ranges, Southern Nechako Plateau, Central British Columbia (93F/2,3,6,7); *in* Interior Plateau Geoscience Project: Summary of Geological, Geochemical and Geophysical Studies, L.J Diakow, P. Metcalfe and J.M. Newell, Editors, *British Columbia Ministry of Energy and Mines*, Paper 1997-2, pages 7-30.

Diakow, L.J. and Levson, V.M. (1997b): Bedrock and Surficial Geology of the Southern Nechako Plateau, Central British Columbia (NTS 93F/2,3,6,7); *British Columbia Ministry of Energy and Mines*, Geoscience Map 1997-2, 1:100 000 scale.

Hrudey, M.G., Struik, L.C., Diakow, L.J., Mahoney, J.B., Woodsworth, G.J., Sparks, H.A., Kaiser, E.A. and Gleeson, T.P. (2002): Plutonic Rocks of the Eastern Bella Coola Map Area, Southwest British Columbia; *Geological Survey of Canada*, Current Research 2002-A.

Israel, S. and Kennedy, L. (2002): Reconnaissance of Structural Geology of the Atnarko Complex, Southern Tweedsmuir Park, British Columbia; *Geological Survey of Canada*, Current Research 2002-A.

Jackaman, W., Lett, R. and Fiske, P. (2002): National Geochemical Reconnaissance Surveys in the B.C. Cordillera to Target and Attract Mineral Exploration; Geological Fieldwork 2001, *B.C. Ministry of Energy and Mines,* Paper 2002-1, this volume.

MacDonald, A.J., Lewis, P.D., Thompson, J.F.H., Nadaraju, G., Bartsch, R.D., Bridge, D.J., Rhys, D.A., Roth, T., Kaip, A., Godwin, C.I. and Sinclair, A.J. (1996): Metallogeny of an Early to Middle Jurassic Arc, Iskut River Area, Northwestern British Columbia; *Economic Geology*, Volume 91, pages 1098-1114.

Mahoney, J.B., Struik, L.C., Diakow, L.J., Hrudey, M.G. and Woodsworth, G.J. (2002): Structural Geology of the Eastern Bella Coola Map Area, British Columbia; *Geological Survey of Canada*, Current Research 2002-A.

Massey, N.W.D., Alldrick, D.J. and Lefebure, D.V. (1999): Potential for Subaqueous Hot-spring (Eskay Creek) Deposits in British Columbia; *British Columbia Ministry of Energy and Mines*, Open File 1999-14, 1:2 000 000 scale.

Poulton, T.P. and Tipper, H.W. (1991): Aalenian Ammonites and Strata of Western Canada; *Geological Survey of Canada*, Bulletin 411, 71 pages.

Ray, G.E., Brown, J.A., Friedman, R.M. and Cornelius, S.B. (1998): Geology of the Nifty Zn-Pb-Ba Prospect, Bella Coola District, British Columbia; *in* Geological Fieldwork 1997, *B.C. Ministry of Energy and Mines*, Paper 1998-1, pages 20-1 to 20-28.

Roth, T., Thompson, J.F.H. and Barrett, T.J. (1999): The Precious Metal-Rich Eskay Creek Deposit, Northwestern British Columbia; *in* Volcanic-Associated Massive Sulphide Deposits: Processes and Examples in Modern and Ancient Settings, C.T. Barrie and M.D. Hannington, Editors, *Reviews in Economic Geology*, Volume 8, pages 357-373.

Rusmore, M.E. and Woodsworth, G.J. (1994): Evolution of the Eastern Waddington Thrust Belt and its Relation to the Mid-Cretaceous Coast Mountains Arc, Western British Columbia; *Tectonics*, Volume 13, pages 1052-1067.

Rusmore, M.E., Woodsworth, G.J. and Gehrels, G.E. (2000): Late Cretaceous Evolution of the Eastern Coast Mountains, Bella Coola, British Columbia; *in* Tectonics of the Coast Mountains, southeastern Alaska and British Columbia; H.H. Stowell and W.C. McClelland, Editors, *Geological Society of America*, Special Paper 343, pages 89-106.

Souther, J.G. (1977): Volcanism and Tectonic Environments in the Canadian Cordillera-A Second Look; *in* Volcanic Regimes in Canada, W.R.A. Barager, L.C. Coleman and J.M. Hall, Editors, *Geological Association of Canada*, Special Paper 16, pages 3-24.

Souther , J,G. (1986): The Western Anahim Belt, Rootzone of a Peralkaline Magma System; *Canadian Journal of Earth Sciences*, Volume 23, pages 895-908.

Souther, J.G. and Yorath, C.J. (1991): Neogene Assemblages, Chapter 10; *in* Geology of the Cordilleran Orogen in Canada, H. Gabrielse and C.J. Yorath, Editors, *Geological Survey of Canada*, Geology of Canada, Number 4, pages 373-401.

Stowell, H.H. and McClelland, W.C. (2000): Tectonics of the Coast Mountains, Southeastern Alaska and British Columbia; *Geological Society of America*, Special Paper 343, 289 pages.

Struik, L.C., Mahoney, J.B., Hrudey, M.G., Diakow, L.J., Woodsworth, G.J., Sparks, H.A. and Kaiser, E.A., Haggart, J. and Poulton, T. (2002): Early Cretaceous Stratigraphy and Tectonics of Eastern Bella Coola Map Area, Southwest British Columbia; *Geological Survey of Canada*, Current Research 2002-A.

Tipper, H.W. and Richards, T.A. (1976): Jurassic Stratigraphy and History of North-Central British Columbia; *Geological Survey of Canada*, Bulletin 270, 73 pages.

van der Heyden, P. (1990): Eastern Margin of the Coast Belt in West-central British Columbia; *Geological Survey of Canada*, Current Research, Part E, Paper 90-1E, pages171-182.

van der Heyden, P. (1991): Preliminary U-Pb Dates and Field Observations from the Eastern Coast Belt near 52°N, British Columbia; *Geological Survey of Canada*, Current Research, Part A, Paper 91-1A, pages 79-84.

Wojdak, P. (2001): Northwest Region; Exploration and Mining in British Columbia - 2000; *British Columbia Ministry of Energy and Mines*, pages 1-8.

Woodsworth, G.J. (1980): Geology of the Whitesail Lake (93E) Map Area, British Columbia; *Geological Survey of Canada*, Open File 708, 1:250 000 scale.

U-Pb Zircon and Titanite Dating in Support of British Columbia Geological Survey Regional Mapping Studies

By Richard M. Friedman and James K. Mortensen[1]

KEYWORDS: Geochronology, U-Pb, zircon, titanite.

INTRODUCTION

In this paper we report U-Pb zircon and titanite data and interpreted ages for sixteen rocks (Figure 1) sampled in support of regional mapping projects conducted by the British Columbia Geological Survey Branch during the mid- to late-1990s. Each sample is reported with geological context, interpretation of U-Pb data and significance of the date. The U-Pb results are also displayed on standard concordia plots (Figures 2, 3, 7 and 8) and compiled in a single table (Table 1). All aspects of sample preparation, clean laboratory work, and data acquisition, reduction and interpretation were carried out at the Geochronology Laboratory of the University of British Columbia following procedures outlined in Mortensen *et al*. (1995) and Friedman *et al*. (2001).

SAMPLE H97BC-43C: SNOWSHOE GROUP, RAMOS SUCCESSION

Geology

Sample H97BC-43c is a tuffaceous metasedimentary rock from the Ramos succession of the Snowshoe Group. The latter consists of fine to coarse siliciclastic, volcanic and carbonate rocks. The depositional age of the Ramos succession and the entire Snowshoe Group are poorly known. Although some workers have suggested lower to upper? Paleozoic ages for the Snowshoe Group, it was inferred by Struik (1988) to be Late Proterozoic in age. These rocks are part of the Barkerville Terrane, which is the northern continuation of the peri-cratonic Kootenay Terrane.

The sample locality lies near the east-verging Eureka thrust fault, which marks the western limit of the Snowshoe Group and juxtaposes this sequence against the late Paleozoic Crooked amphibolite and Mesozoic arc volcanic rocks of the Nicola Group. The rock was selected for U-Pb dating to determine the primary igneous age of its tuffaceous component, which would constrain the depositional age of the succession. The depositional age of this sample, together with that of a similar rock collected for dating from the Downie formation (H97BC-8, see below; also within the Snowshoe Group), would also test a hypothesis proposing that parts or all of the exposed Snowshoe stratigraphic sequence are overturned (Höy and Ferri, 1998).

Geochronology

This foliatied tuffaceous metasedimentary rock yielded abundant rounded and frosted or pitted zircons in a wide range of colours, interpreted to be detrital in origin. A small proportion of the recovered zircons were euhedral and thought to possibly comprise a primary igneous population from the tuffaceous component of the rock. Six single grain analyses of the most euhedral crystals gave nearly concordant to strongly discordant results (1-20% discordant), with Proterozoic and Archaen ^{207}Pb/^{206}Pb dates (Figure 2A; Table 1). These results are taken as strong evidence that the analysed euhedral zircons are also detrital in origin and do not reflect the depositional age of the tuffaceous component of this rock.

Significance

Dating of this sample did not yield an igneous age for the tuffaceous component of the rock and therefore does not provide information that can be used to confirm or refute the hypothesis proposing that much of the Snowshoe Group is overturned. The six analysed detrital zircons give ^{207}Pb/^{206}Pb dates that range from Paleoproterozoic to Neoarchean, consistent with derivation from North American cratonic sources.

SAMPLE H97BC-8: DOWNEY SUCCESSION, SNOWSHOE GROUP (NTS 93A/14)

Geology

Sample H97BC-8 is a tuffaceous metasedimentary rock from the Downey succession of the Snowshoe Group, which consists of fine to coarse siliciclastic, volcanic carbonate rocks. The Snowshoe Group comprises part of the Barkerville Terrane, a northern continuation of the peri-cratonic Kootenay Terrane. The Downey succession is composed of sandstone, phyllite, mafic metavolcanic rocks and limestone. This succession also hosts massive sulphide mineralization at the Ace property in the Little River area. Sample H97BC-8 comes from a highly strained zone and was interpreted as a metaclastic rock with a tuffaceous

[1]*The University of British Columbia*

component. The proximity of the sample to the Ace property suggests that its depositional age is broadly coeval with local massive sulfide mineralization.

Geochronology

This tuffaceous metasedimentary rock yielded only a trace of fine grained (<104 micrometre) rounded, frosted and pitted zircons possessing a variety colours and clarities, which have been interpreted to be detrital in origin. Four single grain analyses of the largest, best quality crystals gave slightly to strongly discordant results (4-19% discordant) with Neoproterozoic to Archaen ^{207}Pb/^{206}Pb dates (Figure 2B, Table 1). The youngest grain (B, ^{207}Pb/^{206}Pb date of 641 Ma) provides a maximum age for the deposition of this unit in the vicinity of the sample locality.

Significance

This sample did not yield primary igneous zircons that could be used to date the age of the tuffaceous component of the rock; detrital zircon ages are consistent with a North American cratonic source.

FFE99-11-2 AND FFE99-12-1: BIG CREEK GROUP (NTS: 94C/12 & 94D/09, RESPECTIVELY)

Geology

The Big Creek Group, which comprises the upper part of Cassiar Terrane in north-central British Columbia, is made up of fine grained dark grey to black clastic rocks with lesser sandstone, conglomerate, limestone and felsic volcanic rocks. Regionally, these rocks lie stratigraphically above platformal carbonates of the Ordovician to Middle Devonian Echo Lake and Otter Lakes groups. The lower part of the Big Creek Group is part of the Earn Assemblage, which was deposited during Cordilleran-wide subsidence of the Ancestral North American margin. (Ferri and Melville, 1994; Ferri, 2000; Ferri *et al*., 1993a, b; 2001).

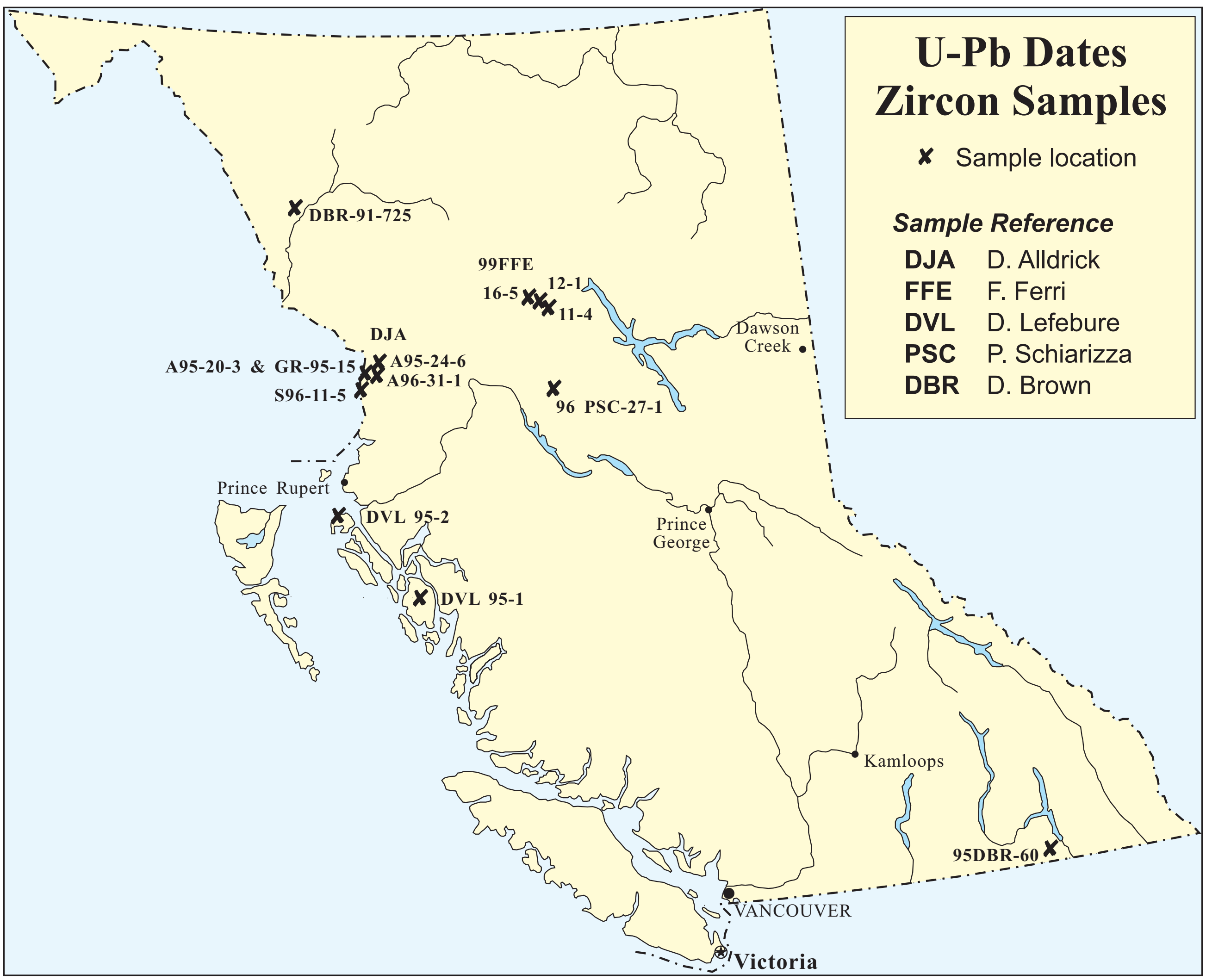

Figure 1. Map of British Columbia showing locations of dated samples.

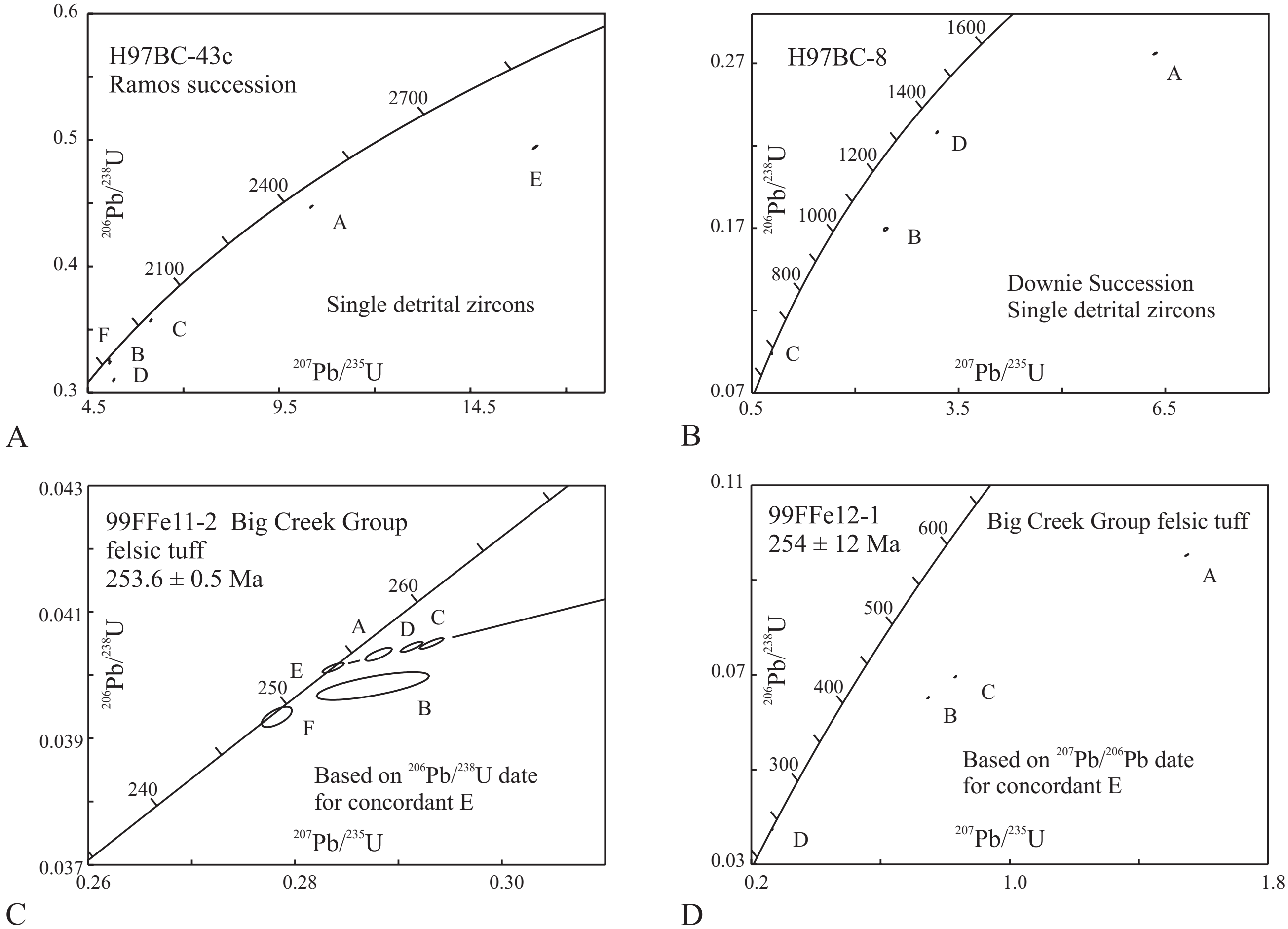

Figure 2. Standard concordia diagrams with error ellipses plotted at the 2-sigma level of uncertainty. *See* plots for sample numbers, names and dates, and text for details of interpretations.

Felsic tuffs within the upper part of the Big Creek Group were sampled for U-Pb dating at two localities near the headwaters of the Swannell River in the northern Lay Range (Fig. 1). Sample FFe99-11-2 consists of approximately 50 metres of light grey weathering, greenish grey, quartz-feldspar tuff to coarse lapilli tuff. The presence of dark grey argillaceous rip-ups indicates that it is conformable with underlying Big Creek Group sedimentary rocks. This tuff unit is sericitic and contains between 10 and 40 per cent plagioclase crystal fragments up to 5 millimetres in size. Quartz crystals are subordinate, comprising less than 10 per cent of the unit. Approximately 25 metres of dark grey argillite similar to that in the underlying Big Creek Group occurs stratigraphically above the felsic tuff. These are structurally succeeded by mafic volcanics of the Upper Mafic Tuff division of the Lay Range Assemblage, the latter having been emplaced into their present position along the east-verging Swannell Fault.

Sample FFe-99-12-1 comes from a 10 to 15 metre-thick unit of rusty to tan weathering, light to dark grey, quartz-feldspar sericitic tuff. Quartz and feldspar crystals are up to 5 millimetres in size and make up to 10 and 20 per cent of the unit, respectively. Dark grey argillaceous streaks are present within the tuffaceous horizon suggesting it is conformable with surrounding Big Creek rocks. Approximately 10 to 20 metres of black argillite lies stratigraphically above the northwest portion of the tuffaceous rocks. Finely laminated tuffs belonging to the Upper Mafic Tuff division of the Lay Range Assemblage sit structurally above this, in the hanging wall of the easterly-directed Swannell Fault. This felsic tuff unit can be traced southeastwards, where it is believed to be cut by the Swannell Fault; it is correlated with the tuff at locality FFe99-11-2 based on similar stratigraphic position, composition and age (*see* below).

Geochronology

Felsic tuff sample FFe99-11-2 yielded clear, pink, euhedral prismatic and rare slightly rounded grains. Six zircon fractions were analysed; the results of four of these plot as a co-linear array on the concordia plot in Figure 2C. A chord fit through these data yields an upper intercept of 2.5 ± 0.3 Ga (MSWD=0.56), which provides an estimate of the average age of inherited zircon in the analysed grains. An igneous age estimate of 253.6 ± 0.5 Ma is based on the $^{206}Pb/^{238}U$ date for concordant fraction E, which lies at the lower intercept of the chord. Fraction F is marginally concordant and is interpreted to have suffered minor Pb loss. Fraction B likely contains inherited zircon and underwent minor Pb loss.

A modest quantity of clear, pink, stubby to elongate, prismatic zircons were recovered from felsic tuff sample FFe99-12-1. Four fractions were analysed, three of which are strongly discordant (A, B and C). The $^{207}Pb/^{206}Pb$ date of 254±12 Ma for nearly concordant fraction D provides the best estimate for the igneous age of the rock. Upper intercept ages of about 1.9-2.7 Ga, based on regressions through the quasi-linear data array (chords ABCD, BCD and ABC; not plotted), suggest the presence of Late Archaen to Early Proterozoic old inherited zircon in three of the analysed fractions (Figure 2D, Table 1).

Significance

The Big Creek Group was previously considered to be Late Devonian to Early Permian in age on the basis of microfossils recovered from rocks that lie between Lay Range and the Omineca River. Dating of felsic tuff samples FFe99-11-2 and FFe99-12-1 extend the upper age range of the Big Creek Group to the Permo-Triassic boundary.

SAMPLE FFE99-16-5: LAY RANGE ASSEMBLAGE (NTS: 94D/09)

Geology

A felsic tuff from within the Upper Mafic Tuff division of the Lay Range Assemblage in the southern Wrede Range, approximately 1.5 kilometres north of Wrede Creek, was sampled for U-Pb dating (sample FFe99-16-5). The Lay Range Assemblage consists of two sequences: the Lower Sedimentary Division composed of peri-cratonic siliciclastics, carbonates and volcanic rocks of late Mississippian to middle Pennsylvanian age and overlying middle Pennsylvanian? to Permian arc-derived mafic volcanic rocks of the Upper Mafic Tuff division (Ferri, 2000a, b; Ferri *et al*., 1992a, b; 1993a, b; 2001a, b; Ferri, 1997). These rocks are basement to Mesozoic arc volcanic and sedimentary rocks of the Quesnel Terrane (Harper Ranch Subterrane).

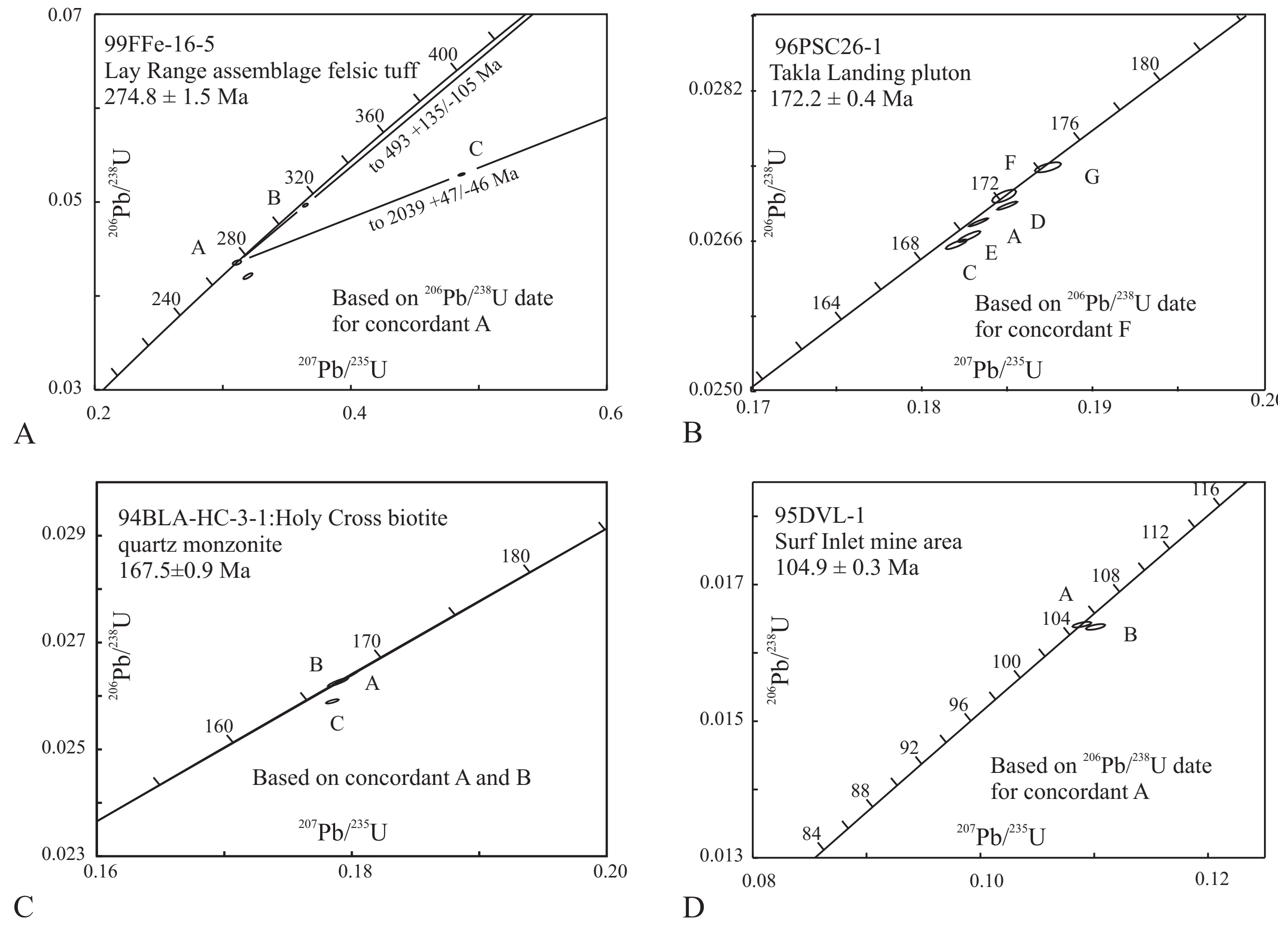

Figure 3. Standard concordia diagrams with error ellipse plotted at the 2-sigma level of uncertainty. See plots for sample numbers, names and dates, and text for details of interpretations.

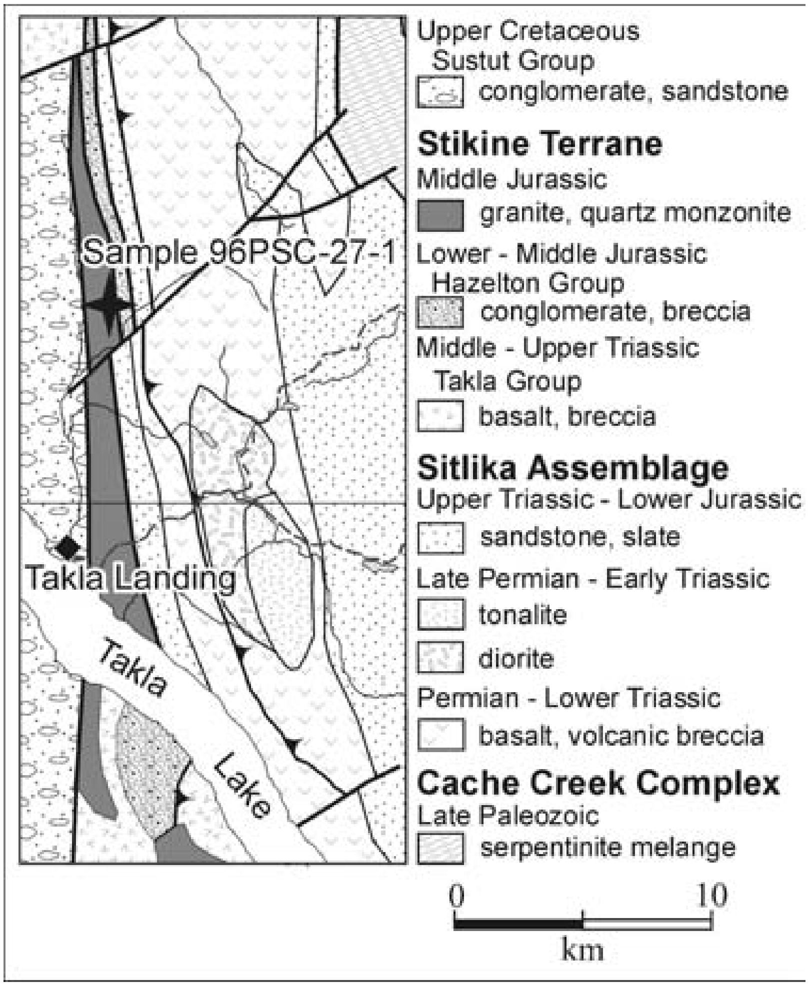

Figure 4. Geologic map showing the location of the Takla Landing pluton sample (96PSC-27-1).

The felsic tuff horizon is approximately 20 metres thick and occurs conformably within fine to coarse grained mafic and lapilli tuffs. The easterly verging Swannell Fault, which places Lay Range rocks above those of the Cassiar Terrane, occurs a few kilometres to the east. The felsic tuff unit is massive, rusty weathering, greenish-grey and distinguished by 10 to 15% quartz crystal fragments and polycrystalline quartz up to several millimetres in size. The remainder is composed of fine-grained muscovite and quartz imparting a sericitic schist or phyllite texture.

Geochronology

This felsic tuff yielded a very modest quantity of clear, pale tan euhedral to very slightly rounded prismatic zircons. The coarser zircons (>74 micrometres) were commonly broken euhedral grains. Due to the scarcity of material abrasion was not carried out. Grains were divided in four multi-grain fractions on the basis of size and shape (euhedral vs. slightly rounded). Three of the four fractions yielded discordant results, with an age estimate of 274.8 ± 1.5 Ma based on the $^{206}Pb/^{238}U$ date for concordant fraction A, which consisted of the coarsest euhedral grains. Two-point reference chords constructed through AB and AC suggest that inherited zircon components with a range of ages was present in the analysed grains (Figure 3A). Results for fraction D are consistent with the presence of minor inheritance and subsequent Pb loss.

Significance

This sample provides a new age constraints for the Upper Mafic Tuff division. The base of the sequence contains Early Permian radiolaria in the southern Lay Range immediately above middle Pennsylvanian limestone of the Lower Sedimentary division, suggesting a lower age limit. In northern Lay Range, felsic tuffs from the unit which was sampled for dating appear to interfinger with this limestone, indicating that they may be as old as middle Pennsylvanian (Ferri, 2000). Prior to the collection of this U-Pb geochronology sample, the age of the remaining section of Upper Mafic Tuff division volcanics was considered to be Permian based on a conodont collection from the Uslika Lake area (Ferri, 1996). The 274.8 ± 1.5 Ma age date demonstrates that this unit is as young as late Early Permian.

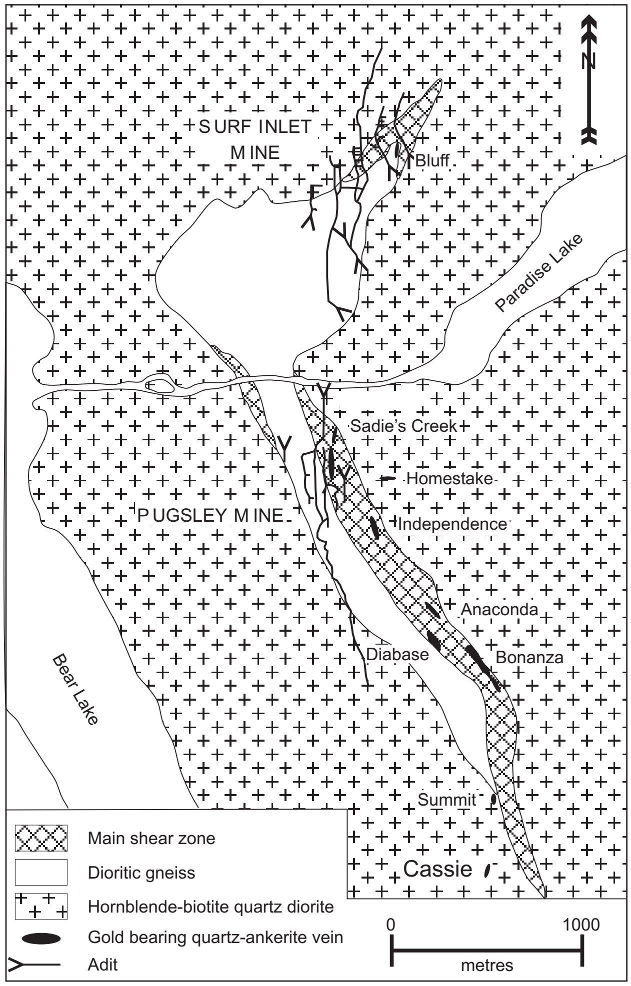

Figure 5. Geology of the Surf Inlet and Pugsley mines area. The zircon sample was collected from a drill hole collared near the Cassie showing at the southern end of the shear zone.

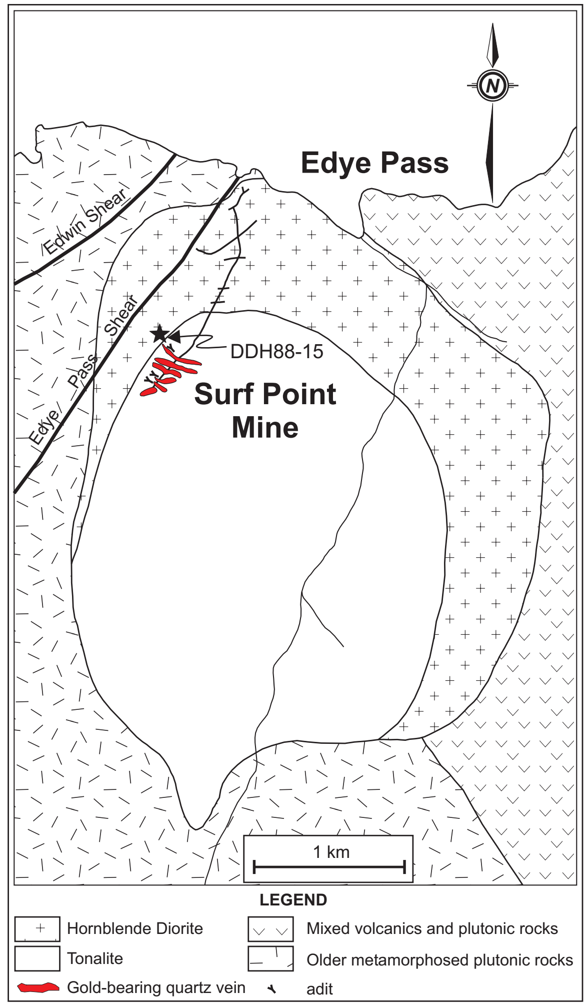

Figure 6. Geology of the Surf Point mine area on Porcher Island derived from Smith (1948). The zircon sample was collected from a drill hole collared just northwest of the mine.

SAMPLE 96PSC-27-1: TAKLA LANDING PLUTON (NTS: 93N/12)

The Takla Landing pluton is represented mainly by sparse exposures of pink-weathering monzogranite and quartz-feldspar porphyry that define a narrow lens that was traced for more than 20 kilometres northward from the northeast shore of Takla Lake (Figure 4), just east of the village of Takla Landing (Schiarizza and Payie, 1997; Schiarizza *et al*., 1998). This lens is juxtaposed against the Cretaceous Sustut Group to the west, across the Takla fault, and is faulted against slivers Triassic-Jurassic sedimentary rocks of the Sitlika assemblage and Stikine Terrane to the east (Schiarizza, 2000). Pink-weathering monzogranite that crops out on the south side of Takla Lake, directly south of Takla Landing, is presumed to be part of the same plutonic body. These rocks are also truncated by the Takla fault to the west, but their contact with Upper Triassic volcanic rocks of the Takla Group to the east is interpreted to be intrusive (Schiarizza *et al*., 2000).

Sample 96PSC-27-1 is a medium grained, isotropic monzongranite containing pink K-spar, saussuritized plagioclase, quartz and 5 - 10 percent chloritized mafic grains. It was collected from the north side of Takla Lake, about 11 km north of Takla Landing.

Geochronology

This sample yielded abundant, high quality, clear, pale yellow, euhedral, prismatic and tabular zircons and a small quantity of pale yellow titanite grains. Five of six analysed multigrain zircon fractions give slightly discordant results (Figure 3B), probably due to the presence of minor inherited components and subsequent Pb loss (especially for C and E). Thin tabular grains analysed in fraction F yielded concordant results. An age estimate of 172.2 ± 0.4 Ma is based on the $^{206}Pb/^{238}U$ date for this fraction.

Significance

At the time sample 96PSC-27-1 was collected it was not known if this lens of plutonic rocks along the Takla fault was derived from Stikine Terrane to the west or from the Permian-Jurassic Sitlika assemblage (western element of Cache Creek Terrane?) to the east (Schiarizza and Payie, 1997). Subsequent work, however, clearly showed that it is part of a plutonic suite within the eastern part of Stikine Terrane represented by several granite to diorite plutons which a belt that extends for more than 80 km southward to Babine Lake. MacIntyre *et al*. (2001) assigned these rocks to the Spike Peak intrusive suite. The date presented here is within the 179 to 166 Ma range of U-Pb and Ar-Ar isotopic dates presented by MacIntyre *et al*. (2001) for other plutons of the Spike Peak suite.

SAMPLE 94BLA-HC-3-1: HOLY CROSS PLUTON (NTS: 93/F15)

This pluton is located in the Intermontane Belt of central British Columbia, near the Eocene Holy Cross epithermal Au-Ag showing, about 33 km south of Fraser Lake (Lane and Schroeter, 1997). It is a poorly exposed biotite quartz monzonite body that cuts reworked andesite crystal tuffs that are mapped as Jurassic Hazelton Group and is nonconformably overlain by conglomerates of the Cretaceous Skeena Group and andesitic volcanic rocks that have given a K-Ar age of 70.3 Ma (Friedman *et al*., 2001). The age of mineralization at Holy Cross is considered to be Eocene or younger (Lane and Schroeter, 1997), because rocks that host the occurrence include rhyolites of the Eocene Ootsa Lake Group.

Geochronology

A small sample (~ 2 kg) of the Holy Cross pluton originally collected for K-Ar dating contained poor quality,

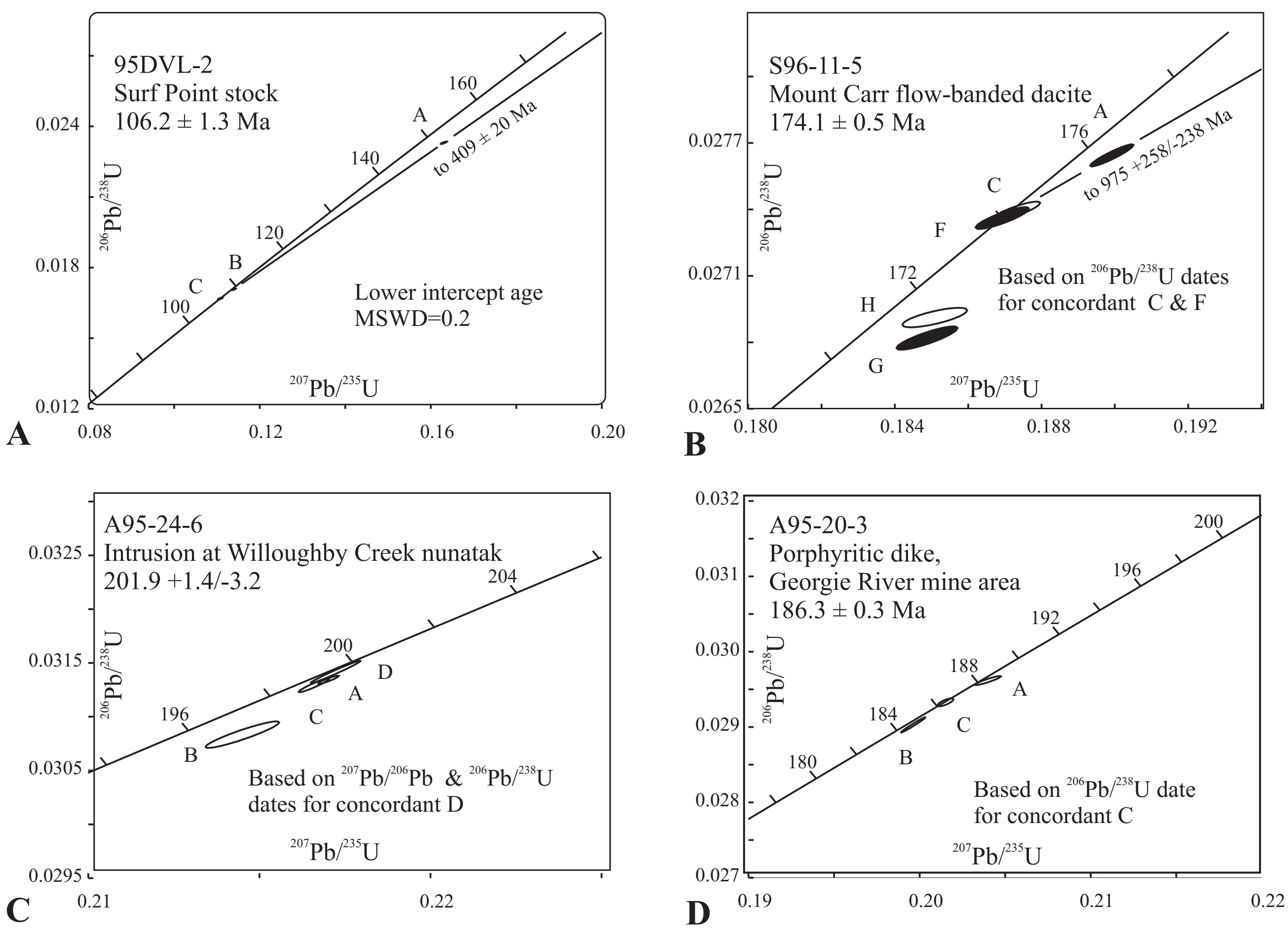

Figure 7. Standard concordia diagrams with error ellipse plotted at the 2-sigma level of uncertainty. See plots for sample numbers, names and dates, and text for details of interpretations.

chloritized biotite but a sufficient quantity of zircons for U-Pb dating. Zircons vary from very clear, pale pink, equant multifaceted and stubby prismatic grains to elongate prismatic and tabular crystals. Three multigrain zircon fractions were analysed and an igneous age estimate of 167.5±0.9 Ma is based on the median value and combined errors for $^{206}Pb/^{238}U$ dates determined for concordant and slightly overlapping A and B (Figure 3C). Discordant fraction C is interpreted to contain inherited zircon components and to have undergone minor Pb loss.

Significance

The Holy Cross pluton is associated with the Stikine terrane; the interpreted crystallization age of 167.5 ±0.9 Ma suggests it belongs to the Jurassic Stag Lake plutonic suite of Anderson *et al.* (1998) and/or the Spike Peak intrusive suite by MacIntyre *et al*. (2001).

SAMPLE DVL95-1: PRINCESS ROYAL ISLAND - SURF INLET MINE AREA (NTS: 103H/02)

Geology

The Surf Inlet and Pugsley mines (both covered by Minfile # - 103H027) are located 160 kilometres southeast of Prince Rupert on Princess Royal Island. The Surf Inlet mine operated from 1917 to 1926 and 1936 to 1942. Total production from the Surf Inlet and Pugsley mines was 918,129 tonnes grading 13.0 grams gold per tonne and 6.8 grams silver per tonne and 0.31% copper. During a regional reconnaissance of gold veins along the North Coast, a sample was collected to establish the age of the host intrusion for the gold-quartz veins. Sample DVL95-1 is a core sample taken from diamond drill hole SI88-1 from a depth of 27 to 70 feet. The drill hole collar is located near the Cassie showing (103H049), which is about 3700 metres south of the Surf Inlet mine (Carl von Einsiedel, personal communication; Figure 5).

Princess Royal Island is largely underlain by diorite to granodiorite intrusions. A large stock of hornblende-biotite quartz diorite outcrops in the centre of the island and hosts the gold mineralization at the Surf Inlet and Pugsley mines. In the area of the mines the stock is cut by westerly-dipping (30 to 60 degrees) shear zone that strikes northerly for more than 30 kilometres. The two mines and several other gold showings, including the Cassie lie along this shear zone (Figure 5). The shear zone has associated gneissic diorite, porphyroclastic diorite, dioritic gneiss, alteration zones and quartz veins. Quartz-ankerite veins with minor calcite generally are aligned parallel or subparallel to the shear zone. The ore-producing veins vary from 1 to 12 metres wide. They contain mainly pyrite with minor chalcopyrite, chalcocite, bornite, covellite, molybdenite and tellurides, but no visible gold.

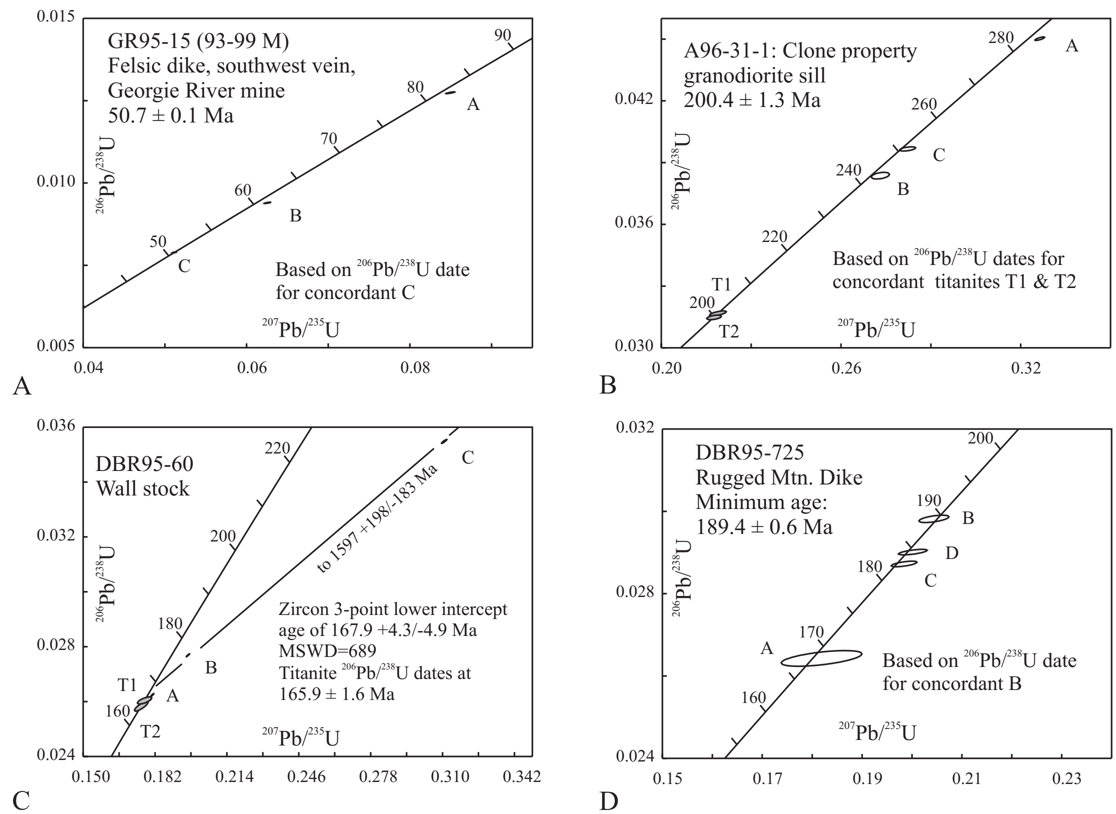

Figure 8. Standard concordia diagrams with error ellipse plotted at the 2-sigma level of uncertainty. See plots for sample numbers, names and dates, and text for details of interpretations. Error ellipses are shaded for titanites T1 and T2 in Figures 8B and 8C.

TABLE 1
U-PB ANALYTICAL DATA

Fraction[1]	Wt	U^2	Pb^{*3}	$^{206}Pb^4$	Pb^5	$^{208}Pb^3$	Isotopic ratios (±1-sigma, %)[6]			Apparent ages (±2-sigma, Ma)[6]		
	mg	ppm	ppm	^{204}Pb	pg	%	$^{206}Pb/^{238}U$	$^{207}Pb/^{235}U$	$^{207}Pb/^{206}Pb$	$^{206}Pb/^{238}U$	$^{207}Pb/^{235}U$	$^{207}Pb/^{206}Pb$
Ramos Succession, H97BC-43c: Single Detrital Zircon Grains; UTM: Zone 10, Easting 566797, Northing 5878051												
A c,N2,pp,b,p,1	0.041	77	38	22466	3.9	8.2	0.44728 (0.10)	10.342 (0.16)	0.16771 (0.07)	2383.1 (3.9)	2466 (2.9)	2534.9 (2.4)
B c,N2,pp,b,p,1	0.025	92	30	8717	5.3	5.2	0.32403 (0.12)	5.0765 (0.17)	0.11363 (0.08)	1809.4 (3.9)	1832.2 (3.0)	1858.2 (3.0)
C c,N2,pp,b,p,1	0.016	74	30	11384	2.3	15.7	0.35719 (0.11)	6.1488 (0.16)	0.12485 (0.07)	1968.8 (3.6)	1997.2 (2.8)	2026.7 (2.6)
D m,N2,co,p,1	0.009	53	19	2962	3.1	17.7	0.31033 (0.16)	5.1823 (0.21)	0.12112 (0.10)	1742.3 (4.8)	1849.7 (3.6)	1972.7 (3.5)
E m,N2,pp,b,p,1	0.011	195	122	13437	4.9	15.9	0.49441 (0.13)	16.191 (0.18)	0.23751 (0.07)	2589.7 (5.5)	2888.2 (3.4)	3103.4 (2.3)
F m,N2,co,p,1	0.009	44	14	2733	3.0	4.3	0.32628 (0.12)	5.0483 (0.18)	0.11222 (0.11)	1820.3 (3.9)	1827.5 (3.1)	1835.6 (3.9)
Downie Succession, H97BC-8: Single Detrital Zircon Grains; UTM: Zone 10, Easting 622600, Northing 5853200; NTS 93A/14												
A f,N2,pp,ov,1	0.005	118	37	839	12	10.7	0.27589 (0.11)	6.3524 (0.20)	0.16700 (0.12)	1570.6 (3.1)	2025.7 (3.5)	2527.8 (4.2)
B f,N2,pp,p,1	0.005	74	14	693	5.8	14.3	0.16941 (0.29)	2.4413 (0.60)	0.10451 (0.52)	1008.9 (1.3)	1254.9 (8.7)	1706 (19)
C f,N2,co,cl,t,1	0.005	232	21	1660	4.1	6.6	0.09385 (0.12)	0.7899 (0.24)	0.06105 (0.18)	578.3 (5.4)	591.1 (2.2)	640.9 (7.9)
D f,N2,pp,b,p,1	0.005	78	19	1125	5.0	9.4	0.22808 (0.14)	3.1877 (0.22)	0.10136 (0.14)	1324.4 (3.3)	1454.2 (3.4)	1649.2 (5.4)
99FFE11-2 Big Creek Group felsic tuff: 253.6±0.5 Ma; UTM: Zone 10, Easting 686921, Northing 6279179; NTS: 94C/12												
A cc,N2,p,1	0.020	364	15	2206	8.4	12	0.04033 (0.13)	0.2881 (0.22)	0.05181 (0.15)	254.9 (0.6)	257.0 (1.0)	276.9 (6.8)
B c,N2,p,7	0.030	696	29	224	255	13	0.03983 (0.28)	0.2875 (0.95)	0.05236 (0.77)	251.8 (1.4)	256.6 (4.3)	301 (35/36)
C c,N2,p,13	0.050	680	28	2328	38	11	0.04050 (0.11)	0.2932 (0.20)	0.05251 (0.12)	255.9 (0.5)	261.1 (0.9)	307.5 (5.3)
D m,M2,p,30	0.040	409	17	3023	14	12	0.04045 (0.10)	0.2913 (0.18)	0.05223 (0.11)	255.6 (0.5)	259.6 (0.8)	295.5 (5.1)
E f,N2,p,p,e	0.040	403	16	5614	7.1	10	0.04012 (0.10)	0.2837 (0.18)	0.05129 (0.12)	253.6 (0.5)	253.6 (0.8)	253.8 (5.3)
F ff,N2,p,p,e	0.015	331	13	5460	2.2	11	0.03934 (0.20)	0.2782 (0.27)	0.05130 (0.21)	248.7 (1.0)	249.3 (1.2)	254.2 (9.6)
99FFE12-1 Big Creek Group felsic tuff: 254±12 Ma; UTM: Zone 10, Easting 683447, Northing 6281436; NTS: 94D/09												
A m,N2,p,s,3	0.025	505	52	16530	4.5	12	0.09526 (0.10)	1.5484 (0.16)	0.11789 (0.07)	586.6 (1.1)	949.9 (1.9)	1924.5 (2.6)
B f,N2,p,s,15	0.035	385	26	4537	12	11	0.06518 (0.10)	0.7475 (0.17)	0.08319 (0.09)	407.0 (0.8)	566.8 (1.5)	1273.5 (3.4)
C f,N2,p,s,23	0.030	215	16	2354	12	15	0.06959 (0.10)	0.8318 (0.18)	0.08669 (0.11)	433.7 (0.8)	614.6 (1.6)	1353.6 (4.2)
D ff,N2,p,e,25	0.010	256	9.8	1336	4.5	11	0.03741 (0.15)	0.2646 (0.31)	0.05130 (0.26)	236.7 (0.7)	238.4 (1.3)	254 (12)
99FFE 16-5 Lay Range assemblage felsic tuff: UTM: Zone 10, Easting 679334, Northing 6283755; NTS: 94D/09												
A f,N2,p,na	0.015	113	5.4	1853	2.5	17	0.04356 (0.29)	0.3110 (0.54)	0.05179 (0.47)	274.8 (1.5)	275.0 (2.6)	276 (22)
B f,N2,b,na	0.015	176	9.7	3794	2.2	19	0.04967 (0.17)	0.3645 (0.27)	0.05322 (0.22)	312.5 (1.1)	315.6 (1.5)	338 (10)
C ff,N2,p,b,na	0.010	357	21	1840	6.5	16	0.05294 (0.13)	0.4864 (0.26)	0.06664 (0.19)	332.5 (0.9)	402.5 (1.7)	826.5 (7.9)
D ff,N2,p,na,3	0.007	154	7.1	755	3.8	17	0.04211 (0.38)	0.3196 (0.57)	0.05504 (0.35)	265.9 (2.0)	281.6 (2.8)	414 (15/16)
96PSC26-1 Takla Landing pluton: 172.2 ± 0.4 Ma; UTM: Zone 10, Easting 313970, Northing 6163330; NTS: 93N/12												
A cc,N2,p	0.072	639	18	10415	7.4	14.5	0.02680 (0.08)	0.1833 (0.15)	0.04961 (0.08)	170.5 (0.3)	170.9 (0.3)	176.7 (3.8)
C m,N2,p	0.058	638	18	6421	9.6	13.8	0.02657 (0.10)	0.1820 (0.17)	0.04969 (0.10)	169.0 (0.3)	169.8 (0.5)	180.7 (4.8)
D m,N2,p,s	0.032	715	20	7181	5.4	12.7	0.02698 (0.08)	0.1850 (0.16)	0.04974 (0.09)	171.6 (0.3)	172.4 (0.5)	182.7 (4.3)
E m,N2,p,s	0.030	647	18	5508	5.9	13.3	0.02665 (0.11)	0.1828 (0.18)	0.04974 (0.10)	169.5 (0.4)	170.4 (0.6)	183.0 (4.6)
F m,N2,t	0.020	487	14	4516	3.7	12.7	0.02708 (0.13)	0.1848 (0.19)	0.04950 (0.14)	172.2 (0.4)	172.2 (0.6)	171.7 (6.4)
G m,N2,t	0.018	528	15	3059	5.3	14	0.2739 (0.10)	0.1874 (0.21)	0.04963 (0.16)	174.2 (0.3)	174.4 (0.7)	177.5 (7.3)
94BLA-HC-3-1 Holy Cross biotite quartz monzonite: 167.5 ± 0.9 Ma; UTM: Zone 10, Easting 370615, Northing 5963860; NTS: 93/F15												
A cc,N2,eq	0.209	487	14	13360	12	15.2	0.02641 (0.11)	0.1801 (0.11)	0.04945 (0.03)	168.0 (0.4)	169.4 (0.4)	169.4 (1.5)
B cc,N2,eq	0.264	605	17	8570	29	16.6	0.02626 (0.15)	0.1789 (0.22)	0.04942 (0.11)	167.1 (0.5)	167.1 (0.7)	167.7 (5.0)
C ff,p,e,na	0.145	553	16	1642	76	18.1	0.02590 (0.08)	0.1785 (0.14)	0.04998 (0.09)	164.8 (0.3)	166.7 (0.4)	194.1 (4.4)
DVL-95-1 (DDH SI-88-1 -27'-70'): 104.9 ± 0.3 Ma; Princess Royal Island: Surf Inlet mine area; NTS: 103H/02												
A cc,N2,eq	0.087	152	2.5	1232	11	8.7	0.01641 (0.12)	0.1089 (0.38)	0.04813 (0.31)	104.9 (0.3)	105.0 (0.8)	106 (15)
B cc,N2,eq	0.094	134	2.2	1089	12	8.1	0.01638 (0.13)	0.1101 (0.38)	0.04876 (0.32)	104.7 (0.3)	106.1 (0.8)	136 (15)
DVL-95-2 (DDH PI-88-15-10'-30') Surf Point stock: 106.2 ± 1.3 Ma; Porcher Island: Surf Point - Edye Pass mine site; NTS: 103J/02												
A cc,N2,p,s	0.224	191	4.5	2448	25	11	0.02330 (0.11)	0.1631 (0.23)	0.05075 (0.14)	148.5 (0.3)	153.4 (0.6)	229.5 (6.3)
B c,N2,p,e,na	0.240	299	4.8	4443	17	7.1	0.01708 (0.10)	0.1139 (0.20)	0.04840 (0.12)	109.1 (0.2)	109.6 (0.4)	118.9 (5.6)
C c,N2,p,t,na	0.119	333	5.3	2576	16	6.1	0.01669 (0.12)	0.1108 (0.25)	0.04815 (0.17)	106.7 (0.3)	106.7 (0.5)	106.7 (8.0)

TABLE 1
U-PB ANALYTICAL DATA, CONTINUED

S96-11-5 Mount Carr flow-banded dacite: 174.1 ± 0.5 Ma; UTM: Zone 9, Easting 435567, Northing 6171200; NTS: 103O

A c,N5,p	0.027	2014	56	16726	5.6	10.9	0.02764 (0.09)	0.1899 (0.16)	0.04983 (0.08)	175.8 (0.3)	176.8 (0.3)	187.0 (3.7)
C m,N5,p,s	0.023	1499	41	3707	16	10.5	0.02739 (0.08)	0.1873 (0.18)	0.04959 (0.12)	174.2 (0.3)	174.3 (0.6)	175.9 (5.5)
F m,N5,p,e	0.035	831	23	2494	20	11	0.02736 (0.09)	0.1869 (0.19)	0.04955 (0.13)	174.0 (0.3)	174.0 (0.6)	174.0 (5.8)
G m,N5,p,s	0.026	1268	34	1480	38	10.4	0.02682 (0.10)	0.1849 (0.22)	0.05000 (0.15)	170.6 (0.3)	172.2 (0.7)	194.8 (7.0)
H f,N5,p,e	0.013	648	18	2246	6.4	11.4	0.02691 (0.08)	0.1851 (0.24)	0.04988 (0.19)	171.2 (0.3)	172.4 (0.8)	189.5 (8.7)

A95-24-6 Intrusion at Willoughby Creek nunatak: 201.9 +1.4/-3.2 Ma; UTM: Zone 9, Easting 463850, Northing 6201900; NTS:

A cc,N2,p,s,t	0.215	481	15	13985	14	6.6	0.03134 (0.06)	0.2170 (0.07)	0.05022 (0.03)	199.0 (0.2)	199.4 (0.2)	205.0 (1.2)
B cc,N2,p,s,t	0.130	421	12	18443	5.4	5.9	0.03083 (0.20)	0.2145 (0.25)	0.05046 (0.10)	195.8 (0.8)	197.3 (0.9)	216.0 (4.6)
C cc,N2,p,s,t	0.213	427	13	21186	8.4	5.8	0.03129 (0.10)	0.2166 (0.10)	0.05020 (0.03)	198.6 (0.4)	199.1 (0.4)	204.3 (1.5)
D cc,N2,p,s,t	0.328	506	15	28514	11	6.9	0.03142 (0.17)	0.2172 (0.17)	0.05015 (0.03)	199.4 (0.7)	199.6 (0.6)	201.9 (1.4)

A95-20-3 Porphyritic dike from Georgie River mine area: 186.3 ± 0.3 Ma; UTM: Zone 9, Easting 434720, Northing 618390; NTS 103O

A cc,N2,p	0.175	385	11	9643	13	7.5	0.02962 (0.10)	0.2040 (0.19)	0.04995 (0.10)	188.2 (0.4)	188.5 (0.6)	192.8 (4.7)
B cc,N2,p	0.371	419	12	16204	17	7.3	0.02903 (0.18)	0.1996 (0.18)	0.04987 (0.03)	184.5 (0.7)	184.8 (0.6)	189.2 (1.4)
C cc,N2,p	0.257	407	12	4557	42	7.7	0.02933 (0.09)	0.2015 (0.12)	0.04983 (0.07)	186.3 (0.3)	186.4 (0.4)	187.2 (3.5)

GR-95-15 (93-99 m) Felsic dike, Georgie River mine: 50.7 +/- 0.1 Ma; UTM: Zone 9, Easting 434295, Northing 6183685; NTS103O

A cc,N2,p,s,eq	0.201	205	2.6	911	37	8.2	0.01274 (0.11)	0.0849 (0.32)	0.04835 (0.23)	81.6 (0.2)	82.8 (0.5)	117 (11)
B cc,N2,p,s,eq	0.230	196	1.9	888	31	11.2	0.00940 (0.11)	0.0626 (0.33)	0.04829 (0.25)	60.3 (0.1)	61.6 (0.4)	113 (12)
C f,N2,p,e,na	0.088	354	2.9	1477	11	11.9	0.00789 (0.10)	0.0512 (0.28)	0.04703 (0.21)	50.7 (0.1)	50.6 (0.3)	51 (10)

A96-31-1 Clone property granodiorite sill: 200.4±1.3 Ma; UTM: Zone 9, Easting 453470, Northing 6185920; NTS: 103P/13

A c,N5,p,s	0.110	77	3.6	1256	19	13.6	0.04502 (0.10)	0.3264 (0.25)	0.05257 (0.18)	283.9 (0.5)	286.8 (1.2)	310.5 (8.3)
B c,N5,p,s	0.061	98	3.7	871	17	9.4	0.03837 (0.21)	0.2731 (0.56)	0.05163 (0.51)	242.7 (1.0)	245.2 (2.4)	269 (23/24)
C c,N5,p,s	0.082	84	3.2	817	21	5.6	0.03966 (0.13)	0.2822 (0.47)	0.05161 (0.42)	250.8 (0.6)	252.4 (2.1)	268 (19/20)
T1 cc,M20	0.360	162	7.5	268	468	38.4	0.03167 (0.19)	0.2189 (0.64)	0.05013 (0.53)	201.0 (0.7)	201.0 (0.7)	201 (24/25)
T2 cc,M20	0.430	184	8.5	395	419	37.9	0.03148 (0.18)	0.2176 (0.56)	0.05013 (0.50)	199.8 (0.7)	199.9 (2.0)	201 (23/24)

DBR95-60 Wall stock: 167.9 +4.3/-4.9 Ma; NTS: 082/02; UTM: Zone 11, Easting 503750,

A cc,N2,p,e,10	0.21	352	9	7801	16	6.8	0.02624 (0.11)	0.1807 (0.19)	0.04996 (0.10)	167.0 (0.4)	168.7 (0.69)	193.0 (4.8)
B c,N2,p,e,17	0.163	361	10	8757	12	8.9	0.02769 (0.09)	0.1966 (0.19)	0.05151 (0.10)	176.1 (0.3)	182.3 (0.6)	263.6 (4.6)
C m,N2,p,e	0.055	433	16	6241	8.5	10.8	0.03548 (0.10)	0.3107 (0.19)	0.06352 (0.10)	224.8 (0.4)	274.8 (0.9)	725.5 (4.4)
T1 cc,M5,b	1.29	199	5	241	188	5.3	0.02604 (0.25)	0.1773 (0.90)	0.04939 (0.75)	165.7 (0.8)	165.8 (2.8)	166 (35)
T2 cc,M5,b	1.31	216	5	250	198	4.6	0.02583 (0.35)	0.1759 (0.87)	0.04938 (0.61)	164.4 (1.1)	164.5 (2.6)	166 (29)

DBR91-725 Rugged Mountain dike: minimum age 189.4 ± 0.6 Ma; NTS: 104G/13; UTM: Zone 9, Easting 343550, Northing 6412100

A f,p,s,na	0.031	2206	67	107	1250	21.2	0.02643 (0.36)	0.1819 (2.22)	0.04991 (2.04)	168.2 (1.2)	169.7 (6.9)	191 (92/98)
B m,p,s	0.010	1319	46	524	46	23.2	0.02982 (0.15)	0.2044 (0.74)	0.04972 (0.66)	189.4 (0.6)	188.8 (2.5)	182 (31)
C m,p,s	0.010	993	34	474	40	25	0.02872 (0.12)	0.1984 (0.65)	0.05011 (0.58)	182.5 (0.4)	183.8 (2.2)	200 (27)
D m,p,s	0.010	2071	69	398	100	21	0.02901 (0.12)	0.2002 (0.72)	0.05004 (0.65)	184.4 (0.4)	185.3 (2.4)	197 (30)

[1] Upper case letter is fraction identifier; T1, T2, etc, for titanites. All zircon fractions air abraded; Grain size, intermediate dimension in micrometres: cc=>149, c=149-134, m=134-104, f=104-74, ff=<74; Magnetic codes: Franz magnetic separator sideslope at which grains are nonmagnetic (N) or Magnetic (M); e.g., N1=nonmagnetic at 1°; Field strength for all is 1.8A; Front slope for all is 20°; Grain codes: b= broken fragments, e=elongate, eq=equant multifaceted ,ov=ovoid; p=prismatic, s=stubby, t=tabular, ti=tips; Additional for detrital grains: colour: co=colourless; pp= pale pink; vp = vivid pink; py= pale yellow; tan = tan; clarity; cl = clear; tr = translucent; Numeral some fractions (listed last) gives number of grains dissolved.

[2] U blank correction of 1pg ± 20%; U fractionation corrections were measured for each run with a double ^{233}U-^{235}U spike (about 0.004/amu).

[3] Radiogenic Pb.

[4] Measured ratio corrected for spike and Pb fractionation of 0.0037-0.0043/amu ± 20% (Daly collector) and 0.0012/amu (Faraday collector), which were determined by repeated analysis of NBS Pb 981 standard throughout the course of this study.

[5] Total common Pb in analysis based on blank isotopic composition.

[6] Corrected for blank Pb (2-10 pg, zircon; 20 pg, titanite), U (1 pg, all) and common Pb concentrations based on Stacey and Kramers (1975) model Pb at the age or the $^{207}Pb/^{206}Pb$ age of the rock.

Sample DVL95-1 is a strongly foliated quartz diorite with a colour index of approximately 30%. It consists of plagioclase, amphibole, quartz, opaques and apatite with minor secondary biotite, epidote and chlorite.

Geochronology

Zircons separated from this sample are very clear and pale pink, with shapes that vary from multifaceted and equant to elongate prismatic. Results for multigrain fractions A and B, composed of strongly abraded equant multifaceted grains, are plotted on Figure 3D. A estimate of 104.9 ± 0.3 Ma for the crystallization age of this intrusion is based on the $^{206}Pb/^{238}U$ date for concordant fraction A. Discordant results for fraction B are interpreted to indicate the presence of inherited zircon and later Pb loss.

Significance

The host intrusion has been considered to be Jurassic to Upper Cretaceous (Harris and Gardiner, 1986) by analogy with other intrusions in the region. This zircon age date shows that the intrusion is 104.9 ± 0.3 Ma or mid-Cretaceous. M. McLaren collected a sample of sericite-altered diorite adjacent to a mineralized quartz vein from drill hole 81-2 (120 to 123.3 feet), and a whole K-Ar date of 80.1 ± 2.8 Ma was obtained by K. Dawson. These two dates therefore constrain the age of the mineralization to between a minimum age of ~80 Ma and a maximum age of ~105Ma.

Acknowledgment

The assistance of Art Freeze, Murray McLaren and Joe Shearer was much appreciated. Surf Inlet Mines Ltd. generously supplied data and permitted use of their camp.

SAMPLE DVL95-2: PORCHER ISLAND - SURF POINT STOCK (NTS: 103J/02)

Geology

The Surf Point (Minfile # 103J017) and Edye Pass (103J015) gold mines, located on the northwest corner of Porcher Island are 30 km south-southeast of Prince Rupert. The Surf Point gold mine produced an estimated 58,962 tonnes grading 10.3 grams gold per tonne and 3.43 grams silver per tonne between 1919 and 1938. Approximately 11,700 tonnes of similar grade ore was mined from the Edye Pass mine.

Sample DVL95-2 consists of core taken from diamond drill hole PI-88-15 from a depth of 10 to 30 feet. The drill collar is located approximately 1 kilometre inland from Edye Pass within the Surf Point stock (Figure 6). The Surf Point stock has a core of light coloured, biotite hornblende tonalite surrounded by a border phase of foliated hornblende quartz diorite (Smith, 1948). In drill core contacts between the two phases are sharp and do not exhibit chilled margins, although distinction of the two phases can be difficult at times. The stock intrudes gneissic diorite with associated pegmatite dikes and agmatite and mixed weakly metamorphosed volcanics and intrusive rocks. Andesite porphyry and basaltic dykes cut the stock.

Gold occurs in mesothermal quartz veins and veinlets throughout the general area, however, ore has only been mined from veins hosted by the tonalite core of the Surf Point stock. These veins trend 070 degrees to 090 degrees and generally dip 60 to 90 degrees north. Individual veins are less than 120 metres in strike length.

The pyritic quartz veins contain lesser amounts of chalcopyrite, sericite, ankerite, calcite and chlorite. Microscopic tetrahedrite with associated free gold has been identified. Individual veins vary from hairline fracture fillings to veins up to several metres in width and "silicified zones" up to 6 metres wide were mined in some cases.

Geochronology

Zircons separated from this sample are clear, colourless, stubby to very elongate prisms and thin tabular grains. The results of three analysed multigrain fractions plot as a co-linear array. A chord fit through these data yields a lower intercept of 106.2 ± 1.3 Ma (Figure 7A), which is interpreted as the best estimate for the crystallization age of the Surf point stock. Results for fraction C, composed of unabraded tabular grains, plot on concordia within error of the lower intercept age. Older, discordant results for strongly abraded stubby prisms of fraction A indicate the presence of inherited zircon. An upper intercept age of 409 ± 20 Ma provides an estimate of the average age of inheritance in the analysed grains. This age is characteristic of Alexander Terrane basement (Gehrels and Saleeby, 1987).

Significance

The sample comes from the northwestern part of the Surf Point stock. It is a fine-grained, equigranular biotite hornblende quartz diorite with a colour index of approximately 40. At least some of the biotite along with epidote is seen to replace the hornblende. Based on its lack of foliation, the sample is interpreted to represent the core tonalite phase of the intrusion. However, the collar of the drill hole is just within the foliated horneblende quartz diorite based on existing maps.

The intrusion was previously believed to be either Cretaceous or Tertiary in age (Smith, 1948). This age date of 106.2 ± 1.3 Ma shows the host intrusion is mid-Cretaceous and provides an upper age constraint on the age of the gold mineralization. Given the spatial relationship of the gold mineralization with Cretaceous age stocks at both Surf Point and Surf Inlet and the Cretaceous age of gold occurrences associated at other gold occurrences, such as Bralorne and Surf Inlet, the Surf Point gold mineralization is most likely Cretaceous age as well.

Acknowledgment

Cathedral Gold Corporation provided logistical support for two field visits and geologist Allan Taylor graciously shared his knowledge of the area.

SAMPLE S96-11-5: MOUNT CARR FLOW-BANDED DACITE (NTS: 103O)

Geology

Flow-banded dacite was sampled (A96-11-5) in the Carr Ridge area, a chain of peaks strung out south of the mouth of the Georgie River in northwestern B.C., in the Stewart area. The northernmost peak on this chain is Mount Carr, which has a ring-like summit. The sample was collected on the southern part of the ridgecrest, just 200 metres west of the southernmost, and highest, point on the rim (TRIM map sheet 103O-070).

The southern half of the summit Mount Carr, and its southern slopes, are composed of a thick (1200 metre) succession of dacite to rhyodacite, which is exposed over a strike length of 4.5 kilometres. These rocks display a variety of textures ranging from flow banding, to fragmental rocks (tuff breccias to lapilli tuffs) to massive felsite. These rocks are variably pyritic ranging up to 10% fine disseminated pyrite. To the north, adjacent black fine-grained metasedimentary rocks are weakly pyritic. To the south, adjacent strata is obscured by Eocene intrusions of the Coast Range batholith.

Due to the high elevation and steep terrain of this peak, these pyritic strata are well exposed and extremely gossanous. Mount Carr is the site of the strongest iron oxide anomaly detected by the LandSat thematic mapper in the Stewart region.

The felsic volcanic textures, lithological associations and widespread pyrite content are similar to features near the Eskay Creek gold-silver mine to the north. There was no clear evidence to indicate whether felsic strata at Mount Carr are deposited in a subaerial or subaqueous setting. This is an important distinction; subaqueous settings are prospective for precious metal enriched volcanogenic massive sulphide deposits (Eskay Creek mine), and subaerial settings are prospective for subvolcanic epithermal and porphyry-style deposits (Premier mine and Sulphurets camp).

Geochronology

A small quantity of clear, colourless, stubby to elongate, prismatic zircons were recovered from this rock. Five multi-grain fractions were analysed. An age estimate of 174.1 ± 0.5 Ma is based on concordant and overlapping results for two fractions composed of elongate prisms. Three fractions of stubby prisms that give discordant results suggest the presence of inherited zircon and two of these (G and H) have likely also undergone subsequent Pb loss. A three point chord through fractions A, C and F with an upper intercept of 975 +258/-238 Ma provides an estimate of the average age of inherited components in the grains analysed in fraction A (Figure 7B).

Significance

This date correlates well with published ages for the host-rock strata at the Eskay Creek mine and hanging wall strata in the Sulphurets camp (Childe, 1996, 1997). Recent GSC research has corroborated these results with a U-Pb zircon age of ca. 176 Ma collected from a site 750 metres northwest of the BCGS sample site (Evenchick *et al*., 1999). The striking gossans along the ridgecrest of Mount Carr has been repeatedly sampled for assay. Results have been only weakly anomalous. However, the steep forested flanks of Mount Carr where most of the 4500-metre strike length of the unit is exposed have not yet been prospected. The Mount Carr area merits thorough prospecting, bearing in mind that the Eskay Creek ores are not localized in the pyritic dacites and rhyolites of the mine sequence, but in adjacent black mudstone units. Stream sediment geochemistry of the many creeks draining of Mount Carr would be useful reconnaissance tool.

SAMPLE A95-24-6: INTRUSION AT WILLOUGHBY CREEK NUNATAK (NTS: 103P/13,14)

Geology

The outcrop area is mapped as intrusive rock of the Texas Creek plutonic suite, which is locally termed the “Goldslide Intrusions” after a prominent stock at the Red Mountain property to the west. The rock is fine to medium grained porphyritic granodiorite with hornblende plus feldspar phenocrysts. Hornblende phenocrysts range up to 6 millimetres across and feldspars up to 1.2 centimetres long. Moderately aligned phenocrysts indicate that the rock is weakly flow-foliated or else tectonically foliated. This sample was collected on the Willoughby Creek property, on the summit of the small peak on the Wilby Zone nunatak. The sample site is just southwest of the Wilby Zone, the North Zone and the North-North Zone (*see* Figure 7 in Alldrick *et al*., 1996 and Gabites *et al*., 1996).

Geochronology

Zircons separated from this felsic porphyry sample are clear, pale pink, stubby prismatic and thick tabular grains with multifaceted terminations. Results for three of four analysed multi-grain fractions composed of strongly abraded, relatively coarse zircons are marginally concordant to slightly discordant and lie in a cluster near concordia at ca. 198-200 Ma (Figure 7C). A crystallization age estimate of 201.9 +1.4/-3.2 Ma is based Pb/U and Pb/Pb dates for marginally concordant fraction D. This fraction is interpreted to have undergone minor Pb loss; the other three are likely to contain traces of inherited zircon and to have also undergone minor Pb loss.

Significance

This Late Triassic-Early Jurassic pluton is probably coeval and cogenetic with the several adjacent mineral prospects. These showings are good examples of the style of intrusion-related gold deposits commonly associated with Early Jurassic plutons throughout the Stewart-Iskut area.

SAMPLE A95-20-3: PORPHYRITIC DIKE FROM GEORGIE RIVER MINE AREA (NTS: 103O)

Geology

The sampled rock is a dike of hornblende-feldspar porphyritic granodiorite identical to the Premier Porphyry dikes of the Early Jurassic Texas Creek plutonic suite in the Stewart mining camp to the north. This medium grained dike is about 15 metres wide and shows chilled margins. It is one of a set of parallel dikes that transect this part of the Georgie River mine property. These dikes are overprinted by the alteration and mineralization of the Southwest Vein, the main mineralized structure at the Georgie River mine. The sample was collected in an area of small knobby hilltops near the Pond Vein, towards the north end of the Georgie River mine property.

Geochronology

Zircons separated from this felsic porphyry sample are clear, pale pink, stubby to elongate multifaceted prismatic grains. Results for three multi-grain fractions of strongly abraded, relatively coarse zircons plot on or near concordia between 184 and 189 Ma (Figure 7D). A crystallization age estimate of 186.3 ± 0.3 Ma is based on the $^{206}Pb/^{238}U$ date for concordant fraction C. Slightly discordant fraction A appears to contain minor inherited zircon and grains in discordant B have probably undergone minor Pb loss.

Significance

The Early Jurassic age of this dike constrains the age of the pyroxene porphyritic basalt flows and interlayered sedimentary rocks cut by the dikes, which must predate these Premier Porphyry dikes. The date also constrains the age of the Southwest Vein, which must postdate the age of this dike (Alldrick *et al*., 1996; Gabites *et al*., 1996).

SAMPLE GR-95-15-93/99: FELSIC DIKE, SOUTHWEST VEIN, GEORGIE RIVER MINE (NTS: 103O)

Geology

The dike rock is fresh, equigranular, unfoliated light grey biotite-hornblende granite. The rock hosts rare xenoliths. This is one of the "Tertiary biotite granodiorite dikes" interpreted to be penecontemporaneous with the main north-trending vein set on the mine property (Alldrick *et al*., 1996, p.105). Dike rock was collected from a diamond drillhole on the Georgie River mine property. DDH 95-15 was sampled from 93 to 95 metres depth. The drillhole intersects the Southwest Vein (see sample site plotted in Figure 6 in Alldrick *et al*., 1996). Lead isotope data from a sample collected from this same vein is reported in Gabites *et al*. (1996)

Geochronology

Two fractions of strongly abraded, relatively coarse-grained zircon, and one fraction of slightly finer, unabraded zircon were analysed. The unabraded fraction (C) is concordant with a $^{206}Pb/^{238}U$ date of 50.7 ± 0.1 Ma, which is taken as a good estimate for the crystallization age of the rock (Figure 8A). The other fractions give somewhat older Pb/U and Pb/Pb ages, indicating the presence of a minor inherited zircon component. Because the data form a non-linear array an upper intercept age was not calculated.

Significance

This mid-Eocene date confirms a Tertiary age for these dikes, which are associated with the north-trending veins on the property. Together with the previously reported lead isotope data from these veins, it supports the interpretation of Tertiary mineralization in the north-trending vein set on the Georgie River mine property. This age contrasts sharply with the Early Jurassic age determined for the east trending veins set on the property, such as the Granodiorite and Pond Veins. These latter veins are probably contemporaneous with the intrusion of the Early Jurassic Premier porphyry dikes reported for the preceding sample.

SAMPLE A96-31-1: CLONE PROPERTY GRANODIORITE SILL (NTS: 103P/13)

Geology

The Clone prospect is characterized by gold-cobalt rich shear zone-hosted mineralization within a mixed volcano-sedimentary succession of Mesozoic age. The sampled rock unit is a sill that cuts strongly hematitic volcaniclastic (epiclastic?) strata near the main mineralized shear zone on the Clone property. Small apophyses from this sill extend out into the enclosing country rock strata of alternating mafic flows, intermediate tuffs and epiclastic sedimentary rocks. The rock is massive to weakly foliated, fine-grained, slightly porphyritic, hornblende granodiorite.

Geochronology

Good quality zircon and titanite were recovered from this sample. Three analysed multi-grain zircon fractions consisting of clear, very pale yellow, stubby prismatic grains contain significant inherited zircon, and were not useful in determining the precise age of this rock. An age estimate of 200.4 ± 1.3 Ma is based on the results for two concordant titanite analyses (Figure 8B). Given the high closure temperature for titanite (greater than 650° C; Frost *et al*., 2000) and the upper crustal emplacement level of the sill, this titanite cooling age can also be regarded as a magmatic age.

Significance

The interpreted age of this sill constrains the minimum age of host-rock strata to Late Triassic. The adjacent shear-hosted gold-cobalt mineralization cuts across the same strata. The mineralized shear zone strikes roughly parallel to the dated sill and may be the same age or younger than the dated intrusion.

SAMPLE 95DBR-60: WALL STOCK (NTS: 082/02)

Geology

The Wall Stock is a biotite hornblende epidote granodiorite intrusion that was emplaced into Proterozoic sedimentary rocks of the Purcell Supergroup in southeastern British Columbia.

Geochronology

This sample of biotite hornblende epidote granodiorite from the Wall stock yielded clear, pale pink, stubby to elongate prismatic zircons and pale yellow, clear to slightly cloudy titanites. The results of three analysed multigrain zircon fractions plot as a quasi-linear array, due to the presence of varying amounts and to a lesser extent variable ages of inherited zircon (Figure 8C). A lower intercept age of 167.9 +4.3/-4.9 Ma is statistically identical to the median $^{206}Pb/^{238}U$ date and combined errors for titanites T1 and T2, 165.9 ± 1.6 Ma. We quote the former value as a conservative age estimate for the Wall Stock. An upper intercept 1597 +198/-183 Ma provides an estimate for the average age of inherited zircon in the analysed grains.

Significance

The interpreted crystallization age of 167.0 +4.3/-4.9 Ma for the Wall Stock confirms that this intrusion is correlative with other bodies of the Nelson suite (Woodsworth *et al*., 1991).

DBR-91-725: RUGGED MOUNTAIN DIKE (NTS: 104G/13)

Geology

A suite of alkaline dikes crop out in the Telegraph Creek map area in northwestern British Columbia (Figure 1; also see Brown *et al*., 1996, Figure 3-4, p. 59). They are spatially associated with Early Jurassic Rugged Mountain pluton, a zoned alkaline body that intrudes Triassic Stuhini Group volcanic rocks of the Stikine terrane. Dikes of the Rugged Mountain swarm are texturally trachytic to subtrachytic and contain potassium feldspar or albite pheoncrysts. A potassium feldspar megacrystic dike from the Rugged Mountain swarm was sampled for U-Pb dating (Brown *et al*., 1996).

Geochronology

A very small quantity of turbid, fractured, subhedral to euhedral, stubby, prismatic zircons were recovered from this sample. The results of four multi-grain zircon fractions plot on concordia between about 167 Ma and 190 Ma with no mutual overlap (Figure 8D). All of the fractions have high U concentrations (~1000-2200 ppm U) and the spread of data is likely due to Pb loss, as there is no visible or analytical evidence of inherited zircon in these grains. Fraction B, which was composed of the coarsest analysed grains, gives the oldest results. The $^{206}Pb/^{238}U$ date of 189.4 ± 0.6 Ma for fraction B is interpreted as a minimum age for the crystallization of the dike. The true age is probably several million years older, as it is likely that these poor quality, high U grains experienced at least some post-crystallization Pb-loss.

Significance

An interpreted minimum crystallization age of 189.4 ± 0.6 Ma for the Rugged Mountain dike and by extension, the swarm as a whole, suggests a possible temporal link with the Early Jurassic Texas Creek plutonic suite or the Early Jurassic-Late Triassic Copper Mountain plutonic suite. The minimum age for the dike is slightly younger than an ^{39}Ar-^{40}Ar plateau date of 195±3 Ma for the spatially associated Rugged Mountain pluton, which has been correlated with the latter suite (Brown *et al*., 1996).

ACKNOWLEDGMENTS

The authors gratefully acknowledge the following people for their help with this study and with the preparation of this report: D. Alldrick, D. Brown, F. Ferri, M. Fournier, J. Gabites, J. Holland, T. Höy, D. Lefebure, B. Lane and P. Schiarizza.

REFERENCES

Alldrick, D.J., Mawani, Z.M.S., Mortensen, J.K. and Childe, F. (1996): Mineral Deposit Studies in the Stewart District (NTS 103O/P and 104A/B); *B.C. Ministry of Employment and Investment*, Exploration in BC - 1995, p.89-109.

Anderson, R.G., Whalen, J.B., Struik, L.C., and Villeneuve, M.E. (1998): Mesozoic to Tertiary Volcanism and Plutonism in Southern Nechako NATMAP Area: Part 2. Triassic to Eocene composite intrusions and molybdenum metallogeny: the Endako Batholith redefined; *in* L.C. Struik and D.G. MacIntyre, editors, New Geological Constraints on Mesozoic to Tertiary Metallogenesis and on Mineral Exploration in central British Columbia: Nechako NATMAP Project; *Geological Association of Canada, Cordilleran Section*, March 27, 1998, Short Course Notes, 19 pages.

Brown, D.A., Gunning, M.H. and Greig, C.J. (1998): The Stikine Project: Geology of the western Telegraph Creek map area, northwestern British Columbia (NTS 104G/5,6, 11W, 12 and 13); *British Columbia Ministry of Employment and Investment*, Bulletin 95, 175 p.

Childe, F.C. (1996): U-Pb Geochronology and Nd and Pb Isotope Characteristics of the Au-Ag-Rich Eskay Creek Volcanogenic Massive Sulfide Deposit, British Columbia; *Economic Geology*, v. 91, p. 1209-1224.

Childe, F.C. (1997): Timing and tectonic setting of volcanogenic massive sulphide deposits in British Columbia; constraints from U-Pb geochronology, radiogenic isotopes, and geochemistry; Ph.D. thesis, *University of British Columbia*, Vancouver, BC, Canada. 325 pages.

Evenchick, C.A., Snyder, L.D. and McNicoll, V.J. (1999): Geology of the Hastings Arm West Half (103P/12W), British Columbia; *Geological Survey of Canada*, Open File 2996, scale 1:50,000.

Ferri, F. (1997): Nina Creek Group and Lay Range Assemblage, North-central British Columbia: Remnants of Late Paleozoic Oceanic and Arc Terranes; *Canadian Journal of Earth Sciences*, Volume 34, pages 854-874.

Ferri, F. (2000): Devono-Mississippian Felsic Volcanism Along the Western Edge of the Cassiar Terrane, North-Central British Columbia; *in* Geologic Fieldwork, 1999; *B.C. Ministry of Energy and Mines*, Paper 2000-1, pages 127-146.

Ferri, F., Dudka, S., Rees, C and Willson, M. (1992a): Geology of the Uslika Lake Area, British Columbia (94C/3,4 and 5); *B.C. Ministry of Energy, Mines and Petroleum Resources*, Open File 1992-11.

Ferri, F., Dudka, S., and Rees, C. (1992b): Geology of the Uslika Lake Area, Northern Quesnel Trough, B.C. (94C/3,4 and 5); *in* Geological Fieldwork 1991, *B.C. Ministry of Energy, Mines and Petroleum Resources*, Paper 1992-1, pages 127-146.

Ferri, F., Dudka, S., Rees, C., and Meldrum, D.G. (1993a): Preliminary Geology of the Aiken Lake and Osilinka River areas, British Columbia (94C/2, 3, 5, 6 and 12); *B.C. Ministry of Energy, Mines and Petroleum Resources,* Open File 1993-2.

Ferri, F., Dudka, S., Rees, C., and Meldrum, D.G. (1993b): Geology of the Aiken Lake and Osilinka River areas, Northern Quesnel Trough (94C/2, 3, 5, 6 and 12); *B.C. Ministry of Energy, Mines and Petroleum Resources,* 1992, Paper 1993-1, pages 109-134.

Ferri, F., Dudka, S., Rees C., Meldrum, D. and Willson, M. (2001): Geology of the Uslika Lake Area, North-Central British Columbia (NTS 94C/2,3,4); *B.C. Ministry of Energy and Mines*, Geoscience Map 2001-4.

Ferri, F., Dudka, S., Rees C. and Meldrum (2001): Geology of the Aiken Lake Area, North-Central British Columbia (NTS 94C/5,6,12); *B.C. Ministry of Energy and Mines*, Geoscience Map 2001-10.

Ferri, F., and Melville, D.M. (1994): Bedrock Geology of the Germansen Landing - Manson Creek Area, British Columbia (93N/9, 10, 15; 94C/2); *B.C. Ministry of Energy, Mines and Petroleum Resources*, Bulletin 91.

Friedman, R.M., Diakow, L.J., Lane R.A. and Mortensen, J.K. (2001): New U-Pb age constraints on latest Cretaceous magmatism and associated mineralization in the Fawnie Range, Nechako Plateau, central British Columbi; *Canadian Journal of Earth Sciences,* Volume 38, pages 619-637.

Frost, B.R., Chamberlain, B.R., and Schumacher, Frost, J.C. (2000): Sphene (titanite): phase relations and role as a geochronometer; *Chemical Geology,* v. 172, p. 131–148.

Gabites, J.E., Mortensen, J.K. and Alldrick, D.J. (1996): Lead Isotope Data from Mineral Prospects in the Cambria Icefield Area, Stewart Mining District (NTS 103O/P and 104A/B); *BC Ministry of Energy, Mines and Petroleum Resources*, Exploration in BC - 1995, p.111-115.

Gehrels, G.E., and Saleeby, J.B. (1987): Geologic Framework, tectonic evolution, and displacement history of the Alexander terrane; *Tectonics*, v. 6, p. 151-173.

Höy, T. and Ferri, F. (1998): Stratabound base metal deposits of the Barkerville Subterrane, central British Columbia (093A/NW); *in* Geological Fieldwork 1997, *British Columbia Ministry of Employment and Investment*, Paper 1998-1, pages 13-1 – 13-12.

Lane, R.A. and Schroeter, T.G. (1997): Metallogeny of the Interior Plateau, central British Columbia (parts of 93B, 93C and 93F) in, Interior Plateau Geoscience Project: Summary of Geological, Geochemical and Geophysical Studies, Diakow, L.J., Metcalf, P. and Newell, J.M., Editors, *British Columbia Ministry of Employment and Investment,* Paper 1997-2.

MacIntyre, D.G., Villeneuve, M.E. and Schiarizza, P. (2001): Timing and tectonic setting of Stikine Terrane magmatism, Babine-Takla lakes area, central British Columbia; *Canadian Journal of Earth Sciences*, Volume 38, pages 579-601.

Mortensen, J. K., Ghosh, D.K. and Ferri, F. (1995): U-Pb Geochronology of Intrusive Rocks Associated with Copper-Gold Porphyry Deposits in the Canadian Cordillera; *in*, Porphyry Deposits of the Northwestern Cordillera of North America, Schroeter, T.G., Editor, *Canadian Institute of Mining, Metallurgy and Petroleum*, Special Volume 46, pages 142-158.

Schiarizza, P. and Payie, G. (1997): Geology of the Sitlika Assemblage in the Kenny Creek - Mount Olson Area (93N/12, 13), Central British Columbia; *in* Geological Fieldwork 1996, *British Columbia Ministry of Employment and Investment*, Paper 1997-1, pages 79-100.

Schiarizza, P., Massey, N. and MacIntyre, D. (1998): Geology of the Sitlika assemblage in the Takla Lake area (93N/3, 4, 5, 6, 12), central British Columbia; *in* Geological Fieldwork 1997, *British Columbia Ministry of Employment and Investment*, Paper 1998-1, pages 4-1 - 4-19.

Schiarizza, P., Massey, N. and MacIntyre, D.M. (2000): Bedrock Geology, Tsayta Lake (93N/3, 4, 5, 6); *British Columbia Ministry of Energy and Mines*, Open File 2000-19; 1:100 000 scale.

Schiarizza, P. (2000): Bedrock Geology, Old Hogem (western part) (93N/11, 12, 13); *British Columbia Ministry of Energy and Mines*, Open File 2000-33; 1:100 000 scale.

Smith, A. (1947): Control of ore by primary igneous structures, Porcher Island, B.C.; *Geological Society of America Bulletin*, Volume 58, pages 245 - 252.

Smith, A. (1948): Surf Point and Edye Pass mines; *in* Structural geology of Canadian ore deposits, a symposium, Canadian Institute of Mining and Metallurgy, *Mercury Press Ltd*. pages 94-99.

Stacey, J.S. and Kramer, J.D. (1975): Approximation of terrestrial lead isotope evolution by a two-stage model; *Earth and Planetary Science Letters,* v. 26, p. 207-221.

Struik, L.C. (1988): Structural geology of the Cariboo Gold Mining District, east-central British Columbia; *Geological Survey of Canada*, Memoir 421, 100 p.

Warren, H.V. and Cummings, J.M. (1936): Mineralogy of the Surf Point and Hunter veins; *The Miner,* Vancouver, British Columbia, June Issue, pages 26-27.

Woodsworth, G.J., Anderson, R.G., and Armstrong, R.L. (1991): Plutonic Regimes, Chapter 15; *in* Geology of the Cordilleran Orogen in Canada, H. Gabrielse and C.J. Yorath, (ed.); *Geological Survey of Canada*, Geology of Canada, no. 4, p. 491-531. (also Geological Society of America, The Geology of North America, no. G-2).

Metal Zoning in the Ecstall VMS Belt, Northwest British Columbia (NTS 103H/103I)

By Dani J. Alldrick and Wayne Jackaman

KEYWORDS: *Economic geology, mineral potential, geologic mapping, Central Gneiss Complex, Coast Plutonic Complex, Coast Crystalline Belt, Ecstall Metamorphic Belt, metavolcanic, greenstone, Devonian, VMS, sulphide, metal zoning, Ecstall, Scotia, Packsack, Prince Rupert, Tasmania, Iberian Pyrite Belt.*

INTRODUCTION

More than a century of prospecting within the Ecstall Greenstone Belt has located 40 sulphide mineral occurrences, including 3 deposits with combined reserves of 10 million tonnes grading 0.5% Cu and 2.1% Zn. The high mineral potential has justified a detailed mapping project, related mineral deposit studies, and a special regional geochemical survey. The third field season of this project focused on mapping and prospect visits in the southern portion of this belt.

The Ecstall belt is 80 kilometres long, 3 to 20 kilometres wide, and extends from the Douglas Channel fiord north northwesterly to the Skeena River (Figure 1). The belt lies midway between the northern port cities of Prince Rupert and Kitimat, and is close to tidewater, the Yellowhead Highway, the Skeena Railway line of VIA Rail and the national power grid (Table 1). Extensive logging road networks are established at the northern and southern ends of the belt (at the mouth of the Scotia River and at Kitkiata Inlet, respectively). Other favourable features of the Ecstall Greenstone Belt are listed in Figure 2.

TABLE 1
KEY DISTANCES FOR DEPOSITS IN THE ECSTALL BELT

Deposit:	Scotia	Ecstall	Packsack
Elevation	758 m	182 m	242 m
Distance to:			
Ocean	27	24	18
Estuary / Tidewater	15	6	15
Hydro Powerline	10	19	29
Highway	15	39	49
Railway	15	39	49
Prince Rupert	49	72	82
Kitimat	67	60	59
Terrace	84	93	98

Elevation ranges from sea level to 1760 metres. Steep-walled, glaciated valleys flank rounded ridgecrests. Despite the precipitous terrain, it is possible to traverse the belt from north to south without exceeding 125 metres elevation by following a route of interconnecting valleys. Rainfall is heavy; average annual precipitation at Prince Rupert is 244 centimetres (96 inches). The low elevation of

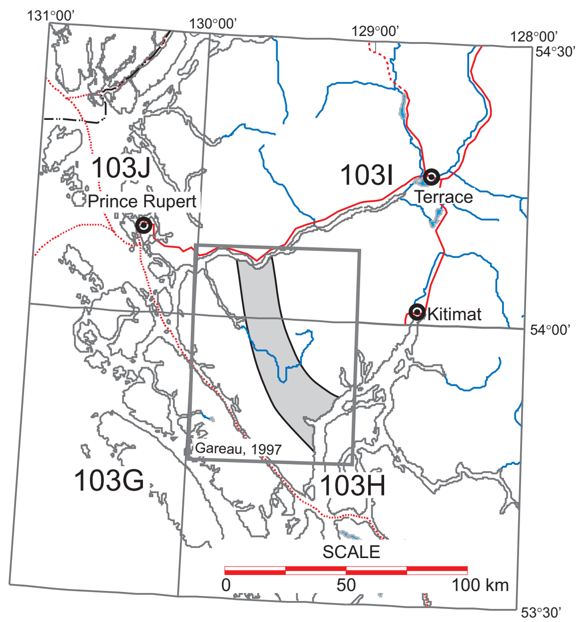

Figure 1. Location of the Ecstall belt in British Columbia.

- Admirable location and infrastructure
- Mid-Devonian metavolcanic belt
- Polymetallic Kuroko-type Zn-Cu VMS
- 3 deposits, all still open
- Coarse-grained sulphides
- Simple mineralogy and metallurgy
- Low levels of deleterious elements
- 40 other sulphide prospects and showings
- Several recent discoveries
- Multiple prospective felsic volcanic horizons
- Detectable by prospecting, geophysics and stream geochemistry
- High exploration / mineral potential
- Underexplored

Figure 2. Favourable features of the Ecstall belt.

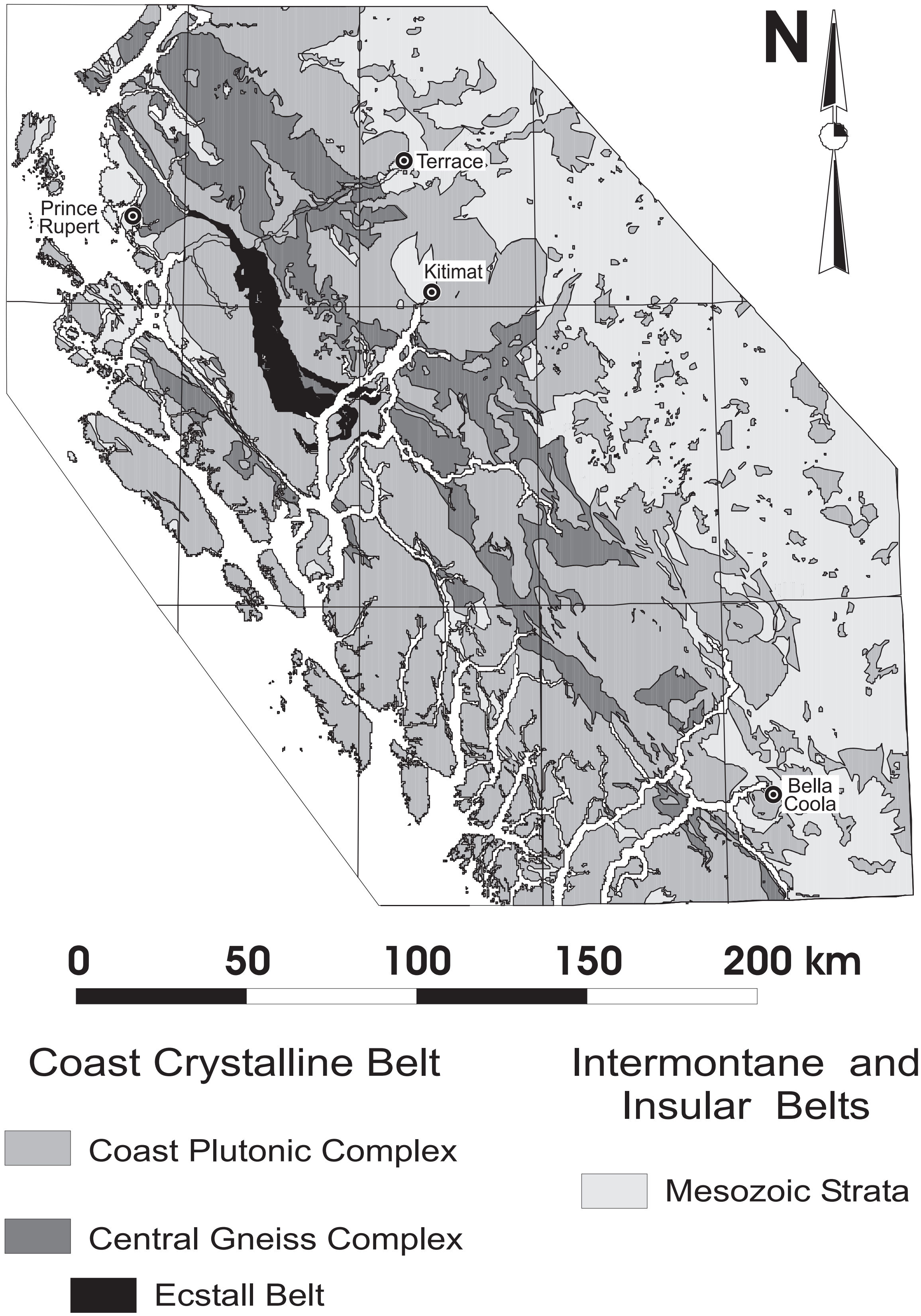

Figure 3. Geology of the mid-coast region of British Columbia, highlighting the location of the Ecstall metavolcanic belt within the Central Gneiss Complex and the Coast Plutonic Complex.

the valley bottoms and their proximity to the coast leaves them free of snow through most of the year. Dense coastal rainforest covers all but the steepest slopes, where bedrock is exposed in cliffs or along avalanche tracks. Terrain above 1100 metres elevation is free of trees and shrubs.

REGIONAL GEOLOGIC SETTING

The Ecstall Greenstone Belt is part of the Central Gneiss Complex, a 2000 kilometre long, anastomosing network of medium to high-grade metamorphosed volcanic, sedimentary and minor plutonic rocks enclosed by younger granitoid rocks of the Coast Plutonic Complex (Figure 3). These two complexes comprise the Coast Crystalline Belt or Coast Belt. The Coast Belt hosts the greatest number of volcanogenic massive sulphide deposits (18) of any of the five physiographic belts in the Cordillera. The following summary is adapted from Greenwood *et al.* (1992), Woodsworth *et al.* (1992), Read *et al.* (1991), Gareau (1991a,b) and Gareau and Woodsworth (2000).

Plutonic rocks of the Coast Plutonic Complex (CPC) make up more than 80% of the Coast Belt; the remainder is metavolcanic rocks, metasedimentary rocks and granitoid gneisses of the Central Gneiss Complex. Plutonic rocks of the CPC range in age from Late Silurian to Eocene. In general, the oldest plutons are exposed along the western edge of the CPC and the plutons young progressively to the east. Rocks range in composition from granite to gabbro, but 70% of all plutonic rocks are tonalite-quartz diorite-diorite. Among the circum-Pacific plutonic terranes, the Coast Plutonic Complex is the largest, the most mafic, and the most deficient in potassium feldspar.

The metamorphic rocks of the Central Gneiss Complex range in age from Proterozoic through Paleozoic and typically occur as screens or pendants surrounded or intruded by the plutonic rocks of the CPC (Figure 3). Evidence of Paleozoic regional metamorphism is preserved locally, but intense mid-Mesozoic and early Tertiary metamorphism, deformation and plutonism have obscured the record of earlier events in many places. Most recrystallization can be attributed to regional metamorphic events, but pluton emplacement can also generate a local contact metamorphic overprint.

The most extensively studied area of the Coast Crystalline Belt lies along the road and rail corridor between Prince Rupert and Terrace (Greenwood *et al.*, 1992; Stowell and McClelland, 2000). This is also the most deeply exhumed part of the Central Gneiss Complex; metamorphic grades range up to kyanite-amphibolite, sillimanite-amphibolite and granulite facies in different parts of this area (Read *et al.*, 1991). Within the Ecstall belt, Gareau (1991a,b) has documented a southwest to northeast progression from lower amphibolite facies to granulite facies, with most rocks falling within the kyanite-amphibolite (upper amphibolite) facies.

The mid-Devonian volcanic arc that evolved into the Ecstall Greenstone Belt (Figure 4) likely developed in a similar setting as the extensive volcanosedimentary successions of the Yukon-Tanana terrane (Gareau and Woodsworth, 2000). The regional geologic history of the Ecstall belt is outlined in Alldrick *et al.* (2001) and summarized in Figure 5; Devonian volcanism, sedimentation and intrusion were followed by four poorly-constrained phases of deformation and four well-dated plutonic episodes. The Jurassic to Eocene plutonic and metamorphic history of the Coast Crystalline Belt is consistent with a model of east-dipping subduction beneath a single, allochthonous Alexander-Wrangellia-Stikinia superterrane, emplaced against North America in Middle Jurassic time (van der Heyden, 1989).

GEOLOGY OF THE ECSTALL BELT

The Ecstall belt is a north-northwest trending, high-grade metamorphic belt bounded by the elongate mid-Cretaceous Ecstall pluton on the west and the Paleocene Quottoon pluton on the east (Figure 4). Gareau (1991a) divided stratified rocks of the belt into four principal units: metavolcanic rocks, metasedimentary rocks, quartzite and layered gneiss (Figure 4). Two new U-Pb zircon ages (Friedman *et al.*, 2001) confirm the stratigraphic succession established for these highly deformed strata (Gareau, 1991a,b and Alldrick *et al*., 2001) and improve the age constraints on the regional stratigraphy (Figure 5).

The mid-Devonian metavolcanic unit consists of mafic and intermediate metavolcanic rocks, interlayered with lesser felsic metavolcanic and clastic metasedimentary rocks and rare limestone and chert. Textures within this metavolcanic unit range from layered gneisses in the north, to pillow lavas and graded beds in the south of the belt. These latter units are too deformed to give reliable tops indicators. This main metavolcanic package hosts 36 of the 40 sulphide prospects in the belt. Felsic volcanic members, preserved as pyritic quartz-sericite schist, typically host these mineral occurrences. Industry exploration programs have traced out many favourable felsic units, as well as exhalative horizons (chert) and extensive stockwork-style mineralized zones.

These mid-Devonian metavolcanic rocks are intruded by three large, elongate, mid-Devonian plutons called the Big Falls tonalite. These coeval, subvolcanic intrusions may be the exposed parts of a single large stock. The mid-Devonian intrusive and extrusive rocks are grouped together as the Big Falls Igneous Complex (Alldrick *et al.,* 2001). In many other greenstone belts, subvolcanic plutons provide camp-scale controls for localization of massive sulphide deposits (Campbell *et al.*, 1981, Galley, 1996 and Barrie *et al.*, 1999) and for metal zoning among deposits (Large *et al.*, 1996). Consequently these plutons are an important component of the evolving metallogenic model for the Ecstall camp.

The metavolcanic unit and its coeval subvolcanic stocks are overlain by a regionally extensive package of late Devonian clastic metasedimentary rocks, consisting of a lower metapelitic unit and an upper quartzite unit. The quartzite unit hosts 3 sulphide prospects (Amber, El Amino and Cheens Creek) in areas where minor limestone units are interbedded with the clastic metasedimentary rocks. Two

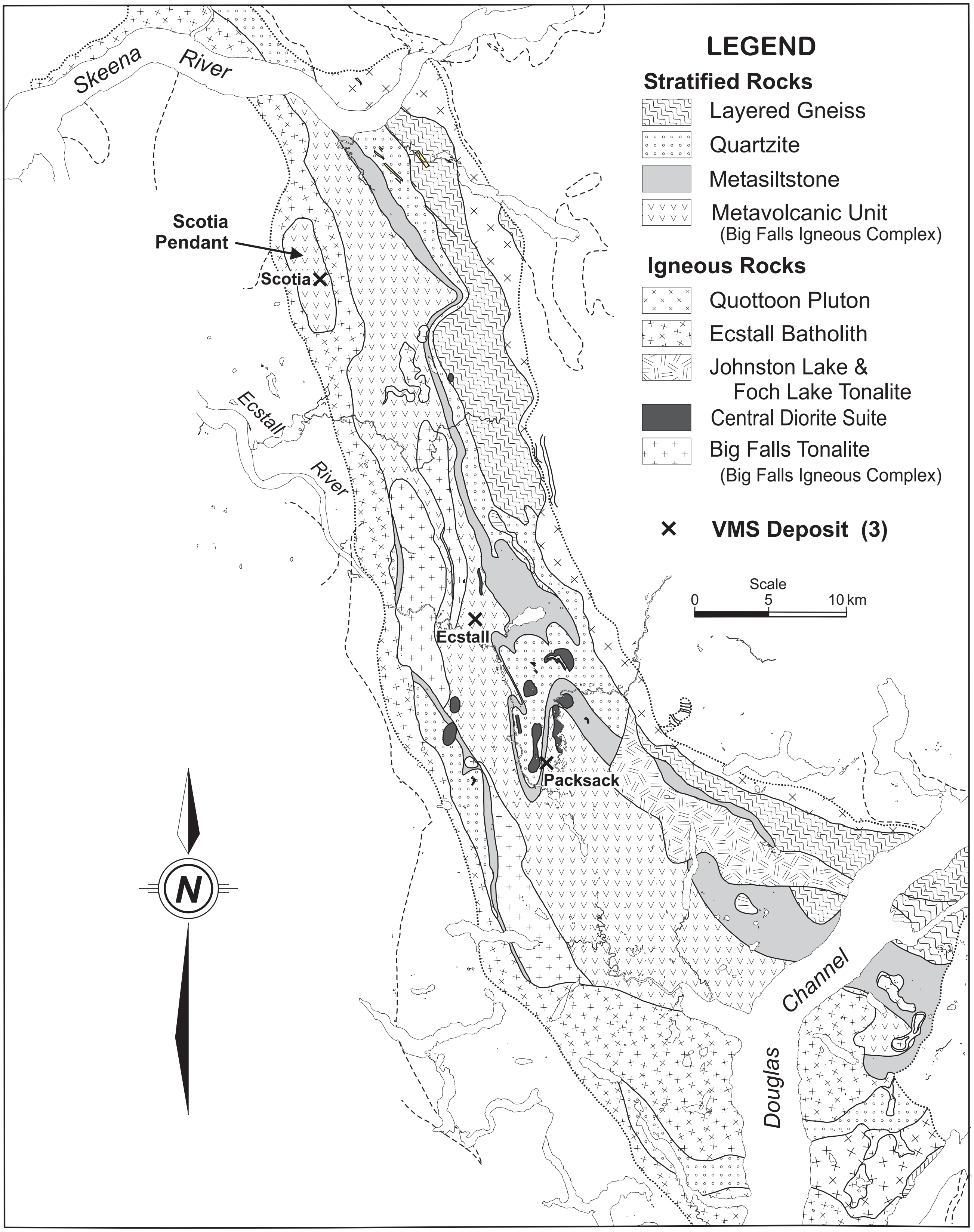

Figure 4. Simplified geology of the Ecstall belt (modified from Gareau, 1997).

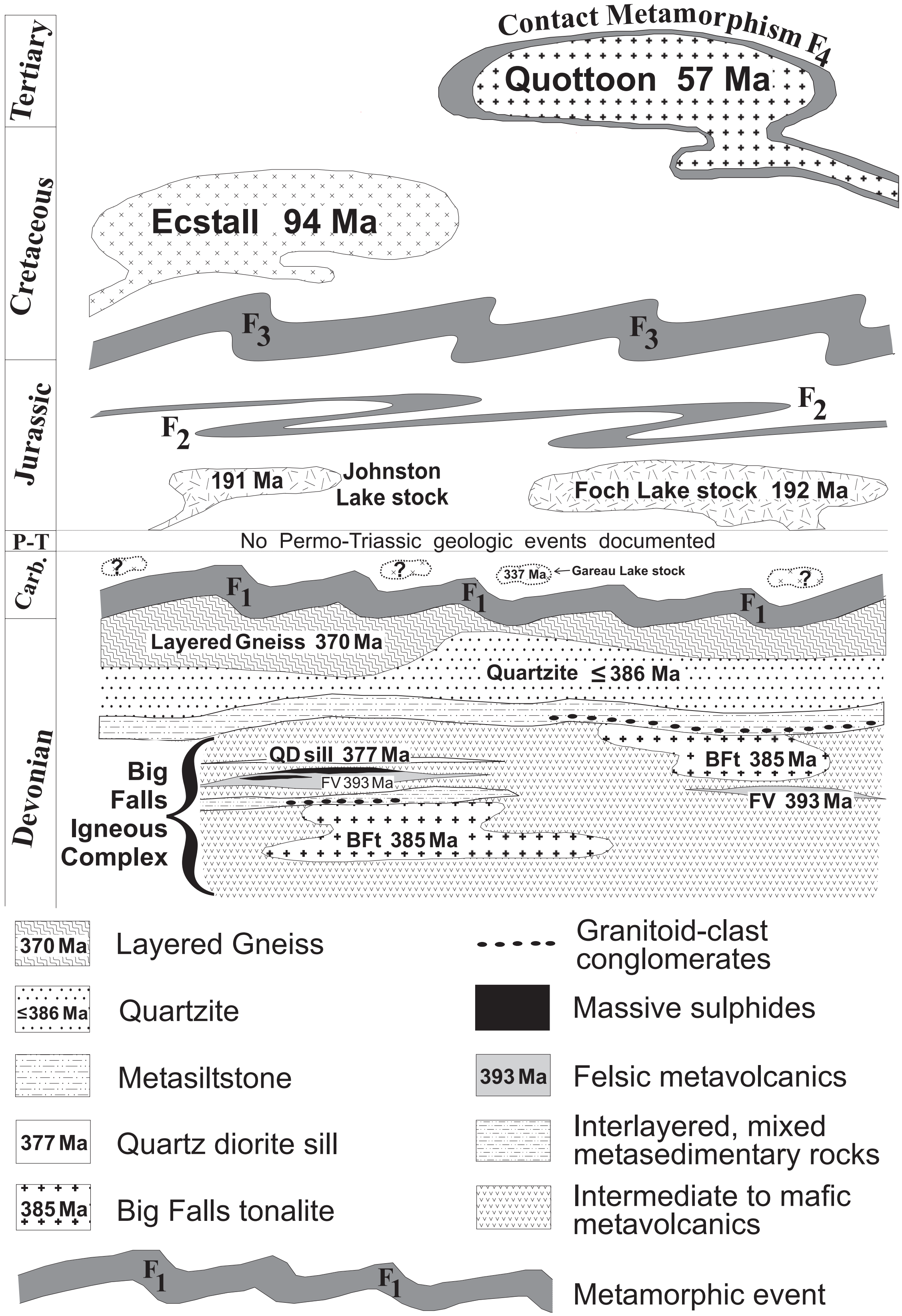

Figure 5. Schematic stratigraphy and geologic history of the Ecstall belt.

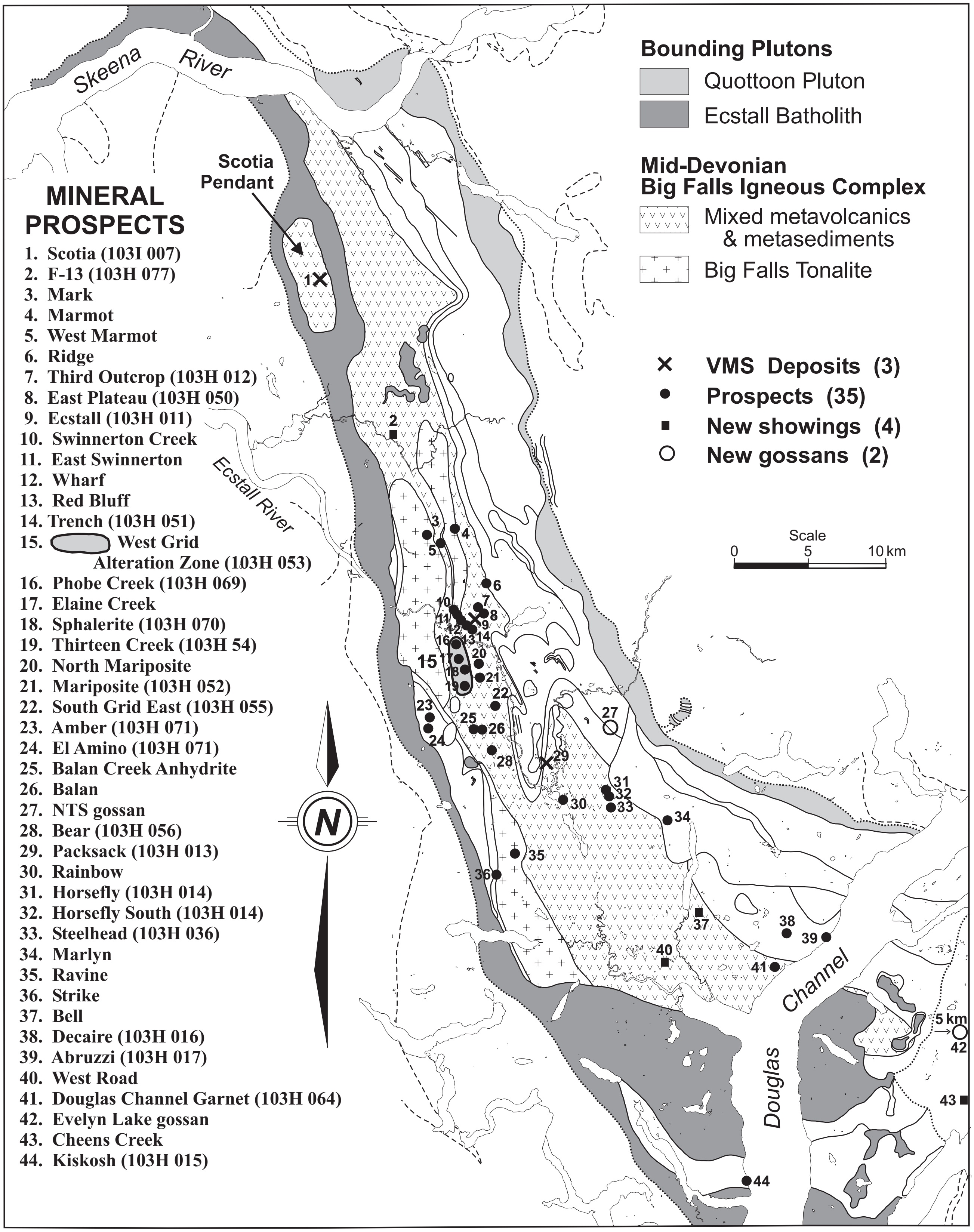

Figure 6. Mineral occurrences of the Ecstall belt.

large gossan areas were also discovered in these units during this season's mapping. Samples show only disseminated to semi-massive pyrite in well foliated quartzite; assay results are forthcoming.

These metasedimentary strata are overlain in turn along the eastern margin of the Ecstall belt by mafic gneiss. The protolith for this black and white banded gneiss is interpreted as a mafic volcanic package of Late Devonian age (Friedman *et al*., 2001).

At least four plutonic events post-date the middle to upper Devonian stratigraphic succession (Figures 4 and 5). An extensive suite of small, weakly deformed diorite stocks are scattered throughout the central Ecstall belt. One stock yielded an Early Mississippian age, which may indicate the age for all these plugs. In addition to Paleozoic intrusions, two elongate Early Jurassic plutons, the Johnston Lake and Foch Lake tonalites, intrude the eastern part of the belt. The two bounding plutons, the mid-Cretaceous Ecstall on the west and the Paleocene Quottoon on the east, have associated dikes, sills and small stocks that cut Ecstall belt rocks.

MINERAL DEPOSITS AND EXPLORATION

The Ecstall belt hosts 40 sulphide and 2 industrial mineral occurrences (Figure 6 and Table 2). These deposits and showings are described in Alldrick (2001a), Scott (2001) and this paper.

In 1890, the specte Ecstall belt (*see* Table 2).acularly exposed sulphide lenses of the Ecstall volcanogenic massive sulphide deposit were discovered in Red Gulch Creek. A series of companies have investigated and developed this deposit over the last 100 years. Prospecting work during the 1930s and 1940s located 12 additional sulphide showings within 8 kilometres of the Ecstall deposit. Regional mapping and exploration programs conducted by Texas Gulf Sulphur Company Limited in 1957 and 1958 discovered the Packsack (1957) and Scotia deposits (1958). Exploration work carried out by many companies and by independent prospectors over the last 30 years, resulted in the discovery of 25 more sulphide occurrences.

Figure 6 shows the location of the 3 deposits and 39 smaller showings in the belt, including four new discoveries. Most of the mineral prospects in the belt are hosted by the mid-Devonian metavolcanic package. These metavolcanic rocks offer the greatest exploration potential for the discovery of more deposits.

NEW CLAIMS

The southern part of the Ecstall belt has seen limited exploration interest and activity over the past century, but a

TABLE 2
RESERVES, RESOURCES, GRADES AND CU:ZN AND CU:PB RATIOS FOR DEPOSITS AND PROSPECTS IN THE ECSTALL GREENSTONE BELT

PROPERTY	SIZE	Cu	Pb	Zn	Ag	Au	Cu:Zn Ratio	Cu:Pb Ratio
	(mt)	%	%	%	g/t	g/t		
Scotia	**1,240,000**	**0.10**	**0.40**	**3.80**	**13.00**	**0.250**	0.03	0.25
Amber		0.01		0.02			0.56	
Bell		0.24	2.56	3.36	112.30		0.07	0.09
Cheens Creek		0.15	0.50	3.74	23.40		0.04	0.31
East Plateau		0.03		0.18			0.17	
Ecstall	**6,878,539**	**0.65**		**2.45**	**17.00**	**0.500**	0.27	
El Amino		0.50		0.60	70.00		0.83	
Elaine Creek		3.04		0.09	11.70	1.525	33.78	
Horsefly		1.16	0.13	4.60	39.00	0.500	0.25	8.92
Horsefly South		5.60	0.09	1.65	30.00	0.860	3.39	62.22
Mariposite		0.03	0.04	0.12	5.50	0.110	0.24	0.66
Mark		0.14	0.01	0.02	0.06	0.002	7.00	14.00
Marlyn		0.01	0.01	0.05	0.05	0.020	0.10	0.50
Marmot		0.01	0.01	0.02	0.01	0.002	0.30	0.60
Packsack	**2,700,000**	**0.50**	**0.01**	**0.20**	**34.00**	**0.300**	2.50	50.00
Phobe Creek		0.69		0.01	2.22	0.251	104.55	
Rainbow		0.04	0.00	0.31	1.80		0.13	40.00
South Grid East		0.12		0.02			5.00	
Sphalerite		0.06	0.00	6.00	1.50	0.015	0.01	20.68
Steelhead		0.03	0.13	0.04	13.80	0.024	0.75	0.21
Strike		0.17	0.27	2.83	1.13	0.010	0.06	0.63
Third Outcrop		0.63		2.30			0.27	
Thirteen Creek		8.05		0.05	350.00	2.400	151.89	
Trench		0.03	0.00	0.12			0.28	7.17

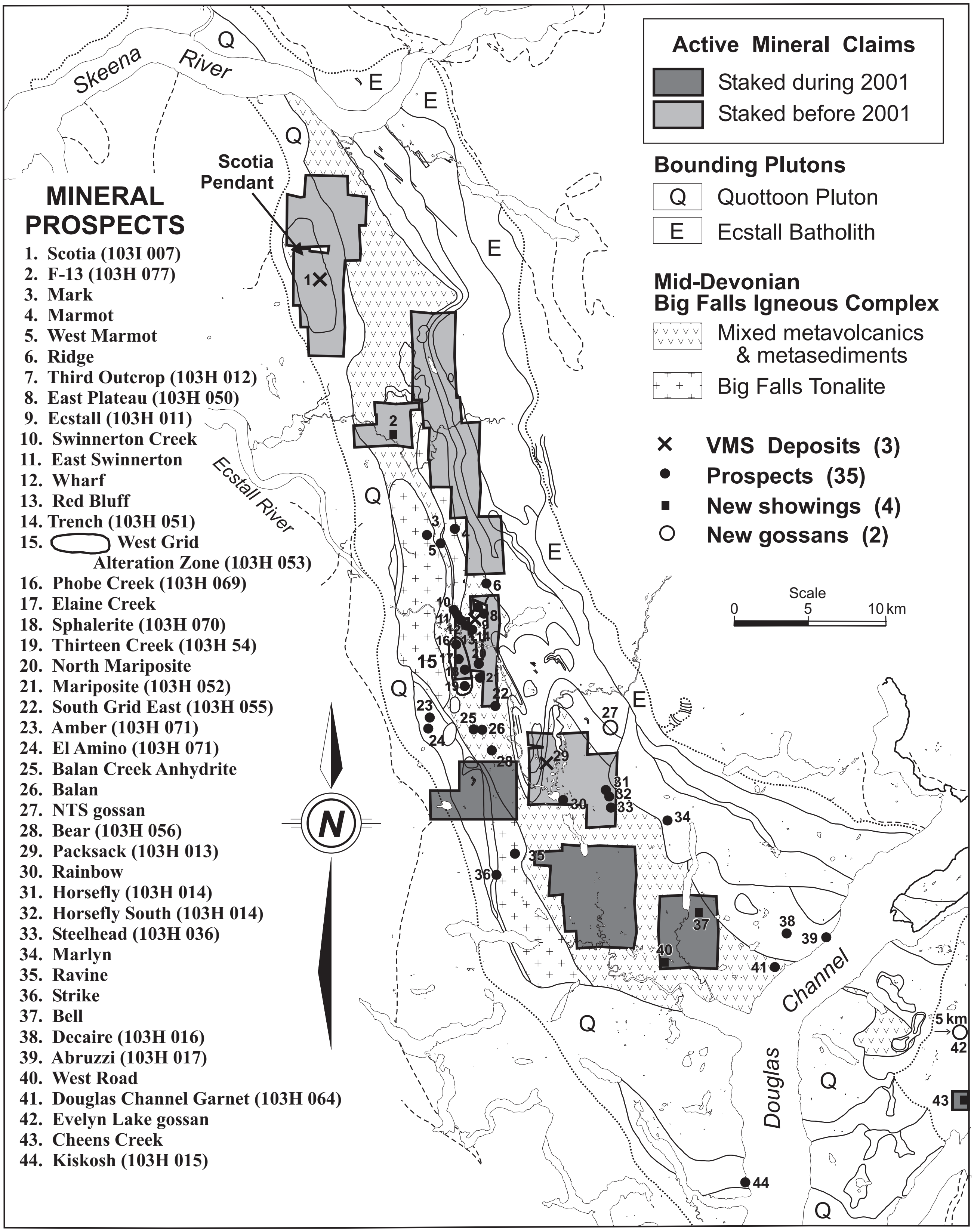

Figure 7. Mineral claims in the Ecstall belt - October, 2001.

number of new claims were staked in this area during 2001 (Figure 7). Staking was carried out just before the publication of Regional Stream Sediment Survey results (Jackaman, 2001) on June 1 to cover areas with known exploration potential. After June 1, claim blocks were staked over areas of multi-element stream sediment survey geochemical anomalies and over three newly discovered mineral showings.

NEW SHOWINGS

Prospectors Ralph Keefe and Shawn Turford have discovered three new polymetallic sulphide showings over the past three summers (Figure 6). These prospects all lie in the southern part of the Ecstall belt and all are exposed in rock cuts along logging roads. Two prospects are hosted by pyritic quartz-sericite schist within the main metavolcanic unit; the other showing is hosted by quartz-biotite schist with minor associated calc-silicate bands within the thick metasedimentary sequence.

The **Bell** prospect is exposed in a rock cut along an upper level logging road southeast of Kitkiata Lake. This zinc-lead-copper prospect is hosted by a 10 metre thick pyritic quartz-sericite schist that strikes 163°. The showing consists of several parallel seams, up to 3 centimetres thick, of medium-grained black sphalerite, with accessory galena and rare chalcopyrite, hosted in well-sheared, weakly to strongly pyritic (5-10 %) quartz-sericite schist. Base-metal-sulphide rich zones are silicified and more resistant, while intervening, less altered, quartz-sericite schist is well-weathered and readily crumbles away. The best assay from five grab samples is 6.24% Zn, 2.07% Pb, 0.163% Cu, 103.6 ppm Ag and 0.78 ppm Au and the average assay from the five samples is 2.63% Zn, 1.58% Pb, 0.106% Cu, 71.4 ppm Ag and 0.53 ppm Au.

This rock unit is exposed again several hundred metres to the northwest on an adjacent logging road. No base metal sulphides are visible in the pyritic quartz-sericite schist at this location and base metal assays are in the ppm range.

The **West Road** showing is a small (7 metres wide) rusty cliff face of pyritic quartz sericite schist exposed alongside a logging road located midway between Kitkiata Lake and the Quaal River valley. One seam of fine-grained black sphalerite, 2 centimetres thick, was exposed during sampling. The pyritic unit crops out for 80 metres subparallel to the road and then extends into the logged off area.

The **Cheens Creek** prospect is exposed in and around a bedrock borrow pit at the end of a new logging road on the south side of Hawkesbury Island, 3.5 kilometres west of Danube Bay (Photo 1). The showing is hosted in thinly laminated biotite-quartz schist with minor associated calc-silicate layers, within the main quartzite unit (Figures 4 and 5). No volcanic rocks have been noted in the area. These strongly foliated metasedimentary strata strike 055°. Mineralization in place consists of abundant disseminated pyrite exposed in the wall of the pit over a thickness of 3 to 4 metres (Photo 2). Large float boulders dispersed along the roadbed include massive sphalerite-magnetite-pyrite rock with minor galena and trace chalcopyrite. Several styles and textures of disseminated to semi-massive to massive sulphides are displayed in the float samples; some incorporate calc-silicate bands consisting of pale green diopside, rusty-red garnet and quartz. Chalcopyrite is more abundant in pyritic samples that have little or no sphalerite, galena and magnetite. One chalcopyrite-rich sample assayed 0.04% Zn, 0.02% Pb, 1.068% Cu, 14.7 ppm Ag, with gold values below detection limit. Assays from sphalerite-galena-rich samples range up to 14.27% Zn, 8.43% Pb, 0.068% Cu, 373.0 ppm Ag and 1.89 ppm Au. The average assay from five grab samples is 6.86% Zn, 2.15% Pb, 1.77% Cu, 99.8 ppm Ag and 0.6 g/t ppm Au. The metasedimentary host rocks, the variable sulphide textures and grades, the presence of magnetite and calc-silicate mineral assemblages and the proximity to stocks and dikes of the mid-Cretaceous Ecstall pluton to the west, all suggest that the mineralization is magmatic-hydrothermal in style. Close analogues in the Ecstall area are the Amber and El Amino prospects (Scott, 2001) which are also hosted by metasedimentary rocks. These three showings may be examples of polymetallic

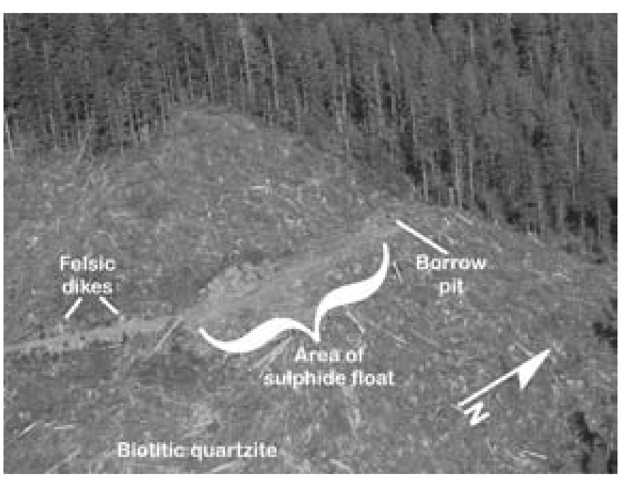

Photo 1. Aerial view of the Cheens Creek sulphide prospect, Hawkesbury Island .

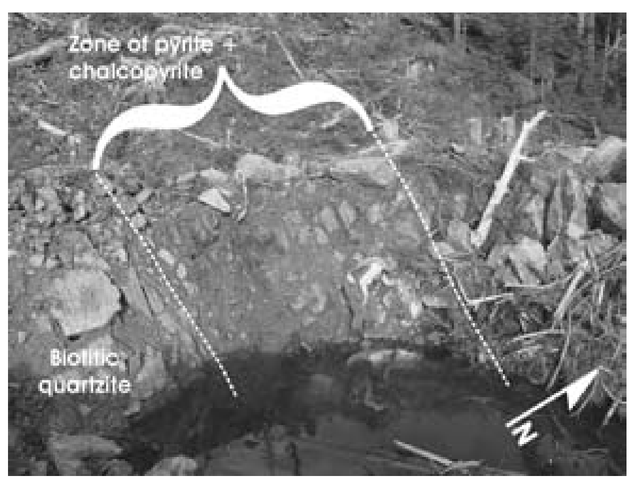

Photo 2. Paul Wojdak in the borrow pit, Cheens Creek prospect.

skarn mineralization developed proximal to the Ecstall batholith.

DISTRIBUTION OF MINERAL PROSPECTS

Sulphide prospects cluster in the central area of the Ecstall belt (Figure 6). Two explanations for this concentration of mineral showings are:

- Favourable geology: Current VMS genetic models emphasize the concentration of massive sulphide deposits on the seafloor in areas directly overlying shallow subvolcanic magma chambers that feed overlying lavas along conduits (Figure 8). Most mineral prospects in the Ecstall belt are concentrated close to the subvolcanic tonalite plugs, so the distribution of prospects at Ecstall fits the genetic model well. Since the model predicts that this type of mineral deposit is preferentially localised in lavas near to, and directly overlying, these buried granitoid bodies, the tonalite stocks become critically important prospecting guides.
- Degree of Exploration: Human factors may be the main influence for the present distribution pattern of mineral prospects in the Ecstall belt. For 20 years (1938-1958) most prospecting teams working in the belt set out on foot, or by boat, from the large mine development camp at the Ecstall deposit. One predictable result of this logistical arrangement is that more showings would be discovered in the immediate area of this base camp and the number of discoveries would drop off further out from the camp.

These two possible explanations raise the question whether the geological factors or the human factors are the dominant control for the obvious clustering of known deposits. The answer is important because, in the former case, future prospecting should concentrate around the tonalite stocks, while in the latter case, the mineral potential at the northern and southern ends of the belt deserve increased attention because they are relatively untested.

Metal Zoning in the Mount Read Volcanic Belt

Metal zoning in VMS deposits spatially related to a large, comagmatic subvolcanic pluton has been documented in the Mount Read volcanic belt of western Tasmania (Large *et al*., 1996). Prospects in this belt demonstrate clear, proximal-to-distal zoning from copper to gold to zinc, both up-section and laterally, away from the regional-scale pluton (Figure 9). Only two small stocks crop out, but the full extent of this buried batholith has been revealed by a recent aeromagnetic survey. These maps clearly illustrate that volcanogenic massive sulphide deposits are distributed throughout the Mount Read volcanics, and are not just concentrated near the coeval pluton.

Metal zoning in the Ecstall Greenstone Belt

The full extent of the exploration potential of the Ecstall belt is revealed in results of a geochemical stream sediment survey (Jackaman, 2001). During the 2000 field season, 228 samples were collected (Figure 10) at double the density of regular mapsheet-scale programs, since this is a well-mineralized district.

All prospects in this belt crop out, and creeks are actively eroding massive sulphide lenses at the Ecstall and Packsack deposits (Photos 3, 4 and 5). Before erosion, the Ecstall deposit is estimated to have been nearly twice its present size (Alldrick, 2001b); therefore, roughly six million tonnes of massive sulphides have been washed downstream. Silt samples from these creeks show high contents of copper, lead, zinc, silver and gold, as expected. However, these are not the most metal-rich samples collected in the survey. The three most metal-rich stream sediment samples collected in the belt come from three streams with no known

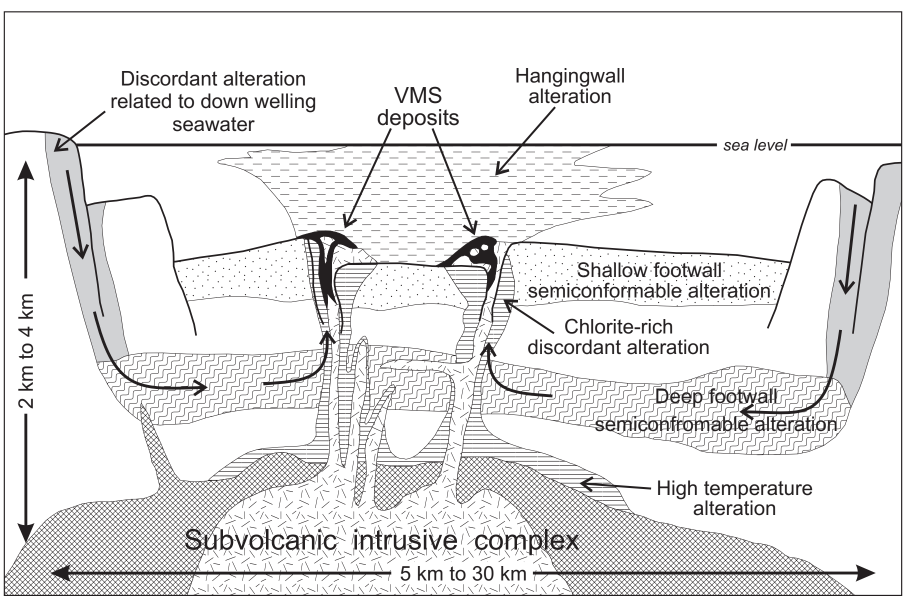

Figure 8. Generalized relationships between VMS deposits, alteration zones and an underlying subvolcanic intrusive complex (from Galley, 1995).

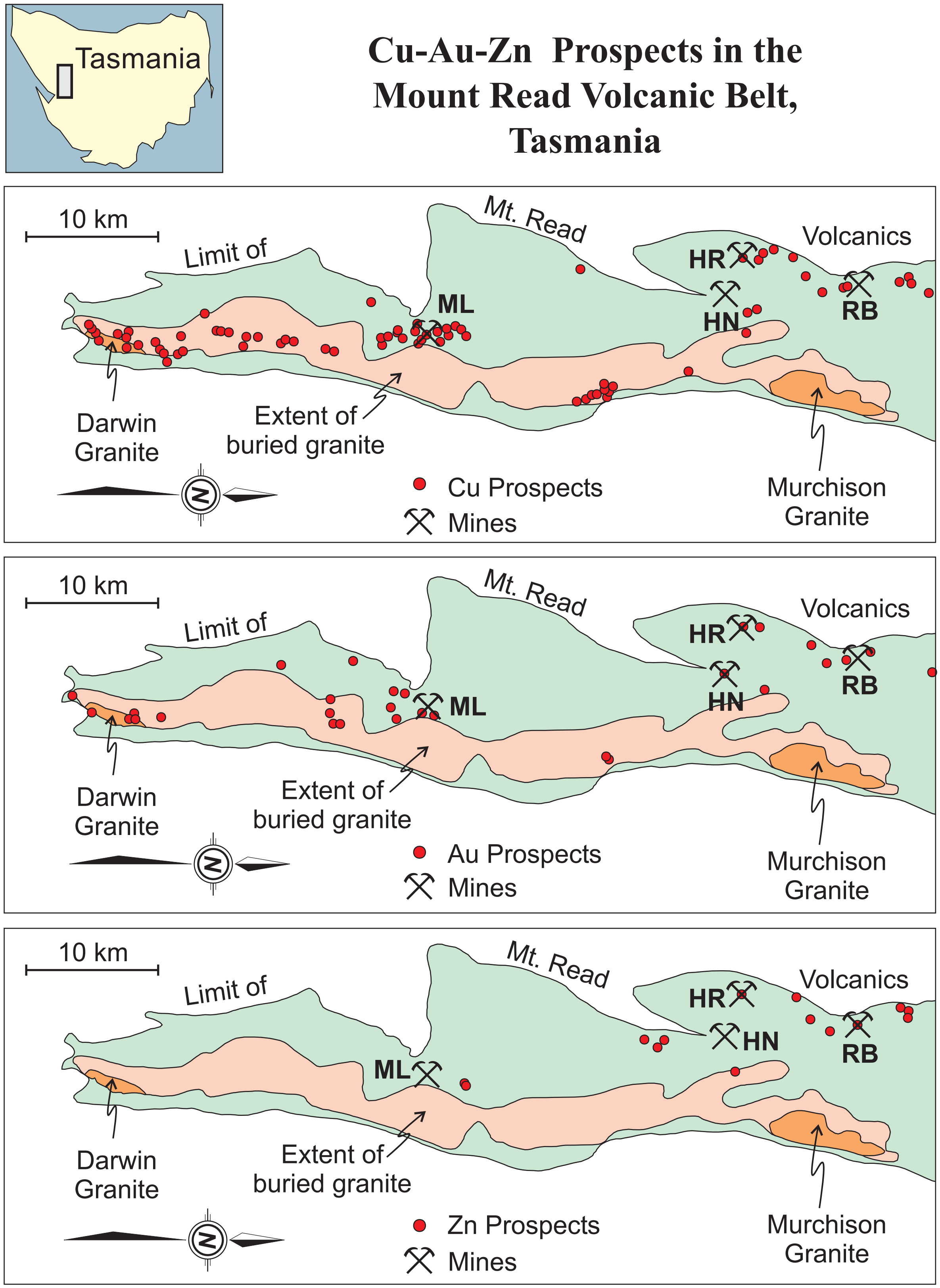

Figure 9. Metal zoning among mineral prospects of the Mount Read Volcanic Belt, western Tasmania (from Large *et al*., 1996). ML-Mount Lyell, HR-Hercules, HN-Henty, RB-Rosebery. Que River and Hellyer mines are off the map edge to the north.

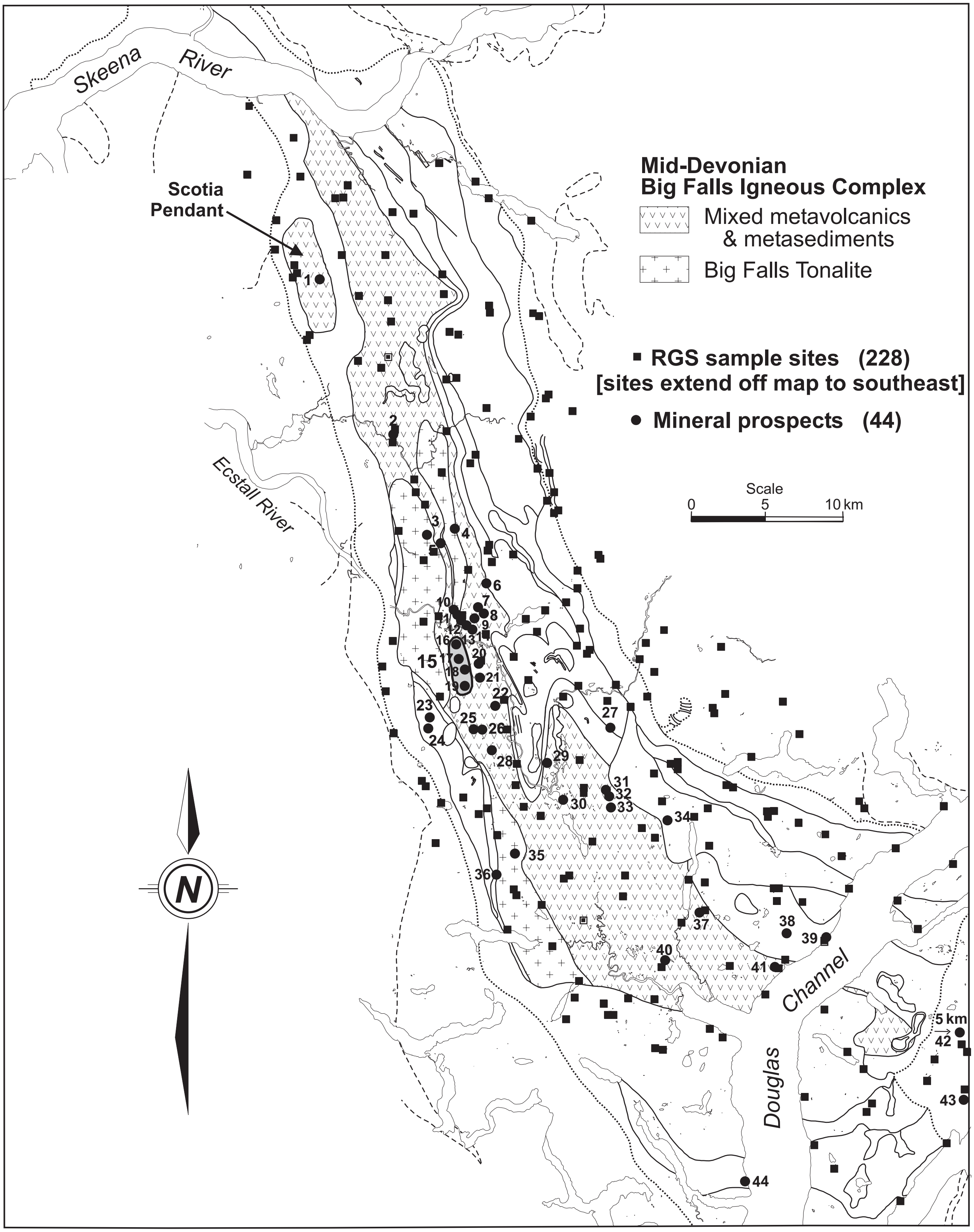

Figure 10. Regional Geochemical Survey sample sites in the Ecstall belt (from Jackaman, 2001).

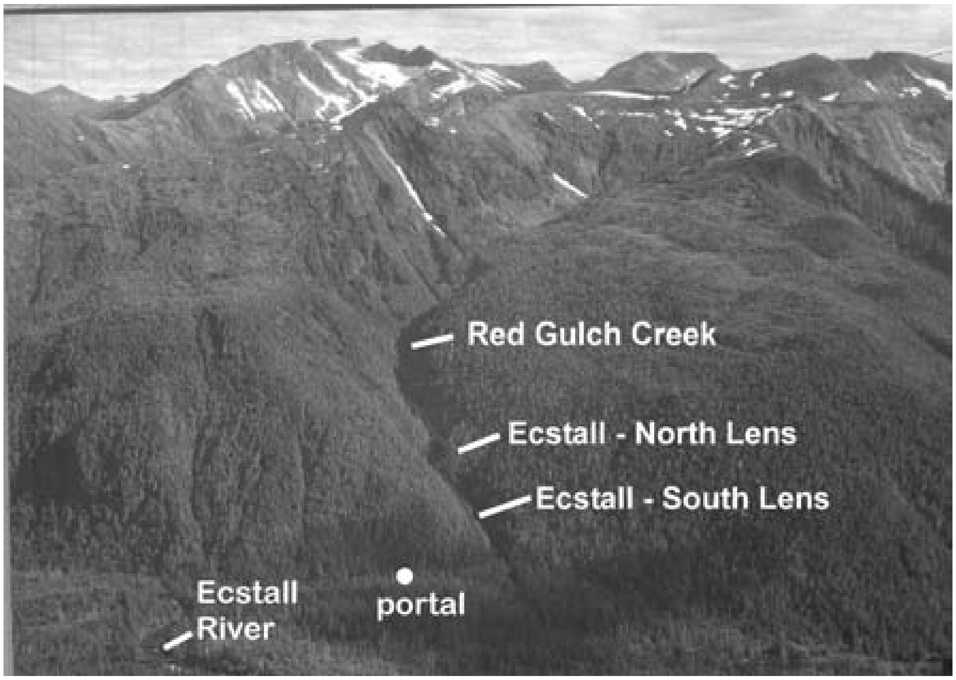

Photo 3. The Ecstall massive sulphide deposit crops out along the floor and canyon walls of Red Gulch Creek for 600 metres. View looking north-northeast.

Photo 4. Part of the continuous exposure of massive sulphides, 25 metres wide and 90 metres long, at the northern end of the Ecstall VMS deposit .

Photo 5. Packsack massive sulphide deposit. Shawn Turford and Paul Wojdak inspect the 5 metre thick lens of massive sulphides at the upper waterfall in Packsack Creek - one of four sulphide lenses exposed along this streambed.

mineral occurrences anywhere within their drainage basins (*see* Table 5 in Jackaman, 2001). And 12 more polymetallic anomalies have been identified from 12 more streams with no known mineral occurrences.

Stream sediment geochemistry results for copper, gold, zinc and lead are shown on the four maps in Figure 11. The strongest copper values are clustered close to the mid-Devonian tonalite bodies (Figure 11a); only a few high copper values are located well away from these intrusions. The highest stream sediment gold values (Figure 11b) overlap with the area of the highest copper values, but also extend further to the south from the high copper values. Thus, the strongest gold values are concentrated a little further outboard from the tonalite bodies than the high copper values.

The strongest zinc anomalies are broadly dispersed along the belt (Figure 11c) compared to the tighter clustering of the copper and gold values. There is also a small area in the center of the Ecstall belt with a noticeable absence of strong zinc values that coincides with an area primarily underlain by the tonalite stocks. The zinc-rich Scotia deposit lies within the northern area of high zinc values. Overall, the zoning pattern of copper, gold and zinc resembles the pattern discovered in the Tasmanian study (Figure 9).

Stream sediment sample results for lead are included in this study of regional metal zoning because they also fit the pattern of lateral zoning well (Figure 11d). The strongest lead values are well dispersed along the whole of the belt. Proximal to the tonalite bodies, there is a conspicuous absence of the strong lead concentrations in the stream sediment samples.

These results from the new stream sediment survey, and the patterns revealed in the Tasmania study, indicate that the

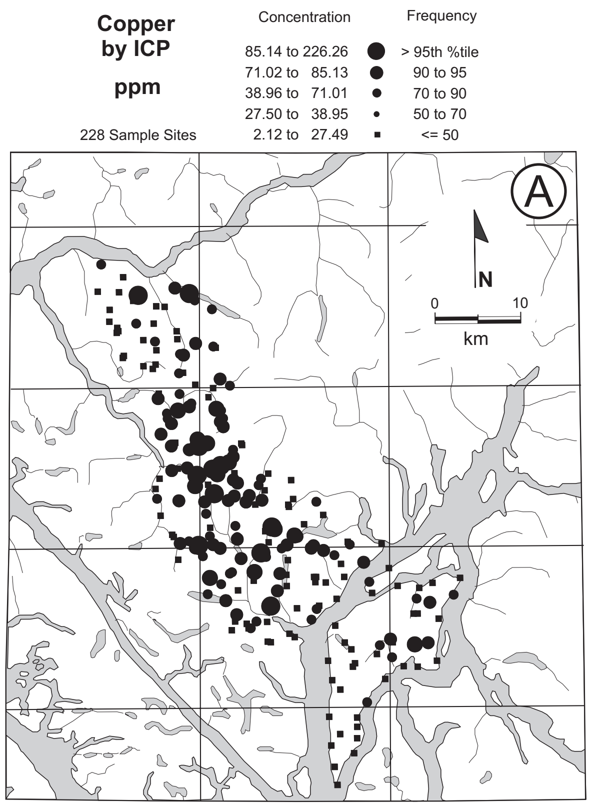

Figure 11a. Copper concentrations in stream sediment samples from the Ecstall belt.

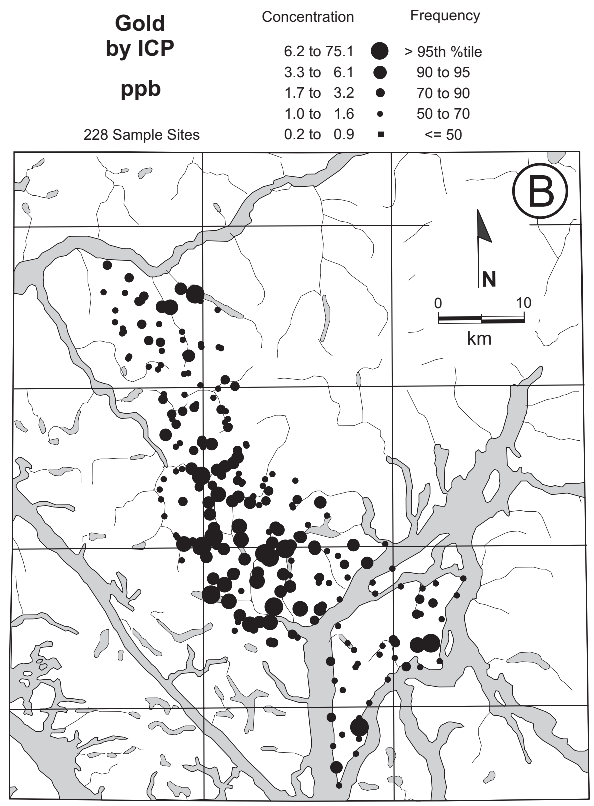

Figure 11b. Gold concentrations in stream sediment samples from the Ecstall belt.

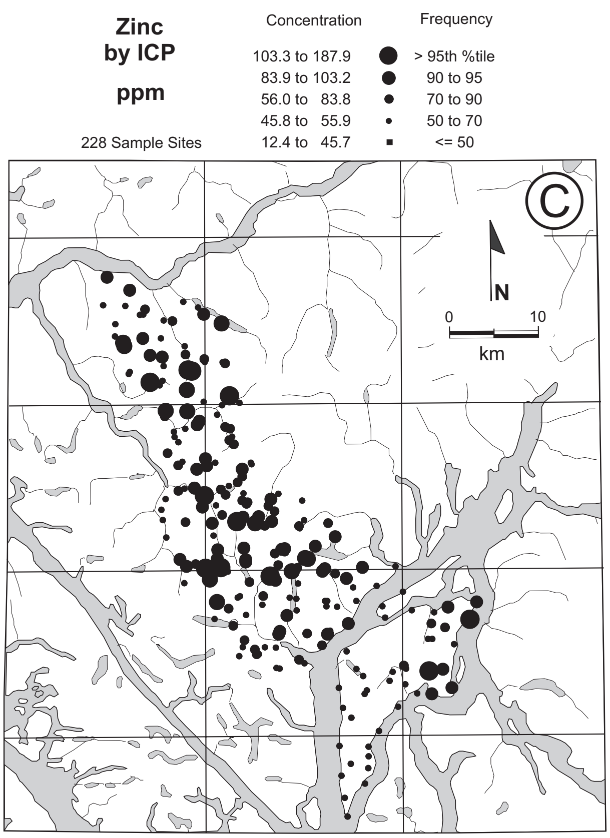

Figure 11c. Zinc concentrations in stream sediment samples from the Ecstall belt.

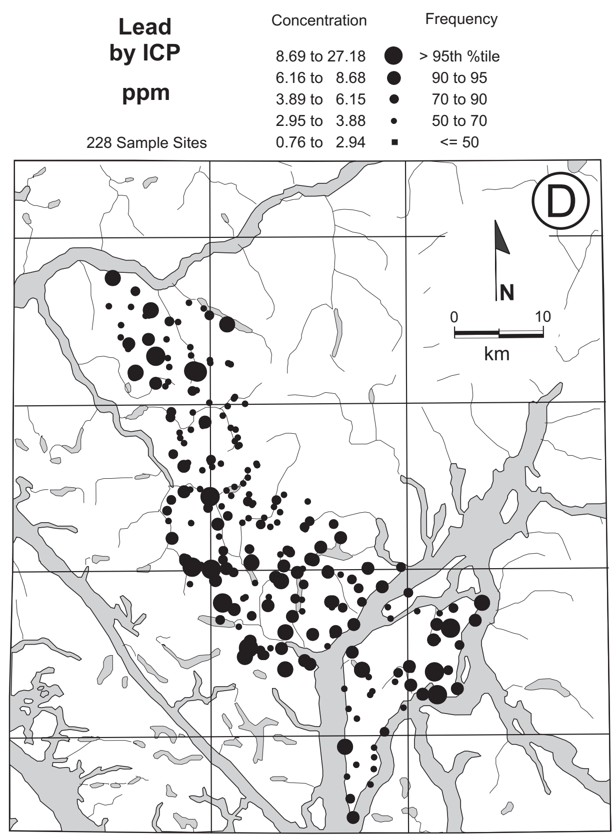

Figure 11d. Lead concentrations in stream sediment samples from the Ecstall belt.

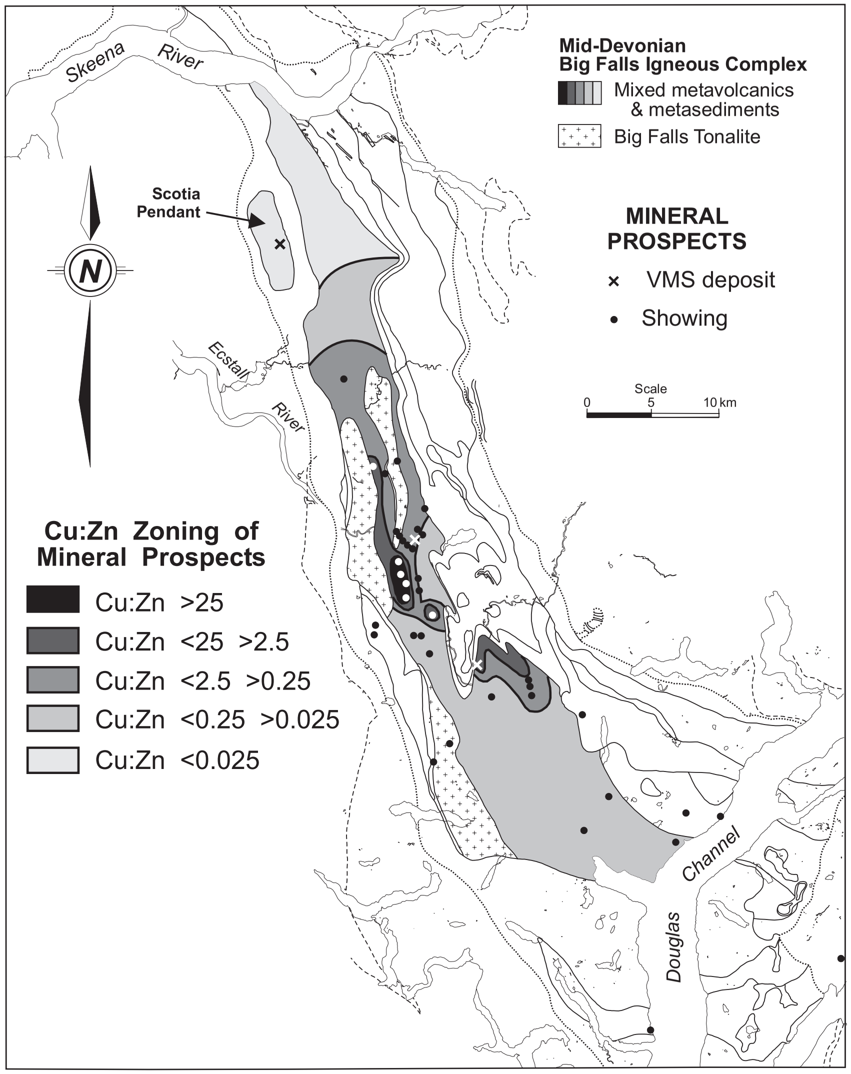

Figure 12a. Contoured Cu:Zn ratios for mineral prospects in the Ecstall belt (*see* Table 2).

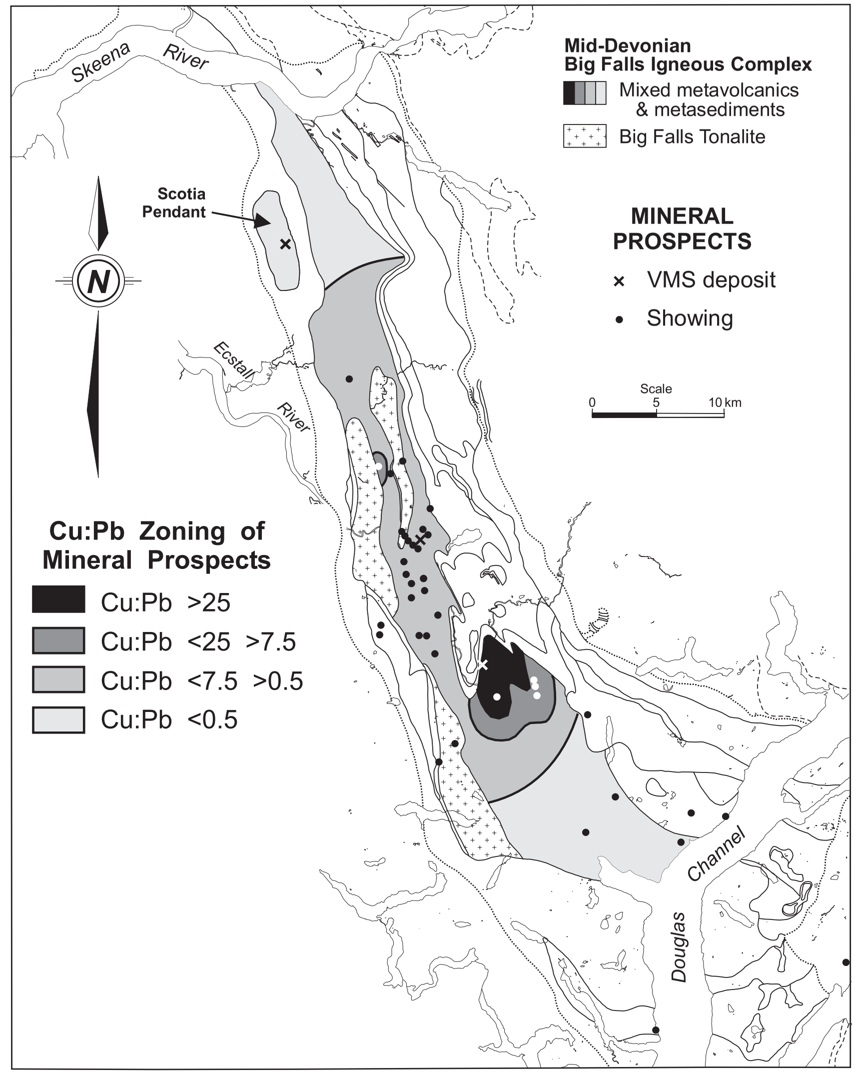

Figure 12b. Contoured Cu:Pb ratios for mineral prospects in the Ecstall belt (*see* Table 2).

high concentration of mineral prospects in the central part of the Ecstall Greenstone Belt is probably an artifact of 20 years of intensive prospecting and exploration work that was based out of the camp at the Ecstall deposit. The exploration potential throughout this belt is high everywhere, but copper-rich deposits will be most abundant near the central tonalite bodies and gold, zinc and lead-rich deposits will be concentrated progressively further away, but still hosted by the metavolcanic rocks of the belt.

The clear pattern of metal-zoning evident in the stream sediment geochemistry results suggested that the same pattern of metal zoning might also be discernible by calculating the Cu:Zn and Cu:Pb ratios for assays from the deposits and prospects in the Ecstall belt (Table 2); these values could then be contoured. In most mining camps, assay data is more readily available than high quality stream sediment survey results, so it offers a more universal database for applying this technique. Nevertheless, there are problems and restrictions encountered when calculating and contouring data derived from assay results:

Just 36 showings in the Ecstall belt are hosted in volcanic strata.

For smaller showings, assays are not always carried out for `accessory' metals such as zinc or lead (Table 2). Copper and zinc analyses are available for 24 prospects; but copper, zinc and lead analyses are only available for 15 prospects.

For very small prospects, the `best assay' is typically reported. This features the highest copper or gold grade, rather than the most representative assay or the average assay.

Showings are unevenly distributed, clustering near the Ecstall deposit (Figure 6).

In general, the contoured maps (Figure 12) show concentric zoning of Cu:Zn and Cu:Pb ratios decreasing outward from the central coeval stocks. An important feature is the presence of a copper-rich zone in the area of the Packsack deposit, despite the apparent absence of mid-Devonian stocks. Tonalite (quartz diorite) intrusions may be present along this part of the valley of the upper Ecstall River where early mapping work (Padgham, 1958; Holyk *et al.,* 1958) identified several small bodies of "diorite". A second significant feature is the absence of any copper-rich zone in the southwest part of the Ecstall belt (Figure 11a, 12a and 12b) where a large tonalite body is shown on the maps by Gareau (1991c, 1997) (Figure 4). The tonalite intrusion in this area was extrapolated from a small exposure mapped far to the north. The absence of any copper-rich geochemical signature, combined with the presence of two relatively low-copper mineral occurrences hosted in schist (Figure 6), suggest that the tonalite body is much less extensive than shown on existing maps. The prominent Cu:Zn high centred over the West Grid Alteration Zone (Phobe, Elaine and Thirteen Creeks prospects) contrasts with a conspicuous absence of a Cu:Pb high at the same location. This reflects the

TABLE 2
RESERVES, RESOURCES, GRADES AND CU:ZN AND CU:PB RATIOS FOR DEPOSITS AND PROSPECTS IN THE ECSTALL BELT

PROPERTY	SIZE (mT)	Cu %	Pb %	Zn %	Ag g/T	Au g/T	Cu:Zn Ratio	Cu:Pb Ratio
Scotia	**1,240,000**	**0.10**	**0.40**	**3.80**	**13.00**	**0.250**	0.03	0.25
Amber		0.01		0.02			0.56	
Bell		0.24	2.56	3.36	112.30		0.07	0.09
Cheens Creek		0.15	0.50	3.74	23.40		0.04	0.31
East Plateau		0.03		0.18			0.17	
Ecstall	**6,878,539**	**0.65**		**2.45**	**17.00**	**0.500**	0.27	
El Amino		0.50		0.60	70.00		0.83	
Elaine Creek		3.04		0.09	11.70	1.525	33.78	
Horsefly		1.16	0.13	4.60	39.00	0.500	0.25	8.92
Horsefly South		5.60	0.09	1.65	30.00	0.860	3.39	62.22
Mariposite		0.03	0.04	0.12	5.50	0.110	0.24	0.66
Mark		0.14	0.01	0.02	0.06	0.002	7.00	14.00
Marlyn		0.01	0.01	0.05	0.05	0.020	0.10	0.50
Marmot		0.01	0.01	0.02	0.01	0.002	0.30	0.60
Packsack	**2,700,000**	**0.50**	**0.01**	**0.20**	**34.00**	**0.300**	2.50	50.00
Phobe Creek		0.69		0.01	2.22	0.251	104.55	
Rainbow		0.04	0.00	0.31	1.80		0.13	40.00
South Grid East		0.12		0.02			5.00	
Sphalerite		0.06	0.00	6.00	1.50	0.015	0.01	20.68
Steelhead		0.03	0.13	0.04	13.80	0.024	0.75	0.21
Strike		0.17	0.27	2.83	1.13	0.010	0.06	0.63
Third Outcrop		0.63		2.30			0.27	
Thirteen Creek		8.05		0.05	350.00	2.400	151.89	
Trench		0.03	0.00	0.12			0.28	7.17

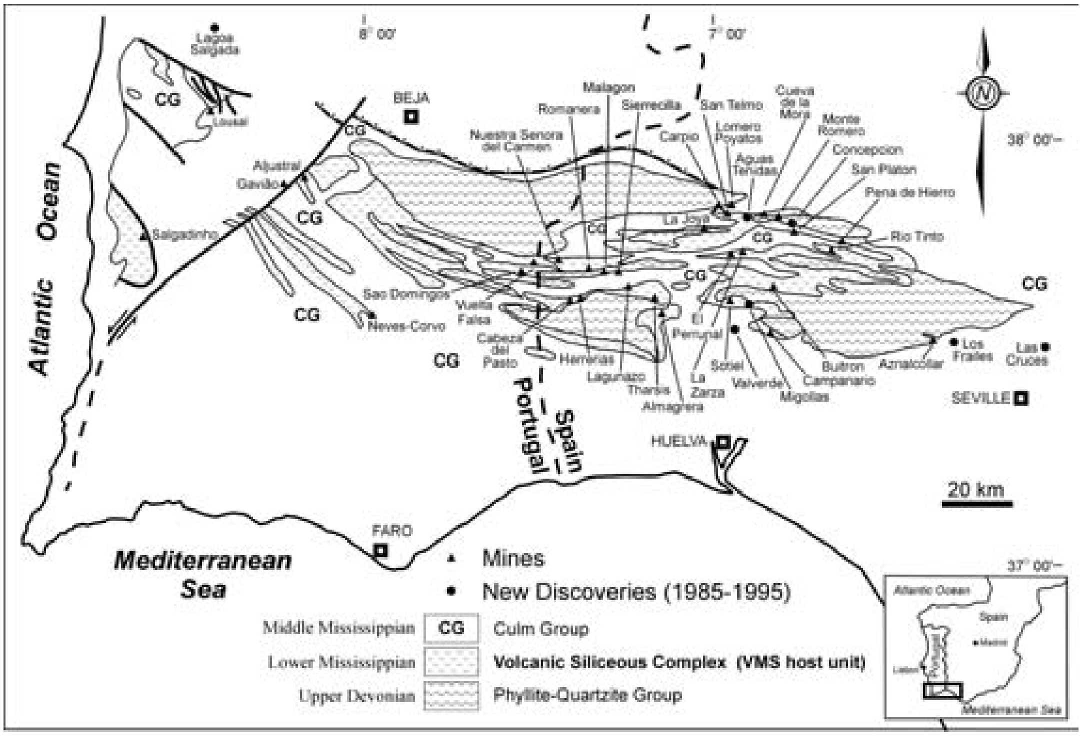

Figure 13. Volcanogenic massive sulphide deposits of the Iberian Pyrite Belt (modified from Leistel *et al.,* 1998).

TABLE 3
PRODUCTION, RESERVES AND CU:ZN AND CU:PB RATIOS FOR DEPOSITS AND PROSPECTS IN THE IBERIAN PYRITE BELT

Mine	Size (mT)	% Cu	% Pb	% Zn	g/t Ag	g/t Au	% Sn	Cu:Zn	Cu:Pb
Aguas Tenidas	41	1.3	0.9	3.1	37	0.5		0.42	1.44
Aljustrel	130	1.2	1.2	3.2	36	1		0.38	1.00
Almagrera	10	0.65	0.8	1.35	40	0.7		0.48	0.81
Aznalcollar	90	0.51	0.85	1.8	37	0.48		0.28	0.60
Cabeza del Pasto	0.6	1	3	1				1.00	0.33
Campanario	0.41	0.97	2	2.58				0.38	0.49
Carpio	3.35	0.5	0.12	2.77				0.18	4.17
Castillo Buitron	0.5	0.6	0.28	1.13				0.53	2.14
Concepcion	55.85	0.57	0.19	0.48	6.68	0.21		1.19	3.00
Cueva de la Mora	4.2	1.45	0.26	0.73				1.99	5.58
El Perrunal	7.55	0.5	0.1	0.2				2.50	5.00
Grupo Malagon	1	1.85	2	4				0.46	0.93
Herrerias	5	0.9	0.54	0.43				2.09	1.67
La Joya	1.19	0.5	0.65	0.2				2.50	0.77
La Romanera	34	0.42	1.18	2.3	44	0.8		0.18	0.36
La Zarza	100	0.7	0.6	1.5				0.47	1.17
Lagunazo	6	0.57	1.1	1.5	65	1.1		0.38	0.52
Las Cruces	42.7	2.95	1	2.14	5	0.2		1.38	2.95
Lomero Poyatos	1.71	0.5	4.5	7.5	120	4		0.07	0.11
Los Frailes	70	0.34	2.25	3.92	62			0.09	0.15
Lousal	50	0.7	0.8	1.4				0.50	0.88
Migollas	57.6	0.88	1.12	2.23				0.39	0.79
Monte Romero	0.8	2	2.5	5				0.40	0.80
Neves Corvo	80.81	3.12	0.74	4.11	37		0.22	0.76	4.22
Nuestra Senora del Carmen	0.04	1.3	10.3	29	153	1		0.04	0.13
Pena de Hierro	5	1.3	0.42	1.39				0.94	3.10
Rio Tinto	334.5	0.39	0.12	0.34	22	0.36		1.15	3.25
San Platon	1.13	1.16	0.53	12.3	69	2.05		0.09	2.19
San Telmo	4	1.2	0.4	12	60	0.8		0.10	3.00
Sao Domingos	27	1.25	1	2				0.63	1.25
Sierrecilla	1	1.5	5	12	500			0.13	0.30
Sotiel	75.2	0.56	1.34	3.16	24	0.21		0.18	0.42
Tharsis	110.06	0.5	0.6	2.7	22	0.7		0.19	0.83
Vuelta Falsa	1	1.27	8.8	20.7	307	9		0.06	0.14

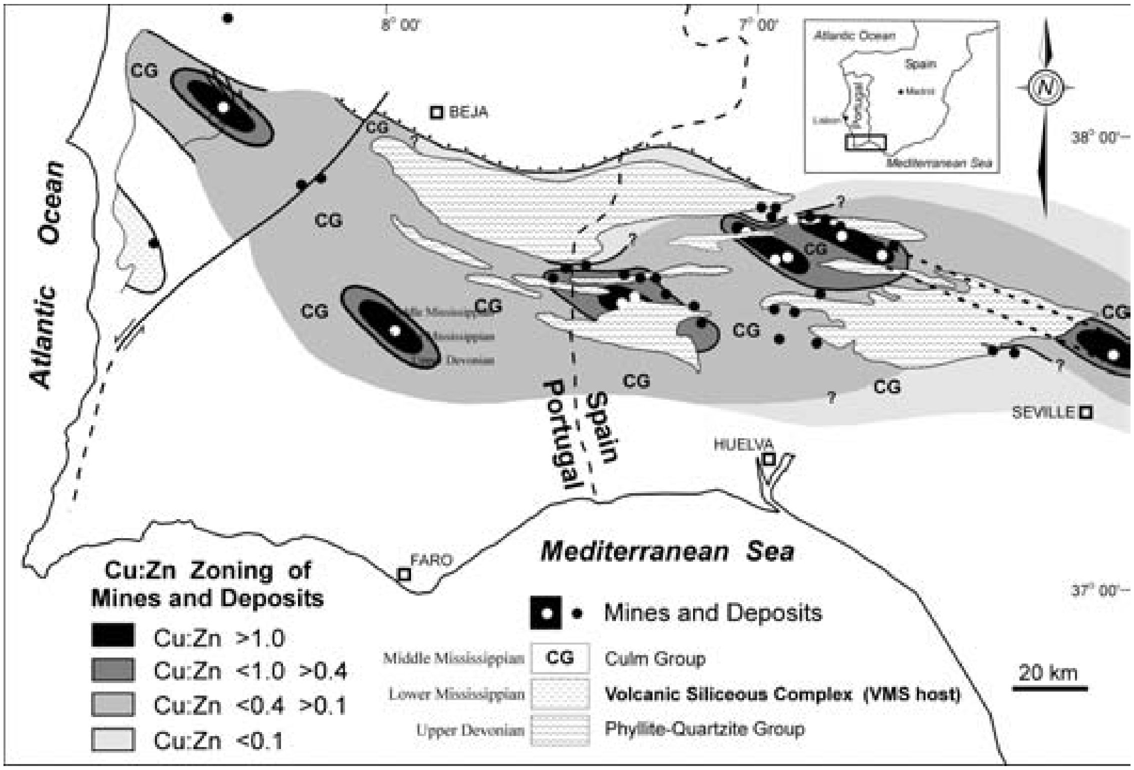

Figure 14a. Contoured Cu:Zn ratios for VMS deposits in the Iberian Pyrite Belt (*see* Table 3).

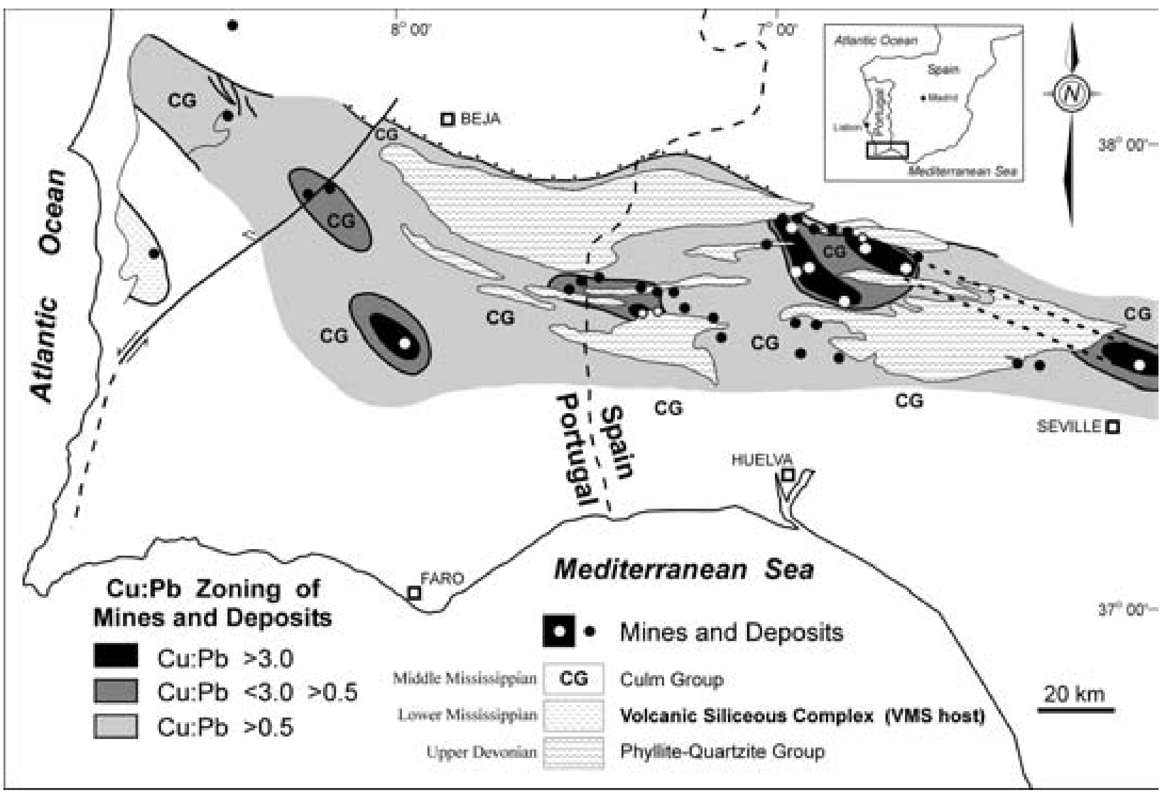

Figure 14b. Contoured Cu:Pb ratios for VMS deposits in the Iberian Pyrite Belt (*see* Table 3).

lack of lead analyses from these showings despite three seasons of exploration work.

Metal Zoning in the Iberian Pyrite Belt

Measuring just 250 kilometres east-west by 20-70 kilometres north-south, the Iberian Pyrite Belt (IPB) straddles the border between southern Portugal and Spain (Figure 13) and hosts more than 140 volcanogenic exhalative massive sulphide deposits within the Late Devonian-Early Mississippian strata of the Volcanic-Siliceous Complex, an average of more than one deposit per 2 km of strike length. The IPB is the setting for the Rio Tinto and Neves-Corvo mines, the second and third largest VMS deposits in the world after the Windy Craggy deposit of British Columbia.

The geology of the IPB is profiled in a special double issue of Mineralium Deposita (Marcoux and Leistel, 1998). No coeval subvolcanic intrusions have been documented through most of this large district. Boulter (1993) describes undated dolerite sills and felsic quartz-feldspar porphyry sills in the Rio Tinto area, and presents textural evidence that the felsic units are synvolcanic.

The technique for contouring Cu:Zn and Cu:Pb ratios was applied to the dataset of assay values for the deposits of the IPB. Published reserves (Leistel *et al.*, 1998) and calculated Cu:Zn and Cu:Pb ratios are listed in Table 3. As in the Ecstall belt, deposit locations are unevenly distributed. Contours are projected up through the unmineralised slates of the Culm Group, which rest as a thin veneer on the VMS host strata in the Volcanic-Siliceous Complex. Many recent discoveries are blind deposits located by drilling through this barren cover sequence (Figure 13).

Contoured maps of Cu:Zn and Cu:Pb ratios (Figure 14) show seven copper-rich centres located around the Lousal, Aljustrel, Neves-Corvo, Cabeza del Pasto, La Zarza, Rio Tinto and Las Cruces massive sulphide deposits. Significantly, other large VMS deposits, such as Tharsis, Aznalcollar and Los Frailes, have relatively low Cu:Zn and Cu:Pb ratios. Contour distributions indicate favourable areas within this extensive belt to search for copper-, gold-, zinc- or lead-rich VMS deposits. These patterns also reveal high Cu:Zn and Cu:Pb areas where coeval plutonic rocks might be preserved and exposed.

Other exploration applications are possible. The Rio Tinto mine and Las Cruces deposit are 55 kilometres apart. They may represent deposits formed near two separate thermal or magmatic centres, shown as separate Cu:Zn and Cu:Pb highs in Figure 14. However, they may lie within one elongate Cu:Zn and Cu:Pb contour high (shown as a dashed outline on Figure 14) that is now dissected where erosion has removed the favourable stratigraphy and exposed the unmineralised footwall strata. In the latter scenario, the area of volcanic rocks immediately east-southeast of the Rio Tinto mine is especially prospective for deposits with relatively high copper and gold grades.

DISCUSSION AND CONCLUSIONS

The high exploration potential and the partially explored status of the Ecstall Greenstone Belt are underscored by the recent discovery of four base metal showings in rock cuts along existing logging roads (Bell, West Road, Cheens Creek and F-13). Stream sediment sampling results from the new Regional Geochemical Survey reliably detect the geochemical signature of the major prospects in the belt, but also reveal 15 more drainage basins where the bedrock sources for the anomalous base metal concentrations in stream sediment samples have yet to be discovered.

The distribution of base metal and gold values in the stream sediment data in the Ecstall region show progressive, overlapping Cu>Au>Zn>Pb zoning outward from coeval subvolcanic plutons. Contours of Cu:Zn and Cu:Pb ratios calculated from assays from mineral prospects and deposits reproduce this same lateral zoning. These two independent lines of data suggest that copper-rich prospects are concentrated near the synvolcanic tonalite stocks while zinc-rich and lead-rich prospects are deposited far from these plutons. This pattern matches the metal zoning sequence demonstrated in an earlier study of the Mount Read volcanic belt in Tasmania (Large *et al*., 1996). Results in the Ecstall belt point to a copper-rich area around the Packsack deposit where synvolcanic plutons are not documented but are likely present. Results also suggest that the large tonalite stock postulated in the southwestern Ecstall belt may be an area primarily composed of volcanic rocks well-removed from the nearest coeval tonalite pluton.

Application of this technique to the world's largest VMS belt in southwestern Spain reveals a simple pattern for the assorted copper-rich and copper-poor deposits of the Iberian Pyrite Belt. Multiple copper-rich centres are present. Each represents an area where coeval subvolcanic plutons might be exposed. The easternmost Las Cruces deposit lies within a copper-rich, `pluton-associated' centre, so exploration potential for proximal copper-rich deposits and then distal zinc- and lead-rich deposits will extend for still farther to the east. The area east-southeast of the Rio Tinto mine is particularly favourable for undiscovered copper- and gold-rich deposits.

In summary, analysis of base metal distributions and contouring of base metal ratios from VMS camps can be accomplished using readily available reserve and assay data. Resolution and reliability can be improved by using an evenly distributed, higher density database, such as a regional geochemical survey. In combination, these two techniques can reveal the location and extent of coeval subvolcanic intrusive rocks, key components of the volcanic complex and the ore-forming process. Identification and delineation of synvolcanic plutons by these methods can be particularly helpful during the early years of exploration and mining in greenstone belts when geochronological confirmation is often lacking. Such analysis can help clarify the original geometry of volcanic belts in highly deformed terranes. Applied during exploration programs, these analytical tools effectively highlight underexplored areas and permit the selection of metal-specific target areas.

ACKNOWLEDGEMENTS

Field work by geologists Pat Desjardins and Mary Dubravcic contributed to the success of the 2001 field season. Ian Swan and Mike Haworth of Quantum Helicopters, Terrace, provided reliable logistical support in less than ideal conditions. Mike Fournier, BCGS, prepared the figures with care. Alan Galley, GSC, and Dave Lefebure, BCGS, improved this report with thorough reviews.

REFERENCES

Alldrick, D.J. (2001a): Geology and mineral deposits of the Ecstall greenstone belt (NTS 103H; 103 I); *BC Ministry of Energy and Mines*, Geological Fieldwork 2000, paper 2001-1, p.279-305

Alldrick, D.J. (2001b): Geology and mineral potential of the Ecstall VMS belt; *British Columbia and Yukon Chamber of Mines,* Annual Cordilleran Exploration Roundup, January, 2001, Abstracts, p.3-4

Alldrick, D.J. Friedman, R.M. and Childe, F.C. (2001): Age and geologic history of the Ecstall greenstone belt, northwest British Columbia; *B.C. Ministry of Energy and Mines*, Geological Fieldwork 2000, Paper 2001-1, p.269-278

Alldrick, D.J. and Gallagher, C.S. (2000): Geology and mineral potential of the Ecstall VMS belt (NTS 103H; 103 I); *B.C. Ministry of Energy and Mines*, Geological Fieldwork 1999, Paper 2000-1, p.249-265

Barrie, C.T., Cathles, L.M., Erendi, A., Schwaiger, H. and Murray, C. (1999): Heat and fluid flow in volcanic-associated massive-sulphide-forming hydrothermal systems; *in* Barrie, C.T. and Hannington, M.D., eds., Volcanic-associated massive sulphide deposits - processes and examples in modern and ancient settings, *Society of Economic Geologists*, Reviews in Economic Geology, v.8, p.201-219

Boulter, C.A. (1993): High-level peperitic sills at Rio Tinto, Spain - implications for stratigraphy and mineralization; Trans. Instn. Min. Metall. (Sect. B: Appl. Earth Sci.), v.102, January-April 1993, p.B30-B38

Campbell, I.H., Franklin, J.M., Gorton, M.P., Hart, T.R. and Scott, S.D. (1981): The role of subvolcanic sills in the generation of massive sulphide deposits; *Economic Geology*, v.76, n.8, p.2248-2253

Friedman, R.M., Gareau, S.A. and Woodsworth, G.J. (2001): U-Pb dates from the Scotia-Quaal metamorphic belt, Coast Plutonic Complex, central-western British Columbia; Radiogenic Age and Isotopic Studies: Report 14, *Geological Survey of Canada*, Current Research 2001-F9, 11p.

Galley, A.G. (1995): Target vectoring using lithogeochemistry: applications to the exploration for volcanic-hosted massive sulphide deposits; CIM Bulletin, May, 1995, Exploration Issue, v.88, n.990, p.15-27

Galley, A.G. (1996): Geochemical characteristics of subvolcanic intrusions associated with Precambrian massive sulphide districts; *in* Wyman D.A., ed., Trace element geochemistry of volcanic rocks - applications for massive sulphide exploration, *Geological Association of Canada*, Short Course Notes, v.12, p.239-278

Gareau, S.A. (1991a): Geology of the Scotia-Quaal metamorphic belt, Coast Plutonic Complex, British Columbia; unpublished Ph.D. thesis, Carleton University, 390p

Gareau, S.A. (1991b): The Scotia-Quaal metamorphic belt: a distinct assemblage with pre-early Late Cretaceous deformational and metamorphic history, Coast Plutonic Complex, British Columbia; Canadian Journal of Earth Sciences, v.28, p.870-880

Gareau, S.A. (1991c): Geology of the Scotia-Quaal metamorphic belt, Coast Plutonic Complex, British Columbia; Geological Survey of Canada, Open File Map 2337, scale 1:50 000, 4 sheets

Gareau, S.A., compiler (1997): Geology, Scotia-Quaal metamorphic belt, Coast Plutonic Complex, British Columbia; *Geological Survey of Canada*, Map 1868A, scale 1:100 000, 1 sheet

Gareau, S.A. and Woodsworth, G.J. (2000): Yukon-Tanana terrane in the Scotia-Quaal belt, Coast Plutonic Complex, central-western British Columbia; *in* Tectonics of the Coast Mountains, southeastern Alaska and British Columbia, *Geological Society of America*, Special Paper 343, p.23-43

Greenwood, H.J., Woodsworth, G.J., Read, P.B., Ghent, E.D. and Evenchick, C.A. (1992): Metamorphism; Chapter 16 *in* Geology of the Cordilleran Orogen in Canada, *Geological Survey of Canada*, Geology of Canada, n.4, p.533-570

Holyk, W., Padgham, W., Money, P. and Read, P.B. (1958): Geological map of the Ecstall River Area; unpublished map for the Texas Gulf Sulphur Company, 1 sheet, scale 1:126,720 (1inch = 2 miles)

Jackaman, W. (2001): Stream sediment and water geochemistry of the Ecstall Greenstone Belt; *B.C. Ministry of Energy and Mines*, Open File 2001-13, 216p.

Large, R.R., Doyle, M., Raymond, O., Cooke, D., Jones, A. and Heasman, L., 1996, Evaluation of the role of Cambrian granites in the genesis of world class VHMS deposits in Tasmania; *Ore Geology Reviews*, v.10, p.215-230

Leistel, J.M., Marcoux, E. Thiéblemont, D., Quesada, C., Sánchez, A. Almodóvar, G.R., Pascual, E. and Sáez, R. (1998): The volcanic-hosted massive sulphide deposits of the Iberian Pyrite Belt - review and preface to the thematic issue; Mineralium Deposita, v.33, n.1-2, p.2-30

Marcoux, E. and Leistel, J.M., editors (1998): Iberian Pyrite Belt Thematic Issue; Mineralium Deposita, v.33, n.1-2, January, 1998, 220p.

Padgham, W.A. (1958): The Geology of the Ecstall-Quaal Rivers area, British Columbia; unpublished M.Sc. thesis, *University of British Columbia*, 202p.

Read, P.B., Woodsworth, G.J., Greenwood, H.J., Ghent, E.D. and Evenchick, C.A. (1991): Metamorphic Map of the Canadian Cordillera; *Geological Survey of Canada*, Map 1714A, scale 1:2,000,000

Scott, B. (2001): Geology of the Amber-El Amino area, northwest British Columbia (NTS 103 H); *B.C. Ministry of Energy and Mines*, Geological Fieldwork 2000, Paper 2001-1, p.307-312

Stowell and McClelland, editors (2000): Tectonics of the Coast Mountains, southeastern Alaska and British Columbia, *Geological Society of America*, Special Paper 343, 289p.

van der Heyden, P. (1989): U-Pb and K-Ar geochronometry of the Coast Plutonic Complex, 53ºN to 54ºN, British Columbia, and implications for the Insular-Intermontane superterrane boundary; unpublished Ph.D. thesis, *University of British Columbia*, 392p.

Woodsworth, G.J., Anderson, R.G. and Armstrong, R.L. (1992): Plutonic Regimes; Chapter 15 *in* Geology of the Cordilleran Orogen in Canada, *Geological Survey of Canada*, Geology of Canada, n.4, p.491-531.

Age of Platinum-Group-Element Mineralization in the Sappho Alkaline Complex, South-Central British Columbia

By Graham T. Nixon[1] and Douglas A. Archibald[2]

KEYWORDS: *Geochronometry, geochronology, argon, Sappho, alkaline complex, platinum-group elements.*

INTRODUCTION

The Sappho mineral occurrence in south-central British Columbia (MINFILE 082ESE147; 49° 00’ 22” N, 118° 42’ 18” W) is part of the Boundary mining camp and one of a number of historical Cu-Ag-PGE(±Au) prospects associated with alkalic intrusive complexes in the province. The property is located approximately 10 kilometres south of Greenwood and 5 kilometres east of Midway (Figure 1). Between 1916 and 1918, 102 tonnes of ore with an average grade of 5.6 wt. % Cu and 61.7 g/t Ag was shipped to the smelter, followed by a further 9 tonnes in 1927-1928. Significant concentrations of platinum were detected in a grab sample of the chalcopyrite-pyrite ore which assayed 3.2 % Cu and 1.03 grams per tonne Pt (Minister of Mines Annual Report 1927). The historical record of copper production, combined with the potential for precious metals, has attracted intermittent interest from exploration companies ever since, especially over the past 40 years. The property is currently optioned to Gold City Industries Ltd. who have re-excavated the old workings and carried out geochemical analyses of soils, till and bedrock. Assays of mineralized bedrock have confirmed anomalous abundances of the platinum-group elements (PGE), and analytical data recently published by Hulbert (2001), for example, show values up to 4.34 g/t Pd, 2.26 g/t Pt, 76 g/t Ag and 0.75 g/t Au for semi-massive and disseminated sulfide-bearing samples.

The style of mineralization at Sappho has been referred to informally as “Coryell-type” due to its association with alkaline rocks correlated with the Tertiary (Eocene) Coryell Batholith in southern British Columbia (Hulbert *et al.*, 1987; Hulbert, 2001). Another alkaline-hosted Cu-Ag-PGE occurrence originally considered to be Eocene in age is the Maple Leaf prospect (82ENE007) which was mined in the early 1900s as part of the Franklin mining camp just north of Grand Forks (Fig. 1). It has since been shown, however, that the intrusion which hosts the Maple Leaf occurrence, the Averill plutonic complex, is Jurassic in age (Keep, 1989; Keep and Russell, 1992). The purpose of this study, therefore, was to provide evidence for the age of the Cu-Ag-PGE

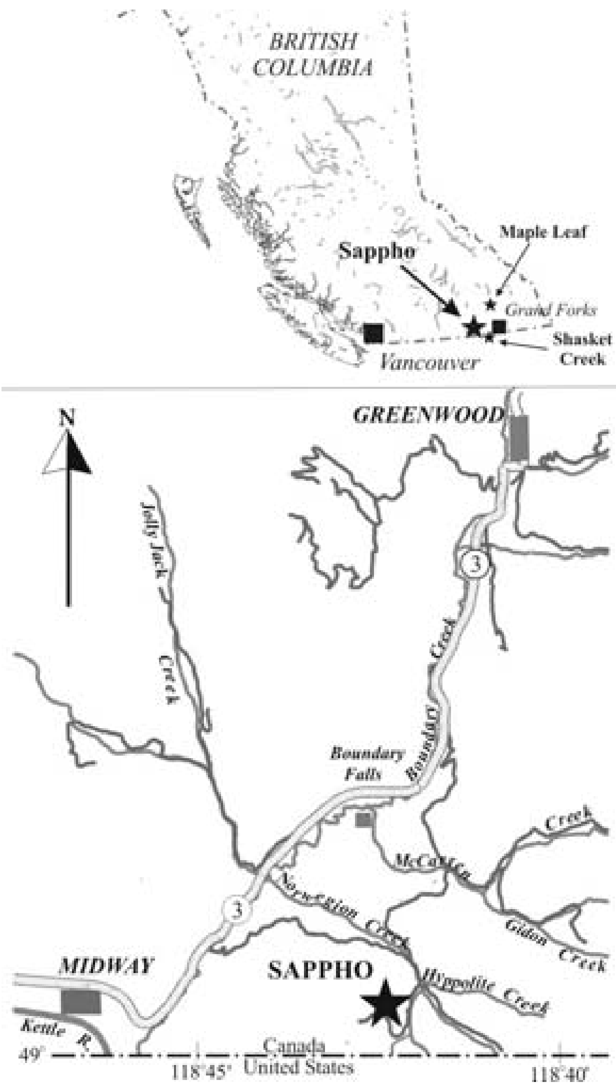

Figure 1. Location of the Sappho alkaline-hosted Cu-Ag-PGE occurrence in south-central British Columbia. Also shown are the locations of the Maple Leaf Cu-Ag-PGE prospect (Averill alkaline plutonic complex) and Shasket Creek alkaline complex in northern Washington State (*see* text).

[1] *British Columbia Ministry of Energy and Mines*
[2] *Queen’s University*

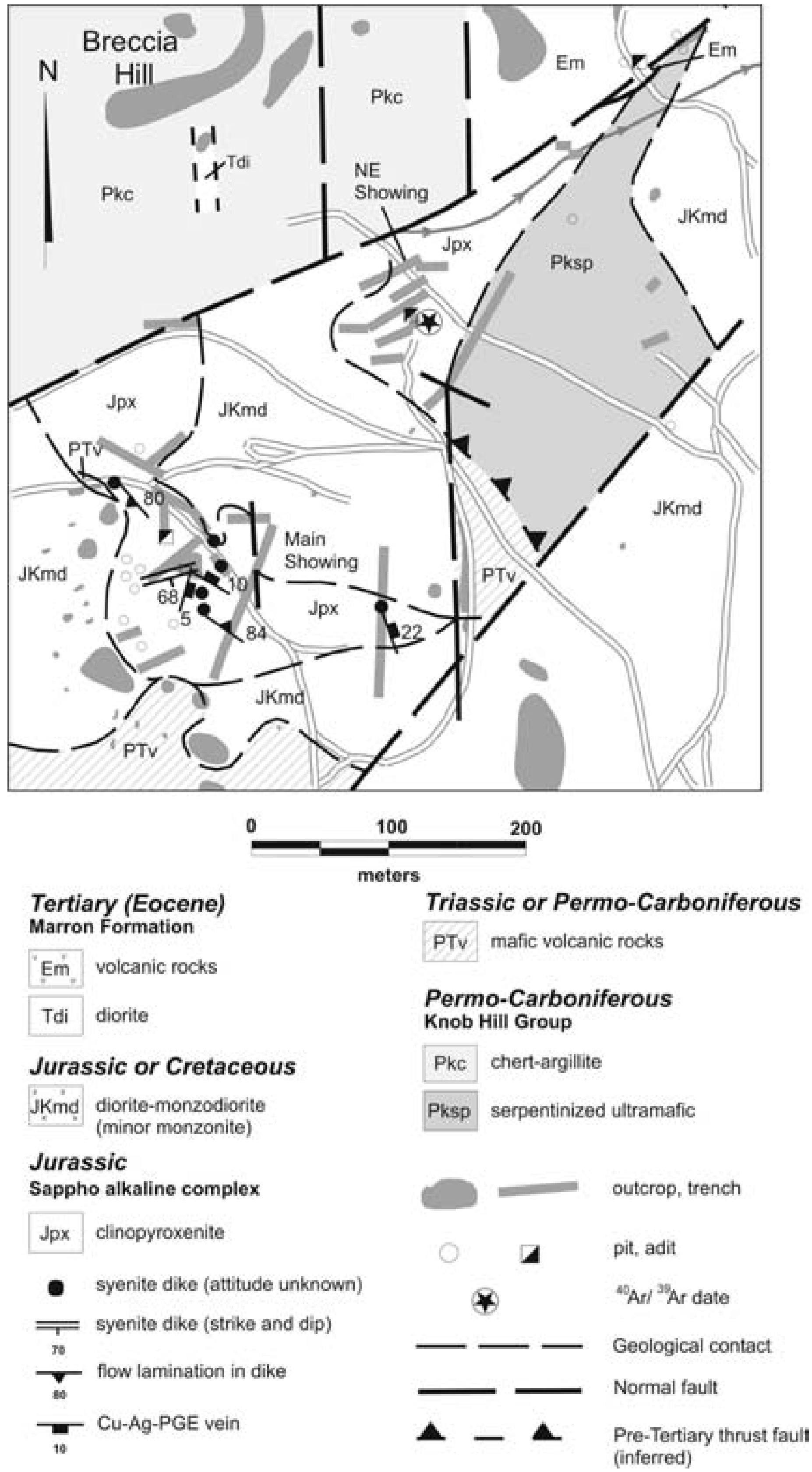

Figure 2. Geology of the Sappho alkaline complex showing location of sample collected for $^{40}Ar/^{39}Ar$ dating.

mineralization at Sappho using $^{40}Ar/^{39}Ar$ dating methods. The results given below are preliminary but sufficient to show that alkaline rocks which host the mineralization are Jurassic in age, and this is also considered to be the age of the mineralization.

CAPSULE GEOLOGY

The geology of the Sappho alkaline complex, named for the mineral occurrence, is shown in Figure 2. Exposure is extremely poor, and the position and nature of contacts between map units are inferred from fieldwork conducted last summer, a compilation of previous exploration work on the property, and detailed maps by Fyles (1990) and Church (1986). This geological compilation of the Sappho alkaline complex is currently available (Nixon, 2002).

In terms of Cordilleran settings, Sappho is located within Quesnellia, an accreted magmatic-arc terrane comprising Late Paleozoic basement rocks (Harper Ranch or Okanagan subterrane) overlain by Early Mesozoic volcanic-sedimentary sequences. The oldest rocks in the area belong to the Permo-Carboniferous Knob Hill and Attwood Groups. Knob Hill lithologies represent a disrupted ocean-floor assemblage of chert, metabasalt, gabbro/diorite and serpentinized peridotite (Fyles, 1990; Dostal *et al*. 2001). The Attwood Group (south and east of the area shown in Fig. 2) comprises argillite, phyllite, limestone and lesser mafic to intermediate volcaniclastic rocks of island-arc or back-arc affinity (Dostal *et al*. 2001). Stratigraphic relationships between these sequences are unknown. These older strata are unconformably overlain by clastic, carbonate and calc-alkaline volcanic rocks of the Middle Triassic Brooklyn Formation which contains detritus derived from erosion of Knob Hill obducted ophiolite sequences and was deposited in a mature island-arc setting (Dostal *et al*., 2001). The mafic volcanic rocks shown in Figure 2 were tentatively assigned to the Brooklyn Formation by Fyles (1990). Further contraction in late Early to Middle Jurassic time accompanied accretion of Quesnel terrane to the cratonic edge of North America (Hoy and Dunne, 1997). Renewed volcanism (Marron Formation) and dike emplacement occurred in the Tertiary (Eocene) accompanied by extensional tectonism which reactivated older structures and generated new ones. The Sappho area lies at the eastern margin of the Toroda Creek graben which is defined by an intersecting set of northeasterly to northerly trending structures (Fig. 2).

The Sappho alkaline complex comprises biotite-hornblende clinopyroxenite, the dominant lithology, minor melanocratic monzonite and dikes of potassium-feldspar porphyritic syenite which cut the pyroxenite. The feldspathic phases of the complex contain melanitic garnet (titanian andradite) with igneous textures, and the syenite dikes locally exhibit a planar alignment of feldspar phenocrysts. Church and Robertson (1983) described the clinopyroxenite as "shonkinite" which, according to Le Maitre *et al*. (1989), requires the presence of essential feldspathoid minerals and none have been observed. The pyroxenite commonly contains veins and disseminations of calcite locally accompanied by epidote, chlorite and white mica; the dikes are typically seriticized. The alkaline rocks are in contact with a larger dioritic intrusion which appears to be younger based on its lesser degree of alteration and lack of syenite dikes. A sample of this intrusion is currently being dated by U-Pb techniques.

The Cu-Ag-PGE mineralization occurs in semi-massive to massive veins, blebs and pods of chalcopyrite-pyrite-magnetite ore and as sulfide disseminations hosted by pyroxenite and syenite dykes. The sulfide veins are predominantly controlled by gently dipping fractures and shears in the pyroxenite (Fig. 2). Thin leucocratic melanite-bearing syenite veins, apophyses of the dikes, have been observed occupying some of these fractures and are found locally at the margins of sulfide-oxide assemblages. The intimate structural and textural relationships between the mineralization and the felsic dykes imply a genetic relationship. Furthermore, the alkalic nature of the pyroxenite and feldspathic phases, underscored by the presence of primary melanite garnet, support previous inferences of a common magmatic lineage (Gilmour, 1981; Church and Robertson, 1983). The Cu-Ag-PGE mineralization is therefore considered to be late magmatic or magmatic-hydrothermal in origin and bears mineralogical traits commonly assigned to the alkalic porphyry deposit-type (Barr *et al*., 1976).

SAMPLE DESCRIPTION

The sample submitted for dating is a biotite-hornblende clinopyroxenite collected from outcrop at the entrance to an adit at the north-east showing (Fig. 2). The rock is a dark grey-green, medium-grained, moderately magnetic clinopyroxenite that is extensively fractured and locally stained by malachite and azurite. The rock contains dark greenish-black hornblende and minor amounts of fresh biotite; hornblende also occurs in localized segregations of coarse subhedral crystals (5-10 mm) intergrown with minor feldspar. The outcrop is cut by numerous white carbonate veinlets several millimetres to a centimeter wide, and calcite also occurs as poikilitic replacements enclosing relatively fresh hornblende. Chlorite, minor epidote and hematitic alteration are locally conspicuous. The copper carbonate stains are derived from local sulfide disseminations (trace to 4 vol. %) and thin veins of chalcopyrite-pyrite-magnetite (≤6 cm in width) which cut the clinopyroxenite and dip shallowly to the north.

In thin section, the rock is a hornblende clinopyroxenite carrying minor amounts of biotite, feldspar, apatite, magnetite and sphene. Colourless to pale green diopsidic pyroxene (2-4 mm) displays mutual intergrowths with primary hornblende and is partially altered to secondary amphibole (?actinolitic) and calcite. Primary hornblende (≤5 mm) exhibits brownish green to deep green pleochroism and may poikilitically enclose magnetite and apatite. The coarser hornblende segregations are observed to contain minor alkali feldspar and rare biotite. The alkali feldspar occurs as anhedral interstitial grains with patchy extinction or perthitic texture and rarely encloses subhedral sodic plagioclase. Biotite (≤2 mm) exhibits dark greenish brown to nearly colourless pleochroism and is partially altered along cleavages to chlorite and secondary granular sphene. Small amounts of apatite (≤0.4 mm; ~2 vol. %) forms euhedral to subhedral grains commonly intergrown with subhedral to anhedral magnetite (£1.5 mm; ~3 vol. %); and primary sphene forms brownish grey anhedral crystals (£0.4 mm; <1 vol. %).

ANALYTICAL METHODS

Mineral separates and flux-monitors (standards) are wrapped in Al-foil and the resulting disks are stacked vertically into a 11.5 cm long and 2.0 cm diameter container, and then irradiated with fast neutrons in position 5C of the McMaster Nuclear Reactor (Hamilton, Ontario) for a duration appropriate for the expected age of the sample. Groups of flux monitors (typically 12 in total) are located at ca. 1 cm intervals along the irradiation container and J-values for individual samples are determined by second-order polynomial interpolation between replicate analyses of splits for each postion in the capsule. Typically, J-values are between ca. 0.003 and 0.03 and vary by <10% over the length of the capsule. No attempt is made to monitor horizontal flux gradients as these are considered to be minor in the core of the reactor.

For total fusion of monitors and step-heating using a laser, the samples are mounted in an aluminum sample-holder, beneath the sapphire view-port of a small, bakeable, stainless-steel chamber connected to an ultra-high vacuum purification system. An 8W Lexel 3500 continuous argon-ion laser is used. For total-fusion dating the beam is sharply focused; for step-heating the laser beam is defocused to cover the entire sample. Heating periods are ca. 3 minutes at increasing power settings (0.25 to 7 W). The evolved gas, after purification using an SAES C50 getter (ca. 5 minutes), is admitted to an on-line, MAP 216 mass spectrometer, with a Baur-Signer source and an electron multiplier (set to a gain of 100 over the Faraday). Blanks, measured routinely, are subtracted from the subsequent sample gas-fractions. The extraction blanks are typically $<10 \times 10^{-13}$, $<0.5 \times 10^{-13}$, $<0.5 \times 10^{-13}$, and $<0.5 \times 10^{-13}$ cm^{-3} STP for masses 40, 39, 37, and 36, respectively.

Measured argon-isotope peak heights are extrapolated to zero-time, normalized to the $^{40}Ar/^{36}Ar$ atmospheric ratio (295.5) using measured values of atmospheric argon, and corrected for neutron-induced ^{40}Ar from potassium, ^{39}Ar and ^{36}Ar from calcium (using production ratios of Onstott and Peacock, 1987), and ^{36}Ar from chlorine (Roddick, 1983). Dates and errors are calculated using formulae given by Dalrymple *et al*. (1981), and the constants recommended by Steiger and Jaeger (1977). Isotope correlation analysis used the formulae and error propagation of Hall (1981) and the regression of York (1969). Errors shown in the tables and on the age spectra and isotope correlation diagrams represent the analytical precision at 2σ, assuming that the errors in the ages of the flux monitors are zero. This is suitable for comparing within-spectrum variation and determining which steps form a plateau (McDougall and Harrison, 1988, p. 89). A conservative estimate of this error in the J-value is 0.5% and can be added for inter-sample comparison. The dates and J-values for the intralaboratory standard (*e.g.*, MAC-83 biotite at 24.36 Ma) are referenced to TCR sanidine at 28.0 Ma (Baksi *et al*., 1996) for young samples and to Hb3Gr hornblende at 1071 Ma for old samples.

RESULTS

The material analyzed consisted of ca. 25 fine-grained, hand-picked crystals of green hornblende. Some grains are intergrown with a small amount of alkali feldspar along grain boundaries and may have had thin overgrowths of a clear to pale green, optically zoned biotite.

The analytical data are given in Table 1 and the age spectrum is shown in Figure 3A. The spectrum is complex and typical of samples that are mixtures of more than one phase. The variation in the calculated Ca/K ratio (Table 1) shows that the low- and high-temperature parts of the spectrum are dominated by Ar release from a K-rich phase whereas the mid-temperature steps (3.75 to 4.25 W) record Ar release from a more Ca-rich phase (with a Ca/K ratio ≥ 5.6).

The first four, low-temperature steps have high atmospheric contamination and large errors but plot on an argon isotope correlation diagram as a linear array with a near-atmospheric $^{40}Ar/^{36}Ar$ ratio (Fig. 3B). The y-intercept yields a date of 100 ± 9 Ma for these steps. The significance of this date is not known. It may reflect argon re-distribution during post-emplacement tectonothermal events (see discussion).

The 4.25 W step yielded 28% of ^{39}Ar and the maximum date in the spectrum (156 ± 3 Ma at the 2σ level of confidence). The calculated Ca/K ratio of 5.6 for this step is typical of many hornblendes. However, because biotite and alkali feldspar release argon over a wider temperature range and fuse at a higher temperature than hornblende both the Ca/K ratio and the date for this step should be taken as minimum estimates. Accordingly, this spectrum shows that the Sappho clinopyroxenite is older than 156 Ma and most likely Jurassic in age.

DISCUSSION

The $^{40}Ar/^{39}Ar$ date reported above for primary igneous amphibole in Sappho pyroxenite places a minimum age of 156 ± 3 Ma (2σ) (Late Jurassic) on emplacement of the alkalic complex and hence the Cu-Ag-PGE mineralizing event with which it is genetically associated. Interestingly, this date is concordant with a conventional K-Ar date of 150 ± 10 Ma (2σ) obtained on an impure mineral separate (hornblende + biotite + clinopyroxene) from the Averill alkaline complex which hosts the Maple Leaf Cu-Ag-PGE occurrence (Keep, 1989). Also of note is the age of the Shasket Creek alkaline intrusive complex situated just across the International Boundary near Danville (Fig. 1) which may also be Jurassic. Syenite porphyry dikes from this complex cut Permian and Triassic limestones and, at the historic Comstock Mine, are intimately associated with copper ores

TABLE 1
RESULTS OF ^{40}AR/ ^{39}AR LASER STEP-HEATING EXPERIMENTS

01GNX1-2-2 Hornblende

J Value: 0.007650±0.000058
Maximum Date: 156±3
Initial $^{40}Ar/^{36}Ar$ Ratio: 312.03±63.15 (MSWD: 1.54)

Volume ^{39}ArK: 123.16
%^{39}ArK for MD: 27.75

Integrated Date: 137.7±2.3
Isotope Correlation Date: 100.1±8.5
%^{39}ArK for CD: 17.48

		Isotope Volumes					Isotope Ratios			
	Laser Power (Watts)	^{40}Ar	^{39}Ar	^{38}Ar	^{37}Ar	^{36}Ar	$^{40}Ar/^{39}Ar$	$^{38}Ar/^{39}Ar$	$^{37}Ar/^{39}Ar$	$^{36}Ar/^{39}Ar$
1	0.75	9.915±0.101	0.068±0.003	0.021±0.003	0.012±0.002	0.031±0.002	145.551±0.041	0.306±0.140	0.175±0.173	0.453±0.078
2	1.50	5.655 0.028	0.257 0.003	0.015 0.003	0.079 0.003	0.015 0.002	22.039 0.014	0.057 0.178	0.308 0.034	0.057 0.149
3	2.25	7.099 0.046	0.517 0.004	0.016 0.003	0.050 0.002	0.013 0.002	13.725 0.010	0.030 0.163	0.096 0.046	0.026 0.154
4	3.00	11.598 0.060	1.335 0.006	0.043 0.003	0.291 0.004	0.008 0.002	8.684 0.007	0.032 0.075	0.218 0.014	0.006 0.265
5	3.75	20.788 0.078	1.895 0.008	0.109 0.004	0.725 0.006	0.004 0.002	10.970 0.006	0.058 0.039	0.383 0.010	0.002 0.507
6	4.25	40.689 0.141	3.441 0.010	0.219 0.007	1.384 0.010	0.006 0.002	11.826 0.005	0.064 0.034	0.402 0.008	0.002 0.391
7	4.75	11.329 0.037	1.043 0.005	0.056 0.003	0.227 0.146	0.002 0.002	10.857 0.006	0.054 0.062	0.217 0.645	0.002 1.141
8	5.50	15.389 0.098	1.511 0.007	0.074 0.004	0.328 0.212	0.003 0.002	10.187 0.008	0.049 0.054	0.217 0.646	0.002 0.782
9	7.00	23.190 0.148	2.348 0.010	0.104 0.004	0.459 0.330	0.003 0.002	9.878 0.008	0.044 0.039	0.196 0.719	0.001 0.720

	Isotope Correlation Data								
	$^{36}Ar/^{40}Ar$	$^{39}Ar/^{40}Ar$	r	Ca/K	Cl/K	%^{40}Ar atm	% ^{39}Ar	$^{40}Ar^*/^{39}ArK$	Age
1	0.002883±0.000221	0.006567±0.000329	0.180	2.235	0.046	85.18	0.53	22.54±9.58	287.0±112.8
2	0.002247 0.000387	0.044824 0.000657	0.014	4.229	0.006	66.31	2.05	7.50 2.55	100.6 33.3
3	0.001584 0.000293	0.072422 0.000752	0.023	1.292	0.002	46.70	4.15	7.35 1.20	98.6 15.7
4	0.000461 0.000183	0.114747 0.000804	0.010	3.001	0.004	13.57	10.75	7.53 0.48	101.0 6.2
5	0.000033 0.000107	0.090674 0.000514	0.003	5.293	0.010	0.95	15.27	10.92 0.35	144.8 4.5
6	0.000019 0.000055	0.084089 0.000386	0.005	5.568	0.011	0.54	27.75	11.83 0.20	156.3 2.5
7	0.000004 0.000370	0.091664 0.000950	0.661	3.000	0.009	0.09	8.40	10.90 0.69	144.5 8.8
8	0.000015 0.000332	0.097750 0.001105	0.635	3.000	0.008	0.41	12.17	10.19 0.42	135.4 5.4
9	0.000003 0.000321	0.100859 0.001102	0.661	2.700	0.007	0.07	18.93	9.91 0.32	131.8 4.0

Isotope Production Ratios: ($^{40}Ar/^{39}Ar$)K = 0.0302; ($^{37}Ar/^{39}Ar$)Ca = 1416.4306; ($^{36}Ar/^{39}Ar$)Ca = 0.3952; Ca/K = 1.83 x ($^{37}ArCa/^{39}ArK$)
All volumes are x10^{9} cm^{3} NTP; all errors are x2 standard error
CD = Correlation date; MD = Maximum date

(chalcopyrite-bornite) which are known to carry anomalous concentrations of PGE (Parker and Calkins, 1964; Mutschler and Mooney, 1993). The only reported isotopic age for these rocks appears to be a $^{40}Ar/^{39}Ar$ date of 168 ± 0.4 Ma obtained on white mica associated with a "mineralizing alkalic intrusion" (Berger *et al*., 1991). The thermal-release spectra of white mica in both this sample and altered pre-Cretaceous metavolcanic rocks and serpentinites in the area indicate thermal disturbances at ≤118.5 ± 1.5 Ma (mid-Early Cretaceous), 103-104 Ma (late Early Cretaceous) and 50-60 Ma (Late Paleocene – Early Eocene). It is possible, therefore, that the inverse isochron date of 100 ± 9 Ma obtained in this study for Sappho hornblende relates to one or more of these events.

In view of the Jurassic age for the Sappho alkaline complex and its associated Cu-Ag-PGE sulfides, it is recommended that use of the term "Coryell-type" be discontinued when referring to this style of mineralization.

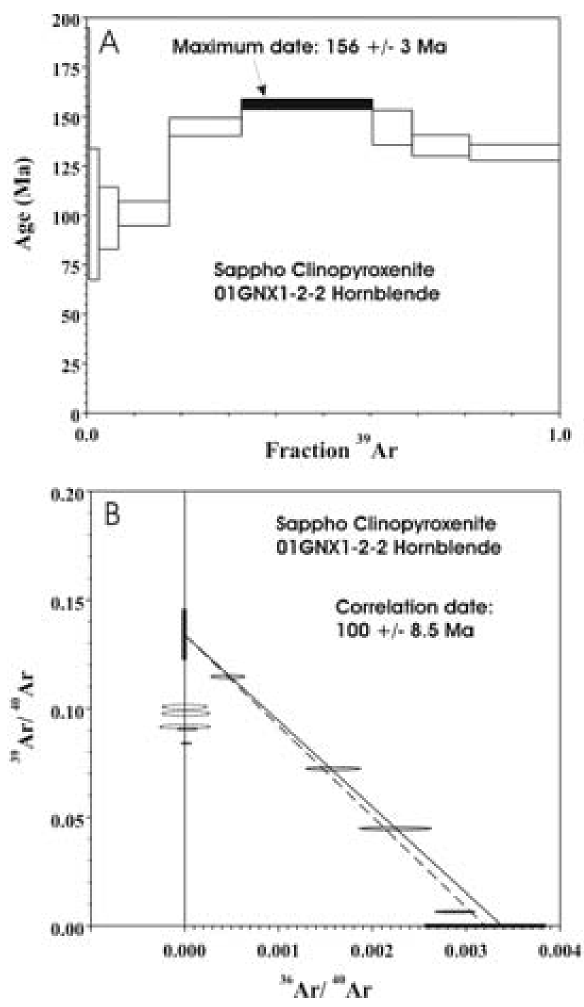

Figure 3. A. Plot of the age spectrum; the solid step indicates the fraction of ^{39}Ar released for the maximum date.
Figure 3. B. Inverse isochron plot. The dashed line is the best-fit line through the solid error ellipses; the size of the ellipse is an indication of the 2σ error associated with the ratios for each step. Ellipses on the ordinate were not included in the age calculation. The solid line connects the best-fit inverse $^{40}Ar/^{39}Ar$ ratio to the inverse atmospheric $^{40}Ar/^{36}Ar$ ratio. The near correspondence of the two lines indicates that the low-temperature steps do not contain excess argon. All quoted errors are given at the 2σ level of confidence.

ACKNOWLEDGMENTS

We would like to thank Gold City Industries Ltd. for providing access to the Sappho property and making available geological information. In particular, GN extends sincere thanks to Linda Caron and Alan Raven for freely sharing their knowledge of the property and geological experience. T. D. Ullrich assisted with the isotopic analysis, Aaron Dow crafted the figures and Dave Lefebure edited the manuscript. The Geochronology Laboratory at Queen's University is supported by a NSERC operating grant to J. K. W. Lee.

REFERENCES

Barr, D. A., Fox, P. E., Northcote, K. E. and Preto, V. E. (1976): The Alkaline Suite Porphyry Deposits. A Summary; in Sutherland-Brown, A. (Editor), Porphyry Deposits of the Canadian Cordillera, *Canadian Institute of Mining and Metallurgy*, Special Volume 15, pages 359-367.

Baksi, A. K., Archibald, D. A. and Farrar, E. (1996): Intercalibration of $^{40}Ar/^{39}Ar$ Dating Standards; *Chemical Geology*, Volume 129, pages 307-324.

Berger, B. R., Snee, L. W., Silberman, M. L. and Box, S. E. (1991): Jurassic to Middle Eocene Tectonic, Magmatic and Geothermal Events in Northeastern Washington; *Geological Society of America*, Abstracts with Programs, Volume 23, page A433.

Church, B. N. (1986): Geological Setting and Mineralization in the Mount Attwood – Phoenix Area of the Greenwood Mining Camp; *B. C. Ministry of Energy, Mines and Petroleum Resources*, Paper 1986-2, 65 pages.

Church, B. N. and Robertson, S. (1983): Geology and Magnetometer Survey of the Sappho Gold-silver-platinum-copper Prospect (82E/2); in Geological Fieldwork 1992, *B. C. Ministry of Energy, Mines and Petroleum Resources,* Paper 1983-1, pages 27-31.

Dalrymple, G. B., Alexander, Jr., E. C., Lanphere, M. A. and Kraker, G. P. (1981): Irradiation of Samples for $^{40}Ar/^{39}Ar$ Dating using the Geological Survey TRIGA Reactor, *U.S. Geological Survey*, Professional Paper 1176, 55 pages.

Dostal, J., Church, B. N. and Hoy, T. (2001): Geological and Geochemical Evidence for Variable Magmatism and Tectonics in the Southern Canadian Cordillera: Paleozoic to Jurassic Suites, Greenwood, Southern British Columbia; *Canadian Journal of Earth Sciences*, Volume 38, pages 75-90.

Freeland, P. B. (1927): Sappho; *B. C. Minister of Mines*, Annual Report, pages 234-235.

Fyles, J. T. (1990): Geology of the Greenwood – Grand Forks Area, British Columbia: *B. C. Ministry of Energy, Mines and Petroleum Resources*, Open File 1990-25, 19 pages.

Gilmour, W. R. (1981): The Sappho Property, Norwegian Creek, Greenwood Mining Division; *B. C. Ministry of Energy, Mines and Petroleum Resources*, Assessment Report 9364, 18 pages.

Hall, C.M. (1981): The Application of K-Ar and $^{40}Ar/^{39}Ar$ Methods to the Dating of Recent Volcanics and the Laschamp Event; Unpublished Ph.D. thesis, *University of Toronto*, 186 pages.

Hoy, T. and Dunne, K. P. E. (1997): Early Jurassic Rossland Group, Southern British Columbia: Part I – Stratigraphy and Tectonics*; B.C. Ministry of Employment and Investment*, Bulletin 102, 123 pages.

Hulbert, L. J. (2001): Digital Map and Database of mafic-ultramafic hosted Ni, Ni-Cu, Cr ± PGE Occurrences and Mafic-ultramafic Bodies in British Columbia; *B. C. Ministry of Energy and Mines,* Geoscience Map 2001-2.

Hulbert, L. J., Duke, M. J., Eckstrand, O. R., Lydon, J. W., Scoates, R. F. J., Cabri, L. J. and Irvine, T. N. (1987): Geological Environments of the Platinum-Group Elements; *GeologicalAssociation of Canada*, Cordilleran Section Workshop, Vancouver, 151 pages.

Keep, M. (1989): The Geology and Petrology of the Averill Plutonic Complex near Grand Forks, British Columbia; Unpublished M.Sc. thesis, *University of British Columbia*, 64 pages.

Keep, M. and Russell, J. K. (1992): Mesozoic Alkaline Rocks of the Averill Plutonic Complex; *Canadian Journal of Earth Sciences*, Volume 29, pages 2508-2520.

Le Maitre, R. W. (Editor) (1989): A Classification of Igneous Rocks and Glossary of Terms*; Blackwell Scientific Publications*, Oxford, 193 pages.

McDougall, I. and Harrison, T. M. (1988): Geochronology and Thermochronology by the $^{40}Ar/^{39}Ar$ Method; *Oxford University Press*, NewYork, 212 pages.

Mutschler, F. E. and Mooney, T. C. (1993): Precious Metal Deposits Related to Alkaline Igneous Rocks – Provisional Classification, Grade-Tonnage Data and Exploration Frontiers; in Kirkham, R. V., Sinclair, W. D., Thorpe, R. I. And Duke, J. M. (Editors), Mineral Deposit Modeling; *Geological Association of Canada*, Special Paper 40, pages 479-520.

Nixon, G. T. and Carbno, B. (2001): Whiterocks Mountain Alkaline Complex, South-central British Columbia: Geology and Platinum-group-element Mineralization; in Geological Fieldwork 2000, *B. C. Ministry of Energy, Mines and Petroleum Resources*, Paper 2000-1, pages 191-222.

Nixon, G. T. (2002): Geology of the Sappho Alkaline Complex, South-central British Columbia; *B. C. Ministry of Energy and Mines*, Open File 2002-7.

Parker, R. L. and Calkins, J. A. (1964): Geology of the Curlew Quadrangle, Ferry County, Washington; *U. S. Geological Survey*, Bulletin 1169, 95 pages.

Onstott, T. C. and Peacock, M. W. (1987): Argon Retentivity of Hornblendes: A field Experiment in a Slowly Cooled Metamorphic Terrane. *Geochimica et Cosmochimica Acta*, Volume 51, pages 2891-2904.

Roddick, J. C. (1983): High-precision Intercalibration of $^{40}Ar/^{39}Ar$ Standards. *Geochimica et Cosmochimica Acta*, Volume 47, pages 887-898.

Steiger, R. H. and Jaeger, E. (1977): Subcommission on Geochronology: Convention on the Use of Decay Constants in Geo- and Cosmo-chronology, *Earth and Planetary Science Letters*, Volume 36, pages 359-362.

York, D. (1969): Least-squares Fitting of a Straight Line with Correlated Errors; *Earth and Planetary Science Letters*, Volume 5, pages 320-324.

Depositional Setting of Silver-Rich Quartz-Sulphate-Carbonate Deposits of the Upper Kitsault River Area, Northwest British Columbia

By Kathryn P.E. Dunne and Robert H. Pinsent

KEYWORDS: *Economic geology, quartz, barite, sphalerite, silver, lead, zinc, epithermal vein deposits, exhalative deposits, subaqueous hot-spring deposits, fluid inclusions, salinity, homogenization temperature, Kitsault River, Alice Arm, Dolly Varden, Torbrit, Northstar, Wolf.*

INTRODUCTION

The Upper Kitsault River area lies approximately 23 to 30 km north of Alice Arm, in the Skeena Mining Division, British Columbia. Mineral occurrences are of three principal types: copper and gold-rich quartz-chlorite stockwork deposits, silver-rich quartz-sulphate-carbonate deposits; and molybdenum-rich quartz stockwork deposits (Alldrick *et al*., 1987). The first two types are hosted by lower Jurassic volcanic and sedimentary strata, near the top of the Hazelton volcanic arc sequence (Alldrick *et al.*, 1987; Godwin *et al.*, 1991). The third is considerably younger and is associated with a suite of Eocene quartz monzonite intrusions (Alldrick *et al.*, 1986).

There are conflicting opinions as to the origins of the silver-rich, quartz-sulphate-carbonate deposits. Originally, they were considered to be structurally-controlled "replacement" veins (Black, 1951; Campbell, 1959; Mitchell, 1973; Thompson and Michna, 1978). However, more recent work suggests that they may be exhalative in origin (Devlin and Godwin, 1986; Devlin, 1987). Pinsent (2001) discusses the previous work and provides descriptions of some of the more important occurrences in the upper Kitsault River area, and comments on similarities between the geological setting of the deposits and those at Eskay Creek (MINFILE 104B 008).

This report presents new fluid inclusion data from the past-producing silver-rich, quartz-sulphate-carbonate Torbrit (MINFILE 103P 191) and Dolly Varden (MINFILE 103P 188) deposits and the nearby Northstar (MINFILE 103P 189) and Wolf (MINFILE 103P 191) prospects (Figure 1). Fluid inclusions in quartz, sphalerite and barite from a variety of "grab-samples" of vein, breccia, disseminated, stringer and semi-massive styles of mineralization have been evaluated. Although the underground workings are no longer accessible and the precise location of only a few of the samples are known, temperature and composition data are used to establish the broad depositional environment of the deposits. The results are compared with published fluid inclusion data from volcanogenic massive sulphide, epithermal and hot-spring-type deposits, including the precious-metal rich Eskay Creek subaqueous hot-spring deposit.

[1] *Consulting Geologist*
[2] *British Columbia Ministry of Energy and Mines*

GEOLOGICAL SETTING

The upper Kitsault River area is underlain by sedimentary and volcanic rocks of the upper Triassic Stuhini (Units 1 and 2; Figure 1) and lower Jurassic Hazelton (Units 3, 4 and 5; Figure 1) groups and sedimentary rocks of the lower-middle Jurassic Salmon River Formation (MacIntyre *et al.*, 1994; Alldrick *et al.,* 1986; Dawson and Alldrick, 1986). Open folds and faults affect the distribution of Hazelton Group andesitic pyroclastic and intercalated sedimentary rocks that host the silver-rich, quartz-sulphate-carbonate deposits (Dawson and Alldrick, 1986). The Dolly Varden, Northstar, Torbrit and Wolf deposits are in green and maroon andesites and related volcaniclastic sediments near the inferred top of the Hazelton volcanic arc. The rocks are disconformably overlain by fossiliferous sediments of the Salmon River Formation. The deposits are on the east side of a major northwesterly-trending, northerly plunging syncline. Dawson and Alldrick (1986) report that the entire Jurassic section in the Kitsault valley has undergone greenschist facies metamorphism. There are relatively few mapped intrusions in the Kitsault River area and virtually none in the vicinity of the deposits (cf., Figures 2 and 3, Pinsent, 2001; Devlin, 1987; Drown *et al.*, 1990).

SILVER-RICH QUARTZ-CARBONATE-SULPHATE DEPOSITS

Pinsent (2001) subdivides the silver-rich quartz-carbonate-sulphate and related deposits on the east side of the upper Kitsault River (Figure 1) into 3 types: 1) epigenetic silver-lead-zinc quartz-carbonate vein (*e.g.* Wolf); 2) syngenetic strontium-barium-lead-zinc-silver (*e.g.* Sault); and 3) epigenetic or syngenetic silver-lead-zinc-barium-strontium (*e.g.* Torbrit, Dolly Varden, Northstar) deposits.

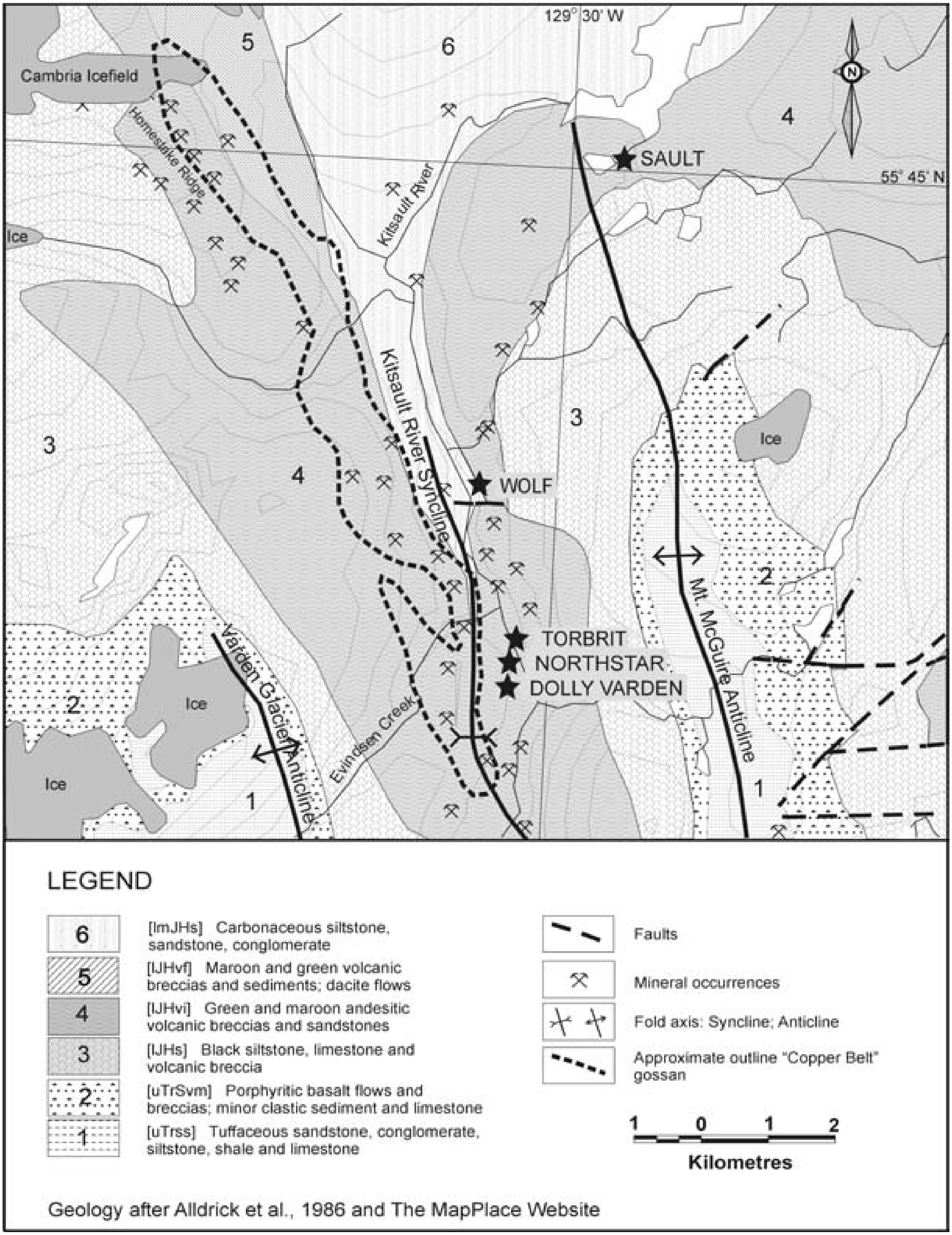

Figure 1. Generalized bedrock geology map of the upper Kitsault River area showing the location of deposits referred to in this study.

EPIGENETIC SILVER-LEAD-ZINC QUARTZ-CARBONATE

These deposits are described by Devlin (1987) and Thiersch (1986) as structurally controlled silver-base metal "replacement" veins that are not restricted to any specific rock unit but are most commonly found in permeable tuffaceous rocks. Devlin notes the presence of breccia and open-space textures, colloform bands of grey, white and jasperoid quartz, comb structures and well-terminated quartz crystals in occurrences of this type. Examples include the Wolf and less well documented David Copperfield, Mitchell, North Musketeer, Surprise and Tiger occurrences (Devlin, op. cit.). Carter (1964) and Thiersch (1986) describe the geology of the Wolf occurrence. The following description is summarized from the work of these authors.

WOLF

The Wolf occurrence comprises three quartz-carbonate "replacement" zones that include local concentrations of barite, jasper and sulphide. The zones may be fault off-set segments of a single discordant vein. The quartz-carbonate "replacement" zones are internally brecciated and bounded by hanging wall and footwall faults. Mineralization was multi-episodic and the vein is irregularly zoned. The following paragenetic sequence of hydrothermal events has been proposed. Early, vein quartz formed in open spaces with colloform banding, comb structures and well-terminated quartz crystals. Pyrite was also deposited with quartz in this open fluid system. The vein was then brecciated and fragments of quartz and pyrite were cemented by gangue, comprised of a second generation of pyrite, galena, sphalerite and minor calcite. After further brecciation, pyrite, galena, sphalerite, magnetite, hematite and unidentified silver-bearing minerals were deposited in small fractures in zones of fine-grained, crushed quartz, interstitial to the larger quartz fragments. The primary sulphide minerals have recrystallized; chalcopyrite has exsolved from sphalerite and pyrite has developed a framboidal texture. As a final mineralizing event, sphalerite and galena precipitated in a carbonate-rich gangue.

New petrographic work on four grab samples taken from the 340 Portal dump at the Wolf occurrence is in broad agreement with the proposed paragenesis. In addition, the following primary growth textures, characteristic of high-level epithermal or hot-spring type, deposits have been identified in early quartz: colloform (botryoidal) and crustiform (alternating) bands of chalcedony and comb quartz, moss-texture similar to that described by Dong *et al.* (1995) in which groups of spheres are highlighted by the distribution of impurities within silica minerals (Photo 1), and euhedral crystal growth zones defined by primary fluid inclusions (Photo 2). Colloform-textured bands of pyrite that probably formed with the quartz are seen in Photo 3.

Early-formed quartz exhibits a number of textures indicative of recrystallization and overprinting by a later metamorphic event. An early stage of this recrystallization is shown by crystals of feathery or flamboyant quartz simi-

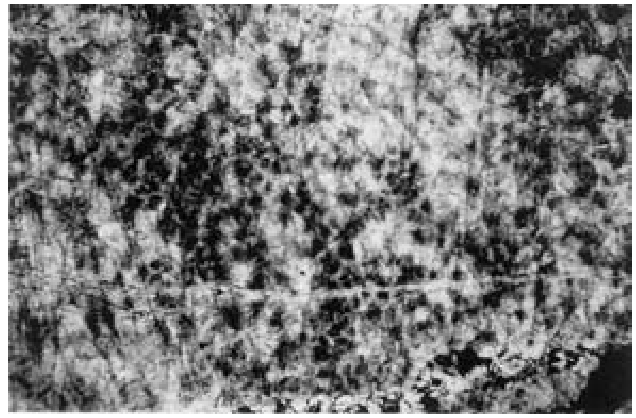

Photo 1. Moss-texture: groups of spheres highlighed by the distribution of impurities within silica minerals, Wolf deposit. Note that the original primary quartz texture is still preserved despite numerous cross-cutting microfractures. Sample RP-W-4. Transmitted plane light. Long field of view is 3.0 mm.

Photo 2. Euhedral quartz crystal growth zones defined by primary fluid inclusions, Wolf deposit. Sample RP-W-1. Transmitted plane light. Long field of view is 3.0 mm.

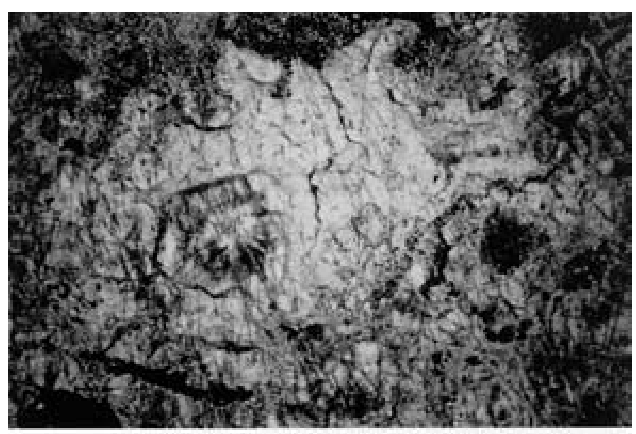

Photo 3. Colloform-textured pyrite with euhedral quartz, Wolf deposit. Note that the original primary growth zones are overprinted by fractures filled with secondary fluid inclusions. Sample RP-W-4. Transmitted plane light. Long field of view is 3.0 mm.

lar to those described by Dong *et al.* (1995). Elsewhere, original primary growth zones are overprinted by fractures filled with secondary fluid inclusions (Photos 1, 2, 3). The early quartz and its late overprinting are distinguished by different fluid inclusion compositions and homogenization temperature ranges (*see* below).

SYNGENETIC STRONTIUM-BARIUM-LEAD-ZINC-SILVER

Mineralization at the Sault (103P 233) occurrence is in a carbonate unit interbedded with andesite to rhyolite pyroclastic rocks just below a disconformity mapped at the top of the Hazelton volcanic arc (Pinsent, 2001). The carbonate unit is 8 metres thick, has been traced for approximately 5 kilometres along strike, and comprises a lower metalliferous carbonate diamictite, limestone and mudstone; a central volcaniclastic interval; and an upper sequence of laminated carbonate, sulphate and sulphide that contains a minor amount of tuff, chert and volcanic rock (Tupper and McCartney, 1990). The sulphide minerals include laminated to bedded and locally framboidal pyrite, fine-grained sphalerite and galena and locally well-bedded celestite (Pinsent, op. cit.).

A single sample of laminated carbonate and sulphate was examined but was found to be unsuitable for fluid inclusion work (Table 1).

EPIGENETIC OR SYNGENETIC SILVER-LEAD-ZINC-BARIUM-STRONTIUM

Mineralization at the Torbrit, Dolly Varden and Northstar deposits has been variously described as: 1) intrusion-related and epigenetic (Campbell, 1959); 2) a replacement vein disrupted by faulting and mineralized during a later epithermal event (Mitchell, 1973); and 3) fault offset segments of a single stratiform deposit (Devlin and Godwin, 1985; Devlin, 1987). They are classified as epigenetic or syngenetic silver-lead-zinc-barium-strontium deposits by Pinsent (2001) in recognition of the conflicting opinions as to their origins. Readers are referred to Black (1951) as well as the authors noted above for details on their geology, which are summarized only briefly below.

TORBRIT

The main deposit at Torbrit is a mineralized lens within an otherwise sub-economic sheeted silica, carbonate, sulphate and sulphide deposit in Hazelton Group volcanic rocks. Black (1951), Campbell (1959) and Mitchell (1973) considered that it formed through hydrothermal replacement of brecciated volcanic rock in a tensional fault system.

Devlin and Godwin (1985) and Devlin (1987) note that the deposit is stratabound and formed at a distinctive horizon within a thick succession of shallow-water Hazelton Group volcanic and related volcaniclastic rocks. They suggest that it may be exhalative in origin and that the Torbrit, Dolly Varden and Northstar deposits may have been part of a single, variable facies, stratabound mineral occurrence. The unit shows gradation from silica-sulphide exhalite at the Dolly Varden East and Northstar deposits to carbonate-sulphate-sulphide exhalite at the Dolly Varden West and Northstar deposits and to sulphate-oxide-sulphide exhalite at Torbrit (Devlin, 1987).

The "vein" or "sulphate-oxide-sulphide exhalite" horizon at Torbrit is composed of quartz, jasper, chalcedony, barite and carbonate and the economically significant portion of the horizon includes up to 20% sulphide and oxide minerals (magnetite, hematite, pyrite, sphalerite, galena, chalcopyrite, tetrahedrite, pyrargyrite and trace native silver) (Campbell, 1959; Devlin, 1987). The gangue minerals are compositionally and colour-banded, commonly subparallel to deposit contacts and to the schistocity of the surrounding rock (Campbell, op. cit.). Campbell describes gangue minerals containing vugs lined with well-terminated quartz crystals and the occurrence of barite with a characteristic crustiform texture. He estimated a temperature of 270 ºC for the formation of sphalerite by plotting the FeS content of the sphalerite on a portion of the system ZnS-FeS-S, and by employing the argentite-silver assemblage as a sulphur barometer (Devlin, 1987).

Fluid inclusion petrography was undertaken on transparent minerals in three samples from Torbrit (Table 1). Sample RP-T-1 is from a drill hole collared northwest of the Torbrit glory hole (McGuigan and Melnyk, 1991). It comprises light-grey subrounded fragments of silicified and sericitized quartz, from 0.1 to 0.5 mm in maximum dimension, infilled by pyrite and pale-green sphalerite. McGuigan and Melnyk (1991) report both honey and blackjack varies of sphalerite in this interval of core. Samples RP-T-2 and RP-T-3 are from the UBC Department of Earth and Ocean Sciences Museum Collection. Sample RP-T-2 comprises primary bladed barite (the bladed texture is common in epithermal deposits) with laths up to 1 cm in length, jasper-sulphides-oxides and colloform quartz. Sample RP-T-3 is similar to RP-T-1; it comprises subrounded fragments of silicified and sericitized (?) quartz infilled by disseminated and stringer sulphides, including pale-green sphalerite, which are cut by later barite and carbonate. Solid inclusions of reddish-brown sphalerite (?) occur along primary growth zones in the pale-green sphalerite (Photo 4).

DOLLY VARDEN

The Dolly Varden mine has been described as a series of ore-shoots within a single "replacement vein" in a package of massive, altered and pyritic volcanic breccias and sandstones (Black, 1951). Similar to Torbrit, the deposit is compositionally and colour-banded; it also contains fragments of locally derived wallrock (Black, 1951). Mitchell (1973) considered the Dolly Varden deposit to be an off-set portion of the same vein that formed the nearby Torbrit and Northstar deposits.

Devlin and Godwin (1986) divide the deposit into East and West segments. The mineralogy of the Dolly Varden East deposit consists of disseminated to massive pyrite, minor chalcopyrite and traces of argentite, pyrargyrite and native silver in a gangue of quartz and sericite and is referred to as a "silica-sulphide exhalite facies" by Devlin (1987). The

TABLE 1
DESCRIPTION OF SAMPLES USED FOR PETROGRAPHIC AND MICROTHERMOMETRIC ANALYSES

DEPOSIT NAME	SAMPLE NUMBER	SAMPLE TYPE [1]	USE [2]	LOCATION DESCRIPTION	MINERALS EVALUATED [3]	MINERAL ASSOCIATION	SOME MINERAL TEXTURES
Wolf	RP-W-1	Grab	P/M	340 Portal Dump #1	quartz*	silica-sulphide	colloform (botryoidal) and crustiform (alternating) bands of quartz
	RP-W-2	Grab	P/M	340 Portal Dump #2	quartz* carbonate	silica-sulphide	colloform and crustiform textures, jasper
	RP-W-3	Grab	P/M	340 Portal Dump #3	quartz*	silica-sulphide	veinlet with well-terminated quartz crystals
	RP-W-4	Grab	P	340 Portal Dump #4	quartz	silica-sulphide	moss-textured quartz, framboidal pyrite
Sault	RP-K-1	Grab	P	Showing Lake	celestite? carbonate	carbonate-sulphate-sulphide	banded ore cut by celestite?-carbonate veinlet
Torbrit	RP-T-1	Core	P/M	DDH 90-22 ~163m	quartz* sphalerite* carbonate barite	silica-sulphate-sulphide	breccia textures, disseminated sphalerite, late carbonate veinlet
	RP-T-2	Grab	P	UBC Collection E 073 001.008	barite quartz	sulphate-oxide-sulphide	bladed barite crystals; colloform and crustiform quartz
	RP-T-3	Grab	P/M	UBC Collection 804 LD 32-56	quartz* sphalerite* barite*	silica-sulphate-(oxide?)-sulphide	breccia textures; sphalerite stringers; late barite veinlet
Dolly Varden	RP-D-1	Grab	P	RP#1 - 152	barite sphalerite	sulphate-sulphide	massive to bladed barite; minor sphalerite
	RP-D-2	Grab	P	RP#2	barite quartz carbonate	carbonate-sulphate-sulphide	breccia textures; massive barite
	RP-D-3	Grab	P/M	RP#4 - No. 3 gloryhole	quartz* sphalerite	silica-sulphide	breccia textures; comb-crustiform-colloform textured quartz; green plus brown sphalerite
	RP-D-4	Grab	P	RP#2 452 stope 125’ from surface	quartz sphalerite	silica-carbonate-sulphide	colliform and crustiform quartz, moss quartz
	RP-D-5	Grab	P/M	UBC Collection #3 No. 16 trench Cu ore	barite* quartz*	silica-carbonate-sulphate-sulphide	prismatic quartz fragments, tabular barite, breccia textures
	RP-D-6	Grab	P	UBC Collection #1 452 A stope 125’ from surface	sphalerite quartz barite	silica-carbonate-sulphate-sulphide	semi-massive sphalerite; breccia textures
Northstar	RP-N-1	Core	P/M	NS89-3 958’	quartz* barite carbonate	silica-carbonate-sulphate-sulphide	breccia textures, fragments euhedral quartz
	RP-N-2	Core	P/M	NS89-3 967’	sphalerite* quartz* barite* carbonate	silica-carbonate-sulphate-sulphide	breccia textures; disseminated sphalerite
	RP-N-3	Core	P/M	NS89-3 988’	barite* quartz* sphalerite	silica-sulphate-sulphide	breccia textures, fragments of euhedral quartz; disseminated sphalerite; massive barite
	RP-N-4	Grab	P	Northstar #1 Barytes NE Raise	barite quartz carbonate sphalerite	silica-carbonate-sulphate-sulphide	breccia textures, fragments of euhedral quartz; bladed barite; disseminated sphalerite

1. Sample Type: Core = split core sample; Grab = surface hand sample,
2. Use: P= fluid inclusion petrography, M = microthermometry,
3. Minerals evaluated with fluid inclusion transmitted light petrography: * = used for microthermometry

same author describes the Dolly Varden West deposit as a "carbonate-sulphate-sulphide" exhalite consisting of layers, disseminations and stringers of sphalerite and galena, minor pyrite, chalcopyrite and tetrahedrite, and traces of native silver in a gangue of calcite, quartz, siderite and barite. Exploration and drilling using the "exhalite" model led to the discovery of several zones of quartz-sulphide breccia composed of jasper, chalcedonic quartz and pyrite with trace amounts of economic sulphides (Drown *et al.*, 1990; McGuigan and Melnyk, 1991).

Petrographic work was undertaken on six grab samples from Dolly Varden taken from the UBC Department of Earth and Ocean Sciences Museum Collection (Table 1). Of particular interest are two samples (RP-D-3 collected from the No. 3 glory hole and sample RP-D-4 collected from the 452 stope at Dolly Varden East) which are breccias with fragments of early-formed comb, colloform and crustiform-textured quartz (Photo 5), moss-textured quartz and euhedral quartz with primary growth zones infilled by stringer and disseminated pyrite, galena and sphalerite. Sample RP-D-3 has two varieties of sphalerite: an earlier euhedral pale-green variety and later reddish-brown variety (equivalent to the honey and blackjack sphalerite described by McGuigan and Meinyk, 1991). Sample RP-D-1, collected from the 152 stope, comprises massive to bladed barite with minor sulphide stringers and trace sphalerite. Sample RP-D-5 (No. 16 trench - Cu ore) is dominantly altered wallrock with a few anhedral fragments of early-formed quartz that exhibits primary growth zones. The rock is infilled by disseminated and stringer sulphides and cut by subsequent late, one-millimetre wide, barite veinlets.

NORTHSTAR

The Northstar occurrence is described as a high-grade lens in a replacement "vein" in Hazelton Group volcanic rocks (Black, 1951; Mitchell, 1973). The deposit comprises barite and quartz with minor amounts of sulphide and sulphosalt minerals (pyrite, marcasite, galena, sphalerite, chalcopyrite, pyrargarite and argentite) and native silver (Pinsent, 2001). Banded and crustiform textures have been described, similar to those reported at the Torbrit mine (Black, 1951).

Alternatively, Devlin (1987) proposed that the Northstar deposit is exhalative in origin. He suggests that mineralized horizon may be stratigraphically zoned from a pyritic basal barite-quartz-carbonate unit upward into a more siliceous and metal-enriched, polymetallic sulphide-bearing unit. Drilling in 1990 based on this model intersected the mineralized horizon and a thick chlorite-calcite-pyrite alteration stockwork in its footwall down-dip of the main adit (Drown *et al.*, 1990). The "exhalite" comprised a lower carbonate-rich barren facies and upper weakly mineralized sulphide and oxide-bearing facies containing pyrite, chalcopyrite, honey-coloured sphalerite, galena and jasper (Drown *et al.*, 1990; McGuigan and Melnyk, 1991).

Fluid inclusion petrography was undertaken on four samples from the Northstar deposit (taken from drill core and the UBC Department of Earth and Ocean Sciences Museum Collection, Table 1). Sample RP-N-1 is a breccia with angular fragments of quartz with primary growth zones; late white carbonate and barite form infill-textures with disseminated and stringer pyrite. Sample RP-N-2 is a similar breccia with fragments of quartz that display primary growth zones (Photo 6). Pale-green sphalerite occurs as disseminations and blebs. Barite and minor carbonate cut the mineralization. This sample came from an interval referred to by Drown *et al.* (1990) as being a "quartz breccia exhalite". Sample RP-N-3 is dominantly massive barite with fragments of euhedral quartz exhibiting primary growth zones; sulphides occur as trace disseminations of pyrite, chalcopyrite and reddish-brown sphalerite. This sample came from an interval of core Drown *et al.* (1990) referred to as "exhalative barite". Sample RP-N-4 is similar to RP-N-3, except that the barite is bladed.

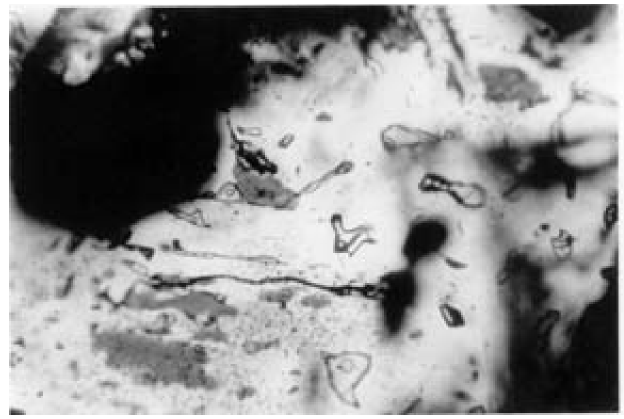

Photo 4. Solid inclusions of reddish-brown sphalerite? with liquid-rich and vapour-rich? fluid inclusions which define primary growth zones in pale-green sphalerite, Torbrit deposit. Sample RP-T-3. Transmitted plane light. Long field of view is 200 µm.

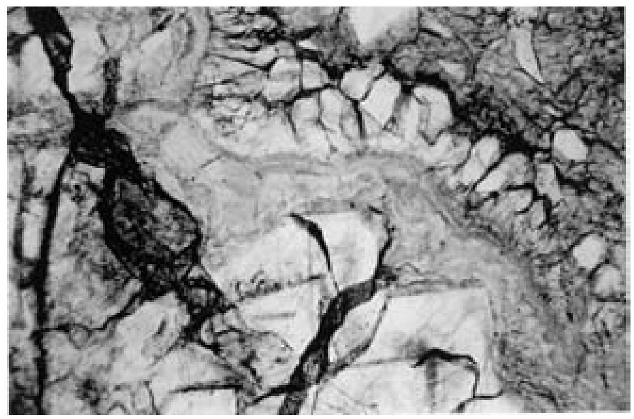

Photo 5. Fragment of early-formed comb, colloform and crustiform-textured quartz, Dolly Varden deposit. Sample RP-D-3. Transmitted plane light. Long field of view is 3.0 mm.

FLUID INCLUSION DATA

Fluid inclusion work has concentrated on quartz from the "epigenetic silver-lead-zinc quartz-carbonate vein" at the Wolf prospect and on quartz, sphalerite and barite from

Photo 6. Fragment of early-formed vein quartz with euhedral crystals and primary growth zones, Northstar deposit. Sample RP-N-2. Transmitted plane light. Long field of view is 3.0 mm.

the "epigenetic or syngenetic silver-lead-zinc-barium-strontium deposits" at the former Torbrit and Dolly Varden silver mines and the related Northstar occurrence (Table 1). The temperature and composition of the hydrothermal fluids present during mineralization have been determined using conventional microthermometric work.

Eighteen 'quick plates' and doubly-polished sections were prepared for fluid inclusion petrography. Quick plates are sections, 80 to 100 microns thick, mounted on glass slides with epoxy and polished on the top surface only. Of these, 10 samples were found to be suitable for microthermometry and were re-prepared, where necessary, as doubly-polished sections. Samples were selected to give broad representation of silica, carbonate, sulphate, oxide and sulphide mineral associations (Table 1).

Quartz and sphalerite were used for the microthermometry because of their high tensile strength and relative translucency. Sphalerite is particularly useful as the microthermometric results can be directly tied to the paragenesis of the deposit. Barite is less useful as it is easily cleaved and highly susceptible to leakage and recrystallization of fluid inclusions (post-entrapment changes). Homogenization temperatures of fluid inclusions in barite were unusable because the inclusions had continued to heal at low temperatures after nucleation of a vapour phase (*i.e.* necked-down; *see* petrography below). The salinity measurements from fluid inclusions in barite were found to be usable.

Fluid inclusions were evaluated using the concept of fluid inclusion assemblages (FIA's). This ensures that the data are not biased by samples containing large numbers of fluid inclusions and helps to eliminate inconsistent results caused by changes in mass, volume or shape of inclusions after entrapment (*i.e.* eliminate non-representative inclusions that are the result of diffusion, stretching, or necking-down processes). A fluid inclusion assemblage (FIA) is a petrographically-associated group of inclusions such as those aligned along primary growth zones or secondary fracture planes. One representative data point, rather than several data points, is used for each FIA.

PETROGRAPHY

Fluid inclusions in quartz, sphalerite and barite in our samples are typically less than 10 microns and rarely reach a maximum of 30 microns in longest dimension. The fluid inclusions vary in shape from irregular to smooth and in some cases they mimic host crystal form and are 'negative-crystal'-shaped.

Fluid inclusions were classified as primary, secondary, pseudosecondary or indeterminate, based on the criteria of Roedder (1984) and Bodnar *et al.* (1985). Primary fluid inclusions were aligned along growth zones in quartz and sphalerite (Photos 6 and 7) and represent the fluid trapped while the host crystal was growing. Secondary inclusions were aligned along fractures that crosscut grain boundaries. Secondary fluid inclusion data represents post-entrapment fluid after primary crystal growth has ceased. Pseudosecondary fluid inclusions were aligned along fractures that do not crosscut grain boundaries and are presumed to represent fluids trapped in fractures at the time the crystal was growing. Fluid inclusions that occur in isolated clusters unrelated to fractures or growth zones were classified as indeterminate origin.

Primary fluid inclusions in quartz from all four deposits studied commonly contain two aqueous phases at room temperature, liquid (5 to 10 percent) and vapour (90 to 95 percent). This type of inclusion is referred to as two-phase aqueous liquid-rich (Type I) using the nomenclature of Nash (1976). Small (less than 5 microns) opaque fluid inclusions, which comprise about 10 percent of the total fluid population, are coeval with the Type I liquid-rich inclusions and aligned along growth zones. They may be vapour rich inclusions (Type II, using the nomenclature of Nash (1976)) that formed through the trapping of phase-separated volatiles. Alternatively, they may be air-filled voids or decrepitated inclusions caused by metamorphism.

Primary Type I fluid inclusions in sphalerite from the Torbrit mine comprise from 5 to 50 volume percent vapour. Opaque fluid inclusions, comprising 10 to 25 percent of the total fluid population, are coeval with the Type I liquid-rich

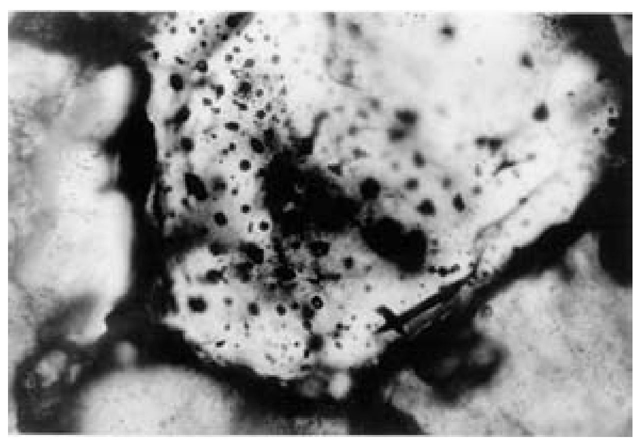

Photo 7. Pale-green sphalerite with primary growth zones defined by liquid-rich and vapour-rich fluid inclusions, Torbrit deposit. Sample RP-T-1. Transmitted plane light. Long field of view is 375 µm.

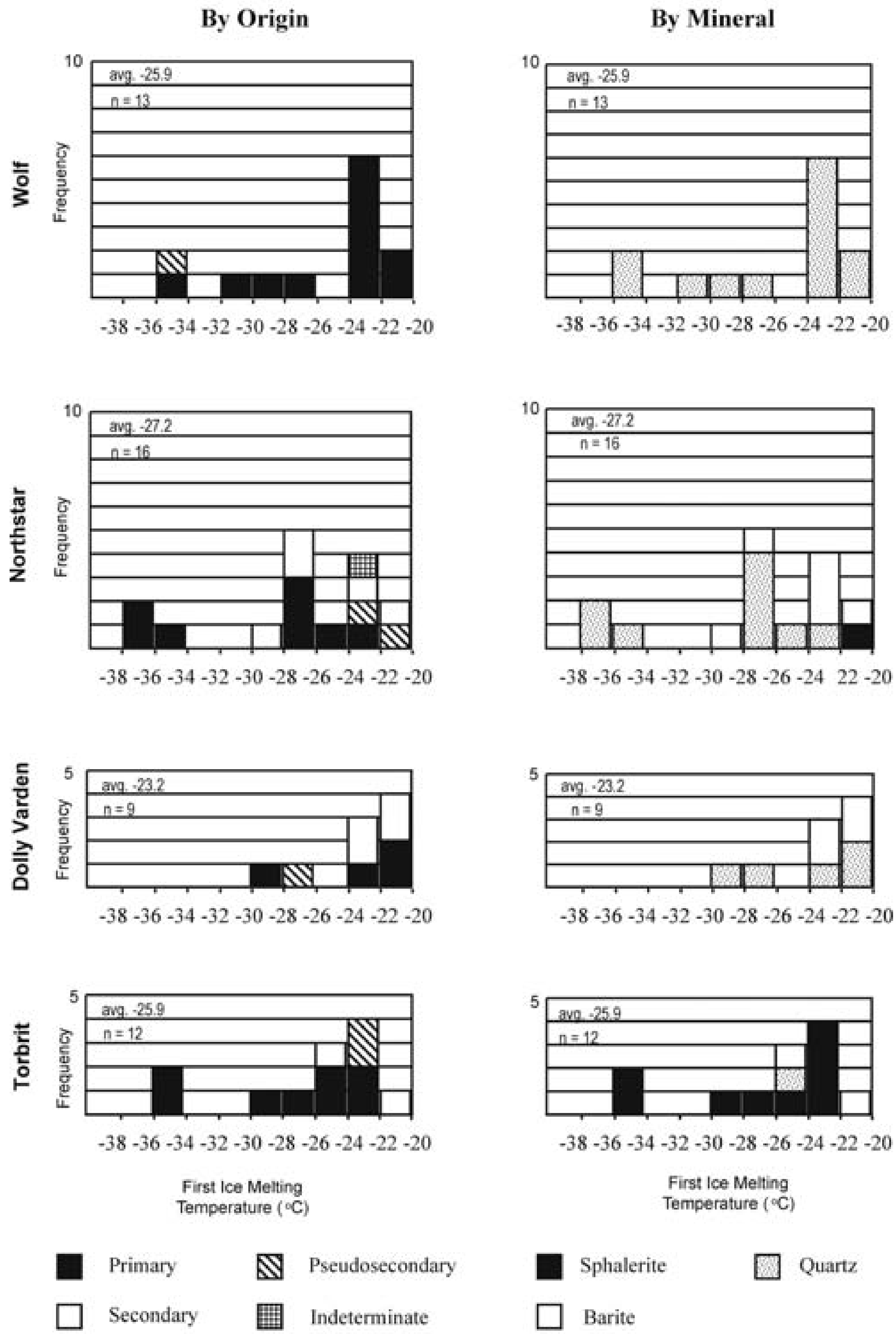

Figure 2. Temperatures of first melt of Type I (aqueous) fluid inclusions by fluid inclusion origin and by host mineral from the Wolf and Northstar occurrences and the former Dolly Varden and Torbrit mines, respectively. The first melt approximates the eutectic temperatures of the fluid inclusions.

inclusions and aligned along growth zones in the sphalerite (Photos 4 and 7). These opaque inclusions may be vapour rich inclusions (Type II), voids filled with air, or decrepitated fluid inclusions as suggested for quartz above.

Secondary multiphase (Type III) fluid inclusions have only been observed in quartz in sample RP-N-1 from the Northstar occurrence. These inclusions comprise liquid brine, vapour and one or more solid phases. The vapour phase typically comprises approximately 10 to 20 volume percent of the inclusion. Many of the solid phases are translucent and some appear to be cubic and are presumed to be salts. Confirmation of the identity of the solid phases as salts has not been possible as the fluid inclusions containing these phases decrepitate prior to solid phase dissolution. Since Type III inclusions typically occur with Type I and Type V (*see* below) fluid inclusions along healed fractures, it is possible that these Type III inclusions may have formed by accidental trapping of the solid phases or post-entrapment changes in the inclusions (necking-down).

Secondary two-phase and three-phase carbonic (CO_2-H_2O) type IV fluid inclusions have been observed healing fractures in quartz at the Wolf and Northstar occurrences. At room temperature (~20^oC), this type of fluid inclusion contains either two immiscible liquids: an outer aqueous liquid and inner CO_2-bearing liquid or two immiscible liquids and a vapour: an outer aqueous liquid, inner CO_2-bearing liquid and a CO_2-bearing vapour. The CO_2 volumetric proportions of Type IV inclusions range from 10 percent to 25 percent.

Very few secondary monophase vapour CO_2-CH_4 (Type V) fluid inclusions have been observed in quartz from the Wolf and Northstar occurrences. Type V inclusions are typically very dark and consist of a single vapour phase at room temperature. Freezing and subsequent melting behaviour of these inclusions indicate the presence of CO_2-CH_4±N_2 phases.

Two-phase liquid-rich Type IV inclusions are coeval with monophase vapour-rich Type V inclusions in secondary fracture planes in quartz in sample RP-W-1 at the Wolf occurrence. The coexistence of CO_2-bearing liquid-rich inclusions with variable liquid-to-vapour ratios and vapour-rich inclusions in the same fracture plane indicates that local effervescence may have occurred.

Secondary Type I fluid inclusions were observed in barite from the Dolly Varden and Torbrit mines and both secondary and primary Type I and Type II fluid inclusions were observed in barite at the Northstar occurrence. For the most part, the Type I barite inclusions are irregular-shaped, sometimes flat, and have inconsistent liquid to vapour ratios. The observation of monophase liquid-filled inclusions coexisting within individual fracture planes with these type I inclusions of variable liquid-to vapour ratio is evidence of post-entrapment changes such as necking-down (Bodnar *et al.*, 1985).

MICROTHERMOMETRIC DATA

Microthermometric data were obtained using a Fluid Inc. adapted USGS gas-flow heating-freezing stage housed at the Mineral Deposit Research Unit, Department of Earth and Ocean Sciences, University of British Columbia. Calibration of the stage was achieved using commercial Syn Flinc synthetic fluid inclusions and ice with the following accuracies: at -56.6±0.0^oC, 374.1±0.5^oC and 0.0±0.0^oC. Temperatures of phase changes are described below for each fluid inclusion assemblage, host mineral, fluid inclusion type, and origin. Variation in temperature and salinity between deposits with respect to fluid inclusion host mineral, origin, and fluid inclusion type are illustrated in Figures 2 though 5.

Type I Fluid Inclusions

Temperatures of first melting were obtained on 50 fluid inclusions from 10 samples representing mineralization at the Wolf, Northstar, Dolly Varden and Torbrit deposits (Figure 2). First melting temperatures for primary and pseudosecondary fluid inclusions range from about -37^oC to -19^oC at the Wolf, Northstar and Torbrit deposits and from -29^oC to -20^oC at the Dolly Varden deposit. These dissimilar ranges may reflect the relative paucity of data obtained from Dolly Varden rather than a truly systematic difference between deposits (Figure 2). The first melting temperature range of secondary fluid inclusions in barite is more restricted than the ranges for of quartz and sphalerite (Figure 2).

First melting temperature approximates the eutectic temperature of the salt-water mixtures. Depression of first melting below -21.2^oC, the stable NaCl-H_2O eutectic, indicates the addition of small concentrations of K^+, Ca^{2+}, Mg^{2+} or other ions to an H_2O-NaCl fluid. For the purposes of this study, the Type I fluid is modeled as an NaCl brine, partly because most formational fluids are NaCl-dominant (Goldstein and Reynolds, 1994) and because comparison of the cotectic surfaces where ice melts for various systems (Crawford, 1981, figure 6) shows only relatively small variations (< 5 wt.% change).

Final ice melting temperatures were obtained from 64 fluid inclusions from the same samples as the first melting temperatures (Figure 3). Final melting temperatures of primary fluid inclusions range from about -11^oC to -1.0^oC (average -3.8±2.9^oC) at the Northstar deposit but from only -5^oC to 0^oC (average -2.5 ±1.6^oC to -1.7±1.1^oC) at the Wolf, Dolly Varden and Torbrit deposits (Figure 3). Salinities for the Northstar deposit, calculated from final melting temperatures and the equation of Bodnar (1993), range from about 2 to 15 weight percent NaCl equivalent (wt. percent NaCl equiv.) and average 6.2± 3.6 wt. percent NaCl equiv. Salinities for the Wolf, Dolly Varden and Torbrit deposits are much lower, ranging from about 0.4 to 8 wt. percent NaCl equiv. and averaging 4.2±2.5, 4.0±3.6 and 2.9±1.8 wt. percent NaCl equiv. respectively. (Figure 3). The final melting temperature range of secondary fluid inclusions in barite and quartz is similar to that for primary fluid inclusions (-8.3^oC to -0.2^oC, Figure 3).

Final homogenization temperatures were obtained on Type I fluid inclusions in quartz and sphalerite from the same samples as the freezing data (above). Homogenization temperatures for primary fluid inclusions in sphalerite range from 104.4 ºC to 352.8ºC and in quartz from 101.8 ºC to 266.4 ºC with significant variation between deposits (Figure 4). Temperatures above 270ºC were only recorded for Type I primary fluid inclusions in sphalerite from the Torbrit mine (Figure 4). Limited Type I primary fluid inclusion data recorded in quartz from the Dolly Varden mine are among the lowest, between 115ºC and 180ºC. Low to moderate-temperature (152ºC to 240ºC) secondary Type I fluid inclusions have only been reported in quartz (Figure 4).

Type II fluid inclusions

Microthermometric data could not be obtained from the primary opaque Type II fluid inclusions observed in quartz from the Wolf occurrence and in pale-green sphalerite at the Torbrit mine due to their opaque nature, and, in the case of the quartz, small size (<3 microns). However, inhomogeneous entrapment of liquid and vapour phases during boiling can be inferred by the coexistance of primary Type I fluid inclusions with variable liquid-to-vapour ratios (see petrography above) and coeval Type II fluid inclusions

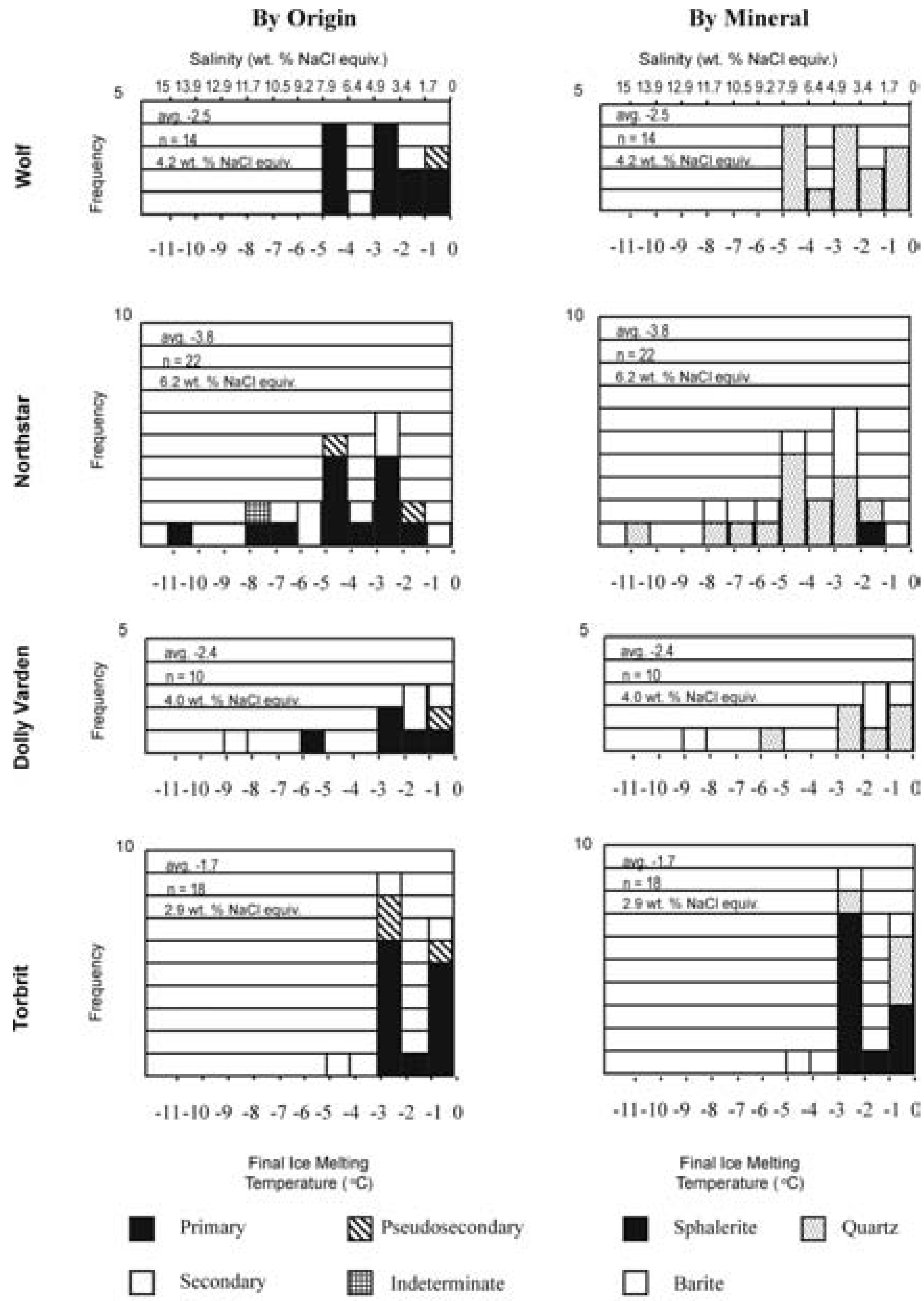

Figure 3. Temperatures of final melt of Type I (aqueous) fluid inclusions by fluid inclusion origin and by host mineral from the Wolf and Northstar occurrences and the former Dolly Varden and Torbrit mines, respectively. The final melt is used to calculate the equivalent salinity.

trapped in the same growth zones in the quartz and sphalerite. This inference is made with the assumption that the Type II fluid inclusions in these minerals are vapour-rich fluid inclusions. Secondary Type II inclusions in barite from the Northstar occurrence were not evaluated.

Type III Fluid Inclusions

Limited data (3 data points) on freezing and subsequent melting behaviours of secondary Type III fluid inclusions in quartz from the Northstar occurrence are different from the behaviour of Type I fluid inclusions (*see* Figures 2 and 3). First melting temperatures between -41ºC and -28.4ºC are significantly lower than those reported from Type I inclusions (above) and may indicate the presence of salts such as $CaCl_2$ (Crawford, 1981; Davis *et al.*, 1990). Last melting temperatures recorded as -2.1ºC and -2.8ºC correspond to salinities of 3.6 and 4.7 wt. percent NaCl equiv.

Homogenization of Type III inclusions, in the presence of contained solid mineral phases, ranges from about 215ºC to 247ºC. On further heating, the fluid inclusions decrepitate at temperatures above 280ºC prior to melting of contained solid phases. Given the limited data, it is difficult to evaluate whether the Type III inclusions contain minerals that are true 'daughter' minerals or if the minerals are trapped accidental solids or the result of 'necking-down'.

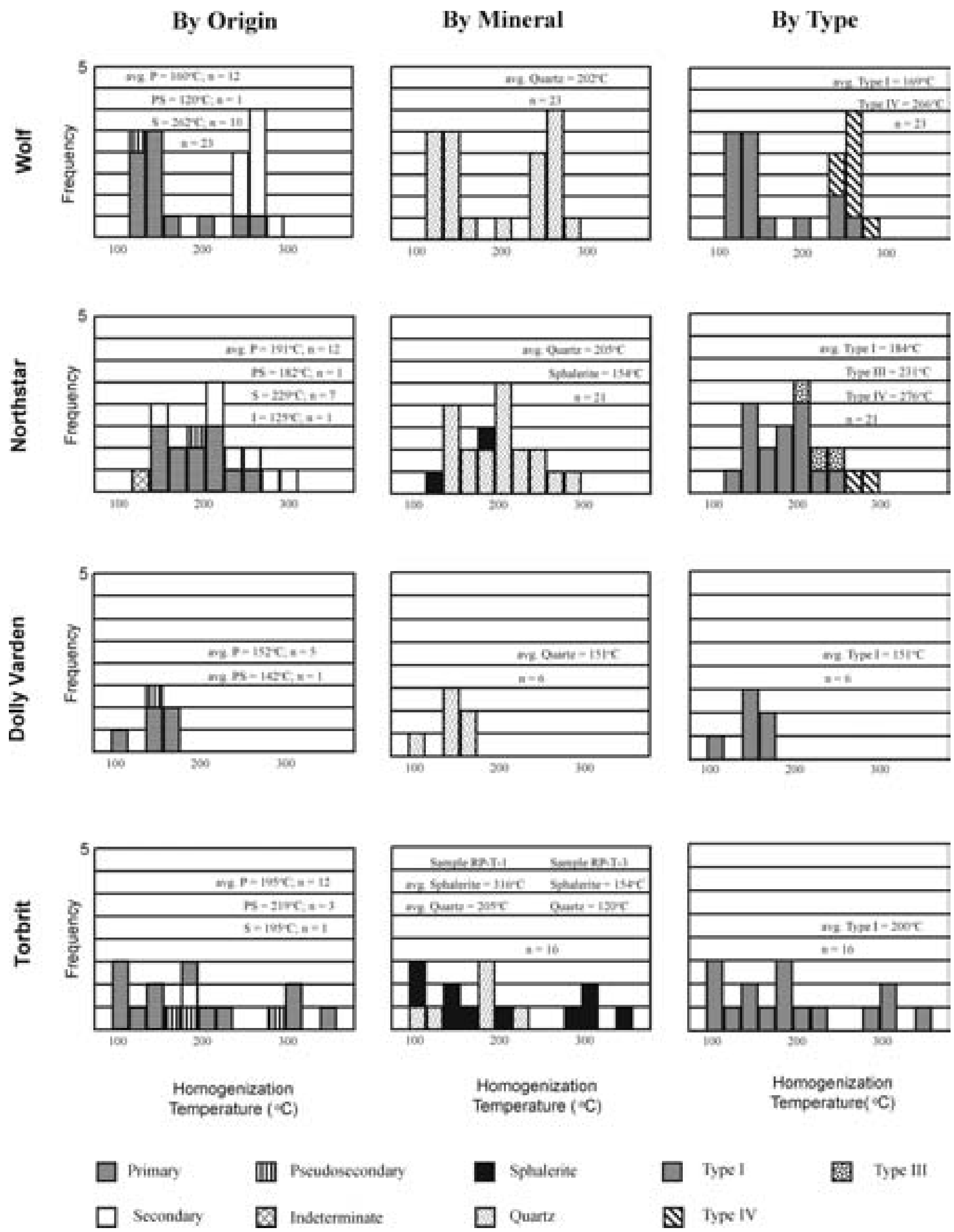

Figure 4. Final fluid inclusion homogenization temperatures (range, average and number), to the aqueous phase by fluid inclusion origin, host mineral and type from the Wolf and Northstar occurrences and the former Dolly Varden and Torbrit mines, respectively.

Type IV Fluid Inclusions

Secondary carbonic fluid inclusions were observed in quartz from the Wolf and Northstar deposits. Carbon dioxide melting temperatures of Type IV inclusions from the Northstar deposit are equivalent to the CO_2 triple point (-56.6°C). Melting temperatures of Type IV inclusions from the Wolf deposit range from -57.8 to -56.6°C with an average of -56.9±0.2°C (Figure 5). This average CO_2 melt temperature is very close to the CO_2 triple point of -56.6°C which indicates that < 2 mole percent, using the method of Thiery *et al.* (1994), or virtually no CH_4 or N_2 are dissolved in the CO_2. Type IV fluid inclusions can therefore be modeled using an H_2O-CO_2-NaCl system.

Temperatures of clathrate (gas hydrate) melting were obtained on 10 fluid inclusions from the same samples as the CO_2-melting temperatures. Clathrate melting, which occurs after ice melting, varies from 3.7 to 8.2°C with an average of 6±1.5°C and 7.7±0.7 °C for the Wolf and Northstar occurrences respectively (Figure 5). Clathrate melting temperatures less than +10°C are another indication of very low CH_4 or N_2 presence in Type IV inclusions. Clathrate melting temperatures in excess of + 10°C are related to CH_4 impurities (Burruss, 1981). Salinities calculated from clathrate melting, using the system H_2O-CO_2-NaCl and the computer program FLINCOR version 1.4 (Brown, 1989), range from 3 to 11.5 wt. percent NaCl equiv.

Homogenization temperatures of CO_2 liquid and vapour were obtained from 7 fluid inclusions from some of the same samples at the Wolf occurrence. Homogenization of the inclusions (always to the liquid phase) ranges from 19.9 to 27.5°C with an average of 24.4±1.9°C (Figure 5). The range in density, calculated as above (using FLINCOR), is 0.67 to 0.75 grams per cubic centimetre for the CO_2 component of the inclusions.

Final homogenization temperatures of the inclusions, again always to the aqueous phase, were obtained from the same samples as the freezing data (above). Homogenization temperatures for secondary Type IV inclusions from both Wolf and Northstar occurrences are moderate ranging from 259.3 to 283.4°C (Figure 4). Figure 4 shows that overall, secondary Type IV fluid inclusions homogenize at significantly higher temperatures than Type I fluid inclusions for data evaluated in this study.

Type V Fluid Inclusions

Secondary Type V fluid inclusions were observed associated with Type III or Type IV fluid inclusions along fracture planes in two quartz samples from the Wolf and Northstar deposits. On freezing the monophase Type V inclusions, phase separation of the vapour bubble into CO_2-bearing liquid and CO_2-bearing vapour phases occurred at temperatures below 20°C. Further cooling resulted in freezing of the CO_2 phase at about -90 to -95°C. Carbon-dioxide melting temperatures are -56.8°C and -57.8°C; which are similar to the range observed for CO_2-melting of Type IV fluid inclusions (Figure 5). Homogenization temperatures of the inclusions to the liquid phase are 3.5 °C in the Northstar sample and 19.9 °C in the Wolf sample. The measured CO_2 melt and homogenization temperatures are used to calculate fluid molar volumes (or the density) and composition of Type V fluid inclusions using the VX diagrams of Thiery *et al.* (1994). The Type V inclusion from Wolf has a molar volume of 59 cubic centimetres per mol with 4 mole percent CH_4 dissolved in the CO_2. The Type V

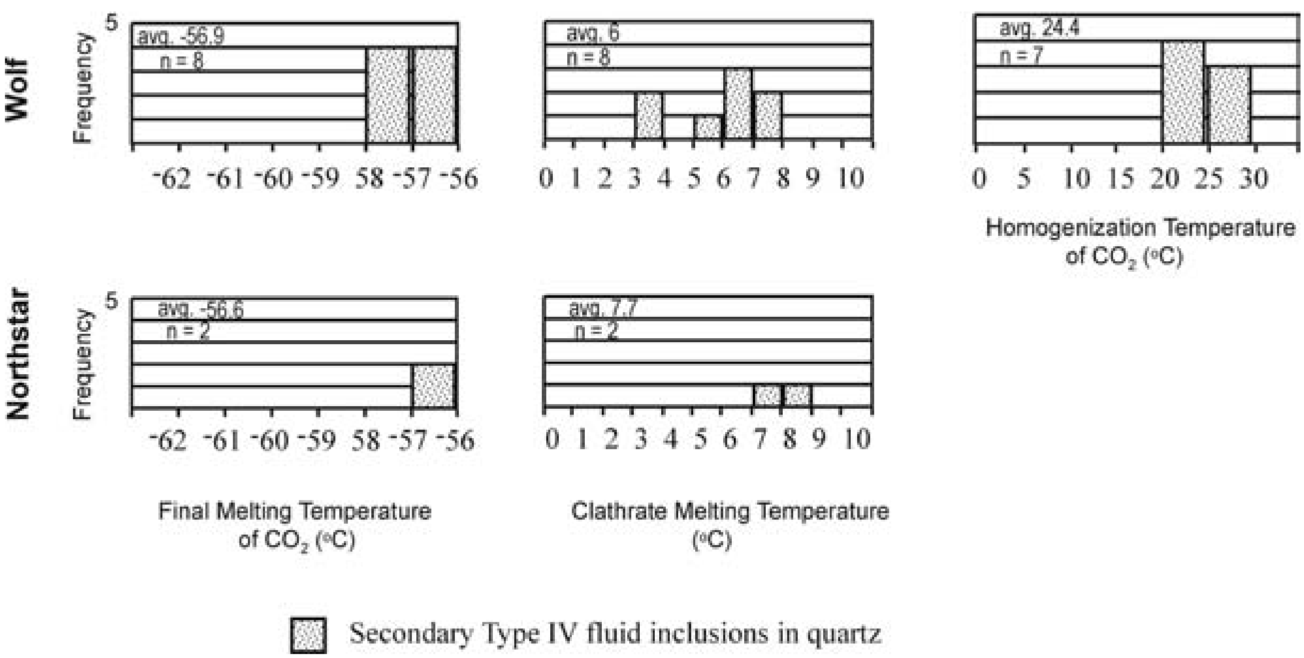

Figure 5. Temperatures of final CO_2 melt, clathrate melt and homogenization of CO_2 phases of secondary Type IV (CO_2-bearing) fluid inclusions in quartz from the Wolf and Northstar occurrences, respectively. The final CO_2 melt temperature is used approximate the proportion of CH_4, N_2 or other volatile phases trapped in the fluid inclusions. The clathrate melt is used to calculated the equivalent salinity. The homogenization temperature of CO_2 is used to calculate the CO_2 density.

inclusion from Northstar has a molar volume of 49 cubic centimetres per mol and 1 mole percent CH_4 dissolved in the CO_2 (Thiery *et al.*, op. cit.).

STABLE ISOTOPE DATA

Devlin (1987, pp. 86-90, table 4.2) reported temperatures of deposition from the former Dolly Varden and Torbrit mines and the Northstar and Wolf deposits as determined from pairs of sulphur and oxygen compounds using data calculated from sulphur and oxygen isotope fractionation equations. Devlin (1987) concluded that the range of realistic calculated temperatures for pairs of sulphur compounds from the Dolly Varden, Northstar and Torbrit deposits was between 143°C and 375°C. He noted that this range is consistent with exit temperatures measured in active hydrothermal vents on the East Pacific Rise, fluid inclusion temperatures determined for sulphide and sulphate minerals in Kuroko deposits and depositional temperatures calculated from sulphur isotope data for sphalerite-galena pairs from stratiform zinc-lead-barite deposits in Alaska. Realistic depositional temperatures for oxygen compounds from the Wolf and Dolly Varden deposits ranged from 152°C to 190°C (Devlin, op. cit.).

DISCUSSION

This discussion focuses on the following: (1) estimated fluid properties of inclusions in quartz and sphalerite from silver-rich quartz-carbonate-sulphate deposits in the upper Kitsault River area, (2) the relationship of fluid inclusions in host minerals to the introduction of metals in both epigenetic epithermal and syngenetic exhalative settings, and (3) proposed analogues to the silver-rich mineralization.

FLUID PROPERTIES

Fluid inclusion assemblages with liquid-rich aqueous (Type I) inclusions (relatively consistent liquid-to-vapour ratios) trapped with vapour-rich (Type II) inclusions in growth zones or fractures have been observed in many samples from silver-rich deposits in the upper Kitsault River area (*see* below). This fluid inclusion evidence for boiling is predicated on the assumption that the Type II inclusions do indeed contain a vapour phase and are not decrepitated, air-filled voids. Since microthermometric data could not be collected from the virtually opaque, often tiny Type II inclusions, fluid inclusion gas chromatographic analysis is required to validate this assumption.

Wolf

Primary Type I and Type II fluid inclusions occur in early, vein quartz that forms colloform banding, comb structures and well-terminated quartz crystals as a result of open-space filling. The Type I inclusions are low salinity (average 4.2 ± 2.5 wt % NaCl equiv., Figure 3) and homogenize at low temperatures (average 169±54°C, Figure 4). These inclusions are similar in appearance to finely crystalline, irregular-shaped < 200°C-type quartz that has been recognized in the subaerial epithermal environment (Bodnar *et al.*, 1985), but have higher average salinity (> 3.4 wt. % NaCl) which may indicate a submarine setting (see Hannington *et al.*, 1999, figure 15). Seawater is 3.1 wt. % NaCl equiv.

Evidence for boiling, given the assumption noted above, was recognized in one fluid inclusion assemblage (FIA) from sample RP-W-1. The estimated pressure of entrapment for fluid inclusions in this FIA, which homogenized at 138°C, is 5 bars, using the equation of Brown and Lamb (1989) and the computer program FLINCOR (Brown, 1989). This equation and program are used throughout this paper for pressure estimates for Type I inclusions. A pressure of 5 bars indicates a near-surface sample depth of between 20 metres (assuming lithostatic load) and 50 metres (assuming hydrostatic load). At such shallow depths, pressure correction of homogenization temperatures for the remaining fluid inclusion assemblages are insignificant, even for unboiled fluids.

Further evidence to support depositional temperatures below 200 °C is the stable isotope data of Devlin (1987, table 4.2). He reports calculated depositional temperatures of 152 °C and 174 °C for quartz-calcite and quartz-witherite pairs.

The low temperatures, salinities typically just above seawater, and calculated depths of formation reported for primary Type I fluid inclusions in early vein quartz at the Wolf occurrence are consistent with formation in a subaerial, or possibly submarine, hot-spring-type setting (Figure 6a).

Secondary high XH_2O (low XCO_2) Type IV (carbonic) fluid inclusions occur in numerous microfractures that cut the original low temperature quartz. These low-to-moderate salinity (average 7.4 ± 2.5 wt. % NaCl equiv.) CO_2-bearing inclusions were introduced at minimum (homogenization) temperatures of between 255 to 280 °C and corresponding minimum pressures of between 1452 and 2776 bars using the equations of Brown and Lamb (1989) and the computer program FLINCOR (Brown, 1989). These pressures translate to minimum depths of formation of between 5.5 and 10.5 kilometres, assuming lithostatic load. Fluid inclusions of similar composition are found in low to medium grade metamorphic rocks and mesothermal to hypothermal ore deposits (Diamond, 1994).

Dolly Varden

Primary Type I and Type II fluid inclusions occur inside subangular breccia fragments of early-formed comb, colloform and crustiform-textured quartz, moss-textured quartz and euhedral quartz with primary growth zones. These fragments are infilled by stringer and disseminated pyrite, galena and sphalerite and veinlet-controlled barite. Sphalerite did not yield any usable inclusions for microthermometric study.

The Type I inclusions in quartz are low salinity (average 4.0 wt % NaCl equiv., Figure 3) and homogenize at low temperatures (average 151±27°C, Figure 4). These inclusions are finely crystalline and irregularly-shaped, similar to those described as < 200°C-type quartz at the Wolf (above). A lower salinity variety of this type of quartz has been recognized in the epithermal environment (Bodnar *et al.*, 1985). The average salinity of the inclusions in quartz from the Dolly Varden deposit may indicate a submarine setting (*see* Hannington *et al.*, 1999).

Evidence for boiling is reported from an FIA in sample RP-D-3. The estimated pressure of entrapment for fluid inclusions in this FIA, which homogenized at 148°C, is 4 bars; which represents near-surface sample depths of between 15 metres (assuming lithostatic load) and 40 metres (assuming hydrostatic load).

Devlin (1987, Figure 4.2) reports calculated depositional temperatures, using sulphur and oxygen isotope data, of 190 °C for quartz-calcite and 192°C for barite-sphalerite pairs. These temperatures are slightly higher than our reported fluid inclusion range (Figure 4).

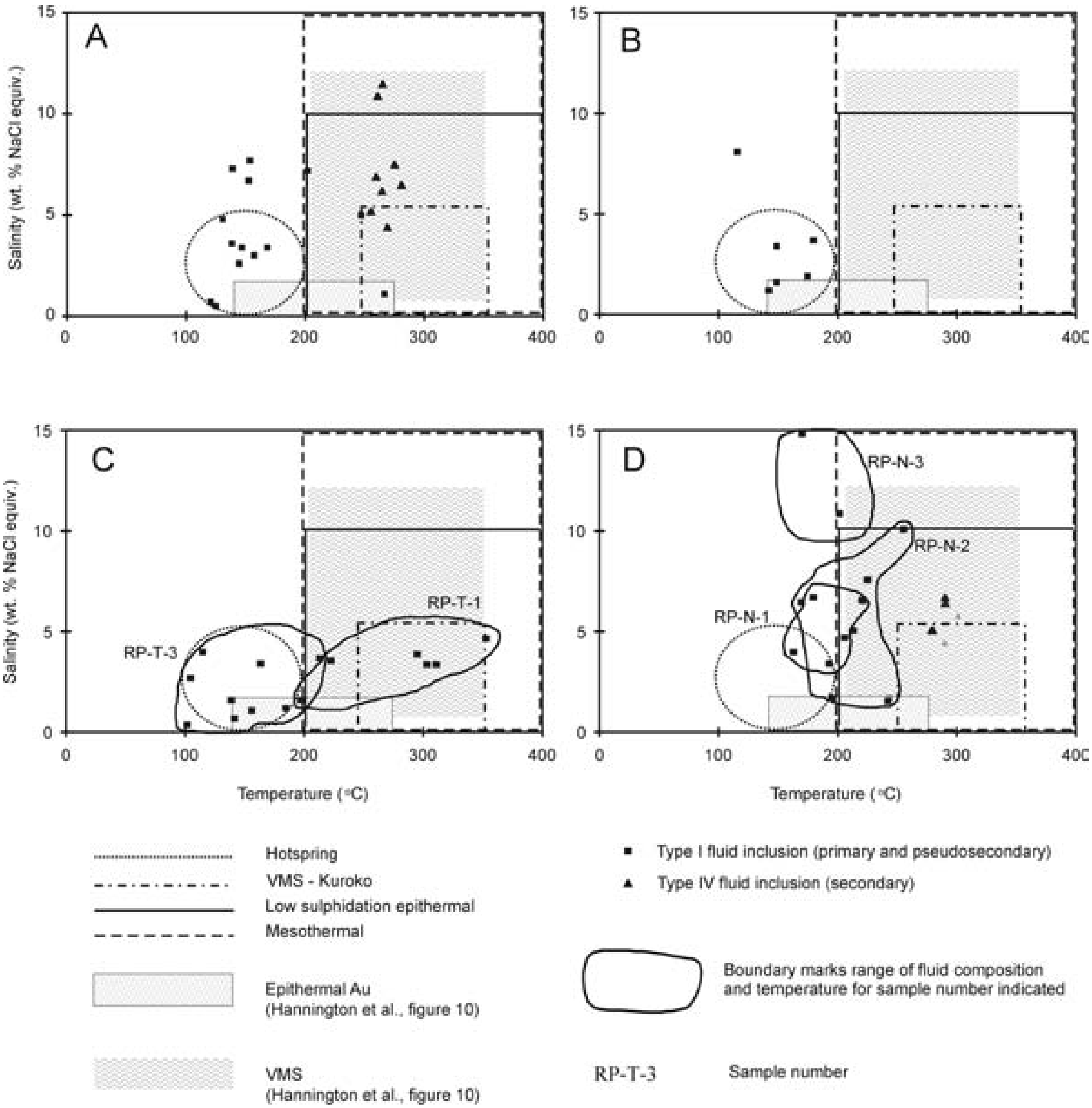

Figure 6. Salinity versus temperature for fluid inclusion assemblages at the a) Wolf occurrence, b) former Dolly Varden mine, c) former Torbrit mine, and d) Northstar occurrence. Groups of fluid inclusion assemblages (FIA's) from specific samples are circled. Boxes represent ranges of salinity and temperature from fluids in different ore deposit environments (after Reynolds, 1991; Dunne, 1992; and Lattanzi, 1991). Note that ranges for epithermal Au (stippled shading) and VMS (wavy-line shading) ore fluids (figure 10 of Hannington et al., 1999) differ from the above boxes.

Low temperatures, salinities near seawater composition and calculated depths of formation reported for primary Type I fluid inclusions in early vein quartz breccia fragments at the Dolly Varden deposit are similar to those observed at the Wolf occurrence, and are consistent with formation in a subaerial, or possibly submarine, hot-spring-type deposit (Figure 6b).

TORBRIT

Primary and pseudosecondary Type I fluid inclusions occur in subrounded to subangular, silicified and sericitized (?) quartz breccia fragments infilled by disseminated and stringer sulphides, including sphalerite. A small number of the finely-crystalline quartz fragments preserve primary growth zones. Primary and pseudosecondary Type I and Type II fluid inclusions occur in minor pale-green sphalerite associated with pyrite in core sample RP-T-1 and pale-green sphalerite associated with galena in grab sample RP-T-3. The final melting temperatures (salinities) of Type I primary and pseudosecondary fluid inclusions in quartz and in sphalerite cannot be distinguished (Figure 3). The salinities for these inclusions average 2.9±1.8 wt. % NaCl equiv. (Figure 3); similar to that of seawater.

Average homogenization temperatures for primary and pseudosecondary Type I fluid inclusions in early quartz fragments from samples RP-T-3 and RP-T-1 are 120 ± 26 ^{o}C and 205 ± 15 ^{o}C respectively (Figure 4). Average homogenization temperatures for Type I fluid inclusions, of similar origin, in pale-green sphalerite associated with pyrite in samples RP-T-1 and associated with galena in RP-T-3 are 316±26 ^{o}C and 154±38 ^{o}C respectively (Figure 4). Additional petrographic and fluid inclusion work on temporally and spatially constrained samples are required to resolve differences in temperature, and possibly composition, between the two apparently distinct populations of sphalerite present at the former Torbrit mine.

The low temperature fluid inclusions in finely-crystalline quartz with irregular shapes and somewhat inconsistent liquid-to-vapour ratios are similar to <200^{o}C -type quartz described from the epithermal environment (Bodnar *et al.*, 1985). The inclusions in quartz from Torbritt have average salinities that fall in the range of low temperature epithermal fluids (< 3.4 wt. % NaCl) and approximate seawater fluids (~ 3.1 eq. wt. % NaCl).

Evidence for boiling was not observed in the finely-crystalline quartz. Based on comparison of emplacement depths (~50 metres) in similar quartz observed at the Wolf and Dolly Varden deposits, it is likely that a maximum pressure correction of about 5^{o}C can be applied to homogenization data from fluid inclusions in quartz at Torbrit. Application of the maximum correction to homogenization temperatures of primary and pseudosecondary Type I inclusions in quartz yields trapping temperatures of approximately 125 ^{o}C (sample RP-T-3) and average trapping temperatures of 210±15^{o}C (sample RP-T-1).

Evidence for boiling can be seen in sphalerite from sample RP-T-3 from FIA 6-1. The estimated pressure of entrapment for fluid inclusions in this FIA that homogenize at 156^{o}C is 6 bars. This represents a near-surface sample depth of between 25 metres (assuming lithostatic load) and 60 metres (assuming hydrostatic load).

Evidence for boiling is reported in sphalerite from two FIA's in sample RP-T-1 that homogenize at 311.0 and 352.8^{o}C, respectively. The estimated pressure of entrapment for these FIA's are 97 and 163 bars which translates to moderate sample depths of between 370 and 620 metres (assuming lithostatic load) and 990 and 1660 metres (assuming hydrostatic load). Because the fluids are interpreted to have been boiling at the time of entrapment, no pressure corrections for conversion of homogenization temperature to trapping temperature for the remaining fluid inclusion assemblages in sphalerite were employed.

Further evidence to support both moderate and low depositional temperatures for sphalerite at Torbrit is from the stable isotope data of Devlin (1987, Table 4.2). He reports calculated depositional temperatures, using sulphur isotope data, of 346 ^{o}C and 405 ^{o}C for barite-sphalerite and 202^{o}C and 328^{o}C for sphalerite-galena pairs. Campbell (1959) estimated a moderate temperature of 270^{o}C for sphalerite formation at the Torbrit deposit using estimated FeS content and phase diagrams.

Low temperatures, salinities that range from nearly pure water to seawater composition (Figure 3), and textural similarities of primary and pseudosecondary Type I fluid inclusions in early vein quartz breccia fragments (sample RP-T-3) at the Torbrit deposit are similar to those observed at the Wolf and Dolly Varden deposits. The quartz breccia fragments and low temperature sphalerite from sample RP-T-3 are consistent with formation in a subaerial, or possibly submarine, hot-spring-type deposit (Figure 6c).

Fluid inclusions in quartz breccia fragments from sample RP-T-1 plot more within the lower temperature range of low sulphidation epithermal deposits or low-temperature subaqueous hydrothermal systems on Figure 6c. Homogenization temperatures for Type I fluid inclusions in sphalerite from RP-T-1 fall within the higher temperature range of low sulphidation epithermal deposits as well as within the range expected for modern black smokers and ancient volcanogenic massive sulphide deposits (Figure 6c).

Northstar

Fluid inclusion work at the Northstar occurrence was undertaken on three core samples from drill hole NS89-3 sampled at 958 feet (RP-N-1), 967 feet (RP-N-2) and 988 feet (RP-N-3). Primary Type I fluid inclusions occur in subangular to subrounded fragments of quartz vein (up to 5 millimetres) that appear to pre-date massive barite and disseminated and stringer sulphides, including sphalerite, as well as late barite and carbonate veinlets. The quartz vein fragments comprise typically euhedral, fine-to-medium grained quartz with well-preserved primary growth zones (Photo 6). Pseudosecondary and indeterminate Type I fluid inclusions occur in pale-green sphalerite associated with pyrite in sample RP-N-2. Microthermometric work on sphalerite from the Northstar is limited to this sample.

Final melting temperatures (salinities) of primary Type I fluid inclusions in the quartz from the drill core appear to vary with the down-hole depth of sampling. Salinities for primary Type I fluid inclusions in quartz from samples RP-N-1, RP-N-2 and RP-N-3 average 5.1±1.5 wt. % NaCl equiv., 6.2±3.1 wt. % NaCl equiv., and 12.9±2.4 wt. % NaCl equiv. (Figure 6d). These salinities are all significantly higher than average seawater. One measured salinity, from a pseudosecondary fluid inclusion in the sphalerite, was much lower at 1.7 wt. % NaCl equivalent.

Homogenization temperatures for both quartz and sphalerite are low (average 191± 30^{o}C for quartz and 182 ^{o}C (n = 1) for sphalerite). The quartz is similar in appearance to finely crystalline, irregular-shaped < 200^{o}C-type quartz with inconsistent liquid-to-vapour ratios and 200 ^{o}C to 230 ^{o}C -type quartz with consistent liquid-to-vapour ratios that forms in the epithermal environment (Bodnar *et al.*, 1985, Reynolds, 1991). Salinities typically less than 10 equiv. wt. % NaCl (Figure 3) are consistent with this interpretation. Low temperature fluids with similar salinities have also been reported in both quartz and sphalerite at Eskay Creek (Sherlock *et al.*, 1999, figures 7 and 8).

Evidence for boiling was not observed in quartz or sphalerite fluid inclusion assemblages from the Northstar occurrence. A confining pressure of about 21 bars is required to suppress phase separation (boiling) for the fluid that precipitated quartz at the maximum recorded homogenization temperature of 243^{o}C (Figure 4) and salinities between 3 to 8 equiv. wt. % NaCl (Figure 3, equation of Bodnar and Vityk, 1994). Similarly, a confining pressure of about 7 bars is required to suppress boiling of the fluid that precipitated sphalerite at a temperature of 182^{o}C and 1.7 eq. wt. % NaCl (equations of Bodnar and Vityk, op. cit.). Using these estimated pressures, the Northstar prospect formed under a water column of between 70 and 210 metres or at depths of 26 to 80 metres assuming a lithostatic pressure regime. The maximum pressure correction for a 210 metre water column overlying the mineralization is about 14^{o}C (Potter, 1977). Application of this correction to homogenization temperatures of primary and pseudosecondary Type I inclusions yields trapping temperatures from 164 to 257^{o}C.

Devlin (1987) reports calculated depositional temperatures, using sulphur isotope data, of 349 ^{o}C and 354 ^{o}C for barite-sphalerite pairs. Fluid inclusions with these moderate temperatures have not been observed in this study.

Pressure corrected homogenization temperatures from fluid inclusions in quartz vein fragments from samples RP-N-1 and RP-N-2 plot mostly within the lower temperature range of low sulphidation epithermal deposits or low-temperature subaqueous hydrothermal systems on Figure 6d. Fluid inclusions in sample RP-N-3 have much higher salinities.

Secondary Type IV (carbonic) and Type V (CO_2-CH_4) fluid inclusions occur in numerous microfractures that cut the original low temperature epithermal/low temperature subaqueous hydrothermal quartz in sample RP-N-1. The low salinity (average 5.9±1.2 wt. % NaCl equiv.) carbonic inclusions were introduced at minimum (homogenization) temperatures of between 268 ^{o}C to 283 ^{o}C, similar to temperatures recorded for secondary carbonic fluids at the Wolf occurrence (Figure 6a,d). In the absence of observed CO_2 liquid-vapour homogenization temperatures (due to the tiny size of Type IV fluid inclusions), minimum pressure estimates cannot be calculated. As discussed for the Wolf occurrence, carbonic fluid inclusions are found in low to medium grade metamorphic rocks and mesothermal to hypothermal ore deposits and may be a product of prograde metamorphism (Diamond, 1994, Marshall *et al.*, 2000). Secondary Type III (multiphase) fluid inclusions with low to moderate homogenization temperatures similar to those recorded in this study (sample RP-N-1) also can occur in metamorphosed and synmetamorphic ore deposits (Marshall *et al.*, op. cit.).

GENETIC MODELS/ANALOGUES

Although the metals present (barium, strontium, silver, lead and zinc) in the mineral deposits east of the Kitsault River are indicative of genetically related deposits (Thiersch, 1986; Devlin, 1987), there are differences in opinion as to the mode of origin of specific deposits. While most authors agree that the mineralization at Sault is syngenetic, and at Wolf is epigenetic, some consider the Dolly Varden, Torbrit and Northstar to be epigenetic “replacement” (Campbell, 1959; Black, 1951; Mitchell, 1973; Thiersch, 1986), and others consider them to be syngenetic (Devlin and Godwin, 1986; Devlin, 1987; Drown *et al.*, 1990; McGuigan and Melnyk, 1991, Tupper and McCartney, 1990).

EVIDENCE FOR HOT-SPRING-TYPE DEPOSITS

New fluid inclusion data from the Wolf, Dolly Varden, Torbrit and Northstar deposits indicates that the hydrothermal fluids responsible for deposition of early vein quartz and vein quartz breccia fragments at the Wolf, Dolly Varden and Torbrit deposits and disseminated sphalerite mineralization associated with galena at the Torbrit and pyrite at the Northstar deposits are low temperature (< 200^{o}C) and low salinity (< 5 wt. % NaCl equivalent.), consistent with formation in either subaerial or near-surface subaqueous hot-spring-type deposits (Figure 6a,b,c,d). These data are supported by calculations of some low depositional temperatures (< ~200^{o}C) for sulphide-sulphate, sulphide-sulphide, silica-carbonate pairs at the Wolf, Dolly Varden and Torbrit deposits using sulphur and oxygen isotope data (Devlin, 1987, table 4.2). Similar low temperature and low salinity hydrothermal fluids are reported from fluid inclusions in quartz and sphalerite at the Eskay Creek deposit (Sherlock *et al.*, 1999).

Calculated fluid pressures are very low, about 5 bars, for primary fluid inclusions in early vein quartz and vein quartz breccia fragments at the Wolf and Dolly Varden deposits and from primary fluid inclusions in sphalerite at the Torbrit deposit that exhibit evidence for boiling. Note that evidence for boiling is inferred by the coexistence of primary Type I fluid inclusions with variable liquid-to-vapour ratios and coeval Type II fluid inclusions trapped in the same growth zones in the quartz and sphalerite. This inference is made with the assumption that the Type II fluid inclusions in these minerals are true vapour-rich fluid inclusions and not air-filled voids. The calculated fluid pressure of 5 bars, assuming boiling fluids, equates to deposition at water depths of about 50 metres or 20 metres of overlying rock.

Examples of active shallow, submarine hot-spring deposits include low temperature pyritic sulphides forming from the Punta Banda hot-springs, California borderlands and related deposits, such as sulphide veins that occur in marine sediments (boiling vents) in Kagoshima Bay, S. Kyushu (Hannington *et al.*, 1999, Table 6). Both examples are forming at < 100 metre depths (Hannington, op. cit.). The Eskay Creek deposit, based on fluid inclusion data, is considered to have deposited from boiling fluids at fluid pressures of 150 bars and water depths of 1500 metres (Sherlock *et al.*, 1999). Interestingly, Sherlock *et al.* (1999) reports tiny, opaque inclusions coeval with Type I fluid inclusions that may be vapour-rich; microthermometric data was unobtainable from these opaque inclusions. Examples of subaerial epithermal hot-spring-type precious metal deposits formed at very shallow levels include Paradise Peak, Nevada (John *et al.*, 1991) and deposits in the Hart Mining District, California (Ausburn, 1991).

EVIDENCE FOR LOW SULPHIDATION EPITHERMAL/VMS DEPOSITS

Primary fluid inclusions in some vein quartz breccia fragments from the Torbrit and Northstar deposits are slightly higher temperature (200ºC to 230ºC), and in the case of the Northstar, higher salinity (>5 wt. % NaCl equiv.). The hydrothermal fluids responsible for initial deposition of these vein fragments formed in the lower temperature range of low sulphidation epithermal deposits or perhaps in the range of volcanogenic massive sulphide deposits as defined by Lattanzi (1991, figure 9).

Primary and pseudo secondary fluid inclusions in pale-green sphalerite associated with pyrite from the Torbrit are moderate temperature (295ºC to 350ºC) and low salinity (<5 wt. % NaCl eq.) consistent with formation in the higher temperature range of low sulphidation epithermal deposits as well as within the range expected for modern black smokers and ancient volcanogenic massive sulphide deposits (Figure 6c). These data are supported by calculations of moderate depositional temperatures (328ºC to 405ºC) for sulphide-sulphate and sulphide-sulphide pairs using sulphur isotope data (Devlin, 1987). Calculated fluid pressures from these moderate temperature fluid inclusions in sphalerite are 97 and 163 bars. These fluid pressures are typical for modern black smokers, ancient volcanogenic massive sulphide deposits and are within the range reported for the Eskay Creek deposit (150 bars, *see* above). The calculated fluid pressure equates to water depths of 970 and 1630 metres or relatively shallow rock sample depths of between 370 and 620 metres.

Devlin (1987) identified a distinctive, silica, carbonate, sulphate and sulphide-bearing horizon that can be traced for several kilometres along strike within a thick succession of shallow-water Hazelton Group volcanic and related volcano-sedimentary rocks. He considered this horizon to be exhalative in origin and host the Dolly Varden, Northstar and Torbrit deposits. He reconciles compositional differences within the horizon and differences between the three deposits by proposing that the ‘facies’ changes (silica-sulphide at Dolly Varden, carbonate-sulphate-sulphide at Northstar and sulphate-oxide-sulphate at Torbrit) are consistent with changing fluid chemistry brought about by mixing of exhalative fluids and sea water and differing depths of deposition. The Dolly Varden deposit is inferred to have formed under less oxidizing, deeper water conditions than the Torbrit (Devlin, 1987; Devlin and Godwin, 1986).

THE TRANSITIONAL EPITHERMAL-VMS GENETIC MODEL

Evidence of early, high-level deposition of silicates, sulphates and sulphides from low temperature, low salinity fluids is indicated by colloform, crustiform, comb, and locally bladed mineral textures and fluid inclusions in quartz, barite and sphalerite. These minerals may have deposited in veins, or possibly, in sea-floor mounds. Collapse and/or erosion of vein or mound material is indicated by local brecciation of this material. Alternatively, the breccia zones may have formed as a result of sealing and over-pressuring of the hydrothermal system followed by explosive brecciation. Later, local introduction of low to moderate temperature and low salinity fluids is indicated by infill textures of sulphides, sulphates and carbonate and fluid inclusions in sphalerite.

The Torbrit, Northstar and Dolly Varden deposits are perhaps best described as transitional epithermal-VMS deposits, a “polygot” category proposed by Galley (2001). He notes that this category of deposits “includes precious metal-rich VMS deposits that usually form within a shallow (<1 km) aqueous environment, are associated with felsic cryptodome complexes emplaced in a mixed volcaniclastic-siliciclastic succession overlying a rifted evolved arc sequence” (Galley, op. cit., p. 24). He suggests that deposits associated with extensive sericite-quartz-pyrite alteration, perhaps with associated Fe-carbonate and/or barite, and with sphalerite, galena and pyrite as common sulphide minerals are included in this category. He proposes that these are the base-metal-rich equivalent of submarine low sulphidation epithermal deposits (Sillitoe *et al.*, 1996). Examples of British Columbia deposits of this type are Eskay Creek (Roth *et al.*, 1999) and Rea Gold and Homestake (Hoy, 1991).

EVIDENCE FOR LATE METAMORPHIC (?) FLUIDS

Microfractures defined by secondary CO_2-bearing fluid inclusions overprint primary growth banding in quartz at the Wolf and Northstar deposits and indicate that both these deposits may have been subjected to a post-mineral (?) regionally extensive, metamorphic event. Abundant microfractures have also been observed in quartz at the Dolly Varden and Torbrit deposits. The composition of fluid inclusions in the microfractures from the latter two deposits has not been evaluated. It is likely that all the silver-rich mineral deposits in the upper Kitsault River area have undergone regional metamorphism.

SUMMARY

This initial study of fluid inclusions in quartz, sphalerite and barite from the Wolf, Dolly Varden, Torbrit and Northstar deposits provides the following new information concerning the nature of fluids that relate to epigenetic Ag-Pb-Zn quartz-carbonate vein deposits and epigenetic or syngenetic Ag-Pb-Zn-Ba deposits in the upper Kitsault River area.

KEY OBSERVATIONS AND RESULTS

- Primary growth textures characteristic of high-level subaerial or submarine hot-spring type deposits have been identified in early quartz veins and vein quartz breccias at the Wolf and Dolly Varden deposits. These textures include: colloform (botryoidal) and crustiform (alternating) bands of chalcedony and finely-crystalline quartz, comb quartz, moss-textured quartz and euhedral crystals defined by primary growth zones.
- Quartz breccia fragments at the Torbrit and Northstar deposits are subangular to subrounded and comprise euhedral to anhedral, fine-to-medium grained quartz with well-preserved primary growth zones.
- The following five compositional types of fluid inclusions have been identified in quartz based on phases present at room temperature and microthermometric data: primary, pseudosecondary and secondary Type I: 'Aqueous' H_2O-NaCl, primary Type II: 'Vapour-rich' H_2O-NaCl, secondary Type III: 'Multiphase', secondary Type IV: 'CO_2-bearing or carbonic' H_2O-CO_2-NaCl and secondary Type V: 'CO_2-CH_4'. It is possible that the Type II fluid inclusions are air-filled voids; their opaque nature precludes microthermometric evaluation.
- Pseudosecondary and secondary Type I fluid inclusions have been identified in barite. Primary and pseudosecondary Type I and II fluid inclusions have been identified in sphalerite.
- Early vein quartz and vein quartz breccia fragments at the Wolf, Dolly Varden and Torbrit deposits contain fluid inclusions that are low temperature (<200^{o}C) and low salinity (< 5 wt. % NaCl equiv.) consistent with formation in subaerial or near-surface submarine hot-spring-type deposits.
- Early vein quartz fragments at the Northstar deposits, and some from Torbrit, are slightly higher temperature (200 to 230^{o}C) and in the case of the Northstar, higher salinity (> 5 wt. % NaCl equiv.) consistent with formation in low sulphidation epithermal deposits or perhaps in volcanogenic massive sulphide deposits.
- Two distinct populations of pale-green sphalerite from Torbrit are apparent, based on homogenization temperatures for primary fluid inclusions. Sphalerite associated with galena formed at low temperature (average 154±38^{o}C) and low salinity (< 5 wt. % NaCl eq.) consistent with conditions for subaerial or submarine hot-spring-type deposits. Sphalerite associated with pyrite was deposited at moderate temperature (average 316± 26^{o}C) and low salinity (< 5 wt. % NaCl eq.) consistent with formation in the higher temperature range of low sulphidation epithermal deposits, modern black smokers and ancient volcanogenic massive sulphide deposits.
- Limited fluid inclusion data from pale-green sphalerite associated with pyrite at the Northstar occurrence indicates low temperature (125 and 182^{o}C) and low salinity (1.7 wt. % NaCl eq.) fluids similar to the low temperature sphalerite variety at the Torbrit deposit.
- The occurrence of liquid-rich and probable vapour-rich fluid inclusions in the same primary growth zones provided evidence for boiling in some quartz samples from the Wolf and Dolly Varden deposits and in sphalerite from the Torbrit deposit.
- The following pressure estimates have been calculated using fluid inclusion data:

  Wolf: 5 bars (primary fluid inclusions in early vein quartz and quartz breccia fragments, evidence for boiling)

  Dolly Varden: 4 bars (primary fluid inclusions in early vein quartz and quartz breccia fragments, evidence for boiling)

  Torbrit(sample RP-T-3): 6 bars (primary and pseudosecondary fluid inclusions in sphalerite, evidence for boiling)

  Northstar (sample RP-N-2): 21 and 7 bars (primary fluid inclusions in early vein quartz and quartz breccia fragments and pseudosecondary fluid inclusions in sphalerite, minimum estimates - no evidence for boiling)
- Pressure estimates from early quartz and sphalerite from the Wolf, Dolly Varden, Torbrit (sample RP-T-3) and Northstar deposits equate to deposition at water depths of approximately 40 to 210 metres or rock depths of about 15 to 80 metres and are consistent with formation in a near-surface hot-spring-type depositional setting.
- Pressure estimates of 97 and 163 bars from primary and pseudosecondary fluid inclusions in sphalerite from the Torbrit deposit (sample RP-T-1) correspond to deposition from boiling fluids at significantly greater water depths of approximately 370 and 620 metres or greater rock depths of about 990 and 1660 metres.
- Secondary CO_2-bearing fluid inclusions define microfractures that overprint the primary growth textures in quartz at the Wolf and Northstar deposits and indicate that these deposits may have been subjected to a regional metamorphic event. The relatively low salinity, CO_2-bearing inclusions were introduced at minimum (homogenization) temperatures of between 255^{o}C to 283^{o}C and corresponding minimum pressures, for the Wolf deposit, of between 1452 and 2776 bars. These pressures translate to minimum depths of formation of between 5.5 and 10.5 kilometres for secondary, metamorphic (?) fluids at the Wolf deposit (assuming lithostatic load).

CONCLUSIONS

This fluid inclusion study, together with existing geological and geochemical data, supports the contention that the silver-rich deposits in the upper Kitsault River area are genetically related. It also suggests that the deposits may be silver-rich analogues to the precious metal-rich Eskay Creek deposit. The Kitsault River deposits all formed at surface or at shallow depth in the waning stages of Hazelton arc volcanism. They have similar tenor (silver, lead, zinc, strontium, barium) and mineralogy. Their mineralization varies from multi-episodic and irregularly zoned to laminated and bedded, perhaps relating to proximity to subaqueous chimneys, surface mounds or collapse-textures in shallow marine basins or emplacement along active faults. Colloform, crustiform and comb textures clearly indicate early, high-level deposition of quartz in veins that formed from low temperature, and for the most part, low salinity hydrothermal fluids in a hot-spring-type setting. These early veins are locally brecciated, perhaps indicating near-contemporary structural activity or collapse. Alternatively, the brecciated zones may be the result of near-surface explosive brecciation. The silver was probably precipitated from low-to-moderate temperature and low salinity fluids that also deposited sphalerite and other sulphide minerals. It could either have been deposited in a subaerial hot-spring - low sulphidation epithermal environment or, possibly, a submarine hot-spring - volcanic-hosted massive sulphide-type depositional setting.

ACKNOWLEDGMENTS

Professor Lori Kennedy in the Department of Earth and Ocean Sciences at the University of British Columbia is thanked for permission to use samples from their collection for this study. The authors gratefully acknowledge the contributions of numerous public and private sector geologists and others in the preparation of this report. In particular, they wish to thank Fred Christiansen, President of Dolly Varden Minerals Inc. for permission to visit and sample the silver deposits in Kitsault River area.

We appreciate the editorial review by Dave Lefebure.

REFERENCES

Alldrick, D.J., Dawson, G.L., Bosher, J.A. and Webster, I.C.L. (1986): Geology of the Kitsault River area (NTS 103P); in Geological Fieldwork 1985, British Columbia Ministry of Energy, Mines and Petroleum Resources, Open File Map 1986-2, scale 1:50 000.

Alldrick, D.J., Brown, D.A., Harakal, J.E., Mortensen, J.K. and Armstrong R.L. (1987): Geochronology of the Stewart Mining Camp (104B/1); *in* Geological Fieldwork 1986, *British Columbia Ministry of Energy, Mines and Petroleum Resources*, Paper 87-1, pages 81-92.

Ausburn, K.E. (1991): Ore-Petrogenesis of Tertiary Volcanic Hosted Epithermal Gold Mineralization at the Hart Mining District, Castle Mountains, NE San Bernardino County, California; *in* Geology and Ore Deposits of the Great Basin, Symposium Proceedings, *Geological Society of Nevada*, pages 1147-1188.

Black, J.M. (1951): Geology and Mineral Occurrences of the Upper Kitsault Valley; *in British Columbia Ministry of Energy, Mines and Petroleum Resources*, Annual Report 1951, pages A76-A83.

Bodnar, R.J. (1993): Revised Equation and Table for Determining the Freezing Point Depression of H_2O-NaCl Solutions; *Geochimica et Cosmochimica Acta*, Volume 57, pages 683-684.

Bodnar, R.J. and Vityk, M.O. (1994): Interpretation of Microthermometric Data for H_2O-NaCl Fluid Inclusions; in Fluid Inclusions in Minerals: Methods and Applications, Short Course of the Working Group (IMA) "Inclusions in Minerals", B. De Vivo and M.L. Frezzotti, Editors, *Virginia Polytechnic Institute and State University*, pages 117-130.

Bodnar, R.J., Reynolds, T.J. and Kuehn, C.A. (1985): Fluid-Inclusion Systematics in Epithermal Systems; *in* Geology and Geochemistry of Epithermal Systems, Berger, B.R. and Bethke, P.M., Editors, Society of Economic Geologists, *Reviews in Economic Geology*, Volume 2, pages 73-97.

Brown, P.E. (1989): FLINCOR: A Microcomputer Program for the Reduction and Investigation of Fluid Inclusion Data; *American Mineralogist*, Volume 74, pages 1390-1393.

Brown P.E. and Lamb W.M. (1989): P-V-T Properties of Fluids in the System H_2O-CO_2-NaCl: New Graphical Presentations and Implications for Fluid Inclusion Studies; *Geochimica et Cosmochimica Acta*, Volume 53, 1209-1221.

Burruss, R.C. (1981): Analysis of Phase Equilibrium in C-O-H-S fluid inclusions; *in* Short Course in Fluid Inclusions: Applications to Petrology, Hollister, L.S. and Crawford, M.L., Editors, *Mineralogical Association of Canada*, Volume 16, pages 39-74.

Campbell, F.A. (1959): The Geology of Torbrit Silver Mine; *Economic Geology*, Volume 54, pages 1461-1495.

Carter, N.C. (1964): Wolf (Dolly Varden Mines Limited); *in British Columbia Ministry of Energy, Mines and Petroleum Resources*, Report of the Minister of Mines, pages 41-43.

Crawford, M.L. (1981): Phase Equilibria in Aqueous Fluid Inclusions; *Mineralogical Association of Canada*, Short Course, Volume 6, pages 75-100.

Davis, D.W., Lowenstein, T.K. and Spencer, R.J. (1990): The Melting Behaviour of Fluid Inclusions in Laboratory-Grown Halite Crystals in the Systems NaCl-H_2O, NaCl-KCl-H_2O, NaCl-$MgCl_2$-H_2O and NaCl-$CaCl_2$-H_2O; *Geochimica et Cosmochimica Acta*, Volume 54, pages 591-601.

Dawson, G.L. and Alldrick, D.J. (1986): Geology and Mineral Deposits of the Kitsault Valley (103P/11,12); *in* Geological Fieldwork 1985, *British Columbia Ministry of Energy, Mines and Petroleum Resources*, Paper 86-1, pages 219-224.

Devlin, B.D. (1987): Geology and Genesis of the Dolly Varden Silver Camp, Alice Arm Area, Northwestern British Columbia; Unpublished M.Sc. Thesis, *The University of British Columbia*, 131 pages plus maps.

Devlin, B.D. and Godwin, C.I. (1986): Geology of the Dolly Varden camp, Alice Arm area, (103P/11,12); *in* Geological Fieldwork 1985, *British Columbia Ministry of Energy, Mines and Petroleum Resources*, Paper 86-1, pages 327-330.

Diamond, L.W. (1994): Introduction to Phase Relations of CO_2-H_2O fluid inclusions; *in* Fluid Inclusions in Minerals: Methods and Applications, Short Course of the Working Group (IMA) "Inclusions in Minerals", De Vivo, B. and Frezzotti, M.L., Editors, *Virginia Polytechnic Institute and State University*, pages 131-158.

Dong, G., Morrison, G. and Jaireth, S. (1995): Quartz Textures in Epithermal Veins, Queensland: Classification, Origin, and Implication, *Economic Geology*, Volume 90, Number 6, pages 1841-1856.

Drown, T., McGuigan, P. and Melnyk, W. (1990): 1989 North Star Exploration Program on the Dolly Varden Property, Skeena Mining Division; *British Columbia Ministry of Energy, Mines and Petroleum Resources*, Assessment Report #20 033, 34 pages plus maps.

Dunne, K.P.E. (1992): Application of Fluid Inclusion Petrography to Mineral Exploration; *Mineral Deposit Research Unit*, Technical Report 2, 27 pages.

Galley, A. (2001): A Review of the Characteristics of Volcanogenic Massive Sulfide (VMS) Deposits; in Massive Sulphides - A Practical Review; *Kamloops Exploration Group*, Short Course Notes, pages 1-24.

Godwin, C.I., Pickering, A.D.R., Gabites, J.E. and Alldrick, D.J. (1991): Interpretation of Galena Lead Isotopes from the Stewart-Iskut area (103 O, P; 104A, B, G); *in* Geological Fieldwork 1990, *British Columbia Ministry of Energy, Mines and Petroleum Resources*, Paper 91-1, pages 235-243.

Goldstein, R.H. and Reynolds, T.J. (1994): Systematics of Fluid Inclusions in Diagenetic Minerals; *Society for Sedimentary Geology*, Short Course 31, 199 pages.

Hannington, M.D., Poulsen, K.H. and Thompson, J.F.H. (1999): Volcanogenic Gold in the Massive Sulfide Environment; in Volcanic-Associated Massive Sulfide Deposits: Processes and Examples in Modern an Ancient Settings, C.T. Barrie and M.D. Hannington, Editors, Society of Economic Geologists, *Reviews in Economic Geology*, Volume 8, pages 325-356.

Höy, T. (1991): Volcanogenic Massive Sulphide Deposits in British Columbia; in Ore Deposits, Tectonics and Metallogeny in the Canadian Cordillera, *British Columbia Ministry of Energy, Mines and Petroleum Resources*, Paper 1991-4, pages 89-123.

John, D.A., Nash, J.T., Clark, C.W. and Wulftange, W.H. (1991): Geology, Hydrothermal Alteration and Mineralization at the Paradise Peak Gold-Silver-Mercury Deposit, Nye County, Nevada; *in* Geology and Ore Deposits of the Great Basin, Symposium Proceedings, *Geological Society of Nevada*, pages 1020-1050.

Lattanzi, P. (1991): Applications of Fluid Inclusions in the Study and Exploration of Mineral Deposits; *European Journal of Mineralogy*, Volume 3, pages 689-701.

MacIntyre, D.G., Ash, C.H. and Britton, J.M. (1994): Geological Compilation, Skeena-Nass area, west central British Columbia (NTS 93 E, L, M; 94D; 103 G, H, I, j, O, P; 104 A, B); *British Columbia Ministry of Energy, Mines and Petroleum Resources*, Open File 1994-14.

Marshall, B., Giles, A.D. and Hagemann, S.G. (2000): Fluid Inclusions in Metamorphosed and Synmetamorphic (Including Metamorphogenic) Base and Precious Metal Deposits: Indicators of Ore-Forming Conditions and/or Ore-Modifying Histories?; *in* Metamorphosed and Metamorphogenic Ore Deposits, Spry, P.G., Marshall, B. and Vokes, F.M., Editors, *Mineralogical Society of America,* Reviews in Economic Geology, Volume 11, pages 119-148.

McGuigan, P. and Melnyk, W. (1991): Diamond Drill Report on the Dolly Varden property, Skeena Mining Division; *British Columbia Ministry of Energy, Mines and Petroleum Resources*, Assessment Report #20 900, 16 pages plus maps.

Mitchell, M.A. (1973): Geology, Dolly Varden Mine; Unpublished Report, *Dolly Varden Mines Limited*, 16 pages and figures.

Nash, J.T. (1976): Fluid Inclusion Petrology - Data from Porphyry Copper Deposits and Applications to Exploration; *United States Geological Survey*, Professional Paper 907-D, 16 pages.

Pinsent, R.H. (2001): Mineral Deposits of the Upper Kitsault River Area, British Columbia (103P/W); *in* Geological Fieldwork 2000, *British Columbia Ministry of Energy, Mines and Petroleum Resources*, Paper 2001-1, pages 313-326.

Potter, R.W. II (1977): Pressure Corrections for Fluid Inclusion Homogenization Temperatures Based on the Volumetric Properties of the System NaCl-H_2O; *United States Geological Survey*, Journal of Research, Volume 5, pages 603-607.

Reynolds, T.J., (1991): Short Course on Fluid Inclusions; *Mineral Deposit Research Unit*, Short Course 6.

Roedder E. (1984): Fluid Inclusions; *Mineralogical Society of America,* Reviews in Mineralogy, Vol. 12, Bookcrafters Inc., Chelsea, Michigan, 644 pages.

Roth, T., Thompson, J.F.H. and Barrett, T.J. (1999): The Precious Metal-Rich Eskay Creek deposit, Northwestern British Columbia; *in* Volcanic-associated massive sulphide deposits: process and examples in modern and ancient settings, *Society of Economic Geologists*, Reviews in Economic Geology, Volume 8, pages 357-372.

Sherlock, R.L., Roth, T., Spooner, E.T.C. and Bray, C.J. (1999): Origin of the Eskay Creek Precious Metal-Rich Volcanogenic Massive Sulphide Deposit: Fluid Inclusion and Stable Isotope Evidence; *Economic Geology*, Volume 94, pages 803-824.

Sillitoe, R.H., Hannington, M.D. and Thompson, J.F.H. (1996): High Sulfidation Deposits in the Volcanogenic Massive Sulfide Environment; *Economic Geology*, Volume 91, pages 204-212.

Thiersh, P. (1986): The Geology of the Wolf Silver Prospect, Upper Kitsault Valley, British Columbia; Unpublished B.Sc. Thesis, *The University of British Columbia*, 45 pages.

Thiery, R., van den Kerkhof, A.M. and Debussy, J. (1994): VX Properties of CH_4-CO_2 and CO_2-N_2 Fluid Inclusions; Modeling for T<31 degrees C and P< 400 bars; *European Journal of Mineralogy*, Volume 6, Number 6, pages 753-771.

Thompson, I.S. and Michna, P.D. (1978): Geochemical and Geological Exploration of the Claims, Crown Grants and Licenses held by Dolly Varden Resources Limited in the Kitsault River valley, Skeena Mining Division; *British Columbia Ministry of Energy, Mines and Petroleum Resources*, Assessment Report #7098, 34 pages plus maps.

Tupper, D.W. and McCartney, I.D. (1990): Geological, Geochemical and Diamond Drilling Report on the Kits-Jade project, Skeena Mining Division; *British Columbia Ministry of Energy, Mines and Petroleum Resources*, Assessment Report #20 167, 23 pages plus maps.

Geology of the East Harrison Lake Belt, Southwestern British Columbia

By Chris Ash

KEYWORDS:*Cogburn ophiolitic assemblage, Giant Mascot Mine, ultramafic xenoliths, Cu-Ni-PGE, Late Triassic basinal clastic metasediments.*

INTRODUCTION

The East Harrison Lake belt (EHLB) refers to a northwest-trending belt of rocks occurring to the east of Harrison Lake in southwest British Columbia (Figure 1) which is currently the focus of exploration for ultramafic-related Cu-Ni (PGE). The geology of the EHLB will also be summarized as a 1: 50 000-scale compilation map (Ash *et al.*, in preparation) incorporating both published and unpublished data sets that include recent industry mapping.

This work is part of a multidisciplinary field study undertaken by the British Columbia Geological Survey in response to significant staking and grassroots exploration activity for PGEs within the EHLB. Since January 2000, over 2000 claims have been staked with four significant exploration projects conducted in 2001 (Houle, 2002). In addition to the geological mapping component described below, detailed aspects of PGE related Cu-Ni mineralization (Pinsent, this volume) and geochemical detection of PGEs in stream samples (Lett and Jackman, this volume) were also examined.

The author conducted intermittent fieldwork totaling six weeks between mid June and late October, 2001. The bulk of this time was focused on mapping two east-northeast trending areas across the EHLB. As well five days of mapping were completed in the area of the Giant Mascot Cu-Ni mine. One transect was mapped from the Bear Creek camp east along Cogburn Creek and beyond and a second from Silver Creek east along Hornet Creek and beyond. These are referred to as the Cogburn and Hornet transects in this report. Active logging roads which feed the Bear and Silver Creek log-sorting and mill areas on the eastern shore of Harrison Lake facilitated access in both these areas. As well, the North Fork and Settler Creek logging roads, branches to the north and south, off the main Cogburn logging road at roughly 4.5 and 12.5 kilometres respectively, were mapped to provide along strike continuity between the two transects.

Observations obtained through this study combined with a detailed assessment of the available data for the region enables recognition of a modified lithotectonic framework for the EHLB. They also help place constraints on the age and origin of ultramafic rocks that host Cu-Ni (PGE) mineralization at the Giant Mascot mine.

PREVIOUS WORK

This area was included in several earlier regional mapping studies by the Geological Survey of Canada (Daly, 1912; Cairnes, 1944). The earliest detailed mapping in the region was at the Giant Mascot Mine (Horwood, 1936; Aho, 1954, 1956). Thesis mapping by Lowes (1967, 1968, 1972), covering the southern three-quarters of the region under discussion, represents the only comprehensive mapping of the area and has been the geology used on most subsequent maps for this region.

In addition to these works the EHLB has been the subject of thesis mapping and related studies over the past three decades (Figure 2). Earlier studies were mainly by students with The University of British Columbia, Vancouver (Read, 1960; Richards, 1971; Richards and McTaggart; 1976; Vining, 1977; Reamsbottom, 1971, 1974; Pigage, 1973; 1976; Bartholemew, 1979 and Gabites, 1985). Most of this early work has been synthesized and augmented by

Figure 1. Location of the East Harrison Lake map area.

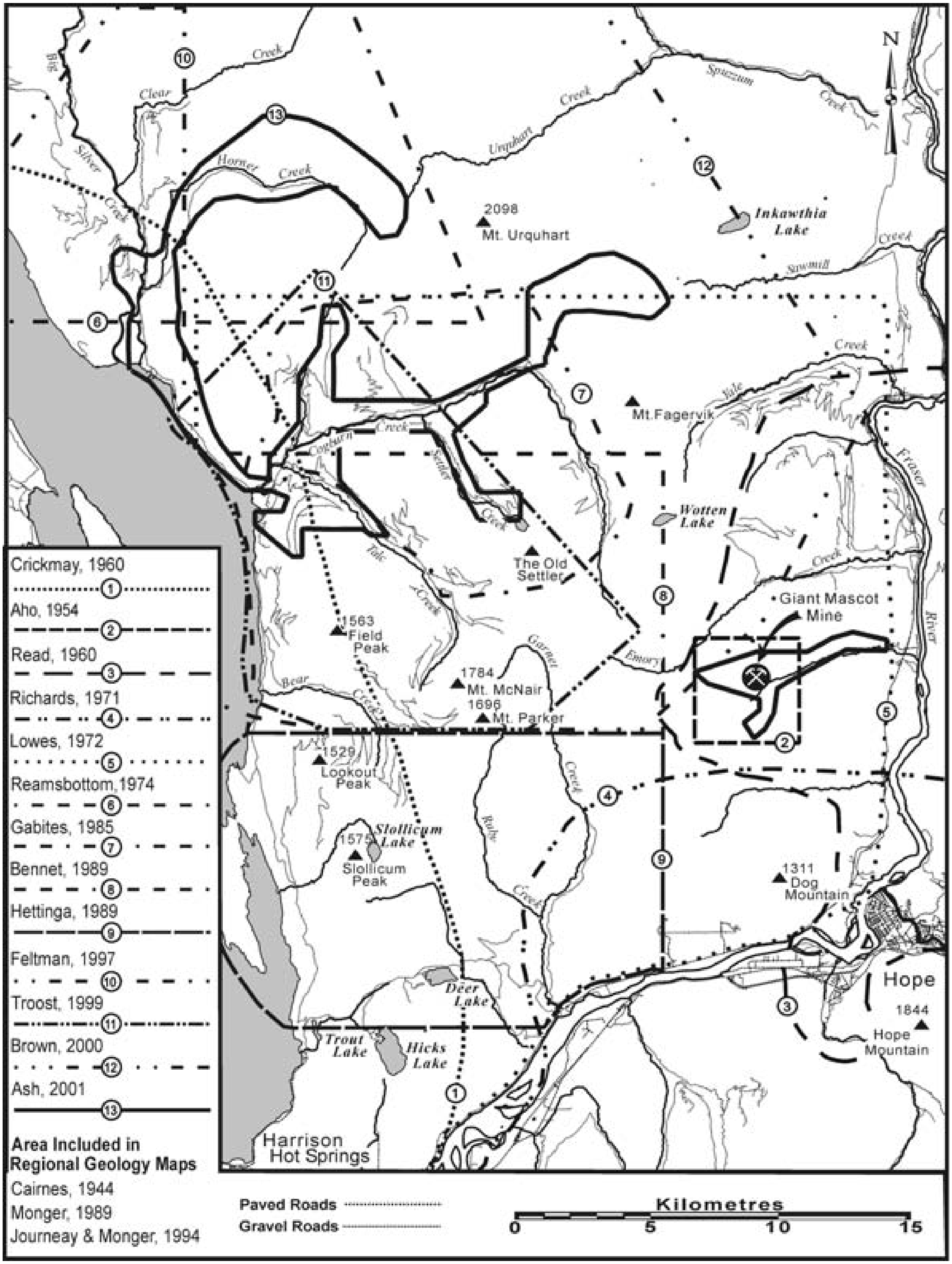

Figure 2. Areas examined during this study and mapping coverage by previous workers.

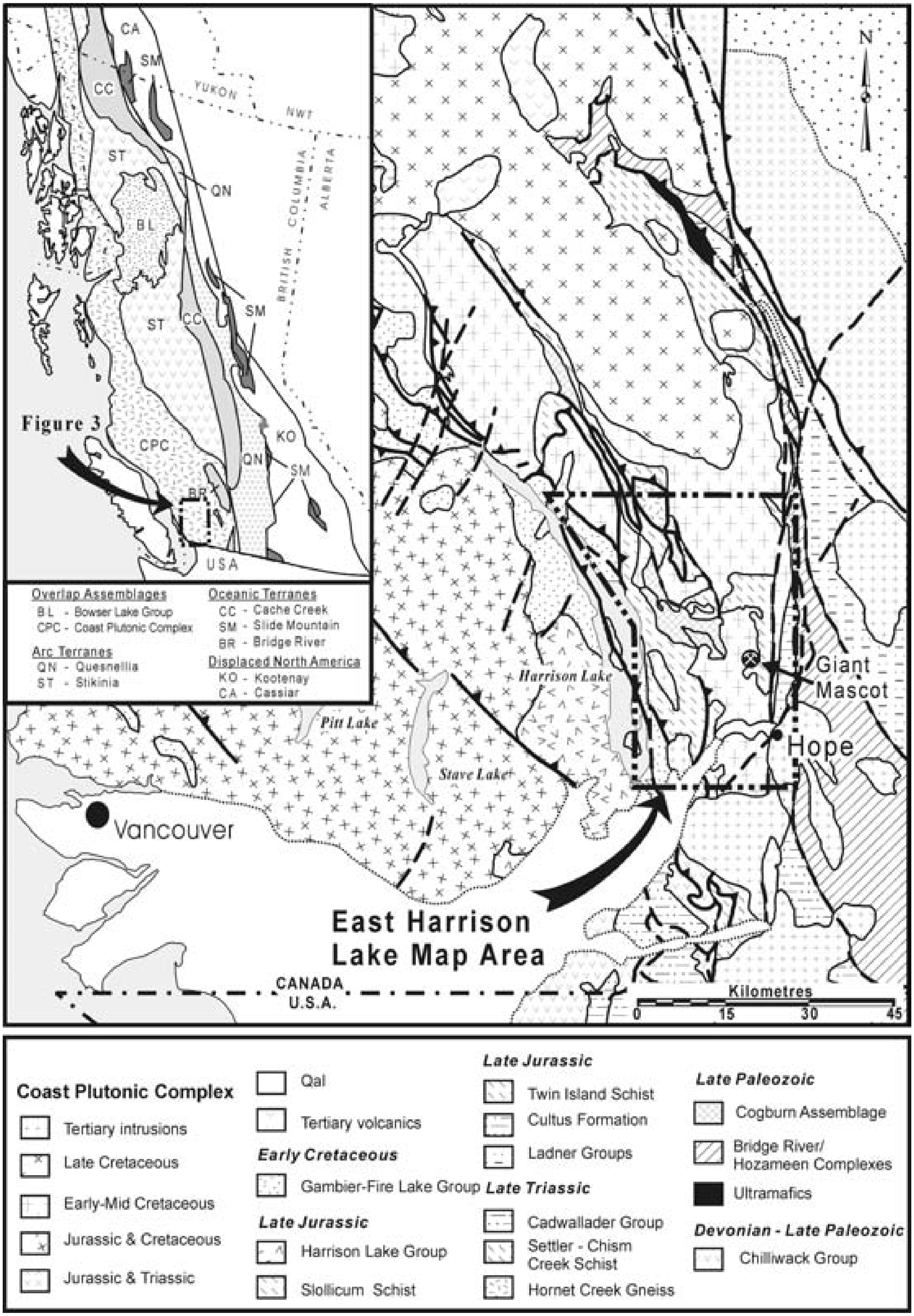

Figure 3. Regional geological setting of the East Harrison Lake map area (after Journeay and Friedman, 1993, with modified legend).

geologists with the Geological Survey of Canada (Monger, 1970; 1986; 1989; Journeay and Friedman, 1993; Journeay and Monger, 1994).

More recent thesis-related studies in the area have been the focus of students from Western Washington University, Bellingham and include works by Bennett (1989), Hettinga (1989), Feltman (1997), Lapen (1998) and Troost (1999). These studies are summarized and augmented with additional data by Brown and Walker (1993), Brown *et al.* (2000) and Brown and McClelland (2000).

The extent of research in this area has resulted in a range of individual approaches to combining lithologic units into packages or terranes, and intrusive rocks into suites. Therefore some discussion of the history of evolution of lithological classification and nomenclature is necessary before introducing a revised lithotectonic framework.

GEOLOGICAL SETTING

The EHLB is the eastern half of a broader belt of supracrustal rocks which crops out on both sides of Harrison Lake (Figures 3 and 4). This broad area of supracrustal rocks is largely surrounded by middle to late Mesozoic intrusions of the Coast Plutonic complex. Within the supracrustal rocks there has been consistent recognition of a general progressive increase in metamorphic grade from subgreenschist to amphibolite from west to east across the belt.

The rocks underlying a large area west of Harrison Lake, and forming the islands within it, are mainly sub greenschist grade, Jura-Cretaceous, calcalkaline, intermediate to felsic, arc volcanic-sedimentary sequences (Authur, 1986; Monger, 1989; Journeay and Monger, 1994) assigned to the Harrison Lake Terrane (Monger, 1991) (Figure 4). The oldest rocks are Middle Triassic (Ladinian), Camp Cove Formation clastic sediments and intermediate volcanic flows (Authur *et al*., 1993). These represent only a minor component of the Mesozoic stratigraphy and are limited to a relatively isolated area along the western shore of Harrison Lake, due east from Echo Island. These early Mesozoic rocks are unconformably overlain by the Middle (Toarcian) and Late Jurassic intermediate to felsic volcanic and related sedimentary rocks of the Harrison Lake Group (Authur, 1986; Authur *et al.,* 1993). Plutons related to the Harrison Lake Group formed during several distinct episodes of magmatism over a 15 Ma period with U-Pb dates indicating magmatic events at 148-145, 158-153 and 162-160 Ma (Journeay and Friedman, 1993). Harrison Lake Group rocks are unconformably overlain by the late Early Cretaceous (Albian) Fire Lake Group or its regional correlative, the Gambier Group.

Harrison Lake and Fire Lake Group rocks are also dominant in the lower half of the west-facing slopes along the eastern shore of Harrison Lake. Lowes (1972) identified vestiges of sheared Buchia shells in metasedimentary rocks at the 460 metre elevation above the eastern shore of Harrison Lake, east of Cascade Bay, indicating Early Cretaceous strata to at least that level.

EAST HARRISON LAKE BELT

The EHLB is underlain by a northwest-trending belt of variably deformed and metamorphosed, greenschist to amphibolite grade, sedimentary, volcanic and lesser plutonic rocks (Figure 5). These rocks extend east from Harrison Lake for several tens of kilometres where they are bounded by younger, mid to Late Cretaceous (84-92 Ma) diorite to tonalite intrusions of the Coast Plutonic Complex. Within the belt there are two lithotectonic packages. The term package is applied as an informal designation referring to a number of lithologically distinctive rock types, which share a spatial and interpreted genetic association. In the EHLB a package of remnant abyssal oceanic (ophiolitic) rocks termed the Cogburn assemblage rests structurally above a succession of basinal, marine, clastic sedimentary rocks.

This twofold subdivision of the EHLB deviates from the threefold subdivision of units as established by Monger (1986) and adopted by all subsequent workers which recognized three lithologically distinctive belts of rocks (Figure 6b). From west to east these three units have been designated as the Slollicum, Cogburn and Settler packages (Monger, 1986) schist belts (Monger, 1989; Journeay and Monger, 1994) or terranes (Brown, *et al*., 2000; Brown and McCelland, 2000). These individual belts have been interpreted to be juxtaposed along west-verging thrust faults. These faults are marked by ultramafic rocks and are interpreted to become more deeply rooted towards the east (Figure 6b).

The revised tectonostratigraphic framework introduced here (Figure 6c) is a significant modification from that presented by previous workers. The first major modification is the inclusion of the upper mafic volcanic component of the previously defined Slollicum as part of the Cogburn ophiolitic assemblage. Reassignment of this unit is based on its 1) structural position in faulted contact above the clastic metasedimentary unit, 2) basaltic composition and local pillowed character (Lowes, 1972), and 3) MORB petrochemical signature (Bennett, 1989; Hettinga, 1989). These rocks are comparable to those that comprise the basaltic volcanic component of the Cogburn assemblage to the east (Figure 6b). This modification reestablishes a correlation between these rocks as suggested by earlier mappers (Lowes, 1972, Figure 6a; Gabities, 1985) based on lithological similarities between the two areas.

A second implication of the revised tectonic framework involves recognition of continuity of the metasedimentary clastic unit across the EHLB. Lithological similarity and a comparable structural setting show that the metasedimentary component of the previously designated Slollicum and Settler (Figure 6b) are part of the same stratigraphic unit (Figure 6c). Previous designation into two separate units has been founded largely on interpreting the belts of ultramafic rocks as delineating deeply-rooted fault zones.

Variations in the macroscopic character of these previously separated clastic metasedimentary units are not particularly evident where examined throughout the map area. Clastic sedimentary rocks along Silver and Hornet Creeks,

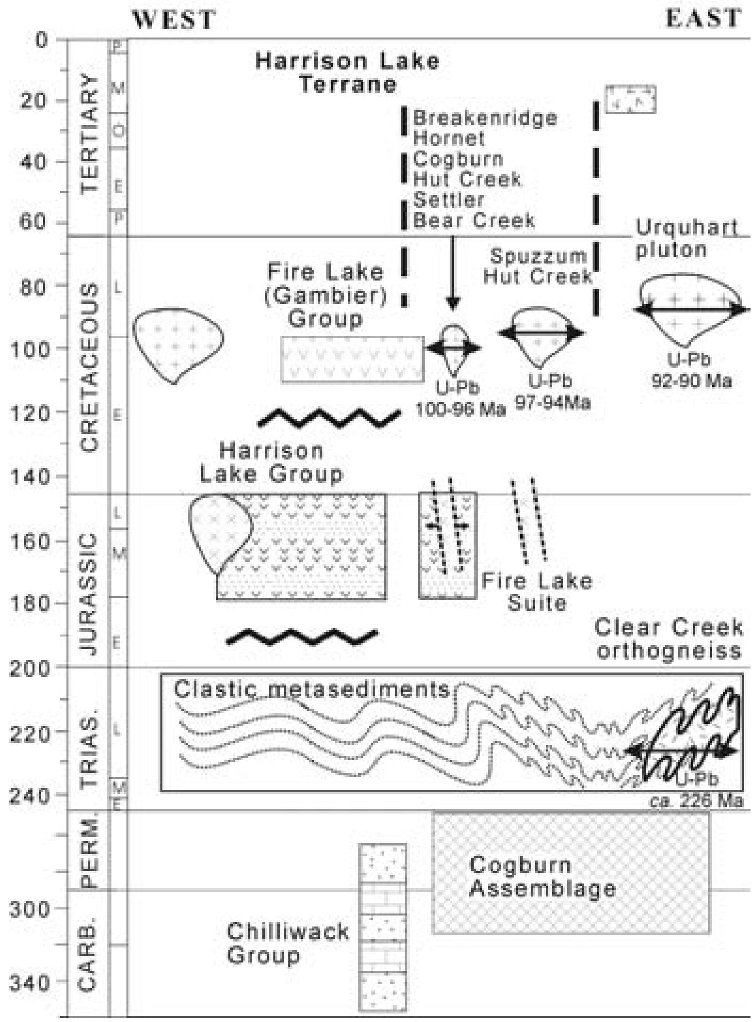

Figure 4. Time correlation chart for lithologies in the East Harrison Lake belt. Age constraints and unit designations are from sources discussed in the text.

the north-trending belt centered on the 6 km point of the Cogburn logging road, those to the north of The Old Settler Mountain and clastic rocks east of Giant Mascot are relatively consistent. These are variably metamorphosed and deformed clastic sedimentary rocks comprising interbedded mudstone, siltstone and fine to medium-grained volcanic wackes (Lowes, 1972). They are generally well bedded at the outcrop scale with individual beds from centimetres to metres in thickness. The most notable variation in the clastic metasedimentary unit is the higher degrees of metamorphism and increase in complexity in styles of ductile deformation towards the east. However, this is considered more likely the result of secondary processes, unrelated to its primary depositional environment.

The age of this unit is poorly constrained, at least in part, due to the metamorphism and recrystallization, which has destroyed any fossils. Two U-Pb monzonite ages of metasedimentary rocks near the southeast portion of the Urquhart Pluton at 90±1 and 89±1 Ma are consistent with metamorphism related to intrusion of the pluton, which is dated by U-Pb zircon methods at 92-91 Ma (Brown *et al.*, 2000).

Bennett (1989) reported a 146 Ma, U-Pb zircon age (attributed to Nick Walker, University of Texas at Austin) for a felsic rock described as being interbedded with the Slollicum metasedimentary unit northeast of Field Peak, roughly 220 meters above the Harrison Lake shore. This reported date has been often invoked to constrain the age of the previously defined Slollicum (Hettinga, 1989; Journeay and Friedman, 1993; Troust, 1999; Brown *et al*., 2000). Felsic volcanic rocks, however, were not recognized as a lithologic component of the clastic medisementary unit in the region previously designated as Slolicum, where examined to the north and east. These Late Jurassic felsic volcaniclastic rocks are largely constrained to the east Harrison Lake shore in the southern half of the map area. The transition from the intermediate to felsic volcaniclastic succession eastward into the calstic metasedimentary unit is interpreted involves a primary stratigraphic contact relationship in which the Late Jurassic rocks overlie the older clastic metasedimentary unit.

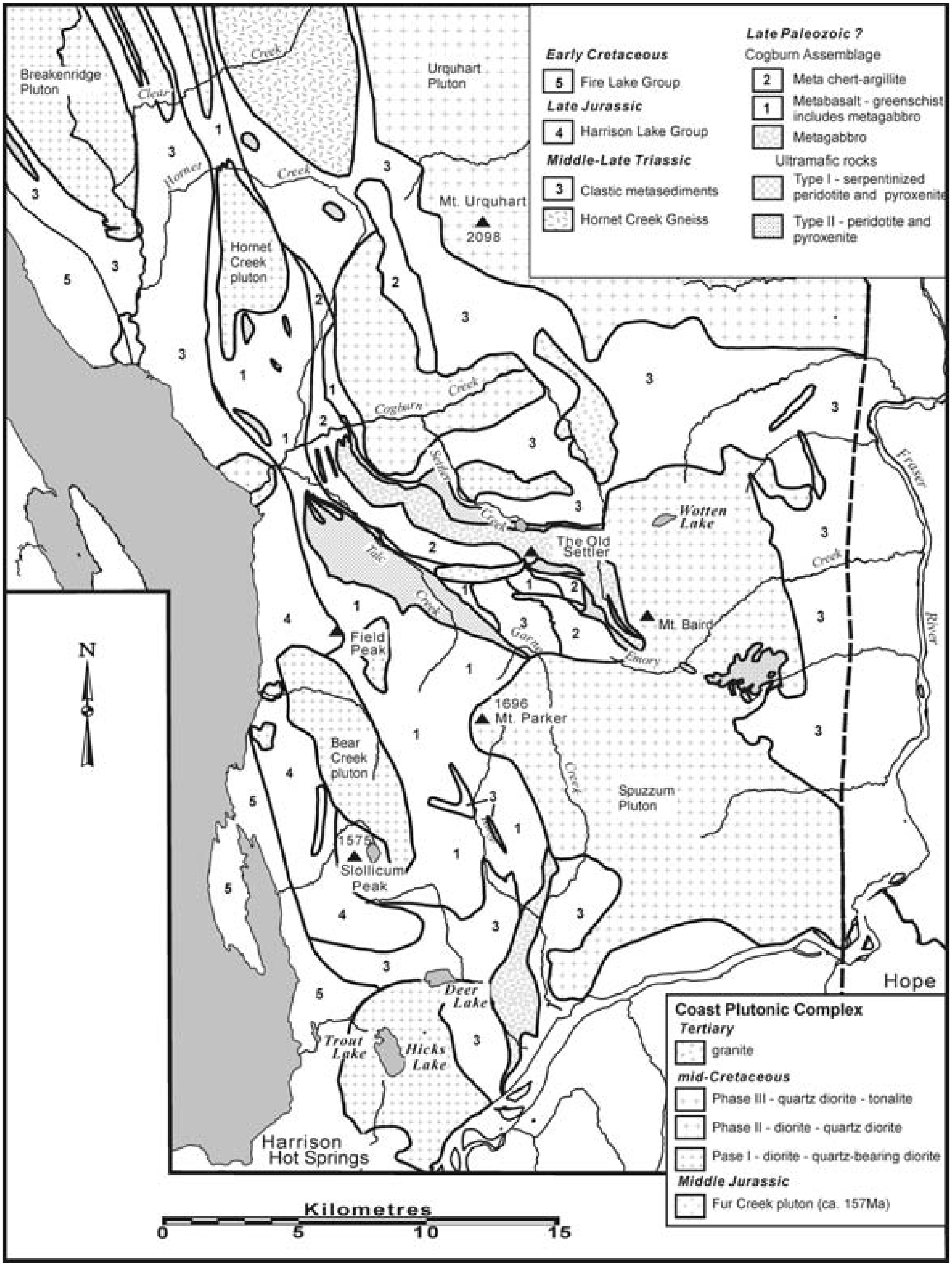

Figure 5. Geology of the East Harrison Lake area, based on preliminary compilation by Ash and Brown (in preparation).

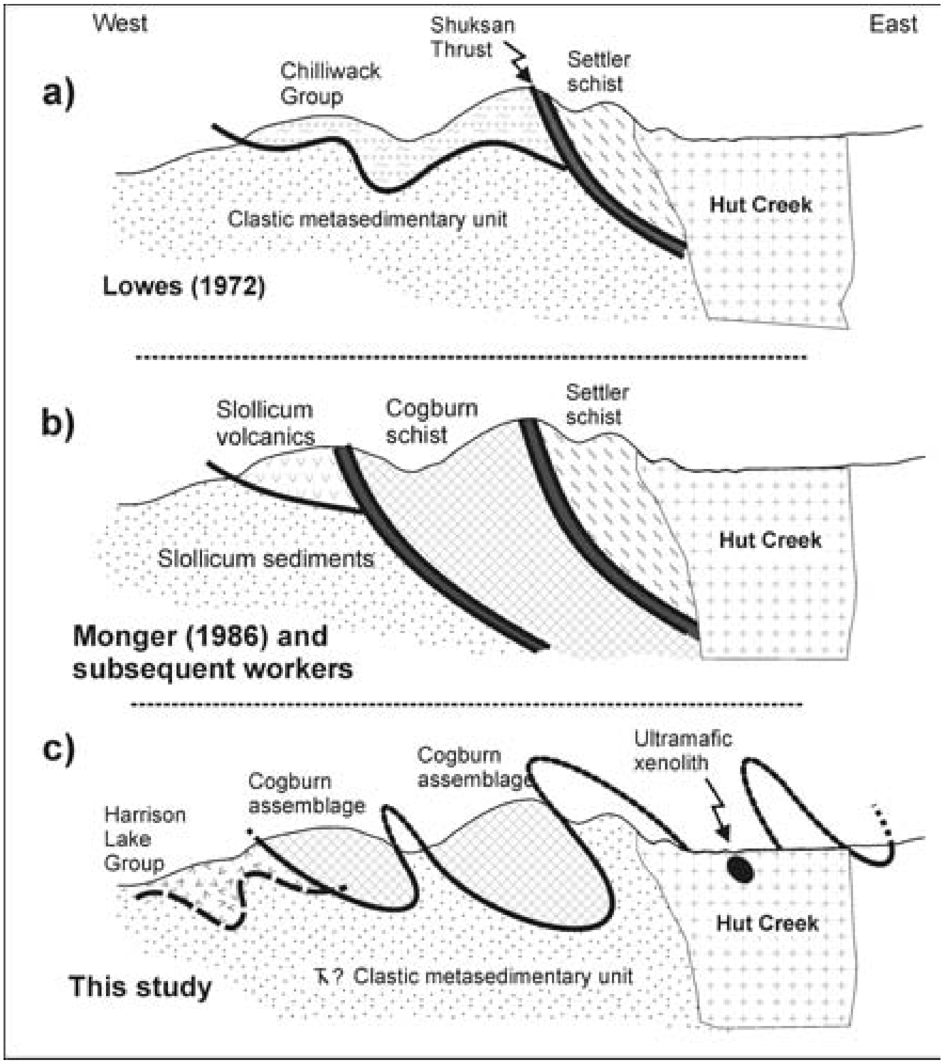

Figure 6. Schematic cross-sections through the central portion of the EHLB illustrating the evolving lithotectonic interpretations. a) Lowes (1972), b) Monger (1986) and subsequent workers, c) this study.

A relative age for the unit is suggested by its association with the Late Triassic Clear Creek orthogneiss, a banded to strongly foliated tonalite situated at the eastern end of the Hornet transect. This deformed pluton is dated by U-Pb zircon methods at ca. 226 Ma. (Monger, 1991). Primary contact relationships between the orthogneiss and clastic metasedimentary rocks are obscured by deformation and metamorphism. Similar styles of deformation suggesting comparable structural histories imply that the clastic metasedimentary rocks are at least as old as the intrusion.

These rocks are clearly typical of Late Triassic basinal sedimentary sequences that are a dominant component of Mesozoic volcanic arc terranes along the Cordillera. The Slollicum metasedimentary-volcanic unit was initially correlated by Monger (1986) with the little metamorphosed Late Triassic Cadwallader Group along regional trend to the north-northwest. Similarities with the Late Triassic Stuhini Group, with which the author is familiar, are particularly evident.

Supporting evidence for the lithotectonic framework presented is provided by regional variations in the geology along the trend of the EHLB. There is significant difference in the structural style of the terrane-bounding faults between the Cogburn and Hornet transects. Along the Hornet transect the terrane bounding structure forms a broad open upright fold (Figure 7), in which ophiolitic assemblage rocks comprise the hangingwall. At its central portion the Cogburn assemblage forms the core of a large-scale synform (Monger, 1986; Brown *et al*., 2000). In detail however, this regional folding produces a crenulation at the scale of several to tens of metres that causes infolding of contrasting units at terrane boundary contacts. The structural complexity of this relationship is demonstrated between the 14 and 15 kilometre point of the Hornet Creek logging road where steeply dipping, bedded clastic metasediments alternate over 5 to 10 m intervals with ribboned chert-argillite of the Cogburn assemblage.

To the south rocks along the Cogburn transect rocks are characterized by tight, west-verging isoclinal folds. The

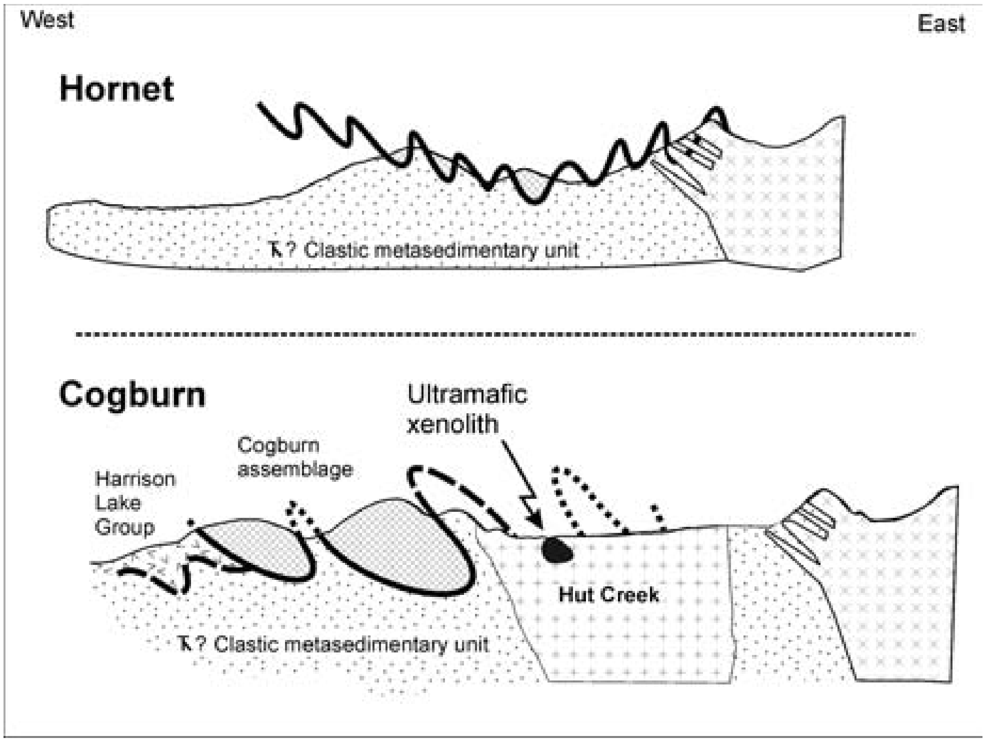

Figure 7. Schematic cross-section through the Hornet and Cogburn transects contrasting their lithotectonic character.

There are also regional lithological variations along the belt that involve a general reduction in the amount of ophiolitic assemblage rocks towards the north. Cogburn assemblage rocks become much more abundant southwards as they form the core of an arcuate, south to southeast plunging anticline. This relationship is consistent with the shallow southeasterly dip of the crust in this region as constrained by increased metamorphic grade of the rocks to the north (Journeay and Friedman 1993).

At the southern extent of the map sheet in lower Garnet Creek area, Lowes (1972) describes clastic sediments underlying volcanics in the core of an antiform indicating continuity of this structural style in that direction (Figure 5).

Isoclinal folding of the terrane bounding structure in the central Cogburn region is attributed to the structural heterogeneity introduced by the Hut Creek pluton during crustal shortening.

Most notable is the loss, or dissipation of the previously interpreted west-verging, terrane-bounding thrust faults, so well delineated by ultramafic belts south of Cogburn Creek. This variation is explained by the combined effects of the changing structural styles and reductions in the relative amount of ophiolitic rocks towards the north. In either case, a preexisting scenario in which the clastic metasedimentary unit is overlain by ophiolitic assemblage rocks that have been modified by subsequent inhomogeneous deformation accounts for the observed lithotectonic relationships.

COGBURN ASSEMBLAGE

The term ‘Cogburn assemblage’ is introduced to refer to an ophiolitic (oceanic crustal) package of variably deformed and metamorphosed chert-argillite, mafic volcanics, gabbros and ultramafic rocks. These units occur as tabular, folded and attenuated bodies that parallel the local and regional foliation. They are most prevalent within the central portion of the map sheet where they are thickened within the core of a large scale synform.

The term Cogburn Creek Group was initially introduced by Gabaites (1985) to include only the sedimentary and volcanic component of the currently defined Cogburn assemblage. The gabbroic and ultramafic units were interpreted as part of a separate and older package of rocks, representing the root zone and northern extension of the ‘Shuksan Thrust’ of the North Cascades in Washington State where similar rocks of the Yellow Aster Complex were considered as being possibly analogous (Lowes, 1972; Gabities, 1985).

Subsequently, Monger (1986) using, ‘Cogburn package’ or Monger (1989) and Journeay and Monger (1994) using ‘Cogburn schist’, unlike Gabites (1985), included the ultramafic rocks with the chert-argillite, and mafic volcanics. They retained the assignment of the metagabbro rocks to the Proterozoic-Paleozoic Yellow Aster Complex. This correlation was maintained in part because of a whole rock Rb-Sr isochron age of 3.2±2.3 Ga obtained by Gabities (1985) for these retrograde metamorphosed gabbroic rocks (Baird metadiorite of Gabities, 1985). This age is not considered reliable due to the sample's exceptionally large error combined with the generally low abundance of these large ion lithophile elements which are known to be easily remobalized. The combined effects of hydrothermal activity during its life as ocean crust as well as the effects of a complex tectonic history involving related metamorphic, magmatic and associated hydrothermal activity suggest ample opportunity for modification of the primary isotopic signature.

Both the mafic and ultramafic igneous bodies display features characterizing their tectonic mode of emplacement. Their are typically completely converted to retrograde schistose rocks while internally they are relatively massive and locally preserve remnant primary texture and mineralogy. A genetic association between these mafic and ultramafic rocks is supported by local variations in the gabbro that range from more mafic melanocratic phases to pyroxene dominant ultramafic phases suggesting the two are compositionally transitional.

Traditionally, this unit has been directly correlated with the Bridge River Terrane (Gabites, 1985; Monger, 1986; Journeay, 1990; Journeay and Monger, 1994). The Bridge River Terrane to the north is dominated by chert-argillite deposits with local remnants of ophiolitic assemblage rocks (Ash, 2000). Although now largely attenuated and converted to schists, the individual units display a well-defined ophiolitic tectonostratigraphy with no indication of internal tectonic disruption and mixing of lithologies to suggest melange development. The term assemblage is applied as outlined by Ash (2000) to help characterize the association of chert-argillite, basalts gabbros and ultramafic rocks as remnants of oceanic crust and distinct from the tectonically disrupted, chaotic chert-argillite dominant complexes.

Chert and Argillite

Chert and argillite beds of the Cogburn assemblage are best represented along the Cogburn transect. They are well exposed in near continuous sections between 6 and 7.5 kilometres along the Cogburn logging road and intermittently from roughly 1 to 5 kilometres along the North Fork logging road. The unit is relatively conspicuous due to the typically ribboned nature with fine grained, 0.5 to 1 cm, light-grey to buff-white chert layers alternating with medium to dark grey argillite that is largely converted to schists. Locally within the unit, either chert or argillite may dominate within intervals of several meters.

Further north at the eastern end of the Hornet transect the appearance of the chert – argillite unit is significantly different due to the amphibolite metamorphic grade. The unit alternates between intervals of black biotite schist (metamorphosed argillite) and fine to medium-grained polygonized quartz bands (recrystallized chert).

Metabasalt Unit

The metabasalt unit is light to dark green in colour and distinctively homogeneous in appearance. It occurs most often as a fine-grained, schistose rock consisting mainly of chlorite and could be adequately referred to as greenschist. It usually displays a well-developed 1-2 cm scale schistosity-parallel, planar cleavage. Locally the chlorite schist contains thin, discontinuous intervals of light-gray to off-white, thinly banded chert. White quartz veinlets and stringers are a commonly developed within and proximal to these cherty intervals. Several localities of less schistose mafic volcanic rock preserve relict pillow structures similar to those first noted by Lowes (1972, his Figure 16) on Slollicum Peak. During this study pillow structures were identified in greenschist-grade metabasalt at roughly the 6 kilometre point along the North Fork logging road. This unit is prominent within the central zone of the Cogburn assemblage, where it is intimately associated with the chert-argillite, metagabbroic and ultramafic units.

Barid Metagabbro

The gabbroic component of the Cogburn ophiolitic assemblage is best represented by a belt of mafic igneous rocks exposed along the eastern slopes of Talc Creek valley (Figure 4). Minor amounts of similar gabbro are also found associated with ultramafic and volcanic rocks in the high ground west of Talc Creek. It is a light grey-green, medium-grained equigranular rock with a weak to moderate foliation defined by alignment of secondary amphibole and chlorite. Near its tectonized contact margins the metagabbro is converted to medium-grained chlorite-sericite schist. Lowes (1972) initially designated the unit as metagabbro and interpreted it to be related to the adjacent belt of ultramafic rocks. He reported that plagioclase contained relict cores in the range of An^{65}, in contrast to the An^{37} content for albitic rims attributed to regional metamorphism. In addition, he recognized relict clinopyroxene cores in hornblende.

The large northwest trending body was later termed the 'Baird metadiorite' by Gabities (1985) with geographic reference to Mount Baird, which is just beyond the eastern limit of the unit and separated from it by a sliver of ultramafic rocks. In light of the relict composition of this mafic igneous rock as gabbro, it is referred to as the 'Baird metagabbro'. This rock name also adequately distinguishes between this older unit and the younger mid-Cretaceous intrusions which are in part dioritic.

Ultramafic Rocks

Ultramafic rocks are recognized along the length of the EHLB. The largest and most continuous exposures form two prominent ridges along opposite sides of the northwest-trending segment of Talc Creek in the central portion of the map area. Starting near Cogburn Creek these ultramafic belts continue to the southeast to where they become disrupted by the Spuzzum pluton near Mount Baird. North of Cogburn Creek exposures of ultramafic rocks are discontinuous and sporadic. These cumulate ultramafic rocks range from dunite to peridotite and pyroxenite. The belt of ultramafic rocks to the southeast appears to be the most olivine rich, consisting mainly of dunite with local intervals of chromite-bearing dunite. Though locally dunitic, the belt east of Talc Creek shows more compositional variation with peridotite and pyroxenite more prevalent. In the peridotites and pyroxenites both ortho and clinopyroxene have been identified as relict primary phases (Lowes, 1972; Gabities, 1985; Pinsent, this volume). Massive dunite is dark-green and weathers a characteristic dun brown. Where serpentinized, ultramafic rocks display characteristic light and dark grey mottled surface with a distinctive purple tinge. Orange rusty-brown exposures typify talc-carbonate altered zones.

On the basis of level of preservation of primary texture and mineralogy, as well as spatial association with younger mid-Cretaceous quartz dioritic intrusions, two distinctive styles of ultramafic rocks are identified. In the first and most prominent type, ultramafic rocks occur as attenuated tabular bodies and lenses that parallel the local foliation fabric. These are consistently found in association with all or some of the ophiolitic assemblage rocks. They are everywhere variably serpentinized (mainly antigorite, Troost, 1999). Intense serpentinization is often associated with talc and local carbonate alteration proximal to tectonic contacts and later crosscutting faults. Relict primary textures and mineralogies show only moderate preservation locally and it is often restricted to the core of these ultramafic bodies. No Cu or Ni sulphides have been found in these ultramafic rocks.

In contrast to the attenuated and altered character of the ultramafic rocks described above, the second type of ultramafic rocks are usually devoid of penetrative fabrics and maintain exceptionally well preserved primary igneous mineralogy and textures. These occur, almost exclusively, as xenoliths or inclusions within the younger mid-Cretaceous Coast Plutonic Complex diorite and quartz diorite intrusions. The largest of these ultramafic xenoliths occurs along the east side of the Spuzzum pluton and is host to Cu-Ni sulpide mineralization at the Giant Mascot mine (Horwood, 1930, Aho, 1956, Pinsent, this volume). The body covers an area of roughly four kilometres. It is very irregular in shape, with lobate tongues of the ultramafics and the quartz diorite protruding into one another. Smaller inclusions tend be subrounded in outline. Irrespective of shape all the ultramafic inclusions display distinctive, black, coarse-grained hornblende-rich metasomatic reaction rims at the intrusive contacts.

The largest exposures of this type are ultramafic rocks that host Cu-Ni (PGE) mineralization at the Giant Mascot mine (Pinsent, this volume). This ultramafic body consists of cumulate pyroxenites and lesser peridotites and is contained largely within the Spuzzum pluton.

Ultramafic xenoliths are also present in the Hut Creek pluton along its western margin where it intrudes the northern extent of the prominent eastern ultramafic belt where it extends north across Cogburn and along Hut Creek Valley. Examples of these ultramafic inclusions are present along the Cogburn logging road and in the high ground near the end of the North Fork logging road. These ultramafic bodies range in size from several centimetres to hundreds of metres. Like the larger ultramafic body at Giant Mascot, these are usually pyroxene-rich ultramafic rocks, often containing interstitial sulphides with elevated concentrations of Cu and Ni. Significantly, the ultramafic xenoliths associated with the younger mid-Cretaceous plutons always contained some sulphides.

The marked contrast in style of preservation between the two types of ultramafic rocks led previous workers to suggest that both types were genetically distinct. Most previous workers interpreted the well-preserved ultramafic rocks as a phase the Spuzzum pluton (Aho, 1954; McLeod, 1975; Vinning, 1977; Gabities, 1985) or as distinct ultramafic intusions, younger than the Spuzzum pluton. Lowes, (1972) interpreted the ultramafic rocks at the Giant Mascot mine to be part of a younger, composite zoned intrusion including peridotite, pyroxenite, hornblendite and diorite.

The relative age of these ultramafic inclusions can be constrained by intrusive contact relationships in the area of the Giant Mascot mine. In this area the Spuzzum pluton displays a characteristic hornblende-rich, banded margin in contact with metasomatically altered country rock. These features are developed along the margin of the quartz-diorite where in contact with both the clastic metasedimentary unit and the ultramafic body hosting the Giant Mascot mine. In addition, small plugs of diorite intrude this ultramafic body and show identical contact features to those developed around its external margin. These contact relationships indicates that the Spuzzum pluton is younger than both the ultramafic and adjacent sedimentary rocks. This relationship eliminates the possibility that the ultramafic rocks are younger than the mid-Cretaceous intrusions as suggested by Lowes (1972). One could still possibly argue that the ultramafic rocks are earlier phases of the pluton. However, the observed contact reaction argues against a co-genetic relationship between the ultramafic rocks and the Spuzzum pluton. Additionally, ultramafic inclusions of this type do not occur elsewhere in the vast expanse of the Cosat Plutonic Complex, except locally in the Harrison Lake area where they interact with older ultramafic rocks. This isolated occurrence of ultramafic rocks suggests that they are not a primary phase of the mid-Cretaceos plutons.

Interestingly, Lowes (1972) also interpreted a narrow zone of ultramafic rocks along the western side of the Spuzzum pluton just east of Mount Baird as being genitically similar to those at Giant Mascot. This zone occurs right at the southeastern extent of the northern ultramafic belt where terminated by the Spuzzum pluton. In light of the relative constraints on the age of ultramafic rocks at the Giant Mascot, and the isolated position of the zone along the contact between the ultramafic belt and the Spuzzum intrusion, it is reasonable to infer that this zone resulted from interaction of the two. Additionally, ultramafic rocks are present in the Emory Creek Valley midway between the Giant Mascot mine and the northwest trending belt of Cogburn assemblage rocks to the northwest. This relationship lends further support to disruption of a once contiguous belt of ultramafic rocks that has been engulfed by a younger intrusion with local preservation of older ultramafic rocks due to the high melting point of the primary silicate minerals. The texture of the ultramafic rocks have survived because of being sheltered by the plutonic competent mass from post intrusion alteration and tectonism.

INTRUSIVE ROCKS

The bulk of intrusive rocks recognized in the EHLB are mainly mid-Cretaceous diorites to tonalites of the Coast Plutonic Complex (Gabities, 1985; Monger, 1989; Parrish and Monger, 1992; Brown and Walker, 1993; Journeay and Friedman, 1993; Brown and McClelland, 2000; Brown *et al*, 2000). Several younger tabular feldspar porphyric intrusions of interpreted Miocene age and a number of older deformed felsic dikes of possible Late Jurassic age are also present.

Mid-Cretaceous intrusions in the EHLB appear to be part of a single evolving suite of intrusion that formed between 103 and 90 Ma. These intrusions show a progressive variation in age, scale, composition, grain size and contact margin relationships from west to east across the belt. Plutons become progressively younger and larger, with an accompanying increase in grain size, quartz content and an increase in the width and complexity of their contact aureoles. Three identifiable phases of this evolving suite are present within the EHLB. A fourth and younger phase is present to the northeast beyond the EHLB map area.

Phase I

The most westerly phase includes a number of smaller, isolated intrusions with their long axis paralleling the dominant structural grain. These are medium-grained diorites and quartz-bearing diorites that range in age from 103 to 96 Ma. Lowes (1972) recognized that the westerly belt of linear plutons and their smaller related stocks were compositionally similar to the larger easterly mid-Cretaceous intrusions. He also recognized that the westerly belt of intrusions were distinctive, being in general finer-grained, lacking foliation fabrics, and displaying relatively narrow static hornfels zones, unlike the broader and complex migmatized zones characteristic of the larger plutons to the east.

Intrusions belonging to the phase include from north to south; the Hornet Creek (at 98.3±2 Ma, Brown and McClellan, 2000), Cogburn (at 97±1 Ma, Parrish and Monger, 1992) and Settler (at 96.7±1Ma, Brown and McClellan, 2000) plutons. The southern portion of Breakenridge plutonic complex extends into the northwestern corner of the EHLB. This intrusion has been designated as a plutonic complex (Journeay and Friedman, 1993) to include a number of larger sheeted bodies that are separated from the main intrusive body. This complex also occurs along the western margin of the belt and its long axis parallels the regional structural grain. It is also of similar magmatic age as the Phase I plutons (at 103.8±0.5 and 96±0.5 Ma, Brown and McClellan, 2000), being the oldest dated among the mid-Cretaceous suite.

The unnamed, northwest-trending body in the south central portion of the map area that is underlain largely by Bear Creek is informally designated the 'Bear Creek pluton'. It is also tentatively included with this suite due to its comparable size, composition, texture, contact margin features and linear nature which parallels the regional structural grain. The Bear Creek pluton has been previously assigned a Tertiary age on the basis of a hornblende K-Ar age 53±1.7 Ma (Monger, 1989). Notably, the physically similar Phase I Hornet Creek pluton to the north, was also designated as Tertiary due to an Eocene hornblende K-Ar age (Monger, 1989). Subsequent U-Pb zircon dating established that the Hornet pluton is mid-Cretaceous. This Tertiary K-Ar isotopic age date is considered unreliable due to potential and likelihood of re-setting of K-Ar systematics of hornblende during younger magmatic or tectonic activity. U-Pb dating is required to verify this interpretation.

The more rounded intrusive body in the southwest corner of the map area underlying Hicks Lake, informally referred to as the 'Hicks Lake pluton', has been previously interpreted as Miocene on the basis of a 24.6±0.8 Ma hornblende, K-Ar age (Richards and White, 1970). This plutons is also of similar composition and texture with comparable contact relationships to plutons characteristic of the Phase I plutons (Lowes, 1972) described above. Its shape however is not characteristic of the Phase I plutons and may be more texturally akin to the Chillawick to the south to which has been previously assigned (J. Monger, personal communication, 2001). An older, mid-Cretaceous age may be more consistent with the interpreted genetic relationship between the intrusion and a number of mesothermal gold-quartz veins at the Harrison Gold mineral occurrence (MINFILE No. 92H092) on Bear Mountain several kilometres northeast of Harrison Hot Springs. U-Pb dating is obviously required to resolve this uncertainty.

Phase II

The second or intermediate phase of the mid-Cretaceous suite in the EHLB includes the Spuzzum (at 96.3±0.5 Ma, Brown, *et al.,* 2000) and Hut Creek plutons (at 94.6±0.5 Ma, Brown, *et al.,* 2000). These are somewhat larger than, and situated mainly to the east of, the phase I plutons. They are medium to coarse-grained and range from diorites to quartz diorites. This plutonic phase of the mid-Cretaceous suite is economically most significant as these are the only plutons to host Cu-Ni mineralized ultramafic inclusions.

Metasomatic contact margins accompanied by ductilely deformed and often well-banded marginal zones, termed 'layered migmatic gneiss zones' by Lowes (1972) are a characteristic feature of the phase two plutons. The width of these metasomatic intrusive contact aureoles is generally on the order of several tens of metres, but may be locally greater than 100 metres. The transition from host rock into the intrusion involves several 10s of metres of migmatized banded country rock, often displaying contorted, complex folded patterns. This is followed inward by a brecciated zone in which black medium to coarse-grained to locally pegmatitic hornblendite forms the matrix to subrounded to angular clasts of both migmatized country rock and host intrusion. Adjacent to this brecciated zone the intrusion is typically well banded, over distances of several metres with alternating dark mafic and light felsic bands from 1 to 2 cm thick and generally steeply dipping. The banding quickly dissipates and gives way to a relatively massive, equigranular rock that is more typical of the intrusions away from the migimatized contact margins. Injection of black hornblendite dikes into both the intrusive diorite and adjoining migmatized host rocks is a common feature that may extend several hundred metres beyond the contact.

Phase III

Underlying most of the northeast portion of the EHLB is the southeastern part of the Urquhart pluton (at 91.3±0.3 and 91.2±0.3, Brown and McCelland, 2000). It consists mainly of coarse-grained quartz-diorite and tonalites and displays a pervasive magmatic foliation fabric. Contact relationships between the intrusion and country rocks were examined at eastern end of both the Hornet and Cogburn transects.

Within 1 to 2 kilometres of the of the pluton contact, medium-grained to more often pegmatitic, white, tonalite dikes and irregular bodies are a minor component. Towards the pluton both the frequency and thickness of these dikes increases. Within several 100 metres or more of the pluton these intrusions form sheeted zones with alternating intrusive sills and screen of country rock up to 10 metres in thickness that dip at moderate to shallow angles towards the core of the pluton. Beyond this sheeted zone the pluton becomes mainly continuous but large concordant country rock screens can occur for 2 to 3 kilometres beyond the pluton margin (Brown and McCelland, 2000, data repository note).

Phase IV

This spatial variation in pluton character also extends regionally to the northeast, beyond the current map area. To the immediate northeast of the Urquhart pluton is the younger (84-90 Ma, Brown and McClellan, 2000), larger and mainly coarse-grained, tonalitic Scuzzy Pluton. Brown and McClellan (2000) describe the margin of the Scuzzy pluton as a, 'spectacular sheeted sill complex'. These marginal sheeted zones of the Scuzzy pluton are up to three kilometres wide, with sills from tens of centimetres to over a 100 meters thick separated by screens of country rock with of similar varied thickness. These contact margin features are obviously akin to that of the somewhat smaller and slightly younger Phase III Urquhart pluton.

CONCLUSIONS

The geology of the East Harrison Lake belt is interpreted to include only two, and not three, major lithotectonic belts of rocks. A lower clastic metasedimetary sequence of interpreted middle to Late Triassic age is structurally overlain by an ophiolitic assemblage of metamorphosed chert-argillite, mafic volcanics, gabbros and ultramafic rocks referred to as the 'Cogburn assemblage'. This proposed twofold subdivision provides a structural framework that allows for continuity of lithologically similar rock types across the EHLB. It distinguishes two lithological distinctive rock packages that can be correlated with two contrasting paleotectonic environments of formation including both basinal-arc and abyssal ocean settings.

The ultramafic rocks hosting the Giant Mascot deposit are older than the mid-Cretaceous quartz-bearing diorites and quartz diorites that surround and locally intrude them. The Spuzzum pluton cross cuts the ultramafic-clastic metasediment contact with similar metasomatic contact aureoles affecting both.

Cu-Ni (PGE) mineralization is consistently found only in ultramafic rocks of the Cogburn assemblage where they occur as xenoliths within the mid-Cretaceous Spuzzum intrusions. Where not proximal to the younger intrusion, ultramafic rocks are devoid of Cu-Ni sulphide mineralization. The reasons for this spatial relationship between intrusion and ultramafic rocks remain uncertain.

This relationship lends itself to the possibility that Giant Mascot ore is not primary but related to metasomatic interaction where the older ultramafic is intruded by the younger felsic plutons.

ACKNOWLEDGMENTS

Enthusiastic and capable field assistance was provided by Mary Dubravcic during a portion of the field program. Ned Brown, (Western Washington University) and Jim Monger (GSC, Vancouver) are graciously acknowledged for enlightened discussions and sharing of their ideas and data.

Ongoing discussions, following field interaction with Robert Pinsent, Jacque Houle (BC Ministry of Energy and Mines), George Nicholson (Nicholson and Associates Natural Resources Development Inc.), Robert Krause (Starfield Resources Inc.), Murray McClaren (Crockite Resources Ltd.), Robert Macdonald and Craig Payne (Crest Geological Consultants Ltd.), Jazi Nikhanj and Mike MacLeod (Leader Mining International Inc.) are continually informative and greatly appreciated.

The paper has been improved by edits from Dave Lefebure and Brian Grant. Michael Green deserves many thanks for producing the illustrations.

Without the assistance, and often tolerance for 'that rock guy' by the staff of Lakeside Pacific Forest Products Ltd. in allowing ready access to gated logging roads, the scope of this work would not have been possible.

REFERENCES

Aho, A.E. (1954): Geology and genesis of ultrabasic nickel-copper-pyrrhotite deposits at the Pacific Nickel property, southwestern British Columbia; unpublished Ph.D. thesis, *The University of California*, Berkeley, California.

Aho, A.E. (1956): Geology and genesis of ultrabasic nickel-copper-pyrrhotite deposits at the Pacific Nickel property, southwestern British Columbia; *Economic Geology*, Volume 51, pages 444-481.

Ash, C.H. (2001): Ophiolite related gold quartz veins in the North American Cordillera; *B.C. Ministry of Energy and Mines*, Bulletin 108, 140 pages.

Ash, C.H. And Brown, E.H. (in preparation): Geology of the East Harrison Lake belt, Southwest British Columbia; *BC Ministry of Energy and Mines*, Open File, 1:50 000 map.

Authur, A. (1986): Stratigraphy along the west side of Harrison Lake, southwestern British Columbia; *in* Current Research, Part B, *Geological Survey of Canada*, Paper 86-1B, pages 715-720.

Authur, A.J., Smith, P.L., Monger, J.W.H, Tipper, H.W. (1993): Mesozoic stratigraphy and Jurassic paleontology west of Harrison Lake, southwestern British Columbia, *Geological Survey of Canada*, Bulletin 441, 62 pages.

Bartholomew, P.R. (1979): Geology and metamorphism of the Yale Creek area, British Columbia; unpublished M.Sc. thesis, *The University of British Columbia*, 105 pages.

Brown, E.H., Talbot, J.L., McClelland, W.C., Feltman, J.A., Lapen, T.J., Bennett, J.D., Hettinga, M.A., Troost, M.L., Alvarez, K.M. and Calvert, A.T. (2000): Interplay of plutonism and regional deformation in an obliquely convergent arc, southern Coast Belt, British Columbia; *Tectonics*, Volume 19, No. 3, pages 493-511.

Brown, E.H. and McClelland, W.C. (2000): Pluton emplacement by sheeting and vertical ballooning in part of the southeast Coast Plutonic Complex, British Columbia; *Geological Society of America Bulletin*, Volume 112, No. 5, pages 708-719.

Bennett, J.D. (1989): Timing and conditions of deformation and metamorphism of the structural packages east of Harrison Lake, British Columbia; unpublished M.Sc. thesis, *The University of Western Washington*, 87 pages.

Cairnes, C.E. (1924): Nickeliferous mineral deposits, Emory Creek, Yale Mining Division, British Columbia; *Geological Survey of Canada*, Summary Report, part A, pages 100-106.

Cairnes (1944): Geology of Hope Area, British Columbia; *Geological Survey of Canada*, Map 737A.

Crickmay, C.H. (1930): The structural connection between the Coast Range of British Columbia and Cascade Range of Washington; *Geological Magazine*, Volume 67, pages 482-491.

Daly, R.A (1912): Geology of the North American Cordillera at the forty-ninth parallel; *Geological Survey of Canada*, Memoir 38.

Feltman, J.A. (1997): Structure, metamorphism and geochronology along the southern margin of the Breakenridge orthogneiss, Coast Range, Southern British Columbia; unpublished M.Sc. thesis, *Western Washington University*, Bellingham, 128 pages.

Gabites, J.E. (1985): Geology and geochronometry of the Cogburn Creek-Settler Creek area, northeast of Harrison Lake, British Columbia; unpublished M.Sc. thesis, *The University of British Columbia*, 153 pages.

Hettinga, M.A. (1989): Metamorphic petrology, geothermobarometry and structural analysis of a portion of the area east of Harrison Lake, British Columbia; unpublished M.Sc. thesis, *Western Washington University*, Bellingham, 85 pages.

Horwood, H.C. (1936): Geology and mineral deposits at the mine of B.C. Nickel Mines Ltd., Yale Mining District; *Geological Survey of Canada*, Memoir 190, 15 pages.

Houle, J. (in preparation): Southwest Region; in Exploration and Mining in British Columbia 2001, *B.C. Ministry of Energy and Mines.*

Journeay, J.M. (1990): A progress report on the structural and tectonic framework of the southern Coast Belt, British Columbia; *in* Current Research, Part E, *Geological Survey of Canada*, Paper 90-1E, pages 183-195.

Journeay, J.M. and Friedman, R.M. (1993): The Coast Belt thrust system: evidence of Late Cretaceous shortening in southwest British Columbia; *Tectonics*, Volume 12, No. 3, pages 756-775.

Journeay, J.M. and Monger, J.W.H. (1994): Guide to the geology and tectonic evolution of the southern Coast Mountains; *Geological Survey of Canada*, Open File 2490, 77 pages.

King, P.N. (1972): Microvariation of nickel in Pyrrhotite and Pentlandite, Climax ore zone, Giant Mascot Mine, British Columbia; unpublished B.Sc. thesis, *The University of British Columbia*.

Lett, R. and Jackman, W. (this volume): PGE Stream Sediment Geochemistry in British Columbia; *in* Geological Fieldwork, *BC Ministry of Energy and Mines.*

Lowes, B.E. (1967): Chilliwack Group, Harrison Lake area; *Geological Survey of Canada*, Paper 67-1, part A, pages 74-75.

Lowes, B.E. (1968): Chilliwack Group, Harrison Lake area; *Geological Survey of Canada*, Paper 68-1, part A, pages 74-75.

Lowes, B.E. (1972): Metamorphic petrology and structural geology of the area east of Harrison Lake, British Columbia; unpublished Ph.D. thesis, *The University of Washington*, Seattle, 162 pages.

McLeod, J.A. (1975): The Giant Mascot ultramafite and its related ores, British Columbia; unpublished M.Sc. thesis, *The University of British Columbia*, 123 pages.

Monger, J.W.H. (1970): Hope map area, west half, British Columbia; Geological Association of Canada, Paper 69-47, 75 pages.

Monger, J.W.H. (1986): Geology between Harrison Lake and Fraser River, Hope map area, southwestern British Columbia; *in* Current Research, Part B, *Geological Survey of Canada*, Paper 86-1B, pages 699-706.

Monger, J.W.H. (1989): Geology, Hope, British Columbia; *Geological Survey of Canada*, map 41-1989.

Monger, J.W.H. (1991): Correlation of Settler Schists with Darrington phyllite and Shuksan greenschists and its tectonic implications, Coast and Cascade mountains, British Columbia and Washington; *Canadian Journal of Earth Sciences*, Volume 28, pages 447-458.

Muir, J.E. (1971): A study of the petrology and ore genesis of the Giant Nickel 4600 orebody, Hope, British Columbia; unpublished M.Sc. thesis, *The University of Toronto*.

Parrish, R.R. and Monger, J.W.H. (1992): New U-Pb dates from southwestern British Columbia; in Radiogenic Age and Isotopic Studies, Report 5; Geological Survey of Canada, Paper 91-2, pages 87-108.

Pigage, L.C. (1973): Metamorphism southwest of Yale, British Columbia; unpublished M.Sc. thesis, *The University of British Columbia*, 95 pages.

Pinsent, R. (this volume): Ni-Cu-PGE Potential of the Giant Mascot and Cogburn Ultramafic-Mafic bodies, Harrison-Hope area, Southwestern British Columbia (092H)

Read, P. (1960): The geology of the Fraser Valley between Hope and Emory Creek, British Columbia; unpublished M.Sc. thesis, *The University of British Columbia*, 154 pages.

Reamsbottom, S.B. (1971): The geology of the Mt. Breakenridge area, Harrison Lake, British Columbia; unpublished M.Sc. thesis, *The University of British Columbia*, 143 pages plus maps.

Reamsbottom, S.B. (1974): Geology and metamorphism of the Mt. Breakenridge area, Harrison Lake, British Columbia; unpublished Ph.D. thesis, *The University of British Columbia*.

Richards, T.A. (1971): Plutonic rocks between Hope, British Columbia, and the 49th parallel; unpublished Ph.D. thesis, *The University of British Columbia*, 178 pages.

Troost, M.L. (1999): Structure and metamorphism of the Talc Creek area, Harrison Lake, British Columbia; unpublished

M.Sc. Thesis, *The University of Western Washington*, 144 pages.

van der Heyden, P., (1992): A Middle Jurassic to Early Tertiary Andean-Sierran arc model for the Coast Belt of British Columbia; *Tectonics*, Volume 11, pages 82-97.

Vinning, M.R. (1977): The Spuzzum pluton northwest of Hope, British Columbia; unpublished M.Sc. thesis, *The University of British Columbia*, 103 pages.

Ni-Cu-PGE Potential of the Giant Mascot and Cogburn Ultramafic-Mafic Bodies, Harrison-Hope Area, Southwestern British Columbia (092H)

By Robert H. Pinsent

KEYWORDS: *Economic Geology, Cogburn Creek, Cogburn Schist, Settler Schist, Spuzzum pluton, Hut Creek pluton, Giant Mascot mine, nickel-copper showings, ultramafic cumulate, pyroxenite, peridotite, mafic cumulate, gabbro, diorite, pyrrhotite, pentlandite, chalcopyrite, nickel, copper, platinum, palladium, platinum-group elements.*

INTRODUCTION

The Giant Mascot mine, near Hope, British Columbia, was the only nickel mine in the province. It produced approximately 4 191 035 tonnes of ore averaging 0.77% Ni and 0.34% Cu, and shipped approximately 3.23 tonnes of nickel and 1.43 tonnes of copper between 1958 and 1974 (Tindall, 1987). The mine is rumoured to have produced small amounts of platinum and palladium; however, there are no records of their production or presence in the concentrate. The ore came from shoots in an ultramafic body that are acknowledged to be magmatic in origin. However, there is considerable uncertainty regarding their precise origin and age of emplacement and of the relationship of the mineralized body to other ultramafic bodies in the area, and to the nearby Spuzzum pluton.

In 2001, the British Columbia Ministry of Energy and Mines conducted mineral deposit studies, and mapping (Ash, 2002) and stream geochemical programs (Lett and Jackaman, 2002) to evaluate the potential for platinum-group elements in the ultramafic rocks in the Cogburn Creek area, east of Harrison Lake. This study compares and contrasts the geology and mineralization found at Giant Mascot with that in the Cogburn Creek area; provides geochemical data; discusses the distribution of platinum-group elements and reviews the exploration potential of the ultramafic rocks.

GEOLOGICAL SETTING

The Cogburn Creek area, located east of Harrison Lake (Figure 1), is underlain by highly deformed, and locally highly metamorphosed, meta-volcanic, meta-sedimentary and plutonic rocks. The area has attracted a considerable amount of study over the past thirty years and several theses have been written. Some, by Aho (1954), Muir (1971), McLeod (1975) and Vining (1977) specifically relate to the geology of the Giant Mascot deposit, while others, by Read (1960), Richards (1971), Lowes (1972), Gabites (1985), Bennett (1989), Hettinga (1989) and Troost (1999) are more concerned with the tectonic and metamorphic history of the belt. Brown and Walker (1993) and Journeay and Monger (1994) discuss various aspects of this latter work and Ash (2002) provides a review of current thinking on the tectonic history of the area.

Monger and Journeay (1994) subdivide the stratabound rocks east of Harrison Lake into three units and provide the following interpretation of the tectonic relationships. The westernmost unit, Unit 1 (MSL, Slollicum Schist) is composed of greenschist facies volcanic and sedimentary strata of probable Triassic to Cretaceous age that the authors assign to the Harrison Terrane, which is stratigraphically linked to Wrangellia Terrane west of Harrison Lake. The central package, Unit 2 (PMCS, Cogburn Schist) consists of Paleozoic to Mesozoic amphibolites, meta-cherts and meta-pelites that are similar, and probably equivalent to rocks of the Hozameen and/or Bridge River Group in the Bridge River Terrane (Journeay and Monger, 1994). Cogburn Schist is intimately associated with two plutonic units, Unit 3 (Pmu, ultramafic rocks) and Unit 4 (PPY, Yellow Aster Complex meta-diorite and meta-gabbro (a.k.a. Baird meta-diorite, Gabites (1985))). The latter units appear to be part of the same rock assemblage as the Cogburn Schist. The easternmost unit, Unit 5 (MS, Settler Schist) is composed of high-grade meta-sedimentary rock of possible Cretaceous or older age that Monger and Journeay (1994) assign to the Cayoosh Assemblage; a sedimentary unit that overlies the Bridge River Terrane.

The layered units are cut by an older, mid- to Late Cretaceous (96 - 104 Ma), foliated, diorite pluton (Unit 6, Spuzzum Pluton) and a younger suite of Tertiary age, post-orogenic quartz diorite to granodiorite intrusions (Unit 7, Scuzzy Pluton, Chilliwack Batholith).

According to Journeay and Monger (1994) the central, Cogburn Schist package (Units 2, 3 and 4) is fault bounded to the northeast and southwest and is tectonically juxtaposed against Units 1 and 5 by steep, regional-scale northeasterly dipping, high-angle reverse faults. However, recent work by Ash (2002, this volume) provides a different structural interpretation. He suggests that the belt includes two tectonostratigraphic packages, an upper package consisting of Unit 2 (PMCS, Cogburn Schist), Unit 3 (Pmu, ultramafic rocks) and Unit 4 (PPY, Yellow Aster Complex) and a lower package comprised of Unit 1 (SML, Slollicum Schist) and Unit 5 (MS, Settler Schist). The rocks are highly deformed and the former is tightly infolded with the latter.

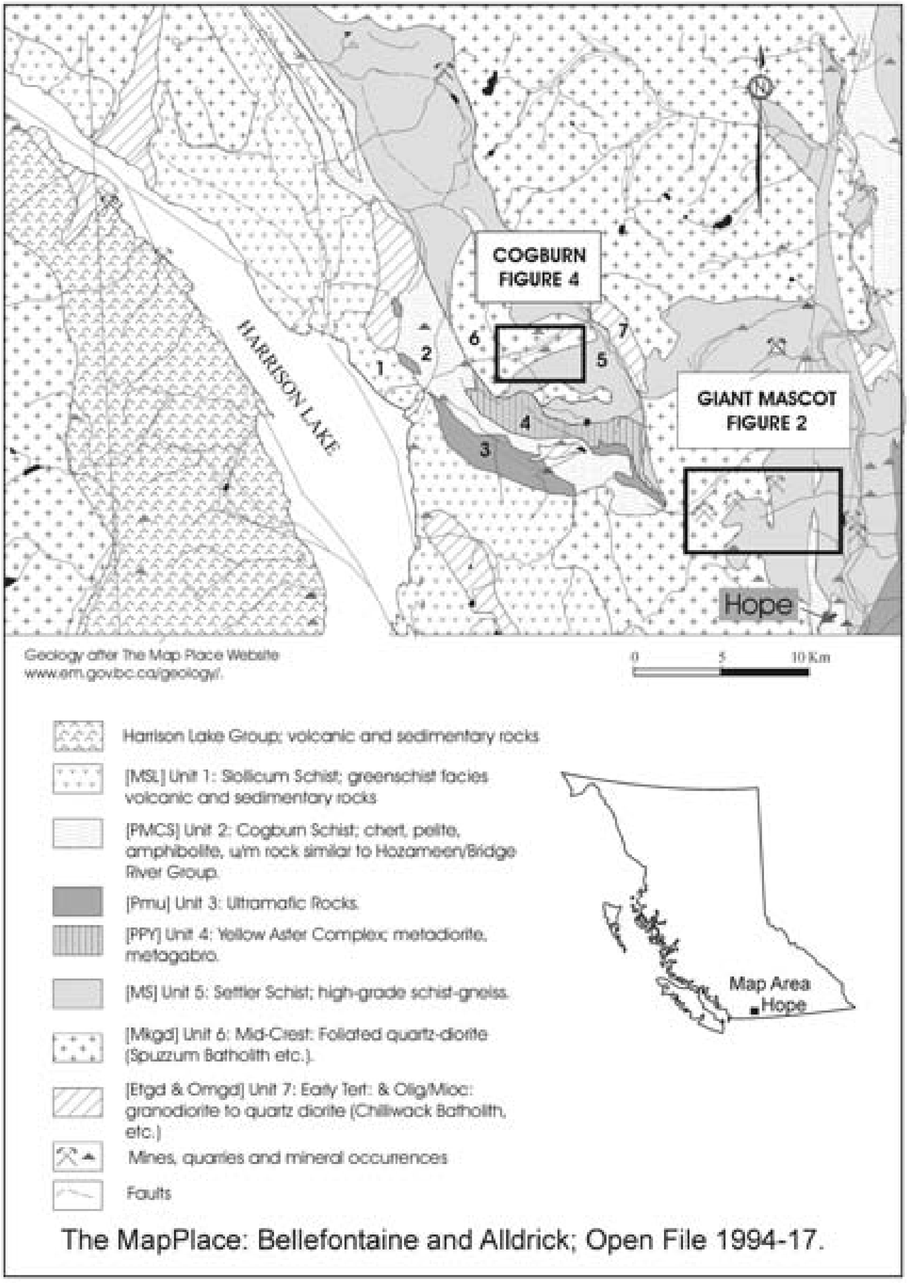

Figure 1. Generalized bedrock geology map of the Harrison - Hope area showing the mineralized areas studied. Data after Bellefontaine and Alldrick (1994), Monger and Journeay (1994), Monger (1970, 1986 and 1989) and “The Map Place” website.

The ultramafic rocks in the area occur in two distinct geological settings. Most occur as large and small, discontinuous lenses in northwesterly-trending belts on either side of the Cogburn Schist and can be seen to the west and east of Talc Creek (Figure 1). The belts can be traced from north of Cogburn Creek, south to Emory Creek, where they appear to be cut-out by the Spuzzum pluton. These lenses show no obvious relationship to the Spuzzum or other, apparently younger, plutons.

By contrast, the remaining ultramafic bodies are intimately associated with rocks of the Spuzzum pluton (Figures 1). They include the Giant Mascot ultramafic body, which hosts the nickel-copper deposit (Figure 2). This is on strike with the northeastern belt of ultramafic lenses discussed above, but is separated from it by several hundred metres of Spuzzum pluton diorite and shows no clear relationship with the Cogburn Schist. There is no indication of a contact between the two, but the ultramafic rocks are partially juxtaposed against high-grade metamorphic rocks of the Settler Schist. The nature of that contact is uncertain, but inclusions of schist are found in the ultramafic body. Further north, the Hut Creek mafic to ultramafic body, which hosts the nickel-copper showings at Cogburn Creek, is similarly enveloped by diorite and separated from the Cogburn Schist unit. It is also in close contact with Settler Schist (Figure 1).

The relationship between the ultramafic rocks found in the two disparate structural settings is uncertain. McLeod (1975) suggests that the Giant Mascot cumulate probably formed through early fractionation of the Spuzzum pluton; however, Ash (2002) suggests that it may be a raft of Unit 3 caught up in the diorite.

GIANT MASCOT MINE AREA (MINFILE 092HSW 004)

INTRODUCTION

The Giant Mascot (Pacific Nickel) deposit is located at the head of Stulkawhits (Texas) Creek, approximately 20 kilometers by road northwest of Hope. It was discovered by a prospector, Carl Zofka, in 1923 and was subject to a considerable amount of surface exploration and underground development prior to the first attempt at production, in 1958. This failed but, with improved metal prices and corporate restructuring, the mine was successfully restarted the following year. Giant Mascot Mines Limited acquired the operation in 1961 and kept it in near-continuous production through to 1974. It was temporarily closed in November 1968, following the collapse of one of the Brunswick stopes, and in August 1970, when the 1270 tonne/day mill burnt down. In the mid-1960s, the mine employed approximately 130 people. The upper part of the Pride of Emory deposit was mined by open pit methods; however, most of the ore was extracted by cut and fill and long-hole mining methods. The mine produced a bulk nickel-copper concentrate, most of which was trucked to Vancouver and shipped to the Sumitomo smelter in Japan (Stephens, 1963). Aho (1954, 1956), Clarke (1969), Christopher (1974) and Christopher and Robinson (1974) discuss the mine's development at different stages in its life. There were no systematic studies of platinum-group element distribution at the mine while it was in production, but there are enough published analyses (Hulbert, 2001) to indicate that platinum and palladium must have been present in the ore.

In 2001, Ministry of Energy and Mines staff revisited the Giant Mascot deposit, examined and sampled the surface rocks and collected a wide range of mineralized samples from the dumps for a study of platinum-group element distribution. Figure 2 is a simplified geology map of the Giant Mascot ultramafic body after Aho (1954). It shows the distribution of the principal ultramafic, mafic and sedimentary rock types and sample locations. The Pride of Emory is the only orebody exposed on surface and access to *in-situ* mineralization was limited. However, the principal lithologies are exposed in zones of near-continuous outcrop along the main road from the mill-site to the 3550 level adit.

HISTORY

The mine consisted of a series of small ore-shoots, most of which were clustered at the west end of a (2.0 km long) ultramafic body that underlies what is now known as Zofka Ridge (Figure 2). The shoots were predominantly northerly plunging "pipe-like" and northerly dipping "tabular" bodies of mineralized peridotite and/or pyroxenite (Figure 3). The mill was developed at the head of Stulkawhits Creek and most of the ore-bodies were developed through an upper portal at the 3550 level, driven through the ridge into the Emory Creek drainage, and a lower, main haulage, portal at the 2600 level. Over the years, the owners undertook a considerable amount of development between these levels, particularly on the 3250 and 2950 sublevels. They also drove a major crosscut on the 3050 level to access two satellite ore-zones north and east of the main development Figure 3). These deposits were also accessed by means of a portal collared at 3275 feet elevation along the main access road over Zofka Ridge.

The Brunswick and Pride of Emory ore-bodies were the only deposits of any size to crop out at surface (Figure 3). Most of the shoots were located and defined by underground drilling. The company systematically drilled off large sections of the main access levels with 200 ft (61 m) spaced, horizontal drill holes. Production came from numerous ore-zones in several deposit clusters. Table 1, after Christopher and Robinson (1974), summarizes the approximate dimensions, tonnages and nickel-copper grades of 26 ore-zones. Most contained a relatively modest tonnage; however, four (Pride of Emory, Brunswick #2, 4600 and 1500) are reported to have each contained in excess of 500 000 tonnes at mineable grade. The table shows that Ni/Cu ratios of the ore-zones range from 1.78 (4300 zone) to 4.03 (2000 zone) with several clustering around values of 2.3 and 3.0. There is no obvious pattern to their distribution among the ore-shoots and, given the intimate association of both high and low values in the Brunswick area, they probably reflect a single episode of deposit formation, possibly followed by some remobilization of the component metals. As of October 1st, 1973, reserves at the mine were 860 000 tonnes grading 0.75 % Ni and 0.30 % Cu (Tindall, 1987).

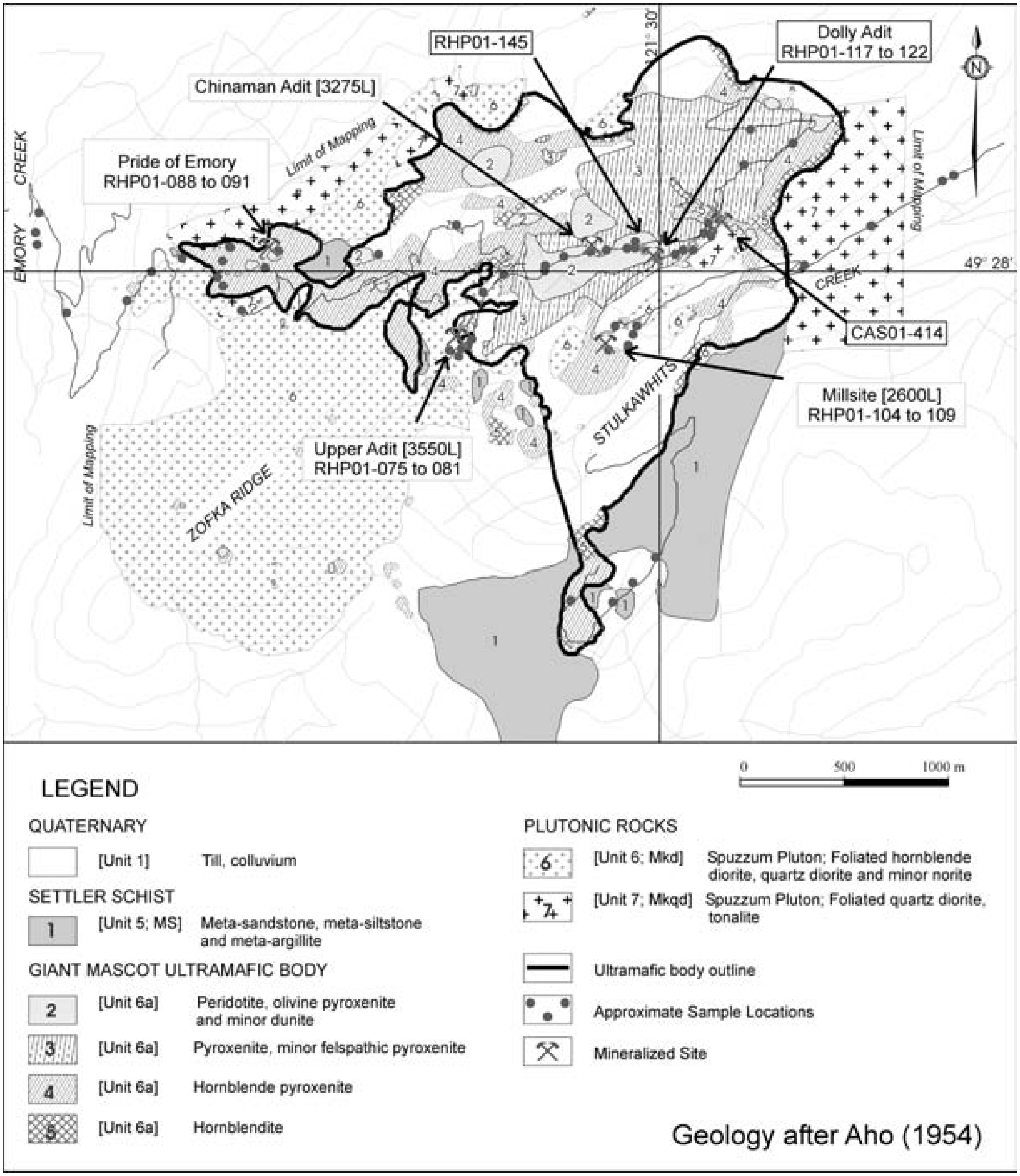

Figure 2. Schematic surface geology map of the Giant Mascot area, after Aho (1954), showing the principal rock units named locations and sample sites.

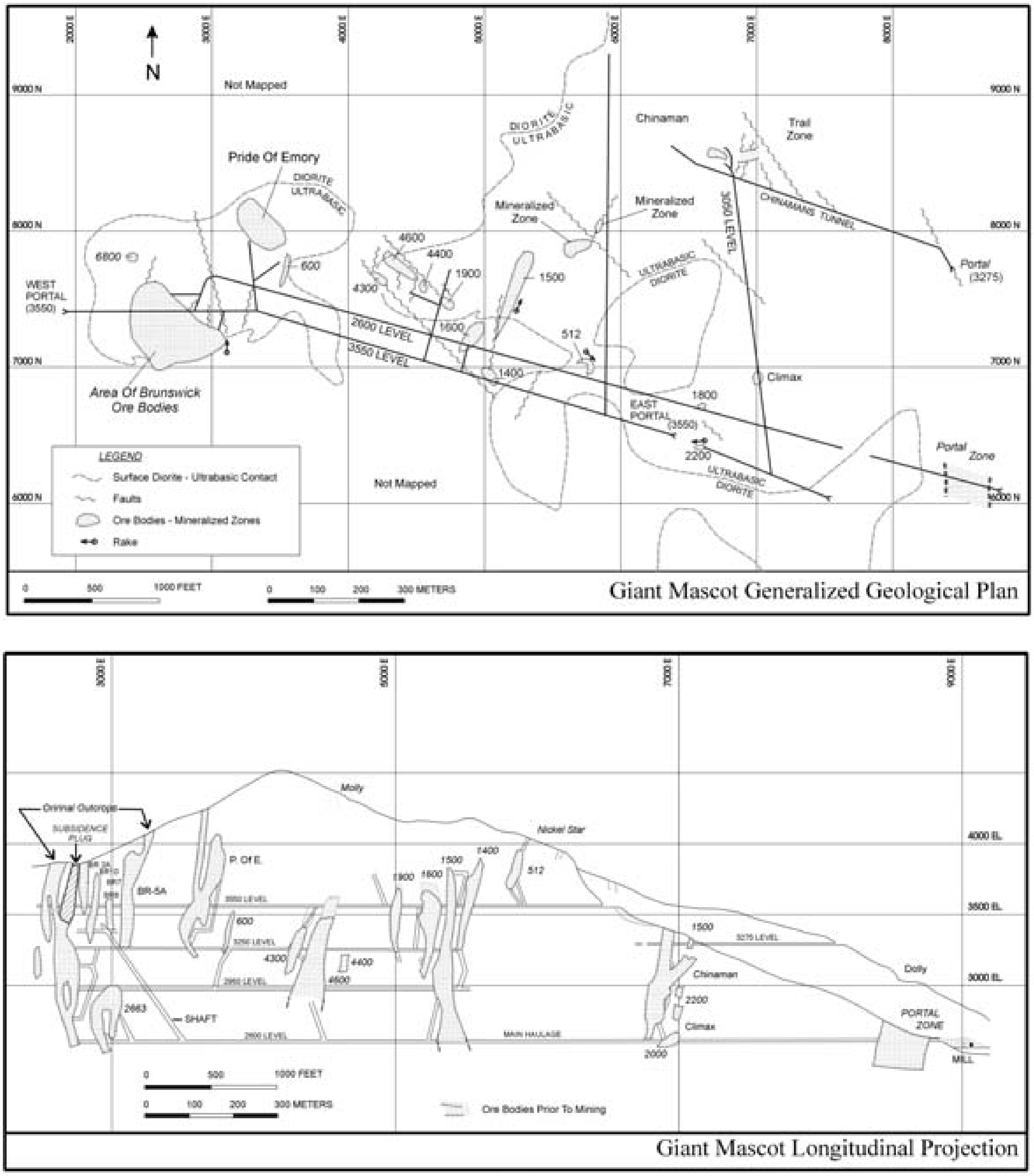

Modified from Clarke (1969) and Christopher and Robinson (1974)

Figure 3. Simplified surface geology map with projections of ore shoots and an, east to west oriented, longitudinal projection of the Giant Mascot mine after Clarke (1996), and Christopher and Robinson (1975). The figures show steeply dipping ore-pipes.

TABLE 1
SUMMARY OF GIANT MASCOT ORE SHOOTS

ID	Dimension Horizontal (m)	Dimension Vertical (m)	Tonnage Tonnes x 1000	Grade Ni %	Grade Cu %	Ratio Ni/Cu	Deposit Type*
Pride of Emory	45.7 x 18.3	266.7	638.6	1.46	0.38	3.84	Unzoned
Brunswick #1	33.5 x 18.3	160.0	111.6	1.1	0.35	3.14	Zoned
Brunswick #2	54.7 x 21.3	251.5	517.0	1.4	0.6	2.33	Unzoned
Brunswick #2A	33.5 x 21.3	106.7	263.0	0.98	0.35	2.8	Unzoned
Brunswick #2G	21.3 x 19.8	91.4	118.8	0.56	0.27	2.07	Unzoned
Brunswick #5	36.6 x 21.3	182.9	371.0	1.49	0.5	2.98	Zoned
Brunswick #7	27.4 x 15.2	61.0	20.9	2.37	0.75	3.16	Zoned
Brunswick #8	6.1 x 15.2	53.3	10.9	1.75	0.61	2.86	Unzoned
Brunswick #10	21.3 x 16.8	61.0	34.5	0.74	0.05	2.11	
2663	15.2 x 18.3	99.1	92.5	0.86	0.32	2.69	Zoned
6800	15.2 x 15.2	91.4	42.6	0.66	0.24	2.75	
600	30.5 x 13.7	91.4	75.3	1.42	0.42	3.04	
Portal		189.0	2154.4	0.25	0.11	2.27	
4600	76.2 x 30.5	196.0	730.2	1.35	0.73	1.8	Zoned
4400	12.2 x 15.2	45.7	24.7	0.51	0.22	2.31	
4300	27.4 x 12.2	68.6	56.2	0.91	0.51	1.78	Zoned
2200	15.2 x 15.2	228.6	122.4	0.68	0.38	1.79	
2000	9.1 x 9.1	15.2	3.1	1.33	0.33	4.03	
1900	15.2 x 24.4	91.4	40.8	0.86	0.45	1.91	Zoned
1800	15.2 x 24.4	45.7	36.3	0.53	0.23	2.3	Zoned
1600	51.8 x 27.4	129.5	195.9	0.97	0.34	2.85	Zoned
1500	61.0 x 21.3	344.4	605.9	1.37	0.45	3.04	Unzoned
1400	15.2 x 18.3	142.6	48.1	0.71	0.32	2.21	
Chinaman	27.4 x 30.5	194.5	341.1	0.73	0.3	2.43	Zoned
Climax	15.2 x 27.4	182.3	191.4	0.78	0.36	2.16	Zoned
512	9.1 x 15.2	68.6	25.4	1.08	0.41	2.63	Zoned
# of deposits			26	26	26	26	
Average			264.33	1.03	0.38	2.59	

After Christopher and Robinson (1974)
* Zoned or Unzoned deposits, where known

In 1980, ownership of the mine was transferred to Mascot Gold Mines Limited, a subsidiary of Giant Mascot Mines Limited. In 1986, after an extended period of inactivity, Mascot Gold Mines Limited resumed exploration. The company was particularly interested in the gold and platinum-group element content and its distribution (Tindall, 1987). International Corona Corporation acquired Mascot Gold Mines Limited as part of its acquisition of the Nickel Plate gold deposit, near Hedley, British Columbia, in 1988. The company continued Mascot Gold's platinum group element study, but did not release the results.

In 1992, Homestake Canada Limited acquired International Corona Corporation and its interests at Giant Mascot as part of its acquisition of the Eskay Creek gold deposit. The company has spent the last few years reclaiming the mine-site. It has now sealed the portals, groomed the dumps and seeded the tailings. In 2001, the company extended an old logging road on the Emory Creek side of Zofka Ridge up to the Pride of Emory and filled a "glory-hole" in the Brunswick area.

PREVIOUS WORK

The geology of the Giant Mascot deposit has been described and discussed by several authors, including Cairnes (1924), Cockfield and Walker (1933) and Horwood (1936, 1937) during its early exploration; Aho (1954, 1956) at the start of production; Clarke (1969) while the mine was in operation and Christopher (1974) at the time of closure. These authors provide similar descriptions of the ultramafic body that hosts the deposit and discussions on the geometry of the ore-zones, and nature of the mineralization; however, they differ slightly in their conclusions as its mode of formation. They also differ in their interpretation of the age of the ultramafic body with respect to the Spuzzum pluton. Cockfield and Walker (1933) and Horwood (1936, 1937) indicate that the diorite intrudes the ultramafic body. However, Cairnes (1924) and Aho (1954, 1956) suggest that the ultramafic body may be younger than the Spuzzum pluton.

There were several detailed studies undertaken shortly before the mine closed. They include petrologic studies of the 4600 zone by Muir (1971) and of the Climax and Chinaman ore-zones by McLeod (1975), and a study of the contact relations around the ultramafic body by Vining

(1977). McLeod (1975) also completed six K/Ar age-date determinations to resolve the relative ages of the igneous rocks. The results suggest that the ultramafic body (119-95 Ma) is older than the Spuzzum pluton (79-89 Ma; McLeod *et al*., 1976); however thermal resetting of the rocks may have occurred during subsequent metamorphism and the ages may not be absolute.

GEOLOGICAL SETTING

The Giant Mascot ultramafic body has a pronounced northeasterly trend (Figure 2). It is enveloped on three sides by two types of diorite and is juxtaposed against meta-sediment on the fourth. It is irregular in outline, but is approximately 2.0 kilometres long and 1.0 kilometre wide. The ultramafic rock is composed of olivine and orthopyroxene-rich cumulate, with variable but lesser amounts of clinopyroxene, feldspar and hornblende. It ranges in composition from peridotite (harzburgite - lherzolite) through olivine pyroxenite (olivine websterite) to pyroxenite (websterite) and hornblende pyroxenite. The cumulate is typically massive and relatively uniform in composition and texture, at least at outcrop scale. Contacts between individual units are either sharp, or they may be transitional over a few centimeters. Contacts are locally crosscutting and rounded inclusions of one variety of pyroxenite can be seen in another, or in peridotite. There is no obvious penetrative fabric but the rocks are faulted and in some localities the olivine crystals are systematically cross-fractured and serpentinized and the pyroxenes are noticeably deformed. Narrow zones of hornblendite are commonly found on the outer contact of the ultramafic body.

ULTRAMAFIC ROCKS

The ultramafic rocks vary considerably in grain-size and bulk composition. The principal rock type is pyroxenite, which is present in several varieties, most of which contain small, scattered, euhedral crystals of olivine (1-2 mm) and spinel (< 1.0 mm). At the eastern end of the ultramafic body the pyroxenite is medium grained (3-6 mm) and porphyritic, with large (10-20 mm), locally poikilitic, phenocrysts of orthopyroxene and small amounts of interstitial feldspar. In the central part, near the 3275 portal, it consists of relatively homogenous, coarse (6-8 mm) and fine-grained (2-4 mm) varieties. Towards the west and locally around the contact, it contains an appreciable amount of hornblende (Figure 2). The hornblende crystals are most commonly poikilitic and large (10-30 cm). Locally, the olivine grain size (3-4 mm) and content increases and the pyroxenite shows rapid transition to olivine pyroxenite and peridotite. The latter forms large, irregular-shaped masses within the pyroxenite in the central part of the body and also occurs in small, mineralized "pipe-like" structures at the west end. Aho (1956) describes several mineralized peridotite pipes in the Brunswick and Pride of Emory area that were developed early in the life of the mine. More recently, Muir (1971) has studied the 4600-zone pipe and McLeod (1975) has examined the Climax and Chinaman deposits on the 3050 level crosscut.

Irrespective of composition, the cumulate displays a consistent paragenetic evolution. Olivines and spinels occur as, euhedral to subhedral, cumulus-textured crystals that are commonly poikilitically-enclosed in larger, euhedral crystals of also cumulus-textured orthopyroxene. Some of the latter contain minute lamellae of clinopyroxene, which also occurs interstitial to, and in an interlocking relationship with, the orthopyroxene. In some samples, large clinopyroxene crystals poikilitically enclose olivine and orthopyroxene. Hornblende is found in pyroxenite near the outer margins of the ultramafic body, where it commonly occurs as large, poikilitic crystals filling inter-cumulus spaces. Alternatively, it occurs as smaller, subhedral crystals. Feldspar is found in small amounts in some of the less olivine-rich pyroxenites, although rarely in those that contain hornblende. It is invariably interstitial to the other minerals.

The cumulate displays modal layering but electron microprobe data, from Muir (1971) and McLeod (1975) show little evidence of appreciable cryptic layering. The silicate minerals are not obviously zoned and their compositions are reasonably consistent from one lithology to another. Muir (1971) analyzed coexisting minerals in samples of olivine pyroxenite and peridotite from the 4600 Zone. He shows that the crystals are unzoned, have a mean forsterite composition of 83.43 +/- 0.27 (mol. %) Fo, and have a mean nickel content of 0.13 % Ni. His work also shows that the mean enstatite content of the orthopyroxene in the peridotite is En 84.3 and that in the olivine pyroxenite is En 81.85. Muir found less enstatite in orthopyroxenes within hornblende-rich cumulates. The mean enstatite content of orthopyroxene in hornblende pyroxenite inside the ore zone was found to be En 80.9, and outside the orebody En 77.0. Muir found that the 4600 Zone orthopyroxenes contain between 1.8 % and 3.6 % Al_2O_3.

McLeod (1975) conducted a similar study of mineral compositions in peridotites and pyroxenites in and around the Climax and Chinaman deposits. He found that olivine crystals range in composition from Fo 80.0 to Fo 86.65, with the higher values in the more olivine-rich rocks. Similarly, he found that orthopyroxene crystals range in composition from En 85.65 to En 75.10 and coexisting clinopyroxenes range from Wo 39.5 to Wo 48.15, En 43.95 to En 52.75 and Fs 5.8 to Fs 10.8.

McLeod *et al*. (1976) show that the crystal compositions are consistent with their formation as cumulate in a magma chamber. They show that distribution coefficients between Ca-rich and Ca-poor pyroxenes (K_D average: 0.729) imply a magmatic origin, and that 15 ortho- and clinopyroxene pairs from the interior of the body (McLeod, 1975) yield an average temperature of 990° +/- 50° C, using the method of Wood and Banno (1973).

The ultramafic rocks are largely unaltered; however, they are weakly to strongly altered in the vicinity of major faults. Deformed and altered rocks commonly take on a crumbly appearance (Christopher and Robinson, 1974) as primary minerals are progressively altered to actinolite, biotite, talc and magnetite. Locally, secondary serpentine veinlets form a network throughout olivine crystals.

HORNBLENDITE

Contact relations between ultramafic rocks and the surrounding rocks commonly show conflicting age relationships because of the development of large amounts of hornblendite on, or immediately adjacent to, the contact. Aho (1956), McLeod (1975) and Vining (1977) discuss the problem. Hornblendite locally (1) cuts diorite, (2) replaces pyroxenite, (3) replaces diorite and (4) forms a coarse-grained, locally pegmatitic, matrix to hornblende-altered pyroxenite fragments along brecciated contacts. Hornblendite is well developed towards the east end of the ultramafic body (Figure 2), where it separates a quartz-rich phase of the diorite from a hornblende-rich phase of the pyroxenite. Sample CAS01-414 is a fine-grained variety of hornblendite collected from a particularly well-developed hornblendite zone on the main access road. It has been submitted for Ar/Ar age dating. The results are pending and will be reported on separately. Narrow (10-20 mm) tonalite dikes in pyroxenite at the east end of the ultramafic body have well-developed (10-20 mm) amphibole-rich alteration envelopes formed as a result of hydration and metasomatic alteration. The envelopes suggest that the contact hornblendite may also have formed as a result of hydration and metasomatism following emplacement of the diorite. Vining (1977) conducted a lithogeochemical study and established that the hornblendite could be formed from pyroxenite or diorite through a moderate amount of chemical transference from either rock type to the other. He concluded that it was formed by metasomatism shortly after emplacement of the Spuzzum diorite.

MAFIC DIKES

The ultramafic cumulate is cut by numerous dikes of fine-grained (1.0 mm) mafic gabbro and/or hornblendite. They have sharp contacts and show little alteration of the surrounding rock. The dikes are commonly narrow (0.1-0.2 m) and anastamozing and locally display disturbed contacts indicative of injection of several phases of differing composition. Most are composed of hornblende with a variable amount of feldspar. The dikes are discussed by Aho (1956) and Vining (1977). The latter concluded that some could be genetically related to the marginal amphibolite discussed above. Sample RHP01-145 was collected from a dike cutting the cumulate along the main access road east of the 3275 portal (Figure 2). It is currently being age dated by Ar/Ar methods. The results are pending.

SPUZZUM DIORITE

The southern part of the Spuzzum pluton is described by Richards (1971) and by Richards and McTaggart (1976) who differentiate the body into three outwardly zoned, gradational diorite phases and a distinctive (but probably related), outer tonalite. Their work, south of American Creek, shows that the pluton has two core areas of hypersthene-augite diorite (Type I) surrounded by zones of augite-hypersthene-hornblende diorite (Type II). The latter is enveloped by biotite-hypersthene-hornblende diorite (Type III) and all of the above are enclosed by biotite-hornblende tonalite. The three phases of diorite vary systematically in modal composition. The quartz (1% - 9%) and hornblende (1% - 20%) contents increase outwards at the expense of hypersthene (13% - 1%). The pyroxenes become progressively altered to amphibole near the outer rim of the diorite complex and feldspar crystals become increasingly zoned from core to margin. The tonalite contains less plagioclase than the diorite, but is appreciably richer in quartz and biotite. The three phases of diorite and the tonalite are strongly foliated. The diorite found at the mine resembles Type III, as defined by Richards (1971).

Aho (1956) and Vining (1977) describe two varieties of foliated diorite in the Giant Mascot mine area (Figure 2). They show that the west side of the ultramafic body is enveloped by "hornblende diorite" and that the east end is in contact with "quartz-diorite". This study shows that most of the diorite to the south and east of the mine is rich in hornblende and relatively quartz poor, although local quartz enrichment occurs adjacent to some of the hornblendite zones at or near ultramafic rock contacts. For example, it was found at the eastern contact of the small diorite body exposed below the switchback on the road to the upper portal (Figure 2). The two phases appear to be gradational and can be treated as a single unit. The diorite is commonly medium grained (3-6 mm) and weakly to strongly foliated. It is composed of up to 40% of mafic minerals (ragged orthopyroxene, hornblende and biotite) with the remainder made up of strongly zoned feldspar and minor amounts of quartz.

Although the Giant Mascot cumulates are deformed, the deformational fabric is weak and previous workers focused on the fault, rather than fold, relations at the mine (Aho, 1956; Clarke, 1969; Muir, 1971; McLeod, 1975) as some of them control the distribution of mineralization. However, internal contact relations described in the literature show considerable three-dimensional complexity to the distribution of rock units in the cumulate body that cannot entirely be attributed to faulting. In the past, much of it has been attributed to remobilization and re-injection of cumulate (Muir, 1971; McLeod, 1975); however, Friesen (1967) suggests that early folding may also have played an important part in controlling the distribution of rock-types and locating some of the ore zones.

The cumulate body underwent a second phase of deformation after emplacement of the diorite. The diorite and hornblendite at the west end of the ultramafic body (Figure 2) are strongly foliated and they, and the cumulate body, appear to have been folded and faulted about a northeasterly-trending axis. Similarly, contact relations in the vicinity of the small body of diorite exposed below the switchback on the main access road to the upper adit (Figure 2) show that both the ultramafic body and the diorite intrusion must have undergone considerable, if local, deformation about a northwesterly-trending axis. The diorite, adjacent hornblendite and the hornblende pyroxenite are all sheared and folded about a shallow, northwesterly-trending, northwesterly-dipping axis. The map pattern displayed by the cumulate body is consistent with two major phases of post-diorite deformation. Structural relations are complicated by late, post-mineral faults.

MINERAL DEPOSITS

Giant Mascot Mines Limited identified twenty-eight mineral deposits within the ultramafic body and mined twenty-two for a total production of 4 319 976 tonnes containing 26 573 090 kilograms of nickel and 13 212 770 kilograms of copper. The mine also produced 140 700 kilograms of cobalt between 1971 and 1973, and 16 516 grams of silver and 1026 grams of gold in 1958 (MINFILE 092HSW004). Christopher and Robinson (1974) describe the size, shape, geological and structural setting, and tonnage and grade of the twenty-six deposits shown in Figure 3. Some of the data are reproduced in Table 1. They show that most of the deposits are “pipe-like” or “tabular”. They range in horizontal section from approximately 80 m x 40 m to 7 m x 15 m. Most plunge at a moderate to steep (55 º to 80 º) angle to the northwest; however a few (1600, 600, 512) plunge at a similar angle to the southwest and one, 1800, has an anomalous plunge to the southeast. Continuity down plunge ranges from 15 m to 350 m. In some localities the ore zones grade out into sub-economic mineralization; at others, they terminate on faults. Some of the ore zones appear to be isolated while others, particularly in the Brunswick area (Figure 3), belong to well-defined clusters. Giant Mascot Mines Limited traced most of the zones from their uppermost expression down to the 2600 haulage level. At closure, it concluded that the ore bodies exposed at that elevation were low grade and that they would likely be cut out by diorite at depth.

The company recognized two principal types of deposit at the mine; zoned deposits, largely comprised of disseminated mineralization in one or more rock type (Brunswick #1, #5, #6 and 4600, 1600, 1900 and 512), and unzoned deposits, largely comprised of semi-massive to massive sulphide lenses (Pride of Emory, Brunswick #2, #8 and #9; Table 1). Narrow sulphide veins occur in both types of deposit.

Aho (1956) describes several zoned deposits in the Brunswick area. Typically, they are concentrically zoned. They are composed of interstitial blebs of sulphide disseminated in olivine-rich peridotite and dunite in or near the core of sub circular, “pipe-shaped” bodies that are enveloped by more pyroxene-rich peridotite and pyroxenite. In most of these deposits, the sulphide content increases locally to form segregations and drops-off rapidly outwards, as the orthopyroxene content of the rock increases. The 4600 zone is unusual in that the greatest sulphide concentrations are found in hornblende pyroxenite (Muir, 1971). The Climax and Chinaman deposits are also zoned (McLeod, 1975). Although the sulphide is fairly uniformly distributed in most of the deposits, some, such as the Climax and Chinaman, are reported to have projectable high-grade concentrations along their structural footwall contacts (McLeod, 1975).

Aho (1956) also describes several unzoned deposits, including the Pride of Emory. These are typically irregularly shaped, tabular, and semi-massive to massive sulphide bodies that have sharp, commonly banded, contacts that are locally controlled by changes in lithology. The ore commonly consists of angular fragments of country-rock peridotite or pyroxenite in a sulphide matrix that contains euhedral to subrounded crystals of olivine and/or pyroxene. The amount of silicate material mixed in the sulphide is variable.

The two ore-types are intimately associated and may be gradational in the Brunswick and Pride of Emory areas. The controls on the distribution of the two types of deposit and their mode of formation are uncertain. However, Clarke (1969) suggests that they may be structurally controlled and related to two principal fault sets. He attributes much of the mineralization in the Brunswick and Pride of Emory area (Figure 3) to northwesterly-trending, northeasterly-dipping structures that appear to dam some of the ore-shoots and to offset others. He attributes the primary control on the orientation of the 600, 1600 and 512 deposits to northeasterly-trending, near-vertical faults. In an in-house proposal for future exploration, Friesen (1967) notes that the ore in the 600 and 1500 ore bodies was far richer at bottom than the top and suggests that these deposits may have been subject to gravity separation after emplacement. Similarly, he describes partial flowing “of sulphide solutions” along a fault plane away from the bottom of the 1500 deposit and suggests that it must have been a pre-ore fault that acted as a dam. In the case of the 2200 orebody, he suggests that its geometry reflects folding.

Table 1 shows that the zoned and unzoned deposits differ considerably in tonnage but are similar in grade. In both cases, the ore is composed of abundant pyrrhotite with lesser amounts of pentlandite, chalcopyrite, magnetite and traces of pyrite. There has been very little work done on the distribution of platinum-group elements in the deposit and there are no public domain references to platinum-group minerals being found. In zoned deposits, the sulphides commonly occur as irregular grains or granular aggregates interstitial to the silicate minerals. The aggregates are composed of large, anhedral grains of pyrrhotite that commonly contain fine-grained pentlandite exsolution lamellae. The pyrrhotite groundmass also contains smaller, more granular crystals of pentlandite. Chalcopyrite crystals are less directly tied to pyrrhotite. They are found either in close proximity, or at some remove, from the pyrrhotite-pentlandite crystal aggregates.

In the more massive ores of the unzoned deposits, there is greater continuity between the pyrrhotite crystals and the rock may become net textured. Where this occurs, large pyrrhotite crystals commonly show a similar texture to poikilitic hornblende found in hornblende pyroxenite. The proportions of sulphides and silicates vary and net-textured ores are gradational into semi-massive ores. Although the latter are not necessarily deformed, some are brecciated and show clear evidence of solid-state deformation of sulphide. In these samples, the sulphide-silicate assemblage becomes grain-size and compositionally banded around country-rock fragments that either contain disseminated mineralization, or are barren. The sulphide appears to enclose and “cement” silicate fragments. In these deformed rocks, there is local evidence of sulphide replacing silicate crystals, particularly along cleavages and fractures. Deformed sulphide aggregates show a similar textural relationship between pyrrhotite and pentlandite to that found in undeformed sulphide aggregates; however, chalcopyrite is less frequently found as isolated grains and more commonly occurs as well-defined, coarse or fine-grained veinlets that cut the sulphide-silicate assemblage (Aho, 1956; Clarke, 1969).

McLeod (1975) studied the distribution of sulphide in the Climax and Chinaman areas of the mine and paid particular attention to the compositions of the sulphides. He notes that the net texture is commonly well developed in the lower-grade portions of the ore shoots. As part of his study, he analyzed coexisting pyrrhotite and pentlandite crystals using an electron microprobe and determined that both display a wide range in composition. He found that their compositions were related both to local differences in bulk sulphide composition and to systematic differences in the silicate composition of the rocks. In general, he found that nickel and iron increase in pentlandite as one approaches the Climax deposits.

THIS STUDY

As part of this study, a total of 22 sulphide-bearing samples were collected from the Giant Mascot nickel-copper deposit. The samples came from the Pride of Emory, 3550 portal dump, 2600 portal dump and the Dolly adit (Figure 2, Table 4). They form a continuum selected to include a range of total sulphide contents and different textures. Some contain small amounts of interstitial sulphide, others contain sufficient sulphide to develop a net texture, and still others are composed of semi-massive and breccia-cement sulphide. Several display elements of more than one textural type.

Samples RHP01-080, -089, -105, -108 and -109 are composed of coarse (5-10 mm) and fine-grained (2-5 mm) peridotite samples that contain small amounts of poikilitic, inter-cumulus hornblende and minor amounts of disseminated sulphide. Sample RHP01-109 is unusual, in that it also contains interstitial plagioclase. In each sample, the sulphide occurs as irregular-shaped, coarse and/or fine-grained blebs in the interstitial spaces between olivine and pyroxene crystals. The sulphide is predominantly pyrrhotite with minor pentlandite and granular crystals of chalcopyrite. The latter are either intimately associated with the other sulphides or are scattered among the silicate crystals at some distance from them. Locally, the pyrrhotite appears to corrode and partially replace pyroxene crystals along fractures. It may have been remobilized.

Samples, RHP01-106, -120 and -121 display sharp, planar contacts between barren and mineralized rock. The interstitial hornblende content drops-off rapidly across the contact and its place is taken up by sulphide. Sample RHP01-120 is brecciated.

Samples RHP01-078, -077, -091, -107, -090, -117, -088, -081, -118 and -075, show a progression from silicate-rich rocks that contain interstitial sulphide to silicate-poor rocks that are net-textured and/or composed of semi-massive sulphide. The transition results from a progressive increase in inter-cumulus sulphide and decrease in inter-cumulus hornblende. As the sulphide content of the rock increases, the olivine and pyroxene crystals appear to be increasingly disaggregated and in the most sulphide-rich rocks individual silicate grains are completely enveloped by sulphide. Most of these ores are semi-massive and homogenous; although some, such as RHP01-088, display a weak, imposed, tectonic fabric. The silicate grains are typically euhedral to subrounded and range in size from 1.0 mm to 5.0 mm. Pyrrhotite and pentlandite are evenly distributed throughout the matrix and chalcopyrite commonly occurs as wispy veinlets, and is more dispersed. Sample RHP01-078 is undeformed but particularly rich in chalcopyrite.

At some localities, most notably around the Dolly adit, the host rocks were clearly deformed and brecciated before they were mineralized and angular to subrounded fragments of barren peridotite and pyroxenite are cemented by net-textured to semi-massive sulphide. The rocks have a knobby appearance caused by preferential weathering of the sulphide-rich matrix that surrounds the barren blocks. Locally, narrow bands of net-textured sulphide appear to feather out into barren, massive peridotite or pyroxenite. The matrix cement in samples RHP01-076, -104, -119, -120 and -122 is similar to that described above; however, the rocks commonly have a crushed, protoclastic texture. The silicate component commonly includes angular fragments of country rock, as well as different grain-sizes of olivine and pyroxene. The sulphide breccia cement commonly contains well-developed stringers and veins of chalcopyrite that also wrap around the country rock fragments. A few semi-massive samples, such as RHP01-076 are extremely deformed. In this sample, the sulphide-silicate matrix contains both fragments of country rock silicate and deformed, coarse-grained pyrrhotite crystals. The sample is also strongly veined by chalcopyrite.

COGBURN CREEK AREA

INTRODUCTION AND HISTORY

In the late 1960s, Giant Explorations Limited formed the "Nickel Syndicate" to explore the Cogburn Creek area for nickel-copper mineralization. It staked 242 claims in 1969 and added a further 322 units the following year, establishing a substantial land position. At the same time, it flew an airborne magnetometer survey from the mine north to Cogburn Creek (Crosby, 1970) and conducted detailed stream sediment and contour soil geochemical surveys (Gayfer, 1970a, 1970b). The company established grids on, and mapped and sampled seven areas and diamond drilled three, two along Cogburn Creek and one at Daioff Creek (Berg and Clarke, 1971a, 1971b). At Cogburn Creek, it identified several areas of low-grade nickel-copper mineralization in an ultramafic to mafic cumulate body west and east of Settler Creek.

PREVIOUS WORK

There was little interest in the nickel-copper potential of the Cogburn area from the mid-1970s to the late-1990s, but the ultramafic cumulates attracted the attention of Granite Creation and Stoneworks Limited. The company extracted a bulk sample of "black granite" from the Raven Quarry (MINFILE 092HNW 078) in 1996 (Sanguinetti, 2000a). Four years later, it drilled 13 diamond drill holes, for a total length of 397 metres, at the quarry site and other localities north of Cogburn Creek (Sanguinetti, 2000b). In 2001, it returned to the Raven Quarry and extracted a larger test sample. Exploration for nickel-copper and platinum group elements resumed in the late 1990s. David Haughton, a prospector working on the Provincial Government's Prospector Assistance Program was one of the first into the area, staking the Jason Claims west of Settler Creek in 1999. Several junior companies acquired large ground holdings in the area in 2000 and 2001.

GEOLOGICAL SETTING

The plutonic rocks in the Cogburn Creek area were considered by Lowes (1972) to be part of the Spuzzum pluton. This was based on inferred map continuity and observed similarities with foliated quartz diorite in the type area near the Fraser River, described by McTaggart (1970) and Richards and White (1970). More recent mapping has shown that the Hut Creek pluton is a separate entity, albeit with strong similarities to the Spuzzum pluton. The Hut Creek pluton was included by Gabites (1985) in a detailed study of age relations in the Cogburn Creek area. She subdivided it into an inner core of "hornblende-hypersthene gabbro" and an outer, more extensive zone of foliated diorite (Figure 4). The former is a composite body composed of ultramafic to mafic cumulate.

ULTRAMAFIC TO MAFIC ROCKS

North of Cogburn Creek, the ultramafic to mafic cumulate body is approximately 3.5 km wide. It is bounded to east and west, and partially to the south by diorite (Gabites, 1985). The cumulate is best exposed on the north side of Cogburn Creek (Figure 4). It is composed of differing compositions, grain-sizes and textural varieties of pyroxenite, feldspathic pyroxenite and gabbro. Most of it is massive and homogenous; however the feldspathic pyroxenite exposed at the Raven quarry is intermittently rhythmically layered as a result of subtle variations in grain-size. At one locality at this site, the layering is distorted around an inclusion of slightly different (more pyroxene-rich) composition. The layers display a pronounced northwesterly-trend and a moderate southwesterly dip. This type of banding is uncommon; most of the cumulate is massive, with both diffuse and sharp transitions between different varieties.

The cumulate is largely fine-grained (2-4 mm), medium-grained (3-6 mm) and coarse-grained (5-8 mm) feldspathic pyroxenite, or gabbro. The modal composition varies, but the rocks commonly contain subhedral to euhedral crystals of orthopyroxene (25-50%), interstitial plagioclase (25-30%), relatively large anhedral to subhedral crystals of clinopyroxene (20-35%), small inclusions of opaques and, locally (1-10%) secondary biotite. However, in some localities, most notably near the mineralized outcrop north of Cogburn Creek, the feldspathic rocks include layers that are richer in pyroxene and include euhedral olivine crystals.

Granite Creation and Stoneworks Limited drilled several exploratory holes in massive pyroxenite and feldspathic pyroxenite cumulate alongside the road north of Cogburn Creek. Most were collared in medium-grained feldspathic pyroxenite ("pyroxene gabbro") and either intersected it throughout, or intersected weakly intercalated layers of fine to coarse-grained, black pyroxene gabbro (Sanguinetti, 2000a).

South of Cogburn Creek, the cumulate has been intruded by diorite and partially disaggregated to form irregularly shaped, northerly-trending bodies. West of Settler Creek, these become fully disaggregated and ultramafic and mafic xenoliths become progressively smaller and less frequent within the main body of diorite (Berg and Clark 1971a; Berg, 1972; Gonzales and Clarke, 1972 and 1973). Although Gonzalez and Clarke (1972, 1973) identified a highly feldspathic, gabbroic phase of the cumulate body south of Cogburn Creek, elsewhere feldspar is less evident and the rocks appear to be more mafic to ultramafic. It is predominantly massive, blackish-brown, medium-to-coarse-grained, orthopyroxene-rich pyroxenite that contains, locally abundant, large crystals of late, interstitial and also secondary amphibole.

HUT CREEK DIORITE

The cumulate is intruded by medium-grained (3-6 mm), weakly to strongly foliated hornblende diorite. The contacts appear to be tectonic and, as at Giant Mascot, they are commonly marked by the development of hornblendite. The plutonic rocks are jointed. The principal joint sets are oriented in a northeasterly direction with a steep northerly dip, and in a northwesterly direction with a moderate northeasterly dip. They are also cut by, northerly-trending, vertical zones of intense shearing. Some of the joints in the cumulate areas contain narrow (centimeter-scale) tonalite and diorite dikelets, clearly indicating that the cumulate was deformed prior to intrusion of the diorite. Some of the steep northeasterly-trending fractures contain aphanitic to fine-grained (1.0 mm) hornblendite dikes with sharp contacts that are similar in texture and composition to those found at Giant Mascot. The Hut Creek pluton is juxtaposed against Settler Schist north and south of Cogburn Creek; however the nature of the contact is uncertain. It may be tectonic.

MINERAL DEPOSITS

SETTLER CREEK: NI: ZONE #4 (MINFILE 092HNW 045)

In 1970, Giant Exploration Limited located mineralized pyroxenite along a logging road that exposed an outcrop of cumulate south of Cogburn Creek (Figure 4). Company staff later mapped the area and conducted soil geochemical and geophysical surveys (Berg and Clarke, 1971a, 1971b). Chip samples assayed 0.4% Ni and 0.2% Cu over an undefined length (Berg and Clarke, 1971a) and three diamond drill holes, with an total length of 500 metres (Eastman, 1971) located a "short interval" grading 0.3% Ni and 0.3% Cu (Berg and Clarke, 1971a). The soil geochemical survey located a strong but relatively restricted, coincident nickel and copper anomaly uphill from the showing (Gonzales and Clarke, 1973).

The Zone #4 showing is underlain by hornblende-rich pyroxenite near a creek controlled by one of the main, northerly-trending faults. At this locality, the mineralized pyroxenite appears to be juxtaposed against coarse-grained,

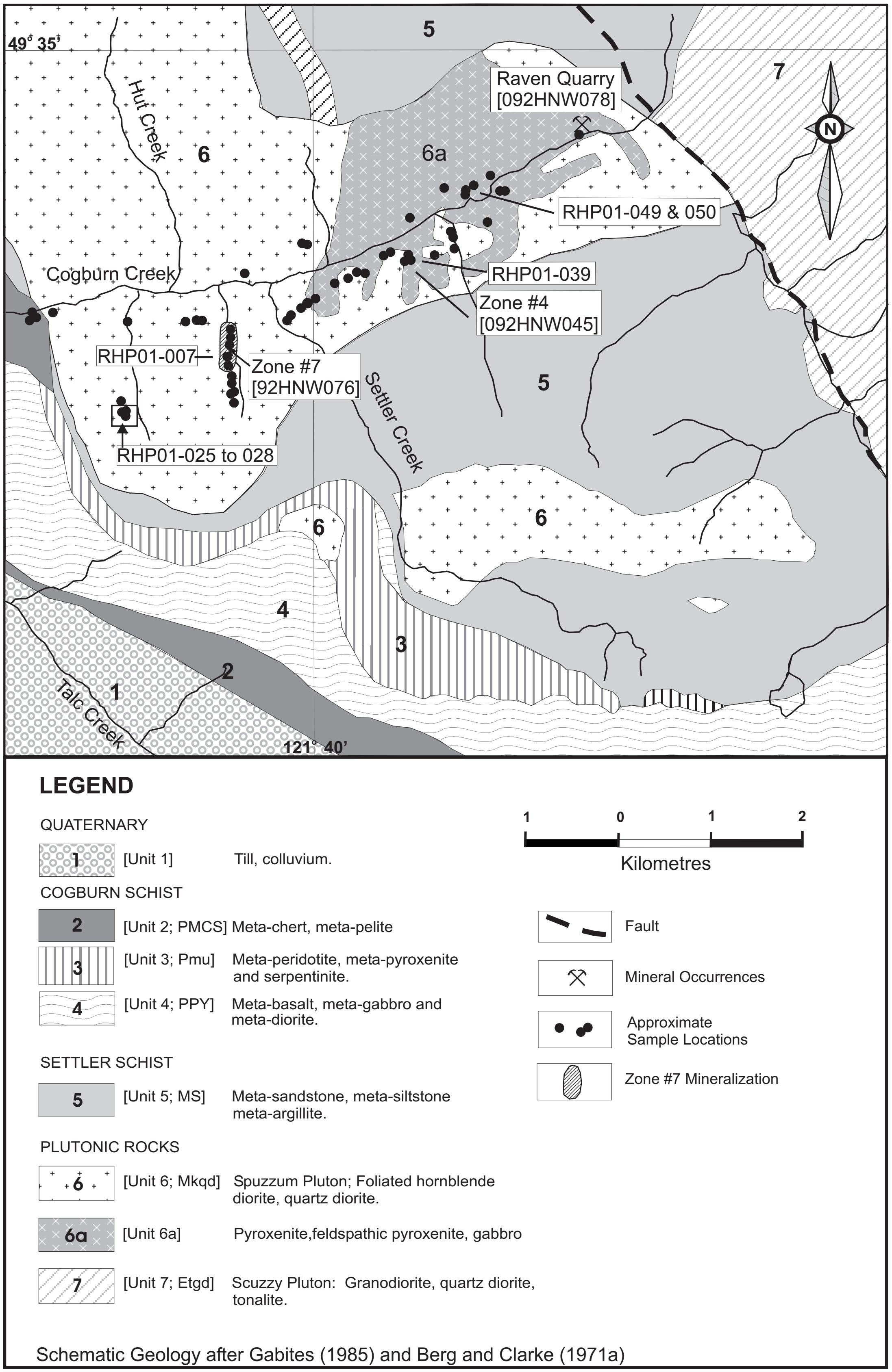

Figure 4. Schematic surface geology map of the Cogburn Creek area, after Gabites, showing the principal rock units, mineral occurrences and sample sites.

pegmatitic hornblendite. The pyroxenite is largely composed of crystals of orthopyroxene (2-3 mm) that are locally poikilitically enclosed in larger (10 mm) hornblendes. In outcrop, the rock contains fine disseminations and rare patches of net-textured sulphide in fresh, undeformed, hornblende-free pyroxenite. Rare float samples show that the net-texture is also to be found in crushed pyroxenite surrounding sub angular to sub rounded fragments of barren hornblende pyroxenite. The silicate minerals in Sample RHP01-039 are crushed and some are partially recrystallized. Small crystals display 120^{o} degree angles and envelope larger crystals. The sulphide occurs as disseminations, net-textured concentrations and wispy veinlets in the silicate matrix and some of the larger sulphide blebs enclose large, isolated crystals of olivine and pyroxene that do not appear to be recrystallized.

Giant Exploration Limited also located trace amounts of sulphide at several localities within a north to northwesterly-trending belt of pyroxene-rich pyroxenite north of Cogburn Creek. The mineralization on this side of the river occurs in three settings, all of which occur in a 200-metre section through the pyroxenite west of the Settler Creek turn-off (Figure 4). It is found as (1) fine, disseminated and lacy, net-textured sulphide, (2) as veins and heavy disseminations in crushed silicate in breccia zones cutting the pyroxenite and (3) as veins and disseminations within inclusions in barren pyroxenite.

Granite Creation and Stoneworks Limited found small amounts of fine, disseminated and net-textured sulphide in one of their diamond drill holes (#5) but report low metal values (Sanguinetti, 2000a). Within a few metres of this drill site, there are several roadside blocks of mineralized pyroxenite float. Sample RHP01-050, from one of them, is similar in appearance and texture to mineralized pyroxenite found south of the river. It is composed of fresh, adcumulate-textured orthopyroxenite that contains a minor amount of interstitial to net-textured sulphide.

Sample RHP01-049 was collected at the same locality. It resembles RHP01-039, which was collected south of the river. It is a foliated, feldspathic pyroxenite, composed of small euhedral orthopyroxene and larger, more ragged, clinopyroxene crystals in a matrix of feldspar. The rock is deformed and cut by a narrow vein (5.0 mm wide) that is partially composed of pyrrhotite. The vein has diffuse outer boundaries and pyrrhotite appears to have permeated outward from the main fracture along micro-fractures and crystal boundaries. Pyrrhotite locally extends several centimeters from the main fracture. The vein also contains chalcopyrite, however it is not found in the surrounding rock.

The third style of mineralization has only been seen at one locality. There are two mineralized pyroxenite inclusions in unmineralized pyroxenite exposed on a glacially polished rock surface by the side of the Cogburn road. The larger of the blocks is irregular in outline and gossanous on surface. It is fractured and appears to be mineralized along the cross-fractures.

JASON: NI: ZONE #7 (MINFILE 092HNW076)

Giant Explorations Limited located small amounts of sulphide in pyroxenite in diorite south of Cogburn Creek and west of Settler Creek (Figure 4) and, in 1972, extended its exploration into what is now known as the Jason area (Gonzales and Clarke, 1972). The company identified and studied an extensive area of near-continuous outcrop of low-grade mineralized pyroxenite along the bed of a north-flowing tributary of Cogburn Creek. It collected channel samples and estimated a grade of 0.03% Ni and 0.02% Cu over 150 metres. The company drilled two short diamond-drill holes for an aggregate depth of 100 metres. One was collared half way up the creek and the other was sited along the access road, near the foot of the main outcrop section. The results are not available (Berg and Clarke, 1972).

The hornblende diorite west of Settler Creek contains numerous small, isolated and large, elongated bodies of hornblende pyroxenite cumulate that is similar in composition and texture to that found east of the creek. The largest of the known bodies underlies a north-flowing creek and its lateral extent is unknown. At this locality, massive to partially deformed hornblende pyroxenite contains intermittent, spotty, sulphide mineralization over a distance of approximately 250 metres. The sulphide appears to be most abundant in rocks that have knobby appearance, possibly indicating early brecciation and recementation of the cumulate. The sulphide is composed of lacy, interstitial crystals of pyrrhotite with traces of pentlandite and chalcopyrite. Sample RHP01-007 is a coarse-grained hornblende pyroxenite composed of relatively small (2-4 mm) crystals of pyroxene that are locally, poikilitically, enclosed in large (20-30 mm) hornblende crystals. The sulphide occurs as rare, scattered blebs in the matrix surrounding the large hornblende crystals. There is no olivine in the rock, but some of the fresh, barren pyroxenites in the creek bed (RHP01-003) do contain small amounts of early-formed, cumulus olivine. Samples RHP01-025; -026; -027 and -028 are float samples collected approximately 1.0 kilometre to the west of the mineralized creek bed (Figure 4). They are texturally similar, but richer in sulphide. In these samples, the matrix pyroxenes are locally recrystallized. They are more ragged and altered and show partial to near complete replacement by the interstitial hornblende. Sample RHP01-027 is almost completely composed of large (10-20 mm), irregular-shaped, poikilitic hornblende crystals. In this sample, there is very little pyroxene remaining in the matrix.

WHOLE-ROCK GEOCHEMISTRY

A total of 27 rock samples from Giant Mascot and 35 samples from the Cogburn Creek area were selected as being representative of the principal ultramafic and mafic rock types found at the two localities. The samples were crushed in a hardened-steel jaw crusher and reduced to a fine powder in a tungsten carbide swingmill. The samples were analyzed for major and minor elements by X-ray fluorescence at the Cominco Research Laboratory, Vancouver. Accuracy and precision were monitored by international standards included in the run. The analytical results for both areas are listed in Table 2. The samples are grouped by lithology as determined by visual estimate of modal abundance, either in hand specimen or thin section. Thirteen samples (RHP01-007, -025, -026, -027, -028, -049, -050, -080, -088, -089, -105, -109 and -119) contain an appreciable amount of sulphur, and the ferrous iron content of the rock was reduced by the amount calculated to be present in sulphide prior to calculation of CIPW norms.

TABLE 2
WHOLE ROCK MAJOR ELEMENT ANALYSES OF THE GIANT MASCOT & COGBURN CREEK AREA

	Elements			SiO_2	TiO_2	Al_2O_3	Fe_2O_3	FeO	MnO	MgO	CaO	Na_2O	K_2O	P_2O_5	Ba*	LOI	SUM	Rb	Sr	Y	Zr	Nb
	Units			%	%	%	%	%	%	%	%	%	%	%	%	%	%	ppm	ppm	ppm	ppm	ppm
	Method			XRF1	XRF1	XRF1	XRF1	TIT	XRF1	XRF1	XRF1	XRF1	XRF1	XRF1	XRF1	FUS	CAL	XRF2	XRF2	XRF2	XRF2	XRF2
	Lab			COM	COM	COM	COM	COM	COM	COM	COM	COM	COM	COM	COM	COM	COM	COM	COM	COM	COM	COM
ID	Sample	Easting	Northing																			
Giant Mascot Area																						
Diorites																						
	RHP01-073	609335	5481185	55.75	0.23	21.60	1.05	2.71	0.07	3.94	7.90	4.63	0.40	0.02	0.03	0.72	99.36	12	697	9	29	10
	RHP01-082	607840	5480406	57.68	0.66	17.90	1.07	5.86	0.14	4.17	7.78	3.50	0.14	0.11	0.02	-0.09	99.60	5	439	13	31	11
	RHP01-102	608924	5480737	55.34	0.76	18.17	0.57	5.95	0.12	4.76	8.18	3.90	0.20	0.15	0.02	0.64	99.43	5	541	15	58	10
	RHP01-112	608958	5480732	59.34	0.60	16.76	1.70	4.55	0.12	4.38	7.09	3.74	0.30	0.10	0.03	0.58	99.80	7	443	17	62	9
	RHP01-114	608860	5480647	52.58	0.68	19.50	1.10	6.22	0.14	4.98	8.10	4.15	0.12	0.14	0.01	0.93	99.35	7	556	11	23	9
Pyroxenites																						
	RHP01-072	609136	5481256	52.31	0.27	2.76	1.61	6.52	0.17	21.17	12.46	0.31	0.01	0.01	0.01	1.02	99.36	6	29	7	19	9
	RHP01-084	607939	5480502	52.45	0.28	2.71	1.22	5.61	0.15	20.84	14.02	0.33	0.01	0.01	0.01	1.05	99.32	<3	45	3	16	10
	RHP01-088*	606600	5480600	37.20	0.17	1.92	5.50	21.20	0.18	18.62	3.21	0.20	0.01	0.01	0.01	5.57	96.16	<3	12	<3	15	7
	RHP01-089*	606600	5480600	44.29	0.18	2.63	1.96	13.01	0.15	29.62	2.93	0.31	0.02	0.01	0.01	1.79	98.36	3	43	8	17	10
	RHP01-096	608356	5480618	53.09	0.18	2.30	1.81	9.62	0.18	27.88	2.80	0.12	0.01	0.01	0.01	0.37	99.46	3	12	6	17	8
	RHP01-100	608577	5480669	48.93	0.23	2.31	2.05	9.00	0.17	28.10	6.88	0.21	0.01	0.01	0.01	0.30	99.22	5	25	8	14	9
	RHP01-101	608716	5480672	52.84	0.23	3.04	2.31	6.85	0.15	24.40	4.42	0.33	0.02	0.01	0.01	3.61	98.99	3	39	8	18	9
	RHP01-109*	608550	5480160	48.77	0.33	3.90	2.52	12.98	0.15	23.59	2.29	0.46	0.15	0.01	0.01	1.69	98.30	<3	47	<3	18	8
	RHP01-110	608973	5480816	49.29	0.70	5.67	1.22	7.01	0.15	17.30	14.92	0.98	0.09	0.01	0.01	1.19	99.33	6	77	13	21	8
	RHP01-116	608770	5480623	52.00	0.37	4.07	1.16	8.41	0.18	21.59	9.78	0.46	0.05	0.01	0.01	0.67	99.70	4	56	6	19	7
	RHP01-119*	608632	5480624	46.79	0.18	2.14	3.05	11.89	0.17	26.39	4.86	0.12	0.01	0.01	0.01	1.39	98.34	<3	17	<3	17	7
	RHP01-074	609105	5481071	52.29	0.33	3.43	1.24	6.95	0.17	20.52	12.81	0.37	0.03	0.01	0.01	0.47	99.41	4	36	12	20	8
Peridotites																						
	RHP01-085	608137	5480523	39.00	0.05	0.87	3.43	9.73	0.15	41.79	1.02	0.10	0.01	0.01	0.01	1.52	98.78	<3	23	<3	16	6
	RHP01-087	608146	5480554	43.29	0.14	1.62	3.02	7.16	0.14	31.90	7.38	0.25	0.03	0.01	0.01	3.28	99.03	3	37	5	16	8
	RHP01-094	608226	5480592	40.33	0.07	1.16	2.45	9.71	0.15	42.29	1.48	0.15	0.01	0.01	0.01	0.23	99.14	3	26	3	17	9
	RHP01-099	608547	5480652	39.22	0.10	1.09	2.93	12.10	0.18	39.25	2.32	0.11	0.01	0.01	0.01	0.30	98.98	<3	14	<3	14	8
	RHP01-080*	607785	5480176	38.11	0.23	3.18	2.80	12.82	0.12	32.20	1.94	0.50	0.07	0.02	0.01	4.15	97.58	<3	62	<3	22	8
	RHP01-105*	608550	5480160	38.47	0.23	2.72	3.67	12.60	0.15	32.38	1.58	0.34	0.03	0.02	0.01	5.42	99.03	<3	41	4	21	8
Hornblendites																						
	RHP01-083	607840	5480406	45.22	1.33	10.92	3.33	6.80	0.14	15.93	11.76	1.90	0.18	0.01	0.01	1.44	99.73	7	168	14	23	11
	RHP01-103	608938	5480779	41.88	2.15	14.28	2.49	9.12	0.12	12.97	11.22	2.38	0.30	0.01	0.01	1.71	99.66	5	245	21	31	9
	RHP01-113	608958	5480732	42.54	1.77	16.26	1.75	8.03	0.10	11.89	11.84	2.49	0.25	0.01	0.01	1.61	99.45	5	414	19	29	9
Dikes																						
	RHP01-097	608356	5480618	45.74	1.49	10.30	3.38	7.39	0.15	17.54	9.71	1.77	0.28	0.01	0.01	1.00	99.60	5	183	22	31	10
		NAD	1983																			

	Elements			SiO_2	TiO_2	Al_2O_3	Fe_2O_3	FeO	MnO	MgO	CaO	Na_2O	K_2O	P_2O_5	Ba*	LOI	SUM	Rb	Sr	Y	Zr	Nb
	Units			%	%	%	%	%	%	%	%	%	%	%	%	%	%	ppm	ppm	ppm	ppm	ppm
	Method			XRF1	XRF1	XRF1	XRF1	TIT	XRF1	XRF1	XRF1	XRF1	XRF1	XRF1	XRF1	FUS	CAL	XRF2	XRF2	XRF2	XRF2	XRF2
	Lab			COM	COM	COM	COM	FeO	COM	COM	COM	COM	COM	COM	COM	COM	COM	COM	COM	COM	COM	COM
ID	Sample	Easting	Northing																			
Cogburn Area																						
Diorites																						
	RHP 01-001	594953	5489862	54.20	1.07	19.90	2.44	4.63	0.10	3.31	8.43	4.11	0.25	0.21	0.03	0.49	99.69	6	882	16	52	10
	RHP 01-008	595044	5490074	54.16	1.04	22.14	0.98	2.49	0.07	3.27	7.84	5.73	0.28	0.28	0.03	1.07	99.66	5	1453	12	90	11
	RHP 01-012	594965	5490145	48.33	1.27	21.40	2.60	5.10	0.09	4.76	10.64	3.77	0.18	0.18	0.01	0.88	99.78	8	1074	16	44	11
	RHP 01-016	595980	5490110	48.08	0.89	17.98	0.56	7.94	0.11	8.25	10.14	2.36	0.46	0.02	0.02	1.37	99.07	14	595	14	49	8
	RHP 01-040	597440	5490800	45.36	1.01	21.73	1.64	6.25	0.12	7.36	11.71	2.08	0.20	0.05	0.01	1.58	99.80	9	926	12	28	8
	RHP 01-053	595359	5490675	53.02	0.88	18.20	0.48	6.92	0.11	6.42	7.88	3.19	0.28	0.15	0.02	1.00	99.33	9	643	11	40	11

Table 2 continued

Feldspathic Pyroxenites																						
	RHP 01-003	594987	5489900	43.72	0.43	4.46	2.37	10.69	0.18	28.01	6.13	0.73	0.11	0.02	0.01	1.14	99.19	6	115	10	23	10
	RHP 01-006	595035	5490009	49.27	0.44	6.01	1.94	8.84	0.18	20.37	8.02	0.89	0.15	0.01	0.01	1.79	98.91	5	143	9	27	10
	RHP 01-007	595048	5490069	48.79	0.77	6.96	2.45	8.80	0.18	20.32	7.69	1.09	0.20	0.03	0.01	0.93	99.20	5	162	13	30	9
	RHP 01-025	594129	5489765	47.93	0.62	5.61	3.21	10.21	0.23	22.10	6.38	0.81	0.14	0.03	0.01	0.64	99.06	11	78	13	33	9
	RHP 01-026	594129	5489765	46.56	0.50	5.34	2.62	8.49	0.18	24.36	8.42	0.86	0.31	0.07	0.02	0.57	99.25	10	112	13	48	9
	RHP 01-027	594129	5489765	47.61	0.87	6.86	2.84	8.79	0.18	21.18	8.02	1.04	0.15	0.01	0.01	0.68	99.22	8	115	13	31	9
	RHP 01-028	594129	5489765	48.02	1.03	5.28	3.25	9.72	0.18	21.03	8.42	0.82	0.11	0.02	0.01	0.70	99.68	<3	95	16	32	10
	RHP 01-017	595955	5490114	50.49	0.68	5.73	0.44	12.62	0.20	17.04	7.59	0.85	0.33	0.01	0.01	1.97	99.37	14	65	22	43	8
	RHP 01-021	596040	5490205	48.75	0.43	18.84	0.35	6.11	0.11	8.84	11.30	1.88	0.33	0.01	0.01	1.80	99.45	15	610	11	34	10
	RHP 01-030	596274	5490412	47.74	0.54	18.31	0.11	9.15	0.15	9.53	10.10	1.50	0.09	0.05	0.01	1.14	99.44	4	603	12	22	10
	RHP 01-034	598407	5491923	51.63	0.40	9.51	1.29	9.60	0.20	16.79	8.25	1.11	0.05	0.01	0.01	-0.09	99.83	5	282	13	21	8
	RHP 01-036	597160	5490671	50.04	0.54	4.73	1.15	9.35	0.18	18.39	12.26	0.41	0.02	0.01	0.01	0.92	99.06	12	82	11	23	10
	RHP 01-038	597145	5490665	50.06	0.40	2.49	1.50	13.02	0.23	21.94	7.51	0.18	0.01	0.01	0.01	0.49	99.30	4	12	8	22	10
	RHP 01-039	597143	5490680	45.04	0.56	3.82	1.74	10.13	0.17	27.18	8.18	0.44	0.11	0.03	0.01	0.34	98.88	6	72	10	36	9
	RHP 01-043	597596	5490925	49.43	1.04	17.30	2.62	6.30	0.15	7.61	10.22	2.75	0.07	0.20	0.01	0.82	99.23	<3	716	13	14	9
	RHP 01-044	597583	5490900	50.43	1.08	17.34	0.29	9.66	0.15	8.30	8.13	2.67	0.07	0.12	0.01	0.31	99.64	4	572	12	29	10
	RHP 01-045	597600	5490873	47.04	1.12	13.15	1.16	9.47	0.17	13.02	9.90	1.49	0.15	0.02	0.01	1.69	99.45	6	350	21	23	10
	RHP 01-049*	597481	5491349	47.15	0.33	2.32	2.60	17.40	0.23	20.90	4.73	0.12	0.01	0.01	0.01	1.40	99.15	<3	10	<3	16	7
	RHP 01-050*	597481	5491349	48.54	0.28	2.27	3.38	16.08	0.25	22.88	2.74	0.05	0.01	0.01	0.01	1.51	99.80	3	4	<3	16	8
	RHP 01-056	597399	5491372	48.41	1.59	19.48	3.07	6.40	0.10	5.69	10.44	2.85	0.15	0.01	0.01	0.70	99.62	9	864	8	16	9
	RHP 01-058	597484	5491357	50.72	0.99	16.35	1.28	7.39	0.14	9.39	9.57	2.42	0.05	0.01	0.01	0.37	99.52	<3	621	6	21	9
	RHP01-030rep			47.93	0.54	18.46	0.17	9.04	0.15	9.46	10.22	1.49	0.09	0.05	0.01	1.19	98.91	<3	592	11	20	9
Hornblendites																						
	RHP 01-015	594210	5490150	48.06	0.91	19.76	2.26	5.19	0.10	6.69	11.23	3.22	0.20	0.09	0.01	1.19	99.49	9	715	15	41	9
	RHP 01-018	595955	5490114	49.43	0.87	11.14	0.83	9.23	0.15	12.84	9.55	1.83	0.57	0.14	0.02	1.32	98.95	15	243	19	50	10
	RHP 01-037	597113	5490663	47.81	1.49	10.52	1.20	8.29	0.12	14.17	11.61	1.47	0.28	0.01	0.01	1.46	99.37	7	189	21	36	10
	RHP 01-052	593995	5490477	47.65	1.05	8.36	2.93	8.61	0.20	14.76	11.42	1.30	0.18	0.07	0.01	1.73	99.23	3	116	19	33	17
Dikes																						
	RHP 01-009	595043	5490089	52.06	0.93	19.63	1.43	5.42	0.10	4.63	8.52	4.71	0.25	0.18	0.02	0.77	99.26	8	727	20	82	10
	RHP 01-010	595045	5490122	57.88	0.81	16.53	1.91	3.66	0.09	2.73	5.53	4.11	1.91	0.18	0.08	3.16	98.99	41	491	27	156	14
	RHP 01-023	596200	5490359	54.06	0.81	14.10	0.84	6.56	0.12	8.75	8.42	3.07	0.33	0.11	0.02	1.38	99.31	13	450	17	66	14
		NAD	1983																			
	Elements			SiO_2	TiO_2	Al_2O_3	Fe_2O_3	FeO	MnO	MgO	CaO	Na_2O	K_2O	P_2O_5	Ba*	LOI	SUM	Rb	Sr	Y	Zr	Nb
	Units			%	%	%	%	%	%	%	%	%	%	%	%	%	%	ppm	ppm	ppm	ppm	ppm
	Method			XRF1	XRF1	XRF1	XRF1	TIT	XRF1	XRF1	XRF1	XRF1	XRF1	XRF1	XRF1	FUS	CAL	XRF2	XRF2	XRF2	XRF2	XRF2
	Lab			COM	COM	COM	COM	FeO	COM	COM	COM	COM	COM	COM	COM	COM	COM	COM	COM	COM	COM	COM
ID	Sample	Easting	Northing																			
	RHP 01-033	596889	5490724	57.06	1.13	16.37	1.47	5.99	0.14	2.29	3.34	4.92	1.61	0.31	0.07	4.23	99.60	35	399	25	141	13
	RHP 01-049*	Total FeO: Value used for CIPW-Norms reduced by % taken up by sulphide.																				
Q/C																						
56054	RHP01-101			52.84	0.23	3.04	2.31	6.85	0.15	24.4	4.42	0.33	0.02	0.01	0.01	3.61	98.99	3	39	8	18	9
56060	RHP01-101rep			52.97	0.25	3.14	2.3	6.82	0.15	24.32	4.53	0.38	0.03	0.01	0.01	3.52	99.19	4	39	5	19	11
	% Difference			0.2	8.3	3.2	0.4	0.4	0.0	0.3	2.5	14.1	40.0	0.0	0.0	2.5	0.2	28.6	0.0	46.2	5.4	20.0
56090	RHP01-030			47.74	0.54	18.31	0.11	9.15	0.15	9.53	10.1	1.5	0.09	0.05	0.01	1.14	99.44	4	603	12	22	10
56099	RHP01-030rep			47.93	0.54	18.46	0.17	9.04	0.15	9.46	10.22	1.49	0.09	0.05	0.01	1.19	99.81	-3	592	11	20	9
	% Difference			0.4	0.0	0.8	42.9	1.2	0.0	0.7	1.2	0.7	0.0	0.0	0.0	4.3	0.4	1400.0	1.8	8.7	9.5	10.5
56080	Std. MRG1			38.97	3.75	8.39	8.09	8.96	0.15	13.42	14.72	0.74	0.15	0.05	0.01	1.3	99.7	9	242	11	96	17
CANMET	MRG-1			39.32	3.69	8.5	8.63	8.26	0.17	13.49	14.77	0.71	0.18	0.06	0.01	0.98	100.1	8.0	260.0	16.0	105.0	20.0
	% Difference			0.9	1.6	1.3	6.5	8.1	12.5	0.5	0.3	4.1	18.2	18.2	0.0	28.1		11.8	7.2	37.0	9.0	16.2
56052	Std. SY4			49.84	0.28	20.54	3.11	2.75	0.1	0.55	7.98	7.11	1.63	0.11	0.03	4.86	99.2	51	1194	116	513	14
CANMET	Std SY 4			49.9	0.287	20.69	2.86	3.45	0.108	0.54	8.05	7.1	1.66	0.131	0.034	4.56		55.0	1191.0	119.0	517.0	13.0
	% Difference			0.1	2.5	0.7	8.4	22.6	7.7	1.8	0.9	0.1	1.8	17.4	12.5	6.4		7.5	0.3	2.6	0.8	7.4

NOTES:

W-C mill grinding @ GSB

XRF1 = Fused Disc - X-ray fluorescence

Ba* = Fused disc analysis for XRF calibration. Values should be used with CAUTION.

COM = Cominco Research Labs

FUS = Loss on ignition @ 1100°C

SUM = Sum of oxides

CAL = Calculated sum

% Difference = ABS ((x1-x2)/(x1+x2)/2)x100

XRF2 = Pressed pellet - X-ray fluorescence

Figures 5a and b show the distinctive chemical and mineralogical trends shown by the two cumulate bodies. The Giant Mascot cumulate contains relatively constant feldspar content and shows significant enrichment towards clinopyroxene. The Cogburn cumulate shows weaker enrichment in clinopyroxene and a strong trend towards feldspar enrichment.

The Giant Mascot cumulates have their compositions controlled by the modal proportions of the principal cumulus phases (olivine, orthopyroxene and clinopyroxene) and the amount of inter-cumulus feldspar and/or hornblende in the rock. Figures 5a and b show that the pyroxenites contain between 7% and 20% normative feldspar; however their modal contents appear to be appreciably lower. Inter-cumulus feldspar is found in the fresh pyroxenites at the east end of the ultramafic body (Figure 2) but it is noticeably absent from the hornblende-rich pyroxenites found further west and round the margin of the body. Its position as a late phase in the rock appears to be taken up by hornblende.

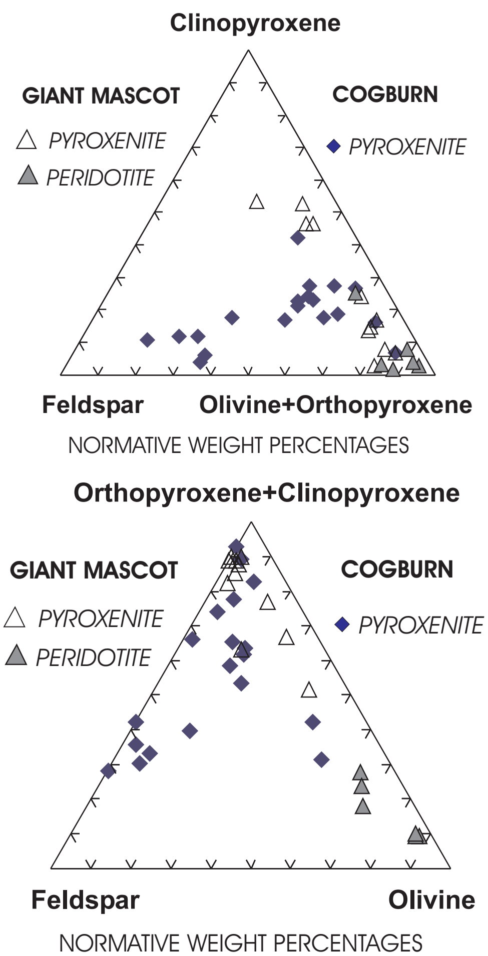

Figure 5. CIPW-normative compositions (wt.%) of peridotite and pyroxenite from the Giant Mascot (closed and open circles) and Cogburn area (diamond) ultramafic to mafic bodies. Figure 5a shows the relationship between feldspar, clinopyroxene and olivine plus orthopyroxene. Figure 5b shows the relationship between feldspar, orthopyroxene plus clinopyroxene and olivine.

The Cogburn cumulate compositions are similarly related to the modal proportions of the principal cumulate and inter-cumulus phases. However, at this locality, the rocks appear to be relatively deficient in modal olivine and enriched in pyroxene, feldspar and inter-cumulus and secondary amphibole. Hornblende is present in large amounts near diorite contacts but is relatively uncommon in the core of the body, north of Cogburn Creek. Figures 5a and b show that most of the Cogburn cumulate contains small amounts of normative olivine; however several samples from the mineralized areas south of the creek contain up to 57% of olivine in their norm. Sample RHP01-003, which contains 50% normative olivine is, as noted above, a fresh unaltered pyroxenite, however the others, including RHP01-026 (57%), RHP01-027 (20%) and RHP01-007 (15%) are hornblende pyroxenites with little or no olivine remaining. The Cogburn cumulates contain between 7% and 66% normative feldspar, however up to 25% may be taken up as hornblende. Most of the "feldspathic pyroxenites" can be classified as olivine gabbro or gabbro.

The plutonic rocks that envelope the Giant Mascot and Cogburn Creek cumulate bodies are mapped as belonging to two separate phases of the Spuzzum pluton. Giant Mascot is on the east contact of the main pluton and Cogburn Creek is on the south side of the Hut Creek pluton (Figure 1). In both instances, the plutonic rock is foliated, hornblende-rich diorite. Analytical data, in Table 2 show that there is broad similarity in composition between the diorites found in each locality. The principal difference appears to be a slight increase in titanium content in the Cogburn area.

Richards (1971) analyzed representative samples of the three types of diorite and the tonalite found in the Spuzzum pluton south of Giant Mascot and, despite differences in modal composition, established that the three types of diorite were chemically similar. Figures 6 to 8 show broad chemical similarity between the diorites found at Giant Mascot, Cogburn Creek and those described by Richards (1971). All three sample populations are sub alkaline (Figure 6) and plot as calc-alkaline on a standard AFM diagram (Figure 7). They also have similar alumina contents (Figure 8). The data support previous contentions that the ultramafic to mafic cumulate bodies are enveloped in calc-alkaline, Spuzzum-type diorite (Aho, 1956; McLeod, 1975; Vining, 1977).

LITHOGEOCHEMICAL ASSAYS

A total of 22 mineralized samples from Giant Mascot, and 8 from the Cogburn Creek area were sent to Acme Analytical Laboratories Limited in Vancouver and analyzed for a selection of major and minor elements including sulphur, base and precious metals and platinum and palladium. The rock powders were digested using four acids (HF-HCLO4-HNO3-HCL) to release near-total amounts of most base, precious element and platinum group elements. However, the digestion only produces partial results for chromium and other rock-forming (lithophile) elements. The solutions were analyzed by inductively coupled plasma mass spectrometry (ICP-MS) and emission spectroscopy.

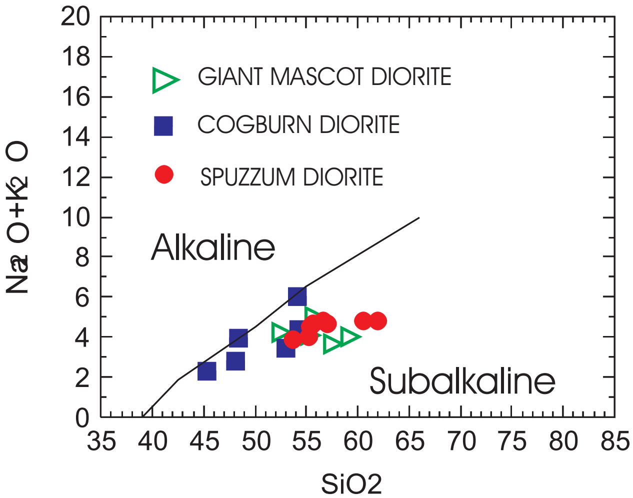

Figure 6. Alkalis versus silica plot (wt.%) of diorite samples from Giant Mascot (triangles); Cogburn (squares), this study and the Spuzzum pluton (circles), (Richards, 1971). The alkaline-subalkaline discrimination line is from Irvine and Baragar, 1971.

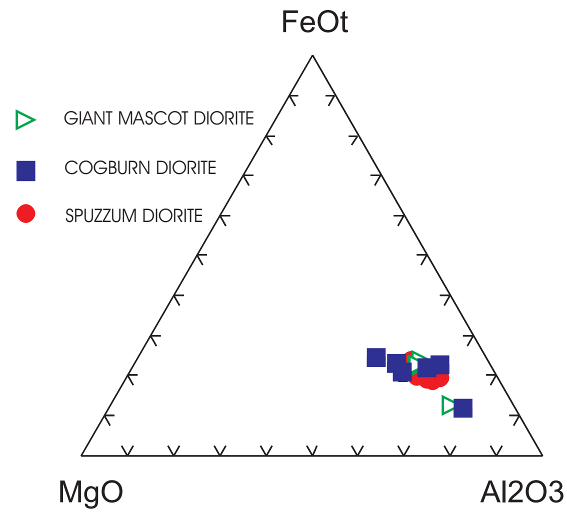

Figure 8. Magnesia-total-iron-alumina plot (wt.%) of diorite samples from Giant Mascot (triangles), Cogburn (squares), this study and the Spuzzum pluton (circles), (Richards, 1971).

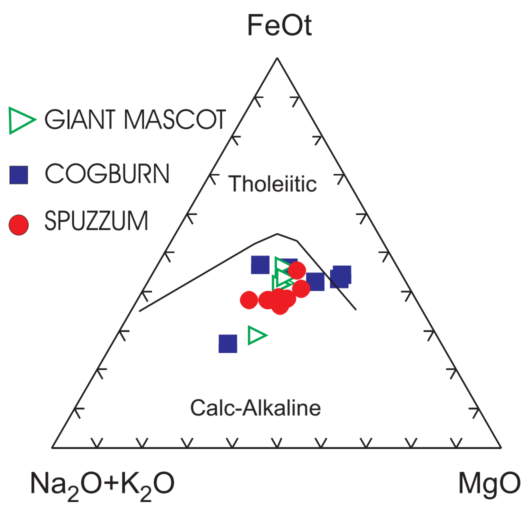

Figure 7. Alkalis-total iron-magnesia plot (wt.%) of diorite samples from Giant Mascot (triangles), Cogburn (squares), this study and the Spuzzum pluton (circles), (Richards, 1971). The calc-alkaline-tholeiitic discrimination line is from Irvine and Baragar (1971).

Gold, platinum and palladium determinations were done by fire-assay with an ICP finish. The results are given in Table 3.

The Giant Mascot samples contain between 1.54% sulphur and 22.65% sulphur (average 8.31% sulphur), depending on the proportions of sulphide and silicate in the rock. Rocks with interstitial sulphide invariably contain less sulphur than those with net-textured or semi-massive sulphide. Although the metal content of the samples might be expected to increase with increase in sulphur content, the results show that this is not always the case. There is a general increase in nickel and copper with increase in sulphur; however, the relationship is far from systematic and there is considerable inter-element variability. This is illustrated in Table 4, which lists the samples according to sulphur content. The table shows that the Giant Mascot samples contain between 0.19% and 2.57% nickel (average 1.16 % Ni) and from 0.12% to 4.01% copper (average 0.98 % Cu). The suite includes a few samples that appear to be particularly enriched in one or other element (Sample RHP01-107 is rich in nickel and Sample RHP01-122 is enriched in copper) and it has clearly been affected by remobilization of chalcopyrite. The results are consistent with rock textures that show that chalcopyrite has been mobile and is commonly found in wispy veinlets and larger veins that cause relative enrichment, or depletion, at the scale sampled.

Figure 9 illustrates the distribution of nickel and copper with respect to sulphur. It shows a poorly defined cluster of samples with a Ni/Cu ratio close to that of the global average of the mine (2.6), as determined from an average of the ore-shoots, and a pronounced trend toward copper enrichment. The samples are numbered to allow for correlation with platinum group element data in Tables 4 and 5.

Tables 3 and 4 also show that the samples contain from 3 ppb to 332 ppb gold (average 49.2 ppb Au), from 1.3 ppb to 1142 ppb platinum (average 107.9 ppb Pt) and from 9.6 ppb to 465.9 ppb palladium (average 173 ppb Pd), again with poor correlation between precious metal content and the amount of sulphur or base metal present. There are significant traces of platinum group elements in both sulphide-rich (RHP01-078, 287 ppb Au, 1142.2 ppb Pt, 889 ppb Pd) and sulphide-poor (RHP01-109, 332 ppb Au, 359.1 ppb Pt, 139.8 ppb Pd) rocks. No platinum-group minerals have been reported from the mine and, in common with other deposits, the platinum group elements are probably present either as minor phases, or in solid solution within the sulphide assemblage.

A subset of 14 samples were sent to Activation Laboratories Limited, Ancaster, Ontario, for neutron activation analysis of the platinum group elements (Os, Ir, Ru, Rh, Pt, Pd), gold (Au) and rhenium (Re) using nickel sulphide pre-concentration. The data are presented in Tables 3 and 5.

TABLE 3
LITHOGEOCHEMICAL ANALYSIS OF THE COGBURN CREEK AND GIANT MASCOT AREAS

			wt% (ACME Analytical Labs)									ppm (ACME Analytical Labs)										
Sample	Easting	Northing	Mg	Ti	Al	Na	K	Fe	Ca	P	S*	Mo	Cu	Pb	Zn	Ag	Ni	Co	Mn	As	U	Au
Giant Mascot																						
RHP01-075	607721	5480101	6.43	0.18	1.18	0.14	0.01	26.89	0.94	< .002	16.92	< 2	9000	< 5	74	1.3	14838	883	678	< 5	< 10	< 4
RHP01-076	607721	5480101	4.07	0.06	0.64	0.08	< .01	30.41	2.63	< .002	22.65	< 2	37786	< 5	117	12.1	25523	1076	568	< 5	< 10	< 4
RHP01-077	607721	5480101	16.41	0.13	1.2	0.19	0.02	18.47	1.1	0.002	7.44	< 2	2426	< 5	80	1	13069	527	1238	< 5	< 10	< 4
RHP01-078	607721	5480101	11.94	0.14	2.09	0.4	0.05	17.81	1.77	< .002	10.72	< 2	36019	< 5	135	13.1	18308	419	950	< 5	< 10	< 4
RHP01-080	607785	5480176	20.84	0.15	1.92	0.39	0.09	13	1.53	0.011	2.4	< 2	2448	< 5	84	1	5944	253	1277	< 5	< 10	< 4
RHP01-081	607761	5480141	14.79	0.09	1.15	0.11	0.02	16.7	0.99	< .002	6.63	< 2	1852	< 5	75	< .5	6761	509	1252	< 5	< 10	< 4
RHP01-088	606600	5480600	11.01	0.09	1.05	0.12	0.02	20.05	1.84	< .002	11.84	< 2	6729	< 5	106	1.5	14733	729	1477	< 5	< 10	< 4
RHP01-089	606600	5480600	18.22	0.11	1.5	0.23	0.04	12.43	2.16	0.003	2.25	< 2	2412	< 5	99	< .5	2429	159	1411	< 5	< 10	< 4
RHP01-090	606600	5480600	7.93	0.11	1.04	0.13	0.01	21.55	4.7	< .002	14.38	< 2	8547	< 5	78	1.9	21986	918	937	7	< 10	< 4
RHP01-091	606600	5480600	16.08	0.09	1.29	0.25	0.05	17.37	1.99	0.006	6.98	< 2	9469	< 5	99	1.4	8261	412	1316	< 5	< 10	< 4
RHP01-104	608550	5480160	11.28	0.17	1.17	0.11	0.01	18.15	3.55	< .002	8.19	13	3210	< 5	91	0.5	10835	489	1352	< 5	< 10	< 4
RHP01-105	608550	5480160	19.45	0.15	1.45	0.24	0.05	12.74	1.15	0.005	1.54	< 2	1339	< 5	96	< .5	1905	186	1249	< 5	< 10	< 4
RHP01-106	608550	5480160	19.98	0.07	1.12	0.25	0.04	14.11	2.14	0.011	3.12	< 2	1172	< 5	54	< .5	3809	338	1217	< 5	< 10	< 4
RHP01-107	608550	5480160	15.7	0.02	0.21	0.03	0.01	23.54	0.21	< .002	13.44	< 2	3789	< 5	73	1.2	22488	1006	1060	14	< 10	< 4
RHP01-108	608550	5480160	12.24	0.18	1.31	0.2	0.03	13.93	3.38	< .002	5.61	< 2	16872	< 5	107	3.7	8470	300	1160	< 5	< 10	< 4
RHP01-109	608550	5480160	14.71	0.21	2.2	0.37	0.15	12.31	1.75	0.005	2.52	< 2	5501	12	100	6	3859	181	1396	< 5	< 10	< 4
RHP01-117	608632	5480624	10.41	0.05	0.5	0.06	< .01	23.58	2.06	< .002	15.51	< 2	7233	< 5	70	1.6	25705	1099	822	7	< 10	< 4
RHP01-118	608632	5480624	10.73	0.09	0.87	0.11	< .01	19.14	3.53	< .002	12.41	< 2	7332	< 5	66	1.9	16983	804	840	< 5	< 10	< 4
RHP01-119	608632	5480624	17.23	0.1	1.13	0.08	< .01	12.19	2.42	< .002	2.68	< 2	1990	< 5	85	< .5	5832	256	1456	< 5	< 10	< 4
RHP01-120	608632	5480624	16.69	0.08	0.93	0.09	0.01	15.6	1.47	< .002	5.55	< 2	7690	< 5	90	1.6	9901	412	1272	< 5	< 10	< 4
RHP01-121	608632	5480624	14.21	0.16	1.51	0.2	0.01	11.37	7.02	< .002	3.09	< 2	3676	< 5	62	0.7	6398	276	1209	< 5	< 10	< 4
RHP01-122	608632	5480624	18.67	0.03	0.34	0.04	< .01	18.42	0.77	< .002	8.21	< 2	40106	< 5	163	7.8	7945	374	1085	< 5	< 10	< 4
Cogburn Creek																						
RHP01-007	595048	5490069	12.44	0.48	4.06	0.87	0.2	8.96	5.61	0.015	0.4	< 2	175	< 5	83	< .5	270	64	1450	< 5	< 10	< 4
RHP01-025	594129	5489765	14.07	0.38	3.26	0.64	0.15	11.08	4.47	0.014	0.25	< 2	77	< 5	136	< .5	396	74	2030	< 5	< 10	< 4
RHP01-026	594129	5489765	14.99	0.29	2.96	0.66	0.31	8.98	5.71	0.039	0.09	< 2	56	< 5	77	< .5	382	75	1489	< 5	< 10	< 4
RHP01-027	594129	5489765	12.71	0.51	3.92	0.81	0.16	9.12	5.61	0.008	0.29	< 2	164	< 5	91	< .5	397	73	1476	< 5	< 10	< 4
RHP01-028	594129	5489765	12.69	0.58	2.92	0.61	0.12	9.86	5.7	0.01	0.13	< 2	60	11	139	< .5	235	73	1465	< 5	< 10	< 4
RHP01-039	597143	5490680	16.58	0.28	1.73	0.18	0.07	12.21	3.24	0.01	1.89	< 2	2325	< 5	101	0.6	2159	166	1437	< 5	< 10	< 4
RHP01-049	597481	5491349	12.84	0.2	1.33	0.1	0.01	15.17	3.5	< .002	3.06	< 2	1465	< 5	127	< .5	1731	199	2001	< 5	< 10	< 4
RHP01-050	597481	5491349	14.13	0.18	1.31	0.06	< .01	14.35	2.13	< .002	2.11	< 2	1545	< 5	142	< .5	1184	157	2175	< 5	< 10	< 4
RHP01-050REP	597481	5491349	13.75	0.18	1.28	0.06	0.01	14.29	2.15	< .002	2.41	< 2	1408	< 5	143	< .5	1332	175	2086	< 5	< 10	< 4
Q/C																						
		Std. WMG1	6.97	0.38	4.83	0.12	0.08	12.98	10.16	0.048	3.39	2	4942	8	100	3.1	2302	166	1209	-5	-10	-4
		CANMET Value	7.15	0.41	4.4	0.13	0.08	11.89	10.7		3.7	1.4	5900	15	110	2.7	2700	200	1170	7	0.65	0.1
		RHP01-050	14.13	0.18	1.31	0.06	-0.01	14.35	2.13	-0.002	2.11	-2	1545	-5	142	-0.5	1184	157	2175	-5	-10	-4
		RHP01-050REP	13.75	0.18	1.28	0.06	0.01	14.29	2.15	-0.002	2.41	-2	1408	-5	143	-0.5	1332	175	2086	-5	-10	-4

Table 3 continued

	ppm (ACME Analytical Labs)																ppb **[ACME]			ppb ***[Activation Labs]							
Sample	Th	Sr	Cd	Sb	Bi	V	La	Cr	Ba	W	Zr	Sn	Y	Nb	Be	Sc	Au	Pt	Pd	Os	Ir	Ru	Rh	Pt***	Pd	Au	Re
Giant Mascot																											
RHP01-075	2	25	< .4	< 5	< 5	114	< 2	3342	11	< 4	< 2	3	< 2	3	< 1	8	3	8.2	31.2								
RHP01-076	2	15	< .4	< 5	< 5	127	< 2	543	4	< 4	< 2	4	2	3	< 1	20	4	5.7	141.6	8	11	10	14.7	66	166	11	130
RHP01-077	< 2	30	1.1	< 5	< 5	91	< 2	1116	12	< 4	3	< 2	2	< 2	< 1	12	4	4.8	88.8	5	5.1	11	7.4	-5	98	6.3	23
RHP01-078	2	61	1.3	< 5	< 5	63	< 2	921	16	< 4	6	2	3	< 2	< 1	10	287	1142.2	889	137	120	180	100	1140	894	280	34
RHP01-080	< 2	96	< .4	< 5	< 5	63	< 2	1841	44	< 4	7	< 2	3	< 2	< 1	8	42	92.9	161.4	3	4.2	-5	5.2	156	182	46	9
RHP01-081	< 2	20	0.7	< 5	< 5	85	< 2	2723	7	< 4	< 2	< 2	< 2	< 2	< 1	14	5	2	19.4	-2	0.5	-5	1.2	-5	26	12	24
RHP01-088	< 2	22	0.8	< 5	< 5	122	< 2	910	15	< 4	< 2	4	< 2	< 2	< 1	21	35	126.3	186.4	5	8.4	10	39.4	110	189	38	21
RHP01-089	< 2	53	< .4	< 5	< 5	163	< 2	879	27	< 4	6	2	2	< 2	< 1	15	8	24.6	34								
RHP01-090	< 2	23	< .4	< 5	< 5	162	< 2	812	7	< 4	< 2	4	2	3	< 1	30	74	1.3	237.1								
RHP01-091	< 2	64	0.9	< 5	< 5	89	< 2	1322	41	< 4	6	4	2	< 2	< 1	13	45	15	44.4								
RHP01-104	< 2	16	1.1	< 5	< 5	434	< 2	2123	5	< 4	4	4	6	2	< 1	31	20	35.6	465.9	10	9	11	9.7	42	413	47	65
RHP01-105	< 2	52	< .4	< 5	< 5	93	< 2	1438	24	< 4	4	< 2	2	< 2	< 1	8	3	9.6	9.6	-2	0.3	-5	0.4	8	9	3.6	-5
RHP01-106	< 2	58	0.5	< 5	< 5	51	< 2	1386	23	< 4	5	3	2	2	< 1	10	5	15.8	27								
RHP01-107	< 2	9	1.3	< 5	< 5	22	< 2	737	5	< 4	< 2	< 2	< 2	3	< 1	3	3	110.4	244.2								
RHP01-108	< 2	82	1.1	< 5	< 5	114	< 2	1233	16	< 4	7	2	4	< 2	< 1	20	24	196.4	149.8	8	12	11	12.7	88	150	24	7
RHP01-109	< 2	61	2.8	< 5	< 5	407	< 2	1442	107	< 4	7	2	4	< 2	< 1	19	332	359.1	139.8	3	0.3	-5	0.4	213	141	300	-5
RHP01-117	< 2	15	< .4	< 5	< 5	58	< 2	835	5	< 4	< 2	4	< 2	3	< 1	13	4	10.1	255.1								
RHP01-118	< 2	20	1.8	< 5	< 5	103	< 2	1140	4	< 4	< 2	4	2	< 2	< 1	24	11	89.2	316.8	18	25	40	31.9	100	285	13	48
RHP01-119	< 2	15	0.5	< 5	< 5	107	< 2	1631	5	< 4	< 2	2	< 2	2	< 1	21	7	34.9	73.8	-2	0.8	-5	2.6	38	81	7.1	7
RHP01-120	< 2	19	1.4	< 5	< 5	74	< 2	1741	8	< 4	2	2	< 2	< 2	< 1	14	3	5	116.4								
RHP01-121	< 2	39	0.6	< 5	< 5	205	< 2	2012	6	< 4	4	< 2	4	3	< 1	37	9	79.4	49.9	2	3.3	-5	4.5	82	60	11	15
RHP01-122	< 2	10	1.8	< 5	< 5	21	< 2	874	4	< 4	< 2	< 2	< 2	< 2	< 1	6	154	5.5	130.8	6	9.1	5	11.7	37	135	44	19
Cogburn Creek																											
RHP01-007	< 2	180	< .4	< 5	< 5	264	< 2	890	80	< 4	13	3	7	< 2	< 1	42	< 1	1.1	1								
RHP01-025	< 2	91	< .4	< 5	< 5	193	< 2	1147	76	< 4	21	2	10	2	< 1	31	< 1	1.4	1.6								
RHP01-026	< 2	123	< .4	< 5	< 5	152	2	1102	164	< 4	32	2	7	2	< 1	35	1	2.6	0.7								
RHP01-027	2	129	< .4	< 5	< 5	233	< 2	952	61	< 4	20	< 2	11	3	< 1	37	< 1	2.7	2								
RHP01-028	2	110	< .4	< 5	< 5	280	< 2	772	97	< 4	16	3	11	2	< 1	38	< 1	1	< .5								
RHP01-039	< 2	53	< .4	< 5	< 5	139	< 2	1943	53	< 4	14	5	6	< 2	< 1	23	12	40.7	28.1	2	0.8	-5	0.8	49	31	15	5
RHP01-049	< 2	14	< .4	< 5	< 5	223	< 2	941	5	< 4	5	4	5	< 2	< 1	38	26	8.5	8	-2	0.3	-5	0.3	23	11	24	11
RHP01-050	< 2	9	< .4	< 5	< 5	209	< 2	923	4	< 4	3	4	3	< 2	< 1	33	41	4.2	6								
RHP01-050REP	< 2	9	0.4	< 5	< 5	204	< 2	1014	4	< 4	3	5	3	< 2	< 1	32	21	4.2	6.1								
Q/C																											
	2	38	1.2	6	-5	160	4	582	106	-4	31	4	12	5	-1	25	91	763.5	367.5								
	1.1	41	1.1	1.8		149		770	114	1.3	43	2.2	12	6	0.6	26	110	731	382								
	-2	9	-0.4	-5	-5	209	-2	923	4	-4	3	4	3	-2	-1	33	41	4.2	6								
	-2	9	0.4	-5	-5	204	-2	1014	4	-4	3	5	3	-2	-1	32	21	4.2	6.1								

Notes:

Prep. Sample jaw crushed & steel milled @ GSB. Quartz wash between each sample milled.

Major (%) and Minor (ppm) elements by %; TICP, HF-HCL04-HN03-HCl digestion - ICPES

ACME = ACME Analytical, Vancouver

* Sulphur % by Leco Combustion

**FAIC = Fire assay-ICP finish (15 g sample)

*** Platinum Group Elements by Instrumental Neutron Activation Analysis

TABLE 4
GIANT MASCOT AND COGBURNAREA ROCK AND SULPHIDE DATA

		#		Rock* Cu ppm	*Sulphide*** *Cu%*	Rock Ni ppm	*Sulphide Ni%*	Rock Au ppb	*Sulphide Au ppb*	Rock Pt ppb	*Sulphide Pt ppb*	Rock Pd ppb	*Sulphide Pd ppb*	Rock S %	*Sulphide S%*	*Sulphide Fe%*
GIANT MASCOT																
RHP01-076	BX-SM	1	UA	37786	*6.32*	25523	*4.27*	4	*6.7*	5.7	*9.5*	141.6	*236*	22.65	*37.87*	*51.55*
RHP01-075	NET	2	UA	9000	*2.06*	14838	*3.39*	3	*7*	8.2	*19*	31.2	*71*	16.92	*38.95*	*55.87*
RHP01-117	NET	3	DA	7233	*1.78*	25705	*6.33*	4	*10*	10.1	*24.8*	255.1	*628*	15.51	*38.17*	*53.72*
RHP01-090	SM	4	PE	8547	*2.27*	21966	*5.84*	74	*197*	1.3	*3.5*	237.1	*631*	14.38	*38.19*	*53.7*
RHP01-107	NET	5	MS	3789	*1.08*	22488	*6.4*	3	*8.5*	110.4	*313*	244.2	*694*	13.44	*38.26*	*54.26*
RHP01-118	NET	6	DA	7332	*2.26*	16983	*5.24*	11	*34*	89.2	*275*	316.8	*976*	12.41	*38.3*	*54.2*
RHP01-088	BX-SM	7	PE	6729	*2.18*	14733	*4.75*	35	*113*	126.3	*409*	186.4	*604*	11.84	*38.4*	*54.64*
RHP01-078	NET	8	UA	36019	*12.3*	18308	*6.25*	287	*979*	1142.2	*3895*	889	*3031*	10.72	*36.59*	*44.86*
RHP01-122	BX-NET	9	DA	40106	*17.73*	7945	*3.51*	154	*681*	5.5	*24*	130.8	*578*	8.21	*36.29*	*42.47*
RHP01-077	NET	10	UA	2426	*1.25*	13069	*6.71*	4	*21*	4.8	*24.4*	88.8	*456*	7.44	*38.17*	*53.87*
RHP01-091	NET	11	PE	9469	*5.15*	8261	*4.5*	45	*24.5*	15	*82*	44.4	*242*	6.98	*37.99*	*52.36*
RHP01-104	BX-NET	12	MS	3210	*1.51*	10835	*5.09*	20	*94*	35.6	*167*	465.9	*2190*	6.98	*38.44*	*54.96*
RHP01-081	NET	13	UA	1852	*1.08*	6761	*3.95*	5	*29*	2	*12*	19.4	*113*	6.63	*38.72*	*56.25*
RHP01-108	INT	14	MS	16872	*11.1*	8470	*5.57*	24	*158*	196.4	*1292*	149.8	*986*	5.61	*36.9*	*46.43*
RHP01-120	BX-NET	15	DA	7690	*5.21*	9901	*6.7*	3	*20*	5	*34*	116.4	*788*	5.55	*37.58*	*50.51*
RHP01-106	INT	16	MS	1172	*1.45*	3809	*4.7*	5	*62*	15.8	*195*	27	*333*	3.12	*38.53*	*55.32*
RHP01-121	INT	17	DA	3676	*4.46*	6398	*7.77*	9	*109*	79.4	*964*	49.9	*606*	3.09	*37.51*	*50.26*
RHP01-119	BX-INT	18	DA	1990	*2.8*	5832	*8.2*	7	*98*	34.9	*491*	73.8	*1038*	2.66	*37.68*	*51.32*
RHP01-109	INT	19	MS	5501	*8.14*	3859	*5.71*	332	*4913*	359.1	*5315*	139.8	*2069*	2.52	*37.3*	*48.85*
RHP01-080	INT	20	UA	2448	*3.81*	5944	*9.24*	42	*653*	92.9	*1445*	161.4	*2510*	2.4	*37.32*	*49.63*
RHP01-089	INT	21	PE	2412	*4.09*	2429	*4.13*	8	*25*	24.6	*418*	34	*578*	2.25	*38.24*	*53.54*
RHP01-105	INT	22	MS	1339	*3.33*	1905	*4.73*	3	*89*	9.6	*283*	9.6	*283*	1.54	*38.27*	*53.67*
COGBURN																
RHP01-049	BX-NET	A	#4	1465	*1.86*	1731	*2.2*	26	*331*	8.5	*108*	8	*102*	3.06	*38.94*	*57*
RHP01-050	BX-NET	B	#4	1545	*2.83*	1184	*2.17*	41	*754*	4.2	*77*	6	*110*	2.11	*38.77*	*45.12*
RHP01-039	BX-NET	C	#4	2325	*4.5*	2159	*4.35*	12	*242*	40.4	*820*	28.1	*566*	1.89	*38.1*	*52.85*
RHP01-025***	INT	D	#7	77		396		<1		1.4		1.6		0.4		
RHP01-027***	INT	E	#7	164		397		<1		2.7		2		0.29		
RHP01-028***	INT	F	#7	60		235		<1		1		<0.5		0.13		
RHP01-007***	INT	G	#7	175		270		<1		1.1		1		0.1		
RHP01-026***	INT	H	#7	56		382		1		2.6		0.7		0.09		

*Lithogeochemical analyses, ACME Analytical Laboratories, Vancouver [*see* Table 3].
**Sulphide analyses by calculation as discussed in text.
***Sulphur and metal values judged to be too low to obtain a meaningful sulphide determination.
INT = Interstitial; NET = Net-textured; SM= Semi-Massive; BX = Breccia Cement
MS = Millsite; PE = Pride of Emery; UA = Upper Adit; DA = Dolly Adit
#4 = Cogburn Area #4; #7 = Cogburn Area #7

The results for the two analytical procedures (FAIC and INAA) produced similar results for palladium and gold and broadly similar results for platinum. However, the platinum values show greater variability and there are small differences in a few samples. Sample RHP01-076, -080 and -122 contain more platinum as determined by INAA than by FAIC and RHP01-109 contains less (Table 5).

The INAA data (Table 5) show that most of the Giant Mascot samples contain low but detectable (ppb level) amounts of most of the platinum group elements. Samples RHP01-078 (a sample with copper-rich interstitial sulphide) and RHP01-118 (mesh-textured sulphide veined by chalcopyrite) are particularly enriched in each of the elements. The minor platinum group metals appear to be strongly correlated; when one is enriched they all are. The table lists the samples in order of decreasing sulphur content, and the data show a general decrease in platinum-group-element content with decrease in sulphur. However, the correlation is only strongly evident in rhenium.

These results can be compared with those of Hulbert (2001), who analyzed 8 samples collected from the mine and 8 from McLeod's thesis collection. The former include a spectrum of sample textures, similar to those analyzed in this study. The latter include a more limited range of interstitial sulphide-bearing samples. Average metal contents are listed in Table 5. Hulbert's samples are similar in nickel and copper content to those analyzed in the present study; however, they appear to be slightly richer in most platinum-group elements. McLeod's samples are, with one exception, less well mineralized than those analyzed in this study and, even including the "higher-grade" sample (46A-1), their average platinum palladium and gold values (Table 5) are lower. There are too many "below-detection" determinations to make a meaningful average determination of the lesser abundant platinum group elements, but McLeod's "higher-grade" sample contains significant amounts of each. The rock contains 1.4% Ni, 1.1% Cu, 240

TABLE 5
PLATINUM GROUP ELEMENTS

ID	Os ppb	Ir ppb	Ru ppb	Rh ppb	Pt ppb	*Pt* ppb*	Pd ppb	*Pd* ppb*	Au ppb	*Au* ppb*	Re ppb
GIANT MASCOT											
RHP01-076	8	11	10	14.7	66	*5.7*	166	*141.6*	11	*4*	130
RHP01-118	18	25	40	31.9	100	*89.2*	285	*316.8*	13	*11*	48
RHP01-088	5	8.4	10	39.4	110	*126.3*	189	*186.4*	38	*35*	21
RHP01-078	137	120	180	100	1140	*1142.2*	894	*889*	280	*287*	34
RHP01-122	6	9.1	5	11.7	37	*5.5*	135	*130.8*	44	*154*	19
RHP01-077	5	5.1	11	7.4	-5	*4.8*	98	*88.8*	6.3	*4*	23
RHP01-104	10	9	11	9.7	42	*35.6*	413	*465.9*	47	*20*	65
RHP01-081	-2	0.5	-5	1.2	-5	*2*	26	*19.4*	12	*5*	24
RHP01-108	8	12	11	12.7	88	*196.4*	150	*149.8*	24	*24*	7
RHP01-120	2	3.3	-5	4.5	82	*79.4*	60	*49.9*	11	*9*	15
RHP01-119	-2	0.8	-5	2.6	38	*34.9*	81	*73.8*	7.1	*7*	7
RHP01-109	3	0.3	-5	0.4	213	*359.1*	141	*139.8*	300	*332*	-5
RHP01-080	3	4.2	-5	5.2	156	*92.9*	182	*161.4*	46	*42*	9
RHP01-105	-2	0.3	-5	0.4	8	*9.6*	9	*9.6*	3.6	*3*	-5
Average (1.07% Ni, 1.22% Cu)	14.2	14.9	17.7	17.3	148	*156*	202	*201.6*	60.2	*66.9*	28
Hulbert (2001) (1.99% Ni, 0.65% Cu)	21	22	39	41	193		382		38		44
McLeod** (0.27% Ni, 0.19% Cu)					57		140		35		
COGBURN											
RHP01-049	-2	0.3	-5	0.3	23	*8.5*	11	*8*	24	*26*	11
RHP01-039	2	0.8	-5	0.8	49	*40.7*	31	*28.1*	15	*12*	5

PGE Analyses from Activation Laboratories (see Table 3)
Pt*, Pd* and Au* data from Acme Analytical Laboratories (see Table 3)
**McLeod *in* Hulbert (2001)

ppb Pt, 940 ppb Pd, 220 ppb Au, 46 ppb Rh, 40 ppb Ru, 24 ppb Os, 29 ppb Ir and 13 ppb Re.

Table 6 shows the extent of the correlation between the various elements (excluding iron) found in the sulphides at Giant Mascot. Correlation coefficients for the rocks analyzed in this study show that there is a strong positive correlation between nickel and sulphur (0.94), a moderate correlation between copper and sulphur (0.50) and a weak correlation between most of the platinum group elements (except rhenium (0.87)) and sulphur (0.10 - 0.39). The platinum group elements (excluding rhenium) are very strongly inter-related (>0.85) and, geochemically, appear to have behaved in a similar manner. Nickel and copper are moderately related (0.36), as might be expected from the observed degree of copper remobilization.

In magmatic rocks, where the sulphides have formed from droplets and the mineralogy is limited to a relatively simple sulphide assemblage, it is possible to reduce the affect of silicate dilution by calculating the "normative" content of the sulphide minerals and recasting the data as if the rock was composed entirely of sulphide. This reduces the differential caused by comparing values from sulphide-rich and sulphide-poor samples. It is done in three steps. Sufficient Fe and S are assigned to the available Cu content to form the mineral chalcopyrite ($CuFeS_2$). Sufficient Fe and S are then allotted to the available Ni content to form the mineral Pentlandite ($Fe_{4.5}Ni_{4.5}S_8$). Lastly, sufficient Fe is allocated to the remaining S to form the mineral pyrrhotite (Fe_7S_8). For a magmatic sulphide assemblage, the total Fe content of the sulphide is taken to be the sum of that required for the chalcopyrite, pentlandite and pyrrhotite. This figure can be used to estimate the percentage of the rock composed of sulphide and this, in turn is used to estimate the composition of the bulk sulphide without its silicate gangue.

Table 4 compares the original metal and sulphide values with calculated, silicate-free, figures using data from Table 3. The data provides a useful approach for comparing samples, but the calculated values should be considered with some caution, as the calculation is predicated on having accurate base, precious metal and sulphur determination and sulphides with "ideal" structural formulae. The nickel content of the rock may be slightly elevated if the silicate gangue contained nickel-rich olivine and it contributed to the total. However, given the small amount of nickel Muir (1971) found in olivine (0.13% Ni), it is not likely to be a significant problem and the pentlandite content should not be significantly overestimated. The samples are estimated to contain between 1.08% Cu and 17.73% Cu (average 4.61% Cu); between 3.39% Ni and 9.24% Ni (average 5.59% Ni); between 6.7 ppb Au and 4913 ppb Au (average 379 ppb Au); between 3.5 ppb Pt and 5315 ppb Pt (average 713 ppb Pt) and between 71 ppb Pd and 3031 ppb Pd (average 893 ppb Pd) when considered in bulk-sulphide form (Table 4). The samples are biased towards high-grade and

TABLE 6
GIANT MASCOT CORRELATION COEFFICIENTS

	Os	S	Ir	Cu	Ru	Rh	Pt	Pd	Ni	Au
Re	0.09	0.87	0.13	0.46	0.1	0.15	0	0.23	0.82	-0.16
Au	0.62	-0.11	0.58	0.25	0.6	0.5	0.74	0.6	-0.01	
Ni	0.41	0.94	0.46	0.36	0.43	0.56	0.19	0.48		
Pd	0.92	0.35	0.93	0.45	0.92	0.89	0.86			
Pt	0.97	0.1	0.96	0.47	0.96	0.9				
Rh	0.93	0.39	0.95	0.49	0.94					
Ru	0.99	0.24	1	0.46						
Cu	0.49	0.5	0.52							
Ir	1	0.27								
S	0.22									

do not constitute a statistically meaningful population; however, they suggest that the concentrate produced at the Giant Mascot mine must have contained several tens of parts per billion of gold and a few hundreds of parts per billion of platinum and palladium. It may also have contained a few tens of parts per billion of the other platinum group elements.

Figure 9, relates the amount of platinum group elements and gold to the sulphur content of the rock and the Ni/Cu ratio. There are no clear correlations; however, there is a suggestion that precious metals may be slightly higher in samples that contain large amounts of nickel and copper relative to the amount of sulphur present. This should be the case if platinum group elements favour pentlandite and chalcopyrite over pyrrhotite.

The mineralized samples from Cogburn Creek generally contain far less sulphide and have lower metal contents (Table 3 and 4). They contain between 0.09% sulphur and 2.11% sulphur (average 1.03% S). The low values are partially a function of the style of mineralization. The disseminated to blebby, sulphide in hornblende pyroxenite south of Cogburn Creek (RHP01-007, -025, -026, -027 and -028) is scattered throughout a large volume of rock and produces a noticeable nugget effect. The analytical results for these samples show low sulphur contents (0.09 - 0.29% S) and only trace amounts of nickel (235 - 397 ppm Ni), copper (56 - 175 ppm Cu), platinum (1.0 - 2.7 ppb Pt) and palladium (0.5 - 2.0 ppb Pd). These are background levels that suggest little metal enrichment.

Samples of fracture-controlled mineralization (RHP01-039, -049, -050), found north and south of Cogburn Creek, are richer in sulphur (1.89 - 3.06% S) and base and precious metals. However, none of the analyzed samples included an appreciable amount of chalcopyrite vein material and the analytical data (Table 3 and 4) show the more disseminated and net-textured sulphides contain only relatively minor amounts of nickel (1184 - 2159 ppm Ni) and copper (1465 - 2325 ppm Cu). However, they also contain a significant trace of gold (12 - 41 ppb Au), platinum (4.2 - 40.7 ppb Pt) and palladium (6 - 28.1 ppb Pd). The rocks appear to be more pyrrhotite-rich, for the amount of nickel and copper present, than those at Giant Mascot.

Two samples, RHP01-039 and RHP01-049 were sent to Activation Laboratories with the samples from Giant Mascot. The samples were analyzed for the same suite of elements and the results are shown in Tables 3 and 5. The platinum, palladium and gold values obtained by instrumental neutron activation analysis are similar to those obtained by conventional fire-assay with ICP finish. The Os, Ir and Ru values, obtained by neutron activation analysis are either below, or barely above, detection (Table 5).

DISCUSSION

Regional mapping by Lowes (1972), Monger (1986, 1989) and Ash (2002) show that the ultramafic bodies east of Harrison Lake are found in two distinct geological settings. Most are clearly deformed and metamorphosed slivers or lenses in Cogburn Schist (Lowes, 1972; Troost, 1999; Ash, 2002); however, some, including those at Giant Mascot and Cogburn Creek are less obviously deformed and metamorphosed. They are irregular-shaped, bodies intimately associated with the Spuzzum and Hut Creek diorite plutons and they are in contact with Settler, rather than Cogburn Schist (Gabites, 1985; McLeod, 1985). The principal areas of nickel-copper mineralization are found in the latter.

The present study shows numerous points of similarity between the mineralized bodies at Giant Mascot and Cogburn Creek and one major point of difference. The cumulate at Giant Mascot is far richer in olivine and contains

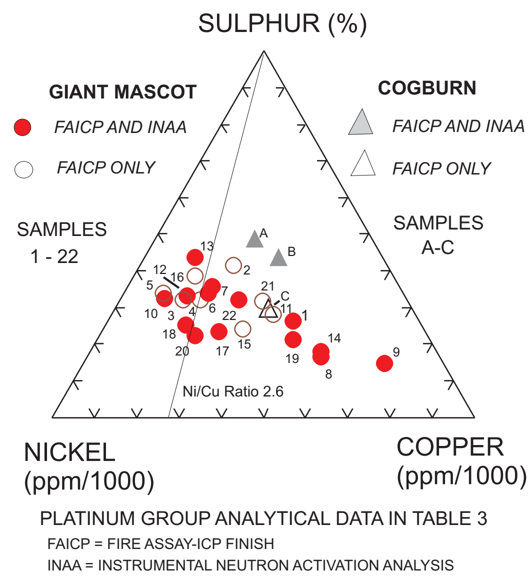

Figure 9. Nickel-sulphur-copper plot (wt.%) of mineralized samples from the Giant Mascot (circles) and Cogburn (triangles) areas. The plot shows the spread of data about the "global" Ni/Cu average of 2.6. Giant Mascot samples are numbered and the Cogburn samples are lettered for reference to Tables 4 and 5. Open samples have been analyzed for platinum-group elements by Fire-assay with ICP finish. Closed samples have been analyzed for platinum group elements by Fire-assay with ICP finish and instrumental neutron activation analysis.

far less feldspar than is found at Cogburn Creek. However, both bodies are composed of thick units of massive, relatively homogenous cumulate of differing compositions that are inter-layered with each other and locally crosscut each other, suggesting that they may have been deformed prior to, and after, final consolidation. In some localities, at Giant Mascot, mineralized cumulate surrounds blocks of barren cumulate; elsewhere, at Cogburn Creek, mineralized inclusions are found in barren cumulate. Delicate layering is uncommon, it has only been observed at one locality along Cogburn Creek.

The sulphides at both localities are found in relatively unaltered rock. They fall within a continuum from rare, scattered interstitial blebs through net-textured, inter-cumulus sulphide to semi-massive sulphide. The latter includes mineralization found in both deformed and undeformed cumulate. At some localities, the sulphide is enriched along well-defined deformation zones cutting fresh rock. In both areas (Giant Mascot and Cogburn Creek), the sulphide is commonly spatially associated with rocks that show late development of inter-cumulus and/or replacement hornblende. However, the relationship may be coincidental as there is very little hornblende with the mineralized rocks north of Cogburn Creek. Net-textured ores at Giant Mascot commonly also contain very little hornblende, however this may be because sulphide displaced silicate magma as the principal inter-cumulus material.

The two cumulate bodies may have been folded but there is little evidence that they were metamorphosed prior to intrusion of the diorite. They were, however, faulted, as diorite and tonalite dikes occur along well-defined fractures at both localities, and contacts between the cumulate body and diorite are commonly brecciated. The contact is commonly defined by hornblendite, which forms in zones several metres in width. In many localities, altered pyroxenite and diorite fragments are cemented by a coarse hornblende-feldspar pegmatite. In both areas, the interstitial, inter-cumulus phase in proximity to the contact is hornblende while feldspar is more abundant at some distance from the diorite. Rock textures suggest that the hornblende is high-temperature and magmatic, formed from hydrated residual magma during the final phase of consolidation, possibly as the diorite was being intruded. Alternatively, it may be porphyroblastic. Secondary amphibole formation continued on cooling, particularly south of Cogburn Creek. The two cumulate bodies were deformed with the Spuzzum and Hut Creek diorite during the mid-Cretaceous, however they behaved in a more competent manner than the diorite and they show little sign of foliation. They have, however, been faulted.

Although Aho (1956) considered the possibility of a hydrothermal origin for the zoned ore shoots at Giant Mascot, more recent workers suggest that the deposit formed as a result of segregation of sulphide droplets from a mafic magma, accumulation of the droplets through gravity settling, and subsequent remobilization and emplacement of a mineralized crystal mush into barren cumulate (Muir, 1971 and McLeod, 1975). They base their conclusion on the inter-cumulus nature of much of the sulphide and on the compositions of coexisting silicates. These indicate high temperatures of formation and a magmatic origin for the pyroxenes (McLeod *et al.*, 1976).

Clarke (1969) studied the geometry of the ore-shoots and concluded that they were controlled by three principal fault sets, although the nature of the control was uncertain. Given the complexity of the distribution of cumulate lithologies in the mineralized areas described by Aho (1956), Muir (1971) and McLeod (1975), it is possible the current distribution of ore-shoots at Giant Mascot is a function of primary sulphide accumulation by gravity followed by folding and faulting, and migration of sulphide-rich material to low-pressure zones prior to intrusion of the diorite. In some localities, there is textural evidence to show that at least some of the sulphide has been remobilized into deformation zones. Current geometric relations will have been complicated by deformation, both folding and faulting, since the emplacement of the diorite.

Magmatic sulphide deposits are formed through accumulation of immiscible sulphide droplets, derived from sulphur-saturated mafic magmas, into ore-grade concentrations. Theoretically, droplets formed during a single sulphur saturation event should be similar in composition and should settle to form deposits with predictable metal ratios. The metal content of a sulphide droplet will be controlled by the composition of the silicate magma; the relative volumes of the sulphide and silicate melt and partition coefficients. Deposits formed from magmas of similar composition commonly display broadly similar metal ratios (Naldrett, 1981; Barnes, 1990; Naldrett and Ebel, 1997). The tenors of the metals will, however, be variable.

Deposits formed from sequential, or non-equilibrium segregation of sulphide will be less consistent in composition, as will those that have undergone substantial remobilization. The timing of introduction of sulphur into a magma chamber is important, as early-formed droplets will preferentially scavenge platinum group metals leaving the silicate magma depleted during subsequent sulphur saturation events. If a significant amount of olivine and trace sulphide has already been deposited as cumulate before the main introduction of sulphur, there will likely be less metal to extract (Naldrett, 1981; Barnes, 1990). Platinum group elements have much higher partition coefficients into sulphide than do nickel and copper, and they can readily be removed from the melt and dispersed in cumulate in small amounts of disseminated, interstitial sulphide.

Hulbert (2001) assigns Giant Mascot to a "Tholeiitic Mafic to Ultramafic" class of deposit, although he acknowledges that limited data suggests some association with the Spuzzum pluton, which is calc-alkaline in character. The average Ni/Cu ratio for the ore-shoots at Giant Mascot is 2.6, which is similar to other nickel-copper deposits formed in other tholeiitic gabbroic intrusions discussed in the literature. The geology at Giant Mascot is very similar to that at the Farley mine, at Lynn Lake in Manitoba (Pinsent, 1980). The "A" plug at Lynn Lake contained 15 ore-shoots with an aggregate 25 771 228 tonnes grading 0.91% Ni and 0.49 % Cu (Ni/Cu ratio 1.86). The smaller, "El" plug contained two ore-shoots with a total of 1 732 264 tonnes grading 2.07% Ni and 0.76% Cu (Ni/Cu ratio 2.72). There has been very little systematic work done on its platinum group element distribution.

Naldrett (1981) describes several other "gabbro-related" deposits including the Pechenga deposit on the Kola Peninsula, in Russia, and the Montcalm deposit, in Ontario. For each of these, and others, he has calculated the average metal content of a "100% sulphide" using the same calculation applied here, allowing for direct comparison.

The Pechenga deposit comprises 20 ore-shoots and prospects in a series of ultramafic to mafic cumulate bodies "intruded" into metasedimentary rock interbedded with thick sequences of submarine basalt. The ore-types include (1) disseminated peridotite-hosted ores, (2) breccia ores in tectonic zones and (3) veinlets in country rocks. The Cu/(Cu+Ni) ratio of the first two ore types is reported to be 0.28 and of the third, 0.51. Based on 13 samples, (Naldrett, 1981) estimated that the sulphide concentrate would contain approximately 600 ppb Pt, 500 ppb Pd and 200 ppb Au. These values are similar to the average values obtained for Giant Mascot (713 ppb Pt, 893 ppb Pd and 379 ppb Au).

The Montcalm deposit (3.56 million tonnes grading 1.44% Ni, 0.68% Cu and 50 ppb total PGE) is similar, but notably depleted in platinum group elements (Barrie *et al.*, 1990). It has a global Ni/Cu ratio of 2.1, but has a very low platinum group element tenor. Naldrett (1981, Table 2) suggests that the "concentrate" from this deposit would likely contain approximately 58 ppb Pt, 17 ppb Pd, 2.4 ppb Rh, 3.7 ppb Ru, 0.7 ppb Ir, <1.5 ppb Os and 82 ppb Au. The data are consistent with sulphide segregation from a primitive magma that has already fractionated much of its olivine, clinopyroxene and chromite, along with trace amounts of sulphide. The deposit formed after the bulk of the platinum group elements had been removed from the magma (Barrie *et al*., 1990).

Similarly, Paktunc (1989) reports finding low platinum group element tenors in sulphides in the St. Stephen "tholeiitic mafic-ultramafic intrusion", that straddles the border between New Brunswick and Maine. The intrusion hosts several deposits, of which the three largest contain 907 000 tonnes grading 1.03% Ni and 0.47% Cu (Ni/Cu ratio 2.19). Paktunc analyzed 19 sulphide-bearing samples by neutron activation analysis and determined concentrations of <5 to 289 ppb Pt, <2 to 150 ppb Pd, <1 to 68 ppb Au, 1 to 5 ppb Rh, <5 to 100 ppb Ru, 0.1 to 1.9 ppb Ir, <3 to 5 ppb Os and <5 to 37 ppb Re. Based on the nickel content of olivines, he concluded that sulphur saturation must have occurred following formation of the main peridotite mass and that early sulphides had already depleted the magma of its platinum-group elements.

The sulphide at Giant Mascot deposit is relatively homogenous at the deposit scale but metal distribution is highly variable on the local, hand-specimen scale. Correlation coefficients suggest that the platinum-group elements and gold are only moderately allied to nickel and copper distribution, which has clearly been, at least in part, affected by remobilization of chalcopyrite into veins and veinlets. The latter may account for the variation in Ni/Cu ratio. The variability in platinum-group element content may be a function of sampling, or it may reflect local remobilization, or sulphide fractionation (Naldrett, 1981; Naldrett and Ebel, 1997). Some of the massive sulphide samples from Giant Mascot contain two generations of pyrrhotite: large, early-formed, and later, finer-grained crystals.

Barnes, *et al.* (1993), discuss the distribution of platinum-group elements in several nickel-copper deposits found in possibly mantle-plume related "synvolcanic gabbros" within the Belleterre-Angliers greenstone belt of the Pontiac sub province, in Quebec. They compare the tenors of metals found in 8 of these deposits and prospects and, by recalculating the values to 100% sulphide established benchmark estimates for platinum-group element contents of "undepleted" and "depleted" deposits. They also examined the possibility of using the Cu/Pd ratios as a tool for exploration. They show that the Cu/Pd ratio for mantle rocks will be in the range 10^3 to 10^4 and that the ratios for palladium depleted and enriched mantle-derived magmas will be somewhat greater, and somewhat lower, respectively (Barnes, *et al.*, 1993; Figure 12). If the palladium content of the Giant Mascot deposit is around 100 - 200 ppb, the Cu/Pd ratio for the deposit will be approximately 10^4. The sulphide ratio plots close to the transition point between mantle-derived and depleted rocks (Barnes, et. al., 1993), suggesting that the source magmas had not been previously depleted in platinum-group metals.

The analytical results for Giant Mascot indicate that the deposit is "gabbro-related", as defined by Naldrett (1981) and that the host magma became sulphur saturated while olivine was crystallizing and was being fractionated. Sulphur was introduced early enough to scavenge a significant, but trace amount of platinum, palladium, gold and detectable amounts of the other platinum group elements as well as copper and nickel. Although there are insufficient data to evaluate the distribution of platinum group elements at Cogburn Creek fully, the abundance of feldspathic cumulate and relative enrichment in pyrrhotite, as opposed to pentlandite and chalcopyrite, and the relatively low platinum and palladium values obtained, suggests that there is greater likelihood of prior platinum group element depletion in this area. This is consistent with the observed presence of mineralized pyroxenite inclusions in feldspathic pyroxenite north of Cogburn Creek. The inclusions indicate an earlier mineralizing event.

CONCLUSION

The study shows that the two principal areas of nickel-copper mineralization east of Harrison Lake (at the Giant Mascot mine and at Cogburn Creek) are similar in their geological setting and style of mineralization. The sulphides are magmatic in origin and the deposits occur in bodies of ultramafic to mafic cumulate that are intimately related to Settler Schist and Spuzzum-type diorite. The principal difference between the two areas appears to be the relative abundance of ultramafic cumulate at Giant Mascot and of mafic cumulate in the Cogburn area.

The age and origin of the cumulate remains in question. Contact relations suggest that the cumulate bodies predate intrusion of the Spuzzum diorite; however, rock textures appear to show inter-cumulus hornblende developed as a late magmatic phase in pyroxenite around the margins of the cumulate bodies. This suggests that the cumulate may have contained a small amount of residual (interstitial) magma that was weakly hydrated when the body was intruded by diorite. The Giant Mascot cumulate body was deformed prior to and after intrusion of Spuzzum diorite and the current configuration of the ore-shoots is probably a result of both primary and secondary influences. The role, if any, of the Spuzzum pluton in the formation of deposit is uncertain.

The Giant Mascot ore-shoots contain nickel, copper, gold and platinum group element concentrations that are similar to other "gabbro-related" deposits that have not suffered appreciable depletion of platinum group elements. The platinum-group elements appear to be present as trace amounts (several 100s of ppb Pt and Pd in "100% sulphide") that would be unlikely to be economic to mine on their own. They would; however, add considerably to the value of a nickel-copper deposit. The ore-shoots are most commonly associated with olivine-rich cumulates, consistent with their early formation in a magma chamber. The Cogburn sulphides are similar, but appear to contain less nickel, copper and platinum-group elements relative to the amount of pyrrhotite present. They are in more feldspathic cumulates and may have formed later than those at Giant Mascot, after the main stage of olivine crystallization and fractionation.

Platinum-group elements are found in magmatic sulphides at both localities and the study suggests that future exploration for these elements should focus on similar, sulphur-saturated, cumulate bodies associated with Settler Schist and Spuzzum-type diorite. The ultramafic lenses found in Cogburn Schist have, to date, proved to be largely sulphide-free and are, consequently considered a less attractive target.

ACKNOWLEDGMENTS

The author wishes to thank Gene Gulajek of Homestake Canada Limited, for permission to review company data and to sample the Giant Mascot mine. He also wishes to thank David Haughton and Mike Sanguinetti for their help in obtaining data and for their comments in the field. The author would like to extend his appreciation to several members of the Ministry of Energy and Mines, including Graham Nixon, Chris Ash, Ray Lett, Nick Massey, Dave Lefebure and Jacques Houle who have each contributed significantly to the project. In particular, the author would like to thank Mary Dubravcic for her help in the field, Maggie Dittrick and Christy Cattermole in the Ministry's Mineral Development Office, and Dave Lefebure and Chris Ash for valuable editorial comments.

REFERENCES

Aho, A.E. (1954): Geology and genesis of ultrabasic nickel-copper-pyrrhotite deposits at the Pacific Nickel property, southwestern British Columbia; unpublished Ph.D. thesis, *The University of California*, Berkeley, California.

Aho, A.E. (1956): Geology and genesis of ultrabasic nickel-copper-pyrrhotite deposits at the Pacific Nickel property, southwestern British Columbia; *Economic Geology*, Volume 51, pages 444-481.

Ash, C. (2002): Geology of the Harrison Lake East Area, Southwestern British Columbia, *in* Geological Fieldwork 2001; *British Columbia Ministry of Energy and Mines;* Paper 2002-1.

Barnes, S.-J. (1990): The use of metal ratios in prospecting for platinum group element deposits in mafic and ultramafic intrusions; *Journal of Geochemical Exploration*, Volume 37, pages 91-99.

Barnes, S.-J., J.-F. Couture, E.W. Sawyer and C. Bouchaib (1993): Nickel-copper occurrences in the Belleterre-Angliers belt of the Pontiac sub province and use of Cu-Pd ratios in interpreting platinum-group element distributions; *Economic Geology*, Volume 88, pages 1402-1418.

Barrie, C.T., Naldrett, A.J. and Davis, D.W. (1990): Geochemical constraints on the genesis of the Montcalm gabbroic complex and Ni-Cu deposit, western Abitibi Sub province, Ontario; *Canadian Mineralogist*, Volume 28, pages 451-474.

Bellefontaine, K. and D. Alldrick (1994): Mineral Potential - Mid Coast; *British Columbia Ministry of Energy, Mines and Petroleum Resources*, Open File 1994-17 [1:250 000-scale].

Bennett, J.D. (1989): Timing and conditions of deformation and metamorphism of the structural packages east of Harrison Lake, British Columbia; unpublished M.Sc. thesis, *The University of Western Washington*, 87 pages plus map [1:19 500-scale].

Berg, N.W. and Clarke, W.E. (1971a): Geological, geochemical and geophysical report on the Ni claim groups, Harrison Lake Area, New Westminster Mining Division; *British Columbia Ministry of Energy, Mines and Petroleum Resources*, Assessment Report #3155, 13 pages plus maps.

Berg, N.W. and Clarke, W.E. (1971b): Geological, geochemical and geophysical report on the Ni claim groups, Harrison Lake Area, New Westminster Mining Division; *British Columbia Ministry of Energy, Mines and Petroleum Resources*, Assessment Report #3356, 25 pages plus maps.

Berg, N.W. and Clarke, W.E. (1972): Geological, geochemical and geophysical report on the Ni claim groups, Harrison Lake Area, New Westminster Mining Division; *British Columbia Ministry of Energy, Mines and Petroleum Resources*, Assessment Report #3615, 20 pages plus maps.

Brown, E.H. and Walker, N.W. (1993): A magma-loading model for Barrovian metamorphism in the Southeastern Coast Plutonic Complex; *Geological Society of America Bulletin*, Volume 105, pages 479-500.

Cairnes, C.E. (1924): Nickeliferous mineral deposits, Emory Creek, Yale Mining Division, British Columbia; *Geological Survey of Canada*, Summary Report, pages 100-106.

Christopher, P.A. (1974): Giant Mascot mine (92H/6), British Columbia; *in British Columbia Department of Mines and Petroleum Resources*; Geological Fieldwork, pages 17-21.

Christopher, P.A. and Robinson, J.W. (1975): Pride of Emory mine, British Columbia; *British Columbia Department of Energy, Mines and Petroleum Resources*, Geology, Exploration and Mining in British Columbia; pages 105-113.

Clarke, W.E. (1969): Giant Mascot Mines Ltd., geology and ore control; *Western Miner*, Volume 42, pages 40-46.

Cockfield, W.E. and Walker, J.F. (1933): The nickel bearing rocks near Choate, British Columbia; *Geological Survey of Canada*, Summary Report, pages 62-68.

Crosby, R.O. (1970): Report on airborne geophysical surveys, Hope Area, New Westminster Mining Division; *British Columbia Ministry of Energy, Mines and Petroleum Resources*, Assessment Report #2583, 4 page, figures and appendices.

Eastwood, G.E.P. (1971): Ni; *British Columbia Department of Mines and Petroleum Resources;* Geology, Exploration and Mining in British Columbia; pages 258-264.

Ebel, D.S. and Naldrett, A.J., (1997): Crystallization of sulphide liquids and the interpretation of ore composition; *Canadian Journal of Earth Sciences*, Volume 34, pages 352-365

Friesen, P.S. (1967): Proposed exploration programme, Giant Mascot Mines Limited, Hope, British Columbia; *Unpublished Company Report*, pages 1-36, plus maps.

Gabites, J.E. (1985): Geology and geochronometry of the Cogburn Creek-Settler Creek area, northeast of Harrison Lake, British Columbia; unpublished M.Sc. thesis, *The University of British Columbia*, 153 pages plus maps [1:20 000 scale].

Gayfer, E. R. (1970a): Geochemical Report on the Ni claims, Harrison Lake Area, New Westminster Mining Division; *British Columbia Ministry of Energy, Mines and Petroleum Resources*, Assessment Report #2469, 6 pages plus maps.

Gayfer, E.R. (1970b): Geochemical Report on the Ni claims, Harrison Lake Area, New Westminster Mining Division; *British Columbia Ministry of Energy, Mines and Petroleum Resources*, Assessment Report #2801, 6 pages plus maps.

Gonzales, R.A. and Clarke, W.E. (1972): Geological, geochemical and geophysical report on the Ni 316 group, Harrison Lake Area, New Westminster Mining Division; *British Columbia Ministry of Energy, Mines and Petroleum Resources*, Assessment Report #4071, 12 pages plus maps.

Gonzales, R.A. and Clarke, W.E. (1973): Geological, geochemical and geophysical report on the Ni 336 group, Harrison Lake Area, New Westminster Mining Division; *British Columbia Ministry of Energy, Mines and Petroleum Resources*, Assessment Report #4070, 15 pages plus maps.

Hettinga, M.A. (1989): Metamorphic petrology, geothermobarometry and structural analysis of a portion of the area east of Harrison Lake, British Columbia; unpublished M.Sc. thesis, *Western Washington University*, Bellingham, 85 pages plus maps [1:20 000-scale].

Horwood, H.C. (1936): Geology and mineral deposits at the mine of B.C. Nickel Mines Limited, Yale, British Columbia; *Geological Survey of Canada*, Memoir 190.

Hulbert, L. (2001): GIS Maps and databases of mafic-ultramafic hosted, Ni, Cu-Ni, Cr +/- PGE occurrences and mafic-ultramafic bodies in British Columbia; *British Columbia Ministry of Energy and Mines*, Geoscience Map 2001-2.

Irvine T. N. and Baragar, W.R.A. (1971): A guide to the chemical classification of the common volcanic rocks; Canadian Journal of Earth Sciences, Volume 8, pages 523-548.

Lett, R. and Jackaman, W. (2002): PGE Stream sediment geochemistry in British Columbia, *in* Geological Fieldwork 2001; *British Columbia Ministry of Energy and Mines;* Paper 2002-1.

Lowes, B.E. (1972): Metamorphic petrology and structural geology of the area east of Harrison Lake, British Columbia; unpublished Ph.D. thesis, *The University of Washington*, Seattle, 162 pages plus maps [1.5" to 1.0-mile scale].

McLeod, J.A. (1975): The Giant Mascot ultramafite and its related ores, British Columbia; unpublished M.Sc. thesis, *The University of British Columbia*, 123 pages.

McLeod, J.A., M. Vining and K.C. McTaggart (1976): Note on the age of the Giant Mascot ultramafic body, near Hope, British Columbia; *Canadian Journal of Earth Sciences*, Volume 13, pages1152-1154.

Monger, J.W.H. (1970): Hope map area, west half (92HW1/2), British Columbia; *Geological Survey of Canada*, Paper 1969-47, 75 pages.

Monger, J.W.H. (1986): Geology between Harrison Lake and Fraser River, Hope map area, southwestern British Columbia; *in* Current Research Part B, *Geological Survey of Canada*, Paper 86-1B, p 699-706.

Monger, J.W.H. (1989): Geology of the Hope and Ashcroft map areas; *Geological Survey of Canada*, Maps 41-1989, 42-1989, [1:250 000-scale].

Monger, J.W.H. and Journeay, J.M. (1994): Guide to the geology and tectonic evolution of the southern Coast Mountains; *Geological Survey of Canada*, Open File 2490, 77 pages plus maps.

Muir, J.E. (1971): A study of the petrology and ore genesis of the Giant Nickel 4600 ore body, Hope, British Columbia; unpublished M.Sc. thesis, *The University of Toronto*, 125 pages plus maps.

Naldrett, A.J. (1981): Nickel sulphide deposits: classification, composition and genesis; *Economic Geology*, 75th Anniversary Volume, pages 628-685.

Paktunc, A. D. (1989): Petrology of the St. Stephen's intrusion and genesis of related nickel-copper sulphide deposits; *Economic Geology*, Volume 84, pages 817-840.

Pinsent, R.H. (1980): Nickel-copper mineralization in the Lynn Lake Gabbro; *Manitoba Department of Energy and Mines*, Mineral Resources Division; Economic Geology Report ER79-3, 109 pages plus appendices.

Read, P. (1960): The geology of the Fraser Valley between Hope and Emory Creek, British Columbia; unpublished M.Sc. thesis, *The University of British Columbia*, 154 pages plus maps [1:50 000-scale].

Richards, T.A. (1971): Plutonic rocks between Hope, British Columbia, and the 49th Parallel; unpublished Ph.D. thesis, *The University of British Columbia*, 178 pages plus maps [1": 1.5-mile scale].

Richards, T.A. and McTaggart, K.C. (1976): Granitic rocks of the southern Coast Plutonic Complex and northern Cascades of British Columbia; *Geological Society of America*, Bulletin, Volume 87, pages 935-953.

Richards, T.A. and White, W.H. (1970): K-Ar ages of plutonic rocks between Hope, British Columbia and the 49th parallel; *Canadian Journal of Earth Sciences*, Volume 7, pages 1203-1207.

Sanguinetti, M.H. (2000a): Geological report on the Raven quarry property, Cogburn Creek area, New Westminster Mining Division; *British Columbia Ministry of Energy and Mines*, Assessment Report #26 226, pages 1-25.

Sanguinetti, M.H. (2000b): Diamond drilling report on the Raven property, Cogburn Creek area, New Westminster Mining Division; *British Columbia Ministry of Energy and Mines*, Assessment Report #26 422, pages 1-10 plus attachments.

Stephens, F.H. (1963): Giant Mascot Mines; *Western Miner and Oil Review*; April 1963, 5 pages.

Tindall, M. (1987): Preliminary rock and tailings geochemistry on the Giant Nickel property, New Westminster Mining Division; *British Columbia Ministry of Energy and Mines*, Assessment Report #16 553, 12 pages plus maps.

Troost, M.L. (1999): Structure and Metamorphism of the Talc Creek Area, Harrison Lake, British Columbia; unpublished M.Sc. Thesis, *The University of Western Washington*, 144 pages plus maps [1:24 000-scale].

Vining, M.R. (1975): Regional setting of Giant Mascot mine (92H/5W, 6E) British Columbia; in *British Columbia Department of Mines and Petroleum Resources*, Geological Fieldwork, pages 49-52.

Vining, M.R. (1977): The Spuzzum pluton northwest of Hope, British Columbia; unpublished M.Sc. thesis, *The University of British Columbia*, 103 pages plus map [1:125 000-scale].

Wood, B.J. and Banno, S. (1973): Garnet-orthopyroxene and orthopyroxene-clinopyroxene relationships in simple and complex systems; *Contributions to Mineralogy and Petrology*, Volume 42, pages 109-124.

Intrusion-Related Gold Mineral Occurrences of the Bayonne Magmatic Belt

By James M. Logan

KEYWORDS: *Economic geology, intrusion-related, gold, Cretaceous, Bayonne magmatic belt.*

INTRODUCTION

Intrusion-related gold deposits, as described by Thompson *et al.* (1999), are a new and economically important class of deposits that occur within felsic magmatic provinces known to host tungsten and/or tin mineralization. Traditionally these magmatic provinces were not believed to host significant gold mineralization and as a consequence are under explored for this type of deposit. Examples of intrusion-related gold deposits occur worldwide (Thompson *et al.*, 1999, Lang and Baker, 2001), but those most applicable to exploration in British Columbia are the well-studied Alaska and Yukon deposits of the Tintina Gold Belt (Newberry *et al.*, 1995; McCoy *et al.*, 1997; Baker *et al.*, 1996). Major deposits include Fort Knox (~210 t Au), Dublin Gulch (~36 t Au), Brewery Creek (~29 t Au) and Pogo (~161 t Au).

The British Columbia Geological Survey initiated a field-based project in 1999 to identify the potential for intrusion-related gold deposits in the province. Southeastern British Columbia (Fig. 1) was selected because it has similarities with the Tintina Gold Belt; including mid-Cretaceous granitic intrusions, intrusion-hosted and peripheral quartz veins with Au-W-Bi metal signatures, and regional geochemical anomalies of pathfinder elements for intrusion-related gold deposits (Lefebure *et al.,* 1999).

In response to encouraging results from the 1999 and 2000 field studies (Logan, 2000; 2001; Cathro and Lefebure, 2000), a regional compilation map of the study area was completed (Logan, 2002). In addition, ongoing research includes; Ar-Ar analysis of alteration and intrusive phases (Douglas Archibald, Queen's University), fluid inclusion studies of selected mineral occurrences and intrusive phases (Kathryn Dunne) and galena and feldspar Pb-isotope studies (Janet Gabites, The University of British Columbia). Preliminary results from these studies are presented below, the final results and interpretations will appear in a separate publication. The compilation map (Geoscience Map 2002-1) shows the distribution, geochemistry and physical characteristics of the intrusions and intrusion-related mineral occurrences that comprise the Bayonne magmatic belt and provides an up-to-date framework in which to assess the applicability of the "intrusion-related gold system model" in southeast British Columbia. Early in the compilation process it was obvious that geological data, and in particular recent geochronological studies, in southeast British Columbia are limited in comparison to data available for the Tombstone-Tungsten magmatic suite (Mortensen, 1999; Mortensen *et al.*, 2000). In contrast to the metaluminous, subalkalic, reduced I-type Tombstone Suite, the Bayonne suite consists of mostly peraluminous, subalkalic hornblende-biotite granodiorite and highly fractionated 2-mica granites, aplites and pegmatites. Some of these intrusions have associated Au-W-Bi-As quartz vein occurrences analogous with intrusion-related deposits in the Tintina Gold Belt. In addition, the metal association and mineral zonation developed around specific Bayonne suite intrusions is most easily explained by depth of emplacement, and can be used to direct exploration into areas of higher potential for undiscovered intrusion-related gold deposits.

INTRUSION-RELATED GOLD SYSTEMS

Intrusion-related gold systems (Lang and Baker, 2001), like many other magmatic-hydrothermal systems, form ore deposits that are characterized by, diverse styles of mineralization, a wide range of mineral and metal assemblages, and spatial association with their related intrusive centers (Fig. 1). Distinctive features of intrusion-related systems are reviewed in recent publications by McCoy *et al.* (1997), Poulsen *et al.* (1997), Thompson *et al.* (1999), Hart *et al.*

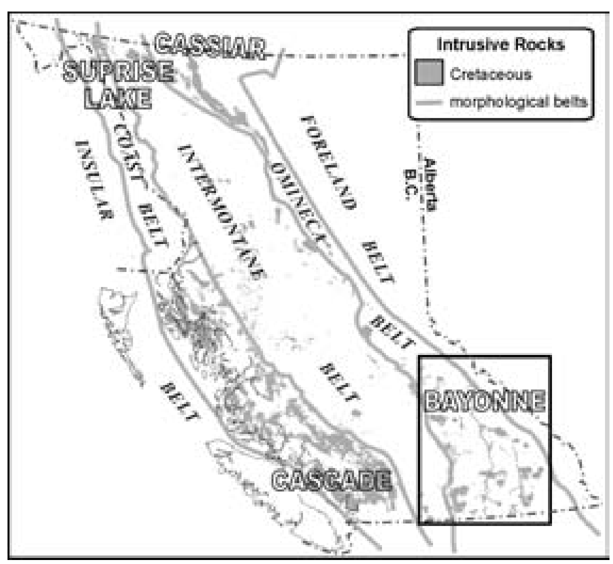

Figure 1. Location map Bayonne magmatic belt.

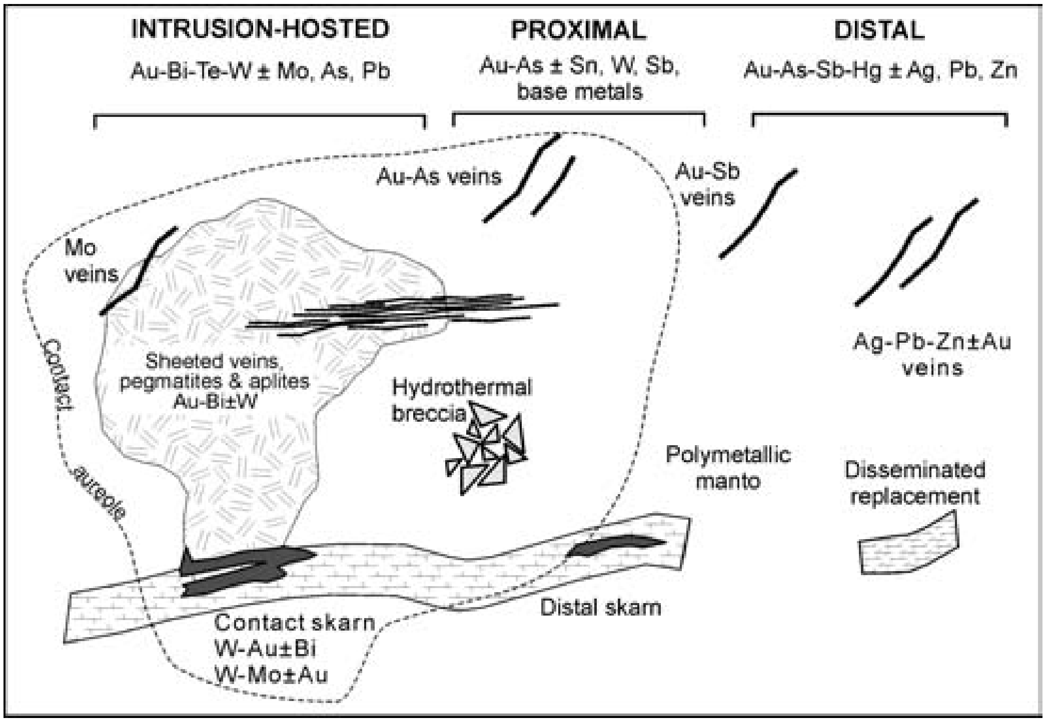

Figure 2. Schematic geological model for intrusion-related gold deposits, showing variations in styles from intrusion-hosted to proximal and distal deposits (Lang and Baker, 2001; adapted from Hart *et al.*, 2000).

(2000) and Newberry (2000). Common features (summarized from Lang and Baker, 2001) include: (1) association with relatively reduced, metaluminous, subalkalic intrusions of intermediate to felsic compositions; (2) location within a continental magmatic arc known for tungsten and/or tin mineralization and characterized by coeval intrusions of alkalic, metaluminous calcalkalic and peraluminous compositions; (3) carbonic hydrothermal fluids; (4) an auriferous metal assemblage containing elevated Bi, W, As, Mo, Te and/or Sb with low concentrations of base metals; (5) a low sulphide mineral content of <5%; and (6) an areally restricted, commonly weak hydrothermal alteration.

Hart *et al.* (2000) separated Yukon deposits into three categories based on their spatial relationship to intrusions (Fig. 2). Intrusion-hosted deposits comprise low grade, large tonnage sheeted and stockwork, low sulphide, auriferous vein systems characterized by metal assemblages containing Au-Bi±Te±Mo±W. For example, at Fort Knox gold mineralization occurs in pegmatites, aplites and quartz veins (Bakke, 1995), while it is found in miarolitic cavities within the Emerald Lake Pluton (Duncan, 1999). Proximal deposits are located in the host rocks adjacent to the intrusion generally within the contact metamorphic aureole. Deposits of this group include contact skarn assemblages of W-Au±Bi and W-Mo±Au±Cu (Dublin Gulch property), disseminated carbonate replacements, tin and copper-rich breccias and vein-deposits. Distal deposits are located beyond the limits of the contact aureole. They include auriferous vein-fault zones (True North), breccias, Ag±Au rich base metal veins and disseminated replacement of carbonaceous and calcareous rocks (Brewery Creek, Poulsen, 1996; Diment and Craig, 1998). Metal assemblages for distal deposits are characterized by a Au-As-Sb±Hg signature.

Similar, *intrusion-hosted* Mo and Au-quartz-As-W vein occurrences (*i.e.* Valparaiso and Rosan), *proximal* W-Cu-Au skarns (*i.e.* Lucky Bear) and Au-Ag-Bi-Cu-Pb fault-veins (*i.e.* Cam-Gloria) and *distal* Pb-Zn-Au-As-Sb ±W quartz-carbonate veins (*i.e.* Ruth Vermont, McMurdo) are located in southern British Columbia associated with the mid-Cretaceous Bayonne Suite (Logan, 2002). The southern end of the Omenica belt that corresponds to the Bayonne Magmatic belt contains extensive magmatic-hydrothermal mineral deposits (Fyles and Hewlett, 1959; Höy, *in press*). Many contain primarily base metals with only minor precious metal but are still important exploration tools that may be used to direct exploration to an intrusion-related gold center. The metal assemblages and metal ratios associated with distal *vs* proximal *vs* intrusion-hosted are also important to establish the position of the causative intrusion.

MESOZOIC INTRUSIONS OF THE CANADIAN CORDILLERAN

Mesozoic granitoid plutons comprise a substantial proportion of the Canadian Cordillera, particularly in the Coast and Omineca belts (Woodsworth *et al.*, 1991; Fig. 1). The plutons of these two belts are markedly different. The granodiorite to tonalite batholiths of the Coast belt were emplaced within large subduction-related magmatic arc complexes that developed along the continental margin (Barker and Arth, 1990; Brandon and Smith, 1994). The volumetrically smaller granodiorite and high-K_2O granites of the Omineca belt were emplaced inboard of the main magmatic arc in continental margin rocks. The mechanisms responsible for magma production in the Cordilleran interior are controversial but likely require a combination of factors involving heat and magma transfer from the mantle to the crust (Hyndman and Foster, 1988; Hoisch and Hamilton, 1990) and crustal thickening (Patiño Douce *et al.,* 1990) which together resulted in crustal anatexis (Brandon and Smith, 1994).

Cretaceous plutons of the Omineca belt extend for more than 1600 km along the Canadian Cordilleran interior from the Yukon to the Canada-US border and comprise six suites that include from north to south Tombstone, Tungsten, Tay River, Anvil, Cassiar and Bayonne (Mortensen *et al.*, 1997; Mortensen, 1999; Woodsworth *et al.*, 1991). A Mo-W±Sn metallogenic province is associated with this Cretaceous magmatic belt. The Tombstone and some of the Tungsten suite plutons are known to host intrusion-related gold deposits (*i.e.* Tintina Gold Belt), but to date only small auriferous vein and skarn occurrences of this particular deposit type and possibly some placer gold deposits are known to be associated with Bayonne suite plutons.

BAYONNE MAGMATIC BELT

The Bayonne magmatic belt is a 50 to 75 km wide arcuate belt extending from the Canadian-USA border northwest to Quesnel Lake (Figure 3). It lies inboard (east) of the terrane accretionary boundary and is bound on the east by the Rocky Mountain Trench. The plutons intrude miogeoclinal rocks of North American affinity. Northwest of the Kootenay Arc, batholiths and large stocks intrude rocks of the Kootenay and Barkerville terranes. Mid-Cretaceous plutons of the Bayonne suite comprise the majority of these magmatic rocks, but volumetrically smaller and fewer Middle Jurassic Nelson suite plutons are present also (Brown *et al.,* 1992), and north of 51^{o} latitude Devonian, Late Cretaceous and Tertiary suites are known (Parrish, 1992; Logan and Friedman, 1997).

The Middle Jurassic suite comprises syn- to late-tectonic plutons that were emplaced during the collapse of the outer margin and accretion of Quesnellia (Monger *et al.*, 1982; Archibald *et al.*, 1984; Price, 1986; Murphy *et al.*, 1995). The younger, mid Cretaceous plutons are discordant with regional structures formed during the early Middle Jurassic accretionary event, and for the most part are undeformed. Assigning syn-, late or post-tectonic categories to plutonic suites can be misleading and oversimplifies younger Cretaceous and Tertiary deformation. For example, in the Shuswap region, the Anstey Pluton (92-94 Ma; Parrish, 1992) was sheared and metamorphosed after ca. 90 Ma at sillimanite stable conditions (5-8 kbar). In the southern Kootenay Arc the *late-synkinematic* Baldy Pluton (117+4/-1 Ma, Leclair *et al.*, 1993) was emplaced during penetrative deformation at crustal levels of 3.5 to 5.5 kbars, while the *postkinematic* Midge Creek Stock (111±1 Ma, Leclair *et al.*, 1993) was emplaced between 4 and 11 Ma later at crustal levels of 2.5 to 3.5 kbars. The Kaniksu/Ryker Batholith (93.8±1 Ma, Brown *et al.*, in prep) was intruded at levels of ~5.5 kbars, deeper than most Cretaceous plutons in the area south of Salmo and also during prograde metamorphism and tectonism. Those examples illustrate how depth of emplacement varies dramatically along the length of the magmatic belt with plutons intruded at structural levels that span both brittle and ductile regimes.

DEPTH OF EMPLACEMENT

In the Cretaceous, between 115 to 90 Ma (Archibald *et al.*, 1984) composite plutons and batholiths were emplaced at mid-crustal levels along the length of the Bayonne belt (Table 1). Contact metamorphic mineral assemblages from the contact aureoles of the mid-Cretaceous plutons in the western Purcell anticlinorium indicate that the plutons intruded into bathozone 2 or 3, at pressures of 2.5 - 4.3 kbar (Archibald *et al.*, 1983, 1984; Warren, 1997). Mineral assemblages from the contact aureoles of the Battle Range batholith and Albert stock indicate pressures of ~3.5 kbar (Sears, 1979) and for Goldstream and Long Creek plutons pressures <3.8 kbar (Logan and Colpron, 1995). At the southern end of the Kootenay Arc pressure data from pelitic assemblages in the contact aureole of the Summit Creek stock and Sheep Creek stock indicate that these plutons were intruded into bathozone 1 or 2, at pressures of ~2.5 kbar (Archibald *et al.,* 1983; Mathews, 1953). At the northern end of the magmatic belt contact metamorphic mineral assemblages from the contact aureole of the Baldy Batholith indicate bathozone 1 or 2, and pressures of ~ 2.5 kbar.

In general the intrusions at the north and southern ends of the belt have contact metamorphic mineral assemblages that indicate pressures of <2.5 kbars. At the center of the arc contact metamorphic mineral assemblages for the Battle Range, Bugaboo, Horsethief, White Creek and Fry Creek batholiths indicate pressures of 3.5 kbars or higher. Higher-pressure mineral assemblages are present adjacent to Big Mouth pluton, located on the western flank of the Windy Range metamorphic culmination and also adjacent to the Shore Line Stock and Corn Creek Gneiss indicating deeper structural levels. The different emplacement depths along the length of the belt are most likely a manifestation of the deeper levels of exhumation at its center, where the shallower plutons (<2.5 kb) have been removed by erosion.

The Middle Jurassic, syn- to late tectonic plutons, on the other hand were intruded at greater depths in the Kootenay Arc and Purcell Mountains (4.3 - 5.6 kbar; Archibald *et al.*, 1984; Warren, 1997) and the Adams Plateau (~3.5 kbar, Logan, 2002) at the north end of the belt.

INTRUSION-RELATED METAL ZONING

The Bayonne suite is the southern component of a 1600 km long W-Sn±Mo province extending from the Yukon territory south to Salmo.

The Bayonne magmatic belt has a well-defined Mo-W±Sn metal association. It is enriched in large-ion lithophile elements, such as uranium, rare earth elements, lead and silver, and is relatively depleted in copper and zinc.

TABLE 1
CHARACTERISTICS OF CRETACEOUS PLUTONS IN THE BAYONNE MAGMATIC BELT, SOUTHEASTERN BRITISH COLUMBIA (AFTER LOGAN, 2002)

PLUTON (area)	COMPOSITION OF PHASES	ASSOCIATED MINERALIZATION	EMPLACEMENT PRESSURE	DEPTH (1 kbar=3.5 km)
Baldy 558 km^2	hb-bi GRNT bi-mu GRNT	Mo, Cu-Mo, W±Au, Au-Cu±Co, Pb-Ag-Zn±Au	BATH 1 (qtz-mu-an-cor) <2.5 kbar	<9 km
Downie 5 km^2	QMDT	Cu	<BATH 2 (qtz-bi-ga-an) <3.5 kbar	<12 km
Goldstream 103 km^2	QMZD, GRNT	Mo, W-Mo, Pb-Ag-Zn±Au	BATH 3 (qtz-mu-an) <3.8 kbar	<13 km
Long Creek 35 km^2	QMNZ, GRNT	W-Mo	<BATH 2 (qtz-bi-ga-an) <3.5 kbar	<12 km
Albert 36 km^2	bi-GRNT GNDT	W-Mo	BATH 2 - 3 (si-an-st-mu) ~3.5 kbar	~12 km
Battle Range 519 km^2	GRNT GRDT	Sn, Mo, W-Mo, Pb-Ag-Zn±Au	BATH 2 - 3 (si-an-st-mu) ~3.5 kbar	~12 km
Bugaboo 151 km^2	leuco-QMNZ	U, Pb-Ag-Zn±Au	BATH 2 and 3 (qtz-mu-an-st) 2.5-3.8 kbar	9-13 km
Horsethief Creek 132 km^2	bi-QMNZ	Mo, U, W-Mo, Pb-Ag-Zn±Au	<4.3 kbar	<15 km
Shoreline 23 km^2	bi-mu GRNT	Ag-Pb-Zn±Au	BATH 5 (ga-bi-ky-si) 5-6 kbar	17-21 km
Fry Creek 611 km^2	leuco- QMNZ	Mo, Au, W-Sn, Ag-Pb-Zn±Au	BATH 2 and 3 (qtz-mu-ga-an-st and qtz-mu-si) 2.5-3.8 kbar	9-13 km
White Creek 435 km^2	leuco- QMNZ porph-QMNZ hb-biGRDT	Be, W, W-Mo, Pb-Ag-Zn±Au	>BATH 3 (qtz-mu-si-st) >3.8 kbar	>13 km
Mount Skelly 302 km^2	bi-GRNT bi-hb GRDT	Mo-W±Cu, As-Pb-Ag-Au, W	BATH 2 and 3 (qtz-mu-an-st) ~3.5 kbar	~12 km
Baldy 35 km^2	leuco-GRDT		(ga-si-bi-mu-qtz-pl) 3.5-5.5 kbar	12-20 km
Midge Creek 17 km^2	bi-GRDT, TNLT	Pb	(an-si) 2.5-3.5 kbar	9-12 km
Lost Creek 24 km^2	leuco- QMNZ	Mo, W-Mo, U	BATH 1 (an, w/ no si) <2.5 kbar	<9 km
Summit 5 km^2	QMNZ, bi-GRNT	Mo, W-Mo, U	BATH 1-2 (qtz-bi-mu-an) ~2.5 kbar	~9 km
Sheep Ck 3 km^2	GRNT	Mo, Au,:Ag-Pb-Zn±Au	BATH 1-2 (qtz-bi-an±ga) ~2.5 kbar	~9 km
Corn Creek Gneiss 3 km^2	bi-mu GRNT	Mo, W	BATH 4 (qtz-mu-ky-si; w/ no an, ga) <5.5 kbar	<20 km
Rykert/Kanisku 27 km^2	bi-GRDT, bi-mu GRNT		BATH 4 (qtz-mu-ky-si; w/ no an, ga) <5.5 kbar	<20 km

Associated Mineralization:
Ag=silver, As=arsenic, Au=gold, Be=beryl, Co=cobalt, Cu=copper, Mo=molybdenum, Pb=lead, Sn=tin, U=uranium, W=Tungsten, Zn=zinc
Emplacement pressures:
BATH=bathozones, kbars=kilobars, an=andalusite, cor=cordierite, gnt=ganet, ky=kyanite, pl=plagioclase, qtz=quartz, si=sillimanite, st=-staurolite.
Composition of Phases:
APLT=aplite, DORT=diorite, GBBR=gabbro, GRDT=granodiorte, GRNT=granite, MNZT=monzonite, QMNZ= quartz monzonite, QMZD=quartz monzodiorite, SYNT=syenite, TNLT=tonalite

In these environments, metal zonation generally reflects depth of emplacement and distance from causative intrusive patterns (Flanigan *et al*., 2000; Hart *et al.*, 2000; Lang and Baker, 2001). Assemblages change from U, Sn, W, W-Mo and Ag-Pb-Zn-Au from deeper to shallower levels and from intrusion/pegmatite hosted to distal structurally controlled veins or replacements. The distribution of known mineral occurrences around the Baldy Batholith defines a simple elliptical pattern extending outward from the western, hornblende-biotite granite phase of the intrusion. At the center are porphyry occurrences containing Mo±Cu±Au, near the margin and beyond are Au-Cu-Bi peripheral veins and W-Cu±Au±Bi skarns, and beyond these are distal veins with low gold values and metal assemblages containing Ag-Pb-Zn±Au and Ag-Pb-Zn±As±Au. No mineral occurrences are known to be associated with the peraluminous, muscovite-biotite granite phase that comprises the eastern portion of the batholith.

Relating intrusion-hosted, sheeted gold-quartz vein mineralization and even peripheral gold-tungsten-bismuth skarn and manto mineralization to late stage magmatic fluids from an intrusion can be straightforward, but understanding the genesis of mineralization that is distal to the causative intrusive or hosted in older intrusive rocks (*i.e.* Cam-Gloria) becomes more difficult. This study collected samples to evaluate the relationships between intrusion and deposits in the areas surrounding the Baldy Batholith, Battle Range and Mount Skelly Pluton and local areas in the Northern Selkirk Mountains and the southern Kootenay Arc.

The focus of this report is on the Baldy Batholith. In the area of the Baldy Batholith there are three separate intrusion-related vein deposits associated with this mid-Creta-

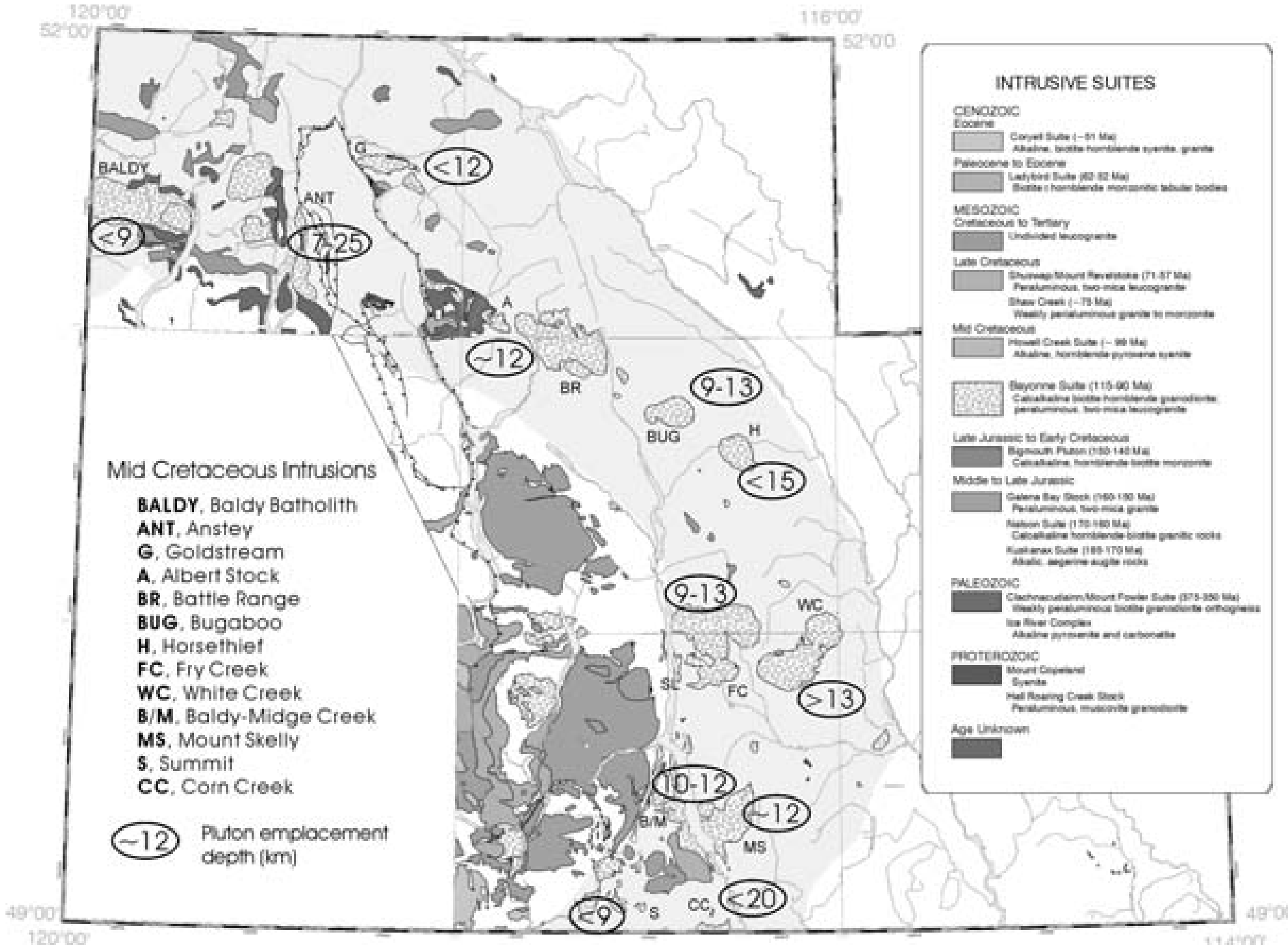

Figure 3. Distribution of plutonic rocks in southeastern British Columbia, illustrates the inboard location of the Bayonne Magmatic belt. Numbers are the mid Cretaceous emplacement depths calculated from contact metamorphic mineral assemblages using pressure limits defined for bathozones (Carmichael, 1978).

ceous felsic body. The San (MINFILE 82M 135), Windpass, Sweet Home (MINFILE 92P 39, 40), and Cam Gloria (MINFILE 82M 266) are quartz fissure veins hosted by a variety of intrusive rocks (Logan, 2000, 2001; and references within). Only the San is hosted in the causative mid-Cretaceous Baldy Batholith; the others are located variable distances from its margins, but are related to its associated Cretaceous hydrothermal activity. The Windpass/Sweet Home veins are hosted in a Permian or older gabbro of the Fennell Formation, approximately 1.5 km west of the Baldy, and the Cam Gloria veins occupy a Middle Jurassic monzodiorite, located approximately 8 km from the southern contact of the Baldy. At the Windpass/Sweet Home deposits the gabbro provided the competent host with open structures. At Cam Gloria the relationship between mineralization and the age of the host monzodiorite is not readily apparent in the field and geochronological (personal communication, D. Archibald, 2000; personal communication, Mortensen, 1999) and geochemical studies were necessary to establish the Cretaceous age of mineralization.

The metal ratios and zonation of these vein systems with respect to the Baldy Batholith generally follows the classic intrusion-related patterns (Figure 1), (Flanigan *et al.*, 2000; Hart *et al.,* 2000; Lang and Baker, 2001). On the other hand the San is a Ag-rich, Pb-Zn-As-Bi±Au quartz vein enveloped by a moderate to strong alteration zone of sericite and iron-carbonate. It does not have the typically low base metal content and high Bi:Au ratios common to intrusion-hosted deposits. The proximal Au-Ag-Cu-Bi quartz veins of the Windpass and Sweet Home mines possess high Bi:Au ratios (Logan, 2001) and the distal auriferous Pb-Ag-Bi±As quartz veins at Cam-Gloria have moderate Bi:Au ratios. ^{40}Ar-^{39}Ar cooling ages from alteration sericite at the San give 93 Ma that correspond with mid Cretaceous biotite and muscovite cooling ages for the batholith (Wanless *et al.*, 1966; Kirkland, 1971; personal communication, D. Archibald, 2000). Galena Pb-isotope compositions from all three cluster together with feldspar leads from the batholith around Cretaceous model ages (personal communication, J. Gabites, 2001).

TABLE 2
CHARACTERISTICS OF ALASKA AND YUKON INTRUSION-RELATED DEPOSITS (FLANIGAN *ET AL.*, 2000)

Deposit	Size (Au)	Mineralization*	Characteristics	Temp*	Pressure	Depth*
True North	1.3 M oz	S-hosted	distal, intermediate depth		~0.5 kb	0.5 km
Ryan Lode	2.4 M oz	I-hosted	proximal, intermediate depth		0.5-.75 kb	<3 km
Dolphin	1.5 M oz	I-hosted	intermediate depth		1 kb	3 km
Cleary Hill		S-hosted	intermediate depth	~300^{o}C	0.9 kb	3 km
Brewery Creek	0.6 M oz	I&S-hosted	shallow level		<1 kb	<3.5 km
Clear Creek		I-hosted	low pressure metam assemblages: and, sill, cor, pyrr, bio, grnt			
Fort Knox	7.2 M oz	I-hosted	deep-level	305±25^{o}C	1.25-1.5 kb	4-5 km
Dublin Gulch	1.5 M oz	I-hosted	bi-qtz-an	200-350^{o}C	>1.5 kb	>5.25 km
Pogo	5.2 M oz	S-hosted	proximal, deep-level	310-640^{o}C	1.75-2.0 kb	6-7 km
Scheelite Dome		I&S-hosted	brittle	240-350^{o}C	up to 2.5 kb	< 8 km
Mactung*		sheeted veins			>2.3 kb	
		W-skarn			2-2.5 kb	8.5 km
Donlin Creek	10.1 M oz	I-hosted	shallow level	<550^{o}C	<0.5 kb	< 2 km
Nixon Fork	0.1 M oz	Skarn	intermediate level		<1 kb	<3.5 km
Shotgun	1.0 M oz	I-hosted	proximal	450-600^{o}C	low pressure	

Mactung data (Atkinson and Baker, 1986)

Mineralization: S-hosted = sediment hosted, I-hosted = intrusion hosted.

Temperature: from fluid inclusion thermometry/barometry and/or sulphide pair thermometry

Depth: conversion from pressure data uses 1 kb = 3.5 km.

IMPLICATIONS FOR EXPLORATION

Contact metamorphic mineral assemblages from country rocks adjacent to the plutons and batholiths of the Bayonne Magmatic belt indicate varying pressures from <2.5 kbars to ~5 kbar (using pressure limits defined for bathozones; Carmichael, 1978). These pressure ranges correspond to emplacement depths of ~8 km to as much as 18 km (assuming 1 kbar = 3.5 km). In comparison, the intrusive-related mineral deposits in Alaska and the Yukon are inferred to have formed at generally shallower levels (Table 2), with several notable exceptions: Pogo and Scheelite Dome. The schematic geological and exploration model of Lang and Baker (2001) show a vertical range from the surface to 7 km depth and a lateral range of 2 km for intrusion-related gold systems. This level of the crust is generally attributed to the brittle regime, and with the exception of the Pogo deposit, the majority of Alaska and Yukon deposits formed under pressure, temperature, fluid content and strain rates associated with brittle deformation. The mid-Cretaceous intrusions of the Bayonne magmatic belt were intruded at structural levels that span both brittle and ductile regimes.

Using the intrusion-related model of Lang and Baker (2001) the explorationist would be focused to areas at the northern and southern ends of the belt where shallower level (<2.5 kbar) mid Cretaceous intusions and related mineralization are preserved. Gold-bismuth quartz veins (Windpass, Sweet Home) at the west end of the Baldy Batholith have mid-1900s production records totaling more than 1.0 M g of Au (Taylor, 1989) and recent discoveries along its southeastern margin at the Cam-Gloria (Evans, 1999). At the south end of the belt near Salmo, tungsten skarn, molybdenum mineralization and bismuth-gold mantos are developed in Paleozoic calcareous sediments adjacent to, and more distal from Cretaceous intrusions on the Emerald Tungsten property (Cathro and Lefebure, 2000). The gold-silver vein deposits of the Sheep Creek camp, located 6 km to the northeast are also Cretaceous or younger (Höy, i*n press*). Biotite granite intrusions with molybdenum occupy the lower levels at the Kootenay Belle gold mine (Mathews, 1953) and infer a spatial relationship to the Au-Ag veins. Mineralization formed at deeper structural levels (~3.5 kbar) is exposed east of Kootenay Lake. Here, there has been limited past production of gold and tungsten from quartz-filled sheeted veins hosted by the Mount Skelly stock at the Valparaiso mine near Creston. There are also low-grade, auriferous, sheeted veins throughout the stock. The characteristics of the Valparaiso veins indicate this is a British Columbia example of a Fort Knox-type deposit (intrusion-hosted) that has formed at substantially deeper levels than its Alaskan counterpart.

ONGOING RESEARCH

Geochronological, fluid inclusion and Pb-isotope investigations of mineral occurrences associated with the Bayonne Suite are ongoing. The ability to establish relationships between mineralization and the intrusive host is paramount to understand the potential of the intrusion and for directing exploration to additional mineralization in the belt.

Age constraints for the plutons are complicated by the composite nature of the larger bodies, discordant U-Pb systematics related to inheritance (xenocrystic zircons), high-grade metamorphism and lead loss. The limited database consists primarily of old K-Ar, Rb-Sr and more recent Ar-Ar ages all which represent relative cooling ages specific to the blocking temperature of the minerals dated. The few uranium-lead zircon age dating studies have focused on the Tertiary extension history of southeastern British Columbia (Parrish *et al*., 1988; Parrish 1995; and references within; Carr, 1992). Preliminary uranium-lead dating studies have been completed on the Battle Range Batholith and identify a 100Ma honblende granodiorite phase, and an approximately 87 Ma, 2-mica granite (personal communication, W. McClelland, 2001). Doug Archibald (Queen's University) has completed $^{40}Ar/^{39}Ar$ step-heating analyses of a substantial number of alteration assemblages associated with Cretaceous intrusion-related mineralization throughout the belt. For the most part, cooling ages of plutons, alteration and mineralization are mid-Cretaceous, but disturbed $^{40}Ar/^{39}Ar$ spectrum indicate some Late Cretaceous and Eocene thermal events for both the Baldy Batholith (north end of the belt) and Mount Skelly Pluton (south end of the belt), respectively.

Pb-isotope analyses of potassium feldspars from intrusions and sulphides from mineralization are currently underway at The University of British Columbia under the direction of Janet Gabites. The study was undertaken to determine the Pb isotope characteristics of a variety of intrusion-related mineral occurrences and selected mid-Cretaceous intrusions that comprise the Bayonne Magmatic belt. These data, in conjunction with the extensive deposit database of southeast British Columbia, will characterize intrusion-hosted, proximal and distal deposits, and permit an assessment of the potential for additional unrecognized intrusive-related mineral deposits. Other studies have utilized initial Pb isotope ratios of plutons to characterize source regions for granitoid rocks (Ayuso, 1986; Bevier, 1987). Isotopic studies of intrusion-related gold systems in the Yukon and Alaska show that Pb-isotope values of potassium feldspars from plutons and galenas from veins and skarns show a similar range in values (McCoy *et al*., 1997, Mortensen *et al*., 1996). Assuming the vein deposits are intrusion-related (magmatic Pb) their galena Pb-isotope compositions should be similar to the initial Pb-isotope compositions of the plutons, which in the case of the mid-Cretaceous suite were derived from anatexis of Precambrian crust in response to crustal thickening.

Fluid inclusion work was carried out by Kathyrn Dunne to characterize the fluids associated with late-stage plutonic phases and pegmatites of the mid Cretaceous suite and to compare them with fluids associated with gold mineralization. The Baldy and Battle Range Batholith areas were selected for fluid inclusion study and microthermometric analyses because they contain late-stage phases as well as intrusion-hosted, proximal and distal styles of mineralization. It was hoped that composition and temperature results could be interpreted with respect to the spatial relationship these categories infer. The preliminary results of the Bayonne study indicate that the fluids are rich in CO_2 and that all of the fluid inclusions homogenize between 150 and 350^o C.

Intrusion-related gold deposits are characterized by low to moderate (0-12%) saline fluids rich in CO_2 (McCoy *et al.*, 1997, Baker and Lang, 1999, 2001). Fluid inclusions from these systems comprise vapour-rich and vapour-poor inclusions that consistently indicate H_20-CO_2 immiscibility occurred during gold deposition (Metz, 1991, McCoy *et al.*, 1997).

In an earlier study Hardy (1993) indicated that the Sheep Creek gold veins formed from H_2O-CO_2±CH_4, low to moderately saline fluids at temperatures of 300±500^{o}C under conditions of variable pressures between 1-2 kbars. These too have similar characteristics and conditions of formation to those described by McCoy *et al.* (1997) and Baker and Lang (1999) for intrusion-related gold deposits in Alaska and the Yukon.

CONCLUSIONS

The Bayonne magmatic suite comprises the southern extension of an extensive mid Cretaceous W±Sn±Mo metallogenic province that follows the Omineca belt north from the Canadian-US border to Alaska. Gold mineralization is associated with the Tombstone and Tungsten suite intrusions at the north end of the belt. The Tombstone intrusions are primarily metaluminous, subalkalic, reduced I-type suite, and are associated with Au-Bi-W-As-Sb mineralization, and while the Tungsten suite also contain sheeted auriferous quartz veins ±Bi-Te similar to Fort Knox style mineralization they comprise a suite of strongly peraluminous 2-mica granites more commonly associated with W skarn deposits. The Bayonne suite intrusions of southern British Columbia are mostly peraluminous, subalkalic granodiorite and highly fractionated 2-mica granites, aplites and pegmatites that have more similarities with the Tungsten than Tombstone suite. In general the intrusions in the Bayonne magmatic belt were emplaced at greater depths (under greater pressures) than either of the Tombstone or Tungsten suites. Many of the Bayonne plutons contain Mo mineralization that reflect the greater depth of emplacement.

The northern and southern ends of the Bayonne Magmatic belt contain structural levels that preserve the shallowest intrusions (<9 km). Intrusion-related mineral assemblages (Au-Bi-W-Te) are concentrated around these intrusions and the potential to discover new occurrences is highest in these areas.

Ongoing research will shed more light on the similarities the Bayonne mineral occurrences share with the Yukon and Alaska deposits but will also recognize those characteristics and exploration criteria unique to the gold mineralization associated with the mid Cretaceous intrusions of southern British Columbia.

ACKNOWLEDGEMENTS

Critical reviews by Dave Lefebure and Brian Grant have improved the manuscript.

REFERENCES

Archibald, D. A., Glover, J. K., Price, R. A., Farrar, E. and Carmichael, D. M. (1983): Geochronology and tectonic implications of magmatism and metamorphism, southern Kootenay Arc and neighbouring regions, southeastern British Columbia. Part I: Jurassic to mid-Cretaceous; *Canadian Journal of Earth Sciences*, Volume 20, p. 1891-1913.

Archibald, D. A., Krogh, T.E., Armstrong, R.L. and Farrar, E. (1984): Geochronology and tectonic implications of magmatism and metamorphism, southern Kootenay Arc and neighbouring regions, southeastern British Columbia. Part II: mid-Cretaceous to Eocene; *Canadian Journal of Earth Sciences*, Volume 21, pages 567-583.

Ayuso, R.A. (1986): Lead-isotope evidence for distinct sources of granite and for distinct basements in the northern Appalachians, Maine; *Geology*, Volume 14, pages 322-325.

Baker, T. and Lang, J.R. (1999): Geochemistry of hydrothermal fluids associated with intrusion-hosted gold mineralization, Yukon Territory; in Stanely C.J. *et al.*, eds., Mineral deposits: processes to processing, *Balkema*, Rotterdam, pages 17-20.

Baker, T. and Lang, J.R. (2001): Fluid inclusion characteristics of intrusion-related gold mineralization, Tombstone-Tungsten magmatic belt, Yukon Territory, Canada; *Mineralium Deposita*, Volume 36, no 6, pages 563-582.

Baker, T., Lang, J.R. and Mortensen, J.K. (1996): Characteristics of mineralization associated with intrusions of the mid-Cretaceous Tombstone-Tungsten magmatic belt, Yukon; *Economic Geology*.

Bakke, A. (1995): The Fort Knox 'porphyry' gold deposit - structurally controlled stockwork and shear quartz vein, sulphide-poor mineralization hosted by a Late Cretaceous pluton, east-central Alaska; *in* Porphyry Deposits of the Northwestern Cordillera, *Canadian Institute of Mining, Metallurgy and Petroleum*, Special Volume 46, p. 795 -802.

Barker, F., and Arth, J.G. (1990): Two traverses across the Coast batholith, southeast Alaska; *in* The Nature and Origin of Cordilleran Magmatism, Anderson, J.L., ed., Memoir *Geological Society of America*, 174, pages 395-4905.

Bevier, M.L. (1987): a Pb isotope study of the Valhalla complex and its surrounding rocks, southeastern British Columbia: preliminary interpretations; *in* Radiogenic Age and Isotopic Studies, *Geological Survey of Canada*, Paper 87-2, pages 13-20.

Brandon, A.D. and Lambert, R.St.J. (1993): Geochemical characterization of mid-Cretaceous granitoids in the Kootenay Arc in the southern Canadian Cordillera; *Can. J. Earth Sci*., 30, p. 1076-1090.

Brandon, A.D. and Smith, A.D. (1994): Mesozoic granitoid magmatism in southeast British Columbia: implications for the origin of granitoid belts in the North American Cordillera; *Journal of Geophysical Research*, volume 99, p. 11,879-11,896.

Brown, D.A, Doughty, P.T., Glover, J.K., Archibald, D.A., Davis, D.W. and Pattison, D. (in prep.): Purcell Anticlinorium to Kootenay Arc, southeastern British Columbia; Hwy 3-Creston Summit Pass, and northern Priest River Complex; *B.C. Ministry of Energy and Mines*, Field Trip Guide and Road Log.

Brown, R.L., McNicoll. V.J., Parrish, R.R. and Scammell, R.J. (1992): Middle Jurassic Plutonism in the Kootenay terrane, northern Selkirk Mountains, British Columbia; *in* Radiogenic Age and Isotopic Studies, Report 5, *Geological Survey of Canada*, Paper 91-2, pages 135-141.

Carmichael, D.M. (1978): Metamorphic bathozones and bathograds: A measure of the depth of post-metamorphic uplift and erosion on the regional scale; *American Journal of Science*, Volume 278, pages 769-797.

Carr, S.D. (1992): Tectonic setting and U-Pb geochronology of the early Tertiary Ladybird leucogranite suite, Thor-Odin-Pinnacles area, southern Omineca Belt, British Columbia; *Tectonics*, v. 11, p. 258-278.

Cathro, M. and Lefebure, D.V. (2000): Several new intrusive-related gold, bismuth and tungsten occurrences in Southern British Columbia; *British Columbia Ministry of Energy and Mines*, Geological Fieldwork 1999, p.207-223.

Crowley, J.L. and Brown, R. L. (1994): Tectonic links between the Clachnacudainn terrane and implications for tectonic setting in the southern Omineca belt, Canadian Cordillea; *Tectonics*, v. 13, p. 1035-1051.

Diment, R. and Craig, S. (1999): Brewery Creek gold deposit, central Yukon; *in* Roots, C.F., and Emond, D.S., eds., Yukon exploration and geology 1998, *Exploration and Geological Services Division Yukon, Indian and Northern Affairs Canada*, pages 225-230.

Duncan, R.A. (1999): Physical and chemical zonation in the Emerald Lake pluton, Yukon Territory; M.Sc. thesis, *The University of British Columbia*, Vancouver, British Columbia.

Evans, G. (1999): Geological & geophysical & geochemical & diamond drilling report on the Cam Gloria Property; *B.C. Ministry of Energy and Mines,* Assessment Report 26 215, 21 pages.

Flanigan, B.P., Freeman, C., Newberry, R.J., McCoy, D., and Hart, C.J.R. (2000): Exploration models for mid and Late Cretaceous intrusion-related gold deposits in Alaska and the Yukon Territory, Canada; *in* Geology and Ore Deposits 2000: *The Great Basin and beyond proceedings volume II*, pages 591-614.

Fyles, J.T. and Hewlett, C.G. (1959): Stratigraphy and structure of the Salmo lead-zinc area, British Columbia; *British Columbia Department of Mines*, Bulletin 41.

Ghosh, D.K. (1995): Nd-Sr isotopic constraints on the interaction of the Intermontane Superterrane with the western edge of North America in the southern Canadian Cordillera; *Canadian Journal of Earth Sciences*, v. 32, p. 1740-1758.

Greenwood, H.J., Woodsworth, G.J., Read, P.B., Ghent, E.D. and Evenchick, C.A. (1991): Metamorphism, Chapter 16: in Geology of the Cordilleran Orogen in Canada; H. Gabrielse, H., and C. J. Yorath, eds., *Geological Survey of Canada*, Geology of Canada, no. 4, p. 533-570 (also Geological Society of America, The geology of North America, v. G-2).

Hardy, R.V. (1993): A light stable isotope and fluid inclusion study of the Sheep Creek gold camp, Salmo, British Columbia; GAC-MAC-CGU Joint Annual Meeting, Edmonton, Ab., page A-40.

Hart, C. J.R., Baker, T. and Burke, M. (2000): New exploration concepts for country-rock-hosted, intrusion-related gold systems: Tintina Gold Belt in Yukon; *in* The Tintina Gold Belt Concepts, Exploration and Discoveries,ed., J.L. Jambour, *British Columbia and Yukon Chamber of Mines*, Cordilleran Exploration Roundup 2000, Extended abstracts volume.

Hoisch, T.D. and Hamilton, W.B. (1990): Granite generation by fluid-induced anatexis; *Eos Trans*., American Geophysical Union, volume 71, pages 694-696.

Höy, T. and Dunne, K.P.E. (1998): Geological Compilation of the Trail map-area, southern British Columbia; *B.C. Ministry of Energy and Mines*, Open File 1998-1.

Höy, T. and Dunne, K.P.E. (in press): Metallogeny and mineral deposits of the Nelson-Rossland map-area; PartII: The early Jurassic Rossland Group, southeastern British Columbia; *B.C. Ministry of Energy and Mines*, Bulletin 109

Hyndman, D.W. and Foster, D.A. (1988): The role of tonalities and mafic dikes in the generation of the Idaho batholith; *Journal of Geology*, volume 96, pages 31-46.

Johnson, B.J. (1994): Structure and tectonic setting of the Okanagan Valley fault system in the Shuswap Lake area, southern British Columbia; unpublished Ph.D. thesis, *Carleton University*, 266 pages.

Kirkland, K.J. (1971): Sulphide deposition at Noranda Creek, British Columbia; Unpublished M.Sc. thesis, *University of Alberta*, Edmonton, Alberta, 107 pages.

Lang, J.R. and Baker, T. (2001): Intrusion-related gold systems:the present level of understanding; *Mineralium Deposita*, Volume 36, no 6, pages 477-489.

Lang, J.R., Baker, T., Hart, C.J.R. and Mortensen, J.K. (2000): An exploration model for intrusion-related gold-systems; *SEG Newsletter*, no 40, p. 6-15.

Leclair, A.D., Parrish, R.R. and Archibald, D.A. (1993): Evidence for Cretaceous deformation in the Kootenay Arc based on U-Pb and 40Ar/39Ar dating, southeastern British Columbia; *in* Current Research, Part A: *Geological Survey of Canada*, Paper 93-1A, p. 207-220.

Lefebure, D.V. and Cathro, M. (1999): Plutonic-related gold-quartz veins and their potential in British Columbia; *in* Short Course on Intrusion-Related Gold- *Kamloops Exploration Group*, p. 185-219.

Lefebure, D.V., Fournier, M.A. and Jackaman, W. (1999): Prospective areas in British Columbia for gold-tungsten-bismuth veins; *British Columbia Ministry of Energy and Mines*, Open File 1999-3, 1:2 000 000 scale map with marginal notes and digital files.

Logan, J.M. (2000): Plutonic-related gold-quartz veins in southern British Columbia; in Geological Fieldwork 1999, *British Columbia Ministry of Energy and Mines*, Paper 2000-1, pages 265-278.

Logan, J.M. (2001): Prospective areas for intrusion-related gold-quartz veins in southern British Columbia; *in* Geological Fieldwork 2000, *British Columbia Ministry of Energy and Mines*, Paper 2000-1, pages 113-134.

Logan, J.M. (2002):Intrusion-related mineral occurrences of the Bayonne magmatic belt, southeast British Columbia; *B.C. Ministry of Energy and Mines*, Geoscience Map 2002-1, 1:500 000 scale map with marginal tables.

Logan, J. M. and Colpron, M. (1995): Northern Selkirk Project - geology of the Goldstream River Map Area (82M/9 and Parts of 82M/10); *in* Geological Fieldwork 1994, Grant, B. and Newell, J. M., Editors, *B. C. Ministry of Energy, Mines and Petroleum Resources*, Paper 1995-1, pages 215-241.

Logan, J.M. and Friedman, R.M. (1997): U-Pb ages from the Selkirk Allochthon, Seymour Arm map area, Southeast British Columbia (82M/8 and 9); *in* Geological Fieldwork 1996, *B.C. Ministry of Energy and Mines*, Paper 1997-1, pages 17-23.

Logan, J.M., Lefebure, D., and Cathro, M. (2000): Plutonic-related gold-quartz veins and their potential in British Columbia; *in* The Tintina Gold Belt Concepts, Exploration and Discoveries, ed., J.L. Jambour, *British Columbia and Yukon Chamber of Mines*, Cordilleran Exploration Roundup 2000, Extended abstracts volume, p. 197-225.

Mathews, W.H. (1953): Geology of the Sheep Creek Camp, *British Columbia Department of Mines,* Bulletin 31, 94 pages.

McCoy, D., Newberry, R.J., Layer, P., DiMarchi, J.J., Bakke, A., Masterman, J.S., and Minehane, D.L. (1997): Plutonic-related Gold Deposits of Interior Alaska; *Economic Geology*, Monograph 9, p. 191-241.

Metz, P.A. (1991): Metallogeny of the Fairbanks district, Alaska and adjacent areas; Mineral Industry Research Laboratory Report 90, School of Mineral Engineering, *University of Alaska*, Fairbanks, Alaska, 370 pages.

Monger, J.W.H. and Berg, H.C. (1984): Lithotectonic terrane map of western Canada and southeastern Alaska; in Lithotectonic Terrane Maps of the North American Cordillera, N.J. Siberling and D.L. Jones Editors, *United States Geological Survey*, Open File Report 84-523.

Monger, J.W.H., Price, R.A. and Tempelman-Kluit, D.J. (1982): Tectonic accretion and the origin of the two major metamorphic and plutonic welts in the Canadian Cordillera; *Geology*, Volume 10, pages 70-75.

Mortensen, J.K. (1999): YUKONAGE, An isotopic age database for the Yukon Territorya; *in* Yukon digital geology, Gordey, S.P., and Makepeace, A., compilers; *Geological Survey of Canada*, Open File D3826.

Mortensen, J.K., Lang, J.R., and Baker T. (1997): Age and gold potential of the Tungsten plutonic suite in the Macmillan Pass area, western N.W.T.; *25th NWT Geoscience Forum*, Yellowknife, N.W.T., November 26-28, 1997, pages 79-80.

Mortensen, J.K., Hart, C.J.R., Murphy, D.C., and Heffernan, S. (2000):Temporal evolution of early and mid-Cretaceous magmatism in the Tintina Gold Belt; ; *in* The Tintina Gold Belt Concepts, Exploration and Discoveries, ed., J.L. Jambour, *British Columbia and Yukon Chamber of Mines*, Cordilleran Exploration Roundup 2000, Extended abstracts volume, p. 49-57.

Mortensen, J.K., Murphy, D.C., Hart, C.J.R. and Anderson, R.G. (1995): Timing, tectonic setting and metallogeny of Early and Mid-Cretaceous magmatism in Yukon Territory; *Geological Society of America*, Abstracts with Programs, v.27, no. 5, p.65.

Murphy, D.C., van der Heyden, Parrish, R.R., Klepacki, D.W., McMillan, W., Struik, L.C. and Gabites, J. (1995): New Geochronological constraints on Jurassic deformation of the western edge of North America, southeastern Canadian Cordillera; *in* Magmatism and tectonics of the North American Cordillera, *ed*., D.M. Miller and C. Busby, *Geological Society of America*, Special Paper 299, p. 159-171.

Newberry, R.J., McCoy, D.T. and Brew, D.A. (1995): Plutonic-hosted gold ores in Alaska: Igneous versus metamorphic origin; *Resource Geology Special Issue*, no. 18, pages 57-100.

Newberry R.J. (2000): Mineral deposits and associated Mesozoic and Tertiary igneous rocks within the interior Alaska and adjacent Yukon portions of the 'Tintina Gold Belt': A progress report; *in* The Tintina Gold Belt Concepts, Exploration and Discoveries, ed., J.L. Jambour, *British Columbia and Yukon Chamber of Mines*, Cordilleran Exploration Roundup 2000, Extended abstracts volume, pages 59-88.

Parrish, R. R. (1992): Miscellaneous U-Pb Zircon Dates from Southeast British Columbia; *in* Radiogenic Age and Isotopic Studies: Report 5, *Geological Survey of Canada*, Paper 91-2, pages 143-153.

Parrish, R.R. (1995): Thermal evolution of the Southeastern Canadian Cordillera; *Canadian Journal of Earth Sciences*, v. 32, p. 1618-1642.

Parrish, R.R., Carr, S.D. and Parkinson, D.L. (1988): Eocene extensional tectonics and geochronology of the southern Omineca Belt, British Columbia and Washington; *Tectonics*, v. 7, p. 181-212.

Patino Douce, A.E., Humphreys, E.D., and Johnston, A.D. (1990): Anatexis and metamorphism in tectonically thickened continental crust exemplified by the Sevier hinterland, western North America; *Earth and Planetary Science Letters*, no. 97, pages 290-315.

Poulsen, K.H, Mortensen, J.K. and Murphy, D.C. (1997): Styles of intrusion-related gold mineralization in the Dawson-Mayo Area, Yukon Territory; *in* Current Research 1997-A, *Geological Survey of Canada*, pages 1-10.

Price, R. A. (1986): The Southeastern Canadian Cordillera: Thrust faulting, tectonic wedging, and delamination of the lithosphere; *Journal of Structural Geology*, Volume 8, pages 239-254.

Scammell, R.J. (1993): Mid-Cretaceous to Tertiary thermotectonic history of former mid-crustal rocks, southern Omineca belt Canadian Cordillera; Ph.D. thesis, *Queen's University*, Kingston, Ont.

Schiarizza, P. and Preto, V.A. (1987): Geology of the Adams Plateau-Clearwater-Vavenby area; B.C. *Ministry of Energy, Mines and Petroleum Resources*, Paper 1987-2, 88 pages.

Sears, J. W. (1979): Tectonic contrasts between the Infrastructure and Suprastructure of the Columbian Orogen, Albert Peak Area, Western Selkirk Mountains, British Columbia; unpublished Ph.D. thesis, *Queen's University*, 154 pages.

Sevigny, J.H., Parrish, R.R., Donelick, R.A., and Ghent, E.D. (1990): Northern Monashee Mountains, Omineca Crystalline Belt, British Columbia: Timing of metamorphism, anatexis and tectonic denudation; *Geology,* volume 18, pages 103-106.

Sinclair, W.D. (1995): Molybdenum, tungsten and tin deposits and associated granitoid intrusions in the Canadian Cordillera and adjacent parts of Alaska; *in* Porphyry Deposits of the Northwestern Cordillera of North America: *Geological Society of the Canadian Institute of Mining, Metallurgy and Petroleum*, Special Volume 46, pages 58-76.

Smith, M., Thompson, J.F.H., Bressler, J., Layer, P., Mortensen, J.K., Abe, I. and Takaoka, H. (1999): Geology of the Liese Zone, Pogo Property, East-Central Alaska; *SEG Newsletter*, No. 38, July 1999 pages 12-21.

Taylor, W.A. (1989): Windpass, Sweet Home (092P039, 49); *B.C. Ministry of Energy, Mines and Petroleum Resources*, Exploration In British Columbia 1988, pages B115-B121.

Thompson, J.F.H., Sillitoe, R.H., Baker, T., Lang, J.R. and Mortensen, J.K. (1999): Intrusion-related gold deposits associated with tungsten-tin provinces; *Mineralium Deposita*, Volume 34, Number 4, p. 323-334.

Wanless, R.K., Stevens, R.D., Lachance, G.R. and Rimsaite, J.Y.H. (1966): Age determinations and geological studies K-Ar isotopic ages, Report 6; *Geological Survey of Canada*, Paper 65-17.

Warren, M. J. (1997): Crustal Extension and subsequent crustal thickening along the Cordilleran rifted margin of ancestral North America, Western Purcell Mountains, Southeastern British Columbia; unpublished Ph.D. thesis, *Queen's University*, 361 pages.

Woodsworth, G.J., Anderson, R.G. and Armstrong, R.L. (1991): Plutonic regimes, Chapter 15: in Geology of the Cordilleran Orogen in Canada; *Geological Survey of Canada*, Number 4, p. 491-531 (also *Geological Society of America*, The Geology of North America, volume G-2).

Overview of Coalbed Methane Geology in Northeast British Columbia

By A.S. Legun

KEYWORDS: *Coalbed methane, Peace River coalfield, Gething Formation, Chamberlain member, Bullmoose Member, Gaylard Member, Bluesky Formation, Gates Formation, "Fourth coal", exploration model, coal isopachs.*

INTRODUCTION

The purpose of this paper is to overview the coalbed methane (CBM) geology of the Peace River District. The CBM potential is examined from regional perspectives relating to coal geology, conventional gas geology, structure and hydrology because there is very limited exploration data. Summary geographic figures are available in several reports and the writer has collated them in a series of overlays. Though some authors have cautioned that each coalbed methane play is unique (Nelson, 2000), a general exploration model for CBM is discussed briefly.

COALBED METHANE

Ryan (2000) provides a good introduction to coalbed methane in British Columbia. How methane is held in coal, reserve estimation and elements of recovery are recapitulated below. These comments draw on Ryan (ibid), Davidson *et al.* (1995), Bowden and Ehrlich (1998).

Methane may be adsorbed (held by weak forces to surfaces of microscopic pores in coals), be present as free gas, or be in solution in water associated with the coal. Adsorbed gas is the most important component and the property of adsorption distinguishes coal from conventional reservoirs for gas.

Adsorption capacity can be estimated roughly using basic parameters of depth and rank, but in detail a number of other parameters influence capacity. These include vitrinite content and micropore volume, which increase capacity, and moisture and ash content which decrease capacity.

Coal is not necessarily saturated with methane, particularly at depth. Also not all adsorbed gas is recoverable. Coal, retrieved at depth, must be tested to assess how methane desorbs from the coal. This leads to an estimate of methane content.

Davidson *et al.* (1995) provide a formula for resource assessment:

$GIP=A*h*Gc*C$

Where GIP=gas-in-place

A=drainage area

h=coal thickness

Gc=methane content from core studies

C=coal density

The well's drainage area depends on permeability, which is difficult to measure. To assess permeability both macro-permeability (open-space cleats, fractures) and micro-permeability (micro-fractures that release gas from matrix) need to be considered. The removal of formation water is also necessary to provide the pressure gradient to initiate and maintain gas flow from the cleat system to the well.

In practice, commercially successful CBM wells intersect coals with high gas yields at shallow depths (Bowden and Ehrlich, 1998). In some CBM fields secondary methane derived from anaerobic bacterial activity in the coal, and free gas under a compressed state (as in a conventional reservoir) contribute significantly to production.

PREVIOUS WORK

The first exploratory petroleum well, drilled by the B.C. government in 1921 at Farrel Creek, a few km east of the W.A.C. Bennet dam on the Peace River intersected water and gas at shallows depths (243 to 290 m) near the top of the Gething Formation, below a permeable conglomerate (Dresser 1922). The gas, used to heat the drilling camp during the winter of 1921/22, may be an early, unrecognised example of methane gas associated with aquifer flow in coal measures in the Peace District.

Subsequent geologic work in the Peace District focused on mapping specific areas near accessible occurrences of coal such as at Carbon Creek (Matthews, 1947) and Pine River (McKechnie, 1955). The first comprehensive regional work was done by Stott (1974) who measured and correlated a series of sections extending from the town of Cadomin in Alberta to the Peace River canyon in B.C. This provided the stratigraphic context for coal exploration in the foothills of Alberta and B.C. Coal exploration expanded rapidly in the 1970's with licenses stretching from the Graham River to the Alberta border. Duff and Gilchrist (1981) used both coal and petroleum well data to correlate Gething and Gates coal trends along the axis of the coalbelt. Leckie (1983,1986) in the north and Carmichael (1983, 1988) in the south, conducted field sedimentological studies on major sandstone bodies in the Gates, correlating them and intervening coal intervals to the subsurface of the plains. The sandstones (known as Fahler A to F) are important gas reservoirs in the subsurface of the plains. Karst and White (1980)

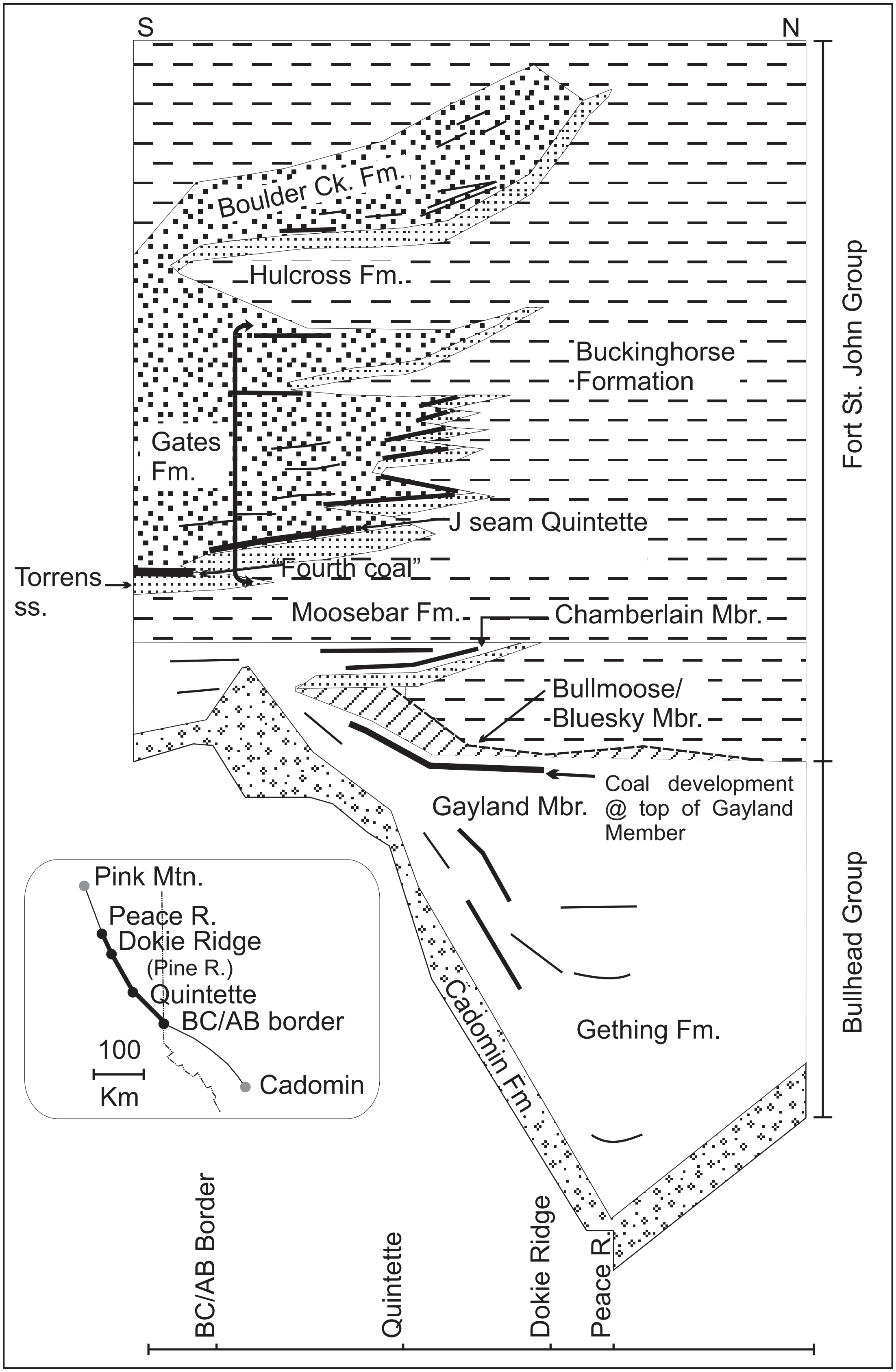

Figure 1. North-south cross section along the foothills of northeastern British Columbia. Modified from Kalkreuth and Leckie (1989).

produced maps showing the distribution of coal reflectance values at the top of the Gething Formation and used the contour plot to discuss the hydrocarbon maturation levels. Kalkreuth *et al.* (1989, 1991) subsequently used reflectance data to interpret the burial and thermal history from the plains to the foothills. Oppelt (1988) showed the Gething marine tongue of Duff and Gilchrist (1981) was a part of the Bluesky Formation, a gas and oil producer in the plains. Broatch (1988) used palynology to identify areas of marine influence in the lower part of the Gething Formation. Legun (1990) researched the extent of upper Gething coals (Chamberlain member) and Gibson (1992) produced a stratigraphic overview of the Gething Formation, formally dividing it into three members. Ryan (1996) compiled coal quality data for the Gething and attempted to gain some understanding of trends in petrography, ash chemistry and rank between coal properties.

Wyman (1984) modeled the coalbed methane potential of the "fourth" coal adjacent to Fahler sandstones in the subsurface of the plains. Lamberson and Bustin (1993) confirmed the high adsorption capacity of Gates coals and studied how maceral composition affected gas content. Ryan (personal communication) made preliminary calculations of CBM resources in the Peace District. Dawson (1995, 2000) formulated CBM exploration models for the foothills and Dawson *et al* (2000) reviewed the drilling results of an exploratory CBM well (Philips Flatbed) near the Monkman coal property.

REGIONAL STRATIGRAPHY

CBM potential in the area of study is largely restricted to two coal-bearing sequences, the Gething and the Gates of Lower Cretaceous age. The two formations are separated by Moosebar marine shale and part of a much larger sequence of interdigitating marine and continental strata that filled the subsiding foreland basin (*see* Figure 1). Though not reviewed in this paper, there is some potential for CBM in the older Minnes Group, the Boulder Creek Formation above the Gates, and the much younger (Upper Cretaceous) Wapiti Formation.

The general area of interest for potential CBM production is east of the coal license blocks of the coalfield shown in Figure 2. A great portion of the potential corresponds to the Gates and Gething formations in the subsurface of the outer foothills.

The structure of the outer foothills in the Peace District is characterized by low amplitude, long wavelength folds, and widely spaced thrusts. A line of section at Sukunka River (Figure 3 after McMechan, 1994) shows shallow depths to the CBM resource. The presence of the upper Fort St. John Group (Goodrich, Hasler and Cruiser formations) indicates areas where there is 1000 metres or less cover to Gates coal.

REGIONAL COAL RANK

In general methane resources in the outer foothills will be in coals of slightly higher rank than that of the coalfield to the west. A contour plot of coal rank (Figure 4) for the uppermost seam of the Gaylard member is taken from Kalkreuth and McMechan (1988). It is based on 664 samples taken from outcrop, mine sites, petroleum well cuttings, and coal borehole core. Reflectance values generally decrease in the direction of the inner foothills reflecting decreasing depth of burial. The axis of maximum rank underlies the outer foothills and is parallel to its trend. A significant area of high rank coal underlies an area centered southwest of Chetwynd. This area of low volatile bituminous coal is underlain by an even larger area of semi-anthracite at the stratigraphic level of the Lower Gething. The Burnt River coal deposit lies at the southwestern margin of the node.

Figure 2. Coal licenses, CBM experimental schemes, CBM land sales in relation to the outer and inner foothills of the Peace District.

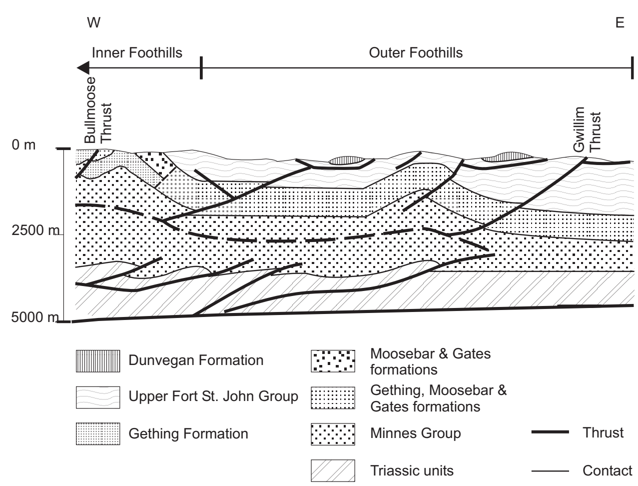

Figure 3. Line of section at Sukunka River from McMechan (1994).

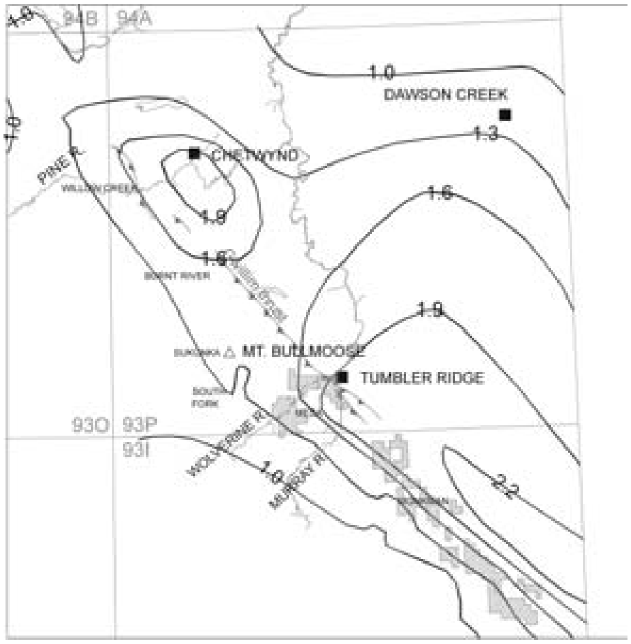

Figure 4. Isoreflectance lines for top of Lower Cretaceous Gething Formation after Kalkreuth and McMechan (1988).

The distribution of reflectance values for Gates coal in the Peace District is shown in Kalkreuth and McMechan (1988, 1991) with additional information provided by Kalkreuth and Leckie (1989). The values appear to follow the same trends as the Gething Formation, although they are at a slightly lower rank due to their shallower depth of burial. The rank varies from low volatile to high volatile bituminous, with low volatile bituminous coal restricted to the outer foothills. The reflectance values at some major coal properties are shown in the table below.

DETAILED STRATIGRAPHY

GETHING FORMATION

The Gething Formation reaches its greatest preserved thickness in the northwest part of the Peace River area (Carbon Creek) where the formation is up to 1100 metres thick with 60 thin seams. The formation is 500 m thick between Peace Canyon and the Pine River, declining to 360 m at Bullmoose Mountain, 200 m at Murray River and less than 100 m at the Alberta border. It also thins eastward, below the outer foothills into the subsurface of the plains.

TABLE 1
REFLECTANCE VALUES OF GATES FORMATION COAL AT SOME MAJOR PROPERTIES

Coal Property	Rank	Reference
Quintette	1.2 to 1.26 (mvb)	Kalkreuth and Leckie (1989)
Bullmoose	1.02 to 1.14 (hvb to mvb)	Kalkreuth and Leckie (1989)
Monkman	1.16-1.27 (mvb)	Leckie, Kalkreuth and Snowdon (1988)

The Gaylard Member represents the Gething Formation between Peace River and the Sukunka River (Figure 1). South of Sukunka River the Chamberlain member, a progradational deltaic wedge, forms the upper part of the Gething Formation and is separated from the Gaylard by a marine tongue of the Moosevale. The marine tongue, known as the Bullmoose member, thins in the Monkman area-its exact southern limit is unclear. South of Monkman the Gething Formation is not differentiated into members.

Duff and Gilchrist (1981), Kilby and Oppelt (1984), Legun (1990), Gibson (1992) drew stratigraphic sections extending from the foothills into the plains. These give a qualitative impression of coal seam distribution in the Gething Formation.

GAYLARD MEMBER

The Gaylard Member was deposited in a lower delta plain environment. Gibson (1992) noted some distributary channel sands, marine to brackish water bivalves and marine foraminifera in the area of Carbon Creek and West Carbon Creek. In the Sukunka and Wolverine River area Broatch (1988) also identified zones of marine influence based on palynological data. However, most Gaylard Member coals were formed in fresh-water environments, as their sulfur content is low. The seams occur en echelon stratigraphically and they are difficult to correlate laterally, suggestive of migrating delta distributary lobes and back swamps. Gaylard coals are not related to major strandplain sands as in the Gates Formation. Ryan (1996) suggests on the basis of inertinite rich coal at the top of many seams that peat swamps may have developed into raised mires.

The distribution of coal seams in the lower part of the Gaylard Member is poorly known due to limited drilling. A few property reports (East Mt. Gething, Rocky Creek, Burnt River, Carbon Creek) describe seams near the contact with the Cadomin Formation. There is more widespread coal development toward the top of the Member. In the Pine River area Ryan (1996) describes coal seam distribution, coal quality and petrography at the Falling Creek, Pine Pass, Lossan, Moberly and Willow Creek properties. Coals average 2-4 metres thick, with occasional coal intercepts exceeding 5 metres. Kilby (1984) used tonstein markers to show at least one seam in this area has a wide extent. He correlated the no. 1 seam at Willow Creek with the Trojan seam at Peace River canyon and southward to the B seam at Sukunka. Kilby and Oppelt (1984) also correlated the Trojan seam at Peace River Canyon eastward, showing it finally pinches out near Hudson Hope in the subsurface.

The B seam at Sukunka and Burnt River east properties is missing or poorly developed in some adjacent drill holes (Gibson 1992). Near the Wolverine River only thin coal intervals are intercepted in boreholes at this stratigraphic position. However further south on the Hermann Gething licenses near the Quintette mine a 5 metre thick seam lies about 45 metres below the top of the Gaylard Member.

The development of coal toward the top of the Gaylard member in the Pine to Murray River area probably reflects a period of low sediment influx and slow subsidence of the delta plain below sea level.

BULLMOOSE MEMBER

The Gaylard is overlain by the Bullmoose member, an upward coarsening shale to sandstone sequence as evident in the gamma trace on geophysical logs. It is not coal-bearing and contains marine to brackish water macro and microfossils. Isolated upward coarsening bodies at this stratigraphic position are present to the east in the subsurface of the plains and identified as the Bluesky.

CHAMBERLAIN MEMBER

Thick, massive sandstone forms the base of the Chamberlain member, which overlies the Bullmoose member. The Chamberlain coal seam lies directly on this shelf strandplain in a similar fashion to sandstone/coal pairs in the succeeding Gates Formation. Significant traceable seams in the Chamberlain member include the Chamberlain, Skeeter and Bird seams with individual thickness to 3 metres. In the subsurface seam development diminishes eastward toward Gwillim Lake and the disappearance of coal kicks on geophysical logs can be used to define the limit of coal measures. The trace of the zero coal isopach defines a lobe-like projection, probably a delta complex that prograded into the Moosebar sea (Figure 5). A sediment buildup is supported by the convergence of the twin tonsteins in the Moosevale and the Gething Formation in this area (Kilby 1984). A narrower deltaic shelf to the northwest flanks the lobe. The Chamberlain member varies from 60 to 100 metres thickness along the coalbelt. Near the Quintette mine the Chamberlain seam is apparently cut out by channel bodies (Legun 1990) but southeast of the Murray River equivalents of the Chamberlain and Bird seams reappear and are well developed (Fig. 5b, Gibson 1992). The Chamberlain delta underlies the outer foothills and is a potentially significant CBM resource due to artesian overpressure potential in continuous seams bounded by shale seals.

GETHING FM. COAL ISOPACHS

The writer is not aware of any regional compilation of total coal thickness for the Gething Formation that incorporates both coalbelt and subsurface plains data. A partial compilation is reported by Ryan (2000a) based on petroleum well data east of the coalbelt, mostly NTS 93P. This data is included in Figure 6; contours should be considered as trends as they omit thicker coal development immediately to the west. The isopach shows a maximum thickness from Pine River to the Murray River at the outcrop belt, and gradual decreasing coal development eastward in the subsurface.

In general the trends from the plains as reported by Ryan (ibid) match trends of thick coal development in the coalfield described above. The thickness in the coalbelt is probably 10-15 metres in a number of properties.

GATES FORMATION FACIES AND COAL ISOPACHS

Coal thickness trends for the Gates Formation are compiled from Carmichael (1983) and Leckie (1986) for the Peace coalfield (Figure 7). Major coals in the Gates tend to be paired with underlying strandline sands. The shoreline oscillated back and forth between Bullmoose Mt. in the north and the Wolverine River to the south. As a result the

Figure 5. Northern limit of coals in Chamberlain Member with section A-A' illustrating underlying marine Bullmoose Member.

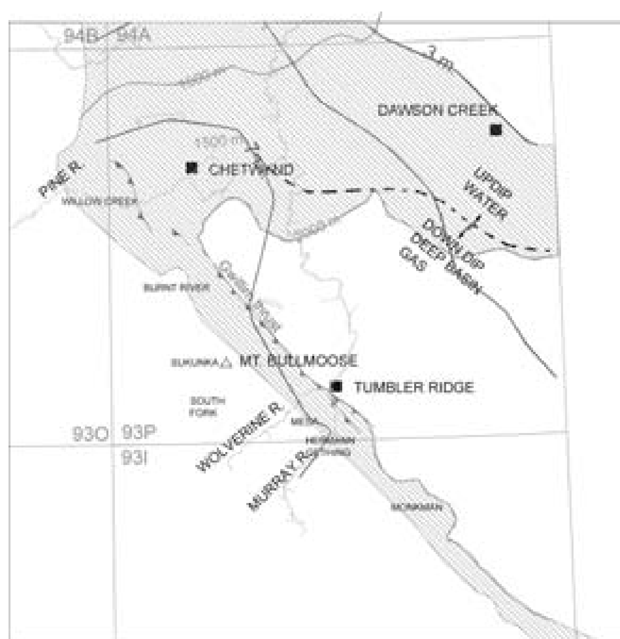

Figure 6. Gething CBM area in outer foothills defined by 2000 metre depth, 3 metre coal isopach and edge of inner foothills. Gething coal isopach after Ryan, (2000a). Note deep basin gas line.

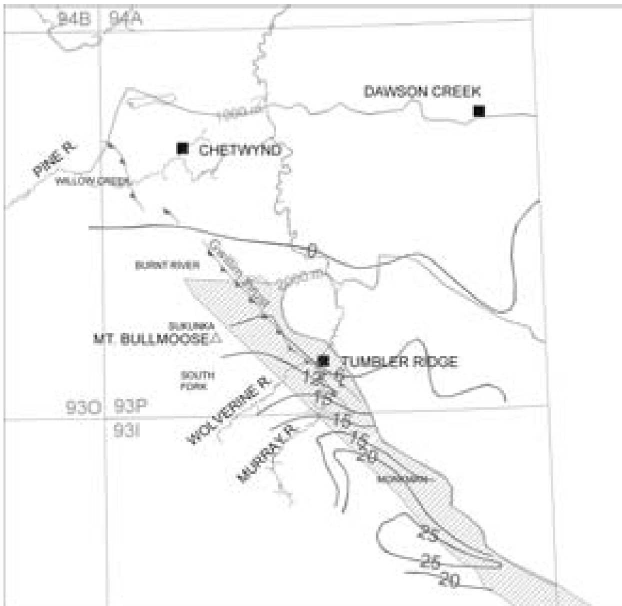

Figure 7. Gates CBM resource area in outer foothills defined by 2000 metre depth, 3 metre coal isopach. Coal thickness data from Carmichael (1983) and Leckie (1986).

coal thickness rapidly increases south of Bullmoose Mt. from 0 to 15 metres. It reaches a maximum of about 25 metres near Monkman and is about 20 metres at the Alberta border. It begins to diminish near Grande Cache in a complicated pattern (Figure 6 in Dawson and Kalkreuth, 1994).

Gates coals are considered to have developed directly on marine strandplains. Longshore drift of sand was an important component in their formation and these strandplains became isolated behind barrier bar delta fronts. Extensive areas were flooded, becoming freshwater lagoons and sites of extensive peat formation. The important strandplains in the Peace District are Fahler F and D. Overlying Fahler F, otherwise known as the Torrens member, is a thick coal that constitutes important coking coal resources at Monkman, Belcourt, Saxon properties in the southern part of the coalfield. Carmichael (1983,1988) noted that the basal J seam at Quintette sat on sandstone "step" above the Torrens, which he labeled Fahler D. He showed a likely correlation of seams from Alberta northward to the Quintette mine area.

Carmichael (1983, 1988) and Leckie (1986) make apparently different designations of the stratigraphic position of the J seam with Carmichael showing it above Fahler D and Leckie above Fahler F. This makes uncertain the correlation of the "Fourth coal" of the plains region, identified as the coal above Fahler F. The Fourth coal is considered a significant source of methane in the Alberta deep basin and has been isopached to the Peace River coalfield (Figure 8, from Kalkreuth and Leckie 1989).

It is uncertain whether the Fourth coal corresponds to J seam at Quintette and seams A and B at the Bullmoose South Fork deposit or only to a lower coal interval that is identified at the Monkman deposit and further south. If Carmichael is correct, the isopach should not extend so far north.

Figure 8. Isopach of "Fourth Coal" after Kalkreuth and Leckie (1989).

The extent of the "Fourth coal" is economically significant as a potential CBM resource in the subsurface and a marketable coking coal in the coalfield.

COALBED METHANE AREA OF INTEREST

The CBM area of interest in the Peace District has been very broadly defined in Figure 3 of the Ministry's publication Coalbed Methane in B.C. Further definition is obtainable by using isopach data, separating potential according to Formation and utilizing depth to Formation data from oil and gas databases, such as ACCUMAP. The next step might be plots of methane capacity as has been done for Gates coal in the Hinton, Alberta area (Dawson and Kalkreuth, 1994).

The intersection of the 2000 metre contour with coal isopach trends identifies the areas of interest for the Gething and Gates Formation. The 2000 metre line marks depth from surface to the formation top (from ACCUMAP). Two thousand metres is a general depth cutoff for CBM production based on reductions of permeability at these depths. The discontinuity of the Gwillim thrust is used in lieu of the contour in part of the area. Contours near the thrust are suspect, as they appear to include intersections in footwall rocks west of the thrust while in fact the CBM resource is upthrown in the hangingwall.

The area of Gething CBM potential is wide and extensive at the level of the Pine River, narrowing southward (Figure 6). Using the same criteria, the CBM potential in the Gates Formation extends from the vicinity of the Sukunka River near Bullmoose Mt. in a southeast direction along the outer foothills to the Alberta border (Figure 7). There is an area in which good potential for Gates and Gething coalbed methane overlap (Figure 9). This is the area from Bullmoose Mt. to Murray River.

HYDROGEOLOGY

High coalbed methane production is favored by artesian overpressure while hydrocarbon overpressure suggests low permeability. Therefore it is important to distinguish basin areas of artesian and hydrocarbon pressuring (Scott

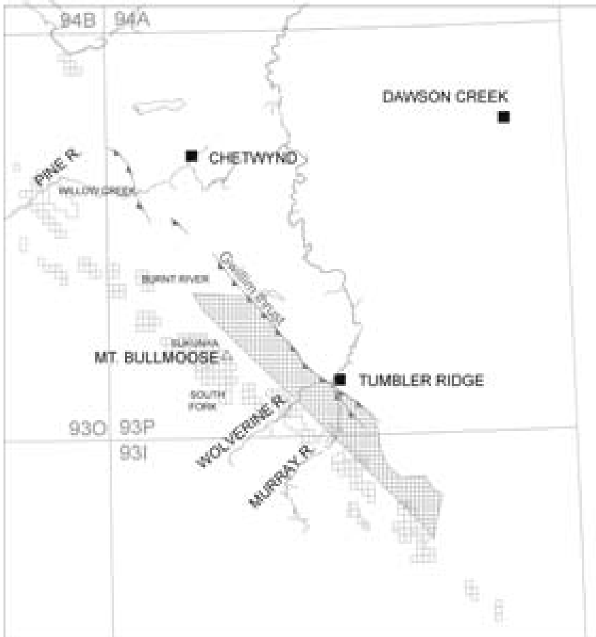

Figure 9. Area in outer foothills with CBM potential in both Gates and Gething Formation coals.

and Kaiser 1996). Hydrocarbon underpressures prevail at the deformation front in Alberta and they suggest insulation of these areas from recharge by the foothills (Karsten and Bachu (2001).

The gas-producing areas within the Alberta deep basin generally show which areas are subject to hydrocarbon pressures. The gas line, distinguishing up dip water from down dip gas for the Gething Formation, is plotted from Smith, Zorn and Sneider (1984) in Figure 6. This line extends to the vicinity of Chetwynd and lies within the depth limit of CBM. The gas line probably extends to the Gwillim thrust or its lateral equivalents. To the north there is recharge between the foothills to the subsurface Gething Formation. Subsurface gravity flow of these waters southward into the deeper part of the foreland basin may be impeded by deep basin gas. This is a "no-flow" boundary (*see* discussion below in the context of an exploration model).

Most of the area identified as a CBM resource area for Gates and Gething coal probably lies within the area of possible artesian overpressures. West of the Gwillim thrust local-scale compartmentalised flow systems are expected in fold structures, with water and gas flow as described by Dawson (2000).

ONE POSSIBLE INTEGRATED MODEL

Tyler *et al*. (2000) developed a general CBM exploration model based on the San Juan, Sand Wash and Piceane basins in the United States. Their model is adapted in Figure 10 and discussed in terms of known data on coal geology, thickness, facies and hydrology in the Peace District.

Tyler *et al.* (ibid) argue favorable conditions for the development of CBM include:

1. Thick laterally continuous coals of high thermal maturity;
2. basinward flow of ground water through coals toward perpendicularly oriented no flow boundaries, such as structural hingelines, faults, facies changes, and discharge areas.
3. generation of secondary biogenic gas; and
4. conventional and hydrodynamic trapping of gas along no-flow boundaries.

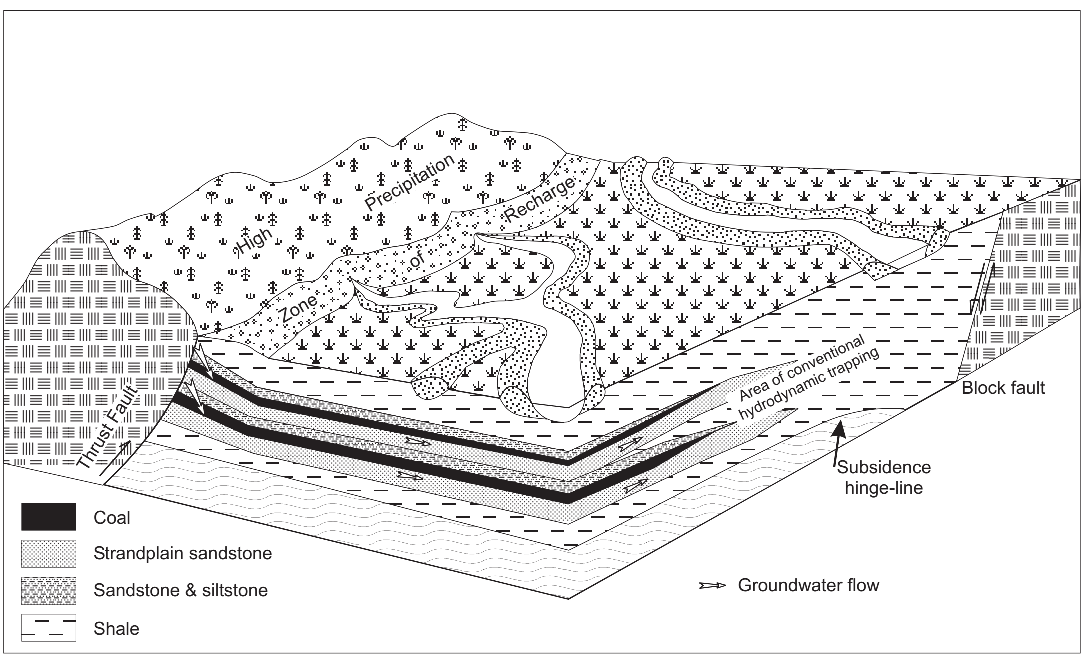

Figure 10. Exploration model showing favorable conditions for the development of CBM in a basin. Adapted from Tyler *et al*. (2000).

The Peace River Coalfield has some of these features:

Condition 1: All coal seams of the Gething and Gates Formation are thermally mature (at least high volatile A) and have moderate to high gas contents of 10-20 cc/g. Coal continuity is very good in the Gates, good in the Chamberlain member of the Gething, and upper part of the Gaylard. The occasional seam in the lower Gaylard is laterally continuous over a coal property.

Condition 2: Basinward flow of groundwater through coal aquifers is uncertain due to very limited data on coal permeability in the Western Canada sedimentary basin. Dawson (2000) suggests permeability averages less than 5 millidarcies and is often less than 0.1 md. Ryan (2000) suggested very low permeability in drilling at Philips Flatbed where Gates Formation coal was intersected in the 1150 to 1550 m depth range. By comparison permeability of the productive San Juan basin is 25md. Finding favorable permeability trends may be the principal challenge in Peace District CBM development.

Wyman (1984) found poor permeability in the "Fourth coal" of the Alberta deep basin, but the sample was derived at an abnormal depth for CBM (>2500 metres). He suggested it might be possible to mitigate poor permeability in coal by tapping an adjacent gas reservoir in permeable conglomerate. His model suggested half the methane content of the coal could be recovered over a period of ten years. In this scenario CBM is produced as an extension to a conventional gas play. Would this model work if there was water or water/gas filled porosity in the permeable sandstone? This is not clear.

Boundaries of "no-flow" perpendicular to presumed regional flow are present in facies changes: shale-outs at the seaward edge of Gates Formation and Chamberlain member "barrier bar" deltas. A structural hinge line at the latitude of Bullmoose Mountain controls the shale-outs. The northeast-trending hinge line marks greater subsidence and marine conditions to the north. However, regional gravity flow in aquifers may be south following the plunge of the major structure, the Alberta syncline. Gravity flow of water from the Sukunka and Murray foothill areas may migrate away from the facies transitions. There are a number of small fold structures west of the Gwillim thrust, some may plunge north and provide for gravity flow to "no-flow" facies traps and seals.

Kalkreuth and McMechan (1988) suggest late north-side up movement on a fault block is responsible for reduced burial and rapid decrease in coal reflectance values north of Chetwynd. The limits of the Alberta deep basin gas near Chetwynd may be related to this structural imprint. As previously mentioned, southward discharge of meteoric waters may be impeded by low permeability deep basin gas. Therefore, this is a "no-flow" boundary of exploration interest.

Condition 3: The writer is not aware of any data indicating generation of biogenic gas in the coals of the Peace District.

Condition 4: Conventional and hydrodynamic trapping of gas along no-flow boundaries may develop in the Chamberlain deltaic wedge. Gibson (1992) notes the Chamberlain sandstones are porous and if the coals have some permeability there may be coalbed methane gas trapped against the Moosevale shale aquitard, which overlies coal seams such as the Bird.

A promising variation on this play occurs where coals are overlain or adjacent to permeable conglomerates. Conglomerates occur at the top of coal measures, in particular the Gaylard (Kilby, 1983), and the upper Gates Formation (Carmichael, 1988). In the latter case Carmichael (1988) has suggested some formed in estuaries where original fluvial deposits were redistributed by marine currents during marine transgression. The association of these conglomerates with coals below shale may facilitate general aquifer permeability and hydrodynamic trapping of gas.

CONCLUSIONS

CBM exploration is at an early stage in northeast British Columbia and requires a further integration of data from coal, petroleum and hydrogeologic datasets. Coal thickness trends, rank and depth to resource suggest the outer foothills between Sukunka and Murray Rivers are particularly prospective due to tiered potential from both Gething and Gates formation coals. It is expected exploration work will develop once the permeability themes relevant to the Peace District are identified.

ACKNOWLEDGEMENTS

The writer thanks Derek Brown for project support. Dave Lefebure provided helpful editorial review and Barry Ryan clarified some CBM concepts for the author. Thanks to Kirk Hancock who drafted several of the figures and Mark Hayes who provided ACCUMAP plots.

REFERENCES

Bowden, W.R. and Ehrlich, R. (1998): Permeability of coals and characteristics of desorption tests: Implications for coalbed methane production; *International Journal of Coal Geology*, volume 35, pages 333-347.

Broatch, J. (1988): A Summary of the results of a palynological investigation of British Columbia's Northeast Coalfield; in Geological Fieldwork 1987, *B.C. Ministry of Energy, Mines and Petroleum Resources*, Paper 1988-1, pages 451-457.

Carmichael, S.M. (1983): Sedimentology of the Lower Cretaceous Gates and Moosebar Formations, Northeast Coalfields, British Columbia; Unpublished Ph.D. thesis, The University of British Columbia, 285 pages.

Carmichael, S.M. (1988): Linear estuarine conglomerate bodies formed during a mid-Albian marine transgression; "upper Gates" Formation, Rocky Mountain foothills of northeastern British Columbia, in D. P. James and D. A. Leckie, editors, Sequences, stratigraphy, sedimentology: surface and subsurface: *Canadian Society of Petroleum Geologists*, Memoir 15, pages 49-62.

Davidson, R., Sloss, L. and Clarke, L. (1995): Coalbed methane extraction; *IEA Coal Research*, 1995, 67 pages.

Dawson, F.M. (2000): Coalbed methane exploration in structurally complex terrain: A balance between tectonics and hydrogeology, in M. Mastalerz, M. Glikson and S. Golding editors, Coalbed Methane: Scientific, Environmental and Economic Evaluation; *Kluwer Academic Publishers*, pages 111-121.

Dawson, F.M. (1995): Coalbed Methane: A comparison between Canada and the United States, *Geological Survey of Canada*, Bulletin 489, 60 pages.

Dawson, F.M., Marchioni, D.L., Anderson, T.C. and McDougall, W.J. (2000): An assessment of coalbed methane exploration projects in Canada, *Geological Survey of Canada*, Bulletin 549, 217 pages.

Dawson, F. M. and Kalkreuth, W. (1994): Coal rank and coalbed methane potential of Cretaceous/Tertiary coals in the Canadian Rocky Mountain Foothills and adjacent Foreland: Hinton and Grande Cache areas, Alberta, *Bulletin of Canadian Petroleum Geology*, V. 42, pages 544-561.

Dresser, J. (1922): Summary report on exploration for oil and gas in the Peace River District; *B.C. Dept of Lands*, 14 pages.

Duff, P. McL. D. and Gilchrist, R.D. (1981): Correlation of Lower Cretaceous coal measures, Peace River Coalfield, British Columbia; *B.C. Ministry of Energy, Mines and Petroleum Resources*, Paper 1981-3.

Gibson, D.W. (1992): Stratigraphy, sedimentology, coal geology and depositional environments of the Lower Cretaceous Gething Formation, northeastern British Columbia and west-central Alberta; *Geological Survey of Canada*, Bulletin 431, 127 pages.

Kalkreuth, W., Langenburg, W. and McMechan, M.E. (1989): Regional coalification pattern of Lower Cretaceous coal-bearing strata, Rocky Mountain foothills and foreland, Canada-implication for future exploration; *International Journal of Coal Geology*, v. 13, pages 261-302.

Kalkreuth, W., and Leckie, D.A. (1989): Sedimentological and petrographical characteristics of Cretaceous strandplain coals: a model for coal accumulation from the North American western interior seaway, in P. C. Lyons and B. Alpern, eds., Peat and coal: origin, facies and depositional models; *International Journal of Coal Geology,* v. 12, pages 381-424.

Kalkreuth W. and McMechan, M. (1988): Burial history and thermal maturity, Rocky Mountain front ranges, foothills, and foreland, east-central British Columbia and adjacent Alberta, Canada; *American Association of Petroleum Geologists Bulletin*, volume 72, no. 11, pages 1395-1410.

Kalkreuth, W. and McMechan, M. (1991): Vitrinite reflectance data for Devonian-Cretaceous strata in the Rocky Mountain front ranges, foothills and foreland, between Pink Mountain, British Columbia and Grande Cache Alberta, *Geological Survey of Canada*, Open File Report 2420.

Karst, R. and White, G.V. (1980): Coal rank distribution within the Bluesky-Gething stratigraphic horizon of northeast B.C.; in Geological Fieldwork 1979, *B.C. Ministry of Energy, Mines and Petroleum Resources*, Paper 80-1, pages 103-108.

Karsten M. and Bachu S. (2001): Fluids and pressure distributions in the foreland-basin succession in the west-central part of the Alberta basin, Canada: Evidence for permeability barriers and hydrocarbon generation and migration; *American Association of Petroleum Geologists Bulletin*, volume 85, no. 7, pages 1231-1252.

Kilby, W. E. (1983): The Character of the Bluesky Formation in the foothills of northeastern British Columbia; in Geological Fieldwork 1983, *B.C. Ministry of Energy, Mines and Petroleum Resources*, Paper 1984-1, pages 108-112.

Kilby, W.E. (1984): Tonstein and bentonite Correlations in northeast British Columbia; in Geological Fieldwork 1984; *B.C. Ministry of Energy, Mines and Petroleum Resources,* Paper 1985-1, pages 257-277.

Kilby, W.E. and Oppelt, H.P. (1984): Numerical depositional modeling - Gething Formation along the Peace River; in Geological Fieldwork 1984; *B.C. Ministry of Energy, Mines and Petroleum Resources*, Paper 1985-1, pages 233-250.

Lamberston, M.N. and Bustin, R.C. (1993): Coalbed methane characteristics of Gates Formation coals, northeastern British Columbia: Effect of maceral composition: American *Association of Petroleum Geologists Bulletin*, v. 77, no. 12, pages 2062-2076.

Leckie, D.A. (1983): Sedimentology of the Moosebar and Gates Formations (Lower Cretaceous), Ph.D. Thesis, *McMaster University*, Hamilton, Ontario, 515 pages (unpublished).

Leckie, D. A. (1986): Rates, controls, and sand-body geometries of transgressive-regressive cycles: Cretaceous Moosevale and Gates formations, British Columbia; *American Association of Petroleum Geologists Bulletin*, V. 70, pages 516-535.

Leckie, D.A., Kalkreuth, W.D. and Snowdon (1988): Source rock potential and thermal maturity of Lower Cretaceous strata: Monkman Pass Area, British Columbia; *American Association of Petroleum Geologists Bulletin*, volume 72, No. 7, pages 820-838.

Matthews, W.H. (1947): Geology and coal resources of the Carbon Creek-Mount Bickford map area; *B.C. Dept. of Mines*, Bulletin 24.

McKechnie, N.D. (1955): Coal Reserves of the Hasler Creek-Pine River area, British Columbia, *B.C. Dept. of Mines*, Bulletin 36.

McMechan, M. E. (1994): Geology, Dawson Creek, west of the sixth meridian, British Columbia; *Geological Survey of Canada*, “A” Series Map, 1858A.

Nelson, C. R. (2000): Coalbed methane potential of the U.S. Rocky Mountain region, in GasTIPS, volume 6, no. 3, Fall 2000, *Gas Technology Institute*, pages 4-12.

Oppelt, H. (1988): Sedimentology and ichnology of the Bluesky Formation in Northeastern British Columbia; in Sequences, stratigraphy, sedimentology, surface and subsurface: *Canadian Society of Petroleum Geologists*, Memoir 15, pages 401-416.

Ryan, B.D. (1996): Coal quality variations in the Gething Formation, northeast British Columbia (93O,J,I); in Geological Fieldwork 1996, *B.C. Ministry of Employment and Investment,* Paper 1997-1, pages 373-397.

Ryan, B.D. (2000): An introduction to coalbed methane potential in British Columbia; *B.C. Ministry of Energy and Mines*, Exploration and Mining in British Columbia 2000, pages 55-69.

Ryan, B.D. (2000a): Coalbed methane and coalbed methane resources of the Peace River Coal Fields; presentation to Mineral North conference, Tumbler Ridge, May 2000.

Scott, A. and Kaiser, W.R. (1996): Hydrogeology in coalbed methane exploration; *Geol. Soc. of America Annual Meeting*, Denver Colorado, Abstract with Programs, page A-41.

Smith, D., Zorn, C. and Sneider, R. (1984): The Paleogeography of the Lower Cretaceous of Western Alberta and Northeastern British Columbia in and Adjacent to the Deep Basin of the Elmworth Area; *American Association of Petroleum Geologists*, Memoir 38, pages 79-114.

Stott, D.F (1974): Lower Cretaceous coal measures of the foothills of west-central Alberta and northeastern British Columbia; *Canadian Mining and Metallurgical Bulletin*, volume 67, no. 749, pages 87-101.

Tyler, R., Kaiser, W.R. and Scott, A.R. (2000): Defining coalbed methane exploration fairways: An example from the Piceane Basin, Rocky Mountain Foreland, Western United States, in M. Mastalerz, M. Glikson and S. Golding eds., Coalbed Methane: Scientific, Environmental and Economic Evaluation; *Kluwer Academic Publishers*, pages 67-88.

Wyman, R. E. (1984): Gas resources in Elmworth coal seams, in J. A. Masters, ed., Elmworth, case study of a deep basin gas field: *Canadian Society of Petroleum Geologists*, Memoir 38, pages 173-187.

The Lustdust Property in Central British Columbia: A Polymetallic Zoned Porphyry-Skarn-Manto-Vein System

By Gerry Ray[1], Ian Webster[1], Peter Megaw[2], Jim McGlasson[2] and Keith Glover[3]

KEYWORDS:*Lustdust, porphyry, skarn, manto, vein, Eocene, Cache Creek Terrane, Pinchi Fault, Takla Silver Mine, molybdenum, copper, zinc, gold, mercury, geochemistry, exploration, economic geology.*

INTRODUCTION AND LOCATION

Alpha Gold Corporation's Lustdust property lies close to the junctions of Canyon and Silver creeks, approximately 210 km northwest of Prince George and 35 km east of Takla Lake in central British Columbia (Figure 1). It includes a skarn-manto-vein system that is discontinuously developed over a 2.5 km strike length. This mineralization is related to an elongate, undeformed, Eocene-age composite Mo-bearing porphyry body, the Glover Stock (Figure 2). The stock lies <2 km west of the Pinchi Fault (Figure 2) and it intrudes deformed oceanic rocks of the Cache Creek Terrane, including mid to Late Permian limestones. The Pinchi Fault is major north-northwest trending structure that separates the Cache Creek rocks from an intrusive suite belonging to the Quesnel Terrane immediately to the east (Gabrielse and Yorath, 1992; Figure 1).

The Lustdust area has a history of exploration and small-scale mining for Hg, Au, Ag and Zn-Pb. The former Bralorne Takla Hg mine (BC MINFILE 093N 008) lies close to the Pinchi Fault (Figure 3), and the southern part of the Lustdust property includes a developed prospect, the "Takla Silver Mine" (093N 009), which only produced some small bulk test samples. The adits at the Takla Silver property were driven to explore veins and carbonate replacements that represent the most southern and distal part of the Lustdust hydrothermal system. Later, it was realized that a metal zoning is present on the property; northwards, the Takla Silver Mine Ag-Pb-Au-Zn-As-Hg-bearing veins pass successively into Zn-rich mantos, Cu-Au (Zn) skarns, and then into Mo porphyry-style mineralization in the Glover Stock (Figure 2).

Previous exploration has concentrated on the more distal Zn-Ag-Au rich mantos and veins, but the economic potential of the more proximal Cu-Au skarns and Mo porphyry is now apparent. Drilling by Alpha Gold in 2000 and 2001 has been centered on these more northerly styles of mineralization.

This paper describes the geology, mineralization and alteration on the Lustdust property and outlines the proximal to distal chemical zoning in the system.

REGIONAL GEOLOGY

The Lustdust mineralization lies in the Cache Creek Terrane (Figure 1) which represents a deformed and imbricated package of Pennsylvanian to lower Jurassic oceanic rocks (Monger 1977, 1998; Paterson, 1974, 1977; Gabrielse and Yorath, 1992). The terrane includes a western element, the Sitlika Assemblage, and an eastern portion that has been designated the Cache Creek Complex (Schiarizza and MacIntyre, 1999; Schiarizza, 2000). The latter, which host the Lustdust mineralization, includes highly deformed phyllites, argillites, cherts and thick carbonates, together with units of oceanic island basalts and mafic tuffs (Paterson, 1974, 1977; Schiarizza and MacIntyre, 1999).

During the Early to Middle Jurassic, the Cache Creek rocks were amalgamated with those of the Stikine Terrane (Figure 1) and imbrication occurred along west-directed thrust faults (Schiarizza and MacIntyre, 1999). In the Lustdust area, this probably coincided with the development of lower greenschist facies metamorphism and several periods of folding. Elsewhere in the terrane, however, some blueschist facies are locally recorded (Paterson, 1977), and these have been dated by K-Ar methods as being Late Triassic (Paterson and Harakel, 1974). Schiarizza and MacIntyre (1999) note that the most important pulses of plutonism occurred during the Middle Jurassic, Late Jurassic to Early Cretaceous and Early Cretaceous times.

The Pinchi Fault (Figure 1) can be traced for >450 km in British Columbia. It is believed to have originally formed during the Late Triassic as a major thrust related to a subduction zone that dipped northwards under Quesnellia (Paterson, 1977; Barrie, 1993). Subsequently, it was reactivated as a north-northwest trending dextral fault.

The Quesnel Terrane in this region comprises a Late Triassic volcanic-sedimentary arc succession that includes both alkalic and sub-alkalic elements. These supracrustal rocks are intruded by a number of major plutons, the largest of which is the multiphase Hogem Batholith (Figure 1). Dating by K-Ar methods (Garnett, 1978) suggests three in-

[1] *British Columbia Ministry of Energy and Mines*
[2] *International Mineral Development & Exploration Inc.*
[3] *Consulting Geologist*

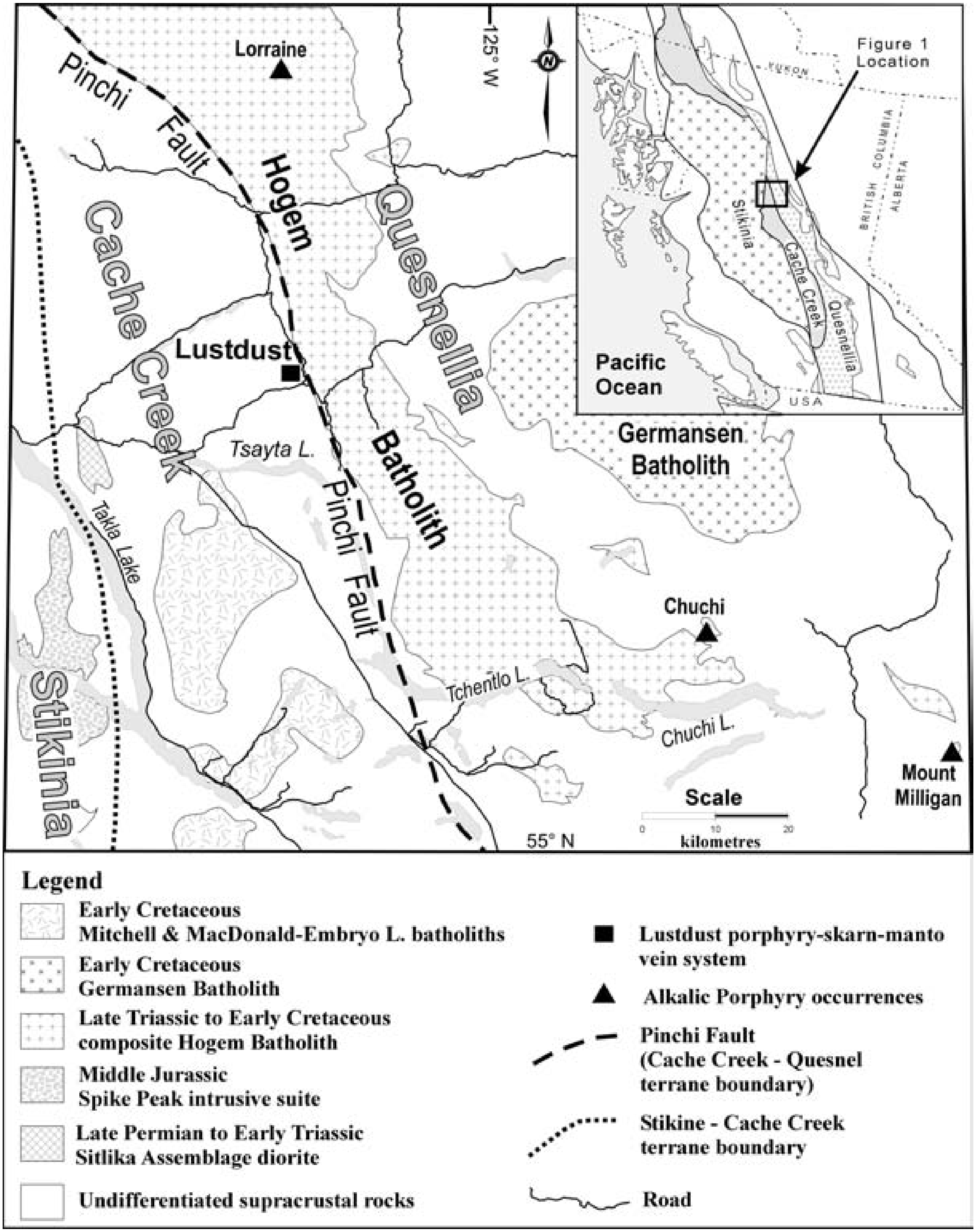

Figure 1. Map of the Takla Lake area showing the locations of the Lustdust property, the Pinchi Fault, the terrane boundaries and the major intrusions. Geology after Wheeler *et al*. (1991) and The MapPlace, October 2001.

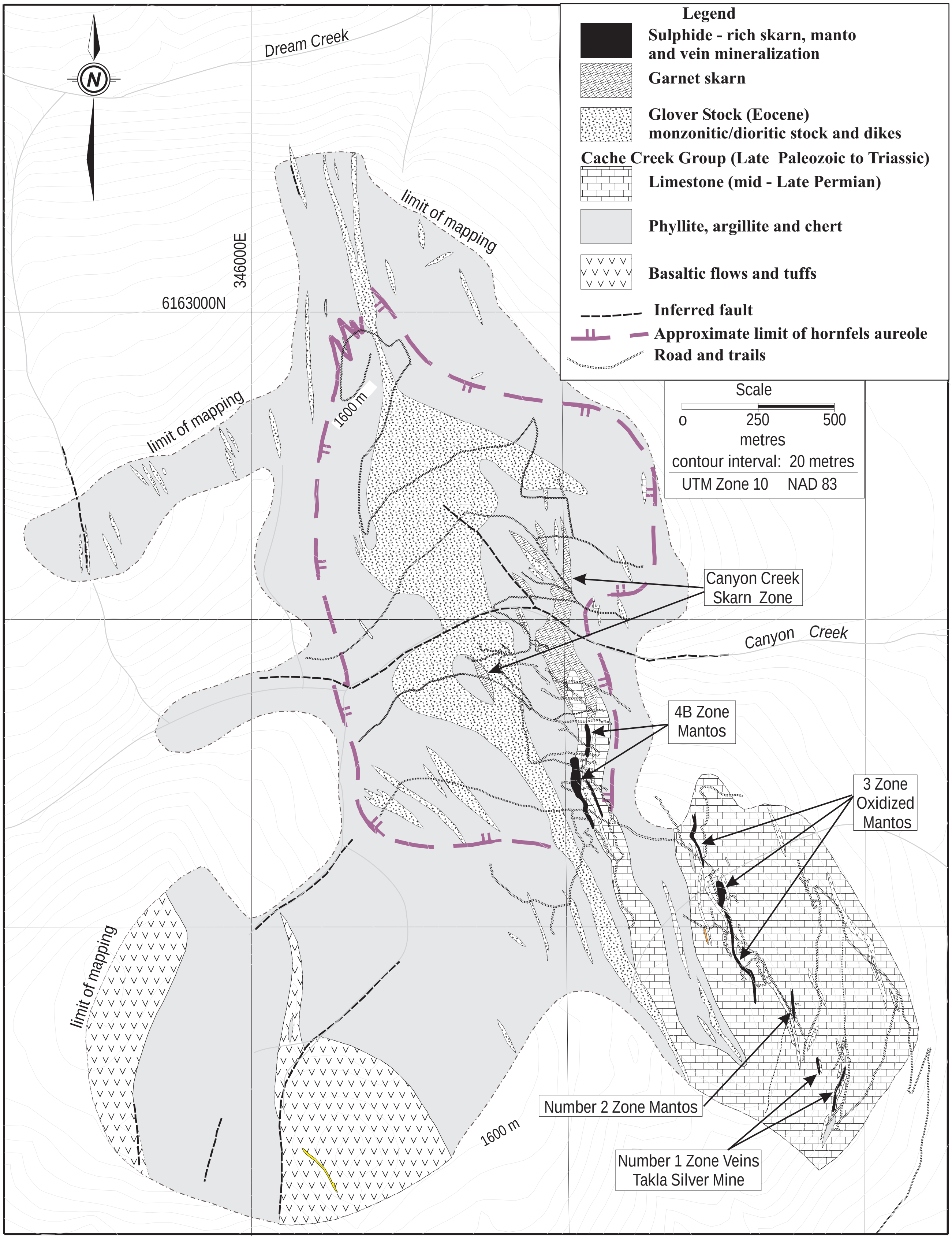

Figure 2. Geology of the Lustdust property showing location of the Glover Stock and the various proximal to distal mineralized zones. Geology compiled from mapping by Evans (1996, 1997, 1998), Megaw (1999, 2000, 2001), Glover, McGlasson, Ray and Webster (unpublished data).

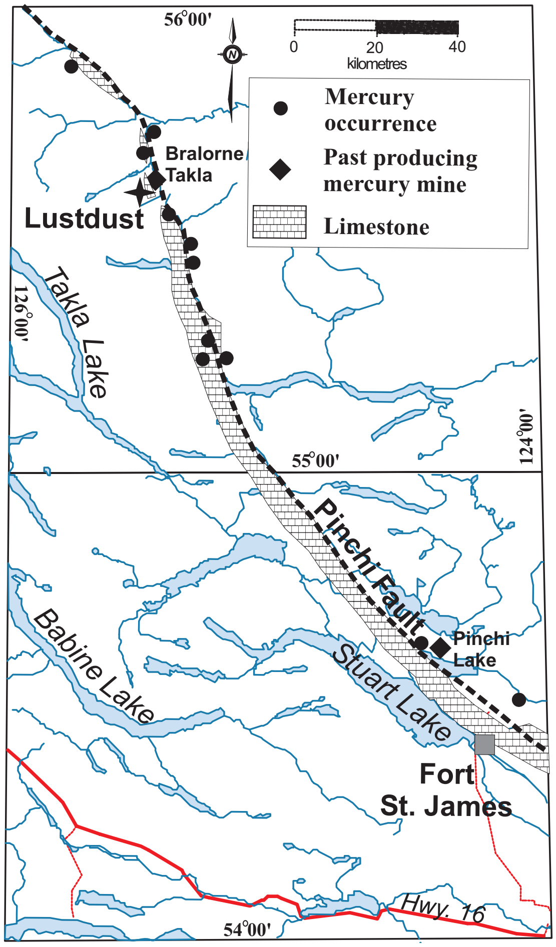

Figure 3. The Pinchi Fault north-west of Fort St. James showing prospective areas for other possible Lustdust targets associated with limestones, Hg occurrences or former Hg mines.

trusive phases, a Late Triassic to Early Jurassic suite of calc-alkaline granodiorites, a Middle Jurassic phase of alkalic syenites, and an Early Cretaceous episode of calc-alkaline granites. Porphyry Cu-Au mineralization is seen at the Lorraine, Chuchi and Mount Milligan properties (Figure 1; Bishop *et al.*, 1995). Garnett (1978) notes that much of this porphyry Cu ± magnetite mineralization is associated with the Middle Jurassic syenites.

PREVIOUS WORK IN THE LUSTDUST AREA

Cinnabar was discovered in 1942 on the west side of Silver Creek, along the Pinchi Fault, at what was to become the Bralorne Takla Mercury Mine (Figure 3; BC MINFILE 093N 008). Total production at the mine amounted to 59 914 kilograms of mercury during 1943 and 1944. In 1944 the Kay claims were staked on veins approximately 1.5 kilometres west of the mine on what later became the Takla Silver Mine. These Ag-Au-Pb-Zn-Hg-bearing sulphide and sulphosalt veins became known as the "Number 1 Zone" and they are now believed to be the most southerly, distal extension of the Lustdust hydrothermal system. The 1945 Minister of Mines Annual Report notes that 350 feet of underground workings had been constructed on the claim group. By 1953, the property was known as the Lustdust. Leta Explorations Ltd undertook considerable diamond drilling and development work up to 1963, and in 1960 a Noranda and Canex joint venture completed extensive trenching. In 1965, Takla Silver Mines Limited drove a new 700-foot long drift on the Number 1 Zone and also dug trenches over surface mineralization at the Number 3 Zone further north (Figure 2; Campbell, 1966). At the Number 1 Zone, Sutherland Brown (1965) reported the presence of an antimony-rich vein-like replacement in limestone and porphyry dike hostrocks. The minerals identified included stibnite, boulangerite, sphalerite, pyrite, some ruby silver and trace realgar and orpiment.

In 1968, Anchor Mines Ltd. extracted a 300-pound bulk sample from the Number 1 Zone for metallurgical testing. A mineralogical study of material taken from underground workings and surface trenches was made by Mathieu and Bruce (1970) who noted the presence of some sulphide, sulphosalt and arsenide minerals, as well as high values of Au, Ag, Pb, Zn and Sb. Zapata Granby Corporation performed geological mapping, soil sampling and geophysical surveys during 1978 and 1979. Noranda Mining and Exploration Company Limited soil sampled and mapped the area during 1979 and 1980. In 1981 they put down a number of diamond drillholes, including some on the north side of Canyon Creek. This was followed in 1986 by survey and sampling work by Welcome North Mines Ltd. and Pioneer Metals.

Alpha Gold Corporation began acquiring the property in 1991 and some exploration was undertaken (Rotzien, 1991; 1992). Later it was optioned to Teck Exploration Limited who completed an extensive exploration and drilling program (Evans, 1996, 1997). Since that time Alpha Gold has done a considerable amount of drilling that has recently focused on skarn and porphyry targets lying north and south of Canyon Creek; details on this work are summarized by Evans (1998), Soregaroli (1999) and Megaw (1999, 2000, 2001). Recently, Alpha Gold Corporation announced intersecting Mo-Cu-bearing porphyry and Cu-Au skarn mineralization along Canyon Creek (Figure 2); intersections through mineralized skarn include hole DDH01-44 which cut 59 m grading 0.8 % Cu and 0.67 g/t Au and hole DDH01-47 which cut 37 m assaying 0.92% Cu and 0.68 g/t Au (Alpha Gold Corp. News release, October 1st, 2001).

Schiarizza (2000) compiled the geology of the district, and Dunne and Ray (2002, this volume) have completed a fluid inclusion study of the Lustdust mineralization.

GEOLOGY OF THE LUSTDUST AREA

INTRODUCTION

The Lustdust mineralization is associated with an elongate, composite igneous body, the Glover Stock, as well as a related north-northwest-trending swarm of felsic dikes and sills (Figure 2). The stock, which crops out both north and south of Canyon Creek, intrudes deformed Cache Creek supracrustal rocks and is surrounded by a 200 to 300 m wide hornfels aureole. The country rocks comprise a steeply west-dipping, north-northwest striking package of slatey carbonaceous or cherty argillites, phyllites, ribbon cherts and mafic metavolcanics and tuffs. Also present are several thick, north-trending units of limestone and marble that host most of the skarn, manto and vein mineralization.

SUPRACRUSTAL ROCKS

Most of the Lustdust area is underlain by a north-northwest striking package of slatey phyllites and cherts, as well as lesser amounts of mafic tuff, greenstone metavolcanics and some limestones (Figure 2). In addition, there are thin, minor units of polymictic volcanic sandstone and conglomerate (Megaw, 2000). The limestones are concentrated in the southeast part of the area but quickly pinch out north of Canyon Creek (Figure 2). It is uncertain whether this northerly disappearance of the limestones in this area reflects facies changes or the northern plunge of the fold axes. Thick units of mafic volcanic and tuffaceous rocks are more common to the southwest (Figure 2), whereas the phyllitic argillites and cherts mainly occupy a north-northwest trending belt in the central portion of the property. The argillites and cherts are commonly interbedded and locally grade from one into another, making it difficult to separate and map out the two units (Figure 2). Limestones form massive to poorly bedded, fine-grained rocks that vary from blue-grey to white in color. Individual carbonate units range from a few centimeters to over 500 m in thickness. During this study, four limestone samples were collected for microfossil identification. Three of these contained no useful fossils, but one massive limestone sample (GR01-38), collected at UTM Zone 10 NAD 83 348069E - 6160847N, yielded fossils of mid to Late Permian age (M.J. Orchard, personal communication, 2001). Many limestones are sugary textured due to recrystallization (Megaw, 1999) and they contain stylolites. Adjacent to intrusive rocks, the carbonates are often bleached, silicified or converted to marble. Evans (1997) identified several different types of limestone, one of which may represent carbonate debris flows. These rocks contain knots or small boudins of white calcite which might represent recrystallized carbonate breccia clasts (Megaw, 2001). Supportive evidence for this idea is that some limestones are interbedded with, or grade into, thin units (maximum 40 m) of a distinctive green, chloritic tuff containing angular to sub-rounded clasts up to 40 cm in diameter (Photo 1). The widely scattered and matrix-supported clasts comprise mainly various types of limestone, but minor quantities of mafic to intermediate volcanics are also present (Megaw, 2000). Evans, (1997, 1999) believed these tuffaceous debris flows represented a single folded horizon. However, later work (Megaw, 1999) suggests there are several units that display considerable lateral variations, including some with graded bedding and Bouma-type sequences. Evans (1996, 1999) reports that these tuffs locally contains up to 2 % finely disseminated pyrite-pyrrhotite and are geochemically anomalous in Pb, Zn and Cu.

The most extensive area of mafic metavolcanic and tuffaceous rocks outcrops in the southwest part of the mapped area (Figure 2). All of these rocks are highly chloritized and many of the original igneous or depositional textures have been destroyed. Unlike the thin tuffaceous units interbedded with limestone further east, no brecciated limestone clasts are seen in these rocks. The volcaniclastic rocks are mostly fine-grained and massive and are believed to represent deformed and altered basaltic ash tuffs. Occasionally they contain small lithic fragments and lapilli, and in some outcrops a weak to moderate layering or sedimentary bedding is observed (*e.g.* at UTM 346476E - 6160321N). Locally, the tuffs include thin horizons of thinly bedded tuffaceous siltstone. The metavolcanic rocks are generally fine grained and massive, but at UTM 346151E - 6160757N, remnant pillow structures are observed.

The phyllites are believed to represent weakly metamorphosed argillites. They make up non-calcareous, massive to thin bedded rocks that vary from light grey to black in colour. Many outcrops contain variable quantities of carbonaceous material as well as pyrite-pyrrhotite that occurs either as disseminations or in thin beds; Megaw (2000, 2001) suggests the latter may indicate syn-sedimentary sulphide deposition. Many of the phyllites are strongly deformed and the original bedding has been transposed and obliterated. In some localities, however, intersections between the bedding and the phyllitic cleavage are recognizable.

Many of the phyllites are cherty and locally these pass into massive or well-bedded ribbon cherts that are white to very dark grey in colour. The ribbon cherts often comprise 1 to 3 cm thick layers of pale chert that are interbedded with thinner (0.25 to 1 cm) horizons of dark phyllite.

INTRUSIVE ROCKS

The Lustdust mineralization is spatially associated with the Glover Stock and a related swarm of felsic sills and dikes that exceeds 3.5 km in strike length (Figure 2; Megaw, 2001). The stock crops out north and south of Canyon Creek and forms an elongate, north-northwest-trending lens-like body whose main portion exceeds 1 km in length and 0.6 km in width. It is enveloped by a 100 to 300 m wide thermal aureole which includes a biotite-dominant hornfels and lesser amounts of calc-silicate and pyroxene-bearing hornfels. Fine-grained, calc-silicate skarnoid overprints the carbonates while the purple-brown coloured biotite hornfels is developed in the argillites and argillitic ribbon cherts. There is a mineral zoning in the hornfels with biotite tending to form more distally and pyroxene occurring more proximal to the stock. The pyroxene hornfels locally includes abundant fine-grained pyrite and pyrrhotite (Megaw, 2001).

To the north and south, the Glover Stock passes out into a series of narrow, north-northwest-striking porphyritic dikes and sills. These elongate minor bodies tend to be more leucocratic and quartz-bearing than the main stock, and some have been classified as “felsites” (Megaw, 2001). Many are feldspar porphyritic but, unlike the main stock, they generally lack significant hornfels development in the wall rocks.

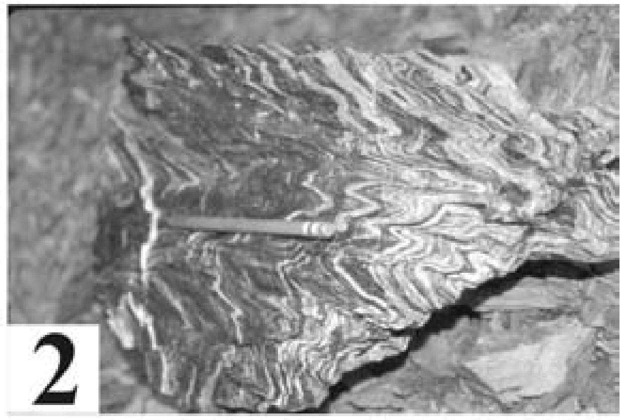

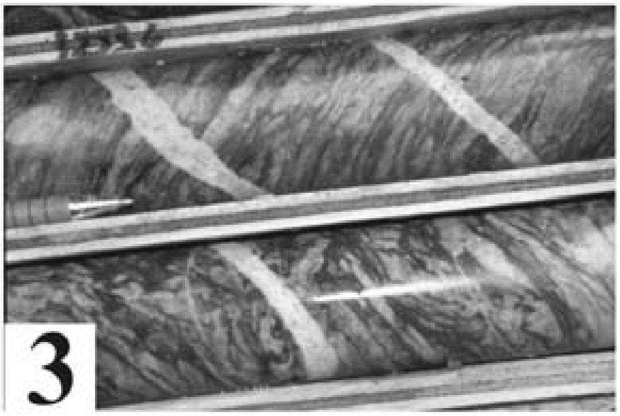

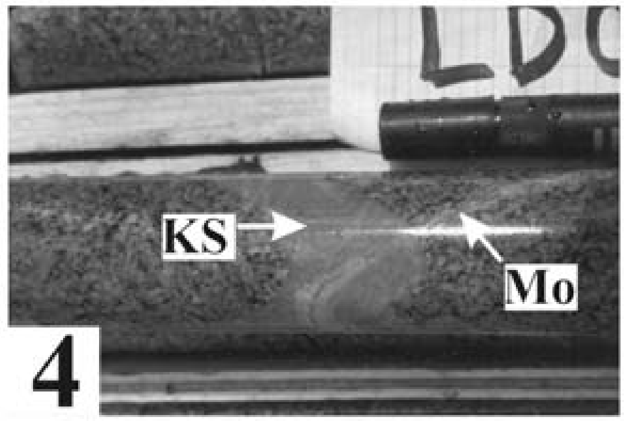

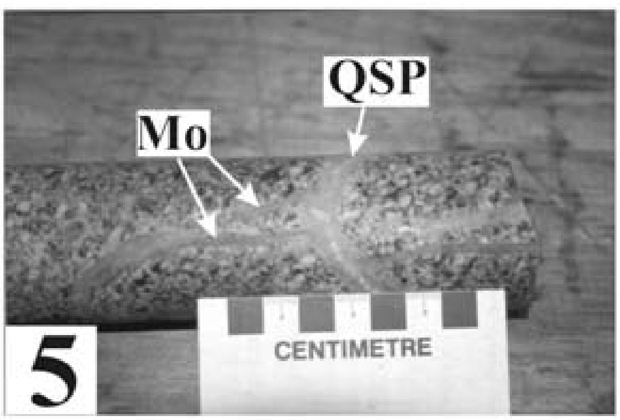

Photo 1. Mafic tuff containing clasts of limestone and minor amounts of mafic volcanic rocks. Holes LD 98-9 and 92-15 at 10 m and 19.8 m respectively.

Photo 2. Argillites, strongly deformed by open to tight F2 folds. Float located 5.2 km southwest of the Takla Silver Mine, UTM 344400E - 6156398N.

Photo 3. Hornfelsed argillitic ribbon cherts cut by early pink, barren quartz-K feldspar veins. Hole LD01-36 at 233 ft. These early veins cut both the Glover Stock (*see* Photo 4) and the hornfels envelope.

Photo 4. Glover Stock porphyry. Early, pink, quartz-K feldspar vein (KS) cut by a thin vein (Mo) containing quartz, molybdenite and trace chalcopyrite. Hole LD01-34 at 436 ft.

Photo 5. Glover Stock porphyry. Two veins (Mo) containing quartz, molybdenite and pyrite cut and displaced by a younger quartz-sericite-pyrite vein (QSP). Hole LD01-34 at 233 feet.

Photo 6. Dioritic Glover Stock cut by a vein with a quartz-feldspar-pyrite core and tourmaline-rich margins. Note the thin bleached and altered zone adjacent to the vein. Hole LD01-30 at 145 ft.

Preliminary U-Pb dating of zircons extracted from both the dioritic and monzonitic phases of the Glover Stock yield Eocene ages of circa 51 to 52 Ma (R. Friedman, personal communication, 2001). The stock represents a multiphase composite intrusive complex, and most of its rocks are weakly to strongly feldspar porphyritic; some of the latter have "crowded" feldspar porphyry textures, in addition to phenocrysts of igneous hornblende and biotite. Chemical plots (Tables 1A and 1B; Figure 4) and thin section studies (Leitch, 2001b, personal communication) indicate the stock ranges compositionally from mafic diorite-monzodiorite to more leucocratic monzonite-quartz monzonite. The age relationships between these phases is complex as the diorites both cut, and are cut by the more leucocratic igneous rocks.

Primary mafic minerals in the dioritic phases include up to 20 % hornblende with lesser biotite and rare relict clinopyroxene. The hornblende is commonly partially to totally replaced by chlorite, actinolite and secondary biotite. Primary igneous biotite comprises up to 5 % and is also chloritized. Phenocrysts of andesine-oligoclase plagioclase may exceed 60 % of the rock and individual crystals reach 3 mm in length. Potassium feldspar, both as megacrysts and small crystals in the fine-grained groundmass, may reach 15 % by volume, but is generally less than 5 %. Groundmass quartz rarely exceeds 10 %. Other accessory to trace minerals identified in the diorites includes calcite, sphene, apatite, zircon and up to 2 % opaque minerals which mainly constitutes magnetite (Leitch, 2001b).

The leucocratic monzonitic phases contain 30 to 35 % plagioclase, up 35 % K feldspar, and between 5 and 10 % quartz. Locally, some of these rocks are megacrystic with K feldspar phenocrysts up to 0.8 cm in length. Leitch (2001b) has identified relict hornblende and biotite crystals which are now replaced by aggregates of carbonate, chlorite, sphene and opaque minerals. Where intense phyllic alteration has taken place, fine grained pervasive sericite may make up 10 % of the rock and this mineral is seen replacing the plagioclase crystals. Sphene may also be replaced by sericite in addition to chlorite, and minute needles of rutile. Accessory and trace minerals in the monzonites include magnetite, apatite, zircon and pyrrhotite (Leitch, 2001b).

Thin (< 1 metre) zones of hydrothermal breccia cut the stock in some localities and many have "pebble" breccia textures. One 20 cm thick breccia zone seen in hole LD 01-36 at 186 feet contains subangular to subrounded fragments up to 3 cm across. The fragments are mostly altered diorite with lesser amounts of mafic volcanics, vein quartz and massive pyrite, that are supported in a fine-grained feldspathic matrix.

Whole rock and trace element analyses of the Glover Stock are listed in Tables 1A and 1B and plots of these data shown in Figure 4. These show that the stock represents a metaluminous, volcanic arc granitoid (Figure 4G, H and O), as defined by Pearce *et al* . (1984). The ferric and ferrous Fe content of the mafic and leucocratic phases indicate the rocks are relatively oxidized, which is typical for plutons associated with Cu skarns (Figure 4M and N). However, plots do indicate significant differences between the more mafic dioritic phases and the leucocratic monzonites which is reflected in their Na, K and Ba contents (Figure 4K and L). The mafic phases are subalkaline, calc-alkaline rocks of diorite-quartz diorite-monzodiorite composition while the leucocratic samples have alkalic affinities, being of monzonite-quartz monzonite-monzodiorite composition (Figure 4A to 4F). The alkalic feature is probably due to secondary potassic (K feldspar, sericite and biotite) and albitic hydrothermal alteration, as suggested by plots in Figure 4K and 4L.

Figure 5 presents comparative chondrite normalized rare earth element (REE) plots for the Hogem Batholith (Barrie, 1993) and the mafic and felsic phases of the Glover Stock. These two phases have virtually identical REE patterns, which indicates their common source. However, the pattern for the Hogem Batholith differs, notably in being comparatively depleted in light REE's (Figure 5). At the start of this project, the Glover Stock was thought to be related to the nearby Hogem Batholith (Figure 1). However, the Eocene age of the stock and its different REE pattern (Figure 5) prove it is not part of the Hogem suite.

STRUCTURE AND METAMORPHISM

The supracrustal rocks in the Lustdust area have undergone a complex history of brittle-ductile deformation that was probably related to both the Jurassic-age accretion of the Cache Creek Group onto the North American continent and later recurrent dextral transcurrent movements along the Pinchi structure. Two phases of deformation are recognized at Lustdust and these correspond with the two main episodes identified in Cache Creek rocks by Paterson (1974, 1977). The earliest of these (D1) was the dominant folding event and was largely responsible for the general north-northwest strike of the supracrustal rocks. It resulted in tight to isoclinal asymmetric F1 folds accompanied by a lower greenschist facies metamorphism and the development of chlorite-sericite-actinolite axial planar phyllitic S1 cleavages. These cleavages are common in the phyllites and ribbon cherts but are absent or less well developed in the more massive cherts, volcanics and limestones. Due to the absence of bedding in many rocks, small scale, outcrop-sized F1 folds are not commonly seen. However, changes in bedding-S1 intersections indicate the presence of relatively large-scale F1 structures in some localities. The F1 folds have steeply west dipping, north-northwest-trending axial planes and their fold axes plunge north to northwest, generally at between 10 and 50 degrees.

The second phase of deformation (D2) resulted in a variety of structures that vary from tight to open flexure folds (Photo 2) as well as a crenulation strain-slip cleavage in the phyllitic rocks. In some localities, two conjugate sets of strain slip cleavage are developed. The F2 folds have a wide variation of strike and plunge, depending on the orientation of the bedding and S1 surfaces. The most common F2 folds have northerly striking axial planes and fold axes that dip between 20 and 75 degrees north-northeast to northwest. The less common set strikes easterly with shallow (<15 degrees) east to west plunging axes. Locally, the F2 folds are also associated with prominent a-c joints that are often

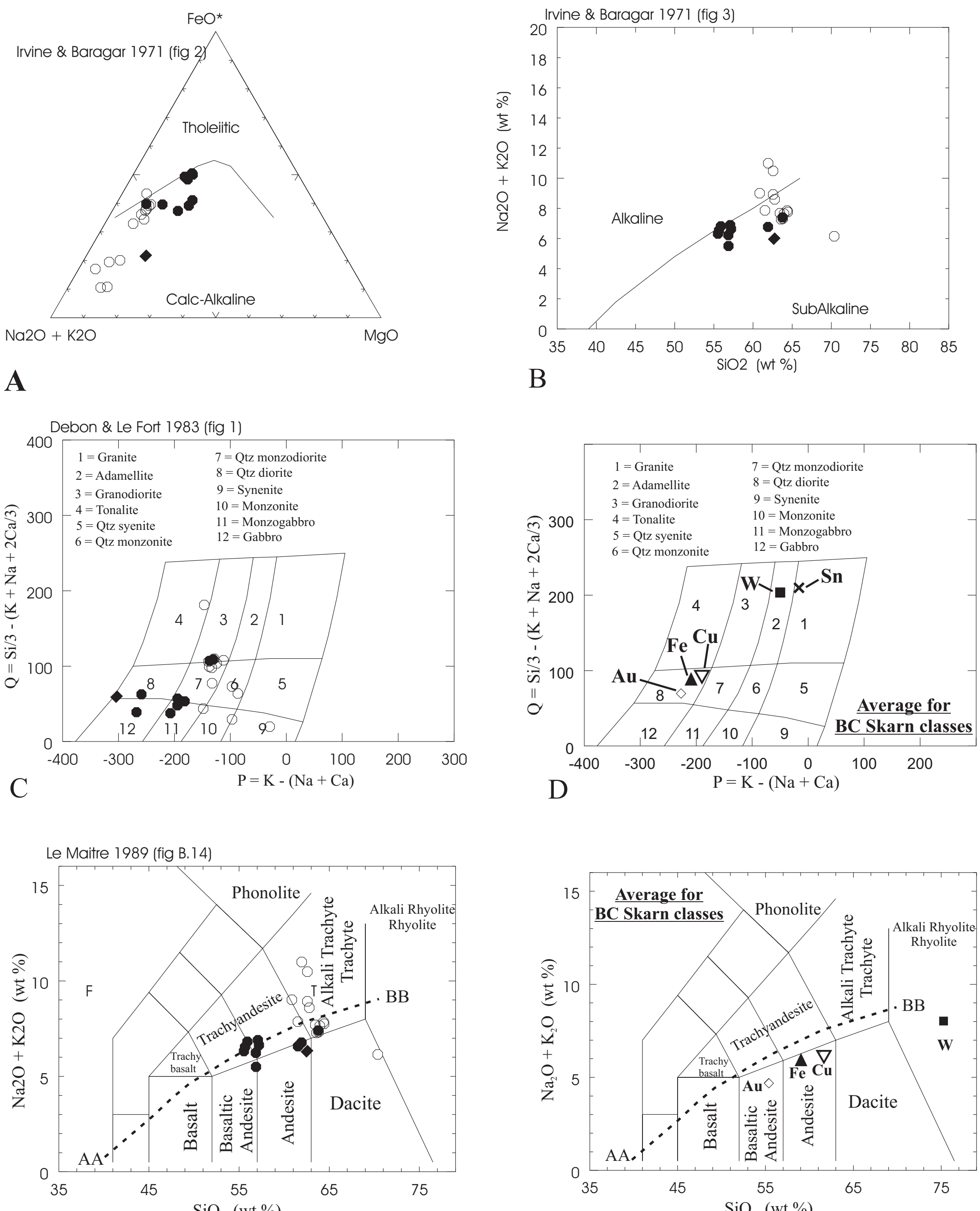

Mean values for other skarn-related intrusions in B.C.

- ◇ Au skarn-related intrusions (n = 27)
- ▲ Fe skarn-related intrusions (n = 49)
- ▽ Cu skarn-related intrusions (n = 59)
- ■ W skarn-related intrusions (n = 21)
- × Sn skarn-related intrusions (n = 19)

- ● Glover Stock mapped as "diorite"
- ○ Glover Stock mapped as "monzonite"
- ◆ Albitized diorite

Figure 4.

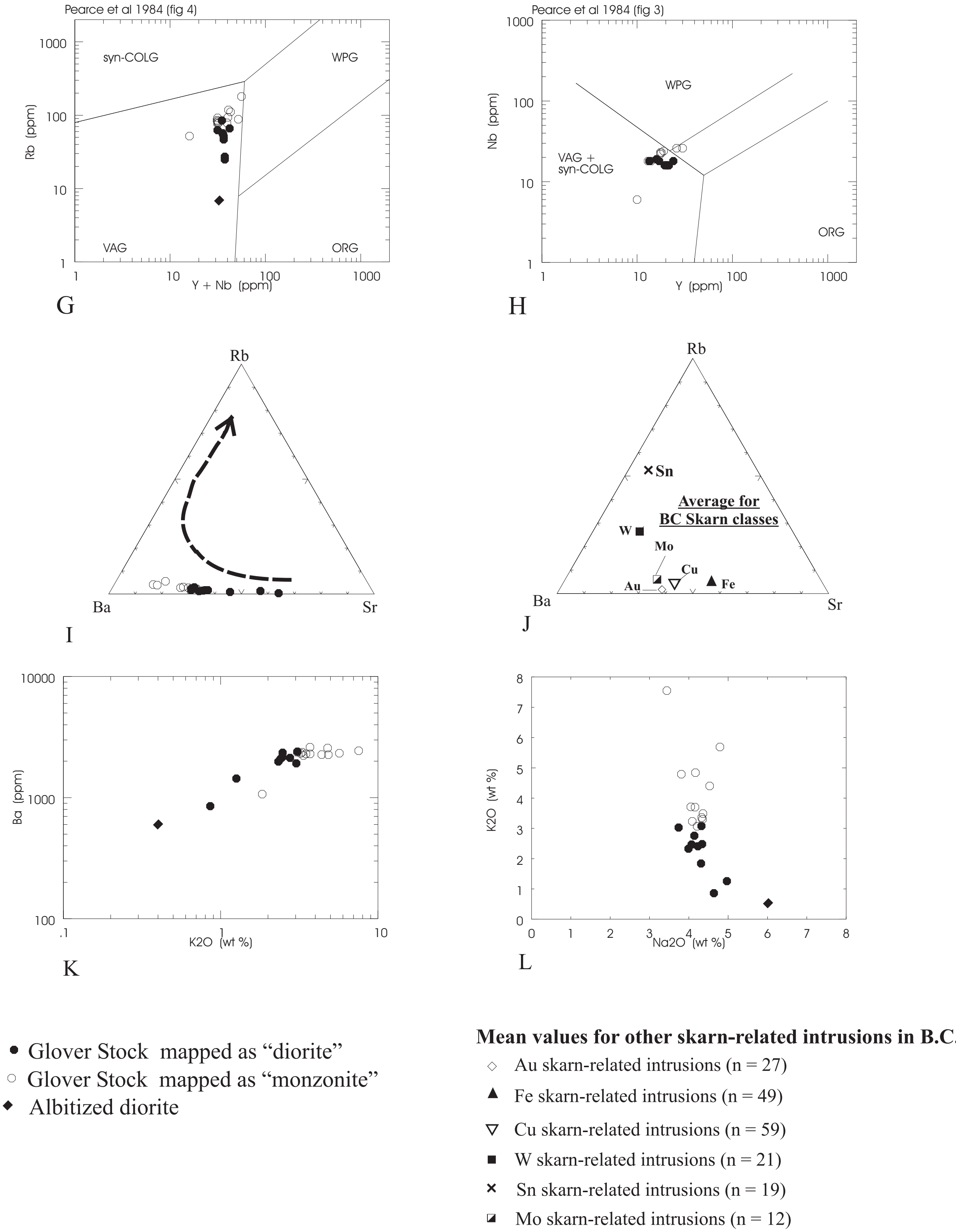

Pearce et al 1984 (fig 4)
syn-COLG
WPG
VAG
ORG
Rb (ppm)
Y + Nb (ppm)
1000
100
10
1
1
10
100
1000
G
Pearce et al 1984 (fig 3)
WPG
VAG +
syn-COLG
ORG
Nb (ppm)
Y (ppm)
1000
100
10
1
1
10
100
1000
H
Rb
Ba
Sr
I
Rb
×Sn
Average for
BC Skarn classes
W
Mo
Cu
Au
Fe
Ba
Sr
J
10000
1000
100
Ba (ppm)
.1
1
10
K2O (wt %)
K
8
7
6
5
4
3
2
1
0
K2O (wt %)
0
1
2
3
4
5
6
7
8
Na2O (wt %)
L
Glover Stock mapped as “diorite”
Glover Stock mapped as “monzonite”
Albitized diorite
Mean values for other skarn-related intrusions in B.C.
Au skarn-related intrusions (n = 27)
Fe skarn-related intrusions (n = 49)
Cu skarn-related intrusions (n = 59)
W skarn-related intrusions (n = 21)
Sn skarn-related intrusions (n = 19)
Mo skarn-related intrusions (n = 12)

Figure 4.

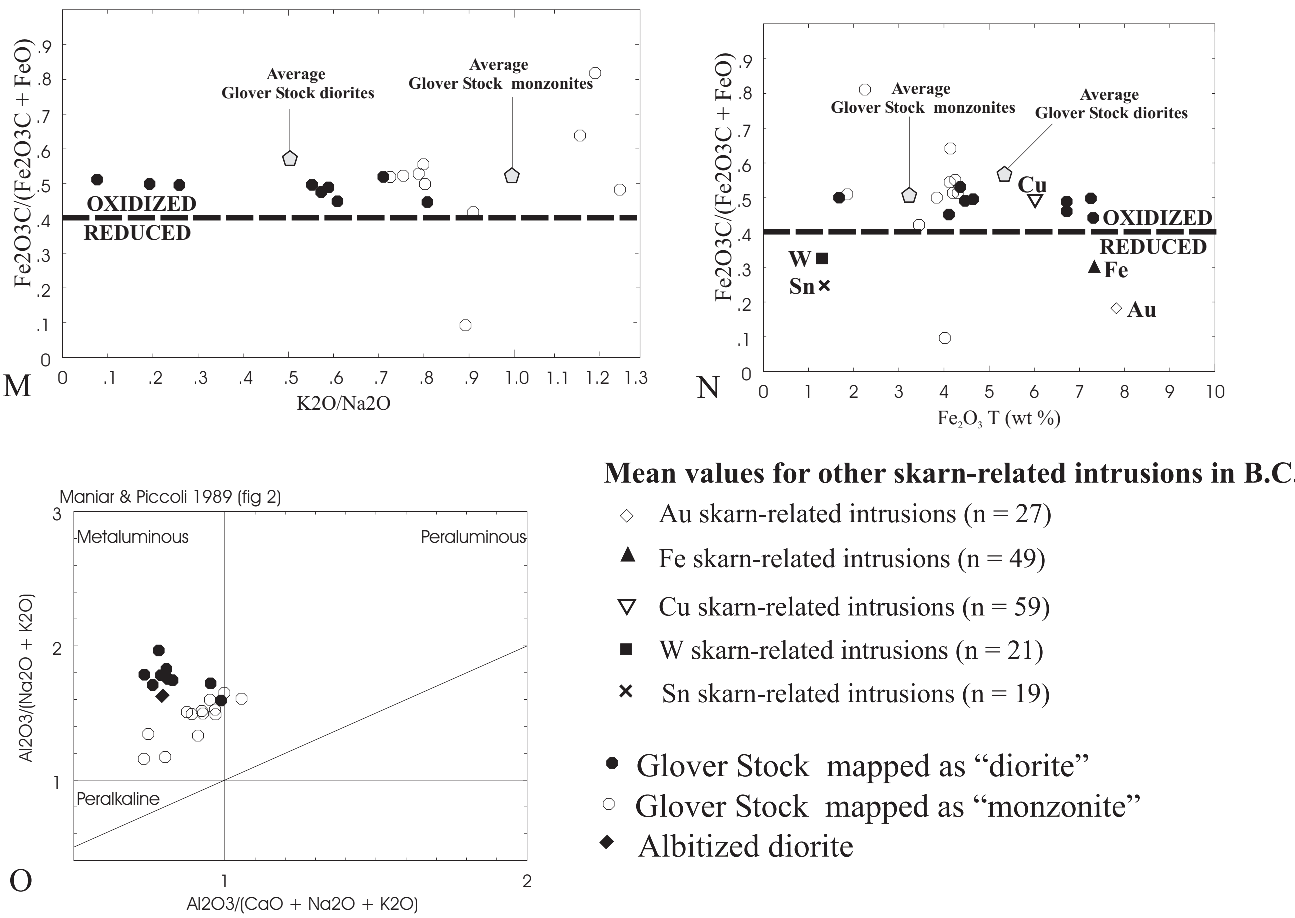

Figure 4. Major and trace element plots of the mafic dioritic and leucocratic monzonitic phases of the Glover Stock (data from Tables 1A and 1B). Also plotted, for comparison, are the average values of other skarn-related plutons in BC (data from Ray and Webster, 1997).A and B: AFM and alkali-silica plots (after Irvine and Baragar, 1971). C and D: Q - P plots (after Debon and Le Fort, 1983). E and F: Alkali *versus* silica plots (after Le Maitre *et al*., 1989). Line AA-BB represent alkaline-subalkaline line in Figure 4B. G and H: Log Rb *versus* Log Y+Nb tectonic discrimination plots (after Pearce *et al*., 1984). I and J: Triangular Ba-Rb- Sr plots (arrow is typical differentiation trend). K: Ba *versus* K_2O plot. L: K_2O *versus* Na_2O plot. M: Calculated Fe_2O3/(calculated Fe_2O3 + FeO) versus K_2O/Na_2O (oxidized-reduced line after Meinert, 1995). N: Calculated Fe_2O_3/(calculated Fe_2O_3 + FeO) versus total Fe as Fe_2O_3. O: Aluminum saturation plot (after Maniar and Piccolli, 1989).

spaced from 1 to 15 cm apart. These a-c joints usually strike easterly and dip northerly at between 10 and 75 degrees.

Much of the intense brittle faulting predates the emplacement of the Glover Stock and has been an important control on the mineralization. However, drilling has identified some faults that post-date the mineralization (Megaw, 2000, 2001). Most faults trend north-northwest, sub-parallel to the dominant strike of the supracrustal and intrusive rocks (Figure 2). A less common set, which may be controlled by the F2 a-c jointing, strikes east to east-northeast, and is best developed along Canyon Creek (Figure 2).

MINERALIZATON AND ALTERATION

INTRODUCTION

The Lustdust mineralization can be discontinuously traced for over 2.5 km, from Glover Stock porphyry-style mineralization in the north, to the quartz-sulphide-sulphosalt-bearing Number 1 Zone veins at the former Takla Silver Mine in the south (Figure 2). Limestone and marble along the eastern flank of the stock host the Cu-Au (Zn)-bearing Canyon Creek skarn which passes southwards into massive sphalerite-dominant mantos and carbonate replacements of the 2, 3 and 4B zones (Figure 2). The most southerly mineralization comprises a series of narrow, en echelon, polymetallic veins comprising the Number 1 Zone. These veins probably represent the most distal part of the

TABLE 1A
WHOLE ROCK AND TRACE ELEMENT ANALYTICAL DATA OF LEUCOCRATIC, MONZONITE SAMPLES, GLOVER STOCK, LUSTDUST PROPERTY

Sample	GR01-16	GR01-17	GR01-45	GR01-52	GR01-55	GR01-59	GR01-63	GR01-95	GR01-96	GR01-97	GR00-28	GR00-29	GR00-30	Average
Al2O3	17.08	16.45	16.34	16.32	16.38	16.28	16.87	16.26	16.11	16.1	14.59	16.41	16.02	16.25
CaO	4.25	3.55	4.31	3.24	3.84	3.38	3.67	3.78	3.07	3.63	2.61	5.37	4.43	3.78
Fe2O3T	1.84	2.14	4.01	3.77	4.27	3.38	4.24	4.14	4.08	4.09	1.84	1.38	1.62	3.14
K2O	4.79	5.69	3.7	3.49	3.07	3.71	3.23	3.3	4.84	3.36	1.84	4.4	7.55	4.07
MgO	1.37	0.68	1.18	1.36	1.55	1.58	1.49	1.47	1.32	1.46	0.68	1.36	1.37	1.30
MnO	0.06	0.05	0.08	0.04	0.06	0.05	0.07	0.06	0.04	0.05	0.04	0.07	0.07	0.06
Na2O	3.81	4.79	4.16	4.36	4.21	4.05	4.09	4.35	4.17	4.33	4.31	4.53	3.44	4.20
P2O5	0.23	0.22	0.28	0.27	0.31	0.33	0.31	0.28	0.3	0.32	0.09	0.27	0.29	0.27
SiO2	62.78	62.57	61.53	64.35	63.6	64.44	63.82	63.96	60.85	63.45	70.39	62.58	61.94	63.56
TiO2	0.58	0.58	0.65	0.58	0.59	0.59	0.64	0.59	0.69	0.6	0.21	0.58	0.56	0.57
LOI	2.34	2.74	2.93	1.1	1.16	1.36	0.81	0.82	2.5	1.33	2.22	2.13	1.41	1.76
Sum	99.13	99.46	99.17	98.88	99.04	99.15	99.24	99.01	97.97	98.72	98.82	99.08	98.70	98.95
FeO	0.85	0.37	3.3	1.8	1.94	1.86	1.84	1.88	1.39	1.8	NA	NA	NA	1.70
Fe2O3C	0.90	1.73	0.34	1.77	2.11	1.31	2.20	2.05	2.54	2.09	1.84	1.38	1.62	1.25
Fe2O3C/ (Fe2O3C+FeO)	0.51	0.82	0.09	0.50	0.52	0.41	0.54	0.52	0.65	0.54	NA	NA	NA	0.51
K/Na	1.26	1.19	0.89	0.80	0.73	0.92	0.79	0.76	1.16	0.78	0.43	0.97	2.19	0.99
Ba	2570	2330	2610	2300	2370	2300	2320	2370	2260	2230	1070	2270	2440	2264.62
Rb	111	118	93.4	82.8	76.8	91.8	77.8	80.6	78.8	85.4	52	88	180	93.57
Sr	971	423	1250	1065	1050	961	1055	1060	1105	993	220	814	600	889.77
Nb	24	23	23	18	18	18	18	18	22	18	6	26	26	19.85
Zr	269	253	254	203	178	187.5	185.5	177	220	169	90	210	204	200.00
Y	19	18	17.5	13.5	13.5	13.5	14	13.5	17.5	13	10	26	30	16.85
Ce	133	134.5	131.5	98	92.5	91	95.5	94	123.5	92.5	NA	NA	NA	108.60
Co	3	3.5	7	6	6	5.5	4.5	5.5	4.5	7.5	NA	NA	NA	5.30
Cs	1.4	2	1.8	1.9	1.9	2.1	1.4	1.8	1.6	2	NA	NA	NA	1.79
Cu	15	45	40	130	55	190	85	90	410	360	NA	NA	NA	142.00
Dy	3.9	4	3.7	2.6	2.6	2.7	3	3	3.7	2.8	NA	NA	NA	3.20
Er	1.7	1.6	1.6	1.3	1.3	1.4	1.3	1.4	1.8	1.3	NA	NA	NA	1.47
Eu	2	1.9	1.9	1.3	1.6	1.5	1.4	1.5	1.7	1.4	NA	NA	NA	1.62
Ga	20	21	21	20	19	19	19	20	21	20	NA	NA	NA	20.00
Gd	5.8	6.2	5.5	4.7	4.5	4.3	4.3	4.5	5.7	4.3	NA	NA	NA	4.98
Hf	6	6	5	4	4	4	4	4	5	4	NA	NA	NA	4.60
Ho	0.6	0.6	0.6	0.5	0.4	0.5	0.4	0.5	0.6	0.4	NA	NA	NA	0.51
La	58.5	59.5	58.5	45	43	41.5	43.5	43.5	55	41.5	NA	NA	NA	48.95
Lu	0.3	0.3	0.2	0.1	0.1	0.2	0.1	0.1	0.3	0.2	NA	NA	NA	0.19
Nd	49	48	47.5	35.5	34.5	33	33.5	35	45.5	33.5	NA	NA	NA	39.50
Ni	30	25	10	<5	<5	<5	<5	<5	<5	15	NA	NA	NA	20.00
Pb	20	10	20	25	30	15	20	20	15	25	NA	NA	NA	20.00
Pr	13.9	14.2	13.9	10.2	10	9.5	9.9	9.9	13.2	9.3	NA	NA	NA	11.40
Sm	7.8	7.8	7.9	5.7	5.4	5.4	5.3	5.8	7.2	5.3	NA	NA	NA	6.36
Sn	1	2	1	<1	1	<1	<1	<1	1	1	NA	NA	NA	1.17
Ta	0.5	0.5	0.5	0.5	0.5	0.5	0.5	0.5	0.5	0.5	NA	NA	NA	0.50
Tb	0.8	0.8	0.8	0.6	0.6	0.6	0.5	0.6	0.7	0.6	NA	NA	NA	0.66
Th	15	15	14	12	12	12	13	14	14	13	NA	NA	NA	13.40
Tl	0.5	0.5	1.5	0.5	0.5	0.5	0.5	0.5	0.5	1	NA	NA	NA	0.65
Tm	0.3	0.3	0.2	0.1	0.1	0.1	0.2	0.1	0.2	0.1	NA	NA	NA	0.17
U	6.5	5	6	5.5	6	6.5	5.5	6	6	6	NA	NA	NA	5.90
V	65	65	75	70	75	85	105	80	85	80	NA	NA	NA	78.50
W	<1	2	1	<1	<1	4	<1	<1	<1	3	NA	NA	NA	2.50
Yb	1.9	1.7	1.5	1.1	1.1	1.2	1.3	1.5	1.6	1.3	NA	NA	NA	1.42
Zn	115	15	30	400	55	25	30	25	15	40	NA	NA	NA	75.00

Analyses completed by ALS Chemex, 212 Brookbank Ave, Vancouver, BC
Major elements in percent; other elements in ppm; NA = sample not analyzed for the element
Major elements except FeO by XRF
FeO by HCl-HF digestion & titrimetric finish
Ba, Nb, Rb, Y and Zr by XRF
Other elements by lithium meta-borate fusion and ICP-MS

Sample description and location

	UTM	UTM	
GR01-16	346939	6162113	LD01-32, 340 ft chlorite-epidote altered crowded feldspar porphyry dike
GR01-17	346939	6162113	LD01-32, 349 ft crowded feldspar porphyry dike with moderate pyrite-sericite alteration
GR01-45	347080	6161207	LD93-7, 9.5m pale altered monzonite with 2% disseminated pyrite, altered hornblende and hydrothermal biotite
GR01-52	346495	6162132	LD01-34, 724 ft, monzonite
GR01-55	346495	6162132	LD01-34, 347 ft monzonite with some K-spar alteration
GR01-59	346495	6162132	LD01-34, 200 ft monzonite with minor pyrite
GR01-63	346495	6162132	LD01-34, 388 ft hornblende monzonite
GR01-95	346495	6162132	LD01-34, 392 ft. hornblende monzonite w pinkish feldspar crystalsstals up to 0.5 cm
GR01-96	346495	6162132	LD01-34, 399 ft. Medium grained hornblende monzonite
GR01-97	346495	6162132	LD01-34, 181 ft. Coarse grained hornblende monzonite with trace disseminated pyrite
GR00-28	346888	6161077	Narrow dike of light grey feldspathic monzonite
GR00-29	346950	6161770	DH20-25, 575 ft, Weakly altered crowded feldspar porphyry ?monzonite
GR00-30	347005	6161740	DH20-05, 415 ft, Megacrystic crowded feldspar ?monzonite. Moderate bleaching

TABLE 1B
WHOLE ROCK AND TRACE ELEMENT ANALYTICAL DATA OF MAFIC, DIORITIC SAMPLES, GLOVER STOCK, LUSTDUST PROPERTY

SAMPLE	GR01-69	GR01-70	GR01-71	GR01-72	GR01-73	GR01-74	GR01-86	GR01-107	GR01-108	GR00-27	Average
Al2O3	16.78	16.69	17.03	16.6	16.84	17.57	16.23	16.79	16.63	17.09	16.83
CaO	6.72	6.49	7.52	6.32	7.14	6.88	4.18	6.11	3.52	5.98	6.09
Fe2O3T	6.85	7.24	4.62	7.26	4.48	1.67	4.09	6.79	4.28	6.69	5.40
K2O	2.48	2.47	1.26	2.33	0.86	0.42	3.03	2.41	3.08	2.76	2.11
MgO	3.44	3.7	3.6	3.48	3.38	1.97	2.06	3.06	1.32	3.21	2.92
MnO	0.12	0.11	0.08	0.09	0.08	0.04	0.04	0.1	0.05	0.13	0.08
Na2O	4.34	4.07	4.97	3.99	4.64	6.08	3.74	4.23	4.32	4.14	4.45
P2O5	0.61	0.62	0.63	0.59	0.57	0.43	0.43	0.56	0.3	0.46	0.52
SiO2	55.91	55.66	56.85	55.54	56.88	62.4	61.93	57.2	63.79	57.09	58.33
TiO2	0.97	1	0.97	0.95	0.93	0.75	0.77	0.91	0.57	0.85	0.87
LOI	0.65	1.18	1.51	1.86	3.05	1.18	2.48	0.85	1.05	0.19	1.40
TOTAL	98.87	99.23	99.04	99.01	98.85	99.39	98.98	99.01	98.91	98.59	98.99
FeO	3.43	3.72	2.18	3.45	2.16	0.76	2.1	3.31	1.9	NA	2.56
Fe2O3C	3.03	3.10	2.19	3.42	2.08	0.82	1.75	3.11	2.17		2.55
Fe2O3C/ (Fe2O3C+FeO)	0.47	0.45	0.50	0.50	0.49	0.52	0.45	0.48	0.53	NA	0.57
K/Na	0.57	0.61	0.25	0.58	0.19	0.07	0.81	0.57	0.71	0.67	0.50
Ba	2350	2160	1440	1985	851	611	1920	2100	2400	2130	1794.70
Rb	46.6	51.4	25	54.6	27.2	6.8	84.8	56.8	62.4	66	48.16
Sr	1200	1180	1210	1175	1140	1090	893	1190	1065	948	1109.10
Nb	16	16	16	16	16	18	19	16	18	18	16.90
Zr	196	182	189	192.5	198	206	182.5	181.5	194.5	162	188.40
Y	20.5	20.5	21.5	20	21.5	17	16	19.5	13.5	24	19.40
Ce	104	102.5	93.5	99.5	106.5	98.5	106	102	93	NA	100.61
Co	11.5	15.5	22	13.5	9	0.5	8	12	7	NA	11.00
Cs	1.2	1.8	0.9	2.8	2	0.5	4.9	3	0.8	NA	1.99
Cu	25	20	50	35	45	55	195	60	85	NA	63.33
Dy	4	4.4	4.4	4.3	4	3.2	3	4.1	3	NA	3.82
Er	2.1	2	2.2	2	2	1.7	1.5	1.8	1.2	NA	1.83
Eu	2.1	2	1.9	2	2	1.7	1.6	2	1.5	NA	1.87
Ga	21	21	20	21	20	21	19	21	21	NA	20.56
Gd	6.1	6.3	6.4	6.5	6.1	5.3	5	6	4.4	NA	5.79
Hf	4	4	4	4	4	4	4	4	4	NA	4.00
Ho	0.7	0.7	0.8	0.7	0.8	0.6	0.5	0.7	0.5	NA	0.67
La	43.5	43	37.5	43	47.5	43.5	47.5	43.5	42	NA	43.44
Lu	0.3	0.3	0.3	0.3	0.3	0.2	0.2	0.3	0.1	NA	0.26
Nd	45	42	41.5	41.5	44	39	39	41.5	34	NA	40.83
Ni	<5	<5	5	<5	<5	<5	<5	5	<5	NA	5.00
Pb	10	15	15	20	15	20	20	20	20	NA	17.22
Pr	11.8	11.4	10.8	11	11.5	10.7	11.3	11.2	10	NA	11.08
Sm	7.3	7.6	7.9	7.4	7.6	6.8	6.3	7.1	5.4	NA	7.04
Sn	<1	1	2	1	3	3	1	1	1	NA	1.63
Ta	<0.5	<0.5	<0.5	<0.5	<0.5	0.5	<0.5	<0.5	0.5	NA	0.50
Tb	0.8	0.8	0.9	0.9	0.9	0.6	0.7	0.8	0.6	NA	0.78
Th	9	8	8	8	9	12	9	10	12	NA	9.44
Tl	<0.5	0.5	<0.5	0.5	0.5	<0.5	0.5	<0.5	0.5	NA	0.50
Tm	0.3	0.3	0.3	0.2	0.3	0.2	0.3	0.3	0.1	NA	0.26
U	3	3	4	3	4.5	4.5	4	3	7	NA	4.00
V	145	150	155	160	160	100	95	140	75	NA	131.11
W	<1	<1	3	1	3	1	6	3	<1	NA	2.83
Yb	1.9	1.8	2.2	1.7	2.1	1.7	1.4	1.8	1.1	NA	1.74
Zn	65	75	55	85	50	100	40	70	35	NA	63.89

Analyses completed by ALS Chemex, 212 Brookbank Ave, Vancouver, BC
Major elements in percent; other elements in ppm; NA = sample not analyzed for the element
Major elements except FeO by XRF
FeO by HCl-HF digestion & titrimetric finish
Ba, Nb, Rb, Y and Zr by XRF
Other elements by lithium meta-borate fusion and ICP-MS

Sample locations & descriptions

	UTM	UTM	
GR01-69	346484	6161771	LD01-30, 395 ft weakly altered hornblende-biotite diorite with 15 % mafics
GR01-70	346484	6161771	LD01-30, 382 ft unaltered diorite
GR01-71	346484	6161771	LD01-30, 397 ft bleached & altered hornblende-biotite diorite
GR01-72	346484	6161771	LD01-30, 350 ft dark hornblende-biotite diorite, moderately chloritized. Some hairline pyrite veinlets
GR01-73	346484	6161771	LD01-30, 356 ft dark hornblende-biotite diorite, moderately chloritized. Some hairline pyrite veinlets
GR01-74	346484	6161771	LD01-30, 847 ft bleached, albitized and, chloritized monzonite with Mo-bearing veinlets
GR01-86	346448	6162051	LD01-36, 327 ft, grey, wkly porphyritic hornblende-biotite diorite. Moderate alteration & disseminated pyrite
GR01-107	346484	6161771	LD01-30, 134 to 150 ft. Unaltered hornblende diorite
GR01-108	346342	6162469	LD01-39, 467-547 ft. Biotite-hornblende diorite with trace pyrite veinlets
GR00-27	347003	6162467	Dark diorite with 8-10 % biotite-hornblende phenocrysts. Pyrite on fractures

Lustdust hydrothermal system; alternatively, they may represent high sulphidation mineralization that formed above another buried intrusion emplaced south of the Glover Stock (*see* Figure 9, Dunne and Ray, 2002, this volume).

Megaw (2001) notes that the manto and vein mineralization is strongly controlled by (1) the presence of carbonate hostrocks, (2) lithological contacts including dike and sill margins or limestone-tuff contacts, (3) bedding planes and faults, and (4) antiformal fold hinges.

Lustdust represents a classic intrusion-related system that exhibits distinct proximal to distal zoning, both in its mineralogy and metal chemistry (Evans, 1996; 1998; Megaw, 1999, 2000, 2001). Changes in the chemistry and estimated formation temperatures of the fluid inclusions throughout the system also reflect this zonation (Dunne and Ray, 2002, this volume). Outboard from the porphyry, Megaw (2001) notes that much of the mineralized belt is auriferous (>0.5 g/t Au). Assay data for the various styles of mineralization are shown in Tables 2A to 2E and the average values of the elements and metal ratios are presented in Table 3.

PORPHYRY MINERALIZATION IN THE GLOVER STOCK

The Glover Stock, which outcrops north and south of Canyon Creek, hosts molybdenite ± chalcopyrite-bearing veinlets with classic porphyry-style alteration selvages. This mineralization is developed in both the dioritic and monzonitic phases; the best intersection are in drillhole LD01-39 which cut an 8.8m wide zone with 0.24 % Mo (Megaw, 2001). Mineralization is often associated with several generations of either barren or mineralized veins containing variable amounts of quartz, K feldspar, sericite, pyrite and rare tourmaline. Assay values on some of the mineralization are presented in Table 2A, and Megaw (2001) notes the following styles of porphyry-related alteration:

1. Tourmaline related to quartz veins that cut the diorite south of Canyon Creek. The tourmaline may occur in the veins (Photo 6), or as replacements of the diorite adjacent to the vein margins.
2. Early, generally barren K feldspar-quartz veins cut the stock (Photo 4) and also extend out into the hornfels (Photo 3).
3. Potassic alteration that includes: (a) secondary biotite selvages on mineralized veinlets, (b) secondary euhedral and/or "shreddy" biotite replacing primary biotite and hornblende, (c) secondary pervasive K feldspar flooding and (d) weak to strong pervasive sericitic alteration of the intrusions.
3. Widespread late chloritization and epidotization of the igneous hornblendes and feldspars.

Porphyry-style mineralization in the Glover Stock includes:

1. Quartz-tourmaline veins containing minor pyrite and chalcopyrite (Photo 6).
2. Quartz-K feldspar-pyrite-chalcopyrite veinlets.

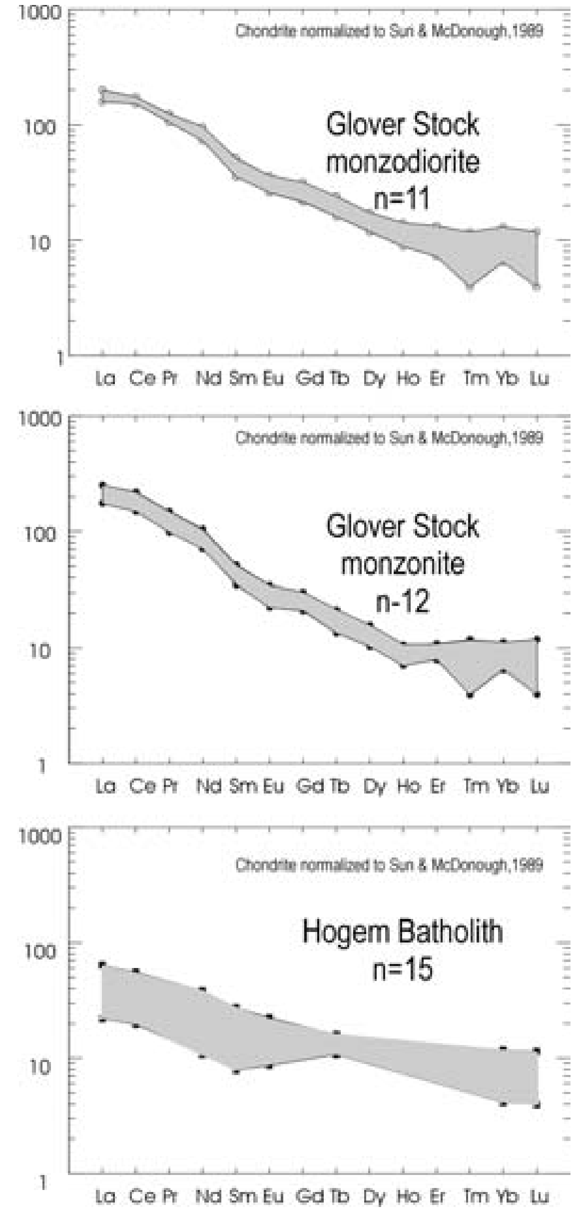

Figure 5. Comparative chondrite normalized rare earth element (REE) plots of the maximum and minimum element ranges (ppm) for the Hogem Batholith and the mafic dioritic and leucocratic monzonitic phases of the Glover Stock. Hogem Batholith data from Barrie (1993). Note the Light Rare Earth Element (LREE) enrichment in the Glover Stock relative to the Hogem Batholith.

3. Quartz-K feldspar-pyrite-molybdenite veinlets (Photos 4 and 5).
4. Younger quartz-K feldspar ± pyrite veinlets that cut the Mo-bearing veins (Photo 5).
5. Igneous hornblendes that are replaced, in turn, by specularite and then magnetite containing interstitial chalcopyrite.
6. Open sigmoidal cavities lined with early quartz-K feldspar-pyrite and then filled with specularite, epidote and rare, late garnet.

TABLE 2A
ASSAY DATA OF GLOVER STOCK PORPHYRY SAMPLES, LUSTDUST PROPERTY

No.	IWE01-2	GR01-50	GR01-51	GR01-53	GR01-58
Ag	0.2	0.4	0.36	0.6	0.42
As	50	66.2	64.6	9.6	5
Au	4	6	2	9	4
Bi	0.4	0.7	0.2	1.1	0.3
Cd	<0.20	6.98	2.1	10.45	2.66
Ce	98	91.5	83.2	78.9	72.6
Co	7	3.5	3.4	6.9	6.2
Cr	90	112	57	177	97
Cu	119.2	80	46.8	165.9	117.1
F	450	660	910	780	740
Fe	3.09	1.2	1.08	1.99	1.38
Ga	22	15.15	19.4	18.55	15.8
Ge	<0.50	0.2	0.2	0.2	0.15
Hg	<10	10	<10	<10	<10
In	0.05	0.09	0.025	0.125	0.03
K	2.41	2.7	3.03	2.57	2.13
La	55	56	50.5	46	43.5
Mg	1.06	0.48	0.71	0.62	0.6
Mn	600	90	120	135	135
Mo	5.5	201	362	866	899
Na	3.08	2.17	2.32	2.24	2.07
Nb	22	10	11.7	12.5	10.4
Ni	16	4.8	4	6.2	5.4
P	1700	1030	970	990	900
Pb	65	15	13.5	51.5	10.5
S	<0.10	0.71	0.35	1.12	0.74
Sb	52	6.95	4.9	45.85	3.4
Se	<10	<1	<1	1	1
Sn	<2.0	0.6	0.8	0.8	0.8
Te	<0.50	0.2	0.05	0.5	0.25
Tl	1	0.86	0.9	0.78	0.9
U	3	4.1	4.7	4.5	3.9
W	1	8.8	2.5	2.4	2.9
Zn	120	708	134	838	38

Analytical methods etc., for Tables 2A - 2F.
Analyses performed at ALS Chemex, 212 Brooksbank Avenue, North Vancouver, B.C. V7J 2C1
Au by fire assay and Induced Coupled Plasma-Mass Spectrometry (ICP-MS); reported in ppb
F by carbonate nitrate fusion and specific ion electrode finish; reported in ppm
All other elements analyzed by combined ICP-MS and ICP-Atomic Emission Spectroscopy. Hg & Au reported in ppb
Fe, K, Mg, Na and S reported in per cent. All other elements in ppm. < = below detection limit.
Note: ICP-MS detections levels were raised for some samples to reflect high-grade sulphide analysis.
Locations using NAD 83, UTM Zone 10 co-ordinates.
Sample descriptions & locations:
IWE01-2: Sub-crop of hornblende-biotite monzonite with pyrite and trace chalcopyrite. 346428E 6162162N
GR01-50: LD01-34; 559 feet. Coarse grained monzonite with disseminations and veinlets of pyrite and trace molybdenite. 346495E 6162133N
GR01-51: LD01-34; 540 feet. Coarse grained monzonite with disseminations and veinlets of pyrite-molybdenite. 346495E 6162133N
GR01-53: LD01-34; 456 feet. Monzonite with molybdenite-quartz-pyrite veins and trace chalcopyrite. 346495E 6162133N
GR01-58: LD01-34; 221 feet. Monzonite cut by quartz-pyrite-molybdenite veinlets. 346495E 6162133N

The paragenesis of the porphyry Mo mineralization is:

1. Quartz-tourmaline-pyrite ± chalcopyrite (early pre-mineralization).
2. Quartz-K feldspar-pyrite-chalcopyrite (early mineralization phase).
3. Quartz-pyrite-molybdenite-chalcopyrite-bornite (main mineralization phase).
4. Quartz-sericite-pyrite-chalcopyrite (late mineralization phase).
5. Quartz-pyrite (post-mineralization).

CANYON CREEK SKARN

The Canyon Creek skarn (Megaw, 1999) forms a north-trending, garnet-dominant body that mostly lies east of the Glover Stock (Figure 2). It is usually hosted by limestones but has also replaced argillite, hornfels and clastic tuff, as well as some intrusive rocks to produce endoskarn. Garnet is the most abundant prograde mineral; it may exceed 80 % of the skarn and forms coarse-grained, euhedral crystals that reach 1 cm in diameter. Clinopyroxene is far less common, forming between 0 and 15 % by volume and occurring as small (<0.25 mm) euhedral to subhedral crystals. Where later hydrous alteration has taken place, the relict clinopyroxene is extensively corroded and partially replaced by fine-grained chlorite, carbonate and possible hydrobiotite (Leitch, 2001a). Other retrograde minerals include up to 20 % calcite, 10 % quartz, and variable quantities of amphibole, biotite and chlorite (Leitch, 2001a). Minor amounts of epidote, vesuvianite and wollastonite have also been seen, the latter tending to occur along the outermost contact between garnet skarn and marble.

In surface outcrop, the garnets mostly form pale yellow-green to pale greenish brown crystals, but locally they are cut by younger veins of dark brown garnet. Megaw (1999, 2001) notes that the younger, darker, and presumably more Fe-rich garnet becomes dominant with depth. In thin section, the pale garnets occur as highly fractured, euhedral to subhedral crystals that have a distinctive yellow-green colour (Leitch, 2001a). They exhibit minor anomalous anisotropism and prominent zoning that is partly due to the

TABLE 2B
ASSAY DATA OF CANYON CREEK SKARN SAMPLES, LUSTDUST PROPERTY

No.	GR01 - 9	GR01-20	GR01-22	GR01-23	GR01-24	GR01-28	GR01-29	GR01-30	GR01-31	GR01-32	GR01-65	GR01-82	GR01-89	GR01-90	GR01-92	GR01-93	GR01-94	GR01-98	GR00-45
Ag	15.75	70.8	17.2	0.42	0.24	0.58	1.42	0.36	0.22	30.7	34	14.8	199	61.6	28	87.2	35.3	182	52
As	1735	124	1510	1485	1565	1470	72.8	371	604	427	257	9380	158.5	123	179	154.5	149	1615	282
Au	350	1920	730	16	8	28	440	19	2	590	2800	230	8500	1600	1210	5100	3100	1060	1170
Bi	1.9	11.9	19.0	10.7	17.1	61.1	11.3	4.5	0.9	4.9	17.8	3.2	71.0	5.9	0.9	3.9	1.8	71.2	81.7
Cd	0.7	>500	6.06	3.84	0.64	0.42	1.76	0.84	0.8	5.44	1.32	1.2	63.9	9.14	8.1	7.48	3.3	9.1	8.18
Ce	59.5	38.3	80.2	72.4	79	60.7	60.5	21.3	44	32.2	10.85	38.5	21.3	33.2	52.4	39.7	48.9	17.2	19.95
Co	5.5	337	4.6	8.7	3	6.6	8.9	4.6	3.3	2.6	428	7	361	26.6	8.4	28.6	21.3	8	9.2
Cr	153	108	109	139	83	100	130	138	61	157	79	90	144	119	90	115	94	70	140
Cu	7910	40300	9490	99.6	71.4	82.2	803	78	213.8	12200	8790	98.6	71000	21400	13800	46600	16600	58000	33600
F	320	190	170	120	140	100	550	300	100	220	300	400	210	300	200	230	200	380	1350
Fe	15.5	13.15	16.4	18	15.95	17.85	14.25	14.3	16.5	14.9	15.45	6.09	20.2	12.3	12.75	14.15	13.15	18.75	15
Ga	15.65	14.55	17.25	13.75	19	18.9	23.65	13.5	14.55	16.55	2.65	20.5	6.25	9.8	20.2	14.35	18.15	13.5	8.25
Ge	0.05	0.5	0.3	0.15	0.2	0.25	0.35	0.3	0.15	0.4	0.25	<0.50	0.55	1.05	0.9	0.5	1	<0.50	7.85
Hg	90	90	10	10	10	<10	30	10	<10	70	10	100	40	10	20	50	20	140	10
In	5.96	33	8.32	2.83	2.95	3.1	1.045	4.93	3.22	7.13	6.53	1.2	15.7	10.6	10	22	11.4	11.3	9.11
K	<0.01	<0.01	<0.01	0.03	0.02	0.09	3.62	0.16	0.21	<0.01	0.03	0.63	<0.01	<0.01	<0.01	<0.01	<0.01	3.03	0.03
La	29	9	35	33	35.5	28	48	10.5	16.5	13	4.5	25	6	8.5	15.5	11	12.5	10	12.5
Mg	0.09	0.64	0.17	0.08	0.11	0.06	0.6	0.63	0.05	0.08	2.67	1.92	2.25	1.59	0.91	0.56	0.77	0.23	0.35
Mn	1785	1820	1700	1580	1870	1710	315	2770	1625	2280	785	2050	1660	1435	1630	1435	1470	900	1760
Mo	2.85	2.05	19.9	3.3	2.6	4.15	587	84	13.95	29.85	7.5	6	5.45	4.05	4.55	4.15	3.05	244	6.95
Na	<0.01	<0.01	<0.01	<0.01	<0.01	<0.01	0.17	<0.01	<0.01	<0.01	<0.01	0.95	<0.01	<0.01	<0.01	<0.01	<0.01	0.18	<0.01
Ni	75.9	509	100.5	17.2	14.6	18.6	32.8	22.4	14.4	123.5	34	20	700	210	156	570	150	32	49.6
P	160	1110	390	70	120	10	1530	1200	<10	340	2270	1900	1560	1470	750	940	730	1600	6660
Pb	4	8	5	22	6	7.5	14	11	8	7.5	7	330	18.5	7.5	8	88.5	12.5	300	207
S	2.45	>10.00	2.15	7.38	1.07	5.88	>10.00	1.77	0.75	1.77	>10.00	0.2	>10.00	2.55	1.44	5.34	1.77	6	3.27
Sb	9.05	7.95	6.45	28.45	5.35	7.85	10.1	11.65	12.9	17.35	18.15	343.5	20.9	13.05	7.25	26	8.3	196.5	225.8
Se	6	79	7	7	<1	8	22	1	<1	2	54	<10	49	5	4	21	7	40	9
Sn	5.6	11	6.2	3.4	3.4	3.4	18.2	14	5.6	8.4	4.4	6	7.4	15	22.6	18.4	18.2	2	8.4
Te	1.5	4.4	3	6.35	0.95	38.2	10.75	3.3	0.3	0.9	7.15	0.5	6.55	2.9	0.15	0.9	0.4	15	35.6
Tl	<0.02	0.8	0.06	0.06	0.04	0.06	1.7	0.12	0.08	0.06	0.16	6.6	0.42	0.22	0.26	2.02	0.34	2.8	0.76
U	19.7	18.3	19	22.4	22.2	18.7	7.2	14.8	13	12.5	2.2	6	10.5	15.8	15.3	12.2	16.8	4	5.3
W	425	209	349	438	404	415	27.4	409	291	206	13.7	5	112	190.5	276	193	269	63	131
Zn	52	214000	642	356	26	<2	10	14	22	416	154	140	8930	920	760	740	286	720	880

Sample descriptions & locations:

GR01-9: LD01-32; 317 feet. Massive brown-green garnet skarn with chalcopyrite. 346939E 6162113N

GR01-20: LD99-17; 275 feet. Green garnet skarn with sphalerite and chalcopyrite.

GR01-22: LD20-12; 211 feet. Massive garnet skarn with chalcopyrite. 346965E 6162128N

GR01-23: LD20-17; 556 feet. Coarse brownish green crystalline garnet skarn with pyrite. 346930E 6162150N

GR01-24: LD20-17; 572 feet. Massive brown garnet skarn with pyrite. 346930E 6162150N

GR01-28: LD01-32; 407 feet. Massive dark garnet skarn with pyrite. 346939E 6162113N

GR01-29: LD01-32; 197 feet. Massive garnet skarn with pyrite. 346939E 6162113N

GR01-30: LD01-32; 229 feet. Brown garnet with retrograde alteration and pyrite veinlets. 346939E 6162113N

GR01-31: LD97-11; 289 feet. Brown garnet skarn with sulphides.

GR01-32: LD 97-11; 494 feet. Greenish garnet skarn with sulphides.

GR01-65: LD20-07; 332 feet. Retrograde altered garnet-chlorite-pyrite-pyrrhotite-chalcopyrite skarn 0.75m from marble.

GR01-82: Pyrite-epidote skarn near dike contact. 346748E 6161809N

GR01-89: LD20-06; 330 feet. Garnet skarn with pyrite and chalcopyrite.

GR01-90: LD20-06; 332 feet. Brown garnet skarn with disseminated pyrite and chalcopyrite.

GR01-92: LD20-09; 267 feet. Brown, green and pink garnet skarn with pyrite and chalcopyrite.

GR01-93: LD20-09: 271 feet. Pale green garnet skarn (minor brown garnet) with pyrite and chalcopyrite.

GR01-94: LD20-09; 282 feet. Pale green coarse grained garnet skarn with disseminated pyrite and chalcopyrite.

GR01-98: Brown and green garnet skarn and massive pyrite-chalcopyrite at drill-pad LD99-04. 347015E 6162122N

GR00-45: North Canyon Zone. Garnet-chalcopyrite-pyrite skarn. 346991E 6162139N

TABLE 2C
ASSAY DATA OF SPHALERITE-BEARING MANTO SAMPLES, NUMBER 3 AND 4B ZONES, LUSTDUST PROPERTY

No.	GR01-43	GR01-78	GR01-79	GR01-80	GR01-99	GR01-100	IWE01-3	GR00-43	GR00-44	GR01-19	GR01-39	GR01-40	GR01-42	GR01-49	GR01-88
Ag	8.8	151	68	36.6	223	13	9.2	10.85	121	20.3	8.62	13.2	64.7	21.8	444
As	235	>10000	>10000	>10000	289	2270	390	651	2420	56	1855	1635	383	627	27.6
Au	16	1430	4700	1200	2500	990	125	91	1190	580	280	340	770	2100	26050
Bi	0.7	193	59.9	87.6	1450	54.3	42	40.1	259	12.9	10.8	9.3	3.9	165.0	44.6
Cd	46.4	230	4.6	210	>500	10.55	>500	>500	>500	>500	>500	>500	257	>500	>500
Ce	1.18	0.9	<0.10	1	1.3	2.6	7.4	7.94	1.39	3.89	2.67	3.48	0.83	6.03	1.52
Co	3.6	<1.0	<1.0	1	<1.0	25	39	19.4	0.8	575	2.3	3.5	17.1	9.6	906
Cr	12	80	20	40	30	160	70	24	103	43	79	93	60	74	12
Cu	168.8	805	247	1320	15000	213	1165	629	330	6510	1025	1680	245	1290	159000
F	90	60	50	60	90	50	80	130	40	120	30	60	380	340	40
Fe	3.99	>25.0	>25.0	>25.0	12.9	>25.0	21.5	12.65	22.8	7.52	>25.0	>25.0	22.1	12.45	>25.0
Ga	0.8	8.5	2.5	5.5	26	1	13	17.9	5.1	2.4	7.9	6.85	1.8	17.15	0.6
Ge	<0.05	0.5	<0.50	0.5	<0.50	<0.50	<0.50	14.35	25.25	0.45	0.7	0.65	0.5	0.45	0.9
Hg	70	3490	510	1240	90	40	470	810	290	190	310	330	170	100	60
In	0.355	31.1	0.55	23.1	13.15	0.3	26.5	29	2.5	27.1	12.65	8.39	3.95	38	26.1
K	<0.01	0.05	<0.01	0.03	<0.01	0.03	0.01	<0.01	<0.01	<0.01	<0.01	<0.01	0.05	0.03	<0.01
La	3	<5.0	<5.0	<5.0	<5.0	<5.0	5	7.5	5	2	3	3	6.5	5	1
Mg	0.19	0.03	0.03	0.01	0.49	<0.01	0.46	0.17	0.01	1.17	0.01	0.03	0.12	0.21	0.14
Mn	840	50	<50	100	3350	50	1600	2060	845	3750	840	845	525	1905	935
Mo	0.45	19	0.5	32.5	2	1	<0.50	1.55	2.6	0.75	2.1	1.35	1	1.1	9.5
Na	<0.01	0.03	0.03	0.03	<0.01	0.03	<0.01	<0.01	<0.01	<0.01	<0.01	<0.01	<0.01	<0.01	<0.01
Ni	19.6	4	6	10	6	8	18	14.6	3.8	93.6	<0.2	<0.2	4.6	8	2460
P	260	1400	<100	1200	<100	<100	200	340	50	590	20	40	30	230	1610
Pb	5010	11600	2820	9830	760	320	120	316	67400	7.5	40.5	34.5	145500	231	11.5
S	4.77	0.4	0.2	0.2	>10.00	>10.00	>10.00	>10.00	>10.00	>10.00	>10.00	>10.00	>10.00	>10.00	>10.00
Sb	>1000.0	>1000.0	>1000.0	>1000.0	164	254.5	107.5	309	>1000.0	4.1	23.25	22.1	>1000.0	152.2	14
Se	2	<10	20	<10	50	50	70	60	113	121	62	57	78	94	190
Sn	0.2	<2.0	<2.0	<2.0	8	<2.0	2	1	3.2	2	1	1	6	1.6	1
Te	0.8	1	12.5	0.5	37	12.5	12.5	4.5	78.4	1.15	4.25	4.75	6	66.4	13.35
Tl	0.06	84.8	56.2	5	1	2.6	0.4	5.24	0.9	0.12	0.04	0.04	0.3	0.12	0.4
U	2.2	16	2	21	2	<1.0	2	1.6	1.6	2.8	2.5	2.4	2.3	4.2	0.5
W	1.6	52	9	30	297	8	20	59.9	0.5	61.2	24.7	36.6	10.2	21.1	5.7
Zn	4500	23000	480	15900	474000	1220	316000	436000	142500	437000	176500	164000	42000	415000	141500

Sample descriptions & locations:

GR01-43: LD93-11; 32.9 metres. Oxidized mineralization in marble.

GR01-78: No. 3 Zone. Light and dark vuggy oxidized material from trench. 347552E 6161102N

GR01-79: No. 3 Zone. Light and dark vuggy oxidized material from trench. 347552E 6161102N

GR01-80: No. 3 Zone. Light and dark vuggy oxidized material from trench. 347552E 6161102N

GR01-99: No. 4B Zone. Massive black sphalerite with coarse pyrite-pyrrhotite. 347096E 6161452N

GR01-100: No. 4B Zone. Massive black sphalerite with coarse pyrite-pyrrhotite. 347096E 6161452N

IWE01-3: No. 4B Zone. Massive sphalerite with coarse pyrite. 347085E 6161470N

GR00-43: 4B Zone. Massive sphalerite-pyrite. 437096E 6161459N

GR00-44: No. 4B Zone. Massive sphalerite-pyrite. 437096E 6161459N

GR01-19: LD99-17; 266 feet; No. 4B (transition) Zone. Sphalerite and chalcopyrite.

GR01-39: LD93-8; 20.4 metres. Massive black sphalerite with pyrite. 347112E 6161510N

GR01-40: LD93-8; 21.5 metres. Massive black sphalerite-pyrite with white quartz veining. 347112E 6161510N

GR01-42: LD93-8; 31 metres. Massive sphalerite with 20% coarse euhedral pyrite. 347112E 6161510N

GR01-49: LD92-15; 32 metres. Massive black sphalerite with pyrite.

GR01-88: LD20-06; 329 feet. Massive to semi-massive sphalerite with pyrite and chalcopyrite. 347005E 6161743N

presence of very large decrepitation fluid inclusions (*see* Photo 5, Dunne and Ray, 2002, this volume). Locally, they contain abundant small fibrous inclusions of unknown composition and origin (Leitch, 2001a).

Where the skarns contain sulphide mineralization, the late, pale to dark green and weakly pleochroic chlorite may make up to 10 % of the rock. Mineralization occurs as Ag and Au-bearing chalcopyrite and lesser bornite with abundant pyrite, variable amounts of sphalerite and rare arsenopyrite and stibnite. It is commonly controlled by fractures but may be disseminated. Megaw (2000, 2001) notes that the conduit structures through the garnetite are often surrounded by zones, several metres wide, of more disseminated mineralization. The density of mineralized structures, the width of their disseminated haloes, and the intensity of retrograde alteration increase with both depth and proximity to the Canyon Creek Fault (Figure 2). Retrograde alteration is often accompanied by a dramatic increase in chalcopyrite, pyrite and magnetite. The latter mineral occurs either as fine-grained masses or as pseudomorphs, up to 2 mm long, after bladed specularite. The chalcopyrite commonly occurs as interstitial blebs and masses up to 6 mm in length. However, chalcopyrite is also seen as small (<0.5 mm), rounded to irregular inclusions in sphalerite and magnetite (Leitch, 2001a). Also present are variable quantities of specular hematite, marcasite and relict pyrrhotite. In rare cases, the skarn may contain up to 30 % sphalerite (Table 2B), as well as trace amounts of a fibrous, dark grey mineral that may be tetrahedrite-tennantite. The dark, red-brown subhedral sphalerite crystals reach 2 mm in length.

TABLE 2D
ASSAY DATA OF MASSIVE PYRITE-PYRRHOTITE REPLACEMENTS, 4B ZONE, LUSTDUST

No.	GR01-21	GR01-41	GR01-44	GR01-46	GR01-47	GR01-48	GR01-67
Ag	54.7	20	5.14	3.24	5	3.04	15.45
As	428	3530	792	1710	>10000	>10000	324
Au	1840	110	400	84	680	550	960
Bi	1165.0	48.5	18.9	14.1	27.6	9.2	74.6
Cd	15.5	>500	4.08	4.8	2.98	1.66	1.76
Ce	1.2	25.8	1.12	7.74	2.37	25.3	12.15
Co	178.2	8	15.4	36.1	21.3	55.2	17.1
Cr	58	59	48	183	103	105	73
Cu	15600	864	891	556	828	405	4750
F	100	2500	320	670	300	210	520
Fe	>25.0	>25.0	>25.0	>25.0	>25.0	24.5	>25.0
Ga	1.1	5.9	1.45	2.85	1.25	7.95	8.45
Ge	0.85	0.9	0.65	0.5	0.75	0.65	1.65
Hg	<10	390	<10	10	30	10	<10
In	3.19	3.95	0.07	0.09	0.07	0.075	3.98
K	<0.01	0.51	0.07	0.03	0.04	0.4	<0.01
La	0.5	28	1	6	2	12.5	9.5
Mg	0.29	0.88	0.38	0.28	0.1	0.69	0.29
Mn	725	910	200	375	385	575	545
Mo	1.2	42.35	0.75	1.65	1.4	5.3	3.8
Na	<0.01	<0.01	<0.01	<0.01	<0.01	<0.01	<0.01
Ni	2.8	22.8	7	17.2	14.8	33.8	31.4
P	380	1110	<10	4060	1420	330	2990
Pb	43.5	27800	325	2360	335	205	29
S	>10.00	>10.00	>10.00	>10.00	>10.00	>10.00	>10.00
Sb	31.05	>1000.0	247.7	>1000.0	434	453.9	15.5
Se	95	29	36	13	5	2	39
Sn	2.4	1.6	0.4	0.2	<0.2	1.2	12
Te	129	6.45	12.3	2.1	0.55	1.4	63.2
Tl	0.02	1.22	0.22	0.1	0.08	0.52	0.12
U	3.4	14.5	4	0.5	0.1	1.2	10.7
W	23.3	15.3	2.3	4.1	12.8	74.9	18.5
Zn	1655	122500	354	410	220	136	164

Sample descriptions & locations:

GR01-21: LD99-17; 192 feet. 4B zone; 1.2 metre wide massive pyrite-pyrrhotite-chalcopyrite in marble.

GR01-41: LD93-8; 27.2 metres. Massive pyrrhotite with sulphosalts. 347112E 6161510N

GR01-44: LD93-11; 46 metres, 1 metre wide zone of massive pyrrhotite in bleached marble.

GR01-46: LD93-4; 88 metres. Massive pyrite-pyrrhotite with sulphosalts.

GR01-47: LD93-4; 90 metres. Massive pyrite-pyrrhotite with white quartz blebs. 347153E 6161265N

GR01-48: LD93-4; 91.5 metre. Massive pyrrhotite-pyrite and white quartz blebs. 347153E 6161265N

GR01-67: LD20-07; 295 feet. Massive pyrite-pyrrhotite-chalcopyrite zone 1 metre from hornfels contact (at 301 feet).

Cross-cutting relationships show that the bulk of the Canyon Creek skarn formed early during an evolving, cyclic process that generated enormous volumes of garnet ± pyroxene assemblages. These features suggest the presence of a potent, long-lived hydrothermal system that resulted in skarn replacement of the limestone, intrusions and previously hornfelsed argillite. The subsequent mineralization was controlled by structures, crystal grain boundaries, and other geologic discontinuities or lithological contacts in the skarn.

The skarn's outer contact with the country rocks is commonly sharp, the very pale brown-green garnet passing out to a narrow (< 2 metres) zone of strongly bleached marble. Locally, the marble-skarn contacts are occupied by irregular blebs and narrow zones of massive sulphide mineralization containing sphalerite, pyrite, pyrrhotite and minor chalcopyrite. Megaw (1999) considers these to be a transitional style of mineralization between the skarns and the more distal mantos.

MANTOS (NUMBERS 2, 3 AND 4B ZONES)

The Canyon Creek skarn passes southwards into a number of more or less stratigraphically concordant massive sulphide mantos and their oxidized equivalents. The mantos are best developed along permeable carbonates, particularly where these rocks are in close proximity to chlorite-altered mafic tuff beds. They tend to occur as

TABLE 2E
ASSAY DATA OF SULPHIDE AND SULPHOSALT-BEARING VEINS, NUMBER 1 ZONE (TAKLA SILVER MINE), LUSTDUST PROPERTY

No.	GR01-5	GR01-26	GR01-27	GR01-101	GR01-42
Ag	167	6277.2	5513.4	1030	840
As	>10000	>10000	>10000	>10000	>10000
Au	4300	6400	4200	12050	4800
Bi	1.1	0.5	0.6	3.5	1.21
Cd	246	301	176	81.6	52.7
Ce	0.9	0.4	<0.10	0.2	0.64
Co	<1.0	<1.0	<1.0	<1.0	0.4
Cr	140	60	80	40	117
Cu	198.3	7980	4110	1000	861
F	40	30	30	30	40
Fe	19.4	7.18	5.34	14.65	9.6
Ga	3	5	2	0.5	1.5
Ge	0.5	<0.50	<0.50	<0.50	7.9
Hg	16510	>100000	62500	11560	19150
In	1.9	0.25	0.25	0.15	0.15
K	0.04	0.01	0.01	<0.01	<0.01
La	5	10	10	10	4
Mg	<0.01	<0.01	0.01	<0.01	<0.01
Mn	50	350	550	300	290
Mo	<0.50	<0.50	<0.50	6	5.1
Na	0.03	0.02	0.02	0.03	<0.01
Ni	2	8	<2.0	4	3.8
P	<100	<100	<100	<100	120
Pb	68300	146000	223000	158000	57300
S	>10.00	>10.00	>10.00	>10.00	8.78
Sb	>1000.0	>1000.0	>1000.0	>1000.0	>1000.0
Se	<10	<10	<10	<10	<1
Sn	6	16	30	16	5.6
Te	<0.50	<0.50	<0.50	0.5	0.05
Tl	>500	>500	>500	310	>500
U	1	2	2	3	0.8
V	<10	<10	<10	<10	3
W	1	<1.0	<1.0	2	0.4
Zn	2920	31900	11000	820	2230

Sample descriptions & locations:
GR01-5: Pyrite, sulphosalts, arsenopyrite, scorodite. 347853E 6160749N
GR01-26: No. 1 Zone. Pyrite, sulphosalts, arsenopyrite, scorodite. 347855E 6160516N
GR01-27: No.1 Zone. Pyrite, sulphosalts, arsenopyrite, scorodite with white quartz. 347860E 6160518N
GR01-101: No.1 Zone. White quartz vein with tetrahedrite-pyrite. 347860E 6160518N
GR00-42: No. 1 Zone. Sphalerite-sulphosalts. 349647E 6159929N

TABLE 3
AVERAGE ASSAY VALUES AND METAL RATIOS FOR THE VARIOUS STYLES OF MINERALIZATION, LUSTDUST PROPERTY

	Glover Stock Porphyry	Canyon Creek Skarn	No. 4B Zone		No. 1 Zone Distal veins
			Pyrrhotite & pyrite-rich masses	Sphalerite-rich mantos	
	(n=5)	(n = 19)	(n = 7)	(n = 15)	(n = 5)
Hg (ppb)	6	38	65	545	41944
Au ppb	5	1520	661	2824	8150
Ag	0.4	43.8	15.2	81	2765.5
As	39	1140	3826	2723	>10000
Ba	1326	59	26	106	77
Bi	0.5	21	194	162	1.4
Cd	4	33	76	351	171
Ce	84.8	43.7	10.8	2.8	0.4
Co	5.4	68	47	107	0.5
Cr	107	112	90	60	87
Cs	2.1	0.9	0.8	0.3	4.5
Cu	106	17955	3413	12642	2830
F	708	304	660	108	34
Ga	18.2	14.8	4.1	7.8	2.4
Ge	0.2	0.8	0.9	3.0	1.8
Hf	2.82	4.86	0.31	3.66	2.80
In	0.1	9.0	1.6	16.2	0.5
La	50.2	19.1	8.5	3.6	7.8
Li	3.5	1.8	7.5	1.1	7.8
Mn	216	1609	531	1181	308
Mo	467	54	8	5	2
Ni	7	150	19	177	4
P	1118	1201	1471	408	64
Pb	31	56	4443	16267	130520
Rb	81.4	17.0	15.1	1.9	1.6
Nb	13.3	2.3	0.9	0.6	1.5
Sb	23	51	455	470	1000
Se	1.6	17.2	31.3	65.1	4.1
Sn	0.8	9.6	2.6	2.1	14.7
Sr	763	23	9	26	9
Te	0.3	7.3	30.7	17.0	0.3
Th	29.9	20.4	0.9	25.9	39.6
Tl	0.9	0.9	0.3	10.5	462
U	4.0	13.5	4.9	4.2	1.8
W	4	233	22	43	1
Zn	368	12056	17920	185673	9774
Al (%)	6.76	1.29	0.46	0.06	0.02
Ca (%)	1.82	13.51	0.85	2.56	0.08
Fe (%)	1.75	14.98	24.93	19.39	11.23
K (%)	2.57	0.42	0.15	0.02	0.02
Mg (%)	0.69	0.72	0.42	0.21	0.01
Na (%)	2.38	0.08	0.01	0.02	0.02
S (%)	0.60	4.41	>10	7.70	9.76
Cu/Au	22848	18043	4583	4123	506
Cu/Ag	296	415	183	88	1
Zn/Pb	16	1460	7	5740	0.1
Zn/Au	63522	8162	160149	670805	1763
Ag/Au	94	41	42	88	519
Cu/Mo	4.50	3563	2352	2828	9898

flat-lying to gently-inclined, elongate zones developed along structurally thickened and deformed antiformal crests. However, drilling has not revealed any substantial chimney feeders for these bodies, which appear to be stacked in successive limestone beds, resulting in “saddle-reef” morphologies (Megaw, 1999). From south to north the clusters of mantos have been designated the Numbers 2, 3 and 4B-Zones (Figure 2; Evans, 1996, 1997; Megaw, 2001). They crop out in an en echelon fashion (Figure 2), and the northernmost bodies, the Number 4B Zone, appear to merge into the Canyon Creek skarn.

The 4B Zone is well exposed in a number of trenches and its mantos and carbonate replacements appear to be developed along a tight, gently northwest plunging antiformal fold whose axial plane is steeply west dipping. The aligned massive sulphide pods follow either the fold crest or a thrust that separates limestones from hornfelsed graphitic phyllites further east (Megaw, 2001). A mafic tuff horizon within the limestone appears to have been an important conduit for fluid movement. There are two styles of mineralization in the 4B Zone. The most common and economically important comprises 10 to 50 % massive, dark brown to black sphalerite with variable amounts of pyrite ± arsenopyrite ± well-zoned pyrrhotite ± chalcopyrite ± an unidentified grey, fibrous sulphosalt mineral that may be boulangerite, bournonite and/or tetrahedrite-tennantite (Leitch, 2001b). Calc silicate minerals generally make up < 1% of the rock and may include thin veins of chloritized clinopyroxene.

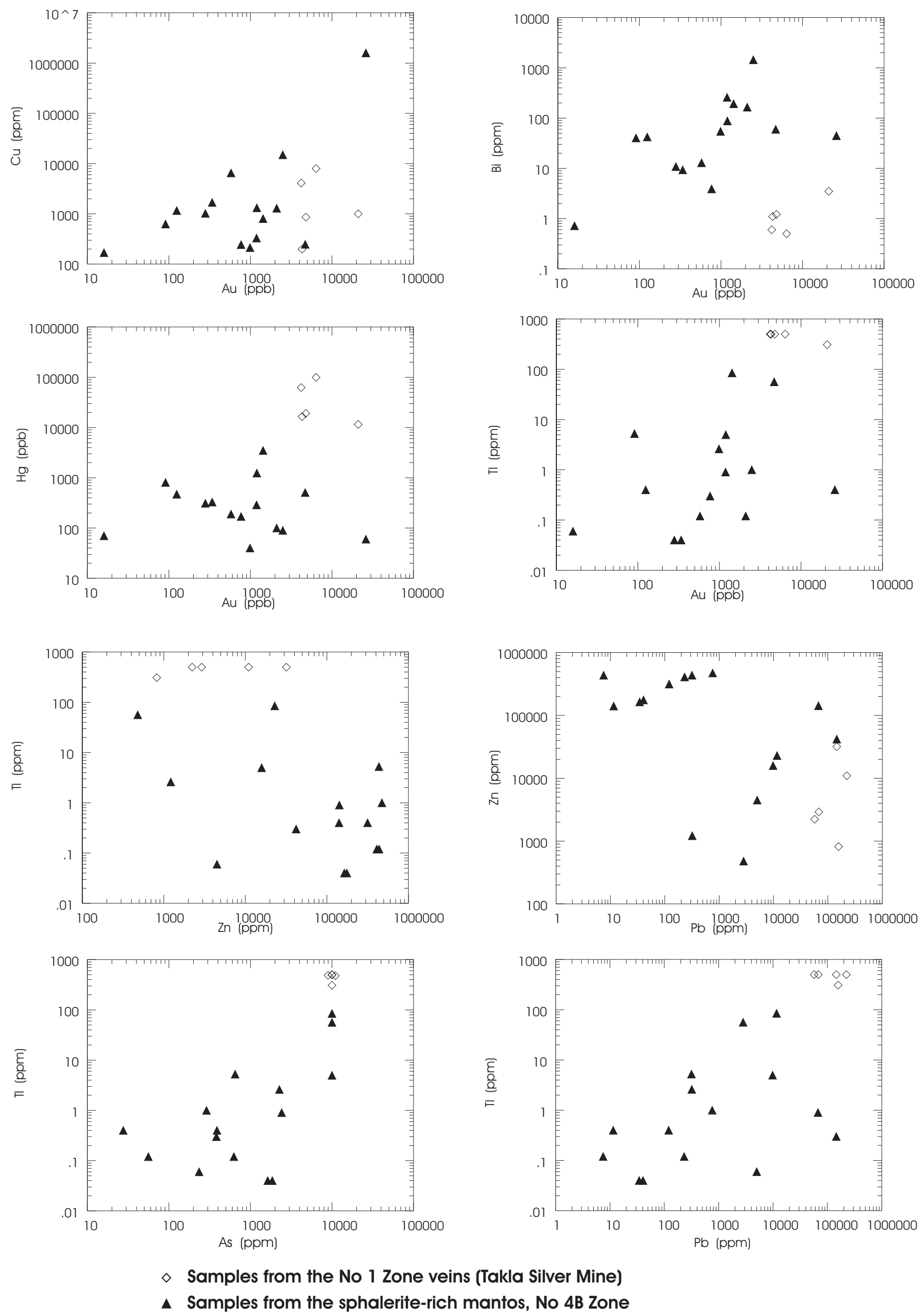

Figure 6. Plots comparing the chemistry of the Number 1 Zone veins (open diamonds) and the sphalerite-rich mantos (filled triangles), Lustdust property. Data from Tables 2C and 2E.

The other style occurs as small (commonly < 1.5 m thick) pods and veins of coarse-grained pyrite-pyrrhotite-dominant mineralization. Pyrite both replaces, and is replaced by, pyrrhotite. Sphalerite in this style of mineralization is generally less abundant (< 10 %), although arsenopyrite, sulphosalt minerals and trace amounts of galena are sporadically developed (Table 2D).

Polished thin section studies (Leitch, 2001a) indicate the subhedral to euhedral sphalerite crystals in the 4B Zone to be almost opaque, suggesting a high Fe content. The crystals reach 3 mm in diameter and contain small (< 25 microns) inclusions of pyrrhotite and larger inclusions of an unidentified bladed silicate. Pyrrhotite and/or pyrite may each locally exceed 50 % of the mineralization. The former mineral comprises subhedral lath-shaped crystals up to 0.5 mm long whereas pyrite cubes, up to 0.75 cm, contain irregular core zones with abundant small silicate inclusions. Gangue minerals include up to 5 % sericite with lesser secondary quartz, calcite and amorphous limonite.

Contacts between the massive sulphides in the 4B Zone mantos and the bleached, recrystallized limestone country rocks are generally very sharp. Replacement features include "scalloped" contacts and in some bodies the massive sulphides contain small, (< 0.3 m) round and isolated remnants of altered limestone. Drilling parts of the 4B Zone between 1992 and 1999 indicates a probable resource of 250,000 tonnes grading 1.3 g/t Au, 12 g/t Ag and 5.5 % Zn with possible Pb, Cu, In, Ge and Ga credits (Megaw, 2001).

The 3-Zone further south (Figure 2) contains the largest manto resource identified at Lustdust. It is entirely oxidized to a 50 m depth, possibly due to pre-glacial weathering. Below this depth, drilling intersects primary pyrite, pyrrhotite and sphalerite with elevated Au grades (Megaw, 2000, 2001). The thickest portions of the 3 Zone mantos occupy the crest of a small-scale anticline and are hosted by carbonates that are interbedded with mafic tuffs. Surface trenching reveals local sections assaying up to 17.9 g/t Au and 69.4 g/t Ag over 4 metres. Drilling from the 1950's to 1991, outlined a probable oxide resource of 650,000 tonnes grading approximately 3 g/t Au, 20 g/t Ag and 5 % Zn (Megaw, 2001).

The Number 2 Zone represents the most southerly development of manto mineralization at Lustdust (Figure 2). It is a minor oxidized replacement zone similar to the 3-Zone further north. However, it is probably controlled by a small synform and mineralization is traceable for 200 m along strike. Surface sampling (Megaw, 2001) indicates an average of 2.3 g/t Au, 109 g/t Ag, 2.16 % Zn and 2.09 % Pb across 5.3 meters true width.

NUMBER 1 ZONE VEINS

The Number 1 Zone veins at the southern end of the property were the target for exploration in the 1940's that led to the underground test workings at the former Takla Silver Mine (Figure 2). In this vicinity, bleached and recrystallized limestones and graphitic phyllites are intruded by numerous thin felsic dikes. At least four, steeply dipping, en echelon, fault-controlled veins and tabular replacements are hosted by the recrystallized limestones or follow dike margins. The veins comprise largely sulphides and sulphosalts with some open-space filling by quartz and calcite. In some outcrops the vein quartz is brecciated and recemented by later quartz and/or calcite. The principal quartz-sulphide vein was explored by underground drifting and drilling in the 1940's and 1960's. Sutherland Brown (1965) and Mathieu and Bruce (1970) identified a number of sulphide, arsenides, and complex sulphosalt minerals, including sphalerite, pyrite, stibnite, boulangerite (Pb5Sb4S11) and realgar. Mathieu and Bruce (1970) noted differences in the mineralogies of the underground and surface trench samples. The latter were oxidized and included a variety of Pb antimonides and secondary Pb-bearing minerals, such as jamesonite, zinkenite, anglesite and Tl-bearing twinnite. In addition, the surface samples contained sphalerite and Ag-bearing tetrahedrite, tennantite and andorite, as well as valentinite, pyrite, arsenopyrite, covellite, chalcopyrite, and scorodite $Fe(AsO_4)$. $2H_2O$) with a gangue of quartz and dolomite. The underground samples had fewer Pb antimonides; the major ore minerals identified included arsenopyrite, pyrite, with lesser sphalerite and jamesonite ($Pb_4FeSb_6S_{14}$) and minor amounts of andorite, argentiferous tetrahedrite, miargyrite, realgar, stibnite and chalcopyrite in a gangue of quartz, calcite and minor dolomite. No gold was observed in the mineralogical study (Mathieu and Bruce, 1970), but their tests suggested the metal was associated with pyrite and arsenopyrite.

In a polished thin section study, Leitch (2001a) tentatively identified the presence of bournonite ($PbCuSbS_3$ ($2PbS.Cu_2S.Sb_2S_3$). The abundant quartz consists of zoned crystals up to 4 mm across, and the arsenopyrite is distinctly more fractured than the pyrite. The sphalerite crystals, which are intergrown with secondary quartz and arsenopyrite, are strongly zoned with dark cores and paler rims.

CHEMISTRY OF THE LUSTDUST MINERALIZATION

For this study, mineralized samples were collected from the Glover Stock porphyry, the Canyon Creek skarn, the sphalerite-rich and pyrite-pyrrhotite replacements in the 3 and 4B zone mantos, and the distal Number 1 Zone veins. The analytical data for these five styles of Lustdust mineralization are presented in Tables 2A to 2E, and the average values and metal ratios are summarized in Table 3. These data demonstrate the north to south chemical zoning at Lustdust. The porphyry has the highest Mo content (average 467 ppm) and there is a progressive decrease in this metal in the skarn, mantos and more distal veins (Table 3). The highest Cu values occur in the Canyon Creek skarn and the 4B sphalerite-rich mantos (averages 17955 ppm and 12642 ppm respectively), while the Number 1 Zone veins and the porphyry have a much lower Cu content.

Unlike Cu and Mo, virtually all the other metals and pathfinder elements listed in Table 3 increase in value towards the more distal, southernmost parts of the mineralized system. The highest average values for Au, As, Hg, Pb, Sb, Sn and Tl are found in the Number 1 Zone veins (Table 3). Exceptions to this include the elements Bi, Cd, Co, Fe, Ni, Se, Te and Zn which occur in far greater abundances in the two styles of mineralization present in the 3 and 4B zone mantos (Table 3).

Figure 6 illustrates some of the chemical differences between the Number 1 Zone veins and the 4B Zone sphalerite-rich mantos. The veins generally contain significantly more Hg, As, Au and Tl than the mantos, and in the latter there is a moderate to good positive correlation between Au:Cu. The Zn versus Pb plot in Figure 6 shows the manto samples are separable into low-Pb and high-Pb populations. The high-Pb population is more chemically similar to the Number 1 Zone veins.

Plots of assay data for the Canyon Creek skarn are shown in Figure 7. These demonstrate good positive correlations between Au:Cu, Au:Ag and Ag:Cu. There is also an excellent positive relationship between Bi:Te, suggesting the presence of trace amounts of bismuth tellurides in the skarn. However, no significant correlations are seen between Au:Te, Au:Bi or Au:Fe, and the Au:As plot indicates a weak negative relationship. Figure 7 strongly suggests that

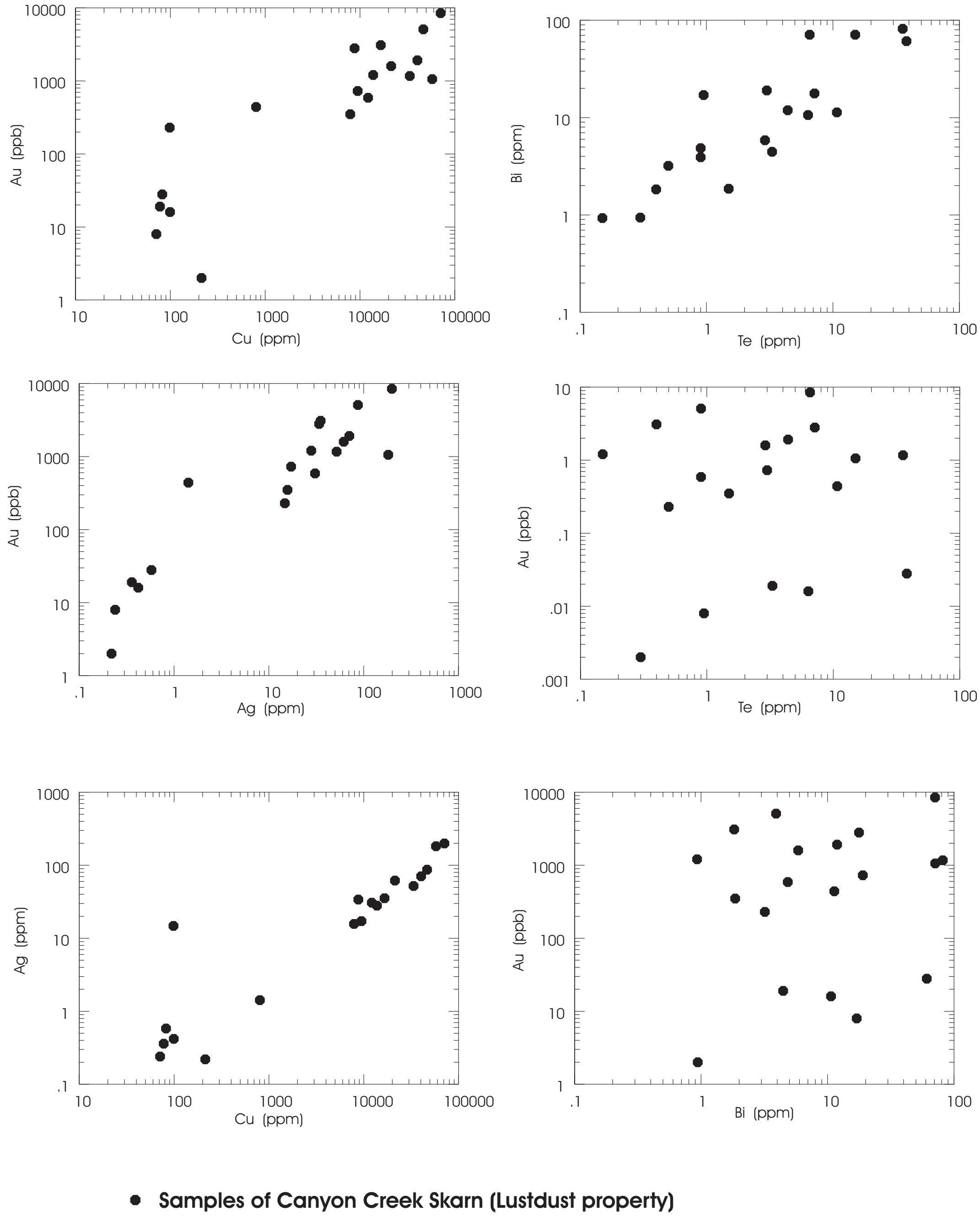

Figure 7. Chemical plots of samples from the Canyon Creek skarn, Lustdust property. Data from Table 2B.

both the Au and Ag in the skarn are associated with chalcopyrite and possibly bornite, and that Au lacks any close association with arsenopyrite or bismuth tellurides. These features, and its Cu:Au, Cu:Ag, Zn:Au and Ag:Au ratios (Table 3; Figure 8) typify Cu skarns rather than the Hedley-type Au skarns (Ray *et al*., 1996; Ray and Webster, 1997).

SUMMARY AND CONCLUSIONS

- Alpha Gold Corporation's Lustdust property, which lies 210 km northwest of Prince George, represents one of the best examples of a zoned porphyry-skarn-manto-vein mineralized system in the Canadian Cordillera.
- Mineralization is developed over a 2.5 km strike length and is related to a small, post-tectonic intrusion, the Glover Stock, and an associated swarm of felsic dikes and sills. The multiphase, composite stock includes mafic dioritic and more leucocratic monzonitic phases, and preliminary U-Pb zircon dates of circa 51-52 Ma on both phases suggest an Eocene intrusive age.
- The stock lies < 2 km west of the Pinchi Fault and it intrudes a deformed package of Cache Creek Terrane argillites, tuffs, cherts and mid to Late Permian lime-

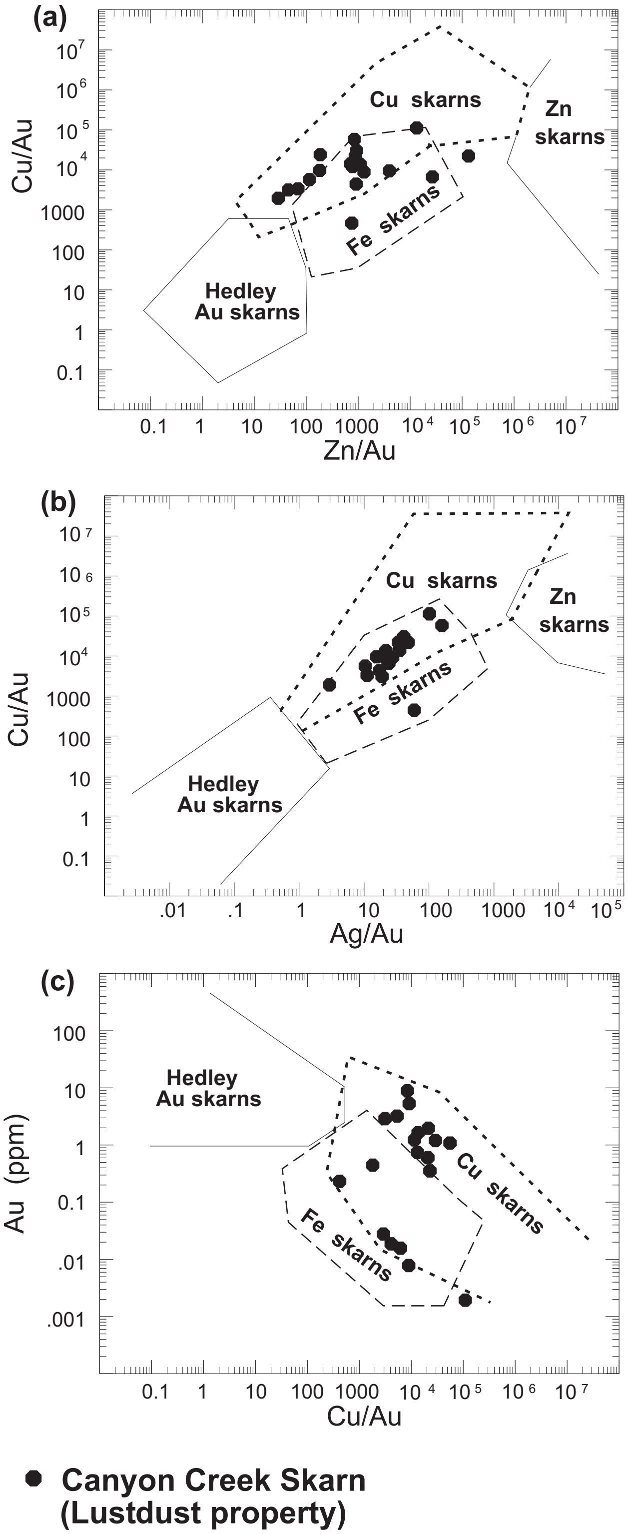

Figure 8. Metal ratio plots for Canyon Creek skarn samples.
(a) Cu/Au *versus* Zn/Au
(b) Cu/Au *versus* Ag/Au
(c) Au *versus* Au/Cu.
Note the Canyon Creek samples plot within the Cu skarn field.Fields for Au, Cu, Fe and Zn skarns in BC from Ray *et al.* (1996); Ray and Webster (1997).

stones. The north-trending Pinchi Fault separates the Cache Creek rocks from the large, multi-phase Jura-Cretaceous Hogem Batholith in the Quesnel Terrane further east.

- The Glover Stock hosts some Mo porphyry mineralization marked by several generations of barren and sulphide-bearing quartz ± sericite ± K feldspar ± tourmaline veins. Mineralization includes molybdenite with lesser chalcopyrite and rare bornite. This is associated with extensive potassic alteration (K feldspar, sericite and biotite) as well as lesser amounts of albitic metasomatism.
- Outboard from the Glover Stock is developed a north-trending, 2.5 km-long discontinuous belt of mineralization. This comprises the proximal Cu-Au (Zn) Canyon Creek skarn, intermediate Zn (Au, Cu, Pb, Bi) mantos (the 2, 3 and 4B zones) and more distal, sulphide and sulphosalt quartz veins enriched in Au, Ag, Pb, Zn, As, Hg and Tl (the Number 1 Zone).
- Controls of the skarn, manto and vein mineralization include the presence of: (1) permeable carbonates, (2) lithological contacts, including sill-dike margins and limestone-tuff contacts, (3) gently north-plunging fold axes, and, (4) faults and shears.
- The lack of ductile structures within the intrusion, the extensive skarn envelope and the brittle-fracture-control of the veins and some mantos are evidence that the Glover Stock was emplaced at a higher structural level. This conclusion is supported by fluid inclusion studies indicating the system formed at depths between 1.1 km and 1.9 km, assuming a lithostatic regime (Dunne and Ray, 2002, this volume). The much higher depth estimates calculated assuming hydrostatic conditions (Dunne and Ray, 2002, this volume) may reflect episodic over-pressuring followed by structural release to produce the hydrothermal breccias seen in the porphyry, skarn and Number 1 Zone veins.
- The Eocene age of the Glover Stock and its REE chemistry (Figure 5) are strong evidence that the stock and the mineralization are not related to the nearby Jura-Cretaceous Hogem Batholith (Figure 1). Instead, the stock may belong to a widespread suite of Eocene plutons, some of which are associated with Cu mineralization. One example includes the intrusions in the Babine porphyry Cu belt (Dirom, 1995; Schiarizza and MacIntyre, 1999), situated approximately 80 km southwest of Lustdust. Another possible body of this type intrudes Cache Creek Terrane rocks at Rubyrock Creek, approximately 100 km south of Lustdust (MacIntyre and Schiarizza, 1999).
- Gold-bearing Cu skarns and Zn mantos associated with Mo porphyry systems are rare and there are few reported analogues to the Lustdust property in British Columbia. Foreign examples may include the Antamina and Magistral porphyry-skarn deposits in Peru (Redwood, 1999; Northern Miner, 2001). These deposits differ in a number of ways from Lustdust, including their geological setting (continental shelf-carbonates versus oceanic carbonates). However, similarities include (1) a large and metal-rich hydrothermal system related to a shallow-level, Mo-bearing, monzonitic pluton, and (2) an extensive skarn envelope comprising abundant distal green garnet and proximal darker brown garnet. Mineralization at Antamina, like Lustdust, is also Zn-rich.
- The presence at Lustdust of high-grade polymetallic mineralization over a 2.5 km distance suggests a powerful,

metal-rich hydrothermal system. The potential for further discoveries of mineralized mantos, skarn and porphyry on the property is excellent because drilling to depth reveals an increased development of retrograde alteration, sulphides and darker-coloured, proximal-type garnet. Drill intersections through skarn during the 2001 season included hole DDH01-44 which cut 59 m grading 0.8 % Cu and 0.67 g/t Au and hole DDH01-47 which cut 37 m assaying 0.92% Cu and 0.68 g/t Au (Alpha Gold Corp. News release, October 1st 2001).

- The Number 1 Zone veins most likely represent distal mineralization related to the Glover Stock. Alternatively, they could be high sulphidation veins that formed above another buried intrusion related to the Glover Stock (*see* Figure 9, Dunne and Ray, 2002, this volume). Either of these possibilities, together with the high Hg content of the Number 1 veins, raises exciting chances that some of the numerous Hg occurrences along the Pinchi Fault (Figure 3) represent distal or upper level expressions of hidden, Eocene-age porphyry systems. Thus, the long belt of Cache Creek carbonates along the Pinchi structure warrant exploration for Lustdust-type porphyry-skarn-manto-vein targets (Figure 3), as well as for the other types of mineral deposits suggested by Nesbitt and Muehlenbachs (1988) and Albino (1988).

ACKNOWLEDGEMENTS

We are grateful to George Whatley, President of Alpha Gold Corp., and his staff for their assistance and hospitality during this project, and for their permission to publish this data. We thank the following: M.J. Orchard (Geological Survey of Canada) for identifying conodont microfossils; R. Friedman (The University of British Columbia) for expediting the preliminary U-Pb zircon dating; C.H.B. Leitch (Vancouver Petrographics Ltd.,) for discussions regarding the ore and plutonic petrography. Editing by Dave Lefebure and Brian Grant is also appreciated.

We dedicate this paper to the memory of our colleague, Keith Glover, who died tragically during this project. The Glover Stock is named for him, as his geological contribution to understanding the deformational history of the area and the structural controls of the mineralization were just beginning to bear fruit.

REFERENCES

Albino, G.V. (1988): The Pinchi Mercury Belt, central British Columbia: near-surface expression of a Mother Lode-type mineralized system; *Geological Society of America*, Abstracts with Programs, 19:7, A141-142.

Barrie, C.T. (1993): Petrochemistry of shoshonitic rocks associated with porphyry copper-gold deposits of central Quesnellia, British Columbia, Canada; *in* Journal of Geochemical Exploration, 48, *Elsevier Science Publishers,* Amsterdam, pages 225-258.

Bishop, S.T., Heah, T.S., Stanley, C.R., and Lang, J.R. (1995): Alkalic intrusion hosted copper-gold mineralization at the Lorraine deposit, north-central British Columbia; *in* Porphyry Deposits of the Northwest Cordillera of North America, Schroeter, T.G., Editor, *Canadian. Institute of Mining, Metallurgy and Petroleum*, Special volume 46, pages 623-629.

Campbell, D.D. (1966): Summary Geological Report Takla Silver Mines Ltd. Manson Creek, B.C.; Unpublished report by Dolmage Campbell & Associates for T*akla Silver Mines Ltd.*,17 pages.

Debon, F., and Le Fort, P. (1983): A chemical-mineralogical classification of common plutonic rocks and associations; *Royal Society of Edinburgh*, Transactions, Earth Sciences 73 (for 1982), pages 135-149.

Dirom, G.E., Dittrick, M.P., McArthur, D.R., Ogryzlo, P.L., Pardoe, A.J. and Stothart, P.G. (1995): Bell and Granisle porphyry copper-gold mines, Babine region, west-central British Columbia; In Porphyry Deposits of the northwestern cordillera of North America, Schroeter, T.G., Editor, *Canadian Institute of Mining, Metallurgy and Petroleum*, Special Volume 46, pages 256-289.

Dunne, K.P.E., and Ray, G.E. (2002, this volume): Constraints on fluid evolution at the polymetallic Lustdust porphyry-skarn-manto-vein prospect, north-central British Columbia; iIn Geological Fieldwork 2001, *British Columbia Ministry of Energy and Mines*, Paper 2002-1.

Evans, G. (1996): Geological and geochemical report on the 1996 exploration of the Lustdust property; *British Columbia Ministry of Energy and Mines*, Assessment Report 24735, 125 pages.

Evans, G. (1997): Diamond drilling and geochemical report on the 1997 exploration of the Lustdust property, unpublished report for *Teck Corporation*, 18 pages.

Evans, G. (1998): Diamond drilling report on the 1998 exploration of the Lustdust property; *British Columbia Ministry of Energy and Mines*, Assessment Report 25739, 77 pages.

Gabrielse, H., and Yorath, C.J., Editors (1992): Geology of the Cordilleran Orogeny in Canada. *Geological Society of America*, DNAG G-2, 875 pages.

Garnett, J.A. (1978): Geology and mineral occurrences of the southern Hogem Batholith; *British Columbia Ministry of Mines and Petroleum Resources,* Bulletin 70, 75 pages.

Irvine, T.N., and Baragar, W.R.A. (1971): A guide to the chemical classification of the common volcanic rocks; *Canadian Journal of Earth Sciences*, Volume 8, pages 523-547.

Johnson, D. (1993): Report on trench, diamond drilling and geophysical surveying on the Lustdust property. Unpublished report for *Alpha Gold Corporation*, 11 pages.

Leitch, C.H.B. (2001a): Petrographic report on polished thin sections of 7 samples; *British Columbia Ministry of Energy and Mines*, internal report, 17 pages.

Leitch, C.H.B. (2001b): Petrographic report on 7 thin sections; *British Columbia Ministry of Energy and Mines*, internal report, 8 pages.

Le Maitre, R.W., Bateman, P., Dudek, A., Keller, J., Lameyre, J., Lebas, M.J., Sabine, P.A., Schmid, R., Sorensen, H., Streckeisen, A., Woolley, A.R., and Zanettin, B., Editors (1989): A classification of igneous rocks and glossary of terms: recommendations of the International Union of Geological Sciences Subcommission on the systematics of igneous rocks, *Oxford Blackwell Scientific Publications*, 193 pages.

MacIntyre, D.G. and Schiarizza, P. (1999): Bedrock geology of the Cunningham Lake map area (93K/ 11, 12, 13, 14), Central British Columbia; *British Columbia Ministry of Energy and Mines*, Open File Map 1999-11, 1:100 000 scale.

Maniar, P.D., and Piccoli, P.M. (1989): Tectonic discrimination of granitoids: *Geological Society of America*, Bulletin, Volume 101, pages 635-643.

Mathieu, G.I., and Bruce, R.W. (1970): Treatment of surface and underground samples of the gold-silver-lead-antimony-zinc ore, from the Omineca Mining District property of Anchor-Takla Mines Ltd., British Columbia; *Department of*

Energy, Mines and Resources, Ottawa, unpublished report, 21 pages.

Megaw, P.K.M. (1999): Report on 1999 drilling and geological study of the Lustdust property, Omineca Mining Division, British Columbia; *British Columbia Ministry of Energy and Mines,* Assessment Report 26069, 151 pages.

Megaw, P.K.M. (2000): Report on 2000 drilling and geological study of Lustdust property, Omineca Mining Division, British Columbia; *British Columbia Ministry of Energy and Mines,* Assessment Report 26466, 396 pages.

Megaw, P.K.M. (2001): Report on 2001 drilling and geological study of Lustdust property, Omineca Mining Division, British Columbia; unpublished report for *Alpha Gold Corporation,* 132 pages.

Meinert, L.D., (1995): Compositional variation of igneous rocks associated with skarn deposits - chemical evidence for a genetic connection between petrogenesis and mineralization; *in* Magmas, fluids, and ore deposits, Thompson, J.F.H., Editor, *Mineralogical Association of Canada,* Short Course Volume 23, pages 401-418.

Monger, J.W.H. (1977): Upper Paleozoic rocks of the western Canadian Cordillera and their bearing on cordillera evolution; *Canadian Journal of Earth Science*, Volume 14, pages 1832-1859.

Monger, J.W.H. (1998): Plate tectonics and northern cordilleran geology: an unfinished revolution; *Geoscience Canada*, Volume 24:4, pages 189-198.

Nesbitt, B.E., and Muehlenbachs, K. (1988): Genetic implications of the association of mesothermal gold deposits with major strike-slip fault systems; in North American conference on tectonic control of ore deposits and the vertical and horizontal extent of ore systems; *University of Missouri-Rolla*, Proceedings Volume, pages 57-66.

Northern Miner (2001): Inca Pacific pushed Magistral to prefeasibility. *Northern Miner*, September 24-30, 2001, page 16.

Paterson, I.A. (1974): Geology of Cache Creek Group and Mesozoic rocks at the northern end of the Stuart Lake Belt, central British Columbia; *Geological Survey of Canada*, Report of Activities, Paper 74-1, Part B, pages 31-42.

Paterson, I.A. (1977): The geology and evolution of the Pinchi Fault Zone at Pinchi Lake, central British Columbia; *Canadian Journal of Earth Science*, Volume 14, pages 1324-1342.

Paterson, I.A., and Harakal, J.E. (1974): Potassium-argon dating of blueschists from Pinchi Lake, central British Columbia; *Canadian Journal of Earth Science*, Volume 11, pages 1007-1011.

Pearce, J.A., Harris, N.B.W. and Tindle, A.G. (1984): Trace element discrimination diagrams for the tectonic interpretation of granitic rocks; *Journal of Petrology*, Volume 25, pages 956-983.

Ray, G.E. and Webster, I.C.L. (1997): Skarns in British Columbia; *British Columbia Ministry of Employment and Investment*, Bulletin 101, 260 pages.

Ray, G.E., Dawson, G.L., and Webster, I.C.L., (1996): The stratigraphy of the Nicola Group in the Hedley District, British Columbia, and the chemistry of its intrusions and Au Skarns: *Canadian Journal of Earth Science*, Volume 33, pages 1105-1126.

Redwood, S.D. (1999): The geology of the Antamina copper-zinc skarn deposit, Peru; *in* The Gangue, *Geological Association of Canada*, Issue 60, pages 1-7.

Rotzien, J. (1991): Diamond Drill Report on the MV 1 Claim; *British Columbia Ministry of Energy and Mines*, Assessment Report 21965, 61 pages.

Rotzien, J. (1992): Diamond Drill Report on the MV 1 Claim; *British Columbia Ministry of Energy and Mines*, Assessment Report 21965, 132 pages.

Soregaroli, A. (1999): Memo on regional geological, geochemical and geophysical studies performed in the Lustdust area by research institutions; unpublished report for *Alpha Gold Corporation*, pages.

Schiarizza, P. (2000): Bedrock geology, Old Hogem (Western Part), NTS 93N/11, 12, 13; British Columbia Ministry of Energy and Mines, Open File 2000-33, 1:100 000 scale.

Schiarizza, P., and MacIntyre, D. (1999): Geology of the Babine Lake-Takla Lake area, central British Columbia (93K/11, 12,13,14: 093N/3,4,5,6); in Geological Fieldwork 1998, *BritishColumbia Ministry of Energy and Mines*, Paper 1999-1, pages 33-68.

Sun, S.S. and McDonough, W.F. (1989): Chemical and isotopic systematics of oceanic basalts: implications for mantle composition and processes; *in* Magmatism in the ocean basins. Saunders, A.D. and Norry, M.J., Editors, *Geological Society*, Special Publication Number 42, pages 313-345.

Sutherland Brown, A., (1965): Lustdust (Takla Silver Mines Limited), *British Columbia Ministry of Mines and Petroleum Resources*, Annual Report 1965, page 105.

Wheeler, J.O., Brookfield, A.J., Gabrielse, H., Monger, J.W.H., Tipper, H.W. and Woodsworth, G.J. (1991): Tectonic assemblage map of the Canadian Cordillera; Geological Survey of Canada, Map 1712a, Scale 1:2 000,000.

Winchester, J.A., and Floyd, P.A. (1977): Geological discrimination of different magma series and their differentiation products using immobile elements; *Chemical Geology*, Volume 20, pages 325-343.

Constraints on Fluid Evolution at the Polymetallic Lustdust Porphyry-Skarn-Manto-Vein Prospect, North-Central British Columbia

By Kathryn P.E. Dunne[1], and Gerald. E. Ray[2]

KEYWORDS: *Fluid inclusions, Lustdust, porphyry, skarn, manto, vein, hydrothermal fluids, salinity, homogenization temperature, pressure, H_2O, NaCl, $CaCl_2$, CO_2, fluid immiscibility, Takla Silver Mine, high sulphidation veins, economic geology, exploration.*

INTRODUCTION

Alpha Gold Corp's Lustdust Cu-Mo-Au-Zn-Pb-Ag property lies approximately 210 km northwest of Prince George and 35 km northeast of Takla Lake in central British Columbia (Figure 1). It includes a skarn-manto-vein system related to an undeformed Mo-Cu-bearing porphyry body, the Glover Stock (Figure 2). A preliminary U-Pb zircon age of 51-52 Ma (Eocene) has been obtained on a dioritic phase of the porphyry (R. Friedman, personal communication, 2001; Ray *et al.* 2002, this volume). The stock intrudes a north-northwest trending belt of deformed oceanic metasedimentary and volcanic rocks which are part of the Carboniferous to Early Jurassic Cache Creek Terrane (Monger 1977, 1998; Paterson, 1977; Wheeler *et al*., 1991; Gabrielse and Yorath, 1992; Schiarizza and MacIntyre, 1999; Schiarizza, 2000). The property lies less than 2 km west of the north-northwest trending Pinchi Fault which is a major dextral transform fault (Patterson, 1974; 1977). It separates the Cache Creek rocks from an intrusive suite immediately to the east belonging to the Quesnel Terrane (Gabriels and Yorath, 1992; Figure 1).

At Lustdust, mineralization is discontinuously traced for 2.5 km, from the porphyry-style mineralization in the north, to the quartz-sulphide-sulfosalt-bearing veins at the old Takla Silver Mine (Minfile 093N 008) in the south (Figure 2). Lustdust represents a classic mineralogically and chemically zoned, intrusion-related system (Evans, 1996; 1998; Megaw, 1999, 2000, 2001; Ray *et al*., 2002, this volume). Proximal Cu-Mo porphyry style mineralization passes southwards into carbonate hosted Cu-Au (Zn) skarns and massive sphalerite-dominant mantos. The most southern expression of mineralization are massive sulphide-sulphosalt veins at the Takla Silver Mine; these veins, also known as the No. 1 Zone (Evans, 1996, 1998; Megaw 1999, 2000), are marked by Zn, Ag, Pb, Au, Hg, Sb and As enrichment (Ray *et al.,* 2002, this volume).

This paper presents the results of a fluid inclusion study of samples taken from the various styles mineralization at Lustdust. The sphalerite present in the skarns and mantos was too opaque for fluid inclusion work; instead, attempts were made to document fluid inclusion characteristics of garnets in the skarns, of igneous quartz phenocrysts in the Glover Stock, and of quartz from barren and mineralized veins in the porphyry, mantos and No 1 Zone veins. This work helped to evaluate changes in temperature and/or fluid composition throughout the system, examine evidence for fluid immiscibility, and estimate depths of emplacement of the intrusion and related mineralization. These data place constraints on fluid evolution at the Lustdust prospect.

GEOLOGIC SETTING

The Lustdust property is underlain by Cache Creek Group rocks, which comprise a steeply dipping, northerly striking package of deformed and weakly metamorphosed phyllites, cherts, mafic tuffs and volcanics, as well as thick (c. 500m) units of limestone. Microfossils, extracted from limestones hosting the Lustdust mineralization, are Mid to late Permian age (M.J. Orchard, personal communication, 2001; Ray *et al*., 2002, this volume).These metasedimentary and metavolcanic rocks have a complex history of brittle-ductile deformation which was probably related to both the accretion of the Cache Creek Group Group onto the north American continent, and later recurrent dextral transcurrent movements along the Pinchi Fault Zone (Monger, 1977, 1998; Paterson, 1977; Gabrielse and Yorath, 1992).

The deformed supracrustal rocks are intruded by a north-northwest-trending swarm of felsic dikes and sills related to the small, post-tectonic Glover Stock (Figure 2). The elongate stock outcrops north and south of Canyon Creek and is surrounded by a narrow (< 300m) hornfelsic aureole. The stock is a multiphase intrusion ranging compositionally from mafic, amphibole-bearing diorite-monzodiorite to more felsic monzonite-quartz monzonite (Ray *et al.,* 2002, this volume). Analyses confirm the mafic phases are calcalkaline but the more felsic monzonitic suites have alkalic affinities; it is uncertain whether the latter chemical feature is primary or the result of hydrothermal overprinting by K-spar and sericite (Ray *et al*., 2002, this volume). The stock hosts porphyry-style, Cu-Mo-bearing quartz veins and either it, or a related intrusive phase at depth, is believed to be genetically related to the adjacent skarn, manto and vein mineralization (Megaw, 2000, 2001).

[1] *Consulting Geologist*
[2] *British Columbia Ministry of Energy and Mines*

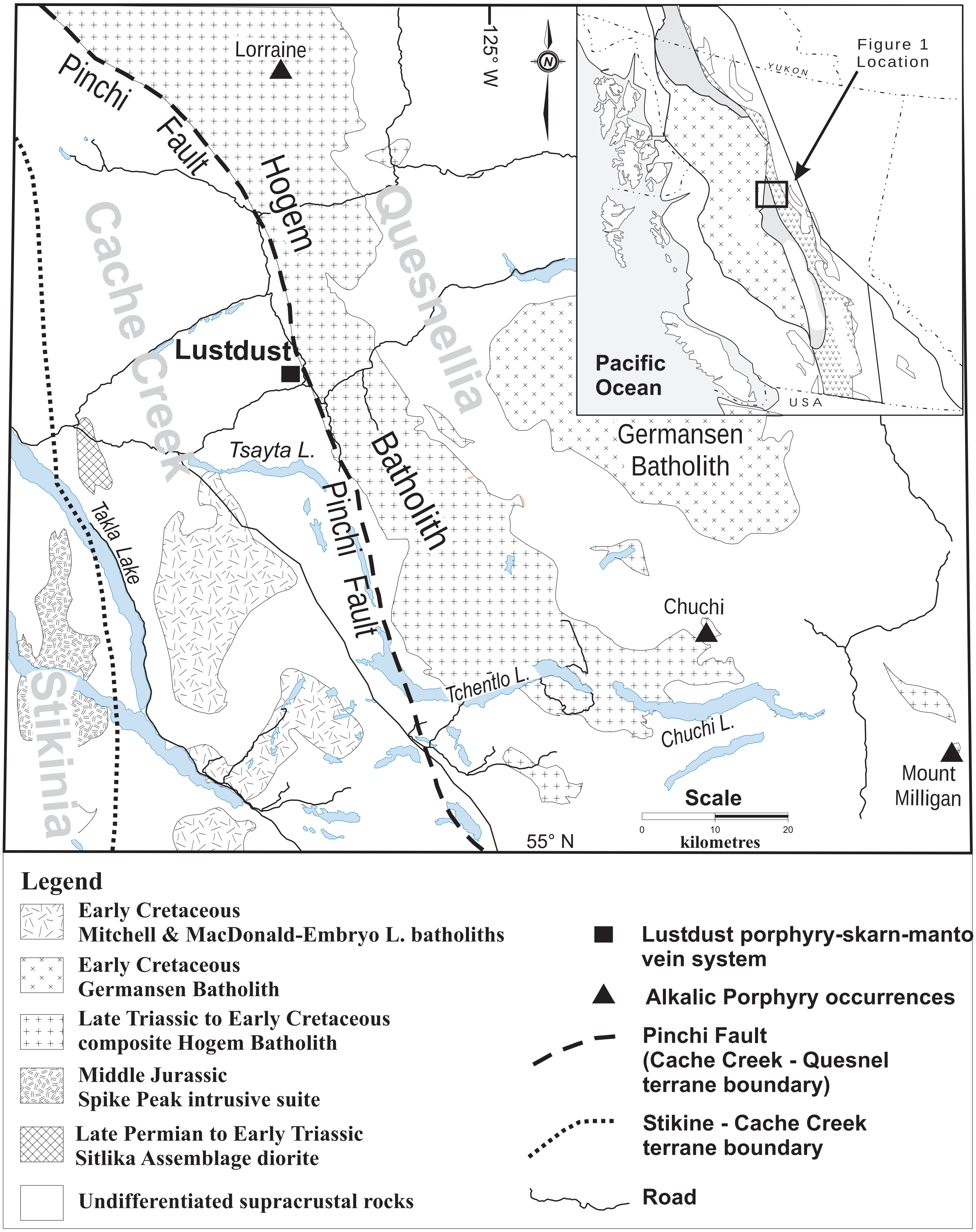

Figure 1. Takla Lake area showing the location of Lustdust property, the Pinchi Fault, the terrane boundaries and major intrusions. Geology after Wheeler *et al.* (1991) and The MapPlace, October, 2001.

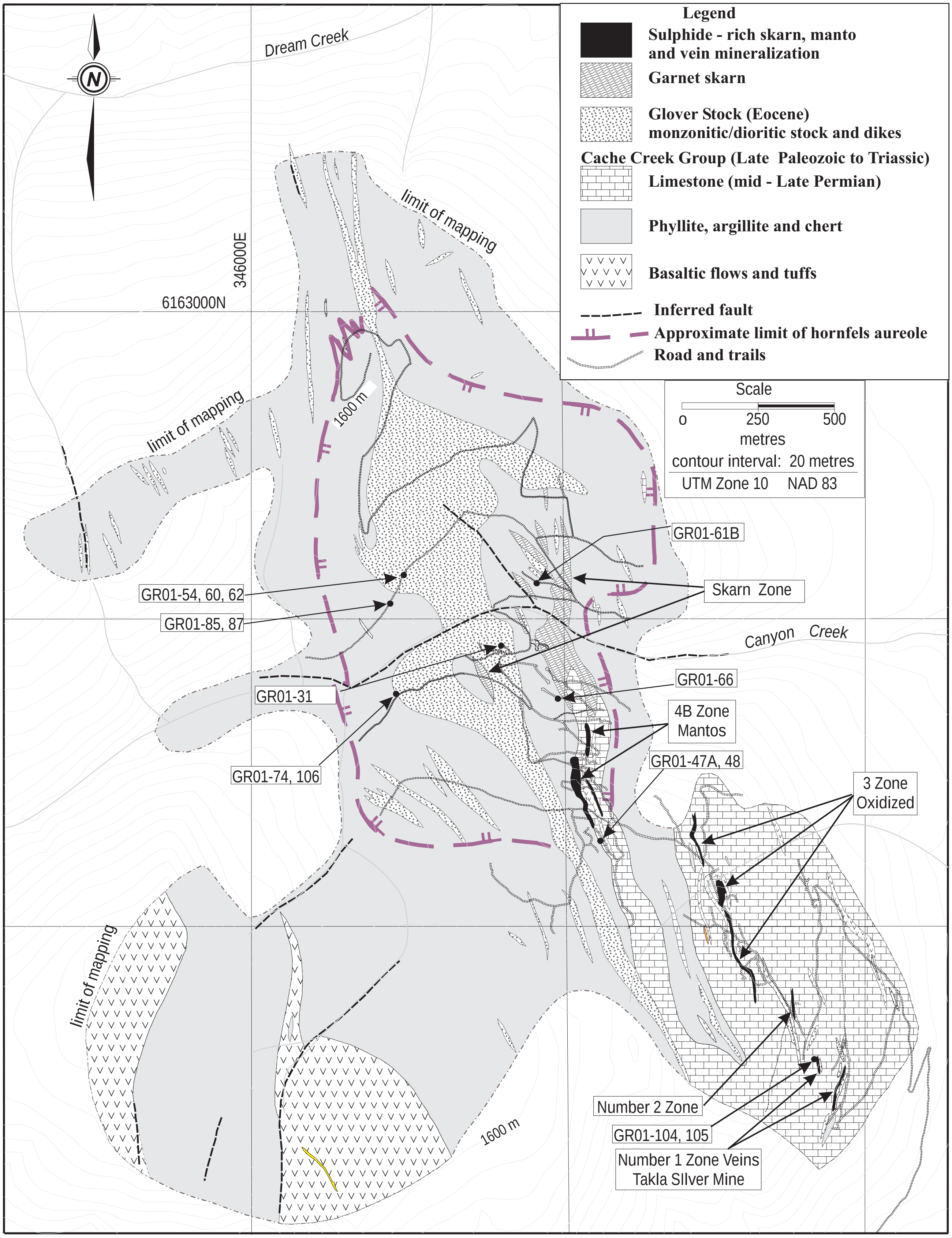

Figure 2. Geology of the Lustdust property showing location of the mineralized zones and samples collected for this study. Geology compiled from mapping by Evans (1996; 1998), Megaw (1999; 2000, 2001), and Ray *et al*. (2002, this volume).

The Lustdust mineralization extends discontinuously over a strike distance of 2.5 km (Figure 2). Samples were collected from the four main styles of mineralization named, from north to south, as follows (Table 1): the porphyry in the Glover Stock which lies north and south of Canyon Creek (Figure 2), the skarn zone, the sphalerite-rich mantos (4B Zone) and the No. 1 Zone veins which lie in the vicinity of the Takla Silver Mine (Figure 2). Megaw (2000, 2001) and Ray *et al*. (2002, this volume) describe details of the mineralization in each of these localities.

METHOD OF FLUID INCLUSION STUDY

Twenty-seven hand samples selected from outcrop and drillcore were collected for fluid inclusion, petrographic examination. They were selected to best represent the different styles of mineralization and alteration observed on the property. The samples included the following minerals which were of particular interest for this study (Table 1): (1) igneous quartz phenocrysts from the Glover Stock diorite and monzonite, (2) hydrothermal quartz from barren and mineralized Cu-Mo veins in the porphyry, (3) garnet and calcite crystals in the skarn, (4) quartz crystals in blebs in the massive 4B Zone sphalerite mantos, and (5) quartz and calcite from the quartz-sulphide-sulfosalt-bearing veins in the No. 1 Zone. Fluid inclusion shapes and sizes, spatial relationships among inclusions and minerals, and phases within inclusions were microscopically observed in doubly-polished thick sections. Based on this preliminary work, fifteen samples containing representative populations of inclusions from the different areas were selected for heating/freezing studies (Figure 2, Table 1).

Microthermometric data were obtained using a Fluid Inc. adapted USGS gas-flow heating-freezing stage housed at the Mineral Deposit Research Unit, Department of Earth and Ocean Sciences, The University of British Columbia. Calibration of the stage was achieved using commercial Syn Flinc synthetic fluid inclusions and ice with the following accuracies: at -56.6± 0.2°C, 374.1 ± 1°C and 0.0±0.1°C. Fluid inclusion data were obtained by first freezing mineral chips and then observing CO_2 melting (if CO_2 present), first and final melting temperatures of ice, melting of salt-hydrates and gas-hydrates (clathrates), and where possible CO_2 homogenization (if CO_2 present) during heating. High temperature data (liquid-vapour homogenization and salt dissolution) were then collected from fluid inclusion assemblages in each mineral chip by incrementally heating above room temperature. Phase transitions in all inclusions were monitored during this heating run to avoid repeat heating and the resultant stretching of fluid inclusions.

Fluid inclusions were evaluated using the concept of fluid inclusion assemblages (FIA's). This ensures that the data was not biased by samples containing large numbers of fluid inclusions and helps to eliminate inconsistent data caused by changes in mass, volume or shape of inclusions after entrapment (*i.e.,* eliminate non-representative inclusions that are the result of diffusion, stretching, or necking-down processes). A fluid inclusion assemblage (FIA) is a petrographically-associated group of inclusions such as those aligned along primary growth zones or secondary fracture planes. One representative data point, rather than several data points is used for each FIA.

RESULTS OF FLUID INCLUSION STUDY

The sphalerite crystals in the mantos were too opaque to determine their fluid inclusion characteristics. Instead, quartz and pale-yellow/green garnet were used for microthemometric analyses because of their optical clarity and high tensile strength; calcite was used in some samples for comparison. Fluid inclusions in quartz and calcite minerals ranged in maximum diameter from less than 1 micron to 30 microns; most measured fluid inclusions averaged 10 to 15 microns. Those in garnet from the skarn were significantly larger, averaging from 20 to 65 microns, and decrepitated inclusions over 100 microns were also observed.

FLUID INCLUSION POPULATIONS

Fluid inclusions were divided into four populations on the basis of phases present at room temperature and their freezing/homogenization behaviour. Microthermometric data are summarized in Tables 2A to 2E.

Type I: Low to Moderate Salinity, Liquid Dominated

Type I inclusions are liquid-rich, low to moderate salinity, and they contain liquid + vapour phases. Rarely, one or two translucent daughter minerals (not halite or sylvite) are present. Type I inclusions are sparse in the igneous quartz phenocrysts and in the porphyry-style quartz veins but are common in the skarn, mantos and No. 1 Zone veins.

First melting of ice between -77 and -26°C indicates that salts such as Ca-, Mg- or Fe-chlorides may present in addition to NaCl (Table 2A). Melting of hydrohalite is observed as a sudden clearing in the inclusions in the presence of ice at temperatures of between -42.6 to -15°C. Final ice melting is observed between temperatures of -24 to 0°C. Homogenization to the liquid phase is recorded at temperatures of 339 to 379°C for 2 inclusions in a quartz phenocryst, 354 to 513.3°C for veins in the porphyry, 305 to 444°C for massive sulphide samples from the mantos and 183 to 323°C for the No. 1 Zone veins. Virtually no difference can be distinguished between melting and homogenization temperatures of fluid inclusions from different origins in the porphyry, skarn and manto (Table 2A). Primary fluid inclusions in the No. 1 Zone veins appear to melt initially at lower temperatures and perhaps homogenize at higher temperatures but the paucity of data precludes any real distinction between primary and secondary fluid inclusions.

Type II: Low-Salinity, Vapour Dominated

Type II inclusions appear to be vapour-rich, as they contain vapour + liquid phases, and homogenize to the vapour (with rare exception to the liquid, *see following*). They are common in both the porphyry and No. 1 Zone vein

TABLE 1
SUMMARY DESCRIPTIONS OF SAMPLES USED FOR FLUID INCLUSION MICROTHERMOMETRIC ANALYSES, LUSTDUST PROPERTY

SAMPLE NUMBER	ZONE	DRILL HOLE 1	DEPTH 2	UTM(E)3	UTM(N)3	DEPOSIT TYPE	HOST ROCK	FEATURE STUDIED	FEATURE TYPE 4 (mineral examined for FI in bold)
GR01-54	porphyry	LD01-34	387 ft	346495	6162133	porphyry	monzonite	vein vein	**qz**+ks+py±cp±mg **qz**+py
GR01-60	porphyry	LD01-34	292 ft	346495	6162133	porphyry	monzonite	vein phenocryst	**qz**+mo+py±cp±bo **qz**
GR01-62	porphyry	LD01-34	232 ft	346495	6162133	porphyry	monzonite	vein vein phenocryst	**qz**+mo+py±cp±bo **qz**+se+py **qz**
GR01-74	porphyry	LD01-30	847 ft	346484	6161771	porphyry	diorite	vein phenocryst	**qz**+mo+py±cp±bo **qz**
GR01-85	porphyry	LD01-36	225 ft	346448	3162051	porphyry	hornfels 48 ft from diorite margin	vein	**qz**+ks+py±cp±mg
GR01-87	porphyry	LD01-36	332 ft	346448	3162051	porphyry	hb-diorite	vein phenocryst	**qz**+mo+py±cp±bo **qz**
GR01-106	porphyry	LD01-30	138.8 ft	346484	6161771	porphyry	hb-diorite	vein phenocryst	**qz**+to+cpy+py **qz**
GR01-20	skarn (porphyry?)	LD99-17	275 ft	-	-	skarn		massive skarn	**gn**+cp+sp+mg (**ca**)
GR01-31	skarn	LD97-11	289 ft	346827	6161912	skarn	garnet skarn	massive skarn	**gn**+cp+sp+mg
GR01-61B	skarn	LD01-33	561 ft	346938	6162115	skarn	garnet skarn	massive skarn	**gn**+cp+sp+mg
GR01-66	skarn	LD20-7	327 ft	347005	6161745	skarn	garnet skarn	massive skarn	**gn**+(cpx+amp+ca)+cp+py
GR01-47A	4B Zone	LD93-4	90 m	347153	6161265	manto	limestone	massive sulphide	py+po+cp+**qz**
GR01-48	4B Zone	LD93-4	91.5 m	347153	6161265	manto	limestone	massive sulphide	py+po+cp+**qz**
GR01-104	No. 1 Zone - Takla Silver Mine	-	-	347860	6160518	vein	limestone	vein	py+as+ss+**qz**±sp (**ca**)
GR01-105	No. 1 Zone - Takla Silver Mine	-	-	347860	6160518	vein	limestone	vein	py+as+ss+**qz**±sp

1. Drill hole year-number; dash = surface grab sample
2. ft = feet, m = metres
3. dash = location uncertain
4. Mineral abbreviations as follows: qz = quartz, py = pyrite, cp = chalcopyrite, gn = garnet, sp = sphalerite, cpx = clinopyroxene, amp = amphibole, ca = carbonate, po = pyrrhotite, as = arsenopyrite, ss = sulphosalt, ks = potassium-feldspar, to = tourm

TABLE 2A
SUMMARY DESCRIPTIONS OF SAMPLES USED FOR FLUID INCLUSION MICROTHERMOMETRIC ANALYSES, LUSTDUST PROPERTY

FEATURE (FEATURE TYPE)	FI ORIGIN 1	FIRST ICE MELT TEMP. range (N) oC (mean ± 1 sig.)	INTERMEDIATE MELT TEMP. 2 range (N) oC (mean ± 1 sig.)	LAST MELT TEMP. 3 range (N) oC (mean ± 1 sig.)	HOMOG. TEMP. range (N) oC (mean ± 1 sig.)
porphyry					
phenocryst (monzonite)	I	-77.4 to -52.2 (2) (-64.8 ± 17.8)	-42.6 (1)	-5.6 (1)	339 to 379 (2) (359 ± 28.3)
phenocryst (diorite)	none noted				
vein (qz+to+cp+py)	PS	-62.9 (1)	-23.8 (1)	-11.6 (1)	not observed
vein (qz+ks+py±cp±mg)	I	-53 to -45 (2) (-49 ± 5.6)	-27 to -25.3 (2) (-26.2 ± 1.2)	-4.3 (1)	489.9 (1)
vein (qz+mo+py±cp±bo)	I	-32.3 (2) (-32.3 ± 0)	-26 (1)	-12.2 to -7.3 (2) (-9.8 ± 3.5)	380.6 to 513.3 (3) (430.6 ± 72.2)
vein (qz+mo+py±cp±bo)	S	-65 to -52.7 (2) (-58.9 ± 8.7)	-27 to -26 (2) (-26.6 ± 0.7)	-16.4 to -7.5 (2) (-12.0 ± 6.3)	467 to 473.9 (2) (470 ± 4.8)
vein (qz+se+py)	I	-37 to -26.6 (2) (-31.8 ± 7.4)	-15 (1)	-7.3 to -6 (2) (-6.7 ± 0.9)	354 to 405.4 (2) (379.7 ± 36.3)
vein (qz+py)	none noted				
skarn					
massive skarn (gn+cp+sp+mg)	P	-55 to -36.5 (7) (-48.7 ± 7.6)	-27.6 to -25.2 (6) (-29.6 ± 3.5)	-16.6 to -7.2 (6) (-13.8 ± 3.6)	not usable
massive skarn (gn+cp+sp+mg)	PS	-40.2 to -54.5 (4) (-43.9 ± 7.1)	-34 to -20.8 (3) (-28.8 ± 7.0)	-17.9 to -13 (4) (-15.3 ± 2.3)	not usable
massive skarn (gn+cp+sp+mg)	S	-45.7 to -39.8 (2) (-42.8 ± 4.2)	-38 to -27 (2) (-32.5 ± 7.8)	-23.6 to -14.8 (2) (-19.2 ± 6.2)	not usable
massive skarn (gn+(cpx+amp+ca)+ cp+py)	P	-40.6 to -39 (2) (-39.8 ± 1.1)	-22.5 (1)	-14.1 to -11 (2) (-12.6 ± 2.2)	not usable
manto					
massive sulphide (py+po+cp+qz)	P	-38.3 to -31.9 (5) (-34.7 ± 2.5)	-27.3 to -21.9 (5) (-25.2 ± 2.5)	-24 to -11.6 (5) (-16.9 ± 4.5)	340 to 444 (6) (386 ± 35.9)
massive sulphide (py+po+cp+qz)	PS	-38.1 to -36.2 (3) (-36.9 ± 1.0)	-28.7 to -28.4 (3) (-28.6 ± 0.2)	-23.9 to -6.1 (4) (-16.2 ± 8.6)	305 to 406 (6) (354.9 ± 33.2)
vein					
massive sulphide (py+as+ss+qz±sp)	P	-64 to -29.3 (5) (-47.7 ± 12.8)	-31 to -26.4 (2) (-28.7 ± 3.3)	-22 to 0 (6) (-9.3 ± 9.9)	218 to 323 (8) (265.7 ± 35.3)
massive sulphide (py+as+ss+qz±sp)	S	-40.5 to -32.9 (3) (-35.4 ± 4.4)	-25 to -15 (2) (-20 ± 7.1)	-11 to -6.1 (3) (-8.0 ± 3)	183 to 309.9 (5) (247.9 ± 48.8)

1. P = primary, PS = pseudosecondary, S = secondary, I = intermediate
2. Assumed to be salt-hydrate (hydrohalite?) melt (see text for description of melting behaviour)
3. Assumed to be last ice melt (see text for description of melting behaviour)

samples. Vapour-rich inclusions from the No. 1 Zone veins homogenize to both vapour (type II) and liquid (type IIQ). The behaviour of the type II inclusions from the veins during heating indicates that they probably represent a single population trapped at near critical conditions.

First and final ice-melting temperatures were difficult to obtain for type II inclusions because of the small amount of liquid present. First melting of ice between -53 and -29.5°C, observed in 6 inclusions, indicates the presence of $CaCl_2$, $MgCl_2$ and/or $FeCl_3$ in addition to NaCl (Table 2B). An intermediate melting event, recorded between -28.6 and -25°C in only 3 inclusions, is interpreted as melting of hydrohalite. Final ice melting is observed between temperatures of -8.8 and -0.4°C. Homogenization to the vapour phase is recorded at temperatures of 333 to 545.6°C in the igneous quartz phenocrysts, 334°C to 573.3°C for veins in the porphyry and 310 to 391.7°C in the No. 1 Zone vein. Homogenization to the liquid is recorded in a tight cluster within the range of type II inclusions (between 353.6 and 365°C) for 4 vapour-rich type IIQ inclusions. Insufficient data precludes evaluation of differences in melting and homogenization temperature between fluid inclusions of differing origin.

Type III: High-Salinity, Liquid Dominated

Type III inclusions are liquid-rich and contain halite other daughter minerals at room temperature. They are the most abundant type present in the igneous quartz phenocrysts and in quartz veins in the porphyry. Typically they contain liquid, vapour and halite.

TABLE 2B
MICROTHERMOMETRIC DATA FOR AQUEOUS, VAPOUR-RICH TYPE II INCLUSIONS

FEATURE (FEATURE TYPE)	FI ORIGIN [1]	FIRST ICE MELT TEMP. range (N) °C (mean ± 1 sig.)	INTERMEDIATE MELT TEMP. [2] range (N) °C (mean ± 1 sig.)	LAST MELT TEMP. [3] range (N) °C (mean ± 1 sig.)	HOMOG. TEMP. range (N) °C (mean ± 1 sig.)	TO PHASE	COMMENT on melt/ homog. behaviour
porphyry							
phenocryst	I				333 (1)	vapour	
(monzonite)							
phenocryst	I	-51.7 (1)	-28.6 (1)	-8.8 (1)	400 to 545.6 (3)	vapour	
(diorite)					(463.9 ± 74.4)		
vein	PS				400 (1)	vapour	
(qz+to+cp+py)							
vein	I					vapour	
(qz+ks+py±cp±mg)							
vein	S	-53 (1)	-23.4 (1)	-5.3 to 3.4 (2)	334 to 573.3 (4)	vapour	
(qz+mo+py±cp±bo)				(-1 ± 6.1)	(407.7 ± 111.3)		
vein	PS					vapour	
(qz+se+py)							
vein	I					vapour	
(qz+py)							
skarn							none noted
manto							none noted
vein							many cannot observe
massive sulphide	P	-48.1 to -32 (2)	-25 (1)	-2.5 to -0.4 (2)	337 to 391.7 (6)	vapour	
(py+as+ss+qz±sp)		(-40.1 ± 11.4)		(-1.5 ± 1.5)	(362 ± 19.0)		
massive sulphide	P	-32.2 to -29.5 (2)		-4.7 to -2.4 (4)	353.6 to 365 (4)	liquid	type IIQ inclusions
(py+as+ss+qz±sp)		(-30.9 ± 1.9)		(-3.4 ± 1.0)	(357.2 ± 5.4)		
massive sulphide	S				310 to 325 (2)	vapour	
(py+as+ss+qz±sp)					(317.5 ± 10.6)		

1. P = primary, PS = pseudosecondary, S = secondary, I = intermediate
2. Assumed to be salt-hydrate (hydrohalite?) melt (*see* text for description of melting behaviour)
3. Assumed to be last ice melt (*see* text for description of melting behaviour)

Type IIIA inclusions form approximately 60% of the type III population in the porphyry samples, and they comprise a vapour bubble with larger diameter than the halite cube. Type IIIA inclusions exhibit halite dissolution at temperatures below liquid-vapour homogenization. Type IIIB inclusions, comprise the remaining 40% of the type III population in the porphyry samples, and exhibit a halite cube with larger diameter than the vapour bubble. Type IIIB inclusions homogenize by halite dissolution after liquid-vapour homogenization. Approximately equal numbers of analyzed type III inclusions homogenize by vapour-bubble disappearance (type IIIA) and halite dissolution (type IIIB), regardless of inclusion origin (Figure 3a). Type III inclusions in the porphyry phenocrysts and veins may contain an opaque mineral (sometimes cubic or hexagonal plate) and/or one or two translucent solids in addition to halite (Photo 1).

Type III inclusions generally exhibit first ice melting between -78 and -40°C, although melting may begin as high as -26°C (Tables 2C and 2D). These observed first melting temperatures compare with the eutectic temperatures for the $CaCl_2$-H_2O, NaCl-$CaCl_2$-H_2O, and $FeCl_3$-H_2O systems that are -49.8°C, -52°C and -55°C (Linke 1958, 1965), respectively. First melting temperatures below -55°C would require additional components in the fluid inclusions. Last ice melting, in the presence of hydrohalite, is recorded between -50.2 and -21°C (generally between -35 and -21°C). Paucity of data precludes comparison of melting temperatures on the basis of fluid inclusion origin.

Little difference is observed in homogenization temperatures between primary versus secondary fluid inclusions (Figure 3a). Final homogenization temperatures of type IIIA inclusions (by vapour bubble disappearance to the liquid) vary widely from 302.6 to 488°C in quartz phenocrysts, 287 to 635.1°C in veins from the porphyry, 266.8 to 271°C (only 2 inclusions) from quartz in the mantos and 167.4 to 178°C (only 2 inclusions) from quartz from the No. 1 Zone vein (Table 2C, Figure 3b). Final homogenization temperatures of type IIIB inclusions (by halite dissolution to the liquid) also vary widely from 329 to 441.2°C in quartz

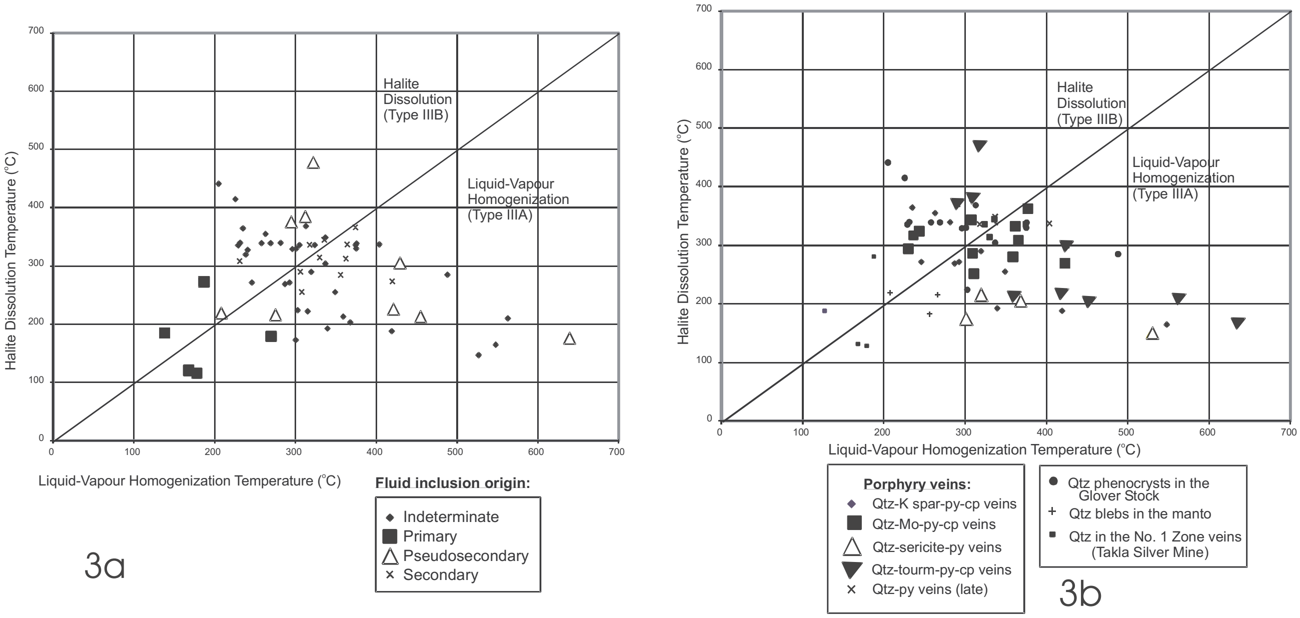

Figure 3. Halite dissolution temperatures as a function of liquid-vapour homogenization temperature for type III inclusions in quartz phenocrysts from the Glover Stock, quartz veins in the porphyry, quartz blebs in massive sulphide from the mantos and quartz from the massive sulphide No. 1 Zone veins, Takla Silver Mine. The diagonal line separates type IIIA from type IIIB inclusions. (a) Temperature of type III fluid inclusions grouped by fluid inclusion origin. Type IIIA and Type IIIB inclusions occur as primary, indeterminate (possibly primary), pseudosecondary and secondary fluid inclusions. (b) Temperature of type III fluid inclusions grouped by deposit and feature type. Type IIIA and Type IIIB inclusions are represented in all deposit/vein types except qtz-sericite-py veins (Type IIIB only). Note: similar symbols from Figures 3a and 3b do not relate to each other.

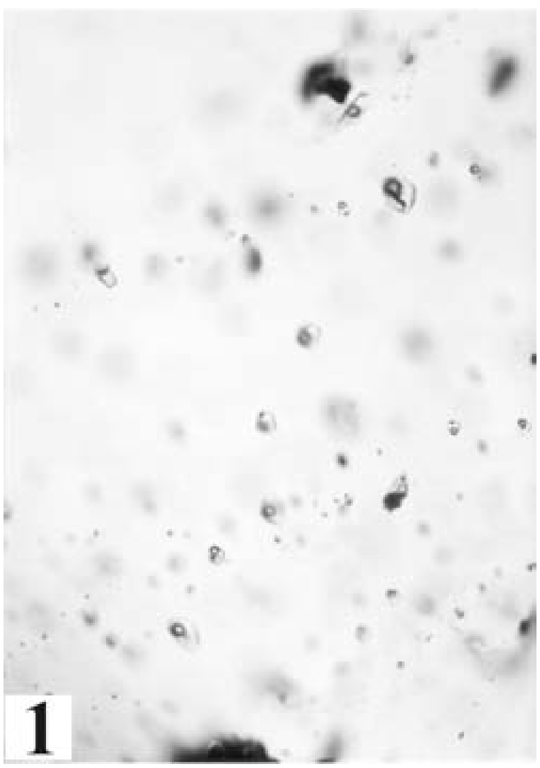

Photo 1. Fracture planes in a Mo-bearing quartz vein from the porphyry defined by secondary type III halite-bearing fluid inclusions, each containing a cubic-shaped, opaque daughter mineral. Sample GR01-60. Transmitted plane light. Long field of view is 0.64 mm.

phenocrysts, 271.5 to 472°C in veins from the porphyry, 213°C (one inclusion) from the mantos, and 189 to 277°C (2 inclusions) from the vein (Table 2D, Figure 3b).

Type IV: Low-Salinity, Vapour Dominated, CO_2-Bearing

Type IV inclusions are vapour-rich, and contain vapour + liquid phases at room temperature. However, CO_2 is detected as a minor, low-density component indicated by phase behaviour at and just below -56.6°C and/or by clathrate formation. Slight depression of the melting point of pure CO_2 (typically less than one degree, Table 2E) indicates trace amounts of CH_4 or N_2. Formation of clathrates (gas-hydrates) at temperatures between -0.5 and +7.9°C indicate that the liquid phase is a low-to-moderate salinity brine. Type IV inclusions are common in the porphyry, manto and No. 1 Zone vein samples. Trace amounts of CO_2 liquid were noted wetting the bubble walls in samples from the mantos and in one sample from the porphyry. This liquid homogenized to the vapour (CO_2 homogenization) a few degrees above clathrate melting (Table 2E).

Homogenization to the vapour phase is recorded at temperatures between 351.6 and 378.9°C for quartz phenocrysts, 325 to 552°C from veins in the porphyry, 309 to 385.4°C from quartz in the mantos, and 304 to 357°C (3 inclusions) from the No. 1 Zone vein (Table 2E).

TABLE 2C
MICROTHERMOMETRIC DATA FOR SALT-SATURATED TYPE III INCLUSIONS THAT HOMOGENIZE BY VAPOUR DISAPPEARANCE (TYPE IIIA)

FEATURE (FEATURE TYPE)	FI ORIGIN [1]	FIRST ICE MELT TEMP. range (N) °C (mean ± 1 sig.)	LAST ICE MELT TEMP. [2] range (N) °C (mean ± 1 sig.)	LIQUID-VAPOUR HOMOG. TEMP. (to liquid) range (N) °C (mean ± 1 sig.)	HALITE MELT TEMP. range (N) °C (mean ± 1 sig.)	COMMENT
porphyry						
phenocryst (monzonite)	I	-75 (1)	-33.9 (1)	337 to 488 (4) (393.9 ± 65.3)	285 to 338.8 (4) (314.4 ± 24.6)	opaques common
phenocryst (diorite)	I			302.6 (1)	224 (1)	
vein (qz+to+cp+py)	PS	-36 (1)	-22.5 (1)	417 to 635.1 (4) (481.9 ± 103.1)	168 to 299 (6) (212.4 ± 47.7)	
vein (qz+ks+py±cp±mg)	I	-46 (1)	-27.4 (1)	287 to 419.1 (7) (338 ± 45.0)	188 to 289.8 (7) (239.8 ± 41.3)	opaques common
vein (qz+mo+py±cp±bo)	I	-78 to -69 (4) (-72.3 ± 4.3)	-50.2 to -30 (4) (-39.4 ± 10.9)	300.4 to 526.6 (5) (376.9 ± 89.7)	146.8 to 336 (5) (216.2 ± 72.9)	opaques common
vein (qz+mo+py±cp±bo)	S	-45 to -40 (2) (-42.5 ± 3.5)	-37.6 to -23.4 (2) (-30.5 ± 10.0)	306.4 to 419.9 (7) (356.0 ± 39.4)	255.1 to 366.2 (7) (302.5 ± 38.6)	opaques common
vein (qz+se+py)						none noted
vein (qz+py)	I	-56 (1)	-26 (1)	403.8 (1)	337 (1)	opaque noted
skarn						none noted
manto						
massive sulphide (py + po + cp + qz)	P	-26 (1)	-21 (1)	266.8 (1)	183 (1)	
massive sulphide (py + po + cp + qz)	PS	-37 (1)	-21.7 (1)	271 (1)	210 (1)	
vein						
massive sulphide (py+as+ss+qz±sp)	P	-48 to -44 (2) (-46 ± 2.8)	-35 (1)	167.4 to 178 (2) (172.7 ± 7.5)	120 to 122 (2) (121 ± 1.4)	

1. P = primary, PS = pseudosecondary, S = secondary, I = intermediate
2. Last ice melting observed before final melting of salt-hydrate (presumed to be hydrohalite)

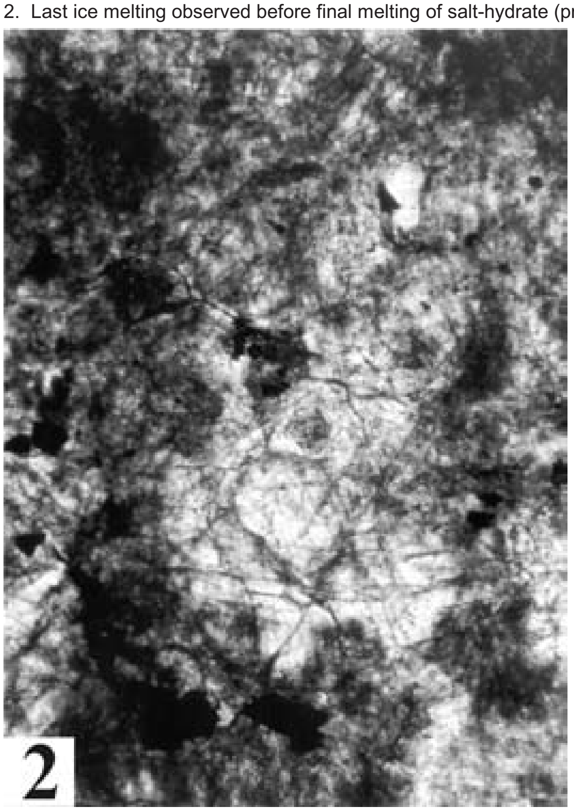

Photo 2. Distinct core zones defined by primary fluid inclusions in quartz crystal aggregates from the No. 1 veins, Takla Silver Mine. Sample GR01-105. Transmitted plane light. Long field of view is 2.63 mm.

TEMPORAL RELATIONSHIPS BETWEEN POPULATIONS

Definitive criteria for primary origin, such as the presence of inclusions in growth zones or geometric arrays of fluid inclusions oriented parallel to crystal faces, were observed in the following mineral assemblages:

- Subhedral ‘cloudy’ quartz crystal aggregates comprise the gangue (possibly secondary) to sulphide and sulphosalt minerals in the No. 1 Zone veins. Distinct core zones in many of the quartz crystals are characterized by abundant coexisting type I-II-III and type I-IV-III fluid inclusions (Photo 2). Leitch (2001) notes that core zones cut across crystal boundaries in sample GR01-26 from the No. 1 Zone veins. He suggests that original larger, zoned crystals up to 4mm across may have been recrystallized. Some of the core zone type II and IV fluid inclusions exhibit final homogenization to the liquid phase and may have formed at near-critical conditions.
- Subhedral to euhedral quartz occurs interstitial to massive pyrrhotite, pyrite and chalcopyrite in the manto samples. The quartz may be secondary (formed after the

TABLE 2D
MICROTHERMOMETRIC DATA FOR SALT-SATURATED TYPE III INCLUSIONS THAT HOMOGENIZE BY HALITE DISSOLUTION (TYPE IIIB)

FEATURE (FEATURE TYPE)	FI ORIGIN [1]	FIRST ICE MELT TEMP. range (N) °C (mean ± 1 sig.)	LAST ICE MELT TEMP. [2] range (N) °C (mean ± 1 sig.)	LIQUID-VAPOUR HOMOG. TEMP. (to liquid) range (N) °C (mean ± 1 sig.)	HALITE MELT TEMP. range (N) °C (mean ± 1 sig.)	COMMENT
porphyry						
phenocryst (monzonite)	I			258 to 301 (3) (285 ± 23.5)	329 to 339 (3) (332.7 ± 5.5)	opaques common
phenocryst (diorite)	I		-27.3 (1)	205 to 313 (6) (245.6 ± 39)	335.4 to 441.2 (6) (373.1 ± 44.9)	
vein (qz+to+cp+py)	PS			290.6 to 318 (3) (305.5 ± 13.9)	370.1 to 472 (3) (407 ± 56.4)	opaques common
vein (qz+ks+py±cp±mg)	I			234.9 to 281.5 (4) (256.3 ± 20.4)	271.5 to 364.7 (4) (332.7 ± 42.1)	
vein (qz+mo+py±cp±bo)	I	-74.5 (1)	-49 (1)	240.7 to 324 (4) (277 ± 44)	319.6 to 336 (4) (329.8 ± 7.9)	opaques common
vein (qz+mo+py±cp±bo)	S			231 to 335.8 (3) (298.9 ± 58.9)	308 to 344.8 (3) (322.3 ± 19.7)	
vein (qz+se+py)						none noted
vein (qz+py)	I			337 (1)	349 (1)	
vein (qz+py)	S			318 (1)	336 (1)	
skarn						none noted
manto						
massive sulphide (py + po + cp + qz)	PS			204 (1)	213 (1)	
vein						
massive sulphide (py+as+ss+qz±sp)	P			135 to 183.5 (2) (159.3 ± 34.3)	189 to 277 (2) (233 ± 62.2)	

1. P = primary, PS = pseudosecondary, S = secondary, I = intermediate
2. Last ice melting observed before final melting of salt-hydrate (presumed to be hydrohalite)

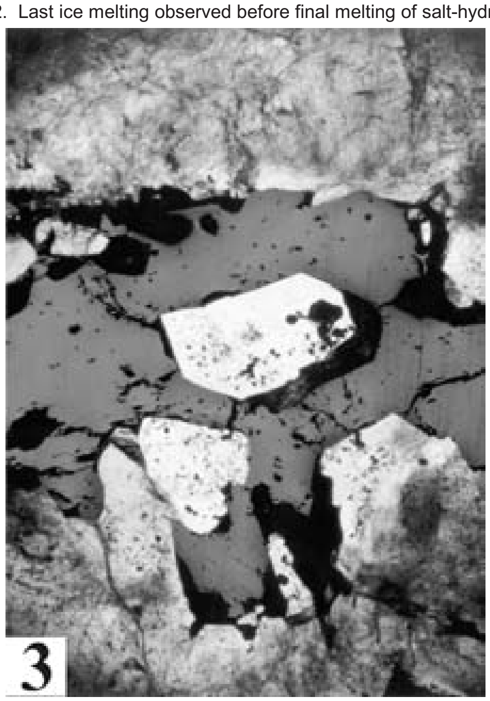

Photo 3. Geometric arrays of primary fluid inclusions in subhedral to anhedral quartz (light minerals) occurring interstitial to massive pyrrhotite (grey minerals) in the manto (No. 4B Zone). Sample GR01-48. Transmitted and reflected light. Long field of view is 2.63 mm.

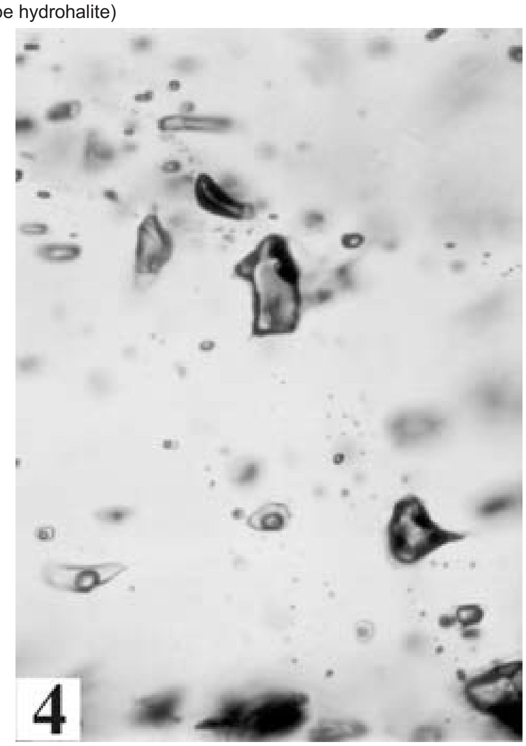

Photo 4. Coexisting liquid-rich type I and vapour-rich type IV primary fluid inclusions in quartz from No. 4B Zone mantos. Sample GR01-47A. Transmitted plane light. Long field of view is 160 µm.

TABLE 2E
MICROTHERMOMETRIC DATA FOR CARBONIC, VAPOUR-RICH TYPE IV INCLUSIONS

FEATURE (FEATURE TYPE)	FI ORIGIN [1]	CO_2 MELT TEMP. range (N) °C (mean ± 1 sig.)	LAST ICE MELT TEMP. range (N) °C (mean ± 1 sig.)	CLATHRATE MELT TEMP. (to liquid) range (N) °C (mean ± 1 sig.)	CO_2 HOMOG. TEMP. range (N) °C (mean ± 1 sig.)	TO PHASE	FINAL HOMOG. TEMP. (to vapour) range (N) °C (mean ± 1 sig.)	COMMENT
porphyry								
phenocryst (monzonite)	I	-56.8 to -56.6 (3) (-56.7 ± 0.1)	-9 to -3.5 (2) (6.3 ± 3.9)	-0.5 to 5.8 (3) (3.5 ± 3.5)			351.6 to 378.9 (2) (365.3 ± 19.3)	
phenocryst (diorite)								none noted
vein (qz+to+cp+py)	PS	-59.9 (1)	-6.6 (1)	6.2 (1)			325 (1)	
vein (qz+ks+py±cp±mg)	I	-58.9 to -56.6 (6) (-57.2 ± 0.9)	-15 to -2.2 (5) (-10.5 ± 5)	4.7 (1)			366 to 494 (6) (448.1 ± 49.4)	
vein (qz+mo+py±cp±bo)	I	-56.9 to -56.6 (5) (-56.7 ± 0.1)	-10.8 to -0.9 (4) (-3.6 ± 3)	-3.1 to 5.1 (4) (1.6 ± 3.1)			347 to 412 (6) (368.3 ± 26.5)	
vein (qz+mo+py±cp±bo)	S	-56.9 (1)	-10.8 (1)	-3.1 (1)			347 (1)	
vein (qz+se+py)	S	-57.4 (1)	-5.2 to -4.4 (2) (-4.8 ± 0.6)	-0.2 to 1.3 (2) (0.5 ± 1.1)			367.1 to 377 (2) (372 ± 7)	
vein (qz+py)	PS	-57.1 (1)					552 (1)	
skarn								none noted
manto								
massive sulphide (py+po+cp+qz)	P	-58.3 to -57.2 (3) (-57.6 ± 0.6)	1.1 (1)	2.3 to 7.9 (3) (5.1 ± 2.8)	4 to 11.4 (3) (8.5 ± 3.9)	vapour	309 to 385.4 (3) (353.5 ±39.7)	
massive sulphide (py+po+cp+qz)	PS	-57.3 to -58.3 (3) (-57.8 ± 0.5)		0.2 to 6 (3) (2.4 ± 3.1)	3.1 to 10.6 (3) (7.4 ± 3.9)	vapour	315 to 354 (3) (329.7 ± 21.2)	
vein								
massive sulphide (py+as+ss+qz±sp)	P	-56.6 (2)	-4.1 to -2.3 (2) (-3.2 ± 1.3)	3.4 to 7.6 (3) (4.9 ± 2.3)			304 to 328 (2) (316 ± 17)	
massive sulphide (py+as+ss+qz±sp)	S	-56.8 (1)		3.6 (1)			357 (1)	

1. P = primary, PS = pseudosecondary, S = secondary, I = intermediate

Photo 5. Growth zones in skarn garnet. Zones are defined by large, irregular-shaped type I fluid inclusions. Sample GR01-31. Transmitted plane light. Long field of view is 2.63 mm.

sulphide minerals). It contains geometric arrays of fluid inclusions oriented parallel to crystal faces (Photo 3). Co-existing types I and IV fluid inclusions characterize the fluid inclusion assemblages in the arrays (Photo 4).

- Zoned garnet crystals in the skarn contain large, irregular-shaped Type I fluid inclusions that define growth zones (Photo 5). The very large, structurally-weak inclusions (~100 microns) have decrepitated (even when 250 micron thick sections were used for observation. The large size, irregular shape and mostly inconsistent liquid-to-vapour ratios of these primary inclusions suggest that they necked down and underwent post-entrapment change in mass and/or volume. Homogenization temperatures from these primary inclusions are unreliable but the salinity values are believed to be valid.
- Primary growth bands were observed in quartz from a 6 mm thick molybdenite-pyrite-bearing quartz veinlet in the porphyry. Fluid inclusions within the growth bands could not be distinguished, as they are less than 1 micron in maximum size. No other evidence of primary origin was noted in the porphyry.

Pseudosecondary and secondary fluid inclusions occurring along fracture planes were observed in samples from the skarn, mantos and No. 1 Zone veins**.** Definitive fluid inclusion fracture planes were observed in a few quartz veins from the porphyry. The majority of fluid inclusions in quartz from porphyry veins and phenocrysts occur as 'clusters', or are 'isolated'. These inclusions have been assigned an indeterminate origin.

Temporal relationships between secondary and indeterminate populations are subtle and will require observation of additional samples to resolve. However, the following observations are noted:

(a)Type II, III and IV inclusions are dominant in the porphyry (type II less abundant) and coexist in both quartz phenocrysts and veins. Fracture planes with coexisting type IIIA and IV fluid inclusions (Photo 6) are common. These fractures crosscut fracture planes with only type IIIB fluid inclusions in sample GR01-106. Type II inclusions can comprise isolated fracture planes (photo 7). Less commonly, Type II or IV inclusions coexist with Type I inclusions in "clusters" of indeterminate origin.

(b) In the skarn garnets, secondary type I fluid inclusions are much smaller than the primary and pseudosecondary inclusions and have smooth to negative-crystal shapes. Fluid inclusion assemblages with variable liquid-to-vapour ratios indicate necking down, consequently, the homogenization temperatures were not used in this study.

(c) In the mantos, pseudosecondary type I and lesser type IV fluid inclusions coexist (Photo 4). Where rare type III fluid inclusions were noted, they sometimes coexist with type I inclusions.

(d) Secondary type I and type II or IV fluid inclusions coexist in the No. 1 Zone veins, but secondary type III inclusions have not been noted.

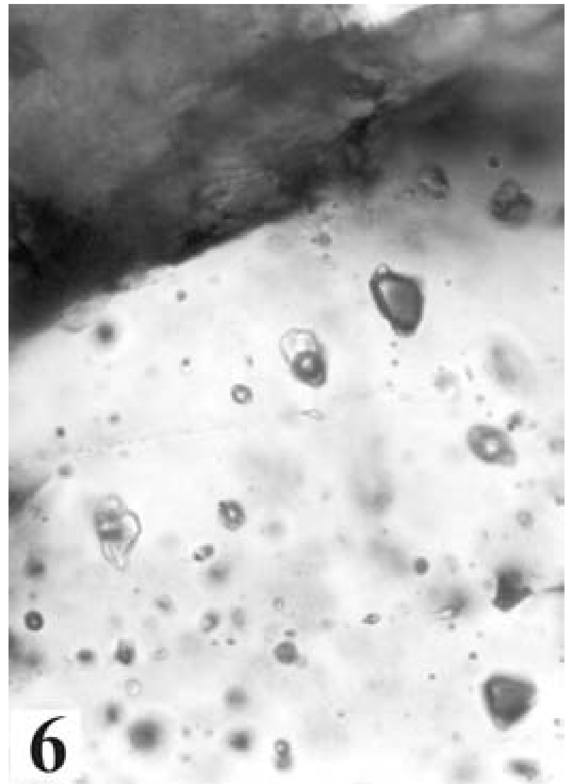

Photo 6. Coexisting halite-bearing type III and vapour-rich type IV fluid inclusions of indeterminate origin in quartz from a Mo-bearing quartz porphyry vein in the Glover Stock. Sample GR01-87. Transmitted plane light. Long field of view is 160 µm.

FLUID INCLUSION COMPOSITIONS

Petrographic and microthermometric data of fluid inclusions from the porphyry, skarn, mantos and No. 1 Zone veins indicate four fluid inclusion populations which can be modeled as varieties of two types of fluids: H_2O-NaCl-$CaCl_2$ (±$FeCl_3$, $MgCl_2$) and H_2O-CO_2-NaCl-CH_4.

H_2O-NaCl-$CaCl_2$ (±$FeCl_3$, $MgCl_2$) Fluids

The dominant salt components in the vast majority of naturally-occurring fluids are NaCl, $CaCl_2$, KCl, $MgCl_2$ and $FeCl_2$ (Shepherd *et al*, 1985, p. 101). At Lustdust, the ternary H_2O-NaCl-$CaCl_2$ system is used to model type I, II and III fluid inclusions for a number of reasons. First, the eutectic (first melting) temperatures for these inclusions are typically < -35 to 40°C (Tables 2A through 2D), which indicates the presence of possible Ca-, Mg- or Fe- chlorides. In fact, first melting temperatures as low as -73°C are reported in synthetic NaCl-$CaCl_2$-H_2O inclusions (Vanko *et al.,* 1988, p. 2454) although temperatures this low are usually attributed to additional components. Second, there is little evidence for KCl (no sylvite daughter minerals and first melting < -22.9°C). Third, KCl and $MgCl_2$ are relatively minor components of most fluids (Shepherd *et al*., 1985) and $FeCl_2$ is not a common chloride species (Goldstein and Reynolds, 1994, Table 7.2 modified from Crawford, 1981). Finally, the physical properties of $CaCl_2$ and $MgCl_2$ hy-

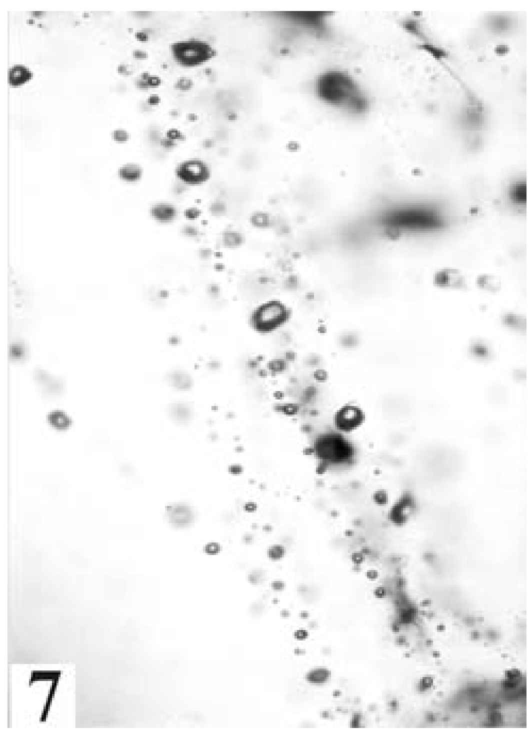

Photo 7. Fracture planes in quartz from a Mo-bearing quartz porphyry vein in the Glover Stock. Planes are defined by secondary vapour-rich type II fluid inclusions only. Sample GR01-60. Transmitted plane light. Long field of view is 0.64 mm.

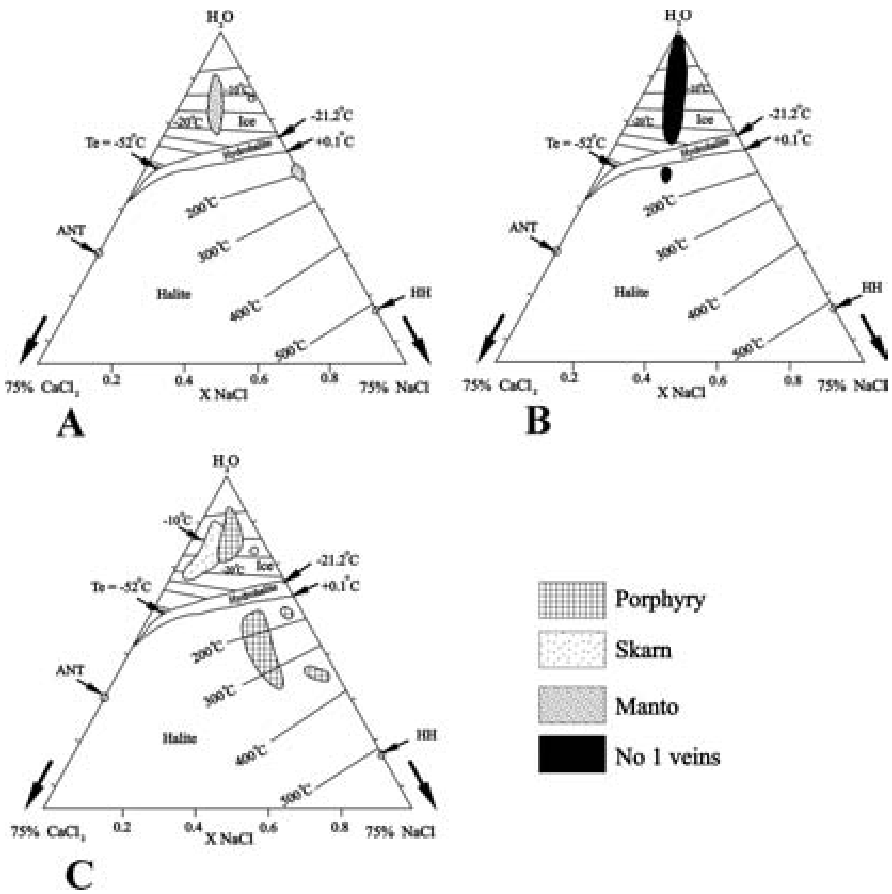

Figure 4. Phase diagrams showing liquidus relations in the ternary system NaCl-$CaCl_2$-H_2O with compositions in weight percent (from Oakes *et al.* 1990 and Vanko *et al.* 1988). The compositional ranges of fluid inclusions in (A) quartz in massive sulphide from the mantos, (B) quartz from the massive sulphide veins at the Takla Silver Mine, (C) porphyry quartz veins and garnet skarn. HH = hydrohalite (NaCl.$2H_2O$), ANT= antarcticite ($CaCl_2$.$6H_2O$).

drates are similar and most aqueous fluids are well represented by the ternary H_2O-NaCl-$CaCl_2$ system (Shepherd *et al.,* 1985).

Assuming an H_2O-NaCl-$CaCl_2$ model system, hydrohalite melting, in the presence of ice, liquid and vapour, is used to estimate the weight fraction of NaCl (XNaCl) for type I and type II inclusions (method of Oakes *et al.,* 1990, Figure 4). Ice melting, in the presence of hydrohalite, liquid and vapour is used to estimate XNaCl for type III inclusions (method of Vanko *et al*., 1988, Figure 4). In type III inclusions where halite never transformed to hydrohalite on cooling, measurements of ice melting in the presence of liquid, vapour and metastable halite were also used to crudely estimate the bulk composition.

Distinct ranges of XNaCl are apparent in the Lustdust porphyry, skarn, manto and vein fluids (Figure 4). Porphyry, skarn and manto fluids record two ranges of XNaCl corresponding evidence for both NaCl-dominant fluids (> 0.8 XNaCl) and mixed NaCl-$CaCl_2$ fluids (< 0.7 XNaCl, Table 3). The difference between the various ranges is not attributable to inclusion origin or type.

Final ice melting is used to estimate the total salinity of type I and II inclusions (method of Oakes *et al.,* op. cit, Figure 4). Ice melting and halite dissolution temperatures are used to determine the bulk composition of type III inclusions (method of Vanko, 1988). The total salinity (weight % salts) ranges in weight percent salts for mixed NaCl-$CaCl_2$ fluids and the total salinity ranges in weight percent salts for NaCl-dominant fluids are in Table 3. In general, the NaCl-dominant fluids have higher salinities than most of the mixed NaCl-$CaCl_2$ fluids.

TABLE 3
FLUID INCLUSION COMPOSITIONS, LUSTDUST PROSPECT

	H2O-NaCl-CaCl2 (± FeCl3, MgCl2) FLUIDS				H2O-CO2-NaCl-CH4 FLUIDS				
	mixed NaCl-CaCl2 FLUIDS		NaCl-dominant FLUIDS		aqueous phase	bulk fluid			
DEPOSIT TYPE	**X NaCl**	**wt. % salts**	**X NaCl**	**wt. % salts**	**eq. wt. % NaCl**	**X NaCl**	**XH2O**	**XCO2**	**XCH4**
igneous phenocrysts	0.4, 0.65*	13, 40*			7.7 to 16.1				
porphyry veins	0.4 to 0.7	6 to 51	0.8 to 1	28 to 44	7.0 to 18.4				
prograde skarn	0.1 to 0.5	9 to 22							
retrograde skarn			0.8	17					
manto	0.3 to 0.4	15 to 24	0.8 to 1	23 to 30	4.1 to 14.3	0.01 to 0.05	0.73 to 0.89	0.06 to 0.21	0 to 0.03
Takla Silver veins	0.3 to 0.6	2 to 31			2.1 to 4.6				

* Based on 2 samples, points not plotted on Figure 4.

H_2O-CO_2-NaCl-CH_4 Fluids

The identification of CO_2 in type IV fluids at Lustdust is based upon clathrate melting between -0.5 and +7.9ºC, less commonly by phase behaviour at or just below -56.6ºC (pure CO_2 melting point), and rarely, in fluid inclusions from the mantos, by wetting of bubble walls by tiny amounts of CO_2 liquid. Because liquid CO_2 was observed in only trace amounts, the CO2 is presumed to exist as a gas in the inclusion bubble and as a minor aqueous component.

Salinity estimates for type IV inclusions (eq. wt. % NaCl) based on clathrate melting were calculated using the H_2O-CO_2-NaCl-CH_4 system (Jacobs and Kerrick, 1981; Brown and Hagemann, 1994).

Salinities from type IV fluid inclusions in the mantos are much lower than those recorded for H_2O-NaCl-$CaCl_2$ (±$FeCl_3$, $MgCl_2$) fluids (Table 3). CO_2 homogenization to vapour, indicating a low-density CO_2 phase, was extremely difficult to observe and only observed in samples from the mantos; it seemed to occur a few degrees above clathrate melting. Bulk compositions of type IV fluid inclusions from the mantos are included in Table 3.

ESTIMATED TRAPPING CONDITIONS

A variety of methods were used to estimate *minimum* trapping pressures of the fluid inclusions in the porphyry, skarn, mantos and No. 1 Zone veins. These methods involve the construction of isochores using fluid inclusion microthermometric data for the H_2O-NaCl and H_2O-CO_2-NaCl-CH_4 systems. The H_2O-NaCl model system is used to construct isochores for the H_2O-NaCl-$CaCl_2$ (±$FeCl_3$, $MgCl_2$) fluids because the pressure-temperature-compositional properties of the latter more complex system are unknown. This substitution is reasonable based on work by Potter and Cline (1978). Their work demonstrates that the volumetric properties of many Na-K-Ca-Mg-Br-SO_4 brines are within ±1% of those of an NaCl solution having the same depression of freezing point. Thus, the isochores of aqueous liquid-vapour fluid inclusions in many multi-component systems will be the same as those for H_2O-NaCl provided that the comparison is on the basis of NaCl equivalent obtained by freezing point depression. However, the actual salinities will be different and the equivalent weight % NaCl will not equal total weight % salts.

TABLE 4
SUMMARY OF PRESSURE ESTIMATES AND TRAPPING CONDITIONS

FEATURE (FEATURE TYPE)	TRAPPING PRESSURE BASED ON CONDITIONS OF FLUID IMMISCIBILITY (bars)		MINIMUM TRAPPING PRESSURE BASED ON		DEPTH ESTIMATE ASSUMING	
	Type IIIA or Type I[1]	Type IV[2]	HOMOGENIZATION BY HALITE DISSOLUTION (bars)[3]	TRAPPING AT NEAR-CRITICAL CONDITIONS (bars)	LITHOSTATIC PRESSURE REGIME	HYDROSTATIC PRESSURE REGIME[3]
porphyry						
phenocryst (monzonite)	150				570 metres?	1.5 km?
		~500 est.			~1.9 km	~5.1 km
			880		3.3 km	9.0 km
phenocryst (diorite)			880		3.3 km	9.0 km
vein (qz+to+cp+py)			1800*		6.8 km*	18 km*
vein (qz+ks+py±cp±mg)			950		3.6 km	9.7 km
vein (qz+mo+py±cp±bo)	150				570 metres?	1.5 km?
		450 to 500 est.			~1.7 to1.9 km	~4.6 to 5.1 km
			230		870 metres	2.3 km
vein (qz+se+py)	120				450 metres	1.2 km
		~450 to 500 est.			~1.7 to 1.9 km	~4.6 to 5.1 km
vein (qz+py)			260		980 metres	2.7 km
manto						
massive sulphide						
(py+po+cp+qz)		320			1.2 km	3.3 km
			170		640 metres	1.7 km
vein						
massive sulphide						
(py+as+ss+qz±sp)				300 to 400	1.1 to 1.5 km	3.1 to 4.1 km
			1700*		6.4 km*	17 km*

1. Pressure estimates based on isochores and final homogenization to liquid phase for type IIIB inclusions
2. Minimum pressure estimates based on estimated composition of 2 mol % CO_2 (minimum), 10 wt. % NaCl and final homogenization to vapour phase for type IV inclusions
3. * = Minimum pressure and depth estimates seem unreasonably high (*see* discussion and summary)

Evidence for immiscible entrapment (coexisting NaCl-saturated inclusions or under-saturated inclusions and vapour-rich inclusions which homogenize at the same temperature) is used to calculate estimated *actual* trapping pressures where possible. Evidence for entrapment of vapour-rich fluid inclusions under near critical conditions is also used to estimate trapping pressures. Geologic estimates of inclusion trapping pressures based on paleodepth or the use of mineral geobarometers have not been calculated.

Pressure estimates and depths of emplacement of fluid inclusions calculated using the following methods are summarized in Table 4.

Evidence for and Trapping Conditions of Phase Separation (Immiscibility)

Evidence for immiscible entrapment is abundant in samples from the porphyry. It was observed in fluid inclusion assemblages of indeterminate (possibly primary) origin from quartz phenocrysts in the monzonite and from the following vein types in the porphyry: quartz+potassium feldspar+pyrite±chalcopyrite±magnetite, quartz + molybdenite+pyrite±chalcopyrite±bornite and quartz+sericite+pyrite. Immiscible entrapment was also observed in planes of secondary inclusions from the quartz + molybdenite + pyrite±chalcopyrite±bornite veins. Outside the porphyry, immiscible entrapment was only observed in quartz from one sample of the mantos. Coexisting liquid and vapour-rich inclusions do occur in quartz in the No. 1 Zone veins but they do not homogenize at the same temperature.

Quartz Phenocrysts in the Monzonite Porphyry

Coexisting type IIIA and type IV fluid inclusions occur as isolated clusters in quartz phenocrysts in the monzonite. Homogenization temperatures, type IIIA to the liquid and type IV to the vapour, for the fluid inclusion assemblages are both at 334±10°C and 377±3°C for samples GR01-62 and GR01-60 respectively. Isochores have been calculated for type IIIA inclusions using equations from Bodnar and Vityk (1994) and the computer program MacFlincor (Brown and Hagemann, 1994). Pressures of trapping based on final homogenization by disappearance of the vapour bubble are approximately 100 bars for sample GR01-62 and 150 bars for sample GR01-60. It is not possible to calculate isochores for the type IV fluid inclusions as CO_2 homogenization was not observed in these inclusions precluding density estimates. Estimates of salinity of the liquid phase for type IV inclusions are 7.7 and 8.5 equivalent weight percent NaCl using clathrate melting temperatures.

The observed melting behaviour of type IV inclusions suggests they contain a low-density, gas-rich fluid, which is probably conjugate to the briney type III inclusions (based on very similar homogenization temperatures for both types of fluids). Phase separation of type III and IV fluids is inferred at maximum pressures of 150 bars and 377°C (using Type IIIA isochore construction and final homogenization data, Table 4). Estimated depths of emplacement based on this pressure estimate are 570 metres under lithostatic load or 1.5 km under hydrostatic load, but neither estimate seems realistic in comparison with the deeper vertical positions of magmatic (early) fluid inclusions in many porphyry copper deposits (Bodnar, 1995, figure 3). If the presence of perhaps as little as 2 mol % CO_2 in combination with a 10 wt % NaCl aqueous fluid is considered for type IV inclusions from quartz phenocrysts in the monzonite, the vapour pressure at 377°C can be estimated at 500 bars (using figure 9 of Bowers and Helgeson, 1983) which corresponds to more realistic trapping depths of 1.9 km under lithostatic load (Table 4).

Porphyry Veins Associated with Potassium Silicate Alteration±Chalcopyrite

In sample GR01-85 coexisting types I and II fluid inclusions of indeterminate origin homogenize to both liquid and vapour phases at 491±1°C (fluid inclusion assemblage 3-1). Unfortunately, the salinity (eq. wt. % NaCl) for inclusions in this assemblage cannot be calculated since inclusions exhibit ice melting above 0°C. Similar type I inclusions in another assemblage (1-3) from the same sample yield salinities of ~7 eq. wt. % NaCl, however, homogenization temperatures for this assemblage were not recorded and the assemblage did not provide evidence for immiscibility.

Porphyry Veins Associated with Molybdenite ± Chalcopyrite Mineralization

In sample GR01-60, types III and IV fluid inclusions coexist in a fluid inclusion assemblage of indeterminate origin. Homogenization temperatures to both liquid (type IIIA) and vapour (type IV) are 366±11 °C. Isochores have been calculated for type IIIA inclusions using equations from Bodnar and Vityk (1994) and the computer program MacFlincor (Brown and Hagemann, 1994). Pressures of trapping based on final homogenization by disappearance of the vapour bubble in type IIIA inclusions are approximately 150 bars. Absence of observed CO_2 homogenization temperatures precludes density estimates and isochore construction. Using the clathrate melting temperature, the salinity of the liquid phase for type IV inclusions is 8.8 equivalent weight percent NaCl.

In sample GR01-60, types III and IV fluid inclusions and separate type IIIA and II fluid inclusions coexist in fluid inclusion assemblages of secondary origin (FIA's 3-1 and 2-1, respectively). Homogenization temperatures for assemblages 3-1 and 2-1 are 351.5±6.4°C and 370.6±5.4°C respectively. Isochores have been calculated for type IIIA inclusions using equations from Bodnar and Vityk (1994) and the computer program MacFlincor (Brown and Hagemann, 1994). Pressures of trapping based on final homogenization by disappearance of the vapour bubble for type IIIA inclusions are approximately 120 bars and 150 bars for assemblages 3-1 and 2-1 respectively. Absence of observed CO_2 homogenization temperatures for assemblage 3-1 precludes density estimates and isochore construction for type IV inclusions. Using the clathrate melting temperature, the salinity of the liquid phase for type IV inclusions in assemblage 3-1 is 18.4 equivalent weight percent NaCl. The salinity (eq. wt. % NaCl) for type II inclusions in assemblage 2-1 cannot be calculated since inclusions exhibit ice melting above 0°C.

The observed melting behaviour of type IV inclusions of indeterminate (possibly primary) and secondary origin suggests they contain a low-density, gas-rich fluid which is probably conjugate to the briney type III inclusions (based on very similar homogenization temperatures for both types of fluids). Phase separation of type III and IV fluids is inferred at maximum pressures of 150 bars and temperatures of 366°C for inclusions of indeterminate origin and at slightly lower pressures of 120 bars and temperatures of 351.5°C for inclusions of secondary origin. Estimated depths of emplacement for indeterminate and secondary fluids are 570 metres and 450 metres under lithostatic load or 1.5 km and 1.2 km under hydrostatic load (Table 4). If the presence of as little as 2 mol % CO2 in combination with a 10 wt % NaCl or 20 wt. % NaCl aqueous fluid is considered for type IV inclusions from molybdenite-bearing veins in the porphyry, the vapour pressure at 351 to 366°C is ~ 450 to 500 bars (using figure 9 of Bowers and Helgeson, 1983) which corresponds to trapping depths of 1.7 to 1.9 km under lithostatic load (Table 4).

Phase separation of type II and III fluids of secondary origin is inferred at maximum pressures of 150 bars and 370°C. Estimated depths of emplacement for these fluids are 570 metres under lithostatic load or 1.5 km under hydrostatic load. There is no evidence for CO_2 in these secondary fluid inclusion assemblages.

Porphyry Veins Assocated with Sericite Alteration

In sample GR01-62, types I and IV fluid inclusions coexist in a fluid inclusion assemblage of indeterminate origin. Homogenization temperatures to both liquid (type I) and vapour (type IV) are 360.6±9.3°C. Isochores have been calculated for type I inclusions using equations from Bodnar and Vityk (1994) and the computer program MacFlincor (Brown and Hagemann, 1994). Pressures of trapping based on final homogenization by disappearance of the vapour bubble in type I inclusions are approximately 120 bars. Absence of observed CO_2 homogenization temperatures for type IV inclusions precludes density estimates and isochore construction. Using the clathrate melting temperature, the salinity of the liquid phase for type IV inclusions is 14.1 equivalent weight percent NaCl.

The observed melting behaviour of type IV inclusions of indeterminate (possibly primary) and secondary origin suggests that they contain a low-density, gas-rich fluid which is probably conjugate to the low salinity (9.2 eq. wt. % NaCl) type I inclusions (based on very similar homogenization temperatures for both types of fluids). Phase separation of types I and IV fluids is inferred at maximum pressures of 120 bars and temperatures of 360°C for these inclusions of indeterminate origin. Estimated depths of emplacement are 450 metres under lithostatic load or 1.2 km under hydrostatic load (Table 4). If the presence of as little as 2 mol % CO_2 in combination with a 10 wt % NaCl or 20 wt. % NaCl aqueous fluid is considered for type IV inclusions from molybdenite-bearing veins in the porphyry, the vapour pressure at 360°C is ~ 450 to 500 bars (using figure 9 of Bowers and Helgeson, 1983) which corresponds to trapping depths of 1.7 to 1.9 km under lithostatic load (Table 4).

Massive Sulphide from the Mantos

In sample GR01-47A, types I and IV fluid inclusions coexist in fluid inclusion assemblage 3-1 of pseudosecondary origin. Homogenization temperatures to both liquid (type I) and vapour (type IV) are 352.5±1.5°C. Isochores have been calculated for all type IV inclusions from the mantos using equations from Jacobs and Kerrick (1981) and the computer program MacFlincor (Brown and Hagemann, 1994). The minimum pressure of trapping based on final homogenization by disappearance of the liquid rim (*i.e.*. to the vapour) from assemblage GR01-47A 3-1 is approximately 320 bars (Figure 5). The minimum pressure range for all measured type IV inclusions in sample GR01-47A is from 304 to 386 bars (Figure 5); type IV inclusions from sample GR01-48 have minimum pressure estimates of between 256 and 460 bars (Figure 5). The salinity (eq. wt. % NaCl) for type I inclusions in FIA 3-1 cannot be calculated since inclusions exhibit ice melting below the NaCl-H_2O eutectic of -20.8°C. This implies a high salinity for the type I inclusions and the existence of halite as a daughter mineral. No solid daughter minerals were observed in fluid inclusion assemblage 3-1.

Phase separation of type I and IV fluids is inferred at minimum pressures of 320 bars and temperatures of approximately 350°C for inclusions in FIA 3-1 from sample GR01-47A. Estimated depths of emplacement are 1.2 km under lithostatic load or 3.3 km under hydrostatic load (Table 4).

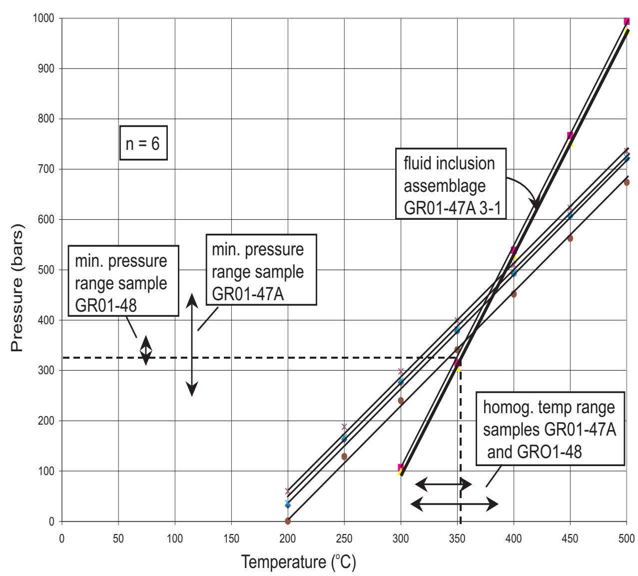

Figure 5. Isochores calculated using the H_2O-CO_2-NaCl-CH_4 system (Jacobs and Kerrick, 1981) and the computer program MacFlincor (Brown and Hagemann, 1995) for type IV inclusions in quartz associated with massive sulphide in the mantos at the Lustdust property. The estimated trapping pressure of coexisting vapour-rich type IV and liquid-rich type I inclusions in sample GR01-47A (fluid inclusion assemblage 3-1) at 352°C is approximately 320 bars (dashed lines). Minimum pressure and homogenization temperature (homog. temp) ranges for samples GR01-47A and GR01-48 are indicated.

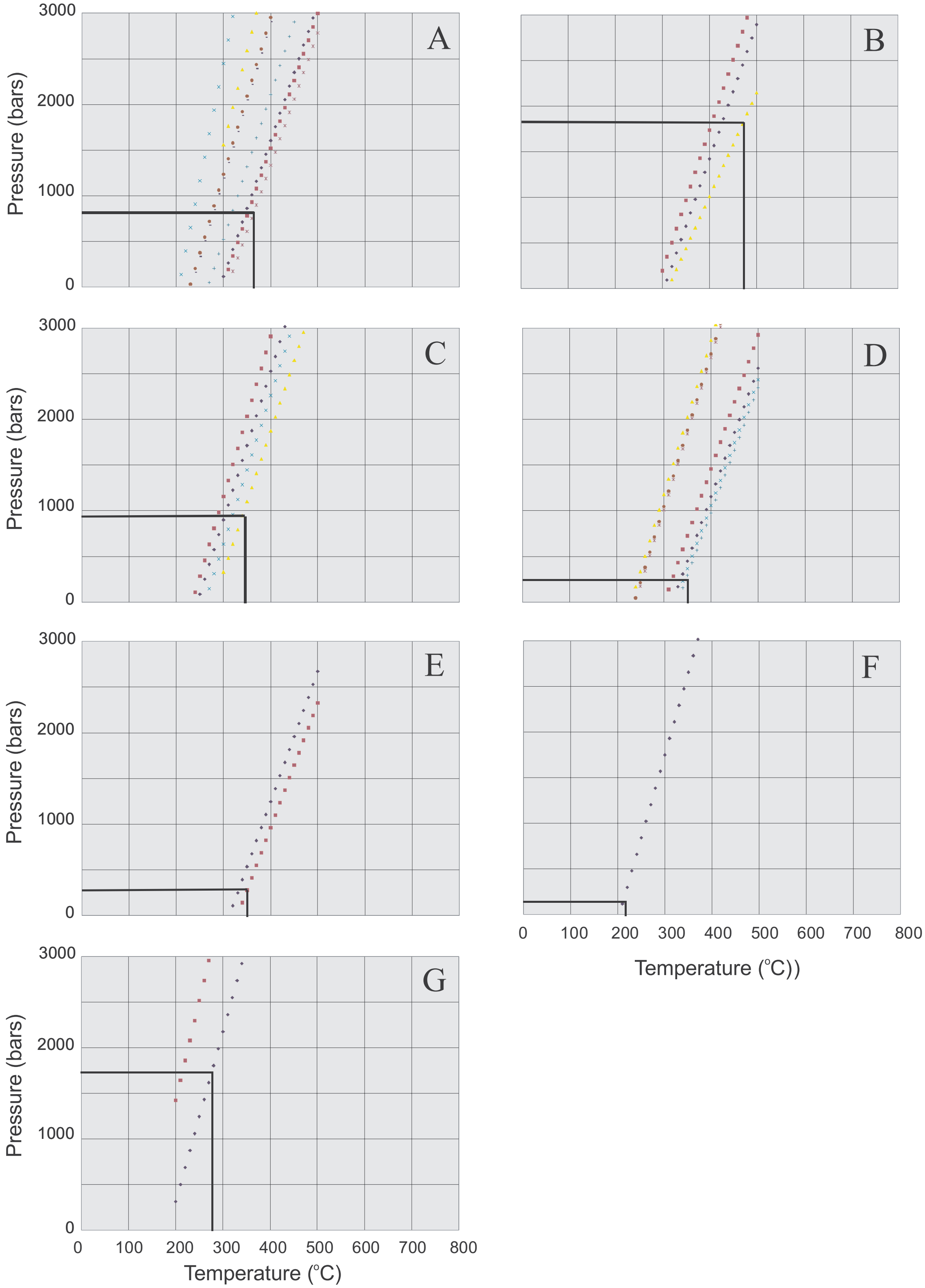

Figure 6. Isochore plots of minimum trapping conditions for type IIIB inclusions. (A) quartz phenocrysts, (B) quartz-tourmaline-chalcopyrite-pyrite vein in porphyry, (C) quartz-potassium feldspar-pyrite veins in the porphyry, (D) quartz-molybdenite-pyrite veins in the porphyry, (E) late quartz-pyrite vein, (F) quartz associated with massive sulphide in the mantos, (G) quartz associated with massive sulphide veins from Takla Silver Mine. Note the diagrams share common x and y axes. Lines defined by symbols are isochores; each line represents data from a single fluid inclusion assemblage. The fine, solid, vertical lines represent the final homogenization temperature (by halite dissolution) for the isochore that gives the minimum trapping condition for each diagram. The fine, solid, horizontal lines represent the corresponding pressure at the final halite dissolution temperature.

Trapping Conditions Based on Homogenization by Halite Dissolution

The relationship between halite dissolution temperatures and liquid-vapour homogenization temperatures for type III inclusions in quartz phenocrysts, veins and massive sulphide mineralization at Lustdust is illustrated in Figure 3. The diagonal line divides inclusions into type IIIA which exhibit final homogenization by vapour-bubble disappearance (lower right of Figure 3) and type IIIB which homogenize by halite dissolution (upper left of Figure 3).

Immiscible entrapment of dense type IIIB brines is precluded by phase-equilibria constraints. In the absence of evidence for fluid immiscibility, isochores of type IIIB inclusions provide better minimum trapping temperature estimates than other types of inclusions trapped in the one-phase field (Shepherd *et al*., 1985). Disappearance of the vapour bubble in type IIIB inclusions at Lustdust generally occurs approximately 40 to 150°C lower than halite dissolution (Figure 3), which indicates moderate to high minimum trapping pressures.

Minimum trapping conditions for type IIIB inclusions in quartz phenocrysts, in veins in the porphyry, in massive sulphide mineralization from the mantos and in the No. 1 Zone vein are illustrated using isochore plots (Figure 6A to G). Minimum trapping pressures for each deposit and feature type are as follows: 880 bars (quartz phenocrysts, Figure 6A), 1.8 kb (quartz-tourmaline-chalcopyrite-pyrite veins, Figure 6B), 950 bars (quartz-potassium feldspar-pyrite veins, Figure 6C), 230 bars (quartz- molybdenite-pyrite veins, Figure 6D), 260 bars (late quartz + pyrite veins, Figure 6E), 170 bars (massive sulphide from mantos, Figure 6F), and 1.7 kb (No. 1 Zone vein, Figure 6G). Estimated depths of entrapment assuming lithostatic and hydrostatic loads are in Table 4.

Trapping Conditions Based on Critical Behaviour of Vapour-Rich Inclusions

Vapour-rich inclusions from the No. 1 Zone veins homogenize to both vapour (type II) and liquid (type IIQ) within an apparently narrow 20°C temperature range from 354 to 373°C. Type IIQ inclusions display unusual homogenization behaviour as the homogenized vapour bubble re-appears in virtually the same location as it disappears. True 'liquid-rich' inclusions typically show a period of a few degrees of cooling before the vapour bubble pops back in a different location (Cline and Vanko, 1995). The vapour bubble of type II inclusions from the outer veins does not appear to "grow" until it exhibits rapid expansion near the homogenization temperature. These types of behaviour indicate that these inclusions contain fluids with near-critical densities (Roedder, 1984; Cline and Vanko, 1995). Measured homogenization temperatures for vapour-rich inclusions may be significantly underestimated due to difficulties in observing disappearance of the liquid rim on the wall of the inclusion (Roedder, 1984; Bodnar *et al*., 1985; Cline and Vanko, 1995).

Trapping conditions for type II fluids from the No. 1 Zone vein are indicated on a pressure-temperature projection of the H_2O-NaCl system for a 5 eq. wt. % NaCl fluid (Figure 7). The inclusions are interpreted to have been trapped during mild fluctuations in pressure (300 to 400 bars), temperature (400 to 440°C) and fluid composition (4 to 7.5 eq. wt. % NaCl) at near-critical conditions (*see* oval in Figure 7). The 'pressure correction' for type II fluid homogenization temperatures is approximately 45 to 70°C. At the maximum pressure of 400 bars and 440°C, rock is ductile, precluding open fractures except during short periods of high strain (Fournier, 1991; Hedenquist *et al*., 1998). The No. 1 Zone vein is interpreted to have formed at depths between 1.1 and 1.5 km under lithostatic load (Table 4).

DISCUSSION AND SUMMARY

The Lustdust property is a polymetallic hydrothermal system in which mineralization is discontinuously developed over a 2.5 km strike length. The system is zoned, and includes Cu-Mo porphyry mineralization, carbonate replacement Cu-Au skarns and Zn mantos, and complex metallic (Zn-Pb-Ag-Au-As-Sb-Hg) massive sulphide-sulphosalt veins in limestones at the No. 1 Zone. Fluid inclusion studies at Lustdust were completed on the following types of minerals:

(1) igneous quartz phenocrysts in the Glover Stock diorite and monzonite porphyry,

(2) hydrothermal quartz in the various porphyry-style mineralized (Cu-Mo) and barren veins which cut the stock,

(3) hydrothermal garnet and calcite crystals in the Cu-Au skarns,

(4) late quartz in the Zn mantos, and

(5) quartz and calcite in the quartz-sulphide-sulphosalt-bearing No. 1 Zone veins.

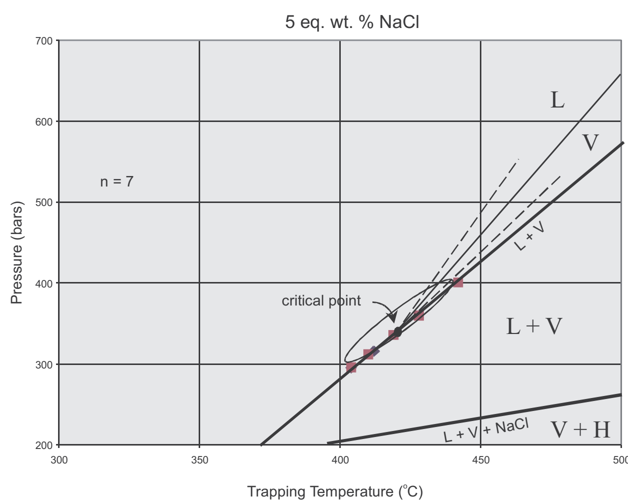

Figure 7. Pressure-temperature projection of the H_2O-NaCl system modified from Bodnar *et al.* (1985). The dark line (L + V) represents the liquid-vapour curve for a 5 eq. wt. % NaCl fluid similar to the composition of type II inclusions in samples GR01-104 and GR01-105 from the Takla Silver Mine No. 1 Zone veins. The critical point for this fluid is indicated. The oval indicates trapping conditions for type II inclusions, which homogenize to the liquid and vapour phases at near-critical conditions.

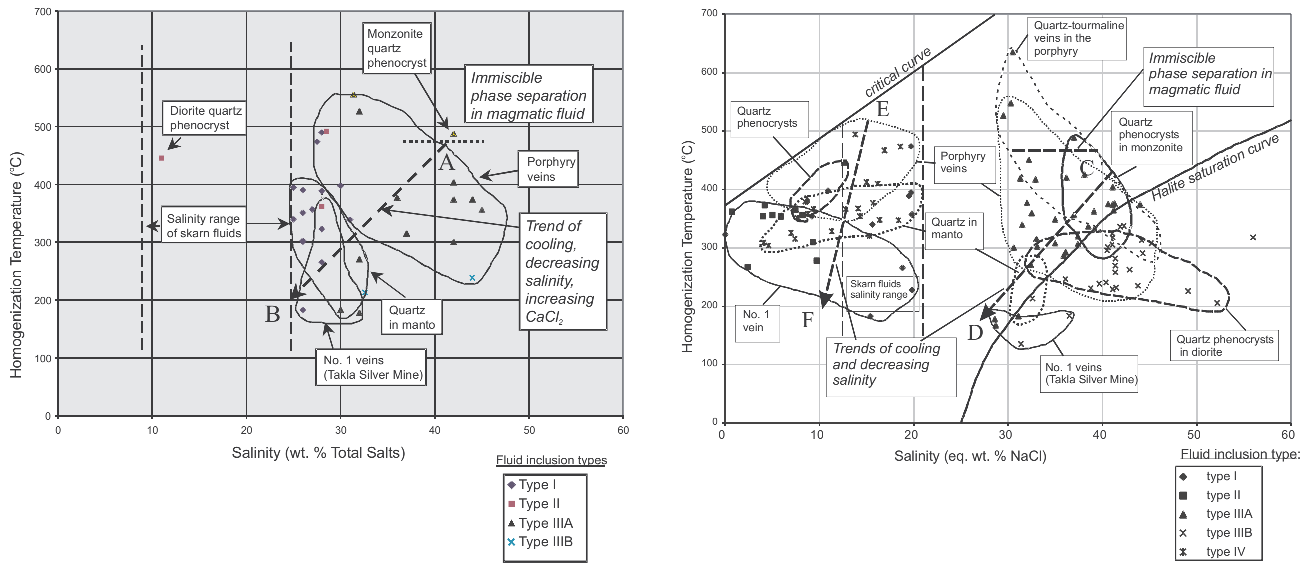

Figure 8. Homogenization temperature - salinity relationships in fluid inclusions from the Lustdust property (format from Lang and Baker, 1999). (a) Salinity is in weight percent total salts calculated from the H_2O-NaCl-$CaCl_2$ ternary diagram in Figure 4. (b) Salinity is in equivalent weight percent NaCl calculated using the equations of Bodnar and Vityk (1994) and freezing point depression data. Note that range of salinity of skarn fluids is indicated by broad dashes. Trends of decreasing temperature and salinity are represented by thick, dark dashed lines with arrows (lines A-B, C-D and E-F).

The studies place constraints on the fluid evolution of the Lustdust hydrothermal system. Each style of mineralization has unique fluid inclusion populations and compositions indicating they were trapped under specific conditions that change spatially and temporally.

Fluid inclusions in the monzonite quartz phenocrysts and the Cu-Mo-bearing porphyry veins comprise coexisting high salinity H_2O-NaCl-$CaCl_2$ $MgCl_{2\pm}$ $FeCl_2$ (Type III) and vapour-rich H_2O-CO_2-NaCl-CH_4 (Type IV) fluids. These fluids were trapped as immiscible phases at maximum homogenization temperatures of approximately 475 to 500^{o}C (*see* horizontal dotted line in Figures 8a and 8b). For comparison, salinities are calculated as weight percent total salts (35 to 45 weight percent at maximum homogenization temperatures) in Figure 8a and as equivalent weight percent NaCl (30 to 40 equivalent weight percent at maximum homogenization temperatures) in Figure 8b. Fluids, in both diagrams, plot along trends of decreasing temperature and salinity (Path A-B, Figure 8a and Path C-D, Figure 8b) and increasing $CaCl_2$ concentration (cf. Figure 4). A second cooling trend, for immiscible Type II or IV and I fluids, at maximum homogenization temperatures of 450 to 500^{o}C and salinities of 12 to 20 equivalent weight percent NaCl is inferred in Figure 8b (Path E-F). Similar temperature-salinity relationships have been reported in high-temperature, carbonate-hosted Zn-Pb-AgCu skarn-manto deposits in Mexico (Lang and Baker, 1999).

At Lustdust, pressure estimates, assuming immiscible entrapment in a lithostatic pressure regime and considering the presence of CO_2, indicate deposition of late magmatic fluids at the following depths (Table 4):

Monzonite quartz phenocrysts: 1.9 km

Porphyry veins: 1.7 to 1.9 km

Mantos: 1.2 km

The No. 1 Zone veins are interpreted to have formed under near critical conditions in a lithostatic pressure regime at depths between about 1.1 to 1.5 km.

Depth estimates at Lustdust, assuming immiscible entrapment in an open system (hydrostatic pressure regime), range from about 3.0 to 5.0 km (Table 4).

Field evidence, including the lack of ductile structures, abundance of brittle faulting and the development of the extensive skarn envelope, suggests the Lustdust mineralization formed at relatively shallow depths (Ray *et al.*, 2002, this volume). Consequently, the minimum estimated trapping pressures for some type IIIB inclusions that homogenize by halite dissolution seem unreasonably high (*see* Table 4: quartz-tourmaline-chalcopyrite-pyrite veins and the No. 1 Zone veins). The discrepancy between geologic and other fluid inclusion evidence, trapping pressure estimates based on observed fluid immiscibility, and the estimates based on halite dissolution may be explained if the composition of the fluids (H_2O-NaCl-CaCl±$MgCl_2$±$FeCl_2$) is considered. Stewart and Potter (1979) show that the introduction of Ca^{2+} ion reduces the slopes of isochores calculated using NaCl-H_2O model composition. Reduced isochore slopes would result in lower calculated pressure estimates for the type IIIB inclusions.

At Lustdust, the temporal and spatial occurrence of early type III (liquid-rich, high salinity) inclusions coexisting with types IV and II (vapour-rich inclusions) followed by later type I (liquid-rich, low salinity) inclusions is characteristic of the productive portions of shallow magmatic-hydrothermal systems associated with porphyry Cu deposits (Beane and Bodnar, 1995). Although CO_2 is not typical in most porphyry Cu deposits, it is more common in

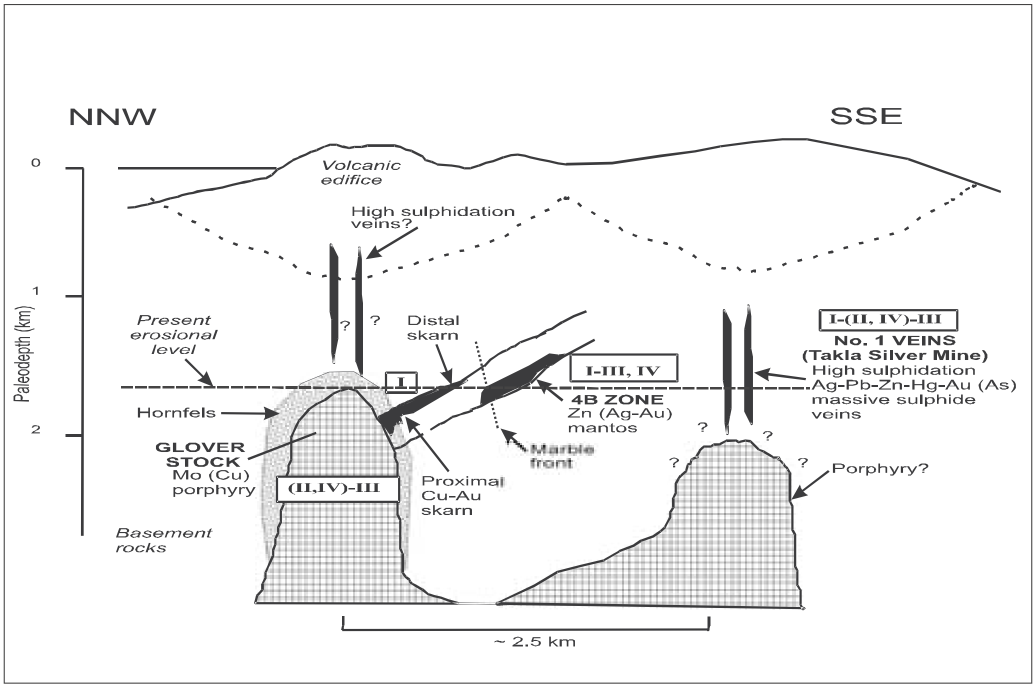

Figure 9. NNW-SSE section showing idealized lateral and vertical zoning of deposit types and principal metals at the Lustdust prospect, adapted from a general exploration model by Sillitoe (1995). Depths are calculated assuming a lithostatic pressure regime. The composition of fluids that characterize different portions of each type of system are indicated: I = low-moderate salinity, liquid dominated; II = low salinity, vapour dominated; III = high salinity, liquid dominated; IV = low salinity, vapour dominated, CO_2 bearing (concept after Lang *et al*., 2000).

porphyry-Mo systems (Beane and Bodnar, 1995; Roedder, op. cit.). CO_2 in vapour-rich inclusions is reported at Santa Rita, New Mexico (Reynolds and Beane, 1985) and is recognized in other deposits such as Bingham, Utah, El Salvador, Chile, and Sar Cheshmeh, Iran (Roedder, 1984).

The Lustdust prospect represents a classic magmatic-related and zoned system similar to those described by Sillitoe (1995), Megaw (1998) and Lang *et al.* (2000). The fluid zoning at Lustdust is characterized as follows (Figure 9):

Porphyry: Hydrothermal fluid types IV and II (vapour-rich ± CO_2-bearing) and type III (liquid-rich, high salinity, halite-bearing)

Skarn: Hydrothermal fluid type I (liquid-rich, low salinity)

Manto: Hydrothermal fluid types I and III (liquid-rich, low and high salinity) and type IV (vapour-rich, CO_2-bearing).

No.1 Zone Veins: Hydrothermal fluid types I and III (liquid-rich, low and high salinity) and types II and IV (vapour-rich ± CO_2-bearing)

The No. 1 Zone veins give estimated depths of 1.1 to 1.5 km, assuming trapping at near-critical conditions. The occurrence of abundant vapour-rich inclusions (Types II and IV) in quartz from the veins suggests that they formed above a magmatic intrusion. The presence of type III (salt-saturated) inclusions, together with the occurrence of sulphosalts and significant arsenopyrite (~7 to 15 %, Leitch, 2001) in dominantly massive sulphide veins suggests that these veins may have formed in a high sulphidation environment above a porphyry, similar to those described by Sillitoe (1995) and Lang *et al*. (2000). Thus, the No. 1 Zone veins may overlie a southern extension of the Glover Stock or be related to a separate buried intrusion (Figure 9). This possibility and the Hg-rich nature of the veins is significant for regional exploration because the presence elsewhere of Hg occurrences and/or Takla Silver-type veins may indicate the existence of a Lustdust-type target.

ACKNOWLEDGMENTS

We are grateful to the management and staff of Alpha Gold Corp for their assistance during this project, particularly George Whatley (President, Alpha Gold). Thanks to M.J. Orchard of the Geological Survey of Canada for identifying conodont microfossils. Many of the geological ideas expressed in this paper were derived from discussions in the office and field with Peter Megaw (President, IMDEX), Jim McGlassen, Ian Webster, the late Keith Glover, and Craig Leitch. Editing by Brian Grant and Ian Webster are also appreciated.

REFERENCES

Beane, R.E. and Bodnar, R.J. (1995): Hydrothermal Fluids and Hydrothermal Alteration in Porphyry Copper Deposits; *in* Porphyry Copper Deposits of the American Cordillera, F.W. Pierce and J.G. Bolm, Editors, *Arizona Geological Society*, Digest 20, pages 83-93.

Bodnar, (1995): Fluid-Inclusion Evidence for a Magmatic Source for Metals in Porphyry Copper Deposits; *in* Magmas, Fluids, and Ore Deposits, J.F.H. Thompson, Editor, *Mineralogical Association of Canada*, Short Course, Volume 23, pages 139-152.

Bodnar, R.J. and Vityk, M.O. (1994): Interpretation of Microthermometric Data for H_2O-NaCl Fluid Inclusions; *in* Fluid Inclusions in Minerals: Methods and Applications, Short Course of the Working Group (IMA) "Inclusions in Minerals", B. De Vivo and M.L. Frezzotti, Editors, *Virginia Polytechnic Institute and State University*, pages 117-130.

Bodnar, R.J., Burnham, C.W. and Sterner, S.M. (1985): Synthetic Fluid Inclusions in Natural Quartz. III. Determination of Phase Equilibrium Properties in the System H_2O-NaCl to 1000^oC and 1500 bars; *Geochimica et Cosmochimica Acta*., Volume 49, pages 1861-1873.

Bowers, T.S. and Helgeson, H.C. (1983): Calculation of the Thermodynamic and Geochemical Consequences of Nonideal Mixing in the System H_2O-CO_2-NaCl on Phase Relations in Geologic Systems: Equation of State for H_2O-CO_2-NaCl Fluids at High Pressures and Temperatures; *Geochimica et Cosmochimica Acta*., Volume 47, pages 1247-1275.

Brown, P.E. and Hagemann, S.G. (1994): MacFlincor: A Computer Program for Fluid Inclusion Data Reduction and Manipulation; in Fluid Inclusions in Minerals: Methods and Applications, Short Course of the Working Group (IMA) "Inclusions in Minerals", B. De Vivo and M.L. Frezzotti, Editors, *Virginia Polytechnic Institute and State University*, pages 231-250.

Cline, J.S. and Vanko, D.A. (1995): Magmatically Generated Saline Brines Related to Molybdenum at Questa, New Mexico, USA; *in* Magmas, Fluids, and Ore Deposits, J.F.H. Thompson, Editor, *Mineralogical Association of Canada*, Short Course, Volume 23, pages 153-174.

Crawford, M.L. (1981): Phase Equilibria in Aqueous Fluid Inclusions; *in* Fluid Inclusions: Applications to Petrology, L.S. Hollister and M.L. Crawford, Editors, *Mineralogical Association of Canada*, Short Course Handbook 6, pages 75-100.

Evans, G. (1996): Geological and Geochemical Report on the 1996 Exploration of the Lustdust Property; submitted by Teck Corp., *British Columbia Ministry of Energy and Mines*, Assessment Report 24735, 125 pages.

Evans, G. (1998): Diamond Drilling Report on the 1998 Exploration of the Lustdust Property; submitted by Alpha Gold, *British Columbia Ministry of Energy and Mines*, Assessment Report 25739, 77 pages.

Fournier, R.O. (1991): Transition from Hydrostatic to Greater Than Hydrostatic Fluid Pressures in Presently Active Hydrothermal Systems in Crystalline Rocks; *Geophysical Research Letters*, Volume 18, pages 955-958.

Gabrielse, H., and Yorath, C.J. (1992): Geology of the Cordilleran Orogeny in Canada. *Geological Society of America*, DNAG G-2, 875 pages.

Goldstein, R.H. and Reynolds, T.J. (1994): Systematics of Fluid Inclusions in Diagenetic Minerals; *Society for Sedimentary Geology*, Short Course 31, 199 pages.

Hedenquist, J.W., Arribas, A. Jr. and Reynolds, T.J. (1998): Evolution of an Intrusion-Centered Hydrothermal System: Far Southeast-Lepanto Porphyry and Epithermal Cu-Au Deposits, Philippines; *Economic Geology*, Volume 93, No. 4, pages 373-404.

Jacobs, G.K. and Kerrick, D.M. (1981): Methane: An Equation of State with Application to the Ternary System H_2O-CO_2-CH_4; *Geochimica et Cosmochimica Acta*, Volume 45, pages 607-614.

Lang, J.R. and Baker, T. (1999): The Role of Fluid Immiscibility in Some Mexican Skarn Deposits; *in* Mineral Deposits: Processes to Processing, C.J. Stanley *et al.* Editors, *Balkema Publishing*, Rotterdam, pages 1047-1050.

Lang, J.R., Baker, T., Hart, J.R. and Mortensen, J.K. (2000): An Exploration Model for Intrusion-Related Gold Systems; *Society of Economic Geologists*, Newsletter, No. 40, pages 1 to 15.

Leitch, C.H.B. (2001): Petrographic Report on Polished Thin Sections of 7 Samples; *British Columbia Geological Survey*, Internal Report.

Linke, W.F. (1958): Solubilities of Inorganic and Metal Organic Compounds, Volume I.; *D. Van Nostrand Col,* Princeton, New Jersey; 1487 pages.

Linke, W.F. (1965): Solubilities of Inorganic and Metal Organic Compounds, Volume II; *American Chemical Society*, Washington, D.C.; 1914 pages.

Megaw, P.K.M. (1998): Carbonate-hosted Pb-Zn-Ag-Cu-Au replacement deposits: An Exploration Perspective; *in* Mineralized Intrusion-Related Skarn Systems, D.R. Lentz, Editor, *Mineralogical Association of Canada*, Short Course Series, Volume 26, pages 337-358.

Megaw, P.K.M. (1999): Report on 1999 drilling and geological study of the Lustdust property, Omineca Mining Division, British Columbia; submitted by *Alpha Gold Corporation*, October 1999, *British Columbia Ministry of Energy and Mines*, Assessment Report 26069, 151 pages.

Megaw, P.K.M. (2000): Report on 2000 drilling and geological study of Lustdust property, Omineca Mining Division, British Columbia; submitted by *Alpha Gold Corporation*, October 2000, *British Columbia Ministry of Energy and Mines*, Assessment Report 26466, 396 pages.

Megaw, P.K.M. (2001): Report on 2001 drilling and geological study of Lustdust property, Omineca Mining Division, British Columbia; submitted by *Alpha Gold Corporation*, October 2001, *British Columbia Ministry of Energy and Mines*, Assessment Report**,** 40 pages.

Monger, J.W.H. (1977): Upper Paleozoic rocks of the western Canadian Cordillera and their bearing on Cordillera evolution. *Canadian Journal of Earth Science*, volume 14, p. 1832-1859.

Monger, J.W.H. (1998): Plate tectonics and northern Cordilleran geology: An unfinished revolution. *Geoscience Canada*, volume 24:4, p. 189-198.

Oakes, C.S., Bodnar, R.J. and Simonson, J.M. (1990): The System NaCl-CaCl2-H2O: I. The Ice Liquidus at 1 Atm Total Pressure; *Geochimica et Cosmochimica Acta*, Volume 54, pages 603-610.

Paterson, I.A. (1974): Geology of Cache Creek Group and Mesozoic rocks at the northern end of the Stuart Lake Belt, central British Columbia;Report of Activities, *Geological Survey of Canada*, Paper 74-1, Part B, p. 31-42.

Paterson, I.A. (1977): The geology and evolution of the Pinchi Fault Zone at Pinchi Lake, central British Columbia; *Canadian Journal of Earth Science*, volume 14, p. 1324-1342.

Potter, II, R.W. and Clynne, M.A. (1978): Solubility of Highly Soluble Salts in Aqueous Media - Part 1., NaCl, KCl, $CaCl_2$, $NaSO_4$, and K_2SO_4 Solubilities to 100^o; *United States Geological Survey*, Journal of Research, Volume 6, pages 701-705.

Ray, G.E., Webster, I.C.L, Megaw, P.K.M., McGlasson, J., and Glover, J.K. (2002, this volume): The Lustdust property in central British Columbia: A polymetallic zoned porphyry-skarn-manto-vein system; *British Columbia Ministry of Energy and Mines*, Geological Fieldwork 2001, Paper 2001-1.

Reynolds, T.J. and Beane, R.E. (1985): Evolution of Hydrothermal Fluid Characteristics at the Santa Rita, New Mexico, Porphyry Copper Deposit; *Economic Geology*, Volume 80, No. 5, pages 1328-1347.

Roedder, E. (1984): Fluid Inclusions; *Mineralogical Society of America*, Reviews in Mineralogy, Volume 12, 644 pages.

Schiarizza, P. (2000): Bedrock geology, Old Hogem (Western Part), NTS 93N/11, 12, 13, 1:100 000 scale compilation map, *British Columbia Ministry of Energy and Mines,* Open File 2000-33.

Schiarizza, P., and MacIntyre, D. (1999): Geology of the Babine Lake-Takla Lake area, central British Columbia (93K/11, 12,13,14: 093N/3,4,5,6). *B.C. Ministry of Energy, Mines and Petroleum Resources*, Geological Fieldwork 1998, Paper 1999-1, pages 33-68.

Shepherd, T.J., Rankin, A.H. and Alderton, D.H.M. (1985): A practical Guide to Fluid Inclusion Studies; *Blackie & Son Ltd.,* London, 239 pages.

Sillitoe, R.H. (1995): The Influence of Magmatic-Hydrothermal Models on Exploration Strategies for Volcano-Plutonic Arcs*; in* Magmas, Fluids, and Ore Deposits, J.F.H. Thompson, Editor, *Mineralogical Association of Canada*, Short Course, Volume 23, pages 511-525.

Stewart, D.B. and Potter, II, R.W. (1979): Application of Physical Chemistry of Fluids in Rock Salt at Elevated Temperature and Pressure to Repositories for Radioactive Waste; in Scientific Basis for Nuclear Waste Management, G.J. McCarthy, editor, *Wiley Interscience*, New York, pages 236-277.

Vanko, D.A., Bodnar, R.J. and Sterner, S.M. (1988): Synthetic Fluid Inclusions: VIII. Vapour-Saturated Halite Solubility in Part of the System $NaCl$-$CaCl_2$-H_2O, with Application to Fluid Inclusions from Oceanic Hydrothermal Systems; *Geochimica et Cosmochimica Acta*., Volume 52, pages 2451-2456.

Wheeler, J.O., Brookfield, A.J., Gabrielse, H., Monger, J.W.H., Tipper, H.W. and Woodsworth, G.J. (1991): Terrane map of the Canadian Cordillera; *Geological Survey of Canada,* Map 1713a, Scale 1:2 000 000.

Platinum-Group-Element (PGE) Placer Deposits in British Columbia: Characterization and Implications for PGE Potential

By Victor M. Levson, David J. Mate and Travis Ferbey

KEYWORDS: *Placer geology, PGE, Platinum, Platinum Group Elements, Palladium, Quaternary geology, Geochemistry.*

INTRODUCTION

A number of techniques are now available that can be used to evaluate the relationships of PGE-Au rich placers with their original lode sources using sedimentological, geochemical and mineralogical data (Levson and Morison, 1995; Youngson and Craw, 1999; Knight *et al.*, 1999a, b; Chapman *et al.,* 2000; Levson and Blyth, 2001). Information about the type of PGE lode deposits can also be obtained from the study of placer deposits (Bowles *et al.,* 2000; Gornostayev *et al.*, 2000). The objective of this study is to use these types of data to lead to the identification of new PGE exploration targets (new deposit types and specific target areas) in British Columbia. Emphasis is placed on areas where high grade proximal placers occur but known lode sources have not been identified, especially where exposure in the probable source areas is poor. This study includes an evaluation of known and suspected platinum placers in BC (Table 1; Figure 1). Field and laboratory verification of reported PGE occurrences was conducted in areas with good potential. The geology of each placer was described and interpreted and the concentration of PGEs and other elements quantitatively assessed.

Platinum group elements occur in a variety of mineral deposit settings including: PGEs associated with Nickel deposits (*e.g.* Giant Mascot, Nickel Mountain areas; MINFILE 92HSW004 and 104B006,); PGE's in Cu-enriched Alkaline complexes (*e.g.* Whiterocks Mountain./Dobbin area; MINFILE 82LSW005); listwanite Au-PGE occurrences (*e.g.* Atlin area); and Alaskan-type complexes. An attempt was made to collect data from placer deposits with PGE potential in each of these settings. A well known example in British Columbia of a placer derived from an Alaskan-type PGE complex is the PGE-bearing placers in the Tulameen area. These placers yielded 620 kg of platinum from 1889 to 1936 (Nixon *et al.* 1990). The Salmon River placers in southwestern Alaska are also derived from an Alaskan-type complex and produced 20 200 kg of PGE, mostly in the form of Fe–Pt alloys (Foley *et al.* 1997).

The platinum-group elements include platinum, iridium, osmium, palladium, rhodium, and ruthenium. They have unique properties that result in a wide range of important applications. Platinum, for example, has a high melting

TABLE 1
PLACER DEPOSITS WITH REPORTED PGE'S IN BRITISH COLUMBIA
(SOURCE: MINFILE DATABASE)

Minfile #	Stream Name(s)	Content	NTS
082ESW026	ROCK CREEK/ JOLLY CREEK	Au Pt	82E/3E
092HNE192	BEAR CREEK/ LAWLESS CREEK	Au Pt	92H/10W
092HNE194	CEDAR CREEK/ MANION CREEK	Au Pt	92H/10W
092HNE196	EAGLE CREEK/ BRITTON CREEK	Au Pt	92H/10W
092HNE197	HINES CREEK	Pt Au	92H/10W
092HNE198	SLATE CREEK/ OLIVINE CREEK	Au Pt	92H/10W
092HNE199	TULAMEEN RIVER	Au Pt Cu	92H/10W
092HSE230	GRANITE CREEK	Au Pt Os Ir Rh Pd Cr Cu	92H/7E, 10E
092HSE232	NEWTON CREEK	Au Pt	92H/7W, 7E
092HSE233	SIMILKAMEEN RIVER	Au Pt Ag	92H/7E, 8W
092HSE235	TULAMEEN RIVER/ RUBY	Au Pt Ir Pd Rh Os Ru	92H/7E, 10E, 10W
092HSE236	WHIPSAW CREEK	Au Pt	92H/7E
092HSW148	SOWAQUA/ PIERRE/ PEERS CREEKS	Au Pt	92H/6E
092INW050	GLASGOW/ BABKIRK	Au Pt Ag	92I/13W
093G 025	COTTONWOOD	Au Pt	93G/1E
093J 007	MCDOUGALL/ LITTLE MCLEOD RIVER	Au Pt	93J/14W
093J 012	MCLEOD RIVER	Au Pt	93J/14E
093O 003	BILL CUST'S BAR	Au Pt Ir	93O/13E, 12E
093O 004	NATION RIVER BAR	Au Pt Ir	93O/5E
093O 005	RAINBOW CREEK	Au Pt Ir	93O/4W
093O 006	PHILIP AND WHEEL CREEKS	Au Pt Ir	93O/4E, 5E
093O 045	PARSNIP RIVER	Au Pt Ag	93O/11W
094B 001	PETE TOYS BAR	Au Pt	94B/4W
094B 002	BRANHAM FLATS	Au Pt	94B/2E
094B 004	PEACE RIVER/ GOLD BAR	Au Pt	94B/2E
094D 007	MCCONNELL CREEK	Au Pt	94D/16W
104J 007	THIBERT CREEK	Au Pt	104J/16E
103F 026	BLUE JACKET CREEK/ MASSET SOUND	Au Pt Fe Ti Zr	103F/16E
092HSE238	DALBY CREEK**	Au Pt Ir	92H/7E
092GNE013	MONTE CRISTO*	Au Pt	92G/16W
092GNE019	CHILCO*	Au Pt Pd Ag	92G/16W
092HNE179	JOY MINING*	Au Pt	92H/10E
092HSE229	CHAMPION CREEK*	Au Pt	92H/7W
092ISW078	VAN WINKLE BAR*	Pt Ir	92I/5E
092JSE022	HEMRICK MINES*	Au Pt Ag	92J/2E
093A 085	MAUD CREEK*	Au Ag Pt	93A/12E
094D 008	INGENIKA RIVER*	Au Pt	94D/16W

* Showing; ** Developed Prospect; all others Past Producers

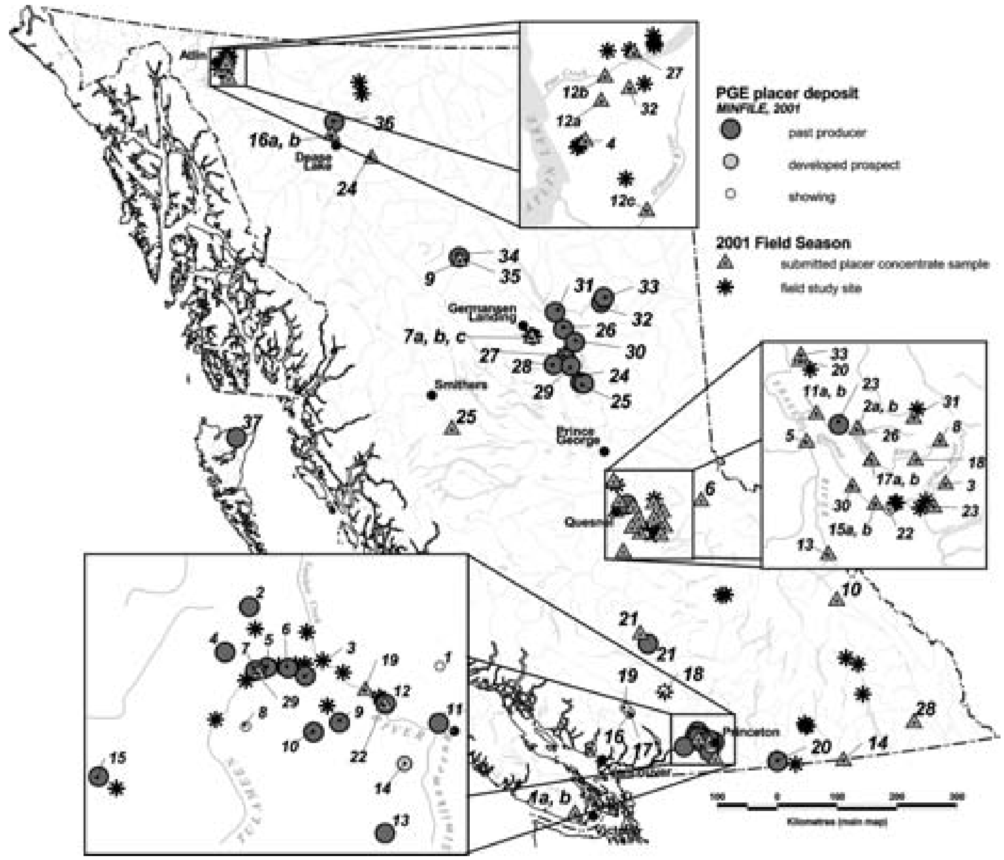

Figure 1. Locations of PGE placer deposits in British Columbia (*see* also Table 1), locations of placer samples analysed in this study (see Tables 3 to 5 for results), and locations of field study sites.

point (1775° C), is a good conductor, and is unusually hard for a metal (4-4.5). Applications include uses as a catalyst in the chemical and petroleum industry, in vehicle pollution control, electronics, power generation, medicine, dentistry, investment and jewellery. The level of demand and supply of PGE's has progressively increased in North America and dramatic increases in price have led to a renewed interest in exploration for the PGEs in recent years.

PREVIOUS STUDIES

Previous work on PGE's in British Columbia has been conducted by a number of authors. Good summaries have been provided by Nixon and Hammack (1991), Nixon *et al.* (1997) and Lefebure (2000). The distribution of PGE occurrences in the province in relation to geology has been mapped by the Ministry of Energy and Mines (2000) and Hulbert (2001). In addition, numerous reports dealing with PGE's in specific areas have been published (*e.g.* in the Tulameen area, Nixon et al., 1990; Cook and Fletcher, 1992). Historical reports dealing mainly with platinum in placer deposits include reports by the Munition Resources Commission (1920), O'Neill and Gunning (1934) and Rublee (1986). An excellent summary of platinum placers around the world is provided by Cabri *et al.* (1996).

OBJECTIVES

This paper reports on the preliminary results of field and laboratory work conducted in the first six months of a two year study. The objectives of the first year of the study are to: 1) substantiate reported PGE placer occurrences; 2) document new PGE occurrences; 3) provide high quality analytical results; 4) determine the nature of any contained PGE and PGMs in order to evaluate source deposit type; and 5) collect data that will help in determining the proximity of the PGE placers to their source areas.

Objectives for further research on the project include: determination of the proximity of selected placers to potential lode sources; evaluation of dispersal mechanisms of PGEs in till, colluvium and other surficial sediments; identification of preferred sample media and size fractions for locating buried PGE targets; identification of pathfinder elements for PGE exploration; and determination of suitable analytical tools (*e.g*. heavy mineral analysis of the coarse fraction versus trace element analysis of the fine fraction). In order to identify areas with the best potential for the discovery of new PGE targets, the distribution and geology of these placers needs to be compared with existing geochemical data, bedrock geology and PGE deposit models. Follow-up till geochemical sampling is planned for the second year of the study in areas where preliminary results indicate potential for discovery of proximal lode sources.

RESEARCH COMPONENTS

OFFICE EVALUATION

The study included an office evaluation of reported platinum placer occurrences in BC from the MINFILE database (Table 1) and from published works (*e.g.* Rublee, 1986). The distribution of these placers was compared with existing geochemical data, the occurrence of known PGE prospects, bedrock geology and PGE deposit models in order to identify areas with the potential for the discovery of new PGE targets. Field sites were selected from this information.

SAMPLE COLLECTION

Placer samples in areas of PGE potential were obtained in three ways:

- Placer property holders in the British Columbia Mineral Titles registry (as of May, 2001) were canvassed for concentrate samples. Data on the sample site location, type of placer, stratigraphic position, size and shape of placer minerals, method of concentration and processing circuit were requested (Table 2). Data useful for characterizing the host sediments including sedimentary structures, clast shape and lithology, alteration and grain-size distribution were also obtained. Submitted sample size was requested to be between 65 grams and 1 kilogram with grains less than 1 mm (finer than # 18 sieve size);

- Bulk samples were collected from streams in areas where geologic data suggested PGE potential. Sites of natural heavy mineral concentration were sampled wherever possible to increase the likelihood of obtaining detectable levels of PGE's. These sites included back-bar eddies, bar-top lags, and winnowed-channel deposits. Sediments

a

b

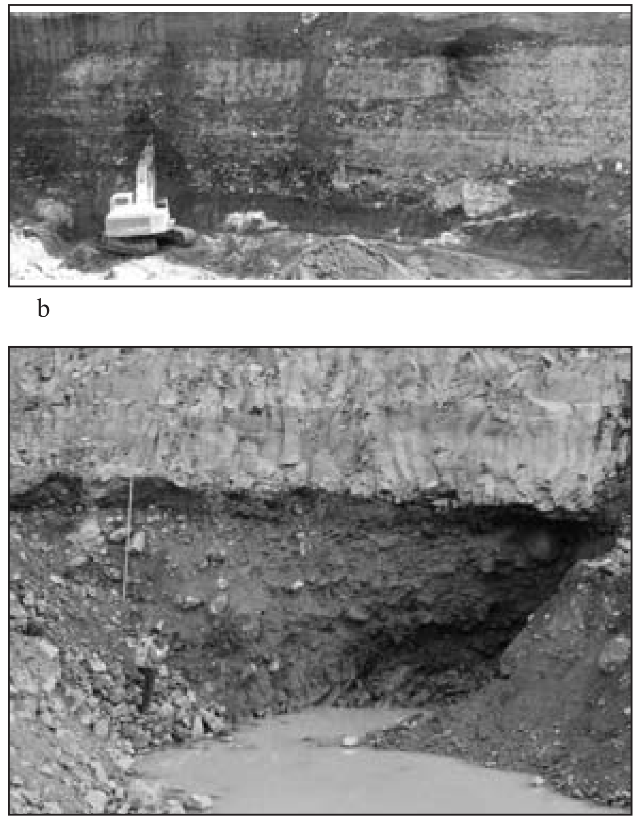

Figure 2. Stratigraphic setting of example placer deposits with PGE potential: 2a) Platinum, palladium and gold bearing gravels underlying glacial deposits at Slate Creek, Manson Creek area (Lloyd Worthing mining operation); 2b) Auiferous gravels underlying Pleistocene basalts at Ruby Creek, Atlin area (Wayne Klippert mine).

TABLE 2
DESCRIPTION COMPONENTS FOR PGE ANALYSIS SAMPLE SUBMISSION

Submitter information:				
Name	Mailing Address	Telephone	Fax	E-Mail
Sample location:				
NTS map	Stream name	Latitude and Longitude	UTM Coordinates	
Description of submitted sample:				
Weight	Grain-size fraction	Method of concentration	Treatment after concentration	
Description of placer mine and deposit from which sample originated:				
Type of mine	Size of mine	Type of deposit	Size of deposit	
Stratigraphic position of sampled horizon:				
Depth of sample	Depth to bedrock	Bedrock lithology	Overburden thickness and description	
Description of sediment from which sample originated:				
Clast shape	Clast lithologies	Stratification	Imbrication	
Cementation	Weathering	Iron staining	Manganese staining	
Description of placer minerals (gold and platinum if present):				
Size range	Shape	Known placer minerals	PGE documentation	
Grain size distribution (estimated percent by volume of each fraction):				
Cobbles and boulders	Coarse pebble gravel	Fine pebble gravel	Sand	Silt and clay
Description of processing circuit:				
Processing operation	Feed rate	Method of screening	Feed size	Concentration ratio
Special equipment	Trommel	Washing process	Riffle type	Sluice box type and slope

TABLE 3
RESULTS OF ICP-MS ANALYSIS OF SELECTED PLACER CONCENTRATE SAMPLES

ELEMENT SAMPLE #	Pt ppb	Au ppb	Mo ppm	Cu ppm	Pb ppm	Zn ppm	Ag ppb	Ni ppm	Co ppm	Mn ppm	Fe %	As ppm	Sb ppm	Cr ppm
VLE2001-1a	< 2	359	6.7	23	6	51	51	117	34	528	37.7	6	0.19	387
VLE2001-1b	< 2	147600	1.2	2581	2412	50	21682	27	15	2746	12.7	1495	27.33	26
VLE2001-2a	3	347800	2.2	32	19	60	10373	142	32	744	22.4	8	1.37	613
VLE2001-2b	< 2	8	57.4	37	13	222	1000	135	11	315	3.4	30	7.39	193
VLE2001-3	< 2	2478000	3.7	220	1124	131	99999	115	35	587	11.8	31	2.8	111
VLE2001-4	5	38184	5.4	86	100	36	3723	229	25	407	11.7	75	99.21	205
VLE2001-5	8592	249300	2.0	27	88	81	11101	186	26	945	20.4	8	1.92	385
VLE2001-6	4	3673	2.8	34	19	77	637	47	19	373	3.7	11	0.48	26
VLE2001-7a	47	1040	1.7	14	61	50	362	85	36	711	36.2	8	0.54	675
VLE2001-7b	20718	1941000	17.9	104	28542	97	99999	357	260	881	30.2	4261	133.06	525
VLE2001-7c	4	60	13.3	196	95	279	2249	100	28	1833	5.2	53	4.2	39
VLE2001-8	4	335000	6.6	513	1233	299	77547	416	456	715	35.2	5041	11.98	54
VLE2001-9	11	89608	3.0	57	22	56	1551	34	27	942	20.5	7	1.33	279
VLE2001-10	< 2	193	1.1	33	106	57	174	68	35	722	6.9	971	1.51	30
VLE2001-11a	3	8459	1.1	30	17	177	869	166	47	1264	35.8	5	0.75	1213
VLE2001-11b	74	3459	2.6	32	20	53	995	57	22	1143	8.5	8	1.53	129
VLE2001-12a	2120	39000	5.8	86	1203	189	4275	1349	113	2228	21.2	17	25.49	2664
VLE2001-12b	3	2171	3.1	34	145	72	660	457	42	811	13.5	19	1.6	1774
VLE2001-12c	84432	4063000	8.9	113	66	105	99999	106	596	1156	17.7	14	2.06	537
VLE2001-13	7941	81579	0.9	18	7	53	6900	43	14	654	6.9	5	0.62	126
VLE2001-14	31	172100	8.4	103	2039	149	7629	92	30	665	33.0	23	11.4	377
VLE2001-15a	7	14116	1.0	40	15	107	876	65	27	991	14.8	11	0.94	308
VLE2001-15b	3	38000	3.0	27	23	138	735	104	35	1002	25.1	7	0.76	575
VLE2001-15c	3	3861	1.2	40	13	84	616	46	24	876	10.8	11	1.02	181
VLE2001-16a	270000	27566000	70.2	3413	3907	196	99999	298	197	534	16.7	197	47.03	103
VLE2001-16b	1692	534000	3.3	114	57	55	15983	127	44	801	36.7	5	0.83	289
VLE2001-17a	1631	1407800	0.9	27	17	153	70709	388	54	1460	19.3	3	0.72	4929
VLE2001-17b	4860	1302900	0.8	29	8	175	82236	432	62	1679	22.0	2	0.61	5569
VLE2001-18	146	97206	3.5	234	605	197	22554	155	52	925	28.6	57	2.43	1440
VLE2001-19	1517	7043	0.5	31	10	47	760	109	54	520	25.5	3	2.43	383
VLE2001-20	20	378000	8.4	15	42	62	10638	80	17	1413	16.8	6	0.93	647
VLE2001-21	19	72597	1.3	26	14	56	5535	29	17	1076	14.0	5	1.35	125
VLE2001-22	11435	527	0.5	27	117	36	161	112	56	561	27.0	3	1.74	386
VLE2001-23	7321	3834	11.1	42	27405	63	99999	123	34	450	23.5	155	56.88	804
VLE2001-24	12	2795	2.4	84	117	128	479	259	21	509	7.6	4	5.54	617
VLE2001-25	195	292600	6.5	30	283	356	89105	44	26	1379	14.1	399	6.64	145
VLE2001-26	44	182100	1.7	26	50	99	8751	234	39	1223	29.1	6	2.29	1406
VLE2001-27	13	3403000	3.1	47	830	74	99999	49	6	25383	6.3	0	2.47	99
VLE2001-28	20	580	0.7	19	18	64	453	42	23	757	36.0	5	0.4	119
VLE2001-29	27850	5653	1.2	27	25	42	1546	114	61	639	33.7	2	0.82	414
VLE2001-30	566	788200	1.8	39	15	115	45005	75	29	1198	22.6	9	1.02	462
VLE2001-31	41	1766	4.9	8907	7456	46471	75139	63	211	7371	19.8	181	28.01	< .5
VLE2001-32	127	1764900	40.3	53	169	88	62121	1372	99	1167	30.7	6	0.97	2770
VLE2001-33	18165	1783900	46.6	29	174	95	92236	149	26	1266	26.5	5	1.02	934
VLE2001-36	266	51834	1.6	42	40	112	5587	27	31	1482	33.0	23	1.63	121

ELEMENT SAMPLE #	Al %	Na %	K %	Pd ppb	U ppm	Th ppm	Sr ppm	Cd ppm	Bi ppm	V ppm	Ca %	P %	La ppm	Mg %
VLE2001-1a	0.34	0.009	0.01	< 10	0.1	0.4	8	0.06	0.05	1486	0.21	0.02	2	0.16
VLE2001-1b	0.88	0.01	0.02	< 10	0.4	0.4	111	0.39	5.47	96	0.95	0.027	4	0.41
VLE2001-2a	0.28	0.005	0.02	< 10	1.7	16.0	9	0.34	13.98	480	0.19	0.05	43	0.13
VLE2001-2b	1.4	0.01	0.2	< 10	1.4	2.0	14	0.29	0.2	157	0.09	0.051	6	1.87
VLE2001-3	0.91	0.017	0.1	< 10	2.0	27.6	25	0.86	3.35	130	0.36	0.079	89	0.51
VLE2001-4	0.23	0.004	0.03	< 10	0.8	0.9	6	0.15	20.45	243	0.11	0.02	5	0.33
VLE2001-5	0.32	0.005	0.02	63	10.9	76.9	16	0.12	2.69	748	0.32	0.087	153	0.19
VLE2001-6	1.03	0.012	0.21	< 10	1.5	14.6	385	0.12	0.37	10	5.66	0.049	29	0.63
VLE2001-7a	0.12	0.005	0.01	< 10	0.6	1.7	10	0.07	0.26	1157	0.28	0.059	5	0.1
VLE2001-7b	0.23	0.007	0.03	735	30.2	8.0	20	5.09	75.65	974	0.43	0.076	9	0.17
VLE2001-7c	1.34	0.011	0.12	< 10	2.2	5.6	75	3.64	0.48	67	1.06	0.119	11	0.81
VLE2001-8	0.13	0.005	0.03	< 10	1.2	4.3	20	2.93	8.93	14	0.53	0.039	11	0.42
VLE2001-9	0.47	0.015	0.04	10	1.6	2.5	30	0.13	0.34	708	0.47	0.097	13	0.22
VLE2001-10	0.67	0.01	0.08	< 10	1.1	5.7	95	0.05	0.37	25	4.52	0.042	22	1.9
VLE2001-11a	0.43	0.015	0.03	10	0.5	1.2	21	0.15	0.13	1242	0.37	0.071	5	0.32
VLE2001-11b	0.93	0.02	0.05	< 10	1.9	16.3	34	0.18	0.24	269	0.64	0.109	46	0.41
VLE2001-12a	0.23	0.008	0.02	38	1.9	36.0	6	0.34	19.12	204	0.3	0.055	59	0.76
VLE2001-12b	0.39	0.009	0.03	< 10	4.0	80.4	8	0.24	8.15	195	0.39	0.042	117	0.71
VLE2001-12c	0.36	0.013	0.04	541	13.1	8.0	18	10.9	12.67	787	0.72	0.125	29	0.3
VLE2001-13	0.68	0.023	0.06	72	1.3	10.0	27	0.15	0.24	242	0.57	0.06	28	0.54
VLE2001-14	0.19	0.008	0.03	< 10	26.7	168.6	15	0.85	6.37	833	0.65	0.115	100	0.24
VLE2001-15a	0.76	0.013	0.05	< 10	1.1	5.7	33	0.23	0.25	516	0.56	0.072	21	0.4
VLE2001-15b	0.42	0.01	0.02	< 10	3.9	11.3	29	0.21	0.77	948	0.52	0.081	22	0.26
VLE2001-15c	0.81	0.014	0.05	11	1.1	5.8	33	0.22	0.36	379	0.55	0.078	24	0.45
VLE2001-16a	0.13	0.011	0.01	6990	57.7	66.0	9	1.01	143.54	132	0.41	0.093	25	0.14
VLE2001-16b	0.09	0.006	< .01	< 10	1.1	4.1	5	0.06	1.48	1192	0.34	0.143	10	0.1
VLE2001-17a	0.7	0.014	0.04	51	2.3	18.7	16	0.17	0.51	959	0.31	0.031	45	0.52
VLE2001-17b	0.77	0.018	0.04	69	1.6	16.3	18	0.14	2.33	1081	0.33	0.028	43	0.59
VLE2001-18	0.65	0.085	0.05	11	1.2	11.0	24	3.74	2.11	681	0.72	0.044	22	0.38
VLE2001-19	0.28	0.01	0.02	22	0.2	0.8	25	0.1	0.1	1053	0.3	0.036	4	0.53
VLE2001-20	0.4	0.005	0.01	< 10	17.4	308.7	11	5.42	10.7	519	0.31	0.103	671	0.11
VLE2001-21	0.4	0.01	0.01	10	5.3	35.7	15	0.15	0.5	566	0.32	0.066	42	0.21
VLE2001-22	0.2	0.007	0.01	44	0.1	0.5	9	0.05	0.16	1104	0.25	0.028	2	0.41
VLE2001-23	0.13	0.011	0.01	< 10	6.8	1.2	18	57.57	2253.17	775	0.1	0.021	2	0.1
VLE2001-24	0.99	0.013	0.05	< 10	0.3	1.5	14	0.24	0.57	129	0.6	0.028	7	3.21
VLE2001-25	0.78	0.048	0.11	< 10	1.0	1.9	42	1.01	41.57	471	0.65	0.116	19	0.55
VLE2001-26	0.3	0.008	0.02	< 10	3.8	30.7	11	0.63	0.66	649	0.15	0.045	131	0.16
VLE2001-27	0.22	0.015	0.08	< 10	43.2	139.3	6	1.33	565.01	< 2	0.38	0.018	204	0.32
VLE2001-28	0.11	0.008	0.01	< 10	1.3	8.4	4	0.04	1.25	640	0.08	0.024	10	0.04
VLE2001-29	0.18	0.01	0.01	96	0.9	1.1	7	0.08	0.44	1305	0.25	0.028	4	0.25
VLE2001-30	0.55	0.027	0.04	20	2.7	10.0	40	0.18	0.46	826	0.67	0.083	14	0.36
VLE2001-31	0.38	0.014	0.06	< 10	0.8	4.7	2	263.94	13.32	4	0.33	0.017	1	0.16
VLE2001-32	0.1	0.007	0.01	< 10	1.9	3.3	2	0.26	3.04	405	0.1	0.025	4	0.52
VLE2001-33	0.3	0.009	0.02	140	22.7	310.6	13	0.17	42.66	756	0.27	0.114	685	0.14
VLE2001-36	0.31	0.022	0.03	< 10	1.7	2.1	14	0.83	1.35	1048	0.26	0.053	9	0.16

Table 3. Con't

ELEMENT SAMPLE #	Ba ppm	Ti %	B ppm	W ppm	Sc ppm	Tl ppm	S %	Hg ppb	Se ppm	Te ppm	Ga ppm
VLE2001-1a	16	0.297	< 1	< .2	1.2	< .02	0.03	417	< .1	< .02	11.5
VLE2001-1b	21	0.098	3	504.0	2.2	1.61	12.48	3513	4.6	0.12	3.0
VLE2001-2a	24	0.19	< 1	10.1	1.4	0.03	0.09	769	0.6	< .02	8.8
VLE2001-2b	89	0.021	4	2.7	5.2	1.17	0.6	10252	28.2	0.19	4.8
VLE2001-3	71	0.052	< 1	1188.3	2.4	0.08	0.18	55347	3.1	0.16	4.4
VLE2001-4	18	0.166	2	141.6	1.2	0.11	1.92	7397	1.5	0.13	2.1
VLE2001-5	51	0.414	< 1	7.2	2.2	0.02	0.07	5480	0.2	0.09	11.8
VLE2001-6	51	< .001	< 1	3.6	1.4	0.05	1.15	175	1.0	0.03	3.5
VLE2001-7a	21	0.245	< 1	1.7	0.7	< .02	0.01	147	0.1	< .02	11.8
VLE2001-7b	43	0.179	< 1	179.1	0.7	0.04	2.51	31010	455.9	4.65	10.4
VLE2001-7c	227	0.048	< 1	< .2	6.1	0.19	0.14	469	87.6	0.19	4.5
VLE2001-8	5	0.027	3	59.4	1.0	0.11	29.03	1463	32.3	13.33	0.9
VLE2001-9	77	0.278	< 1	0.9	2.1	0.02	0.07	548	0.1	0.02	10.2
VLE2001-10	34	0.012	< 1	7.5	1.8	0.04	1.95	913	0.7	0.04	2.3
VLE2001-11a	45	0.699	1	< .2	1.8	< .02	0.01	1249	< .1	< .02	19.9
VLE2001-11b	50	0.31	1	15.6	4.2	0.02	0.02	2936	0.4	0.02	5.0
VLE2001-12a	79	< .001	< 1	237.5	2.1	0.02	0.23	99999	0.3	0.07	4.6
VLE2001-12b	37	0.116	1	853.0	1.7	0.07	0.17	12248	0.3	0.09	7.7
VLE2001-12c	244	0.255	< 1	1373.3	1.9	0.02	0.06	99999	< .1	< .02	11.4
VLE2001-13	54	0.181	1	4.3	2.2	0.03	0.03	309	0.2	< .02	5.1
VLE2001-14	648	0.157	3	103.9	0.8	0.04	0.21	925	< .1	0.06	13.7
VLE2001-15a	45	0.322	2	0.7	2.8	0.03	0.01	1058	0.3	< .02	7.9
VLE2001-15b	38	0.282	< 1	17.6	1.8	< .02	0.38	99999	< .1	< .02	11.7
VLE2001-15c	43	0.288	3	3.0	2.9	0.03	< .01	2973	0.1	0.03	6.3
VLE2001-16a	< .5	0.371	< 1	1569.5	0.7	< .02	13.65	99999	21.4	5.32	2.8
VLE2001-16b	12	0.181	< 1	21.8	0.5	< .02	0.2	7956	< .1	0.04	16.7
VLE2001-17a	49	0.593	1	18.0	2.5	< .02	0.04	9147	0.1	< .02	15.6
VLE2001-17b	55	0.663	2	10.9	2.9	< .02	< .01	3318	0.6	< .02	17.6
VLE2001-18	76	0.22	557	208.2	2.3	0.05	1.33	21426	3.0	0.28	12.9
VLE2001-19	65	0.214	< 1	< .2	1.2	< .02	0.3	471	< .1	< .02	10.1
VLE2001-20	21	0.309	< 1	12.5	2.3	< .02	0.04	578	0.1	0.07	11.3
VLE2001-21	102	0.54	2	0.9	3.0	< .02	0.09	1687	< .1	< .02	6.3
VLE2001-22	52	0.186	< 1	3.5	1.1	< .02	0.23	1216	< .1	0.02	10.1
VLE2001-23	23	0.164	8	8.7	0.7	0.66	3.99	20766	260.2	102.57	6.3
VLE2001-24	60	0.253	5	2.4	3.4	0.03	0.06	315	0.3	0.02	3.0
VLE2001-25	138	0.284	4	3.7	2.7	0.1	0.5	415	0.4	1.6	12.3
VLE2001-26	35	0.261	4	0.9	1.7	0.02	0.04	2570	< .1	< .02	11.4
VLE2001-27	18	< .001	< 1	111.0	24.7	0.06	1.49	99999	20.3	10.75	1.6
VLE2001-28	13	0.038	< 1	28.9	0.3	< .02	0.07	168	< .1	0.03	8.8
VLE2001-29	34	0.233	< 1	5.2	1.0	< .02	0.12	652	< .1	0.04	14.6
VLE2001-30	58	0.341	7	8.8	2.6	0.02	0.06	3982	< .1	< .02	10.9
VLE2001-31	22	< .001	< 1	84.6	0.4	0.1	21.71	1670	16.7	0.05	3.1
VLE2001-32	13	0.049	2	482.9	0.8	< .02	0.05	3159	0.6	0.07	4.0
VLE2001-33	26	0.271	2	42.7	1.6	< .02	0.08	2429	0.8	0.08	16.5
VLE2001-36	159	0.189	4	3.2	2.1	0.02	0.23	1802	0.5	0.33	22.9

were screened in the field and concentrated in the laboratory (*see* below); and

- Samples were collected at active placer mines from representative stratigraphic units. Gravity concentrated samples were obtained where possible from active operations.

FIELD WORK

Field studies were conducted in the vicinity of known and reported PGE placer occurrences (Figure 1). PGE placers were evaluated in a variety of mineral deposit settings. Methods included stratigraphic, sedimentological, geochemical and geomorphological characterization of existing placer deposits and interpretation of depositional environments (Figure 2). The stratigraphic relationships of the placer deposits with the overburden sequences were determined and a detailed description of each sedimentary unit was obtained. Heavy mineral concentrates and representative samples for geochemical studies and size/shape analyses were collected (Figure 3).

LAB WORK AND QUALITY CONTROL

Samples were analyzed for platinum, palladium, gold and 36 other elements by ICP-MS (Table 3) and for gold, platinum and palladium by fire assay (Table 4). All samples received were submitted to the following procedures: 1) Samples were sieved with a #35 mesh screen (0.5 mm); 2) Any coarse visible gold or platinum, the +35 mesh fraction (if present), and any excess (over 50 grams) of the -35 mesh fraction were retained; 3) One split of the sample was milled to produce 40 to 50 g of -150 mesh material for analysis and the other split was archived. A quartz wash was used between each sample milled. If there was insufficient sample for a 30 g mill, 15 g, 10 g or 5 g samples were used for assaying; and 4) The -35 mesh (<0.5 mm) fraction was analyzed at Acme Analytical Laboratories in Vancouver by two methods:

- A 1 gram sample was analyzed for 39 elements (Table 3) by a combination of inductively coupled plasma, emission spectroscopy and mass spectroscopy analyses (ICP/ES & MS) after aqua regia digestion (6 millilitres of 2-2-2 HCL-HNO3-H2O at 95 degrees Celsius for one hour and diluted to 20 millilitres with water). The reported reliable upper limits for these analyses are: 100 ppm for Ag, Au, Hg, W, Se, Te, Tl, Ga and Sn; 2000 ppm for Mo, Co, Cd, Sb, Bi, Th, U and B; and 10,000 ppm for Cu, Pb, Zn, Ni, Mn, As, V, La and Cr (a fire assay is recommended for samples with higher levels.)

- Up to 30 grams (if available) were analyzed by fire assay (with an ICP finish) for Au, Pt and Pd (Table 4). (The reliable upper limit for an ICP finish is 10 ppm; a gravimetric finish is recommended for samples with higher levels.)

ACME and CANMET standards were used to monitor the quality of results.

From this data set, selected samples will be re-analyzed for the entire PGE suite. Results will be used to characterize source deposit types (*e.g.* ophiolites vs Alaskan type complexes) and to highlight areas where field work could be conducted to characterize the placers and determine lode proximity.

Laboratory studies included analyses of magnetic and non-magnetic fractions, fine and coarse fractions, and heavy mineral fractions. Size and shape analyses of placer minerals, and trace element geochemistry of individual placer grains are planned. Concentration of PGE's, gold and other elements was quantitatively assessed but caution is advised in applying grade estimates from these data due to small sample sizes, high natural variability in the placers and inconsistencies in the concentrating systems. Detailed lab analysis to be conducted in year two includes: characterization of PGE, PGM and other minerals in heavy mineral concentrates using reflected light microscopy, electron-microprobe analysis (of exotic phases), SEM microscopy and X-ray diffraction. Documentation of the trace element geochemistry of individual PGM's and the level of trace PGE in common base-metal sulphides is also planned. Results from the ongoing lab component of this study are intended to aid in the identification of the following: specific PGE's present, preferred size fractions for locating PGE targets, heavy mineral suites indicative of PGE potential, pathfinder elements, suitable analytical tools (*e.g.* heavy mineral analysis of the coarse fraction vs trace element analysis of the fine fraction), likely sources of PGE-rich minerals and PGE lode source types in different areas.

RESULTS

More than 150 concentrate samples and 27 bulk samples were submitted for analyses. Preliminary analytical results obtained for platinum, palladium, gold and other elements on 45 samples from 37 different placer properties were available at the time of writing. Results are presented in Tables 3 and 4 and a description of each sample analysed is provided in Table 5. The locations of analysed samples are shown on Figure 1. Results from the remaining 125 samples will be presented at a later date. It is important to emphasize that the results presented in Tables 3 and 4 are based on concentrate samples and therefore they cannot be used to directly calculate grades in the original (unconcentrated) sample material unless the concentration ratio is accurately known. For the purposes of this research, the results are intended to determine if elements such as platinum, palladium, nickel, copper, etc., are present (and not to determine

TABLE 4
FIRE ASSAY RESULTS

Element Sample #	Au** ppb	Pt** ppb	Pd** ppb	Sample Weight (g)
VLE2001-1a	486	< 2	< 2	5
VLE2001-1b	4858980	< 2	14	3
VLE2001-2a	170030	166	3	30
VLE2001-2b	678	< 2	7	10
VLE2001-3	3475900	< 2	27	15
VLE2001-4	102762	2	4	10
VLE2001-5	193300	4010	28	15
VLE2001-6	561	2	3	30
VLE2001-7a	13537	9472	41	15
VLE2001-7b	3051760	51324	901	15
VLE2001-7c	115	2	9	30
VLE2001-8	817470	< 2	6	30
VLE2001-9	42692	7	6	30
VLE2001-10	3656	< 2	< 2	30
VLE2001-11a	27965	1568	8	3
VLE2001-11b	27246	116	< 2	10
VLE2001-12a	30529	2994	15	15
VLE2001-12b	7652	3	8	15
VLE2001-12c	3233200	36992	459	15
VLE2001-13	100110	2608	36	30
VLE2001-14	220250	34	< 2	15
VLE2001-15a	67679	43	< 2	30
VLE2001-15b	60528	358	14	15
VLE2001-15c	41860	5	3	30
VLE2001-16a	2.78E+07	645000	9389	10
VLE2001-16b	480350	11141	208	15
VLE2001-17a	30164	542	< 2	15
VLE2001-17b	792000	7748	234	15
VLE2001-18	170740	391	< 2	10
VLE2001-19	14466	11941	81	15
VLE2001-20	75834	2494	48	15
VLE2001-21	72996	274	< 2	15
VLE2001-22	2719	59744	331	15
VLE2001-23	553	8	< 2	15
VLE2001-24	12107	11	5	30
VLE2001-25	111954	18	< 2	10
VLE2001-26	274516	1060	22	15
VLE2001-27	2930000	343	< 2	15
VLE2001-28	791	8	11	15
VLE2001-29	7892	29386	343	15
VLE2001-30	259000	2489	45	30
VLE2001-31	6407	15	6	15
VLE2001-32	119600	6	< 2	10
VLE2001-33	2615600	40424	568	15
VLE2001-36	36800	760	3	30

TABLE 5
DESCRIPTION OF ANALYSED CONCENTRATE SAMPLES
(*SEE* TABLES 3 AND 4 FOR ANALYSIS RESULTS)

Sample Number	River/Creek Name	Mining District	Mapsheet	Latitude (NAD 27)	Longitude (NAD 27)	Type of Operation[1]	Sample Depth (m)	Fraction Analyzed[2]	Colour[3]	Grain Size[4]	Sorting[5]
1a	Leech R	Shawnigan L	92B/12	48.518	-123.782	testing	0.3	1	bl	f-cS	p
1b	Leech R	Shawnigan L	92B/12	48.518	-123.782	testing	0.3	2	inter	mS	w
2a	Mary, Norton Cr	Cariboo	93G/1E	53.071	-122.078	testing	n/a	3	inter-dg	mS	w
2b	Mary, Norton Cr	Cariboo	93G/1E	53.071	-122.078	testing	n/a	3	dg	mS	w
3	Kiethly Cr	Cariboo	93A/14W	52.750	-121.333	exploration	2	2	inter	fS	p
4	McKee Cr	Atlin	104N/5E	59.483	-133.533	n/a	11	3	bl	mS	w
5	Fraser R	Cariboo	93G/2E	53.016	-122.533	exploration	0.3	3	bl	fS	w
6	Castle Cr	Cariboo	93H/1W	53.100	-120.383	testing	0.5	3	bl	f-mS	p
7a	Slate Cr	Omineca	93N/10E	55.667	-124.533	testing	10-12	3	bl	fS w/ G	p
7b	Slate Cr	Omineca	93N/10E	55.667	-124.533	testing	10-12	3	r-o	S-G	p
7c	Slate Cr	Omineca	93N/10E	55.667	-124.533	testing	10-12	3	dg	Z	n/a
8	Cunningham Cr	Cariboo	93A/13E	52.980	-121.358	production	3-10	3	bl	f-mS	n/a
9	McConnell Cr	Omineca	94D/16W	56.833	-126.467	production	n/a	4	bl	mS	w
10	Quartz Cr	Golden	82N/6W	51.412	-117.323	exploration	1-2	3	br-g	f-mS	p
11a	Cottonwood R	Cariboo	93G/1W	53.161	-122.435	testing	1.5	1	bl	fS	w
11b	Cottonwood R	Cariboo	93G/1W	53.161	-122.435	testing	1.5	3	lg	mS	p-m
12a	Spruce Cr	Atlin	104N/11W	59.556	-133.493	production	n/a	4	bl	f-cS	p
12b	Pine Cr	Atlin	104N/11W	59.599	-133.488	production	n/a	4	bl	f-cS	p
12c	O'Donnel R	Atlin	104N/6W	59.371	-133.295	production	18	4	bl	mS	m
13	Fraser R	Cariboo	93B/8W	52.415	-122.394	testing	n/a	4	inter	f-mS	p
14	Pond O'Reille R	Nelson	82F/3W	49.010	-117.617	exploration	10	3	bl	f-mS	m-w
15a	Quesnel R	Cariboo	93A/12	52.669	-121.961	exploration	2-10	3	inter-dg	f-mS	w
15b	Quesnel R	Cariboo	93A/12	52.669	-121.961	exploration	2-10	4	bl	fS	w
15c	Quesnel R	Cariboo	93A/12	52.669	-121.961	exploration	2-10	4	inter-lg	f-mS	w
16a	Dease Cr	Dease L	104J/9E	58.656	-130.177	production	1-2	2	bl	fS	w
16b	Dease Cr	Dease L	104J/9E	58.656	-130.177	production	1-2	1	bl	fS	w
17a	Swift R	Cariboo	93H/04W	52.900	-121.977	exploration	1	3	bl	fS	w
17b	Swift R	Cariboo	93H/04W	52.900	-121.970	exploration	1	3	bl	fS	w
18	Swift R	Cariboo	93A/13E	52.887	-121.586	exploration	< 1	4	g	fS	w
19	Tulameen R	Similkameen	92H/7, 10	49.500	-120.668	exploration	1	4	inter	S-G	p
20	Government Cr	Cariboo	93G/7	53.448	-122.559	exploration	0.2	4	inter-bl	f-mS	w
21	Fraser R	Cariboo	92O/1E	51.172	-122.085	testing	0.2	3	bl	fS	w
22	Tulameen R	Similkameen	92H/7	49.478	-120.631	exploration	2	3	bl	mS	w
23	Black Bear Cr	Cariboo	93A/11W	52.633	-121.449	production	6	2	bl	fS	w
24	trib. Wheaton Cr	Dease L	104I/7E	58.333	-129.000	exploration	1-3	3	dg	mS	w
25	Bob Cr	Omineca	93L/7E	54.306	-126.635	exploration	1	4	inter	mS	m-w
26	Mary Cr	Cariboo	93G/1E	53.070	-122.083	exploration	n/a	3	bl	mS	w
27	Boulder Cr	Atlin	104N/11	59.647	-133.399	testing	4	2	bl	mS	w
28	Palmer Bar Cr	Fernie	82G/5	49.440	-115.900	exploration	1-3	2	bl	mS	w
29	Tulameen R	Similkameen	92H/10	49.533	-120.883	testing	n/a	3	bl	mS	w
30	Quesnel R	Cariboo	93B/16E	52.767	-122.150	testing	1.5-2	3	bl	mS	w
31	Jack of Club Cr	Cariboo	93H/4	53.110	-121.576	testing	n/a	3	g	f-mS	p
32	Snake Cr	Atlin	104N/11W	59.583	-133.400	exploration	10	2	bl	f-mS	p
33	Government Cr	Cariboo	93G/7	53.475	-122.549	exploration	n/a	4	dg	fS w/ G	p
36	Similkameen R	Princeton	92H/2	49.219	-120.532	testing	0.2-2	4	inter	f-cS	p

n/a = data not available

[1]Type of Operation (at time of sample concentration): exploration - < 10 m^3 of material removed; testing - 10-100 m^3 of material removed; production - operating mine, often with processing rates provided (e.g. yd/hour, tons/day, etc.)

[2]Fraction: 1 = magnetic fraction only, 2 = non-magnetic fraction only, 3 = both magnetic and non-magnetic fractions, 4 = unknown

[3]Colour: bl = black, br = brown, o = orange, r = red, g = grey, dg = dark grey, lg = light grey, inter = mix of felsic and mafic minerals

[4]Grain Size: Z = silt, fS = fine sand, mS = medium sand, cS = coarse sand; G = granule

[5]Sorting: w = well, m = moderate, p = poor

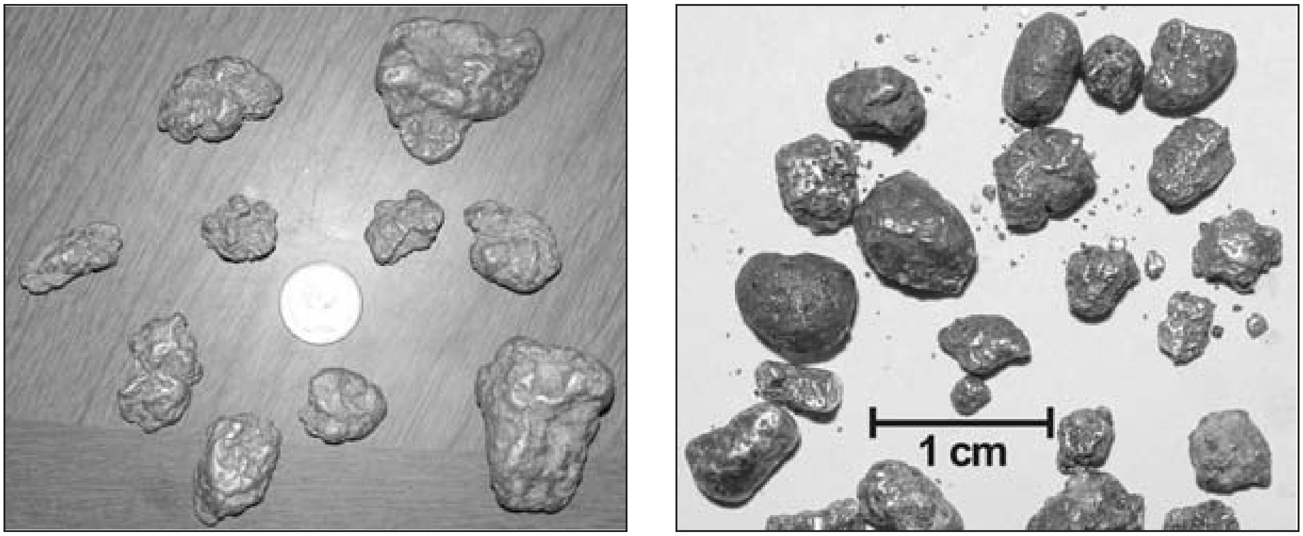

Figure 3. Representative placer mineral samples for size/shape analyses and trace element geochemical studies: 3a) gold nuggets from Birch Creek, Atlin area (Mike Bonnell mine); 25 cent coin for scale; 3b) platinum nuggets from the Tulameen River (supplied by Dave Javorski); note the variety in size, shape, angularity and composition (reflected by color and textural differences).

actual grades). In addition, the results are based on a small sample size and therefore are not representative of the entire deposit or even of a larger volume of the same sample material. In particular, gold and platinum are subject to the "nugget effect". For example, a single large gold grain in the analyzed sample would yield a high gold result even though no gold may occur in the remainder of the sample that was not analyzed. Alternatively, an analyzed sample may show no detectable gold (or platinum) even though nuggets may be present in the remainder of the sample that was not analyzed. For this reason, the larger the sample analyzed the better, and much caution should be exercised in interpreting the significance of small sample results. Samples 15a, b and c provide a good example of the nugget effect. The samples are all from the same site and show little platinum (3-7 ppb) by ICP-MS (Table 3). By fire assay (Table 4), the samples likewise show low levels of platinum (5 and 43 ppb in samples 15c and 15a, respectively) except in sample 15b which contains 358 ppb platinum. These results highlight the fact that a low platinum value in one sample from one location does not preclude the possibility that significant platinum concentrations may still be present at the site.

The following discussion refers to the results of fire assay analyses (Table 4) unless otherwise specified. Platinum was found at 33 of the 37 sites and in 39 of the 45 samples (87% of the samples analysed and 89% of the sites yielded platinum). One additional sample (2001-8) yielded platinum by ICP-MS only (*i.e.* not by fire assay). Palladium was found at 28 sites by fire assay (2 ppb detection level) and at 18 sites by ICP-MS (100 ppb detection level). These data represent a total of 19 new occurrences of platinum in British Columbia (*i.e.* occurrences not reported in MINFILE or by Rublee, 1986). These new occurrences include six areas in the Cariboo region: Mary/Norton Creeks, Castle Creek, Cunningham Creek, Swift River, Black Bear Creek and Jack of Clubs Creek, as well as five new areas in the Atlin region: McKee Creek, Spruce Creek, Pine Creek, O'Donnel River and Snake Creek. Other new platinum occurrences are in the Dease Creek, Alice Shea Creek, Bob Creek (Houston area), Pend Oreille River and Palmer Bar Creek (Fort Steel area) drainages.

New areas with concentrations of platinum in excess of 100 ppb (Tables 3 and 4) occur at Dease Creek (up to 645 000 ppb), O'Donnel River (36 992 ppb), Swift River (three sites - up to 7748 ppb), Spruce Creek (2994 ppb), Mary Creek (1060 ppb), Norton Creek (166 ppb), Black Bear Creek (7321 ppb by ICP-MS), Bob Creek (195 ppb by ICP-MS) and Snake Creek (127 ppb by ICP-MS). Platinum results by fire assay at the latter three sites did not exceed 100 ppb, although for most samples the fire assay results are substantially higher than the ICP-MS results (compare Tables 3 and 4). New areas with levels of platinum between 2 ppb and 100 ppb by fire assay include McKee Creek, Castle Creek, Cunningham Creek (ICP-MS only), Pine Creek, Pend Oreille River, Alice Shea Creek, Palmer Bar Creek and Jack of Clubs Creek (Table 4). Drainages with concentrations of platinum in excess of 100 ppb where PGE's have been previously reported include Slate Creek (up to 51 324 ppb), Government Creek (up to 40 424 ppb), Quesnel River (up to 2489 ppb), Cottonwood River (1568 ppb), Tulameen River (up to 59 744 ppb), Similkameen River (760 ppb), Fraser River (up to 4010 ppb) and Boulder Creek (343 ppb). The presence of platinum was also confirmed at McConnell Creek (Tables 3 and 4).

Stratigraphic and sedimentologic characteristics of PGE placer occurrences were documented at 40 locations throughout BC (Figure 1). Paleoplacer deposits and recent fluvial sediments were studied in the following drainages and areas: Tulameen River, Lawless Creek, Lockie Creek, Blakeburn Creek (tributary of Granite Creek), Rock Creek, Kaslo River, Mobbs Creek, Lardeau River, Franklin Creek, McDonald Creek, Burell Creek, Sappho area, Kaslo River, Thistle Pit, California Gulch, Burns Creek, Grouse Creek, Manson Creek, Slate Creek, Lost Creek, McConnell Creek, Nation River, Wheel Creek, Terry Creek, Fraser River, Sowaqua Creek, Raft Creek, Clearwater River, Quesnel River, Cariboo River, Likely, Keithley Creek, Slate Creek (Figure 2), Rosella Creek, McKee Creek, Ruby Creek, Boulder Creek, Wilson Creek, Wright Creek, and Birch Creek. Detailed case studies to investigate placer proximity criteria and downstream changes in PGE placers were conducted in the Tulameen River, Rock Creek, Slate Creek, and Quesnel River drainages.

For a few samples both magnetic and non-magnetic fractions were analysed (samples 1a, b, 11a, b, 16a, b; Table 5). Results show that both platinum and palladium can occur in significant concentrations in the magnetic fraction (*e.g.* 11 141 ppb Pt and 208 ppb Pd in sample 16b) probably reflecting, for example, the presence of iron in some of the PGE minerals. In sample 11, platinum and palladium concentrations were significantly higher in the magnetic fraction (sample 11a) than in sample 11 b where most of the magnetic minerals had been removed. These results suggest that the common practise of removing and disposing of the magnetic fraction in placer concentrates would be unwise until the PGE content of the magnetic fraction has been thoroughly investigated.

CONCLUSIONS

Preliminary results have identified a surprisingly high number of new areas with anomalous PGE concentrations in placers. A total of 19 new platinum placer occurrences have been identified and concentrations of platinum in excess of 100 ppb occur at nine of these sites. A number of other platinum and palladium occurrences have been verified with laboratory results including 8 sites with up to 100 ppb platinum. The presence of platinum was confirmed and quantified at an additional 14 sites with previously reported PGE placer concentrations. Palladium was detected in samples from 28 sites by fire assay and 18 sites by ICP-MS. Due to the nugget effect, results should be considered with caution and low values of PGE should not be considered insignificant. Preliminary data show that PGE's occur in both the magnetic and non-magnetic/weakly magnetic fractions and, as a result, magnetic concentrates should be evaluated before being discarded. Further work will identify suitable samples for more detailed analysis, determine specific PGE's and PGM's involved, identify new areas with lode source potential and document the stratigraphic, sedimentologic and proximity characteristics of PGE placer occurrences in areas with good potential.

ACKNOWLEDGMENTS

The authors acknowledge those who supplied concentrate samples for analysis including: Sandra Aluisi, Gilbert Anderson, Bjorn Berger, Robert Blom, Jean Pierre Burlot, James Dillon, Don Ferch, Glen Fisher, Thomson George, Paul Gettler, David Gordon, Howard Graham, John Harvey, Tom Hatton, Dennis Hopkins, Gary Hopkins, Andy Horsfield, Patrick Huffman, Wayne Klippert, Lenard Kozak, Roger Lessard, Nick Luschyk, Ronald Mattison, Larry McKay, Barry Pidskalny, Vladimir Pogorevc, Gil Schofield, Bill Schmidt, Peter Shorts, Mike Swenson, Ethel C. Toop, Gary W. Toop, Karl Wabnegger, Steve Wasylenko, Barbara Welsh, Lloyd Worthing and John Zogas. We also thank the following for allowing access to properties and for cooperation in the field: Del Batke, Mike Bonnell, Jennifer and Jillian Bonnell, Stan Brewer, Olmer and Linda Brown, Irvine Broadfoot, Ken Burke, Jean Pierre Burlot, Tex Enemark, Paul Ewaskow, Bob Gauthier, Ed Gordon, Ken Green, Rick Harms, John Harvey, Bud Hellekson, Ken and Ila Herron, Jack Howard, Wayne Klippert, Ron Kohlman, Gord McCauley, Vladimir and Melissa Pogorevc, Jerry Renfro, Dan Rice, Frances Robertson, Joe Sentes, Peter Shorts, Jim Thomas, Jerry Unrau, Bud Wilkinson, Chris and Celine Winther, Lloyd Worthing and John Zogas. In addition, numerous others submitted concentrate samples that have not yet been analysed. We thank them for their cooperation and we will fully acknowledge their contributions when those results are published.

REFERENCES

Bowles J.F.W., Lyon, I.C., Saxton, J.M. and Vaughan, D.J. (2000): The origin of platinum group minerals from the Freetown intrusion, Sierra Leone, inferred from osmium isotope systematics. *Economic Geology,* Volume 95, pages 539-548.

Cabri L.J., Harris, D.C. & Weiser, T.W. (1996): Mineralogy and distribution of platinum-group mineral (PGM) placer deposits of the world. *Exploration and Mining Geology,* Volume 5(2), pages 73-167.

Chapman, R.J., Leake, R.C., Moles, N.R., Earls, G., Cooper, C., Harrington, K. and Berzins, R. (2000): The application of microchemical analysis of alluvial gold grains to the understanding of complex local and regional gold mineralization: a case study in the Irish and Scottish Caledonides. *Economic Geology,* Volume 95, pages 1753-1773.

Cook, S.J. and Fletcher, W.K. (1993): Distribution and behavior of platinum in soils, sediments and waters of the Tulameen ultramafic complex, southern British Columbia. *Journal of Geochemical Exploration,* Volume 46, pages 279-308.

Cook, S.J. and Fletcher, W.K. (1994): Platinum distribution in soil profiles of the Tulameen ultramafic complex, southern British Columbia. *Journal of Geochemical Exploration,* Volume 51, pages 161-191.

Foley, J.Y., Light, T.D., Nelson, S.W. & Harris, R.A. (1997): Mineral occurrences associated with mafic-ultramafic and related alkaline complexes in Alaska. *Economic Geology,* Volume 9, pages 396-449.

Gornostayev, S.S., Dodatko, A.D., Laajoki, K.V.O. and Mochalov, A.G. (2000): Origin of platinum bearing placers in the Aluchin horst, Russian far east. *Economic Geology,* Volume 95, pages 549-558.

Hulbert, L.J. (2001): GIS maps and databases of mafic-ultramafic hosted Ni, Cu-Ni, Cr+/- PGE occurrences and mafic-ultramafic bodies in British Columbia. *Geological Survey of Canada,* Geoscience Map 2001-2, CD ROM.

Knight, J. B., Morison, S. R., and Mortensen J. K. (1999a): The relationship between placer gold particle shape, rimming, and distance of fluvial transport as exemplified by gold from the Klondike District, Yukon Territory, Canada. *Economic Geology,* Volume 94(5), pages 635-648.

Knight, J. B., Mortensen, J. K. and Morison, S. R. (1999b): Lode and placer gold composition in the Klondike District, Yukon Territory, Canada: implications for the nature and genesis of

Klondike placer and lode gold deposits. *Economic Geology,* Volume 94(5), pages 649-664.

Lefebure, D.V. (2000): Potential for palladium and platinum deposits in British Columbia. *British Columbia Ministry of Energy and Mines*, Geofile 2000-5, 11 pages.

Levson, V.M. and Morison, S. (1995): Geology of placer deposits in glaciated environments; *in* Past Glacial Environments - Sediments, Forms and Techniques, J. Menzies, Editor, *Butterworth-Heinemann,* Chapter 16, pages 441-478.

Levson, V.M. and Giles, T.R. (1993): Geology of Tertiary and Quaternary gold-bearing placers in the Cariboo Region, British Columbia. *British Columbia Ministry of Energy and Mines*, Bulletin 89, Victoria, 202 Pages.

Levson, V.M. and Blyth, H. (2001): Formation and preservation of a Tertiary to Pleistocene fluvial gold placer in northwest British Columbia. *Quaternary International*. Volume 82, pages 33-50.

Ministry of Energy and Mines. (2000): Platinum group element mineral occurrences in British Columbia. *British Columbia Ministry of Energy and Mines*, Geofile 2000-2.

Munitions Resources Commission (1920): Platinum mineral investigations; *in* Final Report of the Work of the Commission, *Industrial and Technical Press,* pages 134-194.

Nixon, G.T., Cabri, L.J. & Laflamme, J.H.G. (1990): Platinum-group-element mineralization in lode and placer deposits associated with the Tulameen Alaskan-type complex, British Columbia. *Canadian Mineralologist,* Volume 28, pages 503-535.

Nixon, G.T. and Hammack, J.L. (1991): Metallogeny of ultramafic-mafic rocks in British Columbia with emphasis on the platinum-group elements. *British Columbia Ministry of Energy and Mines*, Paper 1991-4, pages 125-161.

Nixon, G.T., Hammack, J.L., Ash, C.A., Cabri, L.J., Case, G., Connelly, J.N., Heaman, L.M., Laflamme, J.H.G., Nuttall, C., Paterson, W.P.E. & Wong, R.H. (1997): Geology and platinum-group element mineralization of Alaskan-type ultramafic-mafic complexes in British Columbia. *British Columbia Ministry of Energy and Mines*, Bulletin 93, 141 pages.

O'Neill, J.J. and Gunning, H.C. (1934): Platinum and allied metal deposits of Canada. *Geological Survey of Canada,* Economic Geology Series, Number 13, 165 pages.

Rublee, V.J. (1986): Occurrence and distribution of platinum-group elements in British Columbia. *British Columbia Ministry of Energy and Mines*, Open File 1986-7, Victoria, 94 Pages.

Youngson, John H. and Craw, Dave. (1999): Variation in placer style, gold morphology, and gold particle behavior down gravel bed-load rivers: an example from the Shotover/Arrow-Kawarau-Clutha River system, Otago, New Zealand. *Economic Geology,* Volume 94(5), pages 615-634.

Tantalum Market and Resources: An Overview

By George J. Simandl

KEYWORDS: *Tantalum, Industrial Minerals, resources, market, Niobium, carbonatite, pegmatite, specialty granite, peralkaline.*

INTRODUCTION

This paper highlights the world tantalum market, identifies classical tantalum-bearing deposit types that represent major tantalum resources and provides examples of each type. A global approach is required to put potential unconventional tantalum resources, such as some of the British Columbia carbonatites, into proper context.

Recent interest in tantalum is due to increases in spot prices for tantalum raw materials which during 2000 reached US$145 to 175/lb of contained Ta_2O_5 (Platt's Metals Week) and as much as US$ 350 /lb which was the bid rate for the Oct 2000 Davis Langdon Australia (DLA) Tender. As a result, exploration companies targeted a variety of pegmatites, specialty granites, alkaline complexes and carbonatites as possible sources of tantalum.

All these lithologies are enriched in tantalum, relative to the earth's crust, and with the exception of carbonatites are known to host deposits where tantalum is being recovered, at least as a by-product. Carbonatites are well known for associated niobium, REE, phosphate, vermiculite, fluorite, zirconium, uranium, thorium, titanium, copper and iron mineralization (Richardson and Birkett, 1996a; Birkett and Simandl, 1999); several carbonatite-hosted deposits contain relatively high tantalum concentrations.

British Columbia has favorable geological settings for tantalum exploration and is known for a large number of carbonatites and alkaline complexes. It also has a number specialty granite intrusions and pegmatite occurrences (Pell, 1994; Pell and Hora 1990). Tantalum-related mineral occurrences are documented in the BC MINFILE <www.em.gov.bc.ca/Mining/Geolsurv/Minfile>.

TANTALUM USE

Tantalum has a wide variety of uses (Perron, 1995; Cunningham, 2000). It is a hard, but ductile metal, resistant to acid corrosion, with a high melting point (2996 to 3015 ºC depending on source of information), and high density (16.654 g/cm^3). It is a good conductor of electricity and heat. In recent years over 60% of tantalum raw materials went into production of tantalum oxide powders, which are used mainly in manufacturing of electronic components such as capacitors. Tantalum, together with cobalt, nickel and iron, are key ingredients for superalloys used in space/aviation structures and engine components and marine propulsion systems. Because of its high melting point and its corrosion resistance, tantalum alloys are also used in manufacturing of heat exchangers, evaporators, condensers, pumps and liners for reactors and holding tanks for the chemical industry. Tantalum is inert with respect to the human body and is therefore used in hip and knee replacement systems and in the manufacture of a variety of surgical instruments and appliances. Tantalum carbide is used in cutting and drilling tools and wear-resistant parts

TANTALUM MARKET

According to the Tantalum-Niobium International Study Center, world tantalum product shipments for 1998, 1999 and 2000 totaled 3.259, 3.827 and 4.927 million pounds of contained tantalum respectively (Mosheim, 2001). This represents an increase in production of more than 50% in two years. There are no published prices for tantalum metal or intermediate chemicals. Significant proportions of the processor's requirements are met through long term contracts, however, estimated tantalite concentrate spot prices are listed in Platt's Metals Week. Prices, which include cost, insurance and freight to nearest US port, are listed per pound of contained Ta_2O_5. Dealer quotes 60% combined Ta_2O_5 and Nb_2O_5 content.

Year-end average prices of concentrate, per pound of contained Ta_2O_5, between 1959 and 2001 are shown in Figure 1. The trend is relatively steady and upward, but it has a few sharp spikes, notably in 1979-1980, 1988 and most recently in 2000. In November and December 2000, the spot prices for tantalite concentrate, per pound of contained tantalum pentoxide reached from US$ 145-175/lb. The stellar rise in the spot price of tantalite concentrates in late 2000 was largely due to an increase in a demand in a relatively restricted market. Prices have since moved downward and are currently in the US $ 40-50/lb range (Platts Metals Week, November 28, 2001).

There are regulations on the transport of radioactive materials. These regulations depend somewhat on the country or region concerned. There are tantalum/niobium minerals which can not be moved out of their country of extraction because of their levels of radioactivity. The normal limits quoted are 0.1% U_3O_8 and 0.1% ThO_2 (Wickens, J. A. 2001; personal communication).

Australia accounts for most of the Ta_2O_5 concentrate production. Other significant columbite-tantalite producing countries are Brazil, Canada, China, Ethiopia, Nigeria and Democratic Republic of the Congo. Several other African

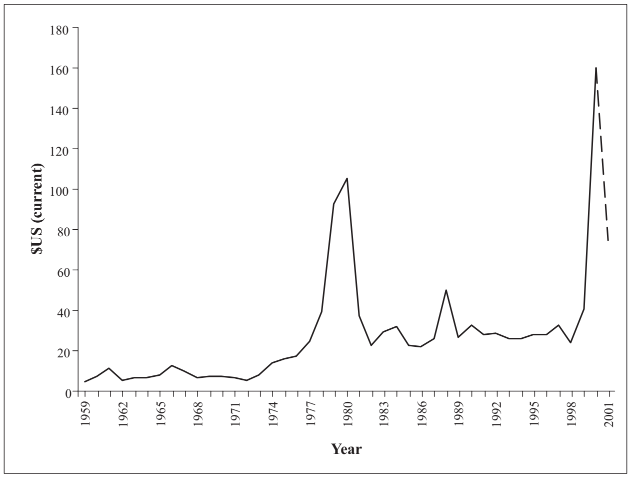

Figure 1: Year-end average tantalum concentrate price per pound of contained Ta_2O_5. The prices are corrected to 2000 US dollars. The price for 2000 is an estimate and the price for 2001 is a projection. Modified from Cunningham (2000).

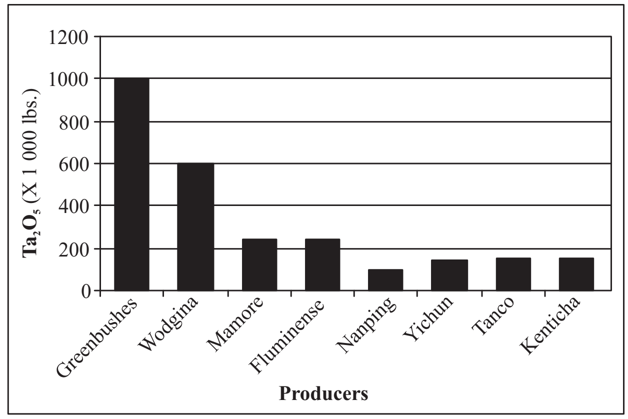

Figure 2. Major Ta_2O_5 concentrate producing mines (source: Sons of Gwalia Ltd.). Greenbushes, Wodgina operations (both in expansion phase) and Tanco are pegmatite-hosted deposits; Nanjing and Yichun and Mamore (Pitinga) are granite related; Kenticha rare metal field, in Ethiopia, contains both granites and pegmatites, in 2001 the production from this locality was greatly reduced because of the legal dispute. Companhia Industrial Fluminense is a unit of Metallurg Inc. It extracts and concentrates Ta and Nb containing ores from Nazareno mine. Concentrates along with other raw materials, are processed into metal oxides at the Sao Joao del Rei plant.

countries, such as Rwanda, Uganda, Zimbabwe, Namibia and Mozambique, also produce concentrates, but no reliable statistics from Africa are available. Ta-bearing slags, legacy of past tin mining in Thailand and Malaysia, were once a major source of tantalum. They are being rapidly depleted and currently supply less than 15% of the world's annual tantalum raw materials. The US Government holds substantial quantities of tantalum-bearing materials, such as tantalum carbide, capacitor grade powder, vacuum-grade metal ingots and ore concentrates in its National Defense Stockpile. Portions of this stockpile were disposed of in 2000 and additional sales were approved for disposal in 2001 (Cunningham, 2001a). Recycling is also an important element of the market (Cunningham, 2001b).

FUTURE MARKET EXPECTATIONS

Tantalum is not entirely irreplaceable; if tantalum prices remain high or shortages persist, then tantalum substitutes will become popular. Ta-based capacitors may have significant advantages over competing products, but in specific segments of the capacitor range they are interchangeable with aluminum, ceramic and niobium varieties. In the past, niobium-based capacitors were considered unstable at current operating temperatures and had substantially higher leakage of current then tantalum-based equivalents.

Recent high tantalum prices prompted. NEC Corp to announce (Press release of July 10, 2001), that it is in position to produce niobium-based capacitors. According to NEC, innovative manufacturing procedures appear to have overcome the stability problem and reduced the current leakage to acceptable level. Vishay Intertechnology Inc. and several European companies are expected to follow with similar products. On the other hand, there are a number of industry players, such as Kemet, that believe that the substitution of Ta_2O_5 by Nb_2O_5 will be limited at current price levels of raw materials.

Niobium is far more abundant and lower priced than tantalum. For example, in November 2000, when the price of tantalite concentrate peaked, the prices for columbite concentrate containing over 65% of combined Nb_2O_5 and Ta_2O_5 was set at US$4.80 to 5.30/lb and steel-making grade ferro-niobium was in range of US$ 6.75-7.00 (Cunningham, 2001c).

It is unlikely that Nb-based capacitors will replace to any large extent the Ta variety; however, the combination of costs of raw materials and technical performance will determine the degree of substitution. If Nb-based capacitors are widely accepted by the electronic industry as a viable substitute for Ta-based ones, the prices of Ta_2O_5-bearing concentrates are likely to further decrease. However, it is possible that the price of the tantalum concentrates will stabilize near pre-2000 year level in the near future.

The likelihood of future Ta_2O_5 shortages is being reduced not only by substitution, but also by production capacity increases of traditional Ta_2O_5 concentrate suppliers and by new exploration and development efforts. For example, Cabot Performance Materials (CPM), a major processor of tantalum, has long-term contracts with Sons of Gwalia Ltd. (SG) currently the world's largest Ta_2O_5 producer. In 2000, SG's combined output from Greenbushes and Wodgina mines was 1.307 million lbs of contained Ta_2O_5 (Figure 2). The A$ 100 million expansion of both mining operations is underway to reach a total capacity of 2.4 million lbs of contained Ta_2O_5 per year (Mosheim, 2001).

CPM plans to double its production capacity of tantalum and niobium products. The expansion started by immediate improvements to an existing electron beam furnace and the purchasse of a 3rd 2400kW electron beam furnace (Anonymous 2001b). The company has also invested in Angus & Ross to explore a deposit within the Motzfeld Centre, South Greenland.

Furthermore, Kemet Corporation, a capacitor producer, invested in the Dalgaranga project in Western Australia (Anonymous, 2001a). The close ties that are currently being developed between miners and downstream users through equity acquisitions and long term contracts may ultimately play an important role in determining which deposits will be developed in the future. At this stage, even major Canadian mining companies are getting a limited exposure to tantalum. This year, SG purchased PacMin Mining Corp. from Teck Cominco Ltd. for cash and shares. The transaction resulted in Teck Cominco holding a 12% stake in SG (Anonymous, 2001c). Placer Dome has ties with Avalon Resources, a company that controls the Separation Rapid pegmatite deposit in Ontario.

WORLD TANTALUM RESOURCES

The Ta content of average upper crust is estimated at 2.1 ppm; average granitic rock contains about 2.3 ppm Ta. Diorite (1.5 ppm), gabbro and basalt (0.9 ppm) and peridotite (<1ppm) have even lower tantalum content (Wedepohl, 1970, Table 73-E-4). Rocks that contain economically significant tantalum concentrations are: pegmatites, specialty granites, alkaline complexes and hyperalkaline rocks, and carbonatites. The only production of tantalum has been from pegmatites and specialty granites. Since the year 2000 rise in tantalite concentrate prices, a number of alkaline complexes and carbonatite occurrences became potential Ta/Nb exploration targets. In some deposits tantalum-bearing concentrate is the main product, but in many cases it is only a byproduct or possible byproduct.

Pegmatite deposits, or their overlying regolith, supply over 70% of world Ta_2O_5 concentrate. The Tanco mine in Manitoba had pre-production reserves of 1.9 million tonnes of 0.216% Ta_2O_5, 6.6 million tonnes of 2.76% Li_2O, 0.3 million tonnes at 23.3 % Cs_2O and 0.8 million tonnes of 0.2% BeO in hard rock (Crouse *et. al*., 1984).

Located in Western Australia, the Greenbushes and Wodgina operations are two of the better-known, world-class deposits with 160 million tonnes grading 0.0214% Ta_2O_5 (with Sn, Li_2O and kaolin as byproducts) and 30 million tonnes at 0.047% Ta_2O_5 respectively. These deposits currently supply the lion's share of the world Ta_2O_5 market (Figure 2).

Significant tantalum resources are contained in **specialty granites**, such as the Beavoir mine in France, which is currently exploited for kaolin and lithium. This deposit is reported to contain a million tonnes of Li at a grade of 1.5% Li_2O, 150 000 tonnes of Sn at a grade of 0.1% Sn, and 20 000 tonnes of Ta at a grade of 0.01% Ta in the upper 300 metres of the host granite (Cuney *et al*.1992). The Orlovka orebody in Russia is another example. A past producer, it had initial resources of 500 tonnes of Ta_2O_5, and 10 000 tonnes of Nb_2O_5, with an average Ta_2O_5 content of 0.013 % (Beskin *et al*., 1994). Yichun and Nanping mines, located in China (Yin *et. all*, 1995 and Mosheim, 2001) are important producers that probably belong to this category (Figure 2). Pitinga mine (Sn, Nb and Ta) orebodies and related placers in Brazil, and Kougarokon deposit on Seaward peninsula in Alaska, which is reported to contain tin and tantalum mineralization, may also belong to this category.

Alkaline Complexes and hyperalkaline rocks host significant tantalum resources (Richardson, D.G. and Birkett, T. 1996b). For example, the "Zone Lake" of the well known Thor Lake property, Northwest Territories has a resource of 64 million tonnes grading 0.04% Ta_2O_5, 0.57% Nb_2O_5, 1.99% REE oxides and 4.73% zirconium (Richardson, D.G. and Birkett, T. 1996b). The Strange Lake deposit located on the Quebec and Labrador border is reported to have a resource of 52 million tonnes grading 3.25% ZrO_2, 0.56% Nb_2O_5, 0.66% Y_2O_3, 0.12% BeO and 1.30% REE oxides (Venkatswaran, 1983). Miller (1988) describes a higher-grade zone with significant Ta_2O_5 content in pegmatite-aplite lenses associated with a roof of a small intrusion within this complex, but no grades and tonnage estimates are given. Within the Motztzfelt Centre, South Greenland, locality 4 has an estimated resource of 38 million tonnes grading 250 ppm Ta_2O_5 or 26 million tonnes grading 350 ppm Ta_2O_5 (Angus & Ross PLC, 2001). The Brockman deposit, located in Western Australia, contains a resource of 4.29 million tonnes grading 1.04% ZrO_2, 0.116% Y_2O_3, 0.44% Nb_2O_5, 0.027% Ta_2O_5, 0.035 % HfO_2, 0.011% Ga and 0.09% REE oxides in tuff (Chalmers, 1990). Unfortunately, the ore minerals are extremely fine grained, most are less than 10 microns in diameter.

Currently, there is no Ta-concentrate production from **carbonatite-related deposits**, although in some cases, tantalum may be recovered by refiners as a niobium byproduct from tantalum-bearing niobium ferroalloy. Two carbonatite-related mineralized zones in Crevier-Lagorce townships, Quebec have a drill-indicated resource of 15.2 million tonnes grading 0.189% Nb_2O_5 and 0.02% Ta_2O_5 (Societé Quebecoise d'Exploration Minière, Annual Report 1981-82). The regolith of the Mount Weld carbonatite in Australia contains resources of 250 million tons grading 18% P_2O_3, 270 million tonnes grading 0.9% Nb_2O_5 and 145 million tonnes grading 0.034% Ta_2O_5 (Duncan and Willett, 1990). The Verity and Fir deposits in the Blue River area of British Columbia, are two more examples that are currently being diamond drilled. Recently, the inferred resource of the Verity-Paradise Carbonatite Complex was reported at 3.06 million tonnes containing 0.0196% Ta_2O_5, 0.0646% Nb_2O_5 and 3.20% P_2O_5 (Commerce Resources Corp. news release, July 25, 2001). Martison Carbonatite, Ontario, containing a resource of 113 million tonnes averaging 21.4 % P_2O_5 is also reported to contain a zone with significant concentrations of Nb_2O_5 and Ta_2O_5.

TABLE 1
TANTALUM/NIOBIUM MINERALS OF ECONOMIC SIGNIFICANCE

Mineral	General formula	$\%Ta_2O_5$	$\%Nb_2O_5$	Density g/cm^3
Microlite	$Ca_2(Ta,Nb)_2O_6(OH,F)_7$	67-70	5-10	6.4
Tantalite	$(Fe,Mn)(Nb,Ta)_2O_6$	42-84	2-40	7.9
Columbite-tantalite	$(Fe,Mn)(Nb,Ta)_2O_6$	20-50	25-60	
Columbite	$(Fe,Mn)(Nb,Ta)_2O_6$	1-40	40-75	5.2
Wodginite	$Mn_4(Sn>Ta,Ti,Fe)_4(Ta>Nb)_8O_{32}$	45-56	3-15	7.1-7.4
Strüverite	$(Ti,Ta,Nb,Fe)_2O_6$	12-13	12-13	5.4
Euxenite	$(Y,Ca,Ce,U,Th)(Nb,Ta,Ti)_2O_6$	2-12	22-30	4.3-5.9
Samarskite	$(Fe,Ca,U,Y,Ce)_2(Nb, Ta)_2O_6$	15-30	40-55	5.2-5.7
Pyrochlore	$(Ca,Na)_2(Nb,Ta,Ti)_2O_6(OH,F)$	<2*	50-70	4.2-4.6

Tantalum minerals of economic significance, their chemical formula, typical Ta_2O_5.and Nb_2O_5 contents and density. Density of minerals is one of the key factors in the selection of processing method required to produce a marketable concentrate. *The Ta content of pyrochlore, given here, is representative of niobium ores. In some deposits, such as Fir and Verity, British Columbia, pyrochlores have much higher Ta content.

ORE DRESSING - TRADITIONAL TA ORE MINERALS VERSUS PYROCHLORE SUBGROUP:

Tantalum is commonly present in a variety of rock-forming minerals, including iron and iron titanium silicates and oxides. The average tantalum content and the average Nb/Ta ratio reported by Wedepohl (1970) for selected rock-forming minerals is indicated in parentheses: biotite (10.1 ppm Ta; Nb/Ta = 11.3), muscovite (14.2 ppm Ta; Nb/Ta = 5.6), pyroxene (6.5 ppm Ta; Nb/Ta = 6.5), hornblende (7.2 ppm Ta; Nb/Ta = 9.8), titanite (330 ppm Ta; Nb/Ta = 11.5), titanomagnetite (100 ppm Ta; Nb/Ta = 6.8), ilmenite (250 ppm Ta; Nb/Ta = 6.4), perovskite (447 ppm Ta; Nb/Ta = 11.3), and zircon (38 ppm Ta; Nb/Ta = 1.0).

The main, economically important, tantalum ore minerals are tantalite columbotantalite (columbite-tantalite group), columbite, wodginite, microlite (Ta-rich mineral of the pyrochlore group) and strüverite. The chemical formula, typical compositional range and the density of these tantalum ore minerals and of pyrochlore are given in Table 1. Simpsonite ($(Al_4Ta_3O_{13}(OH))$ and stibiotantalite ($SbTaO_4$) are less important tantalum-bearing ore minerals. Columbite-tantalite minerals are the most widespread of Ta-Nb minerals, in some occurrences they are replaced by fersmite or microlite. Pyrochlore group minerals are commonly divided into three subgroups: a) pyrochlore (Nb+Ta>2Ti and Nb>Ta), b) microlite (Nb+Ta > 2Ti and Ta > Nb or Ta = Nb) and c) betafite **(**2Ti > Nb+Ta or 2Ti = Nb+Ta**)**. These subgroups may be further subdivided (Hoggarth, 1977), but this is outside the scope of this paper.

Minerals of the pyrochlore subgroup are commonly considered as niobium ores. In unusual circumstances, pyrochlore subgroup minerals may contain high, potentially economic concentrations of tantalum.

There are also other minerals, mostly oxides, that contain much higher tantalum concentrations than rock forming minerals, but they are not as widespread as the minerals listed in Table 1. In specific cases, these minerals may contribute significantly to the tantalum content of the ores and are considered as ore minerals. On the other hand, some of these minerals, especially those that are secondary in nature, may adversely affect the recovery of primary ore minerals during processing.

Pegmatites are currently the main source of Ta_2O_5 concentrates. Pegmatites generally have a significantly higher Ta/Nb ratio than carbonatites. Columbotantalite, wodginite, microlite and strüverite are dense (table 1); consequently Ta-bearing concentrates from pegmatites are produced mainly by relatively simple gravity separation methods, although flotation and magnetic separation may be used as secondary methods. Good descriptions of tantalum ore concentration processes are provided by Burt (1979,1988) and Flemming *et al*. (1982)._Tantalum concentrates usually grade 25% Ta_2O_5 or higher with Ta:Nb ratio greater than unity. The very best concentrates reach 65% Ta_2O_5 with <5% Nb_2O_5, while typical Central African material can go as low as 25%Ta_2O_5 and 40% Nb_2O_5.

Ta_2O_5 may be recovered as a byproduct of Nb_2O_5 production from columbite concentrates, if Ta_2O_5 content exceeds 3% (David Henderson, personal communication, 2001). Concentrates with Ta/Nb ratios around 1/10 or higher are commonly purchased by concentrate-processors for Nb_2O_5 and Ta_2O_5 recovery. In most cases, columbite-tantalite concentrate can be transformed into Nb_2O_5 and Ta_2O_5 products using solvent extraction, prior to conversion to pure metals, oxides, ferroalloys or other high purity tantalum and niobium products.

This is not always the case. At the Pitinga tin mine in western Brazil, cassiterite concentrate is the main product, however cassiterite-columbite middlings that are recovered as part of the process are converted into ferro-niobium-tantalum alloy assaying 50% Nb and 5%Ta. Both niobium and tantalum are recovered from this alloy by subsequent processing.

Carbonatites are the most important source of Nb_2O_5 and in general have a lower Ta/Nb ratio than pegmatites. The regolith that in many cases overlies carbonatite protore may grade over 2.5% Nb_2O_5, while hard rock carbonatites rarely exceed 0.6% Nb_2O_5. The most common ore minerals in carbonatites are of the pyrochlore subgroup and niobium-rich members of columbite-tantalite suite (Table 1). The recovery of minerals of the pyrochlore subgroup from carbonatites commonly necessitates flotation or consists of a combination of physical processing and flotation. A well documented example of such a beneficiation process is the Niobec plant in Quebec (Biss, 1982). Pyrochlore concentrates (55 to 65% Nb_2O_5) are converted directly on site, typically by aluminothermic reduction, to ferroniobium. Villeneuve and Dénommé (1997) summarized the process. Little or no pyrochlore concentrate is sold on the open market. There is no routine recovery of Ta_2O_5 from pyrochlore concentrate, which typically contains 800-2000ppm Ta_2O_5 (David Henderson, personal communication, 2001), although in some exceptional cases it may contain 2 to 5% Ta_2O_5. In such circumstances, tantalum recovery from pyrochlore concentrates may be justified.

Depending on the Ta/Nb ratio of concentrate, solvent extraction could probably be used prior to conversion to ferroalloys and other high purity niobium and tantalum products. If Ta/Nb ratio of a concentrate is low, it may be advantageous to produce a niobium-tantalum alloy as described above for the Pitinga tin mine.

DISCUSSION

The stellar rise in the spot price of tantalite concentrates experienced in late 2000 was largely due to an increase in a demand in relatively restricted market. Since the end of 2000, there has been a significant increase in the production of Ta_2O_5 from conventional sources and strong efforts to recover Ta as a byproduct are also being made. Rapid technological advances are starting to permit substitution of tantalum by other materials even in the field of capacitors. The spot price of Ta_2O_5 has not yet stabilized and in the short term prices are on their way down. It is unlikely that the prices of November and December 2000, will be reached again in the foreseeable future. In short term growth in Ta_2O_5 may be affected by economic slowdown, but in medium and long-term tantalum consumption is expected to continue to grow.

Conservative prices for Ta_2O_5 concentrates should be used in conceptual and pre-feasibility studies. Furthermore, discovery and development of a single large and high-grade tantalum deposit could dramatically change the market situation for years to come.

There are no established guidelines or rules of thumb, as far as evaluation of carbonatite-hosted deposits as a potential primary source of Ta_2O_5-bearing concentrate. Published grade and tonnage data from pegmatite-hosted deposits, as those listed in the previous section, could possibly be used as a starting point but not as a yardstick. The carbonatite deposits under consideration as a potential Ta_2O_5 source, should compare favourably with the more traditional resources in terms of grades, tonnage, mining and processing costs. In general, if Ta_2O_5 is to be recovered from pyrochlore-rich ores, flotation is likely to be needed to produce concentrate and capital costs may be higher.

If the Ta/Nb ore minerals have a high U_3O_8 and ThO_2 content, or high levels of other environmentally problematic impurities, disposal of tailings and/or slags could be a potential problem and cross border transportation of the concentrate may also be a problem.

Key parameters for developing a carbonatite-hosted tantalum mine are: favourable permitting conditions, acceptable environmental constraints, favourable market conditions, infrastructure requirements, open pit mineable reserves in tens of million tonnes, simple mineralogy, and ability to supply concentrates with Ta:Nb ratio of at least around 1:10 .

SUMMARY

Tantalum demand has grown at a rapid pace over the last few years, however, the market base for this commodity is relatively small. Recent expansions of operations supplying Ta_2O_5 concentrate and heavier reliance on long-term contracts between tantalite concentrate suppliers and processors greatly diminished the significance of variations in Ta spot prices. As more and more Ta_2O_5 is sold under contract, the swings in spot prices are expected to be wider but in reality their impact will be less important because of the small amount of product affected.

If a shortage or a prolonged rise in tantalum prices occurs, some of the new tantalum exploration projects will be developed. However, it is likely that substitution of tantalum by cheaper materials, where possible, will also occur in the electronics and other industries.

Future tantalum and niobium markets are the most important factors that will determine the potential of carbonatites and other unconventional resources as a source of tantalum.

It is conceivable, that under favourable market conditions, carbonatites (or alkaline complexes) with favorable grades and high Ta/Nb ratios may supply concentrates or ferroniobium from which tantalum could be economically recovered as a byproduct of niobium. These unconventional deposits will have to compete for part of the tantalum market with pegmatite and specialty granite-hosted resources that require relatively simple processing, and are proven to be viable operations even at the pre-2000 tantalum prices.

ACKNOWLEDGMENTS:

Richard Burt of Cabot Corporation improved the section on mineral processing. David Lefebure, Brian Grant and Garry Payie of the British Columbia Ministry of Energy and Mines and improved clarity of this manuscript. Jody Dahrouge of Commerce Resources Ltd. and Mike Cathro of

the British Columbia Ministry of Energy and Mines provided helpful comments.

REFERENCES

Angus & Ross PLC (2001): Application to Trading on the Alternative Investment Market of the London Stock Exchange; 47 pages.

Anonymous (2001a): Kemet Closes Australian Tantalum Deal; Mining Journal, London, April 20, page 302.

Anonymous (2001b): Cabot Doubling Tantalum Production; Plats Metals Week, 28-May, page 9.

Anonymous (2001c): Teck has deal for PacMin Gold Unit; *Globe and Mail*, Report on Business, October 1. 2001, page B2.

Beskin, S.M., Zagorskii, V.E., Prokof'ev, V.Yu. et al. (1994): Etyka, a Rare-metal Ore Field in East Transbaikalia ; *Geologiya Rudnykh Mestorozhdeniy.* (in Russian), Number 4, pages 310-325.

Biss, R. (1982): Pyrochlore Ore Beneficiation at Les Services TMG Inc. (Niobec) Concentrator; *Canadian Mining Journal*, August 1982, pages 17-25.

Birkett, T.C. and Simandl, G.J. (1999): Carbonatite-associated Deposits (Magmatic, Replacement and Residual); in Selected British Columbia Mineral Deposit Profiles, Volume 3, Industrial Minerals, G.J. Simandl, Z.D. Hora and D.V. Lefebure; Editors, *British Columbia Ministry of Energy and Mines*, pages 73-76.

Burt, R.O. (1979): Tantalum Mining Corporations Gravity Concentrator - Recent Developments, *Bulletin of the Canadian Institute of Mining and Metallurgy*, Volume 72, pages 103-108.

Burt, R.O. (1988): A review of the beneficiation of tantalum ores. An international Symposium on Tantalum and Niobium. *Tantalum Niobium International Study Centre,* Brussels..

Chalmers, D.J. (1990): Brockman Multi-metal and Rare Earth Deposit; in Hughes, T.E. Editor; Geology of Mineral Deposits of Australia and Papua New Guinea. Volume 1, *The Australian Institute of Mining and Metallurgy*, Melbourne, pages 707-709.

Crouse, R.A., Černý, P., Trueman, D.L. and Burt, R.O. (1984): The Tanco Pegmatite, Southeastern Manitoba; in: The Geology of Industrial Minerals in Canada; Editors G.R. Guillet and W.Martin; The Canadian Institute of Mining and Metallurgy, Special Volume 29, pages 169-176.

Cuney, M., Marignac, C. and Weisbrod, A. (1992): The Beauvoir Topaz-Lepidolite Albite Granite (Massif Central, France): The Disseminated Magmatic Sn-Li-Ta-Nb-Be Mineralization, *Economic Geology*, Volume 87, pages 1766-1794.

Cunningham, L.D. (2001a): Tantalum; *US Geological Survey*, Mineral Commodity Summaries, pages 164-165.

Cunningham, L.D. (2001b): Tantalum Recycling in the United States in 1998; *US Geological Survey,* Open File Report OF-01-349, 10 pages,

Cunningham, L.D. (2000): Columbium (Niobium) and Tantalum; Minerals Yearbook, *US Geological Survey*; Volume 1. Metals and Minerals, pages 22.1-22.8:

Cunningham, L.D.(2001c): Columbium (Niobium); *U.S. Geological Survey*, Mineral Commodity Summaries, pages 50-51.

Duncan, R.K. and Willett, G.C. (1990): Mount Weld Carbonatite; in: Hughes, T.E. Editor; Geology of Mineral Deposits of Australia and Papua New Guinea; *The Australian Institute of Mining and Metallurgy*, Melbourne, pages 591-597.

Flemming, J., Mills, C. Burt, R.O. (1982): TANCO's Rare Metal Concentrator; *Canadian Mining Journal*, Volume 103, pages 40-47.

Henderson, D. (2001): Personal communication; Vice President and Director, *Tantalum Operations, Metallurg International Resources* LLC

Hogarth, D.D. (1977): Classification and Nomenclature of the Pyrochlore Group. *American Mineralogist*, Volume 62, pages 403-410.

Kalvig, P. and Appel, P.W. U. (1994): Greenlandic Mineral Resources for Use in Advanced Materials; *Industrial Minerals*, Number 9, pages 45-51.

Miller, R.R. (1988): Yttrium (Y) and other rare metals (Be, Nb, REE, Ta, Zr); in Labrador. Current Research, New Foundland Department of Mines and Energy, Mineral Development Division, Report 88-1, pages 229-245.

Mosheim, C.E. (2001): Tantalum; *in*: Mining Annual Review 2001, *The Mining Journal Ltd.*, CD-Rom, pages Tantalum 1-5.

Pell, J. (1994): Carbonatites, Nepheline Syenites, Kimberlites and Related Rocks in British Columbia; *British Columbia Ministry of Energy and Mines*, Bulletin 88, 133 pages.

Pell, J. and Hora, Z.D. (1990): High-tech Metals in British Columbia; British Columbia; *British Columbia Ministry of Energy and Mines*, Information Circular 1990-19, 28 pages.

Perron, L. (1995): Tantalum: Canadian Minerals Yearbook, *Natural Resources Canada*, pages 21.15-21.19.

Ramsden, A.R., French, D.H. and Chalmers, D.J. (1993): Volcanic-hosted Rare-metals Deposit at Brockman, Western Australia, Mineralogy and Geochemistry of the Niobium Tuff; *Mineralium Deposita*, Volume 28, pages 1-12.

Richardson, D.G. and Birkett, T.C.(1996a): Carbonatite associated Deposits; In Geology of Canadian Mineral Deposit Types, O.R.Ecstrand, W.D. Sinclair and R.I. Thorpe, Editors, *Geological Survey of Canada*, Geology of Canada, Number 8, pages 541-558.

Richardson, D.G. and Birkett, T.C. (1996b): Peralkaline Rock-associated Rare Metals;
In Geology of Canadian Mineral Deposit Types, O.R.Ecstrand, W.D. Sinclair and R.I. Thorpe, Editors*, Geological Survey of Canada*, Geology of Canada, Number 8, pages 523-540.

Venkatswaran, G.P. (1983): A Report on the Geological. Geophysical, and Geochemical Assessment Work, Licenses 1368-1370 and 12128-12131, Strange Lake Area, Newfoundland-Labrador, N.T.S. Sheet 24A/8. Unpublished Report, *Iron Ore Company of Canada.*

Villeneuve, D. and Dénommé, E. (1997): From Ore to Ferroalloy at Niobec Mine: The role of the Geologist in ISO 9002 Implementation; *Bulletin of the Canadian Institute of Mining and Metallurgy*, Volume 90, Number 1007, pages 43-47.

Wedepohl, K.H. (1970): Tantalum; in: K.H. Wedepohl, Executive Editor, *Handbook of Geochemistry*, Volume II-5, Springer-Verlag Berlin, pages 73-A-1 to 73-O-1.

Wickens, J.A. (2001): Secretary General; Tantalum-Niobium International Study Center, Brussels, Belgium. Personal communication.

Note on Desorption Results of Comox Formation Coals from the Courtenay Area, Vancouver Island, British Columbia

By Barry Ryan

INTRODUCTION

There has been increasing interest in the coalbed methane (CBM) potential in the coalfields of British Columbia and some of this interest has been directed at the Comox Basin on Vancouver Island. The CBM resource of the basin has been estimated by a number of authors using published coal data. Most recently by Ryan (2001) quotes a potential resource of 0.8 tcf. These estimates are indeed estimates of the potential resource. Any estimate that is of use for an economic evaluation requires detailed information on gas contents and gas permeability of coal seams. This paper documents some new gas content data for coals from the Comox Basin.

A CBM resource assessment requires drilling, collection of coal samples and a battery of tests. Some of these tests are fairly simple and could, in fact, be included in an exploration program designed to prove reserves for surface or underground coal mining. Other tests are obviously specifically part of a CBM exploration program. Canister tests, which provide estimates of the amount and composition of the gas adsorbed by coal samples, may be part of a coal exploration program, because results impact considerations of mining safety, ventilation and greenhouse gas emissions. On the other hand the results provide the starting point for a realistic CBM resource assessment.

Priority Ventures Ltd. undertook a coal exploration program in the Courtenay area permitted under the mines act and coal regulations. The approval to drill was granted in part on the understanding that the program would not exceed the bounds of what could be expected to be part of a coal exploration program. Data collected by the company have to be submitted to the British Columbia government, but remains confidential for 3 years as specified by the Coal Act Regulations. After three years the data becomes public, with the exception of coal quality information obtained from washed coal samples. The canister tests discussed in this paper were performed at no cost to the company by the author on behalf of the British Columbia Ministry of Energy Mines. In this situation, the company gets data at no cost but looses the right to keep it confidential for an extended period, because the government is obliged to make the information public in a timely fashion. Obviously this applies only to data collected by the government and not other aspects of the exploration program.

The paper presents the gas content and composition data collected from 12 canister tests of samples collected from the three holes drilled by Priority Ventures. Sample depths range from 254 to 486 metres. Gas contents on an as-received basis range from 2.1 to 7.4 cc/g and from 3.6 to 12 cc/g on a dry ash-free basis (daf).

REGIONAL GEOLOGY

The Nanaimo Group, which contains the coal measures of Vancouver Island, is Late Cretaceous (Turonian to Maastrichtian) in age. It was deposited in the Late Mesozoic to Cenozoic sedimentary Georgia basin, which overlaps the Coast and Insular belts of the Cordillera. Deposition of the Nanaimo Group correlates with a period of rapid subsidence, which led to the accumulation of over 5 kilometres of sediments by the close of the Cretaceous (England and Bustin, 1995). Much of the Nanaimo Group in the Mount Washington area near Courtenay is in tectonic contact with the Triassic basement (Muller, 1989), which is often represented by the Karmutsen Volcanics. In places the basement surface is intensely weathered and the resulting lateritic deposits are zones of localized shearing. The group was deformed by the Cowichan fold and thrust system, which is composed of a number of northwest-trending, southwest-verging thrusts, that account for a 20% to 30% shortening of the Nanaimo Group cover over the Wrangellian basement (England and Calon, 1991). This contraction is indirectly dated as Late Eocene.

The Nanaimo Group outcrops in two coal basins on the east side of Vancouver Island (Figure 1). The Nanaimo basin is centered on the town of Nanaimo and covers an area of approximately 780 square kilometres. Between 1849 to about 1950 over 50 million tonnes of coal were extracted from seams in the basin, which is now considered to be largely mined out. The Comox Basin extends from 20 kilometres north of Nanaimo to Campbell River and covers about 1230 square kilometres. Over 15 million tonnes have been mined from the basin in the period 1888 to 1955 (Gardner, 1999) and since then over 6 million tones have been extracted from the Quinsam Mine near Campbell River.

There are at least three coal-bearing formations within the Nanaimo Group (Table 1). The lower Comox Formation outcrops extensively in the Comox Basin, where it is overlain by the Trent River Formation. It occurs at depth in the Nanaimo Basin where it is overlain by marine sediments of the Haslam Formation. The second coal-bearing cyclotherm is marked by the deposition of the Extension and

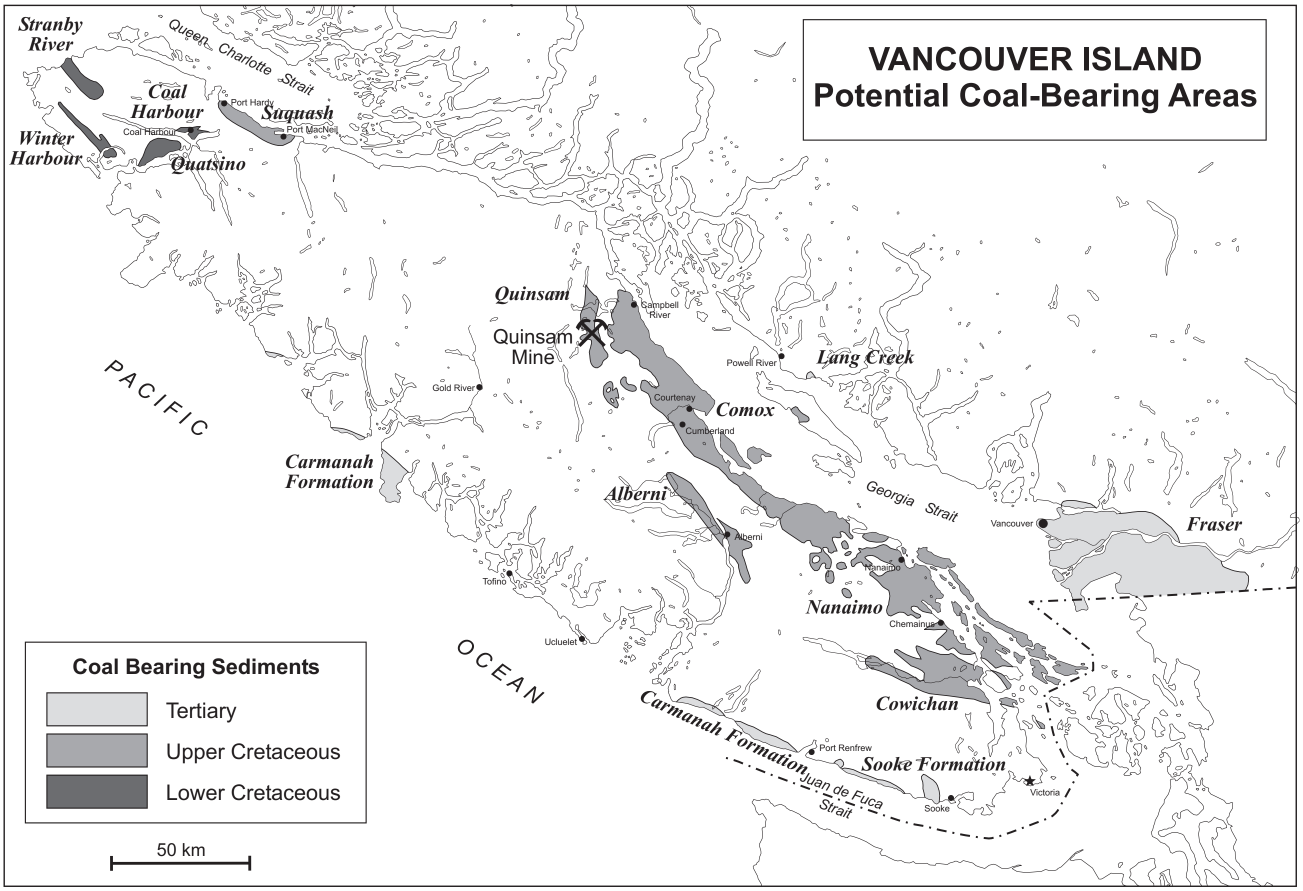

Figure 1. Coal basins of Vancouver Island.

Protection formations, which host the coal seams and mines in the Nanaimo Basin. Coal is reported in the Spray River Formation higher in the Nanaimo Group, but there are no significant deposits (Ward, 1978).

The Comox Formation in the Comox Basin is divided into three members. The lowest Benson Member, which is not always present, underlies or inter fingers with the overlying Cumberland Member, which in turn is disconformably overlain by the Dunsmuir Member. The Benson Member ranges in thickness from 0 to 220 metres and consists of conglomerate, minor red shale and siltstone (Cathyl-Bickford, 1992). The Cumberland Member is composed of 0 to 160 metres of siltstone, shale, minor sandstone and coal. The Dunsmuir Member is composed of 11 to 356 metres of sandstone, minor siltstone and coal.

There are four, economically important seams in the Comox Formation. The lowermost No. 4 seam, which ranges in thickness from 1.2 to 4.5 metres (Cathyl-Bickford, 1991), is in the Cumberland Member near its contact with the underlying Benson member. Near basement highs, where the Benson Member thins, it grades into stony coal or coaly mudstone. The Cumberland Member also contains the Number 3 and the Number 2 seam, which ranges in thickness from 0.8 to 2.2 metres. The Number 1 seam is about 25 metres above the base of the Dunsmuir Member and ranges in thickness from 0.9 to 2.4 metres.

The rank of coals in the Nanaimo and Comox basins is generally high-volatile A bituminous though vitrinite reflectance (Rmax values range from 0.6% to over 2 % near intrusions. In the Quinsam area (Figure 1) rank averages 0.7% (Ryan 1993) with values ranging from 0.53% to 0.85%. Further south in the Comox Basin along Browns River (Figure 2), 8 samples provided an average Rmax% of 1.69% (Kenyon and Bickford, 1989). This location is about 4 kilometres south of the three Priority Ventures drill sites and north and adjacent to an area of Tertiary intrusives. Further south along the Trent River values average 0.84% and between Trent River and Comox Lake values range from 0.84% to 0.99%. In the Tsable River area at the southern end of the Comox Basin Ryan (1996) reports an average of 0.82% and previous values in the area average 0.88%.

LOCAL GEOLOGY

The area explored by Priority Ventures Ltd. is within the Cumberland sub basin of the Comox Basin. An area with a long history of coal mining (MacKenzie, 1922). The three holes were drilled approximately 5 kilometres northwest of Courtenay between the Tsolum and Puntledge rivers (Figure 2). The holes were collared in the Trent River Formation and drilled to a cumulative depth of 1200 metres. In the area a number of members of the Trent River outcrop as well as the Dunsmuir and Cumberland members of the Comox For-

TABLE 1
STRATIGRAPHY OF THE NANAIMO GROUP

	Nanaimo Basin Formations		Comox Basin Formations	
	Campanian			
late Cretaceous	Gabriola		Gabriola	
	Northumberland		Spray River	Coal?
	Northumberland		Geoffrey	
	Northumberland		Lambert	
	De Courcy			
	Cedar District			
	Protection	Coal	Denam	
	Pender			
	Extension	Coal		
	Haslam		Trent River	
	Santonian			
	Comox	Coal	Comox	Coal

mation. A Tertiary intrusion is mapped (Cathyl-Bickford and Hoffman, 1998) approximately 4 kilometres southwest of holes 1 and 3 (Figure 2) and it has increased the rank of coal along the Browns River from 0.79% to 1.69% Rmax (Kenyon and Bickford, 1988). No other reflectance values are published for the area covered by Figure 2. The stratigraphy of the Comox and Trent River formations in the area is discussed by Cathyl-Bickford (2001).

PREVIOUS CBM DATA

There is very little CBM information available for coals on Vancouver Island. Data for the Nanaimo Basin are discussed by Cathyl-Bickford *et al.* (1991), who quote previous references, which provide a range of 5 to 12 cc/g for gas contents in the Douglas Seam. It is not specified if the data is on an as-received or ash-free basis. Gas emission rates range from 8.8 to 128.1 cubic metres/tonne mined. Kissel *et al.* (1973) suggest that for mature mines emission rates divided by 9 provide a rough estimate of gas contents, in which case gas contents range from 1 to 14.2 cc/g. In 1984 Novacorp drilled 14 holes and five intersected the Douglas seam. It has been reported by a number of authors that samples were desorbed but the results have never been published. There are a number of reports of drillers intersecting gassy coals in the Nanaimo and Comox basins (Cathyl-Bickford, 1991) but the reports are not accompanied by desorption data.

There are some desorption data for coals from the Comox Basin. In 1996 Ryan (1997) collected samples from the Tsable River area. Thirteen samples from depths ranging from 127 to 377 metres were desorbed. Gas contents ranged from 2.4 to 6.5 cc/g on a dry-ash free basis. No gas composition analyses were performed. Samples collected from 2 drill holes near the Quinsam Coal Mine in the northern part of the Comox Basin were desorbed in 1993 (Ryan, 1994a). The holes intersected the Number 1 seam at 106 metres and

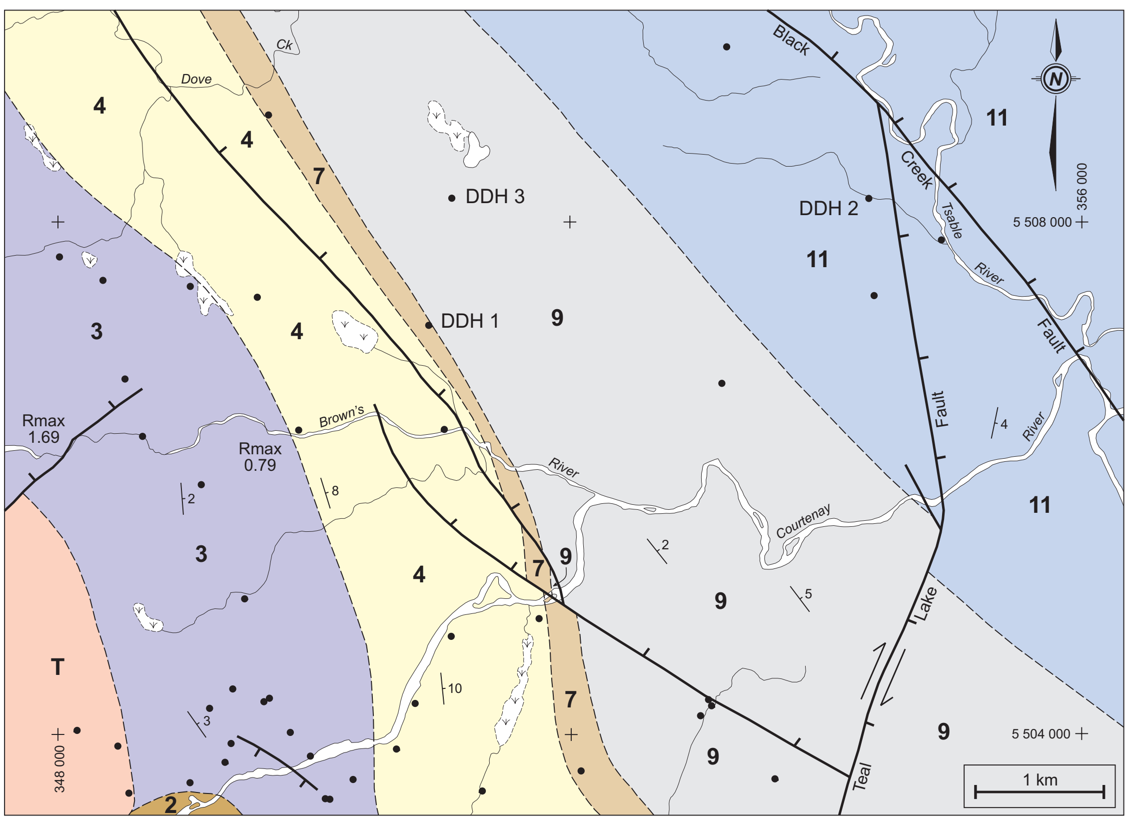

Figure 2. Map of the Comox Basin Courtenay area.

the Number 3 seam at 142 metres. Gas contents were approximately 1 cc/g (dry as-free basis) for 1 seam and from 1 to 1.6 cc/g (dry as-free basis) for the number 3 seam. Based on an adsorption isotherm the seams were under saturated at the shallow depth intersected. The data were collected to provide information for the underground coal mine and not to provide a test for the potential CBM resource of coal in the area.

PROGRAM RESULTS

PROCEDURES

Techniques for desorbing coal in canisters have evolved from those outlined by Kissel *et al.* (1973) to those discussed in McLennan *et al.* (1995). In this study, an excel spread sheet was designed to handle, data input, the multiple corrections to raw data, and curve fitting algorithms (Figure 3). Samples were sealed into canisters capable of holding up to 40 cm of core. Canisters were maintained at about 23ºC and measurements were corrected for the effects of changing temperature and pressure and the effects of water vapour. Data were then corrected to standard temperature and pressure. The spreadsheet calculates cumulative gas contents, gas desorption rates and canister pressure.

Free gas (the gas compressed into the porosity in coal seams) cannot be estimated by canister tests, but there are a number of ways of estimating the amount of gas lost by desorption prior to sealing the samples in canisters. In this study the USBM direct method (McCulloch *et al*., 1975) was used, which plots desorbed gas measurements against the square root of time. Lost times, measured as the time from when the coal was half way up the hole to when it was sealed in a canister, ranged from 10 minutes to 38 minutes and averaged 20 minutes. The amount of lost gas averaged 7.2% of the total gas.

Once the coal was sealed in the canister desorbed gas measurements were made at increasing intervals for periods ranging from 31 to 49 days. After this time, most of the gas had desorbed from the samples and desorption rates were about 0.01 c/g/day. McCulloch *et al*. (1975) suggest that samples should be desorbed in the canisters until the rate is less than 0.05 cc/g/day. The canisters were opened and samples sent for analysis. The remaining desorbable gas was estimated by fitting a desorption curve to the data and projecting to infinite time. The amount of remaining gas averaged 8.3%. The curve used was developed by Airey (1968) and is based on experimental data. The equation:

$$Vt=A^{*}\,(1-e^{\wedge-(t/to)^{\wedge}n})$$

predicts the cumulative gas desorbed (Vt) up to a time t in terms of total desorbable gas (A) and two constants.

to is the time when 63.21% of the total gas (A) has desorbed *i.e.* when t=to Vt/A=(1-1/e). This is in fact the sorption time used in some reservoir simulators for predicting gas production. The term varies based on grain size or degree of fracturing of the coal. By plotting the predicted sorption point on the desorption curve, it is possible to check the agreement of the Airey Curve based on values of A and "to" with the curve defined by the data.

The constant "n" generally does not vary much and is usually in the range 0.3 to 0.4. It does not correspond to the power term discussed by Williams and Smith (1984). The power term they report which is usually approximately 0.5 controls initial desorption ($Vt=D^{*}t^{\wedge Nw}$). The value of Nw can be found by plotting ln(Vt*) versus* Ln(t) where the slope is Nw. For the data presented here the term Nw is approximately 0.5 for all samples ranging from 0.5 to 0.57. Changes in the power term (Nw) can be caused by oxidation of the coal or adsorption of oxygen onto the coal, both effects will tend to decrease the value of Nw.

The Airey Curve was fitted to the data by adjusting values of "n" to fit data points close to the origin and "to" and "A" to fit curve to data points further from the origin. The best fit by eye can be found quickly by setting up the constants to actively change the curve in the gas *versus* time plot in an excel file (Figure 3). Attempts to use a direct mathematical solution for solving for "n" and "to" were not as effective. The fitted curve provided estimates of the total desorbable gas (A) in each sample and the amount of gas left to desorb after the canisters were opened. An additional useful plot is Ln(gas desorption rate*) versus* time (Figure 3). Any problems in the data are immediately apparent as points plot off the trend. Usually this flags minor errors in data entry.

Canisters were purged with argon to eliminate as much air as possible. Spacer pipes were used to decease the void space (dead space) in the canisters. This helps minimize air contamination, but also increases the risk of producing a saw tooth pressure profile as the pressure increases before each desorption measurement. Smaller dead spaces and larger desorbed gas volumes may cause excessive increase in pressure just prior to a measurement. The excel spread sheet calculates the pressure using an estimated dead space or a calculated value. It is generally not possible to measure the dead space until after the canisters are opened. However the manometer used for measuring gas volumes can be used to measure dead space. By lifting the reserve liquid container argon can be pressured by a known amount into the canister. When the argon is released at atmospheric pressure back into the manometer the volume measured and the pressure used to force argon into the canister provide sufficient information to calculate the dead space (Ryan and Dawson, 1994b).

DATA

Approximately 40 cm of core were collected for each canister. To minimize lost time corrections, samples were placed in canisters after minimal description by the project geologist, and as is usual, most of the coal was intersected at night. This in part may explain the variable and sometimes high ash contents of the twelve samples, which range from 8% to 64% (Table2). The gas contents on an as-received basis range from 2.1 cc/g to 7.4 cc/g and on a dry ash-free basis 3.6 cc/g to 12 cc/g.

Sample No 99-99 program uses first 6 readings to estimate lost gas

to change number of points highlight green cells ENTER ---------LINEST(E7:E(7+X),D7:D(7+X),,TRUE) then shft+ctrl+enter

where x is number of data points

excel fills in cells with line fitting details

intercept on Yaxis is lost gas

GAS	LOST	DESORBED	REMAINING	PROJECTED
	initial	measured	left after des test	ultimate
	0.27	2.11	0.38	2.75

HALF LIFE days	1.91	Sorption time hours	135.00	Gas at to	1.74

LOST TIME 0:15 Min

slope	int
0.55	-0.27
0.04	0.03
0.98	0.01
X	Y
0.00	-0.27
0.50	0.01
1.00	0.28
1.50	0.56

head cm	vol ml	dead sp
119.30	205.00	1779.09
120.60	210.00	1802.84
122.20	211.00	1787.71
Average		1789.88

Reading	Cum time	cc /g	sqr time	cc /g	Cm time days	des gas &lost gas	cc/g /day
	0.25	0.00	0.50	0.00	0.01	0.27	0.00
1	0.35	0.06	0.59	0.06	0.01	0.32	13.61
2	0.40	0.08	0.63	0.08	0.02	0.35	10.65
3	0.48	0.11	0.70	0.11	0.02	0.38	8.52
4	0.53	0.15	0.73	0.15	0.02	0.42	20.12
5	0.62	0.17	0.79	0.17	0.03	0.44	5.68
6	0.75	0.20	0.87	0.20	0.03	0.47	5.77
7	1.08	0.26	1.04	0.26	0.05	0.53	4.44
8	1.72	0.35	1.31	0.35	0.07	0.61	3.18
9	3.70	0.51	1.92	0.51	0.15	0.78	1.95
10	7.77	0.67	2.79	0.67	0.32	0.93	0.94
11	10.87	0.73	3.30	0.73	0.45	0.99	0.46
12	18.18	0.80	4.26	0.80	0.76	1.06	0.23
13	24.55	0.87	4.95	0.87	1.02	1.13	0.26
14	31.67	0.93	5.63	0.93	1.32	1.19	0.21
15	38.65	0.97	6.22	0.97	1.61	1.24	0.16
16	44.42	1.03	6.66	1.03	1.85	1.30	0.24
17	59.03	1.11	7.68	1.11	2.46	1.37	0.12
18	69.37	1.15	8.33	1.15	2.89	1.42	0.10
19	82.62	1.21	9.09	1.21	3.44	1.48	0.12
20	92.67	1.26	9.63	1.26	3.86	1.53	0.11
21	105.75	1.36	10.28	1.36	4.41	1.62	0.18
22	115.97	1.40	10.77	1.40	4.83	1.66	0.09
23	129.28	1.44	11.37	1.44	5.39	1.71	0.08
24	140.17	1.48	11.84	1.48	5.84	1.75	0.08
25	152.95	1.51	12.37	1.51	6.37	1.78	0.06
26	164.33	1.54	12.82	1.54	6.85	1.81	0.06
27	177.00	1.57	13.30	1.57	7.38	1.84	0.05
28	199.35	1.63	14.12	1.63	8.31	1.89	0.06
29	225.05	1.67	15.00	1.67	9.38	1.93	0.04
30	249.50	1.69	15.80	1.69	10.40	1.96	0.03
31	273.65	1.73	16.54	1.73	11.40	2.00	0.03
32	297.43	1.76	17.25	1.76	12.39	2.03	0.03
33	320.53	1.79	17.90	1.79	13.36	2.05	0.03
34	344.73	1.81	18.57	1.81	14.36	2.07	0.02
35	368.82	1.83	19.20	1.83	15.37	2.10	0.02
36	393.15	1.86	19.83	1.86	16.38	2.12	0.02
37	424.53	1.88	20.60	1.88	17.69	2.14	0.02
38	448.77	1.89	21.18	1.89	18.70	2.16	0.01
39	516.12	1.93	22.72	1.93	21.50	2.20	0.01
40	645.48	2.00	25.41	2.00	26.90	2.27	0.01
41	859.47	2.06	29.32	2.06	35.81	2.33	0.01
42	981.27	2.11	31.33	2.11	40.89	2.37	0.01
43	0.00	0.00	0.00	0.00	0.00	0.27	0.00
44	0.00	0.00	0.00	0.00	0.00	0.27	0.00
45	0.00	0.00	0.00	0.00	0.00	0.27	0.00
46	0.00	0.00	0.00	0.00	0.00	0.27	0.00
47	0.00	0.00	0.00	0.00	0.00	0.27	0.00
48	0.00	0.00	0.00	0.00	0.00	0.27	0.00
49	0.00	0.00	0.00	0.00	0.00	0.27	0.00
50	0.00	0.00	0.00	0.00	0.00	0.27	0.00

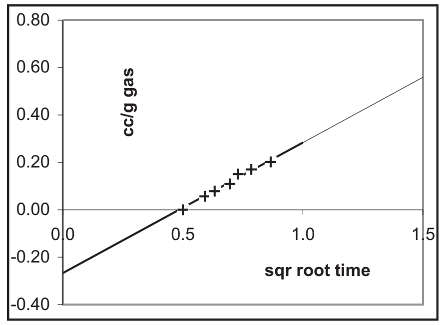

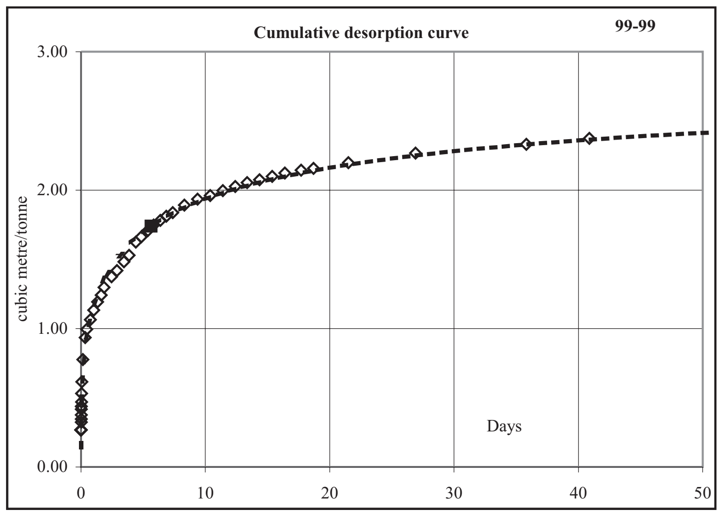

drag XY point in y direction onto curve

Y point is then gas at sorption time (63.2%)

X	Y	Y% of A
5.63	1.74	63.27

Airey const adjust curve to fit data n (0.3-0.4) To hrs A=final vol — n 0.34

to=sorption time — to 135.00

half life in days based on gas content A= 1.91 — A 2.75

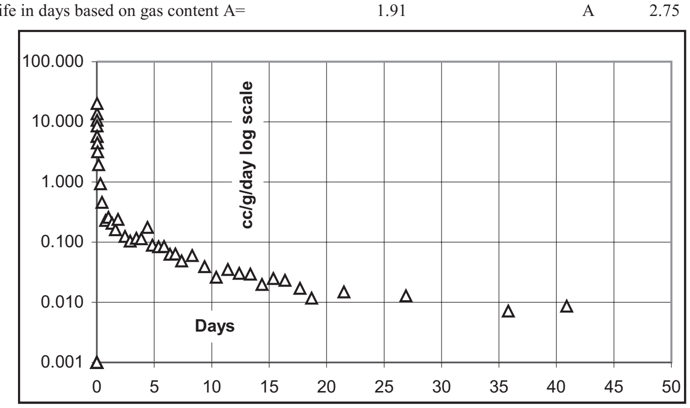

Figure 3. Excel Spread sheet for charting desorption data.

TABLE 2
STRATIGRAPHY OF THE COMOX AND TRENT RIVER FORMATIONS, COURTENAY AREA

Eocene to Oligocene
Mount Washington Intrusive Suite

T	sills and dikes of dacite and quartz diorite

Upper Cretaceous
Nanaimo Group
Campanian

TRENT RIVER FORMATION

11	**Willow Point Member:** shale and siltstone; minor sandstone
9	**Royston Member:** shale and siltstone
8	**Tsable Member:** shale and siltstone
7	**Browns Member:** sandstone and siltstone; locally glauconitic
4	**Puntledge Member:** siltstone and shale; minor sandstone

COMOX FORMATION

3	**Dunsmuir Member:** sandstone; siltstone, shale and coal; minor conglomerate
	Santonian
2	**Cumberland Member:** siltstone and sandstone; coal and shale
	Santonian ?
1	**Benson Member:** conglomerate and sandstone; red shale and siltstone

Upper Triassic
Vancouver Group

V	**Karmutsen Formation:** massive and pillowed basaltic flows; basaltic breccia

Notes: Units 5 and 6 are not recognized within the map area. Units 10a and 10b are probably not present within the map area.

4 Bedding orientation
Geology contact - approximate
Extension fault (ornament on down thrown side)
Strike-slip fault (arrows indicate offset)
Diamond drill hole

The Airey Equation models desorption curves well and values of n, sorption time (to) and total desorbable gas (A) are well defined. The sorption times are short to moderate and correlate inversely with ash content. It appears that coal in thin bands in carbonaceous mudstone tends to be more fractured than thicker low ash coal bands.

A number of samples were collected for gas composition analyses and analyzed on a HP 5710 gas chromatograph. Samples were extracted, using a 50cc syringe, from the manometer feed line adjacent to where it attaches to the canister. The syringe samples were injected into 1litre Tedlar sample bags and sent to B.C. Research Inc. for analysis. Two samples were collected from blow-out-preventors (BOP) on holes 1 and 2. In these cases large plastic exploration sample bags were held over the outlet and allowed to fill. Gas samples were extracted by injecting into the filled bags. Gas composition data (Table 3) indicate that either not all the air was purged out of the canisters or air got into the samples via the manometer or the sampling process. The amounts of gas analyzed are less than 100% because the analysis procedure is not able to measure the argon used to purge the canisters. On average the samples contained 34% air. After correcting the samples for air by removing all the oxygen and air-associated nitrogen based on a volumetric ratio of oxygen/nitrogen= 0.2682, the samples appear to have excess nitrogen. The individual gas composition analyses do not reflect the average gas composition for all the gas desorbed from each canister because the composition of the desorbed gas changes over time as discussed in the next section. However, based on analyses amounts of CO_2 are generally low and less than 10% by volume and average 3%. Methane concentrations range from 9% to 93%. It appears that hole 3 has high nitrogen concentrations. Data from holes 1 to 3 provide averages of 14.1%, 17.7% and 70.3 % nitrogen.

TABLE 3
GAS CONTENT DATA FOR BLOW-OUT-PREVENTOR SAMPLES AND CANISTER SAMPLES

canister	depth top metres	wt ar grams	ar moist	ash% db	mineral matter	lost gas cc/g	desorbed gas cc/g	remaining gas cc/g	total gas cc/g	total gas daf	total gas mmfb
Hole 1											
1	255.2	861	5.8	39.3	42.5	0.62	4.90	0.68	6.20	10.2	10.5
2	298.7	1347	3.0	35.1	37.9	0.25	5.01	0.54	5.80	8.9	9.2
3	299.7	1129	2.7	12.1	13.1	0.24	6.29	0.82	7.35	8.4	8.4
4	325.1	843	3.5	48.0	51.9	0.33	5.43	0.24	6.00	11.5	12.0
5	254.8	1292	6.0	52.5	56.7	0.22	3.10	0.08	3.40	7.2	7.5
Hole 2											
6	485.2	1513	2.3	61.9	66.8	0.32	3.09	0.09	3.50	9.2	9.6
7	486.1	1199	3.6	55.8	60.3	0.33	3.93	0.39	4.65	10.5	11.0
8	512.6	750	4.1	64.4	69.6	0.80	3.10	0.14	4.05	11.4	12.0
Hole 3											
9	237.9	1245	3.0	26.1	28.1	0.11	2.31	0.18	2.60	3.5	3.6
10	237.6	1427	2.7	50.4	54.4	0.11	1.58	0.37	2.05	4.1	4.3
11	297.6	1218	3.6	7.9	8.6	0.23	3.93	0.58	4.75	5.2	5.2
12	298.9	1312	3.2	28.9	31.2	0.19	2.31	0.30	2.80	3.9	4.0

Average Cumberland S%=1.45% from Dolmage and Campbell (1975)
ar = as received moisture daf = dry ash free
dmmf = dry mineral matter free BOP = Blow-out -preventor

DISCUSSION

Dolmage and Campbell (1975) estimate a coal resource of approximately 300 million tonnes to a depth of 1000 metres in the Cumberland sub basin. Based on coal quality data they published for the sub basin, coal has an average Volatile matter daf value of 39% indicating a rank of high-volatile bituminous. In the plot of gas content dmmf basis *versus* depth (Figure 4) a vitrinite reflectance value (Rmax) of 0.9% is used. Samples from holes 1 and 2 appear to be close to saturated based on a predicted gas content using the Ryan Equation (Ryan, 1992). Based on these two holes a gas content of about 8 to 9 c/g (250 to 300 scf/ton) can be assumed for 20% ash coal at about 500 metres. This provides a conservative potential resource of about 0.08 to 0.1 tcf based on a coal resource of 300 million tonnes.

There is evidence that the stratigraphy may be pressured with free gas. This has important implications for the gas content of coal. If the phase in contact with the coal is a CH_4 rich gas rather than water, then it is probable that the coal will be saturated in terms of its ability to adsorb CH_4 and this appears to be the case for coals from the two holes that were over pressured. Coal seams that are in gas pressured stratigraphy will not produce much water during the early stages of production, which will improve the economics of the CBM development. In addition if the porosity in the coal seams is gas filled rather than water filled then there is an additional increment to the total gas that can be produced from the seam. In coal seams the amount of free gas, at any depth, can be calculated using assumed values of porosity, density and a normal hydrostatic gradient. The higher gas content curve (Figure 4) is constructed assuming an additional increment of free gas based on a gas filled porosity of 4%. This might be high for coal, but on the other hand the pressure might be higher than assumed, because there is evidence of over pressuring in holes 1 and 2. It is apparent that at depths greater than 200 metres there could be a significant increment of free gas in the coal seams. The over pressuring could also increase the adsorbed gas content of the seams. Most depth *versus* gas plots assume a normal hydrostatic gradient. An increased gradient would have the effect of producing apparently over saturated samples. The amount of over saturation depends on the constants defining the adsorption curve (Vl and Pl Langmuir constants) or desorption curve (Ryan Equation and Rmax) and the percent increase in the hydrostatic gradient. The amount of over saturation does not change much with depth what ever the curve used. For example in this case an over pressuring of 25% would increase the adsorption capacity at most depths by about 1 cc/g. This increase would be reflected in the desorption results. Adsorption capacity at any rank is very sensitive to

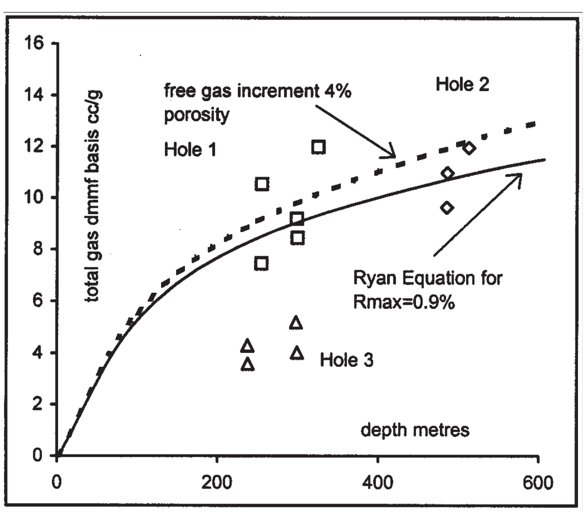

Figure 4. Gas contents (mineral matter free basis) *versus* depth for data from the three holes.

moisture content of coal and it is generally assumed that coals at depth are at equilibrium moisture. However in a situation where there is over pressured free gas in the stratigraphy this might have the effect of reducing the moisture content of the coal and increasing its adsorption capacity.

The ash contents of the samples collected are variable and high, possibly because seams in the Comox Formation sometimes grade laterally into coaly zones. This does not necessarily decrease the CBM resource as long as the amount of carbon in the zone is the same as that in a thinner cleaner seam. In fact a lot of interest is developing in the resource potential of organic rich shales. A 30 metre thick shale bed with total organic carbon of 10% can contain as much gas as a 3.75 metre coal seam.

Samples from hole 3 have unusually high nitrogen contents, which may be an artifact of the sampling process. However there is certainly nitrogen in the stratigraphy as indicated by the composition of the 2 BOP samples and high nitrogen contents may reflect gas compositions in the coal samples. Nitrogen can originate from the sampling process when the oxygen in excess air in the canister is either adsorbed, or chemically bound to the coal by oxidation. This removes oxygen from the gas leaving nitrogen. After correcting for air, using an air oxygen/nitrogen ratio of 0.2682 and the remaining oxygen, there appears to be excess nitrogen in the gas. Oxygen can be adsorbed or can oxidize coal, in which case to some extent CO_2 replaces oxygen in the gas. The samples from hole 3 do not have excessively high CO_2 contents. If the excess nitrogen in samples from hole 3 is caused by adsorption of oxygen in the canisters, then one would expect this to impact the desorption curves. In fact there is no decrease in the power term Nw ($Vt=Dt^{\wedge Nw}$) compared to data from the other holes. On balance it is felt that most of the excess nitrogen probably originates from the coal and surrounding stratigraphy and is not an artifact caused by uptake of oxygen in the canisters. If all the excess nitrogen results from oxidation in the canister, then the percentage of adsorbed oxygen is 19% based on an average of 73% nitrogen in samples from hole 3 and this volume should be added back to the desorption totals. Even a 20% correction to samples from hole 3 is not enough to raise them to the saturation curve in Figure 4.

The high nitrogen contents of the desorbed gases are unusual. Nitrogen is generated as part of the coalification process. Kneuper and Huckel (1972) estimate that 320 scf/ton are released from Carboniferous coals over the rank range of sub-bituminous to anthracite. Scott (1993) estimates from 250 to 500 scf/ton (8 to 15.5 cc/g) are generated during coalification. Coal gas with the highest nitrogen content is found associated with the wet gas generation stage, which occurs in the Rmax range 0.5% to 0.8%. Nitrogen contents in coal gas generally peak at 12% at Rmax 0.7%, with another maximum of 4% nitrogen at Rmax 1.7% (Scott, 1993).

Hole 3 has low total gas contents and high nitrogen contents. If the nitrogen was adsorbed on the coal this would explain the low gas contents because coal has a lower adsorption capacity for nitrogen than CH_4 or CO_2. Nitrogen can originate from the coalification process or from igneous ac-

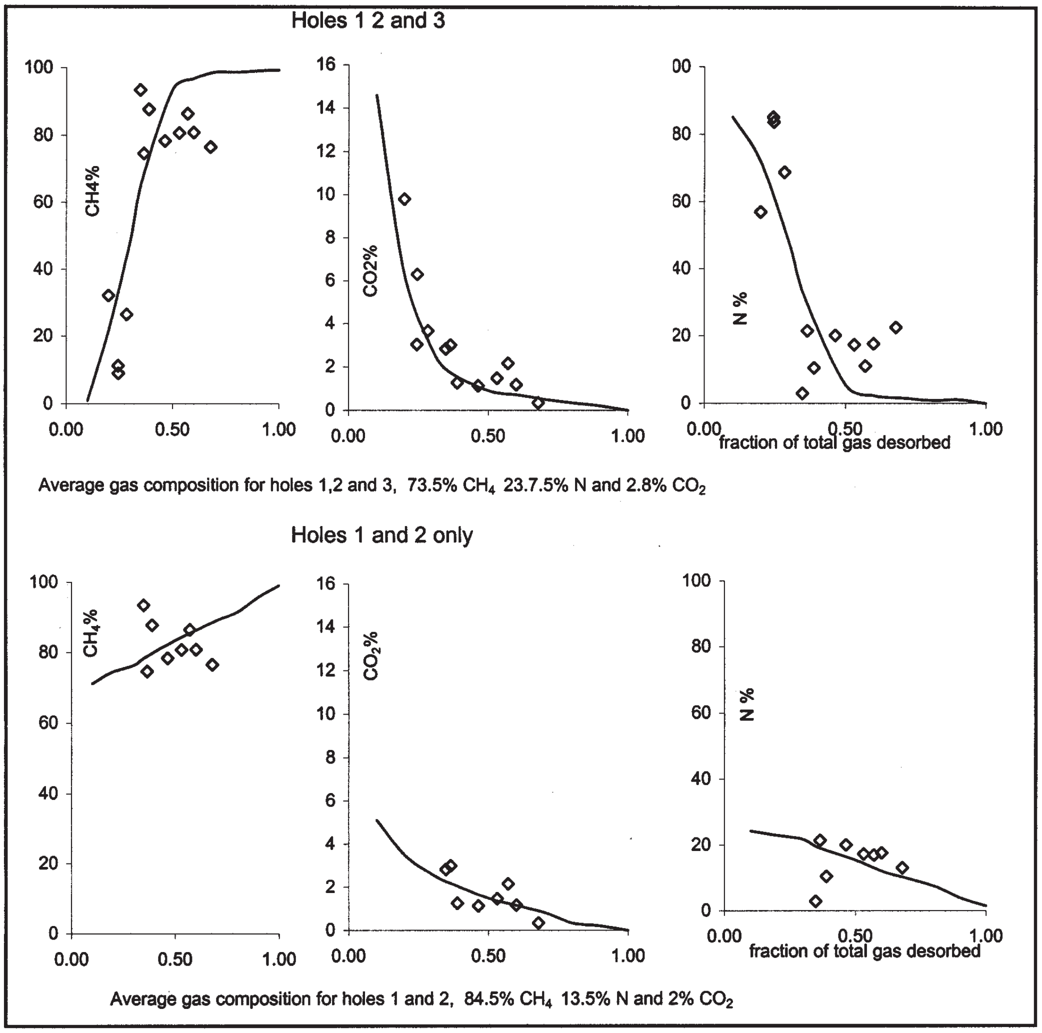

Figure 5. Plots of gas contents versus fraction of totals gas desorbed. Data for all three holes and for holes 1 and 2.

tivity. There were indications in Hole 3 that it might be close to an intrusion but the there is no discernible difference in the rank of the coals from the 3 holes. There is igneous activity in the vicinity and there is excess nitrogen in the stratigraphy as indicated by the composition of the gas from the two BOP samples; 93% for hole 1 and 30% from hole 2. An alternative explanation is that the nitrogen comes from gob gas in abandoned underground coal mines. These mines were originally filled with air, from which oxygen would be removed over time leaving nitrogen that could then penetrate the surrounding stratigraphy.

It is difficult to draw detailed conclusions about the over all gas composition of the desorbed gas from each canister, because the composition changes over time and only 1 or 2 samples were collected from each canister. If however it is assumed that the composition of gases is similar from canister to canister, and the mix changes in a similar way over time, then it is possible to normalize the data to indicate the composition of an average sample over time using all 3 holes (Table 4, Figure 5). This provides an average gas composition of 73.4% CH_4, 23.8% N_2 and 2.8%CO_2. In this case it is probable that the assumptions are not valid, but in many situations the approach might be a poor mans way of producing an average gas composition curve. Data from hole 3 are not representative of the gas compositions in the other two holes and if these data are removed from the analysis, then the average gas composition for holes 1 and 2 becomes approximately 83% CH_4, 15% N and 2% CO_2. The nitrogen is somewhat high but this can be explained easily by some adsorption of oxygen from air contamination in the canisters. The CO_2 contents are low, which makes the gas more attractive as a commercial product.

Nitrogen and carbon dioxide are predicted to come off the coal faster than methane (Figure 6). This has been documented by other authors and is the reverse of what happens during production. Desorption occurs at atmospheric pressure where as production occurs at incremental pressures less than hydrostatic pressure. Under atmospheric conditions, the rate at which different gases enter the canister free space is dependent on diffusion rates through the coal. This is evident in the Airy equation, in which sorption time (to) is dependent on coal fragment size (Airey, 1968). There is no correlation of sorption time to concentrations of nitrogen or carbon dioxide in this study.

CONCLUSIONS

Twelve samples were collected from a drill program in the Courtenay area British Columbia. The samples were desorbed in canisters maintained at about 23ºC until the desorption rate was less than 0.01 cc/day, at which time samples were removed weighted and sent for ash analysis. The equipment used was inexpensive and in part constructed by the author and in part by contractors. Results indicate that the coals in two of the holes are close to saturated with methane and contain moderate concentrations of nitrogen and low concentrations of carbon dioxide. Samples from the third hole are under saturated and appear to contain a lot of nitrogen. One sample of gas from the BOP on hole 1 indicated that there is nitrogen over pressuring of the stratigraphy. A sample of gas from the BOP on hole 2 indicated over pressuring of the stratigraphy by a methane (70%) nitrogen (30%) gas.

This paper documents a cooperative effort between industry and government, in which a balance is struck between timely release of new information, cost saving for the company and recognition of some level of confidentiality for the company.

TABLE 4
GAS COMPOSITION DATA GAS COMPOSITION DATA FOR BLOW-OUT-PREVENTOR SAMPLES AND CANISTER SAMPLES

Hole	Sample	depth metres	% air	GP%	percent mole fraction air free CH_4	CO_2	C_2H_6	H_2	CO	N_2
1	D1-1	BOP	14.7		6.6	0.2	0.1	0.1	0.1	93.0
2	D2-1	BOP	61.59		69.5	0.3	0.3	0.1	0.2	29.6
1	2-1	298.7	42.2	0.35	93.5	2.8	0.5	0.1	0.2	2.9
1	4-1	325.11	37.5	0.37	74.6	3.0	0.5	0.1	0.2	21.5
1	5-1	254.8	33.1	0.57	86.4	2.2	0.2	0.1	0.2	11.0
1	6-1	485.17	47.2	0.53	80.7	1.5	0.2	0.1	0.2	17.4
1	6-2	485.17	31.3	0.60	80.8	1.2	0.1	0.1	0.1	17.6
2	7-1	486.11	35.6	0.39	87.7	1.3	0.2	0.1	0.2	10.5
2	7-2	486.11	22.7	0.46	78.4	1.1	0.2	0.1	0.2	20.1
2	8-1	512.64	31.5	0.68	76.6	0.3	0.2	0.1	0.2	22.5
3	9-1	237.94	40.2	0.20	32.2	9.8	0.1	0.3	0.7	56.9
3	9-2	237.94	31.6	0.28	26.5	3.7	0.5	0.2	0.4	68.8
3	11-1	297.63	21.8	0.24	11.2	3.0	0.2	0.1	0.2	85.1
3	12-1	298.9	31.2	0.25	9.0	6.3	0.4	0.2	0.4	83.7

Sample notation first number=canister

ACKNOWLEDGEMENTS

Project Geologist Gwyneth Cathyl-Bickford provided geological information and other assistance. Priority Ventures Ltd. permitted the project to proceed and supplied donuts on site. Hans-Peter Meier From BC Research Inc. performed the gas composition analyses.

REFERENCES

Airey, E.M. (1968): Gas Emissions from broken coal, An Experimental and Theoretical Investigation; *International Journal of Rock Mechanics and Mineral Sciences*, Volume 5, pages 475-494.

Bickford, C.G.C. and Kenyon, C. (1988): Coalfield geology of eastern Vancouver Island; *in* Geological Fieldwork 1987, *B.C. Ministry of Energy, Mines and Petroleum Resources*, Paper 1988-1, pages 441-450.

Bickford, C.G.C., Hoffman, G. and Kenyon, C. (1990): Geological Investigations in the coal measures of the Oyster River,

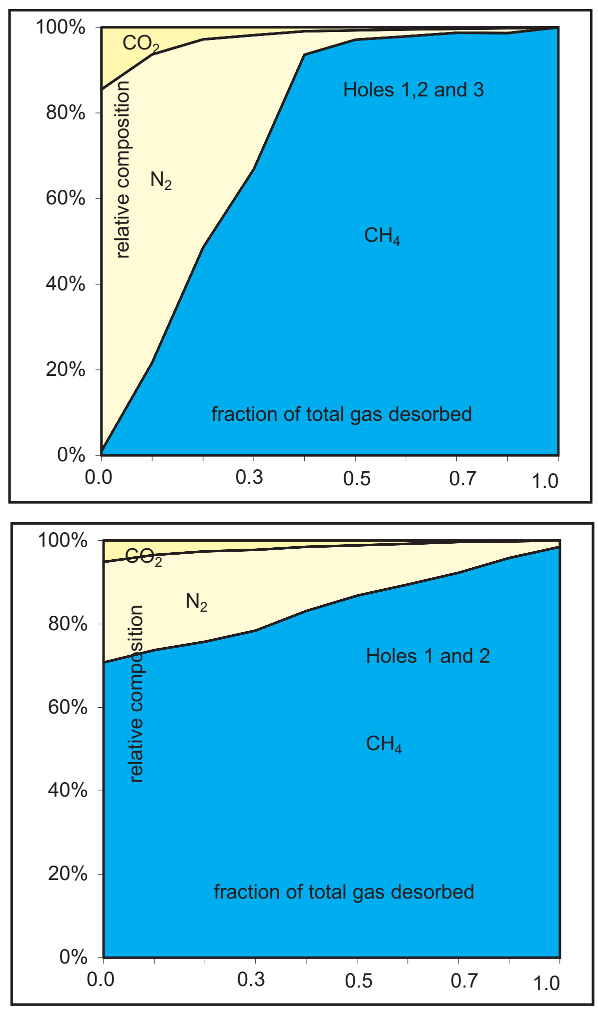

Figure 6. Composite plots of changes of gas composition *versus* amount of gas desorbed for all 3 holes and holes 1 and 2.

TABLE 5
CALCULATIONS OF AVERAGE GAS CONTENTS FOR DATA FROM ALL THREE HOLES COMBINED AND HOLES 1 AND 2

Holes 1, 2 and 3

sample gas data					curve fitting data									
hole	GI%	N_2	CH_4	CO_2	GI%	CH_4	int	GI%	N_2	int	GI%	CO_2	int	
1	0.35	2.9	93.5	2.8	0.0	actual	curve	0.0	actual	curve	0.0	actual	curve	sum
1	0.37	21.5	74.6	3.0	0.1	1.0	0.1	0.1	85.2	8.5	0.1	14.6	1.5	100.8
1	0.57	11.0	86.4	2.2	0.2	21.7	2.2	0.2	72.0	7.2	0.2	6.3	0.6	100.0
1	0.53	17.4	80.7	1.5	0.3	48.0	4.8	0.3	48.0	4.8	0.3	2.8	0.3	98.8
1	0.60	17.6	80.8	1.2	0.4	66.8	3.8	0.4	31.3	1.8	0.4	1.8	0.1	99.9
2	0.39	10.5	87.7	1.3	0.5	93.6	13.4	0.5	5.5	0.8	0.5	0.9	0.1	100.0
2	0.46	20.1	78.4	1.1	0.6	96.8	9.7	0.6	2.2	0.2	0.6	0.7	0.1	99.7
2	0.68	22.5	76.6	0.3	0.7	98.7	9.9	0.7	1.6	0.2	0.7	0.5	0.0	100.8
3	0.20	56.9	32.2	9.8	0.8	98.7	9.9	0.8	0.9	0.1	0.8	0.4	0.0	100.0
3	0.28	68.8	26.5	3.7	0.9	99.1	9.9	0.9	1.1	0.1	0.9	0.2	0.0	100.4
3	0.24	85.1	11.2	3.0	1.0	99.4	9.9	1.0	0.0	0.0	1.0	0.0	0.0	99.4
3	0.25	83.7	9.0	6.3	average% CH_4		73.5	average% N		23.7	average% CO_2		2.8	

Holes 1 and 2 only

0.0	actual	curve	0.0	actual	curve	0.0	actual	curve	sum
0.1	71.1	7.1	0.1	24.3	2.4	0.1	5.1	0.5	100.5
0.2	74.4	7.1	0.2	23.0	2.3	0.2	3.5	0.4	100.9
0.3	76.3	8.0	0.3	21.8	2.2	0.3	2.6	0.3	100.7
0.4	78.7	4.5	0.4	19.4	1.1	0.4	2.2	0.1	100.3
0.5	83.4	11.9	0.5	15.5	2.2	0.5	1.5	0.2	100.4
0.6	86.3	8.6	0.6	12.0	1.3	0.6	1.1	0.1	99.4
0.7	89.1	8.9	0.7	9.7	1.0	0.7	0.8	0.1	99.6
0.8	91.5	9.2	0.8	7.3	0.8	0.8	0.4	0.0	99.2
0.9	95.7	9.6	0.9	4.0	0.4	0.9	0.2	0.0	99.9
1.0	99.1	9.9	1.0	1.5	0.2	1.0	0.0	0.0	100.6
average% CH4		84.8	average% N		13.7	average% CO2		1.7	

Int curve = area under curve for change in GI% GI%=percent of total gas desorbed

Mount Washington and Cumberland areas, Vancouver Island (92F/10,11,14); *in* Geological Fieldwork 1989, *B.C. Ministry of Energy, Mines and Petroleum Resources*, Paper 1990-1, pages 431-437.

Cathyl-Bickford, C.G. (2001): Lithostratigraphy of the Comox and Trent River formations in the Comox Coalfield, Vancouver Island (92F/7, 10, 11, 14), *B.C. Ministry of Energy and Mines*, Paper 2001-1, pages 363-370.

Cathyl-Bickford, C.G. (1992): Geology and energy resource potential of the Tsable River and Denman Island; *in* Geological Fieldwork 1991, *B.C. Ministry of Energy, Mines and Petroleum Resources*, Paper 1992-1, pages 419-426.

Cathyl-Bickford, C.G. (1991): Coal geology and coalbed methane potential of the Comox and Nanaimo coalfields, Vancouver Island , British Columbia; *in* Coalbed Methane of Western North America, *Rocky Mountain Association of Geologists*, pages 155-162.

Cathyl-Bickford, C.G., and Hoffman, G.L. (1998): Geological maps of the Nanaimo and Comox coalfields; *British Columbia Ministry of Energy and Mines,* Open File 1998-7.

Cathyl-Bickford, C.G., Wilson, R. and Hoffman, G.L. (1991): Geology, mineability and coalbed gas potential of the Douglas Coal Zone in the Nanaimo Coalfield, Vancouver Island; in *The Canadian Coal and Coalbed Methane Forum Proceedings*, Parksville, pages 293-309.

England, T.D.J. and Calon, T.J. (1991): The Cowichan Fold and Thrust System, Vancouver Island southwestern British Columbia; *Geological Society of America Bulletin*, Volume 103, pages 336-362.

England, T.D.J. and Bustin, R.M. (1995): Geology of the Georgia Basin; *Geological Association of Canada/Mineralogical Association of Canada,* Annual Meeting, Victoria B.C., Field Guide Number B3.

Gardner, S.L. (1999): Coal resources and coal mining on Vancouver Island; *B.C. Ministry of Energy and Mines* , Open File 1999-8.

Kenyon, C. and Bickford, C.G.C. (1989): Vitrinite reflectance study of Nanaimo Group coals of Vancouver Island; *in* Geological Fieldwork 1988, *B.C. Ministry of Energy, Mines and Petroleum Resources*, Paper 1989-1, pages 543-552.

Kissel, F.N., McCulloch, C.M. and Elder, C.H. (1973): The direct method of determining methane content of coalbeds for ventilation design; *U.S. Bureau of Mines*, Report of Investigations, 7767.

MacKenzie, J.D. (1922): The coal measures of Cumberland and vicinity, Vancouver Island; *Canadian Institute of Mining and Metallurgy*, Transactions, Volume 25, pages 382-411.

McLennan, J.D., Schafer, P/S., and Pratt, J.T. (1995): A guide to determining coalbed gas content; *Gas Research Institute,* No GRI-94/0396

McCulloch, C.M., Levine, R.J., Kissel, F.N. and Deul, M. (1975): Measuring the methane content of bituminous coalbeds; *United States department of the Interior,* Report of Investigations 8043.

Kneuper, G.K. and Huckel, B.A. (1972): Contribution to the geochemistry of mine gas in the Carboniferous coalfield of the Saar Region, Germany; in*, Advances in Organic Geochemistry*, 1971, pages 93-112.

Muller, J.E. and Atchison, M.E. (1970): Geology history and potential of Vancouver Island coal deposits; *Geological Survey of Canada*, Paper 70-53.

Muller, J.E. (1989): Tertiary low angle faulting and related gold and copper mineralization on Mount Washington, Vancouver Island (92F/11,14); *in* Geological Fieldwork 1988, *B.C. Ministry of Energy, Mines and Petroleum Resources*, Paper 1989-1, pages 81-91.

Ryan, B.D. (2001): An introduction to coalbed methane potential in British Columbia; in, Review of Exploration and Mining Activity British Columbia 2000, Part B pages 55-70.

Ryan, B.D. (1992): An Equation for estimation of maximum coalbed-methane resource potential; *in* Geological Fieldwork 1991, *B.C. Ministry of Energy, Mines and Petroleum Resources*, Paper 1992-1, pages 393-396.

Ryan, B.D. and Dawson, M.F. (1994a): Coalbed methane desorption results from the Quinsam Coal Mine and coalbed methane resource of the Quinsam Coalfield, British Columbia; *in* Geological Fieldwork 1993, *B.C. Ministry of Energy, Mines and Petroleum Resources*, Paper 1994-1, pages 215-224.

Ryan, B.D. and Dawson, F.M. (1994b): Coalbed methane desorption techniques; *in* Geological Fieldwork 1993, *B.C. Ministry of Energy, Mines and Petroleum Resources*, Paper 1994-1, pages 245-256.

Scott (1993): Composition and origin of coalbed gases from selected basins in the United States; Proceedings of the 1993 International *Coalbed Methane Symposium, University of Alabama, Tuscaloosa, School of Mines and energy Development,* Volume 1, pages 207-216.

Ward, P.D. (1978): Revisions of the stratigraphy and biochronology of the Upper Cretaceous Nanaimo Group, British Columbia and Washington State; *Canadian Journal of Earth Sciences*, Volume 15, pages 405-423.

Williams, T.B. (1924): The Comox Coal Basin; unpublished Ph.D thesis, University of Wisconsin.

Williams, D.M., and Smith, F.L. (1984): Diffusion models for gas production from coals; *Fuel*, Volume 63, pages 251-255.

Adsorption Characteristics of Coals with Special Reference to the Gething Formation, Northeast British Columbia

By Barry Ryan and Bob Lane

KEYWORDS: *Coalbed methane, Adsorption, Gething Formation, petrography, coal ash.*

INTRODUCTION

There are two major coal-bearing formations in the Peace River Coalfield in northeastern British Columbia, The Gates and the Gething. The younger Gates Formation hosts to the two major coal mines that have operated in the area; therefore there is some coalbed methane (CBM) information available for the formation. In contrast there is very little CBM information available for the older Gething Formation. This paper presents some coal adsorption data for the Gething Formation.

The two major coal-bearing formations in northeast British Columbia (Figure 1) outcrop extensively throughout the Peace River coalfield. The Gates Formation is separated from the older Gething Formation by the marine Moosebar Formation. Coal seams of economic interest in the Gates Formation and Gething formations occur in the southern and the northern parts of the coalfield respectively, which roughly coincides with the north and south of Mount Spieker (Figure 2).

THE GETHING FORMATION

The Gething Formation, which is late Jurassic to early Cretaceous, overlies the Cadomin Formation (Table 1). Therefore it is slightly younger than the Mist Mountain Formation, which underlies the Cadomin in the southeast British Columbia coalfields. The type section for the Formation is in the Peace River Canyon where it is 550 metres thick (Gibson, 1985). It thins to the south and at the Saxon property at the southern end of the coalfield is only 7 metres thick. In the area around the Sukunka property (Figure 2) the upper and lower coal-bearing part of the Gething is separated by a marine tongue (Duff and Gilchrist, 1981 and Legun, 1986) and economic coal seams are found in the upper and lower non-marine sections. The extent of the upper Gething coal-bearing zone is limited to the Sukunka River, Mt. Spieker area, but it has been suggested that there are other marine tongues in the Gething that wedge out to the south (Broatch, 1987). Leckie and Kalkreuth (1990) have suggested that Lower Cretaceous coals formed in a strand plain environment that was distant and protected from the shoreline and storm/tidal inundations. The Formation extends at depth to the east into the Western Canadian Sedimentary Basin, where it hosts a number of gas plays. The Formation has been extensively explored, from Mount Spieker in the south to Williston Lake in the north (Figure 2), for its potential to host surface and underground coal mines as documented by numerous coal assessment reports from the Ministry of Energy and Mines.

There has been very limited mining in the Gething Formation despite the fact that it hosts the first coal to be discovered in British Columbia by Mackenzie in 1793. More recently the Pine Valley Coal Corporation has obtained permits for a mine in the Willow Creek area located 40 kilometres west of Chetwynd (Figure 2). To date they have mined, screened and sold about 70 000 tonnes of coal probably to be used for pulverized coal injection (PCI) and hope to expand into full-scale production soon.

For this study a number of samples were collected in the summer of 2001 from a single seam in the Pine Valley Coal test pit representing a range of petrographic composition. The adsorption characteristics of these seven samples were measured and attempts made to correlate the results with various coal parameters.

TABLE 1
GENERALIZED LOWER CRETACEOUS STRATIGRAPHY, PINE RIVER AREA

			metres
Jurassic to lower Cretaceous	FORT ST JOHN GROUP	CRUISER FORMATION marine shale	115
		GOODRICH FORMATION fine grained sandstone and shale	350
		HASLAR FORMATION marine shale	260
		BOULDER CREEK FORMATION sandstone and conglomerates	150
		HULCROSS FORMATION grey marine shale	100
		GATES FORMATION non marine sandstones and coal seams	110
		MOOSEBAR FORMATION marine shale	250
	BULLHEAD GROUP	GETHING FORMATION non marine sediments and coal	500
		CADOMIN FORMATION conglomerates	150

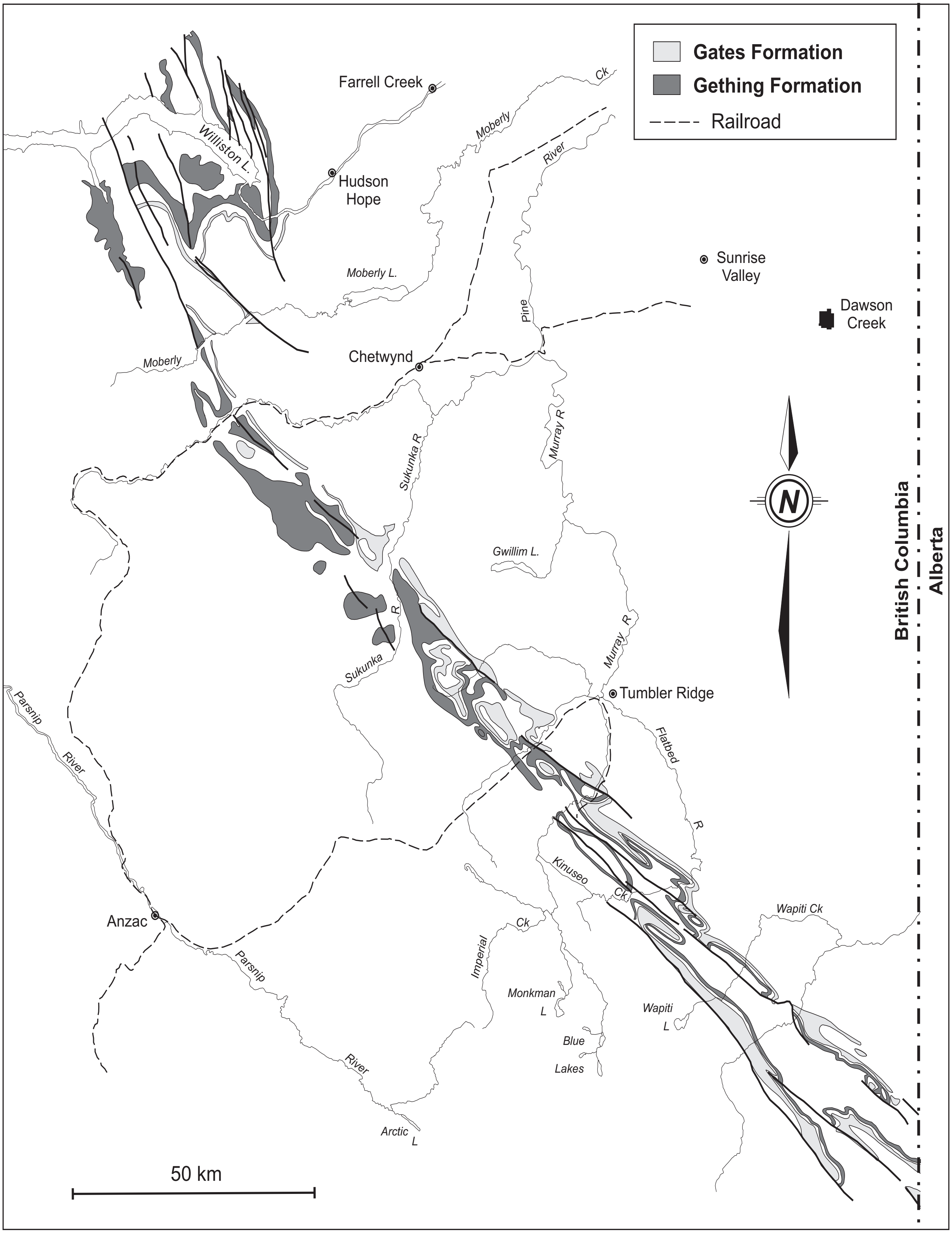

Figure 1. Gething and Gates formations outcrop pattern northeastern British Columbia.

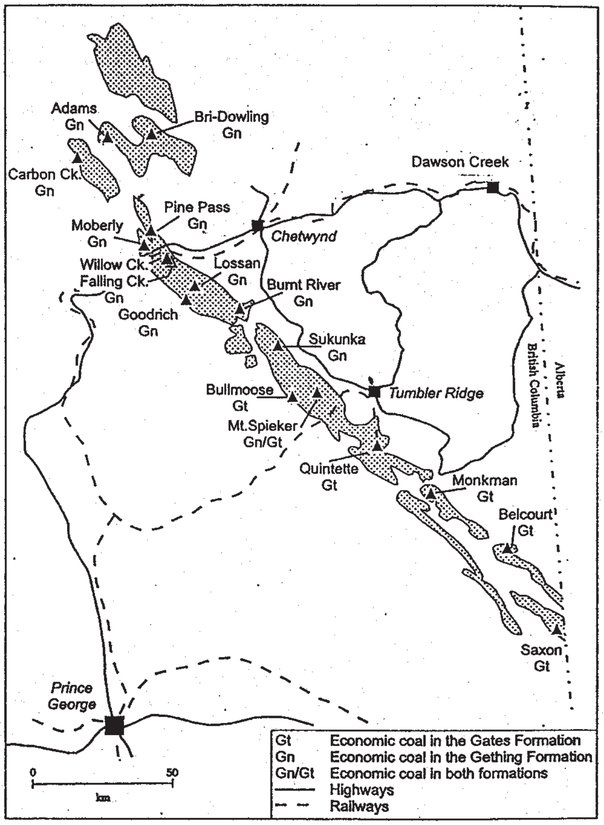

Figure 2. Location of coal mines and deposits in northeastern British Columbia.

PETROGRAPHY

Ryan (1997) has summarized the coal quality and petrography of the Gething Formation. Coal from the Formation is characterized by variable reactives content and low wash ash values. Reactive maceral contents can range from approximately 80% to less than 50%. This variation can explain some of the range of free swelling index (FSI) values seen in exploration coal quality data, but it does not explain the washing characteristics of the coal. The coal samples from Willow Creek have a high content of collodetrinte, which contains fragments of non-structured inert macerals such as macrinite and inertodetrinite. Structured macerals, such as semifusinite and fusinite are less common. Some of the collotelinite could be classified as semifusinite depending on the reflectance cut off. There is a lot of pseudo vitrinite (Photo 1), characterized by small lenses shaped holes, present in some samples. It may be evidence of partial desiccation of partially coalified material. In this temporary dry environment in the coal swamp any forest fires would char partially rotten vegetation, which having lost its cell structure would become macrinite rather than semifusinite after coalification.

The limited amount of structured inert macerals (semifusinite and fusinite) restricts the amount of dispersed mineral matter, which often fills cell lumen in these macerals. There also are few bands of carbonaceous shale in the samples, composed of finely dispersed ash and vitrinite particles, in the coal. These two factors probably explain the low raw ash and very low wash ash concentrations of seams in the formation. Wash-ash contents of Gething coals are consistently lower than those of Gates or Mist Mountain coals.

Preliminary observations of the 7 samples collected from the Willow Creek property indicate that samples contain a lot of particles made up of more than one maceral. Groundmasses of collodetrinite contain fragments of macrinite, collotelinite and occasionally semifusinite (Photo 2). There is little dispersed mineral matter in collodetrinite. In fact most of the finely dispersed mineral matter is associated with telinite or gelovitrinite (Photo 3). Generally compared to coals from the Mist Mountain Formation there is less fusinite and semifusinite and consequently less preserved cell structure

The generation of collodetrinite and macrinite often indicates a prolonged period of humification and destruction of biomass, which is accompanied by a concentration, in the remaining biomass, of the inherent mineral matter derived from the original vegetation. This finely dispersed mineral matter may affect the adsorption characteristics of the coal. The amount of inherent mineral matter in vegetation varies but can be as much as 8% (Renton *et al*., 1979). It contains high concentrations of base oxides, which may be partially lost during coalification. It is estimated that from 1.5% to 2.5% of the mineral matter in bituminous coals may be derived from the original vegetation. The relationship of the amount of biomass destroyed to the volume percent of inherent mineral matter in the remaining coal indicates that very high amounts of biomass must be destroyed to produce

Photo 1. Psuedo vitrinite in Gething coal showing elliptical cavities. Width of photo approximately 0.2 mm.

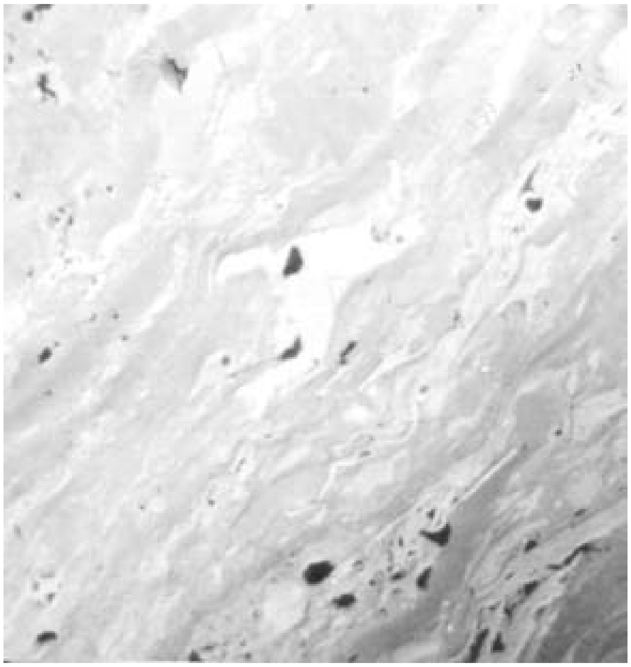

Photo 2. Groundmass of collodetrinite containing fragments of macrinite, collotelinite and semifusinite. . Width of photo approximately 0.2 mm.

significant increases in the volume of inherent mineral matter.

Many post Carboniferous coals are enriched in inertinite with respect to Carboniferous coals. One possible explanation (Taylor *et al*., 1989) is that the high inertinite content of Permian Gondwana coals is caused by a cool climate with wet summers and dry cold winters, during which the coal swamp dried out and inertinite developed. This environment might produce a fine layering of lithotypes similar to varves seen in clays. Possibly the cool climate and lack of ground covering vegetation also allowed dust to blow into the swamp which would explain the high contents of dispersed mineral matter found in some of these coals. Hunt and Smyth (1989) suggest that Australian Permian coals with high inertinite, and low ash contents formed in cratonic basins in fresh water mires, with low subsidence rates, allowing for extensive oxidation. Lamberson *et al.* (1991) emphasize the importance of fires in forming inertinite in Gates coals. There is no obvious explanation for the variable and sometimes high content of inertinite in Gething coals. Gething coal swamps may have experienced more episodes of drying and a greater frequency of forest fires than Gates swamps.

RANK

Karst and White (1979) Kalkreuth and McMechan (1988) and Kalkreuth *et al*. (1989) have all discussed coal rank in the Gething Formation. Rank varies from semi anthracite to high-volatile bituminous. Along the outcrop belt in the foothills the rank is high, in places reaching semi anthracite. To the north and east it decreases to high-volatile bituminous. There is some evidence that outcrops at the western outcrop edge of the formation have lower ranks. Rank was established prior to deformation and variations are related to changes in the thickness of the Gething plus post Gething sedimentary package. Ref Leckie, 1983).

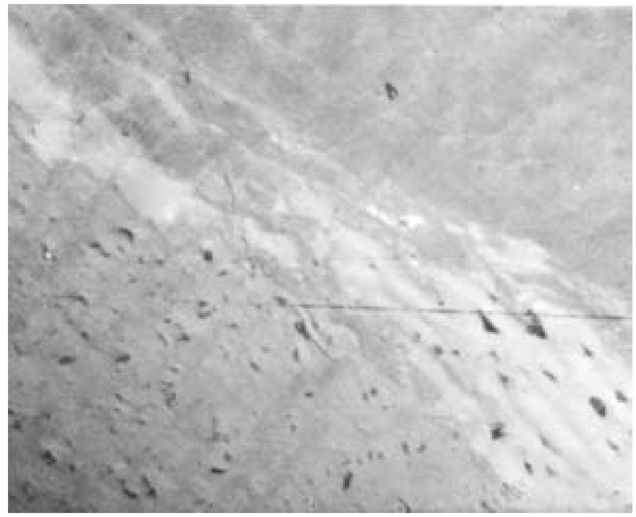

Photo 3. Finely dispersed dark mineral matter associated with telinite. Width of photo approximately 0.2 mm.

The rank at Willow Creek, where the samples were collected ranges from medium to low-volatile bituminous. The rank of 7 seam, which is in the lower part of the section is low-volatile bituminous (WC001-6 Rmax = 1.70% and WC001-4 Rmax=1.73%). Some of the samples have pseudo vitrinite and using this maceral to measure Rmax produced a value that was 0.02% high.

WILLOW CREEK SAMPLE DATA

SAMPLE COLLECTION

Samples were collected from the Pine Valley Coal test pit in the Willow Creek property located on the south side of the Pine River about 40 kilometres west of Chetwynd (Figure 2). In this area the Gething Formation has 8 coal seams ranging in thickness from 1 to over 5 metres and numbered downwards from the top of the formation. Samples were collected from seam 7-0 and seam 7-2 (Figure 3). A mudstone parting (30 cm thick), which separates seam 7-0 from 7-2, was used as a reference plane for sample location. Two samples (WC001-1 and WC001-2) representing a total of 2.74 metres were collected above the parting and a third sample representing 0.7 metres of 7-2 seam was collected adjacent to and below the mudstone parting. The base of seam 7-2, which is 1.1 metres thick, was not exposed. Four grab samples, 2 of bright and 2 of dull coal, were taken from seam 7-0.

Total apparent thickness of 7-0 seam, based on a density log from a nearby hole, is about 3.6 metres; 2 metres of buff-coloured sandstone immediately overlies 7-0 seam, and a 30-40 cm thick coal marker lies just above the sandstone. Seam 7-0 coal is dominantly dull with numerous mm-scale bright coal laminas and one 20 cm thick bright band just above a lower mudstone parting.

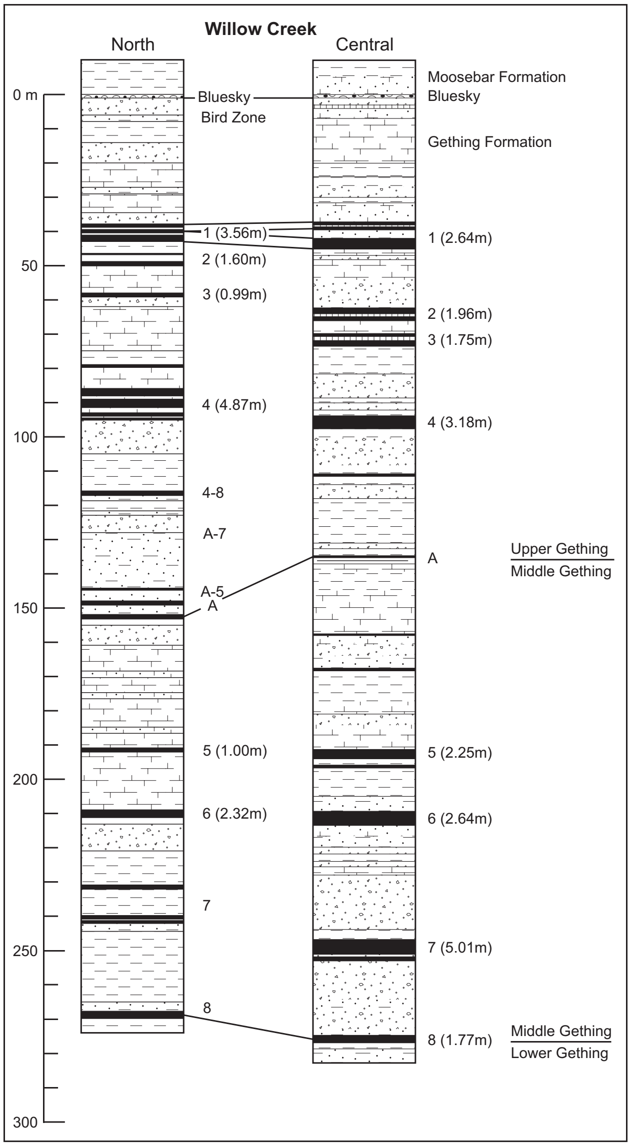

Figure 3. Stratigraphic section of the Gething Formation from the Willow Creek property.

COAL QUALITY AND PETROGRAPHY OF SAMPLES

Proximate analyses were performed on all samples of seam 7-0 and 7-2 (Table 2). With the exception of two samples, ash contents are very low (Table 2) and VM daf concentrations indicate a rank of low-volatile bituminous, which is supported by 2 Rmax determinations of WC001-6 = 1.7% and WC001-4 = 1.73%.

The petrography of the samples (Table 3) indicates a wide range in total reactives contents from 48% to 81% of sample. Some of the samples contain a lot of pseudo vitrinite (Photo 1), the reflectance of which was checked and found to be similar to, or slightly higher than, that of collodetrinite. As previously discussed semifusinite and fusinite with good cell structure makes up less of the inert material than in coals from many other formations.

Coal petrography tends to be a somewhat subjective process that is hard to standardize. For this reason, random reflectance histograms were constructed for each sample to see if they might provide a better estimate of variations of petrography as defined only by reflectance. The histograms are produced using a computerized scanning process in which maceral fragments are scanned for random reflectance under the microscope. The computer is able to extract measurements of minerals or measurements influenced by edge effects from the data. For most samples clear vitrinite and inertinite peaks can be interpreted from the original distribution of random reflectance data (Figure 4). The data (Table 4) indicate that there is a very wide range of total vitrinite contents as recognized by random reflectance (8% to 94% on a dry mineral matter free basis, dmmfb) and that Rmax values calculated from random reflectance (1.65%-1.67%) are some what lower than Rmax values measured on samples WC001-4 and WC001-6.

A comparison of total vitrinite by random reflectance histograms *versus* microscope examinations (Figure 5) provides a good correlation though the best-fit line does not go through the origin because microscope identification has tended to identify more vitrinite in the low vitrinite samples. The reason appears to be that the low vitrinite samples contain more reactive semifusinite as identified by reflectance

TABLE 2
COAL QUALITY DATA FOR ADSORPTION SAMPLES

Sample WC001	Sm	Description	length cm	H_2O% ar	H_2O% ad	VM% dry	Ash% dry	FC% dry	VM% daf
-1	7-0	channel	163	4.3	0.9	12.7	1.8	85.5	13.0
-2	7-0	channel	111	3.1	0.8	12.4	12.7	74.9	14.2
-3	7-2	channel	70	5.1	0.8	12.5	2.4	85.1	12.8
-4	7-0	grab/bright	comp	2.7	0.7	14.9	1.7	83.4	15.2
-5	7-0	grab/dull	1.35	3.6	0.7	13.1	1.4	85.4	13.3
-6	7-0	grab/bright	20	6.7	0.7	14.8	13.2	72.1	17.0
-7	7-0	grab/dull	comp	2.9	0.6	12.7	3.8	83.5	13.2

TABLE 3
PETROGRAPHY FOR SAMPLES 300 POINT COUNT

	VOLUME PERCENTS													
sample	telinite	collotelinite	collodetrinite	vitrodetrinite	liptinite	total reactives	semifusinite	fusinite	inertodetrinite	macrinite	micrinite	total inerts	mineral matter	weight ash%
WC001-1	1	21	39	1	0	62	12	3	11	5	3	33	5	8.3
WC001-2	0	20	39	2	0	61	10	2	9	6	2	28	10	16.3
WC001-3	8	5	32	1	0	47	23	2	6	19	0	51	2	4.0
WC001-4	27	1	48	0	0	76	7	0	4	9	1	22	1	2.3
WC001-5	4	17	36	0	1	58	23	2	4	9	2	40	2	4.0
WC001-6	24	21	34	1	0	81	1	1	1	0	2	6	13	20.5
WC001-7	2	7	44	0	0	53	14	0	9	20	2	44	3	4.5

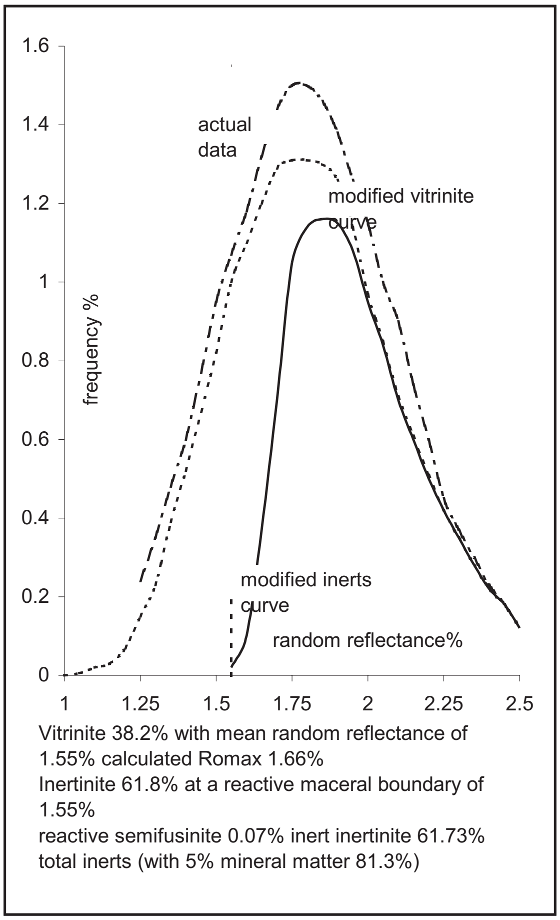

Figure 4. Histogram of random reflectances for sample WC001-4.

profile and this material is identified as telinite during microscope petrography. The vitrinite macerals have a higher volatile content than the inert macerals and both methods of identifying vitrinite contents produce data that correlate well with VM daf (Figure 5). This means that once the quality of a coal seam is understood, VM daf gives a good and very cheap estimate of reactivity and can be used to correlate with adsorption characteristics.

TABLE 4
SUMMARY OF RANDOM REFLECTANCE DATA

Sample WC001-	calculated Rmax%	vitrinite %	random reflectance	reactive semifusinite %	maceral boundary reflectance	inert inertinite %	mean random reflectance inertinite
1	1.67	8.0	1.56	41.7	1.82	50.3	1.82
2	1.66	38.2	1.55	0.1	1.55	61.7	1.84
3	1.66	14.8	1.55	17.3	1.80	67.9	1.88
4	1.65	54.8	1.54	4.8	1.70	40.4	1.54
5	1.67	18.8	1.56	28.6	1.74	52.6	1.80
6	1.65	93.7	1.54	0.8	1.54	5.5	1.65
7	1.67	12.6	1.56	10.7	1.76	76.7	1.90

ADSORPTION DATA

Adsorption isotherms were measured at 25ºC, which probably corresponds to crustal temperatures at a depth of about 1000 metres. This means that using Langmuir volumes (Vl) and Langmuir pressures (Pl) to calculate adsorption at shallower depths will under estimate adsorption capacity and if the depths are greater than 1000 metres adsorption capacity will be over estimated. Adsorption results (Table 5) indicate that in general terms the samples have high adsorption capacities (Figure 6). This is not surprising and is in agreement with the high rank, though based on the Eddy *et al*., (1982) curves and the equation derived from Ryan (1992), they are somewhat higher than the norm. It should be noted that the Ryan Equation was set up to model the Eddy curves and at the same time to be somewhat conservative.

Langmuir volumes (Vl) of the samples do not have a clear relationship to petrography based on a plot of Vl dmmf concentrations *versus* total vitrinite by random reflectance histogram (volume percent basis) (Figure 7). The two samples that have distinctly higher ash contents are highlighted (Figure 7) and if these 2 samples are removed from the data set, then there is a moderate correlation between total

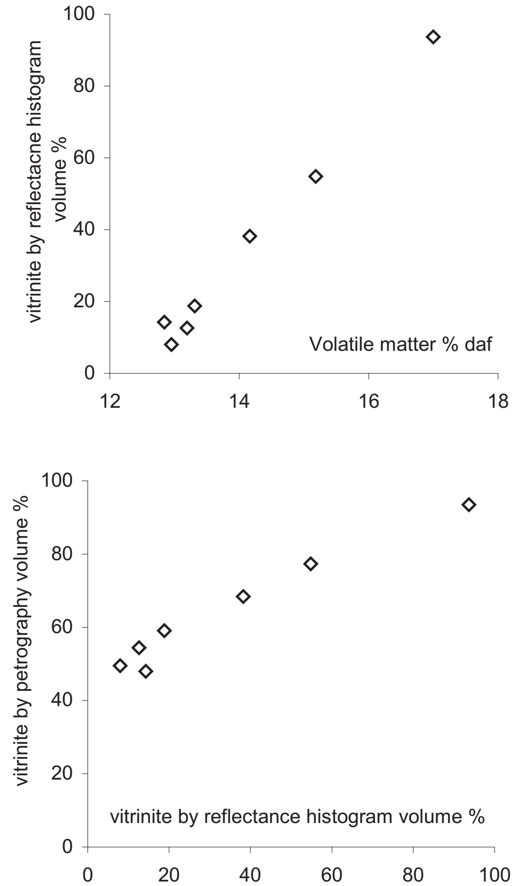

Figure 5. Total reactives by petrography and random reflectance histograms.

TABLE 5
SUMMARY OF ADSORPTION DATA

		isotherms at 25º C			
	ash%	H_2O%	Vl cc/g	Vlcc/g	Pl
sample	ad	equil	ar	daf	Mpa
WC001-1	1.3	5.0	30.2	32.3	2.08
WC001-2	15.6	2.6	24.0	29.4	2.44
WC001-3	2.0	6.2	30.8	33.5	2.57
WC001-4	1.6	3.4	37.1	39.0	3.25
WC001-5	1.1	5.0	33.4	35.6	2.73
WC001-6	13.7	3.6	25.0	30.2	3.63
WC001-7	2.6	3.8	32.5	34.7	3.27

Vl Langmuir volume Pl Langmuir pressure.

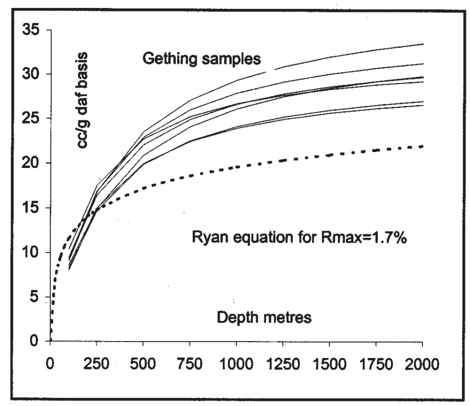

Figure 6. Comparison of Gething coal desorption curves to the curve predicted by the Ryan Equation for a reflectance of 1.7%.

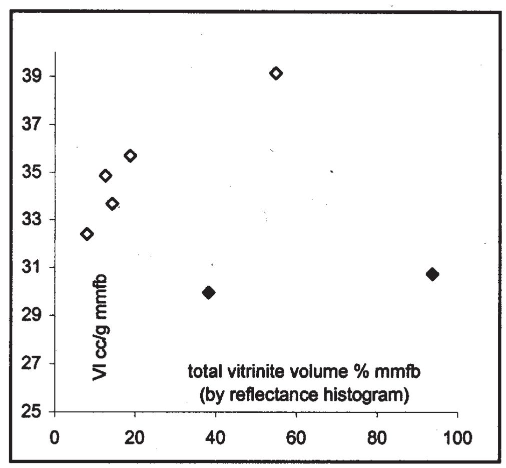

Figure 7. Total reactives versus langmuir volume dmmf basis; filled data points have high ash contents.

vitrinite and adsorption contents. The adsorption *versus* vitrinite content (by random reflectance histogram) relationship is more diffuse if reactive semifusinite is added to vitrinite, implying that reactive semifusinite is not acting as a vitrinite maceral in terms of its adsorption ability. The fact that there is a moderately good relationship between adsorption and vitrinite content as defined by random histograms indicates that in this data set the structure of maceral sub types may not play a major part in influencing adsorption ability. It has been suggested that collodetrinite may have a higher adsorption capacity than telinite and collotelinite (Gurba, 2001).

There is nothing obviously anomalous about the two high ash samples in terms of their petrography or VM daf contents. If there had been a problem with equilibrating the samples back to equilibrium moisture the Vl values would generally increase. It is possible that the low Vl values are caused by ash acting as a more than a simple dilutent.

The Langmuir pressure (Pl) is independent of ash content and may be a better indicator of the effect of petrography on adsorption characteristics. It is dependent on rank, generally decreasing as rank increases (Figure 8) (Olszewski, 1992). Olszewski data were obtained on dry coal and indicate that dry coals of equivalent rank have increased adsorption capacities and reduced Langmuir pressures. There is no obvious relationship between Pl and petrography in this study (Figure 8). If the two high ash samples are removed, then there is weak positive correlation of Pl with total reactives, which would imply that the effect of increased reactives is similar to a decrease in rank. Part of the reason for the weak or absent correlation of Pl to petrography may be the high rank of the samples. The physical properties of macerals, including porosity, tend to converge at higher ranks.

Moisture content, below equilibrium moisture, has a profound influence on adsorption capacity. Joubert (1974) investigated the effect of moisture on the adsorptive capacity of coals of different ranks and found that it increased as the moisture decreased below equilibrium moisture. The equilibrium moisture of individual macerals varies and vitrinite of low to medium rank has higher equilibrium moistures than inertinite. There is no correlation of equilibrium moisture with petrography in this study. However for many British Columbian coals, air-dried and equilibrium moisture correlate positively with vitrinite content and negatively with ash content. This means that, at constant rank, equilibrium moisture may be an indicator of adsorption ability. It appears that iso-rank coals from different basins are characterized by different average equilibrium moisture contents. In fact there is a rough trend for data suites with lower equilibrium moisture to contain more gas (Bustin and Clarkson, 1998). It is not clear if changes in equilibrium moisture content for different suites are related to variations in the vitrinite sub-types, the history of the coal or the original vegetation source. Equilibrium moisture varies by rank and maceral content going through a minimum at the boundary between high and medium-volatile bituminous. Above this rank the difference in equilibrium moisture contents of the various macerals is less pronounced. It is also probably pressure dependent. In coal seams that are pressured by free gas, it is possible that moisture contents of coals are below equilibrium moisture. This would increase the coals ability to adsorb gas and would make it look over saturated, based on desorption data, depth and rank. Just as water movement has been used to explain under saturated coals, free gas movement in seams might remove water and increase the adsorption capacity and gas content of seams.

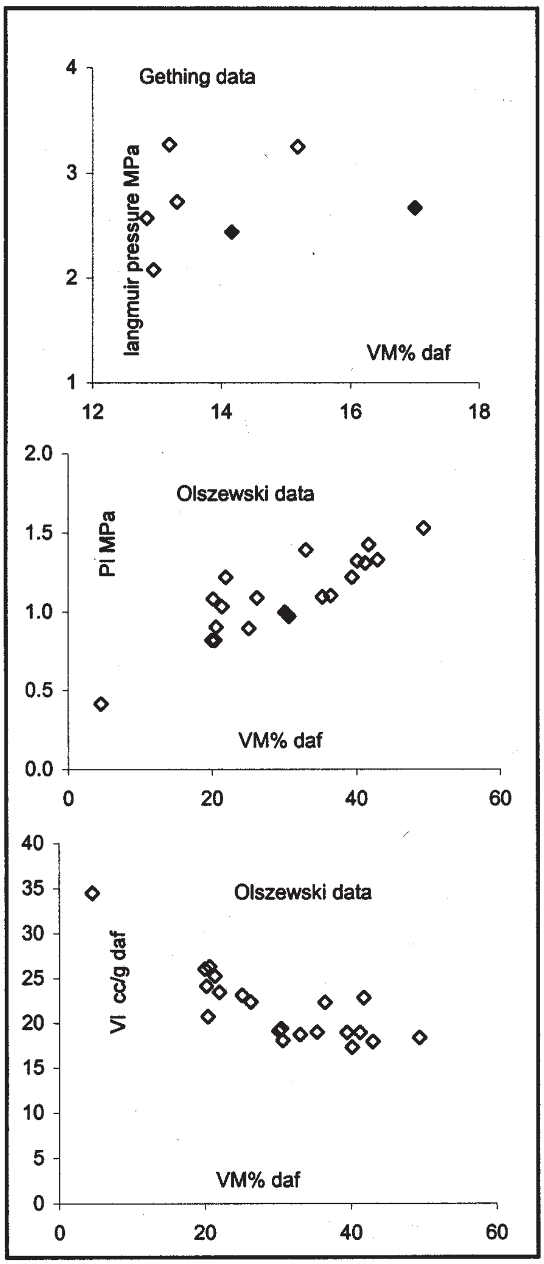

Figure 8. Plot of VM daf versus Langmuir pressure data from Olszewski (1992), and this study.

DISCUSSION

EFFECT OF TEMPERATURE AND PRESSURE ON ADSORPTION CAPACITY AND POTENTIAL GAS CONTENT

This paper discusses adsorption ability, but it is the actual volume of adsorbed gas that is available for recovery that is important. It is revealing to construct a schematic plot (Figure 9) outlining the tract of coal on a downward coalification curve with a number of upward branches representing uplift tracts for coals, which have attained different ranks. The plot does not attempt to exactly reproduce temperatures, depths and adsorption characteristics of coals of different ranks, though numbers are probably within a moderate margin of error. Both Kim (1977) and Olszewski (1992) have developed empirical equations predicting gas contents at varying coal ranks and temperatures. However, they were using data derived from dry coals tested over a temperature range of 0 to 50 degrees. The equations are therefore probably not reliable at the higher temperatures at which bituminous coals form. As vegetation is progressively buried, rank, pressure and temperature all increase. Initially adsorption capacity also increases, but eventually increasing temperature causes it to decrease. Over a temperature range of 20 to 65ºC Levy *et al.* (1997) found that adsorption decreased by 0.12 cc/g per °C. During most of their burial tract coals are producing CH_4 in excess of their adsorption capacity and the excess is expelled into the surrounding rocks. Upon uplift, rank is fixed and temperature and pressure decrease. At depths considerably greater than those equivalent to Pl, adsorption capacity is generally not pressure dependent and adsorption capacity increases as temperature decreases. It is only at depths equivalent to about Pl x 2 that the effect of decreasing pressure becomes dominant and adsorption capacity decreases with uplift.

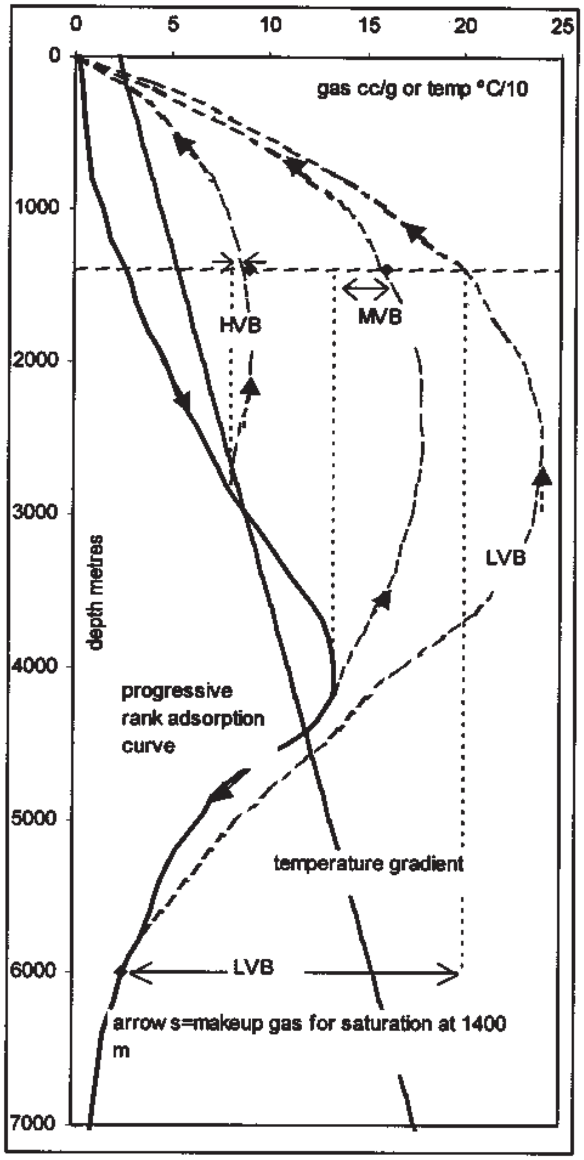

Figure 9. Schematic plot of rank versus adsorption as coal is buried and uplifted.

This means that most coals must scavenge CH_4 during uplift in order to achieve saturation. The plot (Figure 9) indicates that higher rank coals probably have to scavenge large amounts of CH_4 during uplift if they are to achieve saturation at shallow depths. Therefore one should not be surprised that many coals are either under saturated or contain biogenic CH_4 . In fact, based on the importance of biogenic CH_4, which may provide the only viable way of re-saturating coals during uplift, there might well be a negative correlation of degree of saturation with depth in some coalfields.

Coal generates much more gas during coalification than it can adsorb and the excess is expelled into the surrounding rocks. If it is contained in these rocks at depth then the rocks become gas saturated rather than water saturated. It is possible to estimate the amount of gas charged into surrounding rocks. This has been done by Meissner (1984) and by the authors. Estimates need to take account of the effect of increasing temperature and its effect on the adsorption ability of the coal. As an approximate calculation, a coal buried such that its rank reaches 1.5% Rmax will generate enough excess gas to saturate about 5 times its volume of surrounding rock, based on a porosity of 4%. During uplift to 500 metres the gas will expand to fill over 40 times the coal volume. If coals are buried to greater depths, reach higher ranks, and generate more excess gas, then the volumes of surrounding rock that they can saturate are even larger. These calculations require estimates of a number of relationships including, the amount of gas generated by coal during coalification, the effect of temperature on adsorption, temperature gradients, and a relationship between rank and temperature. Obviously only order of magnitude estimates can be made of the effect of coal gas on the surrounding stratigraphy. Oh the other hand if the stratigraphy is gas saturated it is probable that the coal will remain saturated, in terms of adsorption, during uplift. Also it is possible that gas saturation could lead to a reduction in the moisture content of the coal below equilibrium moisture, producing apparent adsorption over saturation when compared to an isotherm run at equilibrium moisture.

RELATIONSHIP BETWEEN COAL COMPOSITION AND ADSORPTION CAPACITY

Different macerals have different adsorption capacities and generate different amounts of gas. Vitrinite generates much more gas during coalification than inertinite, but based on the work of Ettinger *et al*. (1967) may have lower adsorption capacities at high temperatures in conditions where moisture has less influence on adsorption. In banded coals, at high temperatures, inertinite may retain more gas than vitrinite. On uplift a banded or inertinite rich coal would have to scavenge less methane to achieve saturation. Coals in which inertinite has similar adsorption capacities to vitrinite may have a better chance of being saturated during uplift.

There are a number of papers in the literature that study the influence of coal composition on the adsorption ability of coal. Early literature generally dealt with coals dried below equilibrium moisture and is therefore difficult to compare to more recent data. Some of the earlier papers include the work of Ettinger *et al.* (1966). They found distinct differences in the adsorption capacity of vitrinite-rich *versus* inertinite-rich coals. Both types of coals exhibit a minimum adsorption capacity at a rank of about Rmax=0.8%. The minimum increased in intensity with increasing pressure and temperature. Levine (1993) suggests that hydrocarbons generated at about this rank block micro pores and reduce adsorption capacity, especially that of vitrinite, but not necessarily that of inertinite. Ettinger *et al.* (1966) indicated that inertinite rich coals had higher adsorption capacities than the vitrinite rich coals. They do not indicate the moisture contents of samples analyzed and they may have been below equilibrium moisture. The samples studied by Ettinger generally had low ash contents (less than 10%), which is important because it tends to remove the added confusion of ash as a variable when interpreting the results. Based on their results, for coals of medium or low-volatile rank the ratio of adsorptive capacities inertinite/ vitrinite was 1.5 to 2 at high pressures. The ratio decreased at low pressures, but remained greater than 1. Ettinger *et al.* also state that the rate of desorption was faster from inertinite than from vitrinite. Levy *et al*. (1997) found that where as the adsorption capacity of coals at equilibrium moisture contents increased moderately consistently with rank the same was not true for coals dried below equilibrium moisture.

Ulery (1988), studying coals from Pennsylvania, found that desorbed gas content was related to vitrinite reflectance and not maceral content. Gas contents were also influenced by local geological factors such as roof lithology and local folding. Most of his samples contained over 75% vitrinite on a mineral matter-free basis so that it is difficult to use his database of 88 samples to test for any maceral influence on gas content, especially because of the wide range in mean maximum reflectance values (Rmax 0.6% to 1.1%) which strongly influence gas content.

Faiz and Cook, (1992) found that depth of cover had an overriding effect on gas content but that inertinite rich coals of Permian age from southern part of the Sydney Coalfield in Australia tended to contain more gas than vitrinite rich coals. They studied samples collected from the Bulli, Cape Horn and Wongawilli seams with ranks ranging from 1.1% to 1.5%. Within this range and for a wide range of ash contents they derived the following relationship:

m^3/tonne gas = -19.4 + 0.0383 x depth(m) + .0292 x inerts% - 0.153 x MM + 7.63x Rmax% (R^2=0.65).

A review of earlier literature does not indicate a clear maceral control on adsorption capacity or desorbed gas content, possibly because researchers were analyzing coals below equilibrium moisture. More recent literature tends to indicate that vitrinite has a greater adsorption capacity than inertinite. Levine and Johnson (1993) found that over a range of ranks, vitrinite-rich coals from the Bowen Basin, Australia had higher adsorption capacities than inertinite-rich coals. The data were not collected at equilibrium moisture and moisture probably suppresses the adsorption of vitrinite more than inertinite.

Lamberson and Bustin (1993), studied coals from the Gates Formation in northeast British Columbia and found that adsorption capacity correlated with the amount of vitrinite in the ash-free samples of medium-volatile bituminous coals ranging in rank from 1.02% to 1.14% Rmax. Variations in vitrinite content caused greater variation in adsorption capacity than a wide range of rank. Based on their plot of gas *versus* vitrinite %, on a dry mineral matter-free basis (dmmfb), gas concentrations of 0.25 cc/g per 1% vitrinite and 0.1 cc/g per 1% inertinite can be derived. The equivalent values for the Gething samples are 0.45 cc/g for 1% vitrinite and 0.32 c/g for 1% inertinite. They also report adsorption values for CO_2, which have similar relationships to maceral content as CH_4. This is interesting because an argument can be made that inertinite may preferentially adsorb CO_2 where as vitrinite preferentially adsorb CH_4. This is because CH_4 may volume fill the smaller micro pores in vitrinite, where as CO_2 may layer fill the larger meso pores in inertinite.

The maceral influence on adsorption varies with increasing pressure. Bustin *et al.* (1995) studied the Bulli and Wongawilli coals from the Sydney Basin and found that the maceral control of adsorbed gas for these coals was less apparent than for the Gates coals studied by Lamberson and Bustin (1993). Bustin *et al.* looked at the correlation of differential adsorbed gas volume with maceral content at different pressures and found that at low pressure there was a correlation of differential adsorbed gas volume with vitrinite content but at higher pressures the correlation was with inertinite content. The cross-over was at about 2.5 MPa (or about 250 metres).

The data from Bustin *et al.* (1995) plotted in terms of total adsorbed gas at different pressures (Figure 10) emphasizes the lack of maceral influence on adsorption for coals from the Bulli seam. A similar analysis is applied to the Gething and Lamberson and Bustin (1993) data sets (Figure 10). As pressure increases the positive correlation factor for vitrinite *versus* adsorbed gas content improves for the Gething and Gates data suites and the difference in adsorption abilities of the end member macerals increases. The correlation factors are very dependent on the slope of the line and are not reliable for flat lines. The plot is a bit miss leading because the data does not reflect the effect of increased temperature with increased pressure in that the data were acquired at a constant temperature of 25ºC. The Gething data set comes from 5 samples so that not a lot of confidence can be placed in the conclusions.

Bustin and Clarkson (1998) indicated that medium-volatile Permian coals from Australia have higher adsorption capacities than Gates Formation coals of similar rank from northeast British Columbia. It is apparent from Figure 10 that the reason may be that, though the vitrinite from the 2 coals has similar adsorption capacities, inertinite in Australian coals has a higher adsorption capacity than inertinite in Gates coals. This difference may also be apparent in the rheology of the two coals. Australian coking coals tend to have higher Giesler fluidities and FSI values than British Columbian coking coals of similar rank and petrography.

If the type of plot in Figure 10 is valid, then it is possible to pick a depth and therefore a pressure line and predict the adsorption capacity of a coal by sliding along the line to the correct vitrinite percentage. Changes in the maceral influence on adsorption capacity with depth opens the possibility, that depending on depth, coals of high vitrinite or high inertinite content may be better exploration targets. Inertinite is stronger than vitrinite, diffuses gas better (Beamish and Crosdale, 1993) and may retain permeability at depth better, however it would probably under go less matrix shrinkage as gas is produced. Vitrinite on the other hand may have better cleat permeability but may tend to loose gas (Bustin and Clarkson, 1998) and be under saturated.

EFFECT OF MINERAL MATTER ON ADSORPTION CAPACITY

Most of the authors mentioned, used maceral content *versus* adsorption or desorbed gas content plots to support their arguments. Data were corrected either to an ash-free basis or a mineral matter free basis. Although most data indicate that mineral matter acts simply as a dilutent, this may not always the case. It is possible that in some cases a component of the mineral matter may have a negative adsorption capacity. This may be the case for the two samples in this study. Even if this is rare, a useful way of avoiding any confusion about the effect of mineral matter is to plot data into triangular plots. This removes any uncertainty generated by correcting for ash or mineral matter. It is also probably best to use mineral matter volumes determined by microscope work, if available, as they may better estimate the volume of mineral matter that acts as a dilutent.

A number of data suites are re plotted into triangular plots (Figure 11). The plot contains medium-volatile coals from northeast British Columbia (Lamberson and Bustin, 1993), southeast British Columbia (Dawson and Clow, 1992), Australia (Bustin *et al*, 1995 and Walker *et al.,* 2001) and low-volatile Gething coals from this study. There is a trend for adsorption to decrease as mineral matter content increases and to increase as vitrinite content increases. Though there also appears to be a tendency for adsorption capacity to be a maximum for a low mineral matter samples that contain a mixture of a lot of vitrinite and some inertinite. The relationship between gas capacities per unit volume of vitrinite *versus* inertinite should be apparent by looking at data that plots along a single mineral matter concentration line. An adsorption maximum at a specific vitrinite/inertinite ratio rather than at a 100% vitrinite content may indicate that collotelinite, which predominates in mixed maceral coals, may contain more gas than telinite, which predominates in high reactive coals. This is counter to the results from the reflectance histogram data, which seems to indicate that adsorptio is dependent on total vitrinite content only.

It is interesting to consider the effect of mineral matter in a little more detail. It is probably important to differentiate between dispersed mineral matter, which may not act strictly as a dilutent and the discreet crystalline mineral matter, which on a weight or volume basis probably acts only as a dilutent. Therefore attempting to correct data for the effects of mineral matter may be difficult. Dry ash-free corrections will under estimate the weight of mineral matter while mineral matter free corrections such as the Parr equation may over correct the data in terms of the dilutent effect of the mineral matter. It is then important to consider whether dispersed mineral matter directly influences adsorption characteristics of coal by effectively having a negative adsorption capacity. This is similar to the argument made by Thomas and Dam Berger (1976) and Levine (1993) who suggest hydrocarbons generated in the high-volatile bituminous coal block micro pores and reduce adsorption capacity.

It is difficult to determine the proportion of total mineral matter that is dispersed in coal. Generally it is in the range of 2% and comes in part from the original vegetation (equivalent to the ash left after burning clean wood) and in part from salts in solution in the inherent water or adsorbed onto the coal. The amount of dispersed mineral matter decreases as rank increases because some is dispelled with the inherent water and some leaves the organic matrix and crystallizes as discreet mineral phases. Ward *et al*. (2001) used low temperature aching and detailed analysis of RED traces

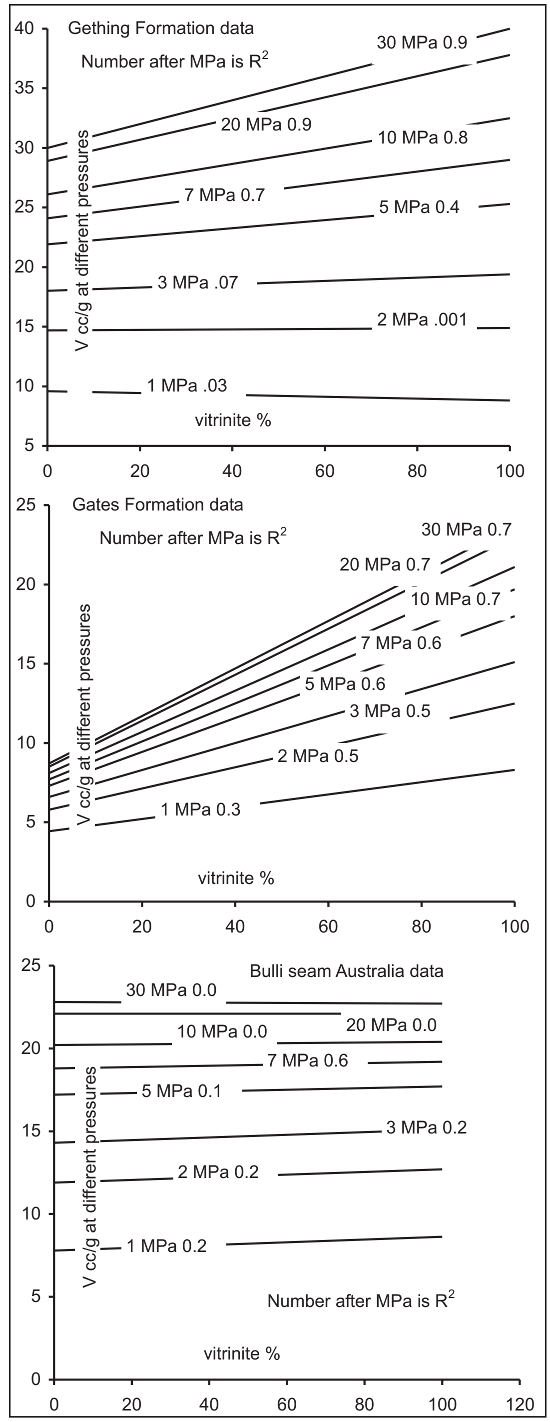

Figure 10. Effect of increasing pressure on vitrinite and inertinite adsorption with R^2 correlation factors for lines. Data from this study, Lamberson and Bustin, (1993) and Bustin *et al.* (1995).

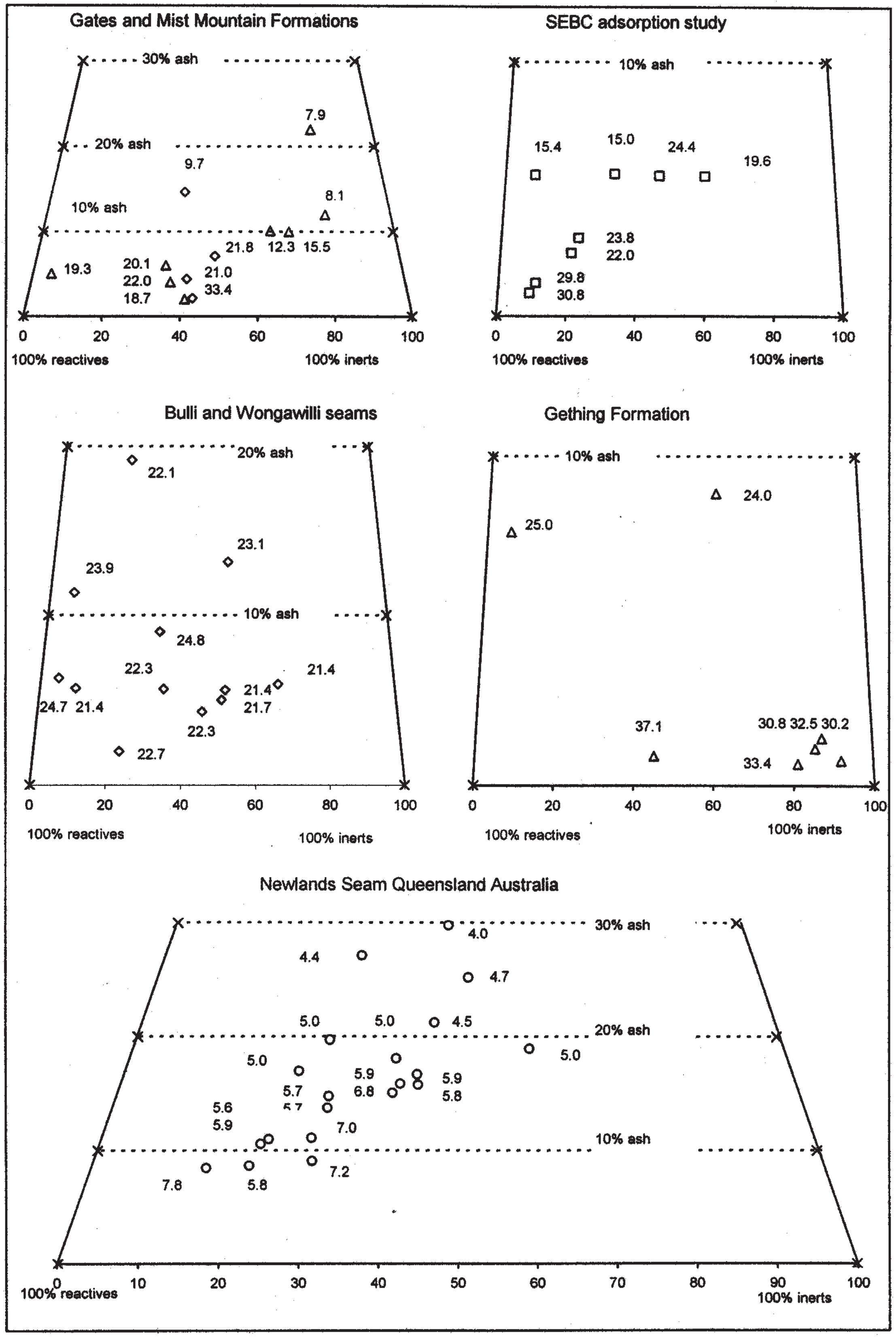

Figure 11. Tertiary plot of vitrinite, inertinite and mineral matter in volume percents. Posted numbers are gas contents. Data from this study, Dawson and Clow (1992), Lamberson and Bustin (1993), Bustin *et al.* (1995) and walker *et al.* (2001).

to identify the proportion of oxides present in crystalline minerals and the proportion present in amorphous form. They were working with Late Permian seams from the Gloucester Basin in Australia. In low rank coals some Ca, Mg, Na, K and Fe may be dispersed in the coal matrix and some may be in solution. In either case these elements may be able to block micro pores acting to decrease the adsorption ability of the coal.

The dispersed mineral matter probably has the same weight as the resultant ash because it is represented by dispersed elements rather than formed minerals that may contain loose CO or OH, which is lost during aching. There does not need to be a miff type correction for this material and as the amount increases in coal there might be a decrease in gas content of more than would be expected based on a weight dilutent effect. At increased ash concentrations represented by the addition of crystalline mineral matter gas contents will decrease based on the dilutent effect of the additional mineral matter. This would imply a 2 stage desorbed gas *versus* ash plot consisting of a line with steep negative slope at low ash and a line with negative slope representing the dilutent effect of ash at higher ash concentrations.

There are a number of data sets that illustrate a progressive decrease in gas contents as ash increases. They usually predict an ash content of less than 100% at zero ash content indicating that mineral matter has a greater weight than the resultant ash, usually by 5% to 20%. However these plots often steeper at low ash contents (Figure 12) (data from Dawson, 1993 and Walker *et al.,* 2001) and a single line does not provide the best fit to the data. This could indicate a negative adsorption effect of dispersed ash or that samples with low ash concentrations have increased vitrinite/inertinite ratios. In some cases the effect is related to petrography as is possibly the case with the desorption data from New lands coals from Queens land Australia (Walker *et al.,* 2001). The desorbed gas *versus* ash indicates a two-slope trend (Figure 12) and at low ash concentrations the reactives/inerts ratio increases. In these cases the two-component line can be taken as more evidence that vitrinite often contains more gas than the inertinite.

There is limited evidence, that in some data suites, ash has a negative adsorption effect. Some medium-volatile Mist Mountain Formation coals from southeast British Columbia (Dawson and Clow, 1992) range in rank from 1.14% to 1.2% Rmax. The four samples are generally enriched in inertinite and have a limited range of vitrinite/inertinite ratios of 1.05 to 1.52, which are not correlated with ash content. The gas contents corrected for ash using the Parr Equation are correlated with ash content implying that the ash may be negatively affecting the gas more than would be expected if it were acting as a dilutent. This is similar to the effect seen by Faiz and Cook whose equation implies that ash has a negative adsorptive capacity of about 0.45 cc/g per 1% ash. Inherent ash contents are probably higher in vitrinite that inertinite, which generally has mineral matter filling cells but in which dispersed mineral matter was probably expelled during charring.

It is possible that some trace elements can be used to estimate dispersed mineral matter. A trace element correlation

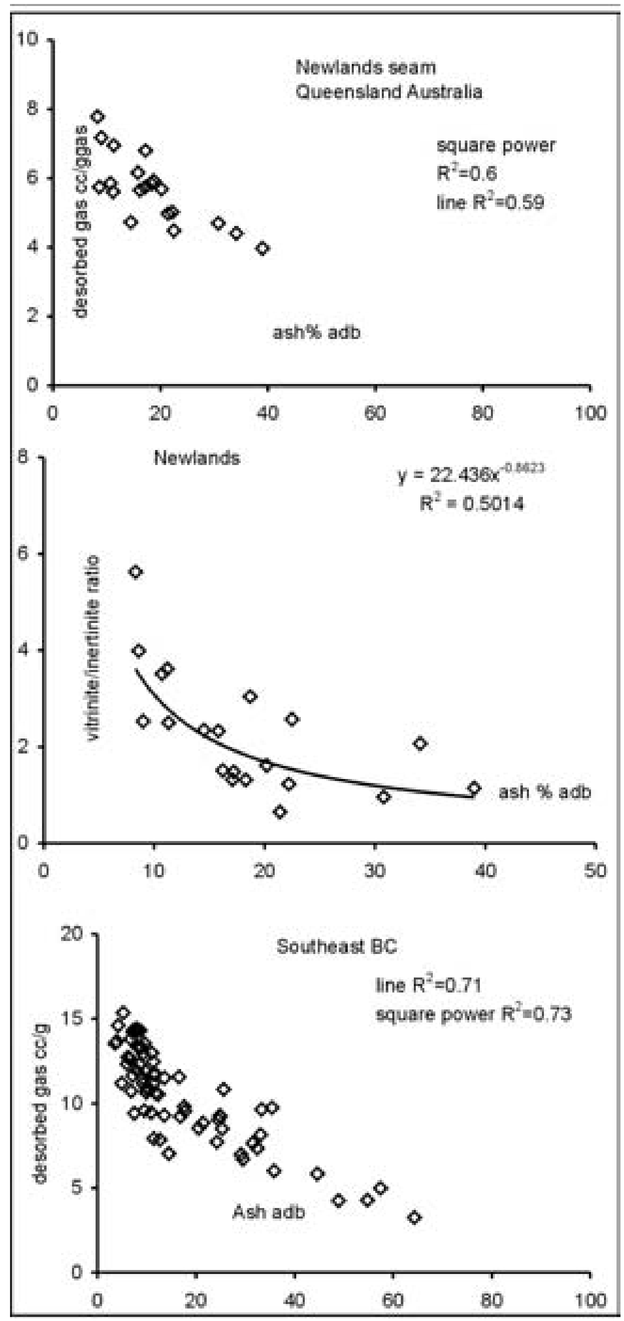

Figure 12. Ash versus gas content plots for southeast British Columbia. Data (Dawson, 1993) and Walker *et al.* (2001) ash versus gas content and from Walker *et al*. (2001) ash% dab versus vitrinite/inertinite ratio.

matrix for the seven Gething samples in this study shows that a number of trace metals correlate negatively with Vl miff and positively with ash. This could imply that they have a direct effect on the adsorption ability of coal. Organic sculpture might also indicate if non-coal elements effect the desorption ability of coal. Unfortunately IMP-MS does not measure organic S and concentrations detected are very low.

CONCLUSIONS

Seven adsorption isotherms of Gething Formation coal have high adsorption capacities. The samples have a rank of 1.7% Rmax and come from a single seam in the mid part of the formation. The data therefore cannot be applied to the formation as a whole, especially considering the wide variation in rank. However it is encouraging that, based on their rank, the samples have, expected or higher than expected adsorption capacities. The adsorption capacity of the five samples with low ash concentrations correlates moderately well with vitrinite content. This is similar to, though not as strong as, the correlation seen between vitrinite and adsorption capacity for the Gates Formation (Lamberson and Bustin, 1993) but better than that seen for some samples from the Bulli seam (Bustin *et al.,* 1995).

Vitrinite measured by conventional petrography and by random reflectance histograms correlate and both correlate with adsorption capacity, as does VM daf. Of the three measures, VM daf is by far the easiest to obtain. A plot of MV daf *versus* adsorption capacity is probably the fastest and easiest way to check for a maceral control on adsorption capacity.

The adsorption capacity of two of the samples seems to be strongly affected by ash content. It is possible that, in some data sets, finely dispersed ash originating from the original vegetation may inhibit adsorption. Based on the expectation that vitrinite adsorbs better than inertinite, a number of data sets imply either an increase in the vitrinite/inertinite ratio at low ash or an ash effect. This ash effect would be greater than the dilution effect of the ash based on its mass or volume.

The adsorption capacities of vitrinite and inertinite change independently as pressure increases and vary between coal seams and fields. Vitrinite/indefinite adsorption ratio is high in Gates coals and increases at high pressure. The ratio is lower for Gething coals but behaves similarly. The ratio is close to 1 for coals from the Bulli seam in the Sydney Basin in Australia and does not vary much with change in pressure.

ACKNOWLEDGEMENTS

R.B.M. Earth Science Consultants (Marc Bustin) provided the isotherms**.** Pearson and Associates Inc provided the random reflectance histograms. Acme labs using ICP-MS performed the trace element analyses. John Price and the carbonization research group at CAN MET provided the two reflectance measurements.

REFERENCES

Beamish, BIB., and Crosdale, P.J. (1993): Characterizing the methane sorption behavior of banded coals in the Bowen Basin Australia; *Proceedings of the International Coalbed Methane Symposium* 1993, pages 145-150.

Broatch, J. C. (1986): A Summary of the results of a palynological investigation of the British Columbia's northeast coalfield*; Paper 1988-1* pages 451-457.

Bustin, R.M., Clarkson, C. and Levy, J. (1995): Coalbed methane adsorption of coals of the Bulli and Wongawilli seams southern Sydney Basin: Effects of maceral composition*; 29th Newcastle Symposium on Advances in study of the Sydney Basin*.

Bustin, R.M. and Clarkson, C.R. (1998): Geological controls on coalbed methane reservoir capacity and gas content; *International Journal of Coal Geology*, Volume 38, pages 3-26.

Diessel, C.F.K. (1992): Coal bearing depositional systems; *Springer-Verlag*

Dawson, F.M. and Clow, J.T. (1992): Coalbed methane research Elk Valley Coalfield; *Canadian Coal and Coalbed Methane Geoscience Forum*, Parkesville, British Columbia February 1992, pages 57-72.

Dawson, F.M. (1993): Fording Joint Venture Project*, Geological Survey of Canada*, Summary Report.

Duff, P, Mc, L and Gilchrist, R.D. (1981): Correlation of Lower Cretaceous coal measures, Peace River Coalfield British Columbia*; Paper 1981-3.*

Eddy, G.E., Rightmire, C.T. and Byren, C.W. (1982): Relationship of methane content of coal rank and depth: theoretical vs. observed; *Proceedings of the Society of Petroleum Engineers*, Department of the Interior, Unconventional Gas Recovery Symposium, Pittsburgh, Pennsylvania, SPE/DOE 10800, pages 117-122.

Ettinger, I., Eremin, B., Zimakov, B. and Yanovskaya, M. (1966): Natural factors influencing coal sorption properties 1-petrography and the sorption properties of coals*; Fuel*, Volume 45 pages 267-274.

Faiz. M.M. and Cook, A.C. (1991): Influence of coal type, rank and depth on the gas retention capacity of coals in the Southern Coalfield N.S.W. Gas in Australian Coals*, Geological Society of Australia*, Symposium Proceedings 2, pages 19-29.

Gibson, D.W. (1985): Stratigraphy and sedimentology of the Lower Cretaceous Gething Formation, Carbon Creek Coal Basin , northeastern British Columbia*; Geological Survey of Canada*, Paper 80-12.

Gurba, L.W., and Weber, C.R. (2001): The relevance of coal petrology to coalbed methane evaluation, using the Gloucester Basin Australia as a model; *International Coalbed Methane Symposium 2001*, Proceedings, May 14-18, 2001, pages 371-382.

Hunt, J.W. and Smyth, M. (1989): Origin of inertinite-rich coals of Australian cratonic basins*; International Journal of Coal Geology*, Volume 11, pages 23-44.

Joubert, J.I., Grein, C.T. and Beinstock, D. (1973): Sorption of methane in moist coal; *Fuel*, Volume 52, pages 181-185.

Kalkreuth, W. and McMechan, M. (1988): Burial history and thermal maturation, Rocky Mountains foothills and foreland east central British Columbia and adjacent Alberta; *Bulletin, American Association of Petroleum Geologists*, Volume 72, pages 1395-1410.

Kalkreuth, W., Langenberg, W. and McMechan, M. (1989): Regional coalification pattern of Lower Cretaceous coal bearing strata, Rocky Mountain Foothills and Foreland, Canada - Implications for future exploration*; International Journal of Coal Geology*, Volume 13, pages 261-302.

Karst, R. and White, G.V. (1979): Coal rank distribution within the Bluesky-Gething stratigraphic horizon of Northeast B.C.*; Ministry of Energy Mines and Petroleum Geology*, Paper 80-1, pages 103-107.

Kim, A.G. (1977): Estimating methane content of bituminous coalbeds from adsorption data; U.S. Bureau of Mines, Report of Investigations 8245.

Lamberson, M.N., Bustin, R.M., and Kalkreuth, W.D. (1991): Lithotype maceral composition and variation as correlated with paleo-wetland environments; Gates Formation northeastern British Columbia, Canada*; International Journal of Coal Geology,* Volme18, pages 87-124.

Lamberson, M.N. and Bustin, R.M. (1993): Coalbed methane characteristics of the Gates Formation coals, northeastern British Columbia: effect of maceral composition; *American Association of Petroleum Geologists Bulletin* Volume 77, pages 2062-2076.

Leckie, D.A. (1983): Sedimentology of the Moosbar and Gates Formations (Lower Cretaceous); Ph.D Thesis, McMaster University.

Leckie, D.A. and Kalkreuth, W. (1990): Formation of coals on wave -dominated strand plains; *International Journal of Coal Geology*, Volume 16, pages 161-162.

Legun. A. (1986): Relation of Gething Formation coal measures to marine paleo shorelines, (93P,93I); *BC Ministry of Energy, Mines and Petroleum Resources*, Paper 1987-1, pages 369-372.

Levine, J.R. (1993): Coalification: the evolution of coal as source rock and reservoir rock for oil and gas; Chapter 3, *American Association of Petroleum Geologists*; Studies in Geology Series, Number 38, pages 39-77.

Levine, J.R., and Johnson, P. (1993): High pressure microbalance sorption studies; *Proceedings of the International Coalbed Methane Symposium,* 1993, pages 187-196.

Levy, J.H., Day, S.J., and Killingley, J.S. (1997): Methane capacities of Bowen Basin coals related to coal properties; *Fuel,* Volume 76, pages 813-819.

Meissener, F.F. (1984): Cretaceous and Lower Tertiary Coals as sources for gas accumulations *in* the Rocky Mountain area; in, Hydrocarbon Source Rocks of the Greater Rocky Mountain Region, Woodward J., Meissener F.F. and Clayton, J.L., Editors, *Rocky Mountain Association of Geologists*, 1984 Symposium, pages 401-431.

Olszewski, A.J. (1992): Development of formation evaluation technology for coalbed methane development*; Quarterly Review of Methane from Coal Seams Technology*; Volume 9, Number 2, January 1992, pages 32-34.

Renton, J.J., Blaine, C.C., Stanton, R., and Dulong, F. (1979): Compositional relationships of plants and peats from modern peat swamps in support of the chemical coal model; Carboniferous Coal Guide*, Department of Geology and Geography West Virginia University*; pages 57-102.

Ryan, BD (1992): An equation for estimation of maximum coalbed-methane resource potential; *BC Ministry of Energy, Mines and Petroleum Resources*, Geological Fieldwork 1991, Paper 1992-1, pages 393-396.

Ryan, BD (1997): Coal quality variations in the Gething Formation northeastern British Columbia; *BC Ministry of Energy, Mines and Petroleum Resources*, Geological Fieldwork 1996, Paper 1997-1, pages 373-397.

Taylor, G.H., Liu, S.Y. and Diessel, C.F.K. (1989): The cold-climate origin of inertinite-rich Gondwana Coals; *International Journal of Coal Geology*; Volume 11, pages 1-22.

Thomas, J. and Damberger, H.H. (1976): Internal surface area moisture content and porosity of Illinois coals variations with coal rank; *Illinois State Geological Surve,* Circular 193.

Ulery, J.P. (1988): Geologic factors influencing the gas content of coalbeds in southwestern Pennsylvania; *United States Department of the Interior,* Bureau of Mines, Report RI 9195.

Walker, R., Glikson, M. and Mastalerz, M. (2001): Relations between coal petrology and gas content in upper Newlands Seam central Queensland, Australia; *International Journal of Coal Geology*, volume 46, pages 83-92.

Ward, C.R., Taylor, J.C., Matulis, C.E. and Dale, L.S. (2001): Quantification of mineral matter in Argonne Premium coals using interactive Rietveld-based X-ray diffraction; *International Journal of Coal Geology*, volume 46, pages 67-82.

Selenium Concentrations in Mine Refuse and Mist Mountain Rocks; Evaluation of Variations Laterally and Over Time

By Barry Ryan, Mike Fournier and Maggie Dittrick

KEYWORDS: *Selenium, coal, tailings, petrography, weathering, Mist Mountain Formation.*

INTRODUCTION

The distribution of Selenium (Se) in the Jurassic-Cretaceous Mist Mountain Formation of southeastern British Columbia was documented in a previous study by Ryan and Dittrick (2001). As part of that study, complete sections of rock types, including coal seams were sampled, as well as various materials segregated by mining such as coarse refuse and solid tailings from tailings ponds. Preliminary results indicate that coal seams of the Mist Mountain Formation have Selenium concentrations similar to the world average for coal seams. The interburden rocks of the Mist Mountain Formation generally contain more Se than expected based on their composition but this is a function of their association with coal seams, which concentrate Se above the crustal average value. Selenium concentrations, within the Mist Mountain Formation, were higher in rocks with higher clay content and those closely associated with coal seams such as hanging wall, footwall and in-seam splits.

The present study deals with samples from mines in the Elk Valley and Crowsnest coalfields (Figure 1). The coal seams are contained in the Mist Mountain Formation, which is part of the Kootenay Group (Table 1). The formation outcrops extensively in the east Kootenays and varies in thickness from 25 to 665 metres (Gibsons, 1985). Typically 8% to 12% of the thickness of the formation is coal and in places this is distributed in over 30 seams. The rest of the formation is composed of non-marine siltstones, mudstones and sandstones. The Morrissey Formation, a sandstone unit that forms the footwall in most mines, underlies it. This formation is underlain by the Fernie Formation, composed predominantly of marine shales. The Elk Formation, a non-marine sandy formation containing thin sapropelic coal seams, overlies the Mist Mountain Formation.

Three aspects of Se distribution, not covered in the previous study are addressed here. These are:

- Changes in Se concentrations within refuse material over time;
- Lateral variations of Se within coal seams;
- Petrographic control on Se concentration in coal seams.

Coarse refuse material is dumped at various locations within the mine site and reclaimed. It is therefore possible to get refuse samples of different, though not accurately defined, ages. Refuse samples, varying in age from over 15 years to less than five years, were collected from three mine sites. The fine refuse material (tailings) from three of the mines is pumped into tailing ponds where it settles and dewaters much like sediments in a lake. Core samples of tailings material from two mines were obtained. These cores provide stratigraphic sections though the tailings, though obviously, because of the way the tailings ponds are filled, it is not possible to assign exact ages to core samples.

During the previous study complete sections of seams and intervening lithology were sampled along the base of high walls. Because of active mining, the base of the high walls had migrated downward about 3 benches (45 metres) by the time the coal seams in the walls were re sampled in 2000. The 1999 and 2000 coal seam samples therefore pro-

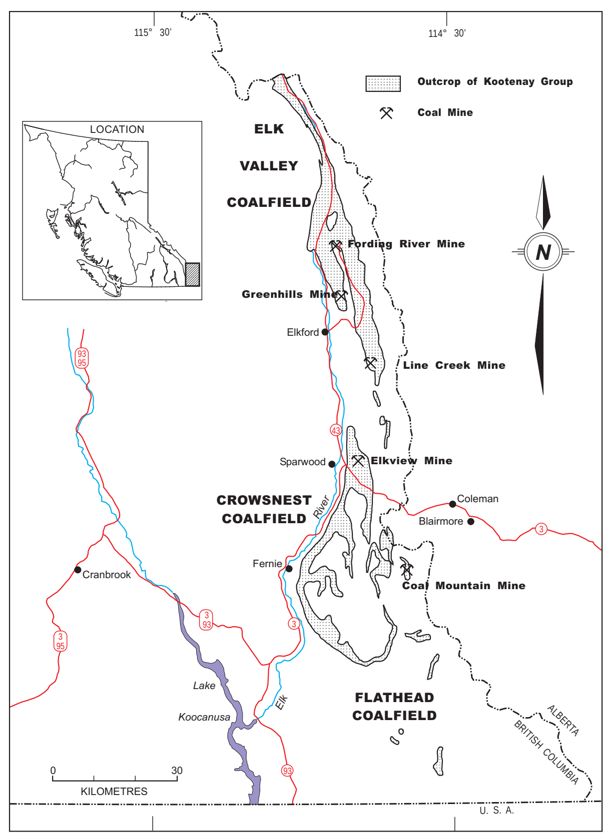

Figure 1. Coalfields and coal mines, southeastern British Columbia.

TABLE 1
KOOTENAY GROUP STRATIGRAPHY

LOWER CRETACEOUS	CADOMIN FORMATION		
JURASSIC AND CRETACEOUS	KOOTENAY GROUP	ELK FORMATION	
		MIST MOUNTAIN FORMATION coal seams	
		MORRISSEY FORMATION	MOOSE MOUNTAIN MEMBER
			WEARY RIDGE MEMBER
JURASSIC	FERNIE FORMATION	PASSAGE BEDS	

vide a good check of the lateral variation of Se concentrations within individual seams.

Fusinite and semi fusinite form as a result of fires in coal swamps. Selenium is very volatile and one would therefore expect concentrations in fusinite and semifusinite to be less than in vitrinite. In this study samples of bright and dull lithotypes were hand picked from a single seam. The samples are used in an attempt to better delineate a maceral influence on Se concentrations.

BACKGROUND

When a study of the Elk River and tributaries in southeast British Columbia (McDonald and Strosher 1998) documented a trend of increasing Se concentrations over the last 15 years, mine operators in the area decided to study the Se distribution, mobility and effects on the environment in more detail. A number of studies are now under way or have been completed. Ryan and Dittrick (2001) studied the distribution of Se in the Mist Mountain Formation and this paper builds on their previous work, and in part details Se distribution in refuse material of variable age. Elevated concentrations of Se in stagnant water (lentic) can concentrate in the food chain and cause reproductive failure and die offs of fish and bird populations as documented in the Kesterton Reservoir in California (Weres, *et. al.,* 1989). In the case of the Kesterton reservoir, agricultural wastewater, enriched in Se, concentrated in the reservoir, which had no outflow. The effects of Se enrichment in flowing water have been less well documented.

DATA COLLECTION

Sampling of lake-bottom unconsolidated sediments has been undertaken using low-cost simple, though moderately labour intensive techniques for collecting cores of a few metres length. The method described in Reasoner (1993) was adapted for sampling in tailings pond areas not submerged by water. The process involved walking out on the near thixotropic material, putting a plywood floor on the tailings to support a stepladder (Photo 1). PCV pipe (7 cm diameter) with a catcher cone on the lower end was forced (with the aid of a sledge-hammer and block of wood held on the top of the pipe) through the plywood and into the tailings. The process was tiring for the sledgehammer operator and somewhat stressful for the person holding the block of wood, however it provided amusement for any passer-by.

Twelve cores with a cumulative length of 43.75 metres were obtained from 2 tailings ponds. Generally about 3 to 4 metres of pipe could be forced into the tailings before progress no longer warranted the effort. At that point the height of tailings in the pipe was measured with reference to the level of tailings out side the pipe. Forcing the pipe into the tailings caused some dewatering and compaction of the material entering the pipe. Consequently after the pipe was forced into the tailings, the level of the tailings in the pipe was always below the level of the tailings outside the pipe.

The core-filled pipes were extracted with the help of a come-along (Photo 1). The suction of the surrounding tailings on the pipe and its contents caused further compaction

Photo 1. Extracting a core from one of the tailings ponds.

of the core. Inspection of the core catcher at the base of the pipe indicated that little core was lost as the pipes were extracted. It is concluded the difference in core length between before and after extracting the core pipe is a result of dewatering and compaction. Total compaction averaged 24% and ranged from about 10% to 32%. The length of cores recovered ranged from 1.27 to 3.84 metres (Table2). Material in the top of the core may not be representative of surface material, because the process of setting up coring equipment inevitably disturbed the surface material around the coring site. Consequently, a surface sample was collected at a nearby locality.

TABLE 2
TAILINGS PONDS CORE DATA SUMMARY

core	length of pipe metres	length of core in pipe before recovery	length of core after recovery	percent total compaction
C00-1	2.7	ND	1.27	53
C00-2	2.7	ND	1.92	29
C00-3	2.7	ND	2.24	17
C00-8	2.7	2.4	2.4	11
C00-9	2.75	2.4	2.2	20
C00-10	4.27	3.67	3.63	15
C00-11	4.25	3.5	3.5	18
B00-45	4.24	3.21	2.88	32
B00-47	4.25	3.34	3.21	24
B00-49	4.26	3.32	3.13	27
B00-50	4.21	3.31	3.25	23
B00-52	4.72	3.77	3.84	19
average compaction				24

Cores were analyzed in Victoria. The filled pipe was placed in a horizontal cradle and cut along its length into two halves (Photo 2) using a bone saw with the blade set to just penetrate the plastic. The top half of the pipe with the tailings was separated from the lower half using a fine pull cord, before being carefully lifted off. The material was uniformly black with horizontal layering sometimes emphasized by changes in grain size, which ranged up to a few mm. A total of 114 (30 centimetre long) samples were collected by excavating a 1 centimetre by 0.5 cm deep channel along the center of the core. The tailings were dried, pulverized and sent for ICP-MS. Some samples were also sent for ash concentration, sulphur form analysis and major oxide analysis using XRF.

Surface samples were collected as channel or chip samples. Samples were crushed, pulverized and sent for ICP-MS analysis; some samples were also sent for ash, proximate and XRF analyses.

Photo 2. A bone cutter used to cut core tubes in preparation for sampling.

At one mine, a number of hand picked samples of bright and dull coal were collected from a single seam. These samples were prepared for petrographic analysis and sent for full proximate analysis.

ANALYTICAL TECHNIQUES

Most Se analyses were done using instrumental neutron activation analysis (INAA) in the previous study by Ryan and Dittrick (2001). The method requires no sample preparation other than pulverizing, consequently Se is not volatilized, as might be the case if the samples were subjected to hot dissolution. Selenium values were checked against a standard and duplicate samples were analyzed at separate laboratories. The data indicated that INAA was providing reliable Se concentration data as long as concentrations were safely above detection limits. However, INAA does have some disadvantages compared to induced coupled plasma mass spectroscopy (ICP-MS). ICP-MS is less expensive, has lower detection limits, and generally requires a smaller sample (1 gm, Table 3). In this study, ICP-MS results were compared to INAA results for samples analyzed previously (Figure 2). There is a tendency for ICP-MS to predict higher concentrations than INAA for concentrations above 4ppm and lower concentrations for samples with less than 4 ppm. On average INAA predicts concentrations 5% higher than ICP-MS.

ICP-MS samples were partially dissolved in aqua regia at a temperature of 90°C. If the wet chemistry sample preparation technique required for ICP-MS analysis was volatilizing Se from samples, or not extracting all the Se, then one would expect ICP-MS results to be consistently low compared to INAA results, which is not the case. It was felt,

TABLE 3
DETECTION LIMITS
(ICP-MS; ALL ELEMENTS ANALYZED. ONLY TOTAL DETERMINATIONS ARE SHOWN IN SUBSEQUENT TABLES)

element	detection			element	detection		
Au	0.2	ppb	T	Mo	0.01	ppm	T
Ag	2	ppb	T	Na	0.001	%	P
Al	0.01	%	P	Ni	0.1	ppm	P
As	0.1	ppm	V	P	0.001	%	P
B	1	ppm	P	Pb	0.01	ppm	T
Ba	0.5	ppm	P	S	0.02	%	P
Bi	0.02	ppm	T	Sb	0.02	ppm	V
Ca	0.01	%	P	Sc	0.1	ppm	P
Cd	0.5	ppm	T	Se	0.1	ppm	T
Co	0.1	ppm	T	Sr	0.5	ppm	P
Cr	0.5	ppm	P	Te	0.02	ppm	T
Cu	0.01	ppm	T	Th	0.1	ppm	P
Fe	0.01	%	P	Ti	0.001	%	P
Hg	5	ppb	T	Tl	0.02	ppm	T
Ga	0.02	ppm	T	U	0.1	ppm	P
K	0.01	%	P	V	2	ppm	P
La	0.5	ppm	P	W	0.2	ppm	P
Mg	0.01	%	P	Zn	0.1	ppm	T
Mn	1	ppm	P				

T total concentration
P partial concentration V some volatilization

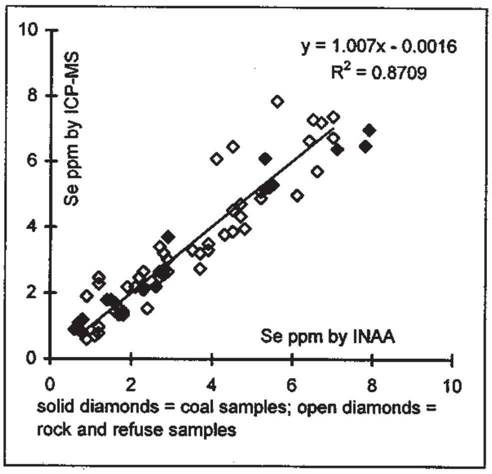

Figure 2. Comparison of Se analyses using INAA and ICP-MS.

therefore, that the ICP-MS method was providing accurate total Se concentrations and all Se analyses in this study were done using the technique. The comparison of methods was made using both coal and rock samples (Figure 2) because the Se has different mineralogy in the two sample types.

Partially dissolving samples in aqua regia at 90°C appears to produce complete extraction of some elements (for example Se) and partial extraction of others such as sulphur and especially rock forming elements such as iron. In these cases comparing ICP-MS data to total concentration data provides information on the partitioning of elements in samples. The relationship of S concentrations derived by ICP-MS and ASTM methods is discussed later.

DATA

The ICP-MS data for the 12 tailings-pond cores are summarized in Table 4, which only lists analyses reported as total concentrations and not those affected by partial extraction or volatilization. Data for some of the elements, which are only partially extracted by ICP-MS, are presented in the discussion. Samples from a hole from the mine B tailings pond were subjected to a number of leaches in an attempt to identify the way in which the Se and other metals are held in the tailings. The leach procedures are those employed by ACME laboratories. In all, 4 leaches each with a different level of aggressiveness, were used (Table 5). The least aggressive leach involved mixing 20 ml of distilled water with 1 g of solid for 1 hour to extract water-soluble components. A 1 M sodium acetate leach for 1 hour was employed to remove exchangeable cations adsorbed on clays. A 0.1 M hydroxylamine leach for one hour was used to remove elements adsorbed by amorphous Mn hydroxide. A 0.25 M hydroxylamine leach for one hour was used to remove elements adsorbed by amorphous iron hydroxide.

Coarse refuse samples were collected from three mines. It is difficult to collect a lot of coarse refuse samples because of the size of each sample, which is determined by the rock fragment size. Generally two, 10 Kg samples of refuse material were collected at each site. One sample of surface material and a second sample from a depth of about 0.7 metres were collected (Table 6). It was usually possible to find locations where the age of the material could be estimated to within a few years and ages ranged from 1 to 7 years to more than 15 years. Samples were analyzed by ICP-MS for Se and other elements; only those elements reported as total analyses are included in Table 6.

A number of outcrop coal samples were collected from Mines B and E. In the previous study the complete section was sampled; in this study only coal seams and some hanging walls and footwalls were sampled. Samples were analyzed by ICP-MS for a number of elements including Se. In addition the ash contents of samples were determined (Tables 7 and 8).

At mine A, a number of samples were hand picked from a single seam representing bright and dull lithotypes. These were analyzed for, proximate values, trace metals by ICP-MS, and for major oxides by XRF. In addition, basic petrography for the samples was recorded using standard microscope techniques and a 300 point count per sample (Table 9).

It is difficult to document the effect of weathering on Se concentrations in coal seams, primarily because of the variation in Se concentrations in the fresh seams. However, in order to better understand potential effects a number of samples of fresh and weathered coal from the same seam were collected and analyzed (Table 10). A few samples of sheared coal were collected (Table 11) to detect any abnormalities in the concentration of Se or any other elements.

TABLE 4
ICP-MS ANALYSES OF TAILINGS POND CORE SAMPLES

Interval	Ash	Se	Mo	Cu	Pb	Zn	Ag	Ni	Co	Au	Cd	Bi	P	La	Hg	Ga
B00-45	%	ppm	ppm	ppm	ppm	ppm	ppb	ppm	ppm	ppb	ppm	ppm	%	ppm	ppb	ppm
surface	71.04	4.5	4.46	35.61	14.95	151.4	271	20	5.3	0.7	1.58	0.26	0.089	6.3	163	1.9
0.0-0.3		6.3	5.23	32.42	16.09	194.9	265	21.6	6.1	0.6	1.93	0.28	0.092	6.6	214	1.8
0.3-0.6		4.9	3.97	30.69	14.73	135	229	18.9	5.2	0.2	1.4	0.27	0.085	6.6	120	1.7
0.6-0.9		4.4	4.4	30.26	14.45	167	232	20.9	5.6	0.9	1.6	0.26	0.079	6.2	165	1.9
0.9-1.2		3.5	3.42	31.87	13.75	122	212	17.8	4.6	1	1.36	0.27	0.078	6.1	108	1.5
1.2-1.5		3.4	3.47	32.83	12.89	112.5	197	16.8	4.5	0.8	1.27	0.26	0.079	5.9	112	1.3
1.5-1.8		3.7	3.47	32.64	14.74	135.6	218	18.7	4.8	0.8	1.42	0.26	0.093	6.1	123	1.5
1.8-2.1		3.2	3.32	30.61	12.84	108	198	16.9	4.1	0.4	1.29	0.24	0.091	6.4	106	1.3
2.1-2.4		3.5	3.37	29.47	13.81	140	227	19.2	4.8	0.6	1.54	0.25	0.082	6.3	140	1.7
2.4-2.7		4.2	4.01	32.8	14.95	161.3	257	20.3	5.1	0.3	1.84	0.28	0.085	6.1	161	2.1
B00-47																
surface	77.21	4.7	4.4	35.03	16.2	156.9	280	20	5.7	0.8	1.69	0.27	0.09	6.3	157	2.1
0.0-0.3		6.6	5.37	32.02	16.95	220	269	24.3	6.4	0.5	2.12	0.27	0.082	5.9	242	2
0.3-0.6		5.1	4.64	30.06	14.83	165.8	250	21.4	5.6	0.3	1.68	0.27	0.085	6.4	170	2
0.6-0.9		4.5	3.89	31.84	14.44	140.7	242	19	5.4	0.4	1.42	0.27	0.081	6	148	1.7
0.9-1.2		4.3	4.26	30.29	14.6	167.7	235	19.4	5.3	0.5	1.56	0.26	0.081	6.2	160	1.9
1.2-1.5		3.6	3.22	31.63	13.73	92.2	194	17	4.1	0.2	1.04	0.25	0.079	6	103	1.2
1.5-1.8		3.3	3.22	30.43	12.65	120	191	15.8	4.1	0.4	1.24	0.24	0.096	6.7	124	1.2
1.8-2.1		4.3	4.08	33.2	15.52	180.8	269	20.7	5.3	0.5	1.93	0.27	0.09	5.9	191	1.9
2.1-2.4		3.2	3.14	29.25	11.8	100.8	210	16.7	3.8	0.3	1.12	0.23	0.082	6	102	1.3
2.4-2.7		4.4	3.98	33.1	14.57	194.8	257	21.1	5.2	0.3	1.99	0.26	0.077	6.1	194	1.8
2.7-3.0		4.3	4	31.49	15.6	187.4	262	20.2	5.1	0.5	1.96	0.27	0.083	6.4	194	1.9
bottom		3.9	3.38	30.71	12.99	338.6	221	17.9	4.5	0.2	1.35	0.24	0.077	6	126	1.4
B00-49																
surface	54.79	3.9	3.59	30.42	13.33	120	217	16.5	4.6	0.7	1.29	0.21	0.089	6.3	113	1.5
0.1-0.4		5.2	4.44	31.18	14.24	138.4	258	19.6	5.4	0.4	1.44	0.27	0.077	5.8	154	2.1
0.4-0.7		4.5	4.14	31.54	14.03	139	248	19.8	5.2	0.2	1.58	0.27	0.074	5.8	159	2.3
0.7-1.0		4.3	4.14	29.2	13.57	137.6	236	19.2	5.1	0.2	1.4	0.26	0.073	5.8	152	2
1.0-1.3		3.2	3.23	29.84	12.56	104.8	195	16.7	4.2	1	1.11	0.24	0.078	5.9	100	1.4
1.3-1.6		3.5	3.68	29.29	12.79	126.3	203	17.4	4.4	0.4	1.25	0.24	0.076	6	126	1.8
1.7-2.0		4.1	4.22	30.87	13.52	182.5	245	20.7	5.4	0.6	1.85	0.24	0.093	5.9	185	2.1
2.0-2.3		4.1	4.15	33.35	14.27	197.7	262	20.3	4.9	0.6	1.84	0.25	0.086	6.3	213	2.3
2.3-2.6		3.8	3.59	32.69	14.15	165.9	269	20.7	5.1	0.4	1.68	0.27	0.075	6.2	175	2
2.6-2.9		3.9	4.13	31.75	14.87	189.6	266	19.8	5.1	0.4	1.77	0.26	0.076	5.7	209	2
bottom		3.8	3.71	31.04	15.17	270.8	251	20.3	4.9	0.3	1.78	0.27	0.076	5.8	177	1.9
B00-50																
surface	76.73	4.5	4.23	34.43	16.59	158.5	275	19.6	5.5	0.7	1.69	0.27	0.087	5.8	185	2.1
0.1-0.4	79.26	5.4	5.61	31.05	14.75	192.5	276	22.1	5.8	0.4	1.93	0.26	0.086	6	224	2.6
0.4-0.7	77.31	5.1	4.55	31.22	14.53	162.4	262	20.3	5.5	0.5	1.76	0.26	0.077	5.6	202	2
0.7-1.0	73.55	3.9	4	30	14.41	132.4	229	17.9	5.1	0.6	1.3	0.26	0.076	5.4	161	2.4
1.0-1.3	67.1	3.4	3.32	30.92	12.94	117	198	16.4	4.3	0.6	1.19	0.24	0.072	5.7	109	2.2
1.3-1.6	58	3.3	3.35	28.65	13.09	114.1	186	14	3.9	0.5	1.05	0.22	0.078	6.3	106	1.6
1.6-1.9	75.51	4.1	4.36	30.57	15.41	187.8	274	20.6	5.1	0.6	2	0.26	0.093	6.6	187	2.8
1.9-2.2	78.19	3.7	3.99	29.3	13.9	172.2	259	18.7	4.5	0.4	1.62	0.26	0.077	6.5	151	2.8
2.2-2.5	72.02	3.4	3.27	31.58	13.85	126.3	250	17.7	4.3	0.2	1.4	0.26	0.066	6.2	119	2
2.5-2.8	75.72	3.7	4.27	30.5	14.44	147.8	253	19.1	4.9	0.4	1.58	0.26	0.068	6.1	142	2.4
2.8-3.1	69.18	3.2	3.09	30.38	13.53	128.1	235	16.6	4.1	0.3	1.37	0.26	0.061	5.8	120	2
bottom	55.92	3.3	3	28.68	12.16	376.9	205	15.2	3.9	0.2	1.14	0.24	0.07	6.7	90	1.3
B00-52																
surface	74.56	4.7	5.22	34.15	16.92	185	313	23.2	6.6	0.3	2.02	0.27	0.094	6	189	2.2
0.1-0.4	79.52	5.6	5.25	31.45	16.19	244.4	298	22.8	5.9	0.4	2.2	0.26	0.077	5.9	316	2.5
0.4-0.7	78.48	4.8	4.19	29.96	15.07	181.1	256	19.8	5.1	0.2	1.77	0.25	0.064	5.8	188	2.4
0.7-1.0	80.08	5	4.98	28.32	16.48	201.8	276	21.7	5.7	0.2	1.88	0.26	0.07	6.1	227	2.5
1.0-1.3	72.17	3.4	3.52	28.77	13.09	142.6	218	15.6	4.2	< .2	1.34	0.25	0.063	6	124	2
1.3-1.6	72.22	3.5	3.48	30.48	13.5	138.3	229	16.4	4.7	0.2	1.4	0.26	0.07	6.5	142	2.1
1.6-1.9	74.63	4.1	4.26	31.33	15.01	198.5	259	19	4.9	0.2	1.88	0.26	0.078	6.4	220	2.6
1.9-2.2	74.99	5.2	5.44	28.3	16.74	326	290	22.8	5.7	0.3	2.82	0.24	0.088	6.6	402	2.7
2.2-2.5	76.81	4.5	4.41	27.92	15.07	239.4	262	20.1	5.1	0.3	2	0.24	0.075	6.2	263	2.5
2.5-2.8	80.03	4.1	4.03	30.4	14.9	186	268	19.6	5	< .2	1.92	0.26	0.07	6	239	2.5
2.8-3.1	73.71	4.2	3.8	28.86	15.44	164.8	255	19.1	4.5	< .2	1.68	0.27	0.068	6.2	188	2.3
3.1-3.4	77.78	3.9	3.46	31.47	15.6	147.7	259	21.1	5.1	0.2	1.55	0.29	0.064	5.4	214	2.5
3.4-3.7	74.6	3.6	4.01	27.82	13.76	140.7	238	19.4	5	0.3	1.49	0.25	0.068	5.6	179	2.4
bottom	75.69	3.6	3.51	29.23	14.08	507.5	256	19.6	4.6	0.4	1.56	0.27	0.073	5.9	165	2.1

TABLE 5
SUMMARY OF LEACH RESULTS FROM HOLE B00-50

Depth	W	SA	0.1 HL	0.25 HL	NL	W	SA	0.1 HL	0.25 HL	NL	W	SA	0.1 HL	0.25 HL	NL	W	SA	0.1 HL	0.25 HL	NL
		Se ppm					As ppm					Pb ppm					Zn ppm			
0-.1	0.153	< .2	< .2	< .2	4.5	<.005	<.1	0.36	0.36	4.4	<0.02	0.41	1.34	3.61	16.59	0.05	5.2	11.8	15.2	158.5
0.1-.4	0.138	< .2	< .2	0.2	5.4	<.005	<.1	0.38	0.90	4.8	<0.02	0.63	1.10	4.46	14.75	< .01	4.8	12.4	18.1	192.5
0 .4-.7	0.109	< .2	< .2	0.2	5.1	<.005	<.1	0.34	1.08	3.9	<0.02	0.81	1.26	4.45	14.53	0.02	5.5	15	19.6	162.4
0 .7-1.0	0.121	< .2	< .2	< .2	3.9	<.005	<.1	0.39	1.02	3	<0.02	0.53	1.12	4.38	14.41	< .01	4.8	12.2	16.6	132.4
1.0-1.3	0.1	< .2	< .2	< .2	3.4	<.005	<.1	0.35	0.80	2.6	<0.02	0.35	0.97	3.27	12.94	0.04	4.1	11.3	10.6	117
1.3-1.6	0.114	< .2	< .2	< .2	3.3	<.005	<.1	0.37	0.51	2.5	<0.02	0.55	0.77	3.19	13.09	0.02	4	8.6	10.1	114.1
1.6-1.9	0.122	< .2	< .2	0.2	4.1	<.005	<.1	0.36	0.67	5	0.026	0.65	0.81	4.07	15.41	0.02	5.1	10.8	19.9	187.8
1.9-2.2	0.1	< .2	< .2	0.2	3.7	<.005	<.1	0.27	0.64	4.4	<0.02	0.77	0.94	4.24	13.9	< .01	5.4	11.3	18.1	172.2
2.2-2.5	0.078	< .2	< .2	< .2	3.4	<.005	<.1	0.39	0.45	3	0.02	0.79	1.01	3.96	13.85	0.01	4.7	10.2	10.6	126.3
2.5-2.8	0.059	< .2	< .2	< .2	3.7	<.005	<.1	0.36	0.75	3.9	0.053	0.62	1.02	4.25	14.44	0.02	4.5	12.2	15.7	147.8
2.8-3.1	0.06	< .2	< .2	< .2	3.2	<.005	<.1	0.28	0.66	2.7	<0.02	0.64	0.91	3.52	13.53	< .01	4.1	10.4	13.3	128.1
bottom	0.067	< .2	< .2	< .2	3.3	<.005	<.1	0.33	0.47	2.3	0.028	0.60	0.81	2.54	12.16	1.5	102.9	50.6	24.6	376.9
		P ppm					cu ppm					Mn ppm					Hg ppb			
0-.1	1	< 5	179	225	870	0.09	0.7	2.7	2.6	34.4	0.2	11	60	79	205	< 1	< 5	< 5	6	185
0.1-.4	0.6	< 5	174	226	860	0.03	0.9	2.8	2.4	31.1	0.16	12	70	136	363	< 1	5	< 5	8	224
0 .4-.7	1	< 5	165	237	770	0.03	2.1	2.8	2.7	31.2	0.24	11	90	105	260	< 1	5	< 5	5	202
0 .7-1.0	1	< 5	199	206	760	0.01	1	3	2.5	30	0.09	12	61	73	184	< 1	8	< 5	< 5	161
1.0-1.3	1	< 5	174	152	720	0.07	< .1	2.5	2.3	30.9	0.15	8	59	32	136	< 1	5	< 5	< 5	109
1.3-1.6	1.4	< 5	191	137	780	0.02	1.3	2.3	1.8	28.7	< .05	7	41	44	164	< 1	< 5	< 5	< 5	106
1.6-1.9	2	< 5	207	245	930	0.04	2.8	2.1	2.7	30.6	0.13	9	107	255	522	< 1	< 5	< 5	5	187
1.9-2.2	0.3	< 5	160	218	770	0.01	3.8	2.6	2.8	29.3	0.07	10	98	196	382	< 1	< 5	< 5	7	151
2.2-2.5	1	< 5	197	145	660	0.02	2.1	2.2	2.2	31.6	< .05	8	67	70	206	< 1	< 5	< 5	< 5	119
2.5-2.8	0.6	< 5	174	217	680	0.04	1.7	2.9	2.9	30.5	0.13	9	87	115	259	< 1	< 5	< 5	< 5	142
2.8-3.1	0.5	< 5	181	195	610	0.02	2.1	2.4	2.5	30.4	0.06	9	53	63	170	< 1	< 5	< 5	< 5	120
bottom	0.8	< 5	187	141	700	0.05	0.6	2.5	1.8	28.7	0.09	8	37	45	109	< 1	< 5	< 5	< 5	90
		Fe %					Mo ppb					U ppb					Cd ppb			
0-.1	<0.005	0.012	0.65	0.87	2.5	27	< 10	72	1538	4230	1.7	107	307	286	1400	17	165	62	72	1690
0.1-.4	<0.005	0.013	0.76	1.23	3.77	21	< 10	75	1744	5610	1.3	114	313	296	1400	19	226	124	116	1930
0 .4-.7	<0.005	0.074	0.95	1.17	2.93	27	< 10	74	1743	4550	1.5	101	324	279	1300	17	262	147	137	1760
0 .7-1.0	<0.005	0.016	0.70	0.88	2.09	39	< 10	97	1505	4000	2	108	268	257	1200	17	179	129	98	1300
1.0-1.3	<0.005	0.011	0.67	0.44	1.5	42	< 10	72	1073	3320	2.8	83	209	204	1200	21	135	61	43	1190
1.3-1.6	<0.005	0.013	0.48	0.61	1.57	66	< 10	94	1038	3350	3.6	73	219	170	1100	13	135	34	77	1050
1.6-1.9	<0.005	0.019	1.05	2.15	4.18	39	< 10	62	1306	4360	2	98	320	290	1400	13	191	83	165	2000
1.9-2.2	<0.005	0.022	1.03	1.62	3.29	37	< 10	55	1084	3990	1.7	96	324	273	1300	18	177	89	132	1620
2.2-2.5	<0.005	0.017	0.71	0.66	1.84	54	< 10	80	887	3270	3	76	329	206	1200	18	222	113	114	1400
2.5-2.8	<0.005	0.011	0.84	1.02	2.31	32	< 10	63	1203	4270	1.9	77	315	275	1300	18	191	101	169	1580
2.8-3.1	<0.005	0.014	0.59	0.67	1.62	36	< 10	59	1068	3090	1.5	68	262	218	1100	16	148	79	108	1370
bottom	<0.005	0.009	0.48	0.48	0.96	53	< 10	71	834	3000	2.1	55	215	199	1100	18	198	70	78	1140

W = distilled water neutral pHSA = 0.1 M sodium acetate   0.1 HL = 0.1 hydroxylamine   0.25HL = 0.25 hydroxylamine   NL = no leach original sample

TABLE 6
COARSE REFUSE DATA

	Age years	Ash %	Se ppm	Mo ppm	Cu ppm	Pb ppm	Zn ppm	Ag ppm	Ni ppm	Co ppm	Au ppm	Cd ppm	P %	Hg ppb	Te ppm	Ga ppm
Mine A	recent		3.7													
L bnch D	15+	75.18	2.5	2.04	28.04	11.82	90.9	265	15.1	3.3	0.3	1.24	0.113	80	0.05	1.3
L bnch S	15+	74.56	1.8	1.55	27.54	11.54	101.1	263	15	3	0.5	1.41	0.093	94	0.06	1.4
U bnch D	15+	74.31	2	1.82	33.02	12.37	140.2	308	14.5	3	0.4	1.76	0.079	131	0.06	1.4
U bnch S	15+	75.91	2	2.09	31.64	12.94	121.1	275	18.5	4.3	< .2	1.68	0.08	121	0.06	1.4
U bnch D	15+	77.74	3.4	3.44	27.14	11.42	116.7	323	14.9	2.6	0.2	1.88	0.452	160	0.08	2.4
U bnch S	15+	77.33	2.4	1.93	27.82	12.36	120.6	377	15.4	3.2	0.2	2.06	0.196	109	0.07	1.7
Mine B	recent		3.5													
pile D	1 to 7	63.26	3.5	2.52	27.32	11.24	96.4	272	13.7	3.2	< .2	1.37	0.07	137	0.05	1
pile D	1 to 7	62.23	3.5	2.43	27.5	11.03	109.3	275	14.7	3.3	< .2	1.48	0.086	126	0.04	1.1
S	1 to 7	68.37	2.2	1.86	29.3	11.14	112.3	224	12.1	3.2	0.2	1.42	0.065	92	0.06	1.2
S	1 to 7	65.42	1.9	1.83	27.52	11.13	83.7	212	9.9	3.1	< .2	1.19	0.06	81	0.05	1.3
Mine C	recent		2.1													
L bnch D	15 +/-	54.02	2.1	1.32	26.48	11.07	77.2	215	9.2	2.6	< .2	1.45	0.076	244	0.05	0.7
U bnch D	15 +/-	59.66	1.8	1.37	31.29	12.12	76.8	207	8.2	3.6	< .2	1.3	0.058	107	0.06	0.9
U bnch S	15 +/-	63.83	1.8	1.39	28.36	11.6	75.8	233	11.3	3.1	< .2	1.24	0.071	151	0.06	1.2
Pile D	5+/-	55.36	2.1	1.77	28.06	10.57	66.6	202	16.9	3.8	< .2	1.03	0.041	85	0.05	1

U=Upper, L=Lower; Bnch = Bench S = surface sample D= sample about 70 cm depth

TABLE 7
SURFACE COAL, HANGING WALL AND FOOTWALL MATERIAL MINE B
SEAM 1 IS LOWEST IN SECTION

Seam		ash %	thick ppm	Se ppm	Mo ppm	Cu ppm	Pb ppm	Zn ppm	Ag ppm	Ni ppm	Co ppm	Cd ppm	P %	Hg ppb	Te ppm	Ga ppm
14	coal	14.1	1	1.4	1.17	13.2	5.3	11.8	109	7.3	1.3	0.38	0.084	7	0.03	0.5
13	coal	5.4	1.5	0.7	0.7	5.4	2.2	8.3	26	5	1	0.1	0.062	< 5	0.02	0.2
12	coal	25.7	1.5	1.4	1.44	16.8	6.2	44.9	114	4.6	1.8	0.71	0.024	18	0.03	0.3
11	HW	64.1	0.5	2.5	3.05	20.8	14.3	98.7	192	26.8	5.1	1.04	0.024	270	0.06	1.3
11	coal	6.4	1.5	0.4	0.65	5.0	1.9	6.2	32	1.6	0.4	0.07	0.129	< 5	0.03	0.2
10	coal	11.1	1.5	0.9	1.02	6.1	3.5	8.5	37	3.7	0.8	0.11	0.081	11	0.03	0.3
10	coal	53.1	1	2.1	1.48	19.6	10.4	56.6	207	5.2	1.7	1.31	0.04	20	0.06	0.8
9	HW	68.5	0.15	3.4	1.95	36.2	19.2	199.1	285	40.4	8.4	2.79	0.142	122	0.12	1.6
9	HW	86.5	0.15	3.1	3.46	28.9	17.8	151.7	259	46.5	9.1	1.49	0.142	93	0.07	3.2
9	coal	8.9	1	0.6	1.49	11.1	3.2	9.4	58	5.6	2.1	0.1	0.1	< 5	0.05	0.3
9	HW	73.7	0.2	2.5	1.69	24.8	14.2	73	431	6.9	1.2	0.96	0.01	33	0.02	1.4
8	coal	18.0	2.5	1.8	1.73	8.4	3.3	52.2	93	4	0.4	0.36	0.054	88	0.03	0.5
8	parting	76.6	2.5	3.7	2.18	31.8	13.5	164.9	547	20.3	5.4	2.56	0.065	53	0.07	1.6
8	coal	16.9	3	1.2	1.65	10.4	4.2	33	108	5.1	0.6	0.51	0.044	14	0.02	0.3
7	HW	82.7	0.2	4.8	4.13	34.0	21.7	185.9	326	65.6	15.9	1.93	0.125	84	0.04	2.1
7	coal	18.4	1.5	1.4	1.09	9.0	4.6	23.4	56	4.2	1.3	0.34	0.012	14	0.02	0.4
7	parting	82.9	0.1	1.7	0.56	20.5	8.5	11.8	139	3.7	1.4	0.42	0.003	9	0.05	1.5
7	coal	18.4	1.5	0.6	1.72	10.7	2.3	25	33	3.4	0.7	0.3	0.008	43	< .02	0.6
7	FW	71.3	0.3	3.7	4.99	26.7	16.9	117.4	156	45.4	11.1	1.08	0.025	263	0.05	1.7
7	FW	44.8	0.5	3.5	6.35	24.7	13.2	150.2	145	30.4	5.7	1.32	0.128	121	0.07	1.3
6	coal	20.8	4	1.6	1.59	25.5	8.9	20.1	75	7	2.1	0.33	0.05	38	0.05	0.3
5	HW	70.1	0.5	2.8	1.34	26.0	16.7	121.2	265	28.1	17.3	0.81	0.051	62	0.07	1.3
5	coal	8.4	1.5	0.4	0.78	5.6	2.6	4.6	19	2	0.2	0.05	0.218	< 5	0.03	0.3
5	FW	63.7	1.5	1.4	1.27	17.0	8.4	96.8	129	7.5	2.5	0.6	0.042	24	0.03	1.6
4	coal	14.2	2	1.2	0.5	10.1	5.4	13.3	38	5.1	1.6	0.22	0.034	12	0.03	0.2
3	coal	21.2	1	1.7	2.21	16.6	6.1	57.5	98	6.7	1.5	0.7	0.029	23	0.03	0.2
3	coal	39.1	2	2.7	1.57	18.8	8.6	61.1	161	10.3	1.6	1.2	0.034	19	0.04	0.3
2	coal	21.3	2	0.5	0.22	5.0	4.0	4.6	21	3.1	0.7	0.04	0.12	< 5	< .02	0.1
1	coal	57.0	3	3.3	4.26	37.3	11.1	98.4	262	21.3	5.1	1.35	0.067	101	0.06	0.9

HW=hanging wall and FW= footwall

TABLE 8
SURFACE COAL, HANGING WALL AND FOOTWALL MATERIAL MINE E
SEAM 1 IS LOWEST IN SECTION

Seam		thick	ash	Se	Mo	Cu	Pb	Zn	Ag	Ni	Co	Cd	P	La	Cr	Hg	Te	Ga
			%	ppm	ppm	ppm	ppm	ppm	ppm	ppm	ppm	ppm	%	ppm	ppm	ppb	ppm	ppm
15	coal	2	13.4	4	0.53	6.0	2.1	13.2	49	7.7	0.4	0.25	0.033	2.9	9.1	12	0.02	0.2
14	coal	1.5	25.3	2.8	0.71	14.0	6.6	11.5	133	3.2	0.7	0.19	0.017	6.6	5.5	11	0.06	0.2
13	coal	1	29.6	5.5	1.25	23.2	8.7	47.3	90	9.9	3.4	0.48	0.187	14	12	51	0.09	0.5
12	coal	1.5	11.7	1	0.67	18.5	3.5	5.5	50	2.2	0.8	0.23	0.199	10.4	2.6	10	0.07	0.2
11	coal	1	11.5	1.9	1.34	9.7	7.0	14.3	58	5.5	1.1	0.18	0.13	8.3	2.3	17	0.04	0.2
10	HW	2	54.4	3.3	2.44	25.5	11.5	109.5	332	18.3	4.9	2.08	0.058	6.3	12.6	59	0.07	0.8
10	coal	6	25.4	2.4	1.69	18.6	7.1	24.4	153	5.6	1.1	0.64	0.052	7.7	10.6	16	0.06	0.3
10	FW	0.3	52.7	3.7	2.89	25.2	10.1	99.5	318	21.6	3.4	2.02	0.062	4.8	15.8	44	0.04	0.5
	interB	6	86.7	3.2	3.11	25.0	15.8	152.1	410	32.6	5.2	1.95	0.123	9.8	31.8	66	0.05	2.3
9	coal	3	40.6	3.5	2.9	20.2	9.9	100.2	173	12.5	3.7	1.36	0.096	10.4	9.2	48	0.07	0.6
	interB	15	87.6	2.5	2.07	24.4	12.0	106.4	375	27.3	5.6	1.52	0.098	9.5	32.6	60	0.06	1.9
8	HW	0.4	32.1	4.7	2.6	20.3	8.1	34.0	188	16.8	2.2	0.87	0.035	2.6	7.7	22	0.03	0.7
8	HW	0.4	88.1	5.1	1.85	34.0	15.5	114.4	384	26.4	4.4	1.9	0.093	5.1	15.2	81	0.08	1.6
8	coal	3	20.2	2.1	1.77	15.1	5.6	43.8	93	6.5	1.5	0.46	0.117	6.9	9.5	19	0.04	0.4
8	coal	0.1	50.6	1.6	1.66	15.4	12.3	6.7	86	3	0.8	0.26	0.006	3.3	< .5	90	0.07	0.6
8	coal	0.3	53.9	5.9	4.12	29.3	14.3	142.4	254	18.9	5.3	1.55	0.003	1.9	9.4	147	0.06	0.4
7	coal	1.5	22.5	5.5	2.82	12.7	6.6	63.6	99	16	1.6	0.38	0.142	10.1	9.5	45	0.08	0.5
6	coal	2	64.0	3.8	3.1	30.2	10.4	95.7	420	12.2	1.6	2.17	0.091	12	20.9	51	0.06	0.9
5	HW	0.2	86.0	4.9	3.58	51.3	17.4	292.3	472	51.2	9.6	4.83	0.145	7.8	22.9	186	0.07	2.2
5	HW	0.2	88.8	3.9	2.27	40.4	15.7	194.3	430	41	6.9	3.37	0.163	8.6	24.8	101	0.07	2.5
5	coal	1.5	20.4	1.8	1.91	16.6	4.8	34.9	101	11.1	2.3	0.69	0.13	10.8	6	31	0.04	0.4
5	FW	1.5	74.6	4.8	3.02	37.4	14.8	216.7	433	26.2	5.5	2.69	0.102	8.4	18.2	146	0.08	1.4
4	coal	3	67.3	2.7	2.49	28.1	12.8	118.9	212	21.9	4.4	1.1	0.06	10.3	10.9	80	0.03	1
3	coal	2.5	14.1	0.7	1.19	14.5	4.8	21.7	58	3.1	1.1	0.6	0.145	8.8	8.1	75	0.03	0.2
	interB	6	85.6	4.7	2.79	37.5	15.8	243.6	553	43.2	6.6	3.87	0.188	17.8	32.8	131	0.07	2.5
2	coal	0.3	42.6	1.5	5.96	20.8	6.2	12.8	296	12.7	1.4	0.23	0.041	8.3	12.6	30	0.04	0.4
	interB	2	84.4	3.9	2.96	30.2	14.9	217.6	525	40.8	8.2	2.65	0.143	14.4	23.9	248	0.06	2.4
	interB	6	87.4	4.8	2.7	39.7	17.0	238.5	548	36.7	6.7	4.11	0.195	14.1	29.9	229	0.08	2.6
1	HW	4	78.5	3.2	2.43	37.8	20.0	193.6	350	28.4	7.5	2.46	0.071	8.3	18.2	122	0.07	1.4
1	coal	2.5	18.1	1.3	1.05	25.1	10.4	28.2	34	3.6	2.2	0.18	0.124	13.4	0.6	22	0.05	0.4
1	parting	0.3	72.3	2.8	2.05	18.1	9.5	230.0	346	25	4.2	2.55	0.049	4.6	24	97	0.05	1.2
1	coal	5	29.8	1.7	4.61	19.8	7.1	34.2	109	5.8	1.3	0.27	0.122	8.9	3.2	26	0.05	1.1
1	FW	4	73.3	5.3	3.62	42.1	14.6	176.7	653	31.8	5	3.62	0.117	9.7	18.9	147	0.08	1.4

TABLE 11
ICP-MS, PROXIMATE AND OXIDE ANALYSES ON SHEARED COAL

	Se	Mo	Cu	Pb	Zn	Ag	Ni	P
	ppm	ppm	ppm	ppm	ppm	ppm	ppm	%
Mine B seam 1								
F	2	0.48	2.65	1.94	17.4	11	1.7	0.02
S	1.3	0.92	10.62	5.68	31	67	2.5	0.083
Mine E seam 8								
F	2.1	1.77	15.1	5.6	43.8	93	6.5	0.12
S	1.6	1.66	15.44	12.33	6.7	86	3	0.006
S	5.9	4.12	29.34	14.26	142.4	254	18.9	0.003
S	5.5	2.82	12.66	6.58	63.6	99	16	0.142

	M% ad	VM% ad	Ash% ad	FC% ad	B/A
F			6.54		
S	0.35	22.89	22.01	54.75	0.083
F			20.2		
S	0.25	19.48	51.92	28.35	0.017
S	0.32	15.62	54.24	29.82	0.089
S	0.36	20.56	23.74	55.34	0.052

B/A raitio of base to acid oxides. F=Fresh S=Sheared

DISCUSSION

TAILINGS POND DATA

Cores were collected from 2 ponds. Seven cores were collected from the pond C (Figure 3), which has been inactive for about 20 years, although it is periodically flooded to stop it from drying out and generating dust. Five cores were collected from pond B, which is active. Tailings enter the ponds via spigots, which are periodically moved. It is therefore impossible to document a detailed and consistent pond stratigraphy. However, based on annual clean coal production, yield and size of the pond it is possible to estimate average accumulation rates, which probably range from 20 to 50 cm per year in compacted material. This means that a 3 metre core probably represents from 5 to 10 years of accumulation.

Tailings pond material consists of the solid tailings and interstitial water. The material has the consistency of wet mud 10 cm below the surface. It is difficult to estimate the water content but core recovery results provide sufficient data to make an informed estimate.. The cores experienced an average compaction of 24% (Table 2) as they were ex-

TABLE 9
ANALYTICAL DATA FOR COAL SAMPLES COLLECTED FOR SE *VERSUS* PETROGRAPHY STUDY

	B/A	Se	Mo	Cu	Pb	Zn	Ag	Ni	Co	Cd	P	La	Cr	Hg	Te	Ga
		ppm	ppm	ppm	ppm	ppm	ppm	ppm	ppm	ppm	%	ppm	ppm	ppb	ppm	ppm
T		4.2	2.3	25.7	11.0	130.3	178	11.4	3.2	1.32	0.059	7	9.2	85	0.03	0.3
1D		1.4	1.61	14.1	5.0	4.1	70	1.6	0.5	0.28	0.051	8.6	2.9	12	0.05	0.1
2B		2.3	1.7	7.0	7.9	5.1	40	2.8	0.7	0.19	0.044	4.7	3.5	5	0.03	0.1
3D	0.027	2.2	1.87	17.7	7.8	4.2	136	2.7	0.5	0.11	0.004	1.1	7	7	0.04	0.1
4B	0.020	2.6	1.8	18.3	9.4	2.5	87	5.2	1.1	0.03	0.003	1.8	5.5	6	0.02	0.1
5D	0.011	1.4	1.69	11.8	4.8	3.7	56	3.2	1.4	0.15	0.002	1.8	3.5	< 5	0.03	0.1
6B	0.015	1.2	1.41	10.6	3.8	2.6	29	1.9	1.5	0.14	0.008	8.1	< .5	< 5	0.02	0.1
7D	0.030	6.5	8.9	10.4	7.9	6.9	40	9.6	4.4	0.21	0.067	14.9	1.7	321	0.06	0.3
8B	0.035	2.5	3.36	6.9	3.7	3.4	17	5.9	2.2	0.07	0.074	15.3	2.7	86	0.03	0.4

		coal analyses					Petrography Volume %		
		M% ad	Ash% ad	VM% ad	VM%daf	FC% ad	Reactives	Inerts	Mineral matter
A	T	0.3	36.4	17.3	27.3	46.0	70	10	20
A	1D	0.32	23.5	18.8	24.7	57.4	43	39	18
A	2B	0.37	5.8	24.5	26.1	69.4	85	14	2
A	3D	0.37	31.1	17.5	25.6	51.0	44	36	20
A	4B	0.46	5.0	26.2	27.7	68.4	93	4	3
A	5D	0.39	12.1	23.3	26.6	64.2	73	20	6
A	6B	0.44	5.9	26.7	28.5	67.0	92	4	5
A	7D	0.44	11.1	21.5	24.3	67.0	53	39	8
A	8B	0.4	4.6	25.1	26.4	70.0	83	15	2
G	1T	0.93	1.8	12.7	13.0	85.5	62	33	5
G	2T	0.81	12.7	12.4	14.2	74.9	61	28	10
G	3T	0.75	2.4	12.5	12.8	85.1	47	51	2
G	1B	0.73	1.7	14.9	15.2	83.4	76	22	1
G	2D	0.7	1.4	13.1	13.3	85.4	58	40	2
G	3B	0.67	13.2	14.8	17.0	72.1	81	6	13
G	4D	0.6	3.8	12.7	13.2	83.5	53	44	3

A samples from Mine A G samples from Gething Formation

T=total seam B= bright lithotypes D=dull lithotypes. B/A ratio of base oxides to acid oxides

tracted, and once at surface they retained water filling intergranular porosity. The measure of compaction using the compression resulting from driving the pipe into the tailings materials vary based on length of core and pond character. In the active pond B, cores of 3 to 4 metres length compacted 22%. In the inactive pond C, cores varying from 2.7 to 3.7 metres length compacted 16%. These compaction amounts are estimates of the water, which was expelled as the cores were forced into the barrel. The resulting cores probably contained 5% to 25% water. After recovery of the core, most of this water was evaporated and the dry tailings held any trace metals that may have originally been held in solution. There are therefore three samples to consider, the expelled water, which was not sampled, the included water, which in terms of dissolved solids, was probably combined with the final tailings sample, and finally the solid tailings sample.

The distilled water leaches for core B00-50 (Table 5) indicate concentrations of elements in the included and expelled water phases as well as any easily leached phase pre-existing on the solid sample. Elements originally in solution were probably precipitated on the solid tailings in a water-soluble form, as the tailings cores dried. Therefore, these elements should be extractable by a distilled water leach.

The different leaches applied did not remove significant Se from the dried samples, and in fact most samples were below detection limits (Table 5). This is not the case

TABLE 10
ICP-MS PROXIMATE AND OXIDE ANALYSES ON WEATHERED COAL

	M% ad	Ash% ad	VM% ad	VM% daf	FC% ad	B/A	Se ppm	Mo ppm	Cu ppm	Pb ppm	Zn ppm	Ag ppm	Ni ppm	Cd ppm	Bi ppm	P %
Seam 1																
weathered	1.5	6.5	26.3	28.6	65.7	0.53	2	0.48	2.65	1.94	17.4	11	1.7	0.1	0.03	0.017
↓	1.3	7.3	26.5	29.0	65.0	0.25	1.1	0.35	2.94	3.42	3.8	11	1.6	0.08	0.03	0.034
	0.9	10.0	26.4	29.6	62.8	0.06	5.7	0.51	5.75	2.15	53.3	27	18.4	0.28	0.07	0.008
fresh	0.5	56.6	14.6	34.1	28.3	0.09	3.6	1.23	25.13	12.55	105.8	224	24.3	1.18	0.22	0.055
seam 2																
weathered	2.6	9.5	31.6	36.0	56.2	1.22	1.5	0.4	11.96	1.52	31.8	30	22.6	0.88	0.03	0.044
↓	0.6	20.8	26.1	33.1	52.6	0.03	8.4	1.83	15.14	7.6	34.5	60	9.9	0.63	0.18	0.05
	0.4	17.1	27.3	33.1	55.1	0.09	2.1	2.38	10.82	7.49	25.5	53	8.8	0.16	0.11	0.336
fresh	0.6	4.9	29.0	30.7	65.5	0.14	0.6	0.89	5.44	2.23	2.8	12	2.4	0.04	0.02	0.003

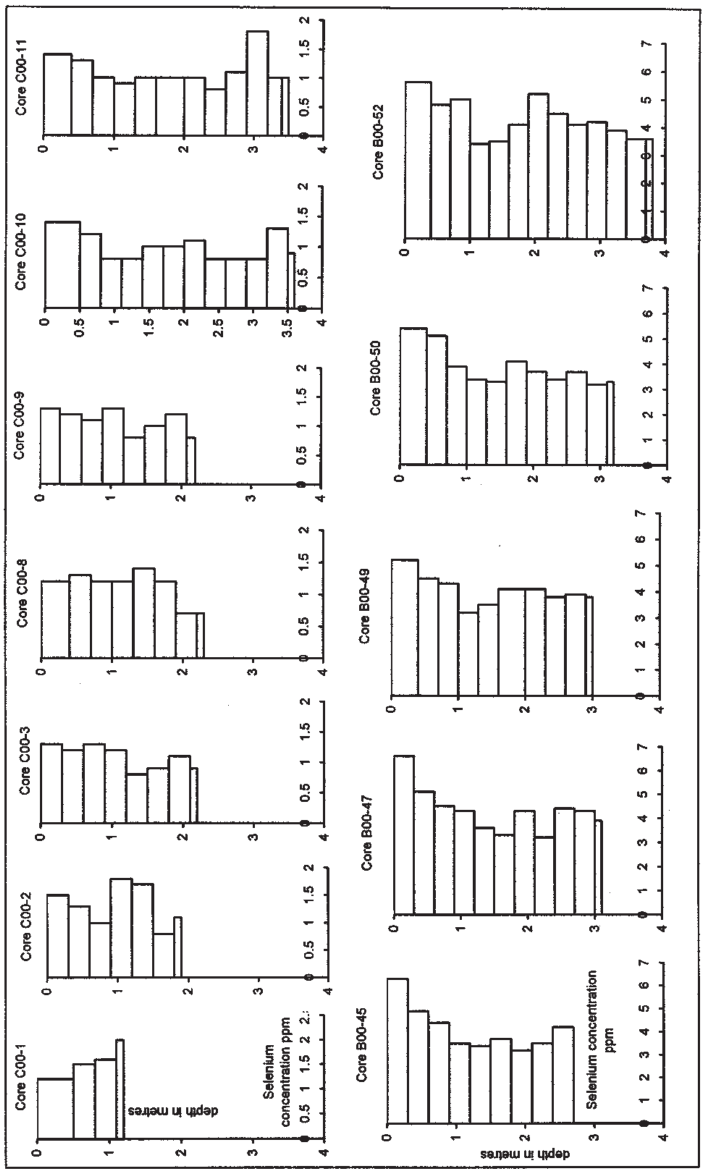

Figure 3.Se stratigraphy for the tailings ponds cores.

TABLE 12
COMPARISON OF RECENT AND OLDER REFUSE MATERIAL
DATA SEMI QUANTATIVE BASED ON LIMITED NUMBER OF ANALYSES

	A mine				C mine				B mine			
	Se	ash	N	yr	Se	ash	N	yr	Se	ash	N	yr
contact material	3.5			0	2.9			0	2			0
raw coal					1.9	24.6						
HW + FW	4.3		13	0	1.8		12	0	3.8		5	0
refuse+tails recent	3.1	61.4	7		2.4		4	0	3.5	48.6	4	0
old refuse	2.45	75.8	6	15 +	2	58.2	4	15+/-	2.8	64.8	4	1--7
old tails					1.1	22.1	59	15+	4.1	74	54	0--10

contact material values from Ryan and Dittrick (2001)
N = number of samples

for the distilled water leach, in part because of increased instrument sensitivity. The water leach removed, on average, 2.6% of the Se in the dried sample. The pH and Eh conditions determine which Se species are in solution. In lower pH environments Se is reduced to Se0 or Se+4 and is more readily adsorbed onto Fe and Mn oxyhydroxides (Belzile *et al.*, 2000). Some of this Se would reenter solution in the distilled water leach, especially considering the proportions of solid to liquid (1 g solid to 20 ml distilled water). The water-leach Se therefore represents Se, which was in the pore water but precipitated onto the tailings as they dried . Se that in the tailings pond was adsorbed onto the tailings but was released into solution in the neutral pH distilled water leach.

It is not possible to differentiate pore water Se from Se adsorbed onto the tailings. However, the maximum amount of Se possible in solution can be estimated by assuming all the leach Se was originally in the pore water. Because leach results are reported in terms of the solid sample some assumptions are made. If the water leach phase represents material that was in the included water associated with the samples after compaction and before drying, then based on an assumed water content of 10% by volume and an assumed dry specific gravity of the tailings of 2, the concentrations reported have to be increased by a factor of about 18. This means that a Se water leach concentration of less than 0.2 ppm (ranges up to 0.153 ppm) removed from the solid could represent a concentration in the pore water of 2.7 ppm. This is much higher than concentrations generally reported for pore waters in sediments (Velinsky and Cutter, 1991), Belzile *et al.*, 2000) (Weres *et al.*, 1989) and indicates that a significant amount of the leach Se must be adsorbed in the tailings pond and not in solution in the pore water. The distilled water leach did not remove high concentrations of any of the elements noted in Table 5, indicating that concentrations reported for tailings approximate those of dry tailings with little influence from pore water material.

It is important to determine if the tailings ponds data indicate:

1. Any substantial loss of Se over time.
2. Any remobilization of Se.
3. Changes in the mineralogical association of Se compared to fresh samples.

It appears that the older tailings pond C (15 years+) has lost Se compared to the younger pond B. However, much of the difference in Se contents can be explained by the difference in ash contents between the two ponds. Cores from pond C average 22.1% ash and those from pond B average 79.4% ash. There is no indication of Se decreasing with depth in the cores (Figure 3). Most of the variations in concentration with depth can be explained by changes in ash content. The average Se concentrations of the tailings are broadly similar to the concentrations of fresh equivalent rock types.

Se concentrations appear to be a bit higher in older material within tailings pond B than for younger, surface materials (Table 12). This is explained by the addition of pyrite to the tailings. In tailings pond C, average Se concentrations are lower than for surface rocks. Part of the reason is the low ash content of the tailings, which should be compared to raw coal rather than hanging wall or footwall material. As a further complication, the tailings represent material from the lower seams in the section that have below average Se concentrations and the raw coal Se and ash data in Table 12 are average values calculated using the full section. Consequently, it cannot be proven that the low Se contents in tailings pond C represent loss of Se over a fifteen-year period, because it is difficult to know what bench mark fresh Se concentration to use for comparison. The pyrite concentration in the tailings pond C is about 0.2% (Figure 4) and there is no correlation of Se with pyrite. If there has been any addition of pyrite to the tailings and formation of a Se pyrite mineral (as discussed later) for pond B, then the pyrite has been removed over the years and this could be reflected in a loss of Se.

The 12 cores from the 2 tailings ponds have a remarkably consistent stratigraphy (Figure 3) The Se concentra-

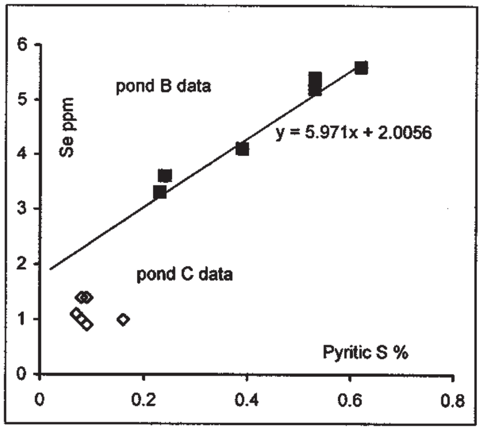

Figure 4. Pyritic S ***versus*** Se for tailings material from ponds B and C.

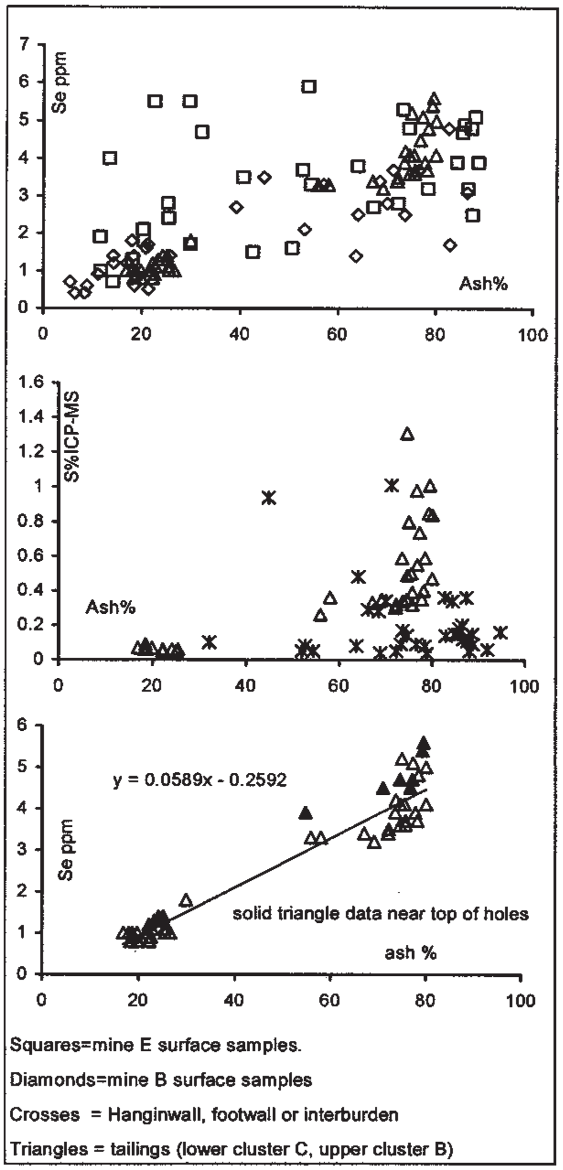

Figure 5. Ash ***versus*** Se and Ash ***versus*** Sulphur plots for surface and tailings samples.

tions peak at the surface and at a depth of about 1 to 2 metres in both ponds. This may indicate an upward migration of Se caused in part by changing pH and Eh with depth in the water column. Any migration of Se will change the inter element correlations and the ash *versus* Se relationship seen in fresh samples. Ash content data are available for four holes and Se *versus* ash data correlate (Figure 5), and have a similar distribution to that seen in fresh samples. Also, the ash and Se stratigraphic profiles for the 4 tailings cores (Figure 6) are similar, indicating that, if Se has been mobilized, then it has retained an ash relationship. However, if the data points from the top of the core holes are identified on an ash *versus* Se plot (Figure 5) they appear enriched in Se relative to ash. This could indicate upward migration of Se probably into higher pH environments in the tailings pore water or the effects of evapo-concentration as the tailings are repeatedly flooded.

Changes in the mineralogical association of Se may effect the correlation of Se with other elements. The data in Table 13 are linear correlation coefficients (R) for Se against other elements. In coal, hanging wall and footwall samples, the most obvious conclusion from the data is an absence of any correlation with S. This may indicate that Se is not associated with organic sulphur or pyrite in these rock types and may occur adsorbed onto clays or as selinides. In Interburden rocks there is a better correlation of Se with S and a number of trace metals. This is compatible with a selinide and or sulphide association. In the coarse refuse of variable age and tailings pond B there is a strong correlation of Se with S and an increased correlation with Fe and Mn (Table 13).

Tailings material contains higher sulphur, at a given ash content, than fresh hanging wall, footwall or interburden material (Figure 5), probably because it is enriched in pyrite liberated from the raw coal during washing. The Fe concentration of tailings is also higher than for hanging wall and footwall material (Figure 7), probably because of the addition of pyrite and siderite liberated from raw coal. Both of these minerals have been identified in coal and in partings associated with the coal. The sulphur-form data (Table 14) for samples from pond B indicate a pyrite content of about 0.8% (calculated assuming pyrite%=Pyritic Sulphur% x 1.87). There may have been removal of some pyrite by oxidation, but a lot of the increase in Fe content may be caused by the addition of siderite. An addition of about 0.8% pyrite to tailings material would increase the average Se concentration above that of the hanging wall, footwall and parting material in the pit, which is the source of much of the tailings. If the concentration of Se in pyrite is in the range of 25 ppm, then this would increase the Se concentration in the tailings by about 0.25 ppm and this is about the increase seen in comparing hanging wall and footwall material to the average Se content of the tailings in pond B (Table 12).

It is important to try to determine the concentration of Se in pyrite associated with the coal seams and with pyrite in the tailings ponds. Some analyses and data from the literature discussed in Ryan and Dittrick (2001) indicate that the Se content in massive pyrite in the Mist Mountain Formation and in coal is low, generally less than 50 ppm. An analy-

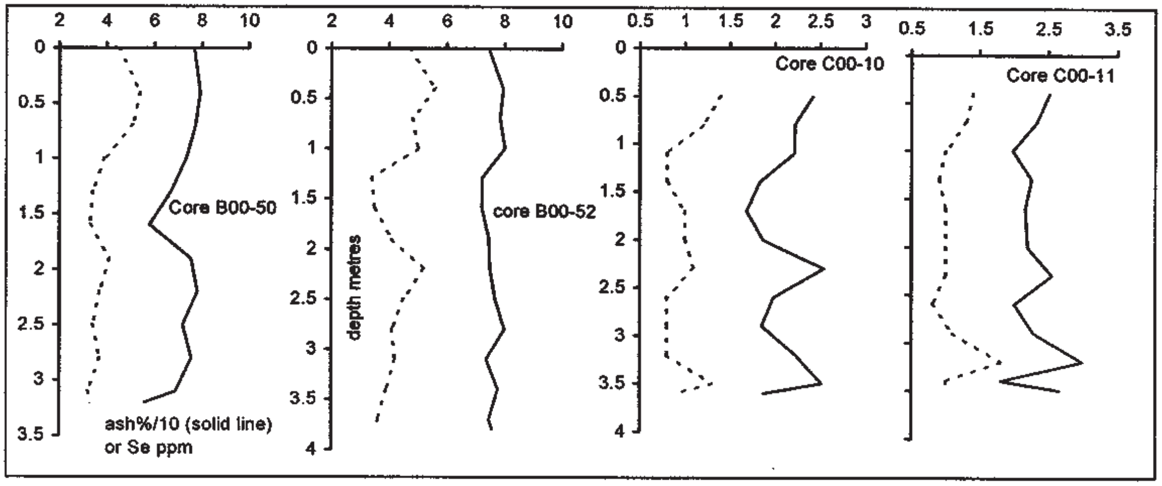

Figure 6. Se and Ash profiles in 4 holes. The X axes are ppm Se or percent ash divided by 10.

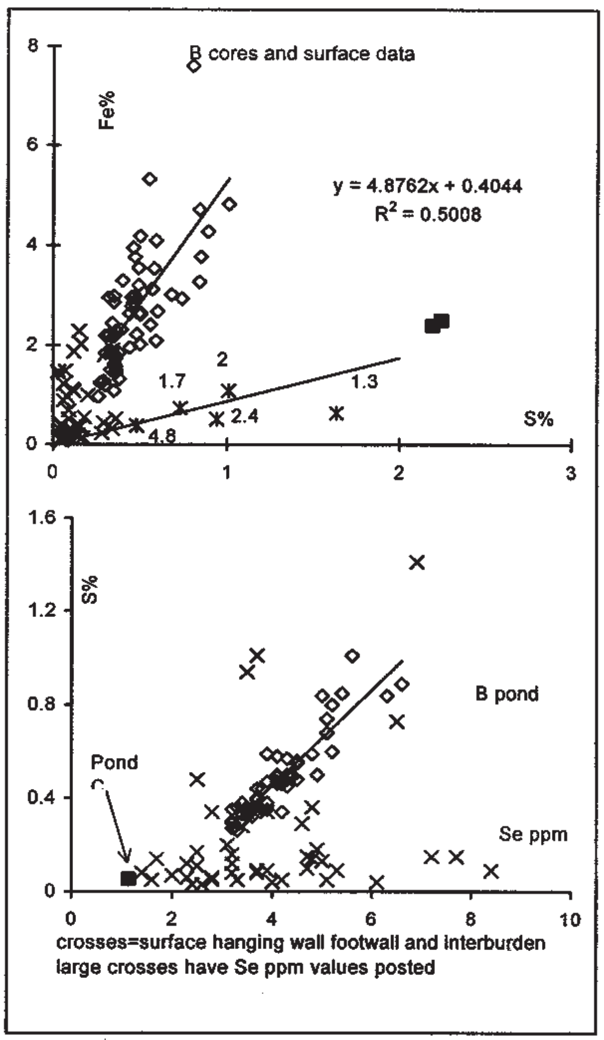

Figure 7. S *versus* Fe plot with pyrite line.

TABLE 13
LINEAR CORRELATION (R) FACTORS OF SE WITH OTHER ELEMENTS FOR DIFFERENT ROCK TYPES

	coal	HW + FW	interB	weathered coal samples	refuse mixed age	B pond cores	C pond cores
number	53	31	14	8	14	53	58
ash%	32.8	76.6	83.9	16.0	67.7	73.9	22.1
S*	.04	.13	.44	.36	.95	.91	-.29
Mo	.42	.43	.89	.35	.84	.90	.46
Cu	.33	.53	.92	.36	-.42	.19	.46
Pb	.45	.30	.91	.33	-.28	.76	.55
Zn	.49	.41	.84	.41	.26	.22	.03
Ag	.30	.56	.92	.22	.42	.67	.58
Ni*	.56	.34	.87	.36	.27	.80	.25
Co	.54	.39	.34	.33	-.23	.90	.17
Mn*	-.14	.05	-.51	.01	.34	.52	.29
Fe*	-.12	-.04	-.35	-.04	.38	.65	.25
As**	.09	.19	.27	.08	.50	.62	.55
U*	.43	.50	.93	-.13	.37	.73	.30
Th*	.13	.35	.53	.46	.20	.27	.34
Sr*	.13	-.12	-.02	.09	.49	-.05	.53
Cd	.39	.40	.89	.32	.27	.68	.73
Sb**	.30	.43	.92	.33	.13	.75	.47
Bi	.33	.37	.79	.60	-.27	.42	.41
V*	.23	-.13	.23	.48	.26	.17	.39
P*	-.07	.34	.46	-.11	.49	.24	.26
La*	.20	.17	.58	.07	.45	.02	.44
Cr*	.28	-.36	-.40	.15	.24	.14	.26
B*	-.32	.11	.56	.15	-.11	-.32	-.36
Na*	.08	.25	-.63	-.18	.17	.57	-.04
Sc*	.41	.03	.42	.67	-.21	.53	.03
Hg	.47	.24	.76	-.01	.17	.67	.31
Te	.40	.43	.77	.24	-.06	.36	.17
Ga	.24	-.19	.25	.51	.29	.37	.60

* partial extraction
** possible loss by volatilization

sis of massive pyrite from a coal seam in this study provided a concentration of 25 ppm. There is, however, always the possibility that the finely disseminated pyrite in coal seams, hanging wall and footwall material has higher Se contents. Some outcrop data in the Fe *versus* S plot (Figure 7) appears to scatter along a pyrite line. The Se contents are posted next to these points and do not indicate any trend of increasing Se with increasing pyrite content making it unlikely that there are higher concentrations of Se in pyrite.

Sulphur-form data in the tailings ponds indicate the presence of some pyrite (Table 14). A pyritic S *versus* Se plot (Figure 4) indicates that pyrite in pond B contains 319 ppm Se (5.971 x 53.4, the slope of the line in Figure 4 is 5.971 and 53.4% S=100% pyrite). This assumes that the ASTM method for identifying pyrite works on tailings material. If the method is appropriate, there is strong evidence for the formation of diagenetic Se-rich pyrite. The Y (Se) intercept in Figure 4 indicates that about 2 ppm Se is not associated with sulphides. There is very little (about 0.2%) pyrite in tailings in pond C and no Se *versus* pyritic S relationship. If this secondary mineral was present it has been removed over the years.

Belzile *et. al*. (2000) studied the distribution of Se in lake sediments. They found that in sediments near the water interface higher pH environments increased Se solubility. Within the sediments, reduced pH favoured the adsorption of Se as Se^{+4} onto Fe-Mn oxyhydroxides, with a preference for Fe oxyhydroxides, (Balistrieri and Chao, 1990). Further reduction of pH deeper into the sediments favoured the formation of Se^0 and precipitation of diagenetic minerals such as achavalite (FeSe) and ferroselite ($FeSe_2$) or the incorporation of Se into pyrite to form Se-pyrite. In tailings pond B there is evidence for the formation a diagenetic Se pyrite. There is also some evidence for the formation of Fe oxyhdroxides. The 0.1 molar and 0.25 molar hydroxylamine leaches, designed to remove Fe and Mn hydroxides, together remove on average 44% of the Fe reported in the unleached samples. Fe and Mn hydroxides have been shown to adsorb Se (Belzile *et al*., 2000). In tailings pond B, there is no clear evidence of a Se rich Fe hydroxide. However, though most of the leaches reported Se concentration below detection limit of 0.2 ppm, the 0.25 molar hyroxylamine leach designed to remove Fe hydroxides reported 4 samples with Se concentrations of 0.2 ppm. These samples correspond to samples with higher total Se and on average could imply a removal of about 4.5% of the total Se as a Se Fe-oxyhydroxide. Low concentrations of Se in the leach samples may be caused by readsorption of Se by the organic phase during the leach experiments. In pond C, in contrast to pond B, there is no correlation of Se with Fe or S (Table 13) and consequently there is no evidence for any Se pyrite.

The ASTM sulphur form analysis reports pyritic sulphur based on the amount of Fe removed by nitric acid. Pyritic-S will therefore not include sulphur in other sulphides. This will be reported as organic S, which is determined by difference after total sulphate and pyritic sulphur have been determined. This may help to explain why S measured by ICP-MS is greater than pyritic S measured by the ASTM

TABLE 14
SULPHUR FORM ANALYSES AND ICP-MS SULPHUR ANALYSES

Mine	rock type	ash %	Se ppm	S% ICP-MS	S% total	S% pyrite	S% sulphate	S% organic
C	T	24.2	1.4	0.06	0.27	0.08	0.07	0.12
C	T	25.4	1.1	0.06	0.24	0.07	0.04	0.13
C	T	18.7	0.9	0.06	0.27	0.09	0.03	0.15
C	T	25.1	1.4	0.04	0.28	0.09	0.03	0.16
C	T	21.6	1	0.03	0.27	0.08	0.02	0.17
C	T	26.5	1	0.07	0.27	0.16	0.07	0.04
B	T	79.3	5.4	0.85	0.99	0.53	0.06	0.4
B	T	75.5	4.1	0.5	0.62	0.39	0.04	0.19
B	T	55.9	3.3	0.26	0.46	0.23	0.04	0.19
B	T	79.5	5.6	1.01	1.17	0.62	0.05	0.5
B	T	75.0	5.2	0.8	0.98	0.53	0.04	0.41
B	T	75.7	3.6	0.32	0.42	0.24	0.05	0.13
B	T	ND	4.5	0.98	1.2	0.62	0.07	0.51
A	T	ND	4.7	1.31	1.42	0.64	0.07	0.71
A	R	ND	ND	0.08	0.2	0.14	0.06	0.01
A	R	ND	ND	0.29	0.42	0.28	0.07	0.07
B	C	ND	ND	0.39	0.8	0.2	0.05	0.55
B	C	ND	ND	0.46	0.9	0.35	0.03	0.52
B	C	ND	ND	0.05	0.42	0.05	0.09	0.28
B	FW	ND	ND	1.1	1.28	0.55	0.04	0.69
B	HW	ND	ND	0.34	0.62	0.22	0.07	0.33
E	C	ND	ND	0.1	0.62	0.12	0.04	0.46
E	IB	ND	ND	0.34	0.43	0.22	0.04	0.17

T=tails R=coarse refuse C=coal IB=interburden

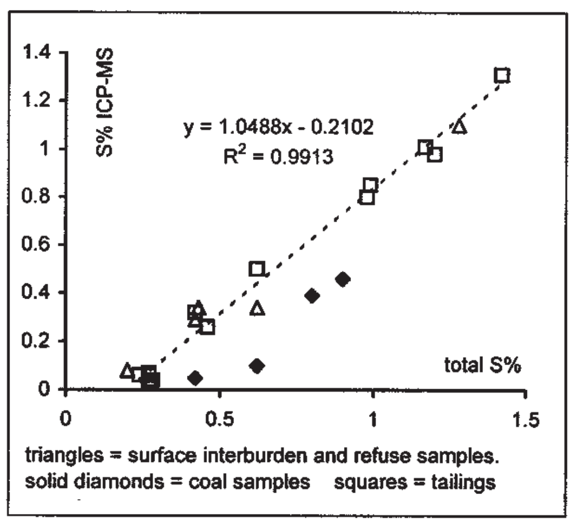

Figure 8. A comparison of S analyses by ASTM and ICP-MS methods.

method. Interpretation of S and Fe ICP-MS data is confused by the fact that the hot aqua regia extraction may not remove all the Fe or S or there may be volatile loss during the digestion. It removes a lot more Fe than that present in pyrite based on a plot of pyritic S *versus* Fe (ICP-MS). A comparison of total S and ICP-MS S analyses (Figure 8) indicates that the ICP-MS S measurement is a constant 0.2% low for rocks and somewhat lower for coal samples. It appears, based on S-form data (Table 13), that ICP-MS extraction measures all the pyritic S and some of the organic S, though it appears to extract less of the organic S in coal.

COARSE REFUSE MATERIAL

It is difficult to collect a lot of coarse refuse samples because of the size of each sample, which is determined by the rock fragment size. The size range of the material is determined by the processing plants and usually has a maximum size of 5 cm. A lot more samples would need to be collected for a comprehensive study. At most mines it was only possible to estimate the age of the refuse material. Though it was possible to collect material ranging in age from recent to about 15 years old.

It is impossible to compare the Se concentrations of old refuse material to those of fresh refuse material because Se concentrations of the material prior to any weathering have probably changed over time. The Se concentration of the old refuse material is not significantly lower than that of recent material (Table 6). However in most cases the older refuse has similar or lower Se concentrations than the average value for recent refuse material. These comparisons should be treated with caution because they are based on only a few samples. There does not appear to have been a major remobilization of Se out of refuse material. The data also appear to indicate some removal of Se from near surface material, though this may be caused by downward migration of fine material. Surface samples have similar or lower Se concentrations than samples collected at the same location but 70 cm below surface (Table 6). The only safe conclusion is that large amounts of Se are not leached out of bulk coarse refuse material over time. This conclusion might not hold for finer material which makes up a small percentage of the total refuse samples. The coarse refuse material is stored above the water table and therefore experiences a different environment from the tailings, which are constantly submerged and probably in a lower pH environment. The constant wetting and drying and oxidizing environment may make coarse refuse material more susceptible to removal of Se, because the conditions are more likely to produce the soluble oxidized forms of Se.

SURFACE DATA

Regional Variation

In 1999 stratigraphic sections were sampled at the five mines and the Se concentrations measured for all rock types, including coal seams (Ryan and Dittrick, 2001). In this study, coal seams in stratigraphic sections previously sampled at two of the mines were resampled. Because of the progression of mining samples in this study (2000) were collected from lower benches, and sample sites (1999 *versus* 2000) for particular seams were probably in the order of 50 metres apart. Comparison of the data (Figure 9) indicates very little lateral consistency of Se concentration within seams. The Se concentration in seams is controlled by ash content and petrography. Both can change markedly along strike within a single seam. It is unlikely, therefore, that individual seams can be characterized by a single Se concentration.

Petrography Data

Nine samples were collected from a single seam at Mine A. In addition, data are used from a study of the Gething Formation from northeastern British Columbia. In that coal quality and petrography data were already available it was only necessary to analyze the samples for Se. Four of the samples from MINE A were handpicked bright

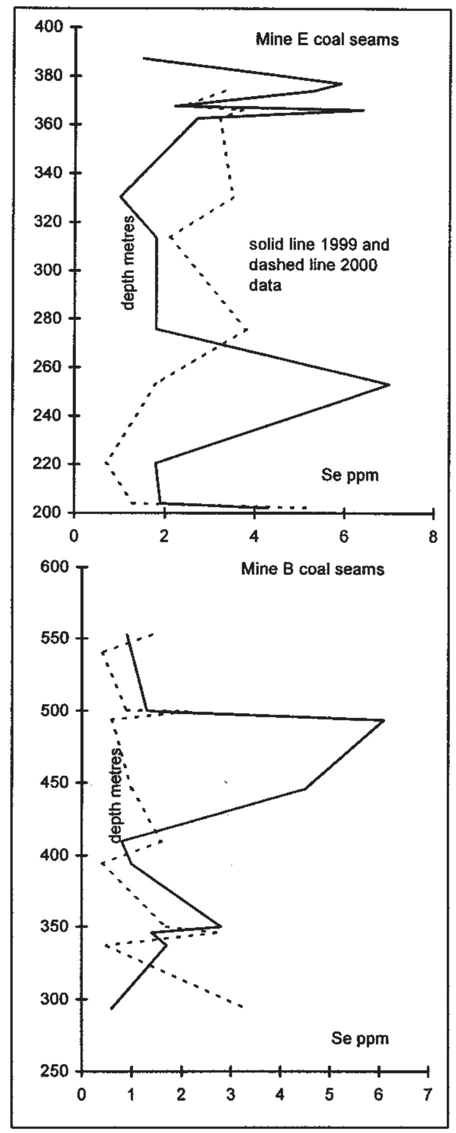

Figure 9. Lateral consistency of Se in coal seams.

coal, four were handpicked dull coal and the last was a channel sample across the whole seam. Similarly, for the Gething samples the first three samples (Table 9) are channel samples and the others are hand picked samples of bright or dull coal. The proximate analyses of the samples (Table 9) indicate dull samples from Mine A have higher ash contents than the bright samples. The volatile matter contents on a dry ash free basis are consistently higher for the bright samples than for the dull samples indicating a high reactives content in the former. This is supported by the petrography summarized in Table 9. In the previous paper washability data was used to support the conclusion that, within the coal, Se concentrates in the reactive macerals. This is because Se is volatile and would be volatilized by forest fires responsible for charring the vegetation and initiating the formation of the inertinite. In this study based on a triangular plots of volume percentages of mineral matter inerts and vitrinite with posted Se concentrations (Figure 10) it appears that the Se is concentrated in the inert coal macerals and mineral matter.

Weathered Samples

Goodarzi, (1987) has documented the effect of weathering on Se concentrations. In this study two sets of samples were collected at Mine B going from bloom coal to fresh coal within the same seam. There is no clear pattern of deletion of Se in the samples (Figure11). There does seem to be a decrease in S% as measured by ICP-MS, which probably indicates a removal of trace amounts of pyrite during weathering. One of the more striking changes is the increase in base/acid ratio for weathered coal. This appears to be caused by the precipitation of Mg, Fe and Ca carbonates in the weathered coal. Many trace metals seem to decrease in the weathered coal (Table 10), but there is no consistent trend.

Sheared Coal

A lot of seams have highly fractured zones or are cut by shear zones. At mines E and B, shear zones and non sheared coal from the same seam were sampled (Table 11). Sheared coal is characterized by an increase in ash content, but no major changes in trace chemistry. The base/acid ratios for the sheared coal remain low indicating that the increase in ash was the result of mixing in ground-up country rock and not the introduction of secondary carbonates. If there was a lot of water movement during shearing it does not appear to have precipitated carbonates or removed trace elements.

CONCLUSIONS

Cores of tailings material up to 4.7 metres long (before compaction) were recovered from two tailings ponds using minimal equipment. The dried tailings were analyzed for a number of elements including Se with the intention of documenting any loss of Se from the tailings ponds, mobility of Se within the tailings ponds and the mineral association of Se in the tailings ponds.

There is no clear evidence for a substantial loss of Se from the tailings. Average Se concentrations for the length

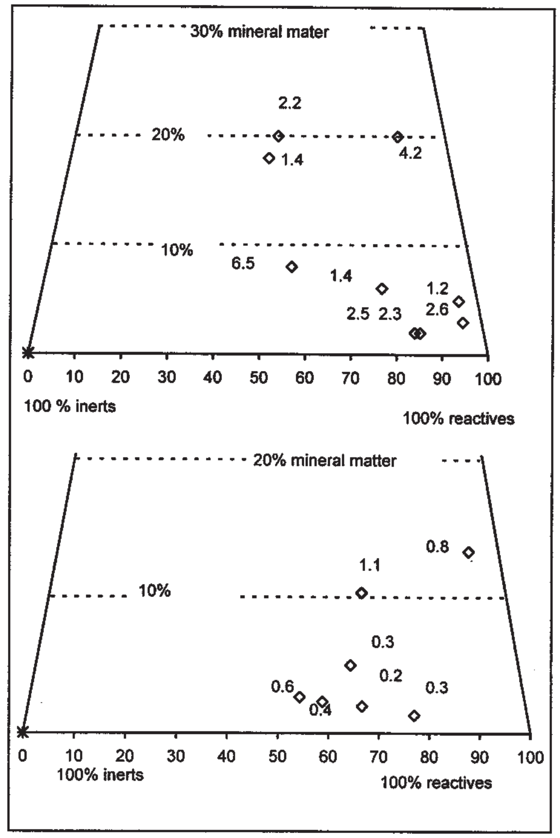

Figure 10. Triangular plot of volume percents of mineral mater, inert and reactive macerals with posted.

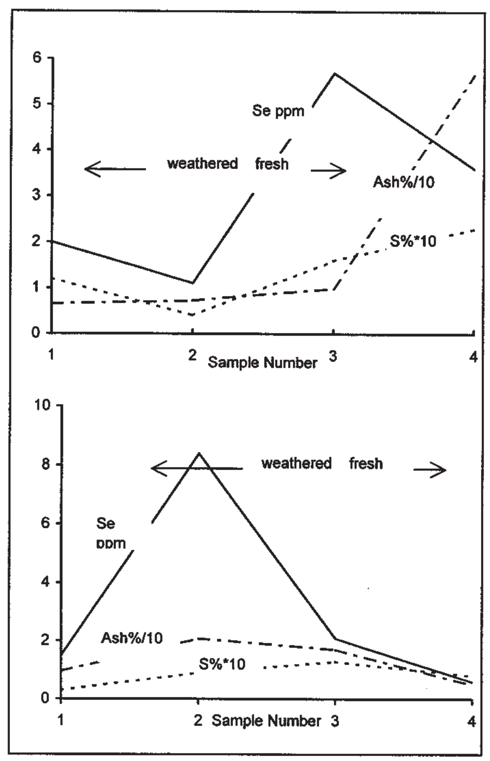

Figure 11. Profiles of Se ppm, S%*10 and Ash%/10 for 2 weathered seams Mine B.

of cores recovered are not markedly lower than what would be expected based on the Se contents of the materials being mined.

There is some evidence of movement of Se within the tailings towards the sediment water interface. Unlike Se in outcrop rocks and coal, Se in the tailings ponds seems to be in part associated with a Se rich pyrite and Fe oxyhydroxides.

There is some indication that small amounts of Se are removed from near surface coarse refuse material but more samples are required to confirm this.

A comparison of Se contents from different locations within the same seams did not reveal any strong lateral consistency in Se concentrations.

Weathering does not markedly decrease Se contents probably because there is not much pyrite in the coal and it has low Se contents. The main change is the introduction of secondary carbonates that increase the base/acid ratio.

Shearing of coal appears to be largely a mechanical process, which produces little change in the seam chemistry but does increase the ash content.

ACKNOWLEDGMENTS

The tedious job of cutting and sampling the cores was carried out with good humour by Graham Giddens and the dusty job of pulverizing 140+ samples was completed by Lara Forbes whose smile was mostly hidden by a dust mask. ICP-MS analyses were conducted by ACME labs; XRF analyses by Cominco Labs and miscellaneous coal analyses by Loring Labs.

The paper benefited from comments by Stephen Day, SRK Consulting, and Jody Frenette, Line Creek Mine. The authors are however unable to avoid responsibility for the content.

REFERENCES

Balistrieri, L.S., and Chao, T.T. (1990): Adsorption of selenium by amorphous iron oxyhydroxide and manganese dioxide; *Geochimica Cosmochim. Acta*, volume 54, pages 739-751.

Belzile, N., Yu-Wei, C, and Xu, R. (2000): Early diagenetic behaviour of selenium in freshwater sediments; *Applied Geochemistry,* volume15, pages 1439-1454.

Gibsons, D.W. (1985): Stratigraphy, sedimentology and depositional environments of the coal-bearing Jurassic-Cretaceous Kootenay Group, Alberta and British Columbia; *Geological Survey of Canada*, Bulletin 357.

Goodarzi, F. (1987): Comparison of elemental distribution in fresh and weathered samples of selected coals in the Jurassic-Cretaceous Kootenay Group, British Columbia, Canada; *Chemical Geology*, volume 63, pages 21-28.

McDonald, L.E. and Strosher, M.S. (1998): Selenium mobilization from surface coal mining in the Elk River Basin British Columbia; a survey of water, sediment and biota*; British Columbia Ministry of Environment, Lands and Parks*, Pollution Prevention Branch Cranbrook, BC.

Reasoner, M.A. (1993): Equipment and procedure improvements for a lightweight inexpensive percussion core sampling system*; Journal of Paleolimnology*, volume 8, pages 273-281.

Ryan, B.D. and Dittrick, M. (2001): Selenium in the Mist Mountain Formation of southeastern British Columbia; in Geological Fieldwork 2000, *B.C. Ministry of Energy and Mines*, Paper 2001-1, pages 337-362.

Weres, O., Jaouni, A and Tsao, L. (1989): The distribution, speciation and geochemical cycling of selenium in a sedimentary environment, Kesterton Resrvoir, California, U.S.A.*; Applied Geochemistry*, volume 4, pages 543-563.

Velinsky, D.J. and Cutter, G.A. (1991): Geochemistry of selenium in a coastal salt marsh; *Geochimica Cosmochim Acta,* volume 55, pages 179-191.

PGE Stream Sediment Geochemistry in British Columbia

By Ray Lett and Wayne Jackaman

KEYWORDS: *Geochemical surveys, PGE's, platinum, palladium, Giant Mascot mine.*

INTRODUCTION

There are few published studies describing the application of regional drainage sediment surveys for platinum group elements (PGE's) in British Columbia. Orientation surveys by Fletcher (1989) and by Cook and Fletcher (1993) revealed that platinum tends to concentrate in the magnetic heavy mineral fraction and the finer grain sizes of stream sediment. These conclusions are partly based on research by Cook (1991) along Grasshopper Creek that drains the Tulameen ultramafic complex. This complex is an Alaskan-type ultramafic intrusion where platinum group (except palladium) minerals are associated with massive chromitite segregations within the dunite core of the complex (Nixon and Hammack, 1991). Platinum in Grasshopper Creek sediment ranged from 8 to 91 ppb whereas in moss mat sediment platinum levels did not exceed 47 ppb (Cook and Fletcher 1993). Concentrations in the sediment along the stream profile were found to be higher at slope breaks suggesting mainly physical dispersion of platinum. Physical transport has also been proposed by Cawthorn, (2001) using platinum:palladium:gold ratios to explain the relationship of stream sediment anomalies to platinum mineralization in the Merensky Reef, South Africa. While recent studies in B.C. have focused on the geochemical behaviour of PGE's in soil and vegetation over platinum-rich copper sulphide mineralization (Dunn, Hall and Nixon, 2000) there have been no published stream geochemical orientations involving PGE's.

A stream geochemical survey was conducted in the Cogburn Creek - Stulkawhits Creek area (Figure 1) during 2001 to expand the knowledge of platinum group element dispersal. The objective of this work is to establish the most effective sample media (stream sediment, moss sediment, heavy mineral) and pathfinder element association for mafic-ultramafic hosted suphide-bearing platinum mineralization. In addition, archived sediment samples (- 80 mesh fraction) from previous regional geochemical surveys in different parts of B.C. (Figure 1) were also analysed for platinum and palladium to identify potentially new PGE-mineralized targets. Both orientation survey and RGS archive sample reanalysis are a contribution to a multi-disciplinary initiative to better understand the occurrence and discovery of PGE's in B.C.

FIELD STUDY AREA DESCRIPTION

PHYSIOGRAPHY

The Cogburn Creek drainage is located in the Lillooet Mountain Range approximately 21 kilometres north of Harrison Hot Springs. The study area, roughly 500 km2 between Harrrison Lake and the Fraser River, covers the Cogburn, Settler, Talc, Emory and Stulkawhits (Texas) creek watersheds (Figure 2). Physiography is typical of the Coast Mountains with high, irregular, steeply sloping mountains dissected by large, steep-sided valleys. Mean annual temperature for the major valleys is 6.5ºC and annual precipitation ranges from 1500 mm to 3400 mm at higher elevations. Vegetation on lower-elevation slopes (< 900 m above sea level) consists of Douglas-fir, western hemlock, western red cedar, amabilis fir and birch. The under-story comprises willow, alder and several shrub species, including abundant devils club. At higher elevation (> 900 m above sea level) vegetation is largely mountain hemlock and amabilis fir.

A predominantly dendritic drainage pattern reflects erosion of bedrock and geological structures. Second and third order streams are fast flowing, typically have steep gradients (10 - 15º) and shoot-to-pool profiles. Stream sediment consists mainly of gravel to boulder size material, al-

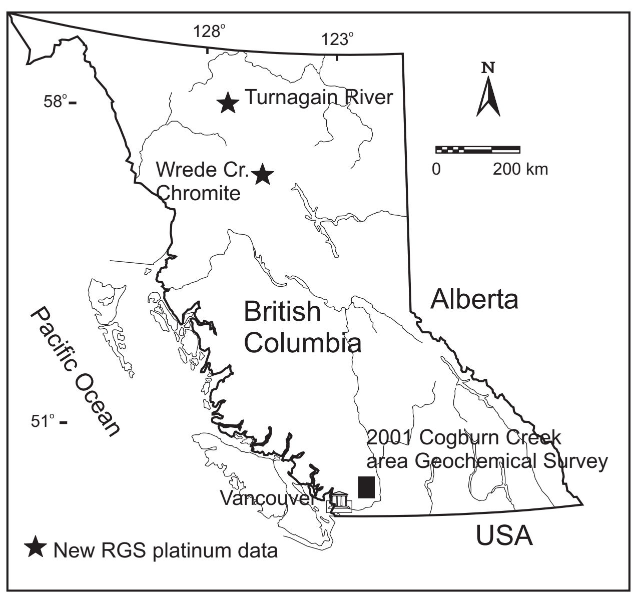

Figure 1. Location of the geochemical survey and re-analysed archive samples.

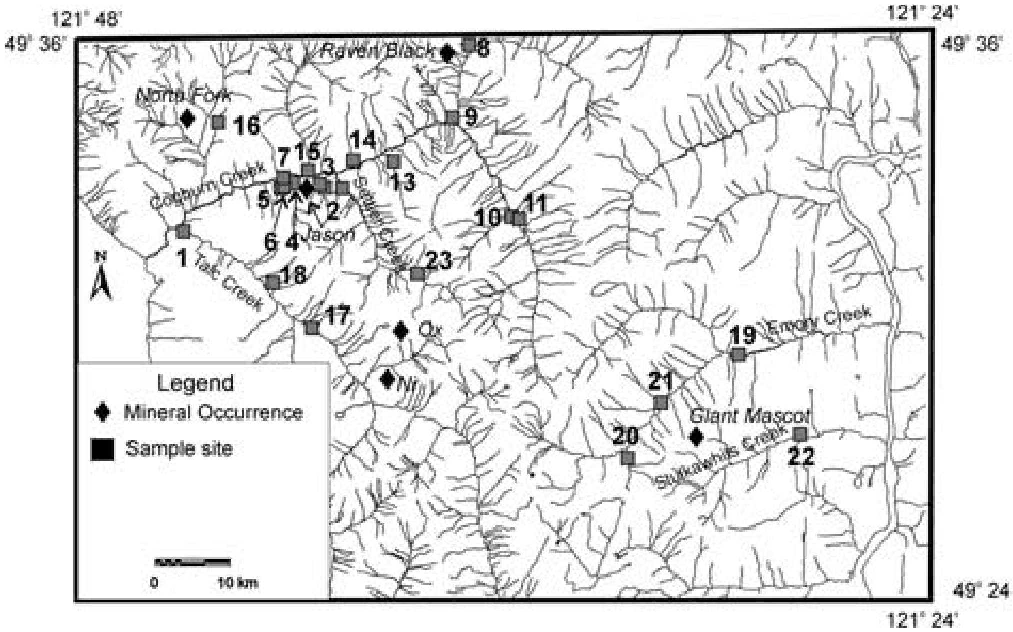

Figure 2. Location of sample stations in the Cogburn Creek-Giant Mascot area.

though sand and silt can be found on scattered channel bars especially where water flow has decreased. Moss is abundant on boulders and logs.

GEOLOGY AND MINERAL DEPOSITS

Bedrock geology has been described previously by Monger (1989), by Ash (2001) and by Pinsent (2001) and will be only briefly outlined in this paper. Proterozic to Paleozoic age metavolcanic and metadiorite (Baird diorite) are the oldest rocks found in the area. These are succeeded by Carboniferous age shale and schist (Cogburn Group), Triassic age arenaceous metasediment (Settler Schist) and by early Cretaceous shale, phyllite, schist and metadiorite (Slollicum Schist). These rocks have been intruded by middle Cretaceous dunite, peridotite, pyroxinite, hornblendite, gabbro and diorite, by middle to late Cretaceous quartz diorite-granodiorite and by Tertiary age granite, tonalite and quartz diorite. Geological structures are parallel east dipping thrust faults, and four other distinct fault systems. Bedrock is covered by surficial sediments in the lower part of valleys. Larger valleys (*e.g.* Cogburn Creek) contain alluvium and a complex of fluvio-glacial silt, sand and gravel. Valley sides are covered by basal till, colluviated till, colluvium and talus.

Among types of mineralization found in the area are copper-nickel sulphides known to be PGE enriched such as the Giant Mascot mine (MINFILE 92HSW 004), Besshi-type copper-zinc massive sulphides (*e.g.* the North Fork occurrence, MINFILE 92HSW 070) and the OX, a copper-gold-silver skarn (MINFILE 92HSW 081). The PGE enriched copper-nickel sulphides are associated with ultramafic (peridotite, olivine pyroxinite, hornblendite, gabbro) intrusive rocks. At the Giant Mascot mine sulphide ore grading 0.77 percent nickel and 0.34 percent copper was found to contain up to 4 ppm platinum-palladium and 8 ppm gold. Ultramafic rocks, similar to those at Giant Mascot, have also been mapped in Cogburn, Settler and Talc watersheds (Pinsent, 2001; Ash, 2001).

SURVEY METHODOLOGY

The survey was carried out to establish the geochemical expression of platinum mineralization in different drainage sample types (*e.g.* moss mat sediment) at an average density of 1 sample per 12 square kilometres. This density is typical of a routine regional stream geochemical survey (RGS) carried out in B.C. Consequently, samples were taken from creeks draining catchments covering 10 - 15 square kilometres and especially from areas where a previous RGS (Jackaman and Matysek, 1989) had detected anomalous nickel and copper levels in the sediment. More detailed stream sampling was conducted near known PGE-bearing sulphide mineralization.

SAMPLE COLLECTION

Stream sediment, moss mat sediment and water samples were collected in August 2001 from tributaries of major creeks including those draining known copper-nickel sulphide mineralization (*e.g.* Giant Mascot Mine, Jason Claims). A total of 23 stream water, 25 stream sediment and 25 moss mat samples (including two field duplicates) were collected from 19 sites in 92H 5 and 12, (Cogburn Creek area), 4 sites in 92H 6 and 11 (Seaton and Stulkawhits Creeks). Locations of the sampling stations are shown in Figure 2. Fifteen bulk sediment samples were also taken at selected stations for preparation of a heavy mineral fraction. These bulk samples were collected in a higher energy stream environment (typically a coarse gravel deposit) by wet-sieving sufficient material through an 18 mesh (<1 millimetre) nylon screen to recover 10 kilograms of <1 millimetre sized sediment. Wet sieving usually required an hour to obtain 10 kilograms of the <1 millimetre fraction and this material was then stored in a heavy-duty plastic bag.

Between 2 to 5 kg of fine-textured sediment, typical of material collected during a regional survey, was taken, generally from the sandy part of a bar in the stream channel, and stored in a high wet strength Kraft paper bag. Live moss (1-2 kg) containing trapped sediment, collected from the surface of boulders or logs in the active stream above the water level, was also stored in Kraft bags. Abundant moss was found at almost all of the stations. Water samples were collected by filling a 125 millilitre high-density polyethylene bottle after previously rinsing the bottle with the stream water.

Where possible the sample stations were chosen upstream from known anthropogenic disturbances such as bridges or culverts or logged areas. During regional sampling where a stream flowed through an obviously disturbed area every effort was made to locate the sample site in an undisturbed riparian zone or where secondary timber growth had stabilized the terrain. Field observations about sample media, sample site, local terrain and float geology were recorded.

SAMPLE PREPARATION

Fine-textured sediment and moss mat sediment samples were prepared in the B.C. Geological Survey Branch Laboratory, Victoria, B.C. The samples were air dried and the - 18 mesh (< 1 mm) recovered by gently disagregating the sediment or by pounding moss mats before dry sieving through a 1 mm stainless steel screen. One half of the 1 mm fraction was then screened to - 80 ASTM mesh (<0.177 mm) and a half screened to - 230 mesh (<0.063mm). Control reference material and analytical duplicate samples were inserted into each analytical block of twenty sediment samples at the Geological Survey Branch Laboratory in Victoria. Any remaining - 80 and -230 mesh sediment was archived for future analyses.

SAMPLE ANALYSIS

The – 80 and –230 mesh stream sediment and moss mat sediment samples with quality control samples were analysed at ACME analytical (Vancouver) for 37 trace and minor elements by a combination of inductively coupled mass spectroscopy (ICP-MS) and inductively coupled plasma emission spectroscopy (ICP-ES) following aqua regia digestion. Platinum, palladium, gold and rhodium in the two fractions of the field survey samples and in the – 80 mesh fraction of archived regional survey samples were also determined at ACME analytical by lead fire assay collection followed by ICP-MS finish. Selected - 80 mesh fraction samples were also analysed for gold and 35 trace elements at ActLabs (Ancaster, Ontario) by instrumental neutron activation analysis (INAA). Table 1 lists detection limits reported for elements determined by the methods described above. Water samples were analysed for pH and sulphate in the Geological Survey Branch laboratory (Victoria). The pH of water samples was measured using a combination glass-reference electrode (GCE) and sulphate was determined by a barium sulphate suspension turbidimetric method (TURB). The detection limit for sulphate is 10 ppm.

TABLE 1
DETECTION LIMITS FOR INSTRUMENTAL NEUTRON ACTIVATION (INAA), INDUCTIVELY COUPLED PLASMA MASS SPECTROSCOPY (ICP-MS), INDUCTIVELY COUPLED PLASMA EMISSION SPECTROSCOPY (ICP-ES) AND FIRE ASSAY- INDUCTIVELY COUPLED PLASMA MASS SPECTROSCOPY FINISH (FA-ICPMS)

Element	Symbol	Method	Detection Limit	Unit
Aluminium	Al	ICP-ES	0.01	%
Antimony	Sb	INAA/ICP-MS	0.1/0.02	ppm
Arsenic	As	INAA/ICP-MS	0.5/0.1	ppm
Barium	Ba	INAA/ICP-MS	50/0.5	ppm
Bismuth	Bi	ICP-MS	0.02	ppm
Bromine	Br	INAA	0.5	ppm
Cadmium	Cd	ICP-MS	0.01	ppm
Calcium	Ca	INAA/ICP-ES	1/0.01	%
Cerium	Ce	INAA	3	ppm
Cesium	Cs	INAA	1	ppm
Chromium	Cr	INAA/ICP-MS	5/0.5	ppm
Cobalt	Co	INAA/ICP-MS	1/0.1	ppm
Copper	Cu	ICP-MS	2/0.01	ppm
Europium	Eu	INAA	0.2	ppm
Gold	Au	INA/ICP-MS	2/0.2	ppb
Hafnium	Hf	INAA	1	ppm
Iron	Fe	INAA/ICP-ES	0.01/0.01	%
Lanthanum	La	INAA	0.5/0.5	ppm
Lead	Pb	ICP-MS	0.01	ppm
Lutetium	Lu	INAA	0.05	ppm
Manganese	Mn	ICP-MS	01-May	ppm
Magnesium	Mg	ICP-ES	0.01	%
Mercury	Hg	ICP-MS	5	ppb
Molybdenum	Mo	ICP-MS	2/0.01	ppm
Neodymium	Nd	INAA	5	ppm
Nickel	Ni	ICP-MS	1/0.1	ppm
Platinum	Pt	FA-ICPMS	0.1	ppb
Paladium	Pd	FA-ICPMS	0.5	ppb
Rubidium	Rb	INAA	15	ppm
Rhodium	Rh	FA-ICPMS	5	ppb
Sulphur	S	FA-ICPMS	0.01	%
Samarium	Sm	INAA	0.5	ppm
Scandium	Sc	INAA	0.1/0.1	ppm
Selenium	Se	INAA	5/0.1	ppm
Silver	Ag	ICP-MS	0.2/0.002	ppm
Sodium	Na	INAA	0.01/0.001	%
Tantalum	Ta	INAA	0.5	ppm
Terbium	Tb	INA	0.5	ppm
Tellurium	Te	ICP-MS	0.02	ppm
Thallium	Tl	ICP-MS	0.02	ppm
Thorium	Th	INAA	0.2	ppm
Tungsten	W	INAA/ICP-MS	1.0/0.2	ppm
Uranium	U	INAA/ICP-MS	0.5/0.1	ppm
Vanadium	V	ICP-MS	2	ppm
Ytterbium	Yb	INAA	0.2	ppm
Zinc	Zn	INAA/ICP-MS	50/0.1	ppm

QUALITY CONTROL

Reliable data interpretation depends on discriminating between real geochemical trends and those variations introduced by sampling and analysis. Control reference standards and analytical duplicates were therefore routinely inserted into the batches of stream sediment and moss sediment samples submitted for commercial analysis to measure the accuracy and precision. The standard National Geochemical Reconnaissance (NGR) and Regional Geochemical Survey (RGS) quality control procedures were used in this project and are based on the analysis of a block of 20 samples. Each block comprises:

- Seventeen routine sediment or water samples,
- One field duplicate sample collected adjacent to one of the routine samples,
- One control reference standard containing known element concentrations.

The location of control reference samples within each batch of samples was selected before sampling, whereas field duplicate sites were chosen randomly during fieldwork. Field duplicate samples were generally collected 2-3 metres apart from the same type of material and stream environment.

THE PRECISION AND ACCURACY OF STREAM AND MOSS SEDIMENT DATA

Element variations in stream and moss sediment can reflect changes in regional geology (bedrock geochemistry, surfical geochemistry, presence of mineralization), within-site variations (combined sampling, analytical and sample preparation variation) or analytical precision alone. Good analytical precision is of little value if the combined sample preparation and collection error is larger than the regional geochemical variation (Fletcher, 1981). Analytical accuracy and precision for gold, platinum and palladium by fire assay and ICP-MS finish was estimated from replicate data for CANMET standard reference material WGB-1 (Bowman, 1994). This standard was included during routine analyses of archived RGS samples and samples collected during the field survey. Results for replicate analyses of this standard are shown in Table 2. Mean values for gold, platinum and palladium in WGB-1 fall within the ranges recommended by CANMET. Platinum precision, expressed as percent relative standard deviation (%RSD), is 16 percent indicating that at 5 ppb the platinum values can be expected to vary between 6.5 and 3.5 ppb in 19 determinations out of 20. Mean and percent relative standard deviation (%RSD) of duplicate analyses of platinum, palladium and other elements in a GSB standard are listed in Table 3. Percent RSD values for most trace elements (*e.g.* Cu, Ni, Co) are less than 6 percent. However, the platinum and palladium precision (%RSD) falls in the 20 to 35 percent range.

A rigorous statistical analysis of duplicate sample data is not feasible because only two field and three analytical duplicates were analysed. Therefore, analytical variation between duplicates is illustrated in Table 4 by the mean and percent difference for selected elements in the - 80 and -230 mesh fractions of two duplicate analytical, stream sediment

TABLE 2
ACCURACY AND PRECISION FOR CANMET STANDARD REFERENCE MATERIAL WGB-1

Sample	Au-ppb	Pt-ppb	Pd-ppb	Rh-ppb
557680	1	5.6	13.8	0.33
953293	4	4.1	10.8	
107060	2	4.8	15.9	0.15
Mean	2	4.8	13.5	0.24
% RSD	65	16.0	19.0	53
CANMET	2.9+/-1.1	6.1+/1.6	13.9+/-2.1	0.32

TABLE 3
ANALYTICAL PRECISION FOR AN INTERNAL GSB STANDARD

Element	Unit	Mean	%RSD
Ag	ppb	51.5	4.1
Al	%	1.6	11.1
As	ppm	5.8	0.0
Au	ppb	16.5	124.3
Au	ppb	2.25	28.3
Ba	ppm	68.75	1.7
Bi	ppm	0.04	0.0
Ca	%	0.86	0.8
Cd	ppm	0.14	10.1
Co	ppm	24.6	0.6
Cr	ppm	75.2	1.1
Cu	ppm	59	1.7
Fe	%	4.51	3.0
Ga	ppm	5.05	4.2
Hg	ppb	31.5	6.7
K	%	0.15	4.9
La	ppm	7.7	5.5
Mg	%	1.38	0.5
Mn	ppm	850	0.3
Mo	ppm	0.5	5.7
Na	%	0.02	4.6
Ni	ppm	39.95	3.0
P	%	0.16	3.4
Pb	ppm	3.68	5.0
Pd	ppb	3.45	34.8
Pt	ppb	12.9	24.1
Rh	ppb	0.13	32.6
S	%	0.03	28.3
Sb	ppm	0.6	5.9
Sc	ppm	4.15	1.7
Se	ppm	0.15	47.1
Sr	ppm	45.95	2.0
Te	ppm	0.02	0.0
Th	ppm	1.05	6.7
Ti	%	0.08	5.9
Tl	ppm	0.04	20.2
U	ppm	0.3	0.0
V	ppm	136	4.2
Zn	ppm	58.25	5.5

and moss sediment samples. The percent difference is given by the expression ABS(X1-X2)/(X1+X2)/2)*100 where X1 and X2 are the first and second analysis of the duplicate sample pair. Large differences (>100%) generally reflect mean concentrations close to detection limit, especially for gold, platinum and palladium. Analytical duplicate sample (ADUP) differences for most elements in the -230 mesh fraction are typically smaller than in the -80 mesh fraction. Similarly, the percent difference for elements is smaller in the -230 mesh fractions of the field duplicate (FDUP) moss mat sediment samples compared to the -80 mesh fraction of the field duplicate stream sediment samples. This pattern could be explained by more uniform distribution of elements in finer grained sediment captured by the moss.

TABLE 4
MEAN AND PERCENT DIFFERENCE FOR ANALYTICAL AND FIELD DUPLICATE SAMPLE DATA

Sample	Type	Ag[2] ppb	Au[2] ppm	Au[1] ppb	Co[2] ppm	Cr[2] ppm	Cu[2] ppm	Fe[2] %	La[2] ppm	Mg[2] %	Ni[2] ppm	Pd[1] ppb	Pt[1] ppb	Rh[1]- ppb
107021 -80	Moss	22	0.7	-1	10.6	55.2	23.55	1.68	3.6	1.03	60.4	-0.5	0.5	0.23
107036 -80	Moss	22	0.5	4	11.0	54.7	23.97	1.70	4.2	1.04	69.7	1.9	0.7	0.09
% Difference	**ADUP**	**0**	**33**	**333**	**4**	**1**	**2**	**1**	**15**	**1**	**14**	**343**	**33**	**88**
107021 -230	Moss	29	1.5	1	13.3	70.2	29.15	1.96	5.4	1.17	74.3	-0.5	1.4	0.09
107036 -230	Moss	25	1.5	68	13.3	67.7	30.15	1.98	5.5	1.17	83.7	2.3	1.3	-0.05
% Difference	**ADUP**	**15**	**0**	**194**	**0**	**4**	**3**	**1**	**2**	**0**	**12**	**311**	**7**	**700**
107034 -80	Sed.	17	1.5	-1	10.2	41.2	23.82	1.55	2.9	0.97	53.4	2.7	0.7	-0.05
107035 -80	Sed.	20	0.4	1	11.1	44.5	25.82	1.65	3.6	0.98	57.9	2.3	1.0	-0.05
% Difference	**FDUP**	**16**	**116**	**0**	**8**	**8**	**8**	**6**	**22**	**1**	**8**	**16**	**35**	**0**
107036 -80	Moss	22	0.5	4	11.0	54.7	23.97	1.70	4.2	1.04	69.7	1.9	0.7	0.09
107037 -80	Moss	19	1.0	2	10.6	52.0	23.53	1.67	3.6	1.03	66.7	1.3	1.1	-0.05
% Difference	**FDUP**	**15**	**67**	**67**	**4**	**5**	**2**	**2**	**15**	**1**	**4**	**38**	**44**	**700**
107036 -230	Moss	25	1.5	68	13.3	67.7	30.15	1.98	5.5	1.17	83.7	2.3	1.3	-0.05
107037 -230	Moss	28	0.8	3	13.0	66.4	30.2	1.96	5.2	1.15	81.0	1.7	1.4	-0.05
% Difference	**FDUP**	**11**	**61**	**183**	**2**	**2**	**0**	**1**	**6**	**2**	**3**	**30**	**7**	**0**
107041 -80	Sed.	31	0.9	-1	7.4	33.5	31.14	0.90	1.9	0.41	31.6	-0.5	0.8	-0.05
107056 -80	Sed.	28	0.7	-1	8.3	35.1	27.17	0.96	2.0	0.44	35.5	0.8	0.9	-0.05
% Difference	**ADUP**	**10**	**25**	**0**	**11**	**5**	**14**	**6**	**5**	**7**	**12**	**867**	**12**	**0**
107041 -230	Sed.	29	0.8	-1	8.9	42.0	31.81	1.01	2.3	0.45	36.3	-0.5	0.6	-0.05
107056 -230	Sed.	34	1.7	-1	9.4	45.2	34.11	1.09	2.6	0.50	36.9	0.8	1.1	-0.05
% Difference	**ADUP**	**16**	**72**	**0**	**5**	**7**	**7**	**8**	**12**	**11**	**2**	**867**	**59**	**0**
107056 -80	Sed.	28	0.7	-1	8.3	35.1	27.17	0.96	2.0	0.44	35.5	0.8	0.9	-0.05
107057 -80	Sed.	29	0.6	-1	8.8	39.3	31.64	1.02	2.3	0.47	36.6	-0.5	0.7	-0.05
% Difference	**FDUP**	**4**	**15**	**0**	**6**	**11**	**15**	**6**	**14**	**7**	**3**	**867**	**25**	**0**
107056 -230	Sed.	34	1.7	-1	9.4	45.2	34.11	1.09	2.6	0.50	36.9	0.8	1.1	-0.05
107057 -230	Sed.	36	1.0	-1	10.6	49.8	35.3	1.18	2.7	0.54	40.6	0.7	1.0	-0.05
% Difference	**FDUP**	**6**	**52**	**0**	**12**	**10**	**3**	**8**	**4**	**8**	**10**	**13**	**10**	**0**
107058 -80	Moss	24	0.2	2	7.7	34.5	34.97	1.08	2.4	0.47	36.2	0.7	0.9	-0.05
107059 -80	Moss	22	0.7	-1	8.1	34.9	30.71	1.11	2.6	0.49	39.6	-0.5	0.8	0.13
% Difference	**FDUP**	**9**	**111**	**600**	**5**	**1**	**13**	**3**	**8**	**4**	**9**	**1200**	**12**	**450**
107058 -230	Moss	29	0.6	-1	9.3	41.6	31.41	1.18	3.3	0.52	39.7	-0.5	0.9	-0.05
107059 -230	Moss	28	1.1	-1	9.1	42.7	32.38	1.16	3.3	0.51	40.2	-0.5	0.8	0.16
% Difference	**FDUP**	**4**	**59**	**0**	**2**	**3**	**3**	**2**	**0**	**2**	**1**	**0**	**12**	**382**

Elements identified with [1] by fire assay and ICP-MS finish; elements identified with [2] by aqua regia digestion and ICP-MS finish

COGBURN CREEK-GIANT MASCOT MINE ORIENTATION SURVEY - RESULTS

An examination of element data reveals that elevated platinum, palladium, copper, nickel, gold and lanthanum values occur together in stream and moss mat sediments. Element values and statistics (median, maximum value, 95 percentile) for the –80 and –230 mesh fractions of moss and stream sediment samples are listed in Tables 5 and 6. Plots showing elements in the two size fractions of the stream and moss sediment at percentiles from 25 to 98 are shown in Figure 3. These plots reveal that the relative concentration of elements in samples generally follows the order: moss -230 mesh> moss -80 mesh> sediment -230 mesh > sediment > 80 mesh. However, the difference between 95 percentile platinum and palladium levels in the -80 mesh fraction of moss sediment compared to the - 230 mesh is small (< 10 ppb). The highest platinum (95.8 ppb) detected by the survey actually occurs in the - 80 mesh fraction of the sediment from a small, steep, slow flowing stream (station 6) on the Jason claims. A chalcopyrite occurrence has been identified close to this creek during previous geological mapping and geochemical surveys on these claims (Haughton, 2001). The -230 mesh of the moss sediment from this site has lower platinum (76 ppb), but the highest palladium (18.6 ppb) found in the survey. This sediment also has up to 345 ppm nickel and 229 ppm copper. The -230 mesh fraction of moss sediment from Stulkawhits Creek downstream from the Giant Mascot mine (station 22) contains the second highest platinum (89.2 ppb) and palladium (10 ppb). Lower levels (68 ppb Pt) occur in the -80 mesh of the stream sediment. Copper and nickel show a reverse trend and are highest in the - 80 mesh of the moss sediment. Weakly anomalous (> 5 ppb) platinum levels are present in the - 230 mesh fraction of moss sediment from Emory Creek. The highest gold detected during the survey (2491 ppb) also occurs in Emory Creek in the -80 mesh fraction of the moss at station 21. Distribution of platinum in the -230 mesh of the moss sediment is shown in Figure 4.

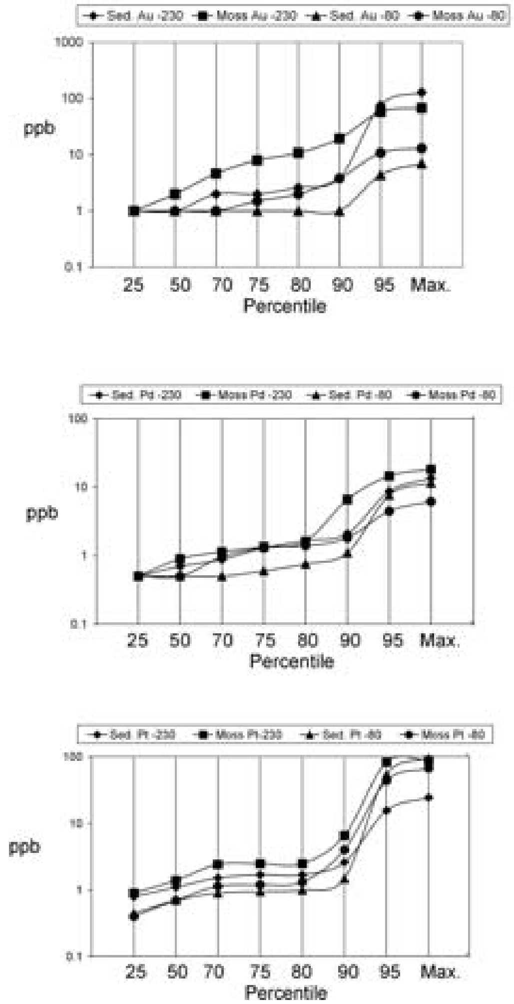

Figure 3. Percentile plots for gold, palladium, platinum and gold in -80 and -230 mesh fractions of stream and moss sediments.

ARCHIVED RGS STREAM SEDIMENT SAMPLES - RESULTS

WREDE CHROMITE NTS 94D/09

Sixteen RGS archive samples (- 80 mesh fraction) from streams draining the Wrede Creek Chromite occurrence (MINFILE 094D 026) were analysed for platinum, palladium and gold by lead fire assay collection followed by ICP-MS finish and for 35 trace elements including chromium, copper, cobalt, nickel and vanadium by ICP-ES following hydrofluoric-perchloric-nitric-hydrochloric acid digestion. The Wrede Creek chromite occurrence (Figure 1) is hosted in a Late Triassic Alaskan-type ultramafic body intruded into middle Triassic to lower Jurassic Takla Group volcanics of the Quesnel Terrane. Mineralization consists of rare chromite grains and blebs within the dunite core of the ultramafic body (Nixon and Hammack, 1991).

Archived sediment samples from two creeks draining the occurrence have more than 11 ppb platinum (Figure 5), up to 2000 ppm chromium and 700 ppm nickel. These results are also compared to instrumental neutron activation (INAA) and aqua regia-AAS RGS survey data (Jackaman, 1997). The presence of chromite in the sediment is indicated by the high INAA chromium compared to lower hydrofluoric-perchloric-nitric-hydrochloric acid digestion-ICP-ES values (Table 7). Nickel levels in samples by the two methods are similar and most likely reflect nickel in olivine weathered from the dunite core of the ultramafic body.

TURNAGAIN RIVER COMPLEX NTS 104I/07

Fifty five RGS archive samples (- 80 mesh fraction) from around the Turnagain River complex were also analysed for platinum, palladium and gold by lead fire assay collection followed by ICP-MS finish. The samples are from a stream draining the Turn nickel occurrence and from a belt of Cache Creek rocks to the south.

TABLE 5
STREAM SEDIMENT AND MOSS MAT SEDIMENT STATISTICS FOR THE - 80 MESH FRACTION

Sample	Stn.	Type	Ag[2] ppb	Au[1] ppb	Au[2] ppb	Cr[2] ppm	Cu[2] ppm	Fe[2] %	La[2] ppm	Mg[2] %	Ni[2] ppm	Pd[1] ppb	Pt[1] ppb	Rh[1] ppb
107022 -80	1	Sed.	43	-1	1.2	160.5	47.37	2.84	1.5	3.75	291.0	0.7	1.0	-0.05
107023 -80	1	Moss	34	2	0.8	180.3	43.49	3.14	1.7	3.53	297.3	1.5	4.4	0.15
107024 -80	2	Sed.	31	-1	5.8	59.1	82.77	1.62	1.6	0.71	66.2	-0.5	0.7	-0.05
107025 -80	2	Moss	27	1	5.6	59.3	72.82	1.71	1.6	0.67	64.3	-0.5	0.7	-0.05
107026 -80	3	Sed.	20	1	1.8	140.4	146.64	2.23	1.6	1.96	160.5	-0.5	1.5	-0.05
107027 -80	3	Moss	28	1	1.7	146.1	174.11	2.25	2.0	1.80	176.8	0.8	2.6	-0.05
107028 -80	4	Sed.	21	-1	0.9	66.3	55.78	1.83	2.0	1.52	106.0	-0.5	0.8	-0.05
107029 -80	4	Moss	15	-1	1.3	87.6	50.18	2.22	1.9	1.83	122.8	0.6	1.2	-0.05
107030 -80	5	Sed.	37	1	1.9	80.6	56.65	2.21	3.3	1.47	115.2	-0.5	1.4	0.15
107031 -80	5	Moss	42	-1	0.7	88.4	59.31	2.15	4.2	1.36	104.9	-0.5	1.4	-0.05
107032 -80	6	Sed.	84	7	5.1	125.9	188.63	2.08	2.0	1.50	261.9	11.6	95.8	0.17
107033 -80	6	Moss	84	3	21.0	134.8	192.52	2.36	2.5	1.60	294.0	6.2	13.3	0.40
107034 -80	7	Sed.	17	-1	1.5	41.2	23.82	1.55	2.9	0.97	53.4	2.7	0.7	-0.05
107036 -80	7	Moss	22	4	0.5	54.7	23.97	1.70	4.2	1.04	69.7	1.9	0.7	0.09
107039 -80	8	Sed.	22	-1	1.1	39.8	16.94	1.91	3.9	0.82	19.1	-0.5	0.3	-0.05
107040 -80	8	Moss	22	-1	0.6	32.6	13.86	1.78	5.5	0.63	16.8	-0.5	0.3	0.09
107042 -80	9	Sed.	18	-1	0.6	34.7	15.98	1.93	4.0	0.66	16.9	-0.5	0.2	-0.05
107043 -80	9	Moss	18	1	0.7	26.6	14.64	1.89	6.0	0.48	13.3	-0.5	0.2	-0.05
107044 -80	10	Sed.	24	-1	0.3	49.9	24.71	1.99	4.5	0.85	23.3	-0.5	0.6	-0.05
107045 -80	10	Moss	31	-1	0.3	41.8	20.91	1.67	3.7	0.68	19.4	-0.5	0.3	-0.05
107046 -80	11	Sed.	9	-1	-0.2	44.8	17.14	1.31	3.8	0.61	34.5	-0.5	0.7	-0.05
107047 -80	11	Moss	23	-1	0.7	65.5	23.43	1.72	4.3	0.79	49.1	-0.5	0.6	-0.05
107048 -80	12	Sed.	34	-1	0.4	86.9	37.15	2.32	4.3	1.90	155.1	0.5	0.6	-0.05
107049 -80	12	Moss	28	-1	0.5	84.6	31.64	2.07	4.1	1.77	143.6	1.4	1.2	0.20
107050 -80	13	Sed.	30	-1	0.6	52.6	29.76	1.92	4.9	0.89	28.4	-0.5	0.4	0.35
107051 -80	13	Moss	19	-1	0.5	38.9	21.72	1.54	4.8	0.66	20.6	-0.5	0.4	0.06
107052 -80	14	Sed.	36	-1	0.9	47.7	28.46	1.82	2.1	0.88	31.1	-0.5	0.4	-0.05
107053 -80	14	Moss	40	-1	0.6	43.8	28.01	1.66	2.3	0.74	30.1	-0.5	0.4	-0.05
107054 -80	15	Sed.	23	-1	0.7	38.7	24.81	1.44	3.6	0.73	40.7	-0.5	0.4	-0.05
107055 -80	15	Moss	19	-1	1.0	43.0	20.92	1.36	3.4	0.60	38.0	-0.5	0.3	-0.05
107056 -80	16	Sed.	28	-1	0.7	35.1	27.17	0.96	2.0	0.44	35.5	0.8	0.9	-0.05
107058 -80	16	Moss	24	2	0.2	34.5	34.97	1.08	2.4	0.47	36.2	0.7	0.9	-0.05
107062 -80	17	Sed.	75	1	1.1	82.4	22.21	2.34	2.8	2.26	190.2	-0.5	0.9	0.17
107063 -80	17	Moss	43	8	1.7	90.5	22.53	2.88	3.1	2.39	203.9	-0.5	0.9	0.13
107064 -80	18	Sed.	25	-1	0.7	59.7	63.10	2.10	2.7	1.36	75.9	1.1	1.0	-0.05
107065 -80	18	Moss	25	-1	0.9	65.5	67.83	2.22	2.9	1.21	66.7	1.4	1.0	-0.05
107066 -80	19	Sed.	28	-1	0.6	37.4	29.65	1.58	4.1	1.53	79.4	-0.5	0.8	-0.05
107067 -80	19	Moss	24	-1	0.8	42.1	28.13	1.56	4.9	1.54	77.6	-0.5	0.3	0.50
107068 -80	20	Sed.	36	1	0.9	123.2	143.09	3.38	2.6	5.31	396.4	1.1	1.5	0.40
107069 -80	20	Moss	30	13	1.4	97.8	101.52	3.09	3.9	4.68	324.6	1.2	1.1	-0.05
107070 -80	21	Sed.	22	-1	0.4	37.3	30.82	1.55	3.2	2.02	101.5	-0.5	0.5	0.30
107071 -80	21	Moss	936	-1	2491.7	46.0	31.76	1.71	4.2	1.98	102.0	-0.5	0.6	0.31
107072 -80	22	Sed.	31	-1	0.2	33.7	41.70	1.32	5.2	0.63	83.1	-0.5	0.4	-0.05
107073 -80	22	Moss	55	-1	1.7	39.2	100.58	1.63	5.8	0.79	188.8	2.3	68.1	-0.05
107074 -80	23	Sed.	33	-1	1.3	45.0	23.93	1.89	4.8	0.75	31.5	-0.5	0.8	-0.05
107075 -80	23	Moss	28	-1	0.8	45.8	23.40	1.78	4.4	0.71	35.0	-0.5	0.4	0.06
Median			28	-1	0.8	51.3	30.29	1.86	3.5	1.01	72.8	-0.5	0.7	-0.05
Maximum			936	13	2491.7	180.3	192.52	3.38	6.0	5.31	396.4	11.6	95.8	0.50
90%ile			49	2.5	3.5	130.4	122.31	2.60	4.9	2.33	276.5	1.7	2.1	0.31
95%ile			82	6	5.8	144.7	167.24	3.04	5.4	3.70	296.5	3.0	11.0	0.39

[1] tire assay - ICP-MS finish [2] aqua regia digestion - ICP-MS

TABLE 6
STREAM SEDIMENT AND MOSS MAT SEDIMENT STATISTICS FOR THE - 230 MESH FRACTION

Sample	Stn.	Type	Ag[2]	Au[2]	Au[1]	Cr[2]	Cu[2]	Fe[2]	La[2]	Mg[2]	Ni[2]	Pd[1]	Pt[1]	Rh[1]
			ppb	ppb	ppb	ppm	ppm	%	ppm	%	ppm	ppb	ppb	ppb
107022 -230	1	Sed.	59	1.2	128	125.5	56.94	2.72	1.6	2.86	244.3	1.0	1.4	-0.05
107023 -230	1	Moss	44	1106.5	2	166.7	46.26	2.67	1.8	3.55	307.4	1.5	2.5	0.20
107024 -230	2	Sed.	69	6.8	3	77.6	121.89	2.44	2.6	0.89	105.7	0.8	1.1	-0.05
107025 -230	2	Moss	40	3.1	2	73.5	105.75	2.26	2.5	0.79	81.9	0.8	1.2	-0.05
107026 -230	3	Sed.	44	2.2	2	214.2	223.76	3.14	2.6	2.34	235.2	1.7	2.8	-0.05
107027 -230	3	Moss	45	2.0	3	205.8	244.54	2.96	3.0	2.05	248.5	1.1	2.0	-0.05
107028 -230	4	Sed.	29	1.3	2	86.8	71.45	2.22	3.2	1.51	132.3	0.8	1.2	0.13
107029 -230	4	Moss	23	1.0	2	110.4	65.37	2.46	3.2	1.78	144.6	1.1	2.3	0.11
107030 -230	5	Sed.	59	0.9	2	97.4	65.92	2.55	4.3	1.58	138.3	0.5	1.7	0.16
107031 -230	5	Moss	57	1.1	2	102.6	72.78	2.46	5.6	1.42	118.8	0.7	2.5	-0.05
107032 -230	6	Sed.	75	23.7	9	164.5	222.01	2.71	3.5	1.67	310.7	13.6	24.5	0.29
107033 -230	6	Moss	75	7.2	12	181.1	229.13	2.83	3.9	1.68	345.4	18.3	76.0	0.91
107035 -230	7	Sed.	34	2.1	-1	62.1	34.72	2.13	5.1	1.19	74.8	3.7	1.0	0.18
107036 -230	7	Moss	25	1.5	68	67.7	30.15	1.98	5.5	1.17	83.7	2.3	1.3	-0.05
107039 -230	8	Sed.	56	0.9	-1	40.1	26.01	2.08	7.5	0.73	22.6	-0.5	0.5	-0.05
107040 -230	8	Moss	56	3.1	-1	38.7	24.12	2.15	7.9	0.69	21.9	1.7	0.6	-0.05
107042 -230	9	Sed.	59	3.6	-1	40.1	25.16	2.16	7.2	0.71	22.7	2.2	-0.1	-0.05
107043 -230	9	Moss	32	0.7	-1	33.5	20.68	2.04	7.7	0.57	18.3	0.9	-0.1	-0.05
107044 -230	10	Sed.	38	0.7	-1	59.9	32.70	2.23	4.9	0.95	27.3	-0.5	0.8	-0.05
107045 -230	10	Moss	26	0.7	-1	52.5	28.18	2.04	4.9	0.84	24.2	0.6	0.6	0.24
107046 -230	11	Sed.	26	1.0	1	96.7	35.83	2.68	6.2	1.21	65.4	1.6	1.7	-0.05
107047 -230	11	Moss	36	0.7	7	81.1	29.68	1.95	5.8	0.89	59.4	1.2	1.4	0.13
107048 -230	12	Sed.	53	1.2	-1	107.6	46.99	2.80	5.6	1.98	167.7	1.7	1.7	0.47
107049 -230	12	Moss	39	0.9	-1	99.4	37.90	2.34	5.4	1.82	158.6	0.9	1.3	0.06
107050 -230	13	Sed.	35	0.4	-1	59.6	35.27	2.11	6.6	0.95	32.2	-0.5	0.5	0.19
107051 -230	13	Moss	29	0.6	-1	48.0	27.79	1.80	6.8	0.77	26.1	-0.5	0.4	0.06
107052 -230	14	Sed.	90	1.0	-1	57.0	46.85	2.23	4.2	0.93	42.8	-0.5	0.2	-0.05
107053 -230	14	Moss	88	1.1	-1	46.6	40.50	1.94	4.2	0.74	37.0	-0.5	0.4	-0.05
107054 -230	15	Sed.	33	1.5	-1	41.9	28.40	1.55	5.4	0.75	42.7	-0.5	0.9	-0.05
107055 -230	15	Moss	25	1.2	2	54.6	27.09	1.68	6.1	0.73	45.9	7.7	2.5	-0.05
107056 -230	16	Sed.	34	1.7	-1	45.2	34.11	1.09	2.6	0.50	36.9	0.8	1.1	-0.05
107058 -230	16	Moss	29	0.6	-1	41.6	31.41	1.18	3.3	0.52	39.7	-0.5	0.9	-0.05
107059 -230	16	Moss	28	1.1	-1	42.7	32.38	1.16	3.3	0.51	40.2	-0.5	0.8	0.16
107062 -230	17	Sed.	73	1.5	4	96.6	29.87	2.77	4.1	2.32	217.4	-0.5	0.9	0.20
107063 -230	17	Moss	54	1.8	21	95.9	28.37	2.77	3.9	2.23	206.3	-0.5	1.8	0.20
107064 -230	18	Sed.	24	0.8	-1	58.5	68.03	2.14	2.9	1.21	65.9	0.7	0.9	-0.05
107065 -230	18	Moss	26	1.6	-1	65.1	72.79	2.35	3.2	1.22	65.1	1.1	1.3	0.09
107066 -230	19	Sed.	57	1.0	-1	46.5	37.83	1.72	5.2	1.02	76.8	0.6	0.8	0.11
107067 -230	19	Moss	30	0.5	45	46.6	31.74	1.50	7.5	0.97	64.4	-0.5	7.2	0.11
107068 -230	20	Sed.	59	1.5	-1	133.4	175.01	3.48	4.9	3.70	419.2	0.8	1.9	0.38
107069 -230	20	Moss	41	2.0	9	111.7	136.59	3.14	6.8	3.50	348.1	1.1	4.2	0.13
107070 -230	21	Sed.	40	0.4	-1	49.7	39.84	1.69	5.1	1.37	95.5	-0.5	4.4	-0.05
107071 -230	21	Moss	42	1.4	-1	56.7	41.35	1.80	6.7	1.37	94.5	-0.5	2.4	0.15
107072 -230	22	Sed.	34	1.0	-1	35.3	46.27	1.45	7.0	0.57	87.5	0.6	1.3	-0.05
107073 -230	22	Moss	41	3.7	13	43.5	84.96	1.70	8.8	0.66	132.0	10.0	89.2	2.02
107074 -230	23	Sed.	43	1.0	3	52.3	30.72	2.19	5.7	0.86	36.3	-0.5	0.8	-0.05
107075 -230	23	Moss	46	1.9	-1	52.7	31.20	2.06	5.7	0.83	41.8	-0.5	0.9	-0.05
Median			41	1.2	-1	59.9	37.90	2.16	5.1	1.02	76.8	0.8	1.3	-0.05
Maximum			90	1106.5	128	214.2	244.54	3.48	8.8	3.70	419.2	18.3	89.2	2.02
90%ile			71	3.6	12.4	145.8	152.00	2.80	7.3	2.30	272.1	2.9	4.3	0.30
95%ile			75	7.1	38	176.8	223.20	3.10	7.6	3.31	335.0	9.3	19.3	0.44

[1] tire assay - ICP-MS finish [2] aqua regia digestion - ICP-MS

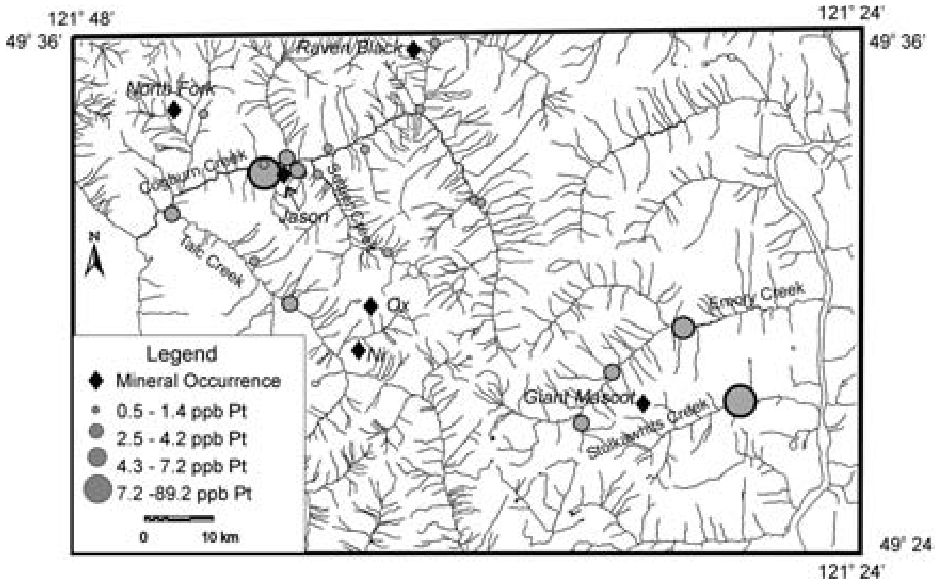

Figure 4. Platinum in -230 mesh fraction of moss sediment in the Cogburn Creek-Giant Mascot mine area.

The Turn (Discovery) (MINFILE 104I 014) prospect is hosted in an Alaskan-type ultramafic intrusive complex consisting of a dunite core enclosed in peridotite, pyroxene-rich peridotite, and olivine pyroxenite. The peripheral ultramafic rocks contain disseminated pyrrhotite, pentlandite, chalcopyrite and bornite with chromite, ilmenite and magnetite. The complex is intruded in the Late Triassic into upper Paleozoic and/or Triassic metavolcanic and metasedimentary rocks (Nixon and Hammack, 1991).

The area south of the Turnagain River is underlain by Cache Creek terrane argillites, chert arenites, limestones and greenstones. Several ultramafic-related mineral deposits, including Letain asbestos (MINFILE 104I 006), occur in Late Mississippian to Permian serpentinized peridotite, dunite, and diorite. No PGE occurrence has been found associated with these ultramafic rocks although chromite showings are common in the Cache Creek Terrane. Possible volcanic massive sulphide (VMS) mineralization, east of the Turnagain River, is represented by the Bow galena-sphalerite occurrence (MINFILE 104I 078). This occurs in lower Ordovician to Devono-Mississippian siliceous mudstone of the Road River Group.

An archive sediment sample (104I953313) from Turnagain creek close to the Turn occurrence has 8.2 ppb platinum (Figure 6), 7.3 ppb palladium and 269 ppm nickel. Another sample (104I953308) from a creek to the west of the Turn has 11.7 ppb palladium. Other creeks within the belt of ultramafic rock in the Cache Creek assemblage to the south also have elevated platinum and palladium in the sedi-

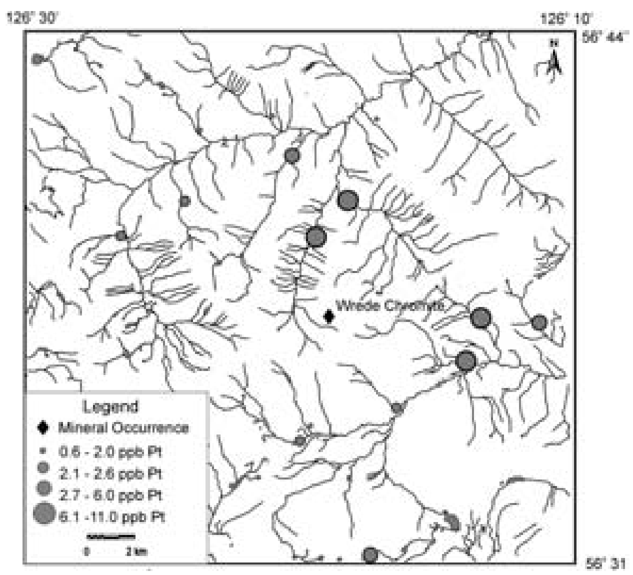

Figure 5. Platinum in RGS samples, Wrede chromite deposit area.

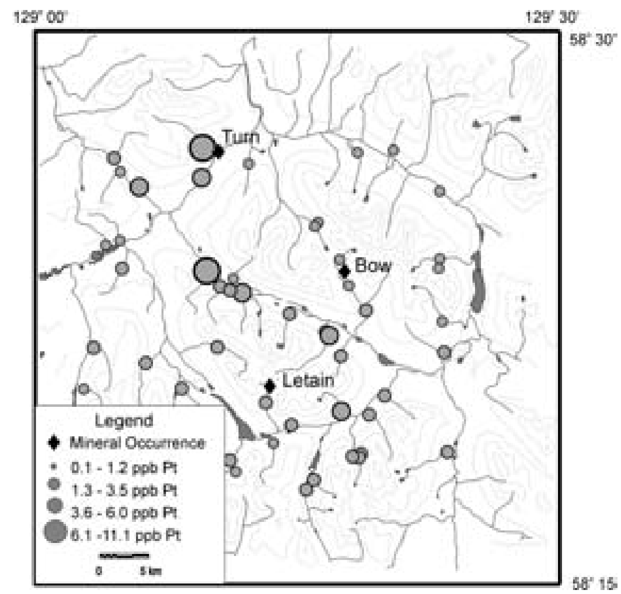

Figure 6. Platinum in RGS samples, Turnagain River area.

TABLE 7
GEOCHEMISTRY OF RGS SAMPLES FROM THE WREDE CHROMITE DEPOSIT AREA

	1311	1314	1337	1338	1339	1342	1343	3373	3374	3375	3376	3378	3382	3383	3384	3385
As-AA	4.7	10.0	9.5	2.7	4.3	7.9	1.0	5.0	16.0	3.2	2.6	7.5	5.2	10.0	11.0	2.2
As-HF	9	8	11	-5	-5	9	-5	-5	14	5	-5	-5	5	13	12	-5
As-NA	4.9	12.0	12.0	4.3	5.7	8.9	0.5	5.4	13.0	4.3	4.2	9.2	4.7	8.9	14.0	3.3
Au-MS	5	7	1	3	2	5	2	1	4	2	7	10	6	12	8	13
Au-NA	16	25	42	46	41	14	11	2	2	38	2	36	9	12	21	17
Ba-HF	367	546	342	246	223	381	235	177	940	694	392	421	258	450	437	579
Ba-NA	370	420	370	270	300	470	370	330	1300	740	390	460	320	500	380	550
Co-AA	20	21	26	46	38	23	16	55	17	7	11	17	55	23	24	9
Co-HF	29	24	32	60	56	31	42	75	21	19	17	23	71	33	33	18
Co-NA	21	18	29	50	46	24	44	56	18	19	15	20	56	24	37	15
Cr-AA	-1	-1	-1	-1	-1	-1	-1	-1	-1	-1	-1	-1	-1	-1	-1	-1
Cr-HF	185	103	526	937	643	169	183	810	169	348	106	151	680	158	157	131
Cr-NA	170	110	1200	2300	1300	160	220	2000	160	340	100	130	1500	140	220	100
Cu-AA	73	66	47	76	103	94	116	40	36	42	49	80	153	140	142	77
Cu-HF	78	73	43	77	107	94	127	42	44	45	60	95	166	153	149	91
Fe-AA	2.30	3.50	3.40	3.50	3.40	3.20	1.60	4.10	3.20	1.70	3.70	2.40	4.50	3.50	3.70	2.00
Fe-HF	5.5	5.11	4.78	6.3	6.88	5.79	6.18	5.36	4.77	8.45	5.33	5.14	6.56	6.48	6.56	5.61
Fe-NA	5.06	4.78	4.88	6.42	6.84	5.69	8.49	5.45	4.86	9.19	5.35	4.90	6.66	5.82	8.66	5.10
La-HF	-2	-2	27	-2	-2	-2	-2	8	44	27	12	17	-2	2	-2	17
La-NA	7.7	9.7	43.0	12.0	6.8	9.0	8.2	22.0	60.0	23.0	9.2	11.0	5.9	11.0	16.0	14.0
LOI	5.2	8.4	9.7	5.7	3.2	6.5	1.9	4.9	20.2	6.8	17.2	6.8	6.1	4.1	4.3	4.8
Mg-HF	3.1	2.32	4.92	11	9.02	2.81	5.52	14.68	1.27	2.27	1.73	2.64	10.58	2.93	2.94	2.28
Mn-AA	361	736	479	430	499	615	178	529	336	225	341	433	755	473	490	178
Mn-HF	1140	1211	828	1085	1357	1319	1320	951	527	1056	865	1122	1441	1231	1246	1020
Ni-AA	33	25	213	430	245	27	37	660	41	21	16	27	425	32	33	15
Ni-HF	51	30	220	461	288	44	89	705	57	58	25	43	479	50	47	34
Ni-NA	20	20	190	400	260	86	20	540	20	120	20	20	290	20	20	20
Pd-MS	2.5	2.5	1.1	2.7	4.2	2.7	4.3	1.3	0.6	1.9	1.6	3.0	4.0	3.8	5.7	2.9
Pt-MS	2.3	1.8	4.8	9.9	11.3	2.6	4.4	11.4	0.6	2.0	2.1	2.2	6.1	3.4	3.8	1.6
V-AA	65	97	17	31	55	62	64	22	14	53	106	61	77	98	102	59
V-HF	264	221	117	182	275	253	289	88	118	348	244	220	206	298	305	236
Y-HF	17	18	14	10	12	18	15	7	7	19	11	16	10	15	15	16
Zr-HF	24	24	48	22	19	19	29	28	65	16	15	19	16	21	21	18

ment. These include sample 104I953294 with 13.7 ppb palladium and 104I953297 with 11.1 ppb platinum.

CONCLUSIONS

The -230 mesh fraction of moss sediment from Stulkawhits Creek downstream from the Giant Mascot nickel-copper sulphide mine contains 89.2 ppb platinum and 10 ppb palladium. In general, platinum and palladium appear to be concentrated in the -230 mesh fraction of moss sediment. However, high platinum values (up to 96 ppb) can also occur in the - 80 mesh fraction of stream sediments. A lead fire assay-inductively coupled plasma mass spectroscopy (ICP-MS) technique allows low (6-10 ppb) platinum and palladium levels to be confidently detected in stream and moss sediments.

Re-analysis of RGS archive samples for platinum and palladium by this method has identified anomalies related to known Alaskan-type ultramafic intrusives and also in areas where no platinum mineralization has been reported.

Only copper and nickel appear to be associated with platinum and palladium in drainage and moss sediment from streams draining sulphide mineralization. Because there are few pathfinders future exploration for new PGE-rich sulphide deposits should integrate existing geological, geophysical data to define target areas for geochemical surveys.

COMPLETION OF THE SAMPLE ANALYSIS

Only data for platinum and palladium and elements determined by aqua regia ICP-MS or hydrofluoric-perchloric-nitric-hydrochloric acid digestion ICP-ES are reported in this paper. The results of INAA and heavy mineral concentrate analysis will be presented in a later publication.

REFERENCES

Ash, C. (2001): Geological of the Cogburn-Settler Creek area, 92H/07; in Fieldwork 2001; *B.C. Ministry of Energy and Mines; Paper 2002-1.*

Cook, S.J. and Fletcher, W.K. (1993): Distribution and behavior of platinum in soils, sediments and waters of the Tulameen ultramafic complex, southern British Columbia, Canada; *Journal of Geochemical Exploration*, Vol. 46, pages 279-308.

Cook, S.J. (1991): Distribution and behavior of platinum in soils of the Tulameen ultramafic complex, southern British Columbia: Applications to Geochemical Exploration for Chromitite-associated platinum deposits. Unpublished M.Sc. Thesis, *The University of British Columbia*, 1991.

Bowman, W.S. (1994): Certified reference materials, Canadian Certified Reference Materials Project (CCRMP); CCRMP publication 94-1E.

Cawthorn, R.G. (2001): A stream sediment geochemical re-investigation of the discovery of the platiniferous Merensky Reef, Bushveld Complex; *Journal of Geochemical Exploration*, Volume 72, pages 59-69.

Dunn, C.E., Hall, G.E.M and G. Nixon (2000): Orientation study of surface geochemical methods to assist in the exploration of platinum group metals in the Whiterocks Mountains Alkalic complex, near Kelowna, British Columbia (82L/4); *in* Geological Fieldwork 2000, *B.C. Ministry of Energy and Mines*, Paper 2001-1, pages 223-229.

Fletcher, W.K. (1989): Preliminary investigation of platinum content of soils and sediments, southern British Columbia (82E/9, 92H/7. 10, 92I14); *in* Geological Fieldwork, 1988; *B.C. Ministry of Energy, Mines and Petroleum Resources*, Paper 1989-1, pages 607-610.

Fletcher, W.K. (1981): Analytical Methods in Geochemical Prospecting; Handbook of Exploration Geochemistry, Volume 1, Govett, G.V.S., Editor, *Elsevier*, 255 pages.

Haughton, D.R. (2001): Geological, geochemical and geophysical assessment report on the Jason Claim Group, NTS 92H/12; *B.C. Ministry of Energy and Mines*, Assessment Report 26519.

Jackaman, W. and Matysek, P.F. (1989): British Columbia Regional Geochemical Survey, NTS 92H - Hope. BC RGS 39/GSC 2665.

Jackaman, W. (1997): British Columbia Regional Geochemical Survey, NTS 94D -McConnell Creek. BC RGS 45.

Monger, J.W.H (1989): Geology of the Hope area, B.C., *Geological Survey of Canada*; Map 41-1989.

Nixon, G.T. and J.L.Hammack (1991): Metallogeny of ultramafic-mafic rocks in British Columbia with emphasis on the platinum-group elements; in Ore Deposits, tectonics and Metallogeny in the Canadian Cordillera, W.J.McMillan, Editor; *Ministry of Energy, Mines and Petroleum Resources*, Paper 1991-4, pages 125-161.

Pinsent, R. (2001): Ni-Cu-PGE potential of the Giant Mascot-Cogburn ultramafic-mafic bodies, Harrison-Hope area, SW British Columbia, 92H; in Fieldwork 2001; *B.C. Ministry of Energy and Mines, Paper 2002-1.*

National Geochemical Reconnaissance Surveys in the B.C. Cordillera to Target and Attract Mineral Exploration

By Wayne Jackaman[1], Ray Lett[1] and Peter Friske[2]

KEYWORDS: *Mineral exploration, multi-element, stream sediment, stream water, National Geochemical Reconnaissance Program, Regional Geochemical Survey, Dease Lake, Bella Coola, Ecstall, Triumph Bay.*

INTRODUCTION

This paper highlights the publication of new regional stream sediment and water geochemical information and also provides details of surveys completed during the 2001 field season (Figure 1). As part of the National Geochemical Reconnaissance (NGR) program, results from a 1:250 000 reconnaissance-scale survey covering the Dease Lake (NTS 104J) map sheet were published, and a new survey was completed in the Bella Coola (NTS 93D) and parts of the Laredo Sound (NTS 103A) map sheets. Funded by the Corporate Resource Inventory Initiative (CRII), results of a survey covering the Ecstall Greenstone Belt (parts of NTS 103H and 103I) were released, and a sample collection program was completed in the Triumph Bay area (parts of NTS 103H).

NGR SURVEYS

The British Columbia Ministry of Energy and Mines (MEM) has been involved in reconnaissance-scale stream sediment and water surveys since 1976. This joint federal-provincial initiative was originally referred to as the Uranium Reconnaissance Program (URP). In 1978 the provincial program was renamed the Regional Geochemical Survey (RGS) and in 1987 the Province began to independently administer surveys conducted in British Columbia. As part of Canada's NGR program, the B.C. RGS continues to maintain sample collection, preparation and analytical standards established by the Geological Survey of Canada. The current database covers close to 70 percent of the province and contains field and analytical information for over 46,000 sample sites. Survey results are used by industry to pinpoint exploration opportunities and by government for resource management, land-use planning and environmental assessments.

DEASE LAKE DATA RELEASE

In July, new field and analytical results for 963 sediment and water samples collected in the Dease Lake (NTS 104J) map sheet were published (Jackaman and Friske, 2001). Stream sediment samples were analysed for more than 40 constituents (Table 1), including base and precious metals, pathfinder and rare earth elements. Water samples were analyzed for pH, uranium, fluoride and sulphate. In addition, 213 stream water samples were analysed for over 40 trace and major elements.

Survey results identified numerous multi-element anomalies including polymetallic volcanogenic massive sulphide (Table 2) and copper-gold porphyry (Table 3) deposits (Lefebure *et al*., 2002). Although the data clearly highlights existing mining camps, many anomalies do not coincide with any recorded mineral occurrence or exploration activity. To the northeast, sediment samples collected from streams draining rocks of the Cache Creek Terrane report elevated levels of zinc, copper and barium values combined with high silver, antimony, selenium and cadmium. These VMS targets are found in rocks that may be related to the intraoceanic arc which hosts the Kutcho Creek (MINFILE 104I 60) massive sulphide deposit (Mihalynuk and Cordey, 1997). Several copper-gold anomalies that appear to be related to Triassic granodiorite intrusions have also been identified in the southern part of the map sheet. A region of known potential, these areas are prime exploration

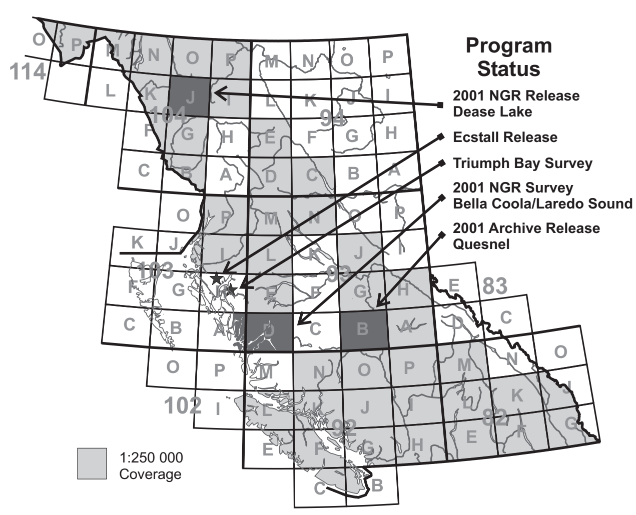

Figure 1. Location map of surveys.

[1] *British Columbia Ministry of Energy and Mines*
[2] *Geological Survey of Canada*

TABLE 1
ANALYTICAL SUITE OF ELEMENTS

Element	Detection	Units	Method
Aluminum	0.01	%	ICPMS
Antimony	0.02/0.1	ppm	ICPMS / INAA
Arsenic	0.1/0.5	ppm	ICPMS / INAA
Barium	0.5/50	ppm	ICPMS / INAA
Bismuth	0.02	ppm	ICPMS
Bromine	0.5	ppm	INAA
Cadmium	0.01	ppm	ICPMS
Calcium	0.01/1	%	ICPMS / INAA
Cerium	5	ppm	INAA
Cesium	0.5	ppm	INAA
Chromium	0.5/2	ppm	ICPMS / INAA
Cobalt	0.1/5	ppm	ICPMS / INAA
Copper	0.01	ppm	ICPMS
Europium	1	ppm	INAA
Gallium	0.2	ppm	ICPMS
Gold	0.2/2	ppb	ICPMS / INAA
Hafnium	1	ppm	INAA
Iron	0.01/0.2	%	ICPMS / INAA
Lanthanum	0.5/2	ppm	ICPMS / INAA
Lead	0.01	ppm	ICPMS
Lutetium	0.2	ppm	INAA
Magnesium	0.01	%	ICPMS
Manganese	1	ppm	ICPMS
Mercury	5	ppb	ICPMS
Molybdenu	0.01	ppm	ICPMS
Nickel	0.1	ppm	ICPMS
Phosphorus	0.001	%	ICPMS
Potassium	0.01	%	ICPMS
Rubidium	5	ppm	INAA
Samarium	0.1	ppm	INAA
Scandium	0.1/0.2	ppm	ICPMS / INAA
Selenium	0.1	ppm	ICPMS
Silver	2	ppb	ICPMS
Sodium	0.001/0.02	%	ICPMS / INAA
Strontium	0.5	ppm	ICPMS
Sulphur	0.02	%	ICPMS
Tantalum	0.5	ppm	INAA
Tellurium	0.02	ppm	ICPMS
Terbium	0.5	ppm	INAA
Thallium	0.02	ppm	ICPMS
Thorium	0.1/0.2	ppm	ICPMS / INAA
Titanium	0.001	%	ICPMS
Tungsten	0.2/1	ppm	ICPMS / INAA
Uranium	0.1/0.2	ppm	ICPMS / INAA
Vanadium	2	ppm	ICPMS
Ytterbium	2	ppm	INAA
Zinc	0.1/50	ppm	ICPMS / INAA
Fluorine	10	ppm	ION
Loss on	0.1	%	GRAV
Fluoride	20	ppb	ION
Sulphate	1	ppm	TURB
Uranium	0.05	ppb	LIF
pH (waters)	0.1		GCE

targets for new porphyry deposits. Some of these sites were staked immediately following the release, but many important anomalies reflecting VMS, porphyry and other exploration targets remain open (Figure 2).

The Dease Lake survey was funded in part by the Geological Survey of Canada Targeted Geoscience Initiative (TGI) and the B.C. Geological Survey Branch.

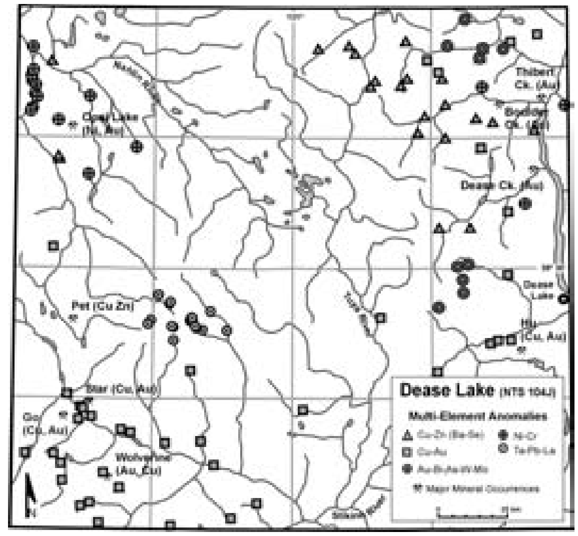

Figure 2. Location map of muli-element anomalies.

QUESNEL ARCHIVE DATA RELEASE

Ongoing since 1991, the RGS Archive program has re-analyzed over 21,000 stream sediment samples by instrumental neutron activation analysis (INAA) for gold and 25 other metals. These sediment samples were saved from reconnaissance-scale stream sediment and water surveys conducted from 1976 to 1985. At this time, RGS open files only presented analytical data for a limited number of metals (*e.g.* zinc, copper, lead, nickel, cobalt, silver, manganese, iron, molybdenum and uranium). To date, new INAA data for nineteen 1:250 000 NTS map sheet areas have been published.

In May of this year, archive data was released for the Quesnel (NTS 93B) map sheet (Jackaman, 2001). Conducted in 1980, the Quesnel reconnaissance-scale stream sediment and water survey included a total of 757 sediment samples and 750 water samples collected from 715 sites over a 14,000 square kilometre area (Figure 3).

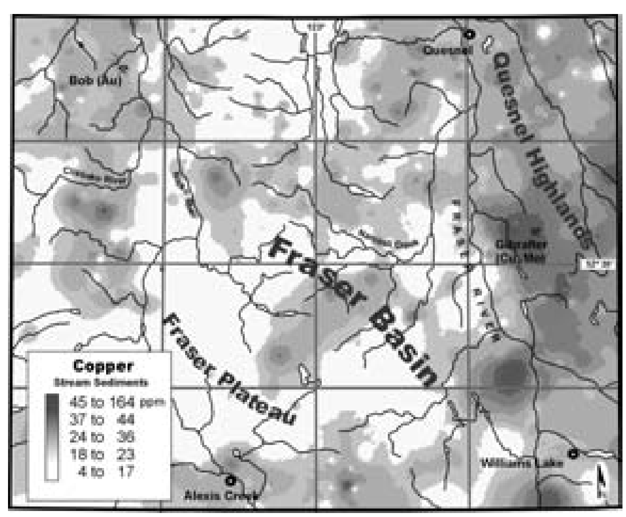

Figure 3. Distribution of copper in the Quesnel map sheet.

TABLE 2
TOP RATED CU-ZN-BA-SE TARGETS

Map	ID	Cu ppm ICPMS	Zn ppm ICPMS	Ba ppm INAA	Se ppm ICPMS
104J15	1056	96.79	204.1	2000	5.8
104J08	1091	62.69	168.6	950	2.4
104J09	1135	68.91	213.7	2800	1.7
104J15	1144	86.55	236.0	990	7.8
104J15	1147	38.15	256.0	1100	3.6
104J15	1148	38.62	253.0	980	3.7
104J15	1167	108.07	418.3	2500	3.4
104J16	1172	186.73	126.5	1200	13.4
104J16	1174	106.12	261.9	1800	2.2
104J16	1197	616.47	46.1	810	7.6
104J15	1218	61.16	443.1	1900	2.8
104J16	1245	38.14	200.0	3800	2.5
104J15	1262	100.49	132.6	1600	4.5
104J15	1263	89.80	195.6	2400	1.3
104J16	1278	68.98	185.3	2500	1.9
104J16	1295	35.24	241.6	2100	1.4
104J09	1297	384.12	140.0	800	8.0
104J12	1418	100.16	150.3	1600	2.0
104J12	1422	88.74	155.3	2600	1.7
104J12	1423	89.83	157.8	2600	2.0
104J10	1437	84.50	153.9	1800	1.2
104J10	1438	53.56	249.0	900	0.6
104J15	1472	48.23	189.2	1300	2.8
104J14	3002	35.54	208.6	1000	1.0
104J04	3229	730.99	491.5	680	2.1
104J04	3231	272.63	126.4	1000	1.1
104J04	3249	464.87	101.8	580	1.0
104J03	3266	142.75	109.2	1200	1.2
104J08	3384	51.20	211.5	810	0.9
104J01	3451	59.23	197.7	880	0.5

TABLE 3
TOP RATED CU-AU-AG TARGETS

Map	ID	Cu ppm ICPMS	Au ppb INAA	Ag ppb INAA
104J07	1086	166.52	<2	54
104J04	1105	161.25	6	175
104J16	1152	64.77	250	176
104J16	1172	186.73	8	2598
104J16	1193	150.95	100	151
104J16	1194	213.33	<2	102
104J16	1197	616.47	<2	509
104J16	1232	115.57	34	131
104J09	1297	384.12	6	354
104J04	3107	256.56	6	74
104J04	3111	159.89	10	90
104J03	3150	155.31	11	303
104J04	3155	175.26	12	180
104J04	3156	273.28	15	193
104J04	3213	321.20	4	79
104J04	3225	691.46	14	453
104J04	3229	730.99	140	643
104J04	3231	272.63	20	189
104J04	3242	129.53	20	158
104J04	3243	134.46	19	81
104J04	3244	138.35	22	95
104J04	3249	464.87	130	324
104J03	3262	138.07	58	205
104J03	3266	142.75	21	331
104J03	3273	38.84	260	51
104J08	3375	160.71	4	82
104J01	3432	200.43	<2	73
104J03	3437	162.84	<2	83
104J02	3471	19.78	140	33
104J06	3479	32.75	349	23

BELLA COOLA/LAREDO SOUND SURVEY

In cooperation with the Geological Survey of Canada (GSC), a new reconnaissance-scale stream sediment and water survey was completed in the Bella Coola (NTS 93D) and Laredo Sound (NTS 103A) map sheets. Truck, boat and helicopter supported sampling was conducted during July and August, 2001. A total of 1060 stream sediment and water samples were collected from 1003 sites at an average density of 1 site every 12 square kilometres.

Stream sediment samples are being analysed by aqua-regia inductively coupled plasma-mass spectroscopy (ICP-MS) and instrumental neutron activation analysis (INAA). Table 1 lists the elements and associated detection limits. Water samples are being analyzed for pH, uranium and fluoride. Additional 125 millilitre water samples collected from 232 sites will be analyzed for trace and major elements. Quality data is maintained by monitoring analytical variation with sample duplicates and control reference standards.

This survey is being funded in part by the Geological Survey of Canada Targeted Geoscience Initiative (TGI) and the B.C. Geological Survey Branch. Results will be published in 2002.

DETAILED GEOCHEMICAL SURVEYS

These surveys are designed to provide baseline regional geochemical data that can be used in the evaluation of the mineral potential of the target areas. Funded under the provincial government's Corporate Resource Inventory Initiative (CRII), these surveys are part of the Ministry of Energy and Mines' contribution to the North Coast Land and Coastal Resource Management Plan (NCLCRMP). Although this work does not cover complete 1:250 000 map sheets the sampling and analyses are carried out to NGR standards and the data are incorporated into the provincial geochemical database.

ECSTALL RELEASE

In May, new field and analytical data for 219 sediment and water samples collected in the Ecstall Greenstone Belt (parts of NTS 103H and 103I) were published (Jackaman, 2001). The report included results for over 48 different metals in stream sediments and pH, uranium, fluoride and sulphate in stream waters (Table 1). A number of sediment samples exhibited anomalous concentrations of copper, lead, zinc, silver and gold (Figure 3). These results clearly

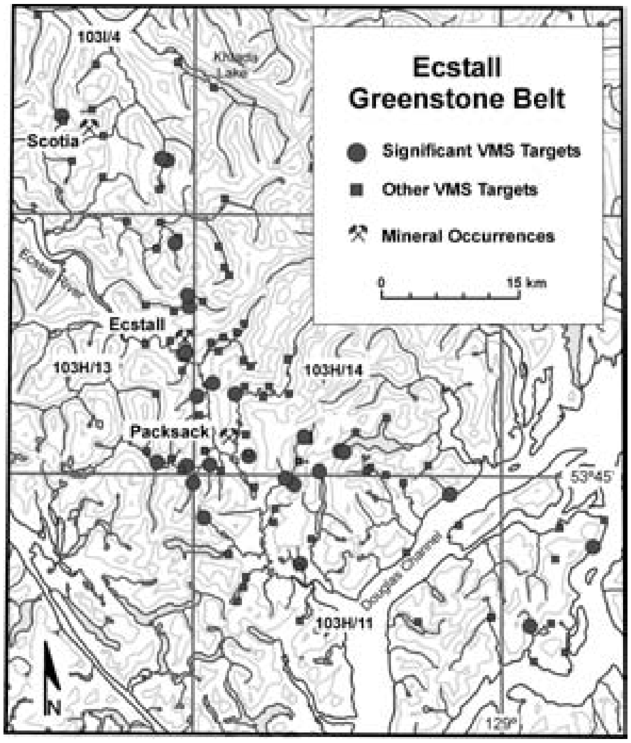

Figure 4. Location map of VMS targets in the Ecstall Belt.

identify areas of known mineralization (Alldrick, 2001; Alldrick and Jackaman, 2002) and outline new regions that may be of interest to mineral explorationists looking for new VMS deposits.

The geochemical signature of samples collected downstream from several known VMS mineral occurrences are shown in Table 4. These samples are anomalous in one or more of the listed metals relative to the Ecstall data set (Table 5) and when compared to the total provincial geochemical database. Table 6 lists the top rated sample sites that are not associated with any recorded mineral occurrence or historical mineral exploration activity and exhibit a multi-element signature characteristic of VMS deposits.

Overall, survey results clearly highlight the high mineral potential of this belt. It can be shown that geochemical data for copper, lead, zinc, silver and gold detect known mineral occurrences, enlarge target areas for currently known prospects and outline new prospective areas for VMS deposits.

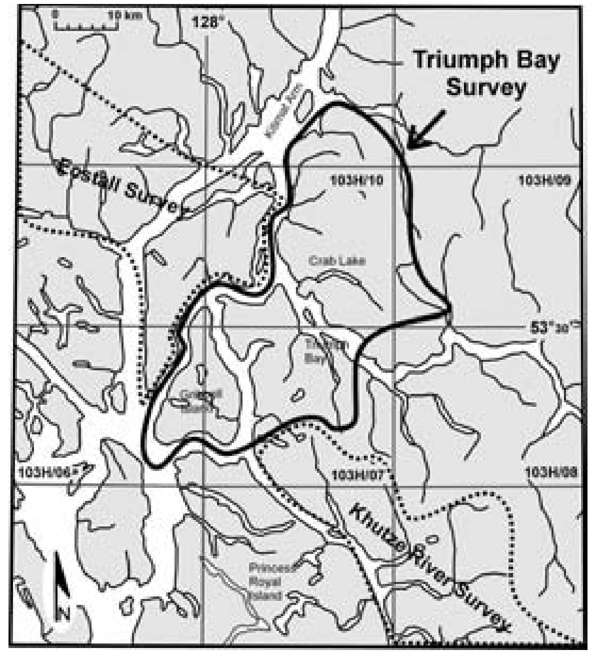

Figure 5. Location map of North Coast surveys.

TRIUMPH BAY SURVEY

In support of previous work completed in the region, the Triumph Bay project covered un-surveyed ground immediately south of the Ecstall survey and north of the Khutze River survey (Jackaman and Pinsent, 2000). Helicopter supported sampling was conducted in late August, 2001. A total of 208 stream sediment and water samples were collected from 196 sites at an average density of 1 site every 7 square kilometres. This area contains mineral deposit environments favourable for the discovery of massive sulphides and gold bearing quartz veins. Results are scheduled to be published in 2002.

TABLE 4
SEDIMENT DATA DOWNSTREAM FROM KNOWN MINERAL OCCURRENCES

MINFILE	ID	Cu ppm ICPMS	Pb ppm ICPMS	Zn ppm ICPMS	Ag ppb ICPMS	Au ppb INAA	Cd Ppm ICPMS	S % ICPMS	Se Ppm ICPMS
Ecstall	9106	125.99	14.07	139.8	304	10	0.57	0.14	0.9
Ecstall	9107	125.00	11.30	158.1	240	7	0.69	0.14	0.6
Strike	9145	74.96	11.88	88.7	99	5	0.13	0.17	1.0
Horsefly	9150	70.88	6.61	69.0	102	92	0.24	0.05	0.6
Ravine	9174	54.31	6.00	104.4	141	2	0.71	0.21	2.4
Steelhead	9179	90.71	3.98	117.2	167	22	0.89	0.10	1.5
Scotia	9038	21.33	9.57	80.1	48	2	0.24	0.05	0.4

TABLE 5
SUMMARY STATISTICS FOR VMS ELEMENTS

Map	Cu ppm ICPMS	Pb ppm ICPMS	Zn ppm ICPMS	Ag ppb ICPMS	Au ppb INAA	Cd ppm ICPMS	S % ICPMS	Se ppm ICPMS
N	228	228	228	228	228	228	228	228
Mean	33.93	3.66	51.85	73	2	0.14	0.05	0.72
Median	27.49	2.94	45.7	48	2	0.07	0.03	0.5
Mode	28.38	1.57	30.3	19	2	0.03	0.02	0.4
St Dev	28.52	3.19	27.87	117.13	11.04	0.20	0.04	1.32
Min	2.12	0.76	12.4	10	2	0.02	0.02	0.1
50th	27.49	2.94	45.7	48	2	0.07	0.03	0.5
70th	38.95	3.88	55.9	69	2	0.12	0.04	0.7
90th	71.01	6.15	83.8	132	7	0.31	0.09	1.1
95th	85.13	8.68	103.2	218	26	0.41	0.14	1.7
98th	104.92	11.88	139.8	287	37	0.57	0.18	2.4
Max	226.26	27.18	187.9	1563	92	2.00	0.33	18.3

TABLE 6
TOP RATED SITES EXHIBITING VMS SIGNATURES

Map	ID	Cu ppm ICPMS	Pb ppm ICPMS	Zn ppm ICPMS	Ag ppb ICPMS	Au ppb INAA	Cd ppm ICPMS	S % ICPMS	Se ppm ICPMS
103H13	9154	106.63	20.99	187.9	1563	70	2.00	0.33	18.3
103H13	9100	55.18	16.92	82.9	319	2	1.18	0.15	6.0
103H10	9230	79.37	20.64	151.2	229	8	0.33	0.04	1.0
103H14	9117	84.25	4.14	92.8	189	26	0.38	0.02	1.2
103H14	9130	71.01	4.84	94.8	218	2	0.31	0.02	2.1
103H14	9104	176.44	3.42	55.8	422	2	0.18	0.03	1.5
103H11	9158	38.92	6.22	72.1	241	64	0.17	0.12	2.8
103H11	9189	95.15	8.22	67.3	203	17	0.24	0.06	1.1
103H10	9410	32.12	3.90	150.5	258	2	1.05	0.18	3.2
103I04	9015	36.46	6.98	83.8	127	2	0.19	0.07	0.7
103I04	9022	226.26	2.63	41.4	50	2	0.04	0.03	0.3
103H14	9177	105.36	3.29	77.4	160	2	0.24	0.02	0.6
103H10	9234	40.22	11.02	52.8	92	2	0.13	0.03	0.5
103H14	9103	74.51	1.57	49.8	259	2	0.37	0.05	1.6
103H14	9165	41.33	1.33	107.1	177	2	0.17	0.02	1.5

REFERENCES

Alldrick, D.J. (2001): Geology and mineral deposits of the Ecstall Greenstone Belt, northwest British Columbia (NTS 103H/I); *in* Geological Fieldwork 2000, *B.C. Ministry of Energy and Mines*, Paper 2001-1, pages 279-302.

Alldrick, D.J. and Jackaman, W. (2002): Metal zoning in the Ecstall VMS Belt, northwest British Columbia (NTS 103H/I); *in* Geological Fieldwork 2001, *B.C. Ministry of Energy and Mines*, this volume.

Jackaman, W. (2001): Stream sediment and water geochemistry of the Ecstall Greenstone Belt (parts of NTS 103H/I), *B.C. Ministry of Energy and Mines,* Open File 2001-13.

Jackaman, W. (2001): British Columbia regional geochemical survey - Quesnel (93B), *B.C. Ministry of Energy and Mines*, BC RGS 54.

Jackaman, W. and Pinsent, R. (2000): Stream sediment and water geochemistry of the Khutze River area (NTS 103H 1, 2, 7), *B.C. Ministry of Energy and Mines*, Open File 2000-12.

Jackaman, W. and Friske, P.W.B. (2001): Regional stream sediment and water data - Dease Lake (NTS 104J), *Natural Resources Canada and the B.C. Ministry of Energy and Mines*, BC RGS 55, GSC Open File 4011.

Lefebure, D.V., Jackaman, W., Mihalynuk, M.G. and Nelson, J. (2002): Anomalous RGS survey results west of Dease Lake - new massive sulphide targets?; *in* Geological Fieldwork 2001, *B.C. Ministry of Energy and Mines*, this volume.

Mihalynuk, M.G. and Cordey, F. (1997): Potential for Kutcho Creek vocanogenic massive sulphide mineralization in the northern Cache Creek Terrane: a progress report; *in* Geological Fieldwork 1996, *B.C. Ministry of Energy and Mines*, Paper 1997-1, pages 157-170.

Anomalous RGS Survey Results West of Dease Lake - New Massive Sulphide Targets

By Dave Lefebure, Wayne Jackaman, Mitch Mihalynuk and JoAnne Nelson

KEYWORDS: *Geochemical survey, silt sample, RGS, volcanogenic massive sulphide, porphyry, intrusion-related gold, Dease Lake.*

INTRODUCTION

The first government regional geochemical survey (RGS) data for the Dease Lake map sheet (104J) in northwestern British Columbia (Figure 1) was released on July 5th, 2001. Stream sediment samples were analysed for more than 40 elements, including precious and base metals (Jackaman and Friske, 2001; Jackaman *et al*., 2002). The survey results include samples with anomalously high values in drainages with no known mineral occurrences. Some of these anomalous values are for elements that are characteristic of polymetallic volcanogenic massive sulphide (VMS), copper-gold porphyry, and intrusive-related gold deposits. The VMS potential of the region is particularly interesting given the number of zinc, copper and barium anomalies associated with a package of poorly known volcanic rocks that includes ferruginous cherts. There are also samples with intriguing, multi-element anomalies, including high tantalum values that are underlain by Level Mountain volcanics, an area that has been generally discounted for its mineral values.

For this preliminary evaluation of the RGS data it was decided to identify only the most highly anomalous element values. Therefore, only samples with an element of interest whose value exceeded the 90th percentile for the 104J data set were used and are shown on the plots in this article. These anomalous samples were assigned scores from a low of 1 to a high of 4 if they exceeded the 90th, 95th, 98th or 99th percentile respectively. Different combinations of indicator elements were chosen to target different styles of mineralization as shown in Table 1.

VOLCANOGENIC MASSIVE SULPHIDE TARGETS

A broad zone of coincident zinc, copper and barium anomalies with associated silver, antimony, selenium and cadmium values extends from Killarney Lake to north of Nuthinaw Mountain in the northeast corner of the Dease Lake map area (Figure 2). Many of the zinc values exceed 145 ppm and are higher than the 90th percentile value of 135 ppm for all 46,591 British Columbia RGS samples. Thirty-six sites from the 104J RGS survey exceed the 95th percentile for zinc values for the province.

TABLE 1
INDICATOR ELEMENTS USED TO IDENTIFY PROSPECTIVE AREAS FOR MINERALIZATION

Main Elements	Subsidiary Elements	Target Mineralization Type
Cu, Zn	Ba, Se	volcanogenic massive sulphide
Au, Cu		porphyry copper-gold
Au, Bi, As	Mo, W	intrusive-related gold
La, Ta, Zn		rare metals
Au, Ag, As, Sb, Hg		epithermal veins
Cr, Ni		ultramafic-related

These anomalies are found in silts from streams draining little known volcanic rocks of the Cache Creek Terrane, including areas with exposures of the mid-Permian French Range Formation (Gabrielse, 1994, 1998). This formation consists primarily of basaltic volcanic rocks, including pillowed sections, with associated argillite and chert. The presence of pillows and sedimentary rocks show that the French Range Formation was deposited in a largely submarine environment.

The French Range was the subject of a preliminary investigation by the British Columbia Geological Survey in

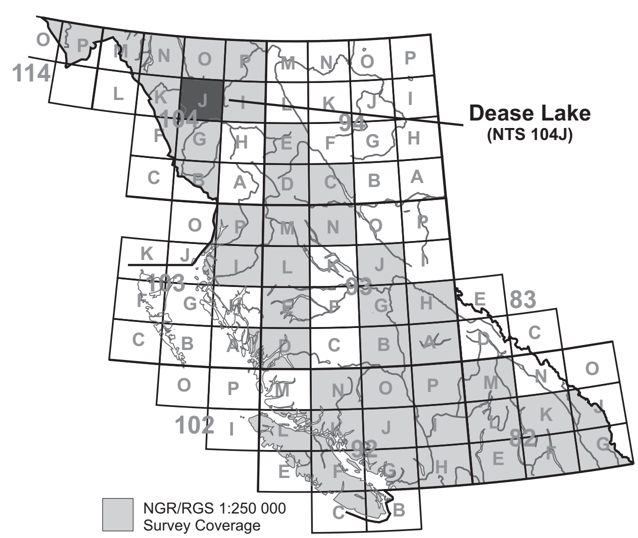

Figure 1. Index map showing the location of the Dease Lake (NTS 104J) map area.

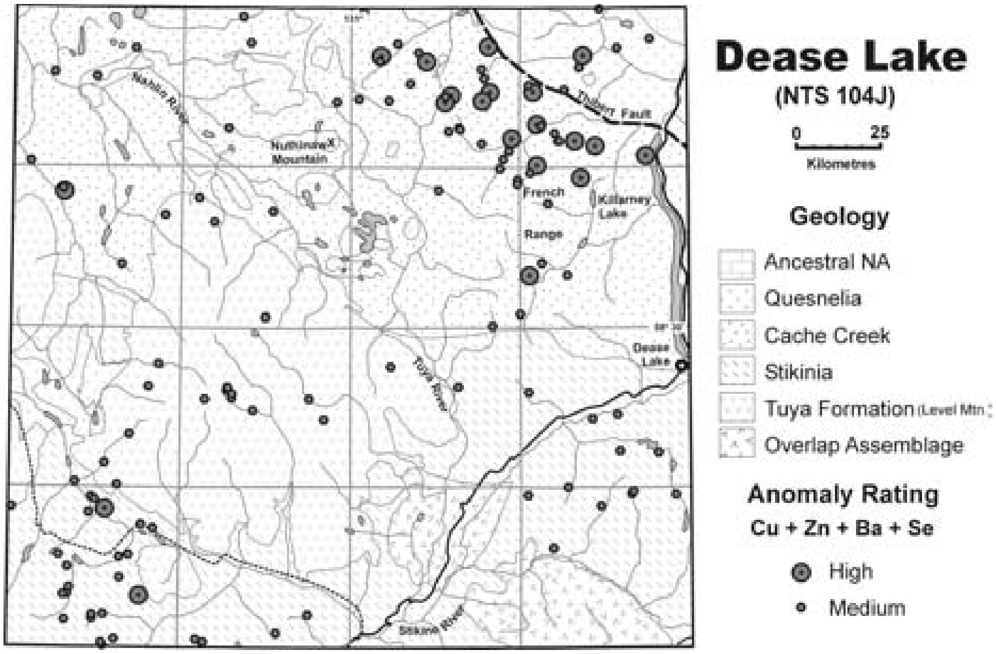

Figure 2. Distribution of Cu-Zn-Ba-Se multi-element anomalies in the Dease Lake map area.

the late 1990s (Mihalynuk and Cordey, 1997). In all, two weeks of 1:50 000 scale mapping were completed during the summers of 1996, 1999 and 2000 to examine the area's potential for the presence of volcanic stratigraphy equivalent to the rocks that host Kutcho Creek deposit (Minfile 104I060). The mapping identified for the first time a felsic volcanic unit and bright red ferruginous cherts, both features associated with some VMS deposits. Recent dating has shown that the Kutcho felsic volcanic rocks at 242 to 246 Ma (Childe and Thompson, 1997) are younger than the only dated volcanic unit from the French Range Formation, which is a felsic tuff that yielded a 263 Ma age (Mihalynuk *et al*., 1999). Therefore, there is no evidence yet of a temporal correlation between the French Range Formation and Kutcho Creek volcanic rocks, although both may be relics of the same intraoceanic arc.

At present, most of the Dease Lake map area has only been covered at 1:250 000 scale (Gabrielse, 1998). Given the lack of detailed geological mapping and the presence of rocks at least as young as Lower Jurassic along strike to the northeast in the Cache Creek terrane (Cordey *et al*., 1991); there is potential south of the Thibert Fault (Figure 2) for Mesozoic volcanic sequences correlative with packages that are known to host VMS deposits. For example, stratigraphy that is age-equivalent to the rocks that host the precious metal-rich Eskay Creek deposit may occur in the area. Several anomalous RGS samples from areas underlain by Cache Creek rocks just south of the Thibert Fault warrant mention as possible indicators of precious metal-rich VMS deposits. Site 1167 just northwest of Vowell Mtn. contains 17 ppb Au (> 90th %tile) and 544 ppb Ag (< 99th %tile) plus significant Cu, Zn, Ba, Se, As and Sb (*see* Jackaman and Friske, 2001 for location of specific sample sites). Sample 1172, at the headwaters of Mosquito Creek northeast of Vowell Mtn, has the highest selenium value (13.4 ppm) encountered during the survey and also contains 2598 ppb Ag. Two other samples, 1152 and 1170, contain elevated gold (250 and 96 pbb), arsenic, antimony, barium and selenium values. Repeat analyses of these samples for gold returned values of 606 and 5 and 8 and 259 ppb Au respectively which suggests a possible nugget effect. The area south of the Thibert Fault has anomalous values for a suite of elements characteristic of epithermal deposits (Au-Ag-As-Sb-Hg, Figure 3) that could be due to Eskay Creek or subaqueous hot spring-type mineralization. Eskay Creek is well known for its high values of contained arsenic, antimony and mercury, as well as gold and silver (Roth *et al*., 1999).

COPPER±GOLD PORPHYRY POTENTIAL

The porphyry potential of the ancient island arcs of this part of the Cordillera is well known. The prospective Stikine and Quesnellia terranes occur in the southern half and northeast corners of the map sheet respectively (Figure 3). These terranes host many of the larger porphyry copper (± gold) deposits in the province, such as Galore Creek, Shaft Creek, Kemess, Bell, Mount Polley and Highland Valley (McMillan *et al*., 1995).

A number of RGS samples with copper-gold anomalies were collected from parts of the Dease Lake map area that are underlain by the Stikine Terrane. The most anomalous area is along the Hackett River near its junction with the Shesley River and east of Kaketsa Mountain. The anomalous drainages extend nearly 15 kilometres east-southeast along the Hackett River valley almost to Kennicott Lake. The anomalous RGS values are close to a number of copper and gold prospects that are related to the differentiated granite of the Triassic Kaketsa stock and related outlying intrusions.

Another set of RGS copper-gold anomalies within the Stikine Terrane are located south of the Hackett River valley (Figure 4). They are near Triassic intrusions (Gabrielse,

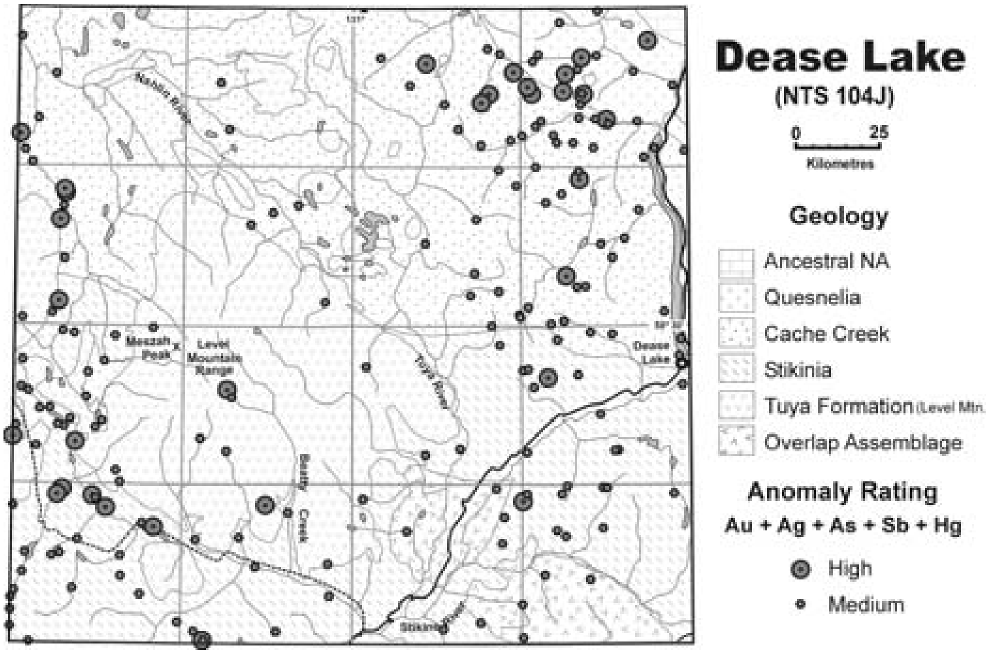

Figure 3. Distribution of Au-Ag-As-Sb- Hg multi-element anomalies in the Dease Lake map area.

1998), but there is no known mineralization in the drainage basins sampled. These anomalies warrant consideration as possible indicators of porphyry-style mineralization. As well, there are a number of unexplained copper-gold anomalies in the Stikine Terrane in the southeast corner of the Dease Lake map sheet in the Hotailuh Range (Figure 4).

Only a small portion of the Quesnel Terrane underlies the Dease Lake map area. Known porphyry mineralization occurs within and near Mesozoic intrusions on Slough Mountain; it is associated with the several Cu-Au RGS anomalies. Another Cu-Au anomaly is near Northwest Mountain and the Anki copper showing (Minfile 104J048).

INTRUSIVE-RELATED GOLD POTENTIAL RELATED TO CRETACEOUS STOCKS

Moderately anomalous gold values (up to 47 ppb) together with elevated molybdenum, tungsten and bismuth occur in drainages around the Cretaceous Snow Peak pluton (Figure 5). These are well known geochemical indicators of plutonic-related gold systems, like the Fort Knox mine in Alaska (Logan *et al*., 2000), associated with differentiated Cretaceous granitic rocks. The Mack (Minfile 104J014) is the only showing hosted by the Snow Peak Pluton. It consists of molybdenite and/or pyrite quartz stringers in slightly porphyritic granodiorite. Surface samples from a trench and

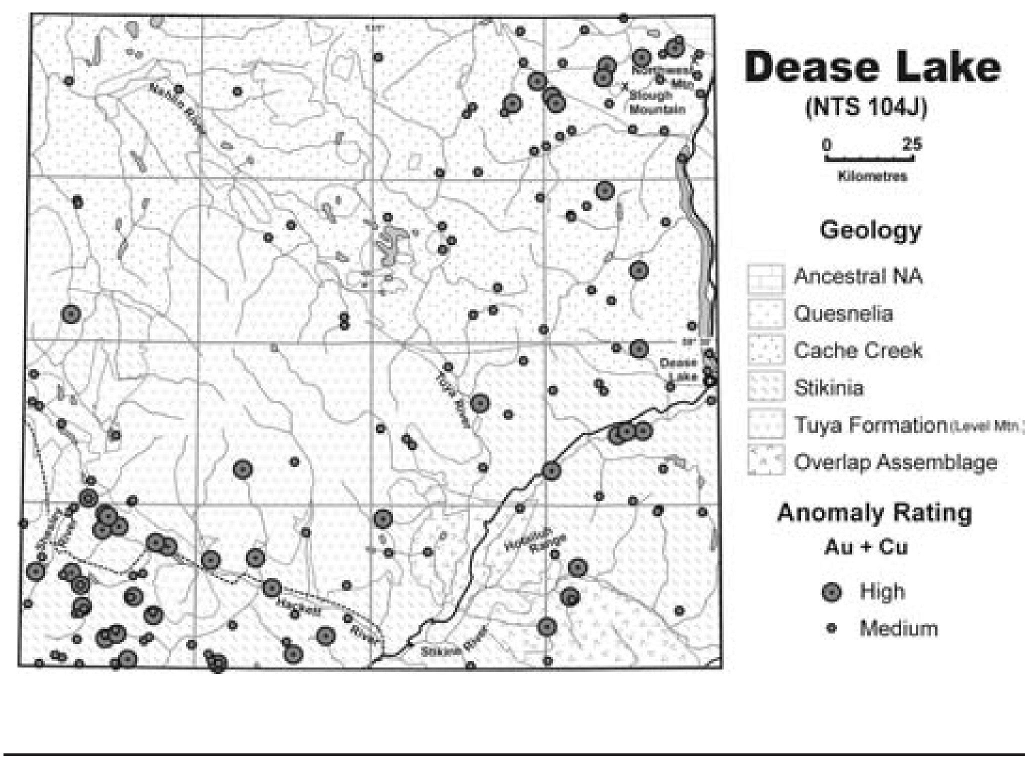

Figure 4. Distribution of Au-Cu multi-element anomalies in the Dease Lake map area.

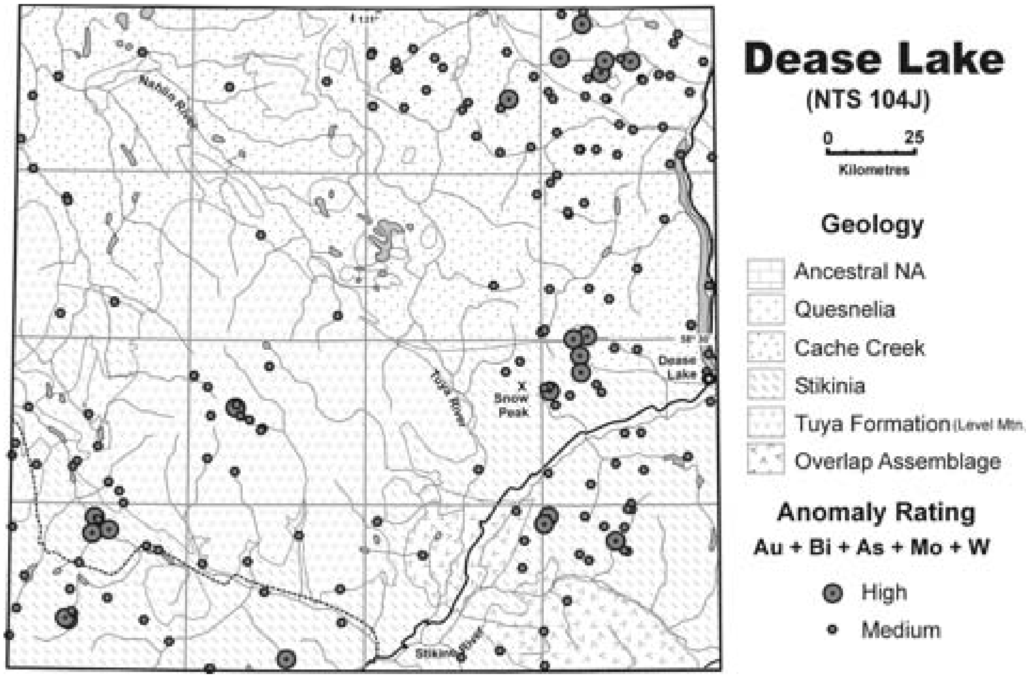

Figure 5. Distribution of Au-Bi-As-Mo-W multi-element anomalies in the Dease Lake map area.

pits yielded up to 0.13% molybdenum, 0.39 % WO_3 and 1.6 grams per tonne gold (Sadlier-Brown and Nevin, 1976).

ANOMALIES AT LEVEL MOUNTAIN RANGE

Highly anomalous levels of zinc, tantalum (values up to 10 ppm) and lanthanum with elevated values of tungsten, cadmium and lead are found in RGS samples from the Level Mountain Range (Figure 6). The Level Mountain Complex is a bimodal assemblage of Miocene to Pleistocene alkaline volcanic rocks. Given the cospatial extent of the drainage basins sampled and the Level Mountain Complex, it appears that these alkaline rocks have high Zn, W, Cd and La background values in contrast with rock types in the map area. There are no previous reports of high Ta values in this area; however, minerals containing tantalum are known to be associated with more differentiated alkaline rocks.

The area southeast of Meszah Peak has attracted some exploration interest because there is a large colour anomaly along the main ridges due to alteration of the highly peralkaline extrusive Level Mountain Complex. The alteration zones are associated with iron- and manganese-stained, weakly brecciated, silicified and kaolinized rhyolites and trachytes (Daly, 1983). There is only one documented showing hosted by Level Mountain rocks, the

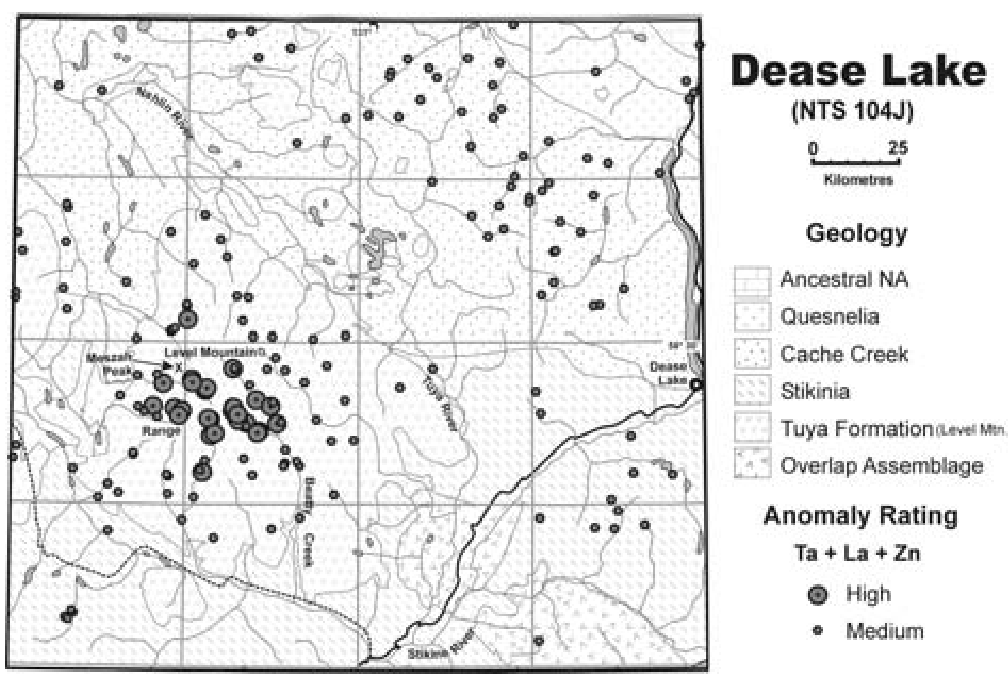

Figure 6. Distribution ofLa-Ta-Zn multi-element anomalies in the Dease Lake map area.

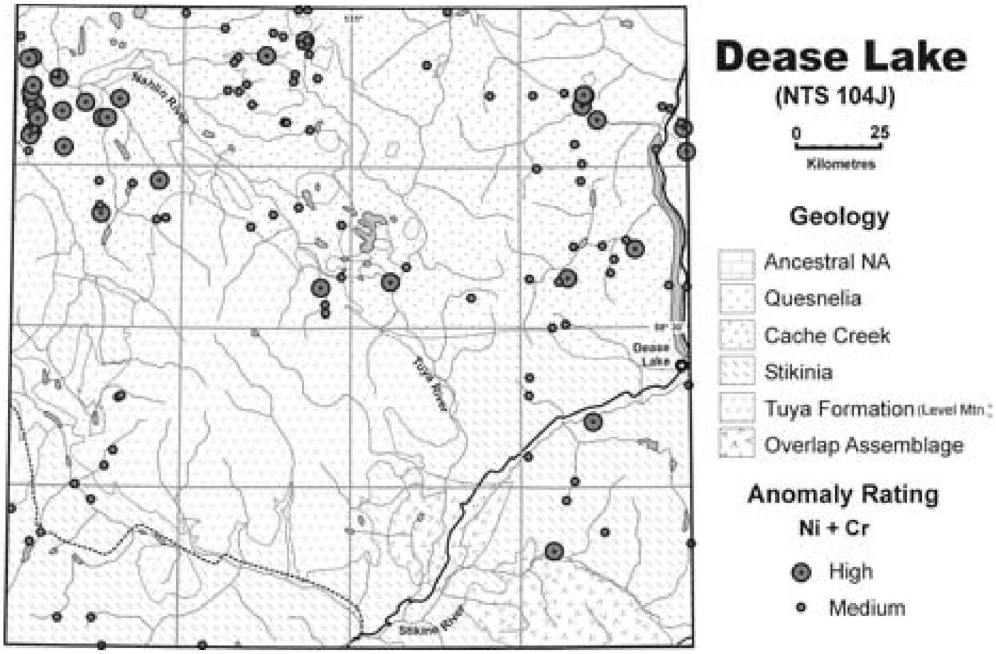

Figure 7. Distribution of Cr-Ni multi-element anomalies in the Dease Lake map area.

Golden Shower Hg occurrence (104J062), which is associated with the colour anomaly. Daley (1983) reports lithogeochemical values of up to 6000 ppb mercury in a brecciated, weakly silicified, limonitic-stained felsite. Many of the 9 stream sediment samples in the same valley, the northern tributary for Beatty Creek, have elevated antimony, mercury and arsenic values. These elements can be indicators of epithermal mineralization which is consistent with the alteration style and geological setting. Unfortunately silver values are only slightly above background and gold contents are not anomalous. When compared to other anomalous RGS samples for Au-Ag-As-Sb-Hg values in the Dease Lake map area (Figure 3), Beatty Creek does not appear to be particularly significant.

NAHLIN RIVER CHROMIUM AND NICKEL ANOMALIES

There are a number of silt samples with anomalous chromium and nickel values from tributaries along the Nahlin River along the northwest edge of the Dease Lake map area (Figure 7). These creeks are draining basins with exposures of the Nahlin ultramafic bodies that may have potential for platinum group elements. Unfortunately there was no sampling for PGEs in the survey.

SUMMARY

The recent release of RGS results for the Dease Lake map area reveal drainage basin areas containing sediment with anomalously high contents of a variety of elements. Elemental suites can be chosen to identify prospective areas for different styles of mineralization. In some areas no mineralization has been reported, and the RGS anomalies remain unexplained. The most interesting exploration targets are:

- volcanogenic massive sulphide deposits in the Cache Creek rocks;
- copper-gold porphyry deposits in the Stikine and Quesnel terranes;
- intrusive-related gold near granitic Cretaceous stocks; and
- an unexplained RGS anomaly with elevated As, Sb and Hg values in the Level Mountain Range.

Anomalously high values of Zn, Ta, La and several other elements are associated with the Level Mountain Complex alkaline volcanic rocks.

REFERENCES

Childe, F. and Thompson, J.F.H. (1997): Geological setting, U-Pb geochronology, and radiogenic characteristics of the Permo-Triassic Kutcho Assemblage, north-central British Columbia; *Canadian Journal of Earth Sciences*, Volume 34, pages 1310-1324.

Daley, F. (1983): Geological and geochemical report on the Steveann, Incan Empire, Golden Shower, White Christmas and Coat of Arms claims at Level Mountain, B.C.; British Columbia Ministry of energy and Mines, Assessment Report 12219, 12 pages.

Cordey, F., Gordey, S.P. and Orchard, M.J. (1991): New biostratigraphic data for the northern Cache Creek Terrane, Teslin map area, southern Yukon; *in* Current Research, Part E, *Geological Survey of Canada*, Paper 91-1E, pages 67-76.

Gabrielse, H. (1994): Geology of the Cry Lake (104I) and Dease Lake (104J/E) map areas, north central British Columbia; *Geological Survey of Canada*, Open File 2779.

Gabrielse, H. (1998): Geology of Cry Lake and Dease Lake map areas, north-central British Columbia, *Geological Survey of Canada,* Bulletin 504, 147 pages.

Jackaman, W., Lett, R. E. and Friske, P.W.B. (2002): National geochemical reconnaissance surveys in the B.C. cordillera to target and attract mineral exploration; *in* Geological Fieldwork 2002, *B.C. Ministry of Energy and Mines*, Paper 2002-1, this volume.

Jackaman, W. and Friske, P.W.B. (2001): Regional stream sediment and water data - Dease Lake (NTS 104J), *Natural Re-*

sources Canada and the B.C. Ministry of Energy and Mines, GSC Open File 4011, BC RGS 55.

Logan, J.L., Lefebure, D. V. and Cathro, M. (2000): Plutonic-related gold-quartz veins and their potential in British Columbia; *in* The Tintina Gold Belt: Concepts, Exploration and Discoveries, Special Volume 2, British Columbia and Yukon Chamber of Mines, pages 197-225.

McMillan, W.J., Thompson, J.F.H., Hart, C.J. and Johnston, S.T. (1995): Regional geological and tectonic setting of porphyry deposits in British Columbia and Yukon Territory; in Porphyry Deposits of the Northwestern Cordillera of North America; T.G. Schroeter, Editor, *Canadian Institute of Mining, Metallurgy and Petroleum*, Special Volume 46, pages 40-57.

Mihalynuk, M. G. and Cordey, F. (1997): Potential for Kutcho Creek volcanogenic massive sulphide mineralization in the northern Cache Creek Terrane: a progress report; in Geological Fieldwork 1996, *B.C. Ministry of Energy and Mines*, Paper 1997-1, pages 157-170.

Mihalynuk, M. G., Erdmer, P., Ghent, E.D., Archibald, D.A., Friedman, R.M., Cordey, F., Johannson, G.G. and Beanish, J. (1999): Age constraints for emplacement of the northern Cache Creek Terrane and implications of blueschist metamorphism; in Geological Fieldwork 1998, *British Columbia Ministry of Energy and Mines*, Paper 1999-1, pages 127-141.

Roth, T., Thompson, J.F.H. and Barrett, T.J. (1999): The precious metal-rich Eskay Creek deposit, northwestern British Columbia, *in* Volcanic Associated Massive Sulphide Deposits: Processes and Examples in Modern and Ancient Settings, Editors, C.T. Barrie and M.D. Hannington, *Society of Economic Geologists*, Review Volume 8, pages 357-373.

Sadlier-Brown, T.L. and Nevin, A.E. (1976): Geological and Geophysical Report on the Mack Group, Snow Peak Area; *British Columbia Ministry of Energy and Mines*, Assessment Report Number 6354, 22 pages.

A Provisional Geochemical Exploration Model (GEM) for the Sappho Property, B.C. (82E/2E)

By Ray Lett[1], Victor Levson[1] and Colin Dunn[2]

KEYWORDS: *Geochemistry, PGE, soil, stream sediment, geochemical exploration model.*

INTRODUCTION

This paper describes an orientation survey on the Sappho mineral property, Greenwood, (MINFILE 82ESE 147) to study the geochemical response of platinum group elements (PGE) and associated metals from massive sulphide mineralization in soil, stream sediment and vegetation (Figure 1). The survey is a contribution to a multi-disciplinary initiative to better understand the occurrence and means of discovering PGE mineralization in B.C. (Nixon, 2002). Results of stream sediment, B and C-horizon soil, basal till and vegetation sampling have been integrated with data from assessment reports and other sources to develop a geochemical exploration model (GEM).

GEM's are designed to simplify data interpretation by visually demonstrating the relationship between bedrock and surficial geochemistry. They are based on a series of conceptual, three-dimensional models first proposed by Bradshaw (1974) for the Canadian Cordillera and later modified by Kauranne (1976), Lovering and McCarthy (1978) and Butt and Smith (1980). The models are formulated from existing geochemical data rather than being based on purely conceptual considerations and can therefore be used with more confidence when designing future surveys.

Several diagrams were used by Bradshaw (1975) to construct the conceptual models. Broad, spatial, element variations were summarized on three-dimensional block diagrams whereas more detailed horizontal and vertical geochemical changes were shown on cross sections and prisms. The diagrams have no scale because geochemical anomaly size is variable and the models were intended primarily to show geochemical relationships and to identify dispersion processes in the near-surface environment. However, anomaly dimensions can be predicted by linking the conceptual models to the supporting data gathered from geochemical case studies and orientation surveys. These predictions can be used when planning geochemical surveys to help, for example, in selecting the appropriate sample type and sampling density.

[1] British Columbia Ministry of Energy and Mines
[2] Consultant

In this paper a GEM has been developed to summarize important features of the geochemical expression associated with PGE-copper-nickel sulphide mineralization found on the Sappho property. Bedrock geology and sulphide mineralization, surficial deposits (soil, till, etc.) and surface drainage are displayed three-dimensionally by a series of stacked, block diagrams. These diagrams are linked to series of geochemical landscape layers showing the observed geochemical expression of mineralization from the bedrock interface into the surficial deposits and vegetation. Ice-flow direction and the projected expression of mineralization at the bedrock surface onto the surficial layers are also shown on the diagrams.

SAMPLING AND ANALYTICAL METHODS

B and C-horizon soil samples were collected from pits dug at eight stations approximately 100 m apart along a traverse extending north from the international boundary to the Main showing on the Sappho property. Duplicate soil samples were taken at one site to measure sampling variability. Douglas-fir (*Pseudotsuga menziesii*) bark samples were also taken at each station by one of the authors (CD). Basal

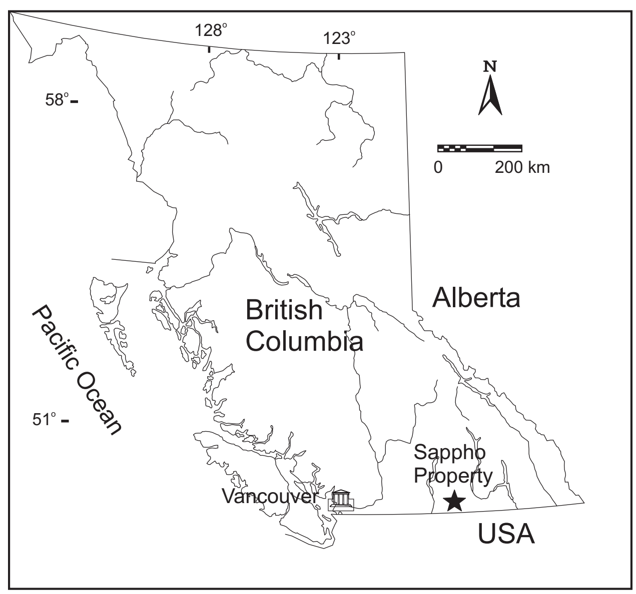

Figure 1. Location of the Sappho Property.

till samples were collected at three sites where thick tills were exposed in trenches (Figure 2). Stream sediment and moss mat sediment samples were collected from the north-flowing Norwegian Creek (Figure 2).

Up to 5 kg of fine-textured sediment, typical of material collected during a regional survey, was taken from the sandy part of a bar in Norwegian Creek, and stored in high wet strength Kraft paper bags. Live moss (1-2 kg) containing trapped sediment, collected from the surface of boulders and logs in the active stream above the water level, was also stored in Kraft bags. Sampling was carried out on June 27 and 28, 2001. Locations of soil, tree bark, stream and moss mat sampling stations are shown in Figure 2. Rock samples were taken from the main showing during geological mapping (Nixon, 2002).

Soil, drainage sediment, moss mat sediment, till and rock samples were prepared in the B.C. Geological Survey Branch Laboratory, Victoria, B.C. The samples were air dried and the - 18 mesh (< 1 mm) recovered by gently disagregating the sediment or by pounding moss mats before dry sieving through a 1 mm stainless steel screen. One part of the 1 mm fraction was then screened to - 80 ASTM mesh (<0.177 mm) and a second part screened to - 230 mesh (<0.063mm). Control reference material and analytical duplicates were inserted into the batch of samples sent for analysis.

The – 80 and –230 mesh of stream sediment and moss mat sediment, tree bark ash, till and soil samples, and the – 150 mesh of milled rock samples were analysed for 37 trace and minor elements by inductively coupled plasma mass spectroscopy (ICP-MS) and inductively coupled plasma emission spectroscopy (ICP-ES) following aqua regia digestion. Platinum, palladium, gold and rhodium in the two fractions of the field survey samples and in the milled rock samples were also determined by ICP-MS following lead fire assay. The samples were analysed by Acme Analytical Laboratories Ltd. (Vancouver).

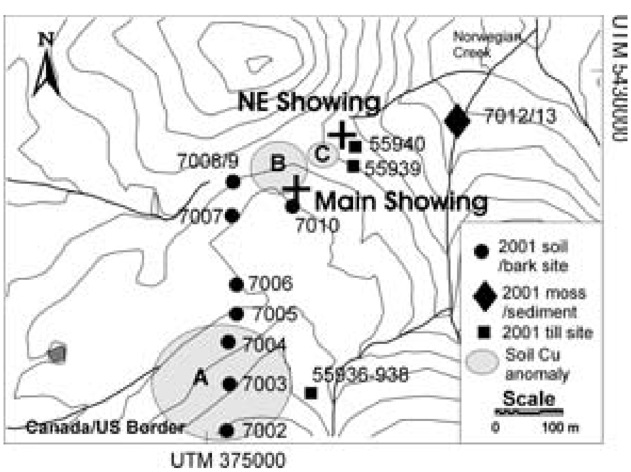

Figure 2. Soil and sediment sample sites and outline of copper anomalies (>90 ppm) from assessment report data (Keating and Fyles, 1984).

COMPILATION OF DATA FOR GEM DEVELOPMENT

Geological and geochemical data from assessment files (Keating and Fyles, 1984) and from results of the orientation survey have been used to formulate a GEM for the Sappho property. This information is briefly summarized:

GEOLOGY

The central part of the property where the orientation survey was carried out is underlain by Jurrassic age greenstone that has been intruded by Tertiary age microdiorite and younger cross-cutting syenomonzonite-shonkinite bodies. These intrusions are the principal hosts for the sulphide mineralization (Keating and Fyles, 1984; Nixon, 2002).

MINERALIZATION

The principal sulphide mineral occurrences on the Sappho property are the Main and Northeast showings where the microdiorite has massive lenses and disseminations of pyrite and chalcopyrite. Grades up to 3.2 per cent copper and 0.9 grams per tonne platinum in grab samples of the suphides have been reported (Keating and Fyles, 1984; Nixon, 2002).

DESCRIPTION OF THE AREA

The Main and Northeast sulphide showings are located on a northeast-facing, moderately steep (20^{o}) hill side that extends for 700 m from the Canada/USA boundary. The property has a maximum elevation of 1125 m and is drained by Norwegian Creek and several smaller creeks. The climate is semi-arid. Bedrock exposure is roughly 10 percent. Surficial sediments are basal till deposited over most of the property, colluvium and colluviated till on steeper hill slopes. Loess and organic accumulations occur in flatter part of the property and in depressions. The regional ice flow direction is southerly. The surficial sediments have been disturbed by road construction and by trenching in some areas. Brunisolic, luvisolic and organic soils have formed on these sediments and support second growth ponderosa pine, Douglas-fir (*Pseudotsuga menziesii*) and birch between patches of open grassland.

SOIL GEOCHEMISTRY

B-soil horizon survey results from assessment reports (Keating and Fyles, 1984) outlined three copper (determined by atomic absorption spectroscopy following nitric-perchloric acid digestion) anomalies (> 90 ppm) on the property (Figure 2). The first anomaly (A) 200 x 300 m size is 500 m south of the main showings and extends to the Canada/USA boundary. The anomaly trends northerly and soils contain up to 270 ppm copper. A second anomaly (B) 150 m by 200 m is centred over the Main showing and a third anomaly (C) 200 m northeast of the main showing is 100 m x 100 m size with up to 280 ppm copper in the soil. Zinc (> 80 ppm) and lead (> 13 ppm) anomalies are smaller than copper and there is a weak spatial correlation between the copper, lead and zinc. Gold values in the B-horizon soil are below 10 ppb.

Results of the 2001 orientation survey reveal an association of platinum, palladium, nickel, gold and copper in B and C-horizon soils. The variation of elements in the B-soil horizon from south to north towards the Main showing (Figure 3) indicates that platinum, palladium, gold, copper and nickel gradually decrease from higher values close to the Canada/USA boundary and then increase over the Main zone sulphide mineralization. Platinum, platinum and gold are generally (but not consistently) higher in the -230 mesh (<0.063 mm) size fraction compared to the - 80 (<0.18 mm) fraction of the soil (Figure 4). Element values for the two size fractions of soil samples from station 10, close to the Main showing, are shown in Table 1. These data demonstrate an association of elevated copper, chromium, manganese, nickel, vanadium, zinc, platinum, palladium and gold in the B and C soil horizons. Values for all elements increase with depth in the soil profile and are similar in the two size fractions. However, anomaly thresholds for elements in the soil cannot be determined because of the small number of samples.

STREAM SEDIMENT GEOCHEMISTRY

Samples from a previous regional geochemical survey (Matysek *et al.*, 1991) covering the Sappho property have not been analysed for platinum and palladium. In Table 2, the 95th percentile values are shown for elements commonly found associated with platinum and palladium (Au, As, Cu, Co, Cr, Ni, Zn), calculated from RGS data for 1500 samples from NTS 82E. The geochemistry of the Norwegian Creek RGS sample (82E765134), shown for comparison, indicates that nickel is the only element above the 95th percentile. Element data for the -80 (<0.180 mm) and -230 (<0.063 mm) mesh size fractions of moss sediment (M) and stream sediment (S) 2001 orientation survey samples from

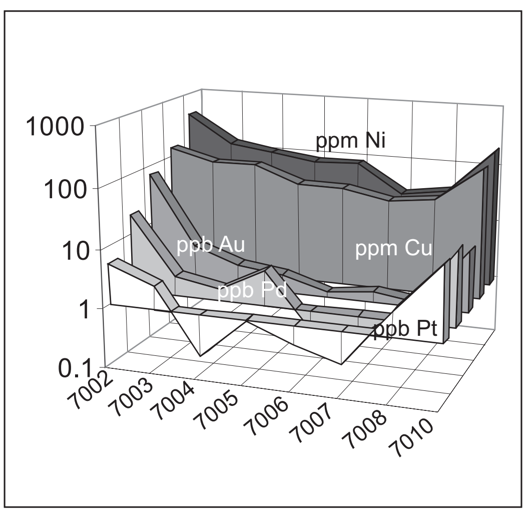

Figure 3. Elements in B-horizon soil (- 80 mesh fraction) across the Sappho property.

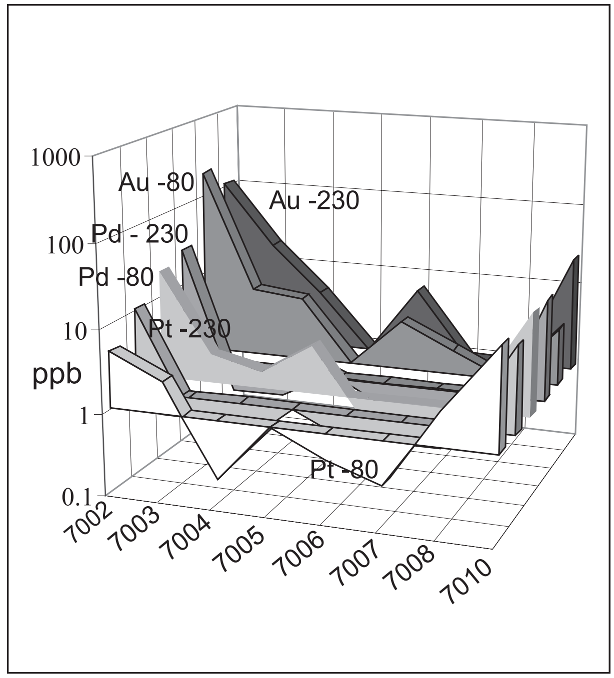

Figure 4. Gold, silver and platinum in -80 and -230 mesh fraction of the B-C soil horizons across the Sappho property.

TABLE 1
GEOCHEMISTRY OF SOIL CLOSE TO THE MAIN SHOWING AT 25 AND 35 CM DEPTH AND IN THE -80 AND -230 MESH FRACTIONS

Sample		55925	55926	55927	55928
Depth		25 cm	25 cm	35 cm	35 cm
Fraction		-80 mesh	-230 mesh	-80 mesh	-230 mesh
Ag-MS	ppb	200	218	255	376
As-MS	ppm	3.5	3.6	4.3	5.3
Au-MS	ppb	4.9	7	10.6	15.3
Au-FA	ppb	5	8	5	25
Co-MS	ppm	27.1	22.1	48.7	41.9
Cr-MS	ppm	162.5	135.1	294.2	269.6
Cu-MS	ppm	163.7	168.0	210.6	247.2
Fe-MS	%	4.19	3.36	7.36	6.13
Hg-MS	ppb	23	22	22	44
La-MS	ppm	19.4	20.6	22.7	26.9
Mg-MS	%	1.87	1.45	3.59	3.03
Mn-MS	ppm	3305	3154	4524	5525
Ni-MS	ppm	101.0	90.1	152.8	133.9
Pd-FA	ppb	9.9	7.2	17.8	16.9
Pt-FA	ppb	6.6	6.4	17.6	11.2
S-MS	%	0.04	0.05	0.04	0.06
Se-MS	ppm	< .1	0.2	< .1	0.1
V-MS	ppm	155	121	299	265
Zn-MS	ppm	172.6	134.7	384.0	316.2

TABLE 2
95 PERCENTILE VALUES FOR ELEMENTS COMMONLY FOUND ASSOCIATED WITH PLATINUM AND PALLADIUM CALCULATED FROM 1500 RGS SAMPLES FROM NTS 82E COMPARED TO DATA FROM ONE RGS SITE (82E765184) ON THE SAPPHO PROPERTY

Element	Au	As	Cu	Co	Cr	Fe	Ni	Pb	Zn
Units	ppb	ppm	ppm	ppm	ppm	%	ppm	ppm	ppm
Method	INAA	INAA	AAS	INAA	INAA	INAA	AAS	AAS	AAS
95th Percentile	31	13.0	58	25	260	6.4	21	21	103
82E765134	11	7.1	24	14	220	3.9	25	2	40

Norwegian Creek are shown in Table 3. Results show that whereas arsenic, copper, cobalt, chromium, iron, nickel, lead and zinc are highest in the -230 mesh size fraction of moss sediment, gold is highest in the -80 mesh fraction of stream sediment. Platinum and palladium are highest in the -80 mesh of moss sediment although concentrations for both elements are below 3 ppb. Higher arsenic, cobalt, chromium and iron in the RGS sample (82E765134), compared to levels found in the orientation moss and stream sediment may be the result of higher concentrations determined in the sample by instrumental neutron activation (INAA) compared to levels released by aqua regia with an ICP-MS finish.

BIOGEOCHEMISTRY

The distribution of elements in bark samples from Douglas-fir close to the soil sites along the orientation traverse are shown in Figure 5. Results are listed in Table 4. Copper and zinc are elevated in the bark at the southern end of the traverse (01-07-002). Elevated palladium (5 ppb) was also detected in the bark at this site. Elevated silver, arsenic, gold and platinum at site 01-07-006 can be explained by higher accumulation of these elements in bark from an older Douglas-fir compared to the bark from younger trees sampled at the other sites. It is noteworthy that the highest platinum (26 ppb) and copper (876) occurs in bark (01-07-010b) from a tree close to the Main showing.

TILL GEOCHEMISTRY

Results of geochemical analysis of tills sampled in the Sappho area are provided in Table 5. Samples 55936 to 38 are from a vertical profile in a pit (old collapsed adit?) in the area of soil anomaly 'A' (Figure 2). Soil development at the site includes about 2-3 cm of an LFH layer, a 0.5 cm Ah horizon, a 30-70 cm thick Bm horizon and a Cca horizon extending to over one m depth. The site is well drained, with an open Douglas-fir forest and a surface slope of about 10°.

Sample 55936 is from a depth of 2.5 m in a moderately dense, massive, matrix-supported diamicton interpreted as a basal till. The matrix is an unoxidized silty-sand to sandy-silt and shows a strong, slope-parallel fissility, highlighted by calcium carbonate precipitate. Clasts are of varied lithologies (*e.g.* pyroxenite, syenite, gabbro, greenstone, rhyolite and schist), and some are striated indicating glacial transport. The till contains about 20-30% clasts and most are subangular to subrounded. Several clasts with sulphide mineralization (mainly pyrite) were observed. Sample 55937 is from 70 cm depth in diamicton that gradationally overlies and is similar to the underlying unit except that it shows weaker fissility, some oxidation and a higher percentage of angular clasts. The diamicton is inferred to be a colluviated till. Sample 55938 is from 25 cm depth in pebbly, fine sand with minor silt. The sand is loose, massive, oxidized, light reddish brown, and contains about 5-10% clasts many of which are quite angular. The lower contact of this unit is gradational and occurs at about 50 cm depth. The unit is interpreted to be of colluvial origin, as indicated by the angular clasts, possibly with an aeolian component. Wind, water and/or gravity sorting of the material are indicated by the loose, fine sandy texture and by the low proportion of fines.

For almost all elements, concentrations increase significantly, with depth (Table 5). Most notably, gold and palladium concentrations are more than 10 times higher in the underlying till and about 5 times higher at 70 cm depth than they are in the B-horizon at 25 cm depth. Gold decreases from 38 ppb in the basal till to 2 ppb in the B horizon, platinum decreases from 3.5 ppb in the till to 1.6 ppb in the B-horizon and palladium decreases from 6.5 ppb in till to below detection (<0.5) in the B-horizon. The analytical duplicate of sample 55936 shows even higher platinum (4.5 ppb) and palladium (13.2 ppb) in the till. Copper, cobalt, chromium, iron and nickel also show progressively increasing concentrations with depth. Other elements show little

TABLE 3
ELEMENT DATA FOR THE -80 (<0.180 mm) AND -230 (<0.063 mm) SIZE FRACTIONS OF MOSS SEDIMENT (M) AND STREAM SEDIMENT (S) FROM 2001 ORIENTATION SURVEY SAMPLES FROM NORWEGIAN CREEK

Element	Au	As	Cu	Co	Cr	Fe	Ni	Pb	Zn	Pt	Pd
Units	ppb	ppm	ppm	ppm	ppm	%	ppm	ppm	ppm	ppb	ppb
Method	ICP-MS	ICP-MS	ICP-MS	ICP-MS	ICP-MS	ICP-MS	ICP-MS	ICP-MS	ICP-MS	FA-MS	FA-MS
5931-80S	2.3	2.7	49.9	9.6	64.5	2.03	66	5.8	52.4	0.8	2.0
5932-230S	10.3	3.0	59.9	10.5	69.8	2.05	79	6.3	57.6	0.9	1.1
5933-80M	1.6	3.7	54.0	13.8	85.8	2.46	96	7.0	61.3	2.6	2.1
5934-230M	1.6	4.0	59.8	13.8	91.3	2.56	112	7.8	66.5	0.9	1.6

TABLE 4
GEOCHEMISTRY OF DOUGLAS-FIR BARK SAMPLES FROM THE SAPPHO PROPERTY

Sample	Ag	As	Ash	Au	Cu	Ni	Pd	Pt	Se	Zn
	ppb	ppm	%	ppb	ppm	ppm	ppb	ppb	ppm	ppm
01-07-002	185	24	2.35	2.4	344	10	5	-2	2.3	1024
01-07-003	162	21	2.08	1.6	352	14	-2	-2	2.1	1511
01-07-004	188	15	2.38	2.5	265	14	6	-2	1.4	697
01-07-005	143	37	2.85	3.4	258	11	-2	-2	2	830
01-07-006	257	119	1.99	12.2	335	13	-2	-2	2.4	476
01-07-007	181	40	3.06	2.2	272	14	9	-2	1.6	906
01-07-008	190	25	3.36	2.4	245	6	-2	-2	1.3	640
01-07-010a	392	33	2.93	3.7	683	10	7	3	1.6	797
01-07-010b	370	33	2.24	4	876	15	-10	26	2.6	936
Median	188	33	2.38	2.5	335	13	2	-2	2	830

variation with depth. Only arsenic is higher in the B-horizon than in the underlying till but the difference is minimal (7.5 vs. 7.2 ppm). Lead and zinc are slightly more concentrated at intermediate depths (sample 55737, Table 5).

Decreasing element concentrations with depth have been observed in several other parts of the Cordillera and probably reflect modifying processes that are most active at the surface (Levson, 2001a, b). The downward migration of metals is probably due to post-depositional, gravity sorting and water washing of the near surface layers. The greater effect on heavy elements, such as gold and palladium, than on lighter elements is consistent with mechanisms of gravity and water sorting. In this area, the addition of windblown fine sands and silty loess may also contribute to lower metal concentrations at the surface. These observations suggest that B-horizon soil sampling in this region would be less effective for exploration than would till sampling. Although concentrations clearly increase with depth, for practical sampling purposes it is probably sufficient to sample near the top of the C-horizon.

Gold concentrations in till at the south end of the property are higher than in soils over the main showing area and other metals such as platinum, palladium and nickel show comparable levels to shallow soils at the showing (compare Tables 1 and 5). Other elements such as copper also are elevated in till at the south end of the property. This suggests that there is potential for discovery of a new mineralized zone in that area, although dispersal from the main showing has not been ruled out.

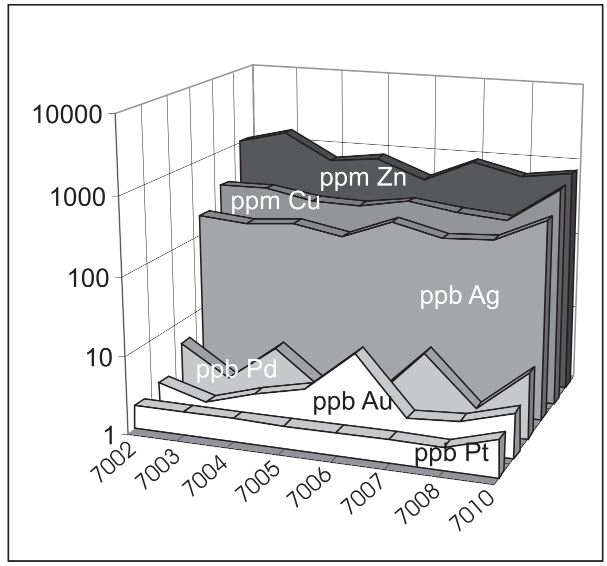

Figure 5. Geochemistry of tree bark samples from the Sappho property.

Samples 55939 and 55940 (Table 5) are from the area around the NE showing area. Sample 55939 is from till in a trench about 30 m south (down-ice and upslope) of the showing whereas sample 55940 is from colluvium about 10 m downhill of the showing. The till is similar to the lowest diamicton unit in the trench described above. It was sampled at a depth of 1.5 m below surface and is overlain by up to 50 cm of pebbly sand. The colluvium is a silty, loose to moderately dense, matrix-supported diamicton with gravelly lenses. Clasts are mostly subangular to angular, medium to large pebbles and cobbles. The diamicton shows crude, slope-parallel stratification and locally contains up to 50% clasts. It was sampled at a depth of 2 m from surface and is overlain by up to 1 m of anthropogenic fill.

Interestingly, concentrations of most elements, including copper, nickel, platinum and palladium (341 ppm, 267 ppm, 15 ppb and 27 ppb, respectively) are much higher in the till down-ice (and up-slope) of the showing than in the colluvium directly down-slope of the showing (189 ppm, 138 ppm, 10 ppb and 10 ppb, respectively). Concentrations

TABLE 5
TILL SAMPLE DATA FOR THE -230 MESH FRACTION OF SAMPLES FROM THE SAPPHO PROPERTY (SAMPLES 55936-38 FROM SOUTH END OF PROPERTY; SAMPLES 55939-40 FROM NE SHOWING AREA

Element	Depth	Au	As	Cu	Co	Cr	Fe	Ni	Pb	Zn	Pt	Pd
Units	m	ppb	ppm	ppm	ppm	ppm	%	ppm	ppm	ppm	ppb	ppb
55936	2.50	37.8	7.2	136.6	20.6	149.6	3.4	93.1	9.6	51.3	3.5	6.5
55937	0.70	11.6	6.6	76.2	19.9	138.5	3.3	89.3	10.5	58.5	3.1	2.1
55938	0.25	2.0	7.5	54.1	15.5	87.2	2.5	65.4	9.0	54.9	1.6	-0.5
55939	1.50	13.1	11.2	341.4	35.1	236.4	5.5	267.2	18.3	80.7	15.4	27.1
55940	2.00	52.7	14.9	189.0	27.8	189.5	4.9	138.4	26.6	68.0	10.5	10.3

of iron, zinc, cobalt and chromium are also higher in the till whereas gold, arsenic and lead are lower in the till. In addition, all element concentrations except zinc are higher in the till than they are in shallow soil samples directly over the main showing (compare Tables 1 and 5). A higher concentration of metals in till than in colluvium is unusual as tills typically reflect a much larger source area and therefore tend to have diluted metal concentrations. Relatively low levels of elements in the colluvium suggests that either the sampled material was not derived from the area of the showing or colluvial processes such as those discussed above have resulted in a significant decrease in metal concentrations in the colluvium in comparison to the original source rocks. The latter interpretation is preferred as the sample site is located directly down-slope from the mineralized zone and almost certainly is derived from it. This interpretation may also explain why elements such as gold and lead are not affected in the same way as most other elements, as variability in the colluvial processes would be expected. Although these results are limited, they suggest that tills in this area may yield higher anomaly contrasts than colluvial materials. The data also support the above conclusion that C-horizon sampling is a better approach for exploration on the property than B-horizon soil sampling.

ROCK GEOCHEMISTRY

The chemistry of sulphide-rich rock samples from the Sappho property is shown in Table 6. Elevated cadmium, cobalt, mercury, lanthanum, antimony and selenium are associated with the high copper, gold, platinum and palladium in the sulphides and can be considered as pathfinders for PGE-rich sulphides.

TABLE 6
GEOCHEMISTRY OF ROCK SAMPLES FROM THE SAPPHO PROPERTY

Sample	Units	56333	56334	56335	56336	Median
Ag-MS	ppm	56	>100	>100	>100	>100
As-MS	ppm	33.2	38.5	10.7	9.3	21.9
Au-FA	ppb	189	609	2263	1876	1243
Au-MS	ppb	156	612	1881	1609	1110
Bi-MS	ppm	1.3	2.4	1.2	1.2	1.3
Cd-MS	ppm	24.6	12.7	26.2	25.4	25
Co-MS	ppm	412	337	102	99	220
Cu-MS	ppm	69175	86734	>100000	>100000	93367
Fe-MS	%	14.56	19.72	25.35	27.09	22.54
Hg-MS	ppb	102	252	326	360	289
La-MS	ppm	140.4	193.7	57.8	49.9	99.1
Mn-MS	ppm	1967	1347	402	299	875
Ni-MS	ppm	162	255	121	102	142
Pd-FA	ppb	729	1226	934	454	834
Pd-MS	ppb	273	1455	986	528	757
Pt-FA	ppb	567	981	2018	3099	1499
Pt-MS	ppb	409	624	424	526	475
Re-MS	ppb	2	<1	2	1	2
Rh-FA	ppb	1.2	1.9	2.9	2.1	2
Sb-MS	ppm	2.4	3	4.5	5.3	3.8
Se-MS	ppm	60.1	85.1	142.8	162.4	114
S-MS	%	6.74	8.78	4.53	5.02	5.88
Zn-MS	ppm	1628	1089	1802	1729	1678

DEVELOPMENT OF A PROVISIONAL GEM FOR PGE MINERALIZATION IN SOUTHERN B.C.

Because exploration for PGE mineralization is currently important, and because there is very little published data for the application of geochemistry for PGE's, a provisional GEM has been developed on limited data. Regional geochemical survey (RGS), assessment file data and the results of an orientation geochemical survey are integrated to illustrate the development of a GEM for massive sulphide bearing platinum-palladium mineralization (Figure 2) in southern B.C. To date data are only available for one PGE occurrence, the Sappho property, and so the GEM must be regarded as provisional. When data are available for other occurrences this GEM can be updated. In Figure 6 three dimensional stacked block diagrams show the relationship between bedrock geology, surficial geology, soils and topography on a GEM for the Sappho property. Mineral deposits can have a distinct multi-element signature that may, to a varying degree, be reflected in the geochemistry of the overlying glacial sediments, soil, vegetation, and water and stream sediment. A copper-silver- gold-nickel-arsenic- platinum-palladium-selenium-lanthanum signature is shown on the bedrock geochemistry layer in Figure 6 because these elements are enhanced in the sulphides at the Main showing.

Glacial dispersal trains (DiLabio, 1990) in till are displayed on the surficial geochemistry layer in Figure 6. In the Cordillera, dispersal trains are typically a few to several km long and elongated parallel to ice-flow (Levson, 2001a). In some parts of southern British Columbia the Quaternary stratigraphy is complex and includes glacial and non-glacial deposits (Fulton and Smith, 1978; Ryder *et al.*, 1991). For this reason the GEM applies to regions where the surficial geology comprises sediments from the last glacial event. The relative magnitude and size of platinum-palladium-copper-nickel C- horizon soil anomalies are represented by shaded vertical patterns on the surficial geochemistry layer. One anomaly reflects a short dispersal down-ice (south) of the Main zone. The second anomaly, partly in colluviated till, may be a part of this dispersal train that has been displaced a greater distance down-ice and incorporated in colluvium on the north-facing hill slope. This anomaly could also be a completely separate dispersal train from a different bedrock source. Additional sampling is needed to determine which interpretation is correct. B-horizon anomalies shown on the sediment-soil layer are of similar strength but generally lower than those in the C soil horizon. A nickel-copper stream-moss sediment anomaly is also shown on the sediment soil layer although values only just exceed regional thresholds (Table 2). Low platinum, palladium and gold values in the sediment could re-

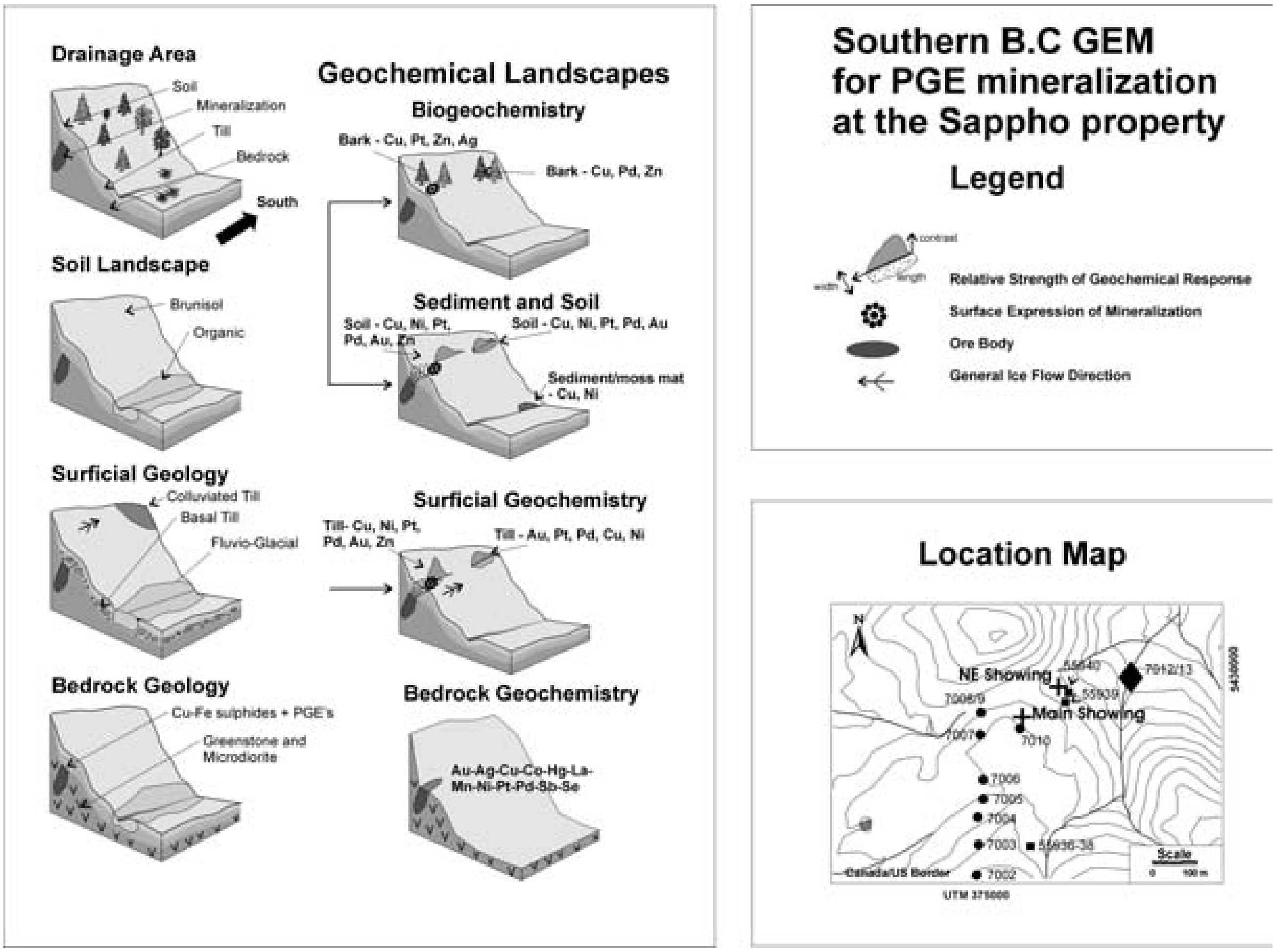

Figure 6. Provisional GEM for PGE mineralization in southern B.C.

flect the limited occurrence of mineralised bedrock or till in the drainage basin. Two patterns are shown on the biogeochemical layer. A strong platinum-copper-silver bark anomaly with additional pathfinders is associated with the Main showing whereas a weaker copper-zinc-palladium signature is associated with the B and C soil anomaly to the south.

CONCLUSIONS

A geochemical exploration model (GEM) for the Sappho property shows that:

- Elevated platinum, palladium, gold, nickel and copper levels in bedrock sulphide mineralization can be detected by B and C-soil horizon sampling but higher values typically occur in the C-horizon.
- Elevated platinum, palladium, copper, silver and zinc levels can be detected by Douglas-fir bark sampling.
- Concentrations of gold, platinum and palladium and most other metals in till increase with depth due to gravity sorting and water washing of the near surface layers and the probable addition of aeolian sediment.
- Basal till down-ice of sulphide mineralization locally yields higher metal values than does down-slope colluvium.
- Soil, till and tree bark anomalies in the southern part of the Sappho property could reflect a second source of bedrock mineralization that has not been discovered.
- Low platinum, palladium, gold, nickel and copper in stream and moss mat sediments can be explained by limited erosion of mineralised bedrock or till into the stream.

Table 7. is a summary of element associations and anomaly characteristics for the Sappho property based on survey results and the relationships summarized by the GEM. While these geochemical associations and anomaly dimensions can be extended to exploration for sulphide-bearing PGE deposits in other areas, any new GEM must be supported by additional field data.

TABLE 7
SUMMARY OF ELEMENT ASSOCIATIONS AND ANOMALY CHARACTERISTICS FOR THE SAPPHO PROPERTY

Mineralization	Media	Pathfinders	Anomaly Size	Remarks
Pyrite-chalcopyrite with high levels of Au, Cd, Co, Cu, Hg, La, Sb, Se, Pt, Pd.	B and C-soil horizon	Cu, Ni, Pt, Pd, Au, (La)	B-horizon soil anomaly (>90 ppm) is 150 m x 200 m over sulphide mineralization. Anomalies are stronger in the C-soil horizon.	Little advantage of using -230 mesh fraction compared to -80 mesh fraction. Colluvial and aeolian effects present at surface.
	Basal till	Au, Pd, Pt, Cu, Ni	No indication on length of dispersal train, but probably >1 km.	Ice flow from north to south. Anomalies stronger with depth.
	Stream sediment		Weak expression in sediment and moss mat may reflect limited occurrence of mineralized source	No advantage to using moss mat compared to stream sediment
	Vegetation	Ag, Pt, Pd, Cu, Zn	Tree bark anomalies are associated with B and C soil anomalies	Extreme differences in tree maturity can introduce spurious variations in element patterns.

ACKNOWLEDGMENTS

The authors would like to thank Gold City Industries Ltd., Vancouver, for funding the tree bark analysis, and granting permission to carry out an orientation survey over the Sappho property. Assistance during the fieldwork by Alan Raven, David Mate and Gwendy Hall is very much appreciated.

REFERENCES

Bradshaw, P.M.D. (1975): Conceptual Models in Exploration Geochemistry, The Canadian Cordillera and Canadian Shield, *Journal of Geochemical Exploration*, Part 4, No 1, pages 1- 270.

Butt, C.R.M and Smith, R.E. (1980): Conceptual models in Exploration Geochemistry –Australia, Journal of Geochemical Exploration, Part 12, pages 89-367.

DiLabio, R.N. (1990): Glacial dispersal trains: *in* Glacial Indicator tracing, Kujansuu, R and Saarnisto, M. (Eds), *A.A.Balkema*, Rotterdam, pages 109-122.

Fulton, R.J. and Smith, G.E. (1978): Late Pleistocene stratigraphy of South-Central British Columbia; *Canadian Journal of Earth Sciences*, Volume 15, pages 971-980.

Kauranne, L.K. (1976): Conceptual models in Exploration Geochemistry – Norden, 1975; *Journal of Geochemical Exploration*, Part 5, pages 175-420.

Keating, J. and Fyles, J.T. (1984): Geological and geochemical survey on the Sappho 83 group of claims; *BC Ministry of Energy and Mines*, Assessment report.

Levson, V.M. (2001a): Regional Till Geochemical Surveys in the Canadian Cordillera: Sample Media, Methods and Anomaly Evaluation; *in* Drift Exploration in Glaciated Terrain, *Geological Society of London*, Special Publication 185, pages 45-68.

Levson, V.M. (2001b): Quaternary Geology of the Babine Porphyry Copper District: Implications for Geochemical Exploration. *Canadian Journal of Earth Sciences*, Volume 38, pages 733-749.

Lovering, T.G. and McCarthy, J.H. (1978): Conceptual models in Exploration Geochemistry – The Basin and Range Province of the Western United States and Northern Mexico. *Journal of Geochemical Exploration*, Part 9, pages 113-276.

Matysek, P.F., Jackaman, W., Gravel, J.L., Sibbick, S.J. and Feulgen, S. (1991): British Columbia Regional Geochemical Survey - Penticton (NTS 82E), *BC RGS 29/GSC* Open File 2354.

Nixon, G.T. (2002): Cu-PGE mineralization hosted by Alkalic Intrusive complexes, Sappho, south central B.C.; *in* Fieldwork 2001, *BC Ministry of Energy and Mines,* Open File 2002.

Ryder, J.M., Fulton, R.J. and Clague, J.J. (1991): The Cordilleran Ice Sheet and the Glacial Geomorphology of Southern and Central British Columbia; *Géographie physique et Quaternaire*, Volume 45, pages 365-377.

Quaternary Geology Reconnaissance Studies 92I/2 and 7

By Peter Bobrowsky, Mike Cathro and Roger Paulen

KEYWORDS: *Till geochemistry, surficial geology, Quaternary geology, ice-flow history, Fox claim, Highland Valley Copper, exploration potential, geology, Merritt, Logan Lake, British Columbia.*

INTRODUCTION

During the summer of 2001, the British Columbia Geological Survey Branch undertook a 6-day reconnaissance excursion to the Merritt-Logan Lake area of southern British Columbia to evaluate the potential for future regional till geochemistry exploration projects (Figure 1). Exploration potential in the area is very attractive, given that this region is already known to host several different types of mineralization including stratiform-base-metal, porphyry and vein targets. The record for previous mining activity in this area includes the prominent Highland Valley Copper and Craigmont mines. More recently, the discovery of a high-grade copper-zinc massive sulphide showing on the Fox claims has triggered a minor staking rush in the region. Within a one-year period nearly 1450 claim units had been staked in the vicinity of the Fox claims. Interesting prospects in the proposed study include the LD barite-gold-silver-zinc-lead-copper prospect at Iron Mountain and the Iron King iron prospect south of Nicola Lake.

The Quaternary geology of the region has been subject to periodic attention for the last four decades, primarily during the process of 1:250,000 scale mapping by the Geological Survey of Canada. Unfortunately, much of the surficial geology work is only relevant at the regional scale and provides minimal insight at a more detailed 1:50,000 scale for the exploration community. Given the recent economic attraction of this area of the province and the lack of detailed surficial data that is of direct importance to the exploration community, a reconnaissance surficial study was clearly warranted. The objectives of the present study were to:

- assess the nature and extent of surficial sediments covering an area corresponding to two 1:50,000 map sheets comprising NTS 92I/02 and 92I/07;
- evaluate the potential to undertake a regional till geochemistry survey;
- establish the regional ice-flow pattern of the study area; and
- identify and recognize sites which should be investigated in detail to help resolve the stratigraphic and glacial history for the region.

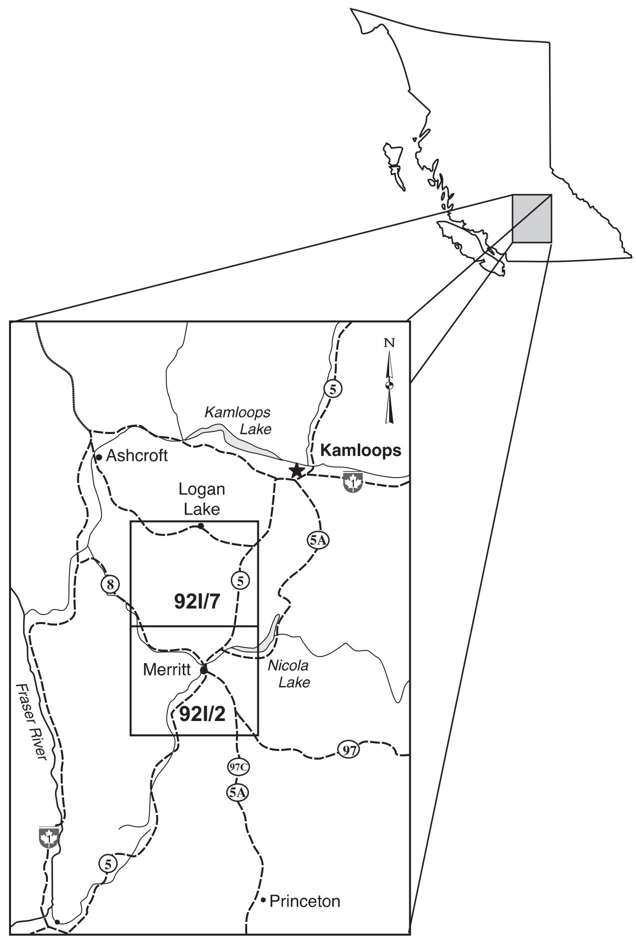

Figure 1. Location map of Quaternary reconnaissance study in the Merritt-Logan Lake area, B.C. (NTS 92 I/2 and 92 I/7).

PREVIOUS WORK

With the exception of work by early geologic explorers working in the Interior Plateau of southern British Columbia, it is the notable mineral deposits in the northwest part of this study (*e.g.* Bethlehem, Highmont, Valley Copper, etc.) that have significantly influenced ongoing geological and mineral exploration study. Previous bedrock geology of the Highland Valley deposit and surrounding area has been detailed in several publications and are well-reviewed by Sutherland Brown (1976) with more recent work by Monger and McMillan (1989) and Moore *et al*. (1990). The surficial geology work is perhaps less well known but equally important. Significant work by R.J. Fulton (Geological Survey of Canada) during the 1960s and 1970s has allowed a good understanding of the region to be developed. Based on his work (Fulton, 1965, 1968, 1969, 1975a, 1975b, 1984; Fulton and Smith, 1978), the Quaternary stratigraphy for this region can be summarized as follows: the oldest deposits consist of Okanagan Centre Drift sediments (type locality near Okanagan Lake) which are Early Wisconsinan in age (>65 000 years old), overlain by Bessette Sediments (type locality near Lumby) of mid-Wisconsinan age (>20 000 - 65 000 years old), which in turn are overlain by Kamloops Lake Drift deposits (type locality near Kamloops Lake) correlative with the Late Wisconsinan (10 000 to 20 000 years old). Even more interesting are much older sediments that have been discovered by Fulton *et al*. (1992) near Merritt, and that are thought to be >790 000 years old based on reversed magnetic polarity (Matuyama age).

The Quaternary stratigraphy of the Merritt area remains the most detailed and comprehensive for the region and should, theoretically be applicable to the full study region. As summarized in Table 1, the oldest deposits consist of the Coldwater silts that are overlain by Sub-Coutlee sediments and Coutlee sediments. These three sediment packages are all known to be in excess of 790 000 years in age and are, in turn, overlain by Valley Basalts and Brown Drift deposits, covering the period from mid-Wisconsinan to the Matuyama reversal. The youngest deposits consist of Kamloops Lake Drift (proglacial sediments, till and postglacial lake sediments).

Perhaps the greatest attention has been paid to the history of deglaciation of the southern Interior Plateau and surficial deposits associated with this event (Fulton, 1967, 1969, 1991; Church and Ryder, 1972; Ryder 1971). The present day physiography, characterized by rolling uplands, steep-walled, flat-floored valleys, as well as open grassland and pine-forested slopes, is strongly influenced by the style of deglaciation. Most of the major valleys and tributaries in the region supported large ice-dammed lakes as ice retreated northward at the end of the Pleistocene (Ryder *et al*., 1991). Such glaciolacustrine deposits typically consist of rhythmically bedded sand and silt, are of varying thickness and pose considerable hazard to transportation corridors and structures given their tendency to fail (Evans and Buchanan, 1976). From an exploration perspective, glaciolacustrine sediments are a hindrance insofar as they effectively conceal mineral deposits, and are of limited use for geochemical studies. Fortunately, only small parts of the study region comprise valley scenarios and thus much of the area is not affected by such sediments.

Other important fundamental and applied Quaternary research in the region includes that of Bobrowsky *et al*. (1993), Kerr *et al*. (1993), Mathews (1944), Ryder (1976, 1979) and Westgate *et al*. (1975).

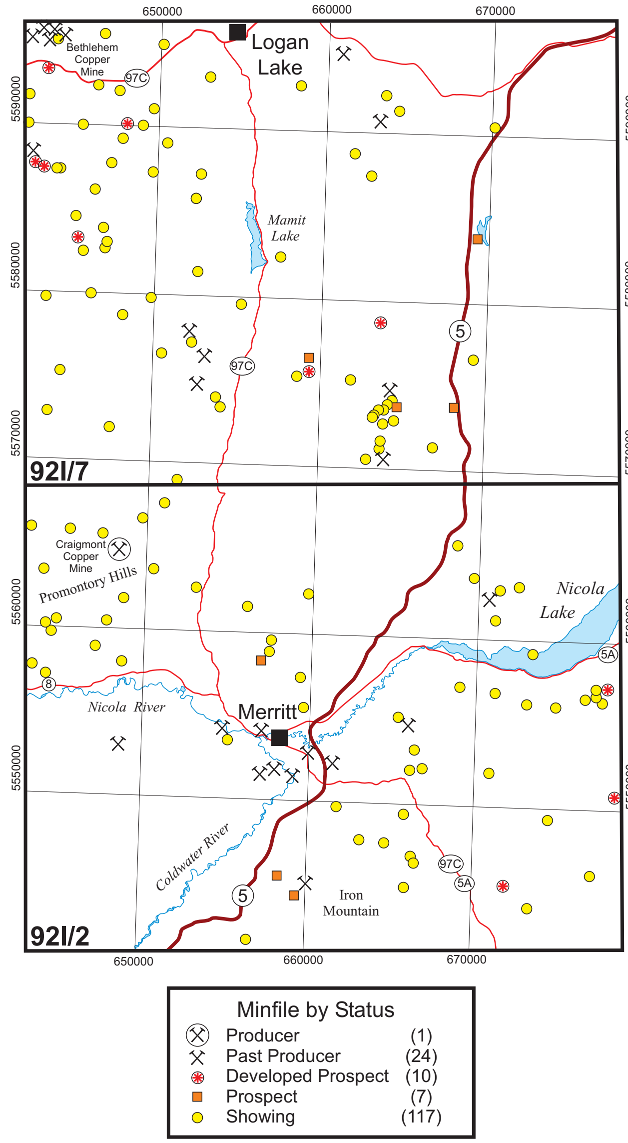

Figure 2. MINFILE occurrence by status in NTS 92I/2 and I/7.

BEDROCK GEOLOGY

The study area (Figure 1) lies within the Intermontane Belt and is part of the Quesnel Terrane. It is primarily underlain by Late Triassic, alkaline to calc-alkaline, predominantly mafic to intermediate but locally felsic, submarine and subaerial volcanic rocks and volcanic-derived sedimentary rocks of the Nicola Group (Preto, 1979). This arc-volcanic package is intruded by large diorite to granite plutons ranging in age from Triassic-Jurassic to early Tertiary (Monger and McMillan, 1989; Moore *et al*., 1990). The largest of these is the Late Triassic to Early Jurassic multiphase Guichon Creek batholith located in the western part of the study.

Clastic and volcanic rocks of Jurassic to Tertiary age (Ashcroft Formation, Spences Bridge Group and Princeton

TABLE 1
QUATERNARY STRATIGRAPHIC UNITS IN THE VICINITY OF MERRITT, BRITISH COLUMBIA

Unit Name	Locality	Interpretation	Age
Merritt silts (Kamloops Lake Drift)	Merritt Lily Lake Road Coldwater	Glacial lake sediments	+/- 11 ka
Till (Kamloops Lake Drift)	Lily Lake Road Coldwater	Glacial deposit	11-20 ka
Proglacial Sediments (Kamloops Lake Drift)	Lily Lake Road	Proglacial deposits	+/- 20-25 ka
Brown Drift	Coldwater River	Glacial deposits	>25 to <790 ka
Valley basalts	Chutter Ranch Quilchena Crk Valley	Volcanic eruption	100 to <790 ka
Coutlee sediments	Lily Lake Road	Interglacial basin fill deposits	>790 ka
Sub-Coutlee sediments	Lily Lake Road	Glacial lake deposits	>790 ka
Coldwater silts	Coldwater	Glacial lake deposits	>790 ka

According to Fulton et al. (1992)
Age is given in thousands of years before present (ka)

Group) unconformably overlie the Nicola Group in local areas. The eastern part of the study area is dominated by the Nicola horst, a fault bounded uplift which comprises metamorphosed Nicola rocks and highly deformed, sedimentary rocks intruded by Triassic, Jurassic and Paleocene plutons (Moore *et al*., 1990). Structurally, there are two predominant fault sets in the area; a northwest striking set of probable Mesozoic age, and a north to northeast striking set of mainly extensional faults of Tertiary age (Moore *et al*., 1990).

The most economically important mineral deposits in the region are the large, calc-alkaline type, porphyry copper-molybdenum-gold-silver deposits hosted by the Guichon Creek Batholith (*e.g.* Highmont, Lornex, Valley, and Bethlehem mines). The study area also includes the past producing Craigmont mine, a large copper skarn in Nicola rocks, and coal mines in Tertiary rocks of the Merritt basin (Figure 2). Throughout its length, the Triassic-Jurassic volcanic and intrusive rocks of the Quesnel terrane host important alkaline-porphyry copper-gold deposits such as Afton mine near Kamloops, and numerous small skarn, vein and stockwork-type base and precious metal occurrences. The recent discovery of the Fox zinc-copper- gold-silver-barite prospect north of Merritt has prompted prospecting for stratiform volcanogenic deposits, particularly in the western volcanic facies of the Nicola Group.

RESULTS

A variety of sediment types were observed within the study area at several sites (Figure 3) including colluvium, glaciolacustrine, lacustrine, fluvial, glaciofluvial, and numerous till facies. Unequivocally, the dominant material encountered throughout the area is basal till. In this case the basal till is characteristically a well-consolidated, massive,

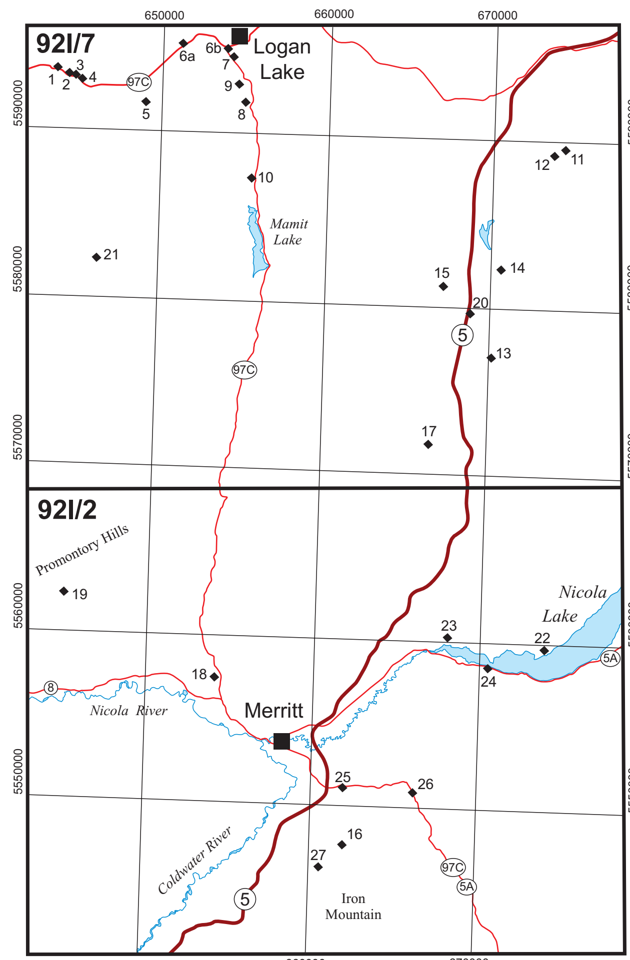

Figure 3. Map showing location of new Quaternary observation points where stratigraphic or ice-flow data were detailed during 2001 reconnaissance study.

moderately stony matrix supported diamicton. Deposits range in thickness from less than a metre to tens of metres, but typically appear to be about 2-5 metres thick. Clast content varies from 5% to 35%, and the majority of stones appear to be subangular in shape. Facets and striae are commonly observed on some of the recovered pebbles. Lithologies reflect the surrounding bedrock geology confirming local provenance sources for the entrained debris.

Bedrock is exposed in small patches throughout the study, thus facilitating an evaluation of the paleo-ice-flow history for the full region. A few dozen locations yielded good evidence for ice flow in the form of striations, rat-tails, grooves, and roche moutonées. Based on the observations conducted in this study it is clear that during the last glaciation ice flowed primarily from the north to the south (Figure 4). Only near the southern margin of the study is there evidence for partial deflection of past ice flow.

Little data are currently available for evaluation regarding the patterns of geochemical distribution in the region. One example of geochemical soil sampling does exist, and is illustrated here to confirm the expected pattern of element dispersion towards the south (Figure 5).

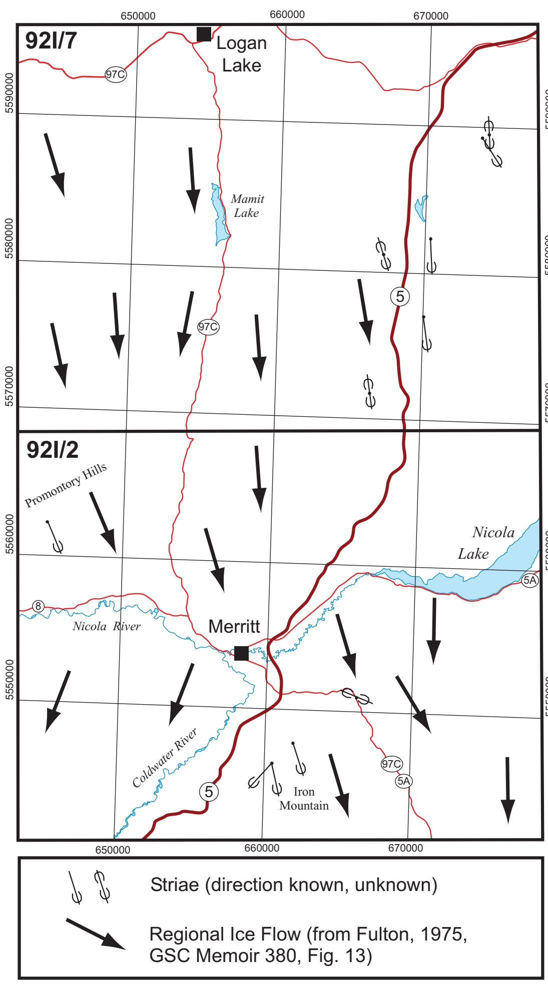

Figure 4. Ice-flow pattern for the study area combining air photographic interpretation by R.J. Fulton and ground based striation evidence from the present study.

CONCLUSIONS

Successful long-term historic mining activity and recently discovered exploration targets suggest that this region contains a high potential mineral exploration framework. From a Quaternary perspective, the predominance of basal till in the area, the relatively thin nature of the surficial overburden cover and the uniform ice-flow direction over the study area all combine to provide an ideal sampling environment for a regional till geochemistry exploration project. During the past few decades expanding ranchland and logging activities have opened previously poorly accessible areas between Merritt and Logan Lake to geological exploration. The improved access, good mineral potential and ideal surficial nature of the region collectively indicate that a reconnaissance level till geochemistry sampling project in NTS 92I/2 and 92I/7 is both feasible and warranted.

ACKNOWLEDGMENTS

The authors appreciate the comments of Nick Massey and Gib McArthur on an earlier version of the manuscript. Janet Holland is thanked for her patience as well as final layout and publication efforts.

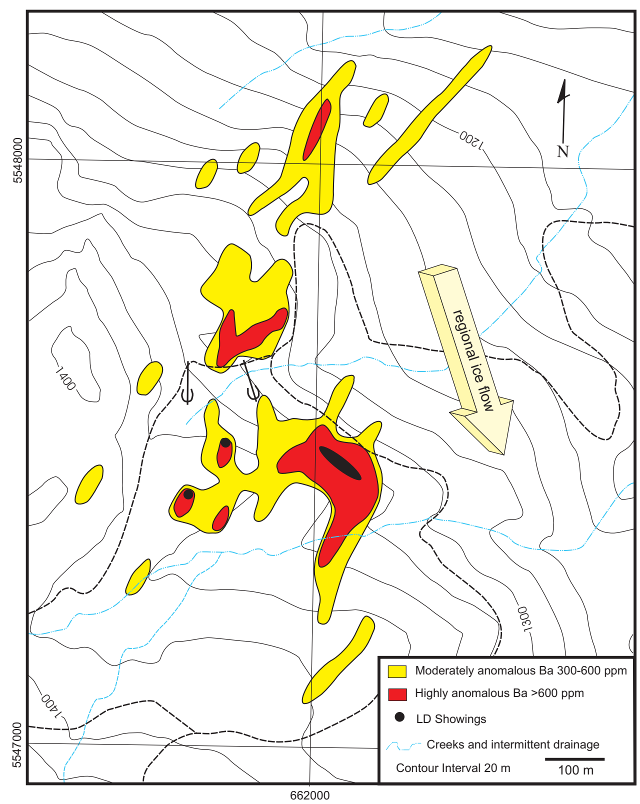

Figure 5. Map showing normalized contour distribution of Ba in soils near the LD showings on the east slope of Iron Mountain. Regional ice flow pattern by GSC compared to site specific detailed ice-flow pattern established at the property scale. Note down ice plume of dispersion of Ba in the sediments.

REFERENCES

Bobrowsky, P.T., Kerr, D.E., Sibbick, S.J. and Newman, K. (1993) Drift Exploration studies, Valley Copper Pit, Highland Valley Copper Mine, British Columbia: stratigraphy and sedimentology (92I/6, 7, 10, and 11); *in* Geological Fieldwork 1992, B. Grant and J.M. Newell (Eds.), *B.C. Ministry of Energy, Mines and Petroleum Resources*, Paper 1993-1, pages 427-437.

Church, M. and Ryder, J. (1972) Paraglacial sedimentation: a consideration of fluvial processes conditioned by glaciation. *Geological Society of America Bulletin*, volume 83, pages 3059-3072.

Evans, S.G and Buchanan, R.G (1976) Some aspects of natural slope stability in silt deposits near Kamloops, British Columbia; *in* Proceedings, 29th Canadian Geotechnical Conference, Session 4, pages 1-32.

Fulton, R.J. (1965) Silt deposition in late-glacial lakes of southern British Columbia. *American Journal of Science*, volume 263, pages 553-570.

Fulton, R.J. (1967) Deglaciation studies in Kamloops Region, an area of moderate relief, British Columbia. *Geological Survey of Canada*, Bulletin 154.

Fulton, R.J. (1968) Olympia Interglaciation, Purcell Trench, British Columbia. Geological *Society of America Bulletin*, volume 79, pages 1075-1080.

Fulton, R.J. (1969) Glacial Lake History, Southern Interior Plateau, British Columbia. *Geological Survey of Canada*, Paper 69-37, 14 pages.

Fulton, R.J. (1975a) Quaternary Geology and Geomorphology, Nicola-Vernon area, British Columbia. *Geological Survey of Canada*, Memoir 380.

Fulton, R.J. (1975b) Quaternary weathering of bedrock, south-central British Columbia. *Geological Survey of Canada*, Paper 1975-1C, pages 91-93.

Fulton, R.J. (1984) Quaternary glaciation, Canadian Cordillera. In: Quaternary Stratigraphy of Canada, a Canadian contribution to IGCP Project 24, R.J. Fulton (Ed.), *Geological Survey of Canada*, Paper 84-10, pages 39-48.

Fulton, R.J. (1991) A conceptual model for growth and decay of the Cordilleran Ice sheet. *Geographie et Physique et Quaternaire*, volume 45, number 3, pages 281-286.

Fulton, R.J. and Smith, G.W. (1978) Late Pleistocene stratigraphy of south-central British Columbia. *Canadian Journal of Earth Sciences*, volume 15, pages 971-980.

Fulton, R.J., Irving, E. and Wheadon, P.N. (1992) Stratigraphy and paleomagnetism of Bruhnes and Matuyama (>750ka) Quaternary deposits at Merritt, British Columbia; *Canadian Journal of Earth Sciences*, volume 29, pages 76-92.

Kerr, D.E., Sibbick, S.J. and Belik, G.D. (1993) Preliminary results of glacial dispersion studies on the Galaxy Property, Kamloops, B.C. (92I/9); *in* Geological Fieldwork 1992, *B.C. Ministry of Energy and Mines*, Paper 1993-1, pages 439-443.

Mathews, W.H. (1944) Glacial lakes and ice retreat in south-central British Columbia; *Royal Society of Canada*, Transactions, Ser. 3, volume 38, pages 39-57.

Monger, J.W.H, and W.J. McMillan (1989) Geology, Ashcroft, British Columbia; *Geological Survey of Canada*, Map 42-1989, Sheet 1, scale 1:250,000.

Moore, J.M., Pettipas, A., Meyers, R.E., and Hubner, T.B. (1990); Nicola Lake Region Geology and Mineral Deposits; *B.C. Ministry of Energy, Mines and Petroleum Resources*, Open File 1990-29, 30 pages.

Preto, V.A. (1979): Geology of the Nicola Group between Merritt and Princeton; *B.C. Ministry of Energy, Mines and Petroleum Resources*, Bulletin 69, 90 pages.

Ryder, J.M. (1971) The stratigraphy and morphology of paraglacial alluvial fans in south-central British Columbia. *Canadian Journal of Earth Sciences*, volume 8, pages 279-298.

Ryder, J.M. (1976) Terrain inventory and Quaternary geology of Ashcroft, British Columbia. *Geological Survey of Canada*, Paper 74-49.

Ryder, J.M. (1979) Terrain inventory and Quaternary geology, Lytton, British Columbia. *Geological Survey of Canada*, Paper 79-25.

Sutherland Brown, A. (1976) Porphyry deposits of the Canadian Cordillera. *Canadian Institute of Mining and Metallurgy*, Special Volume15, 510 pages.

Westgate, J.A. and Fulton, R.J. (1975) Tephrostratigraphy of Olympia Interglacial sediments in south-central British Columbia, Canada. *Canadian Journal of Earth Sciences*, volume 12, pages 489-502.

Sunshine Coast Aggregate Potential Mapping Project

By Ahren J. Bichler, Elizabeth D. Brooks and Peter T. Bobrowsky

KEYWORDS: *Aggregate, aggregate potential mapping, sand and gravel, Sechelt, Powell River, Gibsons, Sunshine Coast, resources, inventory, database.*

INTRODUCTION

The Sunshine Coast has long been a major producer of aggregate products that are readily consumed by the expanding markets of southwestern British Columbia and those south of the border. As part of an ongoing initiative of resource inventory, the Geological Survey Branch of the Ministry of Energy and Mines has undertaken an aggregate potential mapping project along the Sunshine Coast during the 2001 field season. The project's goals follow those of earlier studies conducted by the Branch such as the Prince George (Bobrowsky *et al.*, 1996a), Okanagan (Bobrowsky *et al.*, 1998), Nanaimo (Massey *et al.*, 1998), and Sea-to-Sky (Dixon-Warren *et al.*, 2000; Hickin *et al.*, 2001) projects (Figure 1). Funding and support is provided by the Corporate Resource Inventory Initiative (CRII) with additional logistical support from a variety of organizations including British Columbia Assets and Lands Corporation (BCAL), Ministry of Transportation (MOT), and the Land Use Coordination Office (LUCO) of the Ministry of Sustainable Resource Management.

The desirable outcome of the project is a regional, reconnaissance style survey that will act as a first approximation of aggregate resources within the region. The project will outline exploited and known aggregate resources as well as potential new deposits, in a qualitative manner using distinct landforms.

The basis of the Sunshine Coast Aggregate Potential Mapping Project comes from four major objectives:

1. Compile existing and readily available geological and geotechnical information pertaining to the study area;
2. Examine and record characteristics of known and exploited aggregate deposits;
3. Generate a complete coverage of Level III Aggregate Potential Maps for the study area at a scale of 1:50,000; and
4. Compile all data collected and generated into an interactive geographical information system (GIS) that will be released to government agencies, industry and to the general public.

The purpose of this paper is to describe the methods and progress of this project, provide a summary of the results to date, and to outline the anticipated data that will be released early in 2002.

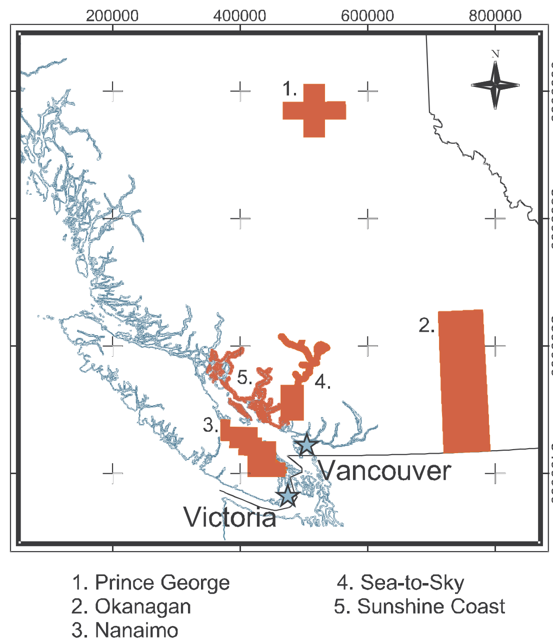

Figure 1. The five aggregate potential mapping projects conducted by the Geological Survey Branch during the past six years. Projects are numbered in accordance to the order in which they were conducted.

STUDY AREA

The study area is located in southwestern British Columbia, northwest of Vancouver (Figure 1), and lies entirely within the Sunshine Coast Forest District. The major communities within the study area are Gibsons, Sechelt and Powell River. It is concentrated along the coastline, stretching from Gibsons as far north as the head of Bute Inlet (Figure 2), with the coastline and a variable buffer extending landward, defining the boundaries of the study area. For the most part this buffer is 3 kilometres wide with exceptions being: between Malaspina Peninsula and Saltery Bay where a 5-kilometre buffer is used; all of Sechelt Peninsula; and Gambier, Texada, Nelson, Read, Cortes and West Redonda islands, which are included in their entirety. Subtracted from the total area are ecological reserves, parks and other protected areas that are greater than 500 hectares. This yields a total study area of approximately 310,000 hectares in portions of NTS map sheets 92F/8-10, 92F/15-16, 92G/5-6, 92G/11-13, 92J/4, 92K1-3 and 92K/6-9.

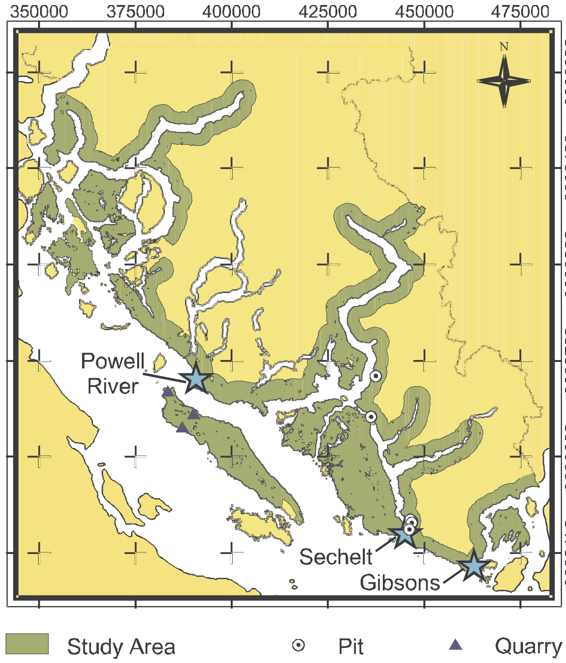

Figure 2. Location of the Sunshine Coast study area and the major aggregate producers and quarries in the region. Natural aggregate pits are indicated by light circles and quarries by dark triangles.

PHYSIOGRAPHY, CLIMATE AND VEGETATION

The Sunshine Coast falls within the Coastal Trough and the Coast Mountains physiographic regions (Holland, 1976). The Coastal Trough is a northwest-southeast structure that lies between the Coast Mountains to the east and the Insular Mountains to the west, stretching the entire length of British Columbia. The Coastal Mountains are an unbroken chain of rugged mountains that, as well, run the length of British Columbia. The study area is contained within a subdivision of the Coastal Trough known as the Georgia Depression, more specifically the Georgia Lowland, with parts of the study area found on the lower slopes of the Coastal Mountains. Adjacent to the study area is the Fraser Lowland, a subdivision of the Georgia Lowland that encloses Greater Vancouver. Except for the Fraser Lowland whose geomorphology is largely due to depositional processes, the Georgia Lowlands are characterized by an undulating Tertiary erosional surface that ascends gently from the Strait of Georgia towards the Coastal Mountains to a maximum elevation of approximately 1300 m asl (Holland, 1976). A relatively thin mantle of sediment covers it, as bedrock outcropping is very frequent.

The study area falls almost entirely within the Coastal Western Hemlock biogeoclimatic zone (Meidinger and Pojar, 1991). This region experiences relatively cool summers and mild winters, having an annual precipitation ranging from 1000 mm to 4400 mm of which, less than 15% occurs as snowfall. The most common tree is the western hemlock but other species such as the western red cedar, douglas fir, amabilis fir, yellow-cedar, lodgepole pine, red alder, black cottonwood and stika spruce are also encountered frequently.

PREVIOUS WORK

Aggregate resources along the Sunshine Coast have been the subjects of numerous studies. The earliest of these studies was that undertaken by Leaming (1968) who from 1961-1962 reviewed sand and gravel resources within the Strait of Georgia area. The resultant report outlines the distribution of unconsolidated sediments on both sides of the Strait as well as up major valleys and reviews available aggregate reserves and presents descriptions of extraction sites. McCammon carried out a similar study from 1974-1975 along the Sunshine Coast (McCammon, 1975; McCammon, 1977). Though the stratigraphy and surficial geology data produced from these studies remains essentially unchanged, the reserve estimates and descriptions of extraction operations are dated. More recently, MOT conducted an investigation into potential aggregate resources within a corridor along a section of Highway 101 between Lund and Powell River (Buchanan and Bergman, 1993), representing a small portion of the current study area.

QUATERNARY HISTORY

Like most of British Columbia, the majority of the unconsolidated surficial deposits along the Sunshine Coast owe their existence to multiple episodes of glaciation and deglaciation that occurred during the Pleistocene. In particular, it is the most recent cycle of glaciation and deglaciation that has produced the current landscape, and left behind the aggregate deposits that are the subject of this paper.

A change in vegetation approximately 29 ka BP, a result of a deteriorating climate, provides evidence for the onset of the last glacial cycle, the Fraser Glaciation (Clague, 1994). Ice normally restricted to high alpine areas began to expand into and advance down low elevation valleys and fjords. These valley glaciers eventually grew sufficient enough to overtop the confining topography and coalesce into a massive ice sheet known as the Cordilleran Ice Sheet. Outwash sediments associated with these advancing ice fronts are known locally as the Quadra Sands and are found in abundance throughout the Strait of Georgia at elevations up to 100 m asl (Ryder and Clague, 1989). These sediments are characterized as being cross stratified, well-sorted, fine to coarse-grained glaciofluvial sands containing minor amounts of gravel and silt (Armstrong and Clague, 1977).

Sometime after 25 ka BP, glaciers had reached the Fraser Lowland through valleys entering from the north and east, only to retreat by 19 ka BP (Clague, 1994). Along the Strait of Georgia, an ice lobe spread south well past the Georgia and Fraser Lowlands, achieving its greatest extent by approximately 14.5 ka BP (Mullineaux *et al.*, 1965). As ice overrode the area, sediments collectively known as Vashon Drift were deposited either ice-proximally or in direct contact with ice. These sediments consist of a complex of silty sandy till and sandy and gravelly glaciofluvial and glaciolacustrine sediments (Hicock and Armstrong, 1985).

After 14 ka BP, the regional climate began to warm and ice retreat followed, with parts of the Strait of Georgia being ice-free by 13 ka BP (Clague, 1980). The most predominant sediments deposited in the Georgia Lowland during this time are the Capilano Sediments. These are retreat-phase glaciofluvial, glaciomarine and marine sediments deposited on the seafloor, and as raised deltas and intertidal and beach sediments (Armstrong, 1981). Capilano sediments can be found in the region up to an elevation of 180 m asl, indicating a relative sea level much higher than that of present day (McCammon, 1977).

Following deglaciation, fluvial and mass wasting processes redistributed glacial sediments during a period of readjustment (Ryder and Clague, 1989). Eventually the system evolved into the modern-day scheme, with gravel, sand and silt sediments being deposited in modern fluvial, beach and bog environments; these deposits are known as the Salish Sediments.

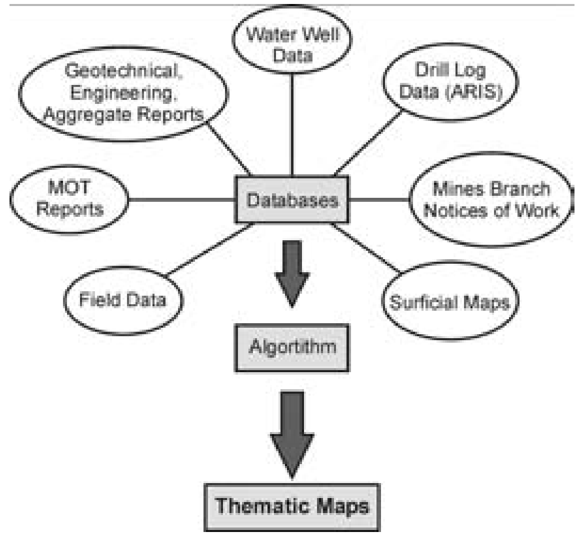

Figure 3. Flow chart depicting the process used for creating the thematic maps. Circles indicate sources of information while boxes represent products generated during the course of the project.

METHODOLOGY

For a number of years now, aggregate potential mapping projects have been implemented across Canada, using various methods (Bobrowsky *et al*., 1995). Within British Columbia, a system was developed based on the methodology established by the Alberta Geological Survey and is discussed in greater detail by Bobrowsky *et al*. (1996b) and Massey *et al.* (in press). This mapping system recognizes five levels of mapping intensity, and while the methods used at each of these levels is essentially the same, the resources that are utilized may vary. Of the five levels of mapping, Level III is favoured for applications of first approximation of aggregate potential within British Columbia (Bobrowsky *et al.*, 1996b).

Figure 3 is a flow chart summarizing the development of the final product for this project, the thematic maps, and the resources used to create it. The initial stage of the project involves the collection and compilation of data from many pre-existing sources into a series of linked databases. Geotechnical, engineering, and aggregate reports, surficial maps, water well data, drill log data, Mines Branch records (Notices of Work) and Ministry of Transportation records (public pits) are then queried for pertinent information such as: type of surficial material; thickness of overburden; aggregate content; and thickness, extent and quality of deposits. This type of information is not always readily available and may even be non-existent in areas.

Next, data collected in the field is added to the databases. The fieldwork component of the project involves visiting all active and inactive aggregate pits that fall within the study area boundaries, which includes commercial and public pits and quarries. The location of each of these mines is determined from previous aggregate studies, Notices of Work, Ministry of Transportation databases, a review of airphotos from the study area and terrain resource inventory management (TRIM) maps. At each field station a variety of observations are made, including:

- verification of mine location (GPS coordinates and elevation);
- type (pit, borrow or quarry);
- status (active, inactive, or reclaimed);
- dimensions of mine;
- surficial material, number of units present and their thickness;
- clast size, roundness, and lithology;
- grain size distribution and degree of sorting (very poor, poor, moderate, well, very well);
- degree of stratification (none, very poor, poor, moderate, well, very well); and;
- geologic interpretation

J.M. Ryder and Associates, Terrain Analysis Inc. completed detailed terrain mapping following the standards set by Howes and Kenk (1997), with the resulting polygons dividing the study area into discrete units. These polygons are then digitized and geo-referenced into a geographic information system (GIS), permitting the information stored in the previously mentioned databases to be linked to their associated polygons. This enables the evaluation of aggregate potential on a polygon-by-polygon basis as well as the ability to perform spatial data queries.

The final step in the generation of the aggregate potential map is to classify polygons (based on their attribute data) into groups that have varying degrees of potential for hosting aggregate resources. Based on select attributes, polygons are assigned a numerical value that is derived from an algorithm that yields an overall score. The construction of the algorithm allows particular attributes to be weighted according to their importance. As previously mentioned, the availability of information pertaining to aggregate potential varies from project to project and so therefore must the structure of the algorithm. The algorithm for this study is yet to be developed.

The desired outcome is a four-tiered classification whereby polygons are ranked in terms of potential by assigning a value of primary, secondary, tertiary, or unclassified. Polygons classified as primary are areas where the potential for aggregate resources is considered to be high. Unclassified polygons on the other hand are those with virtually no potential for aggregate resources, and include areas covered by ice or water. Polygons classified as secondary or tertiary fall in-between these end members.

Once the data capture and compilation stages, data evaluation, and the polygon rankings have been completed, these data are integrated into a GIS format for distribution to clients. ESRI's ArcView (v. 3.2) GIS software is used to produce various thematic maps that display a variety of information relevant to an aggregate potential study. The files used to create these maps, as well as the maps themselves, will be available in CD-ROM format, enabling users to interact with the data, changing the type of information displayed to suit their own needs, as well as be able to query the various databases.

RESULTS

As this project is still in it's early stages, results to report at this time are limited to the data capture and compilation stages. During the 2001 field season a total of 98 field stations were visited (*see* Figure 4). Most sites are located along the coast or near populated areas, rarely more than a couple of kilometres from open water or up a fjord. The primary reason for this is the distribution of surficial sediments within the study area and the added cost of transportation of aggregate products, a limiting factor in the economic viability of an aggregate deposit (Langer and Glanzman, 1993).

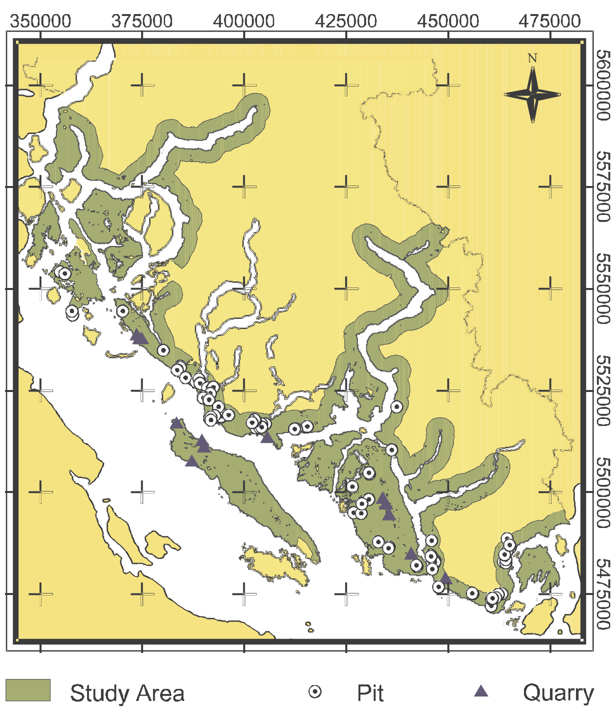

Figure 4. Distribution of the 98 field stations along the Sunshine Coast. Natural aggregate pits are indicated by light circles while quarries by dark triangles.

Table 1 is a summary of the field stations visited. Of the 98 sites, 83 are natural aggregate pits and 15 are rock quarries. In addition, only 33 sites are currently being mined, the remaining 65 are either inactive or have been reclaimed or abandoned.

The size of extraction operations varies throughout the study area from borrow pits and small quarries only tens of square metres in area, to large-scale operations that cover square kilometres such as the Sechelt Pit (Construction Aggregates Ltd.) (*see* Photos 1 and 2). Of the pits that have shut down, approximately half have been abandoned and naturally reclaimed, with the remaining half either re-developed for residential, commercial or industrial use, or serve some other purpose to the local community (Photo 3). Past producing sites that have been re-developed, or that now serve some other purpose to the local community, are considered sterile with regards to aggregate potential.

The most common sediments extracted in the region are the Capilano Sediments, and is consistent with results from earlier aggregate studies by Leaming (1968) and McCammon (1977). As previously mentioned, these are retreat-phase sediments, consisting of glaciofluvial, glaciomarine and marine sediments deposited away from the glacier fronts. In most cases, pits are located in raised glaciofluvial deltas and consist of interbeded sand, sandy

TABLE 1
SUMMARYOF FIELD STATIONS

Mine Type	Active	Inactive	Reclaimed		Total
Sand and Gravel Pit	28	36	19	9 Naturally Revegetated	**83**
				10 Re-developed	
Quarry	5	9	1	1 Re-developed	**15**
Total	**33**	**45**	**20**		**98**

Table 1 shows the classification of field stations according to the type of mine and its status. Also included is a summary of the types of reclamation encountered; either the sites was abandoned and natural re-vegetation has ensued or the site has since been developed and now serves a secondary land-use.

Photo 1. An example of a small borrow pit located near the town of Gibsons where material is being extracted for road construction on private land.

Photo 2. A medium to large-scale aggregate pit located on Jervis Inlet called the Treat Creek Pit (Jack Cewe Ltd.).

Photo 3. Brookman Park; a reclaimed aggregate pit located next to Chapman Creek on the outskirts of Sechelt.

gravel, and gravel (Photo 4) at elevations up to 200 m asl. More rarely, Quadra Sand or Vashon till is being extracted.

Materials being quarried fall under two categories: granitic rock and limestone, with the greater volume being that of limestone. The granite quarries visited are very small in comparison to the massive limestone operations found on Texada Island (Photo 5) (over 6 million tons per year from three quarries). Stockpiles of waste rock at these limestone quarries are a very large potential source of crushed aggregate (in the order of tens of millions of tons).

In addition to field data, other major sources of information related to aggregate potential used in this project have included drill logs taken from the Geological Survey Branch's Assessment Report Index System (ARIS) and water well records from the British Columbia Ministry of Water, Land and Air Protection. Currently there are 455 drill logs and approximately 1300 water well records in the Sunshine Coast Potential Aggregate Mapping Project database.

Terrain mapping has been completed and is in the process of being digitized. In total, 3305 polygons have been delineated, covering an area of approximately 310,000 ha in portions of NTS 92F/8-10, 92F/15-16, 92G/5-6, 92G/11-13, 92J/4, 92K1-3 and 92K/6-9.

Photo 4. Typical sediments found along the Sunshine Coast in aggregate pits. They consist of interbeded sand, sandy gravel and gravel associated with a relict delta.

Photo 5. A photo of the main pit at the Blubber Bay Quarry; a limestone quarry located on Texada Island. This pit is approximately 160 m deep.

SUMMARY

As this project is in it's early stages, it is not possible at this time to comment on aggregate resource potential along the Sunshine Coast. However, some observations on the aggregate industry along the Sunshine Coast can be reported:

1. Glaciofluvial sediments, thought to belong to the Capilano Sediments, are primarily being mined;
2. Mined aggregate deposits lie predominantly below 200 metres asl; and
3. Aggregate pits tend to be near urban centers or near transportation routes such as major roads or waterways.

Once terrain polygons have been digitized, the compiled data will be spatially referenced to the polygons, and an algorithm will be run on this data to rank the polygons in terms of aggregate potential. The release of results from this project is anticipated in spring of 2002.

ACKNOWLEDGEMENTS

Primary funding for this project comes from the Corporate Resource Inventory Initiative and the Ministry of Energy and Mines. Information gathered to date has been provided by: Ministry of Transportation; Ministry of Land, Water and Air Protection; British Columbia Assets and Lands; Ministry of Energy and Mines; Ministry of Forests; Sunshine Coast Regional District; District of Powell River; District of Sechelt; Town of Gibsons; Thurber Engineering Ltd.; Golder and Associates; and Weyerhaeuser Canada. Many thanks go out to the aggregate mines and quarries that have cooperated with us on this project and allowed entry onto their property. Special thanks to Construction Aggregate Ltd., LaFarge Canada, Jack Cewe Ltd., Ash Grove Cement Company and Texada Quarrying Ltd. for their time and hospitality.

REFERENCES

Armstrong, J.E. (1981): Post-Vashon Wisconsin glaciation, Fraser Lowland, British Columbia; *Geological Survey of Canada*, Bulletin 322.

Armstrong, J.E. and Clague, J.J. (1977): Two major lithostratigraphic units in southwest British Columbia; *Canadian Journal of Earth Sciences*, volume 14, pages 1471-1480.

Bobrowsky, P.T., Massey, N.W.D., and Matheson, A. (1996a): Aggregate resource potential of the Prince George area; *BC Ministry of Energy, Mines and Petroleum Resources*, Open-File 1996-24, 5 maps, scale 1:50 000.

Bobrowsky, P.T., Massey, N.W.D., and Matysek, P.F. (1996b): Aggregate Forum, developing an inventory that works for you! Report proceedings March 30-31, 1995; *BC Ministry of Energy Mines and Petroleum Resources*, Information Circular 1996-6.

Bobrowsky, P.T., Massey, N.W.D., and Matheson, A. (1998): Aggregate resource potential map of the Okanagan area (NTS 82E (west) and 82L (west)); *BC Ministry of Energy and Mines*, Open-File 1998-5, 16 maps, scale 1:50 000.

Bobrowsky, P.T., Kilby, C.E., Manson, G. and Matysek, P.F. (1995): British Columbia Aggregate Inventory Project; *in* Geological Fieldwork 1994, Grant, B. and Newell, J.M., Editors; *B.C. Ministry of Energy, Mines and Petroleum Resources*, Paper 1995-1, pages 361-364.

Bobrowsky, P.T., Matheson, A. Paulen, R. and Massey, N. (1999): Aggregate potential project for the Nanaimo area, Vancouver Island (NTS 92B, C, F and G); *in* Geological Fieldwork, 1998; *B.C. Ministry of Energy, Mines and Petroleum Resources*, Paper 1999-1, pages 279-284.

Buchanan, R.G. and Bergman, D. (1993): Aggregate resource investigation- Powel River to Lund- Sunshine Coast District; *Ministry of Transportation and Highways, Geotechnical and Materials Engineering*, unpublished report, File 31-21-09.

Clague, J.J. (1980): Late Quaternary geology and geochronology of British Columbia, Part 1: radiocarbon dates; *Geological Survey of Canada*, Paper 80-13, 28 pages.

Clague, J.J. (1994): The Quaternary stratigraphy and history of south-central British Columbia; *in* Geology and geological hazards of the Vancouver region, southwestern British Columbia, Monger, J.W.H. Editor; *Geological Survey of Canada*, Bulletin 481, pages 181-192.

Dixon-Warren, A.B., and Brooks, E.D. and Bobrowsky, P.T. (2000): Aggregate resource potential of the Sea-to-Sky Highway Area (NTS 92G11 and 14); *B.C. Ministry of Energy and Mines*, digital data, Open File 2000-30.

Hickin, A., and Brooks, E.D. and Bobrowsky, P.T. (2001): Sea-to-Sky Aggregate potential mapping project; *B.C. Ministry of Energy and Mines*, digital data, Open File 2001-12.

Hicock, S.R. and Armstrong, J.E. (1985): Vashon Drift: definition of the formation in the Georgia Depression, southwest British Columbia; *Canadian Journal of Earth Sciences*, volume 22, pages 748-757.

Holland, S.S. (1976): Landforms of British Columbia, a physiographic outline; *B.C. Ministry of Energy, Mines and Petroleum Resources*, Bulletin 48.

Howes, D.E. and Kenk, E. (1997): Terrain classification system for British Columbia (revised edition); *BC Ministry of Environment, Lands, and Parks, Survey and Resource Mapping Branch*, MOE Manual 10.

Langer, W.H. and Glanzman, V.M. (1993): Natural aggregate building America's future; Public Issue in Earth Science, *US Geological Survey*, Circular 1110.

Leaming, S.F. (1968): Sand and gravel in the Strait of Georgia area; *Geological Survey of Canada, Department of Energy, Mines and Resources*, Paper 66-60.

McCammon, J.W. (1975): Sand and gravel deposits on the Sunshine Coast, Port Mellon to Powell River; *in* Geology, Exploration and Mining in British Columbia, 1974; *B.C. Department of Mines and Petroleum Resources*, pages 386-398.

McCammon, J.W. (1977): Surficial geology and sand and gravel deposits of Sunshine Coast, Powell River, and Campbell River areas; *B.C. Department of Mines and Petroleum Resources*, Bulletin 65.

Massey, N.W.D., Matheson, A., and Bobrowsky, P.T. (1998): Aggregate resource potential of the Nanaimo area (parts of NTS 92B/12, 92B/13, 92C/9, 92C/16, 92F/1, 92F/2, 92F/7, 92F/8, 92G/1); *B.C. Ministry of Energy and Mines*, Open File 1998-12, 9 maps, scale 1:50 000.

Massey, N.W.D., Matheson, A. and Bobrowsky, P.T. (in press): Aggregate Resource Potential Maps - a Planning Tool Useful for Explorationists; *in* Industrial Minerals in Canada, 1998, Simandl, G. Editor; *Canadian Institute of Mining*.

Meidinger, D. and Pojar, J. (1991): Ecosystems of British Columbia; *Ministry of Forests*, Special Report Series, no. 6.

Mullineaux, D.R., Waldron, H.H. and Rubin, M. (1965): Stratigraphy and chronology of late interglacial and early Vashon glacial time in the Seattle area, Washington; *United States Geological Survey*, Bulletin 1194-0.

Ryder, J.M. and Clague, J.J. (1989): British Columbia (Quaternary stratigraphy and history, Cordilleran Ice Sheet); *in* Chapter 1 of Quaternary Geology of Canada and Greenland, Fulton, R.J. Editor; *Geological Survey of Canada*, Geology of Canada, no.1, pages 48-58.

The MapPlace - An Internet-based Mineral Exploration Tool

By Larry Jones, Don MacIntyre and Pat Desjardins

INTRODUCTION

The MapPlace, an Internet-based system operated by the British Columbia Geological Survey Branch, provides free interactive map access to data themes, covering a broad range of geospatial data in vector and attribute form. Themes include bedrock geology, surficial geology, metallic and industrial mineral potential ranking, regional silt and water geochemical surveys (RGS), mineral occurrences (MINFILE), exploration assessment reports (ARIS) and mineral title locations. These themes can be combined with other georeferenced datasets such as administrative boundaries, topographic features, aquifers and other related map-based information, including raster images such as digital elevation model (DEM) shaded relief, satellite (LandSat) and aeromagnetics to produce user-defined map views. Table 1 is summary of major datasets accessible through the MapPlace.

With the free Autodesk MapGuide Viewer, users can download data, interactively view, create, print and copy their own maps and reports. In addition to the creation of a map, many of the features that can be displayed on MapPlace are linked to supporting database tables, thus allowing users to access valuable attribute data that is linked to individual map objects. For some themes, clicking on an object links to a separate Internet site such as MINFILE, ARIS or Mineral Titles allowing further search and retrieval capabilities. Other options include buffering, selecting objects within polygons, and digitizing of polygons, points

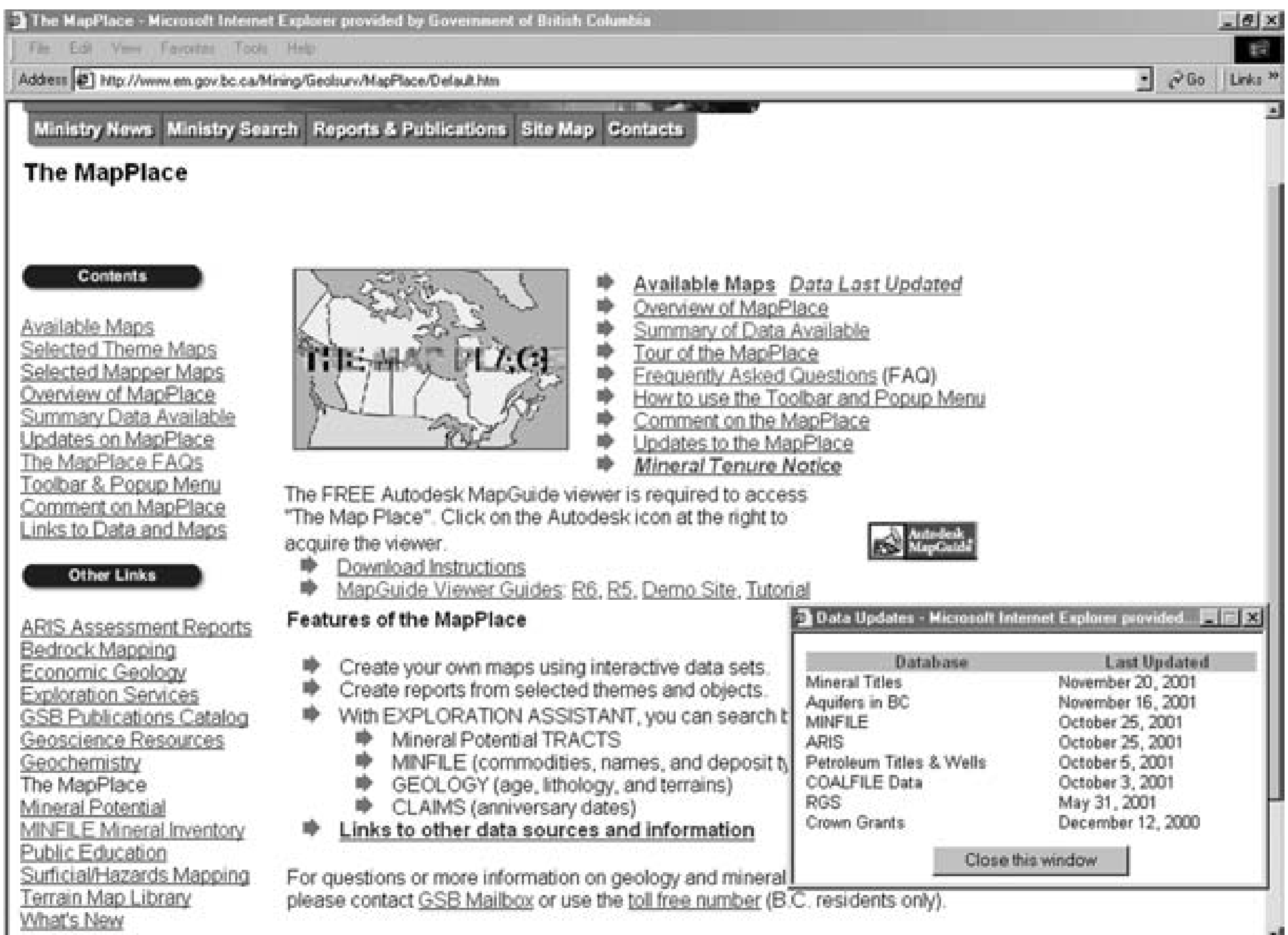

Figure 1. The MapPlace Website.

and lines on screen. Figure 1 shows the startup page for the MapPlace, showing links to more information; the web site is <www.em.gov.bc.ca/MapPlace>.

DEVELOPMENT OF THE MAPLACE

Ward Kilby began developing MapPlace in 1997 around several off-the-shelf software packages including Autodesk MapGuide, Allaire ColdFusion, Microsoft Access and the usual web server software. Databases handle all the tabular information associated with the site. ColdFusion is used as a web database manager, report writer and sophisticated web toolkit. MapGuide Server, Author and Viewer software provide the map displays, GIS functionality and development environment for this style of web presentation.

Several of the datasets displayed on the MapPlace, including the tectonic assemblage map geology, reside on other MapGuide servers. This integration of data from different sources and custodianships is one of the most powerful features of distributed systems (Figure 2).

USING THE AUTODESK MAPGUIDE VIEWER

The free Autodesk MapGuide Viewer transforms your browser (e.g. Microsoft Internet Explorer or Netscape) into a map viewer that works over the Internet. As a type of geo-

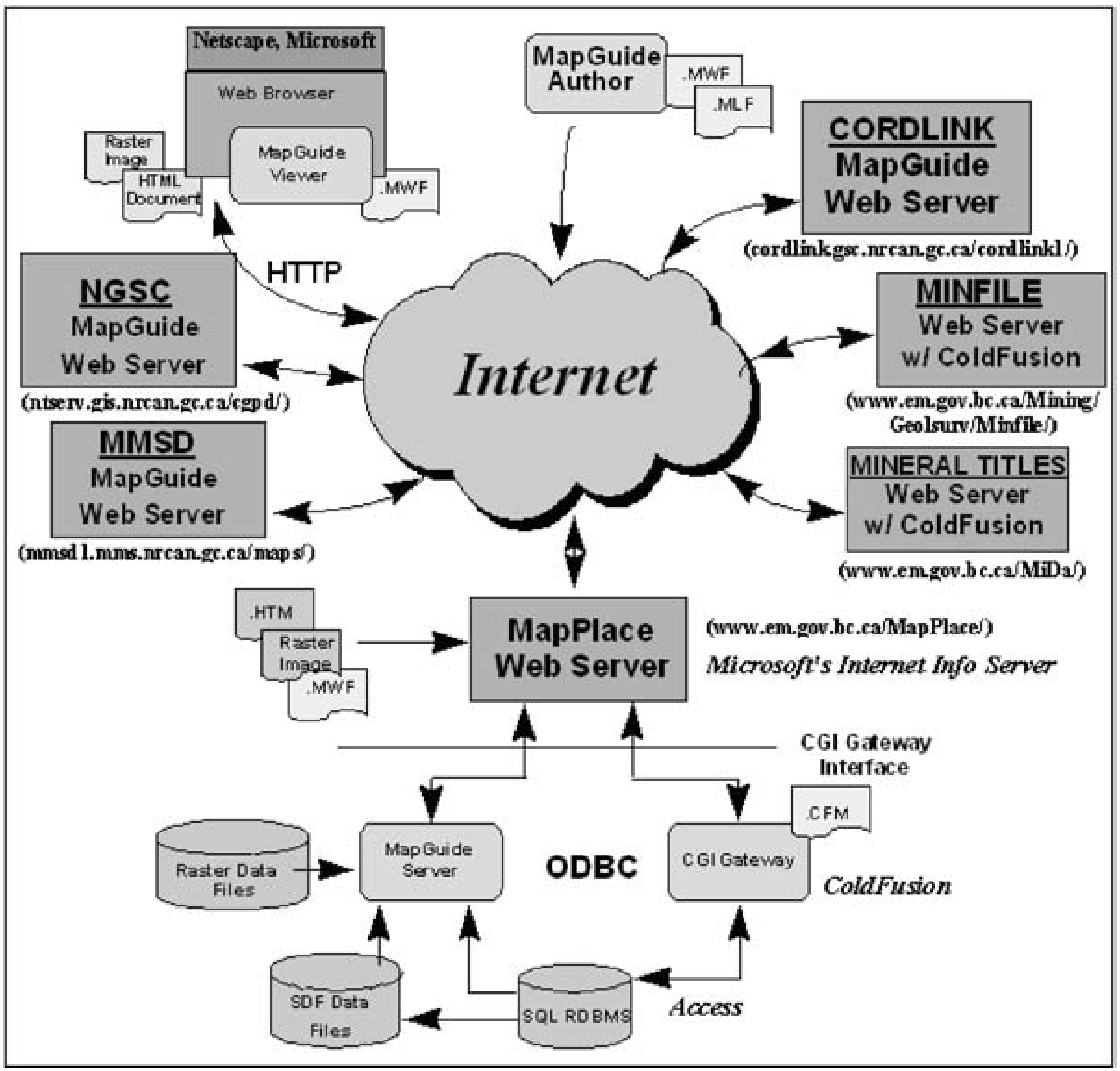

Figure 2. Diagrammatic view of the MapPlace configuration in relation to the Internet, geographic data, attribute databases, other websites and other MapGuide sites.

graphic information system (GIS), the Viewer enables non-technical users to zoom in and out on a map; find, select and display information about specific features; collapse or expand layer groups; make queries; create buffers; print to scale, and much more. The efficient Viewer only downloads the information required or selected to display a map. The Viewer can be downloaded by going to x or through the link at the MapPlace. The MapPlace also contains a link to instructions on how to download and install the Viewer, as well as links to user guides, on-line tutorials, interactive demos, help functions and FAQs.

Organization Of Data Into Layers

Available data in the MapGuide Viewer is presented in the form of layers. Each layer represents one entity, such as rivers, coal boreholes, or BC Mining Divisions (Figure 3a), and performs a function similar to a transparency. The types of data that are available for each map are listed in the legend on the left hand side of the Viewer (Figure 3b). When one or more layers are selected, they appear like stacked transparencies and are displayed as a single map (Figure 3b).

The order in which the layers are 'stacked' or appear on the map, is determined by their position in the legend. Those

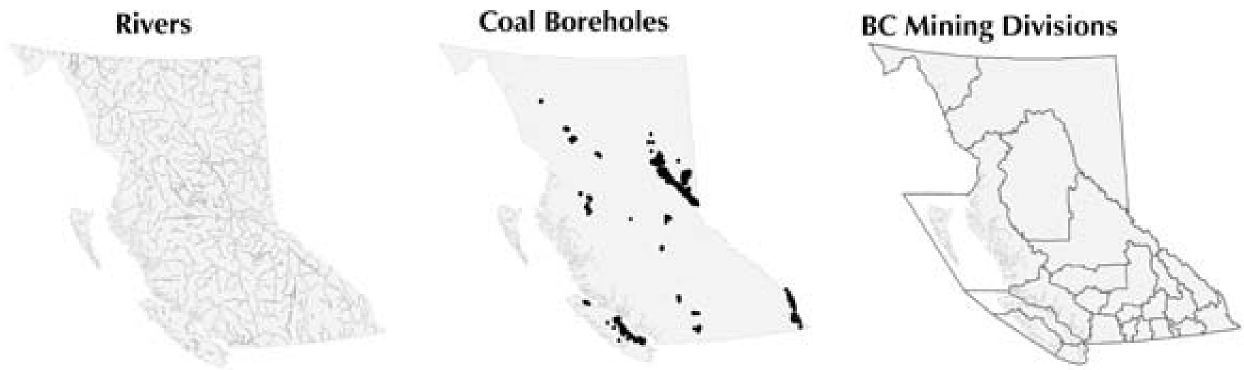

Figure 3a. Layer example selected individually.

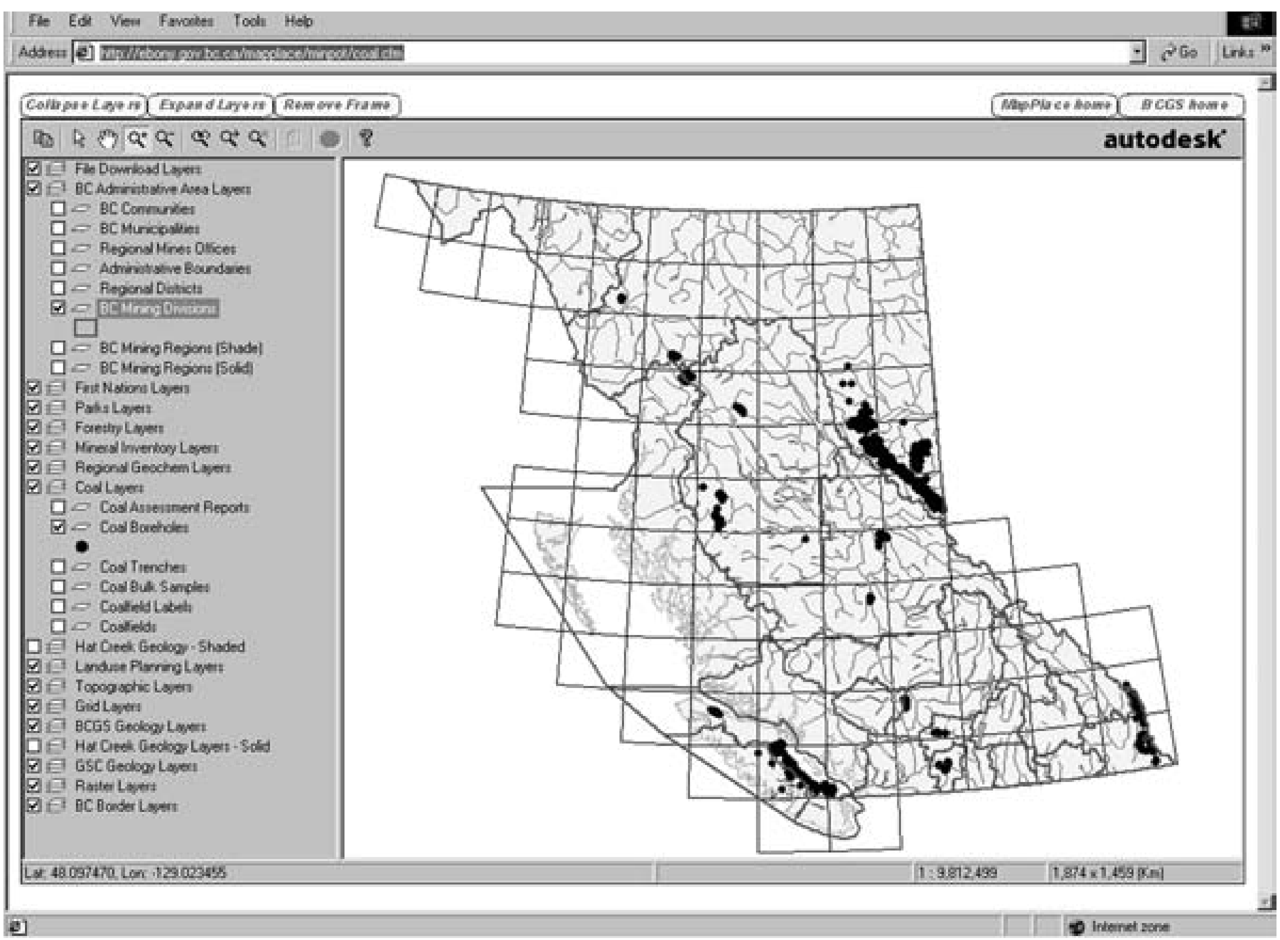

Figure 3b. All 3 layers in Figure 3a were selected together and are displayed on one map.

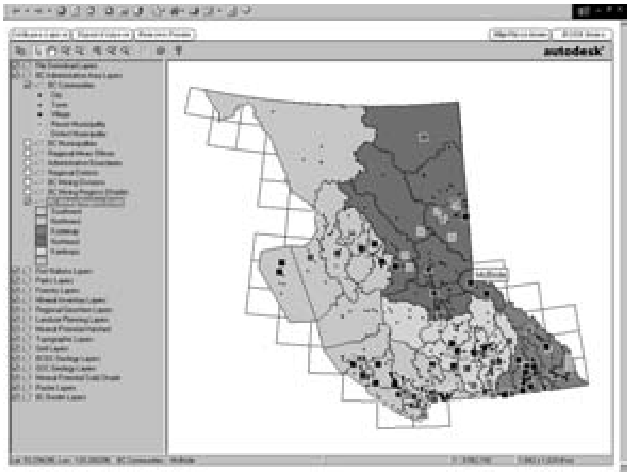

Figure 4a. BCGS Geology Map, viewed at full size. BC Communities and BC Mining Regions (Solid) are selected layers within the BC Administration Layer Group.

layers that are located at the bottom are stacked first, followed consecutively by selected layers above. This means that the layer located at the top most part of the legend will be the last layer stacked and it may appear to overlap or cover up some of the data from the lower positioned layers.

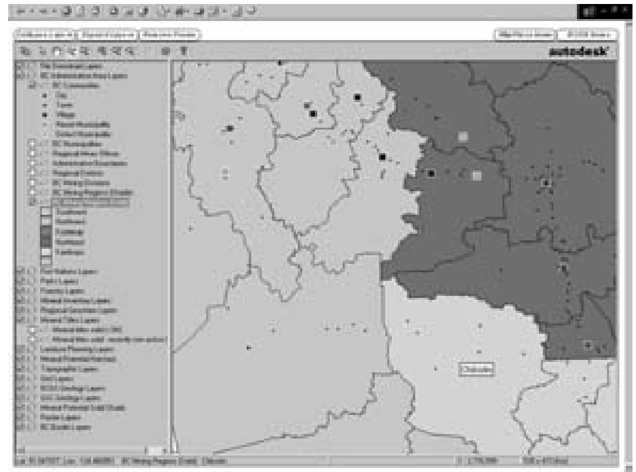

Figure 4b. The ZOOM IN feature used on the map in Figure 4a was used to display a more detailed view. With more detail displayed on the map, another layer 'BC Localities' becomes available and has been selected.

In general the maps are 'authored' to place raster layers at the bottom, vector layers in the middle and point layers at the top.

To further organize the data, layers have been grouped by themes. For example, Figure 4a contains the BC Com-

TABLE 1
SUMMARY OF MAJOR DATASETS ACCESSIBLE THROUGH THE MAPPLACE

Layer Group or Name	Object Type	No. of Objects / Coverage	Date Updated	Reports, Downloads and Links	Visible Scales (M=million, K=thousand)	Sources of Data*
Bedrock Geology (1:5M, 1M, 250K resolution)	Polygon, Line	60,000; 180,570	1994	legend reports	<1M, 2M incremental to 10M	MEM/GSB; NRCan
Geology Map Index	Polygon	298	1998	data report and download	all scales	MEM/GSB
Geology Download	Arcview files (e00)	100% (1:250K maps)	1998	E00 file downloads	all scales	MEM/GSB
Mineral Potential	Polygon	788	1998	data report and download	all scales	MEM/GSB
Aggregate	Point, Polygon	725 pts / Nanaimo, Okanagan, Prince George, Sea-to-Sky	periodically	table download	all scales	MEM/GSB
COAL Assessment Reports, Boreholes, Trenches, Bulk Samples	Point, PDF files	827 reports; 8350 boreholes; 3324 trenches; 459 bulk samples	1990	Reports and table download	all scales	MEM/GSB
Mineral Occurrences - MINFILE	Point	12,091	monthly	data reports and downloads; links to MINFILE	all scales	MEM/GSB
Assessment Reports - ARIS	Point, PDF files	25,941	monthly	data reports and downloads; links to ARIS	all scales	MEM/GSB
Regional Geochemistry - RGS	Point, Polygon	44,428	annually	complete data download	<1M	MEM/GSB
Mineral Tenure	Polygon	41,862	monthly	data report and links to MIDA	<1M	MEM/MTB
Crown Grants	Raster image	100%	periodically	TIFF file downloads	<200K	MEM/MTB
Petroleum Tenure and Wells	Point, Polygon	11,917 titles; 14,405 wells	2001	Reports and table download	all scales	MEM/PLB/OGC
Topography (6M, 2M, 1M, 250K, 50K, 20K resolution; Colour Contours, TRIM Contours, Roads, Rail, Rivers, Lakes, Glaciers, Coast, Bathymetry, Aquifers)	Points, Polygon, Line	very large; 7000 TRIM maps; 1122 aquifers	variable; TRIM 1996	none	variable scales for different resolutions	MSRM; WLAP; NRCan
Geographic Locations (Map Grids, Gazetteer)	Point, Polygon	41,500	1998	none	all scales	MSRM
Administration Areas (First Nations, Parks, Forestry, LRMP areas)	Polygon	multiple	variable	none	all scales	MSRM, MOF
DEM Shaded Relief	Raster image	100%	1999	none	all scales	MSRM; NRCan
LandSat	Raster image	95%	1999	none	all scales	MSRM; NRCan
Aeromagnetics	Raster image	85%	2000	none	all scales	NRCan
Gravity	Raster image	100%	1999	none	all scales	NRCan

Abbreviations: MEM=BC Ministry of Energy and Mines; GSB=Geological Survey Branch; MTB=Mineral Titles Branch; PLB=Petroleum Lands Branch; OGC=Oil and Gas Commission; MSRM=BC Ministry of Sustainable Resource Management; WLAP=BC Ministry of Water, Land & Air Protection; MOF=BC Ministry of Forests; NRCan=Natural Resources Canada munities layer, which is a layer within the BC Administrative Layers group. Layer Groups can either be collapsed or expanded by double clicking on the layer group title. To select a layer group or a layer, use your mouse to click on the box adjacent to the layer or layer group. Selection will be indicated by a checkmark in the box. Layers will only be displayed in the map Viewer if the Layer Group has been selected first. As each layer group is selected, different layers become available and can be selected and deselected with the user's needs. Zooming in on a map area also produces more layer choices and the detail of the map increases. This is demonstrated by comparing the available layers in Figure 4a with Figure 4b. The ZOOM IN feature used to produce the map in Figure 4b allows for the BC Localities layer to be available and selected.

Accessing Commands

The MapGuide Viewer uses either **toolbar buttons** or the **popup menu** to carry out various commands (Figure 5). The toolbar buttons are situated across the top left side of the Viewer window. The popup menu is a menu that appears by clicking the right-hand button on the mouse (referred to as 'right clicking') anywhere in the map window. Right clicking displays the popup menu, and a command can be selected by clicking one of the items in the menu. Those commands that have a right arrow next to them (such as ZOOM) display a secondary popup menu when selected (Figure 5).

The **toolbar buttons** allow the user to COPY the current map view to the clipboard; SELECT features; PAN or slide the map around to display areas that are outside of the current view; ZOOM to an area that is user defined either with a center point or a rectangle; ZOOM OUT from the area defined by a center point; ZOOM PREVIOUS view that was displayed; ZOOM GOTO a specified location; UNZOOM to display the full extents of the map; VIEW REPORTS associated with the selected map objects; STOP or interrupt the updating of the map display; and HELP to link to the Autodesk MapGuide Viewer Help Website.

The **popup menu** provides additional features to the toolbar buttons, such as the PAGE SETUP dialogue box, where map size can be specified by scale; PRINT the current map displayed; RELOAD the viewer to display the original map layout; ZOOM WIDTH dialog box, where map width can be specified at the place of the curser; ZOOM SCALE dialog box, where the scale of the map can be defined; ZOOM SELECTED to selected object(s); BOOKMARKS to add and delete bookmark names for displayed map views; SELECT criteria such as OBJECTS, RADIUS, POLYGON, and WITHIN specified map objects; VIEW DISTANCE between two points; VIEW BUFFER to create buffers around selected areas; and ABOUT which links you to Autodesk MapGuide Viewer Help website and allows you to change PROPERTIES such as viewing scale and map coordinates.

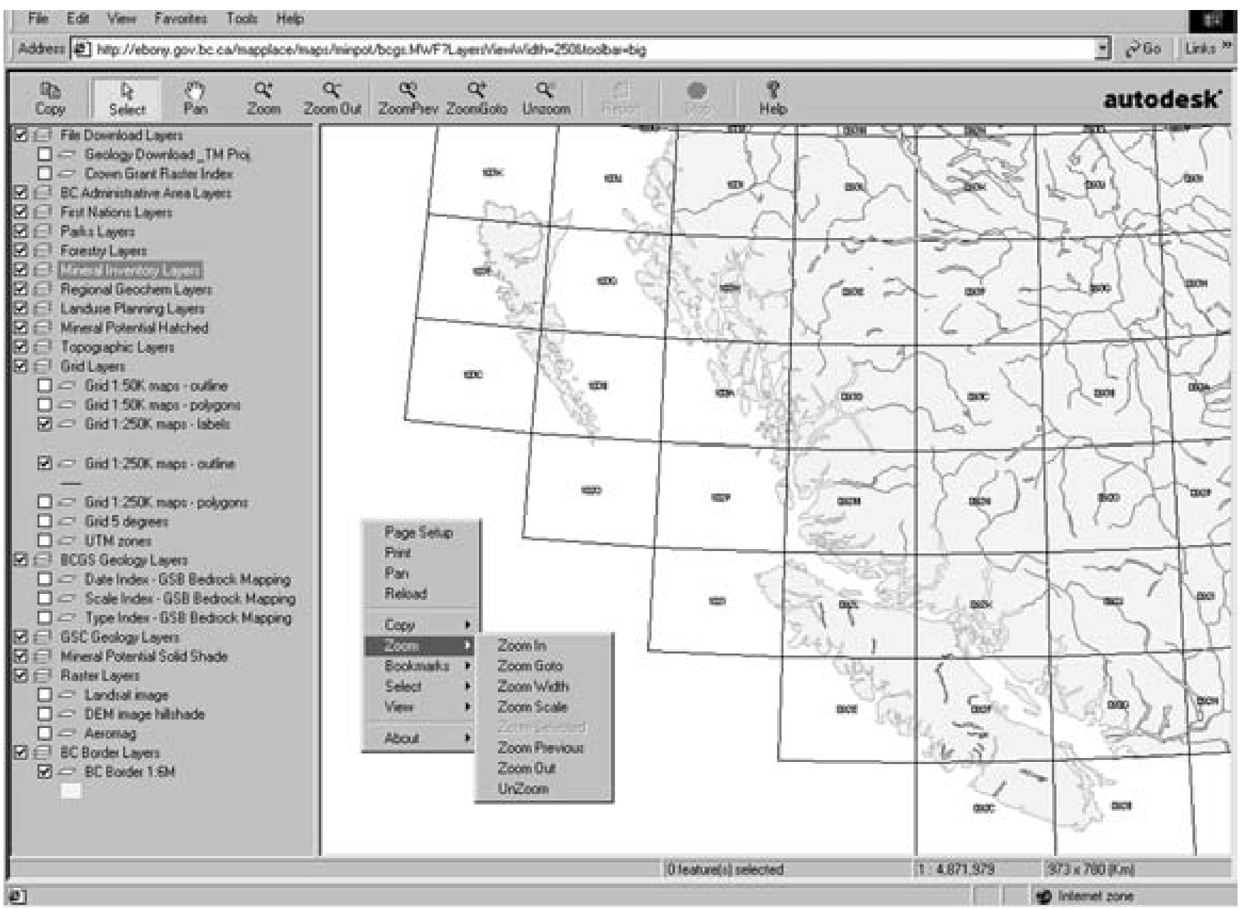

Figure 5. Toolbar Buttons and Popup Menu.

AVAILABLE MAPS

The MapPlace has 21 theme-based maps. The BCGS Geology Map can access all available provincial datasets, whereas the other maps focus on particular areas or themes, such as detailed and surficial geology, geophysics, and geology map indexes. Other maps such as the Exploration Assistant allow users to search and display elements of 4 main databases. Each map has a 'more details' link to provide further information, such as unique layers, special instructions to view certain features, type of projection used, etc. Descriptions of these maps, with examples of their use, are presented here.

Maps Currently Available:

- BCGS Geology Map
- Exploration Assistant
- Mineral Titles Map
- World Map
- Canada Map
- USA Map
- Jennings River Geology Map
- Barkerville Geology Map
- Lillooet LRMP Map
- Guichon Batholith
- Vernon Geology Map
- Aggregate Potential Map
- Terrain Map Index
- Regional Geophysics Map
- Relief and Radar Map
- Southeast BC Geophysics Map
- Petroleum Tenure and Wells Map
- Coal Map
- BC Geology Map Index
- GSC & GSB Geology Map Indexes
- Mineral Statistics Maps: Coal Operations, Metal Operations, Refining & Smelting, Industrial Minerals

BCGS Geology Map

This map is projected in Albers Equal Area for BC. It provides access to all provincial datasets and geology layers. Figure 6 displays the available layer groups (collapsed). The Legend Window is organized into themes. Look for the expanded geology, mineral occurrence, ARIS and mineral title layers at the bottom of the legend window. Administrative layers are at the top. Topographic layers, including TRIM, are in the middle of the legend window. Two sets of Mineral Potential layers are available, a shaded version above the geology layers and a solid version below the geol-

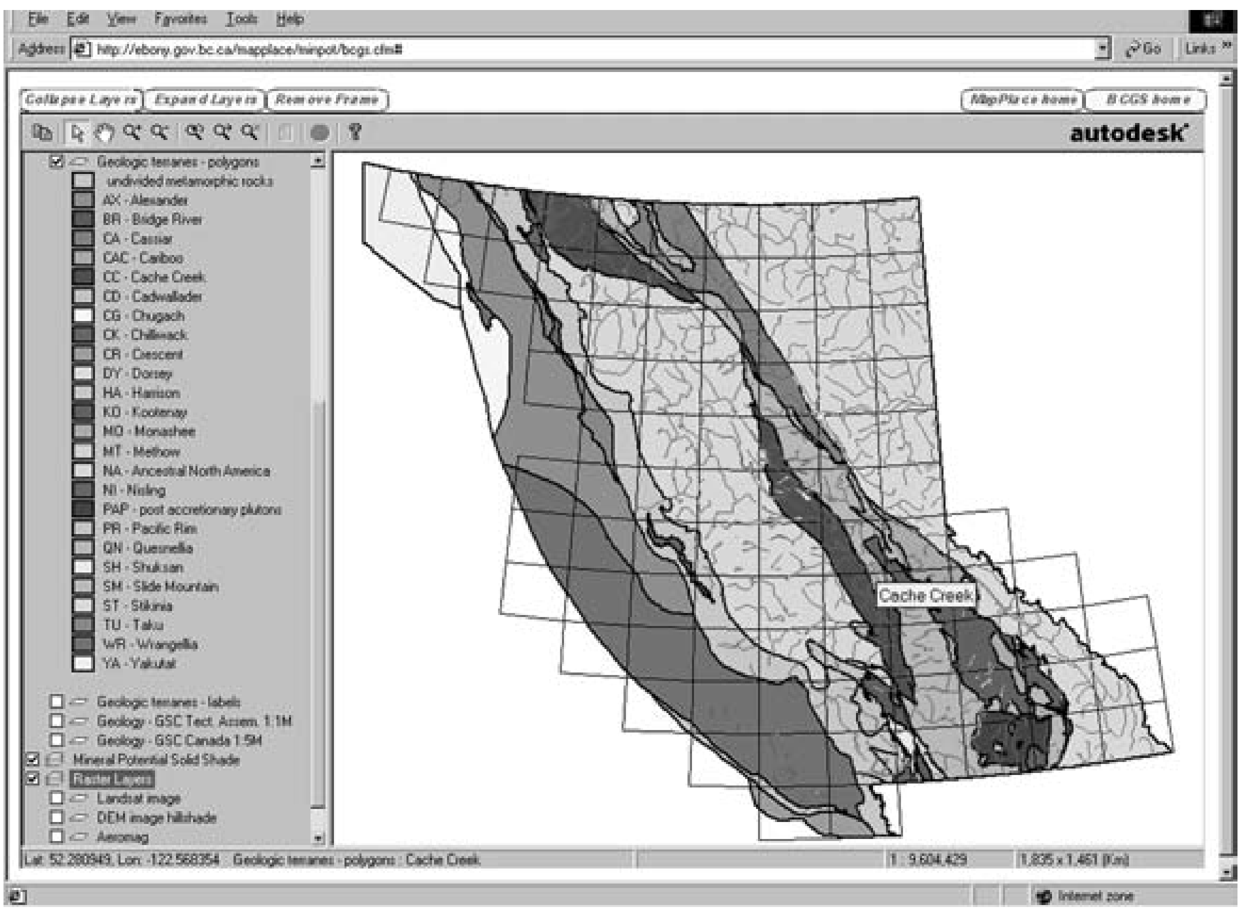

Figure 6. Available layer groups (collapsed) for the BCGS Geology Map are shown in the left hand of the window frame.

ogy layers. This map provides the most flexibility for the combination of available datasets. This is the best map to start with as it allows you to see all the datasets in their most generic form.

Bedrock geology layers are visible under 1:1.5 million scale. Legend reports are attached to the layers which included Faults and Contacts; Geology polygons coloured by age and rock class (sedimentary, intrusive etc.); Geology polygons hatched by rock type (this hatch pattern is transparent and can be superimposed on raster images); Geology labels based on the lithostratigraphic map unit. The cursor flyout also has information on the map unit represented by each polygon, plus it gives the poly-id and previous keycode so that geologic revisions can be done for specific polygons.

To access the Geology Downloads click on the appropriate theme at the top of the legend and double click on the map area of interest. The resultant page display will provide access to the digital files in ArcInfo EXPORT (E00) format in either Albers Equal Area Polyconic or Geographic (decimal degrees) projections. The datum is NAD83. Click on the item you require to download the zipped files. To use the files as shape files they can be translated using the Import71 utility that comes with Arcview. Metadata for the geology of the whole province is also available on this page as a downloadable file (). A describes the download files. To interactively view the bedrock geology with MapPlace, select the Interactive View of the map sheet in either projection and the NTS area will be displayed.

The TRIM (Terrain Resource Information Management) layers are visible at a zoomed scale of 1:100,000, include Transport Structures, Rail, Roads, Rivers, Lakes, Land Cover and Contours in two layers. Aquifers in British Columbia, from Ministry of Water, Land and Air Protection, are available in two layers (above 1:2 million and below 1:2 million scale). Some of the aquifers are directly linked (double click) to the Aquifer Image Portfolio.

Exploration Assistant

This theme map offers 5 different features to perform detailed queries that are displayed on the map. These features include: Gazetteer to find a location; Discovery Potential where Mineral Resource Assessment program predicted new deposits of specific types will be found; MINFILE by commodity or deposit type or name; Regional Geochemistry by provincial or mapsheet statistical threshold for 37 elements; Geology by age, lithology and terrane; and Mineral Titles by claim name and anniversary date. This map has access to other databases such as BC Localities and Communities, Regional Districts, Regional Geochemical Surveys, Assessment Reports, Road, Railways, Rivers, Parks, and many others.

The following are examples of queries that can be performed through the Exploration Assistant: find a particular

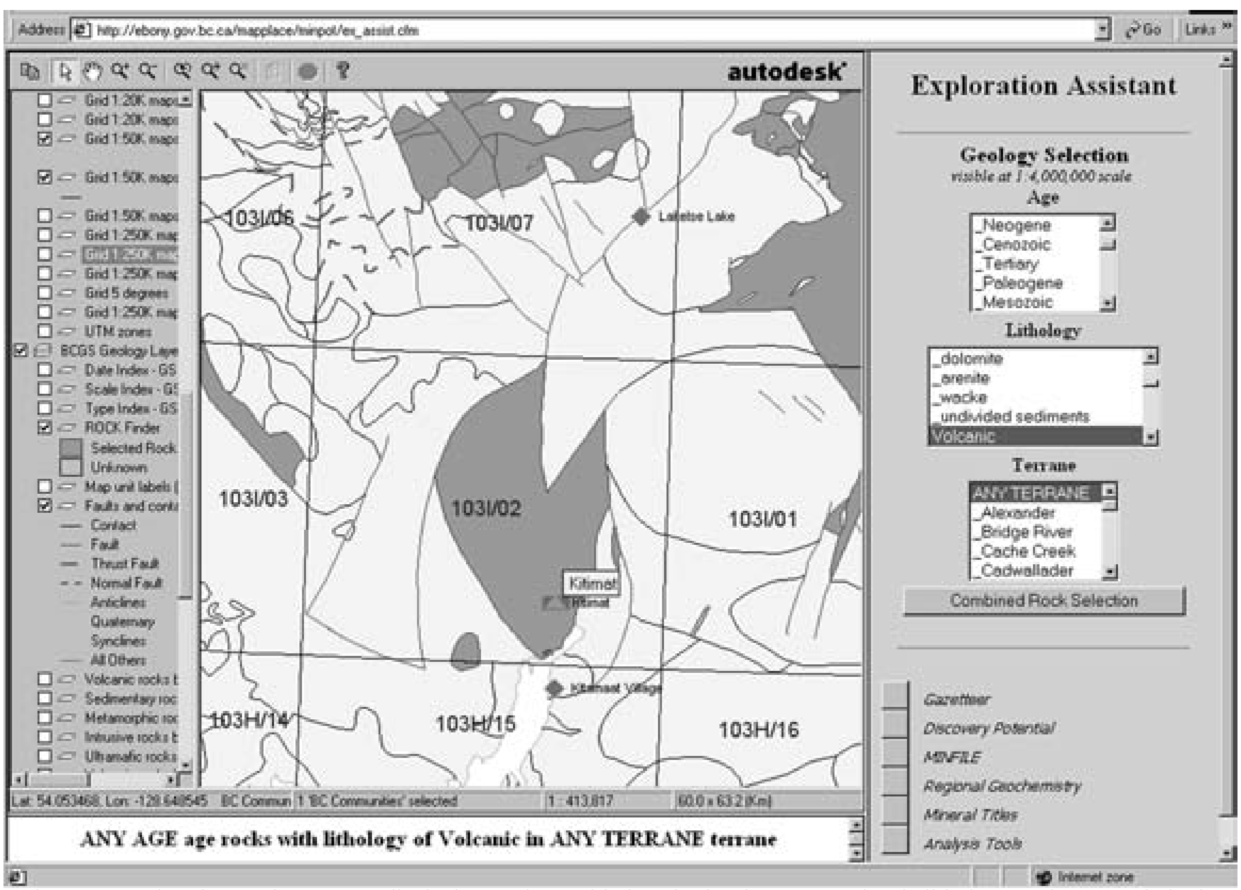

Figure 7. Exploration Assistant Map, displaying geology with the criteria of any age, volcanic lithology, and any terrain in the Kitimat area.

settlement, such as Gold Creek; display areas favourable for garnet skarns; show the location of the Eskay Creek deposit; plot all Jade occurrences; plot the Placer deposits; zoom into an area and display Cretaceous age sedimentary rocks within any terrane; find the Flan claim; display all claims in an area with an anniversary date in the next 40 days. An example of a geology query for the following criteria: any age, volcanic lithology, and any terrain, within the Kitimat area is displayed in Figure 7.

Mineral Titles Map

This map is viewed along with an additional window frame to allow users to conduct a number of Mineral Title related searches:

- **Tenure searches** by number, claim name, tag number, tenures staked by a person, and tenure owned by a person or company
- **Free Miner** searches
- **Maps** searches for a list of all tenures on a specific map and Mineral Title Maps on the web
- **Lot** searches by number and Land District
- **Form** searches for Mineral Tenure Act Forms and Applications
- **Other searches:** Map Index, Tenure Statistics, Links to Mineral Titles Information, and Search Tips

Mineral, Placer and Coal tenures layers are unique to this map and can be viewed at scale of 1:3,000,000 or less. Once these layers have been selected, users can use the SELECTION function on the toolbar buttons, and double-click on any map tenure area to search the database for that particular tenure number (Figure 8). The lower window frame will display related information about the selected tenure as well as provide links to gain access to further information.

A **ZOOM GOTO Mineral Tenure Number** is also available to locate tenures on the map (Figure 9). Right click on the map to display the Popup Menu, select ZOOM, then from the submenu select ZOOM GOTO. A ZOOM GOTO window will appear and in Category use the pull down menu to choose Mineral Tenure Number. Enter the tenure number in Location and click OK. Due to the large size of the Tenure data source, the ZOOM GOTO may take up to a minute to display the tenure map area. Turn on the Mineral Title Layer and the tenure number specified in the GOTO dialogue box will be displayed on the map. Double clicking on the tenure will link to Mineral Titles Registry System (MIDA) for a report on the tenure.

Crown granted two post claims are available in raster format for downloading or viewing Figure 10. To access this layer turn on the Crown Grant Raster Index Layer and double click on the map area of interest. The lower frame win-

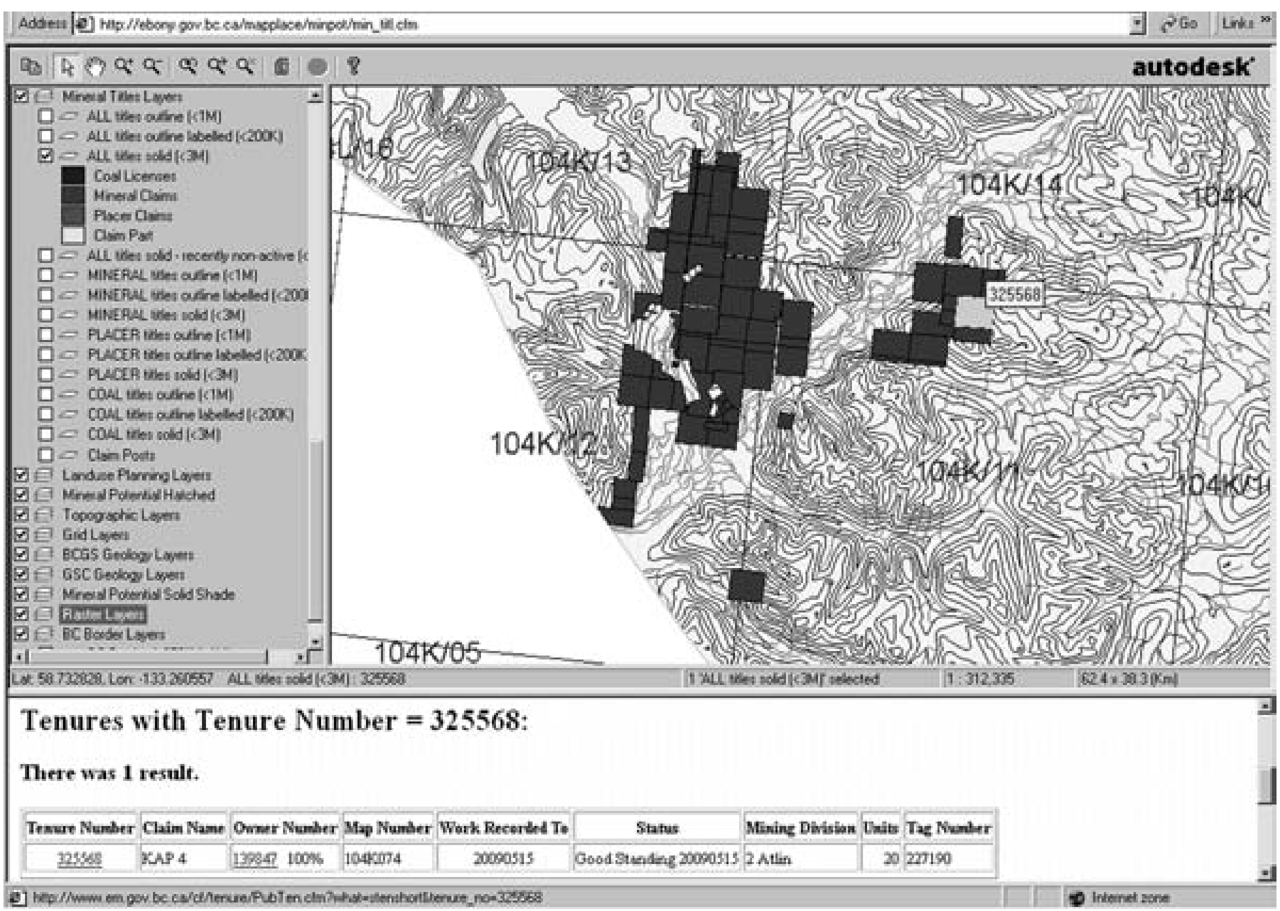

Figure 8. All (mineral) Titles Solid layer was selected. Tenure number 325568 was selected by double-clicking with the SELECT feature on that particular tenure in the map viewer. The lower window frame provides information and links to this tenure.

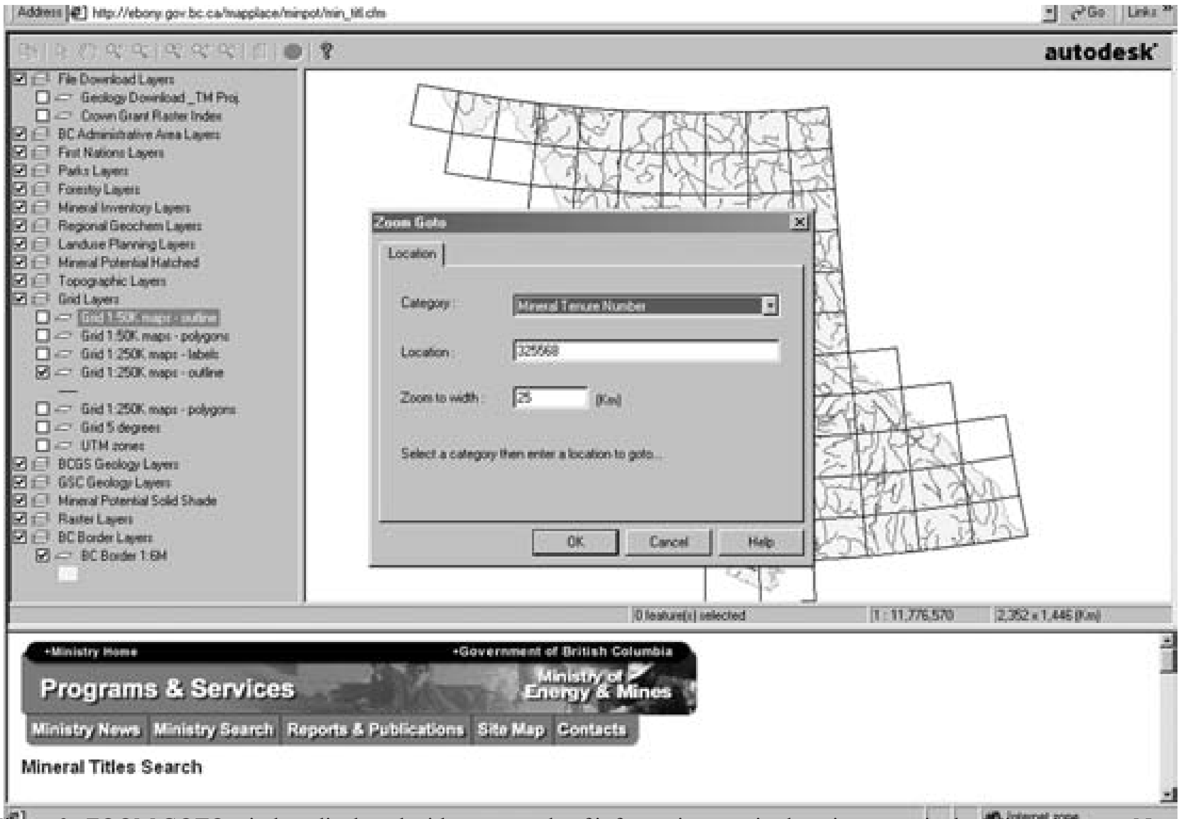

Figure 9. ZOOM GOTO window displayed with an example of information required to view a particular Mineral Tenure Number on the map.

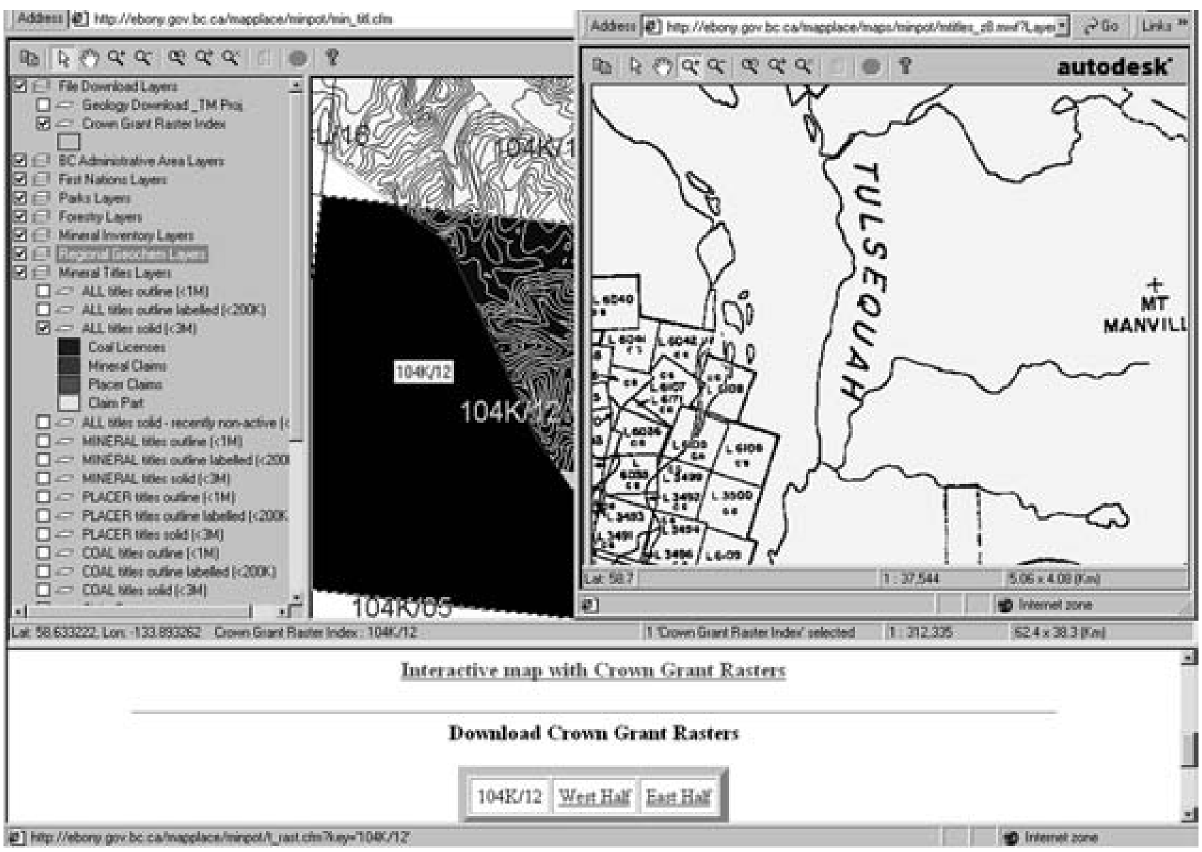

Figure 10. Crown Grant Raster Index layer selected and displayed, NTS map sheet selected by using the SELECT feature on the Toolbar Buttons. Lower window displays link to download or view the NTS map sheet.

dow provides the user with the option to download one of the two possible half sheets for use in some graphics program OR to view the maps interactively and integrated with other MapPlace data. When choosing to interactively view the Crown Grant Raster Index Layer, a new Viewer window will open up allowing further data to be added. The Crown Grant Raster maps are displayed with a UTM83 projection, so caution must be exercised as one nears the UTM zone boundary.

Selected Theme Maps

There are 15 Selected Theme Maps and they contain most of the layers found in the BCGS Geology Map, but also contain layers unique to their theme. Some of these maps when opened will already be zoomed into an associated geographical area.

Jennings River Geology Map

This map is displayed in Albers Equal Area projection and includes the Jennings River area (NTS 104O/14E and 15) geology. The detailed map features: Station Points, Features and Labels; Geology Lines, Polygons (stippled and solid) and Labels; Outcrops; and Eskers. Geology is from of Open File 2001-6 by J. Nelson, T. Harms, C. Roots, M. Mihalynuk and M. de Keijzer.

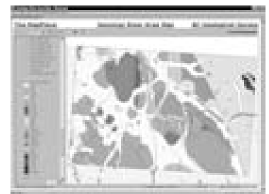

Barkerville Geology Map

This map covers the Barkerville area (NTS maps 093A and H) and unique layers include the Barkerville Cariboo and Kootenay terranes.

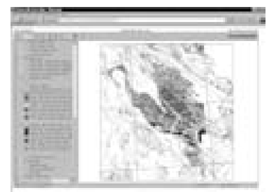

Lillooet LRMP Map

This map covers NTS maps, 092IW, 092J and 092O (south) and is displayed in the Universal Transverse Mercator projection. In addition to the standard data sets, this map has a Lillooet LRMP layer, DEM image hillshade layer, a magnetics map layer, and a magnetics raster map with legend.

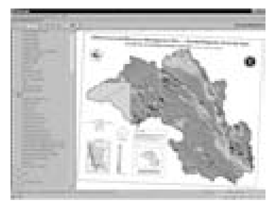

Guichon Batholith Map

This map covers NTS map 92I and is displayed in BC-Albers projection. Unique data layers include the Guichon Magnetic Linears, Guichon Geology Transparent, and Guichon Geology. Mapping was done by W. J. McMillan, J. D. Blanch-Flower, P. McAndless, D. Coombes, P. Garvin; 1969-1974 and linework was digitally captured by Cominco Ltd.

Vernon Geology Map

This map covers NTS maps 082L03, 06, 11, 13, 14 and is displayed in the Universal Transverse Mercator projection. Unique layers to this map are Geology Unit, Lines, Structures, Mapping Stations, and Ages in the Vernon Area.

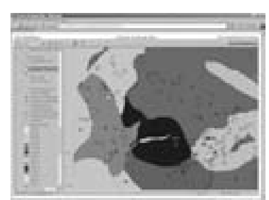

Aggregate Potential Map

This map displays the results of four aggregate potential study areas: Prince George, Okanagan, Nanaimo and Sea-to-Sky. Each of these four study sites are organized into four layers under the Aggregate Potential layer Group. Photos of aggregate pits are available mainly in the north part of the Sea-to-Sky study area. To view the photos, use the select tool and double click if a hand shows while on the pit symbol. Links to the Aggregate Projects and downloads are available in the PopUp Menu on the Map.

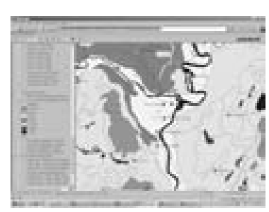

Terrain Map Index (Open File 1992-13)

This published index provides a compilation of data for about 2000 surficial geology/terrain maps of British Columbia. The database is presented both as a tabulated listing, and graphically in a series of provincial base maps. The tabulated database presents the location in relation to the National Topographic System, scale and agency involved. This hardcopy report is available from Crown Publications. A link to the Terrain Map Library provides terrain and slope stability related maps in digital format. The digital maps may be constructed and viewed on-line or downloaded for use in a GIS or Desktop Mapping package.

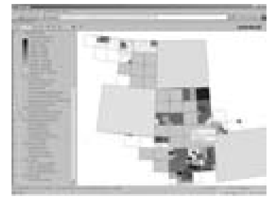

Regional Geophysics Map

This map is projected in Lambert Conformal Conic, NAD 27. Unique layers to this map are Gravity, Aeromagnetics, Landsat and DEM Shaded Relief. These images come directly from the CORDLINK, a collaborative knowledge network initiative between the Geological Survey of Canada and its provincial/territorial and academic partners in western Canada.

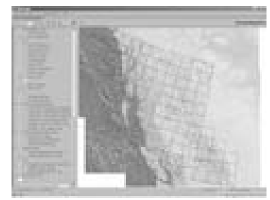

Relief and Radar Map

The Relief and Radar Map contains a colour shaded relief map based on the GTOPO30 data set and a radar mosaic for the southern portion of the province. More detailed colour relief, radar mosaic and digital elevation model (DEM) layers are available for Vancouver Island. These raster layers are from GeoGratis (National Resources of Canada), a web site and FTP site that distribute geospatial data of Canada free of charge.

Southeast BC Geophysics Map

The Southeast BC Geophysics map is displayed in UTM-NAD 83 projection and contains three unique layers geophysical layers: Kootmag, Magnetics and Thorium ratios. These layers are from the Geological Survey of Canada Pacific Geoscience Centre. A sample detailed orthophoto (1 metre pixels) is available for area 082F.099 at scale of 1:35,000.

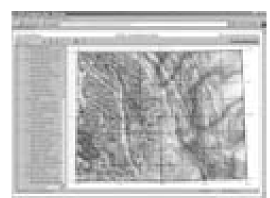

Petroleum Tenure and Wells Map

This map displays northeastern BC Petroleum and Natural Gas well locations, tenure and major pipelines. Tools allow users to query tenure owner, tenure number, range of tenure numbers or BC Gazetteer locations in the right window frame. This queried information can be displayed on the map.

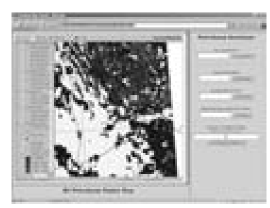

Coal Map

This map features Coal Geology layers, databases from COALFILE and links to Coal Assessment Reports in PDF format on the map.

BC Geology Map Index

This map is displayed in Albers Equal Area Projection. This map contains most of the layers found in the BCGS Geology map, as well as the following Index Map layers: Surficial Mapping Index, Regional Geochemical Survey Index, MINFILE Index, and B.C. Geological Survey of Bedrock by Date, Scale and Type.

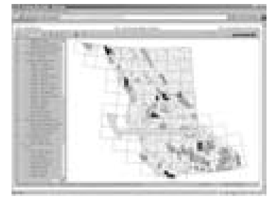

GSC & GSB Geology Map Indexes

This map of the World, is zoomed into Canada and is displayed in Mercator projection. This map contains map index layers from the Geological Survey of Canada (GSC) and B.C. Geological Survey (GSB), as well as a volcano, world countries, major cities layer, U.S. Cities, States and Interstates layers.

Mineral Statistics

These maps display locations of mining, coal, industrial mineral, refining and smelting operations.

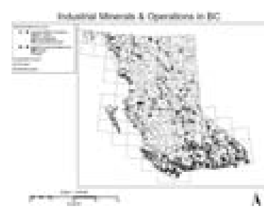

CONCLUSION

The MapPlace has been operational for over five years, providing free Internet access to mineral exploration-related information to the mineral exploration industry, land use planners, government agencies and the general public. It has proven to be an efficient and effective way to disseminate map-based information and its flexibility gives users a powerful tool for building their own custom maps. Visit the MapPlace at http://www.em.gov.bc.ca/MapPlace.